IAEA-SMR-43

NUCLEAR THEORY FOR APPLICATIONS

PROCEEDINGS OF THE COURSE ON NUCLEAR THEORY FOR APPLICATIONS
HELD AT TRIESTE, 17 JANUARY – 10 FEBRUARY 1978
DURING THE WINTER COURSES ON NUCLEAR PHYSICS AND REACTORS
JOINTLY ORGANIZED BY THE
INTERNATIONAL ATOMIC ENERGY AGENCY,
THE INTERNATIONAL CENTRE FOR THEORETICAL PHYSICS
AND THE
CENTRO DI CALCOLO BOLOGNA OF THE
COMITATO NAZIONALE PER L'ENERGIA NUCLEARE OF ITALY
AND HELD AT THE
INTERNATIONAL CENTRE FOR THEORETICAL PHYSICS, TRIESTE
17 JANUARY – 10 MARCH 1978

INTERNATIONAL CENTRE FOR THEORETICAL PHYSICS, TRIESTE, 1980

NUCLEAR THEORY FOR APPLICATIONS

THE INTERNATIONAL CENTRE FOR THEORETICAL PHYSICS (ICTP) in Trieste was established by the International Atomic Energy Agency (IAEA) in 1964 under an agreement with the Italian Government, and with the assistance of the City and University of Trieste.

The IAEA and the United Nations Educational, Scientific and Cultural Organization (UNESCO) subsequently agreed to operate the Centre jointly from 1 January 1970.

Member States of both organizations participate in the work of the Centre, the main purpose of which is to foster, through training and research, the advancement of theoretical physics, with special regard to the needs of developing countries.

IAEA-SMR-43

NUCLEAR THEORY FOR APPLICATIONS

PROCEEDINGS OF THE COURSE ON NUCLEAR THEORY FOR APPLICATIONS
HELD AT TRIESTE, 17 JANUARY – 10 FEBRUARY 1978
DURING THE WINTER COURSES ON NUCLEAR PHYSICS AND REACTORS
JOINTLY ORGANIZED BY THE
INTERNATIONAL ATOMIC ENERGY AGENCY,
THE INTERNATIONAL CENTRE FOR THEORETICAL PHYSICS
AND THE
CENTRO DI CALCOLO BOLOGNA OF THE
COMITATO NAZIONALE PER L'ENERGIA NUCLEARE OF ITALY
AND HELD AT THE
INTERNATIONAL CENTRE FOR THEORETICAL PHYSICS, TRIESTE
17 JANUARY – 10 MARCH 1978

INTERNATIONAL CENTRE FOR THEORETICAL PHYSICS, TRIESTE

NUCLEAR THEORY FOR APPLICATIONS, IAEA, VIENNA, 1980

Printed by the IAEA in Austria
March 1980

FOREWORD

The International Centre for Theoretical Physics has maintained an interdisciplinary character in its research and training programmes in different branches of theoretical physics. In pursuance of this objective, the Centre has organized extended research courses and workshops, including topical conferences, with a comprehensive and synoptic coverage in varying disciplines. The first of these – on Plasma Physics – was held in 1964 and then repeated in 1977; the second, in 1965, was concerned with the Physics of Particles. Between then and now, the following courses were organized: four on Nuclear Theory (1966, 1969, 1971, 1973), six on the Physics of Condensed Matter (1967, 1970, 1972, 1974, 1976, 1978), three on Atomic Physics (1973, 1977, 1979), two on Geophysics (1975, 1977), one on Control Theory and Functional Analysis (1974), one on complex analysis (1975), one on Applications of Analysis to Mechanics (1976), one on Mathematical Economics (1978), one on Systems Analysis (1978), two on Teaching of Physics at tertiary level (in English in 1976, in French in 1977), and two on Solar Energy (1977, 1978). Most of the Proceedings of these courses have been published by the International Atomic Energy Agency (Vienna, Austria).

The present volume forms part of the Proceedings of the Winter Courses on Nuclear Physics and Reactors, conducted from 17 January to 10 March 1978. This volume contains the Proceedings of the Course on Nuclear Theory for Applications, held at Trieste, 17 January to 10 February 1978. A separate volume contains the Proceedings of the Course on Reactor Theory and Power Reactors, held from 13 February to 10 March 1978. The Winter Courses were held in response to the growing need of developing countries which plan to establish a nuclear power programme to familiarize themselves with the nuclear and reactor physics foundations of nuclear energy and their applications in the design of nuclear reactors.

The programme of lectures and working sessions was organized by Drs. J.J. Schmidt and J.A. Larrimore (International Atomic Energy Agency, Vienna, Austria), Professor V. Benzi (Centro di Calcolo of the Comitato Nazionale per l'Energia Nucleare, Bologna, Italy), and Professor L. Fonda (ICTP, Trieste, Italy).

Abdus Salam

PREFACE

This volume contains the text of the invited lectures presented during the Course on Nuclear Theory for Applications which was held at the International Centre for Theoretical Physics (ICTP) in Trieste, Italy, from 17 January – 10 February 1978, within the framework of the nuclear physics activities of the ICTP during the winter of 1978. This Course was jointly organized by the IAEA Nuclear Data Section and ICTP with the collaboration of the Centro di Calcolo, Bologna, of the Comitato Nazionale per l'Energia Nucleare (CNEN) of Italy. The Course was attended by 91 participants from 29 developing countries, 12 participants from six developed countries, and five participants from the Central Bureau for Nuclear Measurements, Geel, and the Joint Research Centre, Ispra, of the Commission of European Communities, and from the Joint Institute for Nuclear Research, Dubna, USSR.

The purpose of this Course was to offer nuclear physicists, nuclear data evaluators and reactor scientists with an interest in nuclear theory and nuclear data particularly from developing countries which have plans to embark on a nuclear power programme a thorough review of the contemporary research in low-energy nuclear reaction theory with a simultaneous training on an advanced level in the application of this theory and associated computer codes to the interpretation and computation of neutron nuclear data needed for nuclear reactor calculations.

The Course was started with introductory lectures on the importance and evaluation of nuclear data for applied purposes and continued with a series of lectures, special seminars, working sessions and computer code workshops on the following major topics and their applications in nuclear data computations:

1. Theory and interpretation of resolved and unresolved neutron resonances including statistical distribution laws for partial resonance widths and resonance spacings;
2. Advanced neutron optical models including the foundations and parameterization of spherical and deformed optical potentials with an emphasis on modern matrix methods;
3. Statistical theory of neutron nuclear reactions including nuclear single-particle and collective level density theories;
4. Theory and models of pre-equilibrium decay in neutron nuclear reactions;
5. Theory of neutron-induced nuclear fission with an emphasis on the double-humped fission barrier, its properties and parametrization.

Since the lectures given at this Course present the first comprehensive review of nuclear reaction theories and models underlying the interpretation and computation of neutron nuclear data needed for reactor physics calculations and other applied purposes, they are expected to be of interest to nuclear scientists both from developing countries where nuclear data and reactor physics research are still in the beginning and from developed countries where such research is in an advanced stage. They can be used as a reference in the field or as an advanced text-book for postgraduate study.

The organizers are most grateful to the lecturers, workshop leaders and scientific coordinators for their very active engagement and co-operation in the objectives of the Course, and to the Staff of the ICTP for their most pleasant and efficient help in the preparation and conduct of the Course.

CONTENTS

IV. PRE-EQUILIBRIUM DECAY
(Scientific co-ordinator: D. Seeliger)

V. FISSION THEORY
(Scientific co-ordinator: J.E. Lynn)

NUCLEAR DATA, THEIR IMPORTANCE AND EVALUATION

J.J. SCHMIDT
Nuclear Data Section,
Division of Research and Laboratories,
International Atomic Energy Agency,
Vienna

ABSTRACT

Nuclear data comprize all quantitative results of nuclear physics investigations and can be subdivided in the three areas of nuclear structure, nuclear decay and nuclear reaction data. For the purposes of fission and fusion reactor design mostly neutron reaction data are needed, while for the nuclear fuel cycle outside the reactor and for a large variety of "non-energy" scientific applications a number of photonuclear and charged particle nuclear reaction data and of nuclear structure and decay data are needed, in addition to selected neutron nuclear reaction data. To meet the needs of nuclear science and technology for accurate nuclear data, comprehensive computer libraries of evaluated nuclear data have been built up from evaluation of a massive volume of experimental data complemented by data calculated from nuclear theory. The basic characteristics and requirements of evaluated data libraries are discussed and evaluation sources and methods illustrated with the example of a few important neutron nuclear reactions. International mechanisms have been developed, coordinated by the IAEA Nuclear Data Section with the cooperation of many nuclear data centres and groups, for the efficient dissemination of bibliographic and numerical experimental and evaluated nuclear data to data users in the whole world.

1. INTRODUCTION

As a general definition, the quantitative results of any scientific investigation of the nuclear properties of matter are called nuclear physics data, or briefly nuclear data.

Nuclear data are generated mostly by nuclear physics experiments, but also by nuclear theory. The application of nuclear theory, nuclear models and nuclear systematics to the generation and interpretation of nuclear data is the main subject matter of the first part of these Winter Courses on Nuclear Physics and Reactors, dealing with Nuclear Theory for Applications.

Nuclear data have a wide-spread use in nuclear science and technology, with neutron nuclear data playing a prominent role. Their most important application as input to the design calculations of nuclear fission reactors will be discussed particularly in the beginning of the second part of these Winter Courses, dealing with Reactor Theory and Power Reactors.

In any application of nuclear data there is a genuine interest to use the "best" information then available in a most convenient form. The results of different nuclear physics measurements do generally not agree with each other. Before their application they have therefore to be compiled, critically compared, renormalized to common standards, selected, averaged, and error bars assigned, i.e. they have to be evaluated to so-called "best" or "recommended" values. Via interpretation, inter- and extrapolation nuclear theory plays an important role in this process. Evaluated data are then made available to the user in computerized and/or published medium.

It seems therefore necessary and appropriate to devote the introductory lectures to these courses to the subject of nuclear data, their detailed definition, importance and evaluation, with an emphasis on neutron nuclear data.

2. DEFINITION OF NUCLEAR DATA

Nuclear data can be subdivided into the following three categories:

- nuclear structure data;
- nuclear decay data; and
- nuclear reaction data.

To understand the meaning of these data a few basic facts from nuclear physics have to be recalled.

2.1 Nuclear structure data

The nucleus of an atom is composed of neutrons and protons called nucleons. They move, individually or collectively, within the spatial boundaries of the nucleus and are held together by strong short-range attractive forces called nuclear forces. Each nucleon thus possesses kinetic and potential energy in given energy states whose characteristics are governed by the Pauli-exclusion principle. The sum of these energies forms the ground state energy of the nucleus.

Individual or collective excitation of nucleons, by taking up energy from nuclear particles or radiations, produces excited states

of the nucleus, called its energy levels. Each of these levels is characterized by its energy above the ground state and spin and parity quantum numbers.

Each isotope of each element, whether stable or unstable, has its own characteristic level scheme. The density of the levels per energy unit increases with increasing excitation energy of the nucleus. At lower excitation energies up to several MeV above the ground state, and at energies just above nucleon binding energy in particular, experimental techniques allow the resolution of individual levels and the determination of their energy and quantum characteristics. At higher energies the levels become so dense that they can no more be discerned experimentally; they form a quasi-continuum of decaying states and only their statistical properties can be investigated.

The totality of this category of nuclear data is called nuclear level scheme or nuclear structure data. They are illustrated in figure 1.

2.2 Nuclear decay data

At present 276 stable isotopes and about 2800 radioactive isotopes are known. While per definition the stable isotopes decay only from excited states, radioactive isotopes decay from their ground and excited states, usually by β- and γ-ray emission or internal conversion, except for the heavy actinide nuclides which in addition exhibit α-decay and spontaneous fission. If a nucleus is excited to levels above the binding energy of a nucleon or a heavier particle, decay will proceed also via single or multiple particle emission, usually followed by γ-ray emission, until a stable end product, i.e. the ground state of a stable nucleus, is reached. If energetically feasible, particle emission is usually preferred to β- or γ-ray emission.

The practically most important data governing nuclear decay are the decay half lives of ground and excited states including metastable states, the branching ratios for the various possible decays and the energies and intensities of the emitted particles and radiations.

The totality of this category of nuclear data is called nuclear decay data.

2.3 Nuclear reaction data

The interaction of nuclear particles and radiations (a) (γ-rays, neutrons, protons, deuterons, or heavier ions) with nuclei (A) are usually described by the equation

$$A + a = B + b$$

or schematically

$$A\ (a,b)\ B$$

where b denotes the emitted particle(s) and/or radiation(s) and B the residual nucleus (or, in the case of fission, the resulting two fission fragments).

The strength of a particular nuclear reaction is expressed in terms of a quantity called the cross section; it is a measure for the probability of the occurrence of a particular reaction between nuclear particles A and a which leads to specific particles B and b. It is usually measured in units of $10^{-24}cm^2$, called barn, which roughly compares to the "geometrical" cross sections of nuclei which range from about 0.02 to 2 barn. Measured cross sections range from about 10^{-6} to 10^{+6} barn.

Usually not only the cross section for a specific nuclear reaction as a function of the kinetic energy of the incoming particle "a" is wanted, but in addition the energy and angular distributions of the emitted secondary particles or radiations "b", or, in fission, the number of prompt and delayed neutrons emitted and their energy distributions, or composite quantities such as the ratio α of neutron capture to neutron fission cross sections.

The totality of this category of data is called nuclear reaction data.

2.4 Neutron nuclear reaction data

The characteristic features of nuclear reactions and their cross section behaviour are illustrated below by the example of neutron nuclear reactions which are the most important nuclear reactions for applications.

Once a neutron is captured by a nucleus A, the nucleus C is formed which is called the compound nucleus with an excitation energy which is the sum of the kinetic energy of the neutron and its binding energy ($\sim$ 5-10 MeV) in the nucleus C. The compound nucleus may now decay in several different ways depending upon the size of its excitation energy. The following reactions are most common at neutron energies below about 15 MeV (see figure 1):

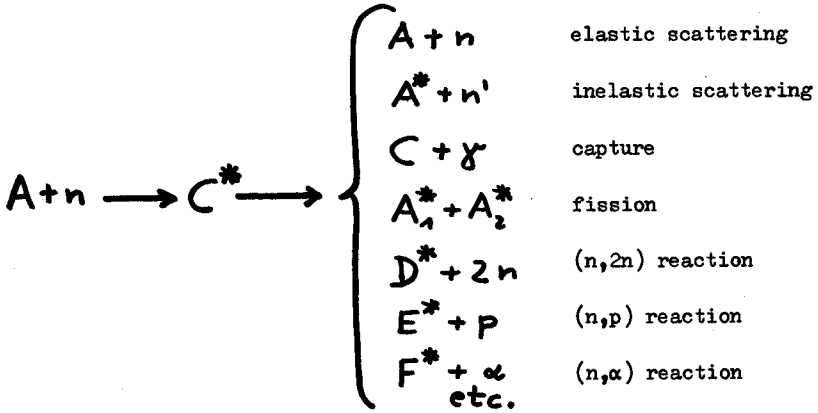

The * means the nucleus in state of excitation; usually the excited nuclei return to their groundstate by single or cascade γ-ray emission, the excited fission fragments decay by delayed neutron, γ-ray, β and neutrino emission. While elastic scattering, capture and (for fissile nuclei) fission are possible at all neutron energies, inelastic scattering is only possible for kinetic energies of the incoming neutrons higher than the first excited state of nucleus A; (n,2n) reactions only for excitation energies in excess of the binding energies of the two nucleons; (n,p) and (n,α) reactions only for excitation energies in excess of the binding energies of the proton and of the α-particle in the compound nucleus (if $E_{exc} > E^{p,\alpha}_{Bind}$: exothermic reaction; if $E_{exc} < E^{p,\alpha}_{Bind}$: endothermic reaction); and fission reactions (for fertile nuclei) only above the fission threshold of the compound nucleus with some subthreshold fission due to "tunnelling" through the fission barrier. The sum of the cross sections for all reactions possible at a given energy is called the total cross section.

Note that the compound nucleus formation and decay is not the only, but, at lower excitation energies up to the MeV range, the most usual reaction mechanism which involves a statistical sharing of the excitation energy imparted to a nucleus by all its nucleons at an intermediate stage of the reaction. Other possible reaction mechanisms at higher excitation energies, leading, however, to the same reaction products, involve direct or semi-direct excitation and emission of nucleons or clusters of nucleons before the formation of a compound nucleus. These can be subsumed under "direct" or "pre-compound" reaction mechanisms; they will form an important subject of the present course.

The general dependence of neutron nuclear reaction cross sections upon neutron kinetic energy is visualized in figure 2 for the capture, fission and elastic scattering of neutrons on a heavy fissile nucleus. According to the structure exhibited by the cross sections the total energy range displayed from 0 to above 10 MeV can be subdivided in the four subranges of

- thermal energies;
- resolved discrete resonances;
- unresolved overlapping resonances; and
- range of smooth energy dependence of cross sections or so-called "continuum" range.

2.4.1 Resolved discrete resonances

Due to the high binding energy of the neutron, the compound nucleus, already for small neutron kinetic energies, is excited in very densely distributed nuclear energy levels called resonances. As the widths of these resonances are usually smaller than their distances, they can be discerned from each other and experimentally resolved. Usually resonances are very complex states whose individual properties cannot be predicted by nuclear theory. Resonance shapes and the energy dependence of cross sections through resonances, however, can be adequately described by nuclear resonance theory with appropriate parameterisation. With sophisticated experimental and theoretical techniques developed over the past 25 years several 10 000 resonances for many nuclei over the whole range of atomic weights have been measured and analyzed for their energy positions, half widths for the various possible decay modes, and the quantum numbers for their spin and neutron orbital angular momentum, altogether called resonance parameters. The range of resolved resonances extends to keV neutron energies for heavy and medium-weight nuclei and to MeV neutron energies for lighter nuclei.

2.4.2 Thermal energies

The thermal range of neutrons, governed by thermal equilibrium between neutrons and the lattice vibrations of the surrounding medium, extends between 0 and about 1 eV neutron energy and thus represents a very small section only of the resonance range. For the resonance range extends also to "negative" energy resonances below the neutron binding energy which, however, can only decay by the emission of γ-rays.

If the thermal range falls between resonances, the cross sections follow a rather simple energy dependence and are fairly small. If resonances fall in the thermal range, then the cross sections can reach very high values. Prominent examples are the exceptionally high capture cross sections of the fission product isotopes ^{135}Xe and ^{149}Sm of $3.4 \cdot 10^6$ b and $1.2 \cdot 10^5$ b in the peaks of resonances located at neutron energies of 0.084 eV and 0.098 eV respectively.

2.4.3 Unresolved overlapping resonances

Due to the combined effects of the broadening of the resonance widths and the increase of the resonance density with increasing neu-

tron energy the resonances eventually begin to overlap and can no more be disclosed from each other. For heavy and medium weight nuclei this range extends to higher keV energies, below about 100 keV, for lighter nuclei to higher MeV energies.

In this range only average resonance properties such as average half widths and average level spacings can be deduced from

- measured cross sections;
- extrapolation of resolved resonance properties to higher energies; and
- nuclear level systematics.

The distribution in size of the resonance partial widths and spacings is theoretically well understood and can also be deduced from known resolved resonances. These data are needed in theoretical predictions of unknown cross sections by means of the statistical theory of neutron nuclear reactions.

2.4.4 "Continuum" range of energies

At high neutron energies any resonance structure is washed out so that the energy dependence of the neutron cross sections becomes smooth. At excitation energies of multiples of the nucleon binding energy multiple particle emission or spallation is observed.

3. IMPORTANCE OF NUCLEAR DATA

Generally speaking an adequate knowledge of nuclear data is required whereever in science and technology nuclear reactions, radiations and isotopes are applied. It will be shown in the following, that nuclear data occur in practically all branches of nuclear science and technology with varying priority and accuracy requirements.

3.1 Fission reactors

In the domain of nuclear energy, the largest and most stringent requirements for accurate nuclear data, particularly neutron cross sections, exist for the physics design of fission reactors. Reactor parameters such as the effective multiplication factor K_{eff}, critical mass, fuel enrichment, critical reactor size, neutron flux, breeding ratio, safety coefficients, kinetic and dynamic characteristics are calculated from mathematical equations in which neutron cross sections and related nuclear data enter as basic parameters. Well known is for example the Boltzmann-equation for the calculation of the energy and space-dependent reactor neutron flux.

The answer to the question which nuclear data are needed for fission reactors and with which priority is closely linked with the material composition and the energy dependent neutron flux or neutron energy spectrum of a given reactor. Generally speaking neutron cross sections are needed for all reactor materials over the whole energy range covered by the reactor neutron energy spectrum. In order to understand the nuclear data needs in detail the neutron energy spectra occurring in typical fission reactors will be considered.

Fission reactors can be roughly subdivided into so-called thermal and fast reactors which are currently the most important reactor types. Thermal reactors contain moderating material of low atomic weight such as light or heavy water, graphite or beryllium which, by elastic scattering collisions, slows the neutrons generated in fission down to thermal energies, thus leading to a thermal neutron energy spectrum. In a fast reactor, which is usually composed of materials of higher atomic weight, fission neutrons are slowed down preferably by inelastic scattering, without reaching thermal energies, thus leading to a fast neutron energy spectrum centered in the keV and MeV ranges of neutron energies.

Figure 2 shows typical neutron energy spectra of thermal and fast reactors. Specifically, the spectrum of a thermal reactor is centered between 0.01 and 1 eV. In this energy range it obeys essentially a Maxwell type distribution, whereas above 1 eV it decreases as 1/E. The fast neutron flux of a thermal reactor, obtained by integration of the neutron energy spectrum over fast neutron energies, is still typically by a factor three larger than the thermal neutron flux, but the much higher fission and capture cross sections cause about 100-fold higher reaction rates at thermal energies. Therefore in a thermal reactor the knowledge of fission, capture and elastic scattering cross sections in the very small energy range between 0 and several eV as well as of the properties of the low-lying resonances in fertile and fissile isotopes is crucial for the determination of the physics characteristics of the reactor. This is easily realized from figure 2, when comparing the neutron flux and cross section curves at low neutron energies. With some exceptions neutron cross sections needed for thermal reactors can be considered today as sufficiently well known.

Fast reactor neutrons, however, are spread over a much larger energy range extending from eV energies to about 15 MeV, with an emphasis on energies between about 1 keV and several MeV. They cover the resonance range as well as the "continuum" range. In addition to fission, capture and elastic scattering, resonance parameters and cross sections over the entire discrete and over-lapping resonance range, cross sections for inelastic scattering, at higher energies also (n,p), (n,α), (n,2n), (n,3n) reactions, and the angular and energy distributions of emitted neutrons have to be known as a function of neutron energy, as can again be seen from figure 2.

For the different variants of both thermal and fast reactors, neutron cross sections have to be known for a large variety of materials and isotopes such as

fissile isotopes:	^{233}U, ^{235}U, ^{239}Pu, ^{241}Pu;
fertile isotopes:	^{232}Th, ^{238}U, ^{240}Pu;
structural materials:	Fe, Cr, Ni, Zr;
cooling materials:	H_2O, D_2O, He, CO_2, Na;
moderating materials:	H_2O, D_2O, Be, C;
control rod materials:	B, Ta;
shielding materials:	Fe, Pb, Ba, Si;

O for oxide fuel and C for carbide fuel, to mention only the most important materials.

Contemporary reactor theory calculations performed with the aid of computers are so refined that they allow very accurate predictions of the physics characteristics of fission reactors under the condition that the neutron cross sections involved are available to sufficient detail and accuracy.

For an adequate description of the energy dependence of the neutron cross sections many data points in an uninterrupted chain are needed, typically of the order of 100 to more than 1000 data points for each reaction, depending upon the complexity of its energy dependence.

In order to illustrate the neutron cross section accuracies required for reactor calculations we will consider two important parameters of a fast reactor, i.e. K_{eff} and the breeding ratio BR, and with simplifying assumptions, the equations which connect these parameters with neutron nuclear data.

3.1.1 K_{eff}

K_{eff} is defined as

$$K_{eff} = \frac{\text{Neutron generation in reactor per unit time}}{\text{Neutron absorption in reactor per unit time} + L}$$

$$= \frac{\bar{\nu} \cdot \Sigma_f}{\Sigma_a + L}$$

where

$\bar{\nu}$ = average number of neutrons per fission;

$\Sigma = N \cdot \sigma$ = macroscopic cross section for fission (f) and capture (γ), averaged over the whole neutron energy spectrum;

N = number of atoms/cm^3;

σ = microscopic cross section;

$\Sigma_a = \Sigma_f + \Sigma_\gamma$ = macroscopic absorption cross section;

L = neutron leakage out of the reactor per unit time.

For simplicity we neglect neutron capture in all reactor materials except ^{238}U and ^{239}Pu and the neutron leakage (small in a typical large fast reactor). Then K_{eff} becomes

$$K_{eff} \cong \frac{\bar{\nu}^9 \Sigma_f^9 + \bar{\nu}^8 \Sigma_f^8}{\Sigma_{f+\gamma}^9 + \Sigma_{f+\gamma}^8}$$

where the superscripts 8 and 9 denote ^{238}U and ^{239}Pu respectively.

Introducing

$$\gamma = N^8/N^9$$
$$\alpha^9 = \sigma_\gamma^9/\sigma_f^9$$

we get

$$K_{eff} \cong \frac{\bar{\nu}^9 + \gamma \cdot \bar{\nu}^8 \sigma_f^8/\sigma_f^9}{1 + \alpha^9 + \gamma\left(\frac{\sigma_f^8}{\sigma_f^9} + \frac{\sigma_\gamma^8}{\sigma_f^9}\right)}$$

K_{eff} thus depends essentially upon four types of neutron nuclear data:

- $\bar{\nu}$
- α^9
- $\sigma_f^8/\sigma_f^9 = F$
- $\sigma_\gamma^8/\sigma_f^9 = G$

They belong to those nuclear data most crucially needed for fast reactor calculations. Reactor designers generally require K_{eff} to be predicted to an accuracy of at least 1%. Starting from the above equation we will now investigate how accurately these nuclear data have to be known

in order to fulfil this requirement. We get upper estimates of the required accuracies, if in each of the four cases we consider the respective other nuclear data as precisely known. The equation shows immediately that $\bar{\nu}$ has to be known to at least 1%. For the three other quantities we get by partial differentiation and by inserting currently known values for α, F and G

$$\frac{\partial \alpha^9}{\alpha^9} \cong (10 \div 20) \left| \frac{\partial K}{K} \right| (\%)$$

$$\frac{\partial F}{F} \cong (5 \div 10) \frac{\partial K}{K} (\%)$$

$$\frac{\partial G}{G} \cong (3 \div 5) \frac{\partial K}{K} (\%)$$

This shows that for K_{eff} to be predicted with 1% accuracy α^9 has to be known with an accuracy between 10 and 20%, σ_f^8/σ_f^9 to 5-10%, and $\sigma_\gamma^8/\sigma_f^9$ to 3-5%. Note that these are upper estimates and that the real requirements for each of these data are more stringent if it is taken into account that each of them has a certain inaccuracy.

3.1.2 Breeding ratio

The breeding ratio is defined as

$$BR = \frac{^{239}\text{Pu nuclei produced in reactor per unit time}}{^{239}\text{Pu nuclei destroyed in reactor per unit time}}$$

and can be written as [1]

$$BR = \eta^9 - 1 - L'$$

where

$$\eta^9 = \bar{\nu}^9 \cdot \frac{\sigma_f^9}{\sigma_\gamma^9 + \sigma_f^9} = \bar{\nu}^9 \cdot \frac{1}{1 + \alpha^9}$$

η^9 = average number of neutrons per neutron absorption in ^{239}Pu;

L' = neutron loss by leakage and by capture in all other reactor materials except fissionable.

Besides $\bar{\nu}$ whose magnitude ($\cong 2.9$) enables ^{239}Pu breeding at fast neutron energies, BR depends essentially upon α^9.

The feedback from the uncertainty in α to that of the breeding ratio is, like in the case of K_{eff}, obtained by partial differentiation with the result

$$\frac{\partial \alpha}{\alpha} \cong \frac{1 + \alpha}{\alpha} \left| \frac{\partial BR}{BR} \right| (\%)$$

$$\cong 5 \left| \frac{\partial BR}{BR} \right| (\%)$$

For the usual requirement of 2% accuracy for the prediction of BR, α^9 has at least to be known to 10% accuracy, i.e. to a better accuracy than for K_{eff}.

3.1.3 Requirements and achievements

In response to these requirements, very extensive efforts of nuclear physicists have been devoted over the past 20 years to the accurate measurement particularly of the capture and fission properties of thermal and fast reactor fertile and fissile isotopes. At thermal energies and for the major isotopes these properties are nowadays almost all known to satisfactory accuracy. For resonance and fast energies only the upper limits of the accuracy requirements have so far been met and much work is still going on to improve the measurement methods and results. A comparison of the presently requested and achieved accuracies for some of the crucial fast reactor capture and fission data is given in the table below. The requested accuracies were taken from reference [2].

Quantity	Accuracy (%)	
	requested	achieved
$\bar{\nu}^9$	0.5 - 1.0	1 - 2
σ_f^9	1 - 3	5
α^9	5 - 10	10 - 20
σ_γ^8	3 - 7	5 - 10

Taking into account the present uncertainties of all relevant nuclear data one can compare the uncertainties of predicted fast reactor design parameters due to nuclear data uncertainties with the accuracies required for these parameters. This is illustrated in the following table.

Reactor parameter	Accuracy required	Accuracy achieved
K_{eff}	1%	1 - 2%
Breeding ratio	2%	5 - 10%
^{239}Pu doubling time	10%	20 - 40%
Fuel cost	0.03 $\frac{\text{mill}}{\text{KW(e)h}}$	$\sim$ 0.10 $\frac{\text{mill}}{\text{KW(e)h}}$

The economic incentive for having accurate nuclear data for fast reactor design is illustrated in the last line of this table by the uncertainties in the fuel cost. Greebler et al. [3] from General Electric estimated that the uncertainty in fuel cost of 0.13 mill/KW(e)h in 1970 due to uncertainties in nuclear data is equivalent to an uncertainty of US $ 900 000/year in the operating cost of a single 1000 MW fast reactor. Simultaneously they requested an improvement in the accuracy of nuclear data to achieve eventually a tolerable fuel cost uncertainty of 0.03 mill/KW(e)h. This goal is still not reached; the present achievement is about 0.10 mill/KW(e)h.

The IAEA Nuclear Data Section publishes biannually a list of requirements for non-existent or improved nuclear data needed for fission reactor design from input provided by about 20 Member States of the IAEA; this list is called WRENDA. In the most recent edition, WRENDA 76/77 [2], about 30% of the 1200 individual requests are high priority requests for improved capture, fission and scattering cross section data for the major fissile, fertile, structural and coolant materials of fast and thermal reactors.

As a typical example figure 3 shows the requests for improved fast reactor capture cross sections for ^{238}U contained in WRENDA 76/77. Each individual request provides information on the requested isotope and quantity, the neutron energy range, the required accuracy and priority, and the origination and purpose of the request. Request lists like WRENDA have proven to be very useful means to stimulate and coordinate required nuclear data measurements.

3.2 Fission product and actinide nuclear data

More recently, due to the growing development of nuclear industries in many countries, which comprise few to many reactor stations, plants for fuel fabrication and chemical reprocessing, transport of fresh and spent nuclear fuel etc., the problem of accumulation of fission products and actinides produced in the reactors becomes more and more severe. Both groups of nuclides are highly radioactive; due to larger half lives the life time of actinides is much longer than that of fission products so that actinides present the stronger long-term radioactivity hazard. With the exception of some specific applications such as the use of the α-decay of ^{238}Pu and ^{244}Cu as a heat source in nuclear batteries of earth satellites, both fission products and actinides can no more be used in the reactor itself (except potential incineration of actinides in special purpose reactors) and have to be disposed of. To give an idea of the size of the future waste disposal problems a forecast made in the United States [4] two years ago estimates the cumulative amount of actinide production in US reactors until the year 2000 at about 1300 metric tons and the annual discharge of actinides in the USA around the year 2000 at about 110 metric tons. These estimates are based on a projection that in the year 2000 1200 reactors of 1000 MW(e) each will be in operation in the USA. This may be an overestimate, but illustrates the order of magnitude of the problem. The production of fission products will be several times higher.

The following experimental and theoretical investigations are thus imperative and are currently being pursued in Member States by short- and long-term projects:

1. build-up of fission products and actinides in reactors and their influence on reactor operation;
2. release of heat after reactor shut-down, so-called afterheat, caused by α, β and γ-decay of fission product and actinide nuclides and by fissions induced by delayed, spontaneous fission and (α,n) neutrons;
3. short-term shielding problems of fission products and actinides during fuel handling, reprocessing and transport; and
4. long-term radioactivity hazards of fission product and actinide wastes and criticality hazard of actinide waste, which represents a neutron source due to spontaneous fissions, (γ,n) and (α,n)-reactions.

For all of these investigations a large amount of nuclear data is needed, many of which are still unknown or only poorly known. The size of the requirements can be partially illustrated by the number of isotopes involved as seen from the table below.

Nuclide species	Total number occurring	Important
Fission products	800	$\approx$ 50
Actinides	200	$\approx$ 30

Long half-lives, high yields and high capture and fission cross sections were used as criteria in this selection. The many nuclides with short half-lives have only short-term importance, such as short-lived fission products in afterheat calculations, and are omitted from the important.

The size of the requirements is furthermore demonstrated by the fact that about 30% of the nuclear data requests for fission reactors contained in WRENDA 76/77 are for various nuclear data for fission product and actinide nuclei.

In summary the nuclear data needs are

inside the reactor: ①	all neutron cross sections, especially capture, yields, and delayed neutron data for fission products; all neutron cross sections, especially fission and capture, for actinides; neutron energy range: 0-15 MeV;
outside the reactor: ②-④	α-, β-, γ-, and spontaneous fission decay characteristics, half lives, radiation energies and intensities for both fission products and actinides; (γ,n) and (α,n) reactions particularly in low Z materials.

In response to the requirements and in assistance to the current national efforts the IAEA Nuclear Data Section has recently started a rather intensive long-term programme by which the needs and status of nuclear data for fission products and actinides are continuously being assessed, the major gaps and discrepancies in the data determined, and national efforts coordinated to avoid unnecessary duplication. This programme is currently being pursued in cooperation with the Nuclear Energy Agency of the OECD by a series of larger specialist meetings of users and producers of fission product and actinide nuclear data [5-7], by issuing bulletins informing the community concerned about work needed, completed and in progress [8,9], by stimulation of sensitivity studies to determine nuclear data priorities, and by initiating and supporting cooperative research projects for the measurement and evaluation of the required data.

For many highly radioactive fission product and actinide isotopes with short to medium half lives the required neutron cross sections cannot be obtained by experiment or only under extreme conditions and have therefore to be calculated from nuclear theory and systematics. In fact the prediction of fission product and actinide cross sections belongs to the major applications of low-energy nuclear reaction theory. The lectures during this course will show how important the fundamental understanding of the nuclear reaction mechanisms is, as well as the appropriate parameterisation of nuclear reaction theories, for satisfactorily accurate predictions of neutron fission, capture and scattering data.

3.3 Other selected nuclear energy applications

In the context of nuclear energy development several other application areas with sometimes important nuclear data requirements should be mentioned, in particular:

(i) Shielding of neutrons, other nuclear particles and γ-radiation in reactors, particle accelerators and space crafts;

(ii) reactor neutron dosimetry, i.e. in-pile activation measurements of neutron fluence and flux needed e.g. to estimate the radiation damage caused to reactor materials by neutron irradiation; and

(iii) nuclear materials safeguards.

For shielding one needs specifically for a number of reactor and shielding materials the cross sections for the production of γ-rays by neutron fission, capture and inelastic scattering and the energy spectra of the produced γ-radiation. The most recent review of the nuclear data requirements for shielding was performed by a Technical Committee Meeting convened jointly by the IAEA and the Nuclear Energy Agency of the OECD [10].

For reactor neutron dosimetry very accurate data for several dozen activation reactions, mostly threshold reactions ((n,p), (n,α), (n,2n), n,n')), but also (n,γ) and (n,f) data are required. Neutron energy spectra are obtained by unfolding measured activation rates

$$A_i = \int_0^\infty \Sigma_i(E)\ \phi(E)\ dE$$

where i denotes the neutron activation reaction, $\Sigma_i(E)$ its macroscopic cross section as a function of neutron energy E, and $\phi(E)$ the neutron energy spectrum. For N measured reaction rates, one gets a system of N integral equations of the Fredholm first order type, which, for known A_i and Σ_i, can be solved to obtain the desired energy spectrum ϕ. Without going into mathematical detail (see e.g. reference [11]) it can be stated that the results for ϕ are the more accurate, the more activation rates are measured, the more the responses of the activation reactions used complement each other to cover the full energy range of ϕ, and the more accurate the cross sections are for these reactions. The current status of the knowledge of reactor dosimetry neutron cross sections is reviewed in reference [12]. In cooperation with the USA and other countries the IAEA Nuclear Data Section is currently pursuing a cooperative measure-

ment, evaluation and testing programme to establish one single internationally accepted neutron cross section file for reactor neutron dosimetry [13].

Research in nuclear materials safeguards is for instance interested in accurate determinations of nuclear fuel composition e.g. by fuel burn-up measurements for which yields and decay characteristics of selected fission products are needed. As another typical example for data requirements, best values for the masses and half lives of the major U- and Pu-isotopes are needed for the correction of analytical and accountability data for radioactive decay.

These few examples must suffice to illustrate the spread of the data needs for some of the fields related to present-day nuclear energy.

3.4 Nuclear fusion

While the production of nuclear energy from nuclear fusion is a long-term challenge, efforts have already been started in various laboratories to measure nuclear data needed for fusion research and technology. In 1976 the Nuclear Data Section published, as part of WRENDA 76/77 [2] a request list for fusion nuclear data which contains more than 300 individual data requests from France, the Federal Republic of Germany, Japan, the UK, USA and USSR.

The requirements can be subdivided into three categories:

- atomic and selected molecular data;
- charged particle nuclear data; and
- neutron cross sections.

The area of atomic data for fusion is outside the scope of these lectures and is therefore only briefly mentioned. The volume of required data is comparable to that of neutron data required for fission reactors, however, much more serious gaps exist in the present knowledge, compilation, dissemination and use of atomic data. The needs are urgent as many of the required data, such as charge exchange reactions between plasma particles and impurities with the effect of plasma cooling, are intimately connected with the realizability of fusion. The IAEA Nuclear Data Section has started a new programme in this most challenging field.

Let me turn to the nuclear data needs for fusion. Fusion reactions are charged particle nuclear reactions between light nuclei. The most common reaction considered in present fusion reactor concepts is the

$$D(T,n)He^3$$

reaction. It is the fusion reaction with the lowest lying maximum of the cross section, i.e. at 100 keV deuteron energy, and thus with the lowest temperature for a nuclear plasma to fuse. Many investigations have resulted in an accurate knowledge of the energy dependence of the cross section for this reaction. Only for low energies below 10 keV where data are needed to calculate the ignition phase of the fusion reactions, measurements are missing. In fusion devices based on the D(T,n) reaction the T-T reaction can not be neglected, but is only very poorly known at present [14].

For potential future more exotic fusion design a selection of about 80 charged particle reactions for nuclides between H and Li is available [15]. Some of them have the advantage of producing no secondary neutrons, all of them the disadvantage to require higher plasma temperatures to reach fusion conditions. Work on these reactions has already started in some laboratories.

The neutron data requirements by far exceed those for charged particle data. With the use of the T(d,n) reaction the fusion reactor is actually a strong source of 14 MeV neutrons with fluxes at the inner plasma wall estimated to about 10^{15} neutrons/cm^2 sec. These neutrons are gradually slowed down when penetrating the Li blanket and assume an energy distribution which is centered in the MeV range as qualitatively shown in figure 2. This energy range becomes thus of major interest regarding required neutron data. Because these energies are only of limited interest for fast breeder reactors, gaps were left mainly in partial neutron cross sections which now have to be filled. (n,p), (n,d), (n,α), (n,T), (n,^{3}He), (n,2n) reactions as well as the angular and energy distributions of the emitted secondary particles become important. The materials for which these and other data are needed are mostly structural materials suggested for use in a fusion reactor such as Ti, V, Cr, Mn, Fe, Ni, Zr, Nb, Mo and W. Of particular interest is the (n,2n) reaction in first wall materials because it leads to a multiplication of the neutrons available for tritium breeding in the Li blanket of a fusion reactor. Tritium is produced in the blanket by the reactions

$$Li^6(n,\alpha)T \quad \text{and}$$
$$Li^7(n,n'\alpha)T.$$

Much work is going on to accurately determine the neutron energy dependence of these and competing neutron-lithium reactions in the MeV range.

Comprehensive surveys of the requirements and status of nuclear data for fusion reactor design have been reported in reference [16].

3.5 "Non-energy" applications

With the increasing use of nuclear techniques, isotopes and radi-

ations for a large variety of scientific, societal and other purposes, the requirements for accurate nuclear data for "non-energy" applications are continuously growing. This fact was for the first time comprehensively brought out by the Symposium on Nuclear Data in Science and Technology held by the IAEA in Paris in 1973 [17].

Contrary to the rather compact requirements for nuclear energy purposes, the requirements for "non-energy" applications are more heterogeneous and wide-spread; their size becomes large due to the large variety of applications. Nuclear data requirements have been expressed in diverse fields such as medical nuclear dosimetry, diagnostics and therapy, nuclear chemistry, geoscience, archeology, hydrology, environmental research, forensic sciences and astrophysics.

Out of the nuclear methods applied in these fields I shall pick out the following four which are the most widely used:

- nuclear activation analysis by neutrons, charged particles and photons;
- use of radioisotopes as tracers;
- production of radioisotopes; and
- nuclear particle irradiation.

3.5.1 Nuclear activation analysis

For nuclear activation analysis mostly nuclear activation cross sections for neutrons, charged particles and photons, half lives, energies and intensities of the emitted secondary radiations have to be known. As one out of many examples we mention the new IAEA project on neutron activation analysis of pollutants in human hair to measure the degree of environmental pollution caused by poisonous non-radioactive substances. For this project best values of neutron activation cross sections, half lives, and γ-ray energies and intensities are needed for all isotopes of the following elements:

As, Au, Br, Cd, Cl, Cu, Hg, K, Mn, Na, Sb, Se and Zn.

3.5.2 Tracer techniques

Tracer techniques require a knowledge of the half lives and characteristic decay properties of the radioisotopes used as tracers. From the many examples of applications of these techniques we quote the use of tritium and other radioisotopes in surface water investigations of nuclear hydrology and the use of iodine radioisotopes in medical diagnostics.

3.5.3 Radioisotope production

To estimate and optimize the production rate and purity of a desired radioisotope one has to consider and select between all the reactions which lead to this isotope with an additional account for competing reactions leading to other unwanted isotopes. A prototype example is the production of pure ^{238}Pu whose α-radiation is used as a heat source for thermoelectric conversion in a heart pace maker [18]. ^{238}Pu can be produced by neutron irradiation of ^{237}Np in a reactor according to the reaction

$$^{237}Np(n,\gamma)^{238}Np \xrightarrow{\beta-} {}^{238}Pu$$

Competing reactions such as

$$^{237}Np(n,2n)^{236}Np \quad \text{and}$$
$$^{237}Np(\gamma,n)^{236}Np$$

occur simultaneously and lead through β-decay of ^{236}Np to ^{236}Pu. This isotope is an undesirable byproduct because it emits more energetic γ-radiation of higher intensity than ^{238}Pu whose γ-radiation has mostly energies below 150 keV and can be easily shielded. The neutron irradiation energy has thus to be optimized so that ^{236}Pu is produced only at the tolerable minimum. To calculate the optimum irradiation conditions the cross sections of the above mentioned ^{237}Np nuclear reactions as well as the γ-ray production cross sections through neutron reactions with the surrounding reactor materials have to be known.

3.5.4 Nuclear particle irradiations

In nuclear irradiations the cross sections for the interactions of the incident nuclear particles with the nuclei of the irradiated specimen have to be known as well as the angular and energy distributions of emitted particles and radiations resulting from these interactions. As an example we mention cancer therapy by neutron irradiation of the afflicted tissue. For the production of the neutrons, for example the $^{9}Be(d,n)$ reaction is used with deuterons accelerated in a cyclotron. In this example one has to know [19]

1. the cross section for the $^{9}Be(d,n)$ reaction as a function of the deuteron energy and, to greater accuracy, the energy spectra of the emitted neutrons for a variety of deuteron energies and target thicknesses;

2. cross sections and secondary particle distributions for the interaction of 15-50 MeV neutrons with the major elements of the human body (H, C, N, O, P, Ca) for calculations of the radiation dose

distributions in the irradiated part of the body. The prime needs concern the cross sections and angular distributions for elastically and inelastically scattered neutrons, (n,p), (n,α), and other neutron reactions which are followed by the emission of several nuclear particles, and the energy spectra of the emitted secondary particles.

The required neutron data are almost non-existent.

3.5.5 Data availability

It is seen that for "non-energy" applications mostly nuclear structure and decay data, but also data for specific neutron, photonuclear and charged particle nuclear reactions are needed. For such applications up-to-date nuclear data handbooks and tabulations are most appropriate. For example, to satisfy some of the nuclear reaction data requirements for nuclear activation analysis, the IAEA Nuclear Data Section, with the cooperation of several nuclear data physicists, has published in 1974 a handbook on nuclear activation cross sections [20] which contains data on neutron, charged particle and photon-induced nuclear activation reactions. Typical nuclear decay data required for the calculation of radiation doses can be found in the table work reference [21]. The Journal on Atomic Data and Nuclear Data Tables represents a general source of tabulations of selected recommended nuclear reaction and nuclear structure and decay data.

Due to the rapid progress in nuclear physics and data research the contents of handbooks and table works become usually obsolete in a few years time. The issue of revised and updated editions is therefore important and can most conveniently be performed from the printout of computer files on which the data are stored and regularly updated.

In the field of nuclear reaction data a cooperation has been established over the past years between the existing pertinent nuclear data centres, which is being coordinated by the IAEA Nuclear Data Section, and which involves the continuous compilation, exchange and dissemination of all neutron and selected charged particle and photonuclear reaction data in computerized medium. The mechanism of such an intercentre cooperation and the associated services are illustrated in chapter 6 by the example of neutron data.

In the field of nuclear structure and decay data a similar internationally coordinated network of data centres has recently been created for the systematic compilation, evaluation and dissemination of all bibliographic and numerical nuclear mass chain data, which include all nuclear structure and decay data. The participating centres committed themselves in 1977 to contribute to a continuous and complete evaluation of nuclear structure and decay data for all isotopes on a four year cycle. The results will be internationally disseminated in the form of a computerized evaluated nuclear structure data file and are continuously being published in the Nuclear Data Sheets Journal and, for lighter nuclei, in the Journal of Nuclear Physics.

4. EVALUATED NEUTRON NUCLEAR DATA LIBRARIES

From chapter 3 it can be concluded that the most extensive requirements for nuclear data concern neutron nuclear data, primarily for fission and fusion reactor design, but also for activation analysis and other "non-energy" purposes. These requirements can only be met by comprehensive computerized libraries of evaluated data which can be used as input to nuclear design and other required calculations. Such libraries have been developed over the past twenty years in several developed countries pioneering in the development of nuclear energy, and a large fraction of these data has been made internationally available.

Experience has shown that a typical evaluated neutron data library to be used for nuclear design and other purposes has to fulfil the following requirements:

(i) It must cover a large range of materials so that it can be used for all conceivable applications.

(ii) It must cover a neutron energy range from 0 to about 20 MeV for fission and fusion reactor calculations, and, if needed to meet for example biomedical requirements, also some specific reactions for neutron energies above 20 MeV to, say, 100 MeV.

(iii) It must cover all neutron nuclear reactions possible for these energies, i.e. the reactions (n,γ), (n,f), (n,n), (n,n'), (n,p), (n,α), (n,T), (n,^{3}He), (n,2n), (n,3n) and other neutron reactions with multiple particle emission plus the angular and energy distributions of the emitted secondary radiations and particles, plus, for fissile and fertile isotopes, the number $\bar{\nu}$ and energy spectra of prompt and delayed fission neutrons, all as a function of the incident neutron energy.

In addition energy-dependent composite quantities are needed such as

$$\alpha = \frac{\sigma_\gamma}{\sigma_f} \qquad \eta = \frac{\bar{\nu}}{1+\alpha} \quad ;$$

$\sigma_T = \sum \sigma\,(\text{partial})$ = total cross section;

$\sigma_X = \sigma_T - \sigma_n$ = non-elastic cross section.

(iv) The data should preferably be represented in both point-wise and parametric forms. For example should the resonance range be described by resonance cross sections as well as resonance parameters; the angular distributions by pointwise $\sigma_n(E,\theta)$ (θ = scattering angle) data as well as for example Legendre polynomial coefficients.

Such double representation is not only required by the calculations to be performed with these data, but also to allow a mutual checking of the data.

For checking purposes it is also useful to tabulate "redundant" data such as σ_T in addition to all partial cross sections, and α in addition to σ_γ and σ_f.

(v) The data should be densely tabulated as a function of the neutron energy, in order to allow an adequate physical representation and simple linear or logarithmic interpolation between adjacent data points. In this way the evaluated data become independent of their specific application and can be used e.g. for multigroup constant calculations with varying energy groups and for design calculations of all types of nuclear fission and fusion reactors with different energy spectra, material compositions, geometries etc.

(vi) Very important is the availability of computer codes for the checking of the correctness and internal consistency of all data contained in an evaluated data library.

The simplest example is that certain sum rules must be obeyed by the data such as

$$\sigma_T = \sum \sigma(\text{partial});$$

$$\Gamma_T = \sum \Gamma(\text{partial}); \quad \Gamma = \text{resonance half width};$$

$$\sigma_n(E) = \int_{4\pi} \sigma_n(E,\Omega)\, d\Omega$$

Such checks presuppose that all data ($\neq 0$) are tabulated at the same neutron energies for a given element.

Secondly, since most of the data are obtained from measurements relative to some standard reaction, all data should be consistent with unique data sets for these standard reactions. If a standard is changed, all data dependent upon this standard have to be changed to maintain consistency.

Among the checks for physical correctness of the data we have already mentioned before the consistency e.g. between resonance parameters and cross sections. For elastic scattering angular distributions the cross section at zero scattering angle, which cannot be measured directly and has to be extrapolated from measurements for $\Theta > 0^\circ$, has to fulfil Wick's limit, i.e.

$$\sigma_n(0^\circ) \geq \left(\frac{k\sigma_T}{4\pi}\right)^2$$

where k is the wave number of the incident neutron.

Furthermore computer programmes must be available which, following the modification of a particular data set, perform the modifications of all those data dependent upon this particular data set. The following is one example for many: In a given energy range the values of σ_n' had to be changed, because new experimental data had become available, different from and more reliable than those stored on the file. As a consequence the following cross sections have to be changed:

$$\sigma_X = \sigma_{n'} + \sigma_p + \sigma_\alpha + \cdots\cdots$$

$$\sigma_n = \sigma_T - \sigma_X$$

$$\sigma_{tr} = \sigma_T - \bar{\mu}_L \sigma_n$$

where $\bar{\mu}_L$ = mean cosine for elastic scattering in the laboratory system.

(vii) Only recently efforts have been started to include error estimates in evaluated data libraries, in order to allow the direct prediction of uncertainties for example in reactor design parameters due to errors in the data. Such errors are composed of statistical errors, which are usually rather small due to the high beam intensities in present-day nuclear physics experiments, and systematic errors which are usually larger than the statistical errors and rather difficult to estimate. Typical systematic errors will be discussed in chapter 5.

(viii) Comparisons of the microscopic evaluated data with so-called integral data help to check the reliability of the microscopic data and can provide some indication for needed re-evaluation or (re-)measurement of certain data.

We can generally discern between so-called "clean" and "dirty" integral data. "Clean" integral data are simple

and well-defined measured integral data such as the infinite dilute resonance integrals for neutron capture, fission and absorption ($x = \gamma, f, a$)

$$RI_x^{\infty} = \int_{0,5\ eV}^{\infty} \sigma_x(E)\ \frac{dE}{E}$$

or average cross sections measured in (normalized) standard fission neutron spectra ($N(E)$) such as the thermal neutron induced fission spectrum of ^{235}U or the neutron spectrum from spontaneous fission of ^{252}Cf:

$$\langle \sigma \rangle = \int_0^{\infty} \sigma(E)\ N(E)\ d\,E$$

The integrals are calculated from the microscopic evaluated data and can be compared with the independently measured integral data.

Under "dirty" integral data we understand data measured under more complex experimental conditions such as reaction rates and spectral indices in research reactors and critical facilities or other so-called benchmark experiments. Usually evaluated data are tested on a variety of such "dirty" integral data and modified if necessary before they are applied to the calculation of power reactors. Such modifications are being performed either by re-evaluation or by mathematical adjustment of the microscopic to the integral data.

(ix) Finally, evaluated data libraries must be well documented. The documentation must give a concise and comprehensive account of all experimental and theoretical sources, decisions and procedures used to obtain the evaluated data and their uncertainties, so that all information is gathered in one reference which is needed for later re-evaluation and updating by other evaluators. Of equal importance is the complete documentation of the formats used for the storage of the evaluated data in computer medium as well as of all data handling and retrieval programmes associated with the library.

Examples of evaluated nuclear data libraries which have been built up in the past, and/or are under continuous development, and which fulfil most of the above requirements except (vii) are

ENDF/B = U.S. Evaluated Nuclear Data File (most comprehensive; addition of errors to the data under development);

ENDL = Evaluated Nuclear Data Library of the Lawrence Livermore Laboratory in the U.S.;

UKNDL = U.K. Nuclear Data Library;

JENDL = Japanese Evaluated Nuclear Data Library;

KEDAK = Karlsruhe Nuclear Data File (= Kerndatenfile Karlsruhe); and

SOKRATOR = Soviet Evaluated Nuclear Data File.

5. NEUTRON NUCLEAR DATA EVALUATION

This chapter will be devoted first to a short description of the basic sources and procedures used in neutron nuclear data evaluations and then to a more detailed outline of some of the methods used in the evaluation of major thermal and fast neutron cross sections. For resonance cross sections we refer to the detailed treatment in the lectures given at this course by M.S. Moore and F. Froehner.

5.1 Basic sources and procedures

Every evaluation starts with the collection of all references on the available experimental data. The most valuable and comprehensive source for neutron data is the CINDA handbook [22] which is periodically published by the IAEA and, which represents an up-to-date international index to the literature on microscopic neutron data. Format and content of this handbook are illustrated by the sample page reproduced in figure 4. In CINDA all references pertaining to the same experiment are grouped together so that an evaluator can easily pursue the history of an experiment. CINDA contains furthermore data index lines which inform the user about the availability of the data referred to from the existing neutron data centres. CINDA finally contains also references to evaluations, evaluated data files and selected theoretical nuclear data articles.

The next step is the collection of all experimental data referenced in CINDA. Most of these data can be obtained by request from the existing neutron data centres whose basic task it is to compile, exchange and disseminate all experimental neutron data (for details see chapter 6). The centres provide a requestor not only with the data, but also with physics information associated with the data

such as method, sample characteristics, experimental errors, standards used, data status and others which helps in the judgement and critical comparison of the data.

The evaluation of the experimental data obtained proceeds in the following steps:

- selection of the data, in particular elimination of data having unusually large errors and/or lying far outside the bulk of the data;

- modification of the retained experimental data, e.g. reduction of the data to common energy scales, renormalization of the data to common standards;

- appraisal and, if needed, estimate or re-estimate of the statistical and, more important, systematic errors attributed by the authors to their data and recalculation of the total error;

- averaging of the data, usually weighted with the inverse square of the total error. This can be done in several ways, e.g. by drawing "eye-guide" curves through the data, by linear, parabolic, spline function etc. curve fitting, or by fitting the data with some nuclear theory function (for example resonance cross sections with appropriate resonance formulae; inelastic scattering energy distributions with an evaporation formula; or elastic scattering angular distributions with an appropriate optical model expression);

- if experimental data are insufficient or non-existant, recourse must be held to nuclear theory, models or systematics in order to fill the gaps by interpolation, extrapolation and prediction. The five most important theoretical tools form the subject of this course, i.e.

  resonance theory;
  optical model;
  statistical theory;
  pre-compound decay theory; and
  fission theory;

- tabulation, coding, checking and final storing of the evaluated data.

5.2 Evaluation of specific neutron cross section data

The whole range of atomic weights ($1 \lesssim A \lesssim 260$) can be subdivided in five subranges with the following characteristics:

(i) $A \lesssim 5$ — Very light nuclei.
The cross section behaviour is smooth up to about 20 MeV with a few very broad resonances.

(ii) $5 \lesssim A \lesssim 20$ — Light nuclei.
The cross sections exhibit a broad resonance structure up to energies $\gtrsim 10$ MeV. The total resonance widths are composed of Γ_n, $\Gamma_{n'}$, Γ_γ, Γ_α and/or Γ_p.

(iii) $20 \lesssim A \lesssim 100$ — Medium-weight nuclei.
The cross sections exhibit resonances up to KeV and sometimes MeV energies. Γ_T is composed of Γ_n, Γ_γ ($\Gamma_n \overset{A \to \infty}{\longrightarrow} \Gamma_\gamma$) and, above the threshold for inelastic scattering, $\Gamma_{n'}$.

(iv) $100 \lesssim A \lesssim 210$ — Heavy nuclei.
Resonances extend in the eV and KeV ranges of neutron energy. $\Gamma_T = \Gamma_n + \Gamma_\gamma$. Generally $\Gamma_n \gtrsim \Gamma_\gamma$; for rare earth isotopes, however, $\Gamma_n \ll \Gamma_\gamma$.

(v) $210 \lesssim A \lesssim 260$ — Very heavy nuclei.
Resonances extend in the eV and KeV ranges. $\Gamma_T = \Gamma_n + \Gamma_\gamma$ (+ Γ_f for $A \gtrsim 220$). For even nuclides generally $\Gamma_f \ll \Gamma_\gamma$, Γ_n (subthreshold fission), for odd nuclides generally $\Gamma_n \ll \Gamma_\gamma$ and Γ_f for fully open fission channels.

In the following we restrict ourselves to the discussion of concrete evaluation problems for medium, heavy and very heavy nuclei which are the most important for applications. The examples will show the mostly complementary role played by experiment and theory.

5.2.1 Thermal neutron cross sections

(i) Non-fissionable nuclei

Only neutron elastic scattering and capture occur, so that only the cross sections for these two reactions plus the sum of both, the total cross section, need to be evaluated over the range 10^{-5} eV $\lesssim E \lesssim 1$ eV.

From experiment usually σ_T and σ_γ (0.0253 eV) data are available, where 0.0253 eV is the most probable neutron energy in a thermal Maxwellian neutron spectrum at room temperature.

Needed are: $\sigma_n(E)$, $\sigma_\gamma(E)$ and $\sigma_T(E)$.

First case: The next (positive or negative) resonance is far from the thermal range.

It can then easily be derived from resonance theory that

$$\sigma_\gamma^{(E)} = \frac{\text{const.}}{\sqrt{E}}$$

A "best" value of the experimental σ_γ (0.0253 eV) data is determined and the constant fixed by matching this value. $\sigma_T(E)$ is evaluated from the experimental data and $\sigma_n(E)$ obtained as the difference $\sigma_T(E) - \sigma_\gamma(E)$.

Second case: The next (positive or negative) resonance is rather close to the thermal range.

$\sigma_\gamma^{(E)}$ has then to be calculated from resonance theory by taking all known positive (s-wave) resonances and one fictitious "negative" resonance into account. For $\Gamma_\gamma = \langle \Gamma_\gamma \rangle$, an assumption which is normally justified due to the large number of exit channels (= γ-decay possibilities) in neutron capture, the neutron width and the energy position of the fictitious "negative" resonance can be derived by matching the contribution of the negative resonance to the difference between the known 0.0253 eV values of σ_γ and σ_T and the total contribution of all positive resonances. Again $\sigma_n^{(E)}$ follows from $\sigma_T(E) - \sigma_\gamma(E)$.

Third case: One or more resonances fall into the thermal range. This case occurs rather seldom; important examples are the fission products ^{135}Xe and ^{149}Sm.

For those resonances $\Gamma_n \ll \Gamma_\gamma$ with the consequence that

$\sigma_n \cong \sigma_{pot}$ = potential scattering cross section

and

$\sigma_\gamma(E) \cong \sigma_T(E) - \sigma_{pot}$

where $\sigma_T(E)$ is evaluated from experimental data and σ_{pot} determined from resonance analysis or nuclear systematics.

(ii) Fissionable nuclei

For the more important isotopes experimental energy dependent and 0.0253 eV data are available for the following quantities:

σ_T, σ_f, α (or η), $\bar{\nu}$, occasionally σ_n.

Needed are energy dependent cross sections for

σ_T, σ_f, σ_γ, σ_n, α, η, $\bar{\nu}$

Normally $\sigma_T(E)$, $\sigma_f(E)$ and sometimes $\alpha(E)$ (or $\eta(E)$) can be evaluated from experimental data. $\sigma_n(E)$ can either be evaluated from experimental data or calculated from resonance theory. It follows that

$\sigma_\gamma(E) = \alpha(E) \cdot \sigma_f(E)$

If α is not known then

$\sigma_\gamma(E) = (\sigma_T - \sigma_f - \sigma_n)(E)$ and

$\alpha(E) = (\sigma_\gamma/\sigma_f)(E)$

$\bar{\nu}$ can be assumed constant over the thermal energy range, an assumption which is confirmed by measurements within the limits of experimental accuracy, and is normally available from measurements relative to the spontaneous $\bar{\nu}$ of ^{252}Cf used as standard.

$\eta(E)$ then follows from

$$\eta(E) = \frac{\bar{\nu}}{1 + \alpha(E)}$$

5.2.2 Fast neutron cross sections

We consider here only cross sections in the so-called "continuum" range, i.e. cross sections which vary slowly as a function of neutron incident energy.

(i) Elastic neutron scattering

Needed are $\sigma_n(E)$ and $\sigma_n(E, \Theta)$ data for a full description of neutron elastic scattering. $\sigma_n(E)$ can be obtained either from direct measurements and/or integration of experimental $\sigma_n(E, \Theta)$ data, or from $\sigma_T(E) - \sigma_X(E)$, when both can be evaluated from measured data, or, in the case of no experimental data, from optical model predictions.

$\sigma_n(E, \Theta)$ can be obtained from experimental data with inter- or extrapolations by e.g. optical model calculations or, if no experimental data are available, from such calculations only. In the neighbourhood of rather spherical magic or

half-magic nuclei spherical optical potentials can be used, for deformed nuclei such as those of rare earth and actinide isotopes deformed optical potentials have to be used. The optical model allows to calculate the following cross sections:

σ_c = compound nucleus formation cross section;

σ_{sn} = shape elastic scattering cross section (differential and integral values); and

$\sigma_T = \sigma_c + \sigma_{sn}$

Needed are, however,

$\sigma_n = \sigma_{sn} + \sigma_{cn}$

with σ_{cn} = compound elastic scattering cross section, which can be calculated from the statistical theory developed by Hauser and Feshbach [23]. For $E \gtrsim 5$ MeV and non-magic nuclei with $A \gtrsim 30$

$\sigma_{cn} \cong 0$; $\sigma_n \cong \sigma_{sn}$

For the conceptual and mathematical details of optical model and statistical theory calculations we refer to the pertinent lectures presented at this course.

In evaluating experimental angular distribution data one has usually to extrapolate the data to 0^o and 180^o scattering angles by hand, by polynomial or, preferably, optical model fits. At 0^o the cross section is usually close to the Wick limit.

A further difficulty can arise through differences in the angular resolution of different $\sigma_n(\Theta)$ measurements. In the minima and maxima of $\sigma_n(\Theta)$ one has then to rely upon the best resolved measurement or on optical model calculations.

$\sigma_n(\Theta)$ measurements may also differ in the energy resolution with the possible consequence, that inelastic neutron scattering to low-lying levels is not separated from elastic scattering. One can correct the experimental $\sigma_n(\Theta)$ data by subtracting evaluated experimental $\sigma_{n'}$ data, if available, or nuclear theory estimates of $\sigma_{n'}$, with due account for the usually anisotropic angular distributions for inelastic scattering to individual levels.

An evaluator of experimental elastic scattering data has furthermore to check whether the reported experimental results have been corrected for end and wall effects in the neutron counter, for neutron beam attenuation and multiple scattering in the sample, and, in the case of fissionable and fertile nuclei, for fission neutrons, to mention several of the more important sources of systematic errors.

(ii) Inelastic neutron scattering

For inelastic neutron scattering data we have to discern between three different incident neutron energy regions:

Region 1, in which individual energy levels are excited in the rest nucleus.

In this region the cross sections for inelastic excitation of individual levels E_j, $\sigma_{n'}(E,E_j)$, and their angular distributions have to be evaluated. The total inelastic scattering cross section is the sum of the partial excitation cross sections

$$\sigma_{n'}(E) = \sum_j \sigma_{n'}(E,E_j)$$

The energy distribution of the inelastically scattered neutrons is simply given by a δ-function

$$f_{n'}(E,E')dE' = \delta(E-E' = E_j > o)dE'$$

where E' is the energy of the inelastically scattered neutron.

Region 2 in which quasi-continuously distributed energy levels are excited in the rest nucleus.

Needed are again the total inelastic scattering cross section and inelastic scattering angular and energy distributions. The major contributions to these quantities are due to the compound mechanism; with increasing energy in the MeV range direct and pre-compound emission increase.

For not too high energies and/or as a first approximation the nuclear evaporation model which corresponds to the compound reaction mechanism may be applied to obtain the energy distribution of the inelastically scattered neutrons. Accordingly

$$f_{n'}(E,E') = C(E)E'e^{-E'/T} \quad \text{for } 0 \leq E' \leq E$$
$$= 0 \quad \text{for } E' > E$$

C(E) is a normalization factor which follows from the normalization condition

$$\int_0^E f_{n'}(E,E')dE' = 1$$

to be

$$C(E) = \frac{1}{T(T - e^{-E/T}(E + T))}$$

The nuclear temperature T is approximately given by the expression

$$T = \gamma\sqrt{E} \quad , E \text{ and } T \text{ in MeV}$$

with a semi-empirical atomic weight dependence of the coefficient γ given by

$$\gamma = \frac{3.2}{\sqrt{A}} \quad [\text{MeV}^{1/2}]$$

The energy at which $f_{n'}$ reaches its maximum is easily calculated to be equal to T. The average energy $\overline{E'}$ of the inelastically scattered neutrons follows from

$$\overline{E'} = \frac{\int_0^E E' f_{n'}(E,E')dE'}{\int_0^E f_{n'}(E,E')dE' \ (=1)} = 2T - \frac{E^2 e^{-E/T}}{T - e^{-E/T}(E+T)}$$

For heavy nuclei and $E \gg T$ we get

$$E' \cong 2T$$

The shape of $f_{n'}$ as a function of E' is qualitatively visualized in the following figure.

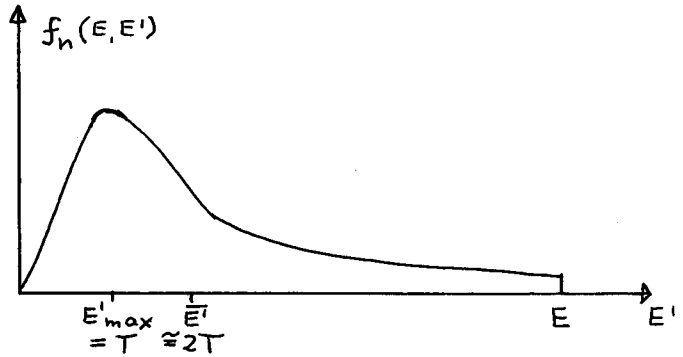

Region 3 is a "grey" area betwen regions 1 and 2, in which there is an overlap between resolved and unresolved rest nucleus levels excited by inelastic scattering. $f_{n'}(E,E')$ can be represented approximately as a superposition of the two expressions valid for regions 1 and 2:

$$f_{n'}(E,E')dE' = C'(E)\left\{\sum_j \delta(E-E' = E_j > o)dE' + f_{n'}^{evap.}(E,E')\right\}dE'$$

with C'(E) = normalization factor.

Now we discuss some detailed problems and procedures connected with the evaluation of inelastic scattering data in regions 1-3.

The general energy dependence of $\sigma_{n'}$ is visualized in the following figure.

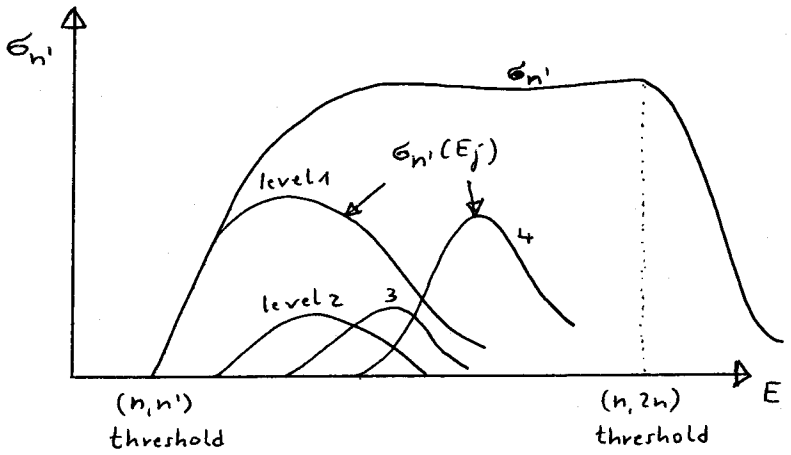

Above the (n,n') threshold $\sigma_{n'}$ rises to a "plateau" and decreases above the (n,2n) threshold due to competition with the (n,2n) process.

$\sigma_{n'}(E,E_j)$ are experimentally obtained by counting the neutrons or the γ-rays which are emitted upon inelastic scattering. If $\sigma_{n'}(E,E_j)$ data are desired, but only $\sigma_{n'}(E,E_{\gamma i})$ measurements are available, a case which occurs frequently, one has to convert them to $\sigma_{n'}(E,E_j)$ data according to

$$\sigma_{n'}(E_j) = \sum_i \sigma_{n'}(E_{\gamma i})$$

as can be seen from the example given in the figure below.

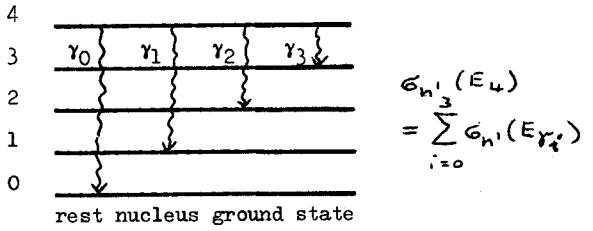

If no or only few $\sigma_{n'}$ data are available the Hauser-Feshbach theory can be applied to calculate the needed data with an accuracy which is about comparable to the accuracies reached in experimental determinations ($\sim$20%) provided that the spins and parities of the excited levels are known. Average capture and, for fissionable isotopes, fission widths are obtained by

extrapolation from known resonance values or from nuclear capture and fission systematics. Average elastic and inelastic scattering widths or transmission coefficients are obtained from optical model calculations. This is only a very short summary of the theoretical procedures, a detailed account will be given in the lectures on the statistical theory and the optical model presented during this course.

$\sigma_{n'}$ for unresolved rest nucleus levels is usually not directly measured, but can be obtained from measured σ_X values by subtracting the other partial reaction cross sections

$$\sigma_{n'} = \sigma_X - (\sigma_p + \sigma_\alpha + \sigma_{2n} + \ldots\ldots)$$

$\sigma_{n'}(\Theta)$ is normally assumed isotropic for resolved as well as unresolved rest nucleus levels. This assumption is neither experimentally nor theoretically always justified: The scarce experimental data available indicate anisotropy already at low neutron energies. For pure compound scattering $\sigma_{n'}(\Theta)$ can be shown to be symmetric to 90° scattering angle, i.e.

$$\sigma_{n'}(90° - \Theta) = \sigma_{n'}(90° + \Theta)$$

not necessarily isotropic. At higher energies ($E \gtrsim 5$ MeV) direct and pre-compound components increase which are forward peaked. In most present-day evaluated neutron data libraries these effects are still not taken into account.

Systematic errors arise first due to normalisation. Typical standards used are $\sigma_n(H)$; $\sigma_n(C)$; $\sigma_{n'}(E_\gamma = 4.43$ MeV from $^{12}C)$; $\sigma_{n'}(E_\gamma = 0.845$ MeV from $^{56}Fe)$. Sometimes $\sigma_{n'}(\Theta)$ data are normalized to measurements of other authors at fixed angles (e.g. 95°). In the error estimates for measured relative $\sigma_{n'}$ data the errors of the standards must not be neglected.

Other effects which are sources of typical systematic errors and which one has to check whether the measured data have been corrected for, are for example multiple neutron scattering, γ-ray attenuation and neutron self-absorption in the sample. Often $\sigma_{n'}$ is measured only at one angle Θ_i, and in order to obtain the total cross section, isotropy is assumed:

$$\sigma_{n'} = 4\pi\sigma_{n'}(\Theta_i)$$

Corrections for anisotropy may be necessary and can be obtained from Hauser-Feshbach calculations.

(iii) Neutron capture

The general shape of $\sigma_\gamma(E)$ is visualized in the figure below in somewhat greater detail than in figure 2.

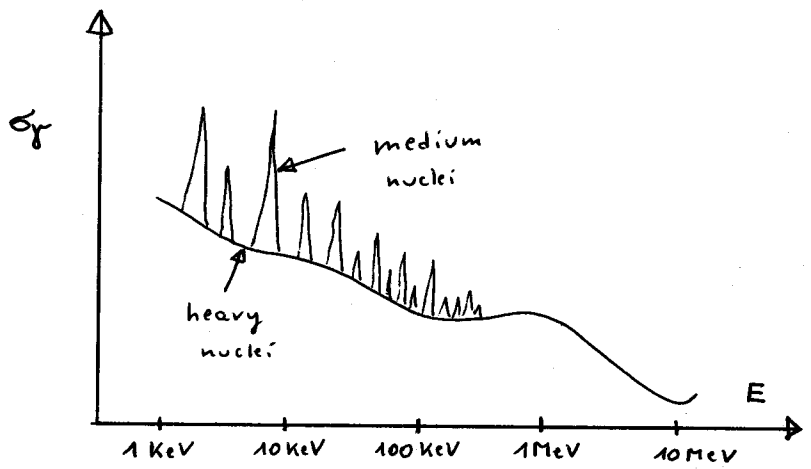

As a function of energy σ_γ is generally decreasing with neutron energy due to the increasing competition with neutron elastic scattering. Due to the accumulating contributions of several neutron orbital angular momenta σ_γ shows usually a plateau or small maximum in the higher keV range up to about 1 MeV and then decreases more strongly due to the onset of inelastic scattering competition. Above 10 MeV, where σ_γ is usually very small of the order of mb, a slight increase is exhibited due to direct capture.

For heavy and very heavy nuclei σ_γ shows generally a smooth energy dependence for keV and MeV energies. Medium-weight nuclei exhibit resonances in the keV range. p- and higher l-wave resonances with $\Gamma_n < \Gamma_\gamma$ dominate the capture in this range; they are usually very sharp and can usually not be resolved in transmission, but only in capture cross section measurements.

The major methods used to measure σ_γ are the following:

- activation method involving the counting of decay β or γ-rays;
- associated activity method;
- slowing-down time spectrometer method (applicable only below ~50 keV); and
- sphere transmission from monoenergetic sources such as the Sb-Be source for the production of ~30 keV neutrons.

The first three methods allow the measurement of σ_γ as a function of the incident neutron energy.

Almost all σ_γ measurements are performed relative to a standard. The most important basic standard reactions used are the following:

$^{6}Li(n,\alpha)$; $^{10}B(n,\alpha)$; $^{197}Au(n,\gamma)$; $^{235}U(n,f)$;

furthermore known thermal σ_γ values for the normalization of slowing-down time spectrometer measurements. Measurements are often normalized to a known σ_γ value of the element under investigation at a specific energy, e.g. a relative $\sigma_\gamma(E)$ measurement for ^{238}U is normalized to a known $\sigma_\gamma(^{238}U)$ value at 30 keV. It may also occur, that σ_γ is measured relative to a secondary standard such as $^{127}I(n,\gamma)$ which in turn is normalized to $^{235}U(n,f)$. Every evaluation of σ_γ data involves a careful checking of the normalizations used, the adoption of unique standard values and the reduction of the experimental σ_γ data to these standard values.

Other sources of systematic errors can be as follows:

- multiple neutron scattering before neutron capture in the sample is particularly important for medium-weight nuclei for which $\sigma_n >> \sigma_\gamma$. The required corrections for multiple scattering can be very significant and are the smaller, the thinner the sample used is;
- γ-background from competing reactions, e.g. (n,n'), has to be determined and subtracted;
- there may be a bias in the γ-detection so that not all γ-rays are detected, the difference has to be accounted for;
- geometrical resonance self shielding effects in the sample have to be corrected for;
- the γ-ray detection efficiency usually changes with the incident neutron energy and the data have to be corrected for these changes

In addition, in the judgement of the reliability of σ_γ measurements the properties of the samples used play an important role. We mention sample homogeneity and dimensions, sample backing and/or canning (dimensions and choice of material), isotopic composition, impurities, chemical compound, temperature (particularly in resonance experiments). These properties and data have to be very well known and/or very carefully chosen. Usually the corrections to be applied to measured capture data are the more severe the thicker the sample is.

If experimental σ_γ data are available the usual evaluation procedures apply. If not, the statistical neutron reaction theory can be applied up to MeV energies with an additional account for direct capture at higher energies.

(iv) Neutron fission

The fundamentals of the fission process and the application of fission theory to the calculation of fission cross sections and other fission data will be discussed in detail in the fission lectures given by Brack and Lynn at this course. Therefore we restrict ourselves to a few remarks only.

Odd-A actinides usually have the fission threshold below, even-A actinides above neutron binding energy. Odd-A actinides therefore exhibit a strong fission component at all neutron energies, even-A actinides only above the fission threshold with some sub-threshold fission at lower energies. The general energy dependence for both cases is very roughly visualized in the figures below (see also figure 2).

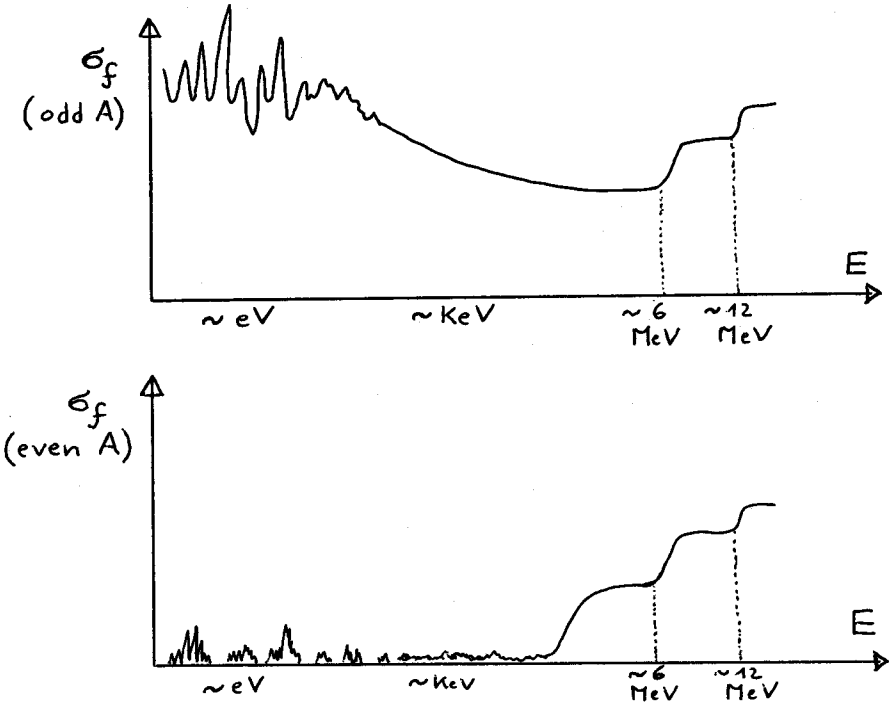

At about 6 and 12 MeV are the thresholds for the (n,n'f) and (n,2n'f) reactions respectively, which lead to a stepwise increase of σ_f.

The "tunneling" through the fission barrier allows some subthreshold fission to occur and is responsible for the rather slow rise of σ_f in the vicinity of the fission threshold as seen in the threshold behaviour of σ_f of even-A actinides. If the fission barrier would have the one-hump shape predicted by the liquid drop model as developed by Bohr and Wheeler [24] (see figure 5) then the subthreshold fission cross sections would vary smoothly as a function of energy. Strutinsky [25] was the first to modify the liquid drop model prediction by taking the shell structure of the nucleus into account; he obtained for most actinides a double-hump-shaped fission barrier (see figure 5). This leads to characteristic modifications of the subthreshold fission cross sections as shown in the above figure for σ_f of even-A actinides. This is due to interaction of the resonance states in the first well with the so-called intermediate states in the second well which lead to an enhancement of resonance subthreshold fission in the neighbourhood of these intermediate states and to very small or zero fission cross sections for resonances lying between the intermediate states. Because of its dependence on these intermediate states this phenomenon is called "intermediate subthreshold fission". It has been experimentally observed in all major even-A actinide isotopes, and these observations represent one of the best proofs for Strutinsky's theory, apart from direct investigations of the properties of these intermediate states. We will come back to this phenomenon in the next section where we discuss the energy dependence of α (^{239}Pu).

Most fission cross section measurements are made relative to σ_f (^{235}U), but also σ_n(H), ^{6}Li(n,α) and ^{10}B(n,α) are used as standards. In the measurements made relative to σ_f (^{235}U) usually fission chambers with back-to-back foils of ^{235}U and the fissile isotope to be investigated are used

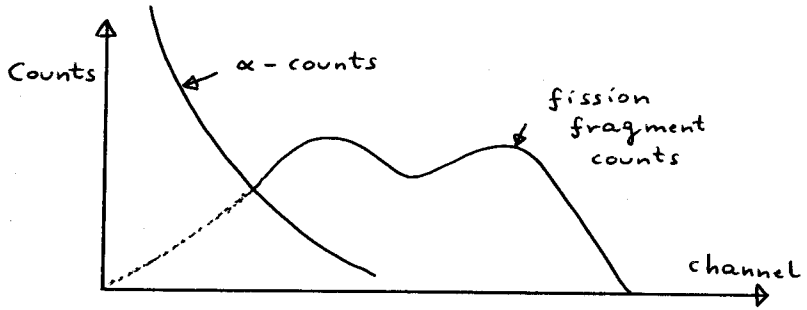

for counting the fission fragments. As all fissile isotopes show a more or less intensive α-decay one has to use very thin foils to minimize the α-background, as is illustrated in the figure below. The lower the α-background the more accurate is the extrapolation of the measured fission fragment distribution in the area shadowed by the α-decay.

In the absence of experimental data statistical theory with appropriate parameterisation can be used to predict $\sigma_f(E)$. Without theoretical foundation, a few empirical laws have been observed in the MeV range whose parameters are obtained from known experimental data and which can be used to calculate unknown σ_f as a function of Z and A of the fissionable nuclide. For example in the region of the first plateau of σ_f at a few MeV it has been observed that σ_f follows a straight line as a function of the parameter $Z^{4/3}/A$:

$$\sigma_f = \sigma_f(Z^{4/3}/A) = a + b\,\frac{Z^{4/3}}{A}$$

With known (n,n'f) and (n,2n'f) thresholds and known ratios of σ_f (2^{nd} plateau)/σ_f(1^{st} plateau) and an average estimate of the slope of σ_f through the thresholds rough estimates of $\sigma_f(E)$ can be obtained in the MeV range.

(v) α- ^{239}Pu

In this section we would like to discuss the example of the evaluation of one of the most important fast reactor neutron data, the energy dependence of $\alpha(^{239}Pu)$ in the lower keV neutron energy range. As has been shown in chapter 2, the breeding ratio for ^{239}Pu which is a measure of the speed of generation of new fissile material ^{239}Pu depends critically upon α. The whole nuclear fuel strategy depends essentially upon the fuel doubling time which is inversely proportional to the breeding gain (BR-1), and thus upon $\alpha(^{239}Pu)$. On the other hand, as will be shown below, the history of the evaluation of $\alpha(^{239}Pu)$ presents an excellent example for the crucial need for correct physical understanding of the fission process in order to obtain reliable data whose behaviour can be physically understood.

Figure 6 shows the status of mostly experimental $\alpha(^{239}Pu)$ values as available in 1970. The most recent data in this figure due to Gwin et al. [29] and Schomberg et al. [30] have in the seventies been confirmed within experimental error limits and are still representative for the present status of knowledge of α.

Before the development of more sophisticated techniques which allowed the much more detailed measurement of the energy dependence of α and the development of Strutinsky's theory in the second half of the sixties, the only α-values known in the lower keV range were a few integral values obtained at the Knolls Atomic Power Laboratory (KAPL) in the U.S. in the mid fifties [26-28]. These values resulted from many years of sample irradiation in Hanford reactors and from reactivity coefficient measurements in different neutron energy spectra of intermediate critical assemblies. These values were considered very reliable and the rather poor knowledge of the fission and capture widths of resolved resonances did not allow an independent check of the KAPL values by extrapolation to higher energies. The low KAPL values led to the prediction of rather high breeding ratios of the order of 1.4 - 1.5 for fast reactors. With such high breeding ratios fast reactor neutron spectra with rather low energies in the keV range could still be accepted as shown e.g. by steam-cooled fast reactors which, apart from corrosion problems, promised to offer some technical advantages over the Na-cooled fast reactor which has a somewhat harder neutron energy spectrum in regions of lower α-values.

Without going into the detail of all the later experimental [29-31, 34, 35] and evaluated data [32, 33] two important conclusions can immediately be drawn from figure 6:

(i) In the energy range 0.1 - 10 keV the "true" α-^{239}Pu values as determined by Gwin et al [29] and Schomberg et al [30] are almost a factor 2 higher than the KAPL-values.

Taking the new data into account reduced the breeding ratio to unacceptably low values for steam-cooled fast reactors which, beside technical shortcomings, was one of the reasons which killed such reactor projects and let only the reactor projects with Na- or He-cooling survive up to the present.

(ii) The recent experimental data [29, 30] show quasi-periodical fluctuations in α as a function of neutron energy.

After the development of Strutinsky's theory in 1967 and more extensive investigations at Saclay [36, 37] and Harwell [38] of the properties of individual resonances of ^{239}Pu in the second half of the sixties this fluctuating behaviour could be well understood, as is shown below.

In the lower keV-range the influence of s-wave resonances is dominant; we need therefore only to consider the properties of the ^{239}Pu s-wave resonances as measured in the Saclay [36, 37] and Harwell [38] experiments. The ^{239}Pu ground state has the spin 1/2, the s-wave resonances of ^{239}Pu fall therefore into two groups with spins J = 0 and J = 1. In summary the resonance measurements disclosed the J = 0 resonances as very broad states with fission widths of eV size and an average spacing of about 9 eV, superimposed by three times closer spaced sharp J = 1 resonances with much smaller fission widths ranging from 0 to about 100 meV. One would therefore expect that the threshold for J = 0 fission lies below and that for J = 1 fission above neutron binding energy. This expectation has indeed been confirmed by independent investigations of both fission thresholds. From (d,pf) measurements Northrop et al [39] deduced the position of the J = 0 fission threshold to be 1.6 MeV below neutron binding energy. From the very steep descent of α above about 20 keV (see figure 6) [40, 41] and from collective model calculations [42] a J = 1 fission threshold energy of the order of 100 keV above neutron binding energy was derived.

A closer examination of the σ_f measurements and the deduced J = 1 fission widths shows the typical intermediate subthreshold behaviour of the J = 1 fission component, with fluctuations in σ_f due to fluctuations in J = 1 fission widths. In figure 7 which displays a sample of the Saclay σ_f measurements on ^{239}Pu [37] for neutron energies between 0.5 and 4 keV one can for example easily discern maxima around 0.5 and 1 keV and a minimum between 0.6 and 0.9 keV corresponding to large and small J = 1 fission widths. Figure 6 shows at the same energies the inverse behaviour of α, i.e. minima in α around 0.5 and 1 keV and a maximum around 0.7 keV. That this behaviour of α is indeed due to the fluctuations in the J = 1 component of σ_f can easily be proven by statistical theory [43]. α is given by

$$\alpha = \frac{\langle\sigma_\gamma\rangle}{\langle\sigma_f\rangle} = \frac{\langle\sigma_\gamma{}^0\rangle + \langle\sigma_\gamma{}^1\rangle}{\langle\sigma_f{}^0\rangle + \langle\sigma_f{}^1\rangle}$$

where $\langle \ldots \rangle$ denotes an average over many neighbouring resonances, 0 and 1 the spins $J;\ell > 0$ contributions can be neglected. Neglecting for simplicity the half-width

fluctuation factor, considering that

$\Gamma_n^{0,1} \ll \Gamma^{0,1}$, $\Gamma_f^{0,1}$ and

Γ_n^{o} , $\Gamma_\gamma^{o} \ll \Gamma_f^{o} \cong \Gamma_T^{o}$

assuming J- independence of the s-wave strength function

$$\left(\frac{<\Gamma_n^{(0)}>}{<D>}\right)_{l=0,\,J=0} = \left(\frac{<\Gamma_n^{(0)}>}{<D>}\right)_{l=0,\,J=1}$$

and with

$g_{0,1}$ = statistical weight factor for spin 0 (= 1/4) and spin 1 resonances (= 3/4) respectively

one gets for

$$\alpha \cong \frac{g_0\left(\frac{<\Gamma_\gamma>}{<\Gamma_T>}\right)_0 + g_1\left(\frac{<\Gamma_\gamma>}{<\Gamma_T>}\right)_1}{g_0\left(\frac{<\Gamma_f>}{<\Gamma_T>}\right)_0 + g_1\left(\frac{<\Gamma_f>}{<\Gamma_T>}\right)_1}$$

$$\cong \frac{3\left(\frac{<\Gamma_\gamma>}{<\Gamma_\gamma>+<\Gamma_f>}\right)_1}{1 + 3\left(\frac{<\Gamma_f>}{<\Gamma_\gamma>+<\Gamma_f>}\right)_1}$$

For very small $<\Gamma_f>_1$ α becomes very large ($\alpha \cong 1.5$ for $<\Gamma_f>_1$ = 10 meV and $<\Gamma_\gamma>_1$ = 40 meV) and vice versa ($\alpha \cong 0.3$ for $<\Gamma_f>_1$ = 100 meV and again $<\Gamma_\gamma>_1$ = 40 meV).

This proves that at least for energies between about 0.5 and 1 keV the fluctuations in α (^{239}Pu) and in particular the high values of α can be quantitatively understood as a consequence of the "intermediate" subthreshold fission in the spin 1 resonances of ^{239}Pu. The numerical values for $<\Gamma_f>_1$ and $<\Gamma_\gamma>_1$ used in the above estimates correspond to measurements on individual resonances below about 400 eV [44]. The maximum of α near 300 eV (see figure 6) is in addition explained by the low Γ_f^1 values observed in these measurements around 300 eV.

6. Nuclear data centres as a link between nuclear data producers and users

Nuclear data are produced by nuclear physicists. Obviously also nuclear physicists need nuclear data for the comparison of the results of other physicists with their own results and for judging the need for the performance of new measurements and the development of new experimental techniques and theories. The link between nuclear physicists as users and producers of nuclear data is a natural byproduct of the development of the science itself.

The transfer of the nuclear data from nuclear physicists to users in applied fields, however, is a much more difficult problem which, because of the volume of data involved, needs a systematic and coordinated approach for its solution: the data produced have to be systematically compiled, their quality assessed and selections made, their formats unified according to the users' needs, and eventually the data disseminated to the users in convenient medium.

A systematic continuous link between data users and producers is thus required. This is schematically represented in figure 8; the bracketed numbers in the following text are the numbers attached to the arrows in figure 8. This link is in general provided by data centres whose two basic functions are to compile the available data from the producers (1), to collate and disseminate them upon request to users (2), and, in the opposite direction, to compile the users' requirements for new or improved data (3), to assess them and to transfer them to the producers (4). For both functions computer storage and retrieval techniques are required in order to cope adequately and economically with the large amount of data to be handled.

The transfer of the data requirements and the compilation and dissemination of the data have to be appropriately organized. If this work is shared among several data centres, it has to be coordinated by regular meetings between the data centres' staff (5). Meetings are held by data centres also between data users and producers to compare data requirements with their status and availability and to derive recommendations for further work needed (6). The data users are assisted by data centres in the adequate use of the data (7), the data producers are assisted in experiment planning (8). Data centre staff and data producers and users visit each other on training and learning missions, (6)-(8). Data centres and producers work together in the production of special data files, handbooks and other publications, (8) and (6). National data centres have often the task of coordinating the evaluation of experimental data among several institutions, (7) and (6).

Implicit to all these partial functions is the third major function of a data centre, which is coordination. This function is essentially performed in an executive way, while the initiation (9) and review (10) of the coordination between data centres, data users and producers normally rests with national, regional and international data committees.

While the flow chart displayed in figure 8 is generally valid, it applies directly to the three data fields with which the Nuclear Data Section is concerned, i.e. nuclear reaction data, nuclear

structure and decay data and atomic data. The similarity of the requirements in many countries, the impossibility to measure all the required data in one or a few countries only, the need to avoid unnecessary multiplication of work, and the large amount of the data involved made it imperative to share the work among various regional data centres, while the overall coordination of the data centres rests with the IAEA Nuclear Data Section.

Its work follows largely the recommendations of the International Nuclear Data Committee and its performance is continuously reviewed by this committee. Similar functions with respect to the cooperating nuclear data centres are performed by national and regional data committees such as the NEA Nuclear Data Committee.

Figure 9 shows the world-wide data flow from producers through data centres to users as organized and coordinated by the Nuclear Data Section in the field of neutron nuclear data. A similar flow of data has been organized with these and other data centres in the fields of charged particle and photonuclear reaction data, and of nuclear structure and decay data.

In the neutron data field the Nuclear Data Section (NDS) co-operates with the following three national and regional data centres:

- the National Nuclear Data Center (NNDC) at the Brookhaven National Laboratory in the United States;
- the Centr po Jadernym Dannym (CJD = Nuclear Data Centre) at the Institute of Physics and Power Engineering, Obninsk, in the Soviet Union; and
- the Data Bank of the OECD Nuclear Energy Agency (NEA-DB) at Saclay in France.

Each of these centres services one part of the world. These service areas are:

for NNDC:	the USA and Canada (area 1);
for NEA-DB:	all Member States of the OECD/NEA including West Europe and Japan (area 2);
for NDS:	all countries in East Europe, Asia, Australia and New Zealand, Africa, Central and South America (area 3); and
for CJD:	the USSR (area 4).

Each of the four neutron data centres compiles all experimental neutron data from its service area (arrows (1) in figure 9), exchanges these data with the other centres in an agreed and jointly used format called EXFOR (arrows (2)), and satisfies requests for such data from users in its service area (arrows (3)). All three operations are fully computerized. The experimental neutron data exchange which has been firmly established in 1970 assures that every user in the world has access to all available data. A similar computer-based flow of information has been developed for most of the available evaluated neutron data. Thirdly the four neutron data centres cooperate in the compilation of CINDA entries; the CINDA master file is held at Saclay, the CINDA publication [22] is performed by the IAEA on behalf of the four cooperating neutron data centres. A final item of cooperation concerns the compilation of entries for WRENDA, the World Request List for Nuclear Data [2], whose master file is maintained in Vienna and which is also periodically published by the IAEA on behalf of the four cooperating neutron data centres.

References

[1] Glasstone, S., "Principles of Nuclear Reactor Energineering", D. Van Nostrand Company, INC., 1955.

[2] WRENDA 76/77, "World Request List for Nuclear Data", INDC(SEC)-55/URSF, published by the IAEA Nuclear Data Section on behalf of the four neutron data centres, August 1976.

[3] Greebler, P., et al; Second IAEA Conference on Nuclear Data for Reactors, Helsinki, June 1970; Proceedings Volume I, p. 17 ff.

[4] Raman, S., "General survey of applications which require actinide nuclear data", Proceedings of the IAEA Advisory Group Meeting on Transactinium Isotope Nuclear Data, Karlsruhe, Fed. Rep. of Germany, November 1975; Technical Report IAEA-186, 1976, Vol. I, p. 39 ff.

[5] Proceedings of the IAEA Panel on Fission Product Nuclear Data, Bologna, Italy, November 1973; Technical Report IAEA-169, Vol. I, II and III, 1974.

[6] Second IAEA Advisory Group Meeting on Fission Product Nuclear Data, Petten, Netherlands, September 1977; Proceedings to be published.

[7] Proceedings of the IAEA Advisory Group Meeting on Transactinium Isotope Nuclear Data, Karlsruhe, Fed. Rep. of Germany, November 1975; Technical Report IAEA-186, Vol. I, II and III, 1976.

[8] Progress Reports on Fission Product Nuclear Data, edited by G. Lammer, IAEA Nuclear Data Section; issue no. 1: INDC(NDS)-70, December 1975; issue no. 2: INDC(NDS)-75, June 1976; issue no. 3: INDC(NDS)-86, May 1977.

[9] Actinide Newsletter, edited by S. Raman, Oak Ridge National Laboratory; issue no. 1, October 1977.

[10] Joint IAEA-OECD/NEA Technical Committee Meeting on Differential and Integral Nuclear Data Requirements for Shielding Calculations, Vienna, October 1976, Proceedings to be published.

[11] McElroy, W.N., Berg, S., Crockett, T., and Hawkins, R.G., Technical Report No. AFWL-TR-67-41, Vol. I, 1967.

[12] Vlasov, M.F., Fabry, A., and McElroy, W.N., Proceedings of the International Conference on the Interactions of Neutrons with Nuclei, Lowell, Massachusetts, USA, July 1976, CONF-760715-P2, Volume II, p. 1187 ff.

[13] Summary Report of the IAEA Consultants Meeting on Integral Cross Section Measurements in Standard Neutron Fields, Vienna, November 1976, edited by M.F. Vlasov, report INDC(NDS)-81, 1977.

[14] Stewart, L., and Hale, G.M., report LA-5828-MS, 1975.

[15] Rand McNally, Jr., J., reference [17], Vol. II, p. 41 ff.

[16] Proceedings of the International Conference on Nuclear Cross Sections and Technology, Washington, March 1975, NBS Special Publication 425, Session HA: Fusion, Vol. II, p. 646 ff.

[17] Proceedings of the IAEA Symposium on Nuclear Data in Science and Technology, Paris, March 1973, Vols. I and II.

[18] Berger, R., Devillers, C., Gervaise, F., and Le Coq, G., reference [17], Vol. I, p. 329 ff.

[19] Cross, W.G., private communication, 1975.

[20] Handbook on Nuclear Activation Cross Sections, edited by D. Brune and J.J. Schmidt, IAEA Technical Report Series No. 156, 1974.

[21] Dillman, L.T., and Von der Lage, F.C., "Radionuclide Decay Schemes and Nuclear Parameters for Use in Radiation Dose Estimation", nm/mird Pamphlet No. 10, 1975.

[22] CINDA, An Index to the Literature on Microscopic Neutron Data, published periodically by the IAEA on behalf of the four neutron data centres; last edition: CINDA 76/77 plus five supplements.

[23] Hauser, W., and Feshbach, H., Phys. Rev. 87, 366, 1952.

[24] Bohr, N., and Wheeler, J.A., Phys. Rev. 56, 426, 1939.

[25] Strutinsky, V.M., Nucl. Phys. A 95, 420, 1967.

[26] Kanne, W.R., et al., Geneva Conference 1955 on the Peaceful Uses of Atomic Energy, P/595, Proceedings Vol. 4, P. 315.

[27] Sampson, J.B., and Molino, D.F., report KAPL-1793, 1957.

[28] Sampson, J.B., and Luebke, E.A., Nucl. Sci. Eng. 4, 745, 1958.

[29] Gwin, R., et al., INDC(US)-2/U, p. 106 f, 1968.

[30] Schomberg, M.G., et al., unpublished, 1968; Rae, E.R., private communication, 1969.

[31] Ryabov, Y.V., et al., At. Energ. 24, 351, 1968.

[32] Pitterle, T.A., et al., Second Conf. on Neutron Cross Sections and Technology, Washington, March 1968; Proceedings Vol. II, p. 1243 ff, 1968.

[33] Ribon, P., et al., CEA-N-989 (EANDC(EUR)-111), 1968.

[34] Hopkins, J.C., and Diven, B.C., Nucl. Sci. Eng. 12, 169, 1962.

[35] Saussure, G. de, IAEA Conf. on Nucl. Data for Reactors, Paris, 1966; Proceedings Vol. II, p. 233 ff, 1966.

[36] Blons, J., et al., EANDC(E)-89/U, p. 179, 1968.

[37] Blons, J., et al., C.R. Acad. Sci. Paris, Vol. 267, 901, Series B, 1968.

[38] Patrick, B.H., et al., EANDC(UK)-96/AL, 1968.

[39] Northrop, J.A., et al., Phys. Rev. 115, 1277, 1959.

[40] Schmidt, J.J., ANS National Topical Meeting on Reactor Physics in the Thermal and Resonance Regions, San Diego, February 1966, Proceedings Vol. II, p. 223 ff, 1966.

[41] Michaudon, A., Colloque de Physique Nucléaire "Noyaux moyens et Lourds", Bordeaux, March 1967.

[42] Griffin, J.J., IAEA Conf. on the Physics and Chemistry of Fission, Salzburg, 1965, Proceedings Vol. I, p. 23 ff, 1965.

[43] Schmidt, J.J., Atomkernenergie 15, 26, 1970.

[44] Derrien, H., et al., IAEA Conf. on Nuclear Data for Reactors, Paris, 1966; Proceedings, Vol. II, p. 195 ff, 1966; Michaudon, A., ibidem, Vol. II, p. 161 ff.

FIGURE CAPTIONS

FIGURE 1 Schematic representation of neutron nuclear reactions.

FIGURE 2 Schematic representation of the energy dependence of neutron cross sections and of the neutron energy spectra of fission and fusion reactors.

FIGURE 3 Requests for improved neutron capture cross sections of ^{238}U for fast reactor calculations taken from WRENDA 76/77 [2].

FIGURE 4 Sample page from the CINDA publication.

FIGURE 5 Schematic representation of the fission barrier in the liquid drop and the shell model.

FIGURE 6 α-^{239}Pu.

FIGURE 7 σ_f (^{239}Pu) measurements by Blons et al. [37].

FIGURE 8 Data flow (➡) and data coordination links (⟶) between data users and producers, centres and committees.

FIGURE 9 World-wide data flow between neutron data producers, centres and users.

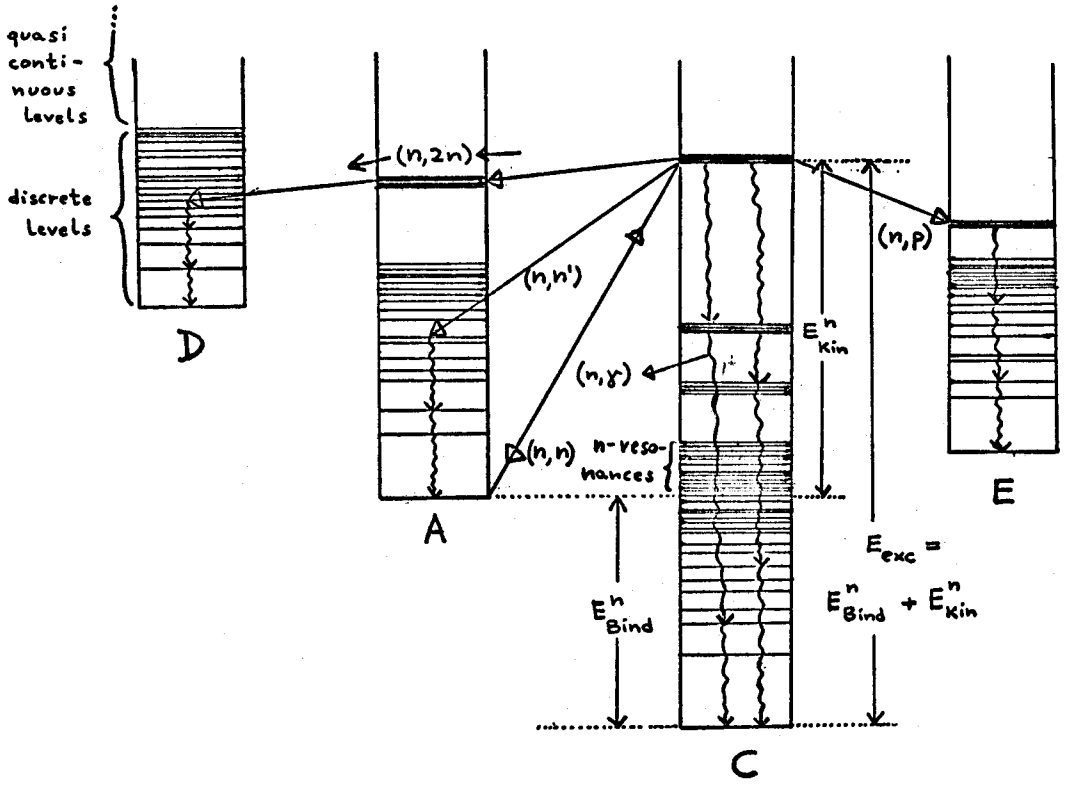

Figure 1

Schematic representation of neutron nuclear reactions

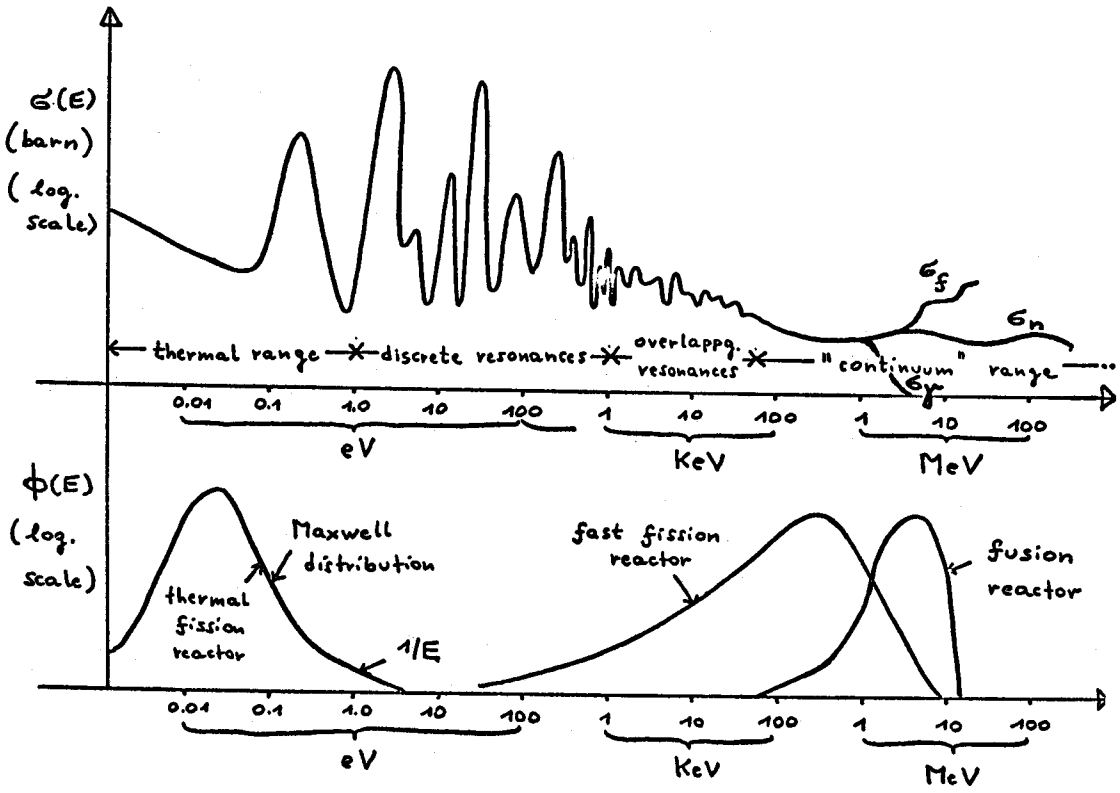

Figure 2

Schematic representation of the energy dependence of neutron cross sections and of the neutron energy spectra of fission and fusion reactors.

Figure 3

Requests for improved neutron capture cross sections of ^{238}U for fast reactor calculations taken from WRENDA 76/77 [2]

Energy range	Accuracy (%)	Priority	Requestor	Organization	Country
500 eV - 10 MeV	4-10	1	C.E. Till	Argonne	USA
			B. Hutchins	General Electric	
			P.B. Hemmig	US Atomic Energy Commission	
10 - 300 KeV	1.5	1	C.E. Till	Argonne	USA
300 KeV - 10 MeV (ratio $\sigma_\gamma^8/\sigma_f^5$)	7	1	B. Hutchins	General Electric	
			P.B. Hemmig	US Atomic Energy Commission	
			A.M. Perry	Oak Ridge	
500 eV - 800 KeV	2-3	1	H. Gerwin	Juelich	FRG
500 eV - 1 MeV	5	2	H. Tellier	Saclay	France
10 KeV - 2 MeV	3	1	C.G. Campbell	Winfrith	UK
5 KeV - 1 MeV	3	2	H. Haeggblom	Studsvik	Sweden
$\lesssim$30 KeV	3	2	M.M. Islam	Dacca	Bangladesh
1 KeV - 1 MeV	<5	1	S. Iijima	Nippon Atomic Industry Group	Japan
500 eV - 1.4 MeV (ratio $\sigma_\gamma^8/\sigma_f^5$)	3	1	M.N. Nikolaev	Obninsk	USSR
1 KeV - 3 MeV	5	1	M. Soleilhac	Bruyeres-le-Chatel	France
5 KeV - 10 MeV	5-10	1	L.N. Usachev	Obninsk	USSR

FIGURE 4 — Sample Page from the CINDA Publication

1 Hydrogen 1

Quantity	Energy (ev) Min	Max	Lab	Type	Documentation Ref	Vol	Page	Author, Comments Date	Data
Evaluation	-3	+7	KFK	Eval Rept	KFK-2233	1		Dec 75 Goel.KEDAK DATA GRAPHS OF TOT,NG,SEL	
Evaluation	1.0-5	2.0+7	LAS	Eval Rept	LA- 6518			Oct 76 Hale+ENDF 4B.TOT,SEL,ANG DISTR.CFD	
Total	1.4+7		LAS	Expt Jour	NP 12 291			Jul 59 Coon+ CF PR 88 562	+
	1.4+7			Data	EXFOR11021.			Aug 76 1PT	+
Total	4.0+5	1.3+9	KFI	ExTh Rept	KFKI-69-10			Mar 69 Hrehuss+ CHARGE-OSCI,TBL+FIG	
	4.0+5	5.0+6		Jour	PL/B 28 585			Mar 69 - +FLUCT IN EN DEP	
	4.0+5	5.2+6		Expt Data	EXFOR30340.002			Sep 76 CS DIFFERENCE H-D, 50 PNTS	+
Total	2.5+6		WIS	Expt Jour	PR/C 4 1061			Oct 71 Davis+.TRANS. 0.12PC ERROR,CFD OTHER	+
Total	8.0+5	2.0+7	RPI	Expt Jour	NP/A 183 51			Mar 72 Clement+ LINAC,TOF,TO 1PC	
	5.0+5	2.0+7		Conf	71Knoxvill	311		Mar 71 Stoler+,TRANS,CURVE	
	1.0+6	2.0+7		Abst	BAP 16 494			Apr 71 Clement+.LINAC+TOF. NO DATA GIVEN	
	5.0+5	2.5+7		Data	EXFOR10173.003			Jul 72 425PTS,SIGMA	+
Total	1.3+2		MUN	Expt Jour	PR/C 11 103			Jan 75 Dilg.H2O.C6H6.CH3OH.C7HB.TARGETS	
				Prog	NEANDC(E)-161U			Aug 74 -.20.491 +- 0.015 B, PRELIM.	
	1.3+2			Data	EXFOR20597.003			Jun 76 4PTS.	+
Total	1.0-3	1.5+7	KFK	Eval Rept	KFK-2233	1		Dec 75 Goel. GRAPH OF KEDAK DATA	
Total	1.1+7	2.5+9	ITY	Comp Jour	NIM 135 337			76 Del Guerra.FOR PLASTIC SCINT TBLGRPH	
Total	1.0+3	2.0+6	GEL	Expt Prog	NEANDC(E)172	3		Feb 76 Boeckhoff+LINAC TOF RES ENERGIES	
Total	5.0+4	5.0+7	LAS	Expt Prog	ERDA-NDC-3	89		May 76 Seagrave+LINAC.STANDARD FOR H003.NDG	
Total	5.0+4	5.0+6	LRL	Expt Prog	ERDA-NDC-3	82		May 76 Phillips+STANDARD FOR TRITIUM MEAS.	
Total	2.0+7	1.4+8	HAR	Eval Conf	76Lowell	1238		Jul 76 Asbury+4LAB+NEW CFD.COMBINED SET.NDG	
	5.0+7	1.5+8		Expt Prog	AERE-PR/NP22			Mar 75 Blair+NO STUCTURE BETWEEN 50-150MEV.	
Elastic	1.3+2		MUN	Expt Jour	PR/C 11 103			Jan 75 Dilg. VARIOUS LIQUIDS.	+
	1.3+2			Data	EXFOR20597.002			Jun 76 1PNT.FREE ATOM.	+
Elastic	Cold		MUN	Expt Jour	ZP/A 272 189			Feb 75 Koester+ COH-SCAT-AMPLIT.=-3.7409 FM	
	1.5-4	4.2-3		Data	EXFOR20609.002			Jun 76 1PNT.COH.SC.AMP.	+
Elastic	1.0-3	1.5+7	KFK	Eval Rept	KFK-2233	1		Dec 75 Goel. GRAPH OF KEDAK DATA	
Elastic	5.6-2		LND	Expt Jour	ACRB 32 2163			Jul 76 Oskarsson.INCOH.SC.CR.SECT.=24 B	
Elastic	None		GEL	Revw Prog	NEANDC(E)182	3		Feb 77 Liskien.FOR LOWELL CONF 76	
Diff Elastic	2.7+6	5.2+6	KFI	Expt Rept	KFKI-69-10			Mar 69 Hrehuss+ SIG(E),4ANGS.FLUCT OBSERVED	
	2.7+6	5.2+6		Data	EXFOR30340.003			Sep 76 REL TO VAL AT 50DEG-CM, 35 PNTS	+
Diff Elastic	2.5+6	2.8+6	KFI	Expt Jour	PL/B 29 105			Apr 69 Czibok+ 0DEG/30DEG RATIO GIVEN	
		1.0+7		Jour	KFI 16 401			Oct 68 - .GRPHS SHOW NO ANG-ISOTROPY	
	2.5+6	2.8+6		Data	EXFOR30327.002			Mar 76 0DEG/30DEG,CM. 3PNTS	+
Diff Elastic	1.4+7		HAM	Expt Diss	KIENLE 50			75 Kienle. POLARISATION.	
Diff Elastic	5.5+7	4.3+8	PTN	Expt Jour	PR/D 13 535			Feb 76 Bersbach+TBL,GRPH.CFD PHAS-SHET ANAL	
	5.5+7	4.3+8		Data	EXFOR10592.002			Aug 76 218PTS CM DIFF CS DATA.	+
Diff Elastic	2.3+7	2.9+7	LAS	Expt Prog	ERDA-NDC-3	101		May 76 Drosg.5ES.180DEG CS.CFD PREDICTION.	
Diff Elastic	5.0+7		DAV	Expt Conf	76Lowell	1356		Jul 76 Romero+2ANGS.POL.CFD PHASE SHIFT.NDG	
Diff Elastic	1.1+7	2.5+7	IRK	Expt Conf	76Lowell	1383		Jul 76 Drosg+E DEP 180 DEG CS.CFD YALE,LRL	
Diff Elastic	2.7+7		HAR	Expt Prog	NEANDC(E)172	8		Aug 76 Cookson+ ANG DIST	
	2.7+7	2.7+7			Prog AERE-PR/NP23			Mar 76 - + N ANGDIST. 6ANGS. NDG	
	2.7+7				Prog AERE-PR/NP23			Mar 76 - + N ANGDIST. 6 ANG. NDG	
					Prog UKNDC(75)P71			Jul 75 - + ANG DIST PROTON RECOIL TBC	
					Prog AERE-PR/NP22			Mar 75 - +ANGDIST.6ANGS.EXPT DETAILS.	
	1.4+7	2.8+7			Prog NEANDC(UK)	160		Jul 74 - + VDG SCAT FORWARD HEMIS TBC	
Diff Elastic	6.5+8		TAM	Expt Abst	DA/B 37 1309			Sep 76 Evans+51TO180DEG.CFD OTH EXPTS.	
	4.6+8	8.0+8		Conf	76Lowell	808		Jul 76 Northcliffe+3ES.GRPHS.TBC	
	6.4+8			Jour	PRL 36 497			Mar 76 Evans+GRPH.145 TO 180 DEG.CFD OTH	
Diff Elastic	2.7+7		HAR	Expt Abst	BAP 22 53			Jan 77 Fowler+VDG.7ANGS,17TO58DEG.CFD PRED.	
Polarization	1.4+7		HAM	Expt Diss	KIENLE 50			75 Kienle. POLARISATION.	
Polarization	3.0+7		DAV	Expt Jour	PR/C 12 1717			Dec 75 Eldred+ TBLS,GRPHS 50-150 DEGS CM	
	3.0+7			Data	EXFOR10565.002			Nov 76 11PTS.POL DATA.11 ANGS 50 TO 150 DEG	+
Polarization	5.0+7		DAV	Expt Conf	76Lowell	1273		Jul 76 Brady+POL N USED.POL,UNPOL H.NDG	
Polarization	5.0+7		DAV	Expt Conf	76Lowell	1356		Jul 76 Romero+2ANGS.CFD PHASE-SHIFT.NDG	
Polarization	1.4+7	1.6+7	DKE	Expt Conf	76Lowell	1358		Jul 76 Tornow+2ES.ANAL PWR.CFD ARNDT.NDG	
Polarization	1.5+7		HAM	Expt Conf	76Lowell	1355		Jul 76 Behrendt+ANAL POWER N,P SCT.CFD.NDG	
Thermal Scat	Pile	2.5-2	ISP	Expt Rept	EUR-4455	D		Apr 70 Seiffert.LIQU.+SOL.NORM+PARA HYDR.	
Thermal Scat	Pile	2.5-2	ISP	Expt Rept	EUR-4496	E		Jun 70 Olivi.ORTHO HYDR	
Thermal Scat	Cold		MUN	Expt Jour	ZP/A 272	189		Feb 75 Koester+ COH-SCAT-AMP, TOT REFLECT	
					Jour PRL 27 956			Oct 71 SUPERSEDED.	
					Rept EANDC(E)140U	14		Aug 71 SUPERSEDED*	
	Maxwl				Rept EANDC(E)127U	20		Mar 70 SUPERSEDED*	
	Cold				Conf 67Juelich	80		Apr 67 SUPERSEDED*	
					Jour ZP 198	187		Dec 66 SUPERSEDED*	
Absorption	Pile		ANL	Expt Rept	ANL-4277	43		Apr 49 Harris+PILE OSC.REL B.	
Absorption	None		ANC	Expt Prog	ERDA-NDC-3	15		May 76 Smith+RATIO OF H/MN ABS CS.	

Figure 5: Schematic representation of the fission barrier in the liquid drop and the shell model.

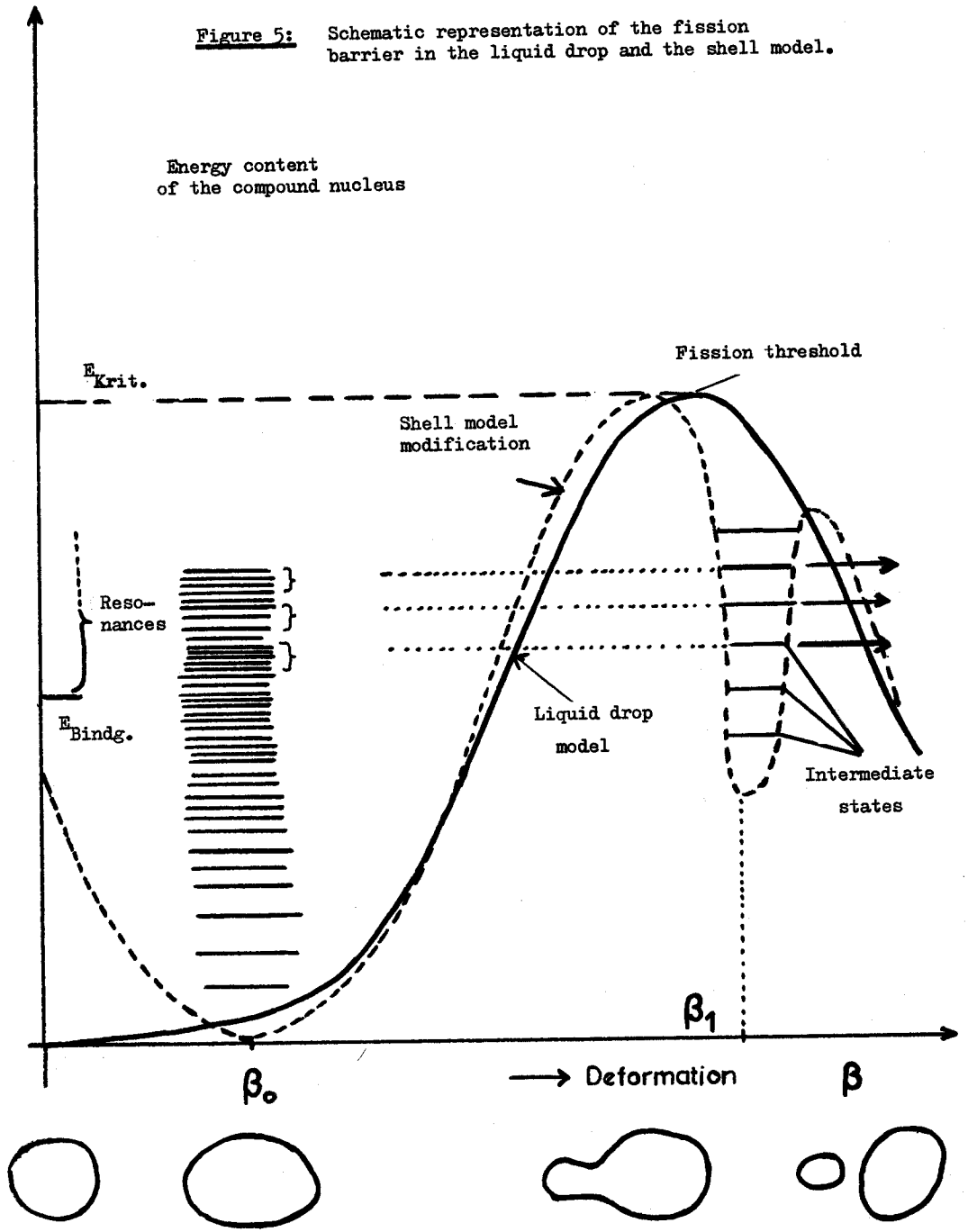

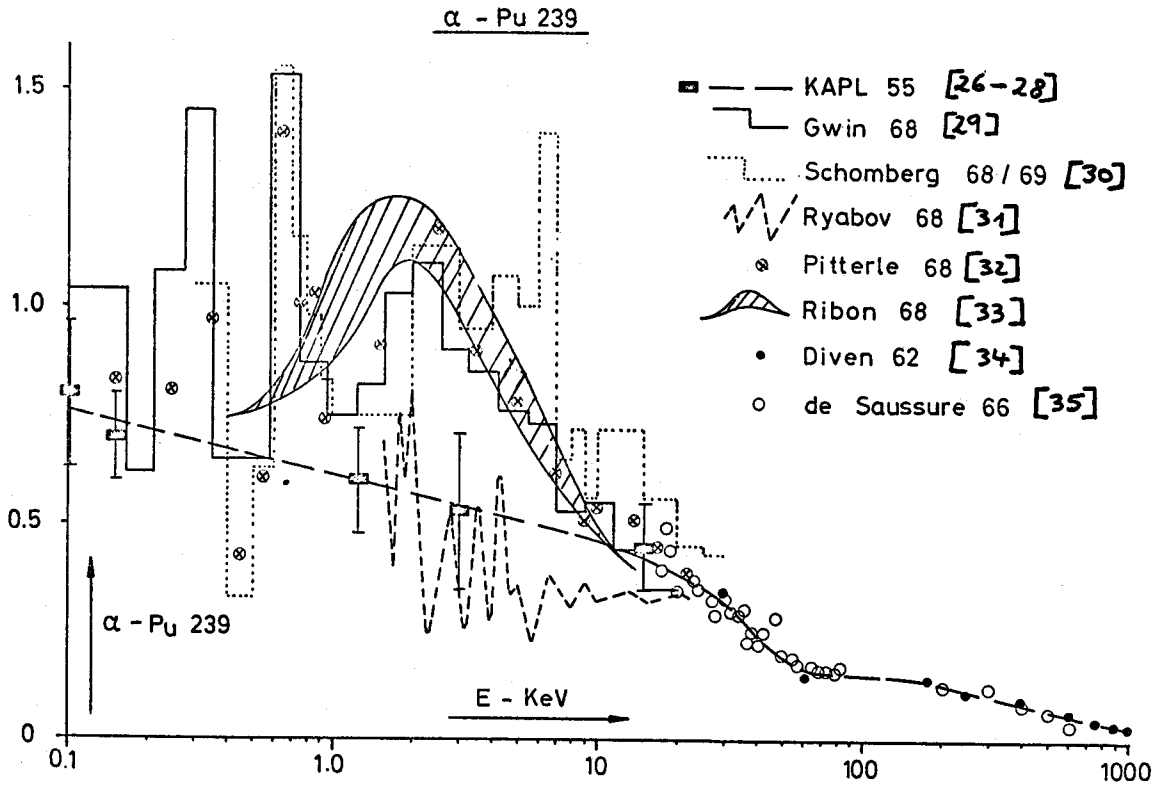

Figure 6:

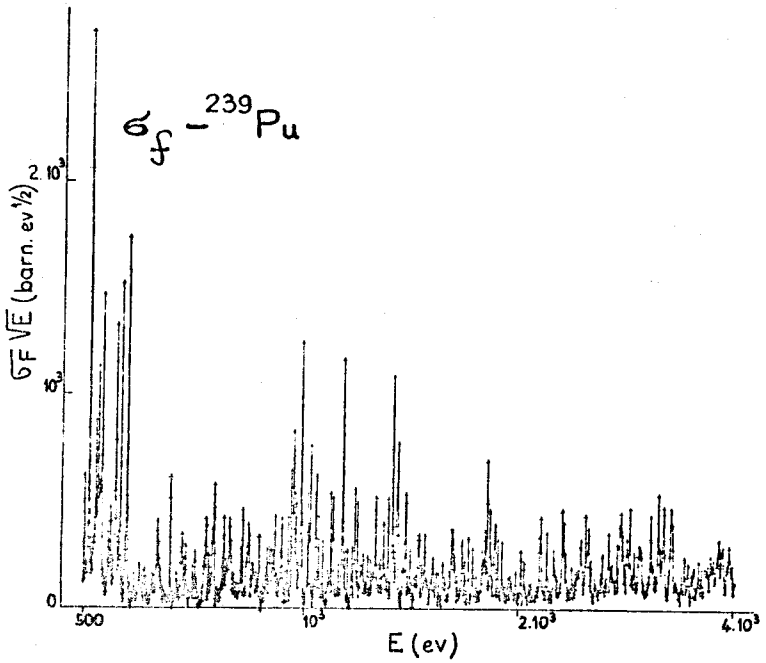

Figure 7: σ_f (^{239}Pu) measurements by Blons et al. [37].

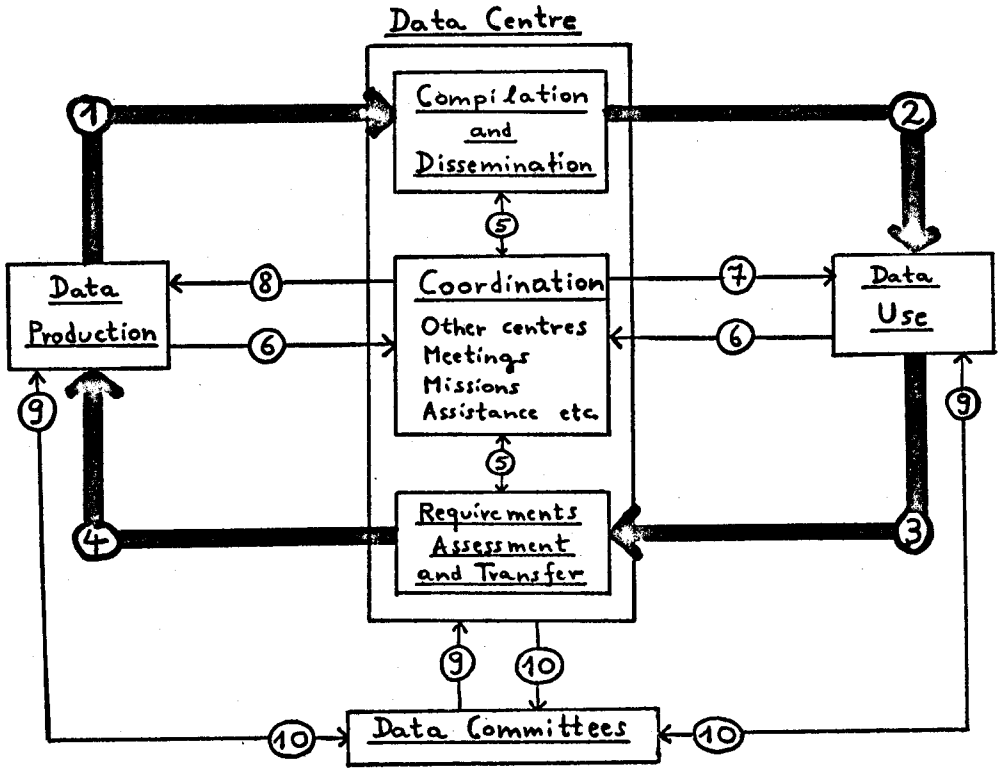

Data flow (▬▬▶) and coordination links (⟷) between data users, producers, centres and committees.

Figure 8:

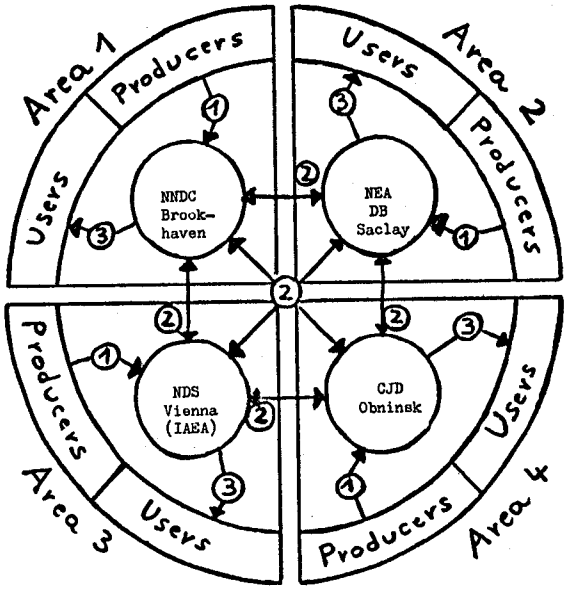

World-wide data flow between neutron data producers, centres and users.

Figure 9:

FUNDAMENTALS AND APPROXIMATIONS OF MULTILEVEL RESONANCE THEORY FOR REACTOR PHYSICS APPLICATIONS

M.S. MOORE
Los Alamos Scientific Laboratory,
University of California,
Los Alamos, NM,
United States of America

ABSTRACT

The formal theory of nuclear reactions leads to any of a number of alternative representations for describing resonance behavior. None of these is satisfactory for applications, and, depending on the problem to be addressed, approximate expressions are used. The specializations and approximations found to be most useful by evaluators are derived from R-matrix theory and are discussed from the viewpoint of convenience in numerical calculations. Finally, we illustrate the application of the theory by reviewing a particular example: the spin-separated neutron-induced cross sections of ^{235}U in the resolved and unresolved resonance regions and the use of these results in the U.S. evaluated nuclear data file ENDF/B.

1. INTRODUCTION

1.1. Requirements of the resonance treatment for application.

It can be estimated that any code which provides an accurate and detailed treatment of resonance cross sections for reactor calculations spends the largest fraction of time on the resolved and unresolved resonance region. For example, in 1973 Hwang [1] noted that the then current version of MC^2, a code that calculated multigroup cross sections from the ENDF/B library, required 45 minutes of running time on an IBM-360/75 computer for a typical fast reactor problem, and that 90% of the time was spent on the resolved resonance region alone. In this paper, Hwang described revised calculational methods used in an option for approximating the resonance treatment for routine calculations. This option was to be incorporated in a second version of MC^2 that resulted in significant time savings (up to a factor of 100 for the resolved range). This example is cited to show the importance of using approximate methods whenever possible. Approximate treatments are based on use of psi and chi-functions (convolutions of a Doppler function, represented by a Gaussian, with a Breit-Wigner line shape). These are also known as Voigt profiles; see Hwang's 1969 review [2] and material in this series to be covered by Fröhner [3]. If a resonance parameterization can be cast in the form of a superposition of symmetric and asymmetric Breit-Wigner profiles with real coefficients, and if one can use the psi-chi approximations for Doppler broadening of these resonances, then the calculations can be done reasonably efficiently. If one or both of these approximations is not adequate, then one must resort to kernel broadening of tabulated cross sections; the most efficient technique is perhaps that described by Cullen and Weisbin [4], which requires a factor of 5 to 7 longer in computation time.

The important point to be made is that resonance treatments must be kept simple, commensurate with the accuracy required of the calculation to be performed. All methods involve approximations of one form or another. The evaluated data set is based on one or more experimental measurements; the best of these measurements are approximate representations of the nuclear cross sections. The question the user must answer is whether the approximate method he has chosen to use is good enough to yield the accuracy required of the calculation.

In principle, the data base consisting of the evaluated set of neutron cross sections should be provided with adequate detail to permit any problem to be addressed to whatever level of accuracy is required. In practice, the data base is a compromise, the most important materials being given the most attention in the evaluation process. For the least important materials, e.g., the heaviest actinides, for which experimental measurements are very limited or nonexistent, the evaluated data base might consist completely of model calculations, based on extrapolations of average parameters, adjusted to give agreement with whatever experimental information might exist. Because in any practical situation the least important materials are present in only trace amounts, it matters very little that the data base is obviously inadequate to calculate neutronics properties in bulk quantities of the material. Only for a few materials is it important to be able to treat temperature effects and calculate Doppler coefficients accurately, to calculate resonance self shielding in heterogeneous systems in deep penetration situations, or to treat accurately the detailed energy and angular dependence of the emitted neutron in inelastic scattering or multiple neutron emission processes.

In short, it is neither necessary nor desirable that the resonance prescription be given with the same degree of accuracy for all materials in the evaluated data base. The simplest representation should always be used if its use is warranted. However, the attempt to use a simple representation when it is unwarranted leads to problems. For example, the evaluator may include a smooth background file of pointwise data to correct the deficiencies of an oversimplified resonance approximation. When this "smooth background" file is not smooth and not small, virtually all the advantages of the oversimpli-

fied resonance treatment are lost. The evaluator might, at this point, consider whether a more complicated resonance prescription may be preferred.

1.2. Limitations imposed by the experimental data.

Even in cases for which the evaluated data base should contain the best and most accurate representation one knows how to provide, the evaluation is a compromise. This is so because the experimental data on which the evaluation is based are inadequate, inconsistent, and incompletely documented. I suspect that this holds to some extent for integral experiments, used as a basis of comparison of eigenvalues, reactivity worths, and reaction-rate ratios in benchmark data-testing calculations of an evaluated library, and which form the basis for data adjustment. It is invariably true for the microscopic cross-section measurements on which the library is based.

In a microscopic or differential measurement, one attempts to observe the "observables" in scattering and reaction theory, i.e., to measure, at infinite separation of a pair of nuclei, the interaction probabilities or cross sections for a particular process to occur. One measures the energy of the incident particle and the reaction rate at that energy; he may measure one or more of several other observables: the energy of the emitted particle or particles, the angle between the incident and emitted particle; if there are two or more emitted particles or radiations, he may measure the angle between them and the energy and intensity of each. He may measure the orientation dependence of the reaction rate by polarizing or aligning the incident particle and/or target nuclei.

We shall consider the specific example of a polarized-neutron and polarized-target measurement on ^{235}U later. At this point it is instructive to look at a typical differential measurement from the point of view of listing the approximations and corrections that may be involved before the evaluator ever sees the experimental data set. If the experiment involves a neutron-induced reaction in the resonance range, one typically measures the count rate of the reaction as a function of neutron time-of-flight over a known flight path, and infers the neutron energy distribution from the time-of-flight spectrum. One might also measure the pulse height or energy of one or more of the reaction products and the angle of emission. To reduce the count-rate data to cross-section, one also needs to measure the neutron flux; generally this is done by placing a material whose cross section is assumed to be known in the neutron beam, and measuring another spectrum of reaction rate vs. time of flight. Finally, one needs to know what the backgrounds are: these generally consist of two components: 1) counts from sources or neutrons interacting with materials other than the target material of interest or the flux monitor, and 2) counts from the target material or flux monitor arising from off-energy neutrons that may be present in the beam. While the method of collecting background data depends on the experiment, the notch-filter method is common. In the beam, one interposes a material that removes all the neutrons at some given energy and perturbs the beam only slightly at other energies. He then infers the background by observing the count rate at the energy at which the neutron flux is zero. By using a series of notch filters, he can infer the background at several energy points in the range of interest.

There are several approximations and/or corrections made in the reduction of experimental data. Only rarely is the documentation adequate to permit an evaluator to judge between two such data sets if they happen to disagree outside the quoted uncertainties. Typical approximations or corrections that might be addressed are listed as follows:

1) The neutron energy scale. Is it absolute or relative to other work? If the energies are determined by time-of-flight, what is the time spread, delay, and uncertainty introduced by the neutron moderator and by the detector? How does one best correct the discrepant energy scales of two or more measurements to be averaged?

2) How were the detector efficiencies and number of target atoms in the sample determined and how large are potential systematic uncertainties? If several measurements are made relative to a common standard, are the correlated uncertainties properly treated?

3) The sample is generally not of negligible thickness; the flux monitor in this case does not experience the same resonance self shielding as does the average target nucleus. Has an appropriate correction been applied to take account of the difference?

4) Multiple-scattering corrections in the sample and flux monitor are often important but rarely discussed in detail.

5) The energy resolution associated with the measurement is often underestimated by the experimenter; the effects of resolution broadening of the data set are rarely studied and documented.

6) The sample temperature is never zero degrees K; the zero-point motion of the target nuclei is dependent on the chemical composition of the sample; and experimentalists also use approximate methods of calculating Doppler-broadening corrections.

The final point to be made in considering experimental limitations on resonance prescriptions is the following: as far as parameterizing experimental data for applications is concerned, resonance analysis is a "black-box" procedure. The experimentalist induces resonance interactions by allowing a neutron beam with known characteristics to strike a sample that also has known characteristics. He observes the interaction products and obtains a spectrum of the reaction rate vs. energy, which he then reduces to cross-section. He then characterizes the bumps and wiggles in the spectrum by a set of parameters, which, when used in a prescribed equation, can be expected to provide a more-or-less accurate representation of the observed spectrum. He may attempt to infer, by studying the distributions of the various parameters, what the properties of the nuclear interaction might be, in order to give some phenomenological means of calculating what he is unable to observe experimentally. However, the methods the experimentalist generally uses to reduce and analyze the measurement, or those the evaluator uses to provide an evaluated data base, are not very different from those used in applied computations. All involve approximations.

2. FUNDAMENTALS

2.1. Assumptions

It is basic to nuclear reaction theory that one observes only quantities at infinite separation; from such observations, one infers the properties of the nuclear interaction that occurred. One fundamental assumption is that the nuclear interaction obeys the laws of quantum mechanics, in particular the time-independent Schrödinger equation. A second is that the interaction is localized in space to the vicinity of the interacting particles, and is representable by some kind of collision operator. This may be a collision matrix if any of the properties of the nuclear species observed at infinity are changed as a result of the interaction, or a collision function if they are not (i.e., if only elastic scattering can occur). We have listed some of the quantities that may reveal whether changes can occur: in addition to determining what nuclear species are involved as a result of the interaction, one can measure the energies, angles, and orientations of the exiting species relative to the incident ones.

The idea of associating a qualitatively different time dependence with different types of nuclear interaction is attributed to Friedman and Weisskopf [5], who in particular, differentiated between shape-elastic scattering and compound-elastic scattering as examples of fast and slow processes that could be distinguished because of the different time delays associated with the two processes. At the present time, one distinguishes at least three such categories. Fast processes generally include direct interactions, the formation and immediate decay into the entrance channel of single particle resonance states, Coulomb excitation if both nuclear species are charged, etc. The second category contains intermediate processes: pre-equilibrium decay, isobaric analogue states, doorway-hallway states. The slow processes are generally assumed to be restricted to compound nucleus formation fulfilling the Bohr hypothesis that the decay probabilities are independent of the formation mechanism, and leading to sharp resonance structure in the interaction probabilities or measured cross sections. In actuality, one knows that this picture is oversimplified: the time spectrum of reaction processes is a continuous one. As a result of the uncertainty principle, one can also associate the width of observed structure with the time dependence of the process: slow processes lead to sharp resonance structure, fast or direct processes to slowly varying or smooth cross sections.

In this series of lectures, we have been asked to treat particularly the category of slow processes in the framework of the R-matrix theory of Wigner and Eisenbud [6]. In this context, the restriction of the treatment to two-body interactions (for which the reaction products observable at infinite separation consist of only a pair of particles) or of sequences of two-body interactions is perhaps adequate for most purposes.

All formulations of reaction theory that contain the basic common assumptions have been shown to be equivalent, in the sense that they are derivable from one of the general unified theories. In the next section, we shall review briefly the various approaches used to demonstrate this equivalency of reaction formalisms. However, at this stage, we should like to note particularly the significant features and relative advantages of particular reaction formalisms for resonance calculations, those of Kapur and Peierls [7], Wigner and Eisenbud [6], and Siegert, Humblet, and Rosenfeld [8,9]. At infinity, the wave function describing the reaction consists of incoming and outgoing waves; the radial parts are spherical Hankel functions, and are complex. If these same functions are used to represent the interaction and the resonance structure, the collision matrix is found to consist of a single-sum expansion with complex and implicitly energy-dependent parameters--the Kapur-Peierls formulation. Adler and Adler [10,11] showed that separating the expansion into real and imaginary parts gives a real expansion that is of the same form as a superposition of single-level terms of the formula of Breit and Wigner [12], and that in certain cases, the parameters are approximately energy independent. This turns out to be very useful in applications, because essentially all the methods of resonance treatment in reactor applications can be used without change.

In other cases, the energy-dependent Kapur-Peierls parameterization is not useful; to obtain an expansion that is both real and energy independent, one must use Wigner and Eisenbud's R-matrix

theory. One introduces the R-matrix as a ratio of value and derivative at the boundary between the interaction region and the external region, and expands the R-matrix in terms of real eigenfunctions and over real eigenvalues. He then must perform a matrix inversion in channel space to obtain the collision matrix expansion. What he has bought with this procedure is simplicity in the parameterization, but the price paid is that the representation cannot readily be put into a form convenient for most calculations. Both these formulations are most often used as "black-box" representations: the compound nucleus is thought of as a black box and the parameters are obtained as a fit to measured cross-section curves.

The Humblet-Rosenfeld formulation is an expansion over outgoing waves. The parameters are complex but energy independent; there is, however, an energy-dependent background that enters. If the expansion is considered as a "black-box" representation, it becomes formally the same as that of Kapur and Peierls. Its greatest strength would appear to come if it is used as a basis of comparison of data to model calculations rather than as a black-box parameterization in its own right, as the eigenfunctions and eigenvalues corresponding to the decaying states (outgoing waves) are those which one would expect to obtain as the natural states in a calculation of quasistationary shell model levels above a finite potential well. This connection was noted by Weidenmüller [13] in his first paper on the shell-model theory of nuclear reactions, and was implicit in the monograph by Mahaux and Weidenmüller [14] on the same subject. However, this approach does not seem to have been exploited; at about the same time, Lane and Robson [15-17] and Tobocman and Nagarajan, et al. [18,19] provided the formalism for addressing the same problem with R-matrix theory. Recently, García-Calderón and Peierls [20-21] reviewed the problem from the viewpoint of the Kapur-Peierls expansion.

The development of R-matrix theory, as reviewed by Lane and Thomas [22] is given in Appendix A. Relations to other resonance formalisms, and in particular to the approximations used in applications, are illustrated in Appendix B.

2.2. Equivalency of the Formulations of Reaction Theory

The earliest treatment of resonance structure in low-energy neutron-induced reactions, in the formula given by Breit and Wigner [12] and by Bethe and Placzek [23-25] was based on the observed similarity in shape of neutron resonances to that in light dispersion. The formal theory of resonance reactions followed two approaches, 1) the real eigenvalue expansion of the R-matrix of Wigner and Eisenbud [6], and 2) the complex eigenvalue expansion of the collision or S-matrix by Kapur and Peierls [7]. In 1950, Lippmann and Schwinger [26] provided an integral-equation representation of the general two-body scattering problem, which formed the foundation for theoretical treatments in many-body scattering theory. Although the Lippmann-Schwinger approach rested on the same basic assumptions as R-matrix and S-matrix resonance theory (i.e., the validity of quantum mechanics, the existence of a localized interaction volume, the restriction to two-body interactions), the aim was rather different: to provide the foundation for a variational approach to nuclear reaction theory. They developed variational principles for the collision operator (S-matrix) and noted problems of unitarity in the results, and then provided a variational method for evaluating the reactance operator (K-matrix) and transition operator (T-matrix) that did satisfy the unitarity requirements. It was not readily apparent how one might reconcile the differences in approach between the general scattering theory of Lippmann and Schwinger and the resonance theories of Kapur-Peierls and Wigner-Eisenbud. This problem was addressed in 1957 by Bloch [27], who introduced a generalized boundary operator based on a Green's function approach, showed the equivalence to the Lippmann-Schwinger treatment, and showed that the Kapur-Peierls and Wigner-Eisenbud dispersion theories can be derived as consequences of this approach in which specified boundary conditions are imposed.

The unified reaction theory of Feshbach [28,29] is rather different from that of Bloch [27]. Feshbach introduced projection operators to modify the Hamiltonian. In effect, the projection operator divides the configuration space into two subsets corresponding to open and closed channels; one then obtains a set of coupled equations, the solution of which gives the modified Hamiltonian. For example, in his 1962 paper Feshbach uses the projection operator formalism to derive the results of R-matrix theory, by choosing P, the projection operator for open channels, to be unity outside the boundary $r = a$, and zero inside. MacDonald [30-32] showed how Feshbach's theory could be derived from the Lippmann-Schwinger integral equation for the transition matrix, and Tobocman [33] recently generalized Feshbach's theory to permit multidimensional projection in configuration space.

In 1966, Lane and Robson [15] showed how the generalized boundary operator Bloch [27] had introduced in 1957 could be used to derive all the reaction theories then in existence. Tobocman [34] later showed how the Bloch operator could be generalized to describe three-body channels. In 1969, Lane and Robson [16,17] showed the connection between R-matrix theory and model calculations with a shell-model Hamiltonian.

3. APPROXIMATIONS

3.1. Constraints introduced by the Doppler-broadening treatment

For reactor physics calculations involving neutronics calculations, all the rigorous formulations of resonance theory are found to

be too cumbersome. This is primarily because reactor codes for routine calculations (i.e., all except those involving Monte-Carlo techniques) are invariably built around a resonance treatment that involves the use of Voigt profiles to take account of Doppler broadening. These functions are defined as follows:

$$\psi = \frac{\xi}{\sqrt{4\pi}} \int_{-\infty}^{+\infty} \frac{\exp[-(q-p)^2\xi^2/4]}{1+p^2}\, dp \quad ,$$

$$\chi = \frac{\xi}{\sqrt{4\pi}} \int_{-\infty}^{+\infty} \frac{2p\, \exp[-(q-p)^2\xi^2/4]}{1+p^2}\, dp$$

Using the notation of Appendix B, the total and reaction cross sections using the single-level Breit-Wigner formula are written as follows, for $\ell = 0$ neutrons:

$$\sigma_{n,T}(E) = \frac{\pi g_J \Gamma_{nr}/k^2}{(E-E_r')^2 + \Gamma_r^2/4} [\Gamma_r \cos 2\phi_o + 2(E-E_r') \sin 2\phi_o] + \frac{4\pi}{k^2} \sin^2 \phi_o$$

and

$$\sigma_{n,x}(E) = \frac{\pi}{k^2}\, g_J\, \frac{\Gamma_{nr}\Gamma_{xr}}{(E-E_r')^2 + \Gamma_r^2/4}$$

(In these expressions, we have simplified the formulas of Appendix B by selecting one level, and by using the identity $1-2\sin^2\phi_o = \cos 2\phi_o$. The reaction x can represent either fission or capture.)

One makes the identifications

$$q = 2(E-E_r')/\Gamma_r, \quad \xi = \Gamma_r/\Delta \quad ,$$

where $\Delta = \sqrt{4EkT/A}$ is the Doppler width, with E the energy; T the absolute temperature, A the reduced mass of the target nucleus; and k the Boltzmann constant in this definition only. (In the cross section equations k is the neutron wave number as defined in the appendices.)

If this is done, then the single-level Breit-Wigner formula for the cross section, convoluted with a Maxwell-Boltzmann distribution assumed to represent the motion of the target nuclei at the temperature T, can be written approximately in terms of the Voigt profiles ψ and χ, multiplied by factors which are only slowly energy dependent. The psi- and chi-functions are tabulated, or can be calculated rapidly; the cross section itself is never calculated in a fine mesh such as would be required if the convolution were to be evaluated numerically. The treatment is an approximation; it does not preserve reaction rates or leave a 1/v cross section invariant, as was noted by Solbrig [35,36] and more recently by Cullen [37]. The accuracy of the approximation has been discussed by Hinman et al. [38], and by Cullen and Weisbin [4] who provide alternate expressions for an exact treatment where it is warranted. In most cases of practical interest, except for very low-energy resonances where the validity of the gas model is also questionable, the approximation is adequate.

The implication is clear, however. Only those resonance representations that can be put into a form suitable for a Doppler-broadening treatment by the use of Voigt profiles will find general acceptance and will be generally used by the reactor community. Three of the four formulations in Appendix B fulfill this requirement.

3.2. Discussion of the approximations used in ENDF/B

The approximations found to be most useful for applications involving the ENDF/B data file are described in a formats and procedures manual by Garber et al. [39]; the formulas are summarized in Appendix B. A revision of the resonance region portion of the manual is in preparation [40]; some of the changes and additions are included in Appendix B. The relations between the approximations and the formal theory are also treated in Appendix B.

The simplest, most often encountered approximation is the single-level formula given by Breit and Wigner (SLBW). When one attempts to represent cross sections by a superposition of single-level terms, according to the prescription given in Appendix B, he occasionally finds that at certain energies the calculated scattering and total cross sections become negative. This unsatisfactory situation is often remedied by including a "smooth file" to be added to the resonance calculation. However, de Saussure et al. [41] have shown that for ^{238}U the SLBW formula is not satisfactory in a strongly self-shielded situation; they recommend the use of the multilevel Breit-Wigner formula introduced by Bethe and Placzek [24] (MLBW, occasionally also called the Gregson formula [42] or the FPW formula, having been derived by Feshbach, Porter and Weisskopf [43] in connection with their formulation of the optical model). The formula takes explicit account of level-level interference; it is derived from an amplitude-squared expression and cannot go negative; and it is valid for $\langle\Gamma\rangle \ll D$. It was shown by de Saussure et al. [41] that this approximation gives quite satisfactory results for a description of the resonance cross sections of (^{238}U + n) even in strongly self-shielded cases; these authors also provided a parameterization suitable for use with Voigt profiles, included in Appendix B.

The next approximation described in Appendix B is not suitable for Voigt-profile broadening. In 1958, Reich and Moore [44] wrote down an expression to be used for s-wave neutron-induced fission. The approach uses the channel-elimination method introduced in 1952 by Teichmann and Wigner [45] to eliminate certain open channels whose off-diagonal matrix elements have random signs; this approach was described in general by Thomas in 1955 [46]. The Reich-Moore specialization of this approach eliminates the open radiative capture channels to give a reduced R-matrix. The further specialization to the case that fission does not occur leads to a reduced R-function treatment of elastic scattering and radiative capture that is also known as the ML formula [41]. Use of the Reich-Moore parameterization for fission has been discontinued in ENDF/B, primarily as a result of the difficulties encountered with processing codes. However, it appears that the simplicity of parameterization permitted in resonance descriptions with higher angular momenta with the reduced R-function or ML formula will lead to its being recommended in the future as an acceptable ENDF/B format in spite of the processing difficulties, in particular for isotopes in the Fe and Ni region.

Moldauer [47] and Adler and Adler [48] have provided computer programs to convert R-matrix parameters to Kapur-Peierls parameters by diagonalizing the level matrix (discussed in Appendix B); de Saussure and Perez [49] showed how the same task could be accomplished by a partial fraction expansion. The Adler-Adler formula as given in Appendix B is found to be a very useful representation for s-wave neutron-induced fission, as the Doppler broadening can be accomplished by Voigt profiles; however, for treating wide energy ranges and higher angular momenta, such as is required for isotopes in the region of iron and nickel, the approximation that the energy dependence of the parameters can be ignored appears to limit the usefulness of the Kapur-Peierls or Adler-Adler representation. The problem of uniqueness of R-matrix parameters has been considered by Adler and Adler [50]; this subject is perhaps best understood by referring to a specific example, and will be deferred to the end of the next section.

4. ANALYSIS AND EVALUATION OF RESONANCE MEASUREMENTS: APPLICATION TO (^{235}U + n)

4.1. The resolved resonances.

In this section we address specific techniques for analysis and evaluation of the resolved and unresolved resonance region, using the cross sections of (^{235}U + n) as the example. There has been a great deal of attention given to (^{235}U + n), and recently there was what we might consider a major breakthrough in contributing to our understanding of the problem: the obtaining of exceptionally high quality fission cross section data by Keyworth et al. [51] with a polarized beam and polarized target. It is the analysis [52] of these data that provides new insight to the general problem of evaluating data in the resonance region, and which is of interest to this review.

The measurement by Keyworth et al. was a second measurement carried out on the Oak Ridge Electron Linear Accelerator (ORELA); it was an extension of an earlier set of data previously analyzed and reported by Keyworth et al.[53,54] The data consisted of time-of-flight spectra of fission events obtained with the polarization vector of the neutron beam oriented both parallel and antiparallel to that of the ^{235}U target, and time-of-flight spectra of the transmitted flux with the same polarizations. If the beam and target polarizations had been complete ($\sim$100%), the data could have been readily reduced to obtain a J=3 fission cross section and a J=4 fission cross section with essentially no sacrifice of statistical accuracy. Even though these polarizations were not exceptionally high (the product $f_n f_N$ of the beam and target polarizations was $\sim$8%), the spectra that were obtained had sufficient statistical accuracy that this could still be done; typical data obtained are shown in Fig. 1 and 2. In these figures, the lower curve is the J=3 fission cross section, the middle curve is the J=4 fission cross section, and the top curve is the sum of the two; i.e., the fission cross section one would measure with an unpolarized beam and/or unpolarized target.

The analysis of these data in the resolved-resonance region has three objectives, which we should note: 1) one wants to provide the user with a set of resonance parameters that will more accurately represent the cross sections in reactor calculations, 2) one wants to derive better average parameters in order to be able to give a more accurate representation in the unresolved resonance region and at higher energies, and 3) one wants to compare the results obtained with other analyses and evaluations, to see if the insight gained for (^{235}U + n) can be applied in a more general way.

Even a casual inspection of the spin-separated fission data on (^{235}U + n) shows that a great many of the resonances previously observed and analyzed as single resonances (i.e., the top curves in these figures) are actually doublets of different spin. Some may even be triplets. However, these data are not good enough to give a completely definitive answer to the question, "What is the resonance spacing in (^{235}U + n)?" No data set by itself can answer this question; the most probable value for the neutron width is zero, and, unless there is strong interference in another channel, such a resonance will not be observed. One must resort to assumptions about the statistical distributions of widths and spacings to arrive at an answer.

We began by dividing the resonances into three categories: those whose existence is 1) definite, 2) probable, and 3) possible or unlikely. Below 62 eV, there are 126 resonances of the first category, 19 of the second, and 20 of the third. We then attempted to use the Δ_3 statistic of Dyson and Mehta [55], in connection with

Dyson's F-statistics[56], to decide which of the resonances of categories 2 and 3 should be included in the set of resonances that actually exist. These statistical tests are to be discussed in detail by Fröhner [3], but their use may be described briefly. Both the Δ- and F-statistics are derived under the assumption that the eigenvalues follow a Gaussian orthogonal ensemble. To obtain the Δ-statistics one calculates the best linear least-squares fit to the stairstep distribution of the number of levels below a given energy versus energy (i.e., the region below ∿ 60 eV in Fig. 3) and compares the observed root-mean-square deviation of the stairstep from the straight line with the theoretical expectation value. The F-statistics considers the spacing of neighboring levels in an interval about the i^{th} level. It is thus a running statistics and is used to point to levels which may be spurious, or to regions in which a level may be missing.

Dyson and Mehta studied the properties of the Δ-statistics and concluded that using the Δ_3 statistics (which has no constraints on slope or intercept), one should be able, in principle, to determine the number of resonances in a given energy region to within ± 1 resonance, provided that the sample is reasonably pure. Unfortunately, this does not appear to be the case in (^{235}U + n), even with spin-separated cross sections. Satisfactory agreement was obtained with the expectation value of the Δ_3 statistics with the 126 resonances of category 1, with the 145 of categories 1 and 2 plus 7 of category 3 for a total of 152, and for a selected set of 139 consisting of the 126 of category 1 and 13 others from categories 2 and 3. One can only conclude that in studying a sample of resonances with this degree of purity, the Δ_3 statistics is not useful.

A comparison of the spacing distribution of the levels of category 1 with that of a Wigner distribution for a mixed sequence (Fig. 4) suggests that there is a significant number of missing levels with small spacing (∿10%). A calculation of the expected peak cross section distribution with the level at which one might expect resonance peaks to be observable (> 2b) is roughly consistent with this estimate. Finally, we devised a missing-level estimator [52] based on the moments of an assumed truncated Porter-Thomas distribution, which led to a recommended average spacing of 0.438 ± 0.038 eV for the mixed sequence. This is to be compared with the 0.38 eV ± 10% estimated by Garrison [57] on the basis of counting observed peaks in computer-generated cross sections.

The second question we should like to address is, "What are the average partial widths for the resolved resonances?" The most direct way of arriving at the answer is to carry out a simultaneous multilevel analysis of these data with other reevaluated total and partial cross section measurements, similar to the approach taken by Smith [58] or by de Saussure et al. [59] This was not done. The approach taken was instead that of an evaluation of evaluations: from various sets of resonance parameters, one can calculate a common set of observables, in this case the total, fission, and capture areas for the resonance structure. These resonance areas were then intercompared, averaged, adjusted as necessary by comparison with the polarization measurements, and eventually an internally consistent set of parameters was obtained. These parameters are those which describe the unpolarized beam, unpolarized sample data on the total, fission, and capture cross sections of (^{235}U + n) in the resonance range, and the polarized beam, polarized sample data on the fission cross section. They were then used to determine the relative average partial widths.

In carrying out an evaluation of this type in the resonance region, one finds parameter sets consisting of R-matrix multilevel results, Kapur-Peierls multilevel results, Breit-Wigner single-level results, and occasionally total and partial resonance areas that may have been determined by using a planimeter and a piece of graph paper. To a first approximation, in comparing such data sets one can assume that the asymmetric term is of equal size and of opposite sign above and below the resonance energy, and that the net area can be calculated from the contribution of the symmetric terms. The appropriate formalism is that given by de Saussure and Perez [60], who note that the assumption is strictly valid only on the average over the entire region spanned by the parameter set.

One recurrent problem, of which evaluators are rarely aware, is that experimentalists are frequently overly optimistic in making corrections and in assigning uncertainties to their measurements. When one compares the various sets of parameters obtained for (^{235}U + n) resonances, it becomes obvious that the resolution functions associated with the experimental data sets are poorly known. While the ratio of capture to fission generally shows good agreement in comparisons of the results from different evaluators, the absolute values of the capture and fission widths are found to be in rather poor agreement because of this resolution problem. We eventually decided to address the problem by using a model calculation of the average radiative capture width, normalized to nonfissile actinide nuclides, and to compute the fission and neutron widths of each resonance from the measured capture-to-fission ratios and fission and/or total areas.

The next step in the evaluation is to establish the statistical distribution of the partial widths, in order to use the results in a calculation of the unresolved region. By considering data obtained by Pattenden and Postma[61] on the angular distribution of fission fragments from aligned nuclei, and in particular the correlation of these data with spin, as shown in Fig. 5, one can conclude that the fission width distribution for (^{235}U + n) is similar to the neutron width dis-

tribution; i.e., it is a chi-squared distribution with two to three degrees of freedom, for both spin-spin states. The distribution of fission widths and the existence of pronounced interference in fission are consistent with this estimate.

4.2. The unresolved resonance region.

As shown in Fig. 6, the neutron cross sections of (^{235}U + n) show pronounced fluctuations which extend to 200 keV or higher. The total cross section [62] of (^{235}U + n) shows similar structure to the absorption; both are strongly correlated with the fission cross section. It has been suggested that the fluctuations in the fission cross section arise because of second-well enhancement: states in the second well are mixed with the usual compound nucleus states in the first well. Others maintained that the fluctuations may be primarily an entrance channel phenomenon.

One would expect the cross sections to be qualitatively different if fluctuations arose from: 1) fluctuations in the average neutron width, or 2) fluctuations in the average fission width. In the first case, fluctuations in radiative capture and fission would be correlated; in the second they would be anticorrelated. One might expect a qualitative difference in the Doppler coefficient, for example, in a highly self-shielded situation. Data presented by Beer and Käppeler [63] on the ratio of fission to capture in (^{235}U + n) from 25 to 60 keV neutron energy strongly support the view that the average fission and capture cross sections are anticorrelated.

Also shown in Fig. 6 are the spin-separated fission cross sections of (^{235}U + n). The evaluated data file in the unresolved region consists of a set of energy dependent unresolved average resonance parameters; from such a table, the partial cross sections can be reconstructed by performing Hauser-Feshbach calculations with width-fluctuation corrections. The energy-dependent average parameters are also of interest in that they permit statistical tests to be made for possible intermediate structure. Several such tests have been described and applied by Baudinet-Robinet and Mahaux [64]. Perhaps the most popular test is the distribution-free runs test of Wald and Wolfowitz [65], suggested by James [66]. If one uses this test on the average fission widths for ^{235}U it is easy to conclude that the average spin-4 fission component shows strong evidence of intermediate structure in fission; as shown in Figs. 7 and 8, the fluctuations in the other spin component are nearly as pronounced. The general conclusions are in qualitative agreement with calculations by James [67], who found that the observed effect could be explained by assuming intermediate structure in one of the two fission components. In this latter paper, James studied two other tests described by Baudinet-Robinet and Mahaux, the Wald-Wolfowitz correlation test [68], and the Levene-Wolfowitz runs-up-and-down test [69]. James concluded that the Levene-Wolfowitz test was not powerful enough to be reliable; Baudinet-Robinet and Mahaux noted in their study that the Wald-Wolfowitz correlation test is perhaps too powerful to be generally useful, as it is therefore very subject to experimental error.

4.3. Uniqueness of multilevel parameters.

The definitive study on the problem of uniqueness of R-matrix parameters of the low-energy cross sections of fissile nuclei is that of Adler and Adler [50]. To understand what the problem is, one needs to be familiar with the ideas involved in developing the various approximations. The reduced R-matrix formulation involves, at each energy point, a summation over resonance amplitudes for however many resonances one needs to consider and a matrix inversion over however many channels one needs to consider. For fission of (^{235}U + n) the number of channels involved is known to be small, but more than one. The fission-width amplitudes can be thought of as a set of vectors in a multidimensional channel space. It is the orientation of these vectors relative to one another that describes the interference observed in the fission cross sections; e.g., if two such fission-width vectors are parallel or antiparallel, the interference is strong; if the vectors are perpendicular, there is no interference. One can, in principle, use this property to assign resonance spins: if the resonances fall into two groups, the fission-width vectors of one group being all mutually perpendicular to those of the other, one infers that these two groups of resonances are characterized by different spins. In practice this method turns out not to be useful, because the parameters are not unique.

If the number of levels to be considered is not very large, then one can use the Wigner level matrix [70] to transform the problem of inverting the R-matrix into one of inverting a level matrix whose rank is equal to the number of levels. (See Appendix B.) This method was used by Vogt [71,72] in analyzing resonance data on fissile nuclides. The parameterization in this case is exactly the same, except that the number of channels is unspecified. What one does is to give the orientation of each fission-width vector relative to each of the others as part of the parameterization. Vogt noted that the number of channels required could be as high as the number of levels treated. One can also think of the Vogt parameterization as an intermediate step in the Kapur-Peierls complex summation over levels; formally all one does to obtain these parameters is to diagonalize the level matrix [10,11]. The problem, therefore, is that there may be several possible sets of off-diagonal elements that give the same eigenvectors.

The problem was first pointed out by Auchampaugh [73], who was addressing the feasibility of making spin assignments by multilevel analysis, and who studied the analysis of computer-generated cross sections with a reduced R-matrix search code MULTI that he had developed [74]. Auchampaugh noted that certain of the multiple solutions he found were simply related to the set used to generate the cross sections, while others were not; the total fission width was always preserved. Adler and Adler [50] solved the general problem, noting that for the case studied by Auchampaugh (two-fission channels permitted), one expects 1 + (N-1)(N-2)/2 possible solutions, where N is the number of resonances in the study.

Finally, it should be noted that the degeneracy is removable if one has additional data. If there are only two fission channels which have different K quantum numbers, then data such as those of Pattenden and Postma [61] are sufficient to determine the reduced R-matrix parameter set uniquely. If more than two channels obtain, one needs additional data.

D. B. Adler [75] has also recently addressed the problem of unitarity of the Kapur-Peierls formulation, in the context of the contraints that exist in the parameterization. She showed that the number of independent parameters is the same as in the R-matrix representation, the remaining parameters being fixed by the requirement that the collision matrix be unitary.

APPENDIX A. FOUNDATIONS OF R-MATRIX THEORY

A1. Introduction

The basis of the R-matrix theory of nuclear reactions has been summarized by Thomas [46] as follows: R-matrix theory is based on the standing-wave Green's function method, and, in fact, the components of the R matrix are the values of the Green's function at the entrances to the various pairs of channels. The definitive review of the R-matrix theory of nuclear reactions is that of Lane and Thomas [22]; the notation used here follows that review, as does the basic development. The scheme of the formal theory is as follows: 1) One defines cross sections $\sigma_{cc'}$ for the production of a pair of nuclei of type c' when two nuclei of type c are bombarded against each other with energy E. 2) A collision matrix is defined from which one can calculate the cross sections. (In R-matrix theory, the collision matrix is designated by U, with elements $U_{cc'}$.) 3) The collision matrix U is related to diagonal matrices L^o, P and Ω as well as to a nondiagonal matrix R, the relation being

$$\vec{U} = \vec{\Omega}\,\vec{P}^{1/2}\,(\vec{I} - \vec{R}\vec{L}^{o})^{-1}\,(\vec{I} - \vec{R}\vec{L}^{o*})\,\vec{P}^{-1/2}\,\vec{\Omega}$$

The L^o, P and Ω matrices take account of long-range nonpolarizing interactions between the separated nuclei; the R matrix is the unknown quantity describing the nuclear interaction. All three matrices depend on parameters a_c, the boundaries outside which the wave functions from each channel c are assumed to be known, and on boundary conditions B_c. 4) The energy dependence of any element of the R matrix is expressible as

$$R_{cc'}(E) = \Sigma_\lambda \frac{\gamma_{\lambda c}\,\gamma_{\lambda c'}}{E_\lambda - E}$$

where λ labels the members of a complete set of states with energy eigenvalues E_λ; the $\gamma_{\lambda c}$ are "reduced width amplitudes." (In the following development, the four steps are derived in reverse order.) The elements of R are real and the $\gamma_{\lambda c}$ are energy independent. The hermiticity of R guarantees the unitarity of the collision matrix. (It is easy to show that if

$$U = e^{-2i\phi}\,(1 - iK)^{-1}\,(1 + iK)$$

and if K is hermitian ($K_{ab} = K_{ba}^*$), then U is unitary, i.e., $U_{ab}\,U_{ba}^* = \delta_{ab}$.)

A2. Assumptions and notations.

Lane and Thomas [22] reviewed the assumptions that are at the basis of R-matrix theory as follows:

1) Applicability of nonrelativistic quantum mechanics as implied by the time-independent Schroedinger equation.

2) Restriction to two-body processes. A treatment of many-body processes can be given insofar as these can be described as a succession of two-body processes.

3) Absence of processes of creation or destruction (although Mahaux [76] showed how this restriction could be removed for photon channels).

4) The existence, for any pair c, of some finite radial distance of separation a_c, beyond which neither nucleus experiences any polarizing potential field from the other.

Lane and Thomas begin by introducing the following channel characterizations, in addition to $a_c = a_\alpha$:

$E_c \equiv E_\alpha$, the energy of relative motion of the particles of the pair c;

$M_c \equiv M_\alpha = \frac{M_{\alpha 1} M_{\alpha 2}}{M_{\alpha 1} + M_{\alpha 2}}$, the reduced mass;

$k_c \equiv k_\alpha = \left(\frac{2M_\alpha |E_\alpha|}{\hbar^2}\right)^{1/2}$, the wave number;

$v_c \equiv v_\alpha = \hbar k_\alpha / M_\alpha$, the relative velocity;

$\eta_c \equiv \eta_{\alpha\ell} = \frac{Z_{1\alpha} Z_{2\alpha} e^2}{\hbar v_\alpha}$, the Coulomb field parameter;

$\sigma_c \equiv \sigma_{\alpha\ell} = \arg\Gamma(1 + \ell_c + i\eta_c)$, the Coulomb phase shift;

$\rho_c \equiv \rho_\alpha = k_\alpha r_\alpha$.

Throughout the whole of configuration space, the wave function of the total system is assumed to satisfy the time-independent Schroedinger equation

$$H\Psi = E\Psi \tag{A1}$$

where E is the total energy, and H = T + V is the Hamiltonian operator.

Preliminary manipulations are carried out to allow one to treat explicitly only that part of the Hamiltonian describing the relative motion of the channel pairs. The wave function describing the relative motion can be expressed as a product of a radial and an angular part:

$$X \sim r_\alpha^{-1} u_{\alpha s\ell}(r_\alpha)[i^\ell Y_m^{(\ell)}(\theta_\alpha,\phi_\alpha)] \ ,$$

and the $u_{\alpha s\ell}(r_\alpha)$ satisfy the radial Schrödinger equation

$$\left[\frac{d^2}{dr_\alpha^2} - \frac{\ell(\ell+1)}{r_\alpha^2} - \frac{2M_\alpha}{\hbar^2}(V_{\alpha s\ell} - E_\alpha)\right] u_{\alpha s\ell}(r_\alpha) = 0 \tag{A2}$$

A3. Standing waves, incoming and outgoing waves, and the Wronskian.

If the interaction in the external region is a Coulomb interaction, Eq. (A2) can be rewritten as

$$u''_{\alpha\ell}(\rho_\alpha) - [\ell(\ell+1)\rho_\alpha^{-2} + 2\eta_\alpha\rho_\alpha^{-1} \mp 1]\, u_{\alpha\ell}(\rho_\alpha) = 0,$$

where the prime denotes differentiation with respect to ρ_α, and where the upper sign denotes positive energy channels ($E_\alpha > V_{\alpha s\ell}$), the lower negative energy channels. If F and G are any two linearly independent solutions, one can show that the Wronskian FG' - GF' is independent of ρ_α. (From the differential equation FG'' - GF'' = (FG' - GF')' = 0.) If, in particular, F_c and G_c are the two real solutions which are regular and irregular at the origin, respectively, and whose asymptotic forms at large ρ_α are

$$F_c \equiv F_{\alpha\ell} \sim \sin(\rho_\alpha - \eta_\alpha \log 2\rho_\alpha - \ell\pi/2 + \sigma_{\alpha\ell}),$$

$$G_c \equiv G_{\alpha\ell} \sim \cos(\rho_\alpha - \eta_\alpha \log 2\rho_\alpha - \ell\pi/2 + \sigma_{\alpha\ell}),$$

then the Wronskian of this pair is

$$F_c'G_c - G_c'F_c = 1.$$

One also needs the positive energy solutions for incoming and outgoing waves, I_c^+ and O_c^+. These have asymptotic forms

$$I_c^+ \equiv I_{\alpha\ell}^+ \sim \exp[-i(\rho_\alpha - \eta_\alpha \log 2\rho_\alpha - \ell\pi/2 + \sigma_{\alpha 0})],$$

$$O_c^+ \equiv O_{\alpha\ell}^+ \sim \exp[i(\rho_\alpha - \eta_\alpha \log 2\rho_\alpha - \ell\pi/2 + \sigma_{\alpha 0})].$$

One immediately sees that the value of the Wronskian for this pair is 2i. The relation between the two sets of solutions is

$$I_c^+ = (G_c - iF_c)\exp(i\omega_c) \ ,$$

$$O_c^+ = (G_c + iF_c)\exp(-i\omega_c) \ ,$$

where

$$\omega_c \equiv \omega_{\alpha\ell} = \sigma_{\alpha\ell} - \sigma_{\alpha 0} = \sum_{n=1}^{\ell} \tan^{-1}(\eta_\alpha/n)$$

A4. The matching conditions at the boundary.

The next stage in the development of R-matrix theory is to match the internal and external wave functions at the nuclear surface. In the internal region, one assumes the existence of a complete orthogonal set of eigenfunctions $X_{\lambda JM}$, where J and M are the angular momenta and projections, such that the wave function Ψ_{JM} in the internal region, satisfying the equation $H\Psi_{JM} = E\Psi_{JM}$ at a particular excitation E, can be expanded as

$$\Psi_{JM} = \sum_\lambda A_{\lambda J} X_{\lambda JM} \ , \tag{A3}$$

the $X_{\lambda JM}$ satisfying the equation $HX_{\lambda JM} = E_\lambda X_{\lambda JM}$.

The functions discussed so far in the external region have been only radial functions $I_{\alpha\ell}^+$ and $O_{\alpha\ell}^+$; the angular part and internal part were split off initially. The complete channel functions, normalized to unit flux crossing any sphere centered at the origin, are written by Lane and Thomas as

$$\bar{I}_{\alpha s\ell vm}^+ = \left(i^\ell Y_m^{(\ell)}\right) \frac{I_{\alpha\ell}^+ \psi_{\alpha sv}}{v_\alpha^{1/2} r_\alpha} \tag{A4a}$$

and

$$\tilde{O}_{\alpha s \ell \nu m}{}^{+} = \left(i^{\ell} Y_m{}^{(\ell)}\right) \frac{O_{\alpha \ell}{}^{+} \psi_{\alpha s \nu}}{v_\alpha^{\frac{1}{2}} r_\alpha} \quad , \tag{A4b}$$

where the notation can be simplified by writing

$$\phi_{\alpha s \ell \nu m} = r_\alpha{}^{-1} \psi_{\alpha s \nu}\left(i^{\ell} Y_m{}^{(\ell)}\right) \tag{A5}$$

for the terms which multiply the radial function $u_{\alpha\ell}$ to give the total channel wave function. One also wants to express the same functions in a different basis (corresponding to the quantum representation of the internal wave functions), as

$$\phi_{\alpha s \ell J M} = \sum_{\nu+m=M} (s\ell\nu m|JM)\ \phi_{\alpha s \ell \nu m} \tag{A6}$$

where the $(s\ell\nu m|JM)$ are vector addition coefficients. Both representations are orthogonal and normalized on the channel surface S, i.e., in either representation,

$$\int \phi_{c'}{}^{*} \phi_c \, dS = \delta_{cc'} \ .$$

The value and derivative of the radial function at $r_c = a_c$ are chosen such that

$$\begin{aligned} V_c &= (\hbar^2/2M_c a_c)^{1/2}\ u_c(a_c) \\ &= (\hbar^2/2M_c a_c)^{1/2} \int \phi_c{}^{*} \Psi dS \end{aligned} \tag{A7a}$$

and

$$\begin{aligned} D_c &= (a_c \hbar^2/2M_c)^{1/2} (du_c/dr_c)_{r_c=a_c} \\ &= (\hbar^2/2M_c a_c)^{1/2} \int \phi_c{}^{*}\ \mathrm{grad}_n\ (r_c \Psi)\ dS \\ &= V_c + (a_c \hbar^2/2M_c)^{1/2} \int \phi_c{}^{*}\ \mathrm{grad}_n\ \Psi\ dS \ , \end{aligned} \tag{A7b}$$

where Ψ is the complete wave function of the system and grad_n is the normal gradient.

In the internal region, the internal functions $X_{\lambda JM}$, evaluated on the surface $r_c = a_c$ satisfy the same form of equation

$$\gamma_{\lambda c} = V_{\lambda c} = (\hbar^2/2M_c a_c)^{1/2} \int \phi_c{}^{*}\ X_{\lambda JM}\ dS \tag{A8a}$$

and

$$\delta_{\lambda c} = D_{\lambda c} = \gamma_{\lambda c} + (a_c \hbar^2/2M_c)^{1/2} \int \phi_c{}^{*}\ \mathrm{grad}_n\ X_{\lambda JM}\ dS \tag{A8b}$$

The quantities $\gamma_{\lambda c}{}^2$ are the reduced level widths; the ratio of derivative and value has to do with the specification of the boundary conditions to be satisfied on S. The normalization of the value and derivative quantities on the surface are chosen for later convenience.

Lane and Thomas provide special symbols for the representations of the logarithmic derivative in the external region. They define

$$L_c = (\rho_c O'_c/O_c)_{r_c=a_c} = S_c + iP_c$$

$$S_c = \rho_c\ (F_c F_c' + G_c G_c')/(F_c{}^2 + G_c{}^2) \tag{A9a}$$

$$P_c = \rho_c/(F_c{}^2 + G_c{}^2) \tag{A9b}$$

$$\phi_c = \tan^{-1}\ (F_c/G_c) \ , \tag{A9c}$$

all of these being evaluated at $r_c = a_c$, and

$$w_c = I_c O'_c - O_c I'_c = 2i \ . \tag{A9d}$$

A5. A simplified case: definition of the R function.

To make the formal derivation more transparent, it is usual to begin by considering a one-channel interaction between spinless particles in which Coulomb interactions are assumed to vanish.

If u_1 and u_2 are two solutions of the internal radial equation, then one writes

$$(d^2u_1/dr^2) + (2M/\hbar^2)\,(E_1-V)\,u_1 = 0$$

$$(d^2u_2/dr^2) + (2M/\hbar^2)\,(E_2-V)\,u_2 = 0\ . \qquad \text{(A10)}$$

The first of these is then multiplied by u_2, the second by u_1, and the difference is integrated from 0 to a, giving

$$\int_0^a \left(u_2 \frac{d^2u_1}{dr^2} - u_1 \frac{d^2u_2}{dr^2} \right) dr + \frac{2M}{\hbar^2}(E_1-E_2)\int_0^a u_1 u_2\, dr = 0. \qquad \text{(A11)}$$

The requirement that u(r)/r be finite as $r \to 0$ allows the first term to be evaluated at r = a. One obtains

$$\left(u_2 \frac{du_1}{dr} - u_1 \frac{du_2}{dr} \right)_{r=a} + \frac{2M}{\hbar^2}(E_1-E_2)\int_0^a u_1 u_2 dr = 0\ . \qquad \text{(A12)}$$

At certain energies E_λ, where $(du_\lambda/dr)_{r=a} = 0$, the solutions are eigenfunctions and the energies are eigenvalues of the internal region.

One can then expand the solution at any energy in terms of these functions, which are also assumed to be normalized, such that

$$\int_0^a u_\lambda\, u_{\lambda'}\, dr = \delta_{\lambda\lambda'}\ . \qquad \text{(A13)}$$

One has, therefore, if $u_E(r)$ is the arbitrary solution

$$u_E(r) = \sum_\lambda A_\lambda\, u_\lambda(r), \quad 0 \leqslant r \leqslant a \qquad \text{(A14)}$$

where $A_\lambda = \int_0^a u_E\, u_\lambda\, dr$. Use of Green's theorem on u_E and u_λ gives

$$-u_\lambda(a)\,(du_E/dr)_a + (2M/\hbar^2)(E_\lambda-E)\int_0^a u_E u_\lambda\, dr$$

or

$$A_\lambda = \frac{\hbar^2}{2M}\frac{u_\lambda(a)}{E_\lambda-E}\left(\frac{du_E}{dr}\right)_a \qquad \text{(A15)}$$

Substituting this in Eq. (A14) gives

$$u_E(r) = \sum_\lambda \frac{\hbar^2}{2M}\,\frac{u_\lambda(a)\,u_\lambda(r)}{E_\lambda - E}\left(\frac{du_E}{dr}\right)_a\ . \qquad \text{(A16)}$$

The dimensionless logarithmic derivative is the R function:

$$R_{cc} = \frac{u_E(a)}{a(du_E/dr)_a} \qquad \text{(A17)}$$

$$= \frac{\hbar^2}{2M_a}\sum_\lambda \frac{u_\lambda(a)\,u_\lambda(a)}{E_\lambda-E}$$

$$= \sum_\lambda \frac{(\gamma_{\lambda c})^2}{E_\lambda-E} \qquad \text{(A18)}$$

A6. The general case: the R-matrix.

In the general case, one goes through exactly the same motions in the derivation, the surface term being replaced by the sum of surface terms for the various channels. The general solutions at two energies E_1 and E_2, corresponding to Eq. (A10), are

$$H\Psi_1 = E_1\Psi_1$$

$$H\Psi_2 = E_2\Psi_2 \qquad \text{(A10')}$$

The first of these is multiplied by Ψ_2^*, the complex conjugate of the second by Ψ_1, and the difference is integrated over the internal region τ to give

$$\int_\tau \left[(H\Psi_2)^* \Psi_1 - \Psi_2^* H\Psi_1\right] d\tau = (E_2-E_1)\int_\tau \Psi_2^*\Psi_1\, d\tau \qquad \text{(A11')}$$

If the interaction term V is self-adjoint ($V^\dagger = V$), then

$$\int_\tau \left[(V\Psi_2)^* \Psi_1 - \Psi_2^* V\Psi_1\right] d\tau = 0$$

and the volume integral of the kinetic energy terms is integrated by Green's theorem to give

$$(E_2-E_1)\int_\tau \Psi_2^*\Psi_1\, d\tau = \int_S \left(\frac{\hbar^2}{2M_c}\right)\left(\Psi_2^* \text{grad}_n\, \Psi_1 - \Psi_1\, \text{grad}_n\, \Psi_2^*\right) dS$$

$$= \sum_c \left(V_{2c}^* D_{1c} - V_{1c}\, D_{2c}^*\right), \qquad \text{(A12')}$$

where the value and derivative on the surface are defined by Eqs. (A7) and (A8).

The generalized boundary condition is $D_{\lambda c}/V_{\lambda c} \equiv \delta_{\lambda c}/\gamma_{\lambda c} = B_c$ (rather than $du/dr = 0$, as in the one-channel case).

Applying Eq. (A12') to two proper solutions X_λ and $X_{\lambda'}$, belonging to energy values E_λ, $E_{\lambda'}$, the right-hand member vanishes with such a boundary condition. The solutions X_λ and $X_{\lambda'}$ are thus orthogonal, and they are assumed to be normalized

$$\int_\tau X_{\lambda'}^* X_\lambda\, d\tau = \delta_{\lambda\lambda'} \qquad \text{(A13')}$$

One then uses these solutions to expand an arbitrary function Ψ as

$$\Psi = \sum_\lambda A_\lambda X_\lambda, \qquad \text{(A14')}$$

where the coefficients $A_\lambda = \int_\tau X_\lambda^* \Psi\, d\tau$. One uses Green's theorem on Ψ and X_λ to obtain

$$(E_\lambda - E)\int X_\lambda^* \Psi\, d\tau = \int_S \left(\frac{\hbar^2}{2M_c}\right)\left(X_\lambda^* \text{grad}_n \Psi - \Psi\, \text{grad}_n\, X_\lambda^*\right) dS$$

$$= \sum_c \left(\gamma_{\lambda c}^* D_c - V_c \delta_{\lambda c}^*\right)$$

$$= \sum_c \gamma_{\lambda c}\, D_c^o,$$

where $D_c^o = D_c - B_c V_c$

or

$$A_\lambda = \sum_c \gamma_{\lambda c} D_c^o \Big/ (E_\lambda - E) \qquad \text{(A15')}$$

Substituting this in Eq. (A14') gives the result

$$\Psi = \sum_c \left[\sum_\lambda \frac{\gamma_{\lambda c} X_\lambda}{E_\lambda - E}\right] D_c^o \qquad \text{(A16')}$$

It is the necessary relation between the value Ψ and generalized derivatives D_c^o on the surface S, and can be considered as the defining equation for $R_{cc'}$.

$$V_{c'} = \sum_c R_{c'c} D_c^o , \qquad (A17')$$

where the quantity in square brackets in Eq. (A16') is the Green's function. The only step remaining is to evaluate Ψ on the surface S, which is done by operating on Eq. (A16') with $\int_S \phi_c^* dS$ and using Eqs. (A7) and (A8). This gives

$$R_{cc'} = \sum_\lambda \frac{\gamma_{\lambda c} \gamma_{\lambda c'}}{(E_\lambda - E)} . \qquad (A18')$$

A.7 The collision matrix.

Let us summarize briefly what has been done so far. The radial configuration space was divided into two regions, an internal region and an external region in which it was assumed that no nuclear or polarizing interactions take place. The boundary between these two regions plays a crucial role in R-matrix theory: the R matrix is defined as a relation between the value and generalized derivative of the standing wave solutions on this boundary. The cross sections and collision matrix, however, are defined in terms of incoming and outgoing traveling waves. The next step is to express the collision matrix U in terms of the R-matrix.

The most general representation of the wave function in the external region is

$$\Psi = \sum_c x_c \bar{O}_c + y_c \bar{I}_c \qquad (A19)$$

where the x_c and y_c are amplitudes of the outgoing and incoming waves in channel c. The collision matrix $U_{cc'}$ is defined by the relationship between these amplitudes, as

$$x_{c'} = - \sum_c U_{cc'} y_c . \qquad (A20)$$

It is noted that the usual treatment assumes incident waves in one channel only; if one puts $y_c = 1$ for that channel, then

$$\Psi = \bar{I}_c - \sum_{c'} U_{cc'} \bar{O}_{c'} . \qquad (A21)$$

On the boundary, the value and derivative in channel c are given by Eq. (A7) as

$$V_c = (\hbar^2/2M_c a_c)^{1/2} v_c^{-1/2} (O_c x_c + I_c y_c)_{r_c=a_c}$$

$$= (\hbar/2)^{1/2} \rho_c^{-1/2} (O_c x_c + I_c y_c)_{\rho_c=k_c a_c} \qquad (A22a)$$

and

$$D_c = (a_c \hbar^2/2M_c)^{1/2} v_c^{-1/2} d/dr_c (O_c x_c + I_c y_c)_{r_c=a_c}$$

$$= (\rho_c^2 \hbar^2/2M_c a_c)^{1/2} v_c^{-1/2} (O_c' x_c + I_c' y_c)_{\rho_c=k_c a_c}$$

$$= (\hbar/2)^{1/2} \rho_c^{1/2} (O_c' x_c + I_c' y_c)_{\rho_c=k_c a_c} \qquad (A22b)$$

where the velocity factors are introduced through the usual method of normalizing incoming and outgoing waves to unit flux.

These must satisfy the fundamental R-matrix Eq. (A17')

$$V_{c'} = \sum_c R_{c'c} (D_c - B_c V_c)$$

or

$$\rho_{c'}^{-1/2} (O_{c'} x_{c'} + I_{c'} y_{c'}) = \sum_c R_{cc'} \left[\rho_c^{1/2} (O_c' x_c + I_c' y_c) - B_c \rho_c^{-1/2} (O_c x_c + I_c y_c) \right] \qquad (A23)$$

The procedure is to solve for the coefficients of x_c and y_c in this expression, and to define the collision matrix in terms of the R matrix by using the definition given by Eq. (A20). To do this, one rewrites Eqs. (A20) and (A23) in matrix notation, as

$$\vec{x} = -\vec{\vec{U}}\vec{y} \tag{A20'}$$

and

$$\vec{\rho}^{-1/2}\vec{\vec{O}}\vec{x} + \vec{\rho}^{-1/2}\vec{\vec{I}}\vec{y} = \vec{R}\left[\vec{\rho}^{1/2}\vec{O}'\vec{x} + \vec{\rho}^{1/2}\vec{I}'\vec{y} - \vec{B}\left(\vec{\rho}^{-1/2}\vec{\vec{O}}\vec{x} + \vec{\rho}^{-1/2}\vec{\vec{I}}\vec{y}\right)\right] \tag{A23'}$$

or

$$(\vec{\rho}^{-1/2}\vec{O} - \vec{R}\vec{\rho}^{1/2}\vec{O}^{o\prime})\vec{x} = -(\vec{\rho}^{-1/2}\vec{I} - \vec{R}\vec{\rho}\vec{I}^{o\prime})\vec{y} ,$$

where

$$\vec{\rho}\vec{O}^{o\prime} = \vec{\rho}\vec{O}' - \vec{B}\vec{O}$$
$$\vec{\rho}\vec{I}^{o\prime} = \vec{\rho}\vec{I}' - \vec{B}\vec{I} .$$

From Eq. (A20'),

$$\vec{U} = (\vec{\rho}^{-1/2}\vec{O} - \vec{R}\vec{\rho}^{1/2}\vec{O}^{o\prime})^{-1}(\vec{\rho}^{-1/2}\vec{I} - \vec{R}\vec{\rho}\vec{I}^{o\prime})$$
$$= \vec{\rho}^{1/2}\vec{O}^{-1}(\vec{1} - \vec{R}\vec{L}^{o})^{-1}(\vec{1} - \vec{R}\vec{L}^{o*})\vec{I}\rho^{-1/2}$$
$$= \vec{\Omega}\vec{W}\vec{\Omega}$$

where

$$\vec{\Omega}_c = (I_c/O_c)^{1/2}_{r_c=a_c} = \exp i(\omega_c - \phi_c)$$

It is convenient to recall the Lane and Thomas definitions of these quantities,

$$L_c = (\rho_c O_c'/O_c) = S_c + iP_c ; \qquad L_c^o = (\rho_c O_c^{o\prime}/O_c) = S_c^o + iP_c$$

$$L_c^* = (\rho_c I_c'/I_c) = S_c - iP_c ; \qquad L_c^{o*} = (\rho_c I_c^{o\prime}/I_c) = S_c^o - iPc$$

$$P_c = (\rho_c/I_c O_c) ; \; S_c^o = S_c - B_c$$

So

$$\vec{U} = \vec{\rho}^{1/2}\frac{\vec{\Omega}}{(\vec{I}\vec{O})^{1/2}}(\vec{1}-\vec{R}\vec{L}^{o})^{-1}(\vec{1}-\vec{R}\vec{L}^{o*})\vec{\Omega}\frac{\vec{I}\vec{O}^{1/2}}{\vec{P}^{1/2}}$$

$$= \vec{\Omega}\vec{\rho}^{1/2}(\vec{1} - \vec{R}\vec{L}^{o})^{-1}(\vec{1} - \vec{R}\vec{L}^{o*})\vec{P}^{-1/2}\vec{\Omega}.$$

or, equivalently,

$$\vec{U} = \vec{\Omega}\left[\vec{1} + 2i\vec{P}^{1/2}(\vec{1} - \vec{R}\vec{L}^{o})^{-1}\vec{R}\vec{P}^{1/2}\right]\vec{\Omega} \tag{A24}$$

A8. The cross sections.

The final step in the formal derivation is the definition of the cross section in terms of the collision matrix. Here, one again finds that the physical principles are obscured by the notational complexity. Even when one restricts the discussion to neutron-induced reactions, notational problems arise because the discussion so far has used J and M, the compound nucleus spin and z-axis projection, whereas the appropriate quantities to use in deriving the cross section formulas are the channel spins s,s', the orbital angular momenta, ℓ,ℓ', and their respective projections ν,ν' and m,m'. The collision matrix can be written in either representation, the relationship is

$$U_{\alpha's'\ell'\nu'm',\alpha s\ell\nu m} = \sum_{JM}(s\ell\nu m|JM)\;\; U_{\alpha's'\ell';\alpha s\ell}^{J}\,(s'\ell'\nu'm'|JM) \tag{A25}$$

where the $(s\ell\nu m|JM)$ are vector addition coefficients.

Following Lane and Thomas, we again consider elastic scattering of spinless particles by a central potential. The method one uses to solve the problem is to express the solution for relative motion in a form which asymptotically is

$$v^{-1/2}\left[\exp(ikz) + \frac{\exp(ikr)}{r} A(\theta)\right], \tag{A26}$$

which represents the sum of a plane wave of unit flux directed along the z axis and a part representing radial motion outward from the scattering center at the origin, of outward density $|A(\theta)|^2/v_r^2$ at the point (r,θ). The cross section $\sigma(\theta)$ for scattering at an angle θ is defined such that $N\sigma(\theta)d\Omega$ is the number of particles scattered per unit time into the solid angle $d\Omega$ at an angle θ to the incident beam, where N is the particle density in the incident beam. Thus $\sigma(\theta) = |A(\theta)|^2$, when the solution has the asymptotic form (A26).

In order to construct a solution with the appropriate asymptotic form, one forms the following linear combination of solutions [cf. Eq. (A21)]:

$$i\pi^{1/2}k^{-1}\sum_{\ell}(2\ell+1)^{1/2}\,(\bar{I}_\ell - U_\ell\bar{O}_\ell) \tag{A27}$$

One then adds and subtracts a wave function of the form

$$v^{-1/2}\exp(ikz)\psi = v^{-1/2}k^{-1}\sum_{\ell}(2\ell+1)r^{-1}F_\ell(\rho)i^\ell P_\ell(\cos\theta)\psi$$

$$= i\pi^{1/2}k^{-1}\sum_{\ell}(2\ell+1)^{1/2}(\bar{I}_\ell - \bar{O}_\ell) \tag{A28}$$

where we have used the usual Legendre expansion of the plane wave in polar coordinates, $F_\ell(\rho)$ being the regular spherical Bessel function of order ℓ, ψ the internal wave function product of the pair of nuclides, and where the last equality follows from the relations between standing wave solutions and incoming and outgoing waves (subsection 3), and the relationship

$$Y_o^{(\ell)}(\theta) = (2\ell+1/4\pi)^{1/2}P_\ell(\cos\theta).$$

The solution (A27) thus takes the form

$$v^{-1/2}\exp(ikz) + i\pi^{1/2}k^{-1}\sum_{\ell}(2\ell+1)^{1/2}(1-U_\ell)\bar{O}_\ell \tag{A29}$$

which has the asymptotic form (A26), where

$$A(\theta) = \frac{i}{2k}\sum_{\ell}(2\ell+1)(1-U_\ell)P_\ell(\cos\theta).$$

The scattering cross section is given by

$$\sigma(\theta) = |A(\theta)|^2 = \frac{1}{4k^2}\left|\sum_{\ell}(2\ell+1)(1-U_\ell)P_\ell(\cos\theta)\right|^2, \tag{A30}$$

and the total elastic cross section by

$$\sigma_{e\ell} = \int\sigma(\theta)d\Omega = \frac{\pi}{k^2}\sum_{\ell}(2\ell+1)\left|1-U_\ell\right|^2 \tag{A31}$$

The derivation of the general expressions for the cross sections follows the same procedure, but the resulting expressions are very much more complicated. In particular, the collision matrix $U_{\alpha's'\ell'\nu'm',\alpha s\ell\nu 0}$ is the representation for which the cross sections are defined, but the collision matrix $U_{\alpha's'\ell',\alpha s\ell J}$ is that which is related to the R-matrix and to the resonance parameters, so that the transformation of Eq. (A25) is generally required. Integrating the cross sections over all angles, adding over final channel spins s', and averaging over initial channel spins s, the transformations of Eq. (A25) result in the usual spin statistical factors, such that

$$\sigma_{\alpha,\alpha} = \frac{\pi}{k_\alpha^2}\sum_{J\ell,\ell',s,s'} gJ\left|\exp(2i\omega_{\alpha'\ell'})\;\delta_{\alpha's'\ell',\alpha s\ell} - U^J_{\alpha's'\ell',\alpha s\ell}\right|^2 \tag{A32}$$

where $gJ = (2J+1)/(2I_1+1)(2I_2+1)$.

The notation can be simplified somewhat by using $c = \alpha s\ell$, $c' = \alpha's'\ell'$. In this case, the elastic cross section is

$$\sigma_\alpha(el) = \frac{\pi}{k_\alpha^2}\sum_{Js\ell} gJ\left\{\left|1 - U^J_{cc}\right|^2 + \sum_{\substack{(\alpha'=\alpha)\\ s'\ell'(\neq s\ell)}}\left|U^J_{cc'}\right|^2\right\} \tag{A33}$$

The cross section for a particular reaction $\alpha' \neq \alpha$ is

$$\sigma_{\alpha\alpha'} = \frac{\pi}{k_\alpha^2}\sum_{\substack{Js\ell\\ s'\ell'}} gJ\left|U^J_{cc'}\right|^2 \tag{A34}$$

The non-elastic is the sum of all processes $\alpha' \neq \alpha$

$$\sigma_\alpha \text{ (nonel)} = \sum_{\alpha' \neq \alpha} \sigma_{\alpha\alpha'} \quad , \tag{A35}$$

and the total cross section is the sum of the elastic and non-elastic, which, from the unitary nature of the collision matrix, can also be written as

$$\sigma_\alpha(\text{total}) = \frac{\pi}{k_\alpha^2} \sum_{Js\ell} 2gJ(1-\text{Re } U_{cc}^{J}) \tag{A36}$$

APPENDIX B. APPROXIMATIONS FOR REACTOR PHYSICS APPLICATIONS

B1. The single-level Breit-Wigner formula (SLBW)

The use of the formal theory in practical applications is done by approximations. The simplest is to assume that there is only one level, such that Eq. (A18') defining the R matrix contains only one term. If the incident particle is a neutron, the Coulomb phase shift ω_c vanishes. The channel parameters S_c, P_c, and ϕ_c of Eq. A24 depend on the energy and orbital angular momentum of the incident neutron. In the U.S. evaluated nuclear data file, the following definitions are used [39]:

$$k = 2.196771 \frac{\text{AWRI}}{\text{AWRI} + 1.0} \times 10^{-3} \sqrt{E} \quad , \tag{B1}$$

where k is the neutron wave number, AWRI is the ratio of the mass of the particular isotope to that of the neutron, and E is the incident neutron energy (laboratory system) in eV.

S_ℓ is the shift factor,

$$S_0 = 0$$

$$S_1 = -\frac{1}{1+\rho^2}$$

$$S_2 = -\frac{18 + 3\rho^2}{9 + 3\rho^2 + \rho^4}$$

P_ℓ is the penetration factor,

$$P_0 = \rho$$

$$P_1 = \frac{\rho^3}{1 + \rho^2}$$

$$P_2 = \frac{\rho^5}{9 + 3\rho^2 + \rho^4}$$

where $\rho = ka$ and "a" is the channel radius (in units of 10^{-12} cm) and is defined as

$$a = [1.23(\text{AWRI})^{1/3} + 0.8] \times 10^{-1}$$

ϕ_ℓ is the phase shift,

$$\phi_0 = \hat{\rho}$$

$$\phi_1 = \hat{\rho} - \tan^{-1}\hat{\rho}$$

$$\phi_2 = \hat{\rho} - \tan^{-1}\frac{3\hat{\rho}}{3 - \hat{\rho}^2}$$

where $\hat{\rho} = k\hat{a}$ and $\hat{a}$ is the effective scattering radius. These are the first few terms of the recursion relations provided by Lane and Thomas:

$$P_\ell = \alpha_\ell P_{\ell-1}/[(b_\ell - S_{\ell-1})^2 + P_{\ell-1}^2] \quad ,$$

$$S_\ell + b_\ell = \alpha_\ell(b_\ell - S_{\ell-1})/[(b_\ell - S_{\ell-1})^2 + P_{\ell-1}^2] \quad , \tag{B2}$$

$$\phi_\ell = \phi_{\ell-1} - \tan^{-1}[P_{\ell-1}/(b_\ell - S_{\ell-1})] \quad ,$$

where

$$\alpha_\ell = \rho^2 + (\rho\eta/\ell)^2 \quad ,$$

$$b_\ell = \ell + (\rho\eta/\ell) \quad .$$

It is customary to define an energy dependent partial level width as $\Gamma_\lambda = 2(P_\alpha^{1/2}\gamma_\lambda)^2$. In the vicinity of a given resonance r ($\lambda = r$) the single-

level formula for elastic scattering and reactions of interest can be derived from Eqs. A18', A24, and A32-A35. The single-level approximation consists of performing a summation over the levels r in the cross section expression, instead of in the R matrix. The resulting formulas are taken from Garber et al. [39], who adopted them from Gregson et al. [42]:

a) Elastic scattering cross section

$$\sigma_{n,n}(E) = \sum_{\ell=0}^{NLS-1} \sigma_{n,n}^{\ell}(E) \quad ,$$

where

$$\sigma_{n,n}^{\ell}(E) = (2\ell+1)\,\frac{4\pi}{k^2}\sin^2\phi_\ell \qquad \text{(B3)}$$

$$+\ \frac{\pi}{k^2}\sum_J g_J \sum_{r=1}^{NR_J} \frac{\Gamma_{nr}^2\cos 2\phi_\ell - 2\Gamma_{nr}(\Gamma_{\gamma r}+\Gamma_{fr})\sin^2\phi_\ell + 2(E-E_r')\Gamma_{nr}\sin 2\phi_\ell}{(E-E_r')^2 + 1/4\ \Gamma_r^2}$$

b) Reaction cross section

$$\sigma_{n,x}(E) = \sum_{\ell=0}^{NLS-1} \sigma_{n,x}^{\ell}(E) \quad ,$$

where

$$\sigma_{n,x}^{\ell}(E) = \frac{\pi}{k^2}\sum_J g_J \sum_{r=1}^{NR_J} \frac{\Gamma_{nr}\Gamma_{xr}}{(E-E_r')^2 + 1/4\ \Gamma_r^2} \qquad \text{(B4)}$$

where the subscript x refers to either radiative capture or fission. The summation on ℓ extends over all ℓ-states to be described (there will be NLS terms in the summation), and the summation on J over all J-states for a particular value of ℓ. NR_J is the number of resonances for a given pair of ℓ and J values.

It is also customary to redefine the resonance energy to remove the shift term in the denominator, as

$$E_r' = E_r + \frac{S_\ell(|E_r|) - S_\ell(E)}{2P_\ell(|E_r|)}\,\Gamma_{nr}(|E_r|) \quad . \qquad \text{(B5)}$$

Usually, one can ignore all energy dependences of the various partial widths except the neutron width. This is specified at a given neutron energy, either at the resonance energy E_r (for bound levels, the absolute value $|E_r|$ is used), or at 1 eV. The special notation Γ_{nr}° is used for the s-wave neutron width of the r'th resonance at 1 eV. Neutron physicists often refer to Γ_{nr}° instead of γ_{nr}^2 as the reduced neutron width of the r'th level. (It differs from γ_{nr}^2 by a constant factor k evaluated at 1 eV.) Neglecting all other energy dependences in the partial widths leads to the definition of the total width as

$$\Gamma_r = \Gamma_{nr}(E) + \sum_x \Gamma_{xr} \qquad \text{(B6)}$$

where the quantity x refers to a given reaction channel--fission or capture.

Occasionally in an evaluated data file, partial cross sections are tabulated in the resonance region for reactions for which no explicit resonance parameterization is given. In such cases, one may wish to include in the total width definition a "competitive width" that allows for the competition of the tabulated cross sections with those described by resonance parameters. In this case the sum over x in Eq. B6 includes the competitive width.

Lane and Thomas provided a way of generalizing the single-level formula, by splitting the R matrix into a single-level term plus a smoothly varying non-resonant background term that contains the contributions of all the other levels. One splits the R matrix into two parts: $\vec{R}=\vec{R}^{\circ}+\vec{R}'$. Consider the matrix inversion implied by $(\vec{1}-\vec{R}\vec{L}^{\circ})^{-1}\vec{R}$. It can be shown that

$$(\vec{1}-\vec{R}\vec{L}^{\circ})^{-1}\vec{R} = (\vec{1}-\vec{R}^{\circ}\vec{L}^{\circ}-\vec{R}'\vec{L}^{\circ})^{-1}(\vec{R}^{\circ}+\vec{R}')$$

can be written as

$$(\vec{1}-\vec{R}^{\circ}\vec{L}^{\circ})^{-1}\vec{R}^{\circ} + (\vec{1}-\vec{R}^{\circ}\vec{L}^{\circ})^{-1}(\vec{1}-\vec{R}'\vec{L}')^{-1}\vec{R}'(\vec{1}-\vec{L}^{\circ}\vec{R}^{\circ})^{-1}$$

where $\vec{L}'$ is defined as $\vec{L}' = \vec{L}^{\circ}(\vec{1}-\vec{R}^{\circ}\vec{L}^{\circ})^{-1}$. In order to show this, one can write

$(\vec{1}-\vec{R}^{\circ}\vec{L}^{\circ}-\vec{R}'\vec{L}^{\circ})^{-1}(\vec{R}^{\circ}+\vec{R}')$ as $(\vec{1}-\vec{R}^{\circ}\vec{L}^{\circ})^{-1}(\vec{R}^{\circ}+\vec{A})$ and solve for $\vec{A}$.

Find $(\vec{1}-\vec{R}'\vec{L}')\vec{A} = \vec{R}'[\vec{1}+\vec{L}^{\circ}(\vec{1}-\vec{R}^{\circ}\vec{L}^{\circ})^{-1}\vec{R}^{\circ}]$, which is nearly the required form.

Note that $\vec{L}^{\circ}(\vec{1}-\vec{R}^{\circ}\vec{L}^{\circ})^{-1}\vec{R}^{\circ} = [\vec{R}^{\circ-1}(\vec{1}-\vec{R}^{\circ}\vec{L}^{\circ})\vec{L}^{\circ-1}]^{-1} = (\vec{R}^{\circ-1}\vec{L}^{\circ-1}-\vec{1})^{-1}$.

Also $(\vec{1}-\vec{L}^{\circ}\vec{R}^{\circ})^{-1}\vec{L}^{\circ}\vec{R}^{\circ} = [\vec{R}^{\circ-1}\vec{L}^{\circ-1}(\vec{1}-\vec{L}^{\circ}\vec{R}^{\circ})]^{-1} = (\vec{R}^{\circ-1}\vec{L}^{\circ-1}-\vec{1})^{-1}$.

Finally, writing $(\vec{1}-\vec{L}^{\circ}\vec{R}^{\circ})^{-1} = \vec{1}+\vec{B}$, one solves for $\vec{B} = (\vec{1}-\vec{L}^{\circ}\vec{R}^{\circ})^{-1}\vec{L}^{\circ}\vec{R}^{\circ}$, which completes the proof.

At this stage, it is not obvious that this development leads to any kind of improved representation. However, as Lane and Thomas note (p. 321ff of Ref. [22]), the collision matrix obtained from the split R matrix is of the form

$$\vec{U} = \vec{U}^{\circ} + 2i\vec{\Omega}\vec{P}^{1/2}\,\frac{\vec{\alpha}_\lambda x\vec{\alpha}_\lambda}{E_\lambda+\Delta_\lambda-E-i\Gamma_\lambda/2}\,\vec{P}^{1/2}\vec{\Omega} \qquad \text{(B7)}$$

where

$$\vec{U}^\circ = \vec{\Omega}[\vec{1}+2i\vec{P}^{1/2}(\vec{1}-\vec{R}^\circ\vec{L}^\circ)^{-1}\vec{R}^\circ\vec{P}^{1/2}]\vec{\Omega} \quad ,$$

$$\vec{\alpha}_\lambda = (\vec{1}-\vec{R}^\circ\vec{L}^\circ)^{-1}\vec{\gamma}_\lambda \quad ,$$

$$\vec{\Delta}_\lambda = [\vec{\alpha}_\lambda^*,(\vec{L}^{\circ *}\vec{R}^\circ\vec{L}^\circ-\vec{S}^\circ)\vec{\alpha}_\lambda] \quad ,$$

$$\frac{1}{2}\Gamma_\lambda = (\vec{\alpha}_\lambda^*,\vec{P}\vec{\alpha}_\lambda) = \frac{1}{2}\sum_c \Gamma_{\lambda c} \quad .$$

In particular, if the background matrix R° is diagonal, then this formalism leads to a single-level formula with modified parameters and a modified phase shift:

$$\frac{1}{2}\Gamma_{\lambda c} = P_c\gamma_{\lambda c}^2/d_c \quad ,$$

$$\Delta_{\lambda c} = \frac{P_c(R_{cc}{}^\circ P_c) - S_c{}^\circ(1-R_{cc}{}^\circ S_c{}^\circ)}{d_c}\gamma_{\lambda c}^2 \quad ,$$

and $U_{cc}{}^\circ = e^{-2i\phi_c'}$,

$$\text{where } \phi_c' = \phi_c - \tan^{-1}\left(\frac{R_{cc}{}^\circ P_c}{1-R_{cc}{}^\circ S_c{}^\circ}\right) \quad , \tag{B8}$$

and where $d_c = (1-R_{cc}{}^\circ S_c{}^\circ)^2 + (R_{cc}{}^\circ P_c)^2$.

Equivalently, one can consider this modification as a modification of the shift and penetration factors, in a form rather similar to that of the recursion relations of Eq. B2.

$$P_c{}' = P_c \,/\, [(1-R_{cc}{}^\circ S_c)^2 + (R_{cc}{}^\circ P_c)]^2$$

$$\text{and } S_c{}' = \frac{S_c(1-R_{cc}{}^\circ S_c) - R_{cc}{}^\circ P_c{}^2}{(1-R_{cc}{}^\circ S_c)^2 + (R_{cc}{}^\circ P_c)^2} \quad . \tag{B9}$$

B2. The multilevel Breit-Wigner formula (MLBW)

Taking the summation over the various levels r in the cross section formula rather than in the R-matrix leads to problems even when $\langle\Gamma_r\rangle$ << D and when all level-level interference in the reaction channels vanishes. deSaussure et al. [41] show that such problems can be effectively circumvented by including the level-level interference term of Bethe and Placzek [24] in the elastic scattering expression, as

$$\frac{\pi}{k^2}\sum_J g_J \sum_{r=2}^{NR_J}\sum_{s=1}^{r-1} \frac{2\Gamma_{nr}\Gamma_{ns}\left[(E-E_r')\ (E-E_s') + 1/4\ \Gamma_r\Gamma_s\right]}{\left[(E-E_r')^2 + 1/4\ \Gamma_r^2\right]\left[(E-E_s')^2 + 1/4\ \Gamma_s^2\right]} \quad . \tag{B10}$$

This expression contains a double sum, the evaluation of which is very tedious. deSaussure et al. show that one can make a partial fraction expansion, in the same way as that done by Adler and Adler (to be discussed below). The interference term can then be rewritten in a form that avoids the double sum and permits evaluation of the expression by Voigt profiles: the interference term becomes

$$\frac{2\pi}{k^2}\sum_r \frac{G_r(\Gamma_r/2) - H_r(E_r-E)}{(E_r'-E)^2 + \Gamma_r^2/4} \tag{B11}$$

$$\text{where } G_r = \frac{1}{2}\sum_{s\neq r}\frac{\Gamma_{nr}\Gamma_{ns}(\Gamma_r+\Gamma_s)}{(E_r'-E_s')^2 + (\Gamma_r+\Gamma_s)^2/4}$$

$$H_r = \sum_{s\neq r}\frac{\Gamma_{nr}\Gamma_{ns}(E_r-E_s)}{(E_r'-E_s')^2 + (\Gamma_r+\Gamma_s)^2/4}$$

Occasionally, one finds MLBW used in describing interference in a reaction channel x. (To do this, one replaces $\Gamma_{nr}\Gamma_{ns}$ in the numerator of B10 or B11 by $\sqrt{\Gamma_{nr}\Gamma_{xr}\Gamma_{ns}\Gamma_{xs}}$. This procedure is not as satisfactory as it was found to be in describing elastic channel interference, the reason being that MLBW is valid if $\langle\Gamma_r\rangle$ << D, but strong reaction channel interference implies $\langle\Gamma_r\rangle \sim$ D.

B3. The reduced R matrix (RM, ML formulas)

a) The level matrix A

As we have noted, the basic difficulty with applying the formal R-matrix theory lies in the inversion of the matrix (1-RL°), whose dimensions equals the number of channels. Wigner [70] showed how one can introduce another matrix (the Wigner level matrix A), and convert the problem into one of inverting a matrix of dimensions equal to the number of levels.

The collision matrix is written, according to Eq. A24, as

$$\vec{U} = \vec{\Omega}(\vec{1} + 2i\vec{P}^{1/2}(\vec{1}-\vec{R}\vec{L}^\circ)^{-1}\vec{R}\vec{P}^{1/2})\vec{\Omega}$$

and one wants to invert $(\vec{1}-\vec{R}\vec{L}^\circ)$. Wigner's inversion procedure is to assume an expansion of the form

$$(\vec{1}-\vec{\vec{R}}\vec{\vec{L}}^{\circ})^{-1} = \vec{1} + \sum_{\mu\nu} (\vec{\gamma}_\mu \times \vec{\beta}_\nu) A_{\mu\nu} \qquad \text{(B12)}$$

Where $\vec{\beta}_\lambda = \vec{L}^{\circ}\vec{\gamma}_\lambda$ and where the $A_{\mu\nu}$ are the elements of the level matrix. If the expansion (B12) is valid, the elements can be found by multiplying by

$$(\vec{1}-\vec{\vec{R}}\vec{\vec{L}}^{\circ}) = \vec{1} - \sum_\lambda \frac{\vec{\gamma}_\lambda \times \vec{\beta}_\lambda}{E_\lambda - E} \quad .$$

This gives

$$-\sum_\lambda \frac{(\vec{\gamma}_\lambda \times \vec{\beta}_\lambda)}{(E_\lambda - E)} + \sum_{\mu\nu} (\vec{\gamma}_\mu \times \vec{\beta}_\nu) A_{\mu\nu} - \sum_{\lambda\mu\nu} \frac{(\vec{\gamma}_\lambda \times \vec{\beta}_\nu)}{(E_\lambda - E)} (\vec{\gamma}_\mu \times \vec{\beta}_\nu) A_{\mu\nu} = 0. \qquad \text{(B13)}$$

The definition of the outer product of two column vectors $\vec{x}$ and $\vec{y}$, $(\vec{x} \times \vec{y})_{cc'} = x_c y_{c'}$, and the inner product, $(\vec{x},\vec{y})_c = \sum_c x_c y_c$, leads to the general property that

$$(\vec{x} \times \vec{y})(\vec{z} \times \vec{w}) = (\vec{y},\vec{z})(\vec{x} \times \vec{w}) \quad .$$

Thus the last term in Eq. (B13) can be written

$$-\sum_{\lambda\mu\nu} \frac{(\vec{\gamma}_\lambda \times \vec{\beta}_\nu)}{(E_\nu - E)} (\vec{\beta}_\lambda,\vec{\gamma}_\mu) A_{\mu\nu}$$

and the entire equation rearranged to give

$$\sum_{\lambda\nu} (\vec{\gamma}_\lambda \times \vec{\beta}_\nu) \left[\frac{-\delta_{\lambda\nu}}{(E_\lambda - E)} + A_{\lambda\nu} - \sum_\mu \frac{(\vec{\beta}_\lambda,\vec{\gamma}_\mu) A_{\mu\nu}}{(E_\lambda - E)} \right] = 0 \qquad \text{(B14)}$$

This is satisfied if for all λ,ν the bracket is zero, or

$$A_{\lambda\nu}(E_\lambda - E) - \sum_\mu (\vec{\beta}_\lambda,\vec{\gamma}_\mu) A_{\mu\nu} = \delta_{\lambda\nu} \qquad \text{(B15)}$$

The quantity one really wants to evaluate is

$$\begin{aligned}(\vec{1}-\vec{\vec{R}}\vec{\vec{L}}^{\circ})^{-1}\vec{\vec{R}} &= \left[\vec{1} + \sum_{\mu\nu} (\vec{\gamma}_\mu \times \vec{\beta}_\nu) A_{\mu\nu}\right] \left[\sum_\lambda (\vec{\gamma}_\lambda \times \vec{\gamma}_\lambda)/E_\lambda - E)\right] \\ &= \sum_\lambda \frac{(\vec{\gamma}_\lambda \times \vec{\gamma}_\lambda)}{(E_\lambda - E)} + \sum_{\mu\nu\lambda} \frac{(\vec{\gamma}_\mu \times \vec{\gamma}_\lambda)(\vec{\beta}_\nu,\vec{\gamma}_\lambda) A_{\mu\nu}}{(E_\lambda - E)} \\ &= \sum_\lambda \frac{(\vec{\gamma}_\lambda \times \vec{\gamma}_\lambda)}{(E_\lambda - E)} + \sum_{\omega\lambda} \frac{(\vec{\gamma}_\mu \times \vec{\gamma}_\lambda)}{(E_\lambda - E)} \sum_\nu (\vec{\beta}_\nu,\vec{\gamma}_\lambda) A_{\mu\nu} \\ &= \sum_\lambda \frac{(\vec{\gamma}_\lambda \times \vec{\gamma}_\lambda)}{(E_\lambda - E)} + \sum_{\mu\lambda} \frac{(\vec{\gamma}_\mu \times \vec{\gamma}_\lambda)}{(E_\lambda - E)} [A_{\lambda\mu}(E_\lambda - E) - \delta_{\lambda\mu}] \\ &= \sum_{\mu\lambda} (\vec{\gamma}_\mu \times \vec{\gamma}_\lambda) A_{\lambda\mu} \quad . \end{aligned} \qquad \text{(B16)}$$

The collision matrix is then written

$$\vec{U} = \vec{\Omega}[\vec{1} + 2i\vec{P}^{1/2} \sum_{\mu\lambda} (\vec{\gamma}_\mu \times \vec{\gamma}_\lambda) A_{\lambda\mu} \vec{P}^{1/2}]\vec{\Omega} \quad , \qquad \text{(B17)}$$

where the level matrix A is defined in terms of its inverse

$$(A^{-1})_{\lambda\mu} = (E_\lambda - E) - i \sum_c \gamma_{\lambda c} \beta_{\mu c} \quad .$$

Since

$$\vec{\beta}_\lambda = \vec{L}^{\circ}\vec{\gamma}_\lambda = \vec{S}^{\circ}\vec{\gamma}_\lambda + i\vec{\vec{P}}\vec{\gamma}_\lambda \quad ,$$

$$(A^{-1})_{\lambda\mu} = E_\lambda - \Delta_{\lambda\mu} - E - i \sum_c P_c \gamma_{\lambda c} \gamma_{\mu c} \quad , \qquad \text{(B18)}$$

where $\Delta_{\lambda\mu} = \sum_c S_c \gamma_{\lambda c} \gamma_{\mu c}$.

If there are only a few levels of interest, then one can invert the matrix A^{-1} and calculate the elements of the collision matrix and the cross sections. This was the approach of Vogt [71, 72] in analyzing a few resonances in the fission cross sections of ^{233}U, ^{235}U, and ^{239}Pu. In general, the number of resonances is far too large for the direct inversion of A^{-1} to be practical. However, it may be noted that the inversion of A^{-1} is particularly easy if it happens to be diagonal; then

$$(A^{-1})_{\lambda\mu} = (E_\lambda - \Delta_\lambda - E - i \sum_c P_c \gamma_{\lambda c}^2)\delta_{\lambda\mu}$$

$$\text{Since } \Gamma_\lambda/2 = \sum_c P_c \gamma_{\lambda c}^2 \quad ,$$

$$A_{\lambda\mu} = \delta_{\lambda\mu}/(E_\lambda - \Delta_\lambda - E - i\Gamma_\lambda/2). \tag{B19}$$

b) Channel elimination and the reduced R-matrix

The channel elimination method of Teichmann and Wigner [45] was devised to eliminate negative-energy or closed channels. Thomas [46] noted that if the signs and sizes of the off-diagonal elements in the A^{-1} matrix are random, then the above approximation for the elements of $A_{\lambda\mu}$ could be used to eliminate positive energy channels as well. One partitions the R-matrix into submatrices

$$\vec{R} = \begin{pmatrix} \vec{R}_{rr} & \vec{R}_{re} \\ \vec{R}_{er} & \vec{R}_{ee} \end{pmatrix} \tag{B20}$$

where the r subscript denotes retained channels, the e subscript eliminated channels. The eliminated channels will be assumed to have outgoing waves only; one then writes Eq. (A17') in the form

$$\vec{V}_e = \vec{R}_{ee}\vec{D}_e^{\,o} + \vec{R}_{er}\vec{D}_r^{\,o}$$

$$\vec{V}_r = \vec{R}_{rr}\vec{D}_r^{\,o} + \vec{R}_{re}\vec{D}_e^{\,o}$$

with the auxiliary equation

$$\vec{L}_e^{\,o} = \vec{D}_e^{\,o}\vec{V}_e^{-1} - \vec{B}_e = \vec{L}_e - \vec{B}_e \quad .$$

This leads to the definition of the "reduced" R matrix, by

$$\vec{V}_r = \vec{R}'_{rr}\vec{D}_r^{\,o}, \quad \vec{V}_e = \vec{R}'_{er}\vec{D}_r \tag{B21}$$

where

$$\vec{R}'_{rr} = \vec{R}_{rr} + \vec{R}_{re}\vec{L}_e^{\,o}(\vec{1} - \vec{R}_{ee}\vec{L}_e^{\,o})^{-1}\vec{R}_{er} \quad ,$$

$$\vec{R}'_{er} = (\vec{1} - \vec{R}_{ee}\vec{L}_e^{\,o})^{-1}\vec{R}_{er} \quad ,$$

both of which can then be expressed in terms of the level matrix A for the eliminated channels

$$\vec{R}'_{rr} = \sum_{\lambda\mu}(\vec{\gamma}_{\lambda r} \times \vec{\gamma}_{\mu r})A_{\lambda\mu} \tag{B22}$$

$$\vec{R}'_{er} = \sum_{\lambda\mu}(\vec{\gamma}_{\lambda e} \times \vec{\gamma}_{\mu r})A_{\lambda\mu} \quad .$$

The reduced R-matrix is complex if the eliminated group contains positive-energy (open) channels; the corresponding collision matrix is symmetric but not unitary in this case. The expression for the reduced R-matrix takes a particularly simple form if $A_{\lambda\mu}$ is diagonal; in this case

$$R'_{rr} = \sum_\lambda \frac{\vec{\gamma}_{\lambda r} \times \vec{\gamma}_{\lambda r}}{(E'_\lambda - E - i\Gamma_{\lambda e}/2)} \tag{B23}$$

where $E'_\lambda = E_\lambda + \Delta_{\lambda e}$ and where $\Gamma_{\lambda e}$ is the partial width for all eliminated channels. Reich and Moore [44] arrived at the same result by partitioning the matrix $(1\text{-}RL^o)^{-1}$ and carrying through the matrix multiplications explicitly under the assumption that $A_{\lambda\mu}$ for the eliminated channels (radiative capture channels, in this case) was diagonal. The advantage of using the reduced R-matrix is, of course, that all the fundamental R-matrix equations (A24, A32-36) are valid. All one does is to replace the R-matrix of Eq. A18' with the reduced R-matrix of Eq. B21, and then carry out the inversion of A24 with the much smaller reduced R-matrix having dimensions r X r.

The explicit use of the reduced R-matrix equations has been summarized by Garber et al. [39] as follows:

Neutron cross sections with an exit channel c are given by

$$\sigma_{nc} = \pi \lambda\!\!\!^{-2}_n \sum_J g_J |\delta_{nc} - U^J_{nc}|^2 \quad , \tag{B24}$$

$$U^J_{nc} = e^{-i(\phi_n+\phi_c)}\left\{2\left[\left(I-K\right)^{-1}\right]_{nc} - \delta_{nc}\right\} \quad , \tag{B25}$$

where

$$(I-K)_{cc'} = \delta_{cc'} - \frac{i}{2}\sum_{\lambda}\frac{\Gamma_{\lambda c}^{1/2}\Gamma_{\lambda c'}^{1/2}}{E_\lambda - E - \frac{i}{2}\Gamma_{\lambda\gamma}} \quad , \tag{B26}$$

where the summation in Eq. (B26) is over the resonance levels λ; E_λ is the resonance energy; $\Gamma_{\lambda\gamma}$, the corresponding radiation widths; and $\Gamma_{\lambda c}$ and $\Gamma_{\lambda c'}$ are the widths for the λ-th level and channels c and c', respectively.

If we define

$$\rho_{nc} = \delta_{nc} - [(I-K)^{-1}]_{nc} = \delta_{nc} - \frac{m_{nc}}{\Delta} \quad ,$$

where $\Delta = |I-K|$ is the determinant of the matrix I-K and m_{nc} is the cofactor of the element $(I-K)_{nc}$ of the matrix I-K, we obtain

$$\sigma_{nT} = \sum_J \sigma_{nT}^J = 2\pi\,\lambda\!\!\!^{-}_n^2 \sum_J g_J R_e\left(1-U_{mn}^J\right)$$

$$= 2\pi\,\lambda\!\!\!^{-}_n^2 \sum_J \left[g_J\left(1-\cos 2\phi_n\right) + 2g_J Re\left(e^{-2i\phi_n}\,\rho_{nn}\right)\right] \quad . \tag{B27}$$

$$\sigma_{nn} = \Pi\,\lambda\!\!\!^{-}_n^2 \sum_J g_J\,|1-U_{nn}^J|^2 \quad . \tag{B28}$$

$$\sigma_{nAbs} = \sigma_{nT} - \sigma_{nn} = 4\Pi\,\lambda\!\!\!^{-}_n^2 \sum_J g_J\left[Re\left(\rho_{nn}\right) - |\rho_{nn}|^2\right] \quad . \tag{B29}$$

$$\sigma_{nFiss} = 4\pi\,\lambda\!\!\!^{-}_n^2 \sum_J g_J\left(\sum_c |\rho_{nc}|^2\right) \quad . \tag{B30}$$

$$\sigma_{n\gamma} = \sigma_{nAbs} - \sigma_{nFiss} \tag{B31}$$

In these expressions $\lambda\!\!\!^{-}_n = 1/k$, where k, ϕ_n have the same definitions as in the previous sections. The summation over c in Eq. (B30) refers to fission channels.

The R-matrix reduces to a complex R-function if only radiative capture and neutron elastic scattering exist; this equation is known as the ML formula [41], and can be written explicitly as

$$\sigma_{n,\gamma}^J = \frac{\pi g_J}{k_n^2}\sum_c |U_{nc}|^2 = \frac{4\pi g_J}{k_n^2}\,\frac{b_{nn}}{(1+b_{nn})^2 + a_{nn}^2} \tag{B32}$$

where a_{nn} and b_{nn} are the real and imaginary parts of $\Sigma_\lambda\ \Gamma_{\lambda n}/(E_\lambda - E - i\Gamma_{\gamma\lambda}/2)$, respectively. We note that this is not formally the sum of single-level Breit-Wigner terms, although when $\langle\Gamma_n\rangle \ll \Gamma_\gamma$, the single-level formula is a good approximation.

B4. The Adler-Adler multilevel formula

a) Diagonalizing the level matrix: the Kapur-Peierls expansion

The use of the Wigner level matrix $\vec{\vec{A}}$ has converted the problem of inverting a very large matrix $(\vec{\vec{1}} - \vec{\vec{R}}\vec{\vec{L}}_o)$ in channel space into that of inverting a very large matrix $\vec{\vec{A}}^{-1}$ in level space. If the matrix $\vec{\vec{A}}^{-1}$ were diagonal, then the problem of inverting it would be trivial. In the previous section, what was done was to reduce the R-matrix by eliminating that part for which the A matrix could be treated as diagonal. In this section, the approach is to diagonalize the A matrix by a similarity transformation with the complex orthogonal matrix $\vec{\vec{T}}$ to form a diagonal matrix $\vec{\vec{C}} = \vec{\vec{\mu}} + i\vec{\vec{\nu}}$ (the notation is that of Adler and Adler [10, 11]).

In matrix notation, the A matrix can be written, in terms of its inverse, as

$$\vec{\vec{A}}^{-1} = (\vec{\vec{e}} - \vec{\vec{E}} - \vec{\vec{\xi}})$$

where the elements of $\vec{\vec{e}}$ are E_λ, those of $\vec{\vec{\xi}}$ are the shift and width terms of Eq. B18, the elements of ξ being given by

$$\xi_{\lambda\lambda'} = \sum_c (S_c^o + i\,P_c)\gamma_{\lambda c}\gamma_{\lambda' c} \quad .$$

The energy matrix $\vec{\vec{E}}$ is already diagonal (it is just E times the unit matrix), so the similarity transformation is applied to $(\vec{\vec{e}} - \vec{\vec{\xi}})$. This gives

$$\vec{\vec{C}} = \vec{\vec{\mu}} + i\,\vec{\vec{\nu}} = \vec{\vec{T}}(\vec{\vec{e}} - \vec{\vec{\xi}})\vec{\vec{T}}^{-1} = \vec{\vec{T}}(\vec{\vec{e}} - \vec{\vec{\xi}})\vec{\vec{T}}^{\dagger *} \tag{B33}$$

where $\vec{\vec{T}}^{\dagger *}$ is the transpose of $\vec{\vec{T}}$. Thus

$$\vec{\vec{A}} = \vec{\vec{T}}^{\dagger *}(\vec{\vec{C}} - \vec{\vec{E}})^{-1}\vec{\vec{T}} \tag{B34}$$

or, from Eq. (B7)

$$(\vec{\vec{1}} - \vec{\vec{R}}\vec{\vec{L}}^o)^{-1}\vec{\vec{R}} = \sum_\lambda (\vec{\omega}_\lambda \times \vec{\omega}_\lambda)/(\vec{C}_\lambda - \vec{E}) \tag{B35}$$

where $\omega_{\lambda c} = \sum_{\lambda'} T_{\lambda\lambda'}\gamma_{\lambda' c}$ are complex and energy dependent.

Using the definitions (B7), the complex eigenvalue expansion (that of Kapur and Peierls) becomes

$$\vec{S} = \vec{U} = \vec{\Omega}\left(\vec{I} + 2i\vec{P}^{1/2}\sum_{\lambda}\frac{\vec{\omega}_\lambda \times \vec{\omega}_\lambda}{\mu_\lambda - E - i\nu_\lambda/2}\right)\vec{P}^{1/2}\vec{\Omega} \quad . \tag{B36}$$

b) The Adler-Adler formula

Let us consider the case of $\ell = 0$ neutron-induced reactions for which $P_n = k$. If the other P_c are constants one can show that the appropriate expression to use for the reaction cross section from Eq. (B36) is

$$\sigma_{reaction} = \frac{c}{\sqrt{E}}\sum_{\lambda}\frac{\nu_\lambda G_\lambda^f + (\mu_\lambda - E)H_\lambda^f}{(\mu_\lambda - E)^2 + \nu_\lambda^2} \quad . \tag{B37}$$

This expression is compatible with Doppler broadening by Voigt profiles. In order to derive Eq. (B37) from (B36) one explicitly carries out the absolute squaring procedure, obtaining

$$\sigma_{reaction} = \frac{\pi g_J}{k^2} P_n P_x \left[\sum_{\lambda}\sum_{\lambda'}\frac{N_{\lambda\lambda'}}{(\mu_\lambda - E + i\nu_\lambda)(\mu_{\lambda'} - E - i\nu_{\lambda'})}\right]$$

One notes that an expression of the form

$$\sum_{k\ell}\frac{N_{k\ell}}{(C_k - E)(C_\ell^* - E)} = \sum_{k\ell}\left[\frac{N_{k\ell}}{(C_k - E)(C_\ell^* - C_k)} + \frac{N_{k\ell}}{(C_\ell^* - E)(C_k - C_\ell^*)}\right]$$

$$= \sum_{k\ell}\left[\frac{N_{k\ell}}{(C_k - E)(C_\ell^* - C_k)} + \frac{N_{k\ell}}{(C_k^* - E)(C_\ell - C_k^*)}\right]$$

$$= \sum_{k,\ell}\left[\frac{N_{k\ell}(C_k^* - E)}{|C_k - E|^2(C_\ell^* - C_k)} + \frac{N_{\ell k}(C_k - E)}{|C_k - E|^2(C_\ell - C_k^*)}\right]$$

Making the identifications

$$G_k = -i\nu_k\sum_{\ell}\frac{N_{k\ell}}{(C_\ell^* - C_k)} + i\nu_k\sum_{\ell}\frac{N_{\ell k}}{(C_\ell - C_k^*)}$$

$$H_k = \sum_{\ell\neq k}\frac{N_{k\ell}}{C_\ell^* - C_k} + \frac{N_{k\ell}}{C_\ell - C_k^*} \tag{B38}$$

and $C_k = \mu_k + i\nu_k$ leads to Eq. (B37).

The total and scattering cross sections can also be put in a form suitable for Voigt profile broadening. Garber et al. [39] give the following explicit formulation for ENDF/B:

Total Cross Section:

$$\sigma_T(E) = \frac{2C}{E}(1 - \cos\omega)$$

$$+ \frac{C}{\sqrt{E}}\sum_{R=1}^{NRS}\frac{\nu_R^T\left(G_R^T\cos\omega + H_R^T\sin\omega\right) + \left(\mu_R^T - E\right)\left(H_R^T\cos\omega - G_R^T\sin\omega\right)}{\left(\mu_R^T - E\right)^2 + \left(\nu_R^T\right)^2} \tag{B39}$$

$$+ \frac{C}{\sqrt{E}}(AT_1 + AT_2/E + AT_3/E^2 + AT_4/E^3 + BT_1 * E + BT_2 * E^2) \quad .$$

Capture or Fission Cross Section:

$$\sigma_{n,x}(E) =$$

$$\frac{C}{\sqrt{E}}\sum_{R=1}^{NRS}\frac{\nu_R^x\left(G_R^x\cos\omega + H_R^x\sin\omega\right) + \left(\mu_R^x - E\right)\left(H_R^x\cos\omega - G_R^x\sin\omega\right)}{\left(\mu_R^x - E\right)^2 + \left(\nu_R^x\right)^2} \tag{B40}$$

$$+ \frac{C}{\sqrt{E}}(Ax_1 + Ax_2/E + Ax_3/E^2 + Ax_4/E^3 + Bx_1 * E + Bx_2 * E^2) \quad .$$

In these formulas, $\omega = 2k\hat{a}$, $C/E = \pi/k^2$, and $\mu_R^T = \mu_R^x$, $\nu_R^T = \nu_R^x$.

REFERENCES

[1] Hwang, R. N., Nuc. Sci. Eng. 52, 157 (1973).

[2] Hwang, R. N., Nuc. Sci. Eng. 36, 82 (1969).

[3] Fröhner, F., Winter Courses on Nuclear Physics and Reactors, Part I (Neutron Resonance Data for Applications), IAEA, Vienna (1978).

[4] Cullen, D. E., and Weisbin, C. R., Nuc. Sci. Eng. 60, 199 (1976).

[5] Friedman, F. L., and Weisskopf, V. F., in Niels Bohr and the Development of Physics, Pergamon Press, London (1955).

[6] Wigner, E. P., and Eisenbud, L., Phys. Rev. 72, 99 (1947).

[7] Kapur, R. L., and Peierls, R., Proc. Roy. Soc. London A166, 277 (1938).

[8] Siegert, J. F., Phys. Rev. 56, 750 (1939).

[9] Humblet, J., and Rosenfeld, L., Nuc. Phys. 26, 529 (1961).

[10] Adler, D. B., and Adler, F. T., Trans. Am. Nuc. Soc. 5, 53 (1962).

[11] Adler, D. B., and Adler, F. T., in Proc. Conf. on Breeding, Economics, and Safety in Large Fast Reactors, USAEC Report ANL-6792, 695 (1963).

[12] Breit, G., and Wigner, E. P., Phys. Rev. 49, 519 (1936).

[13] Weidenmüller, H. A., Nuc. Phys. 75, 189 (1966).

[14] Mahaux, C., and Weidenmüller, H. A., "Shell Model Approach to Nuclear Reactions," North Holland, Amsterdam (1969).

[15] Lane, A. M., and Robson, D., Phys. Rev. 151, 774 (1966).

[16] Lane, A. M., and Robson, D., Phys. Rev. 178, 1715 (1969).

[17] Lane, A. M., and Robson, D., Phys. Rev. 185, 1403 (1969).

[18] Tobocman, W., and Nagarajan, M. A., Phys. Rev. 138, B1551 (1965).

[19] Nagarajan, M. A., Shah, S. K., and Tobocman, W., Phys. Rev. 140, B63 (1965).

[20] García-Calderón, G., Nuc. Phys. A261, 130 (1976).

[21] García-Calderón, G., and Peierls, R., Nuc. Phys. A265, 443 (1976).

[22] Lane, A. M., and Thomas, R. G., Revs. Mod. Phys. 30, 257 (1958).

[23] Bethe, H. A., Phys. Rev. 50, 332 (1936).

[24] Bethe, H. A., and Placzek, G., Phys. Rev. 51, 450 (1937).

[25] Bethe, H. A., Revs. Mod. Phys. 9, 69 (1937).

[26] Lippmann, B. A., and Schwinger, J., Phys. Rev. 79, 469 (1950).

[27] Bloch, C., Nuc. Phys. 4, 503 (1957).

[28] Feshbach, H., Ann. Phys. (N.Y.) 5, 357 (1958).

[29] Feshbach, H., Ann. Phys. (N.Y.) 19, 287 (1962).

[30] MacDonald, W. M., Nuc. Phys. 54, 393 (1964).

[31] MacDonald, W. M., Nuc. Phys. 56, 636 (1964).

[32] MacDonald, W. M., Nuc. Phys. 56, 647 (1964).

[33] Tobocman, W., Phys. Rev. C12, 741 (1975).

[34] Tobocman, W., Phys. Rev. 182, 989 (1969).

[35] Solbrig, A. W., Jr., Am. J. Phys. 29, 257 (1961).

[36] Solbrig, A. W., Jr., Nuc. Sci. Eng. 10, 167 (1961).

[37] Cullen, D. E., Nuc. Sci. Eng. 52, 498 (1973).

[38] Hinman, G. W., Kuncir, G. F., Sampson, J. B., and West, G. B., Nuc. Sci. Eng. 16, 202 (1963).

[39] Garber, D., Dunford, C., and Pearlstein, S., USERDA Report BNL-NCS-50496 (ENDF-102), (1975).

[40] Lubitz, C. R., private communication (1977).

[41] de Saussure, G., Olsen, D. K., and Perez, R. B., Nuc. Sci. Eng. 61, 496 (1976).

[42] Gregson, K., James, M. F., and Norton, D. S., UKAEA Report AEEW-M-517 (1965).

[43] Feshbach, H., Porter, C. E., and Weisskopf, V. F., Phys. Rev. 96, 448 (1954).

[44] Reich, C. W., and Moore, M. S., Phys. Rev. 111, 929 (1958).

[45] Teichmann, T., and Wigner, E. P., Phys. Rev. 87, 123 (1952).

[46] Thomas, R. G., Phys. Rev. 97, 224 (1955).

[47] Moldauer, P. A., Phys. Rev. 136, B947 (1964).

[48] Adler, F. T., and Adler, D. B., in Neutron Cross Sections and Technology (P. B. Hemmig, ed.) USAEC Report CONF 660303, Vol. II, p. 873 (1966), and COO-1546-4 (1967).

[49] de Saussure, G., and Perez, R. B., USAEC Report ORNL-TM-2599 (1969).

[50] Adler, D. B., and Adler, F. T., Phys. Rev. C6, 986 (1972).

[51] Keyworth, G. A., Olsen, C. E., Moses, J. D., Dabbs, J. W. T., and Hill, N. W., in Nuclear Cross Sections and Technology, NBS Spec. Pub. 425, 576 (1975).

[52] Moore, M. S., Moses, J. D., Keyworth, G. A., Dabbs, J. W. T., and Hill, N. W., to be published (1978).

[53] Keyworth, G. A., Olsen, C. E., Seibel, F. T., Dabbs, J. W. T., and Hill, N. W., Phys. Rev. Letters 31, 1077 (1973).

[54] Keyworth, G. A., Lemley, J. R., Olsen, C. E., Seibel, F. T., Dabbs, J. W. T., and Hill, N. W. in Physics and Chemistry of Fission 1973, IAEA, Vienna, Vol. I, p.97 (1974).

[55] Dyson, F. J., and Mehta, M. L., J. Math. Phys. 4, 703 (1963).

[56] Dyson, F. J., as described by M. L. Mehta in Statistical Properties of Nuclei (J. B. Garg, ed.) Plenum Press, N.Y., p. 179 (1972).

[57] Garrison, J. D., Phys. Rev. Letters 29, 1185 (1972).

[58] Smith, J. R., USAEC Report ANCR-1129, p. 10 (1973).

[59] de Saussure, G., Perez, R. B., and Kolar, W., Phys. Rev. C7, 2018 (1973).

[60] de Saussure, G., and Perez, R. B., Nuc. Sci. Eng. 52, 412 (1973).

[61] Pattenden, N. J., and Postma, H., Nuc. Phys. A167, 225 (1971).

[62] Böckhoff, K. H., Dufrasne, A., Rohr, G., and Weigmann, H., J. Nuc. Energy 26, 91 (1972).

[63] Beer, H., and Käppeler, F., Int. Conf. on the Interaction of Neutrons with Nuclei, Lowell, Mass., USERDA Report CONF-760715 P2, 1408 (1976).

[64] Baudinet-Robinet, Y., and Mahaux, C., Phys. Rev. C9, 723 (1974).

[65] Wald, A., and Wolfowitz, J., Ann. Math. Stat. 11, 147 (1940).

[66] James, G. D., Nuc. Phys. A170, 309 (1971).

[67] James, G. D., in Proc. NEANDC/NEACRP Specialists Meeting on Fast Neutron Fission Cross Sections of U-233, U-235, U-238, and Pu-239 (W. P. Poenitz and A. B. Smith, eds.) USERDA Report ANL-76-90, 382 (1976).

[68] Wald, A., and Wolfowitz, J., Ann. Math. Stat. 14, 378 (1943).

[69] Levene, H., and Wolfowitz, J., Ann. Math. Stat. 15, 58 (1944).

[70] Wigner, E. P., Phys. Rev. 70, 606 (1946).

[71] Vogt, E., Phys. Rev. 112, 203 (1958).

[72] Vogt, E., Phys. Rev. 118, 724 (1960).

[73] Auchampaugh, G. F., Nuc. Phys. A175, 65 (1971).

[74] Auchampaugh, G. F., USAEC Report LA-5473-MS (1973).

[75] Adler, D. B., Phys. Rev. C14, 2050 (1976).

[76] Mahaux, C., Nuc. Phys. 68, 481 (1965).

[77] Moore, M. S., and Reich, C. W., Phys. Rev. 118, 718 (1960).

FIGURE CAPTIONS

Fig. 1. Fission cross sections of (^{235}U+n) from 0 to 12 eV. The lower curve is the spin-3 fission cross section; the center curve is the spin-4 fission cross section; the top curve is the sum of the two lower curves, corresponding to the fission cross section measured with an unpolarized beam and target. The spin-3 fission cross section contains a significant amount of apparent structure that was previously unobserved.

Fig. 2. Fission cross sections of (^{235}U+n) from 48 to 60 eV. The lower curve is the spin-3 fission cross section; the center curve is the spin-4 fission cross section; the top curve is the sum of the two lower curves, corresponding to the fission cross section measured with an unpolarized beam and target. Previously unobserved resonance structure is apparent in both the spin-separated curves.

Fig. 3. The number of observed and probable resonances of each spin having $E_o < E$ as a function of neutron energy below 380 eV. The top curve represents spin-4 resonances; the bottom curve spin-3 resonances. The fraction of missing resonances is independent of neutron energy below $\sim$ 60 eV.

Fig. 4. The resonance spacing distribution for (^{235}U+n) below 62 eV. The histogram shows the spacings obtained from the analysis of Ref. [52]; the curve shows the spacing distribution calculated from a Wigner distribution of a mixed sequence having the relative densities appropriate for (^{235}U+n).

Fig. 5. The variation of A_2, the coefficient of the P_2 term in the angular distribution of (^{235}U+n) fragments obtained by Pattenden and Postma [61], versus $J_{effective} = 3 + J_4/(J_3 + J_4)$. The straight line shows a linear least-squares fit to these data. The open circles show A_2 data for resonance structure, the closed circles data for the unresolved region below 2 keV, and the plus signs data for the between-resonance background regions reported by Pattenden and Postma.

Fig. 6. Partial cross sections and $\langle\alpha\rangle$, the average capture-to-fission ratio for (^{235}U+n) from 0.1 to 30 keV, from ENDF/B-V. The spin-separated fission cross sections shown in the middle two curves were obtained by renormalizing in each bin such that the sum gives the ENDF/B-V recommended fission cross section.

Fig. 7. Average spin-3 fission width for (^{235}U+n) from 0.1 to 25 keV obtained from the unresolved resonance analysis described in Ref. [52]. The curve has no theoretical significance; it is simply the authors' eyeguide.

Fig. 8. Average spin-4 fission width for (^{235}U+n) from 0.1 to 25 keV obtained from the unresolved resonance analysis described in Ref. [52]. The curve has no theoretical significance; it is simply the authors' eyeguide.

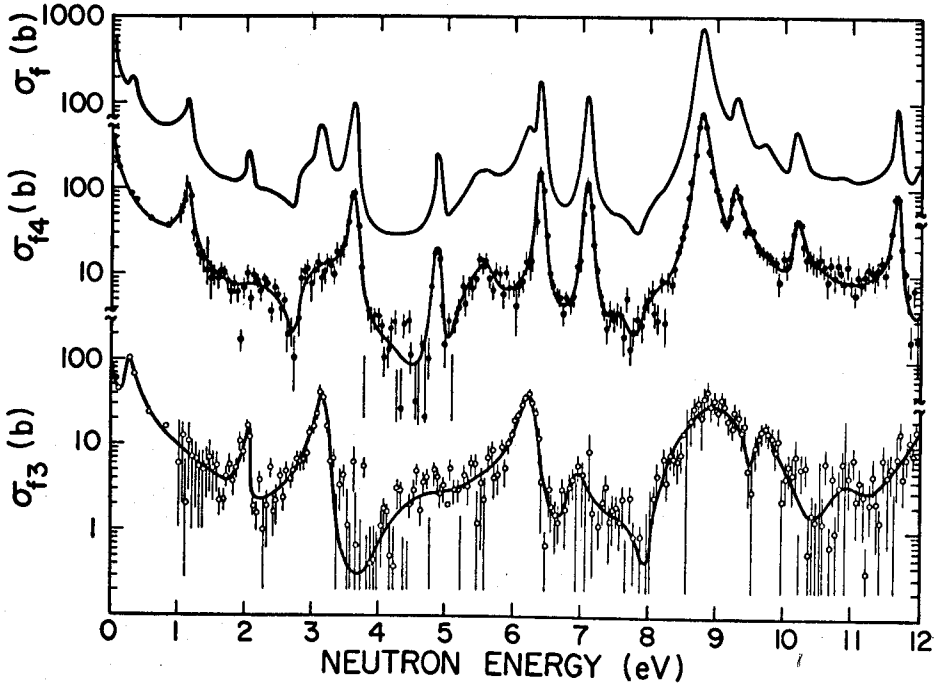

Fig. 1

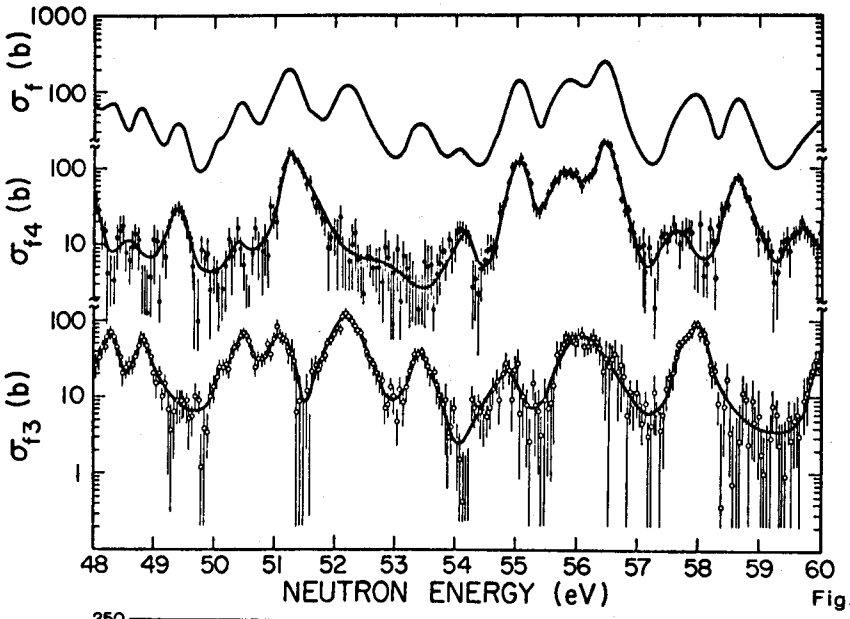

Fig. 2

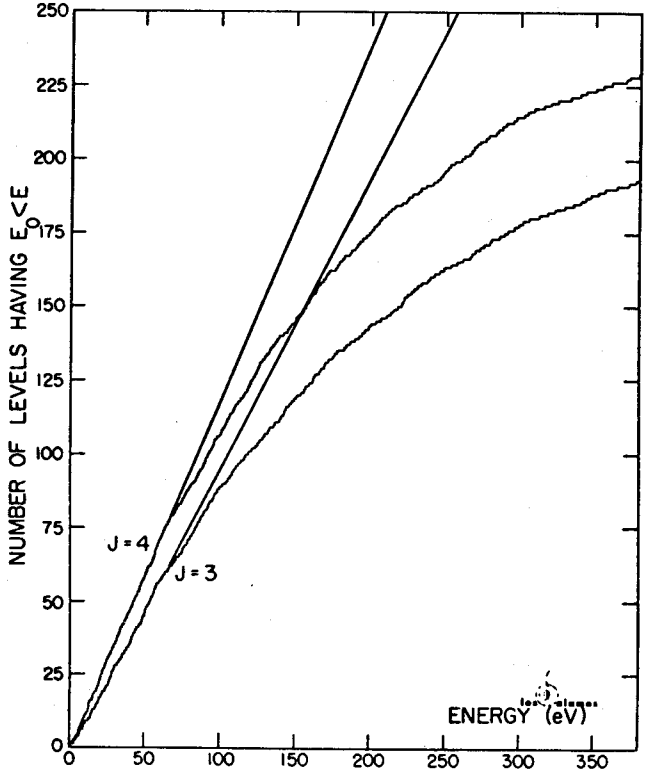

Fig. 3

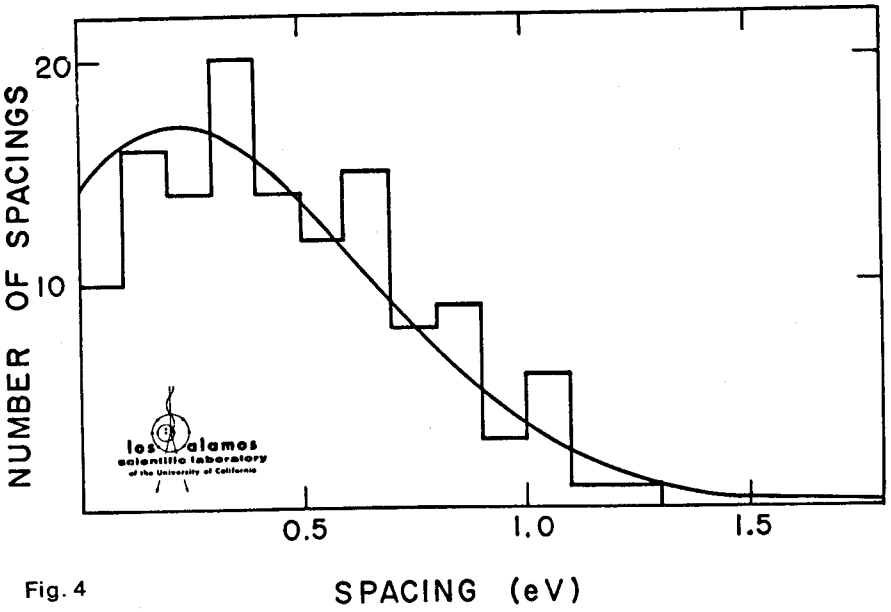

Fig. 4

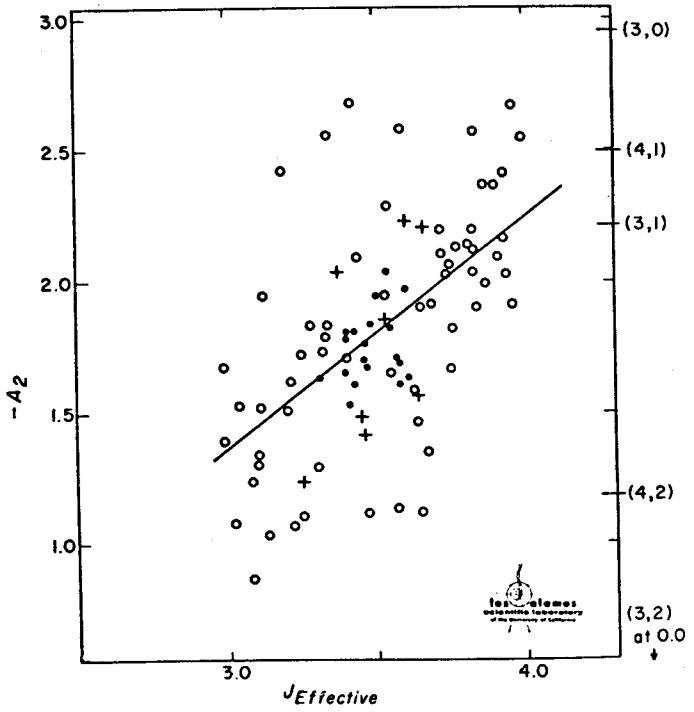

Fig. 5

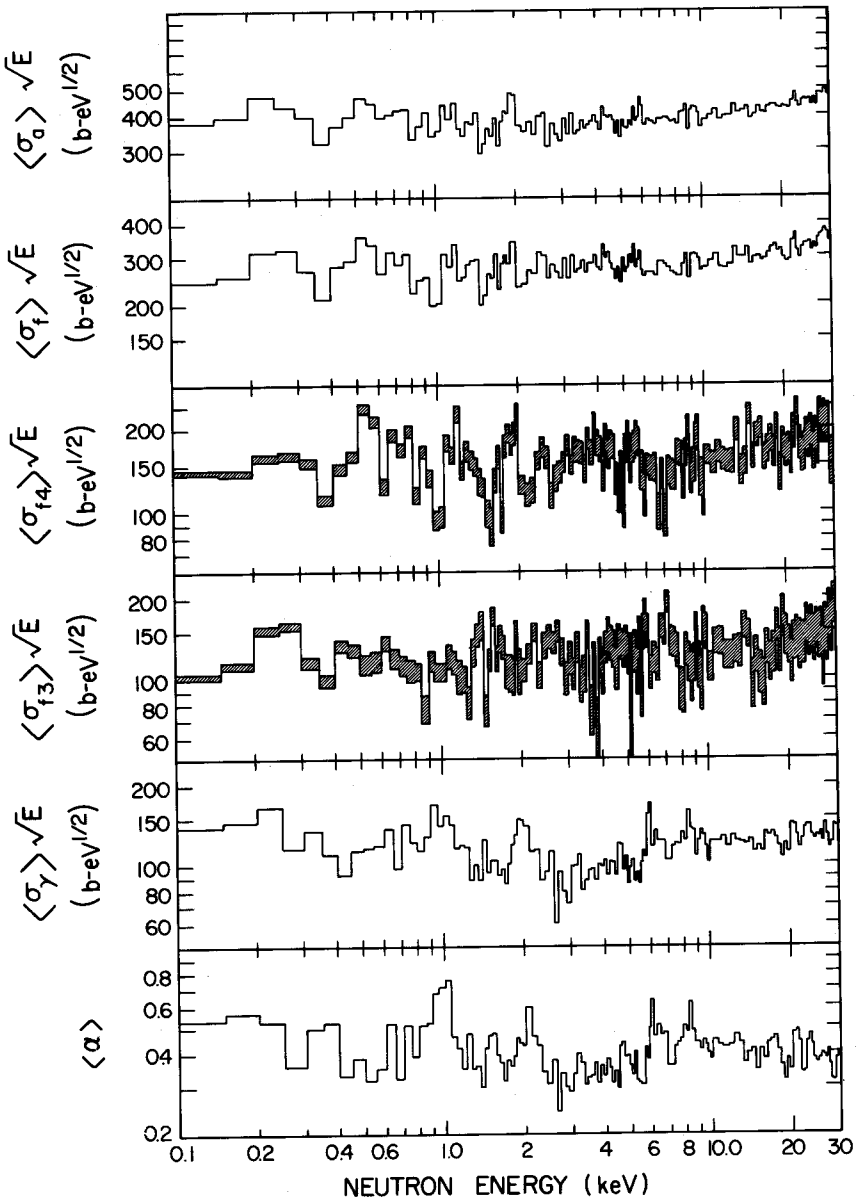

Fig. 6

APPLIED NEUTRON RESONANCE THEORY

F.H. FRÖHNER
Institut für Neutronenphysik und Reaktortechnik,
Kernforschungszentrum Karlsruhe G.m.b.H.,
Karlsruhe,
Federal Republic of Germany

ABSTRACT

Utilisation of resonance theory in basic and applications-oriented neutron cross section work is reviewed. The technically important resonance formalisms, principal concepts and methods as well as representative computer programs for resonance parameter extraction from measured data, evaluation of resonance data, calculation of Doppler-broadened cross sections and estimation of level-statistical quantities from resonance parameters are described.

1. INTRODUCTION

In contrast to the preceding lectures (Ref. 1) on the formal apparatus of resonance theory we shall now discuss mainly its practical applications. The basic reaction formalism, in particular R-matrix theory, will be assumed to be known but we shall not hesitate to retrace the practically important parts of the theory. Although the basic principles of resonance theory are rather simple the general expressions can look quite formidable. A certain amount of repetition may help the reader to overcome this initial barrier and to realize that for practical work only few but thoroughly understood key formulae are needed.

We shall be concerned mainly with compound resonances, those prominent features of particle- and phonon-induced nuclear reactions which are due to excitation of relatively long-lived (quasi-stationary) states of the compound system. At low bombarding energies they appear fairly well separated, but as the energy increases their spacings decrease and their widths increase. Finally the overlap washes out all compound resonance structure and only broader structures like the single-particle or size resonances described by the optical model survive.

The more nucleons belong to the compound system the finer is the compound resonance structure. Typical level spacings observed in neutron reactions are of the order

- MeV for the lightest,
- keV for medium-mass and
- eV for the heaviest nuclei.

2. ANALYSIS OF RESONANCE DATA

The importance of resonance reactions for nuclear technology is obvious. Interpretation and prediction of reactor properties such as

- resonance absorption,
- resonance escape probability,
- resonance self-shielding,
- temperature-dependent reactivity (Doppler coefficient)

require both a detailed understanding of resonance cross sections and comprehensive, machine-readable resonance data files.

2.1 The various steps in the preparation of resonance data for applications

The resonance data for reactor calculations and other applications (e.g. as cross section standards) are usually produced in several steps.

(1) Measurement: Experimenters take data at pulsed accelerators or with the help of nuclear explosions. The time-of-flight technique is employed to cover broad energy ranges with high resolution and under exactly the same experimental conditions for all energies, isotopically pure or highly enriched samples to get reliable isotopic assignments and, in the most advanced experiments, polarized neutrons and targets to get reliable spin assignments for the observed resonances.

(2) Reduction of raw data: Constant and time-dependent backgrounds are subtracted, sample impurities are corrected for, and, in the case of partial cross section (yield) data, flux and detector efficiency are factorised out.

(3) Analysis of clean data: Resonance parameters (E_o, Γ_n, Γ_γ, Γ_f,...$J\pi$) and potential-scattering parameters (R',...) are extracted. At the same time instrumental resolution and (except for transmission data) multiple scattering are accounted for.

(4) Data evaluation: Resonance parameters from all available sources are collected by evaluators who try to understand and to reconcile the discrepancies. Gaps are filled with the help of level statistics, nuclear models and systematics. The complete sets of recommended cross section parameters (E_o, Γ_n, Γ_γ, Γ_f,...$J\pi$; $\bar{R}'$,...) and the deduced level statistical parameters (D_J, S_ℓ, R^*_ℓ, $\Gamma_{\gamma,\ell}$, $\bar{\Gamma}_{f,J\pi}$,...) are put into a machine-readable (card, tape or disk) file.

(5) Generation of group constants: Doppler-broadened point cross sections for various temperatures and all energetically possible reactions can now be calculated from the evaluated cross section parameters and averaged in a special way over relatively large energy intervals. The result is a set of group cross sections and self-shielding factors suitable as input for reactor codes.

International coordination

All these steps require time and years may pass before resonance data needed for technological applications become available in the required form of machine-readable evaluated data files. The great effort to speed up this

process and to coordinate the work on an international scale was described earlier in the course (Ref. 2). It may suffice here to mention that regional and international nuclear data committees (INDC, NEANDC,...) collect and screen formal requests for data which are periodically published by IAEA/NDS in WRENDA, the World Request List for Nuclear Data. Measured data are collected by data centres, neutron data in particular by the four-centre network consisting of

- NNDC (National Nuclear Data Centre) at Brookhaven, servicing the US and Canada,
- CCDN (Centre de Compilation de Données Neutroniques, now part of the NEA Data Bank) at Saclay, France, servicing the non-American OECD countries,
- CJD (Centr po Jadernym Dannym) at Obninsk, servicing the Soviet Union, and
- NDS (Nuclear Data Section, IAEA) in Vienna, servicing all other countries.

Regular data exchange ensures that the data base is essentially the same at all four centres. Evaluated data are also collected, the most important evaluated files being

- ENDF, the US Evaluated Nuclear Data File,
- UKNDL, the UK Nuclear Data Library,
- KEDAK, the German file Kerndaten Karlsruhe,
- SOKRATOR, the USSR file.

Moreover, the Four Centres produce periodically such widely used handbooks as the Computer Index of Neutron Data (CINDA) (Ref. 3) or the "barn book" BNL 325 (Ref. 4) which contains resonance parameters and cross section plots.

Associated computer programs, for instance resonance analysis programs or codes generating cross sections from resonance parameters, are collected and distributed to requestors by the

- US Code Center at ANL, USA;
- CPL, the Computer Program Library of NEA/OECD at Ispra, Italy (now part of the NEA Data Bank);
- RSIC, the Radiation Shielding Information Center at Oak Ridge, USA.

Information as to where other types of data and programs are available can be obtained from NDS/IAEA, Vienna.

2.2 Why parametrize?

Practically all resonance cross section data that go into reactor calculations (in group constant form or directly, e.g. in Monte Carlo calculations) are generated from resonance parameters. It might be asked why one cannot use the best measured high-resolution cross sections directly and thus eliminate the need for resonance parameter extraction. There are several reasons:

(1) Resonance parameters along with consequent utilisation of resonance theory enable us to represent the often staggering detail of cross section structure by relatively few numbers.

Example: The 400 presently known resonances of the compound system $^{238}U+n$ are specified by 1600 parameters (E_o, Γ_n, Γ_γ, $J\pi$ for each level) whereas a reasonably accurate point-wise representation of the capture and the scattering cross section requires about $2\cdot10^4$ data points, i.e. $4\cdot10^4$ numbers. If one considers also angular distributions and different temperatures one gets easily several 10^6 cross section points that would be needed to describe the behaviour of ^{238}U in a fast reactor.

(2) Temperature broadening of resonances is often more easily calculated in terms of resonance parameters than from point data.

(3) Resonance parameters and an inherently unitary cross section formalism such as R-matrix theory guarantee consistency with physical limits such as the unitarity limits for the total cross section in each reaction channel ($0<\sigma_c<4\pi\lambda_c^2 g_c$ where g_c is the spin factor, see below) or Wick's limit for scattering in the forward direction ($d\sigma_{cc}(0)/d\Omega_c \geq \sigma_c^2/(4\pi\lambda_c)^2$).

Another consistency is more subtle but practically at least equally important, especially for the calculation of self-shielded group cross sections. Theory tells us that there is a very rigid relationship between the line shape in one reaction channel and the line shape corresponding to the same compound level in other channels. This relationship is guaranteed if cross sections are generated from a coherent set of resonance parameters, but not with measured data.

(4) At least equally important is the fact that even the best measured resonance data are affected by resolution and Doppler broadening and (except transmission data) by multiple scattering. The most reliable way to correct for these effects is full-scale resonance parameter analysis of the data.

(5) Extrapolation into the region of non-measured or unresolved resonances by level-statistical (Hauser-Feshbach) cross section calculations require statistical parameters such as average level spacings and strength functions. These in turn must be estimated from resonance parameters.

2.3 Practical resonance formalisms

In applications-oriented neutron resonance work and especially in evaluated neutron data files the following formalisms are used almost exclusively.

- BB (Blatt-Biedenharn formalism),
- SLBW (single-level Breit-Wigner formulae),
- MLBW (multi- " " " "),
- RM (" " Reich-Moore "),
- AA (" " Adler-Adler "),

The first one is quite general. It shows how cross sections can be expressed in terms of the unitary, symmetric collision matrix with special emphasis on angular distributions and the influence of particle spins. It can be combined with any of the other four which provide different approximations to the collision matrix.

In the following sections the notation of the comprehensive review written by Lane and Thomas (Ref. 5) will be used.

2.3.1 The Blatt-Biedenharn formalism

We remember that in reaction theory one employs the concept of reaction channels which are fully specified by

α, the partition into reaction partners, e.g. $^{235}U+n$ or $^{236}U+\gamma$,
J, the total angular momentum in units of $\hbar$,
ℓ, the orbital " " " " " $\hbar$,
s, the channel spin " " " " $\hbar$,

with $$\vec{J} = \vec{\ell}+\vec{s}, \text{ i.e. } |\ell-s| \leq J \leq \ell+s, \tag{1}$$

$$\vec{s} = \vec{I}+\vec{i}, \text{ i.e. } |I-i| \leq s \leq I+i, \tag{2}$$

where I and i are the spins of the (two) collision partners. Because of the invariance properties of the Hamilton operator total energy, total angular momentum and parity are conserved quantities in nuclear reactions.

We further remember that for spinless, neutral particles one can solve the Schrödinger equation for the boundary condition "ingoing plane wave + outgoing spherical wave" with the result that the differential cross section for elastic scattering is given by

$$d\sigma_{\alpha\alpha} = \pi\lambda_\alpha^2 \Big| \sum_{\ell=0}^{\infty} (2\ell+1)(1-U_\ell)P_\ell(\cos\theta)\Big|^2 \frac{d\Omega}{4\pi} \tag{3}$$

where P_ℓ is the ℓ-th order Legendre polynomial (angular-momentum eigenfunction). The sum terms with ℓ=0,1,2,3,... are said to belong to the s-, p-, d-, f-,... wave, a nomenclature taken over from atomic spectroscopy. The collision function U_ℓ describes the modification of the ℓ-th outgoing partial wave relative to the case without interaction, its absolute value giving the reduction in amplitude, its argument the phase shift. With $P_\ell P_{\ell'} = (\ell\ell'00,L0)^2 P_L$, where $(\ell\ell'00,L0)$ is a Clebsch-Gordan coefficient (vanishing unless $|\ell-\ell'| \leq L \leq \ell+\ell'$ and $(-)^{\ell+\ell'} = (-)^L$), one can write this as a simple expansion in Legendre polynomials,

$$d\sigma_{\alpha\alpha} = \lambda_\alpha^2 \sum_{L=0}^{\infty} B_L P_L(\cos\theta)d\Omega, \text{ with} \tag{4}$$

$$B_L = \frac{1}{4} \sum_{\ell,\ell'} (2\ell+1)(2\ell'+1)(\ell\ell'00,L0)^2(1-U_\ell^*)(1-U_{\ell'}). \tag{5}$$

Blatt and Biedenharn (Ref. 6) worked out the generalisation for particles with spins and for partition-changing (rearrangement) collisions. For zero Coulomb interaction they obtained

$$d\sigma_{\alpha\alpha'} = \frac{\lambda_\alpha^2}{(2i+1)(2I+1)} \sum_{s,s'} \sum_{L=0}^{\infty} B_L(\alpha s,\alpha' s')P_L(\cos\theta)d\Omega \tag{6}$$

$$B_L(\alpha s,\alpha' s') = \frac{(-)^{s-s'}}{4} \sum_{J_1J_2} \sum_{\ell_1,\ell_2} \sum_{\ell_1',\ell_2'} \bar{Z}(\ell_1J_1\ell_2J_2sL)\bar{Z}(\ell_1'J_1\ell_2'J_2s'L)$$

$$\cdot (\delta_{\alpha\alpha'}\delta_{\ell_1\ell_1'}\delta_{ss'} - U^{J_1}_{\alpha\ell_1 s,\alpha'\ell_1' s'})^*(\delta_{\alpha\alpha'}\delta_{\ell_2\ell_2'}\delta_{ss'} - U^{J_2}_{\alpha\ell_2 s,\alpha'\ell_2' s'}), \tag{7}$$

$$\bar{Z}(\ell_1J_1\ell_2J_2,sL) = \sqrt{(2\ell_1+1)(2\ell_2+1)(2J_1+1)(2J_2+1)}$$

$$\cdot (\ell_1\ell_200,L0)W(\ell_1J_1\ell_2J_2,sL), \tag{8}$$

where $W(\ell_1J_1\ell_2J_2,sL)$ is a Racah coefficient (see e.g. Ref. 7). Our phase convention for the $\bar{Z}$ is that of Ref. 5, a slightly different convention is used in the $\bar{Z}$-coefficient tabulation Ref. 8. The $\bar{Z}$ coefficients vanish unless the triangle conditions for the vector sums

$$\vec{\ell}_1 + \vec{\ell}_2 = \vec{L} = \vec{\ell}_1' + \vec{\ell}_2', \tag{9}$$

$$\vec{\ell}_i + \vec{s} = \vec{J}_i = \vec{\ell}_i' + \vec{s}' \quad (i = 1,2) \tag{10}$$

are fulfilled. Parity conservation in nuclear reactions demands that $(-)^{\ell_i}\Pi_\alpha = \Pi_i = (-)^{\ell_i'}\Pi_{\alpha'}$, where Π_α, $\Pi_{\alpha'}$, are the eigen-parities of the in- and outgoing particles (positive for neutrons, protons and alpha-particles) and Π_i is the parity of the compound system with total angular momentum J_i (i = 1,2).

If there is Coulomb interaction between the collision partners additional terms must be included (see Ref. 5).

Let us now integrate Eq. 6 over all angles. Because all terms with L > 0 vanish due to the orthogonality of the P_L and because of

$$\bar{Z}(\ell_1J_1\ell_2J_2,s0) = (-)^{J_1+s}\sqrt{2J_1+1}\,\delta_{J_1J_2}\,\delta_{\ell_1\ell_2} \tag{11}$$

(cf. Ref. 7) one finds

$$\sigma_{\alpha\alpha'} = \pi\lambda_\alpha^2 \sum_J \sum_{\ell,\ell'} \sum_{s,s'} g_J \left|\delta_{\alpha\alpha'}\delta_{\ell\ell'}\delta_{ss'} - U^J_{\alpha\ell s,\alpha'\ell' s'}\right|^2 \tag{12}$$

where

$$g_J = \frac{2J+1}{(2i+1)(2I+1)} \tag{13}$$

is the so-called spin factor.

We shall not go into the details of angular distributions but point out that they show interference between different partial waves, e.g. s- and p-wave interference, whereas angle-integrated cross sections do not. The latter are simple sums over terms with given ℓ and s without mixed terms. Nevertheless,

a certain connexion exists between different partial waves provided they can excite the same compound states. As mentioned already the compound system and its quasi-stationary states are characterised, apart from energy, by the total angular momentum J and the parity Π. Table 1 shows, for given target spin I and positive target parity, the possible combinations of ℓ, s and J if the incident particles have spin i = 1/2. (If the target parity is negative all signs in the table must be reversed.)

Table 1: Possible combinations of target spin I, orbital angular momentum ℓ and channel spin s resulting in total spin and parity JΠ and spin factor g for positive target parity Π_o and incident particles with spin 1/2:

$I\Pi_o$	ℓ	s	JΠ	g	Σg	spectroscopic symbol
0+	0	1/2	1/2+	1	1	s
	1	1/2	1/2−, 3/2−	1, 2	3	p
	2	1/2	3/2+, 5/2+	2, 3	5	d
		etc.				
1/2+	0	0	0+	1/4	1	s
		1	1+	3/4		
	1	0	1−	3/4	3	p
		1	0− 1− 2−	1/4, 3/4, 5/4		
	2	0	2+	5/4	5	d
		1	1+ 2+ 3+	3/4, 5/4, 7/4		
		etc.				
1+	0	1/2	1/2+	1/3	1	s
		3/2	3/2+	2/3		
	1	1/2	1/2−, 3/2−	1/3, 2/3	3	p
		3/2	1/2−, 3/2−, 5/2−	1/3, 2/3, 3/3		
	2	1/2	3/2+, 5/2+	2/3, 3/3	5	d
		3/2	1/2+, 3/2+, 5/2+, 7/2+	1/3, 2/3, 3/3, 4/3		
		etc.				

We see that certain JΠ values can be formed through more than one channel if ℓ>0 and I>0. If $I\Pi_o$=1/2+, for instance, resonances with JΠ=1− can be excited by the two p-waves (ℓ=1) with s=0 and s=1, and the 2+ levels can be excited by the two d-waves (ℓ=2) with s=0 and s=1. The SLBW neutron widths (see below) of 1− and 2+ levels are therefore sums of two partial widths, for s=0 and s=1. For $I\Pi_o$=1+ the 1/2+ levels can even be excited by two partial waves with different ℓ (s-wave with ℓ=0, d-wave with ℓ=2) while the 3/2+ levels are accessible to three partial waves, the s-wave with s=3/2 and the two d-waves with s=1/2 and s=3/2, etc.

This means that the same resonances (with the same total widths) may show up in channels with different ℓ and s if the spin and parity selection rules allow this. In this context it should be understood that the term s- or p-wave resonance actually means that the resonance can be excited by the s- or p-wave but possibly also by the next higher partial wave with the same parity. As an example the 3/2+ s-wave resonance peaks of a target nucleus with $I\Pi_o$=1+ contain also a d-wave component. The fact that certain d-, f- etc. resonance sequences are masked by s-, p- etc. sequences, respectively, must be kept in mind if the J-dependence of level densities is discussed and compared to resonance data. Finally we note that the sum of all spin factors for a given ℓ is always equal to 2ℓ+1 as shown in the table.

2.3.2 The practically important R-matrix formulae

The angle-integrated cross section $\sigma_{\alpha\alpha'}$, Eq. 12, is a sum over partial cross sections $\sigma_{cc'}$, summed over all those entrance channels c = {αJℓs} and exit channels c' = {α'Jℓ's'} which lead from partition α to partition α'. In slightly simplified notation we can write

$$\sigma_{cc'} = \pi\lambda\!\!\!^{-2}_c g_c |\delta_{cc'} - U_{cc'}|^2 \ . \qquad (14)$$

Due to the unitarity of U one gets for the total cross section

$$\sigma_c = \sum_{c'} \sigma_{cc'} = 2\pi\lambda\!\!\!^{-2}_c g_c (1 - \mathrm{Re}\ U_{cc}) \ , \qquad (15)$$

while the symmetry of U yields the reciprocity relation for the cross section $\sigma_{c'c}$ describing the inverse reaction,

$$\frac{\sigma_{c'c}}{g_{c'}\lambda\!\!\!^{-2}_{c'}} = \frac{\sigma_{cc'}}{g_c\lambda\!\!\!^{-2}_c} \ . \qquad (16)$$

These equations are quite general. The wave length $2\pi\lambda\!\!\!^{-}_c$ is that corresponding to the total kinetic energy in the centre-of-mass system, $\lambda\!\!\!^{-}_c = \lambda\!\!\!^{-}_\alpha = \hbar/(\mu_c v_{rel})$, where μ_c is the reduced mass and v_{rel} the relative speed. It should be noted that σ_c being a linear function of U is easier to calculate and to average etc. than $\sigma_{cc'}$.

Next we invoke R-matrix theory. It teaches us that one can express the collision matrix either in terms of the channel matrix (resonance parameter matrix) R,

$$U_{cc'} = e^{-i(\phi_c+\phi_{c'})} P_c^{1/2} \{[1-R(L-B)]^{-1}[1-R(L^*-B)]\}_{cc'} P_{c'}^{-1/2}$$

$$= e^{-i(\phi_c+\phi_{c'})} \{\delta_{cc'} + 2iP_c^{1/2}[(1-RL^o)^{-1}R]_{cc'} P_{c'}^{1/2}\}, \qquad (17)$$

$$R_{cc'} = \sum_\lambda \frac{\gamma_{\lambda c}\gamma_{\lambda c'}}{E_\lambda - E} \ , \qquad (18)$$

$$L^o_{cc'} \equiv (L-B)_{cc'} = L^o_c\delta_{cc'} = (L_c-B_c)\delta_{cc'} \equiv (S_c+iP_c-B_c)\delta_{cc'} \quad (19)$$

or, alternatively, in terms of the level matrix A,

$$U_{cc'} = e^{-i(\phi_c+\phi_{c'})}(\delta_{cc'} + i\sum_{\lambda,\mu}\Gamma^{1/2}_{\lambda c} A_{\lambda\mu}\Gamma^{1/2}_{\mu c'}) , \quad (20)$$

$$\Gamma^{1/2}_{\lambda c} = \gamma_{\lambda c}\sqrt{2P_c} , \quad (21)$$

$$(A^{-1})_{\lambda\mu} = (E_\lambda-E)\delta_{\lambda\mu} - \sum_c \gamma_{\lambda c}L^o_c\gamma_{\mu c} . \quad (22)$$

Here ϕ_c is the potential-scattering phase, S_c and P_c are level shift factor and centrifugal-barrier penetrability, B_c is the arbitrary boundary constant at the channel radius, E_λ an energy eigenvalue (resonance energy), $\gamma_{\lambda c}$ a reduced width amplitude and $\Gamma_{\lambda c}$ the corresponding partial width. Roman subscripts refer to reaction channels, Greek subscripts to compound levels. We mention here that in applied work all energies, resonance widths etc. are given in the laboratory system, i. e. in the reference frame in which the target nucleus is at rest.

It is useful to remember that ϕ_c and L_c depend only on the values of the precisely known in- or outgoing radial wave functions I_c and O_c at the channel radius a_c,

$$\phi_c = \arg O_c(a_c) = \text{arc tan}\ \frac{\text{Im } O_c(a_c)}{\text{Re } O_c(a_c)} , \quad (23)$$

$$L_c = a_c\frac{O'_c(a_c)}{O_c(a_c)} = a_c\left(\frac{\partial}{\partial r_c}\ln O_c\right)_{r_c=a_c} \quad (24)$$

For neutral particles one has, with $k_c \equiv 1/\lambda\!\!\!^{-}_c$,

$$O_c = I^*_c = ik_cr_c\, h^{(1)}_\ell(k_cr_c) \ (\simeq i^{-\ell}e^{ik_cr_c} \text{ for } k_cr_c >> \sqrt{\ell(\ell+1)}), \quad (25)$$

where $h^{(1)}_\ell$ is a spherical Hankel function of the first kind. With the recursion relations for spherical cylinder functions (cf. e.g. Ref. 5) one gets Table 2.

Table 2: Channel wave functions and related quantities for neutral particles ($\rho \equiv k_cr_c$, $\alpha \equiv k_ca_c$)

ℓ	O_c	ϕ_c	$-S_c$	P_c
0	$e^{i\rho}$	α	0	α
1	$e^{i\rho}(\frac{1}{\rho}-i)$	α-arc tan α	$\frac{1}{\alpha^2+1}$	$\frac{\alpha^3}{\alpha^2+1}$
2	$e^{i\rho}(\frac{3}{\rho^2}-\frac{3i}{\rho}-1)$	α-arc tan $\frac{3\alpha}{3-\alpha^2}$	$\frac{3(\alpha^2+6)}{\alpha^4+3\alpha^2+9}$	$\frac{\alpha^5}{\alpha^4+3\alpha^2+9}$
	etc.			

Note that $S_c=0$ for $\ell=0$, so that one can choose $B_c=S_c=0$ which simplifies all s-wave formulae. S_c and P_c for photon and fission channels are usually taken as constant.

The basic resonance parameters E_λ, $\gamma_{\lambda c}$ depend on the very complicated nuclear interaction and can therefore normally not be calculated. In most technological applications they are just fit parameters of the theory. Depending on the choice of B_c they can be real and constant or complex and energy-dependent.

The Wigner-Eisenbud version of R-matrix theory (Ref. 9) is obtained if the boundary quantities B_c are chosen as real constants. Then the resonance parameters E_λ and $\gamma_{\lambda c}$ are also real and constant, and the energy dependence of U is exclusively due to ϕ_c and L^o_c, i.e. it is explicitly specified. This renders the Wigner-Eisenbud version the most suitable formalism for most purposes. A major problem, however, is the required inversion of either a channel matrix ($1-RL^o$ in Eq. 17) or a level matrix (A^{-1} in Eq. 22). In practice it is overcome by various approximations to the level matrix A^{-1} as we shall see below.

The Kapur-Peierls version of R-matrix theory (Ref. 10) is obtained with the choice $B_c=L_c$, i.e. $L^o_c=0$. This removes the matrix inversion problem completely ($1-RL^o=1$) but leads to complex E_λ, $\gamma_{\lambda c}$ which implicitly depend on energy in a rather obscure way. Nevertheless formulae of the Kapur-Peierls type are convenient in narrow energy ranges, for instance for Doppler broadening.

The R-matrix equations reviewed so far are practically all that is needed in applied work from the whole apparatus of resonance theory. They should be thoroughly understood, however, and experience shows that this is not easy for the beginner. He might therefore wish to look at a simple illustration which shows the essential steps in the development of R-matrix theory and exhibits the meaning of the various quantities without the complexities of spin algebra and matrix notation. The more experienced reader can immediately go to Sect. 2.3.4.

2.3.3 Illustration: R-matrix formulation of single-particle interaction with a complex potential

(1) Schrödinger equation and boundary conditions:

Consider the interaction of a spinless, neutral particle with a spherical complex potential V+iW. From the Schrödinger equation

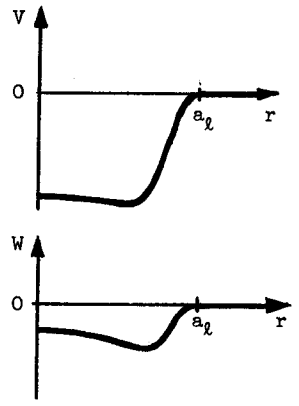

Fig. 1

$$\left(\frac{-\hbar^2}{2m}\nabla^2+V+iW\right)\psi=E\psi \qquad (26)$$

one finds with the usual partial-wave expansion in Legendre polynomials, $\psi = \sum_\ell u_\ell(r)P_\ell(\cos\theta)/r$, the radial wave equation

$$u_\ell'' + \left[k^2 - \frac{2m}{\hbar^2}(V+iW) - \frac{\ell(\ell+1)}{r^2}\right]u_\ell = 0. \qquad (27)$$

($E=\hbar^2k^2/(2m)$). The boundary conditions

$$u_\ell(o)=o, \quad u_\ell(r)=I_\ell-U_\ell O_\ell \text{ for } r\geq a_\ell \qquad (28)(29)$$

follow from the requirements that probabilities, i.e. $|\psi|^2$, remain finite and that outside the range of the potential (which is assumed to vanish for radial separations $r\geq a_\ell$) one has ingoing and outgoing spherical waves I_ℓ, O_ℓ, where the outgoing wave O_ℓ is modified, relative to the case without interaction, by a complex factor U_ℓ, the collision function. The channel wave functions I_ℓ, O_ℓ are given by Eq. 25. Note that in our example a channel is completely specified by the orbital (or, since $\ell=J$, the total) angular momentum.

(2) Orthogonal base in the internal region ($r\leq a_\ell$)

Next we introduce, for each ℓ, a base of real, orthogonal functions $u_{\lambda\ell}$ by demanding

$$u_{\lambda\ell}''+\left[k_\lambda^2-\frac{2m}{\hbar^2}V-\frac{\ell(\ell+1)}{r^2}\right]u_{\lambda\ell} = 0, \qquad (r\leq a_\ell) \qquad (30)$$

$$u_{\lambda\ell}(o) = o, \quad a_\ell u'_{\lambda\ell}(a_\ell) = B_\ell u_{\lambda\ell}(a_\ell), \qquad (31)\ (32)$$

where B_ℓ, the boundary parameter, is seen to be essentially the logarithmic derivative of the internal eigenfunctions $u_{\lambda\ell}$ at the channel radius a_ℓ. Compare the similar definition of L_ℓ in terms of external wave functions, Eq. 24. Since we omitted the imaginary part of the potential in the differential equation (30) everything becomes real, including the eigenfunctions, if we choose B_ℓ real. (Similarly the self-adjoint Hamiltonian in the general theory leads to real eigenfunctions for real B_c.) The orthogonality of the eigenfunctions is checked as follows. The wave equation (30) yields

$$\int_o^{a_\ell} dr\ (u''_{\lambda\ell}u_{\mu\ell}-u_{\lambda\ell}u''_{\mu\ell}) = (k_\mu^2-k_\lambda^2)\int_o^{a_\ell} dr\ u_{\lambda\ell}u_{\mu\ell}$$

$$= u'_{\lambda\ell}(a_\ell)u_{\mu\ell}(a_\ell) - u_{\lambda\ell}(a_\ell)u'_{\mu\ell}(a_\ell)\ . \qquad (33)$$

The integration by parts leading to the last line corresponds to the application of Green's theorem in the general R-matrix case. The whole expression vanishes because of the boundary condition (32). This proves the orthogonality, i.e.

$$\int_o^{a_\ell} dr\ u_{\lambda\ell}u_{\mu\ell} = a_\ell\,\delta_{\lambda\mu}, \qquad (34)$$

where the normalisation constant a_ℓ ensures the correct dimensions.

(3) Surface equation

We can now expand the true wave function inside the interaction sphere as follows

$$u_\ell = \sum_\lambda c_{\lambda\ell}u_{\lambda\ell} \qquad (r\leq a_\ell) \qquad (35)$$

with

$$c_{\lambda\ell} = \frac{1}{a_\ell}\int_o^{a_\ell} dr\ u_{\lambda\ell}u_\ell. \qquad (36)$$

Specific information about the last integral, i.e. about the expansion coefficients $c_{\lambda\ell}$, must come from the wave equations and boundary conditions. We employ the same procedure that we just used to study the quite similar orthogonality integral. From the wave equations (27), (30) we get

$$\int_o^{a_\ell} dr(u_\ell''u_{\lambda\ell}-u_\ell u''_{\lambda\ell}) = (k_\lambda^2-k^2+i\tfrac{2m}{\hbar^2}\bar{W}_\lambda)\int_o^{a_\ell} dr\ u_\ell u_{\lambda\ell} \qquad (37)$$

where

$$\bar{W}_\lambda \equiv \frac{\int_o^a dr\ u_\ell u_{\lambda\ell}W}{\int_o^a dr\ u_\ell u_{\lambda\ell}} \qquad (38)$$

is a volume average over the absorptive potential. Integrating by parts ("Green's theorem") and using the boundary conditions (Eqs. 28, 31, 32) one finds

$$\left[a_\ell u'_\ell(a_\ell)-B_\ell u_\ell(a_\ell)\right]u_{\lambda\ell}(a_\ell) = \frac{2m}{\hbar^2}(E_\lambda-E-i\bar{W}_\lambda)a_\ell^2c_\ell \qquad (39)$$

where $E_\lambda=\hbar^2k_\lambda^2/(2m)$. Inserting c_ℓ from this equation in the expansion (35) one obtains

$$u_\ell = R_\ell(a_\ell u'_\ell-B_\ell u_\ell) \qquad \text{for } r=a_\ell, \qquad (40)$$

where

$$R_\ell \equiv \sum_\lambda \frac{\gamma_{\lambda\ell}^2}{E_\lambda-E-i\Gamma_{\lambda a}/2} \qquad (41)$$

with

$$\gamma_{\lambda\ell} \equiv \sqrt{\frac{\hbar^2}{2ma_\ell}}\,u_{\lambda\ell}(a_\ell), \quad \Gamma_{\lambda a} \equiv -2\bar{W}_\lambda\ . \qquad (42)(43)$$

The "surface equation" (40) is the analogue of the matrix equation V=R(D-BV) of the general theory which connects the "value" and "derivative quantities" V and D at the surface by means of the R matrix. Eq. (42) shows that the reduced width amplitudes $\gamma_{\lambda\ell}$ are essentially the values of the eigenfunctions at the channel radius.

(4) R-function expression for the collision function

Our ultimate goal is an expression of the collision function U_ℓ (from which the cross sections can be calculated) free of the unknown quantities u'_ℓ and u_ℓ. In general this requires matching of the external and internal wave functions

at $r=a_\ell$. With the surface equation this is surprisingly easy. We simply replace the internal quantities in Eq. 40 by the channel quantities I_ℓ and O_ℓ with the help of the matching conditions,

$$r=a_\ell: \qquad u_\ell = I_\ell - U_\ell O_\ell, \tag{44}$$

$$a_\ell u'_\ell = a_\ell(I'_\ell - U_\ell O'_\ell) = L^*_\ell I_\ell - U_\ell L_\ell O_\ell, \tag{45}$$

and solve for U_ℓ. The final result,

$$U_\ell = \frac{I_\ell}{O_\ell}\,\frac{1-R_\ell(L^*_\ell-B_\ell)}{1-R_\ell(L_\ell-B_\ell)} = e^{-2i\phi_\ell}\left(1+\frac{2iR_\ell P_\ell}{1-R_\ell L^o_\ell}\right), \tag{46}$$

with R_ℓ given by Eq. 41, is the analogue of the general Eqs. 17, 18.

In contrast to the Wigner-Eisenbud R-matrix, Eq. 18, our R-function, Eq. 41, is complex. It looks, in fact, exactly like the reduced R-matrix of the Reich-Moore approximation (see below) where $\Gamma_{\lambda a}$ is the radiation width and originates from elimination of all photon channels by means of the Teichmann-Wigner prescription (Ref. 11) if the width amplitudes $\gamma_{\lambda c}$ of the eliminated channels are relatively small and have random signs. The absorptive potential W is thus equivalent to reactions leading from the entrance channel to other eliminated channels.

A more rigorous connexion with the theory of compound resonances is established as follows. One averages the collision matrix element U_{cc} over an energy interval that is so wide that it contains many compound levels but small enough that weak energy dependences (of λ, ϕ_ℓ, L_ℓ and of level statistics) can be neglected. With a Lorentzian weight function centered at E and having the width I (FWHM) one finds, because U_{cc} has no poles above the real axis,

$$\bar{U}_{cc}(E) = U_\ell(E) \text{ with } R_\ell(E) = R_{cc}(E+iI). \tag{47)(48}$$

Thus $\bar{U}_{cc}$ is given by the optical-model expression (46), with R_ℓ replaced by R_{cc} evaluated at the complex energy E+iI. This means that the average total cross section can be calculated from the optical model. If in R_{cc} the summation over levels is replaced by an integration, and I is treated as a small quantity, one gets

$$R_{cc}(E+iI) \equiv R^\infty_c + i\pi s_c \tag{49}$$

with

$$s_c = \frac{\overline{\gamma^2_c}}{D_c} \qquad \text{(pole strength function)}, \tag{50}$$

$$R^\infty_c(E) = \oint_{-\infty}^{\infty} dE\,\frac{s_c(E')}{E'-E} \qquad \text{(distant-level parameter)}, \tag{51}$$

where D_c is the average level spacing and $\oint$ denotes Cauchy's principal value. At low energies (E→0) the effective potential-scattering radius that follows from Eqs. 33 and 36 is

$$R'_c = a_c(1-R^\infty_c). \tag{53}$$

The strength function $S_{\ell J}$ normally used in applied work is related to s_c by

$$S_{\ell J} = 2k_c a_c s_c \sqrt{1eV/E}. \tag{54}$$

The important fact for us is that level-statistical quantities such as $\overline{\gamma^2_c}/D_c$ can be used to adjust the parameters of the optical potential.

(5) Square-well optical potential

For a little numerical exercise let us specialise to a three-dimensional complex square-well potential as in Fig. 2, with the same well radius a for the real and the imaginary part. The natural choice for the channel radii is $a_\ell=a$ for all ℓ.

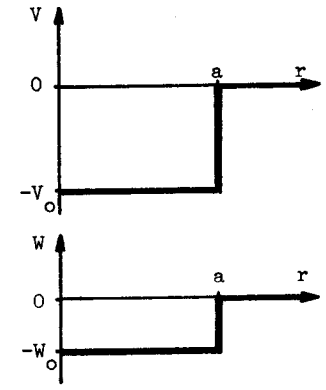

Fig. 2

The eigenfunctions for r<a can now be expressed in terms of the spherical Bessel functions j_ℓ:

$$u_{\lambda\ell}(r) = K_\lambda r\, j_\ell(K_\lambda r) \quad \text{with} \quad K^2_\lambda = \frac{2m}{\hbar^2}(E_\lambda - V_o). \tag{55}$$

$$(u_{\lambda 0}(r)=\sin K_\lambda r,\ u_{\lambda 1}(r)=\sin K_\lambda r/(K_\lambda r)-\cos K_\lambda r, \text{ etc.})$$

For the eigenvalues K_λ or E_λ one has, from Eq. 32,

$$\text{for } \ell=0 \quad B_o \sin K_\lambda a = K_\lambda a \cos K_\lambda a \tag{56}$$

$$\text{for } \ell\geq 1 \quad B_\ell K_\lambda a\, j_\ell(K_\lambda a) = (K_\lambda a)^2\, j_{\ell-1}(K_\lambda a) - \ell K_\lambda a\, j_\ell(K_\lambda a) \tag{57}$$

The last equation follows from the recursion relations for spherical Bessel functions. With $B_\ell=-\ell$, the choice suggested by Eqs. 56 and 57, one finds

$$\text{for } \ell=0 \quad \cos K_\lambda a = 0, \text{ i.e. } E_\lambda = \left(\frac{2\lambda+1}{2}\pi\right)^2 \frac{\hbar^2}{2ma^2} - V_o,\ \gamma^2_{\lambda o} = \frac{\hbar^2}{2ma^2}; \tag{58}$$

$$\text{for } \ell=1 \quad \sin K_\lambda a = 0, \text{ i.e. } E_\lambda = (\lambda\pi)^2 \frac{\hbar^2}{2ma^2} - V_o, \quad \gamma^2_{\lambda 1} = \frac{\hbar^2}{2ma^2};$$

$$\text{for } \ell=2 \quad \tan K_\lambda a = K_\lambda a \qquad \text{etc.}$$

As could be expected from an optical, i.e. wave-mechanical, model the eigenvalues correspond to certain simple ratios between the internal wave length $\Lambda = 2\pi/K$ and the diameter of the potential:

$$2a = \Lambda/2,\ 3\Lambda/2,\ 5\Lambda/2,\ \ldots \qquad \text{for } \ell=0,$$

$$2a = \Lambda,\ 2\Lambda,\ 3\Lambda,\ \ldots \qquad \text{for } \ell=1.$$

The $\gamma^2_{\lambda o}$ and $\gamma^2_{\lambda 1}$ for the square well are the same for all λ and depend only on the range (a) of the real potential. Furthermore, Eqs. 43 and 38 show that $\Gamma_{\lambda a}/2 = W_o$ for all λ and ℓ.

Inserting numbers that are compatible with average neutron cross sections,

$$a = 1.4 \text{ fm} \cdot A^{1/3}, \quad V_o = 50 \text{ MeV}, \quad W_o = 3 \text{ MeV}$$

one gets for a heavy nucleus with A = 238 the resonance parameters of Table 3.

The scattering widths given in Table 3 are defined as usual by

$$\Gamma_{\lambda\ell}(E) = 2P_\ell(E)\gamma_{\lambda\ell}^2 = \Gamma_{\lambda\ell}(|E_\lambda|)P_\ell(E)/P_\ell(|E_\lambda|), \qquad (59)$$

the absolute values ensuring the validity of this definition for subthreshold ("negative") single particle states (E_λ<0) as well as for continuum states with E_λ>0. The levels are rather broad, with total widths $\Gamma_{\lambda a}+\Gamma_{\lambda\ell}$ of about 10 MeV and spacings of about 30 MeV near threshold (E=0).

Table 3: Resonance parameters for a three-dimensional complex square-well potential with a = 1.4 fm $A^{1/3}$, A = 238, V+iW = { $-(50+3i)$MeV for r≤a, 0 for r>a.

ℓ	spectroscopic symbol	E_λ (MeV)	$\gamma_{\lambda\ell}^2$ (MeV)	$2P_\ell(\|E_\lambda\|)$	$\Gamma_{\lambda\ell}(\|E_\lambda\|)$ (MeV)	$\Gamma_{\lambda a}$ (MeV)
0	1s	-49.32	0.275	26.77	7.37	6
	2s	-43.89	"	25.26	6.95	"
	3s	-33.02	"	21.91	6.03	"
	4s	-16.73	"	15.59	4.29	"
	5s	5.00	"	8.52	2.34	"
	6s	32.17	"	21.62	5.95	"
		etc.	"			
1	1p	-47.28	0.275	13.03	3.59	6
	2p	-39.14	"	11.84	3.26	"
	3p	-25.55	"	9.53	2.62	"
	4p	- 6.54	"	4.68	1.29	"
	5p	17.91	"	7.94	2.19	"
	6p	47.78	"	13.10	3.61	"
		etc.				

One can also compare with the neutron strength functions and effective radii observed in the region of resolved resonances (E < 1 MeV) as a function of A (or a). For E=0 our model yields

$$R_\ell^\infty + i\pi s_\ell = \sum_\lambda \frac{\gamma_{\lambda\ell}^2 E_\lambda}{E_\lambda^2+\Gamma_{\lambda a}^2/4} + i\sum_\lambda \frac{\gamma_{\lambda\ell}^2 \Gamma_{\lambda a}/2}{E_\lambda^2+\Gamma_{\lambda a}^2/4} \quad . \qquad (60)$$

The maxima ("size resonances") of s_ℓ are seen to occur where $E_\lambda(a)$=0, i.e. at

$$a = \frac{2\lambda+1}{2}\pi \frac{\hbar}{\sqrt{2mV_o}} \quad \text{for } \ell=0, \qquad (61)$$

$$a = \lambda\pi \frac{\hbar}{\sqrt{2mV_o}} \quad \text{for } \ell=1, \quad \text{etc.}$$

With a = 1.4 fm $A^{1/3}$, V_o = 50 MeV one finds the size resonance positions that are listed in Table 4 together with the observed positions.

Table 4: Size resonance peak positions

ℓ	spectroscopic symbol	nucleon number at peak calculated[a]	observed
0	3s	47	~55
	4s	129	~150
1	2p	24	~25
	3p	81	~90
	4p	193	~210

a) Eqs. 61 with a = 1.4 fm $A^{1/3}$, V = - 50 MeV for r<a.

This should suffice to show the use of level-statistical data in the adjustment of optical-model parameters. Let us now return to the discussion of the various resonance approximations.

2.3.4 The principal approximations to the inverse level matrix

A convenient starting point for the various practically important approximations is the inverse level matrix:

Wigner-Eisenbud representation (exact)

with B_c real and constant,

$$(A^{-1})_{\lambda\mu} = (E_\lambda - E)\delta_{\lambda\mu} - \sum_c \gamma_{\lambda c} L_c^o \gamma_{\mu c} \qquad (20)$$

Kapur-Peierls representation (exact)

with $B_c = L_c$, i.e. $L_c^o = 0$,

$$(A^{-1})_{\lambda\mu} = (\mathcal{E}_\lambda - E)\delta_{\lambda\mu} \tag{62}$$

(eigenvalues $\mathcal{E}_\lambda$ complex, E-dependent).

SLBW approximation

Only one level is retained,

$$(A^{-1})_{\lambda\mu} \to A^{-1} = E_o - E - \sum_c L_c^o \gamma_{\lambda c}^2 \equiv E_o + \Delta - E - i\Gamma/2 \tag{63}$$

(Δ: level shift, $\Gamma = \sum_c \Gamma_c$: total width, both E-dependent, real).

MLBW approximation

All off-diagonal elements are neglected,

$$(A^{-1})_{\lambda\mu} = (E_\lambda - E - \sum_c L_c^o \gamma_{\lambda c}^2)\delta_{\lambda\mu} \equiv (E_\lambda + \Delta_\lambda - E - i\Gamma_\lambda/2)\delta_{\lambda\mu} \tag{64}$$

(Δ_λ: level shift, $\Gamma_\lambda = \sum_c \Gamma_{\lambda c}$: total width, both E-dependent, real).

Reich-Moore approximation

Off-diagonal contributions from photon channels ($c \in \gamma$) are neglected,

$$(A^{-1})_{\lambda\mu} = (E_\lambda + \Delta_{\lambda\gamma} - E - i\Gamma_{\lambda\gamma}/2)\delta_{\lambda\mu} - \sum_{c\in\gamma} \gamma_{\lambda c} L_c^o \gamma_{\mu c} \tag{65}$$

($\Delta_{\lambda\gamma}$: level shift caused by photon channels, $\Gamma_{\lambda\gamma} = \sum_{c\in\gamma} \Gamma_{\lambda c}$: radiation width).

Adler-Adler approximation

The energy dependence of L_c^o is neglected:

$$(A^{-1})_{\lambda\mu} = (E_\lambda - E)\delta_{\lambda\mu} - \sum_c \gamma_{\lambda c} \sqrt{L_c^o(E_\lambda) L_c^o(E_\mu)}\, \gamma_{\mu c} \quad , \tag{66}$$

It should be remembered that for $\ell=0$ everywhere, for $\ell \geq 1$ locally at a given energy, Δ_λ and $\Delta_{\lambda\gamma}$ can be made to vanish in all these expressions, and that the P_c contain (at least) a factor $\sqrt{E}$ for elastic channels (cf. Table 1) but are practically constant for fission and capture channels.

2.3.5 Kapur-Peierls cross section formulae

The Kapur-Peierls collision matrix is

$$U_{cc'} = e^{-i(\phi_c + \phi_{c'})} \left(\delta_{cc'} + i \sum_\lambda \frac{G_{\lambda c}^{1/2} G_{\lambda c'}^{1/2}}{\mathcal{E}_\lambda - E}\right) \tag{67}$$

where we write $\mathcal{E}_\lambda$, $G_{\lambda c} = 2P_c g_{\lambda c}^2$ to distinguish the complex eigenvalues and partial widths from their real Wigner-Eisenbud counterparts E_λ, $\Gamma_{\lambda c} = 2P_c \gamma_{\lambda c}^2$. The corresponding cross section expressions are, in a notation that is convenient for the discussion of Doppler broadening,

$$\begin{aligned}\sigma_c &= 4\pi\lambda\!\!\!^{-2} g_c \left[\sin^2\phi_c + \sum_\lambda \frac{|G_{\lambda c}|}{\Gamma_\lambda}(\psi_\lambda \cos 2\phi_\lambda + \chi_\lambda \sin 2\phi_\lambda)\right] \\ &= 4\pi\lambda\!\!\!^{-2} g_c \left[\sin^2\phi_c + \sum_\lambda \frac{\mathrm{Re}\, G_{\lambda c}}{\Gamma_\lambda}(\psi_\lambda \cos 2\phi_c + \chi_\lambda \sin 2\phi_c)\right. \\ &\qquad \left. + \sum_\lambda \frac{\mathrm{Im}\, G_{\lambda c}}{\Gamma_\lambda}(\psi_\lambda \sin 2\phi_c - \chi_\lambda \cos 2\phi_c)\right],\end{aligned} \tag{68}$$

$$\begin{aligned}\sigma_{cc} = 4\pi\lambda\!\!\!^{-2} g_c \Big[\sum_\lambda \frac{|G_{\lambda c}|^2}{\Gamma_\lambda^2}(\psi_\lambda\, \mathrm{Re}\, C_{\lambda cc} + \chi_\lambda\, \mathrm{Im}\, C_{\lambda cc}) \\ + \sum_\lambda \Big(-\frac{\mathrm{Re}\, G_{\lambda c}}{\Gamma_\lambda}\psi_\lambda + \frac{\mathrm{Im}\, G_{\lambda c}}{\Gamma_\lambda}\chi_\lambda\Big)\Big] + \sigma_c \,,\end{aligned} \tag{69}$$

$$\sigma_{cc'} = 4\pi\lambda\!\!\!^{-2} g_c \sum_\lambda \frac{|G_{\lambda c}\, G_{\lambda c'}|}{\Gamma_\lambda^2}(\psi_\lambda\, \mathrm{Re}\, C_{\lambda cc'} + \chi_\lambda\, \mathrm{Im}\, C_{\lambda cc'}), \tag{70}$$

with

$$\phi_\lambda = \phi_c - \arg g_{\lambda c} = \phi_c - \frac{1}{2}\arctan\frac{\mathrm{Re}\, G_{\lambda c}}{\mathrm{Im}\, G_{\lambda c}} \quad , \tag{71}$$

$$C_{\lambda cc'} = 1 + \sum_{\mu\neq\lambda} \frac{g_{\mu c}}{g_{\lambda c}} \frac{g_{\mu c'}}{g_{\lambda c'}} \frac{i\Gamma_\lambda}{\mathcal{E}_\lambda^* - \mathcal{E}_\mu} \quad , \tag{72}$$

$$\mathcal{E}_\lambda \equiv E_\lambda - i\Gamma_\lambda/2, \qquad G_{\lambda c} = 2P_c g_{\lambda c}^2, \tag{73)(74}$$

and

$$\left.\begin{aligned}\psi_\gamma &= \frac{\Gamma_\lambda^2/4}{(E-E_\lambda)^2 + \Gamma_\lambda^2/4} \equiv \frac{1}{1+x_\lambda^2} \quad , \qquad (75)\\ \chi_\lambda &= \frac{(E-E_\lambda)\Gamma_\lambda/2}{(E-E_\lambda)^2 + \Gamma_\lambda^2/4} = \frac{x_\lambda}{1+x_\lambda^2} \quad . \qquad (76)\end{aligned}\right\}$$ zero-temperature Voigt profiles

In the derivation of Eqs. 69 and 70 we used the partial-fraction decomposition

$$\frac{1}{\mathcal{E}_\lambda - E}\frac{1}{\mathcal{E}_\mu^* - E} = \frac{1}{\mathcal{E}_\mu^* - \mathcal{E}_\lambda}\left(\frac{1}{\mathcal{E}_\lambda - E} - \frac{1}{\mathcal{E}_\mu^* - E}\right). \tag{77}$$

It is thus seen that apart from the potential-scattering term $4\pi\lambda\!\!\!^{-2}g_c \sin^2\phi_c$ all cross sections can be expressed by the symmetric (Lorentzian) and asymmetric Breit-Wigner line shape functions ψ_λ and χ_λ with coefficients that contain a factor P_c (which in turn contains a factor $E^{-1/2}$) and are otherwise weakly energy-dependent. The line shape functions themselves are also slightly distorted because E_λ and Γ_λ are weakly energy-dependent. Note that $\Gamma_\lambda \neq \sum_c |G_{\lambda c}|$ in contrast to the Wigner-Eisenbud relationship $\Gamma_\lambda = \sum_c \Gamma_{\lambda c}$.

2.3.6 SLBW and MLBW cross section formulae

Rather than writing down the well-known SLBW formulae we go immediately to the MLBW case. The collision matrix obtained with Eq. 64 is

$$U_{cc'} = e^{-i(\phi_c+\phi_{c'})}\left(\delta_{cc'} + i\sum_\lambda \frac{\Gamma_{\lambda c}^{1/2}\Gamma_{\lambda c'}^{1/2}}{E_\lambda+\Delta_\lambda-E-i\Gamma_\lambda/2}\right) . \qquad (78)$$

Comparison with the Kapur-Peierls collision matrix (67) shows that we can take over the Kapur-Peierls cross section formulae with the change $E_\lambda \to E_\lambda+\Delta_\lambda$, $\Gamma_\lambda \to \sum_c \Gamma_{\lambda c}$, $g_{\lambda c} \to \gamma_{\lambda c}$. The result is

$$\sigma_c = 4\pi\lambda\!\!\!^{-2}g_c\left[\sin^2\phi_c + \sum_\lambda \frac{\Gamma_{\lambda c}}{\Gamma_\lambda}\left(\psi_\lambda \cos 2\phi_c + \chi_\lambda \sin 2\phi_c\right)\right] \qquad (79)$$

$$\sigma_{cc} = 4\pi\lambda\!\!\!^{-2}g_c \sum_\lambda \left[\frac{\Gamma_{\lambda c}^2}{\Gamma_\lambda^2}\left(\psi_\lambda \,\mathrm{Re}\, C_{\lambda cc} + \chi_\lambda \,\mathrm{Im}\, C_{\lambda cc}\right) - \frac{\Gamma_{\lambda c}}{\Gamma_\lambda}\psi_\lambda\right] + \sigma_c \qquad (80)$$

$$\sigma_{cc'} = 4\pi\lambda\!\!\!^{-2}g_c \sum_\lambda \frac{\Gamma_{\lambda c}\Gamma_{\lambda c'}}{\Gamma_\lambda^2}\left(\psi_\lambda \,\mathrm{Re}\, C_{\lambda cc'} + \chi_\lambda \,\mathrm{Im}\, C_{\lambda cc'}\right), \qquad (81)$$

with
$$C_{\lambda cc'} = 1 + \sum_{\mu\neq\lambda} \frac{\gamma_{\mu c}}{\gamma_{\lambda c}} \frac{i\Gamma_\lambda}{E_\lambda+\Delta_\lambda-E_\mu-\Delta_\mu+i(\Gamma_\lambda+\Gamma_\mu)/2} \frac{\gamma_{\mu c'}}{\gamma_{\lambda c'}} \qquad (82)$$

The SLBW formulae are obtained by specialisation to a single level, with $C_{\lambda cc}=1$. (The sum in Eq. 82 describes level-level interference.)

In contrast to the Kapur-Peierls and the SLBW collision matrices the MLBW collision matrix is not unitary. Therefore non-physical cross sections ($\sigma_c<0$ or $\sigma_c>4\pi\lambda\!\!\!^{-2}g_c$) can occur, but for mild level overlap the MLBW approximation is quite good. In any case it is better than the very popular but often very bad approximation, sometimes termed "many-level Breit-Wigner approximation", that results from omission of the level-level interference sum in Eq. 82 and amounts to simply adding SLBW resonance terms (plus the potential-scattering term in σ_c and σ_{cc}).

The MLBW definition used in the US file ENDF (Ref. 12) is such that Eq. 80 is used for σ_{cc} but level-level interference is neglected by putting $C_{\lambda cc'}=1$ for $\sigma_{cc'}$. The total cross section must then be computed as the sum of all partial cross sections rather than from Eq. 79. This is often justified because level-level interference is usually quite weak for capture (if not for fission or inelastic-scattering) cross sections.

The MLBW approximation corresponds to the first term of the expansion

$$A = (D-N)^{-1} = D^{-1} + D^{-1}ND^{-1} + D^{-1}ND^{-1}ND^{-1} + \ldots \qquad (83)$$

of the level matrix in powers of the nondiagonal part -N of its inverse,

$$N_{\lambda\mu} = (1-\delta_{\lambda\mu})\sum_c \gamma_{\lambda c}L_c^o\gamma_{\mu c} , \qquad (84)$$

$$D_{\lambda\mu} = (E_\lambda+\Delta_\lambda-E-i\Gamma_\lambda/2)\delta_{\lambda\mu} . \qquad (85)$$

Retaining also the second term (Ref. 13) one gets an improved collision matrix,

$$U_{cc'} = e^{-i(\phi_c+\phi_{c'})}\left(\delta_{cc'} + i\sum_\lambda \frac{\Gamma_{\lambda c}^{1/2}W_{\lambda cc'}\Gamma_{\lambda c'}^{1/2}}{E_\lambda+\Delta_\lambda-E-i\Gamma_\lambda/2}\right) \qquad (86)$$

with
$$W_{\lambda cc'} = 1 + \sum_{\mu\neq\lambda}\left(\frac{\gamma_{\mu c}}{\gamma_{\lambda c}} + \frac{\gamma_{\mu c'}}{\gamma_{\lambda c'}}\right)\frac{\sum_{c''}\gamma_{\lambda c''}L_{c''}^o\gamma_{\mu c''}}{E_\mu+\Delta_\mu-E_\lambda-\Delta_\lambda-i(\Gamma_\mu-\Gamma_\lambda)/2} . \qquad (87)$$

Again one can take over the Kapur-Peierls cross section expressions with $E_\lambda \to E_\lambda+\Delta_\lambda$, $\Gamma_\lambda \to \sum_c \Gamma_{\lambda c}$, $G_{\lambda c} \to \Gamma_{\lambda c}W_{\lambda cc}$, $G_{\lambda c}G_{\lambda c'} \to \Gamma_{\lambda c}W_{\lambda cc}^2\Gamma_{\lambda c'}$. The partial widths are now complex but the complex poles of the improved collision matrix, Eq. 85, are still the same as those of the MLBW collision matrix, Eq. 78. This is no longer true if higher-order terms of the von Neumann series Eq. 83 are retained as in Ref. 14.

2.3.7 The Reich-Moore cross section formulae

The inverse level matrix in Reich-Moore approximation, Eq. 65, is exactly what one would derive from a "reduced" R-matrix for particle channels only, with E_λ replaced by $E_\lambda+\Delta_{\lambda\gamma}-i\Gamma_{\lambda\gamma}/2$. In fact, exactly such a reduced R-matrix results if one eliminates the photon channels by means of the Teichmann-Wigner channel elimination method which is the usual way to derive the Reich-Moore formulae (Ref. 15). One can thus calculate all cross sections except that for radiative capture from Eqs. 14, 15 and 17 where R is to be taken as the reduced R-matrix

$$R_{cc'} = \sum_\lambda \frac{\gamma_{\lambda c}\gamma_{\lambda c'}}{\mathcal{E}_{\lambda\gamma}-E} \qquad (c,c' \notin \gamma) \qquad (87)$$

with
$$\mathcal{E}_{\lambda\gamma} = E_\lambda+\Delta_{\lambda\gamma}-i\Gamma_{\lambda\gamma}/2. \qquad (88)$$

The capture cross section can be either calculated as difference,

$$\sigma_{c\gamma} = \sigma_c - \sum_{c'\notin\gamma} \sigma_{cc'} , \qquad (89)$$

or, by generalisation of a result obtained for $\ell=0$ by Harris (Ref. 16), as

$$\sigma_{c\gamma} = \pi\lambda\!\!\!^{-2}g_c \sum_\lambda \Gamma_{\lambda\gamma}\left|\frac{\sum_{c'\notin\gamma}\left|(1-P^{1/2}RL^oP^{-1/2})^{-1}\right|_{cc'}\Gamma_{\lambda c'}^{1/2}}{\mathcal{E}_{\lambda\gamma}-E}\right|^2 \qquad (90)$$

The calculation is quite fast since double sums over levels as in MLBW approximation (cf. Eq. 81) are not needed. The inversion of the reduced matrix $1-RL^o$ is unproblematic since it is usually of rank 1, 2 or 3.

In the most frequent case the only open particle channel is the elastic channel and all matrices reduce to scalar functions. With the definitions

$$\rho_{cc} \equiv \frac{-iR_{cc}P_c}{1-R_{cc}L_c^o} = \frac{-i\sum_\lambda \frac{\Gamma_{\lambda c}/2}{\mathcal{E}_{\lambda\gamma}-E}}{1-\frac{L_c^o}{P_c}\sum_\lambda \frac{\Gamma_{\lambda c}/2}{\mathcal{E}_{\lambda\gamma}-E}} \qquad (91)$$

$$x \equiv \frac{\mathrm{Im}\,\rho_{cc}}{\mathrm{Re}\,\rho_{cc}}\,, \qquad y^2 \equiv \frac{|\rho_{cc}|^2}{\mathrm{Re}\,\rho_{cc}} \qquad (92)\ (93)$$

one gets then expressions which have the formal (and in single-level situations the factual) SLBW form, viz.

$$\sigma_c = 4\pi\lambda\!\!\!^{-2}_c g_c\left(\sin^2\phi_c + y^2\,\frac{\cos 2\phi_c + x\sin 2\phi_c}{1+x^2}\right), \qquad (94)$$

$$\sigma_{c\gamma} = 4\pi\lambda\!\!\!^{-2}_c g_c\, y^2(1-y^2)\,\frac{1}{1+x^2}\,. \qquad (95)$$

For pure elastic scattering, $y^2=1$, one gets, of course, the exact single-channel R-function with

$$x^{-1} = \sum_\lambda x_\lambda^{-1} = \sum_\lambda \frac{\Gamma_\lambda/2}{E-E_\lambda}\,. \qquad (96)$$

The Reich-Moore formalism is thus exact in the limit of one level or one channel and otherwise very accurate. It is fast. Its (nonreduced) collision matrix is unitary (as long as the number of levels does not exceed the number of photon channels which can always be assumed without loss of generality) so that non-physical cross sections are not produced.

2.3.8 The Adler-Adler cross section formulae

The approximation Eq. 66 to the inverse level matrix means essentially that the energy dependence of level shifts (if any) and total widths is ignored. This works very well for fissile nuclei in restricted energy ranges where $\Gamma_\lambda \simeq \Gamma_{\lambda\gamma} + \Gamma_{\lambda f} \simeq$ const, but not for light or medium-mass nuclei for which $\Gamma_\lambda \simeq \Gamma_{\lambda n} = 2P_\ell(E)\gamma_{\lambda n}^2$ with $P_\ell(E)$ given in Table 1. Diagonalising the inverse level matrix Eq. 66 by orthogonal transformation one finds a collision matrix of the Kapur-Peierls form, Eq. 67. Its poles $\mathcal{E}_\lambda$ and reduced width amplitudes $g_{\lambda c}$ are energy-independent as in the S-matrix formalism developed by Siegert, Humblet and Rosenfeld (Refs. 18, 19), but unitarity is not automatically guaranteed.

The Adler-Adler cross section formulae (Refs. 17, 20, 21) are usually written not for specific channels (c, c') but for specific reaction types (total, n, f, γ, ...) and restricted to $\ell=0$:

$$\sigma \equiv \sum_{c\in n}\sigma_c = \sigma_p + \frac{1}{\sqrt{E}}\sum_\lambda \frac{1}{\nu_\lambda}\left(G_\lambda^{(T)}\psi_\lambda - H_\lambda^{(T)}\chi_\lambda\right), \qquad (97)$$

$$\sigma_x \equiv \sum_{c\in n}\sum_{c'\in x}\sigma_{cc'} = \frac{1}{\sqrt{E}}\sum_\lambda \frac{1}{\nu_\lambda}\left(G_\lambda^{(x)}\psi_\lambda - H_\lambda^{(x)}\chi_\lambda\right), \quad (x=\gamma,f,n)\,, \qquad (98)$$

where σ_p is the potential-scattering cross section, the $G_\lambda^{(x)}/(\sqrt{E}\nu_\lambda)$, $H_\lambda^{(x)}/(\sqrt{E}\nu_\lambda)$ are sums over all coefficients of ψ_λ, χ_λ in Eqs. 68-70, respectively, with $\nu_\lambda \equiv \Gamma_\lambda/2$ and $\sqrt{E}$ stemming from $P_c(E)$. The λ-sums extend over all contributing levels irrespective of JΠ, the spin factors g_c being absorbed in the coefficients $G_\lambda^{(x)}$, $H_\lambda^{(x)}$. In principle one could even define Adler-Adler parameters for isotopic mixtures by similarly absorbing the relative abundances also in the $G_\lambda^{(x)}$, $H_\lambda^{(x)}$.

Inversion of the usually quite high-dimensional matrix A^{-1} is possible by brute force on modern computers (Refs. 17, 20, 21) but the orthogonal transformation involved is so complicated that simple conversion formulae giving the $\mathcal{E}_\lambda$, $g_{\lambda c}$ (or $G_\lambda^{(x)}$, $H_\lambda^{(x)}$) in terms of the E_λ, $\gamma_{\lambda c}$ are not available except for the case of a single level (see Sect. 3.2 below). As a consequence the statistical laws for Adler-Adler or, generally, Kapur-Peierls parameters could not be derived from the known statistics of the Wigner-Eisenbud parameters. An improvement of the conversion with respect to energy-dependent partial widths was recently discussed by Segev (Ref. 22).

Further discussion of the advantages and weaknesses of the various approximate resonance formalisms will be deferred until Doppler broadening has been treated.

2.4. Theory of Doppler broadening

In most practical applications of resonance cross sections these are needed in Doppler-broadened form. It is sometimes argued that for light nuclei Doppler broadening can be neglected. This, however, is true only for the broad s-wave levels but certainly not for the very narrow p-, d- ...wave levels of these nuclei which in the case of structural materials contribute significantly to resonance absorption and Doppler coefficient in fast reactors.

2.4.1 Free-gas approximation

Doppler broadening is caused by thermal motion of the target nuclei. Consider a parallel beam of monoenergetic particles with lab velocity v colliding with target nuclei whose velocities $\vec{u}$ are distributed in such a way that $p(\vec{u})d^3u$ is the fraction with velocities in a small three-dimensional region d^3u around $\vec{u}$. If ρ_1 and ρ_2 are the densities of beam and target particles, respectively, the number of reactions occurring per unit time and unit volume is

$$\rho_1\rho_2 \int d^3u\; p(\vec{u})\;|\vec{v}-\vec{u}|\;\sigma(|\vec{v}-\vec{u}|) \equiv \rho_1\rho_2 v\,\bar{\sigma}(v) \qquad (99)$$

where $\bar{\sigma}(v)$ is the effective or Doppler-broadened cross section for incident particles with speed v. Obviously a 1/v cross section is not affected by Doppler broadening. Let us now assume that the target nuclei have the same velocity distribution as the atoms of an ideal gas, i.e. the Maxwell-Boltzmann distribution,

$$p(\vec{u})d^3u = \frac{1}{\pi^{3/2}}\exp\left(-\frac{u^2}{u_T^2}\right)\frac{d^3u}{u_T^3}, \qquad \frac{M}{2}u_T^2 \equiv kT, \qquad (100)$$

where M is the nuclear mass and kT the gas temperature in energy units. Integrating over all possible relative velocities $\vec{w}=\vec{v}-\vec{u}$ and using polar coordinates, $d^3u = d^3w = w^2dw\,d(\cos\theta)d\phi$, with the polar axis parallel to the beam, one finds the exact free-gas expression for the Doppler-broadened cross section,

$$\bar{\sigma}(v) = \frac{1}{v\sqrt{\pi}}\int_0^\infty \frac{dw}{u_T}\frac{w^2}{v^2}\left(e^{-(v-w)^2/u_T^2} - e^{-(v+w)^2/u_T^2}\right)\sigma(w) \qquad (101)$$

In terms of lab energies, $E = mv^2/2$, this is

$$\bar{\sigma}(E) = \frac{1}{\Delta\sqrt{\pi}} \int_0^\infty dE' \left(e^{-4(E-\sqrt{EE'})^2/\Delta^2} - e^{-4(E+\sqrt{EE'})^2/\Delta^2}\right) \sqrt{\frac{E'}{E}}\, \sigma(E') \qquad (102)$$

where
$$\Delta = \sqrt{\frac{4kTE}{M/m}} = 2\frac{u_T}{v} E \qquad (103)$$

is called the Doppler width. For $E \gg \Delta$, i.e. $v \gg 2u_T$, which is the case above a few eV, one can simplify by retaining only the first two terms of the expansion

$$\sqrt{EE'} = E + \frac{E'-E}{2} + \ldots , \qquad (104)$$

by neglecting the second exponential and by replacing $\int_0^\infty$ by $\int_{-\infty}^\infty$ in the first integral. The result is

$$\sqrt{E}\,\bar{\sigma}(E) = \frac{1}{\Delta\sqrt{\pi}} \int_{-\infty}^\infty dE'\, e^{-(E'-E)^2/\Delta^2} \sqrt{E'}\, \sigma(E') . \qquad (105)$$

2.4.2 Cubic crystal

Lamb (Ref. 23) obtained the same expression for radiative capture by the bound atoms of a Debye crystal if $\Gamma+\Delta \geq 4\,kT_D$, where T_D is the Debye temperature. The only difference is that one must use an effective ("Lamb-corrected") temperature

$$T_L = T\left(\frac{T}{T_D}\right)^3 \frac{3}{2} \int_0^{T_D/T} dx\, x^3 \coth\frac{x}{2} = T\left(1 + \frac{1}{20}\frac{T_D^2}{T^2} - + \ldots\right) \qquad (106)$$

that is usually only a few percent higher than the actual crystal temperature T. Using the theory of quasi-free scattering one can extend these results to scattering and to cubic crystals in general (Ref. 24). It is common practice to compute Doppler-broadened cross sections with Eq. 105. For very low energies it may be better to use Eq. 102, i.e. the exact free-gas kernel. In any case the Doppler width, Eq. 104, must be calculated with the Lamb-corrected temperature, Eq. 106, for which a curve is given in Ref. 23 (see also Ref. 56, p.26).

2.4.3 Voigt profiles vs. numerical broadening

Let us now consider Doppler broadening of resonances. We saw that all resonance cross sections in SLBW, MLBW and Adler-Adler approximation can be written as sums of terms of the form $c/(1+x^2)$ or $cx/(1+x^2)$ where the coefficients c contain a factor $E^{-1/2}$ and otherwise depend only weakly on energy. As a consequence one needs the convolutions of $1/(1+x^2)$ and $x/(1+x^2)$ with a Gaussian, the so-called Voigt profiles (Ref. 25),

$$\psi(x,\beta) = \frac{1}{\beta\sqrt{\pi}} \int_{-\infty}^\infty dx'\, e^{-(x-x')^2/\beta^2} \frac{1}{1+x'^2} \qquad (107)$$

$$\chi(x,\beta) = \frac{1}{\beta\sqrt{\pi}} \int_{-\infty}^\infty dx'\, e^{-(x-x')^2/\beta^2} \frac{x'}{1+x'^2} \qquad (108)$$

with
$$x = \frac{E-E_o}{\Gamma/2} , \qquad \beta = \frac{\Delta}{\Gamma/2} . \qquad (109)(110)$$

The quantity β is called the Doppler parameter, Δ,Γ and possibly a level shift (here absorbed in E_o) are to be calculated at the energy for which the broadened cross section is needed. These functions, which occur also in the theory of atomic spectra, are well known (Refs. 25, 26). Fast algorithms are available for computer calculations (Ref. 27). This explains the popularity of SLBW and MLBW formulae even in cases of strongly interfering levels where they are quite inadequate.

The Kapur-Peierls, MLBW and Adler-Adler cross section expressions (Eqs. 68-70, 79-81, 97-98) remain valid also for Doppler-broadened cross sections if the zero-temperature Voigt profiles $\psi_\lambda, \chi_\lambda$ are replaced by the broadened profiles, Eqs. 107-108.

An interesting property of both the exact and the approximate free-gas formulae (Eqs. 102 and 105) is that if one knows the effective cross section for a temperature T_1 one can get that for a higher temperature T_2 by simply broadening with a Doppler width calculated for the difference T_2-T_1, without going back to the unbroadened cross section (Ref. 28). Likewise one can combine Doppler and resolution broadening (see below) of a cross section if the resolution function has the same form as the Doppler kernel, e.g. Gaussian. One simply replaces Δ by $\sqrt{\Delta^2+W^2}$ where W is the resolution width defined analogously to Δ (Ref. 28).

Cross sections of the Reich-Moore type must be numerically broadened. Once enough unbroadened cross section points for linear interpolation with a given accuracy are calculated the problem is reduced to piece-wise convolution of a straight line and a Gaussian which results in error functions and exponentials, again well known and rapidly calculated functions (cf. also Ref. 27). With modern computers these methods can be quite fast, and the Reich-Moore formalism is so attractive, that the recent decision to strike it from the ENDF conventions appears ill-considered.

Assessing merits and drawbacks of the various approximate resonance formulae one should realise that the fastest way to calculate unbroadened cross sections on a computer is not by way of explicit cross section expressions such as Eqs. 68-70, 79-81, 97-98. It is much faster to compute the required collision matrix elements and then to use Eqs. 14 and 15. Use of the explicit cross section expressions is necessary only if resonance broadening is to be calculated by means of the Voigt profiles. In other words, the Voigt profiles require considerable preparatory computations that are not needed for numerical broadening. The convenience of MLBW or Adler-Adler parameters for Doppler broadening should therefore not be overestimated - in multi-level situations it is at least partially offset by the need to utilize the explicit cross section expressions with their time-consuming double sums. Furthermore, the approximations involved lead to cross sections that differ from the exact R-matrix cross sections. The difference is sometimes added as a "smooth" cross section which is considered as unaffected by Doppler broadening (e.g. in the ENDF system). This entails additional preparatory work and, since the "smooth" component is not really smooth near strongly interfering resonances (cf. Ref. 20b) still does not remove all discrepancies for Doppler-broadened cross sections.

In the case of Adler-Adler parameters additional problems exist: If they are derived from Wigner-Eisenbud (e.g. Reich-Moore) parameters one must invert large level matrices, if they are directly determined in a fit procedure one has the consistency problems connected with the unitarity of the collision matrix. There are twice as many real parameters as in the Wigner-Eisenbud case.

In conclusion it is perhaps fair to say that the real, constant R-matrix parameters of the Wigner-Eisenbud or Reich-Moore type should be considered as basic, whereas the complex Kapur-Peierls or Adler-Adler parameters should be considered as an auxiliary representation for Doppler broadening.

2.4.4 Temperature-dependent self-shielding, importance of level spins

In reactor calculations cross sections are usually not required in the form of "microscopic" data with the whole detailed resonance structure. Instead one employs group cross sections. These are defined as flux-weighted averages over certain energy (or rather lethargy) intervals, the group intervals. In the widely used narrow-resonance approximation, which is based on the assumption that the Doppler-broadened resonances are narrow compared to the average energy loss of a scattered neutron, $(\Delta^2+\Gamma^2)^{1/2} << 2AE/(A+1)^2$, the flux over a resonance is proportional to the inverse total cross section. The group cross section of a given nuclide (or element) for the (n,x) reaction can then be written as

$$\bar{\sigma}_x = \frac{\left\langle \frac{\sigma_x}{\sigma+d} \right\rangle}{\left\langle \frac{1}{\sigma+d} \right\rangle} , \qquad (111)$$

where σ_x and $\sigma=\sum_x \sigma_x$ are the (n,x) and total Doppler-broadened cross sections of the nuclide (or element), d is the so-called dilution cross section describing the admixture of other elements, and

$$\langle \ldots \rangle \equiv \int_{\Delta E} dE\, N(E) \ldots \qquad (112)$$

is an integral over the group interval ΔE with the smooth collision function N(E) as weight function. The dilution cross section d is usually taken as constant in ΔE. The self-shielding factors f_x are defined by the factorisation (T denotes the temperature)

$$\bar{\sigma}_x(d,T) \equiv \bar{\sigma}_x(\infty,T)\cdot f_x(d,T), \qquad \text{with} \qquad (113)$$

$$\bar{\sigma}_x(\infty,T) = \langle \sigma_x \rangle . \qquad (114)$$

The group cross section for infinite dilution is just the (collision-function-weighted) average cross section in the usual sense. It is independent of d and, apart from edge effects at the interval boundaries, also of T. Thus f_x contains all d and almost all T dependence. With the usual definition of the covariance,

$$\mathrm{cov}(x,y) = \left\langle (x-\langle x\rangle)(y-\langle y\rangle) \right\rangle , \qquad (115)$$

one can write

$$f_x(d,t) = 1 + \mathrm{cov}\left(\frac{\sigma_x}{\langle \sigma_x \rangle} , \frac{1/(\sigma+d)}{\langle 1/(\sigma+d)\rangle}\right). \qquad (116)$$

Now peaks in σ_x coincide usually with dips in $1/(\sigma+d)$ and vice versa. The covariance is then negative and

$$0 < f_x < 1. \qquad (117)$$

Growing dilution or growing temperature both tend to reduce the covariance so that normally

$$\frac{\partial f_x}{\partial d} > 0, \qquad \frac{\partial f_x}{\partial T} > 0 . \qquad (118)(119$$

Exceptional behaviour may be caused by

- edge effects at the group boundaries, or
- inadequacy of the narrow-resonance approximation near very broad resonances, or
- pronounced resonance-potential interference dips ("windows") in the total cross section. These have no counterparts in the fission or capture cross section and can therefore over-compensate the influence of the peaks on the covariance.

We get more insight with explicit cross section expressions. Neglecting edge effects, level-level interference and resonance-potential interference we write

$$\sigma = \sum_\lambda (\sigma_o \psi)_\lambda + \sigma_p , \qquad (120)$$

$$\sigma_x = \sum_\lambda (\sigma_o \psi \frac{\Gamma_x}{\Gamma})_\lambda , \qquad (121)$$

where $\sigma_o = 4\pi\lambda\!\!\!^{-}(E_o)^2 g\Gamma_n/\Gamma$ is the peak total cross section (unbroadened), ψ the symmetric Voigt profile and σ_p the potential scattering cross section. If the resonances are very narrow and well separated one can treat their contributions to $\bar{\sigma}_x$ independently which results in

$$\bar{\sigma}_x(d,T) \approx \frac{1}{\Delta E} \sum_\lambda N(E_\lambda) A_{\lambda x}\, f(\beta_\lambda,\kappa_\lambda) , \qquad (122)$$

$$\bar{\sigma}_x(\infty,T) \approx \frac{1}{\Delta E} \sum_\lambda N(E_\lambda) A_{\lambda x} , \qquad (123)$$

with

$$A_{\lambda x} = \int dE\, (\sigma_o \psi \frac{\Gamma_x}{\Gamma})_\lambda = 2\pi^2 \lambda\!\!\!^{-}(E_\lambda)^2 (g\frac{\Gamma_n \Gamma_x}{\Gamma})_\lambda \text{ (peak area)}, \qquad (124)$$

$$f(\beta,\kappa) = \frac{2}{\pi}\kappa \int_0^\infty dx \frac{\psi(x,\beta)}{\psi(x,\beta)+\kappa} = \frac{2}{\pi}\kappa J(\beta,\kappa) , \qquad (125)$$

$$\beta_\lambda = \frac{\Delta(E_\lambda)}{\Gamma_\lambda/2} , \qquad \kappa_\lambda = \frac{d+\sigma_p}{\sigma_{o\lambda}} . \qquad (126)(127)$$

The universal function $f(\beta,\kappa)$ can be interpreted as the self-shielding factor of an isolated, symmetric, narrow resonance which depends on the Doppler parameter β and the dilution parameter κ. It obeys the inequalities 117-119 as can be seen from Fig. 3. With Eqs. 122 and 123 one gets

$$f_x(d,T) \approx \frac{\sum_\lambda N(E_\lambda) A_{\lambda x}\, f(\beta_\lambda,\kappa_\lambda)}{\sum_\lambda N(E_\lambda) A_{\lambda x}} . \qquad (128)$$

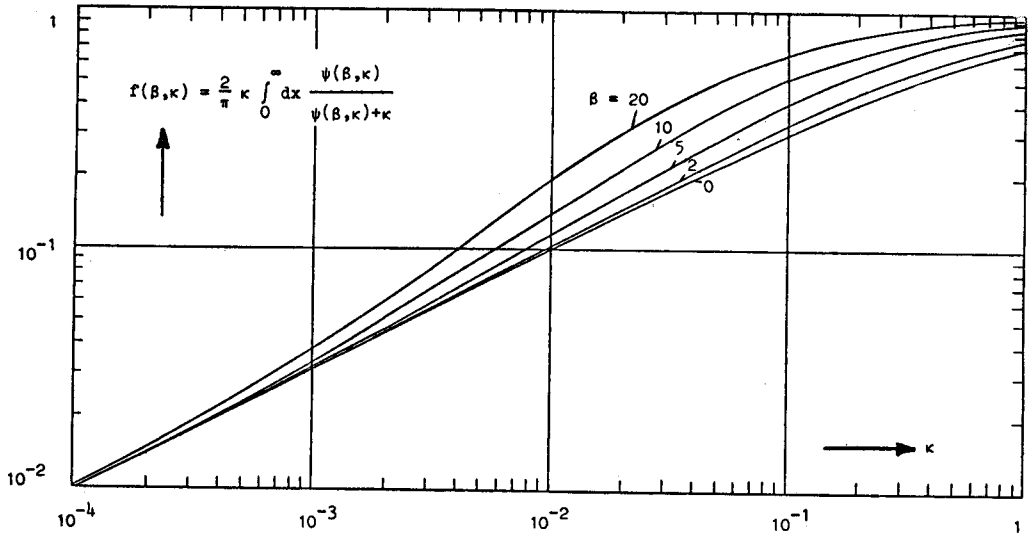

Fig. 3 - Dependence of the narrow-resonance self-shielding factor $f(\beta,\kappa)$ on temperature ($\beta = 2\Delta/\Gamma$) and dilution ($\kappa = (d+\sigma_p)/\sigma_o$).

Thus f_x is a weighted average of the individual narrow-resonance self-shielding factors, the weights being proportional to the areas of the (n,x) cross section peaks $A_{\lambda x}$ and to the local collision densities $N(E_\lambda)$. Eqs. 120-128 were derived for a single isotope. They are also valid for isotopic mixtures if $\sigma_{o\lambda}$ and $A_{\lambda x}$ are taken as containing the isotopic abundance as a factor.

An important remark concerns the **level** spins. The SLBW peak area is proportional to $g\Gamma_n\Gamma_x/\Gamma$. For narrow resonances this quantity is, apart from E_o, usually the only information one has. For broad resonances one knows frequently also $g\Gamma_n$ and, mostly for s-wave levels, even g. Now knowledge of E_o and $g\Gamma_n\Gamma_x/\Gamma$ enables one to calculate $\bar{\sigma}_x(\infty,T)$, cf. Eq. 123, but not $\bar{\sigma}_x(d,T)$ or $f_x(d,T)$. The reason is that in order to calculate $f(\beta,\kappa)$ one must know Γ and this requires knowledge of g, $g\Gamma_n$ and $g\Gamma_n\Gamma_x/\Gamma$. In other words, the peak area alone does not tell whether the peak is broad or narrow, and even the quantity $g\Gamma_n$ does not help much. For a given peak area it is mainly the spin that determines the width and thus the contribution to the self-shielded cross section and especially to its temperature variation: The narrower a resonance, the stronger its response to temperature changes.

An illustration is provided by the so-called structural materials (iron, nickel and other steel components). Their capture cross sections are dominated by very narrow p-, d-...wave levels for which capture peak areas are measured but not Γ or g (excepting very recent data on ^{56}Fe, Ref. 31). In order to calculate realistic self-shielded group constants one must resort to Monte Carlo sampling of spin and neutron widths based on level statistics (Ref. 32). In a fast reactor the increase of neutron capture with temperature (due to increasing f, see Fig. 3 and Eq. 122) expressed by the so-called Doppler coefficient, is the only inherent, automatically functioning safety feature. Hence the practical importance of good data on g (besides $g\Gamma_n$ and $g\Gamma_n\Gamma_x/\Gamma$) is obvious. Experimental spin determination for p, d,...wave levels is at present a widely open field.

2.4.5 Westcott factors

The energy distribution of the neutrons in a thermal reactor is well described by the Maxwell-Boltzmann energy distribution obtained from Eq. 100 by integration over all angles,

$$p(E)dE = \frac{2}{\sqrt{\pi}} \exp(-\frac{E}{kT})\sqrt{\frac{E}{kT}}\ \frac{dE}{kT}, \qquad (129)$$

and a 1/E tail. The (n,x) reaction rate induced by this spectrum can be written as

$$\int_0^\infty dE\ p(E)\sqrt{E}\ \bar{\sigma}_x(E) \equiv \sqrt{kT}\ \bar{\sigma}_x(kT)g_W \qquad (130)$$

where $\bar{\sigma}_x(E)$ is the Doppler-broadened (n,x) cross section for temperature T and $\sqrt{kT}\bar{\sigma}_x(kT)$ is the result one would get for a 1/v cross section. The factor g_W defined by Eq. 130, the so-called Westcott factor, is thus seen to correct the reaction rate for deviations from 1/v behaviour of the Doppler-broadened cross section. Westcott factors are conventient for reaction rate calculations in thermal fluxes since usually the (Doppler-broadened) thermal cross sections $\bar{\sigma}_x(kT)$ are well known, and since low-energy reaction cross sections show 1/v behaviour more or less modified by nearby positive or negative levels. Westcott factors are normally tabulated for room temperature, kT = 0.0253 eV.

2.5 Observables

Cross section measurements, as a rule, do not yield cross sections directly but more or less complicated functions or functionals of the cross sections.

2.5.1 Transmission

The simplest measurement is that of the total cross section σ. One measures that fraction of beam particles of a given energy which traverses without interaction a sample of given thickness n (atoms/b). This fraction, the transmission, for a very small thickness of material Δn is $1-\sigma\Delta n$. For finite thickness it is

$$T = \lim_{n/\Delta n\to\infty} (1-\sigma\Delta n)^{n/\Delta n} = e^{-n\sigma}. \qquad (131)$$

The cross section is thus essentially the logarithm of the observable.

2.5.2 Reaction yield

The (n,x) reaction yield Y_x (x=f,γ,...), i.e. the fraction of beam particles that undergoes an (n,x) reaction in the sample, is composed of contributions from multiple-collision events with zero, one, two etc. preceding scattering collisions,

$$Y_x = Y_{xo} + Y_{x1} + Y_{x2} + \ldots \tag{132}$$

where

$$Y_{xo} = \frac{1-T}{\sigma}\,\sigma_x,$$

$$Y_{x1} = \frac{1-T}{\sigma}\,\sigma_n \left\langle \frac{1-T_1}{\sigma_1}\,\sigma_{x1} \right\rangle_1, \tag{133}$$

$$Y_{x2} = \frac{1-T}{\sigma}\,\sigma_n \left\langle \frac{1-T_1}{\sigma_1}\,\sigma_{n1} \left\langle \frac{1-T_2}{\sigma_2}\,\sigma_{x2} \right\rangle_2 \right\rangle_1$$

etc.

The numerical subscript indicates the number of preceding collisions so that $1-T_1$, for instance, is the probability that after the first collision the scattered neutron interacts again in the sample. The brackets $\langle\,\rangle_1$, $\langle\,\rangle_2$ etc. denote averages over all first, second etc. scattering collisions, which means over all possible spatial coordinates and scattering angles. Note that in each elastic scattering collision the energy of a beam particle changes from E to E' according to

$$E' = E\,\frac{A^2+2A\mu_c+1}{(A+1)^2} \tag{134}$$

if the target particle is at rest initially. Here μ_c is the cosine of the c.m.s. scattering angle and A the mass ratio (target to beam particle). In the resonance region this means that the cross sections to be used before and after the collision can differ dramatically. The multiple-collision yields Y_{x1}, Y_{x2} etc. are therefore very complicated functionals of σ_x, σ_n and σ. If inelastic scattering is energetically possible σ_n is to be taken as the sum of the elastic and inelastic scattering cross sections, and $\langle\,\rangle_1$ etc. include averaging over all possible scattering modes. The thin-sample approximation,

$$Y_x \approx n\sigma_x \qquad \text{for} \qquad n\sigma \ll 1\ , \tag{135}$$

is often accurate enough for fission yields (x=f) where the sample must be so thin that the fission fragments can get out. In capture data analysis, however, one must usually include multiple-collision terms and the self-shielding factors (1-T)/(nσ) because samples are thicker and the ratios σ_n/σ are much greater than in fission data analysis.

2.5.3 Differential scattering yield

Sample thickness effects, i.e. self-shielding and multiple scattering, are also quite important in scattering measurements. In analogy to Eqs. 132-133 one has

$$dY_n = dY_{n1} + dY_{n2} + dY_{n3} + \ldots \tag{136}$$

where

$$dY_{n1} = \frac{1-T}{\sigma}\,\frac{d\sigma_n}{d\Omega}\left\langle T_1 \right\rangle_1 d\Omega$$

$$dY_{n2} = \frac{1-T}{\sigma}\,\sigma_n \left\langle \frac{1-T_1}{\sigma_1}\,\frac{d\sigma_{n1}}{d\Omega_1} \left\langle T_2 \right\rangle_2 \right\rangle_1 d\Omega \tag{137}$$

$$dY_{n3} = \frac{1-T}{\sigma}\,\sigma_n \left\langle \frac{1-T_1}{\sigma_1}\,\sigma_{n1} \left\langle \frac{1-T_2}{\sigma_2}\,\frac{d\sigma_{n2}}{d\Omega_2} \left\langle T_3 \right\rangle_3 \right\rangle_2 \right\rangle_1 d\Omega$$

etc.

Here dΩ is a solid-angle element covered by the detector.

2.5.4 Self-indication (n,x) data

From our discussion of (n,x) yields it is clear that (except for very thin samples) extraction of the (n,x) cross section σ_x from (n,x) yields requires also the total cross section σ. Quite generally one can state that the availability of good total cross section data is a prerequisite for good partial cross section data analysis. Another data type which is valuable especially for area analysis (see below) is obtained with the self-indication method. One uses two samples of the same material, a filter sample (thickness n_1) and a detector sample (thickness n_2). The probability for a beam particle to undergo an (n,x) reaction in the second sample is

$$S_x(n_1,n_2) = T(n_1)Y_x(n_2). \tag{138}$$

The result is essentially a measurement of the filter-sample transmission with a detector system (detector sample plus detector) that has enhanced efficiency across the transmission dips (at the resonance energies).

2.5.5 Semi-empirical determination of self-shielded group cross sections

An interesting application of the self-indication method is the semi-empirical determination of self-shielded group cross sections (Ref. 33). Observed data are always resolution-broadened. Indicating this broadening by average brackets we can write self-indication data taken with a thin detector sample

$$\frac{1}{n_2}\left\langle T(n_1)Y_x(n_2) \right\rangle = \left\langle e^{-n_1\sigma}\,\sigma_x \right\rangle \qquad \text{for } n_2\sigma \ll 1. \tag{139}$$

Suppose this quantity and also the average transmission was measured with a sufficient number of different filter samples to permit numerical evaluation of the integrals

$$\int_0^\infty dn \left\langle e^{-n\sigma} \right\rangle = \left\langle \frac{1}{\sigma} \right\rangle \qquad (140)$$

$$\int_0^\infty dn\, e^{-nd} \left\langle e^{-n\sigma} \right\rangle = \left\langle \frac{1}{\sigma+d} \right\rangle \qquad (141)$$

$$\int_0^\infty dn\, e^{-nd} \left\langle e^{-n\sigma}\sigma_x \right\rangle = \left\langle \frac{\sigma_x}{\sigma+d} \right\rangle \qquad (142)$$

where e^{-nd} with arbitrary d is applied artificially. Comparison with the definition of group cross sections, Eq. 111, shows that this method yields group cross sections for zero dilution as well as for arbitrary dilution cross section d, for the temperature of the samples and for a group interval that corresponds to the resolution width (which can be arbitrarily enlarged by additional numerical broadening, of course).

Various types of observables are shown in Figs. 10-12, 15-19.

2.6 Experimental complications

We shall now briefly review the main causes for corrections and uncertainties in nuclear resonance data measurements.

2.6.1 Backgrounds

In time-of-flight measurements there are always two types of background: constant and time-dependent. Constant background may be due to radioactivity of the sample and its environs, time-dependent backgrounds are produced by the accelerator pulses and the sample. An example is the background caused by resonance-scattered neutrons in neutron resonance capture measurements (Refs. 34,35) that reflects the resonance structure of the scattering cross section and is thus violently energy-dependent. This influence of the sample on backgrounds makes "sample-out" background determinations often quite doubtful. Therefore one uses "notch filters", special samples placed in front of the sample under study. The ideal notch filter has a few widely spaced resonances and is so thick that at their peaks all beam particles are removed. Counts observed at these notch energies are then pure background. This allows background measurements at a few points during the actual run. Of course no "true" data can be measured across the notches, so one uses a few complementary notch filters.

2.6.2 Resolution broadening

It was already mentioned that observed data are always resolution-broadened. Strictly speaking the observables are

$$\bar{T}(E) = \int dE'\, r(E',E)T(E'),\ \bar{Y}_x(E) = \int dE'\, r(E',E)Y_x(E'),\ \ldots \qquad (143)(144)$$

where $dE'r(E',E)$ is the probability that an event observed at energy E (or the corresponding flight time) was actually due to a beam particle with an energy E' in dE'. The main causes are:

- finite accelerator pulse width (t_b),
- finite time channel width (t_c),
- electronic drifts, jitter (t_d),
- uncertain starting point (e.g. in moderator slab or booster) and end point (e.g. in sample or ^{6}Li glass detector) of flight path (δL),
- finite angular resolution in scattering experiments ($\delta\theta$).

The resolution function r(E',E) is normally not well known. Frequently a Gaussian is assumed in data fitting work,

$$r(E',E) = \frac{1}{W\sqrt{\pi}}\, e^{(E'-E)^2/W^2} \qquad (145)$$

with, for instance (cf. Refs. 36-38)

$$W = 2E\left[2\left(\frac{\delta L}{L}\right)^2 + \frac{E}{3mL^2}\left(t_b^2+t_c^2+t_d^2\right)\right]^{1/2} = E\sqrt{c_1+c_2E}\ . \qquad (146)$$

Often slight variation of c_1, c_2 improves the fit but sometimes it is necessary to use other, asymmetric resolution functions, e.g. χ^2 functions (Ref. 38) or Gaussians with tails (Ref. 39).

2.6.3 Detector efficiency and flux

In partial cross section measurements the raw data are count rates,

$$c = \phi Y_x \varepsilon \quad (\simeq \phi n\sigma_x\varepsilon \text{ for } n\sigma \ll 1). \qquad (147)$$

Absolute determination of the flux ϕ and the detector efficiency ε is difficult and is therefore almost always avoided. One usually measures relative to a reference sample (subscript r),

$$\frac{c}{c_r} = \frac{Y_x\varepsilon}{Y_r\varepsilon_r} \quad \left(\simeq \frac{n\sigma_x\varepsilon}{n_r\sigma_r\varepsilon_r} \text{ for } n\sigma \ll 1,\ n_r\sigma_r \ll 1\right), \qquad (148)$$

for which Y_r is known with good accuracy. This eliminates the need to know the flux but still one may have problems with n/n_r and $\varepsilon/\varepsilon_r$ as the thin-sample expression shows. Frequently used reference cross sections are listed in Table 5 together with the accuracies achieved at present.

Table 5: Reference cross sections and accuracies
(1 standard deviation, indicative only)

Reaction	Accuracy	Energies	Detector systems
^{1}H(n,p)	± 1 %	< 10 MeV	plastic and liquid scintillators, counter telescopes
^{6}Li(n,t)	± 2 %	< 100 keV	glass scintillators, semiconductor detectors
^{10}B(n,αγ)	± 2 %	< 100 keV	slab samples viewed by γ-detectors
^{12}C(n,n)	± 2 %	< 5 MeV	graphite samples
^{197}Au(n,γ)	± 4 %	< 3.5 MeV	metal foils viewed by γ-detectors
^{235}U(n,f)	± 3 %	< 8 MeV	fission chambers

If the energy dependence of $\varepsilon/\varepsilon_r$ is known one can determine the absolute value, i.e. the calibration, by normalising to an accurately known cross section value, for instance the thermal cross section. If no suitable known value exists one can often use the saturated-resonance (black-sample) technique: One uses a special sample which is so thick that at a well known resonance the transmission is practically zero (cf. Fig. 11 below). Quite generally one has

$$(1-T)\,\frac{\sigma_x}{\sigma} < Y_x < 1-T. \qquad (149)$$

With $c=\phi Y_x \varepsilon$ this gives at the resonance peak, $E=E_o$, where the sample is black,

$$c < \varepsilon\phi < c\,\frac{\sigma(E_o)}{\sigma_x(E_o)}\,. \qquad (150)$$

If $\sigma \approx \sigma_x$ (i.e. $\Gamma \approx \Gamma_x$) one gets, without further calculation, a quite accurate value for $\varepsilon\phi$. The 4.91 eV resonance of ^{197}Au+n, for example, was frequently used for black-sample normalisation of capture data. With the resonance parameters in the "barn book" (Ref. 4) one calculates in SLBW approximation $\sigma(E_o)/\sigma_\gamma(E_o) \approx 1.12$, i.e. a ± 6 % uncertainty of $\varepsilon\phi$ which is easily reduced further by a multiple-scattering calculation which obviously need not be very accurate. Serious problems are created if the detector efficiency varies from isotope to isotope or, even worse, from resonance to resonance. This is a persistent source of difficulties, for example, with capture measurements. Here the detector response depends on the gamma spectrum (binding energy, transition strength to low-lying levels etc.) and thus fluctuates from level to level in an unpredictable way, especially for relatively light nuclei. A reliable estimation of $\varepsilon/\varepsilon_r$ is then impossible without supplementary data on the gamma spectra of individual resonances (Ref. 40).

2.6.4 Self-shielding and multiple scattering

All partial cross section data are more or less affected by self-shielding and multiple scattering. The corresponding corrections are practically most important for neutron capture and scattering data. Fission cross section measurements based on the observation of fission fragments, on the other hand, require such thin samples that self-shielding and multiple scattering are much less important than self-absorption of fission fragments in the sample. The effect of self-shielding is described by the beam-attenuation factors $(1-T)/(n\sigma)$ in Eqs. 133 and 137 whereas multiple scattering leads to the higher-order terms in the collision expansions Eqs. 132 and 136. As these equations show the two effects are interrelated and cannot be treated separately. Both together are referred to as sample-thickness effects.

As mentioned above the multiple-collision yields are complicated functionals of the cross sections. This means that they depend not simply on the cross sections for the primary energy but on all cross sections for the whole range of energies that a neutron can attain successively during a multiple-collision event (cf. Eq. 134). The average brackets $\langle \ldots \rangle_k$ in Eqs. 133 and 137 denote averages for the k-th collision over

- the distribution of scattering angles θ,

$$p(\mu)d\mu = \frac{4\pi}{\sigma_{nk}}\,\frac{d\sigma_{nk}}{d\Omega}\,\frac{d\mu}{2},\quad -1 < \mu \equiv \cos\theta \le 1, \qquad (151)$$

- the distribution of azimuths ϕ (uniform for zero polarisation)

$$p(\phi)d\phi = \frac{d\phi}{2\pi}\,, \qquad 0 < \phi \le 2\pi \qquad (152)$$

- the distribution of the number s of mean free paths to the next collision,

$$p(s)ds = \frac{e^{-s}}{1-e^{-s_k}}\,, \qquad 0 < s \le s_k \equiv n_x\sigma_k \qquad (153)$$

where n_k is the material thickness (nuclei/b) that a neutron would have to traverse after the k-th collision in order to reach the sample surface and to escape. Since n_k and σ_k depend on the particulars (spatial coordinates, angles, corresponding energy losses) of all preceding collisions one sees that the multiple-collision yields are given by multi-dimensional integrals of rapidly increasing dimensionality. Already the second-collision yield for the simplest sample geometry, viz. infinite slab, looks fairly complicated:

$$Y_{x1} = (1-e^{-n\sigma})\,\frac{4\pi}{\sigma}\int_{-1}^{1}\frac{d\mu}{2}\,\frac{d\sigma_n}{d\Omega}\,\left(1-\frac{1-e^{t-t'}}{t-t'}\,\frac{t}{1-e^{t}}\right) \qquad (154)$$

with

$$t \equiv \mu\,\frac{n\sigma}{|\mu|}\,, \qquad t' \equiv \frac{n\sigma_1}{|\mu|}\,, \qquad (155)(156)$$

The simplest way to calculate such complicated integrals on a computer is to sample the multi-dimensional integrands at random and then to average, which is tantamount to simulation of multiple-collision events with the Monte Carlo technique. For each subsequent collision of such an event one must sample the distributions (151)-(153) and, if inelastic scattering is energetically allowed, also the relative probabilities for elastic or inelastic scattering.

Practical sampling methods employ a random-number generator. This is a function subroutine that is usually part of the computer software just as exponentials, sines, cosines etc. Each time it is called it returns a floating-point number picked at random (i.e. from a uniform distribution) in the interval 0...1. Two principal methods exist to sample a distribution p(x)dx with the help of a random-number generator:

(1) Call the random-number generator once. Equate the random number ρ to the integral distribution,

$$\rho = P(x) = \int_0^x p(x')dx', \qquad (157)$$

and solve for x. The frequency distribution of the x values thus obtained is just p(x)dx. This method is convenient if x can be expressed in closed form (examples: Eqs. 152, 153, counter-example: Gaussian distribution).

(2) Rejection method (v. Neumann): Rescale, if necessary, so that $0 < x' < 1$, $0 < p(x') < 1$. If the range of the distribution is infinite one can substitute e.g. $x=x'/(1-x')$ (if $0\le x<\infty$) or $x'=(1+\tanh x)/2$ (if $-\infty<x<\infty$) etc. Get two numbers ρ_1, ρ_2 from the random-number generator. Accept $x'=\rho_1$ if $\rho_2 \le p(\rho_1)$, reject otherwise and begin again. This works always, even for very complicated or tabulated p(x).

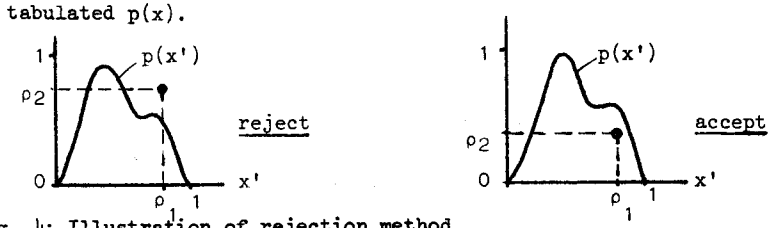

Fig. 4: Illustration of rejection method

Usually it is most convenient to sample the c.m.s. scattering angles and then to convert to the lab system (cf. Ref. 38). At low energies, for example, s-wave scattering is isotropic in the c.m.s. system so that $p(\mu_c)d\mu_c = d\mu_c/2$ with $\mu_c = \cos\theta_c$ (the subscript c indicates c.m.s. quantities). From μ_c one gets the energy of the scattered neutron (Eq. 134) and thus the new cross sections. The latter must be available in tabulated form for convenient interpolation. The new total cross section and the distance to the sample surface determine the total interaction probability ($1-T_k$ in Eqs. 133, 137). A flow diagram for multiple-collision capture yield calculation is shown in Fig. 5.

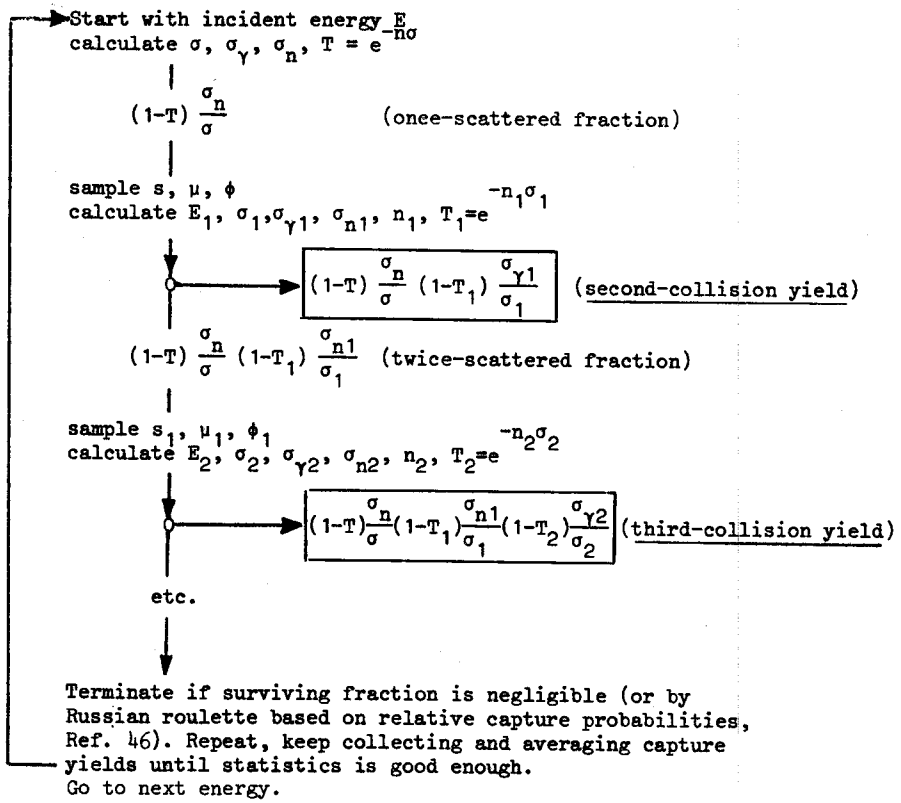

Fig. 5: Flow diagram for multiple-collision capture yield calculation by Monte Carlo simulation

2.7 Resonance parameter estimation

The ideal resonance parameter analysis is based on data measured with isotopically pure samples and proceeds as follows.

(1) From transmission data one determines essentially

$$E_o,\ \Gamma_n,\ \Gamma,\ g \quad \text{for } \ell = 0,$$
$$E_o,\ g\Gamma_n \quad \text{for } \ell \geq 1.$$

(2) The transmission results permit calculation of sample-thickness corrections for yield data from which one gets essentially

$$E_o,\ \Gamma_x \quad \text{if } \Gamma_n, g \text{ are known},$$
$$E_o,\ g\Gamma_x \quad \text{if } g\Gamma_n \text{ is known}.$$

(3) If transmission results are not available (p-, d-, ... levels are not easily observed in transmission experiments) one gets only

$$E_o,\ g\Gamma_n\Gamma_x/\Gamma \quad \text{if } g\Gamma_n \text{ is not known}.$$

The determination of JΠ (and thus g) is usually based on transmission or scattering data. Apart from complications for fissile nuclei or strong level overlap one can usually use the interference between resonant and potential scattering to determine ℓ or at least to distinguish between ℓ=0 and ℓ≥1, whereas the resonance peak height (see Eq. 195 below) and level-level interference allow determination of J.

The best way to extract resonance parameters from transmission, yield, self-indication etc. data is by least-squares analysis. Because of its practical importance and for convenient reference we briefly review the least-squares formalism with explicit account of statistical and systematic errors.

2.7.1 The least-squares method

Let us consider

observables y_i $(i = 1,2,\ldots I)$,

parameters x_μ $(\mu = 1,2,\ldots M<I)$,

and a mathematical model

$$y_i = y_i(x_1,x_2,\ldots x_M) \equiv y_i(\vec{x}) \tag{158}$$

that allows us to calculate the observables (e.g. resolution-broadened transmissions, yields etc.) from the (resonance) parameters. Let us further assume that all y_i were measured with the results $\eta_i \pm \sigma_i$ (σ_i: standard deviation), which actually means that the true value y_i lies in dy_i with the probability

$$p(y_i)dy_i = \exp\left[-\frac{1}{2}\left(\frac{y_i-\eta_i}{\sigma_i}\right)^2\right]\frac{dy_i}{\sigma_i\sqrt{2\pi}} \tag{159}$$

if we assume a Gaussian distribution of the errors as is usual in error estimation. What is the parameter vector $\vec{x}$ which best explains the observed data η_i? It is not very difficult to see (Ref. 41) that it is determined by the requirement that the

joint probability $\Pi_i p(y_i)dy_i$ for all the measurements be maximal, or

$$\frac{\partial \chi^2}{\partial x_\mu} \equiv \frac{\partial}{\partial x_\mu} \sum_i \left(\frac{y_i - \eta_i}{\sigma_i}\right)^2 = 0, \qquad \mu = 1,2,\ldots M. \tag{160}$$

This is the least-squares principle. The M Eqs. 160 for the M unknown parameters x_μ can be solved immediately if the relationship between y_i and $\vec{x}$ is linear. In our case it is definitely not linear so we must iterate. Let $\vec{x}'$ be an approximation to $\vec{x}$ so that

$$y_i(\vec{x}) = y_i(\vec{x}') + \sum_\mu y_{i,\mu}(\vec{x}')(x_\mu - x'_\mu) + \ldots \tag{161}$$

with

$$y_{i,\mu} \equiv \frac{\partial y_i}{\partial x_\mu}. \tag{162}$$

Truncating the Taylor series (161) after the linear term and introducing the notation

$$(B^{-1})_{\mu\nu} \equiv \sum_{i=1}^{I} \frac{y_{i,\mu}(\vec{x}')}{\sigma_i} \frac{y_{i,\nu}(\vec{x}')}{\sigma_i} = (B^{-1})_{\nu\mu} \tag{163}$$

$$c_\mu \equiv \sum_{i=1}^{I} \frac{y_{i,\mu}(\vec{x}')}{\sigma_i} \frac{\eta_i - y_i(\vec{x}')}{\sigma_i} \tag{164}$$

we get the linear system of "normal equations"

$$\sum_{\nu=1}^{M} (B^{-1})_{\mu\nu} (x_\nu - x'_\nu) = c_\mu \quad \text{or} \quad B^{-1}(\vec{x} - \vec{x}') = c \tag{165}$$

Its solution,

$$x_\mu = x'_\mu + \sum_{\nu=1}^{M} B_{\mu\nu} c_\nu \quad \text{or} \quad \vec{x} = \vec{x}' + Bc \tag{166}$$

can be improved by iteration until χ^2 remains constant. It is seen that in each step the MxM matrix B^{-1} must be inverted and values for all observables and their derivatives must be computed.

2.7.2 Error propagation in least-squares fits

What uncertainty in the adjusted parameters x_μ follows from the data uncertainties σ_i? If we denote the unknown errors of the η_i by $\delta\eta_i$ we have, in linear approximation,

$$\delta x_\mu = \sum_i \frac{\partial x_\mu}{\partial \eta_i} \delta\eta_i = \sum_i \sum_\nu B_{\mu\nu} \frac{y_{\nu,i}}{\sigma_i^2} \delta\eta_i \tag{167}$$

(cf. Eq. 166). The uncertainty to be quoted for x_μ is the square root of $\mathrm{var}(x_\mu) = \langle \delta x_\mu^2 \rangle$ where the average brackets indicate the expectation value. Generalising slightly we calculate

$$\langle \delta x_\mu \, \delta x_\nu \rangle = \sum_{i,j} \sum_{\kappa,\lambda} B_{\mu\kappa} \frac{y_{i,\kappa}}{\sigma_i^2} \langle \delta\eta_i \delta\eta_j \rangle \frac{y_{j,\lambda}}{\sigma_j^2} B_{\lambda\nu}. \tag{168}$$

If the data uncertainties $\delta\eta_i$ are mutually independent,

$$\langle \delta\eta_i \delta\eta_j \rangle = \mathrm{var}(\eta_i)\delta_{ij} = \sigma_i^2 \delta_{ij}, \tag{169}$$

one gets simply

$$\langle \delta x_\mu \, \delta x_\nu \rangle = (B\, B^{-1}\, B)_{\mu\nu} = B_{\mu\nu}. \tag{170}$$

In most cases, however, $\sigma_i^2 = \mathrm{var}(x_\mu)$ is a sum of squared statistical and systematic uncertainties. The statistical errors are usually uncorrelated but the systematic errors are not. One has then instead of Eqs. 169, 170

$$\langle \delta\eta_i \delta\eta_j \rangle = \sigma_i^2 \delta_{ij} + \tau_{ij}(1 - \delta_{ij}), \tag{171}$$

$$\langle \delta x_\mu \delta x_\nu \rangle = B_{\mu\nu} + \sum_{i,j \neq i} \sum_{\kappa,\lambda} B_{\mu\kappa} \frac{y_{i,\kappa}}{\sigma_i^2} \tau_{ij} \frac{y_{j,\lambda}}{\sigma_j^2} B_{\lambda\nu} \tag{172}$$

where τ_{ij} describes the correlation. Let us take, for example, the η_i as time-of-flight count rates all affected by the same error δb in background subtraction. Then $\tau_{ij} = (\delta b)^2$ and $\sigma_i^2 = (\sqrt{\eta_i})^2 + (\delta b)^2$, $\sqrt{\eta_i}$ being the statistical error. If there is also a common normalisation error δc one has $\tau_{ij} = (\delta b)^2 + \eta_i \eta_j (\delta c/c)^2$, $\sigma_i^2 = (\sqrt{\eta_i})^2 + (\delta b)^2 + \eta_i^2 (\delta c/c)^2$ etc. This illustrates how important it is that experimenters state clearly and in as much detail as possible the statistical and systematic error components. One might add that it is similarly important that those who extract cross section parameters from experimental data should state not just the parameters x_μ and the variances $\langle \delta x_\mu^2 \rangle$ or the corresponding standard deviations but also at least the more important elements of the covariance matrix $\langle \delta x_\mu \delta x_\nu \rangle$. The uncertainty of a function f of the parameters x_μ, for instance a calculated cross section or transmission value, is given by the variance

$$\langle \delta f^2 \rangle = \left\langle \left(\sum_\mu \frac{\partial f}{\partial x_\mu} \delta x_\mu\right)^2 \right\rangle = \sum_{\mu,\nu} \frac{\partial f}{\partial x_\mu} \langle \delta x_\mu \delta x_\nu \rangle \frac{\partial f}{\partial x_\nu}, \tag{173}$$

so that a good error estimation or sensitivity study is not possible without the covariance matrix or at least its more important elements.

2.7.3 Goodness of fit

The minimal χ^2 obtained provides a means to check the consistency of mathematical model (Eq. 158) and data and the goodness of fit. The probability that a measurement of I observables y_i results in a χ^2-value within $d\chi^2$ is derived as follows: The range $\chi^2 \ldots \chi^2 + d\chi^2$ corresponds to a "spherical" shell in the I-dimensional space of the y_i/σ_i. Replacing the volume element $\Pi_i (dy_i/\sigma_i)$ in Eq. 159 by the volume of this infinitesimal shell and normalising properly one finds the probability

$$p(\chi^2)d\chi^2 = \Gamma\left(\frac{I}{2}\right)^{-1} \left(\frac{\chi^2}{2}\right)^{I/2-1} \exp\left(-\frac{\chi^2}{2}\right) \frac{d\chi^2}{2}. \tag{174}$$

In practice one does not know the true χ^2 (relative to the true y_i) but only that relative to the most likely estimate. This can be taken into account if I is replaced by I-M, the effective degree of freedom (M: number of estimated parameters), so that

$$p(\chi^2)d\chi^2 = \Gamma\left(\frac{I-M}{2}\right)^{-1} \left(\frac{\chi^2}{2}\right)^{(I-M)/2-1} \exp\left(-\frac{\chi^2}{2}\right) \frac{d\chi^2}{2} \tag{177}$$

with the expectation values

$$\langle \chi^2 \rangle = I - M, \qquad \mathrm{var}\,\chi^2 = 2(I-M). \tag{178)(179}$$

Thus χ^2 can be expected to be about equal to the effective degree of freedom: $\chi^2 \approx (I-M) \pm \sqrt{2(I-M)}$. If it is much larger the fit must be considered as bad because either

- the mathematical model is inadequate, or
- the data are faulty, or
- the data errors were underestimated.

Frequently the last explanation is the correct one: systematic errors are often underestimated or not recognised at all. One should then rescale all errors as follows,

$$\sigma_i \to \sigma_i \sqrt{\frac{\chi^2}{I-M}}\,, \qquad \delta x_\mu \to \delta x_\mu \sqrt{\frac{\chi^2}{I-M}}\,. \tag{180)(181}$$

Inadequacy of the mathematical model can mean that an unrecognised resonance is present or a resonance spin is wrong.

2.7.4 Area analysis

The simplest method to extract resonance parameters from measured data is area analysis. The fitted quantities (y_i in the least-squares formulae of the preceding sections) are taken to be the areas of transmission dips

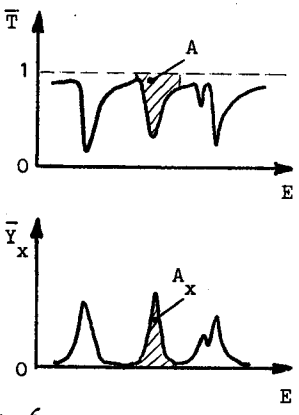

Fig. 6

$$A = \int dE(1-e^{-n\bar{\sigma}}) \simeq \frac{\Gamma}{2}\int_{-\infty}^{\infty} dx\,(1-e^{-n\sigma_o\psi(x,\beta)}), \tag{182}$$

(n,x) peaks,

$$A_x = \int dE(1-e^{-n\bar{\sigma}})\,\frac{\bar{\sigma}_x}{\bar{\sigma}} \simeq A\,\frac{\Gamma_x}{\Gamma}\,, \tag{183}$$

or ratios of such areas, e.g. the (n,x) self-indication ratio

$$R = \frac{\int dE\; e^{-n'\bar{\sigma}}(1-e^{-n\bar{\sigma}})\,\frac{\bar{\sigma}_x}{\bar{\sigma}}}{\int dE(1-e^{-n\bar{\sigma}})\,\frac{\bar{\sigma}_x}{\bar{\sigma}}} \simeq \frac{A(n+n')-A(n')}{A(n)} \tag{184}$$

where the bars denote Doppler broadening, ψ is the Voigt profile, Eq. 75, and

$$\sigma_o = (4\pi\lambda^2\, g\frac{\Gamma_n}{\Gamma})_{E=E_o}\,, \qquad x = \frac{E-E_o}{\Gamma/2}\,. \tag{185)(186}$$

Ideally all these quantities are measured with the same set-up in the same flux. A capture measurement, for example, is easily extended to yield transmission and self-indication data, too, by insertion of a filter sample in front of the capture sample. One can then measure in alternating cycles filter transmission (capture sample out), self-indication data (both samples in) and capture yield (filter sample out). In order to optimise the sample thicknesses and choice of observables one considers (Refs. 42, 43) the SLBW thin- and thick-sample expressions that follow from the properties of the Voigt profiles if potential and multiple scattering is neglected (or subtracted out),

$$A = \pi n\sigma_o\Gamma/2, \qquad A_x = \pi n\sigma_o\Gamma_x/2 \qquad (n\bar{\sigma} \ll 1), \tag{187)(188}$$

$$A = \Gamma\sqrt{\pi n\sigma_o}, \qquad A_x = \Gamma_x\sqrt{\pi n\sigma_o} \qquad (n\bar{\sigma} \gg 1). \tag{189)(190}$$

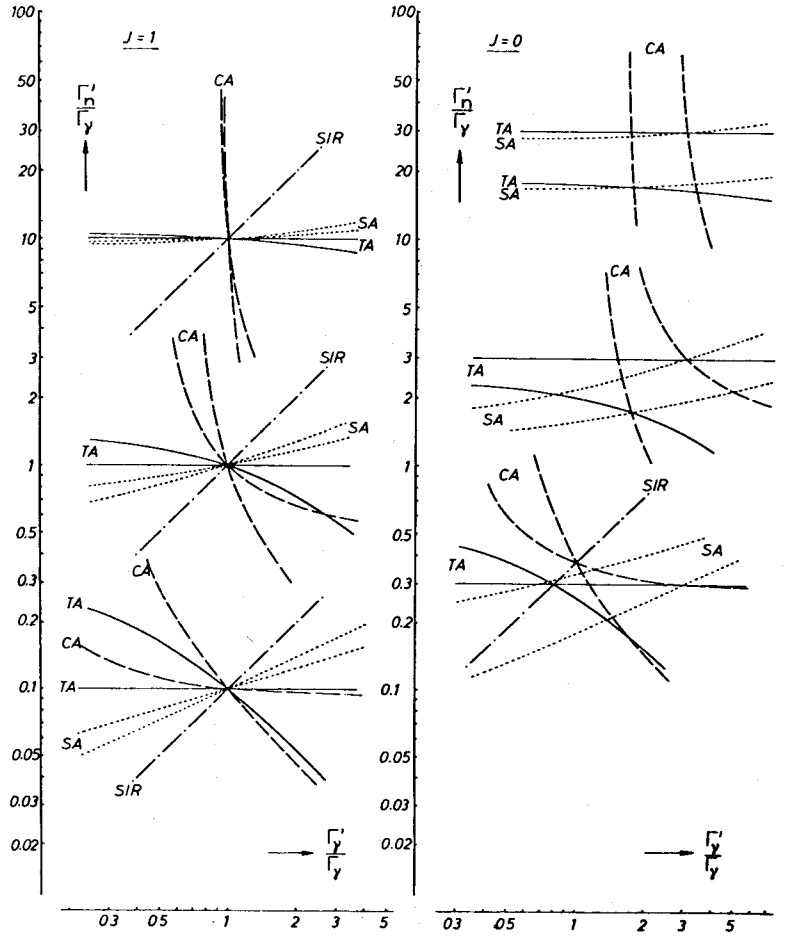

Fig. 7 - Idealised area analysis curves derived under the assumption that the samples are either very thin or very thick for transmission areas (TA), capture areas (CA) and scattering areas (SA), and that self-indication ratios (SIR) were measured with a thick filter and a thin detector sample, or vice versa. Abscissae and ordinates are calculated values Γ'_γ and Γ'_n in units of the true radiation width Γ_γ, on a log-log scale. Three cases are shown: strong, intermediate and weak scattering ($\Gamma_n:\Gamma_\gamma$ = 10, 1, 0.1, respectively). The curves on the left were derived with the correct spin factor - they are independent of J. The curves on the right demonstrate what happens if the spin factor is taken three times too small - this corresponds to an incorrect compound spin J = 0 and a correct spin J = 1. A realistic example is shown in Fig. 9.

Similarly one gets for thick filter and thin detector sample

$$R_x = \frac{1}{\sqrt{\pi n' \bar{\sigma}_o}} \qquad (n'\bar{\sigma} \gg 1,\ n\bar{\sigma} \ll 1). \qquad (191)$$

Equating these theoretical expressions to the measured quantities one sees that, for given level energy E_o and spin factor g, each one defines an equation between the partial widths of the form $\eta_i = y_i(\Gamma_n,\Gamma_\gamma,\Gamma_f,\ldots)$. The most important case for non-fissile nuclei, $\Gamma = \Gamma_n+\Gamma_\gamma$ is represented by 2-dimensional plots (Ref. 43) in Fig. 7. Each equation defines a curve, for the correct g and zero experimental errors all curves intersect in one point. In practice the intersection is not perfect but usually much better than that for an incorrect spin, so that the correct spin is readily recognised. One wants the curves to intersect at angles approaching 90° so that the parameter pair is well defined. For which choice of observables this is achieved depends on the ratio Γ_n/Γ_γ, see Table 6. Very weak resonances are difficult to see in transmission data, even with thick samples.

Table 6: Best Combinations of Observables for Area Analysis if $\Gamma = \Gamma_n+\Gamma_\gamma$

Resonance Type	Best Combinations	Uncertainties (%) $\delta\Gamma_n/\Gamma_n$	Uncertainties (%) $\delta\Gamma_\gamma/\Gamma_\gamma$
$\Gamma_n > \Gamma_\gamma$, strong scattering	(A_γ,A), (R_γ,A)	∿ 2	10 - 20
$\Gamma_n \sim \Gamma_\gamma$, intermediate "	(R_γ,A), (R_γ,A_γ)	∿ 5	5 - 10
$\Gamma_n < \Gamma_\gamma$, weak "	(R_γ,A), (R_γ,A_γ)	5 - 10	10 - 20
$\Gamma_n \ll \Gamma_\gamma$, very weak "	(R_γ,A_γ)	5 - 10	≳ 20

The uncertainties $\delta\Gamma_\gamma$ for strong resonances are mainly due to those of multiple-collision calculations while those for weak levels are mostly caused by backgrounds and statistics.

The principal advantage of area analysis is the insensitivity of areas to resolution broadening, at least as far as the resonance dips or peaks are well separated.

2.7.5 Shape analysis

If adjacent resonances (doublets, triplets etc.) are incompletely resolved instrumentally and the resolution function is well known shape analysis is superior to area analysis. The same is true if very many levels must be analysed. In general shape analysis is more convenient and utilises all the information contained in the data.

The y_i in our least-squares formulae are now the individual data points. There is nothing in the formalism that restricts one to a single resonance or a single set of data points. In a single computer run one can adjust all resonance parameters within a given energy range by simultaneously fitting all relevant transmission, capture, fission ... data points irrespective of experiment, sample thickness, instrumental resolution etc. The only condition is that for all η_i the corresponding theoretical values y_i and their derivatives $y_{i,\mu}$ with respect to the adjusted parameters can be calculated. Of course this is normally beyond hand calculation and one relies heavily on computer codes which in turn have their own limitations as to data types, number of data points, number of cross section parameters that can be handled etc. As mentioned already it is best to analyse all transmission data before one starts fitting yield data.

2.7.6 Computer codes

The initially employed graph methods for area analysis of neutron resonances (Refs. 37, 44) are no longer needed since least-squares computer codes have been developped. A widely used area analysis code was written by Atta and Harvey (Ref. 45) for transmission data analysis. The TACASI code (Ref. 46) for combined transmission area, capture area and self-indication ratio analysis contains the necessary Monte Carlo subroutines for simulation of multiple-collision events. Both these codes employ the "many-level" Breit-Wigner formalism (simple sums over SLBW resonance terms), Doppler broadening by means of Voigt profiles and resolution broadening with a Gaussian. The Atta-Harvey code, however, uses the approximation $\phi_c \ll 1$ which may cause difficulties with s-wave levels at keV energies. An area analysis code for scattering data is under development at CBNM Geel (Ref. 47). As an example TACASI handles simultaneously

≤ 20 observed transmission areas, capture areas and/or self-indication ratios,

≤ 7 resonances, i.e. one main resonance with adjusted Γ_n and Γ_γ, plus up to 6 subresonances with fixed parameters for the calculation of resonance overlap and sample impurity corrections.

TACASI versions that also handle a single observed quantity and adjust one parameter, e.g. Γ_γ, were developped at KfK (Ref. 48) and CBNM Geel (Ref. 49).

The next generation of codes was developed for shape analysis. Some shape analysis codes require data reduced to cross section form, the more convenient ones handle transmission and yield data directly. The following codes fit Doppler- and resolution-broadened cross sections:

- the Reich-Moore code for σ_T and σ_f developped by Derrien, described in Ref. 50;
- the very flexible Reich-Moore program ACSAP (Ref. 51) for $\sigma_T,\sigma_n,\sigma_\gamma,\sigma_f$;
- the Adler-Adler program CODILLI (Ref. 52) for σ_T and σ_f, restricted to heavy nuclei.

Examples for automatic shape analysis codes for transmission data are

- the Atta-Harvey many-level Breit-Wigner shape code, Ref. 45, restricted to nonfissile nuclei and cases with $\phi_c \ll 1$ (below few keV for s-wave levels);
- The MLBW code SIOB ("seven in one blow", i.e. 7 transmission runs fitted simultaneously) suited for heavy non-fissile nuclei (Ref. 53);
- the elaborate and ponderous one-channel Reich-Moore code REFIT (Ref. 54) that fits up to 20 transmission runs simultaneously by adjustment of up to 100 cross section parameters; suited for heavy as well as for light nuclei;
- the FANAL code (Ref. 36) that was written for light and medium-mass nuclei below 400 keV. It employs two-channel Reich-Moore formulae without Doppler broadening for (1 elastic, 1 inelastic) s-wave channels, SLBW formulae for p-, d-... wave channels, fits 5 runs simultaneously by adjustment of up to 50 parameters and is very fast due to the hybrid cross section representation.

All these codes include Doppler-broadening (numerical for Reich-Moore cross sections, exception: s-wave levels in FANAL) and resolution broadening.

Automatic shape analysis programs for yield data are not so numerous yet. The multiple-collision yield, usually calculated by Monte Carlo simulation, presents difficulties in the least-squares formalism because its derivatives are not normally available. One operational shape code is

- FANAC (Ref. 38). It is written for light and medium-mass nuclei below 400 keV, employs the same hybrid cross section formalism as FANAL (see above) but contains, in addition, Monte Carlo subroutines for multiple-collision simulation. It fits up to 5 experimental runs by adjustment of up to 20 resonance parameters.

- The REFIT program (see above) is being extended to include capture shape analysis, too.

Illustrations for some of these codes are given in Figs. 9-19.

2.8 Miscellaneous useful resonance-theoretical expressions

2.8.1 Maxima and minima (windows) in the total cross section

Setting the cross section derivative with respect to energy equal to zero one finds expressions for the energies where the extrema of the cross section occur. Neglecting slow energy dependences (of $\lambda\!\!\!^{-}_c$, L_c, ϕ_c) one gets in SLBW approximation for the maximum

$$E_+ = E_o + \frac{\Gamma}{2}\tan\phi_c, \qquad \sigma_c(E_+) = 4\pi\lambda\!\!\!^{-2}_c g_c \,, \qquad (192)(193)$$

and for the minimum ("window") caused by interference between potential and resonant scattering

$$E_- = E_o - \frac{\Gamma}{2}\cot\phi_c, \qquad \sigma_c(E_-) = 4\pi\lambda\!\!\!^{-2}_c g_c\left(1-\frac{\Gamma_n}{\Gamma}\right), \qquad (194)(195)$$

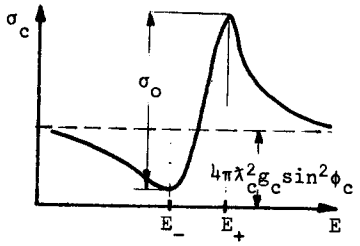

Fig. 8

whence

$$E_o = E_+ \cos^2\phi_c + E_- \sin^2\phi_c \,, \qquad (196)$$

$$\Gamma = (E_+ - E_-)\sin 2\phi_c \,, \qquad (197)$$

$$\sigma_o = 4\pi\lambda\!\!\!^{-2}_c g_c \frac{\Gamma_n}{\Gamma} = \sigma_c(E_+) - \sigma_c(E_-). \qquad (198)$$

For light and medium-weight nuclei, for which Doppler and resolution broadening are often negligible, these relationships are quite useful to determine g_c, i.e. J (Eq. 193), as well as first guesses for E_o, Γ and Γ_n (Eqs. 196-198) directly from the observed extrema. Note that the nominal resonance energy, E_o, is different from the energy at the peak, E_+. The interference dip is the deeper the less absorption one has. For pure elastic scattering ($\Gamma=\Gamma_n$) one gets $\sigma_c(E_-) = 0$. In the minima the observed total cross section may therefore be dominated by other channels (partial waves), other levels and impurities. Other relationships that can provide starting values for least-squares analysis are the SLBW area expressions

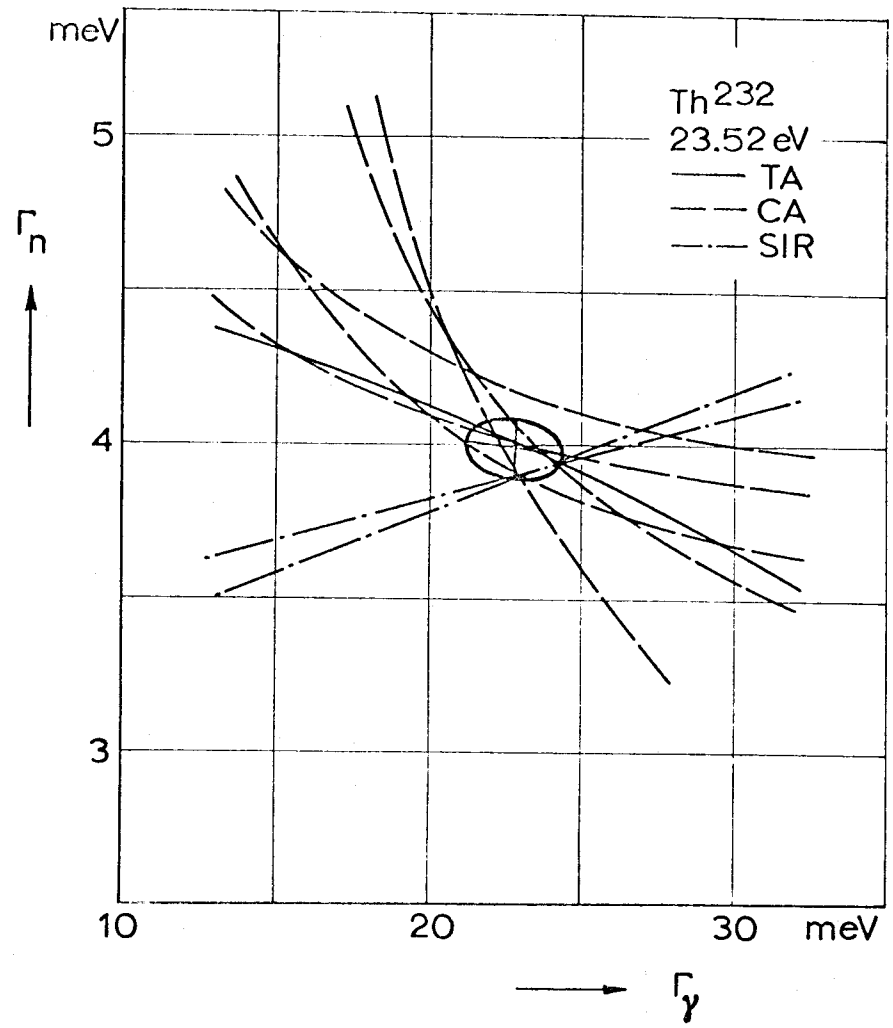

Fig. 9 - Area analysis curves from transmission areas, capture areas and self-indication ratios (TA, CA, SIR) measured for a resonance of ^{232}Th+n with different sample thicknesses. The error ellipse illustrates the final result of a simultaneous fit with the TACASI code, viz. Γ_γ, Γ_n, the uncertainties and the correlation (see Ref. 46).

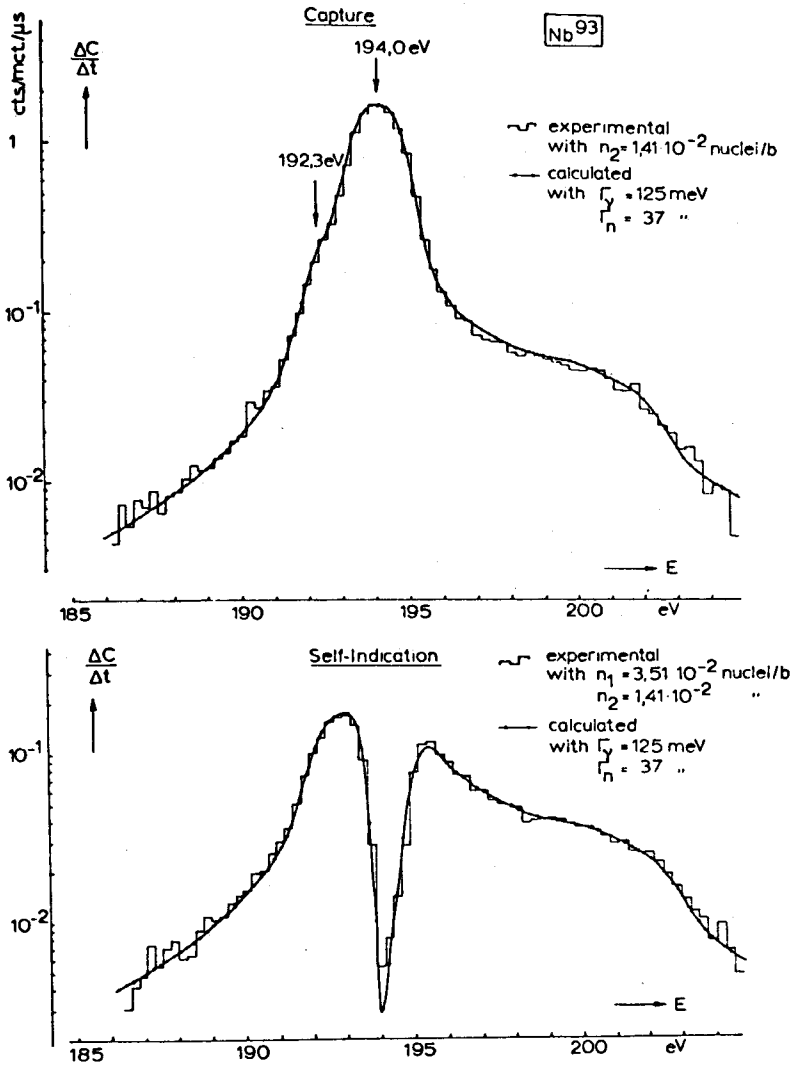

Fig. 10 - Measured (histograms) and calculated (smooth curves) capture and self-indication count rates near the 194 eV resonance of ^{93}Nb+n. The enhancement around 200 eV is due to multiple scattering: The low-energy maximum of the self-indication curve is higher than the high-energy one because of the "window" produced by interference between potential and resonance scattering. The calculated curves were obtained with the TACASI code which actually fits the areas under the histograms but for checking purposes also prints the shapes in tabular form (Ref. 46).

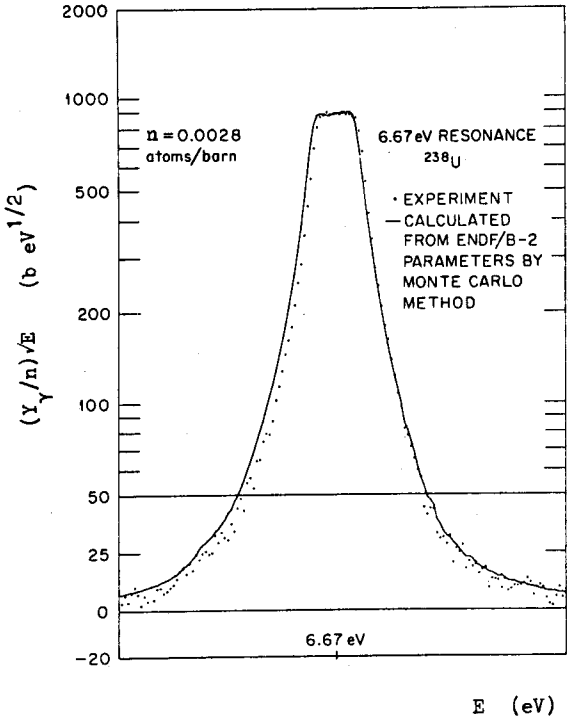

Fig. 11 - Thick-sample capture peak suitable for εφ determination with the saturated-resonance calibration technique. The flat top is typical for thick-sample yield data and indicates the region where the sample is black so that, apart from multiple scattering, $\sigma_\gamma/\sigma \simeq \Gamma_\gamma/\Gamma$ (from Ref. 89).

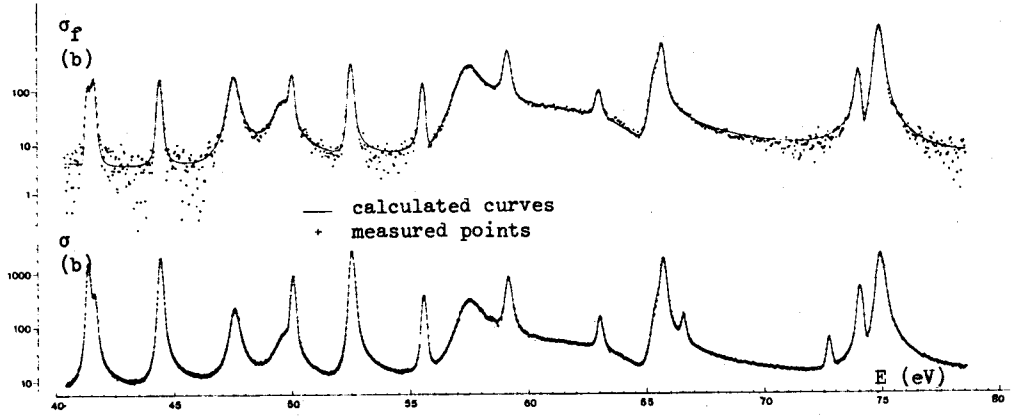

Fig. 12 -
Fission and total cross section data for ^{239}Pu measured by time of flight. The smooth curves are least-squares fits obtained with Derrien's three-channel Reich-Moore shape analysis code (Ref. 50).

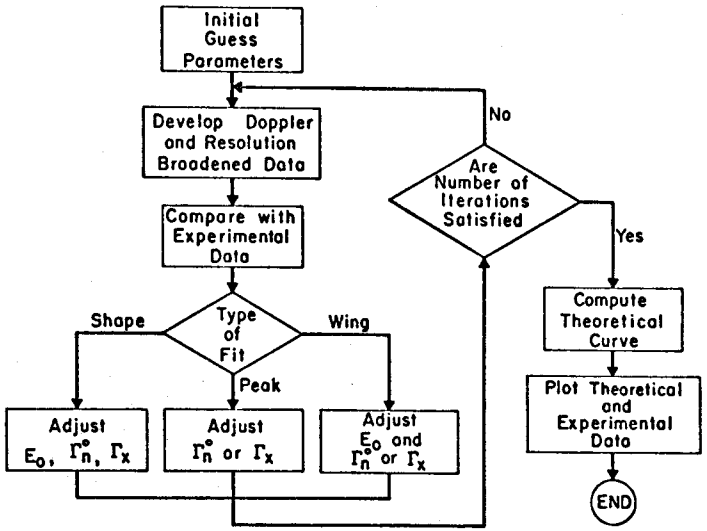

Fig. 13 Flow diagram of the shape analysis program ACSAP. Theoretical cross section data are computed from initial guess parameters, then Doppler and resolution broadened, finally compared with the input data. After adjusting the desired parameters the program reiterates a specified number of times before producing an output listing and plot of the results (from Ref. 51).

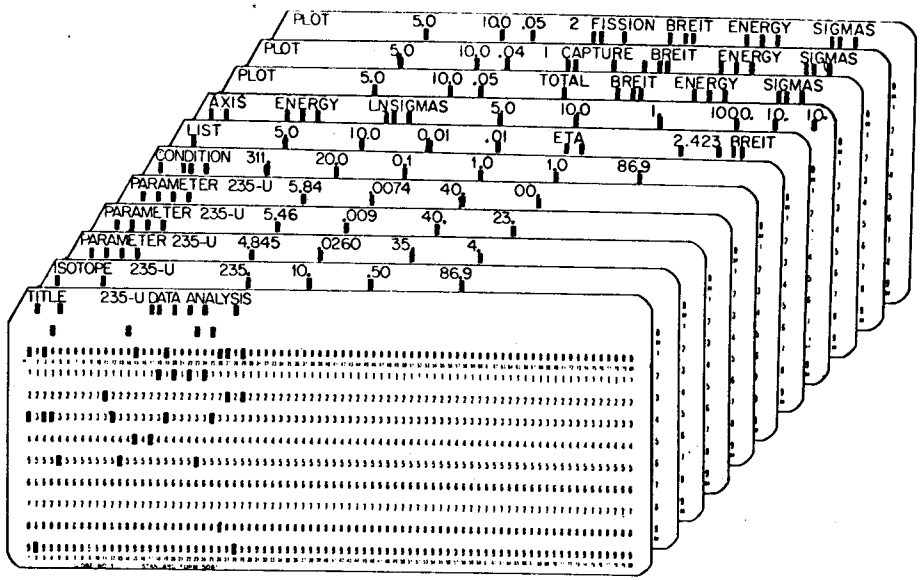

Figure 14 - Input function cards for a short ACSAP run. Key words at the first of each card provide programmability. (Ref. 51)

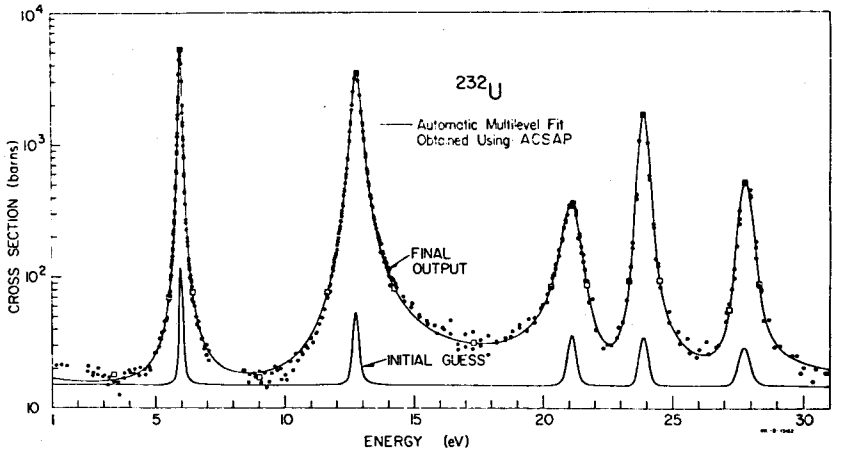

Figure 15 - A theoretical fit to the ^{232}U cross section using ACSAP. Initial guess parameters were deliberately chosen "far from correct" to emphasize power of ACSAP algorithms (from Ref. 51).

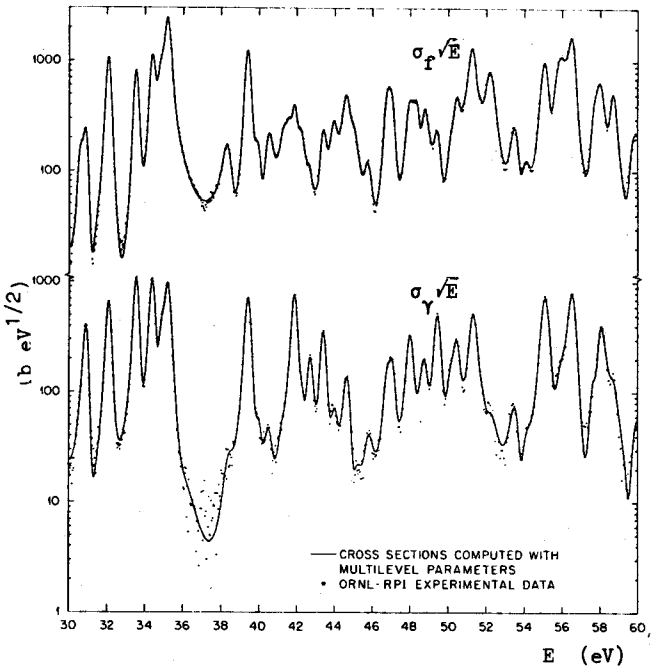

Fig. 16 - Fission and capture cross sections of ^{235}U from 30 to 60 eV. The curves are obtained in a simultaneous fit with the Adler-Adler formalism (Ref. 89).

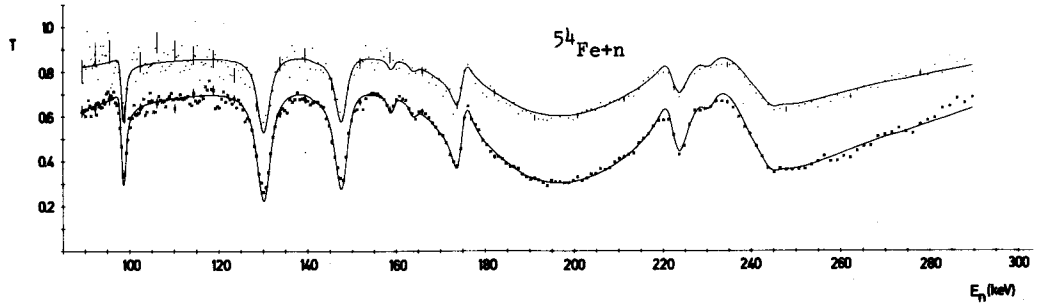

Fig. 17 - Two sets of transmission data on ^{54}Fe and a simultaneous fit obtained with the transmission shape analysis code FANAL (Ref. 36). Note the very severe level-level interference caused by the unusually broad s-wave resonances at 191 and 246 keV. As a consequence the resonance shapes above 120 keV are quite unlike single-level Breit-Wigner shapes. Nevertheless they are properly described by the employed Reich-Moore formalism (from Ref. 90).

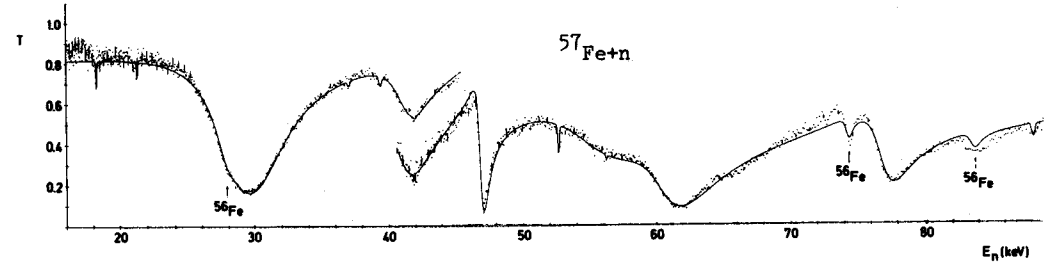

Fig. 18 - Two sets of transmission data on ^{57}Fe and a simultaneous fit obtained with the transmission shape analysis code FANAL (Ref. 36). The interpretation here is complicated by the fact that no less than three s-wave channels are open, two elastic (J = 0 and J = 1) and one inelastic channel (J = 1). Additional elastic and especially inelastic scattering data would have been helpful to resolve the many ambiguities (from Ref. 90).

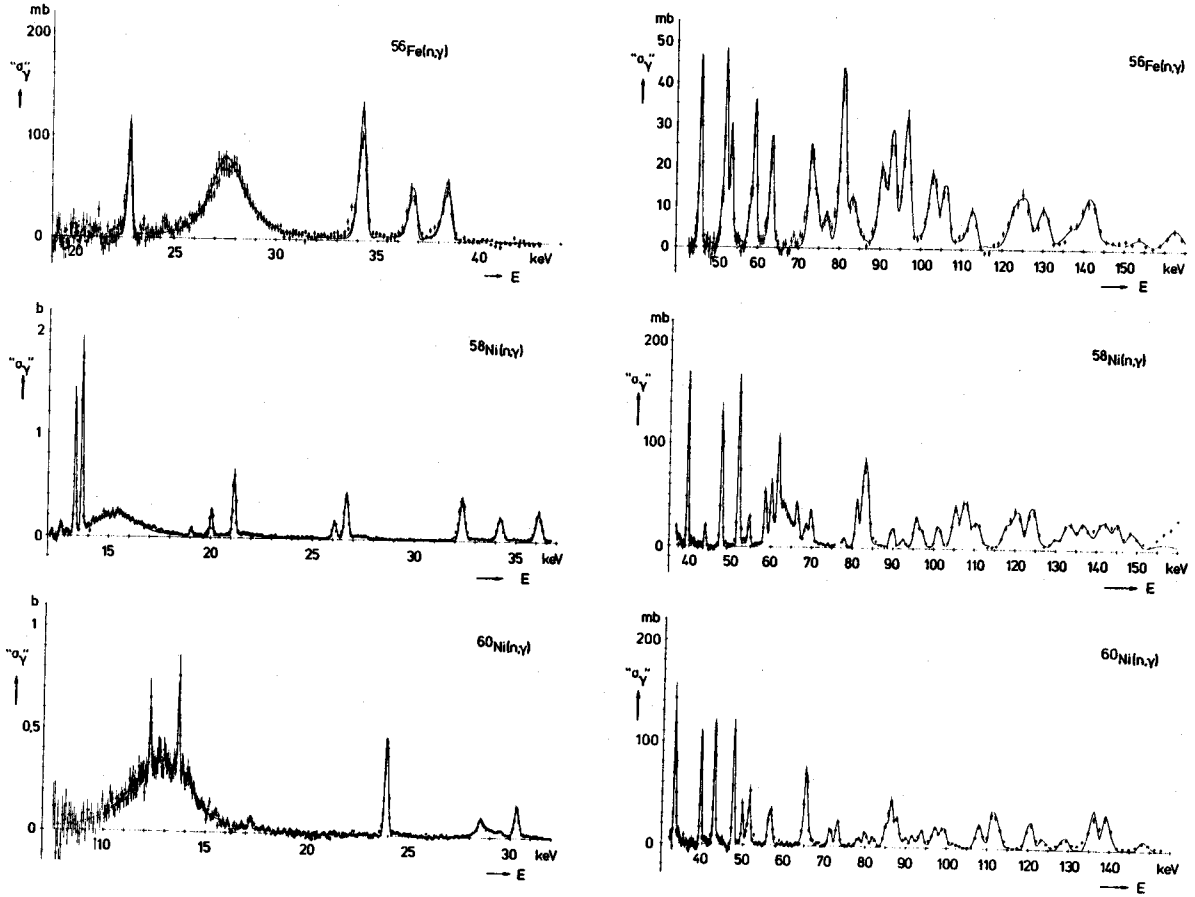

Fig. 19 - Capture yield data on structural-material isotopes and automatic fits obtained with the capture shape analysis program FANAC (Ref. 38). Most of the resonances seen here are p- and d-wave levels. The two curves for the low-energy data on ^{56}Fe correspond to the two data sets taken with slightly different resolution. (From Ref. 40c)

$$\int dE(\sigma-\sigma_p) = 2\pi^2\lambda\!\!\!^{-2}_c \; g\Gamma_n \cos 2\phi_c, \tag{199}$$

$$\int dE\;\sigma_x \;\; = 2\pi^2\lambda\!\!\!^{-2}_c \; g\,\frac{\Gamma_n\Gamma_x}{\Gamma}\,, \tag{200}$$

which do not depend on resolution or Doppler broadening.

2.8.2 Distant levels

So far we glossed over the problems associated with the infinite number of eigenvalues E_λ. In practice one knows only a finite number Λ of them and splits the R-matrix or reduced R-matrix in a smooth part R^0 due to the "distant" levels outside a given energy range and a resonant part R^1 due to the levels explicitly considered,

$$R_{cc'} = R^0_{cc'} + R^1_{cc'} = R^0_{cc'} + \sum_{\lambda=1}^{\Lambda} \frac{\gamma_{\lambda c}\gamma_{\lambda c'}}{E_\lambda - E}\,. \tag{201}$$

In SLBW approximation the sum contains one term only, in Reich-Moore approximation E_λ is to be replaced by $E_\lambda+\Delta_{\lambda\gamma}-i\Gamma_{\lambda\gamma}/2$ (see Sect. 2.3.7). In the resonance region non-resonant, i.e. "direct" transitions between channels can usually be neglected and so can off-diagonal elements of R^0 which represent such transitions. We write therefore

$$\left[1-R^0L^0\right]_{cc'} = (1-R^0_{cc}L^0_c)\delta_{cc'} = q_{cc'}\,e^{i\xi_c} \tag{202}$$

with $$q_{cc'} = |1-R^0_{cc}L^0_c|\,\delta_{cc'}, \qquad \xi_c = \arg\,(1-R^0_{cc}L^0_c) \tag{203)(204}$$

and get $$\left[(1-RL^0)^{-1}\right]_{cc'} = e^{-i\xi_c}\left[(1-q^{-1}R^{-1}_q(1-R^0L^{0*})L^0)^{-1}\right]_{cc'}\frac{1}{q_{c'c'}} \tag{205}$$

$$\left[1-RL^{0*}\right]_{cc'} = q_{cc}\left[1-q^{-1}R^{-1}_q(1-R^0L^0)L^{0*}\right]_{cc'}e^{-i\xi_{c'}} \tag{206}$$

Inserting this in the expression (17) for U we see that all R-matrix equations are preserved if we redefine as follows,

$$\gamma_{\lambda c} \to \frac{\gamma_{\lambda c}}{|1-R^0_{cc}L^0_c|} \equiv \alpha_{\lambda c} \qquad \text{affecting } R_{cc'},\ \Gamma_{\lambda c},\ \Delta_\lambda,\ (A^{-1})_{\lambda\mu} \tag{207}$$

$$\phi_c \to \phi_c + \arg(1-R^0_{cc}L^0_c), \qquad " \qquad \sigma_p, \tag{208}$$

$$\gamma_{\lambda c}L^0_c\gamma_{\mu c} \to \alpha_{\lambda c}(L^0_c-R^0_{cc}|L^0_c|^2)\alpha_{\mu c} \qquad " \qquad \Delta_\lambda,\ (A^{-1})_{\lambda\mu}\,. \tag{209}$$

We can use level statistics to estimate R^0_{cc}. Denoting length and midpoint of the interval of explicitly given levels by I and $\bar{E}$ we have

$$R^0_{cc} = \sum_\lambda \frac{\gamma^2_{\lambda c}}{E_\lambda - E} - \sum_{\lambda=1}^{\Lambda}\frac{\gamma^2_{\lambda c}}{E_\lambda - E} \approx \oint_{-\infty}^{\infty} dE'\,\frac{s_c(E')}{E'-E} - \oint_{\bar{E}-I/2}^{\bar{E}+I/2} dE'\,\frac{s_c(E')}{E'-E}\,, \tag{210}$$

where we replaced sums by integrals and introduced the strength function s_c, Eq.50. With the definition of the distant-level parameter R^∞_c (Eq. 51) and the assumption that neither R^∞_c nor s_c varies significantly over the interval I one gets

$$R^0_{cc} = R^\infty_c(\bar{E}) + 2s_c(\bar{E})\;\mathrm{ar\,tanh}\,\frac{E-\bar{E}}{I/2}, \tag{211}$$

a result which in practice is only needed for neutron channels ($c\in n$). Usually derived from a picket fence model (e.g. in Refs. 36, 55) it is seen to be quite general. It has the great advantage over expansions in powers of $E-\bar{E}$ with adjustable coefficients (e.g. Refs. 54, 56) that only two parameters with a clear physical meaning are involved, R^∞_c (or R'_c, cf. Eq. 53) and s_c (or $S_{\ell J}$, cf. Eq. 54). Both are tabulated extensively (e.g. in Ref. 4) or can be estimated with the optical model. Only slight adjustment (if any) is usually needed for a very satisfactory reproduction of potential scattering over very wide energy ranges. As an example Fig.20 shows R'_c vs. A as calculated from an optical model (Ref. 59) and R'_c values for medium-mass nuclei obtained empirically by adjusting R^∞_c (together with s_c and the resonance parameters) in shape fits to transmission data in the range 10^c to 300 keV (Refs. 57, 58), see also Figs.17,18). Since Eq. 211 is valid on the average but not in cases where untypically weak or strong levels are located just outside the interval I it is good practice to include such "nearby" levels explicitly in R^1 and to use Eq. 211 only for the more distant levels. This means that the interval I is chosen wider than the interval in which one actually wants to calculate cross sections.

2.8.3 Subthreshold ("negative") levels

An example of the "nearby" levels just mentioned are levels with $E_\lambda < 0$ ("negative" levels) corresponding to compound states just below the neutron binding energy. Although low-energy cross sections are mainly determined by the "positive" levels their exact description frequently requires one or at most two additional levels with $E_\lambda < 0$. Let us assume that for a non-fissile target nucleus ($\Gamma=\Gamma_n+\Gamma_\gamma$) we know the positive levels up to a certain energy and want to determine the parameters E_0, Γ_n, Γ_γ for one negative level so that the thermal cross sections are reproduced. At thermal energies the P_ℓ for $\ell\geq 1$ are so small that only s-wave interaction need be considered. With the usual choice $B_c=0$ the Reich-Moore collision function for a given s-wave channel is given by

$$U_{cc} = e^{-2i\phi_c}\;\frac{1+i\sum_\lambda \dfrac{\Gamma_{\lambda n}/2}{E_\lambda-E-i\Gamma_{\lambda\gamma}/2}}{1-i\sum_\lambda \dfrac{\Gamma_{\lambda n}/2}{E_\lambda-E-i\Gamma_{\lambda\gamma}/2}} \qquad (c\in n). \tag{212}$$

The resonance parameters for all positive levels and the one negative level are contained in the sum, and in this way they enter into all cross section expressions. The explicit relationship between the sum and the cross sections is obtained if we solve Eq. 212 for the sum and eliminate U_{cc} by means of

$$\mathrm{Re}\;U_{cc} = 1 - \frac{\sigma_c}{2\pi\lambda\!\!\!^{-2}_c g_c}\,, \quad \mathrm{Im}\;U_{cc} = \pm\sqrt{\frac{\sigma_{cc}}{\pi\lambda\!\!\!^{-2}_c g_c} - \left(\frac{\sigma_c}{2\pi\lambda\!\!\!^{-2}_c g_c}\right)^2}\,, \tag{213)(214}$$

which follows from Eqs. 14 and 15. The resulting expression can then be specialised to the thermal energy, E = 25.3 meV, for which $\phi_c = k_c R' = k_c a_c(1-R^\infty_c) << 1$ (cf. Eqs. 53, 208, 211). Furthermore we assume that no resonance is very close to E which means $\sigma_c << 4\pi\lambda\!\!\!^{-2}_c g_c$, $E << |E_\lambda|$ and $\Gamma^2_{\lambda\gamma} << E^2_\lambda$ for all λ. Under these conditions we get from the real and imaginary part

$$\frac{\Gamma_n}{E_o} = -\sum_{\lambda \neq 0} \frac{\Gamma_{\lambda n}}{E_\lambda} \pm \sqrt{\frac{\sigma_{cc}}{\pi \lambda\!\!\!^{-2}_c g_c} + 2k_c R'_c} \quad , \tag{215}$$

$$\frac{\Gamma_\gamma \Gamma_n}{E_o^2} = -\sum_{\lambda \neq 0} \frac{\Gamma_{\lambda\gamma}\Gamma_{\lambda n}}{E_\lambda^2} + \frac{\sigma_{\gamma c}}{\pi \lambda\!\!\!^{-2}_c g_c} \quad , \tag{216}$$

where $\sigma_{\gamma c} = \sigma_c - \sigma_{cc}$ is the capture cross section for channel c, and where we placed the unknown sum terms on the left-hand sides, the known positive-level terms together with the other known quantities on the right-hand sides. The sign ambiguity is due to the fact that the cross sections depend on $(\mathrm{Im}\, U_{cc})^2$ rather than $\mathrm{Im}\, U_{cc}$. In most cases the positive sign can be immediately discarded because it would make Γ_n/E_o positive contrary to the assumption $E_o < 0$. If this criterion fails one chooses the sign that gives better overall results in the thermal region.

With only two equations for the three unknown quantities E_o, Γ_n, Γ_γ we can choose one of the three and then calculate the other two. The fact that radiation widths do not fluctuate much from level to level suggests to take Γ_γ as the mean radiation width obtained from the positive resonances. Note that in Eqs. 215 and 216 all neutron widths must be calculated at the (thermal) energy E, by specialisation of the general relationship

$$\Gamma_n(E) = \Gamma_n(|E_o|)\, \frac{P_\ell(E)}{P_\ell(|E_o|)} = \Gamma_n^\ell \sqrt{\frac{E}{1\mathrm{eV}}}\, \frac{v_\ell(E)}{v_\ell(|E_o|)} \tag{217}$$

(with $v_\ell \equiv P_\ell/P_o$) to $\ell=0$. The energy-independent quantity $\Gamma^\ell_{\lambda n}$ is the reduced neutron width. In many resonance parameter tables it is listed together with, or instead of, the nominal neutron width $\Gamma_{\lambda n}(|E_\lambda|)$.

For target spin I=0 only one elastic s-wave channel (J=1/2) is open, and $\sigma_c = \sigma$, $\sigma_{cc} = \sigma_n$, $\sigma_{c\gamma} = \sigma_\gamma$. Otherwise one has to consider both elastic channels ($J = I \pm 1/2$) separately which may be problematic since the two σ_c, σ_{cc}, $\sigma_{c\gamma}$ are usually not known separately but only their sum σ, σ_n, σ_γ. Only in rare cases is one negative level per channel not enough to fit known low-energy cross sections. One can then replace the left-hand sides of Eqs. 215, 216 by appropriate sums over negative levels and determine the parameters by a regular shape fit.

3. EVALUATION OF RESONANCE DATA

We shall now briefly discuss some of the problems encountered by the evaluator. He has to construct complete resonance parameter sets from published resonance parameter data and to determine the level-statistical parameters needed for interpretation and prediction of average cross section data in the region of unresolved resonances.

3.1 Intercomparison of resonance parameter sets

The following discussion will be restricted to the intercomparison of resonance parameters of the R-matrix type. It is very rare that different authors use the same potential-scattering parameters (e.g. nuclear radii) in their resonance fits. One should therefore put all available resonance parameter information on a common basis before a detailed comparison and evaluation is started.

3.1.1 Different potential-scattering parameters

Such a common basis can be established by means of the expressions for level shifts and partial widths

$$\Delta_\lambda = \sum_c \frac{\gamma_{\lambda c}^2}{|1 - R^o_{cc} L^o_c|^2} (B_c - S_c + R^o_{cc} |L^o_c|^2), \tag{218}$$

$$\Gamma_{\lambda c} = \frac{2P_c \gamma_{\lambda c}^2}{|1 - R^o_{cc} L^o_c|^2} \quad , \tag{219}$$

which follow from Eqs. 64, 207, 209. With a given author's information on his treatment of potential scattering, e.g. his choice of R'_c as a function of E, we can calculate $\phi_\ell(k_c R'_c)$ at each resonance and compare it to $\phi_\ell(k_c a_c)$ where a_c is the nuclear radius to which we want to refer all resonance parameters, defined e.g. by $a_c = 1.4\ \mathrm{fm}\ A^{1/3}$ or (ENDF, Ref. 12) $a_c = 1.23\ \mathrm{fm}\ A^{1/3} + 0.8\ \mathrm{fm}$. The difference between $\phi_\ell(k_c R'_c)$ and $\phi_\ell(k_c a_c)$ can be formally ascribed to a certain value of R_c, i.e. R^{oc}_{cc}, which in turn can be inserted in Eqs. 218, 219. Thus one gets from the author's resonance energies and widths those which correspond to the adopted a_c convention, with the influence of distant levels removed. These effects are usually negligible at eV energies but can be important in the higher keV region.

3.1.2 Different boundary parameters B_c

Less frequent is the choice of different boundary parameters by different authors. Nevertheless we shall treat this problem in some detail because a very simple method for conversion between the Wigner-Eisenbud (or Reich-Moore) and the Kapur-Peierls representation can be derived from it.

We consider two choices of the boundary parameters, B and B', and the corresponding quantities R, L^o and R', $L^{o\prime}$. Now the collision matrix does not depend on a particular choice, so that (cf. Eq. 17)

$$(1 - RL^o)^{-1} R = R(1 - L^o R)^{-1} = (1 - R'L^{o\prime})^{-1} R', \tag{220}$$

whence
$$(1 - R'L^{o\prime})R = R'(1 - L^o R) \tag{221}$$

or
$$R' = (1 - \delta B \cdot R)^{-1} R \tag{222}$$

with
$$\delta B \equiv B' - B = L^o - L^{o\prime} \ . \tag{223}$$

The poles and residues of R are the E_λ and $\gamma_{\lambda c}\gamma_{\lambda c'}$, those of R' will be denoted by E'_λ, $\gamma'_{\lambda c}\gamma'_{\lambda c'}$. Eq. 222 shows that the poles of R' are the solutions of

$$\det\left[1 - \delta B \cdot R(E'_\lambda)\right] = 0. \tag{224}$$

The residues can be obtained as follows. From Eq. 222 we get

$$\frac{\partial}{\partial E}(R'^{-1}) = \frac{\partial}{\partial E}(R^{-1} - \delta B), \tag{225}$$

or, denoting differentiation with respect to E by a dot,

$$-R'^{-1}\dot{R}'R'^{-1} = -R^{-1}\dot{R}R^{-1} - \dot{\delta B}. \tag{226}$$

Multiplying from both sides with $R' = (1+R'\delta B)R$, which follows from Eq. 221, and going so close to the pole E'_λ of R' that $R' \approx \gamma'_{\lambda c}\gamma'_{\lambda c'}/(E'_\lambda - E)$, $E \approx E'_\lambda$, we find

$$1 = \sum_{c,c'} \gamma'_{\lambda c}\, \delta B_c\, \dot{R}_{cc'}(E'_\lambda)\delta B_{c'}\, \gamma'_{\lambda c'} + \sum_c \gamma'_{\lambda c}\, \dot{\delta B}_c\, \gamma'_{\lambda c}$$

$$= \sum_\mu \Big(\sum_c \frac{\gamma'_{\lambda c}\, \delta B_c\, \gamma_{\mu c}}{E_\mu - E'_\lambda} \Big)^2 + \sum_c \gamma'^2_{\lambda c}\, \dot{\delta B}_c . \qquad (227)$$

Especially simple expressions are obtained from Eqs. 224 and 227 if the boundary parameter is changed for one channel only, namely

$$1 = \delta B_c \sum_\mu \frac{\gamma^2_{\mu c}}{E_\mu - E'_\lambda} , \qquad (228)$$

$$1 = \gamma'^2_{\lambda c}\Big(\delta B_c^2 \sum_\mu \frac{\gamma^2_{\mu c}}{(E_\mu - E'_\lambda)^2} + \dot{\delta B}_c\Big). \qquad (229)$$

Eq. 228 can easily be solved for E'_λ by iteration (see below) whereupon Eq. 229 yields $\gamma'_{\lambda c}$. If δB_c does not depend on energy, as in the Wigner-Eisenbud representation, $\dot{\delta B}_c$ vanishes, of course.

3.2 Conversion from Wigner-Eisenbud to Kapur-Peierls resonance parameters

The results of the preceding section can be applied to the special case $B_c = S_c$, $B_{c'} = L_c$, i.e. $\delta B_c = iP_c$, which corresponds to conversion from Wigner-Eisenbud (s-wave or locally defined p-, d-...wave) parameters to Kapur-Peierls parameters or vice versa (Ref. 48). With the notation introduced in Sect. 2.3 for Kapur-Peierls parameters ($E'_\lambda = \mathcal{E}_\lambda$, $\gamma'_{\lambda c} = g_{\lambda c}$, $2P_c\gamma'^2_{\lambda c} = G_{\lambda c}$) we get from Eqs. 228 and 229

$$\mathcal{E}_\lambda = E_\lambda - \frac{i\Gamma_{\lambda c}/2}{1 - \sum_{\mu \neq \lambda} \frac{i\Gamma_{\mu c}/2}{E_\mu - \mathcal{E}_\lambda}} , \qquad (230)$$

$$\frac{iG_{\lambda c}}{2} = \Big(\sum_\mu \frac{i\Gamma_{\mu c}/2}{(E_\mu - \mathcal{E}_\lambda)^2} \Big)^{-1} \qquad (231)$$

or

$$G^{1/2}_{\lambda c} = \frac{\Gamma^{1/2}_{\lambda c}}{+\sqrt{\Big(1 - \sum_{\mu \neq \lambda} \frac{i\Gamma_{\mu c}/2}{E_\mu - \mathcal{E}_\lambda}\Big)^2 - \sum_{\mu \neq \lambda} \frac{\Gamma_{\lambda c}\Gamma_{\mu c}/4}{(E_\mu - \mathcal{E}_\lambda)^2}}} \qquad (232)$$

where the square root is taken with the positive sign so that for isolated levels $G^{1/2}_{\lambda c} = \Gamma^{1/2}_{\lambda c}$. The term with $\dot{\delta B}_c$ has been omitted since we consider the dependence of δB_c as parametric rather than functional so that the argument of $\delta B_c = iP_c(E)$ coincides only "accidentally" with the bombarding energy. As a consequence all widths ($\Gamma_{\mu c}$, $G_{\lambda c}$) are to be calculated at the energy E for which we want to calculate the Kapur-Peierls parameters (rather than at $\mathcal{E}_\lambda$).

Eq. 230 is convenient for iteration starting from $\mathcal{E}_\lambda = E_\lambda - i\Gamma_{\lambda c}/2$. Convergence is rapid even with severe level overlap (Ref. 48). Having determined $\mathcal{E}_\lambda$ with sufficient accuracy one can caluclate $G_{\lambda c}$ as a simple sum over levels (Eq. 231). The method is formally simpler than the conversion techniques based on matrix inversion (Ref. 17) or on partial-fraction expansion of the determinant in Eq. 224 (Refs. 20,22). In particular large numbers of resonances are easily dealt with. Computation of determinants and matrix inversion are replaced by a perturbation approach which clearly exhibits the influence of interfering levels. Their importance is essentially proportional to $\Gamma_{\mu c}/(E_\mu - E_\lambda)$. In SLBW approximation the sums in Eqs. 230 and 231 vanish and one gets immediately, for conversion in all channels,

$$\mathcal{E}_\lambda = E_\lambda - i\sum_c \Gamma_{\lambda c}/2 = E_\lambda - i\Gamma_\lambda/2, \qquad G^{1/2}_{\lambda c} = \Gamma^{1/2}_{\lambda c}. \qquad (233)(234)$$

In the two-channel case iteration of Eq. 230 produces the continued-fraction representation of the tangent,

$$\mathcal{E}_\lambda = E_\lambda - \frac{i\Gamma_{\lambda c}}{2}\Bigg(1 + \frac{\Gamma^{1/2}_{\mu c}}{\Gamma^{1/2}_{\lambda c}} \cfrac{x/2}{1 - \cfrac{(x/2)^2}{1 - \cfrac{(x/2)^2}{1 - \cdots}}}\Bigg)$$

$$= E_\lambda - \frac{i\Gamma_{\lambda c}}{2}\Big(1 - \frac{\Gamma^{1/2}_{\mu c}}{\Gamma^{1/2}_{\lambda c}} \tan\alpha\Big) \qquad (235)$$

where $$\sin 2\alpha \equiv x \equiv \frac{\Gamma^{1/2}_{\lambda c}\Gamma^{1/2}_{\mu c}}{(E_\mu - i\Gamma_{\mu c}/2) + (E_\lambda - i\Gamma_{\lambda c}/2)}, \quad (\lambda,\mu = 1,2). \qquad (236)$$

This is what one also obtains as solution of the characteristic equation (224) in the diagonalisation of the part $(E_\lambda - E)\delta_{\lambda\mu} - i\Gamma^{1/2}_{\lambda c}\Gamma^{1/2}_{\mu c}/2$ of the inverse level matrix, Eq. 22. We shall not go further into details. It should be sufficiently clear by now that our perturbation approach is most useful for many levels and few channels, that is for the Reich-Moore formalism. With the Kapur-Peierls choice $L^o_c = 0$ for all particle channels the essential Reich-Moore formulae assume the simple form

$$U_{cc'} = e^{-i(\phi_c + \phi_{c'})}\Big(\delta_{cc'} + \sum_\lambda \frac{iG^{1/2}_{\lambda c}G^{1/2}_{\lambda c'}}{\mathcal{E}_\lambda - E - i\Gamma_{\lambda\gamma}/2}\Big) \qquad (c,c' \notin \gamma), \qquad (237)$$

$$\sigma_{c\gamma} = \sum_{c' \in \gamma} \sigma_{cc'} = \pi\lambda^2_c g_c \sum_\lambda \frac{|G_{\lambda c}|\Gamma_{\lambda\gamma}}{|\mathcal{E}_\lambda - E - i\Gamma_{\lambda\gamma}/2|^2} , \qquad (238)$$

where $\mathcal{E}_\lambda$, $G^{1/2}_{\lambda c}$ are the conversion results for the particle channels ($\mathcal{E}_\lambda - i\Gamma_{\lambda\gamma}/2 \approx E_\lambda - i\Gamma_\lambda/2$ for relatively isolated levels).

In this way one can convert Reich-Moore to Kapur-Peierls parameters. The corresponding cross sections can be Doppler broadened by means of the Voigt profiles (see Sect. 2.4.3), but we stress again that the price for this is heavy: One must convert parameters for each energy grid point and then calculate complicated coefficients for the Voigt profiles involving double sums over levels (Eqs. 69, 70, 72) which is time-consuming if many levels are involved. Direct numerical broadening of Reich-Moore cross sections is usually simpler, faster and more accurate.

3.3 Applied level statistics

It was already mentioned that one of the reasons for parametrisation of resonance cross section data is the need to determine level-statistical parameters such as mean level spacings, average widths and strength functions which permit extrapolation of average cross sections and simulation of cross section fluctuations in the unresolved-resonance region. As in resonance theory we shall need only very few formulae from the impressive but often still speculative edifice of the statistical theory of spectra (Refs. 60, 61).

3.3.1 The Porter-Thomas hypothesis

The reduced width amplitudes $\gamma_{\lambda c}$ of Wigner-Eisenbud R-matrix theory are essentially values of the internal wave function taken at the channel radius a_c, as our little single-particle exercise (Sect. 2.3.3, Eq. 42) showed. They can be expressed by the overlap between the λ-th eigenfunction and the channel wave function at the channel entrance ($r_c=a_c$). In the multi-channel (A+1)-nucleon case this is a (3A+2)-dimensional configuration space integral over the surface of the interaction sphere. The very complicated integrand oscillates rapidly so that negative and positive contributions nearly cancel. The integral is thus almost equal to zero and is positive or negative with presumably equal probabilities depending on the particulars of the λ-th eigenstate. Under these circumstances a Gaussian distribution of the $\gamma_{\lambda c}$ for given c is a reasonable guess. Omitting the level subscript we write

$$p(\gamma_c)d\gamma_c = \frac{1}{\sqrt{\pi}} e^{-x^2} dx, \qquad -\infty < x \equiv \frac{\gamma_c}{\sqrt{2\langle\gamma_c^2\rangle}} < \infty . \tag{239}$$

This is the Porter-Thomas hypothesis (Ref. 62) which, with $d\gamma_c^2 = 2\gamma_c d\gamma_c$, $p(\gamma_c)d\gamma_c \equiv p(\gamma_c^2)d\gamma_c^2$ immediately yields the famous Porter-Thomas distribution

$$p(\gamma_c^2)d\gamma_c^2 = \frac{e^{-y}}{\sqrt{\pi y}} dy , \qquad 0 < y \equiv \frac{\gamma_c^2}{2\langle\gamma_c^2\rangle} < \infty . \tag{240}$$

It applies to reduced neutron widths whenever the resonances are excitable only via one channel so that $\Gamma_n^\ell/\langle\Gamma_n^\ell\rangle = \gamma_c^2/\langle\gamma_c^2\rangle$ (e.g. for I=0 or ℓ=0, see Table 1), but also to partial radiation widths for single radiative transitions not only in nuclear but also in atomic and molecular resonance spectroscopy. Many observable widths, however, are sums of single-channel widths, for instance many reduced neutron widths for I>0 and ℓ>0, or the total radiation width or fission widths. If the averages $\langle\gamma_c^2\rangle$ were the same for all ν contributing channels one would get the generalised Porter-Thomas distribution, a χ^2-distribution with ν degrees of freedom,

$$p(\gamma_x^2)d\gamma_x^2 = \Gamma(\tfrac{\nu}{2})^{-1} e^{-y} y^{\nu/2-1} dy, \quad 0 < y \equiv \frac{\nu\gamma_x^2}{2\langle\gamma_x^2\rangle} < \infty, \tag{241}$$

where $\Gamma(\nu/2)$ is the gamma function and

$$\gamma_x^2 \equiv \sum_{c\in x} \gamma_c^2 , \qquad \langle\gamma_x^2\rangle = \nu\langle\gamma_c^2\rangle . \tag{242)(243}$$

The single-channel Porter-Thomas distribution (ν=1) agrees well with observed distributions of single-channel reduced neutron widths (Ref. 63) and partial radiation widths (Ref. 64). The general χ^2 distribution is useful for two-channel reduced neutron widths (ν=2, exponential distribution) and, with an effective number ν of channels, also for fission widths (ν small) and total radiation widths (ν very large). That ν is large for total radiation widths could be expected because usually there is a huge number of allowed radiative transitions to lower-lying compound states, each giving rise to a sum term in Eq. 242. That ν is small for fission widths, however, surprises at first sight. The hundreds of possible pairs of fission fragments, each with many possible excitations, would seem to imply equally many reaction channels or partial fission widths, and a correspondingly large ν.

The puzzle was solved by A. Bohr (Ref. 65). He pointed out that before scission can occur the compound system must cross the saddle point of the potential-energy surface (in deformation parameter space) beyond which Coulomb repulsion prevails over nuclear cohesion. At the saddle point most energy is tied up as deformation energy, only little being available for other modes of excitation whose spectrum resembles somewhat the low-lying (collective) states observed for the ground-state deformation. Energy, angular momentum and parity requirements allow access to only very few of these transition states. This introduces quite rigid correlations between partial widths for the many different fission fragment channels in such a way that the fission width can be approximated as a sum of terms, one for each accessible transition state (or "saddle-point channel"), each term being governed by a single-channel Porter-Thomas distribution (Ref. 66). For fission, therefore, ν is the number of saddle-point channels rather than reaction channels in the usual sense.

This illustrates that the level-statistical "laws" are nowhere as rigid as the formal resonance theory discussed in previous sections. They hold mainly for typical compound levels where all single-particle, collective or other simplicity has been lost. Reflecting more our ignorance than truly statistical phenomena they may fail if the states considered are simple and well understood. Thus the collective transition states of a fissioning nucleus enabled us to modify and, in fact, to simplify the reaction channel concept. In the single-particle exercise with square-well complex potential, Sect. 2.3.3, nothing at all was random or unspecified, and the reduced neutron widths, Eqs. 58, turned out to obey a δ-distribution instead of the Porter-Thomas "law".

3.3.2 Wigner's surmise and Hamiltonian ensemble theory

To find the distribution p(D)dD of nearest-neighbour spacings, $D_\lambda = E_{\lambda+1} - E_\lambda$, in a JΠ level sequence turned out to be much more difficult than to find the width distributions. Very early Wigner tried a bold guess("Wigner's surmise" , Ref. 67). He took issue with the exponential distribution tried by others which is obtained if the probability to find a level in a small energy interval dD is just $dD/\langle D\rangle$, independent of its distance D from the preceding level. He asserted that because of "level repulsion" at least for small D this probability should be proportional to DdD and assumed tentatively that this is true also for large D so that

$$p(D)dD = \exp(-c\int_0^D D'dD')cDdD = e^{-cD^2/2}\, cDdD \tag{244}$$

Expressing the proportionality constant c by the mean level spacing $\langle D\rangle$ one can write the Wigner distribution as

$$p(D)dD = 2e^{-x^2} x\, dx, \qquad 0 < x \equiv \frac{\sqrt{\pi}}{2}\frac{D}{\langle D\rangle} < \infty. \tag{245}$$

Wigner illustrated the level repulsion by pointing to the spacing $D=\sqrt{(H_{11}-H_{12})^2+4H_{12}^2}$ between the eigenvalues of a two-dimensional (real, symmetric)Hamiltonian matrix H which can be visualised as the distance of a point with coordinates $H_{11}-H_{22}$ and $2H_{12}$ from the origin. If the H_{ij} are considered as random variables the probability to obtain a given D within dD is proportional to the two-dimensional area element

$2\pi DdD$, at least in a small domain arround the origin in which nonuniformity of the unknown probability distributions of the $H_{\lambda\mu}$ can be neglected. D=0 is seen to be infinitely unlikely, which is related to the fact that two conditions, $H_{11}=H_{22}$ and $H_{12}=0$, must be fulfilled instead of one as for $D\neq 0$. This latter argument is also true for 3-, 4- ... dimensional Hamiltonian matrices, coincidence of two characteristic values always requiring two conditions instead of one.

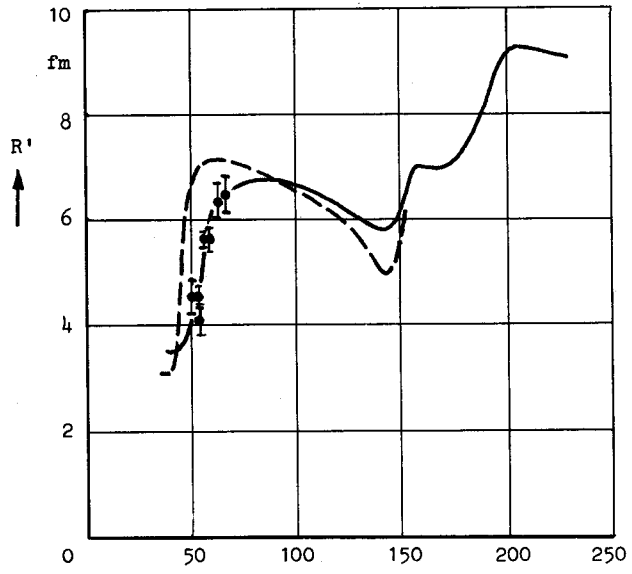

Fig. 20 - Effective radii obtained for Cr, Fe and Ni isotopes by shape fits to transmission data below 300 keV (see Figs. 17 and 18) with the FANAL code (Refs. 36, 57, 58). The broken curve was calculated by Moldauer (Ref. 91) for a complex spherical potential, the solid curve by Jain (Ref. 59) for a complex potential with vibrational and rotational coupling.

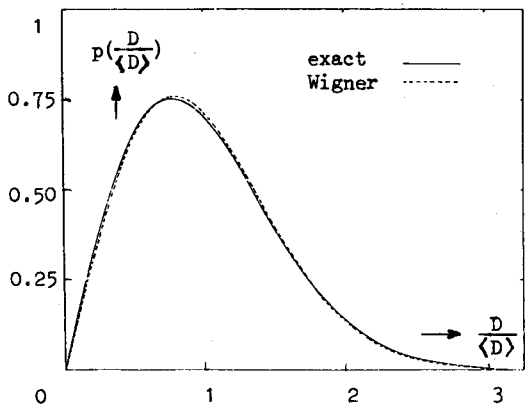

Fig. 21 - Next-neighbour spacing distributions for the Gaussian orthogonal ensemble. Solid line: very large N×N matrices, limit $N\to\infty$ (Gaudin, Ref. 69). Broken line: 2×2 matrices (Wigner distribution). From Ref. 69.

A more rigorous theory of statistical ensembles of Hamiltonians was developped in a brilliant mathematical tour de force by Wigner, Porter, Mehta, Dyson and others (Refs. 60, 61) in an attempt to establish a kind of statistical thermodynamics of quantum systems. First the so-called Gaussian orthogonal ensemble was studied which consists of real symmetric Hamiltonian matrices H whose elements $H_{\lambda\mu}$ are uncorrelated and whose density function p(H) is invariant under rotations in Hilbert space (so that all representations including the diagonal form are put on an equal footing). For 2x2 matrices the Wigner distribution was obtained. For very large matrices Mehta and Gaudin (Refs. 68, 69) found expressions that are fairly complicated but as Fig.21 shows differ only slightly from the 2x2 curve, i.e. Wigner's surmise.

A major difficulty with the Gaussian ensemble is that it leads to a rather unrealistic level density formula, viz. Wigner's semi-circle law for NxN matrices with very large N,

$$p(E) \propto \begin{cases} \frac{4N}{\pi I}\sqrt{1-\left(\frac{E-\bar{E}}{I/2}\right)^2} & \text{for } (E-\bar{E})^2 < I/2 \\ 0 & \text{otherwise} \end{cases} \qquad \text{(N large)} \qquad (246)$$

where $\bar{E}$ and I are midpoint and length of the energy interval in which the eigenvalues occur. This is quite different from the exponentially rising level densities obtained for instance from the Fermi gas independent-particle model.

Dyson gave up the hypothesis of statistically independent matrix elements $H_{\lambda\mu}$ and introduced the circular orthogonal ensembles (Ref. 70). He could show that with these one could reproduce any reasonable energy dependence of the level density ρ apparently without changing less global results such as the spacing distribution obtained with the Gaussian ensembles.

Recently French, Wong and others studied the statistical shell model where not the elements $H_{\lambda\mu}$ but only those of the residual interaction are considered as random variables (cf. Ref. 71). This model, more physical than the Gaussian and circular orthogonal ensembles, nevertheless confirmed their results for nearest neighbor level spacings, whereas ρ(E) turned out to be Gaussian instead of semi-circular.

Both the orthogonal ensembles and the statistical shell model indicate that nuclear (or atomic) level sequences have a nearly "crystalline" regularity in the sense that the familiar staircase diagram (number of levels vs. energy) follows very closely the practically straight line with slope ρ(E), deviations by more than one unit being extremely unlikely (Ref. 72). This implies that adjacent nearest-neighbour spacings are correlated in such a way that a large spacing is followed by a short spacing more often than not and vice versa. In fact, for orthogonal ensembles the expected correlation coefficient is

$$C(D_\lambda, D_{\lambda+1}) = \frac{\mathrm{cov}(D_\lambda, D_{\lambda+1})}{\sqrt{\mathrm{var}(D_\lambda)\mathrm{var}(D_{\lambda+1})}} \approx -0.27 \qquad (247)$$

for large matrices. The exact value $(8\pi-27)/(11\pi-27) \approx -0.253$ for the simplest case of 3x3 matrices (Ref. 73) is already a good approximation. Empirical evidence from long and pure sequences of s-wave neutron resonances supports these theoretical results (Ref. 74).

The Porter-Thomas distribution of single-channel widths, the Wigner distribution of level spacings and the quasi-crystalline long-range regularity of level sequences is about all the level statistics we need for applications.

3.3.3 Maximum-likelihood estimation of $\langle \Gamma_n^\ell \rangle$ and $\langle D \rangle$ from perfect samples

Suppose we know all level energies E_λ and reduced neutron widths $\Gamma_{\lambda n}^\ell$ for a pure $J\pi$ level sequence in a given energy range. What can we infer about the true mean values $\langle D \rangle$ and $\langle \Gamma_n^\ell \rangle$, and about their ratio, the strength function $S_\ell \equiv \langle \Gamma_n^\ell \rangle / \langle D \rangle$? This is the typical statistical problem of parameter estimation. It was tackled by Slavinskas and Kennett (Ref. 75) with the maximum-likelihood method. Consider first the reduced neutron widths which we shall write here simply as Γ_λ. The probability to find Γ_1 in $d\Gamma_1$, Γ_2 in $d\Gamma_2$, ..., Γ_N in $d\Gamma_N$ is a product of Porter-Thomas probabilities (we consider here the single-channel case, $\nu=1$, e.g. s-wave resonances),

$$\prod_{\lambda=1}^{N} p(\Gamma_\lambda)d\Gamma_\lambda = (2\pi \langle \Gamma \rangle)^{-N/2} \exp\left(-\frac{1}{2\langle \Gamma \rangle} \sum_{\lambda=1}^{N} \Gamma_\lambda\right) \prod_{\mu=1}^{N} \frac{d\Gamma_\mu}{\sqrt{\Gamma_\mu}}. \qquad (248)$$

The value of the true average $\langle \Gamma \rangle$ that leads with greatest probability to the experimental result obviously maximises the likelihood function $L \equiv \Pi_\lambda\, p(\Gamma_\lambda)$. From $\partial L/\partial \langle \Gamma \rangle = 0$ or, more conveniently, from $\partial \ln L/\partial \langle \Gamma \rangle = 0$, one finds the maximum-likelihood estimator

$$\langle \Gamma \rangle = \frac{1}{N} \sum_{\lambda=1}^{N} \Gamma_\lambda. \qquad (249)$$

This is just the sample average $\bar{\Gamma}$. In the language of mathematical statistics $\bar{\Gamma}$ is a minimal sufficient statistics, i.e. a quantity that can be calculated from the sample $\Gamma_1, \ldots \Gamma_N$, contains all information about $\langle \Gamma \rangle$ that the sample itself contains, and has the smallest variance of all possible estimators. It is an unbiased estimator for $\langle \Gamma \rangle$ because for very large samples it tends towards $\langle \Gamma \rangle$.

In order to assign confidence limits we need the probability distribution of the random variable $\bar{\Gamma}$. This we know already from the discussion of sums of partial widths to be a χ^2-distribution with N degrees of freedom (compare Eq. 241),

$$p(\bar{\Gamma})d\bar{\Gamma} = \Gamma\left(\frac{N}{2}\right)^{-1} e^{-y}\, y^{N/2-1}\, dy, \qquad 0 < y \equiv \frac{N\bar{\Gamma}}{2\,\Gamma} < \infty. \qquad (250)$$

Confidence limits y_- and y_+ can now be assigned for instance at the 68 % confidence level, in analogy to the standard deviation of a Gaussian distribution. One demands that y lie with $\mathrm{erf}(1/\sqrt{2}) = 68$ % probability within the interval $(y_- \ldots y_+)$, and with equal probability below and above,

$$\Gamma\left(\frac{N}{2}\right)^{-1} \int_0^{y_-} e^{-y}\, y^{N/2-1}\, dy \equiv \Gamma\left(\frac{N}{2}\right)^{-1} \int_{y_+}^{\infty} e^{-y}\, y^{N/2-1}\, dy \equiv \frac{1}{2}\,\mathrm{erfc}\,\frac{1}{\sqrt{2}}. \qquad (251)$$

The confidence limits y_-, y_+ thus defined depend only on the sample size N and can be found e.g. in tables of χ^2-distributions or numerically from Eqs. 251. One knows now that with 68 % probability $y_- < y < y_+$ and thus

$$\frac{N}{2y_+}\,\bar{\Gamma} < \langle \Gamma \rangle < \frac{N}{2y_-}\,\bar{\Gamma}. \qquad (252)$$

For very large samples the χ^2 distribution is nearly Gaussian so that

$$y_\pm = \langle y \rangle \pm \sqrt{\mathrm{var}(y)} = \frac{N}{2}\left(1 \pm \sqrt{\frac{2}{N}}\right) \quad \text{for } N \gg 1. \qquad (253)$$

So far we neglected experimental errors $\delta\Gamma_\lambda$ of the Γ_λ which cause an uncertainty $\delta\bar{\Gamma} = \sqrt{\Sigma_\lambda (\delta\Gamma_\lambda)^2}/N$ of $\bar{\Gamma}$. They are usually accounted for in sufficient approximation if the confidence limits are extended so that the squares of the statistical and experimental errors are added,

$$y_\pm \to y_\pm \pm \left[\sqrt{\mathrm{var}(y) + (\delta\bar{\Gamma})^2} - \sqrt{\mathrm{var}(y)}\right]. \qquad (254)$$

Slavinskas and Kennett found maximum-likelihood estimators also for $\langle D \rangle$ and $\langle \Gamma_n^\ell \rangle / \langle D \rangle = S_\ell$ but we shall not follow their derivation because they neglected the level-spacing correlations, Eq. 247, cf. Ref. 76. Dyson and Mehta (Ref. 72) showed that due to the regularity of level sequences the number N of levels in a given energy interval is already a rather good statistics for the estimation of the average level density, and that the optimum statistics for the orthogonal ensemble is

$$\rho = \frac{1}{\langle D \rangle} = \frac{4}{\pi I} \sum_{\lambda=1}^{N} \sqrt{1 - \left(\frac{E_\lambda - \bar{E}}{I/2}\right)^2} \qquad (255)$$

where I and $\bar{E}$ are length and midpoint of the energy interval from which the energy sample comes. This statistics may be considered as a kind of level count with semicircle weighting. Its variance is

$$\mathrm{var}\,\rho = \frac{1}{2}\left(\frac{4}{\pi I}\right)^2. \qquad (256)$$

3.3.4 Maximum-likelihood estimation of $\langle \Gamma_n^\ell \rangle$ and $\langle D \rangle$ in the case of missed levels

The estimators for $\langle \Gamma_n^\ell \rangle$ and $1/\langle D \rangle$ presented so far are not very useful in practice because they are applicable only to perfect samples from which no levels are missing. In practice the smallest, but according to the Porter-Thomas distribution most frequent, widths are always missing. As a consequence all observed width and especially spacing distributions are badly distorted. It is therefore best to use the width distribution to estimate $\langle \Gamma_n^\ell \rangle$ which then permits estimation of the number of missing levels and thus of $\langle D \rangle$ and S_ℓ.

Let us assume that levels with reduced widths $\Gamma_\lambda < \Gamma_o \equiv 2x_o \langle \Gamma \rangle$ are undetectable and missing from the sample. The distribution of detectable widths is then the truncated Porter-Thomas distribution

$$p(\Gamma_\lambda)d\Gamma_\lambda = \frac{1}{\mathrm{erfc}\,\sqrt{x_o}}\,\frac{e^{-x}}{\sqrt{\pi x}}\,dx, \qquad x_o < x \equiv \frac{\Gamma_\lambda}{2\langle \Gamma \rangle} < \infty, \qquad (257)$$

properly normalised to unity by the complementary error function. Maximising the corresponding likelihood function one gets

$$\langle \Gamma \rangle \left(1 + \frac{2}{\sqrt{\pi}}\,\frac{e^{-x_o}\sqrt{x_o}}{\mathrm{erfc}\,\sqrt{x_o}}\right) = \frac{1}{N} \sum_{\lambda=1}^{N} \Gamma_\lambda = \bar{\Gamma}. \qquad (258)$$

The term in brackets is clearly a missing-level correction factor depending on $\langle \Gamma \rangle$. The equation is readily solved by iteration starting from $\langle \Gamma \rangle = \bar{\Gamma}$. This simple approach works well whenever the detectability threshold Γ_o can be considered as constant and is sufficiently well known.

Often Γ_o varies significantly over the energy range from which the width sample is taken. The truncation of the Porter-Thomas distribution is then not sharp but fuzzy. Fuketa and Harvey (Ref. 77) developed a widely used estimation procedure for $\langle \Gamma \rangle$ with an energy dependence of the form $\Gamma_o = aE^b$, where a is an adjustable constant and b is determined by the experimental details ($b = 2$ in many experiments).

Of course the observed level density reflects the energy dependence of Γ_o, and in fact one can devise a procedure which utilises the level energies E_λ, ... E_N as well as the reduced widths Γ_1, ... Γ_N and obviates the need to know anything about the detection threshold and experimental details. This is especially useful if the latter are not known or if the resonance parameter data stem from many different experiments. Due to the regularity of level sequences and smooth behaviour of $\Gamma_o(E)$ (at least for single experiments) the typical level density staircase curve (number of levels versus energy) fluctuates but little around a smooth curve which usually can be taken as a parabola,

$$\bar{N}(E) = c_o + c_1 E + c_2 E^2. \qquad (259)$$

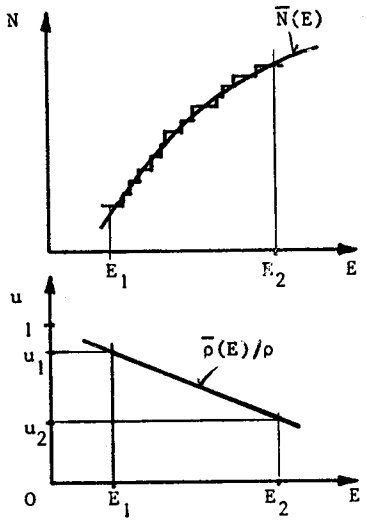

Fig. 22

The coefficients can be determined in a least-squares fit and will be considered as known. The energy derivative is the apparent level density,

$$\bar{\rho}(E) = c_1 + 2c_2 E, \qquad (260)$$

which is smaller than the true level density $\rho \equiv 1/\langle D \rangle$, whose energy dependence we shall neglect as well as that of $\langle \Gamma \rangle$. The detectable fraction of levels (on the average) is then

$$u \equiv \frac{\bar{\rho}(E)}{\rho} = (c_1 + 2c_2 E)\langle D \rangle = \mathrm{erfc}\sqrt{x_o}, \qquad (261)$$

where the complementary error function has the same meaning as in Eq. 255: it is the integral over the Porter-Thomas distribution above the detectability threshold $x_o = \Gamma_o/(2\langle \Gamma \rangle)$. We have thus found from the observed level energies the energy dependence of Γ_o, at least in implicit form and in terms of $\langle \Gamma \rangle$ and $\langle D \rangle$.

The parabolic fit to the staircase diagram is seen to be equivalent to a linear decrease of the detectable fraction from $u_1 = u(E_1)$ to $u_2 = u(E_2)$. The probability that at some unspecified energy within the interval $(E_1 \ldots E_2)$ the detectable fraction has the value u is therefore a constant between u_1 and u_2 and vanishes elsewhere. We can thus write the width distribution with fuzzy truncation edge as

$$p(\Gamma_\lambda)d\Gamma_\lambda = \frac{p_1 p_2 d\Gamma_\lambda}{\int_0^\infty p_1 p_2 d\Gamma_\lambda}, \qquad (262)$$

where $p_1 d\Gamma_\lambda$ is the (a priori) Porter-Thomas probability for a reduced width Γ_λ in $d\Gamma_\lambda$, and p_2 the conditional probability that Γ_λ, for unspecified E_λ, exceeds the detection threshold,

$$p_2 = \begin{cases} 1 & \text{if } \mathrm{erfc}\sqrt{x_\lambda} < u_2 \\ \dfrac{u_1 - \mathrm{erfc}\sqrt{x_\lambda}}{u_1 - u_2} & \text{if } u_2 < \mathrm{erfc}\sqrt{x_\lambda} < u_1 \\ 0 & \text{if } \mathrm{erfc}\sqrt{x_\lambda} > u_1 \end{cases} \qquad (263)$$

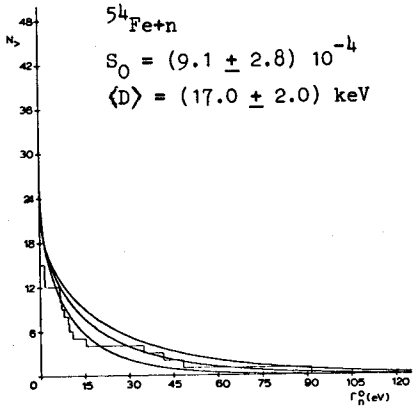

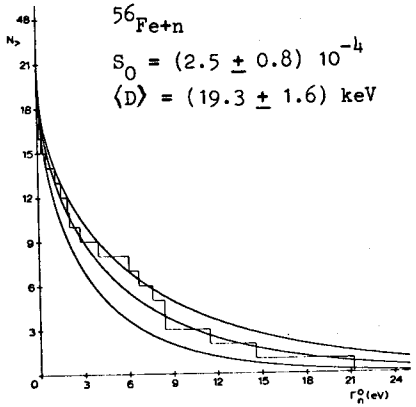

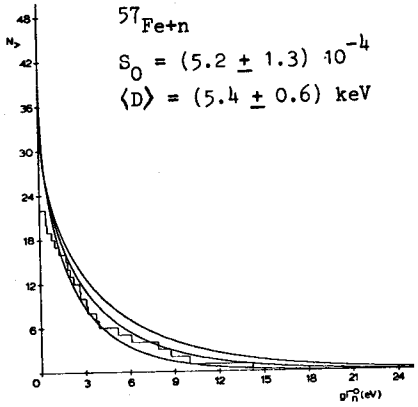

Fig. 23 - Results of statistical resonance analysis for iron isotopes obtained with the maximum-likelihood code STARA (Ref. 78). The histograms are observed integral width distributions for s-wave levels below 400 keV (below 200 keV for ^{57}Fe). The curves are the most likely distributions and the 68% confidence limits. Note that the curves are no fits to the histograms but correspond to the solution $\langle \Gamma_n^o \rangle$ of Eqs. 265, 266.

with $u_i = u(E_i) = (c_1+2c_2E_i)\langle D\rangle$ $(i=1,2)$ (264)

and $x_\lambda \equiv \Gamma_\lambda/(2\langle\Gamma\rangle)$. The denominator in Eq. 262 is equal to the average observable fraction in the interval $(E_1 \ldots E_2)$, $\bar{u} = u(\bar{E}) = [c_1+c_2(E_1+E_2)]\langle D\rangle$. The likelihood function $L = \Pi_\lambda p(\Gamma_\lambda)$ depends on the (known) fit parameters and the unknown level-statistical parameters $\langle\Gamma\rangle$ and $\langle D\rangle$. Thus its maximum is obtained for $\partial L/\partial\langle\Gamma\rangle = 0$ and $\partial L/\partial\langle D\rangle = 0$, whence

$$\langle\Gamma\rangle\left(1 + \frac{1}{N}\sum_\lambda{}' \frac{2}{\sqrt{\pi}} \frac{e^{-x_\lambda}\sqrt{x_\lambda}}{u_1-\mathrm{erfc}\sqrt{x_\lambda}}\right) = \bar{\Gamma}\ , \tag{265}$$

$$\frac{1}{N}\sum_\lambda{}' \frac{\mathrm{erfc}\sqrt{x_\lambda}}{u_1-\mathrm{erfc}\sqrt{x_\lambda}} = 1\ . \tag{266}$$

The primes indicate that the sums contain only terms from the "fuzzy edge" of the width distribution, for which $u_2 < \mathrm{erfc}\sqrt{x_\lambda} < u_1$ with $u_1 = (c_1+2c_2E_1)\langle D\rangle$, $u_2 = (c_1+2c_2E_2)\langle D\rangle$, $x_\lambda = \Gamma_\lambda/(2\langle\Gamma\rangle)$. The equations are again convenient for iteration, starting e.g. from $\langle\Gamma\rangle = \bar{\Gamma}$, $\langle D\rangle = (E_2-E_1)/N$. A program based on this approach (Ref. 78) yielded the results shown in Fig. 23.

So far we restricted the discussion to pure level sequences for a given $J\pi$. Some of the results remain approximately valid also for mixed sequences. Consider, for instance, the p-wave levels for target spin I=0. Their spin is either J=1/2 or J=3/2, i.e. they belong to two different sequences. It is consistent with empirical evidence to consider their strength functions as independent of J, so that $S_{\ell J} = S_\ell$. The spin dependence of the level densities was derived by Bethe (Ref. 79, cf. also Ref. 80) from the Fermi-Gas model as

$$\rho_J \propto \exp\left[-\frac{J^2}{2\sigma^2}\right] - \exp\left[-\frac{(J+1)^2}{2\sigma^2}\right] \propto \sinh\left(\frac{J+1/2}{2\sigma^2}\right)\exp\left[-\frac{(J+1/2)^2}{2\sigma^2}\right] \tag{267}$$

The spin cut-off factor σ has values around 4 so that for small spins one has $\rho_J \propto 2J+1$. In this approximation and with $S_{\ell J} = S_\ell$ one finds that the $g\Gamma_n^1$ values of the combined p-wave sequences have the Porter-Thomas distribution, the average being

$$\langle g\Gamma_n^1\rangle = \frac{S_1}{\rho_{1/2}+\rho_{3/2}} = \langle D\rangle_1 S_1, \tag{268}$$

where $\langle D\rangle_1$ is the average spacing of all p-wave levels and S_1 the strength function of each separate sequence. We can therefore employ essentially the same estimation procedure as for pure sequences with $\nu=1$, with Γ_n^1 conveniently replaced by $g\Gamma_n^1$ so that the mostly unknown level spins are not needed.

Generalisation to $\nu=2$ (exponential distribution) is straightforward.

3.3.5 Spin assignment for given resonance areas with Bayes' theorem

It was already mentioned that resonance peak areas are sufficient for the calculation of average cross sections or zero-dilution group constants but not of Doppler effect or self-shielding. For these one requires spins. Level statistics can give us a handle to assign unknown spins if the area parameters $g\Gamma_n$, $g\Gamma_n\Gamma_x/\Gamma$ are known, at least in the sense that the resulting average spin distribution over many levels is realistic. Let us consider the typical case that enough information on s-wave resonance parameters is available to permit estimation (including missing-level correction) of $\langle D\rangle_o$ and S_o, and that S_1, S_2, ... are known from analysis of average cross sections and optical-model calculations. All required mean level spacings $\langle D_J\rangle$ can then be found from the s-wave spacing with the help of Eq. 267, and the average neutron widths from $\langle\Gamma_{n,\ell J}\rangle = \nu_{\ell J}\langle D_J\rangle S_\ell\sqrt{E/1\mathrm{eV}}\, v_\ell(E)$, where $\nu_{\ell J}$ is the number of channel spins (1 or 2) compatible with ℓ and J. We can now calculate the probabilities

$$p_{\ell J}\, d(g\Gamma_n) = \Gamma\left(\frac{\nu_{\ell J}}{2}\right)^{-1} e^{-x} x^{\nu_{\ell J}/2-1}\, dx, \quad o < x \equiv \frac{\nu_{\ell J}}{2}\frac{g\Gamma_n}{g_J\langle\Gamma_{n,\ell J}\rangle} < \infty \tag{269}$$

with $\ell = 0,1,2,\ldots$ for an observed value $g\Gamma_n$ in $d(g\Gamma_n)$. Bayes' theorem (see e.g. Ref. 41) tells us that we may take the probability for a given ℓJ combination as proportional to $p_{\ell J}$ if all combinations are equally probable a priori. The probability for a given spin J is then

$$p_J = \frac{\sum_\ell p_{\ell J}(g\Gamma_n)}{\sum_{\ell,J} p_{\ell J}(g\Gamma_n)}\ , \tag{270}$$

where the sum in the denominator is over all ℓ that are compatible with J. Often one sees immediately that a certain spin is probably correct, the others being too unlikely. In general one must make a probabilistic choice, for example with the Monte Carlo technique.

If additional types of resonance areas are known one can utilise this information also. Let us take, for instance, the capture peak areas $2\pi^2\lambda(E_\lambda)^2 g\Gamma_n\Gamma_\gamma/\Gamma$ with $\Gamma = \Gamma_n + \Gamma_\gamma$ (non-fissile target nucleus). From $g\Gamma_n$ and $g\Gamma_n\Gamma_\gamma/\Gamma$ we get $g\Gamma_\gamma$, for which an expression similar to Eq. 277 holds. If we know the effective degree of freedom and the average width for the (n,γ) reaction we can calculate the probability $p_{\ell J}(g\Gamma_\gamma)$ and base the spin selection on the joint probabilities $p_{\ell J}(g\Gamma_n)p_{\ell J}(g\Gamma_\gamma)$. Unfortunately $g\Gamma_n$ is often unknown. One must then consider the probability (for each allowed ℓJ)

$$p(\zeta)d\zeta = \int_{\zeta\ \mathrm{in}\ d\zeta}\int d\xi\, d\eta\, p_1(\xi)\, p_2(\eta) \tag{271}$$

$$= d\zeta \int_\zeta^\infty d\xi\, p_1(\xi)\, p_2\left(\frac{\xi\zeta}{\xi-\zeta}\right)\left(\frac{\xi}{\xi-\zeta}\right)^2 \tag{271}$$

where we omitted the subscripts ℓ,J and simplified the notation with $\xi \equiv g\Gamma_n$, $\eta \equiv g\Gamma_\gamma$, $\zeta \equiv g\Gamma_n\Gamma_\gamma/\Gamma$, p_1 and p_2 being the χ^2-distributions for $g\Gamma_n$ and $g\Gamma_\gamma$.

The effective degree of freedom ν for a width distribution can again be estimated with the maximum-likelihood method from a width sample $\Gamma_1, \Gamma_2, \ldots \Gamma_N$ if the average Γ is sufficiently well known. The likelihood function is maximised if ν is chosen as the solution of

$$\psi\left(\frac{\nu}{2}\right) - \ln\frac{\nu}{2} = \frac{1}{N}\sum_\lambda \ln\frac{\Gamma_\lambda}{\langle\Gamma\rangle} = \overline{\ln\Gamma} - \ln\langle\Gamma\rangle \tag{272}$$

where $\psi(\ )$ is the logarithmic derivative of the gamma function $\Gamma(\ )$ and the bar denotes the sample average as before (Ref. 62). Curves for the function on the right-hand side and for the asymptotic variance of the maximum-likelihood estimate ν are given in Ref. 56.

3.3.6 Monte Carlo generation of level sequences

There are situations in applied neutron physics where the resonance structure of the cross sections is important but unobservable due to finite instrumental resolution. For instance the average transmission in a given energy (group) interval can be written as

$$\langle e^{-n\sigma}\rangle = e^{-n\langle\sigma\rangle}\langle e^{-n(\sigma-\langle\sigma\rangle)}\rangle = e^{-n\langle\sigma\rangle}(1+\frac{n^2}{2}\,\mathrm{var}(\sigma)+\ldots). \qquad (273)$$

The variance and the higher-order terms are mainly due to the resonances in the interval. The reduction of raw transmission or yield data to average cross sections requires thus information on the resonance structure, the corresponding corrections being especially large for thick samples and for wildly fluctuating cross sections. Enhanced temperature, i.e. Doppler broadening, implies less fluctuation, hence less variance, so that average transmission and self-shielding of yields are reduced, reaction rates increased.

In the region of unresolved resonances (typically above a few keV for heavy, above a few hundred keV for medium-mass nuclei) these effects must be calculated from level statistics. One can sample the Wigner distribution to build up ladders of resonances, then find their widths from the Porter-Thomas or other appropriate χ^2 distributions, and finally obtain Doppler-broadened cross section values at equidistant or randomly chosen energy points along the ladder. Sorting the results into cross section bins one gets a histogram representation or tables of the cross section probability distributions $p(\sigma_x)d\sigma_x$, from which one can calculate the needed cross section functionals, e.g. the average, the variance etc., e.g.

$$\langle e^{-n\sigma}\rangle = \int_0^\infty d\sigma\; p(\sigma)e^{-n\sigma} = \sum_i \Delta\sigma p(\sigma_i)e^{-n\sigma_i}. \qquad (274)$$

This is the principle of the so-called probability table method (Ref. 81).

A more direct but somewhat slower method is the generation of "resonance environments" or "mini-ladders" (Ref. 82, 83) for each energy required in a Monte Carlo calculation (e.g. simulation of multiple-collision events). One samples, for each relevant JΠ level sequence, the distribution of "central" spacings,

$$p(D)dD \propto D\, p_w(D)dD, \qquad (275)$$

where $p_w dD$ is the Wigner distribution and the extra factor D accounts for the fact that the probability for a randomly selected energy to fall in a given energy interval is proportional to the interval size. Then one samples the (uniformly distributed) actual position of E within the central interval D which fixes the distance to the nearest two levels. Sampling the (bare) Wigner distribution one can generate further resonance energies above and below. Then the widths are sampled from the appropriate χ^2-distributions, and the cross section at E is calculated. With a reasonable level-statistical representation of distant levels (cf. Sect. 2.8.2) two to three levels below and above are usually enough to yield adequate cross section distributions. Addition of more distant levels does not change the results significantly, as experience with the SESH code (Ref. 82) for self-shielding and multiple-scattering correction of yield data showed (Ref. 83).

It should be noticed that in these Monte Carlo calculations the level spacing correlations as given by Eq. 247 were always neglected because there seems to be no simple recipe to produce them. The methods employed in theoretical studies of level spacings and their correlations, namely diagonalisation of Hamiltonian matrices belonging to the orthogonal ensemble etc., are by far too complicated for applied Monte Carlo calculations. The practical importance of the correlations is not very clear either, no systematic studies being available.

3.3.7 Test statistics for purity of level sequences

The theory of the orthogonal ensemble predicts that the level-density staircase curve N(E) of a pure sequence deviates very little from a straight line with slope $\rho = 1/\langle D\rangle$. The mean-square deviation from a best-fit straight line $\bar{N}(E) = c_0 + c_1 E$ in the interval $(E_1 \ldots E_2)$, called the Δ_3 statistic by Dyson and Mehta,

$$\Delta_3 = \frac{1}{E_2 - E_1}\int_{E_1}^{E_2} |N(E) - \bar{N}(E)|^2 dE, \qquad (276)$$

was shown (Ref. 77) to have the expectation value

$$\Delta_3 = \frac{1}{\pi^2}\left[\ln(2\pi N) + \gamma - \frac{\pi^2}{8} - \frac{5}{4}\right] \approx \frac{1}{\pi^2}(\ln N - 0.0687) \qquad (277)$$

($\gamma = 0.5772\ldots$ is Euler's constant) and the variance

$$\mathrm{var}(\Delta_3) = \frac{1}{\pi^4}\left[\frac{4\pi^2}{45} + \frac{7}{24}\right] \approx \frac{1.1690}{\pi^4}. \qquad (278)$$

Absence of mixed levels or presence of spurious levels from other sequences obviously increases Δ_3. One has therefore tried to use Δ_3 as a test statistic for the purity of levels, see Refs. 84, 86.

An optimum statistic for the presence of spurious or missing levels is, according to Dyson (see Refs. 84, 85),

$$F_\lambda \equiv \sum_{\mu\neq\lambda} \mathrm{ar\ cosh}\,\frac{I/2}{E_\mu - E_\lambda} \qquad (279)$$

where μ runs through all levels between $E_\lambda - I/2$ and $E_\lambda + I/2$ and I is an arbitrary fixed interval (for instance 20 times $\langle D\rangle$). Expectation value and variance are, with $n \equiv \pi I/(2\langle D\rangle)$,

$$F_\lambda = n - \ln n - \gamma + 2 \approx n - \ln n - 0.656 \qquad (280)$$

$$\mathrm{var}(F_\lambda) \approx \ln n, \qquad (281)$$

if E_λ is a true member of the sequence. If E_λ is the energy of a spurious level in an otherwise pure sequence one gets

$$F_\lambda = n, \qquad (282)$$

so that a spurious or missing level produces, on the average, a peak or a dip in F_λ of magnitude $\sim \ln n$. The catch lies in the words "on the average" (see Ref. 84). It should be stressed that none of these tests permits unambiguous identification of spurious or missed levels but, as the Columbia group demonstrated (Refs. 84, 86), by combining all available tests one can purify almost pure level sequences further, to a degree which is wholly satisfactory for applied purposes.

4. CONCLUDING REMARKS

We reviewed those aspects of neutron resonance theory, including level statistics, that are most important for applications in neutron cross section metrology and nuclear technology. Among the topics which were not treated are the double-humped fission barrier and its consequences, and resonance-averaged cross sections. These are treated by J.E. Lynn and P. Moldauer in

special parts of this course. For other recent developments in the area of level statistics or rather limitations of it caused by phenomena such as doorway states, valence nucleon transitions, precompound reactions we refer the reader to Refs. 87 and 88. We close by restating a few main points:

1. Multi-level cross sections should be calculated from the collision matrix rather than from explicit cross section expressions. This avoids double sums over levels that are very time-consuming when many levels are involved.

2. If explicit cross section expressions must be used the total cross section is the easiest, the elastic-scattering cross section the most difficult to calculate. The latter is therefore best obtained as difference.

3. The Reich-Moore formalism requires a minimum of real parameters, is virtually exact and not slower than the other multi-level approximations.

4. The applicability of the Voigt profiles ψ and χ to Doppler broadening of MLBW or Adler-Adler cross sections should not be overestimated in view of the necessary preparatory work and the inferior accuracy obtained. Numerical broadening of Reich-Moore cross sections need not be slower, on the contrary, and avoids consistency and accuracy problems. Adler-Adler parametrisation is restricted to relatively small energy intervals, i.e. to heavy nuclei.

5. Partial cross section (yield) data cannot be analysed properly without transmission data of comparable energy resolution and detection power for narrow levels.

6. Measurers and analysts of resonance data should state the errors as clearly as possible, with statistical and systematic components separated, and at least some indication of correlations between deduced resonance parameters.

7. To state resonance parameters without the corresponding channel radii and other potential-scattering or distant-level parameters is a cardinal sin.

8. The Porter-Thomas distribution is the most efficient tool for missing-level corrections. The Wigner distribution is less important for data analysis than for generation of artificial (mock) cross sections for the calculation of resonance effects in the unresolved-resonance region.

References

1. Winter Courses on Nuclear Physics and Reactors, Part I: Nuclear Theory for Applications, Trieste, 16 January - 10 February 1978, to be published

2. J.J. Schmidt, contribution to Ref. 1

3. CINDA 76/77, An Index to the Literature on Microscopic Neutron Data, IAEA Vienna, 1977

4. S.F. Mughabghab and D.I. Garber, BNL 325, 3rd ed., vol.I (1973), vol. II (1976)

5. A.M. Lane and R.G. Thomas, Rev. Mod. Phys. 30 (1958) 257

6. J.M. Blatt and L.C. Biedenharn, Rev. Mod. Phys. 24 (1952) 258

7. U. Fano and G. Racah, Irreducible Tensorial Sets, New York, 1959; cf. also A de-Shalit and I. Talmi, Nuclear Shell Theory, New York-London, 1963, ch. 15 and Appendix

8. L.C. Biedenharn, Report ORNL-1501 (1953)

9. E.P. Wigner and L. Eisenbud, Phys. Rev. 72 (1947) 29, E.P. Wigner, J. Am. Phys. Soc. 17 (1949) 99

10. P.L. Kapur and R.E. Peierls, Proc. Roy. Soc. (London) A166 (1938) 277; R.E. Peierls, Proc. Cambridge Phil. Soc. 44 (1947) 242

11. T. Teichmann and E.P. Wigner, Phys. Rev. 87 (1952) 123

12. M.K. Drake (ed.), Report ENDF 102 (1970)

13. D.R. Harris, Report LA-4327 (1970)

14. J. Krebs, G. le Coq, J.P. l'Hériteau, P. Ribon, Nuclear Data for Reactors, IAEA Vienna, 1970, p. 789

15. C.W. Reich and M.S. Moore, Phys. Rev. 111 (1958) 929

16. D.R. Harris, Neutron Cross Sections and Technology, Washington D.C., 1966 (CONF 660303), p. 833

17. D.B. Adler and F.T. Adler, Proc. Conf. Breeding Economics and Safety in Large Fast Power Reactors, Argonne, 1963, p. 695; F.T. Adler and D.B. Adler, Neutron Cross Section Technology, Washington D.C., 1966, vol. II, p. 873; F.T. Adler and D.B. Adler, Nucl. Data for Reactors, IAEA Vienna, 1970, p. 777

18. A.J.F. Siegert, Phys. Rev. 56 (1939) 750

19. J. Humblet and L. Rosenfeld, Nucl. Phys. 26 (1961) 529

20. G. de Saussure and R.B. Perez, Report ORNL-TM-2599 (1969); Nucl. Sc. Eng. 52 (1973) 412

21. G.de Saussure, R.B. Perez, H. Derrien, Nucl. Data for Reactors, IAEA Vienna, 1970, vol. II, p. 757

22. M. Segev, Report TNSD-R/462 (1977)

23. W.E. Lamb, Phys. Rev. 55 (1939) 190

24. F.H. Fröhner, unpublished

25. W. Voigt, Sitz-Ber. Bayer. Akad. Wiss. (1912) p. 603

26. M. Born, Optik, Berlin 1933

27. D.E. Cullen, C.R. Weisbin, Nucl. Sc. Eng. 60 (1976) 199

28. F.H. Fröhner, Nucl. Instr. Meth. 49 (1967) 89

29. L.P. Abagjan, N.O. Bazazjanc, I.I. Bondarenko, M.N. Nikolaev, Group Constants, KFK-tr-144 (German translation)

30. E.Kiefhaber et al., Report KFK 1572 (1972)

31. F.G. Perey, Specialist Meeting on Neutron Data of Structural Materials for Fast Reactors, Geel, 5-8 Dec. 1977

32. F.H. Fröhner, Specialist Meeting on Neutron Data of Structural Materials for Fast Reactors, Geel, 5-8 Dec. 1977

33. A. Arnaud, C. le Rigoleur, J.P. Marquette, Nuclear Cross Sections and Technology, NBS Spec. Publ. 425 (1975) vol. II, p. 961

34. M.C. Moxon, D.B. Gayther, M.G. Sowerby, KFK 2046 (1975) p. 73

35. B.J. Allen, A.R. de L. Musgrove, R. Taylor, R.L. Macklin, Specialist Meeting on Neutron Data of Structural Materials for Fast Reactors, Geel, 5-8 Dec. 1977, to be published

36. F.H. Fröhner, Report KFK 2129 (1976)

37. F.H. Fröhner and E. Haddad, Nucl. Phys. 71 (1965) 129

38. F.H. Fröhner, Report KFK 2145 (1978)

39. M.R. Bhat, R.E. Chrien, I.W. Cole, Neutron Cross Sections and Technology, Washington D.C. 1966, vol. 1, p. 522

40. A. Ernst, F.H. Fröhner and D. Kompe, Nuclear Data for Reactors, IAEA Vienna, 1970, vol. I, p. 633; F.H. Fröhner, Report KFK 2046 (1975) p. 1; F.H. Fröhner, Nuclear Cross Sections and Technology, NBS Spec. Publ. 425 (1975), vol. II, p. 929

41. J. Mathews and R.L. Walker , Mathematical Methods of Physics, New York-Amsterdam, 1965, p. 365

42. J.A. Harvey, Neutron Cross Sections and Technology, Washington D.C., 1966, vol. I, p. 31

43. F.H. Fröhner, E. Haddad, W.M. Lopez and S.J. Friesenhahn, Neutron Cross Sections and Technology, Washington D.C., 1966, vol. I, p. 55

44. D.J. Hughes, J. Nucl. Energy 1 (1955) 237; Progress in Nucl. Energy, Series I (1959) 1

45. S.E. Atta and J.A. Harvey, Report ORNL-3205 (1961)

46. F.H. Fröhner, Report GA-6909 (1966)

47. E.M. Cornelis, private communication

48. F.H. Fröhner, to be published

49. G. Rohr, private communication

50. H. Derrien, J. Blons, A. Michaudon, Nucl. Data for Reactors, IAEA Vienna, 1970, vol. I, p. 481

51. N.H. Marshall, J.W. Codding , O.D. Simpson, J.R. Smith, Neutron Cross Sections and Technology, Knoxville, 1971, vol. I, p. 354

52. D.B. Adler and F.T. Adler, Report COO-1546-3 (1966)

53. G. de Saussure, private communication

54. M.C. Moxon, Proc. Specialist Meeting on Neutron Data of Structural Materials for Fast Reactors, Geel, Dec. 1977 (to be published)

55. G. de Saussure, D.K. Olsen, R.B. Perez, Nucl. Sci. Eng. 61 (1976) 496

56. J.E. Lynn, Neutron Resonance Reactions, Oxford, 1968, p. 278

57. H. Beer and R.R. Spencer, Nucl. Phys. A240 (1975) 29

58. H. Beer, Li Dy Hong, F. Käppeler, Report KFK 2337 (1976)

59. A.P. Jain, Nucl. Phys. 50 (1964) 157

60. C.E. Porter (ed.), Statistical Theories of Spectra: Fluctuations, New York-London, 1965 (contains all important papers on level statistics up to 1964)

61. J.B. Garg (ed.), Statistical Properties of Nuclei, New York-London, 1972

62. C.E. Porter and R.G. Thomas, Phys. Rev. 104 (1956) 483 (reprinted in Ref. 60)

63. J.D. Garrison, Ann. Phys. 30 (1964) 269

64. H.E. Jackson, J. Julien, C. Samour, A. Block, C. Lopata, J. Morgenstern, Phys. Rev. Letters 17 (1966) 656

65. A. Bohr, Proc. Conf. on Peaceful Uses of Atomic Energy, Geneva, 1955, vol. 2, p. 151

66. J.E. Lynn, Neutron Resonance Reactions, Oxford, 1968, p. 377, see also contribution to this course

67. E.P. Wigner, Conf. on Neutron Physics by Time-of-Flight, Gatlinburg, Tennessee, 1956, Report ORNL-2309 (1957) p. 59 (reprinted in Ref. 60)

68. M.L. Mehta, Nucl. Phys. 18 (1960) 395 (reprinted in Ref. 60)

69. M. Gaudin, Nucl. Phys. 25 (1961) 447 (reprinted in Ref. 60)

70. F.J. Dyson, J. Math. Phys. 3 (1962) 140 (reprinted in Ref. 60)

71. P.A. Mello, J. Flores, T.A. Brody, J.B. French, S.S.M. Wong, Proc. Int. Conf. Interactions of Neutrons with Nuclei, Lowell, 1976, vol. I, p. 496

72. F.J. Dyson and M.L. Mehta, J. Math. Phys. 4 (1963) 701 (reprinted in Ref. 60)

73. C.E. Porter, Nucl. Phys. 40 (1963) 167 (reprinted in Ref. 60)

74. H.I. Liou, H.S. Camarda, S. Wynchank, M. Slagowitz, G. Hacken, F. Rahn, J. Rainwater, Phys. Rev. C5 (1972) 974

75. D.D. Slavinskas and Kennett, Nucl. Phys. 85 (1966) 641

76. Kh. Maletski, L.B. Pikelner, I.M. Salamatin, E.I. Sharapov, Report JINR-P3-4484 (1969)

77. T. Fuketa and J.A. Harvey, Nucl. Instr. Meth. 33 (1965) 107

78. F.H. Fröhner, program STARA, to be published

79. H.A. Bethe, Rev. Mod. Phys. 9 (1937) 69

80. A. Gilbert and A. G. W. Cameron, Can. J. Physics 43 (1965) 1446

81. L.B. Levitt, Nucl. Sci. Eng. 49 (1972) 450

82. F.H. Fröhner, Report GA-8380 (1968)

83. F.H. Fröhner, Report GA-8072 (1967) and F.H. Fröhner, Nucl. Data for Reactors, IAEA Vienna, 1970, vol. I., p. 197

84. H.I. Liou, H.S. Camarda, F. Rahn, Phys. Rev. C5 (1972) 1002

85. M.L. Mehta, Statistical Properties of Nuclei, New York-London, 1972, p.179

86. H. Camarda, H.I. Liou, F. Rahn, G. Hacken, M. Slagowitz, W.W. Havens, Jr., J. Rainwater, Statistical Properties of Nuclei, New York-London, 1972, p. 205

87. J.A. Bird, J.W. Boldeman, B.J. Allen, A.R. de L. Musgrove, M.J. Kenny, Interaction of Neutrons with Nuclei, Lowell, 1976, vol. I, p. 76

88. A.M. Lane, Interaction of Neutrons with Nuclei, Lowell, 1976, vol. I. p. 525

89. E.G. Silver, G. de Saussure, R.B. Perez, R.W. Ingle, Neutron Cross Sections and Technology, Knoxville, 1971, vol. 2, p. 728

90. H. Beer and R.R. Spencer, Report KFK 2063 (1974)

91. P.A. Moldauer, Nucl. Phys. 47(1963)65

THEORETICAL ASPECTS OF THE OPTICAL MODEL

C. MAHAUX
Institut de physique nucléaire,
Liège, Belgium
University of Liège, Sart Tilman,

Abstract

We first recall the definition of the optical-model potential for nucleons and the physical interpretation of the main related quantities. We then survey the recent theoretical progress towards a reliable calculation of this potential. The present limitations of the theory and some prospects for future developments are outlined.

1. INTRODUCTION

The optical-model potential (OMP) is a basic ingredient of practically any nuclear data evaluation : it enters in the analysis of elastic scattering and of total cross sections, of radiative capture, of compound nuclear as well as of direct reactions, of strength functions, of potential scattering lengths, etc. Clearly, a minimal theoretical understanding of the optical model is a prerequisite to all practitioners, and its detailed theoretical investigation is fully justified.

Many previous theoretical studies had been focused on formal aspects of the optical model, or on the qualitative rendering of the gross phenomenological properties of the OMP. In recent years, however, the theory has made sufficient progress to yield semi-quantitative results, i.e. to provide meaningful theoretical constraints on the parameters of the potential. We hope that these lectures will give off a bit of the flavour of this sprouting.

Our main purpose is twofold. Firstly, we recall the definition, the practical interest and the physical interpretation of the OMP. Secondly, we survey some of the recent theoretical calculations of this potential; we try to indicate not only their interest but also their present limitation.

In view of our limited aim, we avoid technical details whenever possible, at the risk of shocking the purists. For instance, we almost indifferently write $\vec{r}$ or r, we omit explicit reference to spin indices, drop Clebsch-Gordan coefficients and spin statistical factors, usually consider only neutron channels, etc. In the same spirit, we quote only very few original papers: an exhaustive list of references can be found in recent books or reviews, e.g. [1-8].

2. PHYSICAL CONTENT

2.1. Scattering matrix

A reaction channel is characterized by a set of quantum numbers (channel spin s_c, relative orbital angular momentum ℓ_c, ...) that we generically denote by $\underline{c}$.

The scattering wave function Ψ_E^c at energy E is an eigenstate of the full Hamiltonian H

$$H \Psi_E^c = E \Psi_E^c \quad ; \tag{2.1}$$

the upper index $\underline{c}$ specifies the channel in which there exists an incoming wave. At a large distance $r_{c'}$ between the two fragments in channel c', one has the asymptotic behaviour

$$\Psi_E^c \sim r_{c'}^{-1} \{\delta_{cc'} e^{-i(k_c r_c - \frac{1}{2}\ell_c \pi)} - (\frac{v_c}{v_{c'}})^{\frac{1}{2}} S_{c'c}(E) \cdot e^{i(k_{c'} r_{c'} - \frac{1}{2}\ell_{c'} \pi)}\} \phi_{c'} \quad . \tag{2.2}$$

Here,

$$v_c = \frac{\hbar k_c}{m} \tag{2.3}$$

is the relative velocity; $\phi_{c'}$ essentially denotes the wave function of the residual nucleus, multiplied by appropriate spin eigenstates and spherical harmonics, coupled to the total angular momentum of channel $\underline{c}$.

The scattering matrix $S_{cc'}$ is symmetric (time reversal invariance of H) and unitary (conservation of flux) :

$$\sum_{c''} S^{*}_{cc''}(E)\, S_{c''c'}(E) = \delta_{cc'} \quad , \tag{2.4}$$

where the sum runs over the channels which are open at the energy E .

Because of the existence of compound nuclear resonances, the scattering matrix is a violent function of energy. It is usually written in the parametric form

$$S_{cc'}(E) = [Q_{cc'} - i \sum_{n} \frac{\Gamma_{nc}^{\frac{1}{2}}\, \Gamma_{nc'}^{\frac{1}{2}}}{E-E_n + \frac{1}{2} i\, \Gamma_n}] \exp(i\,\delta_c + i\,\delta_{c'}) \quad . \tag{2.5}$$

The quantity $Q_{cc'}$ and the potential scattering phase shifts δ_c, $\delta_{c'}$ are smooth functions of energy. If direct reactions can be neglected, one has [9]

$$Q_{cc'} = \delta_{cc'} \quad , \tag{2.6}$$

$$\overline{\Gamma_{nc}^{\frac{1}{2}}\, \Gamma_{nc'}^{\frac{1}{2}}} = \overline{\Gamma_{nc}}\, \delta_{cc'} \quad , \tag{2.7}$$

where the bar denotes an average over resonances.

2.2. Optical-model phase shift

The success of the shell-model indicates that for many purposes one can represent the interaction between a bound nucleon and the rest of the nucleus by an average potential well, or more precisely by a non-local single particle potential. By continuity, one expects a similar picture to be applicable to unbound nucleons. In the latter case, the average potential well may depend on the nucleon energy, besides being non-local. Let us denote this "optical-model potential" (OMP) in channel c and at energy E by $V_c(E)$; the spatial variables $\vec{r}$, $\vec{r}'$ are omitted. We shall progressively reach a specific definition of this OMP.

Let us call $\tilde{S}_{cc'}$ the scattering matrix that corresponds to the scattering of a nucleon by the OMP:

$$\tilde{S}_{cc'} = \tilde{S}_c\, \delta_{cc'} = \exp(2\, i\, \xi_c)\, \delta_{cc'} \quad . \tag{2.8}$$

It is not practical to choose V_c in such a way that $\tilde{S}_{cc} = S_{cc}$: since S_{cc} is a complicated function of energy (see Eq. (2.5)), the same would be true for the corresponding OMP. Hence, one rather requires the OMP to be such that its scattering function $\tilde{S}_c$ is equal to the energy-average $\langle S_{cc} \rangle$ of the diagonal element of the scattering matrix :

$$\tilde{S}_c = \langle S_{cc} \rangle \quad . \tag{2.9}$$

Since this requirement does not fully determine the OMP, we shall further refine the definition below.

The energy average, taken over an averaging interval I centered on E , of a quantity $q(E')$ is conveniently defined by

$$\langle q(E) \rangle = \frac{I}{\pi} \int_{-\infty}^{\infty} \frac{q(E')}{(E-E')^2 + I^2}\, dE' \quad . \tag{2.10}$$

Equations (2.5),(2.10) yield, in the absence of direct reactions (see Eqs. (2.6),(2.7))

$$\tilde{S}_c = \langle S_{cc} \rangle = S_{cc}(E + iI) = (1 - \pi \frac{\overline{\Gamma}_{nc}}{d}) \exp(2\, i\, \delta_c) \quad , \tag{2.11}$$

where d is the average distance between neighbouring resonances. Since

$$|\tilde{S}_c|^2 = |\langle S_{cc} \rangle|^2 < 1 \quad , \tag{2.12}$$

the optical-model phase shift ξ_c is complex and the same must be true for the OMP :

$$V_c = V_c + i\, W_c \quad . \tag{2.13}$$

One finds that (2.12) implies

$$W_c < 0 \quad , \tag{2.14}$$

if W_c is assumed to be a local potential with standard shape.

2.3. Sources of the imaginary part

The existence of an imaginary (or absorptive) component W_c in the OMP is thus directly related to the lack of unitarity of $\langle S_{cc} \rangle$. We mentioned that the unitarity property (2.14) of the scattering matrix expresses the conservation of flux. Correspondingly, the lack of unitarity of $\tilde{S}_c$ expresses a loss of flux.

This lack of unitarity must exist if channels $c' \neq c$ are open since the quantity

$$\langle |S_{cc}|^2 \rangle = 1 - \sum_{c' \neq c} \langle |S_{c'c}|^2 \rangle \qquad (2.15)$$

is larger than $|\langle S_{cc} \rangle|^2$. However, Eq. (2.11) shows that V_c is complex even if no channel other than c is open; the reason is that V_c involves the quantity $\langle S_{cc} \rangle$, i.e. implies an average over compound nuclear resonances.

We conclude from these arguments that the origin of the imaginary component of the OMP is twofold. Part of the incoming flux feeds the compound nuclear resonances; part of it goes into the inelastic channels $c' \neq c$ via direct reactions. Thus, we must be prepared to find these two sources of absorption in the formal expression for the OMP : we return to this point in section 3.4.

2.4. Calculable observables

We mentioned in section 1 that the OMP plays an essential role in the analysis of many types of reaction data. It is not possible to discuss these applications in any detail here; many of them will be reviewed by other lecturers. We first consider those which only involve the optical-model phase shift, and then briefly emphasize that the optical-model wave function is needed in the evaluation of direct reaction data. We recall that for the sake of simplicity, we omit spin statistical factors, Clebsch-Gordan coefficients, ...

The total cross section in channel c is given by

$$\sigma_{c,tot} = \sum_{c'} \sigma_{cc'} = 2\pi k_c^{-2} (1 - \mathrm{Re}\, S_{cc}) \quad . \qquad (2.16)$$

Its energy average can thus directly be obtained from the optical-model phase shift :

$$\langle \sigma_{c,tot} \rangle = 2\pi k_c^{-2} (1 - \mathrm{Re}\, \tilde{S}_c) \quad . \qquad (2.17)$$

For examples, we refer to the reviews by Wilmore and Hodgson (Ref. [5] vol. 2, p. 131) and by Wiedling, Ramstroem and Holmqvist (ibid., p. 205).

The angle-integrated cross section $\sigma_{cc'}$ reads

$$\sigma_{cc'} = \pi k_c^{-2} |S_{cc'} - \delta_{cc'}|^2 \quad . \qquad (2.18)$$

Its energy average can be written as a sum of two terms :

$$\langle \sigma_{cc'} \rangle = \sigma^{SE}_{cc'} + \sigma^{CN}_{cc'} \quad . \qquad (2.19)$$

The first term is

$$\sigma^{SE}_{cc'} = \pi k_c^{-2} |\langle S_{cc'} \rangle - \delta_{cc'}|^2 \quad . \qquad (2.20a)$$

It is diagonal in the absence of direct reactions. The quantity σ^{SE}_{cc} is called the shape elastic scattering cross section and can be expressed in terms of the optical-model phase shift :

$$\sigma^{SE}_{cc} = \pi k_c^{-2} |\tilde{S}_c - 1|^2 \quad ; \qquad (2.20b)$$

it usually dominates the cross section for energies larger than a few MeV (Ref. [2], p. 142).

At low energy, the shape elastic cross section approaches a constant; the potential scattering radius R' is defined by

$$R' = \lim_{E \to 0} (\sigma^{SE}_{cc}/4\pi)^{\frac{1}{2}} \quad . \qquad (2.21)$$

For an example, see Fig. 7.3 of Ref. [8].

The compound nuclear cross section $\sigma^{CN}_{cc'}$ is given by

$$\sigma^{CN}_{cc'} = \pi k_c^{-2} \{ \langle |S_{cc'}|^2 \rangle - |\langle S_{cc'} \rangle|^2 \} \quad . \tag{2.22}$$

In the absence of direct reactions, the second term in the curly brackets vanishes for $c \neq c'$; the first term can then be written in the Hauser-Feshbach form

$$\langle |S_{cc'}|^2 \rangle = \frac{T_c \, T_{c'}}{\sum_{c''} T_{c''}} \quad , \tag{2.23}$$

where the transmission coefficient T_c reads

$$T_c = 1 - |\tilde{S}_c|^2 \quad . \tag{2.24}$$

These relations can be extended to the differential cross sections; significant progress has recently been accomplished to extend their range of validity by including the effect of direct and of precompound reactions : see, e.g., the review by Moldauer (Ref. [5], vol. 1 page 167).

The strength function in channel c is by definition

$$s_c = \left(\frac{E_o}{E}\right)^{\frac{1}{2}} \frac{\overline{\Gamma}_{nc}}{d} \quad , \quad E_o = 1 \text{ eV} \quad ; \tag{2.25a}$$

the factor $(E_o/E)^{1/2}$ is introduced in order to render s_c practically independent of E . Equations (2.11) and (2.23) show that

$$\pi \frac{\overline{\Gamma}_{nc}}{d} \approx \frac{1}{2} T_c \quad . \tag{2.25b}$$

For an example, see Fig. 7.2 of Ref. [8].

The optical-model wave function $\tilde{u}^c_E$ calculated from the OMP plays a fundamental role in the analysis of direct reactions, including direct radiative capture. The index E refers to the total energy in channel c :

$$E = \frac{\hbar^2}{2m} k_c^2 + \varepsilon_c \quad , \tag{2.26}$$

where ε_c is the threshold energy. The function $\tilde{u}^c_E(r)$ is normalized to unit incoming amplitude at $r \to \infty$. In the distorted wave Born approximation, the direct reaction amplitude is proportional to the quantity

$$S^{DI}_{cc'} = \int_o^\infty \tilde{u}^{c'}_E(r) \, F_{c'c}(r) \, \tilde{u}^c_E(r) \, dr \quad , \tag{2.27}$$

where the quantity $F_{c'c}(r)$ represents the operator which is responsible for the direct transition from channel c to channel c' (see, e.g., Ref. [2] p. 67).

The physical interpretation of Eq. (2.27) is that the probability amplitude for a direct reaction to occur at a distance r from the target centre is proportional to the probability amplitude $(\tilde{u}^c_E)$ of finding at that distance a nucleon on top of the unperturbed target state ϕ_c , and to that $(\tilde{u}^{c'}_E)$ of finding a nucleon on top of the residual nucleus $\phi_{c'}$, at the distance r .

2.5. Mean free path

According to its physical interpretation given at the end of the preceding section, we expect $|\tilde{u}^c_E(r)|$ to decrease with decreasing r . Indeed, when a nucleon penetrates into the target (see Fig. 1(a)), it interacts with other nucleons and it thereby excites the target. Two types of excitation are possible. In the first one, all nucleons (including the incoming one) occupy bound shell-model orbitals after the interaction : this collision corresponds to the formation of a quasi-bound state, i.e. of a compound nuclear resonance (see Fig. 1(b)). In the second type of interaction, one nucleon remains in a scattering orbital : this corresponds to a direct excitation of an inelastic channel (see Fig. 1(c)). We recognize the two sources of absorption described at the end of section 2.3.

For simplicity, let us consider the motion of a nucleon with energy E and momentum k in the z-direction, inside a "target" of infinite size (nuclear matter). The latter is

characterized by its density ρ (nucleons/fm^3), which is related to the Fermi momentum k_F by

$$\rho = \frac{2}{3\pi^2} k_F^3 \quad . \tag{2.28}$$

The nucleon wave function is a plane wave $\exp(ikz)$. If the potential energy $V = V + iW$ is complex, the wave number k is complex :

$$k = k^{(R)} + i\, k^{(I)} = \{\frac{2m}{\hbar^2} (E - V - iW)\}^{\frac{1}{2}} \quad . \tag{2.29}$$

Let us expand the square root and retain terms of first order in the ratio $W/(E - V)$. This yields

$$k^{(R)} = \{2m\,(E - V)\}^{\frac{1}{2}} / \hbar \quad , \quad k^{I} = -W / \hbar v \quad , \tag{2.30a}$$

where

$$v = \hbar\, k^{(R)}/m \tag{2.30b}$$

is the velocity. Equation (2.29) shows that the probability of finding a nucleon with unperturbed wave number $k^{(R)}$ decreases exponentially; its "mean free path" is equal to

$$L = \{2\, k^{(I)}\}^{-1} = - \hbar v/2W \quad , \tag{2.31}$$

where the factor 2 occurs because we deal with probabilities rather than amplitudes. In Fig. 2, we sketch the propagation in the z-direction of a wave-packet associated with a nucleon with momentum k on top of an infinite medium. At $z = 0$, the target is unperturbed : all nucleon momenta up to k_F are filled. On its way from $z = A$ to $z = D$, the incoming nucleon collides with target nucleons and excites on particle-one hole (B), two particle-two hole (C), ... target configurations. At $z = D$, the probability of finding a nucleon with momentum k on top of the initial ground (unperturbed) target states has decreased by a factor $\exp(- |DA|/L)$.

The mean free path plays an important role in the analysis of precompound reactions [10]. For an illustration, see Fig. 2.4 of Ref. [11]. The associated "mean life time" τ is given by

$$\Delta t = \tau = L/v = - \hbar/2W \quad . \tag{2.32}$$

The uncertainty relation

$$\Delta E \,.\, \Delta t = \hbar \tag{2.33}$$

shows that the energy of the "single-particle state" is not well defined : the quantity $\Delta E = - 2W$ measures the energy interval over which its strength is distributed because of the collisions. It is called the "single-particle spreading width".

3. NUCLEAR REACTION THEORY

3.1. Introduction

From the physical picture drawn in the preceding section emerges a definition of the OMP which is more specific than the one given in section 2.2 : the OMP should not yield the energy-average of S_{cc} but also, in addition, the energy-average $\tilde{u}_E^c$ of the wave function u_E^c that describes the relative motion of the nucleon and of the target (or residual nucleus). This suggests the following theoretical approach to the problem of calculating the OMP : one should first find a Schroedinger equation for the radial wave function u_E^c and then a similar one for its energy average. Feshbach's projection operator formalism [12] is well suited for this purpose, but will only be used implicitly below.

Before proceeding, we mention another theoretical approach, which is suggested by the content of section 2.5 : it consists in studying the potential energy and the mean free path of a nucleon in infinite nuclear matter with density ρ, and then to construct the OMP in a finite nucleus by allowing ρ to depend on r, namely to be density distribution $\rho(r)$ of the target. This line of approach will be discussed in section 4.

3.2. Coupled channels

The full wave function Ψ_E^c has components in all channels c' which have same parity and angular momentum as the entrance channel c. We want to derive coupled equations for these components, whose asymptotic behaviour is given by Eq. (2.2).

We omit antisymmetrization, and also the spin variables. The ground and the excited target states are eigenstates of the target Hamiltonian $H_t(r_1,\ldots,r_A)$:

$$H_t\,\phi_{c'} = \varepsilon_{c'}\,\phi_{c'} \quad . \tag{3.1}$$

Let us write Ψ_E^c as a sum over its channel components

$$\Psi_E^c = \sum_{c'} u_{c'}^c(r_o;E)\,\phi_{c'}(r_1,\ldots,r_A) \quad . \tag{3.2}$$

This full wave function is the solution, with appropriate boundary conditions, of the Schroedinger equation (2.1) which reads, more explicitly,

$$\left[-\frac{\hbar^2}{2m}\nabla^2_{r_o} + \sum_{j=1}^{A} v(r_o,r_j) + H_t\right]\Psi_E^c = E\,\Psi_E^c \quad . \tag{3.3}$$

We substitute expression (3.2) in Eq. (3.3) and multiply the result to the left by ϕ_c^* , $\phi_{c'}^*$, ... , ϕ_N^* . We integrate over the coordinate r_1 , ... , r_A of the target nucleons : below, this integration is indicated by round brackets. We obtain the following coupled system of equations

$$(E - H_{c'c'})\,u_{c'}^c(r_o;E) = -\sum_{c''} V_{c'c''}\,u_{c''}^c(r_o;E) \quad , \tag{3.4}$$

where

$$H_{c'c'} = \varepsilon_{c'} + V_{c'c'} - \frac{\hbar^2}{2m}\nabla^2_{r_o} \tag{3.5}$$

$$V_{cc'} = \left(\phi_c \,\middle|\, \sum_{j=1}^{A} v(r_o,r_j) \,\middle|\, \phi_{c'}\right) \quad . \tag{3.6}$$

With matrix notations, it is easy [3,12] to solve the set of linear equations (3.4) for $u_{c'}^c$, $(c' \neq c)$, and to obtain an equation for the elastic radial wave function, i.e. for

$$u_c^c(r_o,E) = u_E^c(r_o) \quad . \tag{3.7}$$

For illustrative purposes, it is convenient to perform this elimination of the inelastic components in the framework of second order perturbation theory with respect to the coupling strengths $V_{cc'} = V_{c'c}$, and to set $V_{c'c''} = 0$ $(c' \neq c'' \neq c)$. We have then

$$u_{c'}^c(r_o;E) = -V_{cc'}\,\frac{1}{E^+ - H_{c'c'}}\,u_c^c(r_o;E) \quad , \tag{3.8}$$

where

$$E^+ = \lim_{\eta \to +0} E + i\eta \tag{3.9}$$

insures that $u_{c'}^c$ is purely outgoing for r_o large. Equations (3.4) and (3.8) give

$$\left[E - \varepsilon_c - V_{cc} + \frac{\hbar^2}{2m}\nabla^2_{r_o} - \sum_{c' \neq c} V_{cc'}\,\frac{1}{E^+ - H_{c'c'}}\,V_{c'c}\right] u_E^c(r_o) = 0 \quad . \tag{3.10}$$

This result and Eq. (2.11) yield the expression of the OMP in our simplified model :

$$V_c = V_{cc} + \sum_{c' \neq c} V_{cc'}\,\frac{1}{E - H_{c'c'} + iI}\,V_{c'c} \quad . \tag{3.11}$$

3.3. Hartree-Fock approximation

The first order contribution to V_c (Eq. (3.11)) is V_{cc} , which reads more explicitly

$$V_{cc}(r_o) = \int \phi_c^*(r_1,\ldots,r_A) \sum_{j=1}^{A} v(r_o,r_j)\,\phi_c(r_1,\ldots,r_A)\,dr_1 \ldots dr_A \quad . \tag{3.12}$$

Since the function ϕ_c is antisymmetric and normalized, V_{cc} can be written in terms of the density $\rho(r')$ of the target :

$$V_{cc}(r) = \int \rho(r')\,v(r,r')\,d^3r' \quad ; \tag{3.13}$$

we recall that we do not bother to distinguish between $\vec{r}'$ and r' , unless really useful.

Expression (3.13) is the Hartree approximation $V^H(r)$. Following the work of Greenlees and collaborators [13], this "folding" formula has often been used during the last decade for estimating the real part of the OMP [14].

The effect of antisymmetrization should be included : it is not possible to find out whether the outgoing nucleon is the same as the incoming one, or whether it is one of the original nucleons. As well-known from atomic physics, this leads to replace (3.13) by the Hartree-Fock approximation V^{HF} , which is a non-local field. In other words, the value of $V^{HF}\, u_E^c$ at point r depends on the value of $u_E^c(r')$ at distances $r' \neq r$: the Schroedinger equation reads

$$-\frac{\hbar^2}{2m}\nabla^2 u_E^c(\vec{r}) + \int V_c^{HF}(\vec{r},\vec{r}')\, u_E^c(\vec{r}')\, d^3r' = E\, u_E^c(\vec{r}) \quad . \qquad (3.14)$$

The Hartree-Fock approximation involves the one-body density matrix $\rho(\vec{r},\vec{r}')$ $(\rho(r,r) = \rho(r))$:

$$\int V^{HF}(\vec{r},\vec{r}')\, u_E^c(\vec{r}')\, d^3r' = u_E^c(\vec{r}) \int \rho(\vec{r}')\, v(\vec{r},\vec{r}')\, d^3r' - \int \rho(\vec{r},\vec{r}')\, v(\vec{r},\vec{r}')\, u_E^c(\vec{r}')\, d^3r' \quad . \qquad (3.15)$$

The quantity $\rho(\vec{r},\vec{r}')$ is usually evaluated in the framework of the independent particle model, where the target state ϕ_c can be represented by a Slater determinant constructed with single-particle orbitals θ_m . Then,

$$\rho(\vec{r},\vec{r}') = \sum_{m=1}^{A} \theta_m(\vec{r})\, \theta_m(\vec{r}') \quad . \qquad (3.16)$$

The Hartree-Fock self-consistent field results from requiring that the single-particle states θ_m should be eigenstates of the calculated optical-model Hamiltonian. We note that the Hartree-Fock field is real and independent of energy.

3.4. Second order contribution

The second term on the right-hand side of Eq. (3.11) is energy-dependent and complex. One can see from Eq. (3.27) below that these two properties are intrinsically related. We continue to ignore antisymmetrization.

In order to obtain a more explicit expression for the second order term, let us introduce the eigenstates of $H_{c'c'}$. These are of two types, namely bound states $(u_{nc'})$ and scattering states $(u_{E'c'})$:

$$H_{c'c'}\, u_{nc'} = E_n\, u_{nc'} \quad ; \quad H_{c'c'}\, u_{E'c'} = E'\, u_{E'c'} \quad . \qquad (3.17)$$

The contribution of the bound states reads

$$V_c(CN) = \sum_{n,c'\neq c} \frac{(\phi_c|\sum_j v(r,r_j)|\phi_{c'})\, u_{nc'}(r)\, u_{nc'}(r')}{E - E_n + iI} \cdot (\phi_{c'}|\sum_j v(r',r_j)|\phi_c) \quad ; \qquad (3.18)$$

it is non-local and energy-dependent. Since the configurations $u_{nc'}$, $\phi_{c'}$ are bound (Fig. 1(b)), they correspond to the compound nuclear resonances. Hence, $V_c(CN)$ arises from the feeding of the resonances from the entrance channel. This is one of the two sources of absorption expected from the discussion carried out in section 2.3. Note that $V_c(CN)$ is complex only because an average is performed : it becomes real in the limit $I \to 0$.

The contribution of the scattering states reads

$$V_c(DR) = \sum_{c'\neq c} \int \frac{(\phi_c|V|\phi_{c'})\, u_{E'c'}(r)\, u_{E'c'}(r')\, (\phi_{c'}|V|\phi_c)}{E - E'}\, dE' - i\pi \sum_{c'\neq c} (\phi_c|V|\phi_{c'})\, u_{Ec'}(r)\, u_{Ec'}(r')\, (\phi_{c'}|V|\phi_c) \quad , \qquad (3.19)$$

where the integral is a principal value and is thus real. The imaginary part of $V_c(DR)$ arises from the energy-conserving direct transitions from the entrance channel c to the configuration $u_{Ec'}\, \phi_{c'}$, i.e. to the inelastic channel c' (Fig. 1(c)).

3.5. Local equivalent potentials

One can expand $u_E^c(r')$ about the point $r' = r$:

$$u_E^c(r') = u_E^c(r) + (r-r') \frac{d}{dr} u_E^c(r) + \frac{1}{2} (r-r')^2 \frac{d^2}{dr^2} u_E^c(r) + \ldots . \quad (3.20)$$

Taking the derivative d/dr amounts to multiplying by $- ip/\hbar$, where p is the momentum. Thus,

$$u_E^c(r') = u_E^c(r) \{1 - ip(r-r')/\hbar - \frac{1}{2} (r-r')^2 p^2/\hbar^2 + \ldots\} \quad . \quad (3.21)$$

By inserting this expansion in Eq. (3.14), one sees that a non-local potential formally amounts to a momentum-dependent potential. This relationship has been investigated in detail by Perey and collaborators [15-17] and by Frahn [18], in particular for real "separable" potentials of the form

$$V_N(\vec{r},\vec{r}') = U_N(r) H(s^2) \quad , \quad (3.22)$$

where

$$\vec{s} = \vec{r}' - \vec{r} \quad . \quad (3.23)$$

Let us call $\tilde{H}(k^2)$ the Fourier transform of $H(s)$. It has been shown that the non-local potential $V_N(\vec{r},\vec{r}')$ leads to practically the same scattering phase shift as the <u>local</u> potential $U_L(r)$ defined by

$$U_N(r) \tilde{H} [\frac{2m}{\hbar^2} (E - U_L(r))] = U_L(r) \quad . \quad (3.24)$$

The physical meaning of this relation will become apparent in section 4.3.

While V_N and U_L yield almost the same wave function outside the target, the corresponding wave function <u>inside</u> the target differs by a factor :

$$u_N^c(r) = (\frac{\tilde{m}}{m})^{\frac{1}{2}} u_L^c(r) \quad , \quad (3.25)$$

where the "effective mass" $\tilde{m}$ is defined by

$$\frac{\tilde{m}}{m} = \{1 + 2m\hbar^{-2} U \frac{d}{dk^2} H(k^2)\}^{-1} \quad ; \quad (3.26)$$

the derivative is evaluated at the momentum given by $\hbar^2 k^2/2m = E - U_L$. This scaling correction can play a significant role in some direct reactions. For an illustration, see page 127 of [16].

Note that the local equivalent potential U_L depends on energy even if U_N is energy-independent. We have seen in section 3.3 that U_N depends on energy. Hence, the origin of the energy dependence of the phenomenological <u>local</u> OMP is twofold, namely the "true" nonlocality of the OMP on the one hand, and its "true" (or dynamical) energy dependence on the other hand. In practice, it is not possible to distinguish between these two effects in the analysis of the experimental data. Since the scaling factor $\tilde{m}/m$ arises solely from the nonlocality, a theoretical calculation of the non-local energy dependent field is of interest.

Attempts have been made [19] to disentangle non-locality and energy-dependence on the basis of a dispersion relation. By integrating $(E' - E)^{-1} V_c(E')$ (Eq. (2.11)) along the real axis and by closing the contour in the upper half of the complex E-plane, one finds

$$V_c(E) = \frac{1}{\pi} \int \frac{W_c(E')}{E' - E} dE' \quad . \quad (3.27)$$

One practical difficulty with Eq. (3.27) is that it involves $W_c(E')$ for large values of E'. Another problem is that the quantities V_c and W_c in Eq. (3.27) are the energy-dependent <u>non-local</u> quantities. This is illustrated by the fact that the dispersion relation yields

$$\frac{\bar{m}}{m} = 1 - \frac{d}{dE} V_c > 1 \quad (3.28)$$

at low energy, in apparent contradiction with the fact that the depth of the empirical <u>local</u> OMP decreases in magnitude with increasing energy.

3.6. Empirical potentials

In the following sections, we survey some recent theoretical calculations of the OMP. Their degree of success should be evaluated by considering the number of adjustable parameters that they involve on the one hand, and their agreement with experimental data on the other hand. The latter part of the discussion is often side-stepped by comparing theoretical and empirical OMP, rather than observables proper, e.g. cross sections, strength

functions, ... One must be aware, however, that theoretical expressions of the OMP may be widely different from the assumed empirical ones (non-locality, energy dependence, form factors, ...). Moreover, the experimental data do not uniquely determine the empirical OMP. When possible, the comparison between calculated and empirical OMP is nevertheless quite instructive, since practitioners are eager to be provided with theoretical constraints which would restrict the freedom in the parameter search.

Accurate descriptions of the elastic scattering differential cross section, of the strength function, of the scattering length, etc. can only be obtained if the parameters of the OMP are allowed to vary in a somewhat scattered manner from target to target. One must admit that the theory is not yet, and will probably never be, able to yield such accurate predictions. Nevertheless, "global" parametrizations which depend smoothly on mass number, on energy and on neutron excess are quite useful in providing estimates of the physical observables. In fact, the existence of such simple parametric forms is at the origin of the development of the optical model. By their very nature, these global OMP average out shell- and many other finiteness effects; they are probably characteristic of the nuclear medium. This will be exploited in section 4.

A survey of OMP for individual nuclei has recently been compiled by Perey and Perey [20]. Most parametrizations are of the following form, for spherical nuclei

$$V(r) = - V_o f(x_V) + (V_{SO} + i W_{SO}) \left[\frac{d}{dr} f(x_{so})\right] \vec{\sigma}.\vec{\ell} - i \left[W_o f(x_W) - 4 W_D \frac{d}{dx_D} f(x_D)\right] , \quad (3.29)$$

where the second term is a spin-orbit coupling, while

$$f(x_j) = \{1 + \exp[(r - r_j A^{\frac{1}{3}})/a_j]\}^{-1} \quad (3.30)$$

is the Woods-Saxon form factor. The surface absorption term (with strength W_D) is sometimes assumed to have a Gaussian shape :

$$W_G \exp -[(r - r_D A^{\frac{1}{3}})/a_D]^2 . \quad (3.31)$$

A popular global set of parameters is due to Becchetti and Greenlees [21] :

$$V_o = 56.3 - 0.32 E - U_1(N-Z)/A \quad (3.32a)$$

$$r_V = 1.17 , \quad a_V = 0.75 , \quad U_1 = 24 \quad (3.32b)$$

$$W_o = 0.22 E - 1.56 \text{ or zero, whichever is larger} \quad (3.32c)$$

$$W_D = 13 - 0.25 E - W_1(N-Z)/A \text{ or zero, whichever is larger} \quad (3.32d)$$

$$r_W = r_D = 1.26 , \quad a_W = a_D = 0.58 , \quad W_1 = 12 \quad (3.32e)$$

$$V_{so} = 6.2 , \quad W_{so} = 0 , \quad r_{so} = 1.1 , \quad a_{so} = 0.75 , \quad (3.32f)$$

where units are MeV and fm . This "global" OMP gives fair results for $A > 40$ and $10 < E < 24$ MeV .

At lower energy, the OMP of Wilmore and Hodgson [22] appears somewhat more satisfactory. It is the local equivalent (see section 3.5) of a non-local potential proposed by Perey and Buck [15] who adopted the separable expression (3.22), with a Gaussian non-locality :

$$H(s^2) = \exp -(s^2/\beta^2) . \quad (3.33)$$

The existence of several global (or even individual) parametric forms illustrates our previous warning that the experimental data do not uniquely determine the OMP. Thus, the set (3.32) should only be regarded as an example.

Several general remarks can be made :

(a) The effective mass m^* defined by

$$\frac{m^*}{m} = 1 - \frac{d(-V_o)}{dE} \approx 0.68 \quad (3.34)$$

is smaller than unity, in apparent contradiction with (3.28). This reflects the fact that the energy dependence of the local equivalent potential $V(r)$ has little connection with that of the original non-local potential $V(r,r';E)$ to which (3.28) refers. One can show [4] that

$$\frac{m^*}{m} = \frac{\bar{m}}{m}\frac{\tilde{m}}{m} \quad , \tag{3.35}$$

where $\tilde{m}/m$ is related to the non-locality of the OMP (see Eqs. (3.22) and (3.26)). We conclude that the energy dependence of the depth of the empirical local OMP is mainly due to the non-locality of the original OMP.

(b) One has separated out in the parametrization of V_o a term proportional to the neutron excess

$$\alpha = \frac{N-Z}{A} \quad . \tag{3.36}$$

This is not necessary. Indeed, one could obtain fits of similar quality by modifying the assumed law $R_V = r_V A^{1/3}$ for the potential radius. However, the introduction in V_o of a term proportional to α is logical : it can easily be shown theoretically that the depths of the OMP for protons and for neutrons, respectively, mainly differ by a term proportional to α , besides the Coulomb term. Thus, it is meaningful to write the potential depths for protons and for neutrons as follows

$$V_o = U_o - 0.32\ E \pm U_1 \frac{N-Z}{A} \quad . \tag{3.37}$$

This is not exactly the form adopted in the analyses by Becchetti and Greenlees [21]; they take $U_o = 56.3$ MeV for neutrons and $U_o = 54.0$ MeV for protons. However, parametrization (3.36) is adopted in more recent work [19]. Note that the empirical value of U_1 is sensitive to that of r_V ; moreover, there exists no theoretical reason why the (isovector) part of the OMP which is proportional to α should have the same form factor (radius r_V , diffuseness a_V) as the (isoscalar) other component , or why a term proportional to α should be absent in W_o and present in W_D.

(c) The absorptive part $W(r)$ is surface peaked for $E \lesssim 50$ MeV and takes the same ("volume") form as $V(r)$ for $E \gtrsim 50$ MeV . This "observation" should be taken with caution because it is probably based on theoretical prejudice : very good fits can be obtained with a volume absorption.

(d) The fits are consistent with the assumption

$$W_{so} = 0 \quad ; \tag{3.38}$$

this of course does not mean that (3.38) holds : theoretical work on this topic is still lacking but would be of interest.

(e) We emphasized that a comparison between theoretical and empirical OMP is difficult. Fortunately, it appears that the calculated cross sections are mainly sensitive to the first moments of the OMP, in particular to the volume integrals per nucleon [3,13,23-25]

$$J_V/A = -A^{-1} \int V(r)\ d^3r \quad , \tag{3.39}$$

$$J_W/A = -A^{-1} \int W(r)\ d^3r \quad , \tag{3.40}$$

and to the mean square radii [3,25]

$$\langle R_V^2 \rangle = [\int V(r)\ r^2\ d^3r]/[\int V(r)\ d^3r] \quad , \tag{3.41}$$

$$\langle R_W^2 \rangle = [\int W(r)\ r^2\ d^3r]/[\int W(r)\ d^3r] \quad . \tag{3.42}$$

This empirical observation holds for protons as well as for neutrons, but has only limited validity for light nuclei. It has not been checked whether it applies at low energy, and to strength functions for instance.

3.7. Hartree-Fock calculations

We saw in section 3.3 that the Hartree-Fock field is the first order contribution to the perturbation expansion of the OMP in powers of the nucleon-nucleon interaction. Since the latter is too strong for perturbation theory to converge rapidly, the Hartree-Fock approximation can be meaningful only if a weak effective interaction is used. The interest of such a calculation is somewhat doubtful if the effective interaction contains adjustable parameters, since it would then almost amount to a different fitting procedure. Hence, one should

ideally take the effective interaction from calculations of other nuclear properties than the OMP.

Dover and Van Giai [26] computed the Hartree-Fock self-consistent potential associated with various three-body contact interactions of the Skyrme-type, fitted to ground state properties of nuclei and to low-lying single-particle levels. The calculated energy dependence of the OMP, i.e. the effective mass m^* (Eq. (3.34)), sensitively depends on the variant of the Skyrme interaction that is chosen. In Fig. 3, we show a comparison between the volume integral per nucleon calculated (dashes) by Dover and Giai [26] and empirical values (dots), for the targets ^{12}C , ^{16}O , ^{27}Al , ^{40}Ca and ^{208}Pb , in the case of protons. The agreement is fair, in view of the absence of adjusted parameters; it shows that the same effective interaction can reproduce bound and low-energy scattering properties. Similar work has been performed by Manweiler [27].

To our knowledge, these are the only two examples of the application of the Hartree-Fock approximation to the real part of the OMP (see, however, section 3.8). It would be of great interest to perform calculations of the scattering by the Hartree-Fock field generated by the effective interaction of Gogny et al. [28], which has proved quite successful in reproducing bound state properties.

A poor man's version of the Hartree-Fock approximation consists in using the folding formula (3.13). Many calculations [14] of this type have been performed, stimulated by the work of Greenlees et al. [13]. Self-consistency is not required : $\rho(r')$ is the experimental density distribution of the target and v is a semi-phenomenological interaction. The usefulness of this approach is somewhat doubtful. While the number of fitted parameters is indeed reduced as compared to the expression (3.29), it is not clear at all that the constraints thus imposed have a physical foundation. In particular, it would be dangerous to draw conclusions on $\rho(r)$ from this type of analysis, in view of the number of approximations that are involved. For instance, any "derivation" of an effective interaction leads to a non-local, energy-dependent and density-dependent effective interaction. These complications are usually omitted. A non-local v would lead to the following non-local Hartree (not Hartree-Fock !) approximation :

$$V(r,r') = \int \rho(r_o)\, v(r-r_o, r'-r_o)\, d^3r_o \quad . \qquad (3.43)$$

The effect of a density-dependence of v has been found significant by various authors [29-31].

Exchange corrections (see Eq. (3.15)) to the Hartree field have been estimated, usually on the basis of the expression (3.16) for the density matrix [28,32,33] : they appear able to reproduce approximately the observed energy-dependence of the empirical local equivalent OMP, but this may be accidental in view of the approximations that are involved (neglect of the true energy-dependence, of the non-locality of the effective interaction, of higher order corrections, ...).

We mentioned at the beginning of section 2.2 that the OMP is the natural extrapolation to positive energy of the shell-model potential for bound single-particle states. This is illustrated by the recent work by Giannini and Ricco [34]. These authors fit observed single-particle energies, density distributions and elastic scattering cross sections, for nuclei with $N = Z \lesssim 20$, with a non-local OMP whose real part has the Perey-Buck form, Eqs. (3.22) and (3.33). The depth of the local equivalent potential is shown in Fig. 4, in the energy range minus 60 MeV < E < plus 130 MeV : we see that it is remarkably smooth. The scattering near $E = -10$ MeV is probably due to polarization and rearrangement effects, which are not contained in the Hartree-Fock approximation and are more pronounced in finite nuclei [35-37] than in nuclear matter [4,38]. Similar work has been done by Manweiler [27].

3.8. Second order corrections to the real part

At the end of the preceding section, we alluded to higher corrections. The second order corrections to the Hartree-Fock field in ^{16}O have recently been studied by Bassichis et al. [39], who improved an earlier work by MacKellar et al. [40]. These authors fully include antisymmetrization; they use Tabakin's nucleon-nucleon interaction, and calculate the Hartree-

Fock field and its second order corrections in the case of ^{16}O. It turns out that the second order corrections to the real part almost cancel at low energy. The comparison between the theoretical elastic scattering phase shift and the experimental one ($n + {}^{16}O$ below 5 MeV) is poor. This is expected because low energy scattering by light nuclei is very sensitive to details of nuclear structure.

Most other authors have calculated part of the second order contribution without computing the first order Hartree-Fock field. They were particularly interested in the imaginary part of these terms (see, however, Ref. [41]), and we therefore discuss them in the next section.

3.9. Second order contributions to the imaginary part

The main interest of the second order contributions is that they yield the leading term of the perturbation expansion of the imaginary part of the OMP. We saw in section 3.4 that there exist two main types of second order contributions.

The first one corresponds to the feeding of compound nuclear states (Eq. (3.18)). The structure of the latter is very hard to guess. Most of the available calculations (see, however, [42]) assume that they consist of a particle state (wave function $u_{nc'}$ in Eq. (3.18)) coupled to a vibrational excited state $\phi_{c'}$. The density of these states is rather low, and the averaging procedure is unable to yield a smooth OMP. Thus, the imaginary parts calculated in the cases of ^{58}Ni [43,44] and of ^{208}Pb [45-47] are highly non-local and strongly energy-dependent.

The second type of contribution corresponds to the feeding of open inelastic channels (see Eq. (3.19)). Vinh Mau and Bouyssy [48] studied the imaginary part of this contribution in the case of ^{40}Ca. They describe the excited states $\phi_{c'}$ in the framework of the random phase approximation, and treat antisymmetrization very carefully. They use a zero-range effective interaction fitted to the low-lying collective states of ^{40}Ca. Figure 5 shows that the main contribution to the calculated local equivalent imaginary part arises from the excited target states with odd parity. The main drawback of this work probably lies in the use of plane waves for the functions $u_{Ec'}$ (Eq. (3.19)). It is found that most of the flux goes to collective excited states.

The latter observation is expected on physical grounds, and led Satchler and collaborators [49,50] to evaluate the matrix elements $V_{cc'}$ (Eq. (3.6)) in the framework of the deformed potential model. These authors take into account the distortion of the wave function $u_{Ec'}$ (Eq. (3.19)) by a real [49] or complex [50] potential $V_{c'c'}$. The effect of this distortion, which had been neglected in Ref. [48], is found to be significant. A real and local Woods-Saxon potential well simulates the first order contribution. In the case of ^{208}Pb and of 30 MeV protons, the couplings to 24 open channels (including deuteron channels) yield about 90 per cent of the measured absorption cross section, but only about one-half of the empirical absorptive component of the OMP. It was not found possible to construct a local OMP which would give the same cross sections as the calculated non-local potential. This probably reflects the fact that the separable form (3.22) does not apply here. The authors conclude that the equivalent "local" OMP should at least depend on angular momentum. The second order contribution to the real part of the OMP turns out to be positive, but this may be related to the approximations involved in the calculation.

3.10. Discussion

The main problem encountered by nuclear reaction theory in evaluating the OMP is that it involves an effective interaction, which is by necessity at best a semi-phenomenological quantity. In order to obtain meaningful theoretical constraints, it appears most desirable to adopt a parameter-free effective interaction, which has for instance been fitted to the properties of the ground and of the low excited states of the target nucleus or of neighbouring nuclei.

Besides this drawback, the nuclear reaction approach presents two advantages over the global one to be described in

section 4. Indeed, it enables one to investigate the contribution of individual open channels to the absorptive part of the OMP, and to include the collectivity effects.

4. NUCLEAR MATTER APPROACH

4.1. Introduction

The observation that the volume integral per nucleon of the OMP varies smoothly with mass number and with energy suggests that useful information on the OMP can be derived from the study of an infinite nuclear medium. According to the qualitative description given in section 2.5, one should in this case calculate the mean free path and the potential energy of a nucleon with energy E. The relevant theoretical tools are briefly presented in section 4.2. We shall see that the investigation of nuclear matter also enables one to discuss some details alluded to in the preceding sections. For instance, one can distinguish between the contributions of the non-locality or of the true energy dependence of the theoretical OMP to the energy dependence of the empirical local OMP.

The "local density approximation" offers a simple but crude way of constructing the OMP in a finite nucleus from the results obtained in nuclear matter. It consists in assuming that the value of the OMP at the distance $\underline{r}$ from the nuclear centre, where the density is ρ, is the same as in an infinite medium with density ρ.

4.2. Theoretical tools

For time $t > 0$, the Green function is defined by

$$G(\vec{r},\vec{r}';t) = -i \langle \phi_c | a(\vec{r}',t)\, a^{\dagger}(\vec{r},0) | \phi_c \rangle \quad ; \qquad (4.1a)$$

ϕ_c is the wave function of the ground state and $\underline{a}^{\dagger}$, $\underline{a}$ are creation and annihilation operators, respectively. The Green function gives the probability amplitude of finding on top of the initial target state at time t and at point $\vec{r}'$, a nucleon that had been created at time $t = 0$ and at point $\vec{r}$. Hence, it contains the information relevant to the optical model.

In an infinite medium, G only depends on the combination $s = |\vec{r}-\vec{r}'|$ of the spatial variables. Let us perform a Fourier transform and call

$$k \leftrightarrow |\vec{r}-\vec{r}'| \qquad (4.2)$$

the variable associated to s. The Fourier transform of G reads

$$G(k,t) = -i \langle \phi_c | a(k,t)\, a^{\dagger}(k,0) | \phi_c \rangle \quad ; \qquad (4.1b)$$

it describes the propagation of a nucleon with momentum $\underline{k}$. For simplicity, we used the same notation to refer to a function and to its Fourier transform (see also Eqs. (4.17),(4.18)). According to the optical model, this nucleon should have a rather well defined energy $E(k)$ (see Eq. (2.33)) and the probability amplitude $G(k,t)$ should decrease exponentially in time. Thus, the optical model consists in making the approximation ($W < 0$)

$$G(k,t) \simeq -i\, R(k) \exp(-i\, E(k)\, t/\hbar) \exp(W(k)/t) \quad , \qquad (4.3)$$

where $R(k)$ is a proportionality constant that may depend on $\underline{k}$. By performing a Fourier transform on t, (4.3) amounts to assuming that

$$G(k,E) \simeq \frac{R(k)}{E - E(k) - i\, W(k)} \quad . \qquad (4.4)$$

In the independent particle model, all nucleons move independently of one another in a real common potential $U(k)$ which may be non-local, as indicated by its dependence on $\underline{k}$. The corresponding Green function has the following simple form

$$G^{(o)}(k,E) = \frac{1}{E - \frac{\hbar^2}{2m} k^2 - U(k)} \quad . \qquad (4.5)$$

With the help of the quantity

$$V(k) = E(k) + i\,W(k) - \frac{\hbar^2}{2m}k^2 \quad , \tag{4.6}$$

(4.4) reads

$$G(k,E) \simeq \frac{R(k)}{E - \frac{\hbar^2}{2m}k^2 - V(k)} \quad . \tag{4.7}$$

The comparison between (4.5) and (4.7) suggests to identify the OMP with the momentum-dependent (i.e. non-local) potential $V(k)$. We see that $R(k) \to 1$ when $W \to 0$, i.e. in the limit of the independent particle model.

In order to obtain a more general definition of the OMP, let us introduce the mass operator $V(k,E)$, which is by definition related to the Green function as follows

$$G(k,E) = \frac{1}{E - \frac{\hbar^2}{2m}k^2 - V(k,E)} \quad . \tag{4.8}$$

Note that $V(k,E)$ is complex, non-local and energy-dependent. By Fourier transformation, we obtain

$$V(k,E) \leftrightarrow V(|\vec{r}-\vec{r}'|),E) \quad . \tag{4.9}$$

Equations (4.5) and (4.8) show that one can identify $V(k,E)$ with a complex mean field, i.e. with the OMP.

These considerations can be extended to finite nuclei. There, the mass operator reads

$$V(\vec{r},\vec{r}';E) \quad . \tag{4.10}$$

The corresponding Schroedinger equation is (cf Eq. (3.14))

$$-\frac{\hbar^2}{2m}\nabla^2 u_E^c(\vec{r}) + \int V_c(\vec{r},\vec{r}';E)\, u_E,(\vec{r}')\, d^3r' = E\, u_E^c(\vec{r}) \quad . \tag{4.11}$$

It has been proved by Bell and Squires [51] that $u_E(r)$ is the projection of the full wave function Ψ_E^c on the target ϕ_c :

$$u_E^c(r) = (\phi_c|\Psi_E^c) \quad . \tag{4.12}$$

We recall (section 3.2) that a round bracket indicates an integration over all coordinates of the nucleons contained in the target. The asymptotic form of $u_E^c(r)$ for $r \to \infty$ is given by Eq. (2.2). Thus, $V_c(r,r';E)$ contains more information than the OMP which is only required to yield the average $u_{E+iI}^c(r)$: the OMP proper is given by the energy average $V(r,r';E+iI)$ [52]. In the case of nuclear matter, all quantities depend smoothly on E , and no average needs to be taken.

4.3. Local equivalent potential

The identification of $V(k,E)$ with a single-particle field is rigourous. We must, however, keep in mind that the shell model or the optical model is only an approximation, i.e. that the concept of a mean field cannot lead to an exact description of the elastic scattering process, which is obviously quite complicated : it only aims at describing averages.

The optical model is useful if approximation (4.7) is reasonably accurate. This approximation is obtained as follows from the exact relation (4.8). Let

$$E(k) = \frac{\hbar^2}{2m}k^2 + V(k,E(k)) \tag{4.13}$$

denote the complex pole of $G(k,E)$. We have

$$G(k,E) = \frac{R(k)}{E - \frac{\hbar^2}{2m}k^2 - V(k,E(k))} + \text{rest} \quad , \tag{4.14}$$

where $R(k)$ is the residue

$$R(k) = \{1 - \frac{\partial}{\partial E}V(k,E)\}^{-1}_{E=E(k)} \quad . \tag{4.15}$$

The optical model (4.7) consists in neglecting the "rest" in Eq. (4.15), i.e. to retain only the exponentially decaying part of the wave packet associated with the nucleon.

Equation (4.13) expresses that the total energy is equal to the kinetic energy plus the (complex) potential energy.It

relates the energy to the momentum or, equivalently, the momentum to the energy. In other words, the equation

$$E = \frac{\hbar^2}{2m} k^2 + V(k,E) \qquad (4.16)$$

defines $E(k)$ or $k(E)$. Equation (4.14) shows that the optical model requires the value of the mass operator $V(k,E)$ only when the energy-momentum relation (4.16) is satisfied, i.e. the following quantity

$$V(k,E(k)) = V(k) = V(k) + i\,W(k) \quad , \qquad (4.17)$$

which is identical to

$$V(k(E),E) = V(E) = V(E) + i\,W(E) \quad . \qquad (4.18)$$

By Fourier transformation,

$$V(k) \leftrightarrow V(|\vec{r}-\vec{r}'|) \qquad (4.19)$$

becomes a non-local, energy-independent potential; the quantity $V(E)$ is a local, energy-dependent potential.

In order to obtain a local potential from $V(k,E)$, we have in fact performed exactly the transformation expressed by Eq. (3.24). Indeed, no dependence on $\underline{r}$ appears in nuclear matter and Eq. (3.24) reads

$$U_L = \tilde{H}(k^2) \qquad (4.20a)$$

for the value of k^2 given by

$$E = \frac{\hbar^2}{2m} k^2 + U_L \quad , \qquad (4.20b)$$

which is the energy-momentum relation (4.16).

4.4. Calculational methods

There exist three main approaches to the calculation of the mass operator in nuclear matter.

(a) The first method consists in expanding $V(k,E)$ in powers of the nucleon-nucleon interaction $\underline{v}$. This is justified only if the latter is weak enough, i.e. in practice if it is an effective interaction. The leading term of this perturbation expansion is the Hartree-Fock approximation. It has been discussed in section 3.3, and its expression is given by Eqs. (3.15),(3.16) where, in the case of nuclear matter,

$$\theta_m(\vec{r}) = \exp(i\,\vec{k}_m.\vec{r}) = |k_m\rangle \quad ; \qquad (4.21)$$

in Eq. (3.16), the summation over m extends over all occupied states, i.e. from 0 to the Fermi momentum k_F, which is related to the density by Eq. (2.28). The Hartree-Fock approximation thus reads

$$V(k) = \sum_{k_m<k_F} \langle k_m\, k|v|k_m\, k\rangle + \text{exchange} \quad , \qquad (4.22a)$$

or equivalently

$$V(r,r') = \rho \int v(r')\, dr' + \text{exchange} \quad . \qquad (4.22b)$$

As expected from section 3.3, this approximation yields an OMP which is non-local (because of exchange), real and independent of energy. We note that the direct (Hartree) term is proportional to ρ and is local. Let us call this term $V_H(r)$:

$$V_H(r) = \rho \int v(r')\, dr' \qquad (4.23a)$$

$$J_V = \int V_H(r)\, dr = \int \rho\, dr \int v(r')\, dr' = A \int v(r')\, dr' \quad . \qquad (4.23b)$$

In the Hartree approximation, the volume integral per nucleon of the OMP (Eq. (3.39)) is equal to the volume integral of the effective interaction and is independent of A ; it is also independent of energy, but the exchange term is non-local and thus introduces an energy dependence in the local equivalent OMP.

(b) The second computational method consists in writing down an infinite set of equations which couple the one-, two-, ...-body Green functions. This set is truncated in a suitable way. The simplest truncation yields the Hartree-Fock approximation. There exist three variants of the next-to-simple one; they are usually called approximations Λ_{00} , Λ_{10} , and Λ_{11} , respectively [53]. The results obtained so far from this method are not as detailed as those derived from the Brueckner approach. For a recent list of references, see [54].

(c) In the Brueckner approach, one expands $V(k,E)$ in terms of a small parameter which is, roughly speaking, proportional to the density. The leading term of this low density expansion is called the Brueckner-Hartree-Fock (BHF) approximation,because of its close formal analogy with the Hartree-Fock field. It is obtained from the latter by replacing in Eqs. (4.22a),(4.22b) the effective nucleon-nucleon interaction $\underline{v}$ by an operator $g_E(r,r')$ which is non-local, energy- and density-dependent and complex. This operator is called the "reaction matrix". It can be calculated from the nucleon-nucleon interaction by solving an integral equation (the Bethe-Goldstone equation), which essentially amounts to summing up the first and a number of selected higher order terms of the perturbation series [4]. One interest of the BHF approximation is that it can be used with a realistic nucleon-nucleon interaction with a strong repulsive core at small distance.

4.5. Real part of the optical-model potential

The results shown in the present and in the following sections have been calculated in the framework of the BHF approximation by Jeukenne, Lejeune and the author [4,25]. Let us denote the BHF contribution by

$$V_\rho(k,E) \quad , \tag{4.24}$$

thus omitting the BHF label and writing explicitly the density dependence. The sole input of these calculations is Reid's hard core nucleon-nucleon interaction [55].

We mentioned that one can consider $V_\rho(k,E(k))$ either as a function $V_\rho(k)$ of momentum or as a function $V_\rho(E)$ of the energy (Eqs. (4.17),(4.18)). The function $V_\rho(k)$ is a non-local potential, whose Fourier transform is (see Eq. (4.19))

$$V_\rho(|\vec{r}-\vec{r}'|) = V_\rho(s) = U_\rho(s) + i\, W_\rho(s) \quad . \tag{4.25}$$

In Fig. 6, we show the quantity $-U(s)$, for the Fermi momentum $k_F = 1.35$ fm^{-1} ($\rho = 0.166$ nucleon/fm^3) which closely corresponds to the density at the centre of a nucleus. We see that the Perey-Buck Gaussian parametrization (3.33) is quite well justified; the small difference between the dashed and the full curves can be interpreted as a dependence of the non-locality range β ($\simeq 0.9$ fm) upon energy.

Most empirical forms of the OMP are local and energy-dependent, i.e. correspond to Eq. (4.18) :

$$V_\rho(E) = V_\rho(E) + i\, W_\rho(E) \quad . \tag{4.26}$$

In Fig. 7, we plot versus energy the quantity $V = |V_\rho(E)|$, for three values of the density, namely $\rho = 0.166$ fm^{-3} ($k_F = 1.35$ fm^{-1}) , $\rho = 0.090$ fm^{-3} ($k_F = 1.10$ fm^{-1}) and $\rho = 0.037$ fm^{-3} ($k_F = 0.82$ fm^{-1}) . These are typical of the nuclear interior, surface and tail, respectively. Although the potential depth decreases with the density, these two quantities are not proportional to one another : one has

$$V \propto \rho\,(1 - d\,\rho^{\frac{2}{3}}) \quad , \quad d \simeq 2 \text{ fm}^2 \quad .$$

If we compare this result with the Hartree approximation (4.23a), we conclude that the dependence of the "effective interaction" on the density is close to that proposed by Myers [30]. An algebraic form of $V_\rho(E)$ can be found in Ref. [25].

In order to construct the OMP in a finite nucleus, $V(r,E)$, we use the local density approximation (section 4.1) which consists in writing

$$V(r,E) = V_{\rho(r)}(E) \quad , \tag{4.27}$$

where $\rho(r)$ is the experimental density distribution. In the example of ^{208}Pb, this leads to the potential wells which are drawn in Fig. 8 for several energies. The arrow indicates the half-density radius (Eq. (4.31)). In Fig. 9, we compare the theoretical (full curves) and the empirical (dots) values of the volume integral per nucleon and of the potential root mean square radius, in the case of protons (see Eqs. (3.39), (3.41)). Corrections have been made for the effects of the Coulomb field and of neutron excess (section 4.7). We see that the calculated volume integral per nucleon is in good agreement with the data (up to 170 MeV !), but that the root mean square radius is too small. The latter defect can be corrected if one assumes that the distribution of the neutrons extends beyond that of the protons (see short dashes), but by a fairly large and unreasonable amount [25]. A more likely explanation lies in the inaccuracy of the local density approximation, as we now explain.

For simplicity, let us consider the Hartree approximation (4.23a). The local density approximation leads to

$$V_H(r,E) = \rho(r) \int v(r')\, dr' \quad , \tag{4.28}$$

while the correct Hartree approximation in a finite system is given by Eq. (3.13) :

$$V_H(r,E) = \int \rho(r')\, v(r-r')\, dr' \quad . \tag{4.29}$$

The simplified form (4.28) is correct in two limiting cases, namely a uniform medium (ρ constant : nuclear matter), or a zero-range effective interaction. Hence, we see that in the local density approximation one starts from an expression which is correct in nuclear matter, but leads to an inaccurate value in a finite nucleus because the effective interaction has a finite range. A phenomenological way of introducing this range consists in using the folding formula

$$\tilde{V}(r,E) = (t\sqrt{\pi})^{-3} \int V(r',E) \exp\left(-\frac{|r-r'|^2}{t^2}\right) dr' \quad , \tag{4.30}$$

which amounts to giving a Gaussian form factor to the effective interaction. The value $t \simeq 1.2$ fm for the range parameter yields fair agreement between the theoretical and the empirical root mean square radii; the volume integral per nucleon of $\tilde{V}$ and V are practically equal, and the good agreement obtained in this case remains unaffected.

Similar results have been obtained for protons on the targets ^{12}C, ^{16}O, ^{27}Al, ^{40}Ca, ^{58}Ni and ^{120}Sn [25]. The density distributions used in the calculations are taken from Ref. [56] : the diffuseness is $a_\rho = 0.54$ fm and the half-maximum radius is equal to

$$R_\rho = (0.978 + 0.0206\, A^{\frac{1}{3}})\ \text{fm} \quad . \tag{4.31}$$

It turns out that the diffuseness of the OMP computed from Eq. (4.30) is 0.62 fm, while its half-depth radius is

$$R_V \simeq 1.21\, A^{\frac{1}{3}} \quad . \tag{4.32}$$

The simple law (4.32) is striking in view of the fact that R_ρ is not proportional to $A^{1/3}$ (see Fig. 8 of Ref. [57]).

One drawback of this procedure is that it introduces an adjustable parameter t. A more satisfactory approach would consist in constructing a finite-range effective interaction from the nuclear matter data, and then to introduce it in the Hartree-Fock expression. Progress in this direction has recently been accomplished by Brieva and Rook [58]. This method unfortunately does not lead to analytic expressions for the OMP.

4.6. Imaginary part of the potential

Figure 10 shows the dependence on energy of the quantity $|W_\rho(E)|$, for $\rho = 0.166$ fm^{-3} (short dashes), 0.090 fm^{-3} (long dashes) and 0.037 fm^{-3} (full curve), respectively. For $E < 50$ MeV, the absorption is largest at the smallest density, while the opposite is true for $E > 50$ MeV. This leads to the fact that the absorptive part is surface-peaked at low energy and takes a volume form factor for $E > 50$ MeV, as confirmed by Fig. 11.

In Fig. 12, we show the volume integral per nucleon and the root mean square radius of the imaginary part of the OMP (Eqs. (3.40),(3.42)), in the case of protons on ^{208}Pb. The agreement with empirical values is fair for J_W/A, but the calculated $\langle R_W^2 \rangle$ is too small.

The nuclei ^{12}C, ^{16}O, ^{27}Al, ^{40}Ca, ^{58}Ni and ^{120}Sn have also been investigated, and the calculated J_W/A are found to be too large. This might be due to the fact that these nuclei are close to magic [59] or have important vibrational or rotational excited states. However, it is not clear why these effects would not show up even more strongly in the case of ^{208}Pb, unless we admit that this is a consequence of the large density of states in this case; this appears doubtful.

4.7. Symmetry and Coulomb components

The depths (3.32a) and (3.32d) of the real and of the imaginary parts of the OMP contain a "symmetry" component, which is proportional to the neutron excess parameter α (Eq. (3.36)). This component can be computed from the nuclear matter approach by introducing a difference $\rho_n - \rho_p$ between neutron and proton densities [57]. The calculated U_1 turns out to be 11.5 MeV, i.e. two times smaller than the empirical value (3.32b). On the other hand, the calculated half-depth radius is larger ($r_{U_1} = 1.31$ fm) for this symmetry component than that ($r_V = 1.17$ fm) assumed in the empirical analyses. As a consequence, the calculated volume integral per nucleon of the symmetry potential is in good agreement with experimental evidence. This is shown in Fig. 13, where calculated values of J_V/A (crosses) in the case of 11 MeV neutrons are compared with empirical ones (full and open dots; full straight line).

We note that many phenomenological analyses of neutron scattering data yield values for U_1 which are typically about 13 MeV [60], i.e. smaller than the value 24 MeV (Eq. (3.32b)) given by Becchetti and Greenlees [21], and also smaller than the value ($\simeq$ 24 MeV) derived from proton scattering data [21]. It has been suggested that the latter discrepancy may reflect an underestimate of the Coulomb correction [57].

The latter arises from the fact that the OMP for protons with energy E is given by

$$V(r,E - V_C) + V_C(r) \tag{4.33}$$

where $V_C(r)$ is the value of the Coulomb potential at distance r from the nuclear centre. Expanding (4.33), we find

$$V(r,E - V_C) + V_C(r) = V(r,E) - V_C(r) \frac{d}{dE} V(r,E) + V_C(r)$$

$$= V(r,E) + V_C(r) + \left(\frac{m^*(r)}{m} - 1\right) V_C \quad , \tag{4.34}$$

where $m^*(r)$ is the effective mass (Eq. (3.34)) at location r, i.e. at the density $\rho(r)$. The density dependence of m^* is impossible to determine empirically. The calculation carried out in Ref. [57] leads to a Coulomb correction

$$\Delta_C = V_C \left(1 - \frac{m^*}{m}\right) \tag{4.35}$$

whose volume integral is larger than the assumed empirical value. The latter is obtained by adding the estimate

$$\Delta_C = 0.4 \, Z \, A^{-\frac{1}{3}} \tag{4.36}$$

to the depth of the OMP [21].

Very little theoretical work has been accomplished concerning the spin-orbit component at low energy. It would be of interest, in particular, to compute its imaginary strength W_{so}, and to see whether it contains a significant dependence on the asymmetry parameter α or on energy.

There should exist other components of the OMP that depend on the target spin $\vec{I}$. The simplest is the spin-spin component $\vec{I} \cdot \vec{\sigma}$, which has been evaluated by Dabrowski and Haensel [61] in the case of nuclear matter. The application of their result to finite nuclei is rather delicate.

In the preceding and in the present section, we compared calculated and empirical OMP, and concluded to fair agreement. This is confirmed by recent work by Hodgson [24] and by Kailas and Gupta [62]. A more detailed discussion requires the comparison between experimental and theoretical cross sections. This is discussed in the next section.

4.8. Elastic scattering cross sections

Lejeune and Hodgson [63] have recently computed the elastic differential cross sections for the OMP obtained from the nuclear matter approach (Eq. (4.30)), in the case of 10-70 MeV protons on ^{12}C , ^{16}O , ^{27}Al , ^{40}Ca , ^{58}Ni , ^{68}Zn , ^{90}Zr , ^{116}Sn , ^{208}Pb , as well as of 1-15 MeV neutrons on ^{12}C , ^{27}Al , ^{40}Ca , ^{58}Ni , ^{116}Sn , ^{208}Pb and ^{209}Bi . They found that the agreement with the experimental data is not very good (full curves in Fig. 14) but becomes quite satisfactory (dashed curves) if one multiplies the calculated depths by correction factors. Let us call these C_V and C_W , for the real and the imaginary parts, respectively. It turns out that $C_V \approx 1.1$ and $C_W \approx 0.85$ for 60 MeV protons; $C_V \approx 1.0$ and $C_W \approx 0.8$ for 30 MeV protons. In the case of 1-15 MeV neutrons, C_V remains close to unity : it varies between 0.96 (^{209}Bi) and 1.03 (^{12}C) . In contrast, C_W ranges from 0.38 (^{40}Ca) to 0.97 (^{27}Al) . In general, the calculated imaginary part is thus significantly too large, especially at low energy. We mentioned in section 4.6 that this might be due to the fact that most of the studied nuclei have a closed shell [59] or are strongly deformed, but it is also likely that the local density approximation is a poor one in the case of the imaginary part.

5. CONCLUSIONS

We hope that the reader has been convinced that significant progress has recently been achieved in the physical understanding of the optical model and in the calculation of the optical-model potential. One must of course remain aware that theoretical considerations are only able to yield rather inaccurate cross sections.We believe that their main interest consists in providing information on properties that are very difficult to reach experimentally, for instance the non-locality of the OMP, its symmetry component, the Coulomb correction, the density and the energy dependence of the effective mass, etc.

REFERENCES

[1] FESHBACH, H., Ann.Rev.Nucl.Sci. 8 (1958) 49

[2] HODGSON, P.E., Nuclear Reactions and Nuclear Structure, Clarendon Press, Oxford, 1971

[3] PEREY, F.G., Nuclear Spectroscopy and Reactions (CERNY, J., Ed.), Academic Press, New York (1974) 137

[4] JEUKENNE, J.-P., LEJEUNE, A., MAHAUX, C., Phys.Reports 25C(1976)83

[5] Nuclear Theory in Neutron Data Evaluation, IAEA-190 (1976) volumes 1 and 2

[6] JEUKENNE, P.-P., LEJEUNE, A., MAHAUX, C., Proceedings of the International Conference on the Interactions of Neutrons with Nuclei, Lowell (SHELDON, E., Ed.), ERDA (1976) 451

[7] BOFFI, S., PASSATORE, G., Nuclear Optical Model Potential, Springer Verlag, Berlin, 1976

[8] BARRETT, R.C., JACKSON, D.F., Nuclear Sizes and Structure, Clarendon Press, Oxford (1977)

[9] MAHAUX, C., WEIDENMULLER, H.A., Shell-Model Approach to Nuclear Reactions, North-Holland Publ. Comp., Amsterdam (1969)

[10] BLANN, M., Phys.Lett. 67B (1977) 145

[11] KIKUCHI, K., KAWAI, M., Nuclear Matter and Nuclear Reactions, North-Holland Publ. Comp., Amsterdam (1968)

[12] FESHBACH, H., Ann. Phys. (N.Y.) 19 (1962) 287

[13] GREENLEES, G.W., PYLE, G.J., TANG, Y.C., Phys.Rev. 171 (1968) 1115

[14] SINHA, B., Phys.Reports 20C (1975) 1

[15] PEREY, F., BUCK, B., Nucl.Phys. 32 (1962) 353

[16] PEREY, F., Direct Interactions and Nuclear Reaction Mechanisms (CLEMENTEL, E., VILLI, C., Eds.), Gordon and Breach, New York, (1963) 125

[17] PEREY, F., SAXON, D.S., Phys.Rev. 10 (1964) 107

[18] FRAHN, W.E., Nucl.Phys. 66 (1965) 358

[19] PATTERSON, D.M., DOERING, R.R., GALONSKY, A., Nucl.Phys. A263 (1976) 261

[20] PEREY, C.M., PEREY, F.G., Atomic Data and Nuclear Data Tables 17 (1976) 1

[21] BECCHETTI, F.D., GREENLEES, G.W., Phys.Rev. 182 (1969) 1190

[22] WILMORE, D., HODGSON, P.E., Nucl.Phys. 55 (1964) 673

[23] AGRAWAL, D.C., SOOD, P.C., Phys.Rev.C11 (1975) 1854

[24] HODGSON, P.E., Phys.Lett. 65B (1976) 331

[25] JEUKENNE, J.-P., LEJEUNE, A., MAHAUX, C., Phys.Rev. 16C (1977) 80
[26] DOVER, C.B., VAN GIAI, N., Nucl.Phys. A177(1971) 559; ibid. A190 (1972) 373
[27] MANWEILER, R.W., Nucl.Phys. A240 (1975) 373
[28] GOGNY, D., PIRES, P., DE TOURREIL, R., Phys.Lett. 32B(1970) 591
[29] SLANINA, D., McMANUS, H., Nucl.Phys. 116 (1968) 271
[30] MYERS, W.D., Nucl.Phys. A204 (1973) 465
[31] SRIVASTAVA, D.K., GANGULY, N.K., HODGSON, P.E., Phys.Lett. 51B (1974) 439
[32] OWEN, L.W., SATCHLER, G.R., Phys.Rev.Lett. 25 (1970) 1720
[33] LOVE, W.G., OWEN, L.W., Nucl.Phys. A239 (1975) 74
[34] GIANNINI, M.M., RICCO, G., Ann.Phys. (N.Y.) 102 (1976) 458
[35] BROWN, G.E., GUNN, J.H., GOULD, P., Nucl.Phys. 46 (1963) 598
[36] BERTSCH, G.F., KUO, T.T.S., Nucl.Phys. A112 (1968) 204
[37] HAMAMOTO, I., SIEMENS, P., Nucl.Phys. A269 (1976) 199
[38] JEUKENNE, J.-P., LEJEUNE, A., MAHAUX, C., Phys.Lett. 59B(1975)208
[39] BASSICHIS, W.H., STRAYER, M.R., READING, J.F., SCHEERHAUM, R.R., Submitted to Nucl.Phys. (1977)
[40] MACKELLAR, A.D., READING, J.F., KERMAN, A.K., Phys.Rev. C3 (1971) 460
[41] BOUYSSY, A., NGÔ, H., VINH MAU, N., International Conference on Nuclear Structure and Spectroscopy (BLOK, H.P., DIEPERINK, A.E.L., Eds.), Amsterdam (1974) vol 1, 153
[42] CUGNON, J., Nucl.Phys. A208 (1973) 333
[43] O'DWYER, T.F., KAWAI, M., BROWN, G.E., Phys.Lett. 41B (1972) 259
[44] AZZIZ, N., MENDEZ-PLACIDO, R., Phys.Rev. C.8 (1973) 1849
[45] LEV, A., BERES, W.P., DIVADEENAM, M., Phys.Rev.Lett. 31(1973)555
[46] LEV, A., BERES, W.P., DIVADEENAM, M., Phys.Rev. C9 (1974) 2416
[47] LEV, A., BERES, W.P., Phys.Lett. 58B (1975) 263
[48] VINH MAU, N, BOUYSSY, A., Nucl.Phys. A257 (1976) 189
[49] RAO, C.L., REEVES III, M., SATCHLER, G.R., Nucl.Phys. A207 (1973) 182
[50] COULTER, P.W., SATCHLER, G.R., Nucl.Phys., in press (1977)
[51] BELL, J.S., SQUIRES, E.J., Phys.Rev.Lett., 3 (1959) 96
[52] LIPPERHEIDE, R., Z.Phys. 202 (1967) 58
[53] WEIGEL, M., WEGMANN, G., Forts.Phys. 19 (1971) 451
[54] MARVILLE, C., HAENSEL, P., Z.Phys. A284 (1978) 83
[55] REID, R.V., Ann.Phys. (N.Y.) 50 (1968) 411
[56] NEGELE, J.W., Phys.Rev. C1 (1970) 1260
[57] JEUKENNE, J.-P., LEJEUNE, A., MAHAUX, C., Phys.Rev. C15 (1977) 10
[58] BRIEVA, F.A., ROOK, J.R., Nucl.Phys. A291 (1977) 299; ibid. A291 (1977) 317
[59] EDER, G., LEEB, H., OBERHUMMER, H., J.Phys.G:Nucl.Phys. 3 (1977) L127
[60] HOLMQVIST, B., WIEDLING, T., Nucl.Phys. A188 (1972) 24
[61] DABROWSKI, J., HAENSEL, P., Can.Journ.Phys. 52 (1973) 1768
[62] KAILAS, S., GUPTA, S.K., Phys.Lett. 71B (1977) 271
[63] LEJEUNE, A., HODGSON, P.E., Nucl.Phys. (in press)
[64] VAN OERS, W.H.T., HAW, H., Phys.Lett. 45B (1973) 227
[65] FERRER, J.C., CARLSON, J.D., RAPAPORT, J., Nucl.Phys. A275 (1977) 325.

FIGURE CAPTIONS

Fig. 1. Part (a) represents the entrance channel configuration $u^c\ \phi_c$. In (b) and (c), we show configurations that can be reached from (a) by a collision with one of the target nucleons : configuration (b) is bound and given by u_{nc}, ϕ_c, ; configuration (c) is unbound and of the type u_{Ec}, ϕ_c, .

Fig. 2. Schematic representation of the propagation from A to D of a wave packet through an infinite medium. Its amplitude gives the probability of finding a nucleon with momentum k on top of the target ground state. It decreases because on its way the propagating nucleon excites one particle-one hole, two particle-two hole, ... target configurations.

Fig. 3. Comparison between empirical (dots and full straight lines) volume integrals per nucleon and theoretical (dashes) values calculated by Dover and Giai from the Hartree-Fock approximation with a Skyrme interaction; T_p is the proton kinetic energy (from Ref. [64]).

Fig. 4. The full dots (protons) and the crosses (neutrons) represent the depth of the potential that reproduces single-particle properties of bound and unbound orbitals, for nuclei with $N = Z$ and $A \lesssim 40$. The full curve is drawn through these points (from Ref. [34]).

Fig. 5. Contributions of the odd parity states and of all states to the local equivalent of the imaginary part of the OMP calculated by Vinh Mau and Bouyssy (from Ref. [48]).

Fig. 6. Comparison with a Gaussian (full curve) of the calculated (dashes) dependence upon $s = |\vec{r}-\vec{r}'|$ of the real part of the OMP, for $k_F = 1.35$ fm^{-1} (from Ref. [4]).

Fig. 7. Dependence on energy of the modulus of the real part of the OMP, for the Fermi momenta $k_F = 1.35$, 1.10 and 0.82 fm^{-1} , respectively (from Ref. [6]).

Fig. 8. Real part of the OMP in ^{208}Pb , for the energies E = 1 , 50 , 100 and 200 MeV , respectively (from Ref. [6]).

Fig. 9. Comparison between calculated and empirical (dots) values of J_V/A and $\langle R_V^2\rangle^{1/2}$ (Eqs. (3.39), (3.41)), in the case of protons on ^{208}Pb . The full curves correspond to the local density approximation, the short dashes to the assumption that there exists a neutron-rich skin and the long dashes to the expression (4.30); these coincide with the full curve in the case of J_V/A (from Ref. [25]).

Fig. 10. Dependence on energy of the modulus of the imaginary part of the OMP, for the Fermi momenta $k_F = 1.35$, 1.10 and 0.82 fm^{-1} , respectively (from Ref. [6]).

Fig. 11. Imaginary part of the OMP in ^{208}Pb , for the energies E = 1 , 25 , 50 and 100 MeV , respectively (from Ref. [6]).

Fig. 12. Comparison between calculated and empirical (dots) values of J_W/A and of $\langle R_W^2\rangle^{1/2}$ (Eqs. (3.40),(3.42)), in the case of protons on ^{208}Pb . The conventions are the same as in Fig. 9. The dash-dotted curve represents a Coulomb correction (see section 4.7) (from Ref. [25]).

Fig. 13. Plot versus the asymmetry parameter (N-Z)/A of the volume integral per nucleon. The open and the full dots represent empirical values for 11 MeV neutrons [65], the crosses are the corresponding calculated values; the full line is a fit to empirical values for 8 MeV neutrons [60] (from Ref. [25]).

Fig. 14. Comparison between experimental neutron differential cross sections on ^{120}Sn , ^{208}Pb and ^{209}Bi with the values calculated from the theoretical OMP without renormalization corrections (full curves) and with the following renormalization corrections (dashes, see section 4.8) : $C_V = 0.97$, $C_W = 0.87$ (^{120}Sn at 11 MeV) ; $C_V = 0.98$, $C_W = 0.68$ (^{208}Pb at 14.5 MeV) and $C_V = 0.96$, $C_W = 0.72$ (^{209}Bi at 11 MeV) (from Ref. [63]).

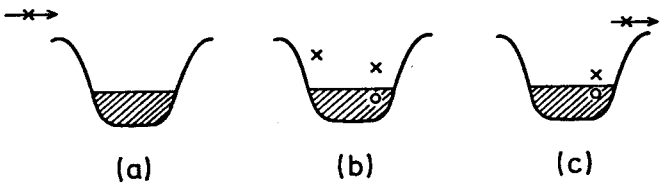

FIG. 1.

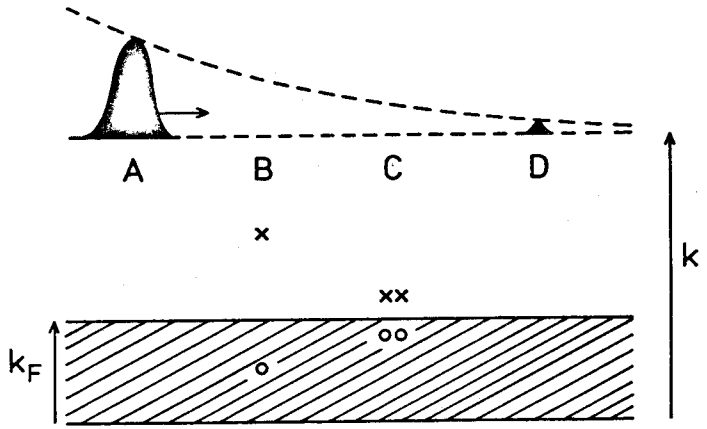

FIG. 2.

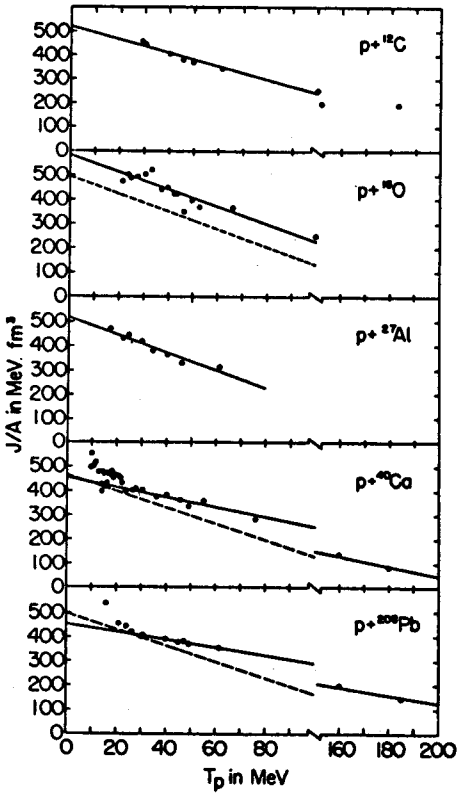

FIG. 3.

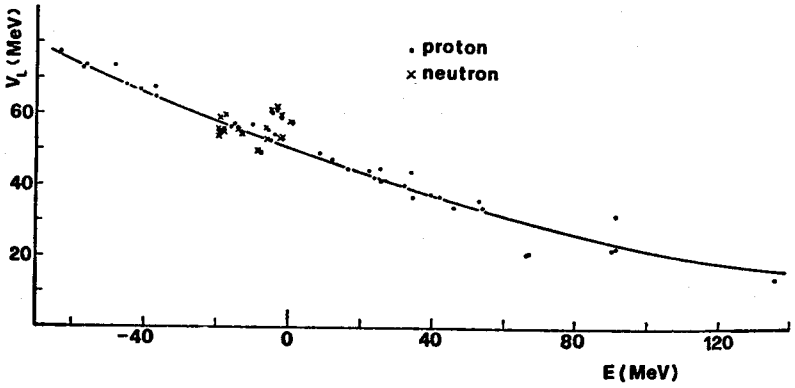

FIG. 4.

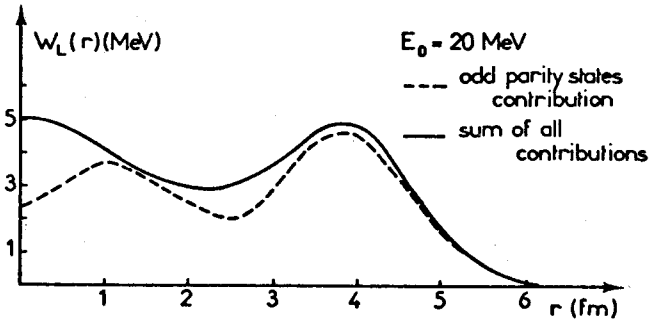

FIG. 5.

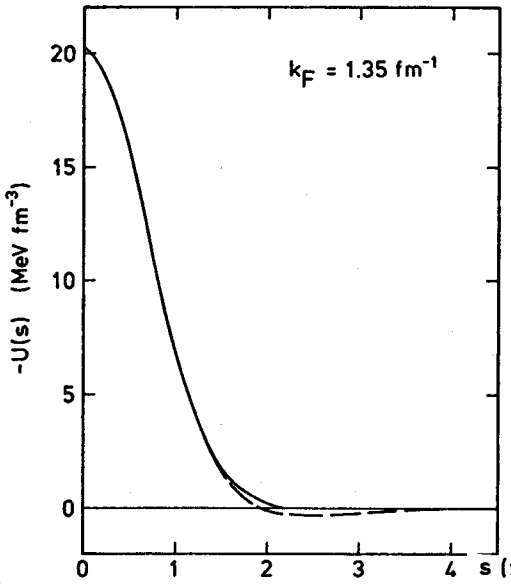

FIG. 6.

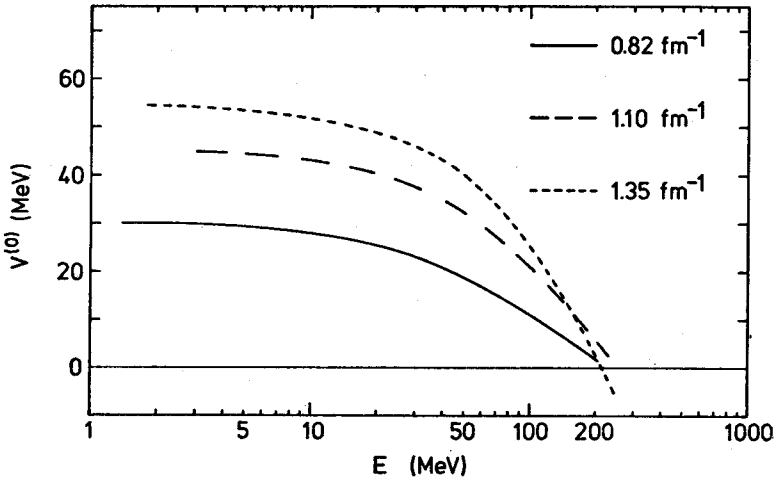

FIG. 7.

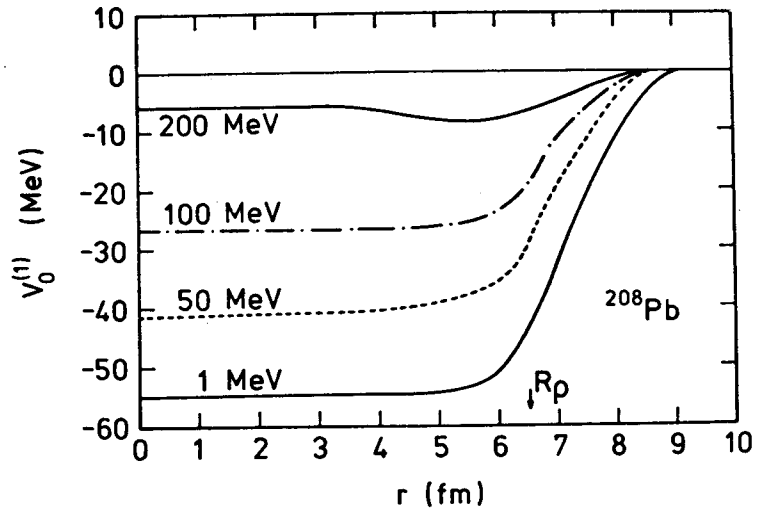

FIG. 8.

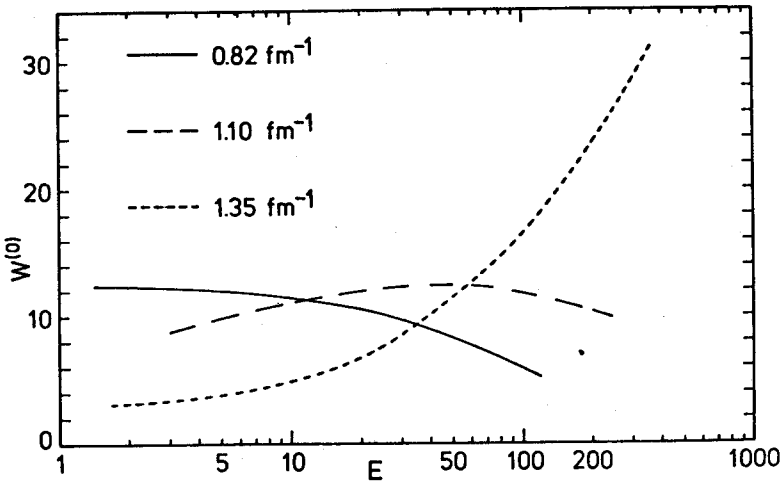

FIG. 10.

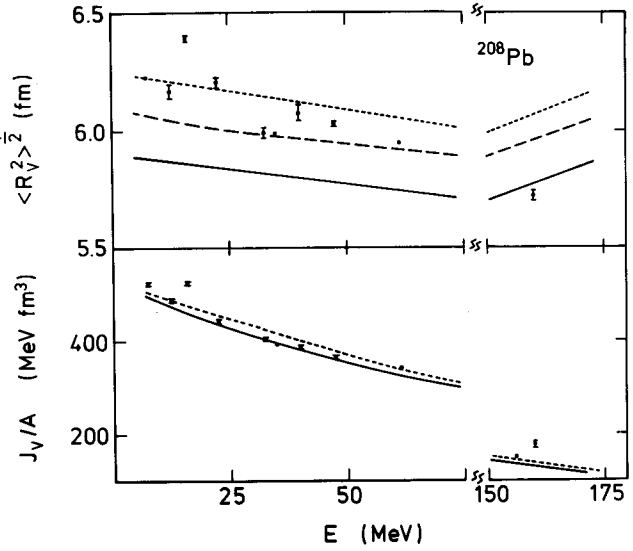

FIG. 9.

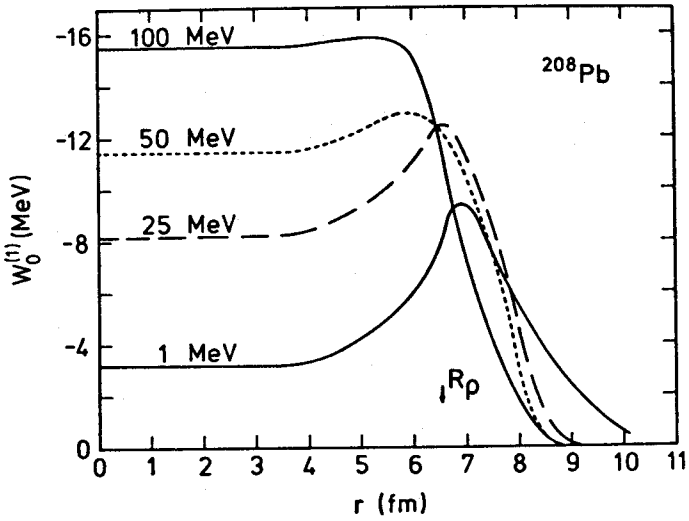

FIG. 11.

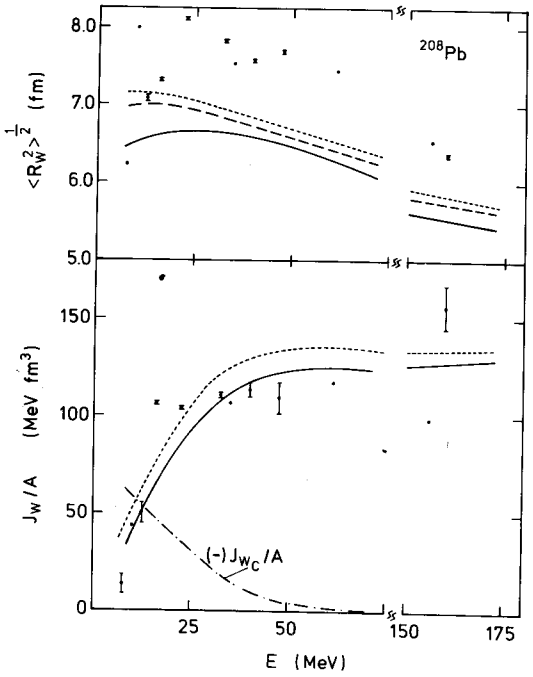

FIG. 12.

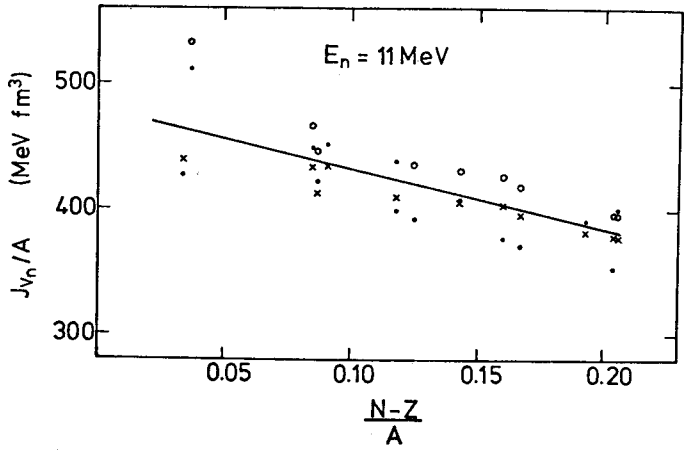

FIG. 13.

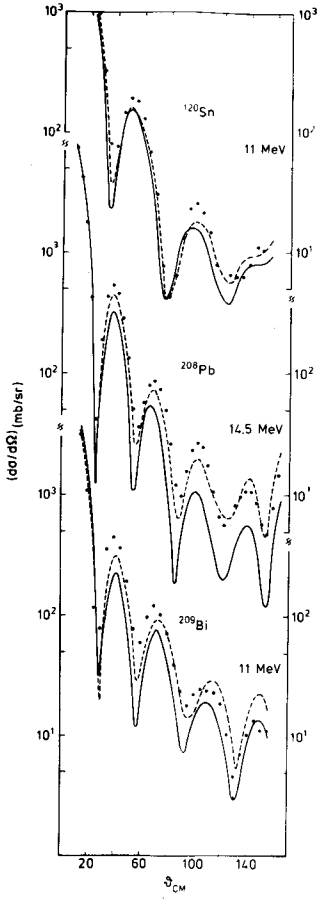

FIG. 14.

MATRIX METHODS IN THE OPTICAL MODEL

Spherical nuclei

J. SALVY
Service de physique nucléaire,
CEA, Centre d'études de Bruyères-le-Châtel,
Montrouge, France

Abstract

The calculable R matrix theory developed by Lane and Robson by using the Bloch boundary condition operator $\mathcal{L}$ is shown to be useful in the frame of practical aspects of the optical model. We first recall the general formalism. We then apply it to spherical nuclei and develop practical methods for constructing all the elements of the matrices which are to be inverted. A non local nuclear potential of the folding type is examined as a possible alternative or improvement of the conventional phenomenological Woods-Saxon potential. From a more fundamental point of view, matrix methods are also shown to be adapted to the treatment of Hartree-Fock type real parts. Finally the applicability of such matrix methods for practical evaluation purposes is illustrated with some simple examples. Other possible developments are suggested.

1. INTRODUCTION

Conventional optical model codes generally use numerical integration methods to solve the Schrödinger equation describing the scattering of a nucleon from a complex potential. In this way very general potential shapes can in principle be treated. However, from a practical viewpoint, such methods encounter for example particular difficulties in directly dealing with non local potentials. The subterfuge of an approximate equivalent local potential has been useful in the frame of global and phenomenological cross section analyses, but it introduces extra energy-dependences in the parametrology and its use is not always suitable. The presence of non locality in the numerical integration methods leads to solve integro-differential equations [1] by generally using iteration procedures with storage at each step of numerical wave functions to generate approximate expressions for the non local term. Besides, large part of the calculation is usually performed again when any parameter or the neutron energy changes. In view of evaluation purposes, coherent and accurate enough calculations of various neutron cross sections for a given target over a wide energy range generally involve at first a specific optimization of optical parameters [2]. Thus computer time problems arise. It may also be desirable to try and limit the number of free parameters or understand physical aspects of the model by using potentials, generally non local, suggested by microscopic studies of nuclear structure. In these lectures we intend to point out some possible advantages brought up by matrix methods, instead of numerical ones, for treating generalized neutron optical potentials. After having summarized the general formalism employed we shall first apply it to the case of neutron scattering from spherical nuclei. Some detailed considerations will be devoted to folding type non local potentials as an illustration of the usefulness of such matrix methods in connection with cross section evaluation problems [3,4]. Some indications will be given on how to treat in the same frame Hartree-Fock type real potentials as an illustration of possible utilization of results from microscopic studies of nuclear structure for scattering problems.

2. SUMMARY OF THE FORMALISM

The method to be employed is based on the so-called generalized or extended R-matrix theory. Following an initial work by Tobocman and Nagarajan [5] this theory has further been developed by Lane and Robson [6] by using the boundary operator method of Bloch [7] which allows to include different nuclear reaction theories into the same framework.

As usual in R-matrix methods, the configuration space of the global system is assumed to be divided into internal and external regions by a certain finite domain D. The systems of interest here are described by a total Hamiltonian H which commutes with the total angular momentum J, the third component of the total angular momentum M and the parity π. All the physical quantities to be calculated depend only on collision matrix elements obtained for each $(J\pi)$ set separately. Hence, even though these labels are omitted, the following considerations hold for a given $(JM\pi)$ set. The total wave-function Ψ, that is $\Psi^{JM\pi}$, to be found for the total center of mass energy E is solution of the Schrödinger equation :

$$(H - E)\,\Psi = o \qquad (1)$$

subject to appropriate boundary conditions. Given a set of practical basis functions $\{\Phi_i\}$, it is assumed that Ψ can be expanded with sufficient accuracy over a finite set of them (i = 1,2,...,NMAX) within and at the boundary D. From a practical viewpoint, the so-called "calculable" R-matrix theory [6] introduces as Φ_i energy independent functions which do not need also to be orthogonal within D. So, convenient such functions can be chosen to be those used for nuclear structure calculations and orthogonal over all space. In practice it must also be possible to impose the appropriate boundary conditions for Ψ at the surface of D. These surfaces are defined by a set of channel radii, $a_{c'}$, associated to channel or surface functions $\phi_{c'}$ in the sense of Lane and Thomas [8]. For the elastic and inelastic neutron processes considered here, these surface functions have the structure $\phi_{c'} \sim \{\chi_n \chi_{1/2} Y^{\ell c'}(r)\}$ (2) where χ_n are the internal wave functions of different excitation states of the target, $\chi_{1/2}$ the spin wave function of the incident or scattered neutron, and $Y^{\ell}(r)$ is a spherical harmonic. The braces in (2) symbolize the chosen angular momentum coupling which is required to complete the description of $\phi_{c'}$. The indices c, instead of c', will be preferentially used to specify only entrance channels $\phi_c \sim \{\chi_1 \chi_{1/2} Y^{\ell c}(r)\}$. The functions $\phi_{c'}$ are chosen to be orthogonal with respect to integrations over the intrinsic coordinates and relative angles :

$$(\phi_{c'} \mid \phi_{c''}) = \delta_{c';c''} \qquad (2)$$

As usual the channel radii have to be chosen so that beyond them there are negligible nuclear interactions between the neutron and the target nucleus. So, in the regions external to D, the wave function Ψ_c associated to an entrance channel c has the asymptotic form :

$$\Psi_c \sim \sum_{c'} (I_c \phi_c \delta_{c,c'} + S_{cc'} O_{c'} \phi_{c'}) \qquad (3)$$

where I_c and O_c are unit-flux ingoing and outgoing radial functions, and the coefficients $S_{cc'}$ are related to the collision matrix elements needed to calculate the cross sections $\sigma_{cc'}$.

In the possible case when a channel c' is closed at the energy E, the corresponding function rO_c becomes essentially a decaying exponential at large distance.

Following Lane and Robson [6], the Schrödinger equation (1) satisfied by Ψ within and at the surface of D is conveniently modified as :

$$(H + \mathscr{L}(b) - E)\, \Psi = \mathscr{L}(b)\, \Psi \qquad (4)$$

The Bloch [7] operator $\mathscr{L}(b)$ is defined as :

$$\mathscr{L}(b) = \sum_{c'} |\phi_{c'}) \frac{\hbar^2}{2m_{c'}a'} \delta(r - a_{c'}) \left[\frac{d}{dr_{c'}} r_{c'} - b_{c'}\right] (\phi_{c'}| \qquad (5)$$

where the constants $b_{c'}$ have to be chosen later. In (5) m_c, is the reduced mass in channel c' and the round bracket $|\phi_{c'})$ (or $(\phi_{c'}|$) means that the relative coordinate r is not concerned. The introduction of the operator $\mathscr{L}(b)$ into equation (4) allows to get more easily Ψ as an expansion over the interior basis states $|\phi_i>$ (the angular brackets here are used to denote functions defined only within and at the boundary of D). By formally operating on equation (4) from the left with the operator $[H + \mathscr{L}(b) - E]^{-1}$, Ψ turns out to be expressed in terms of its asymptotic value (3) to be taken at $r = a_{c'}$ because of the delta "functions" in (5) :

$$\Psi = [H + \mathscr{L}(b) - E]^{-1} \mathscr{L}(b)\, \Psi \qquad (6)$$

A variational form of Ψ [6,7] is obtained by representing within D the operator $[H + \mathscr{L}(b) - E]^{-1}$ in terms of the basis functions Φ_i as :

$$[H + \mathscr{L}(b) - E]^{-1} \approx \sum_{i,j}^{NMAX} |\Phi_i> A^{-1}_{ij} <\Phi_j| \qquad (7)$$

In (7) A^{-1} is the inverse of the matrix A whose elements are :

$$A_{ij} = <\Phi_i| H + \mathscr{L}(b) - E\, |\Phi_j>_o^a \qquad (8)$$

Although the functions Φ_i are actually rather arbitrary, given the channel radii $r_{c'}$, they must in practice be chosen so that the representation (7) ensures a sufficient convergence of the results with a relatively small number NMAX of them. In view of practical applications, it is important to notice, as indicated in (8), that the use of a R-matrix theory implies that the integrations involved in the matrix elements A_{ij} and in the operator $<\Phi_j|$ in (7) have to be performed over the full range of the angular and internal coordinates but over the radial variable r only up to $r = a_{c'} + \varepsilon$ ($\varepsilon \to o$). In this manner the delta functions in $\mathscr{L}(b)$ are included within the integration domain.

Substituting (7) in (6) gives the approximate expansion of Ψ within D :

$$\Psi = \sum_{i,j}^{NMAX} \Phi_i\, A^{-1}_{ij} <\Phi_j| \mathscr{L}(b) |\Psi> \qquad (9)$$

Using (3) and (5), the matrix element of $\mathscr{L}(b)$ in (9) can be expressed as a sum over the channels c', for which, specializing to scattering processes, we shall choose for convenience the same values $m_{c'} = m$ and $a_{c'} = R \equiv RMAX$:

$$<\Phi_j| \mathscr{L}(b) |\Psi> = \frac{\hbar^2 R}{2m} \sum_{c'} (\Phi_j|\phi_{c'}) \left[(rI_c)' \delta_{c,c'} + S_{c,c'} (rO_{c'})' - b_{c'} (I_c \delta_{c,c'} + S_{c,c'} O_{c'})\right]_{r = RMAX} \qquad (10)$$

where the prime means derivative with respect to r.

The unknown elements $S_{cc'}$ can be calculated from a system of linear equations obtained by projecting onto the surface functions $\phi_{c'}$ the continuity condition of Ψ at the boundary of D. From (3) and (9), (10), **for** given c' :

$$\left[I_c \delta_{c,c'} + S_{c,c'} O_{c'}\right]_R = \sum_{i,j}^{NMAX} (\phi_{c'}|\Phi_i)_R\, A^{-1}_{ij} <\Phi_j| \mathscr{L}(b) |\Psi> \qquad (11)$$

that is, using (10) :

$$\left[I_c \delta_{c,c'} + S_{cc'} O_{c'}\right]_R = \sum_{c''} \mathscr{R}_{c'c''} \left[(rI_c)' \delta_{c,c''} + S_{cc''} (rO_{c''})' - b_{c''} (I_c \delta_{c,c''} + S_{cc''} O_{c''})\right]_R \qquad (12)$$

where $\mathscr{R}$ is a channel matrix with the elements :

$$\mathscr{R}_{c'c''} \equiv \frac{\hbar^2 R}{2m} \sum_{i,j} (\phi_{c'}|\Phi_i)_R\, A^{-1}_{ij}\, (\Phi_j|\phi_{c''})_R \qquad (13)$$

The number of equations (12) is equal to the number of open and closed channels being considered. They contain the same dynamical information as the conventional coupled channel equations but they appear to be much easier to deal with. The converged solutions of (12) with respect to the choices of R and NMAX should be identical to the converged solutions of the equivalent generally integro-differential coupled equations. After having solved (12) for the elements $S_{cc'}$, the substitution of (10) into (9) gives the wave function Ψ (that is each $\Psi^{JM\pi}$) in the convenient form of an expansion over a limited number of the basis functions Φ_i. However this representation, even after convergence, holds only for $r \leqslant R$. Following the above formulas, it appears that an obvious choice for Φ_i is to express them in terms of channel states $\phi_{c'}$:

$$\Phi_i \equiv \Phi_{n,c'} = \Phi_{n,c'}(r)\phi_{c'} \qquad (n = 1,2,..,NMAX_{c'}) \qquad \sum_{c'} NMAX_{c'} = NMAX \tag{14}$$

where a set of suitable radial functions $\Phi_{n,c'}(r)$ has to be chosen for each channel c'.

In the following, the above general formalism will first be applied to the simple case of the elastic scattering of neutrons from spherical nuclei with an optical model Hamiltonian $H = T + \mathcal{U}$, where T is the kinetic operator and $\mathcal{U}$ the complex, possibly non local, optical potential. We shall assume as usual that $\mathcal{U}$ contains no terms depending on the spin of the target nucleus. So, choosing $b_{c'} = b_c = o$ and setting $c \equiv \alpha = (\ell j)$ where ℓ and $j = \ell \pm \frac{1}{2}$ are the orbital and total angular momentum associated to the relative motion neutron-nucleus, the following simplified relations will be used.

$$A_{ac} = \langle a|T + \mathcal{U} + \mathcal{L} - E|c\rangle \tag{8'}$$

$$\mathcal{L}(o) = \sum_{\alpha=(\ell,j)} |\alpha) \frac{\hbar^2}{2mR} \delta(r-R) \frac{d}{dr} r\,(\alpha| \tag{5'}$$

Setting :

$$\mathcal{R}_\alpha(r;E) \equiv \frac{\hbar^2 R}{2m} \tilde{\Phi}_\ell(r).\ A^{-1}.\ \Phi_\ell(R) \tag{15}$$

where Φ_ℓ is the one-column matrix consisting of the N≡NMAX independent radial basis functions $\Phi_{n\ell}(n = 1,2,--,N)$ chosen to calculate the matrix A (8'), the "α"-projected radial wave functions Ψ_α are connected to their asymptotic form $[I_\ell + S_\alpha O_\ell]$ in the expansion over the functions $\Phi_{n,\ell}(r)$:

$$\Psi_\alpha(r) = \mathcal{R}_\alpha(r;E)\left[\frac{d}{dr} r(I_\ell + S_\alpha O_\ell)\right]_R \qquad (r \leqslant R) \tag{9'}$$

Setting $\mathcal{R}_\alpha \equiv \mathcal{R}_\alpha(R,E)$, the elements S_α are calculated from the relation :

$$[I_\ell + S_\alpha O_\ell]_R = \mathcal{R}_\alpha[(rI_\ell)' + S_\alpha (rO_\ell)']_R \tag{12'}$$

For such a matrix method to be practical from a computational point of view, the following objectives must be achieved :

a) carrying out easy procedures to calculate all the matrix elements needed in (8') and especially for every term of a realistic enough nuclear potential $\mathcal{U}$,

b) obtaining a quick enough convergence of the physical quantities of interest as a function of increasing values of the order NMAX of the matrix A.

The following chapters are intended to give preliminary answers to these practical constraints.

3. CHOICE OF BASIS FUNCTIONS

The Hartree-Fock methods which carry out matrix diagonalisations to determine the best average field undergone by a bound nucleon inside a nucleus make currently use of the so-called harmonic oscillator functions as basis states. It is known that these functions are indeed good first approximations to describe bound state wave functions in actual nuclei. Moreover, due to their remarkable properties, they lend themselves to unexpected easy construction of two-body matrix elements even in presence of a finite range two-body interaction [9]. One of the purposes of these lectures is to show how much useful are these basis states i) to construct all the matrix elements needed in matrix procedures of optical model, and ii) to describe the corresponding continuum wave functions within the sphere (0,R) as a linear combination of a very limited number of them.

Leaving aside for the moment any spin consideration, the spherical harmonic oscillator functions are the normalized eigen-functions of the single particle Hamiltonian

$$h_{osc}(r) = T + \tfrac{1}{2}\mu\omega^2 r^2 = \frac{\hbar^2}{2\mu}(-\Delta_r + \beta^2 r^2) \tag{16}$$

They can be written as :

$$\Phi_{n_a \ell_a m_a}(\vec{r}) \equiv \langle \vec{r}|a\rangle = N(n_a \ell_a, \beta) \frac{1}{r} \tilde{\phi}_a(r)\ Y^{\ell_a}_{m_a}(\hat{r}) \qquad (n_a = 1,2\ldots\ ;\ \ell_a = 0,1,\ldots) \tag{17}$$

where $N(n_a\ \ell_a,\ \beta)$ is the normalization factor :

$$N(n_a\ell_a,\beta) = \beta^{\frac{2\ell_a+3}{4}} \left[\frac{2\,\Gamma(n_a)}{\Gamma(n_a+\ell_a+\frac{1}{2})} \right]^{\frac{1}{2}} \tag{18}$$

and $\widetilde{\phi}_a(r)$ the "reduced" radial function :

$$\widetilde{\phi}_a(r) = r^{\ell_a+1}\, e^{-\frac{\beta r^2}{2}}\, L_{n_a-1}^{\ell_a+\frac{1}{2}}(\beta r^2) \tag{19}$$

Writing (17) as $\Phi_{n_a\ell_a}(r).\, Y_{m_a}^{\ell_a}(\hat{r})$, the complete radial function $\Phi_{n_a\ell_a}(r) \equiv \frac{1}{r}\phi_{n_a\ell_a}(r)$ is depending on the oscillator parameter β which will have to be conveniently chosen.

According to the relation :

$$h_{osc}\, \Phi_{n_a\ell_a m_a}(\vec{r}) = \left[2(n_a - 1) + \ell_a + \frac{3}{2}\right] \hbar\omega\, \Phi_{n_a\ell_a m_a}(\vec{r}) \tag{20}$$

$\widetilde{\phi}_a$, for example, is solution of the second order differential equation :

$$\left(\frac{d^2}{dr^2} - \frac{2\mu}{\hbar^2}\,\frac{\ell(\ell+1)}{r^2} - \beta^2 r^2\right)\widetilde{\phi}_a = -\,\varepsilon_a \widetilde{\phi}_a \tag{21}$$

where

$$\varepsilon_a = 2\beta(2n_a + \ell_a - \tfrac{1}{2}) \tag{22}$$

The presence of Laguerre polynomials in the above radial functions allows one to use remarkable properties such as the following ones :

$$\left\{ \begin{array}{l} n\, L_n^\alpha(z) = (2n + \alpha - 1 - z)\, L_{n-1}^\alpha(z) - (n + \alpha - 1)\, L_{n-2}^\alpha(z) \\ \\ L_o^\alpha(z) = 1 \quad , \quad L_1^\alpha(z) = 1 + \alpha - z \end{array} \right. \tag{23}$$

$$L_n^\alpha(z) = L_{n-1}^\alpha(z) + L_n^{\alpha-1}(z) \tag{24}$$

$$z\frac{dL_n^\alpha(z)}{dz} = n\, L_n^\alpha(z) - (n + \alpha) L_{n-1}^\alpha(z) \tag{25}$$

$$\int_o^\infty e^{-z} z^\alpha L_n^\alpha L_m^\alpha\, dz = \delta_{n,m}\, \frac{\Gamma(n+\alpha+1)}{\Gamma(n+1)} \quad \text{(orthogonality relation)} \tag{26}$$

When n_a is increasing, the functions $\Phi_{n_a,\ell_a}(r)$ are readily calculated by recurrence using (23). The following useful relations can be deduced from (23) and (25) (with $\dot{\phi} \equiv \frac{d\phi}{dr}$) :

$$\beta r^2 \Phi_{n_a\ell_a} = -\left[n_a(n_a+\ell_a+\tfrac{1}{2})\right]^{\frac{1}{2}} \Phi_{n_a+1,\ell_a} + (2n_a+\ell_a-\tfrac{1}{2})\Phi_{n_a\ell_a} - \left[(n_a-1)(n_a+\ell_a-\tfrac{1}{2})\right]^{\frac{1}{2}} \Phi_{n_a-1,\ell_a} \tag{27}$$

$$\dot{\Phi}_{n_a\ell_a} = (\ell_a+2n_a-1-\beta r^2)\Phi_{n_a\ell_a} - 2\left[(n_a-1)(n_a+\ell_a-\tfrac{1}{2})\right]^{\frac{1}{2}} \Phi_{n_a-1,\ell_a} \tag{28}$$

4. CONSTRUCTION OF SOME MATRIX ELEMENTS

We suppose here that the potentials are spherical. So, no couplings exist between two different angular momenta ℓ and all the matrix elements needed in (8') are of the form $\langle n_a\ell|\sigma|n_c\ell\rangle$.

1 - Case $\sigma = f(r)$

At first, let us give a general recurrence procedure to construct matrix elements of the form $\langle n_a\ell|f(r)|n_c\ell\rangle$ ($n_a, n_c = 1$ to NMAX), where $f(r)$ represents for example any local spherical potential.

Given ℓ and leaving aside normalization factors, we have to calculate :

$$\langle n_a|f(r)|n_c\rangle = \int_o^R \widetilde{\phi}_a(r) f(r) \widetilde{\phi}_c(r)\, dr \qquad (n_c \geq n_a) \tag{29}$$

Two different expressions of $\langle n_a|\beta r^2 f(r)|c\rangle$ can be obtained by using (23) to express either $\beta r^2\widetilde{\phi}_c$ or $\beta r^2\widetilde{\phi}_a$. Their equality leads to the relation :

$$\begin{aligned} n_a \langle n_a+1|f|n_c\rangle = &-(n_a+\ell-\tfrac{1}{2})\langle n_a-1|f|n_c\rangle + (n_c+\ell-\tfrac{1}{2})\langle n_a|f|n_c-1\rangle \\ &- 2(n_c-n_a)\langle n_a|f|n_c\rangle + n_c\langle n_a|f|n_c+1\rangle \end{aligned} \tag{30}$$

As can be seen (30) defines a "parachute" recurrence from (2NMAX-1) matrix elements belonging only to the first row and to be separately calculated. For $\ell \neq o$ these first row matrix elements can be deduced from their 2NMAX in number homologous in the matrix associated to $(\ell - 1)$ owing to the general relation :

$$\beta(\langle n_a,\ell|f|n_c,\ell\rangle - \langle n_a,\ell|f|n_c-1,\ell\rangle)$$

$$=(n_a+\ell-\tfrac{1}{2})\langle n_a,\ell-1|f|n_c,\ell-1\rangle - n_a\langle n_a+1,\ell-1|f|n_c,\ell-1\rangle \tag{31}$$

This recurrence for obtaining "ℓ" élements from "ℓ - 1" elements can be easily deduced from properties (23) and (24) of Laguerre polynomials. Finally, if use is made of (30) and (31) to construct the elements of (ℓ_{max} + 1) different matrices associated to f(r), a separate calculation of (2NMAX + ℓ_{max} - 1) integrals (27) is needed for ℓ = o, n_a = 1 and n_c = 1 to (2NMAX + ℓ_{max} - 1). If numerical integrations are necessary a single set of r-values within the range [o,R] can be advantageously employed, for example in a Gauss-Legendre integration procedure. Examples of such calculations will be given later.

2 - Case $\mathcal{O}$ = E

Let us denote by $\widetilde{I}_{n_a,n_c}$ the quantities involved here, which are obtained from (29) by the substitution f(r) = 1. For $n_a \neq n_c$ very simple expressions can be deduced for $\widetilde{I}_{n_a,n_c}$ in the following manner. The function $\widetilde{\phi}_c$ is solution of :

$$(\frac{d^2}{dr^2} - \frac{2\mu}{\hbar^2}\frac{\ell(\ell+1)}{r^2} - \beta^2 r^2)\widetilde{\phi}_c = -\varepsilon_c\widetilde{\phi}_c \tag{32}$$

Subtracting (32) multiplied from the left by $\widetilde{\phi}_a$ and (20) multiplied from the left by $\widetilde{\phi}_c$, and then integrating from o to R gives :

$$(\varepsilon_a-\varepsilon_c)\widetilde{I}_{n_a,n_c} = \int_o^R [\widetilde{\phi}_a\frac{d^2}{dr^2}\widetilde{\phi}_c - \widetilde{\phi}_c\frac{d^2}{dr^2}\widetilde{\phi}_a]dr = [\widetilde{\phi}_a\dot{\widetilde{\phi}}_c - \dot{\widetilde{\phi}}_a\widetilde{\phi}_c]_R \tag{33}$$

Denoting by I_{n_a,n_c} the corresponding matrix elements needed in (8') which involve the complete radial functions (17), (33) and (22) lead to the result :

$$I_{n_a,n_c} = \frac{[\phi_a\dot{\phi}_c - \dot{\phi}_a\phi_c]_R}{4\beta(n_a-n_c)} \qquad (n_c > n_a) \tag{34}$$

where ϕ and $\dot{\phi}$ are generated from (27) and (28).

For $n_a = n_c = 1$, the first diagonal element can be determined as :

$$I_{1,1} = \beta^{\frac{3}{2}}\frac{2}{\Gamma(\ell+\frac{3}{2})}\int_o^R(\beta r^2)^\ell e^{-\beta r^2}r^2dr \equiv \frac{1}{\Gamma(\ell+\frac{3}{2})}\gamma(\ell+\tfrac{3}{2},\beta R^2) \tag{35}$$

In order to determine the other diagonal elements parachute recurrences (30) and (31) are of interest.

3 - Case $\mathcal{O}$ = T

The matrix elements $\langle a|T|c\rangle_o^R$ needed in (8'), i.e associated to the complete basis functions (17) and to the limited integration range [o,R], are easily deduced from the relation :

$$T|c\rangle = \frac{\hbar\omega}{2}\{(2n_c+\ell-\tfrac{1}{2})|c\rangle + [(n_c-1)(n_c+\ell-\tfrac{1}{2})]^{\frac{1}{2}}|n_c-1\rangle + [n_c(n_c+\ell+\tfrac{1}{2})]^{\frac{1}{2}}|n_c+1\rangle\} \tag{36}$$

In fact, multiplying (36) from the left by $\langle a|$ and integrating from o to R, $\langle a|T|c\rangle_o^R$ is obtained in terms of the elements I_{n_a,n_c} previously determined :

$$\langle a|T|c\rangle_o^R = \frac{\hbar\omega}{2}\{(2n_c+\ell-\tfrac{1}{2})I_{n_a,n_c} + [(n_c-1)(n_c+\ell-\tfrac{1}{2})]^{1/2}I_{n_a,n_c-1} + [n_c(n_c+\ell+\tfrac{1}{2})]^{1/2}I_{n_a,n_c+1}\} \tag{37}$$

The leading relation (36) is a consequence of (20), i.e :

$$\langle a|h_{osc}|c\rangle \equiv \langle a|T|c\rangle + \langle a|\tfrac{1}{2}\mu\omega^2r^2|c\rangle = \delta_{a,c}(2n_c+\ell-\tfrac{1}{2})\hbar\omega \tag{38}$$

where, using (23) to express $\beta r^2.I_{n_a-1}^{\ell+1/2}$ and then (26), the matrix of $\frac{1}{2}\mu\omega^2r^2$ is easily found to be tridiagonal with the elements :

$$\langle a|\tfrac{1}{2}\mu\omega^2r^2|c\rangle = \begin{cases} \frac{\hbar\omega}{2}(2n+\ell-\frac{1}{2}) & \text{for} \quad n_a=n_c=n \\ -\frac{\hbar\omega}{2}[n(n+\ell+\frac{1}{2})]^{\frac{1}{2}} & \text{for the two cases} \\ & n_c=n_a-1=n \quad \text{and} \quad n_a=n_c-1=n \end{cases} \tag{39}$$

4 - Case $\mathcal{O}$ = $\mathcal{L}$

According to the definition (5) of $\mathcal{L}$:

$$\langle n_a|\mathcal{L}(b)|n_c\rangle = \frac{\hbar^2}{2\mu R}\lim_{\varepsilon\to o}\int_o^{R+\varepsilon}\Phi_{n_a\ell}(r)\delta(r-R)\left[\dot{\phi}_{n_c\ell}-b_\ell\Phi_{n_c\ell}\right]r^2\,dr$$

$$= \frac{\hbar^2 R}{2\mu}\Phi_{n_a\ell}(R)\left[\dot{\phi}_{n_c\ell}(R) - b_\ell\,\Phi_{n_c\ell}(R)\right] \qquad (40)$$

Once more relations (27) and (28) are of interest in order to conveniently generate these "$\mathcal{L}$" matrices.

5. MATRIX ELEMENTS OF A PHENOMENOLOGICAL NON LOCAL NUCLEAR POTENTIAL OF THE FOLDING TYPE

5.1. Real central term

Our main purpose here will be to define realistic enough phenomenological potentials that lend themselves to practical calculations of matrix elements. As an illustration of such a possibility, let us consider at first only the real part of a local nuclear potential written as :

$$\mathcal{U}(\vec{r}) = -V\,\mathcal{V}(\vec{r}) \qquad (41)$$

where V is the strength of this real part and the form factor $\mathcal{V}(\vec{r})$ is of the folding type :

$$\mathcal{V}(\vec{r}) = \int \tilde{v}_\mu(|\vec{r}-\vec{r}_1|)\,\rho(\vec{r}_1)\,d\vec{r}_1 \qquad (42)$$

The normalized "two-body" function $\tilde{v}_\mu$ will be taken to be a Gaussian function of range μ, namely :

$$\tilde{v}_\mu(|\vec{r}-\vec{r}_1|) = (\pi^{\frac{3}{2}}\mu^3)^{-1}\,e^{-|\vec{r}-\vec{r}_1|^2/\mu^2} \qquad \left(\int\tilde{v}_\mu(|\vec{x}|)d\vec{x} = 1\right) \qquad (43)$$

In the simplest case, the "density" function $\rho(\vec{r}_1)$ in (42) will be chosen to be constant, and equal to 1, only inside a sphere (O,R_R) of radius R_R. Thus R_R will be the radius parameter of this real potential $\mathcal{U}$.

Making this choice it clearly appears that the finite range μ of $\tilde{v}_\mu$ stands for the diffuseness of $\mathcal{U}$. Indeed, for $\mu = o$, $\tilde{v}_o$ is a representation of the delta "function" $\delta(|\vec{r}-\vec{r}_1|)$ and $\mathcal{U}$ has the same square form as ρ with a discontinuity at $r = R_R$. When μ is increasing the diffuseness of $\mathcal{U}$ around $r = R_R$ is increasing too. So, the representation (41) can be considered at least as a means to generate a potential which has geometrical characteristics quite analogous to those of the more common Saxon-Woods potential.
Now, using the non localization procedure of Perey and Buck [1], we shall consider, instead of the local form (41), the generalized non local one :

$$\mathcal{U}(\vec{r},\vec{r}') = \mathcal{U}\left(\frac{\vec{r}+\vec{r}'}{2}\right)\tilde{v}_\Delta(|\vec{r}-\vec{r}'|) \qquad (44)$$

In (44) $\tilde{v}_\Delta$ is the Gaussian function (43) where the diffuseness μ is replaced by the non locality range Δ.

For such a potential (44) to be treated by matrix methods, it is necessary to calculate its matrix elements of the form :

$$\langle a|\mathcal{U}|c\rangle = \iint d\vec{r}\,d\vec{r}'\;\Phi_a^*(\vec{r})\;\mathcal{U}\left(\frac{\vec{r}+\vec{r}'}{2}\right)\tilde{v}_\Delta(|\vec{r}-\vec{r}'|)\;\Phi_c(\vec{r}') \qquad (45)$$

where, in principle, the integration domains for r and r' are the sphere (O,RMAX). However, because the nuclear terms have to be negligible beyond RMAX, it has been verified that these integrations may practically be extended up to infinity. Anyway, in order to calculate (45) it is convenient to use the following Moshinsky transformation of a product of two oscillator functions :

$$\Phi_a^*(\vec{r})\Phi_c(\vec{r}') = \sum_{b,d}{}' F_{a,c}^{b,d}\,\Phi_b^*(\vec{R})\Phi_d(\vec{u}) \qquad (46)$$

where :

$$a = (n_a\ell_a m_a),\ b = (N,L,M),\ c = (n_c\ell_c m_c),\ d = (n\ell m) \qquad (46')$$

$$\vec{R} = \frac{1}{\sqrt{2}}(\vec{r}+\vec{r}'),\ \vec{u} = \frac{1}{\sqrt{2}}(\vec{r}-\vec{r}') \qquad (47)$$

and all the oscillator functions Φ have the same parameter β.

The main property of the sum in (46), where the numerical coefficients $F_{a,c}^{b,d}$ are not dependent on β, is its limitation by the energy conservation condition :

$$(2n_a+\ell_a) + (2n_c+\ell_c) = (2N+L) + (2n+\ell) \qquad (48)$$

This condition is due to the fact that (45) turns out to be a relation between eigenfunctions of the same two-oscillator Hamiltonian :

$$h_{osc}(r) + h_{osc}(r') \equiv h_{osc}(R) + h_{osc}(u) \qquad (49)$$

Substituting (46) into (45) gives $\langle a|\mathcal{U}|c\rangle$ in the factorized form :

$$\langle a|\mathcal{U}|c\rangle = -V \sum_{b,d}{}' F^{b,d}_{a,c} \; C_b(\mathcal{V}) C_d(\Delta) \tag{50}$$

where :

$$C_b(\mathcal{V}) = \int d\vec{R}\, \Phi^*_b(\vec{R}) \mathcal{V}\left(\frac{\vec{R}}{\sqrt{2}}\right) \tag{51}$$

and

$$C_d(\Delta) = \int d\vec{u}\, \Phi_d(\vec{u})\, \widetilde{v}_\Delta(\sqrt{2}|\vec{u}|) \tag{52}$$

So, all the non locality effects are included **only in the** factors C_d, whereas the geometric characteristics of the potential are brought up by the factors C_b. According to the scalar form of $\widetilde{v}_\Delta$ and $\mathcal{V}$ (spherical nuclei), these integrals imply :

$$L = M = \ell = m = o \tag{53}$$

Therefore C_b and C_d will also be denoted (cf 46') as respectively C_N and C_n.

Calculation of $C_n(\Delta)$

Using (17) with $\ell = o$ and (43), one obtains :

$$C_n(\Delta) = N(no,\beta)(\pi^{\frac{3}{2}}\Delta^3)^{-1} \int e^{-\frac{2u^2}{\Delta^2}} e^{-\frac{\beta u^2}{2}} L^{\frac{1}{2}}_{n-1}(\beta u^2) u^2 du \int Y^o_o(\hat{u})\, d\hat{u}$$

where the last integral gives an extra factor $\sqrt{4\pi}$. By putting $x = \beta u^2$ and making use of the result :

$$\int_o^\infty e^{-sx} x^\alpha L^\alpha_n(x) dx = \frac{\Gamma(\alpha+n+1)(s-1)^n}{n!\, s^{\alpha+n+1}} \quad (\Re e\ \alpha > -1,\ \Re e\ s > o) \tag{54}$$

$C_n(\Delta)$ has the final form :

$$\begin{cases} C_n(\Delta) = C_n(o)\,(1-\frac{\beta\Delta^2}{4})^{n-1}\,(1+\frac{\beta\Delta^2}{4})^{-n-\frac{1}{2}} \\ C_n(o) = \beta^{\frac{3}{4}}\,\frac{1}{2\pi}\,\left[\frac{\Gamma(n+\frac{1}{2})}{\Gamma(n)}\right]^{\frac{1}{2}} \end{cases} \tag{55}$$

The analytical but more complicated result obtained when the integration domain over u is taken to be limited is given in Appendix 1.

Calculation of $C_N(\mathcal{V})$

Because of the folding form (42) of $\mathcal{V}$, $C_N(\mathcal{V})$ given by (51) involves a six-dimensional integration. However we will show that a completely analytical result may be obtained when use is made of the following separable expansion of the Gaussian function (Mehler's expansion) :

$$\widetilde{v}_\mu(|\vec{r}_1-\vec{r}_2|) = \sum_{k=1}^{\infty} \sum_{\ell} f_{k,\ell}(\alpha r_1^2) g_{k,\ell}(\mu,\alpha r_2^2) \sum_m Y^{\ell *}_m(\hat{r}_1) Y^\ell_m(\hat{r}_2) \tag{56}$$

with :

$$f_{k,\ell}(\alpha r_1^2) = \frac{\Gamma(k)}{\Gamma(k+\ell+\frac{1}{2})}\,(\sqrt{\alpha} r_1)^\ell\, L^{\ell+\frac{1}{2}}_{k-1}(\alpha r_1^2) \tag{56'}$$

$$g_{k,\ell}(\mu,\alpha r_2^2) = \frac{2}{\mu^3}\,\frac{(G-1)^{\frac{3}{2}}}{G^{k+\ell+\frac{1}{2}}}\,(\sqrt{\alpha} r_2)^\ell e^{-\alpha r_2^2/G} L^{\ell+\frac{1}{2}}_{k-1}\left(\frac{\alpha r_2^2}{G}\right) \tag{56''}$$

$$G \equiv 1 + \alpha\mu^2 \tag{56'''}$$

and α is an arbitrary real parameter to be chosen later.

This separable expansion has recently been proved very convenient, in the framework of Hartree-Fock calculations [9], for expressing the two body matrix elements of a two-body effective force with finite ranges of the Gaussian type. Obviously another expansion for $\widetilde{v}_\mu$ exists which is obtained by inverting r_1 and r_2 in (56), but the one written above will be proved much more useful. An interesting property of such expansions consists in concentrating the dependence on the "diffuseness" μ (actually on $\alpha\mu^2$) only into one of the factors f and g, i.e. over one of the two variables r_1 and r_2.

In case $\rho(\vec{r}_1)$ in (42) has the spherical symmetry, only the part $\ell = o$ in (56) is useful, namely :

$$\begin{aligned} &\widetilde{v}_\mu(|\vec{r}_1-\vec{r}_2|)\ \underset{(\ell=o)}{\approx}\ \frac{1}{4\pi} \sum_{k=1}^{\infty} f_{k,o}(\alpha r_1^2)\, g_{k,o}(\mu,\alpha r_2^2) \\ &= \frac{\alpha^{3/2}}{2\pi} \sum_{k-1}^{\infty} \frac{\Gamma(k)}{\Gamma(k+\frac{1}{2})} L^{1/2}_{k-1}(\alpha r_1^2)\, \frac{1}{G^{k+1/2}}\, e^{-\alpha r_2^2/G} L^{1/2}_{k-1}\left(\frac{\alpha r_2^2}{G}\right) \end{aligned} \tag{57}$$

leading to the following infinite expansion of the form factor (42) :

$$\mathcal{V}(r) = \sum_{k=1}^{\infty} \mathfrak{N}_k(\alpha,G)\, L^{1/2}_{k-1}(\alpha r_2^2) \tag{58}$$

where :

$$\mathcal{M}_k(\alpha,G)=\frac{\alpha^{3/2}}{2\pi}\,\frac{\Gamma(k)}{\Gamma(k+\frac{1}{2})}\,\frac{1}{G^{k+1/2}}\int e^{-\frac{\alpha r_1^2}{G}}\,L_{k-1}^{1/2}\left(\frac{\alpha r_1^2}{G}\right)\rho(r_1)d\vec{r}_1 \qquad (58')$$

In these coefficients $\mathcal{M}_k$ are concentrated all the geometric characteristics of the nuclear form factor.

Finally $C_N(\mathcal{V})$, cf (51), is written as follows :

$$N(No,\beta)\sum_{k=1}^{\infty}\mathcal{M}_k\int e^{-\frac{\beta R^2}{2}}L_{N-1}^{1/2}(\beta R^2)L_{k-1}^{1/2}\left(\frac{\alpha R^2}{2}\right)R^2\,dR\int Y_0^0(\hat{R})d\hat{R} \qquad (59)$$

Putting $u=\frac{\beta R^2}{2}$, hence $R^2dR=\frac{\sqrt{2}}{\beta^{3/2}}\,u^{1/2}\,du$, for later convenience we shall write (59) in the following form which defines the quantity $\mathcal{G}_N(\mathcal{V})$:

$$C_N(\mathcal{V}) = C\,\mathcal{G}_N(\mathcal{V}) = C\sum_{k=1}^{\infty}\mathcal{M}_k(\alpha,G)\,\mathcal{G}_{N,k} \qquad (60)$$

where :

$$C=(-)^{N-1}\,\frac{4\sqrt{\pi}}{\beta^{3/4}}\left(\frac{\Gamma(N)}{\Gamma(N+\frac{1}{2})}\right)^{1/2} \qquad (61)$$

and

$$\mathcal{G}_{N,k}=(-)^{N-1}\int_0^{\infty}u^{1/2}e^{-u}L_{N-1}^{1/2}(2u)L_{k-1}^{1/2}\left(\frac{\alpha}{\beta}u\right)du \qquad (61')$$

Taking account of the expansion :

$$L_n^{\alpha}(\mu z)=\sum_{m=0}^{n}\binom{n+\alpha}{m}\mu^{n-m}(1-\mu)^m\,L_{n-m}^{\alpha}(z) \qquad (62)$$

and the orthogonality property (26), it is evident that $\mathcal{G}_{N,k}=0$ for $k>N$ when the choice $\alpha=\beta$ is made. In this case the sum over k in (60) is limited to $k=N$:

$$\mathcal{G}_N(\mathcal{V})\underset{(\alpha=\beta)}{=}\sum_{k=1}^{N}\mathcal{M}_k(\beta,G)\,\mathcal{G}_{N,k} \qquad (60')$$

with

$$\mathcal{G}_{N,k}\underset{(\alpha=\beta)}{=}\begin{cases}\dfrac{(-2)^{k-1}\Gamma(N+\frac{1}{2})}{\Gamma(k)\Gamma(N+1-k)} & \text{for } k\leq N\\ 0 & \text{for } k>N\end{cases} \qquad (63)$$

If the limitation of the integration domain has to be taken in consideration in (61'), more general formulae for $\mathcal{G}_N(\mathcal{V})$ and $\mathcal{G}_{N,k}$ are given in Appendix 1.

Calculation of the coefficients $F_{a,c}^{b,d}$

Bearing in mind the condition (53) giving $\ell=0$, the relation (46) can be written in the particular case $\vec{u}=0$, because :

$$\Phi_{n\ell m}(0)=\delta_{\ell,0}\delta_{m,0}\,\frac{1}{\sqrt{4\pi}}\,\beta^{3/4}\left[\frac{2\Gamma(n)}{\Gamma(n+\frac{1}{2})}\right]^{1/2}L_{n-1}^{1/2}(0) \qquad (64)$$

with, cf (A1),

$$L_{n-1}^{1/2}(0)=\binom{n-1/2}{n-1}=\frac{2}{\sqrt{\pi}}\,\frac{\Gamma(n+1/2)}{\Gamma(n)} \qquad (65)$$

Noting $\vec{R}=\sqrt{2}\,\vec{r}=\sqrt{2}\,\vec{r}'$, multiplying (53) from the right by $\Phi_b(\vec{R})$ and integrating over $\vec{R}$, $F_{a,c}^{b,d}$ is given by :

$$\begin{aligned}F_{a,c}^{b,d}\,\Phi_{n00}(0) &= \int\Phi_a^*(\vec{R}/\sqrt{2})\Phi_c(\vec{R}/\sqrt{2})\Phi_b(\vec{R})\,d\vec{R}\\ &= \int_0^{\infty}\Phi_{n_a\ell_a}(R/\sqrt{2})\,\Phi_{n_c\ell_c}(R/\sqrt{2})\,\Phi_{NL}(R)R^2dR\int Y_{m_a}^{\ell_a*}\,Y_{m_c}^{\ell_c}\,Y_M^L\,d\hat{R}\end{aligned} \qquad (66)$$

In (66) the angular integration gives :

$$\int Y_{m_a}^{\ell_a*}\,Y_{m_c}^{\ell_c}\,Y_M^L\,d\hat{R}=(-)^{m_a}\,\frac{\hat{\ell}_a\hat{\ell}_c\hat{L}}{\sqrt{4\pi}}\begin{pmatrix}\ell_a & \ell_c & L\\ 0 & 0 & 0\end{pmatrix}\begin{pmatrix}\ell_a & \ell_c & L\\ -m_a & m_c & M\end{pmatrix} \qquad (67)$$

where $\hat{\ell}\equiv(2\ell+1)^{1/2}$ and $\begin{pmatrix}\ell_1 & \ell_2 & L\\ -m_1 & m_2 & M\end{pmatrix}$ is a Wigner 3j-coefficient.

As for the radial integration, use can be made of the general result :

$$\begin{aligned}&\int\Phi_{n_a\ell_a}^{(\beta_1)}(R)\,\Phi_{n_c\ell_c}^{(\beta_1)}(R)\,\Phi_{NL}^{(\beta_2)}(R)\,R^2\,dR=\frac{1}{2}\,\beta_2^{3/4}\left(\frac{\beta_2}{\beta_1}\right)^{L/2}D_1\cdot\\ &\sum_{\omega=0}^{n_a+n_c-2}(-)^{\omega}\,C(n_a\ell_a,n_c\ell_c,\omega)\int x^{\frac{\ell_a+\ell_c+L+1}{2}+\omega}\,e^{-x(1+\frac{\beta_2}{2\beta_1})}\,L_{N+1}^{L+1/2}\left(\frac{\beta_2}{\beta_1}x\right)dx\end{aligned} \qquad (68)$$

where

$$D_1=\left[\frac{2\Gamma(n_a)2\Gamma(n_c)2\Gamma(N)}{\Gamma(n_a+\ell_a+\frac{1}{2})\,\Gamma(n_c+\ell_c+\frac{1}{2})\,\Gamma(N+L+\frac{1}{2})}\right]^{1/2}$$

and the coefficients C are defined by the expansion (cf A1-1) :

$$L_{n_a-1}^{\ell_a+1/2}(x)L_{n_c-1}^{\ell_c+1/2}(x) = \sum_{\omega=o}^{n_a+n_c-2} (-)^{\omega}\, x^{\omega}\, C(n_a\ell_a,n_c\ell_c,\omega) \qquad (69)$$

$$C(n_a\ell_a,n_c\ell_c,\omega) = \sum_t \frac{1}{t!}\binom{n_a+\ell_a-1/2}{n_a-1-t}\frac{1}{(\omega-t)!}\binom{n_c+\ell_c-1/2}{n_c-1-\omega+t}$$

In (68) the integral can be evaluated by using the result :

$$\int_o^{\infty} e^{-sx} x^{\beta} L_n^{\alpha}(x)dx = \frac{\Gamma(\beta+1)\Gamma(\alpha+n+1)}{n!\,\Gamma(\alpha+1)}\, s^{-\beta-1}\, F(-n,\beta+1,\alpha+1,\frac{1}{s}) \qquad (70)$$

$$(\ \mathcal{R}e\ \beta > -1\ ,\quad \mathcal{R}e\ s > o)$$

Gathering the above results and noting that $\Phi^{(\beta)}(R/\sqrt{2}) \equiv 2^{3/4}\Phi^{(\beta/2)}(R)$, the use of (68) with $\beta_1 = \beta/2$ and $\beta_2 = \beta$ leads to the final form of $F^{b,d}_{a,c} \equiv F^{NL,no}_{a,c}$:

$$F^{NL,no}_{a,c} = D_2 \sum_{\omega}^{n_a+n_c-2} \frac{(-)^{\omega}}{2^{\omega}}\, C(n_a\ell_a,n_c\ell_c,\omega)\, \frac{\Gamma(\frac{\ell_a+\ell_c+L+3}{2}+\omega)\Gamma(\frac{\ell_a+\ell_c-L}{2}+\omega+1)}{\Gamma(\frac{\ell_a+\ell_c-L}{2}-N+2+\omega)} \qquad (71)$$

where

$$D_2 = (-)^{ma}\frac{\sqrt{\pi}}{2}(-)^{N-1}\, 2^{-\frac{\ell_a+\ell_c}{2}}\, \hat{\ell}_a\,\hat{\ell}_c\,\hat{L}\, \begin{pmatrix} \ell_a & \ell_c & L \\ o & o & o \end{pmatrix}\begin{pmatrix} \ell_a & \ell_c & L \\ -m_a & m_c & M \end{pmatrix}.$$

$$\cdot \left[\frac{\Gamma(n)\Gamma(n_a)\Gamma(n_c)}{\Gamma(N)\Gamma(N+L+\frac{1}{2})\Gamma(n+\frac{1}{2})\Gamma(n_a+\ell_a+\frac{1}{2})\Gamma(n_c+\ell_c+\frac{1}{2})}\right]^{1/2}$$

According to the conditions (53) the only coefficients needed are of the form $F^{No,no}_{a,c}$. When L = o, D_2 becomes independent of m_a, and ℓ_a and ℓ_c must be equal to a same value we shall denote (without confusion) by ℓ. In this particular case, (71) reduces to :

$$F^{No,no}_{n_a\ell,n_c\ell} = (-)^{N-1}\frac{\sqrt{\pi}}{2}\left[\frac{\Gamma(n)\Gamma(N+\frac{1}{2})}{\Gamma(N)\Gamma(n+\frac{1}{2})}\right]^{1/2} f(N,n_a,n_c,\ell) \qquad (72)$$

where, following (48)

$$n + N = n_a+n_c+\ell \qquad (72')$$

and

$$f(N,n_a,n_c,\ell) = \frac{1}{\Gamma(N+\frac{1}{2})}\left[\frac{\Gamma(n_a)\,\Gamma(n_c)}{\Gamma(n_a+\ell+\frac{1}{2})\Gamma(n_c+\ell+\frac{1}{2})}\right]^{1/2} \cdot \qquad (73)$$

$$\cdot \sum_{\omega=\omega_o}^{n_a+n_c-2} \frac{(-)^{\omega}}{2^{\ell+\omega}}\, C(n_a\ell,n_c\ell,\omega)\, \frac{\Gamma(\ell+\omega+1)\ \Gamma(\ell+\omega+3/2)}{\Gamma(\ell+\omega-N+2)}$$

with ω_o = maximum of o or $(N-\ell-1)$

and $C(n_a\ell,n_c\ell,\omega)$ is defined in (69)

- Final form of the matrix element of the non-local real central term

Taking into account the partial results (72), (60), (60') and (55), the matrix element (50) takes the simple separable form :

$$\langle a|\mathcal{U}|c\rangle = -V \sum_{n=1}^{n_a+n_c+\ell-1} \left[\frac{(1-\frac{\beta\Delta^2}{4})^{n-1}}{(1+\frac{\beta\Delta^2}{4})^{n+\frac{1}{2}}}\right] f(N,n_a,n_c,\ell)\ \mathcal{G}_N(\mathcal{V}) \qquad (74)$$

where

$$N = n_a+n_c+\ell-n$$

$f(N,n_a,n_c,\ell)$ is a "geometrical" factor given by (73), and $\mathcal{G}_N(\mathcal{V})$ has the simple expression (60') which includes the geometric characteristics of the form factor $\mathcal{V}$ by the intermediate of a limited number of the coefficients $\mathcal{M}_k(\beta,G)$ given by (58'). In addition to its convenient separable form, the remarkable property of the main optical potential term (74) consists of the exact limitation of the sum over n, together with that over k in $\mathcal{G}_N(\mathcal{V})$, cf (60). For a local potential (Δ = o) the same simplified expression (74) is also useful.

- Determination of the coefficients $\mathcal{M}_k$ (β,G)

In the most general cases, the nuclear density function $\rho(r_1)$ will be given by points in a finite range of r_1. A practical method for determining the corresponding $\mathcal{M}_k$ coefficients will perform all the necessary integrations (58') by using a single net of integration points. Such a procedure has been proved helpful even when $\rho(r_1)$ can be expressed in an analytical form, for example in the form of a finite sum of products of essentially two harmonic oscillators as given for example from Hartree-Fock type calculations. In these cases $\rho(r_1)$ is generally normalized so that $\int\rho(r_1)d\vec{r}_1 = A$, say, and the strength V in front of (41) has to be expressed in units of, say, MeV-fm^3.

In the simplest case when ρ is taken to be equal to 1 inside a sphere of radius R_R, the corresponding diffuse well $\mathcal{M}_k(\beta,G)$ have particularly simple forms.

a) For k = 1, putting $x = \frac{\beta r_1^2}{G}$ and using the definition $\gamma(a,x) \equiv \int_o^x e^{-t}t^{a-1}dt$ and $\Gamma(3/2) = \sqrt{\pi}/2$, (58') gives the simple result :

$$\mathcal{M}_1(\beta,G) = \frac{2}{\sqrt{\pi}}\,\gamma\,(\tfrac{3}{2}\,,\,\frac{\beta R_R^2}{G}) \qquad (75)$$

b) For $k \geq 2$, the property $L_n^{\alpha}(x) = \frac{1}{n!}e^{x}\,x^{-\alpha}\,\frac{d^n}{dx^n}(e^{-x}x^{n+\alpha})$ easily leads to the final result :

$$\mathcal{M}_{k\geq 2}(\beta,G) = \frac{(k-2)!}{(k-\frac{1}{2})!}\,\frac{1}{(\beta R_R^2)^{k-1}}\,x_R^{k+\frac{1}{2}}\,e^{-x_R}\,L_{k-2}^{3/2}(x_R) \qquad (76)$$

$$x_R = \frac{\beta R_R^2}{G}\,,\quad G = 1 + \beta\mu^2$$

5.2. Spin-orbit term

In the spirit of a folding phenomenological nucleon-nucleus potential, and in analogy with the Saxon-Woods form factor, a local spin-orbit term proportional to the scalar product $\vec{\ell}.\vec{s}$, where $\vec{\ell}$ is the angular momentum of the incident nucleon and $\vec{s}$ its spin operator, will be chosen as :

$$\mathcal{U}_{so}(r) = 2\lambda_\pi^2\,(V_{so}+iW_{so})\,\frac{1}{r}\,\frac{d\mathcal{V}_{so}(r)}{dr}\,\vec{\ell}.\vec{s} \qquad (77)$$

where the "folding" form factor $\mathcal{V}_{so}(r)$ is given by (42) with its appropriate geometry characteristics : the "diffuseness" μ_{so} and, if the spherical density function $\rho(r)$ is taken to be square, a spin-orbit radius R_{so}.

Using now the spin coupled harmonic oscillator basis states :

$$\langle\vec{r},\sigma|i=n\ell jj_z\rangle \equiv \Phi_i(\vec{r},\sigma) = \left[\Phi_{n\ell}(\vec{r})\times\chi_{1/2}(\sigma)\right]_{j_z}^{j=\ell\pm\frac{1}{2}} \qquad (78)$$

which are eigen-states of $2\vec{\ell}.\vec{s}$ for the eigen-values, respectively, $+\ell$ and $-(\ell+1)$, the matrix elements of (77) are :

$$\langle a|\mathcal{U}_{so}(r)|c\rangle = \lambda_\pi^2(V_{so}+iW_{so})\binom{+\ell}{-\ell-1}\langle n_a\ell|\frac{1}{r}\,\frac{d\mathcal{V}_{so}(r)}{dr}|n_c\ell\rangle \qquad (79)$$

A procedure to construct a non-local spin orbit term from the local form (77) is quite analogous to that **deserved before** for the real term, but with an appropriate $\Delta \equiv \Delta_{so}$ non-locality range.

Following (50) and (77), its matrix elements will have the similar factorized form :

$$\langle a|\mathcal{U}_{so}|c\rangle = \lambda_\pi^2(V_{so}+iW_{so})\binom{+\ell}{-\ell-1}\sum_{b,d}{}' F_{a,c}^{b,d}\,C_b(\tfrac{1}{r}\,\frac{d\mathcal{V}_{so}}{dr})C_d(\Delta) \qquad (80)$$

where only the factor $C_b = \int d\vec{R}\,\Phi_b^*\,\frac{\sqrt{2}}{R}\,d\mathcal{V}_{so}(R/\sqrt{2})/d(R/\sqrt{2})$ remains to be evaluated. Using the relation :

$$\frac{d}{dz}L_n^{\alpha}(z) = -\sum_{m=o}^{n-1} L_m^{\alpha}(z) \qquad (81)$$

this factor C_b is written as :

$$N(No,\beta)\sum_{k=1}^{\infty}\mathcal{M}_k^{so}\int e^{-\frac{\beta R^2}{2}}L_{N-1}^{1/2}(\beta R^2)2\alpha\Big[-\sum_{t=1}^{k-1}L_{t-1}^{1/2}(\tfrac{\alpha R^2}{2})\Big]R^2dR\,Y_o^o(\hat{R})d\hat{R} \qquad (82)$$

By comparison of (82) with (59), the choice $\alpha = \beta$ directly leads to the result :

$$C_N(\frac{1}{r}\,\frac{d\mathcal{V}_{so}}{dr}) = C\,\mathcal{G}_N(\frac{1}{r}\,\frac{d\mathcal{V}_{so}}{dr}) \qquad (83)$$

where C is the constant (61) and :

$$\mathcal{G}_N(\frac{1}{r}\,\frac{d\mathcal{V}_{so}}{dr}) = -2\beta\sum_{k-2}^{\infty}\mathcal{M}_k^{so}(\beta,G)\sum_{t=1}^{MIN[k-1,N]}\mathcal{G}_{N,t} \qquad (84)$$

with $\mathcal{M}_k$ given by (58'), or (75) and (76), and the factors $\mathcal{G}_{N,t}$ are the same as used in (63).

The final form of (80) has the same structure as (74) :

$$\langle a|\mathcal{U}_{so}|c\rangle = \lambda_\pi^2(V_{so}+iW_{so})\binom{+\ell}{-\ell-1}\sum_{n=1}^{n_a+n_c+\ell-1}\Big[\frac{(1-\frac{\beta\Delta^2}{4})^{n-1}}{(1+\frac{\beta\Delta^2}{4})^{n+1/2}}\Big]f\,\mathcal{G}_N(\frac{1}{r}\,\frac{d\mathcal{V}_{so}}{dr}) \qquad (85)$$

where Δ is obviously the non-locality range associated to the spin-orbit term.

When $\Delta = o$, it can be shown that there are no longer contributions in (85) arising from $k > n_a + n_c + \ell - 1$ in (84). In practical calculations, where generally $\Delta \neq o$ and the coefficients $\mathcal{G}_N$ are separately calculated once for all, it has been proved to be sufficient to take the sum over k in (84) up to the available maximum value kMAX = 2NMAX + ℓMAX - 1.

5.3. Absorptive terms

Several kinds of imaginary absorptive terms of a folding optical potential can be constructed.

5.3.1. Volume absorptive term

Such a term is simply given by (41) where the real strength V_R is replaced by the purely imaginary strength iW_V. Following (74), its matrix elements are :

$$\langle a|\mathcal{U}_v|c\rangle = -iW_v \sum_{n=1}^{n_a+n_c+\ell-1} \left[\frac{(1-\frac{\beta\Delta^2}{4})^{n-1}}{(1+\frac{\beta\Delta^2}{4})^{n+1/2}}\right] f\, \mathcal{G}_N(\mathcal{V}_v) \qquad (86)$$

where the parameters Δ, μ and R can be chosen to be different (Δ_v, μ_v, R_v) from those associated to the real term (namely Δ_R, μ_R, R_R).

5.3.2. Gaussian absorptive term

It is defined as :

$$W_G(r) = -iW_G\, e^{-(r-R)^2/a^2} \qquad (87)$$

where W_G is the strength parameter, and R and a (actually R_G and a_G) are respectively radius and diffuseness parameters.

The matrix elements of this term can be constructed by using a separable expansion of the Gaussian function in (87) analogous to (56) but for one dimension :

$$e^{-(r-R)^2/a^2} = \left(\frac{G-1}{G}\right)^{1/2} e^{-\frac{\alpha R^2}{G}} \sum_{n'=o}^{\infty} \frac{1}{2^{n'} n'!\, G^{n'/2}} H_{n'}(\sqrt{\tfrac{\alpha}{G}}R)\, H_{n'}(\sqrt{\alpha}r) \qquad (88)$$

$$(G = 1 + \alpha a^2)$$

where $H_{n'}$ is an Hermite polynomial and α an arbitrary real constant. For later convenience we shall make use of the following relations between these functions and the Laguerre polynomials :

$$H_{n'}(\sqrt{x}) = (-)^{n'/2}\, \frac{n'}{2}!\, 2^{n'} \left[L^{1/2}_{n'/2}(x) - L^{1/2}_{n'/2-1}(x)\right] \qquad (n' \text{ even})$$

$$H_{n'}(\sqrt{x}) = (-)^{\frac{n'-1}{2}}\, (\tfrac{n'-1}{2})!\; 2^{n'}\, \sqrt{x}\, L^{1/2}_{\frac{n'-1}{2}}(x) \qquad (n' \text{ odd}) \qquad (89)$$

Substituting into (87), the form factor of the absorptive term can be written in a manner similar to (58) :

$$W_G(r)/-iW_G = \sum_{n'=o}^{\infty} \mathcal{M}^G_{n'}(\alpha,G)\, f^G_{n'}(\alpha r^2) \qquad (90)$$

where only the coefficients $\mathcal{M}^G_{n'}$ contain the geometry parameters :

$$\mathcal{M}^G_{n'}(\alpha,G) = \alpha^{1/2}\, a\, e^{-\frac{\alpha R^2}{G}}\, C_{n'}\, \frac{1}{n'!\, G^{\frac{n'+1}{2}}}\, H_{n'}(\sqrt{\tfrac{\alpha}{G}}R) \qquad (91)$$

($C_n = (-)^{n'/2} \cdot \frac{n'}{2}!$ for n' even and $(-)^{\frac{n'-1}{2}} \cdot \frac{n'-1}{2}!$ for n' odd)

and :

$$f^G_{n'}(\alpha r^2) = \begin{cases} L^{1/2}_{\frac{n'}{2}}(\alpha r^2) - L^{1/2}_{\frac{n'}{2}-1}(\alpha r^2) & (n,\text{even}) \\ (\alpha r^2)^{1/2}\, L^{1/2}_{\frac{n'-1}{2}}(\alpha r^2) & (n'\text{odd}) \end{cases} \qquad (92)$$

Thus a Perey-Buck non-localization procedure leads to the following structure of the corresponding matrix elements (compare to (74)) :

$$\langle a|\mathcal{U}_G|c\rangle = -iW_G \sum_{n=1}^{n_a+n_c+\ell-1} \left[\frac{(1-\frac{\beta\Delta^2}{4})^{n-1}}{(1+\frac{\beta\Delta^2}{4})^{n+1/2}}\right] f\, \mathcal{G}^G_N \qquad (93)$$

where $\Delta \equiv \Delta_G$ is the corresponding non-locality range. Following (60) and (61') with $u = \frac{\beta R^2}{2}$,

$$\mathcal{G}^G_N = \sum_{n'=1}^{\infty} \mathcal{M}^G_{n'}(\alpha,G)\, \mathcal{G}^G_{N,n'} \qquad (94)$$

with :

$$\mathcal{G}^G_{N,n'} = (-)^{N-1} \int_o^{\infty} u^{1/2} e^{-u} L^{1/2}_{N-1}(2u) f^G_{n'}(\tfrac{\alpha}{\beta}u)\, du \qquad (95)$$

Two cases have to be examined for calculating this last integral :

a) n'even - Comparison of (95) with (61') in this case leads to the result :

$$\mathcal{G}^G_{N,n'} = \mathcal{G}_{N,\frac{n'}{2}+1} - \mathcal{G}_{N,\frac{n'}{2}} \qquad (96)$$

Besides, the choice $\alpha = \beta$ implies $\mathcal{G}^G_{N,n'} = o$ for $n' > 2N$

b) n'odd - In this case, (92) gives, with $\alpha = \beta$:

$$\mathcal{G}^G_{N,n'} = (-)^{N-1} \int_o^{\infty} u\, e^{-u} L^{1/2}_{N-1}(2u) L^{1/2}_{\frac{n'-1}{2}}(u)\, du \equiv (-)^{N-1} J_{N,\frac{n'+3}{2}} \qquad (97)$$

Following (97), the integrals $J_{N,k}$ are :

$$J_{N,k} = \int_0^\infty x\, e^{-x}\, L^{1/2}_{N-1}(2x) L^{1/2}_{k-2}(x)\, dx \qquad (98)$$

Applying the following relation (cf (23)) :

$$zL^{1/2}_{n-1}(z) = -\, n\, L^{1/2}_{n}(z) + (2n-\tfrac{1}{2})\, L^{1/2}_{n-1}(z) - (n-\tfrac{1}{2})\, L^{1/2}_{n-2}(z)$$

first to $2x.L^{1/2}_{N-1}(2x)$ and then to $x.L^{1/2}_{k-2}(x)$ in (98), leads respectively to the results :

$$J_{N,k} = \begin{cases} \frac{1}{2}\left[-N\, K_{N+1,k} + (2N-\tfrac{1}{2})K_{N,k} - (N-\tfrac{1}{2})K_{N-1,k}\right] & (99) \\ \text{or} \quad -(k-1)K_{N,k+1} + (2k-\tfrac{5}{2})K_{N,k} - (k-\tfrac{3}{2})K_{N,k-1} & (100) \end{cases}$$

where the integrals $K_{N,k}$ are defined by :

$$K_{N,k} = \int_0^\infty e^{-x}\, L^{1/2}_{N-1}(2x)\, L^{1/2}_{k-2}(x)\, dx \qquad (k \geq 2) \qquad (101)$$

As shown in Appendix 2 these quantities $K_{N,k} \equiv K^{L=o}_{N,n=k}$ can easily be calculated by means of simple recurrence properties. After having generated a sufficient number of $K_{N,k}$, $J_{N,k}$ is obtained from (99) for $k = 2$ and from (100) for $k > 2$.

5.3.3. Derivative absorptive term

This kind of absorptive term is more commonly used. In the spirit of a folding type optical potential, such a term, in analogy with its Saxon-Woods form factor, will be taken, if local, in the form :

$$\mathcal{U}_D(r) = -i\gamma W_D\, \frac{d\mathcal{V}_D(r)}{dr} \qquad (102)$$

where the folding form factor $\mathcal{V}_D(r)$ is given by (42) with the geometry characteristics μ_D and R_D appropriate to this potential term. In (102) the strength parameter W_D is multiplied by a correction factor γ in order to make $-i\, W_D$ equal, as usual, to the value of this absorptive potential at the radius R_D (if $\rho(r)$ in $\mathcal{V}_D(r)$ is taken to be square).

If the Perey-Buck non-localization procedure is chosen to construct a more general non-local absorptive potential from (102) and (44) with the appropriate non-locality range Δ ($\Delta \equiv \Delta_D$), the corresponding matrix elements have the factorized form (cf (50)) :

$$\langle a|\mathcal{U}_D|c\rangle = -i\gamma W_D \sum'_{b,d} F^{b,d}_{a,c}\, C_b \left(\frac{d\mathcal{V}_D}{dr}\right) C_d(\Delta) \qquad (103)$$

where only the factor $C_b = \int d\vec{R}\, \Phi^*_b\, \frac{d\mathcal{V}_D(R/\sqrt{2})}{d(R/\sqrt{2})}$ remains here to be evaluated.

Using the relation $\frac{d}{dz}L^\alpha_n(z) = -L^{\alpha+1}_{n-1}(z)$, this factor $C_N(d\mathcal{V}_D/dr)$ is :

$$N(No,\beta) \sum_{k=1}^{\infty} \mathcal{M}^D_k \int e^{-\frac{\beta R^2}{2}} L^{1/2}_{N-1}(\beta R^2)\, 2\alpha\, \frac{R}{\sqrt{2}}\left(-L^{3/2}_{k-2}\left(\frac{\alpha R^2}{2}\right)\right) R^2 dR \int Y^o_o(\hat{R})\, d\hat{R} \qquad (104)$$

that is, putting $u = \frac{\beta R^2}{2}$, $R^3 dR = \frac{2}{\beta^2}\, u\, du$:

$$C_N\left(\frac{d\mathcal{V}_D}{dr}\right) = C\ \mathcal{G}_N\left(\frac{d\mathcal{V}_D}{dr}\right) \qquad (105)$$

where C is the constant (61), and :

$$\mathcal{G}_N\left(\frac{d\mathcal{V}_D}{dr}\right) = (-)^N \frac{2\alpha}{\sqrt{\beta}} \sum_{k=2}^{\infty} \mathcal{M}^D_k \int u\, e^{-u}\, L^{1/2}_{N-1}(2u)\, L^{3/2}_{k-2}\left(\frac{\alpha}{\beta}u\right) du \qquad (106)$$

Making the choice $\alpha = \beta$, the integral $I_{N,k}$ in (106) is identical to the integral $I^{L=o}_{N,n=k}$, a practical calculation of which is described in Appendix 2. Finally, the matrix element (103) takes the final form similar to (74) :

$$\langle a|\mathcal{U}_D|c\rangle = -i\gamma W_D \sum_{n=1}^{n_a+n_c+\ell-1} \left[\frac{(1-\frac{\beta\Delta^2}{4})^{n-1}}{(1+\frac{\beta\Delta^2}{4})^{n+1/2}}\right] f\ \mathcal{G}_N\left(\frac{d\mathcal{V}_D}{dr}\right) \qquad (107)$$

where :

$$\mathcal{G}_N\left(\frac{d\mathcal{V}_D}{dr}\right)_{(\alpha=\beta)} = (-)^N\, 2\sqrt{\beta} \sum_{k=2}^{\infty} \mathcal{M}^D_k(\beta, G)\, I_{N,k} \qquad (108)$$

In practical calculations, it has been found very sufficient to take the sum over k in (108) up to the available maximum value of k necessary for calculating the matrix elements (74) of the real term, namely $kMAX = 2NMAX + \ell MAX - 1$.

An estimation of the correction factor γ can be made in the local case $\Delta = o$.

For a square density ρ of radius R the "Gaussian" folding integral (42) has the analytical result :

$$2\mathcal{V}(r) = \mathrm{erf}\left(\frac{R+r}{\mu}\right) + \mathrm{erf}\left(\frac{R-r}{\mu}\right) + \frac{\mu}{r\sqrt{\pi}}\left[e^{-(R+r)^2/\mu^2} - e^{-(R-r)^2/\mu^2}\right] \tag{109}$$

where erf(x) is the "error" function :

$$\mathrm{erf}(x) = \frac{2}{\sqrt{\pi}} \int_0^x e^{-t^2}\, dt$$

Consequently, from direct differentiation :

$$\gamma \equiv \left(\frac{d\mathcal{V}_D(r)}{dr}\right)^{-1}_{r=R} = -\mu\sqrt{\pi}\left\{1 - \frac{\mu^2}{2R^2} + \left[1+\frac{\mu^2}{2R^2}\right] e^{-4R^2/\mu^2}\right\}^{-1} \tag{110}$$

This value of γ has been adopted even for $\Delta \neq o$. In case when the density function ρ is not square, an equivalent radius, to be specified, can be introduced in (110), but the choice $\gamma = -1$ is always possible if comparisons with more conventional potentials are out of interest.

5.4. Total phenomenological folding potential

Gathering the above partial terms and leaving aside some of them judged to be non-important in the scattering of low energy neutrons, a common total phenomenological folding potential will be written, with evident notations, as

$$\mathcal{U}(r) = -V_R \mathcal{V}_R(r) - i\gamma W_D \frac{d\mathcal{V}_D(r)}{dr} + 2\lambda_\pi^2 V_{so} \frac{1}{r} \frac{d\mathcal{V}_{so}(r)}{dr} \vec{l}.\vec{s} \tag{111}$$

The successive terms describe respectively the real central (R), surface derivative imaginary (D) and the real spin-orbit (so) potentials. The matrix elements of all these terms have been shown to have the same structure : they are given respectively by the formulas (74), (107) and (85) where, apart from the corresponding strength factors, only the factors $\mathcal{G}_N$ are different and given respectively in (60') and (63), (108) and (84). These quantities contain the corresponding geometry parameters only by means of the coefficients $\mathcal{M}_k$ given generally by (58') and which reduce to the very simple forms (75) and (76) when constant densities ρ are limited by corresponding radii R. In this case such radii can be generally expressed as a function of the mass number A by the common relation

$$R_i = r_i A^{1/3} \qquad (i = R, D, so) \tag{112}$$

Finally, adopting (111) and (112) the model parameters are the following ones :

3 strengths : V_R, W_D, V_{so}

3 diffuseness parameters : μ_R, μ_D, μ_{so} (113)

3 "reduced" radii : r_R (or r), r_D, r_{so},

which all have their analogues in the local Saxon-Woods type potentials. Nevertheless, the present formulation allows one to add, without extra computational difficulty, the corresponding and possibly different non-locality range parameters :

$$\Delta_R, \Delta_D, \Delta_{so} \tag{113'}$$

Remarks

1- Let $J_{\mathcal{V}}$ be the volume integral $J_{\mathcal{V}} \equiv \int \mathcal{V}(r).4\pi r^2 dr$ of the spherical distribution $\mathcal{V}(r)$. Taking account of its folding form (42), one obtains :

$$J_{\mathcal{V}} = J_{\tilde{v}_\mu} J_\rho = J_\rho \tag{114}$$

If the density function $\rho(r)$ is normalized to the number of nucleons, that is $J_\rho = A$, the strength -V in (41) is nothing but the volume integral of the potential $\mathcal{U}(r)$ per nucleon (generally in units of MeV-fm^3).

If $J_\rho = \frac{4}{3}\pi R^3$ (case of a square density), the potential strength V which gives the same volume integral as a Woods-Saxon potential of strength V_{WS}, diffuseness a and same radius R is equal to :

$$V \simeq V_{WS}\left(1 + \pi^2 \frac{a^2}{R^2}\right) \tag{115}$$

Let $\langle r^2\rangle_{\mathcal{V}}$ be the mean square radius $\langle r^2\rangle_{\mathcal{V}} \equiv \frac{1}{J_{\mathcal{V}}} \int r^2 \mathcal{V}(r) 4\pi r^2 dr$ of the distribution $\mathcal{V}(r)$. Following the folding form (42) of $\mathcal{V}$:

$$\langle r^2\rangle_{\mathcal{V}} = \langle r^2\rangle_{\tilde{v}_\mu} + \langle r^2\rangle_\rho \tag{116}$$

or

$$\langle r^2\rangle_{\mathcal{V}} = \frac{3}{2}\mu^2 + \frac{3}{5}R^2 \tag{116'}$$

This last quantity is to be compared to the corresponding value of the Woods-Saxon form factor :

$$\langle r^2\rangle_{WS} \simeq \frac{7}{5}\pi^2 a^2 + \frac{3}{5}R^2 \qquad (117)$$

2- In the case of the **proton-nucleus scattering**, a Coulomb potential $\mathcal{U}_C$ should be added to the nuclear potential (111). Such a term can be easily introduced in different ways into the formalism developed above. For example, by remarking that :

$$\frac{1}{|\vec{r}-\vec{r}_1|} = \int_0^\infty d\mu\ 2\pi\mu\ \tilde{v}_\mu\ (|\vec{r}-\vec{r}_1|) \qquad (118)$$

where $\tilde{v}_\mu$ is the normalized Gaussian function (43), $\mathcal{U}_C$ can be written in the local folding form (42) where ρ becomes a charge density and an extra integration over μ is involved. Such a μ (or G)-integration is only to be performed in the $\mathcal{M}_k(\alpha,G)$ coefficients, and leads to practical results especially when applied to the case of a uniform charge inside a sphere of radius R_C. However, due to the long range of the Coulomb potential, the corresponding $\mathcal{J}_{N,k}$ integrals (61') have to be limited (cf Appendix 1). We shall say no more here about the case of charged particles.

3- Instead of a Gaussian folding potential, a Yukawa folding potential can also be developed along the same formalism. In this case it is possible to take advantage of recursion relations for evaluating the integrals $C_N(\nu)$.

4- The construction obtained here for the real terms (central and spin-orbit) of the non-local potential (111) can advantageously be **used for** determining the energies and wave functions of bound states. In this case, the only diagonalization of the matrices $T + \mathcal{U}$, with consideration of RMAX = ∞, provides simultaneously all the bound states for each ℓ value. Moreover the corresponding eigenfunctions automatically are obtained in the very convenient form of an expansion over a limited number of oscillator basis functions.

6. MATRIX ELEMENTS OF A HARTREE-FOCK TYPE REAL POTENTIAL

Single-particle average fields calculated from Hartree-Fock type microscopic methods are expected to represent a good first approximation for the real part of the optical potential. Such fields are depending only on a fundamental two-body force chosen for example so as to reproduce bulk properties of the bound states of the actual nuclei. It has been shown [10] that new computation techniques allowing the use of a well adapted effective two-body force are able to **yield** a satisfactory description of the nuclear properties such as nuclear masses, density distributions, equilibrium deformations,..., over a large range of spherical as well as deformed nuclei. So, a practical utilization of such non-local potentials in optical model calculations would be suitable in order to test their usefulness to decrease the number of free parameters. Hartree-Fock densities can be introduced in the coefficients $\mathcal{M}_k$ (73') of the above folding potential. However the only aim of this chapter will be to point out that the spherical Hartree-Fock potentials can easily be taken into account directly in the frame of matrix methods.

For sake of definiteness, let us choose the following density-dependent and finite range two-body interaction carried out by D. Gogny (D1 interaction [10]) :

$$V = \sum_{i=1}^{2} e^{-|\vec{r}_1-\vec{r}_2|^2/\mu_i^2}(W_i+B_iP_\sigma - H_iP_\tau - M_iP_\sigma P_\tau) + i\,W_{LS}(\vec{\sigma}_1+\vec{\sigma}_2).\overleftarrow{\nabla}_{12}\times$$

$$\times\delta(\vec{r}_1-\vec{r}_2)\vec{\nabla}_{12} + t_o(1+x_oP_\sigma)\delta(\vec{r}_1-\vec{r}_2)\rho^\alpha(\frac{\vec{r}_1+\vec{r}_2}{2}) \qquad (\vec{\nabla}_{12}\equiv\frac{\vec{\nabla}_1-\vec{\nabla}_2}{2}) \qquad (119)$$

Such a two-body potential is seen to contain successively central, spin-orbit and density-dependent terms. The values of the different constants are given in Table I. The following radial terms of the Hartree-Fock potential can be deduced [11] for a given (ℓj) set.

6.1. Direct term

It is of the local folding form, with q = neutron or proton :

$$\Gamma_D^q(r) = \sum_{i,q',\ell'}\left\{W+\frac{B}{2} - (H+\frac{M}{2})\delta_{q,q'}\right\}_i \int v_o^{(i)}(r,r_1)\,\mathcal{R}_D^{q'\ell'}(r_1;\beta')r_1^2dr_1 \qquad (120)$$

where

$$\mathcal{R}_D^{q'\ell'}(r_1;\beta') = \frac{1}{2\pi}\sum_{n_\beta n_\delta}\left\{(\ell'+1)\rho^{\ell' j'_+ q'} + \ell'\rho^{\ell' j'_- q'}\right\}_{n_\beta n_\delta}\Phi^{(\beta')}_{n_\beta\ell'}(r_1)\Phi^{(\beta')}_{n_\delta\ell'}(r_1) \qquad (120')$$

$$(j'_\pm \equiv \ell' \pm \tfrac{1}{2})$$

In (120) the coefficients $v_k^{(i)}(r_1,r_2)$ are the radial parts of the multipole expansion of the Gaussian function :

$$e^{-|\vec{r}_1-\vec{r}_2|^2/\mu_i^2} = \sum_k v_k^{(i)}(r_1,r_2)\left[Y^k(\hat{r}_1).Y^k(\hat{r}_2)\right] \qquad (121)$$

In (120') the functions $\Phi_{n\ell}$ are the same radial oscillator functions as described in chapter 3, with specification of the value of the parameter β' used in the HF calculations. Given a set (ℓ',j',q') the density matrix elements $\rho_{n_\beta n_\delta}$ are defined by :

$$\rho^{\ell' j' q'}_{n_\beta n_\delta} = \sum'_\nu u^{(\nu)}_{n_\beta}\,u^{(\nu)}_{n_\delta}$$

where the u's are the coefficients of the expansion of the HF occupied orbitals over the oscillator basis functions, and Σ' is a sum over these occupied orbitals of the type (ℓ',j',q').

From (56) to (56''') where r_1 and r_2 can be inverted, we shall write here, following (121) :

$$v_k^{(i)}(r_1,r_2)=2\pi^{3/2}\frac{(G_i-1)^{3/2}}{G_i^{(k+1)/2}}\sum_{n=1}^{\infty}\frac{\Gamma(n)}{G_i^n\Gamma(n+k+\frac{1}{2})}(\sqrt{\frac{\alpha}{G_i}}r_1)^k.e^{-\frac{\alpha r_1^2}{G_i}}\cdot \tag{122}$$
$$\cdot L_{n-1}^{k+\frac{1}{2}}(\frac{\alpha r_1^2}{G_i})(\sqrt{\alpha}r_2)^k L_{n-1}^{k+1/2}(\alpha r_2^2)$$

with

$$G_i \equiv 1 + \alpha\,\mu_i^2$$

In view of optical model applications, matrix elements of the type $\langle\alpha|\,\Gamma_D^q|\gamma\rangle$ have to be calculated, where the basis oscillator functions $\Phi_{n_\alpha,\ell}$ and $\Phi_{n_\gamma,\ell}$ are associated to a "scattering" oscillator parameter β. Substituting (122) into (120) leads to the form :

$$\langle\alpha|\,\Gamma_D^q|\gamma\rangle = \pi^{1/2}\sum_{i,q'}(G_i-1)^{3/2}\left\{W+\frac{B}{2}-(H+\frac{M}{2})\,\delta_{q,q'}\right\}_i\cdot \tag{123}$$
$$\cdot\sum_{\ell' n_\beta n_\delta}\left\{(\ell'+1)\rho^{\ell' j'_+ q'}+\ell'\rho^{\ell' j'_- q'}\right\}_{n_\beta n_\delta}\sum_{n=1}^{n_\beta+n_\delta+\ell'-1}J^{\ell\ell o}_{n_\alpha n_\gamma n}\,I^{\ell'\ell' o}_{n_\beta n_\delta n}$$

where, for later convenience, the following more general definitions are adopted :

$$J^{\ell_a\ell_c k}_{n_a n_c n}\equiv C_J\int_o^\infty u^{\frac{\ell_a+\ell_c+k+1}{2}}e^{-u\left[1+\frac{\alpha}{\beta G}\right]}L^{\ell_a+1/2}_{n_a-1}(u)L^{\ell_c+1/2}_{n_c-1}(u)L^{k+1/2}_{n-1}(\tfrac{\alpha u}{\beta G})\,du \tag{124}$$

with

$$C_J(\tfrac{\alpha}{\beta})=\left[\frac{\Gamma(n_a)\Gamma(n_c)}{\Gamma(n_a+\ell_a+\frac{1}{2})\Gamma(n_a+\ell_c+\frac{1}{2})}\right]^{1/2}(\tfrac{\alpha}{\beta})^{\frac{k}{2}}\;\frac{1}{G^{n+k+1/2}\Gamma(n+k+\frac{1}{2})}$$

and :

$$I^{\ell_a\ell_c k}_{n_a n_c n}\equiv C_I\int_o^\infty u^{\frac{\ell_a+\ell_c+k+1}{2}}e^{-u}L^{\ell_a+1/2}_{n_a-1}(u)L^{\ell_c+1/2}_{n_c-1}(u)L^{k+1/2}_{n-1}(\tfrac{\alpha u}{\beta'})\,du \tag{125}$$

with

$$C_I(\tfrac{\alpha}{\beta'})=\left[\frac{\Gamma(n_a)\Gamma(n_c)}{\Gamma(n_a+\ell_a+1/2)\Gamma(n_c+\ell_c+1/2)}\right]^{1/2}(\tfrac{\alpha}{\beta'})^{\frac{k}{2}}\,\Gamma(n)$$

Using the formulas (69), (A1-1), and the result :

$$\int_o^\infty e^{-x}\,x^{\gamma-1}L_n^\mu(x)dx=(-)^n\frac{\Gamma(\gamma)\Gamma(\gamma-\mu)}{n!\,\Gamma(\gamma-\mu-n)} \tag{126}$$

the coefficients I take the following form :

$$I\sim\sum_{\omega=o}^{n_a+n_c-2}(-)^\omega C(n_a\ell_a,n_c\ell_c,\omega)\sum_{m=o}^{n-1}\frac{f(\ell_a\ell_c k n\omega m)}{\Gamma(\frac{\ell_a+\ell_c-k}{2}+\omega-n+2+m)}(\tfrac{\alpha}{\beta'})^{n-m-1}(1-\tfrac{\alpha}{\beta'})^m \tag{127}$$

As the quantity f remains finite **contrary to** the Γ-function in the denominator when its integer argument is no longer positive, it is clearly seen that the choice $\alpha=\beta'$, that is m = o, limits the possible values of n. Hence the very practical limitation of the sum over n in the matrix element (123). Choosing $\alpha=\beta'$, the simple result obtained for I is :

$$I^{\ell_a\ell_c k}_{n_a n_c n}=(-)^{n-1}\left[\frac{\Gamma(n_a)\Gamma(n_c)}{\Gamma(n_a+\ell_a+1/2)\Gamma(n_c+\ell_c+1/2)}\right]^{1/2}\sum_{\omega=o}^{n_a+n_c-2}(-)^\omega\,C(n_a\ell_a,n_c\ell_c,\omega).$$
$$.\,\Gamma(\tfrac{\ell_a+\ell_c+k}{2}+\omega+\tfrac{3}{2}).\;\frac{\Gamma(\frac{\ell_a+\ell_c-k}{2}+\omega+1)}{\Gamma(\frac{\ell_a+\ell_c-k}{2}+\omega-n+2)} \tag{128}$$

with the limitation

$$n\leqslant(\ell_a+\ell_c-k)/2+n_a+n_c-1\equiv N_\Delta^{(k)} \tag{128'}$$

As for the coefficients J, analogous explicit expansions could be deduced. However, all those coefficients can advantageously be calculated only from the coefficients I by means of the following relation valid for $\beta'=\beta$:

$$J^{\ell_a\ell_c k}_{n_a n_c n}=A\sum_{q=1}^{N_\Delta^{(k)}}(\tfrac{1}{1+G})^{q-1}\frac{(k+n+q-\frac{3}{2})!}{(q-1)!\,(k+q-\frac{1}{2})!}I^{\ell_a\ell_c k}_{n_a n_c q} \tag{129}$$

$$A=(\tfrac{1}{1+G})^{k+n+1/2}\;\frac{1}{(n-1)!\,(k+n-\frac{1}{2})!},\qquad G=1+\beta\mu^2$$

6.2. Exchange terms

The antisymetrization effects lead to the following non-local and ℓ-dependent radial potential :

$$\Gamma_E^q(r,r') = -\sum_{ikq'\ell'} \left\{ (B+\frac{W}{2})\delta_{q,q'} - (M+\frac{H}{2}) \right\}_i \hat{k}^2 \begin{pmatrix} \ell & k & \ell' \\ o & o & o \end{pmatrix}^2 v_k^{(i)}(r,r') \mathcal{R}_E^{q'\ell'}(r,r';\beta') \tag{130}$$

where

$$\mathcal{R}_E^{q'\ell'}(r,r';\beta') = \frac{1}{2\pi} \sum_{n_\beta n_\delta} \left| (\ell'+1)\rho^{\ell' j'_+ q'} + \ell' \rho^{\ell' j'_- q'} \right|_{n_\beta n_\delta} \Phi^{(\beta')}_{n_\beta \ell'}(r') \Phi^{(\beta')}_{n_\delta \ell'}(r) \tag{130'}$$

$\hat{k} \equiv (2k+1)^{1/2}$ and the "3J" coefficient $\begin{pmatrix} \ell & k & \ell' \\ o & o & o \end{pmatrix}$ permits contributions from multipoles satisfying $|\ell - \ell'| \leq k \leq \ell + \ell'$ and $(k+\ell+\ell')$ even.

In order to take into account such non-local terms, which are very different in structure from Perey and Buck type ones, in optical model matrix methods, their matrix elements $\langle\alpha|\ \Gamma_E^q\ |\gamma\rangle$ are to be calculated as linear combinations of integrals of the type :

$$\iint \Phi^{(\beta)}_{n_\alpha \ell}(r) v_k^{(i)}(r,r') \mathcal{R}_E^{q'\ell'}(r,r';\beta') \Phi^{(\beta)}_{n_\gamma \ell}(r') r^2 dr\, r'^2 dr' \tag{131}$$

The separation of the two variables r and r' in such integrals leads to nothing but products of the type J.I where the coefficients J and I are given by (124) and (125). However this simple result implies $\beta = \beta'$. The final form is :

$$\langle\alpha|\Gamma_E^{\ell q}|\gamma\rangle = -\pi^{1/2} \sum_{iq'} (G_i - 1)^{3/2} \left\{ (B+\frac{W}{2})\delta_{q,q'} - (M+\frac{H}{2}) \right\}_i \cdot$$
$$\cdot \sum_{\ell' n_\beta n_\delta} \left\{ (\ell'+1)\rho^{\ell' j'_+ q'} + \ell' \rho^{\ell' j'_- q'} \right\}_{n_\beta n_\delta} \sum_k \hat{k}^2 \begin{pmatrix} \ell & k & \ell' \\ o & o & o \end{pmatrix}^2 J^{\ell\ell' k}_{n_\alpha n_\delta n} I^{\ell\ell' k}_{n_\gamma n_\beta n} \tag{132}$$

In the following, as suggested up to now, we shall take $\beta = \beta'$. Using $\frac{\hbar^2}{m} = 41.8137$ MeV-fm^2-amu (^{16}O) and, for not too low mass numbers A, the approximations $\mu \approx 1$ amu (^{16}O) and $\hbar\omega \approx 41\ A^{-1/3}$ MeV, the values of β' are expected to be :

$$\beta' = \left(\frac{\hbar\omega}{\hbar^2}\right)^{1/2} \mu \approx A^{-1/3}\ \text{fm}^{-2} \tag{133}$$

Hence, as examples, $\beta' \approx 0.22$ for ^{93}Nb and $\beta' \approx 0.17$ for ^{208}Pb. So, the convenience of such values for β will have to be tested in the optical model matrix methods.

6.3. Local central term arising from two-body spin-orbit interaction

The spin-orbit potential in (119) is taken to have a zero range. In this case, like for the so-called Skyrme two-body interaction [12] it is shown that a local central term is generated in the HF average field with the following expression :

$$\Gamma^q_{cso}(r) = -W_{LS} \sum_{\ell' j'} \langle \ell' s \rangle \frac{d}{dr} \left[\frac{\rho^{\ell' j'}(r)}{r} + \frac{\rho^{\ell' j' q}(r)}{r} \right] \tag{134}$$

where

$$\langle \ell' s \rangle = \begin{cases} \ell'/2 & \text{for } j' = j'_+ \\ -\dfrac{\ell'+1}{2} & \text{for } j' = j'_- \end{cases}$$

and the partial density distributions :

$$\rho^i(r) = \sum_{n_\beta n_\delta} \frac{2j'+1}{4\pi} \rho^i_{n_\beta n_\delta} \Phi^i_{n_\beta}(r)\, \Phi^i_{n_\delta}(r) \qquad (i = \ell' j' \text{ or } \ell' j' q)$$

The construction of the matrix elements $\langle\alpha|\ \Gamma^q_{cso}\ |\gamma\rangle$ in view of optical model calculations is facilitated by the methods stressed in chapter 4.1.

6.4. Spin-orbit terms

The matrix elements of the above three terms depend on the value of the orbital angular momentum ℓ but not on the total angular momentum j. Other terms, that is the so-called "spin-orbit" ones, can arise from the first two terms in the two-body interaction (119) and depend on both ℓ and j.

6.4.1. Non-local spin-orbit term arising from two-body central interaction

This term can be written in the following radial form :

$$\Gamma^{\ell j q}_{soc}(r,r') = \frac{-\langle \ell s \rangle}{\bar{\ell}} \sum_{ikq'\ell'} \left[\frac{W\delta_{q,q'} - H}{2} \right]_i \hat{k}^2 \begin{pmatrix} \ell & k & \ell' \\ o & o & o \end{pmatrix}^2 (\bar{\ell} + \bar{\ell}' - \bar{k}) v_k^{(i)}(r,r') \mathcal{R}^{q'\ell'}_{so}(r,r';\beta') \tag{135}$$

where

$$\mathcal{R}^{q'\ell'}_{so}(r,r';\beta') = \frac{1}{2\pi} \sum_{n_\beta n_\delta} \left[\rho^{\ell' j'_+ q'} - \rho^{\ell' j'_- q'} \right]_{n_\beta n_\delta} \Phi^{(\beta')}_{n_\beta \ell'}(r')\, \Phi^{(\beta')}_{n_\gamma \ell'}(r) \tag{135'}$$

and

$$\bar{\ell} \equiv \ell\,(\ell+1)$$

The structure of the expression (135) is very analogous to that of the main exchange term (130). Thus the matrix elements $\langle\alpha|\ \Gamma^{\ell j q}_{soc}\ |\gamma\rangle$ needed for optical model matrix methods resemble those given in (132). However, as seen from (135), only high lying ($\ell'j'q'$) HF orbitals contribute in such a term and on the condition ($\ell'j_{\uparrow}q'$) is occupied but not ($\ell'j_{\downarrow}q'$) (spin-non-saturations). Thus this non-local term is generally negligible.

6.4.2. Local spin-orbit term arising from spin-orbit two-body interaction

This term can be expressed as follows :

$$\Gamma^{\ell j q}_{so}(r) = W_{LS} \langle \ell s \rangle \frac{1}{r} \frac{d}{dr} (\rho + \rho^q) \qquad (136)$$

where

$$\rho^q(r) = \sum_{\ell' j'} \rho^{\ell' j' q}(r) \qquad \text{and} \qquad \rho(r) = \sum_q \rho^q(r) \qquad (136')$$

Once again it has been proved very efficient to use the method described in chapter 4.1 to construct the corresponding $\langle\alpha|\ \Gamma^{\ell j,q}_{so}|\gamma\rangle$ matrix elements.

6.5. Density-dependent term

Taking account of exchange effects and of an energy-rearrangement term due to the density dependence of the two-body interaction, the last term in (119) induces a density-dependent contribution Γ_ρ in the HF average field. For neutrons for example, this central and local repulsive contribution is [12] :

$$\Gamma^n_\rho(r) = \frac{3}{2} t_0 \frac{\rho^p(r)\left[\rho(r) + 1/3\rho^n(r)\right]}{\left[\rho(r)\right]^{2/3}} \qquad (137)$$

The matrix elements $\langle\alpha|\ \Gamma_\rho|\gamma\rangle$ of such terms can also be generated according to the method given in chapter 4.1.

All the components of the HF potential described above are shown as a function of r in figures 1 and 2, for the two nuclei ^{208}Pb and ^{93}Nb. The density-matrix elements ρ_{n_β, n_δ} have been generated from self-consistent HF calculations [11] using, respectively, the values $\beta' = 0.175$ fm^{-2} and $\beta' = 0.214$ fm^{-2}, to be compared to the approximation (133). In figures 1 and 2, the non-local terms are represented only in relative values of their diagonal components defined by $r = r'$. It can be seen that such HF potentials, essentially non-local, are difficult to compare to the phenomenological Woods-Saxon form factors. Given the practical possibility to construct matrix elements of folding as well as Hartree-Fock type potentials, we have just stressed the ability of matrix methods to take account, without particular difficulty, of relatively general potentials.

7. SOME TESTS OF THE MATRIX METHOD AND APPLICATIONS

Several practical applications have recently been performed in the frame of the calculable R-matrix theory by a number of authors. Only some of these calculations are given in reference [13]. They are dealing with the application of the method in the case of low-energy scattering between light systems (ex.: $\alpha + \alpha$, $n + {}^{12}C$, $n + {}^{16}O, \cdots$) due to real and generally local Woods-Saxon interactions. Here the usefulness of the method is investigated [3,4] in the spirit of the application of the optical model to a large range of target mass-numbers and over a relatively wide range of incident neutron energy. Besides, essentially folding type potentials, as described above, are intended to be used for evaluation purposes.

For preliminary calculations it appeared that sufficient convergence is more difficult to achieve when the matching radius $R \equiv RMAX$ is large, and therefore in cases of heavy targets. It was found also that the choice of a convenient range of values for the oscillator parameter β is less crucial than that of RMAX. We shall first illustrate the convergence properties in some of such difficult situations.

7.1. Convergence of phase shifts

The matrix methods can easily be tested in comparison with numerical integration ones when folding potential terms are taken to be local. Indeed simple analytical expressions of such terms are available following the result (109). Table II gives comparisons between real or imaginary parts of scattering matrix elements S_ℓ as obtained from conventional and matrix methods applied to neutron scattering from a spherical ^{238}U target. Some incident neutron energies have been chosen within the range 1 MeV - 20 MeV and the results are given for the angular momenta $\ell = o$ to 4. The values of the joining radius RMAX have been taken to be large. The corresponding numbers N of oscillator basis states needed to ensure the stabilization of the phase-shifts indicated are given in parentheses.

Despite large values of RMAX, a reasonable convergence is obtained for $N \leq 18$. The presence of non-locality and spin-orbit terms does not modify this conclusion. It has been found the convergence is generally less easy to achieve in case $\ell = o$ compared to $\ell \neq o$. Figure 3 shows how convergence is obtained as a function of N for the s-wave phase shift, actually $\mathcal{R}e\ S_o$, of the neutron scattering from the targets ^{40}Ca and ^{238}U at 2 MeV and 20 MeV. The simple real folding potential refered to as (a) in Table II has been employed. The convergence results are shown for different values of the oscillator parameter β. It is seen that β values smaller than the "nuclear structure" β' values (133) are preferable to achieve an improved convergence in these "scattering" calculations. When β is chosen within reasonable limits, the same value has been proved to be convenient over a very large energy range.

7.2. Convergence of wave-functions

After having determined the elements S_α, the corresponding wave function $u_\alpha(r) = r\,\Psi_\alpha(r)$ calculated following (9') as a linear combination of the N basis oscillator functions $\Phi_\alpha(r)$, can be compared for $r \leq RMAX$ to its analogous $\chi_\alpha(r)$ from the numerical integration method. Putting into (9') $I_\ell = \frac{1}{r}(F_\ell + i\,G_\ell)$ and $O_\ell = \frac{1}{r}(F_\ell - i\,G_\ell)$, where F_ℓ and G_ℓ are the regular

and irregular Coulomb functions, the commonly adopted asymptotic form $\chi_\alpha(r) \sim F_\ell + C_\alpha (G_\ell + iF_\ell) \to e^{i\delta_\alpha} \sin(kr - \ell \frac{\pi}{2} + \delta_\alpha)$ where $C_\alpha \equiv \frac{1}{2i}(e^{2i\delta_\alpha} - 1) = \frac{1}{2i}(S_\alpha - 1)$, leads to the relation $u_\alpha(r) = 2\chi_\alpha(r)$.

As an illustration, such a comparison is shown in figure 4 (and 5) as regards the $\ell = o$ (and $\ell = 4$) neutron scattering from ^{40}Ca at $E_n = 20$ MeV and in presence of satisfactory convergence onto the phase-shifts. The relative difference $D = \frac{1}{\chi_\alpha}(\chi_\alpha - \frac{u_\alpha}{2})$ is represented as a percentage versus the radial distance r. Apart from the immediate vicinity of zeros of the wave function $\chi_\alpha(r)$ where D is normally large, this difference is seen to be very small. Similar conclusions remain valid in cases of a heavy target such as ^{238}U as illustrated in figures 6 (for $\ell = o$) and 7 (for $\ell = 8$). Thus the matrix methods seem to be able to provide a satisfactory and practical representation of the wave functions in the internal region. However, it is important to notice that this representation becomes rapidly bad as r increases beyond the matching radius.

7.3. Convergence tests for practical calculations

In view of practical applications whose purposes are centred on cross-section evaluations, it seems to be possible to improve the convergence of the present matrix method by choosing the least matching radius RMAX compatible with sufficient accuracy of the calculated physical quantities of interest. The use of some folding type potentials as given by (111) has pointed out that reasonable RMAX values should be $RMAX \approx R_R + 2\mu_R$. As an example, in figure 8 are compared results obtained for different choices of RMAX, β and NMAX, concerning the interaction neutron - ^{93}Nb at relatively low neutron energy. The physical quantities examined are : s and p-wave strength functions (S_0, S_1), elastic scattering radius (R') (all calculated at 10 keV), and elastic scattering ($\sigma_{e\ell}$), reaction (σ_R) and total (σ_T) cross-sections at 10 keV and 1 MeV. For β values of the order of 0.12 fm^{-2} reasonable results are obtained with NMAX = 8 for RMAX = 10 fm (that is $RMAX \approx R_R + 2\mu_R$) as can be verified by comparison to converged results obtained with NMAX = 14 and RMAX = 13 fm. It is seen also that the use of the β-value employed in Hartree-Fock calculations [11] to generate the average potential of ^{93}Nb (that is $\beta' = 0.214$ fm^{-2}, to be compared to (133)) is possible in scattering calculations at the expense of a slightly larger value of NMAX, namely NMAX = 10. From similar calculations performed in the case of a heavy target such as ^{208}Pb, the choice RMAX = 11 fm has been seen to ensure reasonable convergence of analogous physical quantities with NMAX = 9, even with the "Hartree-Fock" value $\beta = 0.175$ (to be compared to (133)). In conclusion, optical model calculations using tentative but realistic folding type potentials suggest that a practical number of basis states not exceeding 10 should be convenient within a wide range of mass-numbers A. Moreover the choice of β values particularly helpful (cf chapter 6) for testing Hartree-Fock type potentials remains probably compatible with practical calculations.

7.4. An example of practical application

In view of describing the interaction n-^{93}Nb, a folding type potential (111) has been determined in the frame of the SPRT method [2] so as to obtain a good overall agreement with measured low-energy physical quantities (S_0, S_1, R') and the energy variation of the experimental total cross-section in the MeV region. For that, practical choices of RMAX, β and NMAX have been made according to the tests described above. Without, for the present time, introducing non-locality but using strengths linearly dependent on energy as usual, the following parameter set (cf 112) has been obtained, with energies in MeV and lengths in fm :

$$\begin{aligned} V_R &= 54.51 - 0.3\,E_n \;, & \mu_R &= 1.882 \;, & r_R &= 1.21 \\ W_D &= 2.118 + 0.3\,E_n \;, & \mu_D &= 1.76 \;, & r_D &= 1.26 \\ V_{so} &= 6.73 \;, & \mu_{so} &= 1.43 \;, & r_{so} &= 1.12 \end{aligned} \qquad (138)$$

This "folding" set can be compared to the "Woods-Saxon" one which has been determined in the same spirit by Ch. Lagrange in ref. [14] :

$$\begin{aligned} V_R &= 49.5 - 0.28\,E_n \;, & a_R &= 0.62 \;, & r_R &= 1.24 \\ W_D &= 3.4 + 0.37\,E_n \;, & a_D &= 0.58 \;, & r_D &= 1.26 \\ V_{so} &= 6.2 \;, & a_{so} &= 0.47 \;, & r_{so} &= 1.12 \end{aligned} \qquad (139)$$

Concerning the comparison between the respective diffusenesses μ and a, compare (116') and (117).

In Table III-a the calculated values of S_0, S_1, R' and σ_T at 0.01, 0.2 and 1 MeV from the potential (138) can be compared to the corresponding experimental (or recommended) values. The calculated total cross section over the energy range 10 keV - 3 MeV is compared to experimental values [15] in figure 9. The fit obtained in this low energy region is quite analogous to that resulting from the Woods-Saxon potential (139). The values calculated in this case for S_0, S_1 and R' are respectively 0.433, 5.26 and 6.63. Thus the folding type potential (111), when considered as a local phenomenological one, seems to be able to reproduce experimental data with results comparable to those of conventional Woods-Saxon potentials, but not significantly better. The suitability of some non-locality remains an open problem which the matrix methods are particularly convenient for. For example, it is not yet clear if the introduction of non-locality is able to replace the energy dependence of parametrizations such as (138) or (139) when an overall agreement is searched for with a maximum of nuclear data of a given nucleus as required by locally adapted parametrizations.

As suggested from the application of the SPRT method in case of this target ^{93}Nb [14], a comparison between calculated and experimental elastic scattering angular distributions is of interest. In figure 10 such a comparison is shown at 8.05 MeV between calculations from the folding potential (138) and measurements from ref. [16]. A good, but perhaps fortuitous, agreement is obtained. It is worth-while to notice that at such an energy only shape-elastic scattering is expected to occur.

7.5. On some other advantages of the matrix methods

Apart from the convergence properties described above, we summarize here some advantages of these methods :

a/ Change of parameters

In the folding-potential formulation we have already noticed that the geometry parameters are concentrated only in a limited number of the factors

$\mathcal{M}_k$ (58'). The non-locality ranges Δ appear also only in separated factors. Concerning changes of multiplicative factors in front of different terms of the matrix A given by (8) or (8'), this formalism appears to be advantageous because the corresponding partial matrices can be constructed once for all. This property concerns changes of potential strengths such as V_R, W_V, W_D, W_G or V_{so} but also of the energy E. So, given a parameter set, matrix methods are particularly adapted to the exploration of a large number of energies. At each energy the A matrix is simply rebuilt as a new linear combination of two unchanged matrices and then inverted.

b/ Calculation of sensitivities

The derivatives of the physical quantities with respect to any parameter p (ex.: energy, potential parameters) of the model are simple functions of the corresponding derivatives of the $\mathcal{R}_\alpha$ matrix elements. Following (15) and the definition $\mathcal{R}_\alpha \equiv \mathcal{R}_\alpha$ (R;E), this derivative can be written as :

$$\frac{d\mathcal{R}_\alpha}{dp} = -\frac{\hbar^2 R}{2m} \tilde{\Phi}_\ell(R).\ (A^{-1}\frac{dA}{dp}A^{-1}).\ \Phi_\ell(R) \qquad (140)$$

This expression involves the replacement of A^{-1} in $\mathcal{R}_\alpha$ by the product $-A^{-1}.\frac{dA}{dp}.A^{-1}$. The matrix $\frac{dA}{dp}$ is automatically known when the derivative is taken with respect to any multiplicative parameter of different terms of A (that is p = E, V_R, W_D,...). On the contrary $\frac{dA}{dp}$ is to be constructed when p is a geometry parameter (μ,R) or the non-locality range Δ by derivating the only factors which contain these parameters. In particular, very simple expressions can be obtained for the derivatives with respect to μ or R of the "square-density" coefficients $\mathcal{M}_k$ given by (75) and (76).

Given a set of sensitivities calculated in a single computer run, fitting limitations or improvements can generally be easily inferred from simple examination. As illustrative results, a number of so calculated sensitivities are shown in Table III for various physical quantities associated to the interaction n-^{93}Nb. These quantities are those described in Chapter 7.3 and calculated from the folding potential (138). The examination of such results is very instructive on how to progress or not towards a better overall agreement. Another example is given in Table IV concerning the sensitivities of the elastic scattering angular distributions n + ^{208}Pb at 14.6 MeV to the parameters of two folding non-local optical potentials whose results are compared in figure 11 to experimental data. These potentials referred to as (1) and (2) have the following parameters :

$$\begin{array}{lllll} V_R = 69.66 & \mu_R = 1.624 & r_R = 1.235 & & \\ W_D = 6 & \mu_D = 1.624 & r_R = 1.235 & & (141) \\ V_{so} = 8.55 & \mu_{so} = 1.624 & r_R = 1.235 & \Delta_{so} = o & \end{array}$$

and (1) $\Delta_R = \Delta_D = 0.947$

(2) $\Delta_R = \Delta_D = 0.85$

The version (1) above has been adjusted onto the neutron bound state energies and root mean square radius obtained from Hartree-Fock calculations [11] for the nucleus ^{208}Pb. In this sense it can be considered as an "equivalent" Hartree-Fock potential. It is seen in Figure 11 that such a potential gives an improved agreement when the non-locality ranges are decreased by about 10%. Tables such as III-b and IV show clearly the angular and non-locality dependences of most of the calculated sensitivities.

c) Extension to deformed nuclei

Deformed potentials can be generated for example by introducing non-spherical density functions $\rho(\vec{r}_1)$ in the folding form factor (42). The methods described in Chapter 5 for spherical nuclei can easily be extended for calculating the matrix elements of such deformed potentials even in the presence of non-locality. However, the existence of deformation terms coupling the collective states of the target which are explicitly taken into account increases notably the order of the matrices A to be inverted, cf (8) and (13). Problems related to such a difficulty are dealt with elsewhere in this Course [17] in the general frame of the R-matrix methods applied to inelastic scattering from light nuclei. Concerning the treatment of deformed optical potentials even in case of heavy targets, the practical applicability of such matrix methods remains an open problem to be investigated for evaluation purposes.

REFERENCES

[1] PEREY, F.G., BUCK, B., Nucl. Phys. 32 (1962) 353
PEREY, F.G., ORNL-3429 (1963)

[2] DELAROCHE, J.P., LAGRANGE, Ch., SALVY, J. Nuclear Theory in Neutron Nuclear Data Evaluation, Trieste (Dec.75), IAEA-190 Vol.I, p.251 Vienna (1976).

[3] SALVY, J., BONNET, M., Proc. of the National Soviet Conference, Kiev (1975), Vol.3 p.79.

[4] DUFOUR, J.M., SALVY, J., Symposium on Nucleon Interactions with Nuclei, Gaussig (Nov.1977).

[5] TOBOCMAN, W., NAGARAJAN, M.A., Phys. Rev. 138 (1965) B1351.
GARSIDE, L., TOBOCMAN, W., Phys. Rev. 173 (1968) 1047 ; Ann. of Phys. 53 (1969) 115.

[6] LANE, A.M., ROBSON, D., Phys. Rev. 151 (1966) 774 ; 178 (1969) 1715 ; 185 (1969) 1403.

[7] BLOCH, C., Nucl. Phys. 4 (1957) 503.

[8] LANE, A.M., THOMAS, R.G., Rev. Mod. Phys. 30 (1958) 257.

[9] GOGNY, D., Nucl. Phys. A237 (1975) 399.

[10] GOGNY, D., In Proc. of the Int. Conf. on Nuclear Self-consistent Fields, I.C.T.P. Trieste, Fev. 1975 (G. RIPKA, M. PORNEUF Eds), IAEA (1975).

[11] GOGNY, D., DECHARGE, J., Private communication, and to be published.

[12] VAUTHERIN, D., BRINK, D.M., Phys. Rev. C5 (1972) 626.
QUENTIN, Ph., Thesis (Fac. Orsay, 1975).

[13] CHATWIN, R.A., PURCELL, J.E., J. Math Phys. 12 (1971) 2024.
PURCELL, J.E., Phys. Rev. 185 (1969) 1279.
AYAD, A.A., ROWE D.J., Nucl. Phys. A218 (1974) 307.
PHILPOTT, R.J., GEORGE, J., Nucl. Phys. A233 (1974) 164.
PHILPOTT, R.J., Nucl. Phys. A266 (1976) 109.

[14] LAGRANGE, Ch., Proc. of the Soviet Nat. Conf. on Neutron Phys., Kiev (1975) Vol.3, p.65.

[15] UTTLEY, C.A., et al., Nuclear Data for Reactors, IAEA (1967) Vol.1, p.165.

[16] HOLMQVIST, B., WIEDLING, T., Report AE-430 (1971).

[17] AHMAD, S.S., The iterative R-matrix method for the accurate calculation of nuclear reaction cross sections, this Course.

μ_1,μ_2	W	B	H	M
0.7	-402.4	-100	-496.2	-23.56
1.2	-21.30	-11.77	37.27	-68.81
$\alpha=1/3$ $x_o=1$ $W_{LS}=115$ MeV-fm^5 $t_o=1350$ MeV-fm^6				

TABLE I - Parameters of the D1 interaction
(Units : MeV and fm)

ENERGY (MeV)		1.2 (a)	2 (b)		2 (c)	12 (a)	20 (a)
PHASE-SHIFTS		Re S_ℓ	Re S_ℓ	Im S_ℓ	Re S_ℓ	Re S_ℓ	Re S_ℓ
CONVENTIONAL METHOD (RMAX= 15 fm)	1 = 0	- 0.2569	0.5570	0.4073		- 0.1690	0.9986
	1 = 1	0.7441	- 0.2107	0.1424		- 0.0302	0.9728
	1 = 2	0.7946	0.1723	- 0.7357		0.2603	0.9347
	1 = 3	- 0.9418	0.5398	- 0.3828		0.7707	0.7371
	1 = 4	0.999998	0.9445	- 0.0292		0.9623	0.4119
MATRIX METHOD	1 = 0	- 0.2568 (14)	0.5571 (17)	0.4073 (17)	-0.7934 (18)	- 0.1688 (17)	0.9986 (18)
	1 = 1	0.744 (14)	- 0.2107 (16)	0.1424 (16)	-0.99919(16)	- 0.0300 (16)	0.9728 (18)
	1 = 2	0.794 (12)	0.1723 (15)	- 0.7357 (15)	-0.90418(17)	0.2604 (16)	0.9347 (17)
	1 = 3	- 0.9417 (18)	0.5396 (15)	- 0.3829 (16)	0.96708(16)	0.7708 (15)	0.7371 (17)
	1 = 4	0.999998(11)	0.9444 (14)	- 0.0294 (15)	0.9639 (16)	0.9623 (17)	0.4118 (16)
	Rmax (fm)	15	18	18	18	18	18

(a) Real folding potential with the parameters r_R= 1.374fm, μ_R= 1.5fm, V_R= 41.1MeV and Δ_R= 0

(b) Potential (a) + the gaussian imaginary term $-8i \exp\left[-(r-8.515)^2/\ 1.5^2\right]$ MeV

(c) Potential (a) but with Δ_R= 0.9fm

TABLE II - Comparison between scattering phase-shifts from matrix and conventional methods (case n+^{238}U). In parentheses are the values of the number of basis states N for which the given phase-shifts are converged, with the choice β = 0.123 fm^{-2}.

(a)

	$S_0\times10^4$	$S_1\times10^4$	R'	σ_T(0.01)	σ_T(0.2)	σ_T(1)
exp.val	0.36±0.06 (a)	5.16±0.24 (a)	7.±0.2 (a)	7800 (b)	9430 (b)	6500 (b)
calc.val	0.39	5.01	6.82	8377	9064	6483
d/dE	-0.29	9.09	-4.74	-48201	2073	-3005
d/dV_R	-0.019	1.645	-0.159	-66.61	992.7	599.7
d/dR_R	-0.328	30.6	-2.2	532	21127	12367
$d/d\mu_R$	0.222	3.635	0.67	2724	4107	1673
d/dW_D	0.175	1.097	-0.028	881.2	167	-136.1
d/dR_D	0.008	1.765	0.016	370	474.7	19.63
$d/d\mu_D$	0.214	2.347	0.004	1320	674.9	33.26
d/dV_{so}	0.	0.075	$0.3\ 10^{-4}$	13.18	46.49	23.42
d/dR_{so}	0.	0.081	$0.3\ 10^{-4}$	14.33	58.59	37.44
$d/d\mu_{so}$	0.	0.220	$0.9\ 10^{-4}$	38.81	137.3	35.95

(a) BNL-325,vol.I (1973) - (b) BNL-325,suppl.n°2,vol.IIB (1966)

(b)

θ_{CM}(deg)	1	45	90	135	179
$\sigma(\theta)$mbarn/sr	4581	25.42	17.05	23.44	36.88
d/dE	711.9	7.946	-8.012	-4.319	9.356
d/dV_R	-73.02	0.463	-1.453	0.468	4.171
d/dR_R	1082	42.93	-32.58	10.20	114.5
$d/d\mu_R$	1167	38.29	-6.519	-7.245	17.33
d/dW_D	-40.74	-14.92	-7.254	-6.975	-19.17
d/dR_D	636.5	-27.53	-12.80	-6.321	-15.99
$d/d\mu_D$	709.5	-41.19	-31.37	-26.32	-45.13
d/dV_{so}	-31.83	1.259	-0.433	-3.144	-13.07
d/dR_{so}	-127.1	2.151	1.349	-0.241	-2.225
$d/d\mu_{so}$	93.91	-3.320	-1.289	-0.156	-1.963

TABLE III - Values of some physical quantities of n + ^{93}Nb interaction and their sensitivities to the parameters of the folding optical potential (138). (units : mbarn, MeV, fm).

θ_{CM} (deg)		1	15	25	55	65	80	105	140	179
$\sigma(\theta)_{mbarn/Sr}$	1	16799	5613	391.1	75.13	51.53	75.67	43.79	18.96	23.70
	2	14627	4107	131.9	59.23	96.93	60.15	47.14	18.95	28.81
d/dV_R	1	-190.4	-169	-35.44	-3.075	5.575	-0.686	1.750	0.228	2.375
	2	-274.2	-204.3	-26.82	1.371	8.245	-1.254	1.195	0.348	2.036
d/dR_R	1	3373	-1974	-600.3	-82.61	121.1	-10.6	69.02	7.833	101.1
	2	1806	-2948	-431.7	48.89	182.5	-34.0	43.06	4.990	91.39
$d/d\mu_R$	1	2840	15.06	-36.36	-45.70	23.90	-33.85	-0.084	25.34	15.54
	2	2195	-104.9	94.02	23.14	19.98	-36.80	-17.48	24.09	-16.54
$d/d\Delta_R$	1	18067	13700	2788	249.6	-412.7	88.73	-90.49	-10.22	-104.4
	2	24427	15276	1976	-74.28	-569.3	115.8	-45.66	-20.41	-48.91
d/dW_D	1	-19.29	-114.5	-57.28	-16.13	-5.992	-112.2	-6.893	-3.302	-5.296
	2	-0.034	-18.16	-31.80	-16.40	-6.933	-12.23	-8.908	-4.297	-5.758
d/dR_D	1	1308	-102.5	-213.9	-50.22	-3.810	-20.89	-9.314	-8.082	-16.80
	2	1607	113.1	-115.4	-54.43	-6.202	-30.16	-13.92	-13.16	-17.19
$d/d\mu_D$	1	1824	-300.8	-324.4	-99.13	-20.48	-60.11	-29.01	-18.90	-38.48
	2	2180	96.39	-162.4	-88.38	-31.34	-67.35	-39.53	-24.77	-38.97
$d/d\Delta_D$	1	280.7	511.4	225.6	70.16	30.64	53.77	33.70	15.65	22.63
	2	229.6	67.55	109.6	63.08	35.22	51.72	39.99	17.18	23.19
d/dV_{so}	1	-2.056	-11.03	-5.180	0.497	2.762	-0.330	-0.750	-0.926	-12.26
	2	-110.8	-26.92	-2.457	0.832	1.873	-0.153	-1.031	-0.372	-17.89
d/dR_{so}	1	10.94	5.576	-21.61	-1.055	2.438	4.073	5.164	-5.004	-40.98
	2	-16.96	-31.60	-22.84	-3.520	5.948	1.409	4.166	-2.989	-41.48
$d/d\mu_{so}$	1	460.8	67.53	-31.73	-8.900	8.523	-4.039	3.790	2.270	-24.68
	2	423.9	13.03	-12.49	-0.788	8.196	-5.509	-0.228	5.739	-19.30

TABLE IV - Values of differential elastic scattering cross sections for n + ^{208}Pb at 14.6 MeV (cf fig.11) and their calculated sensitivities to the parameters of the folding non-local optical potentials (140), 1 and 2. (units : mbarn, MeV, fm).

FIGURE CAPTIONS

Fig. 1 . Different terms of the Hartree-Fock neutron potential in ^{208}Pb as a function of the radial distance r. The different terms are described in chapter 6.

Fig. 2 . Different terms of the Hartree-Fock neutron potential in ^{93}Nb as a function of the radial distance r. The different terms are described in chapter 6.

Fig. 3 . Real part of the "s" wave elastic scattering matrix element S_o. The convergence is shown versus the number N of basis oscillator functions, for different values of the oscillator parameter β (in fm^{-2}). Calculations are shown at 2 MeV and 20 MeV for ^{40}Ca and ^{238}U. For both of them a spherical shape is assumed. RMAX (R_N) is the matching (nuclear) radius, in fermi. Results of numerical integration are also indicated (dashed lines). The folding potential is that refered to as (a) in Table II.

Fig. 4 . Relative difference (upper part) in percentage between the numerical wave-function (lower part) and the matrix method one for the ℓ = o scattering n + ^{40}Ca (RMAX = 10 fm and potential (a) from Table II).

Fig. 5 . Relative difference in percentage between the numerical wave-function (dashed curve and right scale) and the matrix method one for the "ℓ = 4" scattering n + ^{40}Ca (RMAX = 10 fm and potential (a) from Table II).

Fig. 6 . Relative difference in percentage between the scattering "s" wave-functions from numerical (dashed curve and right scale) and matrix methods for n + ^{238}U. (RMAX = 18 fm and folding potential (a) from Table II).

Fig. 7 . Relative difference in percentage (upper part) between the "ℓ = 8" wave-functions from numerical (lower part) and matrix methods for n + ^{238}U. (RMAX = 18 fm and folding potential (a) from Table II).

Fig. 8 . Convergence properties of some calculated quantities for n + ^{93}Nb interaction as a function of the number NMAX of basis states and for different choices of RMAX and β. Units are barn for the total (σ_T), shape elastic ($\sigma_{e\ell}$) and reaction (σ_R) cross sections, and fermi for the potential scattering radius (R'). S_o et S_1 are the s and p-wave strength functions calculated at 10 keV.

Fig. 9 . Adjustment theory-experiment [15] for the neutron total cross-section of ^{93}Nb (calculations are from the folding potential (138)).

Fig. 10 . Comparison theory-experiment [16] for neutron differential elastic scattering from ^{93}Nb at 8.05 MeV. Calculated values are from the folding optical potential (138).

Fig. 11 . Neutron elastic scattering from ^{208}Pb at 14.6 MeV : comparison between experimental data and calculations using the folding non local optical potentials (141), 1 and 2. Corresponding sensitivities to the parameters are given in Table IV at the nine angles indicated.

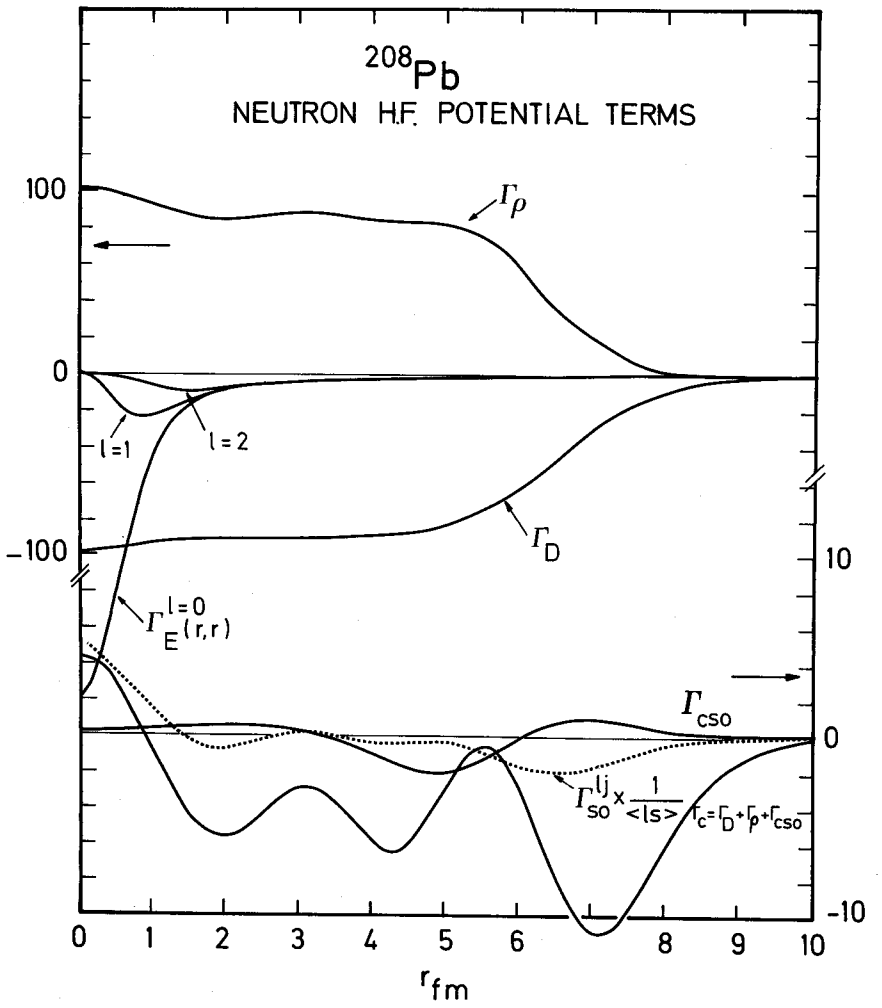

Fig. 1 . Different terms of the Hartree-Fock neutron potential in ^{208}Pb as a function of the radial distance r. The different terms are described in chapter 6.

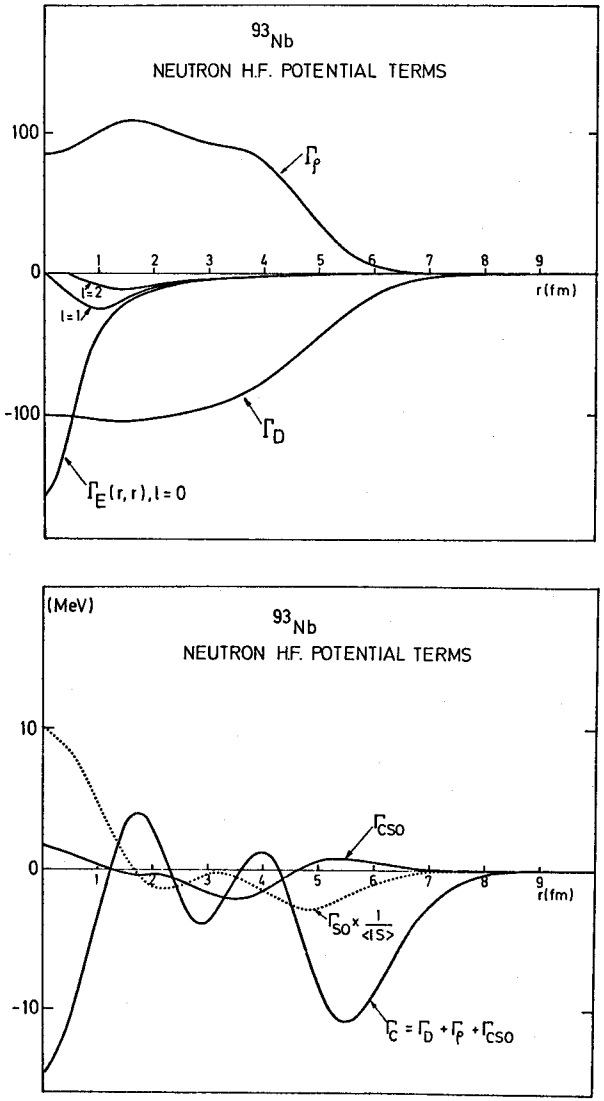

Fig. 2 . Different terms of the Hartree-Fock neutron potential in ^{93}Nb as a function of the radial distance r. The different terms are described in chapter 6.

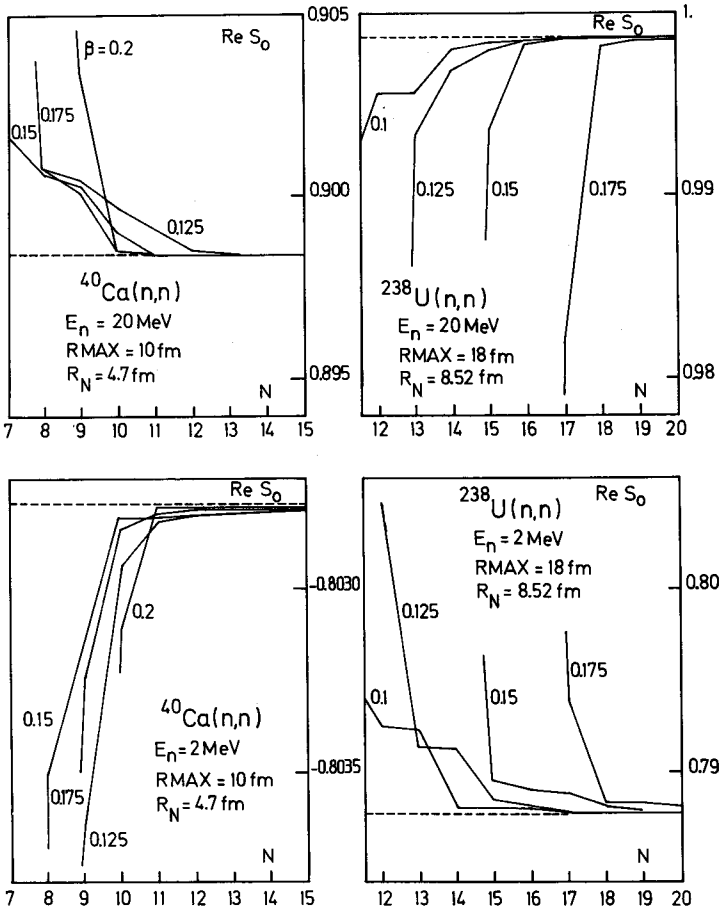

Fig. 3 . Real part of the "s" wave elastic scattering matrix element S_o. The convergence is shown versus the number N of basis oscillator functions, for different values of the oscillator parameter β (in fm^{-2}). Calculations are shown at 2 MeV and 20 MeV for ^{40}Ca and ^{238}U. For both of them a spherical shape is assumed. RMAX (R_N) is the matching (nuclear) radius, in fermi. Results of numerical integration are also indicated (dashed lines). The folding potential is that refered to as (a) in Table II.

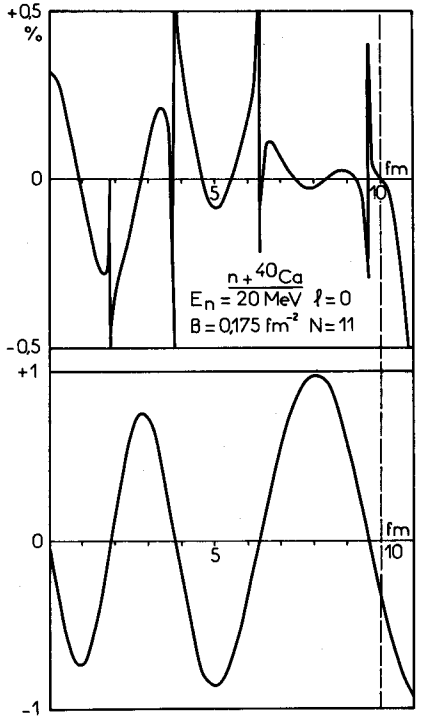

Fig. 4 . Relative difference (upper part) in percentage between the numerical wave-function (lower part) and the matrix method one for the ℓ = o scattering n + ^{40}Ca (RMAX = 10 fm and potential (a) from Table II).

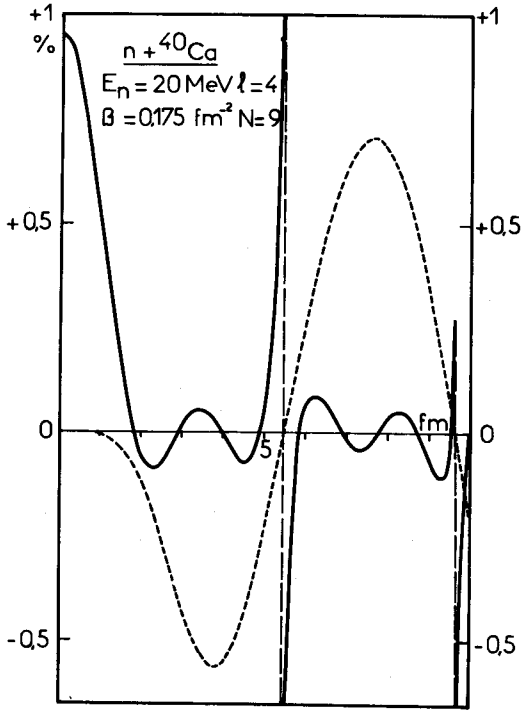

Fig. 5 . Relative difference in percentage between the numerical wave-function (dashed curve and right scale) and the matrix method one for the "ℓ = 4" scattering n + ^{40}Ca (RMAX = 10 fm and potential (a) from Table II).

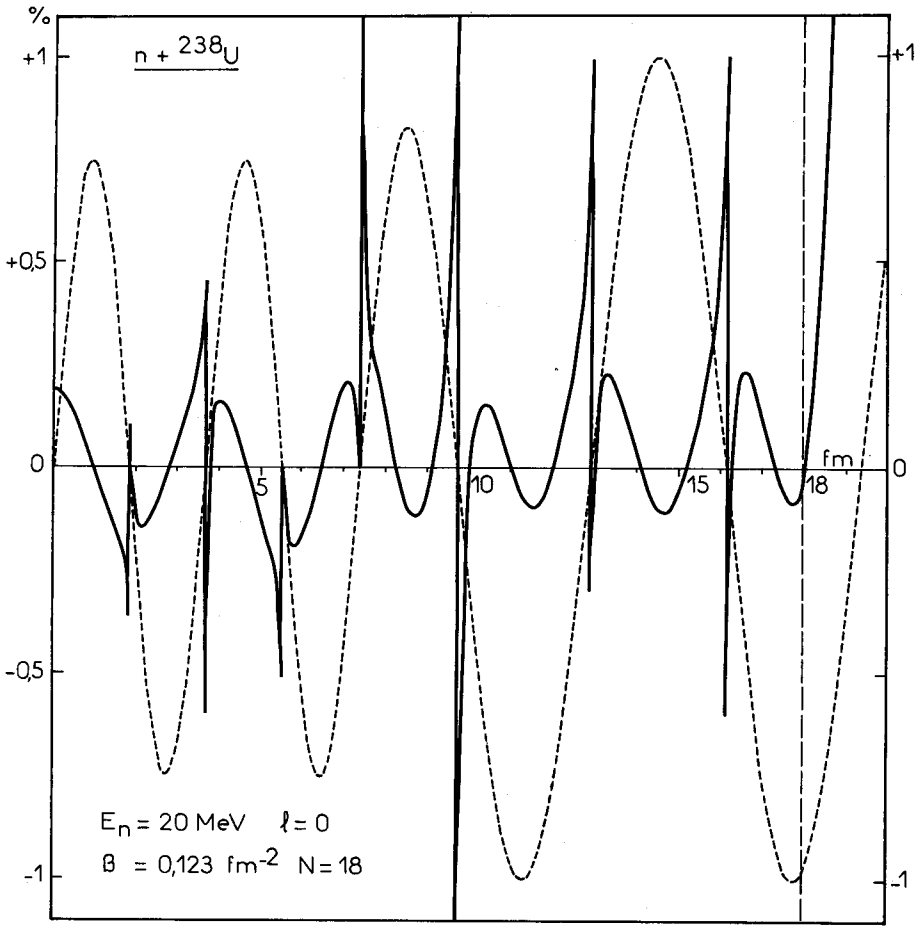

Fig. 6 . Relative difference in percentage between the scattering "s" wave-functions from numerical (dashed curve and right scale) and matrix methods for n + ^{238}U. (RMAX = 18 fm and folding potential (a) from Table II).

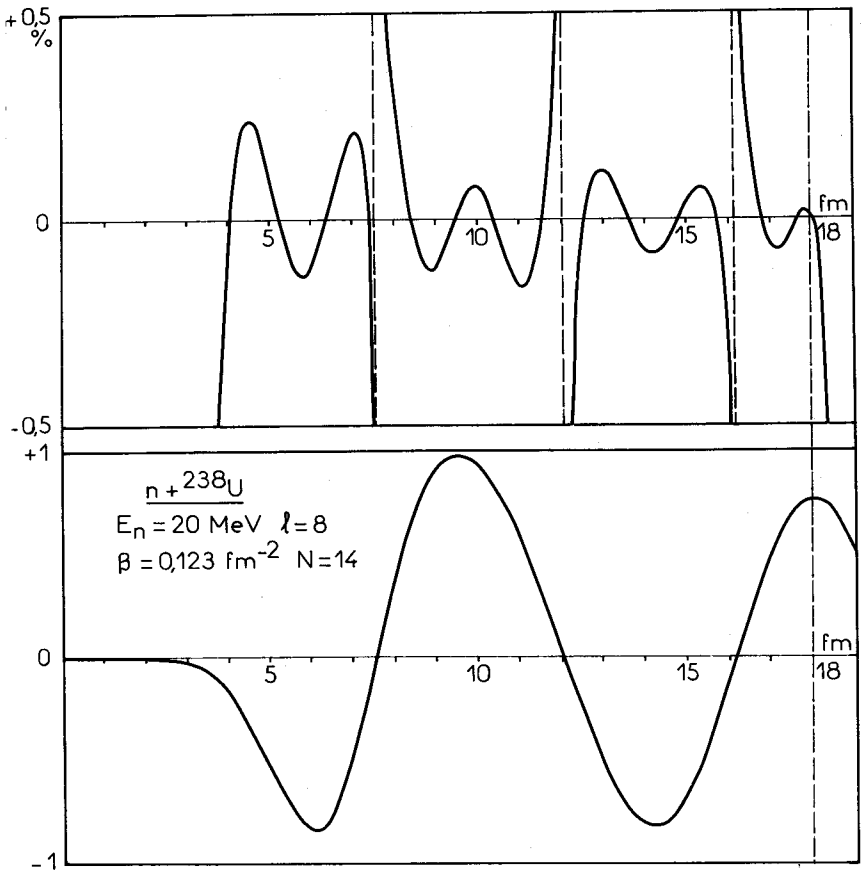

Fig. 7 . Relative difference in percentage (upper part) between the "ℓ = 8" wave-functions from numerical (lower part) and matrix methods for n + ^{238}U. (RMAX = 18 fm and folding potential (a) from Table II).

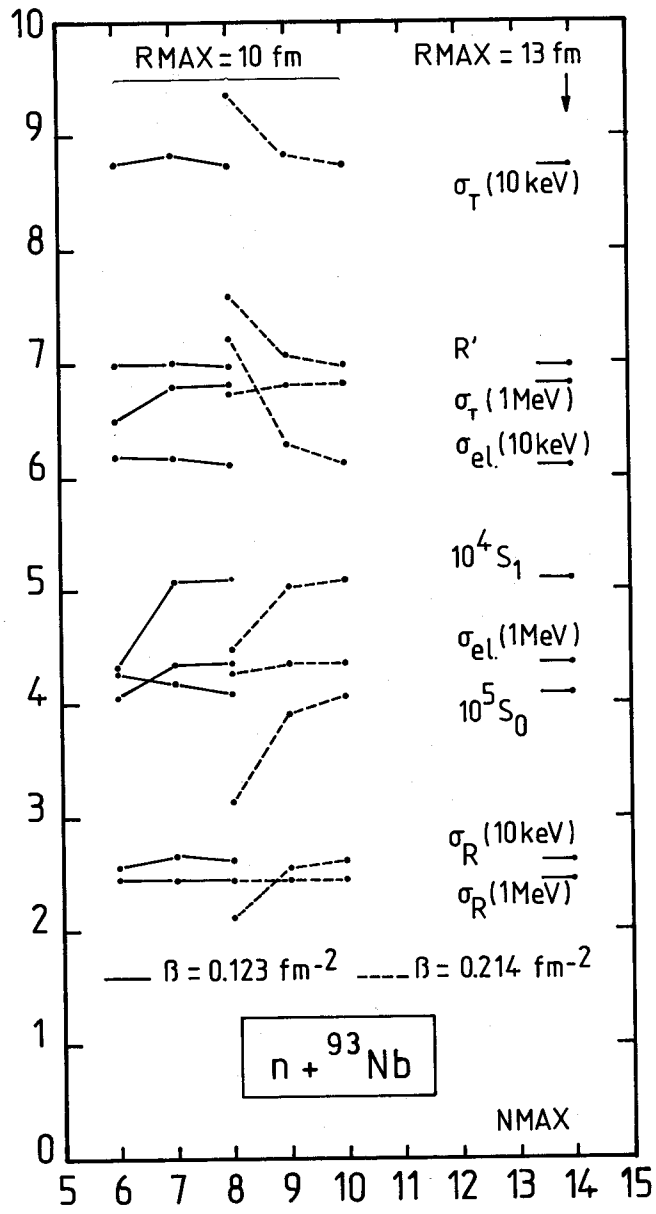

Fig. 8 . Convergence properties of some calculated quantities for n + ^{93}Nb interaction as a function of the number NMAX of basis states and for different choices of RMAX and β. Units are barn for the total (σ_T), shape-elastic (σ_{el}) and reaction (σ_R) cross sections, and fermi for the potential scattering radius (R'). S_0 et S_1 are the s and p-wave strength functions calculated at 10 keV.

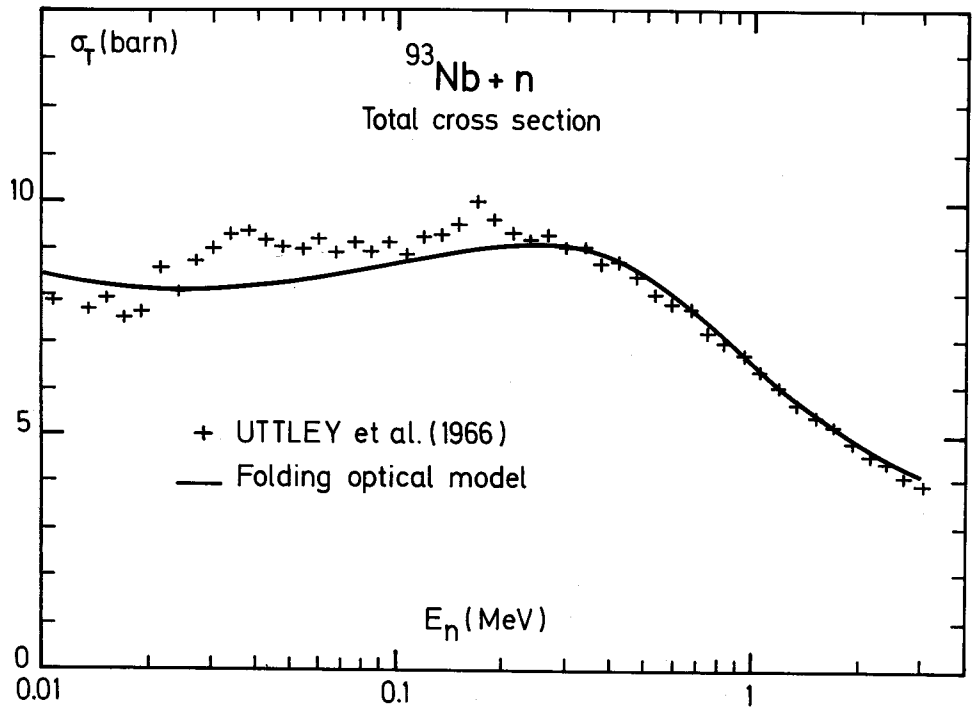

Fig. 9 . Adjustment theory-experiment [15] for the neutron total cross-section of ^{93}Nb (calculations are from the folding potential (138)).

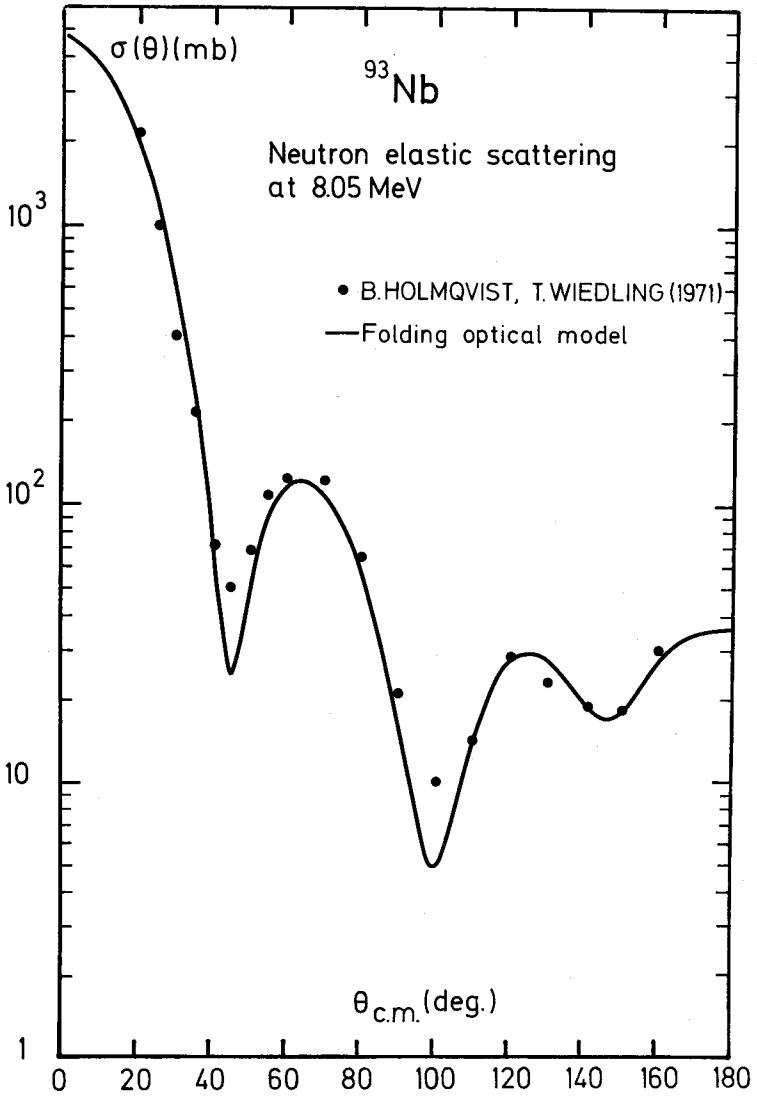

Fig. 10 . Comparison theory-experiment [16] for neutron differential elastic scattering from ^{93}Nb at 8.05 MeV. Calculated values are from the folding optical potential (138).

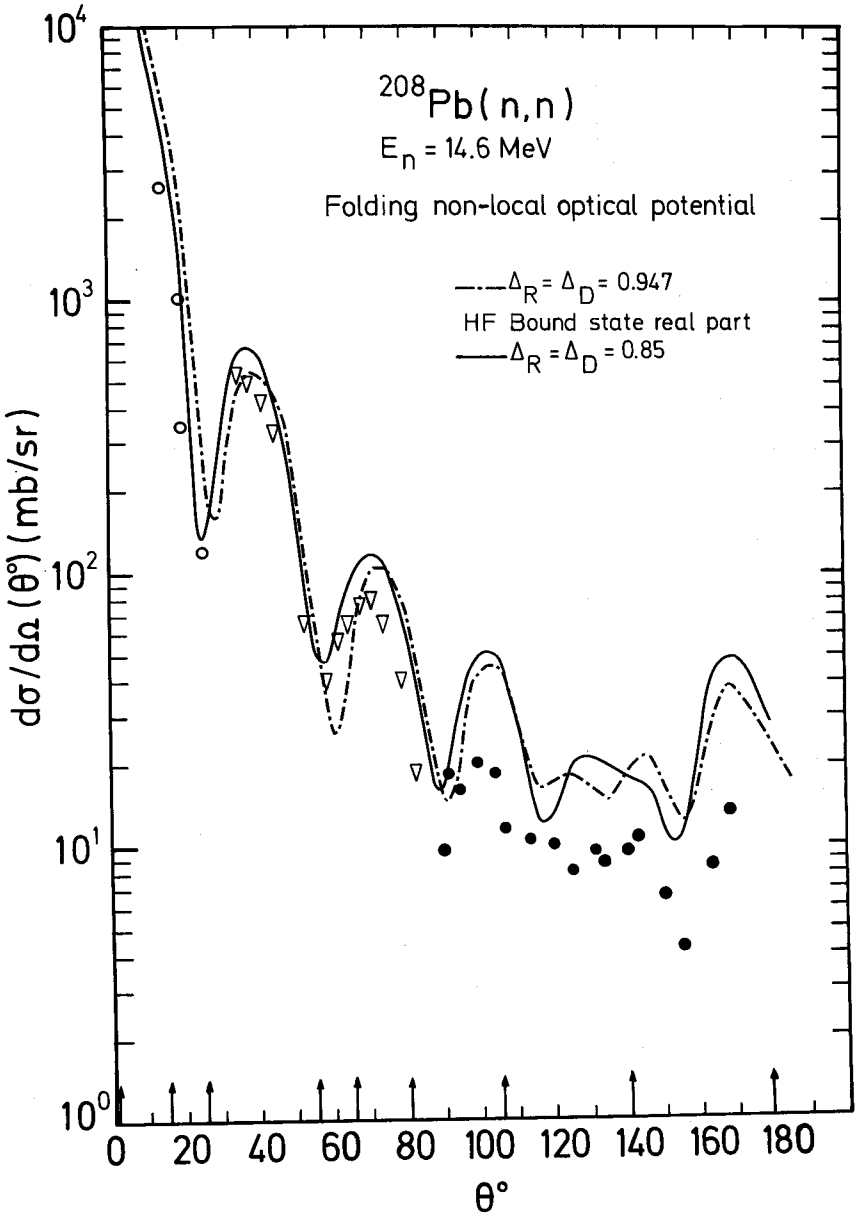

Fig. 11 . Neutron elastic scattering from ^{208}Pb at 14.6 MeV : comparison between experimental data and calculations using the folding non-local optical potentials (141), 1 and 2. Corresponding sensitivities to the parameters are given in Table IV at the nine angles indicated.

APPENDIX 1

- FORMULAS FOR LIMITED INTEGRATION DOMAINS -

1/ Calculation of $C_n(\Delta)$ when $o \leq |\vec{u}| \leq \sqrt{2}$ RMAX

In this case the integral (54) is limited to $x \leq 2\beta.RMAX^2$. Using the expansion :

$$L_n^{\alpha}(x) = \sum_{m=o}^{n} \left[(-)^m \binom{n+\alpha}{n-m} \frac{1}{m!}\right] x^m \qquad (\alpha > -1) \qquad \text{(A1-1)}$$

and the definition of the incomplete γ function :

$$\gamma(a,x) \equiv \int_o^x e^{-t}\, t^{a-1}\, dt \qquad \text{(A1-2)}$$

the result for $C_n(\Delta)$ can be written as :

$$C_n(\Delta) = \frac{\beta^{3/4}}{2\pi\left(\frac{\beta\Delta^2}{4}\right)^{3/2}} \left[\Gamma(n).\Gamma(n+\tfrac{1}{2})\right]^{1/2} \sum_{q=o}^{n-1} \frac{(-2)^q}{q!} \frac{\gamma\left[q+\frac{3}{2}, \beta RMAX^2\left(1+\frac{4}{\beta\Delta^2}\right)\right]}{\Gamma(n-q).\Gamma(q+\frac{3}{2})} \left(\frac{\beta\frac{\Delta^2}{4}}{1+\frac{\beta\Delta^2}{4}}\right)^{q+\frac{3}{2}} \qquad \text{(A1-3)}$$

In case when $\Delta = o$, this expression has the limit value $C_n(o)$ given by (55).

2/ Calculation of $C_N(v)$ when $o \leq |\vec{R}| \leq \sqrt{2}.RMAX$

By putting $x = \beta R^2$, and expanding the two Laguerre polynomials of (59) according to (A1-1), the first integral in (59) becomes :

$$\frac{1}{2\beta^{3/2}} \int_o^{2\beta RMAX^2} x^{1/2}\, e^{-\frac{x}{2}}\, L_{k-1}^{1/2}\left(\frac{\alpha}{2\beta}x\right) L_{N-1}^{1/2}(x)\, dx \qquad \text{(A1-4)}$$

$$= \frac{1}{2\beta^{3/2}} \sum_{q=o}^{k-1} \frac{(-1)^q}{q!} \binom{k-1/2}{k-1-q} \left(\frac{\alpha}{2\beta}\right)^q \sum_{t=o}^{N-1} \frac{(-1)^t}{t!} \binom{N-1/2}{N-t-1} \int_o^{2\beta RMAX^2} x^{q+t+1/2}\, e^{-\frac{x}{2}}\, dx$$

Using (A1-2), $C_N(\nu)$ takes the general form :

$$C_N(\nu)=(-)^{N-1}C \sum_{k=1}^{\infty} \mathcal{M}_k \sum_{q=o}^{k-1} \frac{(-)^q}{q!}\binom{k-1/2}{k-q-1}\left(\frac{\alpha}{\beta}\right)^q \sum_{t=o}^{N-1} \frac{(-2)^t}{t!}\binom{N-1/2}{N-t-1}.\gamma\left[q+t+\tfrac{3}{2},\beta RMAX^2\right] \qquad (A1\text{-}5)$$

where C is the factor (61) and, even for $\alpha=\beta$, the sum over k has practically to be limited.

Following (60), in the case of the real term, $\mathcal{G}_{N,k}$ has to be replaced by :

$$\mathcal{G}_{N,k}=(-)^{N-1} \sum_{q=o}^{k-1} \frac{(-1)^q}{q!}\binom{k-1/2}{k-q-1}\left(\frac{\alpha}{\beta}\right)^q \sum_{t=o}^{N-1} \frac{(-2)^t}{t!}\binom{N-1/2}{N-t-1}.\gamma\left[q+t+\tfrac{3}{2},\beta RMAX^2\right] \qquad (A1\text{-}6)$$

Concerning the spin-orbit matrix element, $\mathcal{G}_{N,t}$ in (84) has to be calculated following (A1-5).

APPENDIX 2

- CALCULATION OF SOME INTEGRALS INVOLVING LAGUERRE POLYNOMIALS -

Let us define the following integrals (with $N \geqslant 1$ and $n \geqslant 2$) :

$$I^L_{N,n} \equiv \int_o^{\infty} e^{-x}\, x^{L+1}\, L^{L+1/2}_{N-1}(2x)\, L^{L+3/2}_{n-2}(x)\, dx \qquad (A2\text{-}1)$$

$$= -\int_o^{\infty} e^{-x}\, x^{L+1}\, L^{L+1/2}_{N-1}(2x)\, \frac{d}{dx} L^{L+1/2}_{n-1}(x)\, dx \qquad (A2\text{-}2)$$

$$J^L_{N,n} = \int_o^{\infty} e^{-x}\, x^{L+1}\, L^{L+1/2}_{N-1}(2x).L^{L+1/2}_{n-2}(x)\, dx \qquad (A2\text{-}3)$$

$$K^L_{N,n} = \int_o^{\infty} e^{-x}\, x^{L}\, L^{L+1/2}_{N-1}(2x)\, L^{L+1/2}_{n-2}(x)\, dx \qquad (A2\text{-}4)$$

a) By expanding $x\, L^{L+3/2}_{n-2}(x)$ in (A2-1) according to the relation :

$$-z\, L^{\alpha+1}_{k-1}(z) = k\, L^{\alpha}_{k}(z) - (k+\alpha)\, L^{\alpha}_{k-1}(z) \qquad (A2\text{-}5)$$

one obtains an expression of I in terms of K :

$$I^L_{N,n} = (L+n-\tfrac{1}{2})\, K^L_{N,n} - (n-1)\, K^L_{N,n+1} \qquad (A2\text{-}6)$$

b) The relation $L^{\alpha+1}_k(x) = L^{\alpha+1}_{k-1}(x) + L^{\alpha}_k(x)$ applied to $L^{L+3/2}_{n-2}(x)$ in (A2-1) leads to :

$$I^L_{N,n} = I^L_{N,n-1} + J^L_{N,n} \qquad (A2\text{-}7)$$

c) Performing the integration by parts (A2-2) and applying (A2-5) to $2x.L^{L+3/2}_{N-2}(2x)$ give the relation :

$$I^L_{N,n} = (L+N)\, K^L_{N,n+1} - (L+N-\tfrac{1}{2})\, K^L_{N-1,n+1} - J^L_{N,n+1}$$

which, changing n into n-1, and using (A2-7) leads to :

$$I^L_{N,n} = (L+N)\, K^L_{N,n} - (L+N-\tfrac{1}{2})\, K^L_{N-1,n} \qquad (A2\text{-}8)$$

The relations (A2-6) or (A2-8) permit to calculate the integrals I from the knowledge of **only the** integrals K. From comparison of these two relations, the following recurrence property is obtained for the integrals K :

$$(n-1)\, K^L_{N,n+1} = (n-N-\tfrac{1}{2})\, K^L_{N,n} + (L+N-\tfrac{1}{2})\, K^L_{N-1,n} \qquad (A2\text{-}9)$$

Together with (A2-9) the values of $K^L_{1,n}$ and $K^L_{N,2}$ have to be evaluated in order to start the recurrence. Making use of the general result :

$$\int_o^{\infty} e^{-x}\, x^{\gamma-1}\, L^{\mu}_n(x)\, dx = (-)\frac{\Gamma(\gamma)\Gamma(\gamma-\mu)}{n!\,\Gamma(\gamma-\mu-n)} \qquad (A2\text{-}10)$$

and $\Gamma(\frac{1}{2}-n) = \frac{(-)^n.\pi}{\Gamma(n+1/2)}$, one simply obtains for $K^L_{1,n}$:

$$K^L_{1,n} = \frac{L!}{\sqrt{\pi}}\, \frac{(n-5/2)!}{(n-2)!} \qquad (A2\text{-}11)$$

As for the integrals $K^L_{N,2} \equiv \int_o^{\infty} e^{-x}\, x^{L}\, L^{L+1/2}_{N-1}(2x)$, analytical expressions slightly more complicated can be obtained, but their accurate evaluation by Gauss-Laguerre type numerical integration is also very practical.

PHENOMENOLOGICAL OPTICAL POTENTIALS AND OPTICAL MODEL COMPUTER CODES

A. PRINCE
National Nuclear Data Center,
Brookhaven National Laboratory,
Upton, NY,
United States of America

ABSTRACT

A. Theoretical Description

An introduction to the Optical Model is presented. Starting with the purpose and nature of the physical problems to be analyzed, a general formulation and the various phenomenological methods of solution are discussed. This includes the calculation of observables based on assumed potentials such as local and non-local and their forms, e.g. Woods-Saxon, folded model etc.

Also discussed are the various calculational methods and model codes employed to describe nuclear reactions in the spherical and deformed regions (e.g. coupled-channel analysis).

An examination of the numerical solutions and minimization techniques associated with the various codes, is briefly touched upon.

B. Workshop (Problem Session)

Several computer programs are described for carrying out the calculations. The preparation of input, (formats and options), determination of model parameters and analysis of output are described.

The class is given a series of problems to carry out using the available computer.

Interpretation and evaluation of the samples includes the effect of varying parameters, and comparison of calculations with the experimental data. Also included is an intercomparison of the results from the various model codes, along with their advantages and limitations.

A. Introduction

1.0 Purpose and Nature of Physical Problems

The strong fluctuations of neutron cross sections with energy are commonly referred to as resonances. The widths of these resonances increase with energy. For nuclei of intermediate mass these widths approach or become larger than the level spacings above a few MeV. At these higher energies, therefore, the cross sections are rather smooth functions of energy. The lower energy interval is generally called the "resonance region," the upper the "continuum region."

The behavior of cross sections in the resonance region does not immediately lend itself to a description by a simple model with few parameters because of the rapid fluctuations with energy, which, moreover, depend upon the nature of the particular compound nuclear state at each resonance. The averages of the cross sections over an interval which includes many resonances, (as shown by Feshbach, Porter, and Weisskopf (FPW)[1]) are those corresponding to a new scattering problem with slowly varying amplitudes, called the "gross-structure" problem. Making the assumption that one can average over the fluctuations, FPW defined an average reflection factor $\langle \eta_\ell \rangle$ which is a function of the energy of the incident particle given by

$$\langle \eta_\ell(E) \rangle = \frac{1}{\Delta} \int_{E-\Delta/2}^{E+\Delta/2} \eta_\ell(E')\, dE' \qquad 1.1$$

The width of the energy interval Δ contains many resonances but is small enough to be a smooth function of energy.

The model proposed by FPW replaced the many-body problem with a one-body potential which acts upon the incident nucleon.

The potential is complex of the form

$$V = V_0 + i W \qquad 1.2$$

where the real part represents the average potential, causing scattering, and the imaginary part the absorption, which describes the formation of the compound nucleus.

The quantity η_ℓ in Equation 1.1 is related to the phase shift δ_ℓ by $\eta_\ell = e^{2i\delta_\ell}$, where δ_ℓ is derived from the solution of the radial part of the Schrödinger equation using the potential given in 1.2.

1.1 General Formulation

The scattering and reaction processes that result from nucleon-nucleus interactions have generated an enormous amount of experimental data. The variety of nuclear reactions that occur is large and attempts to explain them concisely have not been completely successful due to the properties inherent in the nuclear many-body system. However, quantum mechanics has provided a means whereby a formalism for describing nuclear reactions exists through

parameters which have a fundamental relationship with the properties of the many-body system.

The foundation for this approach is manifested in the so-called Optical Model of the nucleus where it is assumed that the nucleons are scattered by nuclei in much the same way as light is scattered by a semi-transparent optical medium. The essence of the model conforms to the notion that the scattering of nucleons by complex nuclei may be described as a solution to the problem of diffraction of the nucleon wave by a particular type potential. Thus, the scattering problem is analyzed not as a many-body problem, but as one of the motion of a nucleon in a certain time-independent field produced by the target nucleus.

The nucleon's motion in this potential or, correspondingly, its wave function $\phi(r)$ is determined by the radial Schrödinger equation

$$\{ d^2/dr^2 - \ell(\ell+1)/r^2 + (K^2/E)[E - (V_{coul}(r) + V_{CR}(r) + iW_{CI}(r)) - (V_{SR}(r) + iV_{SI}(r))\hbar^2(j(j+1) - \ell(\ell+1) - s(s+1))/2]\} \phi_\ell^j(r) = 0 \qquad 1.3$$

where the various terms in Eq. (1.3), which depend only on the distance r between the incident and the target particles, represent, respectively, the Coulomb, central real, central imaginary, spin-orbit real, and spin-orbit imaginary potentials.

The wave function $\phi_\ell^{(j)}(r)$ is the radial wave function for the angular momentum quantum number j, which is composed of orbital angular momentum ℓ and intrinsic spin s of the incident particle (neutrons $s=\frac{1}{2}$):

$$|\ell - s| \leq j \leq \ell + s$$

The wave number in Eq. 1.3 is defined by

$$k = (2\mu E/\hbar^2)^{1/2} \qquad 1.4$$

where μ and E are reduced mass and relative energy between an incident particle and a target nucleus, respectively. They are given as follows:

$$\mu = \frac{mM}{m+M}, \qquad 1.5$$

and

$$E = \frac{M}{m+M} E_0, \qquad 1.6$$

where m and M are masses of incident particle and target nucleus, and E_0 the energy in the laboratory system.

The radial wave function $\phi_\ell^{(j)}(r)$ must satisfy certain boundary conditions, namely (a) it must vanish at the origin and (b) the asymptotic form in the region where the nucleus potential becomes small should be matched to a plane wave plus an outgoing wave. This asymptotic form is written as

$$\phi_\ell^{(j)}(r) \longrightarrow u_\ell^{(j)}(\rho) = u_\ell^{(+)}(\rho) + \eta_\ell^{(j)} u_\ell^{(-)}(\rho) \qquad 1.7$$

The wave functions $u_\ell^{+}(\rho)$ and $u_\ell^{(-)}(\rho)$ represent the incoming and outgoing waves, respectively, and are written as

$$u_\ell^{(\pm)}(\rho) = G_\ell(\rho) \pm i F_\ell(\rho) \qquad 1.8$$

For neutrons, the wave functions $G_\ell(\rho)$ and $F_\ell(\rho)$ are the spherical Neumann function and the spherical Bessel function multiplied by their argument ρ (=kr), respectively.

The coefficient of the outgoing wave, $\eta_\ell^{(j)}$, is related to the scattering phase shift $\delta_\ell^{(j)}$ by

$$\eta_\ell^{(j)} = \exp(2i\delta_\ell^{(j)}) \qquad 1.9$$

The values of $\eta_\ell^{(j)}$ are determined by integrating Eg. (1.3) from the origin to a point where the nuclear potential becomes negligibly small and then matching the logarithmic derivative of $\phi_1^{(j)}$

$$f_\ell^{(j)} = r_M \left[\frac{d\phi_\ell^{(j)}}{dr} \Big/ \phi_\ell^{(j)} \right]_{r=r_M} \qquad 1.10$$

at the matching radius r_M.

For neutrons ($s=\frac{1}{2}$) the shape elastic scattering cross section is written in terms of $\eta_\ell^{(j)}$ as

$$\sigma_{SE} = \frac{\pi}{K^2} \sum_{\ell=0}^{\infty} \{(\ell+1)|1-\eta_\ell^{(\ell+1)}|^2 + \ell|1-\eta_1^{(\ell-1)}|^2\} \qquad 1.11$$

and the differential cross section is given by

$$\frac{d\sigma_{SE}}{d\Omega} = \{|A(\Theta)|^2 + |B(\Theta)|^2\} \qquad 1.12$$

where

$$A(\Theta) = \frac{i}{2k} \sum_{\ell=0}^{\infty} \left\{ (\ell+1)\left(1-\eta_\ell^{(\ell+1)}\right) + \ell\left(1-\eta_\ell^{(\ell-1)}\right) \right\} P_\ell(\cos\Theta) \qquad 1.13$$

and

$$B(\Theta) = \frac{1}{2k} \sum_{\ell=0}^{\infty} \left\{ \eta_\ell^{(\ell-1)} - \eta_\ell^{(\ell+1)} \right\} P_\ell^1(\cos\Theta) \qquad 1.14$$

Legendre function $P_\ell(\cos\Theta)$ and its associated function $P_\ell^1(\cos\Theta)$ are used. The cross section for compound nucleus formation is given by

$$\sigma_c = \frac{\pi}{k^2} \sum_{\ell=0}^{\infty} \left\{ (\ell+1)\, T_\ell^{(\ell+1)} + \ell\, T_\ell^{(\ell-1)} \right\} \qquad 1.15$$

and the total cross section by

$$\sigma_T = \sigma_{SE} + \sigma_C \qquad 1.16$$

where the quantity $T_\ell^{(j)}$ is called transmission coefficient and is related to the quantity $\eta_\ell^{(j)}$:

$$T_\ell^{(j)} = 1 - \left|\eta_\ell^{(j)}\right|^2 \qquad 1.17$$

For protons or charged particles ($^2_1$H, $^4_2$He etc.) the potential must include the Coulomb interaction, and the various quantities used in describing the cross section must take the phase shift of Coulomb scattering into consideration.

2.0 Phenomenological Method of Solution

One of the earliest quantum-mechanical calculations of the elastic scattering cross section using a complex central potential was carried out by Le Levier and Saxon[2].

Subsequent experiments by Barschall[3,4] were analyzed by Feshbach et al.[1] who assumed a complex square well potential

$$V = V_o + iW \qquad r < R$$
$$= 0 \qquad r > R$$

This simple potential reproduced the overall features of the total cross sections for a wide range of nuclei, however it resulted in too little absorption and excessive scattering cross sections at large angles.

Further investigations[5] based on the observed properties of nuclear matter and the nucleon-nucleon interaction showed that a diffuse potential is preferable.

The shape of this diffuseness has taken many forms as seen in Refs. 6&7, however, the most extensively used central complex potential is written as

$$V_C(r) = V_{CR}(r) + iW_{CI}(r) \qquad 2.1$$

where $V_{CR}(r)$ is the real part and $W_{CI}(r)$ the imaginary part. The real potential $V_{CR}(r)$ is assumed to have Woods-Saxon form factor and is represented as follows:

$$V_{CR} = V_c\, f_{CR}(r) \qquad 2.2$$

where $f_{CR}(r)$ is the Woods-Saxon form factor and is written as

$$f_{CR}(r) = \frac{1}{1+\exp\left\{(r-R_o)/a_o\right\}} \qquad 2.3$$

and V_c is the potential strength (or potential well depth) parameter, which is negative for an attractive potential, and $R_o = r_o A^{1/3}$.

The imaginary potential $W_{CI}(r)$ consists of nuclear surface part and nuclear interior part, and is expressed as

$$W_{CI}(r) = \left[W_S f_{CS}(r) + W_I f_{CI}(r) \right] \qquad 2.4$$

The form factor of the surface part, $f_{CS}(r)$, is assumed to be Gaussian type or derivative Woods-Saxon type. On the other hand, the form factor of the interior part, $f_{CI}(r)$, is assumed to be Woods-Saxon form. These three types of the form factor are given by the following expressions:

Surface absorption:

(i) Gaussian absorption:

$$W_{CI}(r) = W_s \exp\left[-\left(\left(r-R_I\right)/b\right)^2\right] \qquad 2.5$$

(ii) Derivative absorption:

$$W_{CI}(I) = 4a_I W_S\left[-\frac{d}{dr}\left(\frac{1}{1+\exp\left(\left(r-R_I\right)/a_I\right)}\right)\right] \qquad 2.6$$

where W_v and W_s are negative for an absorptive potential and $R_I = r_I A^{1/3}$. Both forms of surface absorption have also been combined with a volume absorption.

Volume absorption (Woods-Saxon form factor):

$$V_{CI}(r) = W_v\Big/\left[1+\exp\left(\left(r-R_I\right)/a_I\right)\right] \qquad 2.7$$

The spin-orbit potential is usually assigned a Thomas form factor such as

$$V_{SR}(r) = V_{so}\left(2.0^{-2}r^{-1}\right)\left[\frac{d}{dr}\left(\frac{1}{1+\exp\left(\left(r-R_R\right)/a_R\right)}\right)\right] \qquad 2.8$$

$$V_{SI}(r) = W_{so}\left(2.0^{-2}r^{-1}\right)\left[-\frac{d}{dr}\left(\frac{1}{1+\exp\left(\left(r-R_I\right)/a_I\right)}\right)\right] \qquad 2.9$$

The Coulomb potential $V_{coul}(r)$ is usually taken to correspond to a constant charge density within the nucleus extending to a distance $r_c = R_c A^{1/3}$. Thus

$$V_{coul}(r) = \left(ZZ'e^2/2R_c\right)\left(3 - r^2/R_c^2\right) \qquad r \le R_c \qquad 2.10$$

$$= ZZ'e^2/r \qquad r \gg R_c$$

Thus the parameters of the model are as follows:

Geometrical parameters:

R_c = Coulomb radius parameter
R_o = real potential radius parameter
R_I = imaginary potential radius parameter
a_o = real potential surface parameter
a_I = imaginary potential surface parameter
b = Gaussian absorption width

Dynamic parameters:

V = real potential depth
W_v = volume absorption potential depth
W_s = surface absorption potential depth
V_{so} = real spin-orbit potential depth
W_{so} = imaginary spin-orbit potential depth.

The large amount of experimental data accumulated in recent years has demonstrated that many important properties of nuclei in regions $90 \lesssim N \lesssim 112$ and $88 \lesssim Z$ and $Z \approx 13$ may be correlated by the strong-coupling unified model which assumed that various nuclei and their related average potential fields possess large equilibrium deformations. These large deformations have been shown to exert strong influence on the scattering and absorption of neutrons when analyzed by an optical model. Thus any attempt to describe differential elastic scattering cross sections, penetrabilities, and all other subsequent scattering and reaction characteristics must consider the deformation.

The theory of explaining the scattering mechanism when the collective levels are directly excited by inelastic scattering without formation of a compound nucleus, and the effect of level excitation by formation and decay of a compound nucleus was first pointed out by Bohr and Mottelson.[8] The earliest application of this coupled-channel analysis was by Margolis, et al.[9], and Chase, et al.,[10] who applied the idea to the calculation of low-energy neutron strength functions. Yoshida,[11] also around the same time, described elastic and inelastic scattering of higher-energy neutrons with the same concept.

The Hamiltonian for the interaction of a deformed target nucleus with an incident particle is given as[12]

$$H = T + H_t + V(r,\theta,\phi) \qquad 2.11$$

The optical potential $V(r,\theta,\phi)$ used is assumed to be, in general, non-spherical and is defined in Ref. (12) as

$$V(r,\theta,\phi) = -(V+iW)\frac{1}{1+\exp\left[\frac{r-\bar{R}}{a}\right]} - \frac{4iW_D \exp\left(\frac{r-\bar{R}}{\bar{a}}\right)}{\left[1+\exp\left(\frac{r-\bar{R}}{\bar{a}}\right)\right]^2} \qquad 2.12$$

$$- V_{so}\left(\bar{\sigma}\cdot\bar{\ell}\right)\lambda_\pi^2 \frac{1}{a_r}\left[\frac{\exp\left(\frac{r-\beta}{a}\right)}{\left\{1+\exp\left(\frac{r-\bar{R}}{a}\right)\right\}^2}\right] + V_{coul}$$

When R and $\bar{R}$ are assumed to be independent of angle, Eq. (2.12) becomes the usual optical model potential. When R and $\bar{R}$ are made to be dependent on θ

and ϕ according to the collective nature of the target nucleus, then the following relationships hold.

If the target nucleus is spherically symmetric but is capable of vibration about that shape, then the vibrational deformity is described by

$$R = R_0 \left\{ 1 + \sum_{\lambda\mu} \alpha_{\lambda\mu} Y_{\lambda\mu}(\theta, \phi) \right\}$$
$$\bar{R} = \bar{R}_0 \left\{ 1 + \sum_{\lambda\mu} \alpha_{\lambda\mu} Y_{\lambda\mu}(\theta, \phi) \right\} \qquad 2.13$$

However, if the nucleus is characterized by a permanently deformed surface of cylindrical symmetry (axial symmetric), then the rotational deformity is defined as

$$R = R_0 \left\{ 1 + \sum_{\lambda} \beta_\lambda Y_{\lambda 0}(\theta') \right\}$$
$$\bar{R} = \bar{R}_0 \left\{ 1 + \sum_{\lambda} \beta_\lambda Y_{\lambda 0}(\theta') \right\} \qquad 2.14$$

where β is the usual nuclear deformation parameter. ($\beta > 0$ for prolate deformation; $\beta < 0$ for oblate deformation).

An alternative method of analyzing nuclear scattering from deformed nuclei is the distorted wave Born approximation (DWBA), and has been used very extensively, especially in those areas where the deformation is small ($\beta \simeq 0.1$). For values of $\beta > 0.2$ the shape for the differential inelastic scattering is adequately described, but its magnitude is greatly overemphasized.

The differential elastic cross section is even more difficult to describe for large deformation, and it is more feasible to use the conventional coupled-channels approach than DWBA.[12-15]

Other methods for handling inelastic scattering based on the shell model have also been investigated as a means of microscopic descriptions of collective motion in nuclei, however, they have not been used as often as an evaluation tool, so their significance cannot be commented on at this time.

J. Raynal[16] has reported the development of a "sequential iteration method for coupled equations" called ECIS, which is an approximation between DWBA and coupled channel computations.

Using the phenomenological potential V(r) the computational methods for solving the radial wave equations must be carried out numerically with the aid of computers. Many automatic techniques have been developed in the form of computer programs, for calculating the differential elastic scattering cross sections $\sigma(\theta)$, the total reaction cross section σ_R and the polarization $P(\theta)$, for particles of spin 0, 1/2 and 1.

These calculations involve the numerical integration of the radial Schrödinger equations for the effective partial waves, where as previously mentioned the scattering complex phase shifts are obtained by matching the logarithmic derivatives of the numerically obtained wave functions to those of the Coulomb or spherical Bessel functions.

There are several possible numerical procedures used for finding the radial Schrödinger function.

The most often used are the Runge-Kutta method, (sometimes referred to as the Fox-Goodman method), the Cowell and the Noumerov method (a modification of the Cowell method).

The numerical integration is determined primarily by three parameters:

a) Matching radius R_M
b) The step length Δ
c) Number of partial waves (ℓ_{max})

In general most computer programs have certain parameter criteria built in, however, if more accuracy is desired then the option to vary them is necessary.

A very detailed treatment of numerical methods used in the optical model analysis may be found in Ref. (17).

3.0 Determination of Model Parameters

The preceding sections have outlined the optical model formalism and have set the stage for determining its role in the evaluation of nuclear data necessary for fission and fusion applications.

There now exists a vast body of experimental data for elastic scattering of nucleons and other reactions. Yet, in spite of this abundance, there are many gaps which must be filled by model calculations.

Extensive studies have provided adequate confidence that the optical model can be employed to give precision fits, in the non-fluctuating region, to elastic scattering differential cross sections, reaction cross sections, total cross sections, and polarizations provided the phenomenological parameters are optimized for each nucleus at every energy.

In general it is not possible to determine the best potential for a particular set of data by direct calculation. The usual procedure is to assume a starting potential and then vary the parameters systematically, until an optimum fit to the data is achieved. When realistic potentials are used the calculations require rather complicated computer programs.

These potentials have several disadvantages in that they usually are over-parametrized such that many different potentials exist that give equally good fits to the data. This potential ambiguity raises the questions regarding the physics of the situation. The following section discusses these ambiguities along with ways that have been used to either overcome them or at least minimize them.

3.1 Non-Local Potential

A method for acquiring a somewhat consistent set of parameters over a wide range of nuclides and energies has been introduced, in which the local potential is replaced by a non-local potential. This method for computing the various cross sections from an optical model code was first introduced by Perey and Buck.[18] Whereas the optical model potential given earlier is both energy dependent and local, i.e.,

$$V(\bar{r}', \bar{r}) = V(r)\,\delta(\bar{r}' - \bar{r}), \qquad 3.1$$

the optical potential of Perey and Buck is energy independent and non-local.

The interpretation is that the potential acting on a particle centered at position $\bar{r}$ does not only depend on $\bar{r}$, but also on the value of the wave function over all space and thus takes into account the finite size of the incident particle and the dispersive properties of the nucleus. The non-locality enters through the application of a potential term which leads to an integro-differential Schrödinger equation

$$\left\{\frac{\hbar^2}{2m}\nabla^2 + E\right\}\psi(\bar{r}) = \left\{V_{SR}\,S(r)\,\bar{l}\cdot\bar{\sigma}\right\}\psi(\bar{r}) + \int V(\bar{r},\bar{r}')\,\psi(r')\,d\bar{r}' \qquad 3.2$$

where $V(\bar{r}, \bar{r}')$ is the non-local potential. This potential may be represented phenomenologically by

$$V(\bar{r},\bar{r}') = V\left\{\tfrac{1}{2}(\bar{r}+\bar{r}')\right\}\frac{1}{\pi^{3/2}\beta^3}\exp\left\{-\left(\frac{\bar{r}-\bar{r}'}{\beta}\right)^2\right\} \qquad 3.3$$

where β is the range of the non-locality.

As β approaches zero the non-local potential tends toward a local potential. The forms of the shape factors are analogous to those of the local potential. Perey and Buck[18] found that the scattering cross sections given by the non-local potential could also be adequately fitted by a local potential, and vice versa, which led to a single non-local potential that produced satisfactory agreement over an energy range of 1 to 25 MeV. The relation between the equivalent local and non-local potentials may be expressed as

$$V_L(r) = V_N(r)\exp\left\{\frac{-m\beta^2}{2\hbar^2}\left(E - V_L(r)\right)\right\} \qquad 3.4$$

Wilmore and Hodgson,[19] following the work of Perey and Buck,[18] produced an analytical set of equivalent local potentials based on energy and mass number which yielded very good cross section results from 1 to 15 MeV for medium and heavy nuclei. This method of using an equivalent non-local potential has also been used by Lane, et al.,[20] and Engelbrecht and Fiedeldey.[21]

3.2 Folding Model

The use of the equivalent-local potential, while yielding good fits to a wide range of nuclei, still does not quite overcome the ambiguities derived from the inter-relationship between various potential parameters.

One method for overcoming this difficulty was offered by Feshbach[6] who suggested using a volume integral of the potential

$$J = \int V(\bar{r})\,d\bar{r} \qquad 3.5$$

which is a better measure of the potential strength. This is due to the inclusion of the contributions from the well depths along with the geometry. Such an approach was made by Greenlees, et al.[22,23] who analyzed the real part of the optical model potential in terms of an overlap integral of the nuclear density distribution with an assumed nucleon-nucleon interaction.

This folding procedure manifested itself in what Greenlees et al.[22,23] called the Reformulated Optical Model (ROM).

Greenlees and his collaborators expressed the optical model potential in the following form

$$U_{opt}(r) = -VI(r)/I(0) - iW_v f(r, r_I, a_I) + iW_D 4a_I \frac{d}{dr} f(r, r_I, a_I) + V_s \lambda^2 \frac{1}{r}\frac{d}{dr} f_m(r)\, \bar{\sigma}\cdot\bar{l} + V_c(r) \qquad 3.6$$

where $V_c(r)$ is the potential due to a uniformly charged sphere of radius $R_c = r_c A^{1/3}$, $f(r,r_I,a_I)$ is a Woods-Saxon form factor, and $f_m(r)$ is related to the matter distribution,

$$f_m(r) = \rho_m(r)/\rho_m(0) = \left\{1 + \exp\left(\frac{r-R_m}{a_m}\right)\right\}^{-1} \qquad 3.7$$

The Woods-Saxon form factor is given by

$$f_I(r) = \left\{1 + \exp\left(\frac{r-R_I}{a_I}\right)\right\}^{-1}$$

The folded potential I(r) is represented as

$$I(r) = \int \rho_m(\bar{r}')\, U_d(|\bar{r}-\bar{r}'|)\, d^3r' + \int \rho_{ne}(\bar{r}')\, U_\lambda(|\bar{r}-\bar{r}'|)\, d^3r' \qquad 3.8$$

$$\rho_m(\bar{r}) = \rho_n(r) + \rho_p(r)$$

where ρ_p, ρ_n, and ρ_m are the proton, neutron, and matter distributions of the target nucleus.

$\rho_{ne}(r) = \rho_n(r) - \rho_p(r)$ is the neutron excess distribution and $\lambda = +1$ for protons, -1 for neutrons.

A Yukawa form was chosen to describe the central potential

$$U_d(r) = \exp(-ur)/ur \qquad 3.9$$

As a first approximation, it was assumed that the protons and neutrons had the same density distribution, such that

$$\rho_p(r) = \frac{Z}{A}\rho_m(r)$$

$$\rho_n(r) = \frac{N}{A}\rho_m(r) \qquad 3.10$$

and

$$U_\lambda(r) = \xi U_d(r) \qquad (\xi \text{ being a constant})$$

Thus, the real central potential given by Eq.(3.6) may now be expressed as

$$VI(r) \equiv U_{RS}(r) = \int (1 + \epsilon\xi)\, \rho_m(\bar{r})\, V_d |\bar{r}-\bar{r}'|\, d^3r \qquad 3.11$$

where $\epsilon = (N - Z)/A$.

In order to overcome the various ambiguities inherent in a multiparameter search procedure, Greenlees, et al. following Feshbach[6] derived a volume integral for this real part of the potential. The volume integral of U_{RS} is designated by J_{RS} and is related to J_d, the volume integral of the two-body interaction by

$$-\int U_{RS}\, d\bar{r} = J_{RS} = A J_d \left(1 + \frac{N-Z}{A}\xi\right) \qquad 3.12$$

or

$$\frac{J_{RS}}{A} = J_d + \xi \cdot J_d \left(\frac{N-Z}{A}\right) \qquad 3.13$$

The strength V_{RS} of the central potential U_{RS} was treated as a parameter and the radial parameters for the spin-orbit potential were taken to be the same as the central potential. This reduced the number of parameters from the conventional ten to eight.

The model was applied to proton elastic scattering data at 14.5, 30.3, and 40.0 MeV[22] and neutron scattering at 14.5 MeV[23] and yields results comparable to the conventional phenomenological analyses, although the number of adjustable parameters have been decreased by two.

Further investigation,[14-26] using a Gaussian effective interaction $u_d(r) = \exp(-kr^2)$ in Eq. (3.6) reduced the number of adjustable parameters to six (V, W_v, W_D, V_S, r_I and a_I).

The reasonable success of the folding model concept, while not fully tested at lower energies, e.g., E < 10 MeV, does provide a means for relating some of the nuclear structure characteristics such as the range of the two-body forces and the geometrical properties of the nucleus to the scattering data by means of the optical model. Thus, the folding integral given by Eq. (3.12) constitutes a rather meaningful approach to parametrizing the optical model.

Further details concerning this approach not only for neutrons and protons, but also in the analysis of the scattering of composite projectiles, may be found in Jackson[27] and Hodgson.[28]

4.0 Minimization Technique

In order to determine an optimum set of parameters for the calculation of cross sections, the usual procedure is to carry out a least squares fit and to minimize the quantity χ^2 given by

$$\chi^2=\left\{W_t\left(\frac{\sigma_t^{cal}-\sigma_t^{exp}}{\Delta\sigma_t}\right)^2+W_{el}\left(\frac{\sigma_{el}^{cal}-\sigma_{el}^{exp}}{\Delta\sigma_{el}}\right)^2+W_1\left(\frac{\sigma_1^{cal}-\sigma_1^{exp}}{\Delta\sigma_1}\right)^2\right.$$
$$\left.+W_{cls}\sum_\theta\left|\frac{\left(\frac{d\sigma_{el}^{cal}(\theta)}{d\Omega}-\frac{d\sigma_{el}^{exp}(\theta)}{d\Omega}\right)}{\Delta\frac{d\sigma_{el}(\theta)}{d\Omega}}\right|^2+W_{1s}\sum_\theta\left|\frac{\left(\frac{d\sigma_1^{cal}(\theta)}{d\Omega}-\frac{d\sigma_1^{exp}(\theta)}{d\Omega}\right)}{\Delta\frac{d\sigma_1(\theta)}{d\Omega}}\right|^2\right\} \qquad 4.1$$
$$/(W_t+W_{el}+W_1+\sum_\theta W_{cls}+\sum_\theta W_{1s}),$$

where σ_T, σ_{el}, σ_1 are the total, elastic and inelastic cross sections, and $\frac{d\sigma(\theta)}{d\Omega}$ the corresponding differential scattering cross sections. $\Delta\sigma$ is the error and Wi the weighting factors. Most analyses consider only the differential scattering cross sections. When polarization data exists, this is also taken into account by

$$\chi^2_{pol}=\sum_\Theta\left(\frac{P(\Theta)^{calc.}-P(\Theta)^{exp}}{\Delta P(\Theta)^{exp}}\right)^2 \qquad 4.2$$

The search is made on any number of the parameters given in Eq. 4.1.

Often when one is attempting to define a "global" set of parameters the data for one type of target nucleus at various energies will produce a set of parameters which exhibit wide fluctuations. This is also true for different target nuclei at a single energy. The usual procedure is to hold one set constant or limit the range and then calculate optimum values for those remaining.

The number of variable parameters given on page (8) can be reduced by recognizing that $V_R r_R^n$ = constant where $n \approx 2$ will produce equivalent fits for different values of V_R and r_R (the same holds true for $W_D a_D^m$ = constant where $m \approx 0.8$).

Thus, by holding r_R and a_D constant only V_R, a_R, W_D, r_D need be varied, where it is assumed that $r_D=r_{so}=r_R$ and $a_D=a_{so}=a_R$. In the case of a coupled-channel calculation, the deformation β may also be varied.

It should be mentioned that the χ^2 method is merely a selection procedure with no absolute significance and comparing values of χ^2 with different experiments has no real meaning. This non-uniqueness manifests itself usually in attempts to calculate the inelastic cross section. While a set of parameters from a χ^2 test might produce excellent agreement with the elastic cross section, it might fail totally in reproducing an acceptable value for the inelastic.

A typical example of the χ^2 fitting procedure was carried out for both neutrons and protons by Becchetti and Greenlees[29] to determine an optimum set of nucleon-nucleus OM parameters for A > 40 and for energies less than 50 MeV.

The criterion function F of the theoretical fit was taken to be

$$F=\sum_{n=1}^{n_{max}}\left\{\frac{\chi^2}{N_{\sigma(\theta)}}+\frac{\chi^2}{N_{P(\theta)}}+\chi^2_{\sigma_R}\right\} \qquad 4.3$$

where

$\chi^2/N_{\sigma(\theta)}$ = the χ^2 per point value of the differential cross sections $\sigma(\theta)$ for the nth data set

$\chi^2/N_{P(\theta)}$ = the χ^2 per point value of the polarization data $P(\theta)$ for the nth data set;

and

$\chi^2_{\sigma_R}$ = the χ^2 value of the reaction (protons) or total (neutrons) cross section for the nth data set.

A quantity χ^2/N is defined by

$$\frac{\chi^2}{N}=\frac{1}{N}\sum_N\left\{\frac{g^{OM}(\theta)-g^{obs}(\theta)}{\Delta g^{obs}(\theta)}\right\}^2 \qquad 4.4$$

where $g^{OM}(\theta)$, $g^{obs}(\theta)$, and $\Delta g^{obs}(\theta)$ are the OM prediction,

the experimental value and the error in $g(\Theta)$, where $g(\Theta)$ was taken to be $\sigma(\Theta)$, (differential elastic scattering), σ_R (reaction cross section), σ_T (total cross section) and $P(\Theta)$ (polarization).

Further details of the fits may be found in Reference (29).

Many other systematic studies have also been made to produce a "best set" of optical model parameters. The most complete compilation of these sets has been tabulated by Perey and Perey.[30]

In addition, Aver'yanov and Purtseladze[31] have analyzed experimental data on neutrons and protons having energies ranging from 2.5 to 96 MeV, and have described a set of parameters for nuclei ranging from C to Pb.

Englebrecht and Fiedeldey[21] have also proposed a set of OM parameters for energies between 1 and 100 MeV.

In another attempt to avoid the ambiguity of the real and imaginary potentials, the mean values for the volume integrals of U and W were determined, using the least squares procedure for a range of nuclei of mass 20 to 210, by Holmqvist and Wiedling.[32] These generalized OM potentials provided fits that were almost as good as those from a five parameter best fit set.

References

1. Feshbach, H., Porter, C. E. Weisskopf, V. F., Phys. Rev. 96 (1954) 448.
2. Le Levier, R. E., Saxon, D. S., Phys. Rev. 87 (1952) 40.
3. Barschall, H. H., Phys. Rev. 86 (1952) 431.
4. Walt, M., Barschall, H. H., Phys. Rev. 93 (1954) 1062.
5. Woods, R. D., Saxon, D. S., Phys. Rev. 95 (1954) 377.
6. Feshbach, H., Ann. Rev. Nucl. Sci. 8 (1958) 49.
7. Ulehla, I., et al., "Optical Model of the Atomic Nucleus (Academic Press, N. Y. 1964).
8. Bohr, A., Mottelson, B. R., kgl. Danske Videnskab. Selskab, Mat Fys. Medd. 27 (16) (1953).
9. Margolis, B., Troubetzkoy, E. S., Phys. Rev. 106 (1957) 105.
10. Chase, D. M., Wilets, L., Phys. Rev. 110 (1958) 1080.
11. Yoshida, S., Proc. Phys. Soc. (London A69 (1956) 668.
12. Tamura, T., Rev. Mod. Phys. 37 (1965) 679.
13. Buck, B., Phys. Rev. 130 (1963) 712.
14. Satchler, G. R., Nucl. Phys. 44 (1963) 607.
15. Satchler, G. R., Nucl. Phys. 53 (1963) 1.
16. Raynal, J., "Computing as a Language of Physics" IAEA-SMR 9/8 (1972).
17. Melkanoff, M. A. et al. - "Methods in Computational Physics"; Alder, B. et al., eds. Academic Press 1966.
18. Perey, F., Buck, B., Nucl. Phys. 32 (1962) 353.
19. Wilmore, D., Hodgson, P. E., Nucl. Phys. 55 (1964) 673.
20. Lane, R. O., et al., Phys. Rev. 133B (1964) 80.
21. Engelbrecht, C. A., Fiedeldey, H., Ann. Phys. 42 (1967) 262.
22. Greenlees, G. W., et al., Phys. Rev. 171 (1968) 1115.
23. Pyle, G. J., Greenlees, G. W., Phys. Rev. 181 (1969) 1444.
24. Thomas, G. L., Sinha, B. C., Phys. Rev. Lett. 26 (1971) 325.
25. Battey, J. C., Friedman, E., Nucl. Phys. A179 (1972) 701.
26. Morgan, C. G., Jackson, D. F., Phys. Rev. 188 (1969) 1758.
27. Jackson, D. F., Reports Prog. Phys. 37 (1974) 55.
28. Hodgson, P. E., Reports Prog. Phys. 34 8 (1971) 765.
29. Becchetti, F. D., Jr., Greenlees, G. W., Phys. Rev. 182 (1969) 1190.
30. Perey, C. M., Perey, F. G., Atomic Data and Nuclear Data, Tables 13 (1974) 293.
31. Aver'Yanov, I. K., Purtseladze, Z. Z., Sov. J. Nucl. Phys. (Eng. Trans.) 6 (1968) 212.
32. Holmqvist, B., Wiedling, T., AE-430, Studsvik, Sweden 1971.

B. Workshop (Problem Session)

Code Description

In order to gain experience and obtain a real feeling for carrying out optical model calculations, a series of optical model computer programs will be examined.

The sample codes that have been chosen are:

1. ABACUS-2 E.H. Auerbach, BNL 6592 (1964)
2. CERBERO-2 G. Reffo et al., RT/FI(77) 6
3. CRAPONE Fabbri et al., RT/FI(77) 3
4. RAROMP G.J. Pyle (unpublished), Uni. of Minnesota
5. JUPITOR T. Tamura, ORNL 4152 (1967)

1. ABACUS-2

NAME OF PROGRAM: ABACUS-2 (revised)
AUTHOR: E.H. Auerbach
INSTITUTION: Brookhaven National Laboratory
DOCUMENTATION: BNL-6562 (unpublished), 1964

NATURE OF PHYSICAL PROBLEM: ABACUS is one of the oldest optical model programs still in use. ABACUS-2 is a combination of the Optical Model and the Hauser-Feshbach formalism. It is designed to carry out four classes of calculations, each one based on generating an optical potential and the integration of the radial Schrödinger equation.

Class 1 - Scattering by an optical potential: gives σ_T, σ_{SE}, and σ_R only.

Class 2 - Computes the bound state radial wave function for a specific ℓ and j.

Class 3 - Uses method and information from Class 1 to generate transmission coefficients for use in Hauser-Feshbach calculations. Computes σ_T, σ_{SE}, σ_{CE}, and $\sigma_{nn'}$ (see my lecture on Statistical Theory Applications and Associated Computer Codes).

Class 4 - Calculates radial integrals from partial waves generated by Classes 1 and 2.

A multidimensional search procedure is included for obtaining best optical model parameters.

PROGRAM LANGUAGE: Fortran IV
SIZE: 32 K
STATUS: Converted for PDP-10, CDC 6600, IBM-360

Introduction

Class 1: Scattering and Reaction Cross Sections

A potential well is generated and the Schrödinger equation solved by partial waves. Phase shifts (more precisely, $\eta_{\ell j} = e^{2i\delta_{\ell j}}$), transmission coefficients, $T_{\ell j}$ ($T_{\ell j} = 1 - |\eta_{\ell j}|^2$), and partial reaction cross sections, $\sigma_{\ell j}$, are calculated for each ℓ,j up to an ℓ_{max} which is either given as input or determined by an internal criterion. The reaction cross section, σ_r, is calculated; for neutral incident particles, σ_{total} and $\sigma_{shape\ elastic}$ are also given. Where an angular distribution is desired, $d\sigma/d\Omega$ and the polarization $P(\theta)$, are calculated; results are given in both the lab and center of mass system. For charged particle interactions, the ratio $d\sigma/d\sigma_{rutherford}$ is also given. The incident particle may have either a spin of 0 or a spin of ½.

There are several well forms available in the program and cover the range of those currently of interest. In addition, provision is made for addition, by special subroutine, of new forms; the wells may also be given point-by-point for each point of the integration mesh. In ABACUS the real and imaginary wells are given as:

$$V_c(r) = -V_o f(r) = i(-W_o) \propto f(r) = (1 - \propto) g(r) \quad ; \qquad 1.0$$

$$V_{so}(r) = -(V_{so} = iW_{so}) \left(\frac{h^2}{\mu_\pi c^2} \right)^2 \frac{1}{r} \frac{df(r)}{dr} \quad ; \qquad 1.1$$

$$f(r) = \frac{1}{1 + e^{(r-R_S)/a}} \quad ; \quad g(r) = e^{-(r-R_G)^2/b^2} \quad ; \qquad 1.2$$

$$V_{coul}(r) = \frac{ZZ'e^2}{2R_c} \left(3 - \frac{r^2}{R_c^2} \right) \qquad r \leq R_c \qquad 1.3$$

$$= \frac{ZZ'e^2}{r} \qquad r \geq R_c$$

The central potential is an imaginary part of both the same and different functional form as the real part, and it is assumed, as is customary, that the spin-orbit potential is that of the Thomas form, and V_o, W_o, V_{so}, and W_{so} are respectively the strengths of the real and imaginary central, and the real and

imaginary spin-orbit potentials. The mixing parameter, α, defines the relative amount of volume and surface imaginary components ($\alpha \geq 0$). All of the potential well strengths are taken to be positive. The ranges are defined as follows: R_S, Saxon radius; R_G, Gaussian radius; a, is the diffuseness parameter; b, Gaussian width; R_c, Coulomb Potential radius.

2. CERBERO-II

Name of Code: CERBERO-II: Improved Version of the CERBERO Code for Calculating Nuclear Reaction Cross Sections, CNEN Rpt. RT/FI(77)6

Authors: F. Fabbri, G. Fratamico, G. Reffo

Establishment: CNEN, Bologna, Italy

Nature of Problem Solved: Using an optical model to generate the transmission coefficients, reaction cross sections for discrete and continuous states may be calculated.

Program Language: Fortran IV (IBM 370/165)

Program Size: Less than 240k bytes using an overlay structure.

Introduction

This code is an extension of CERBERO, (RT/FI(74)36) which uses the optical and statistical models in a theoretical calculation of cross sections.

Optical Potential Forms

The optical potential has the conventional form

$$V_{TOT}(r) = -V\, f_V(r) - i\left[W_I\, f_I(r) + W_S\, g_S(r)\right] - V_{SO}\, \hbar(r)\, \bar{\sigma}.\bar{\ell} + V_C(r) \qquad 2.0$$

where V and W are the depths of the real and imaginary parts of the central nuclear potential, V_{SO} the spin orbit strength and f(r), g(r), h(r) their corresponding nuclear form factors, while $V_C(r)$ is the Coulomb potential.

Real Potential

The real part of the potential is given in energy-dependent (non-local characteristic) form and with a symmetry term as

$$V = V_0 + V_1 E + V_2 E^2 - V_3 \frac{ZZ'}{A^{1/3}} + V_4 \frac{(N-Z)\,(N'-Z')}{A.A'} \qquad 2.1$$

V_0, V_1, V_2, V_3, V_4 being input parameters. The corresponding form factor $f_V(r)$ is Woods-Saxon.

Imaginary Potential

The imaginary term in 2.1 is assumed to consist of a volume and surface form given as:

$$W_I = W_{I0} + W_{I1} E + W_{I2} E^2 \qquad 2.2$$

$$W_S = W_{S0} + W_{S1} E + W_{S2} E^2 + W_{S3} \frac{N-Z}{A} \qquad 2.3$$

W_{I0}, W_{I1}, W_{I2}, W_{S0}, W_{S1}, W_{S2}, W_{S3} being input parameters.

The form factor of the volume term is assumed to be Woods-Saxon's

$$f_I(r) = \left[1 + \exp(r-R_I)/a_I\right]^{-1} \qquad 2.4$$

while the form factor for the surface part may be of either Gaussian or derivative Woods-Saxon type

$$g_S(r) = \begin{cases} \exp\left[-\left(\frac{r-R_S}{a_S}\right)^2\right] \\ \\ \dfrac{4 \exp (r-R_S)a_S}{\left[1 + \exp(r-R_S)/a_S\right]^2} \end{cases} \qquad 2.5$$

the radial parameters R_I and R_S are defined as

$$R_I = r_I A^{1/3} + K_I \qquad 2.6$$

$$R_S = r_S A^{1/3} + K_S \qquad 2.7$$

the constants K_I and K_S, the nucleon radii r_I, r_S and the diffusenesses a_I, a_S are input parameters.

Spin orbit potential

The spin orbit potential general form is assumed to be of the Thomas-Fermi type, characterized by a Woods-Saxon derivative form factor

$$h(r) = \left(\frac{\hbar}{m_\pi c}\right)^2 \frac{1}{r\, a_{SO}} \frac{\exp\,(r-R_{SO})/a_{SO}}{\left[1 + \exp(r-R_{SO})/a_{SO}\right]^2} \qquad 2.8$$

where $\left(\frac{\hbar}{m_\pi c}\right)^2 \simeq 2\ f^2$ and $R_{SO} = r_{SO}\ A^{1/3} + K_{SO}$ provided a_{SO} , r_{SO} , K_{SO} are input parameters.

The strength of the spin orbit potential V_{SO} is assumed to be a real and energy-independent quantity to be given in input.

Coulomb potential

The strength of the Coulomb repulsion is that of a uniform charge distribution

$$V_C = \frac{ZZ'\,e^2}{2\,R_C}\left(3 - \frac{r^2}{R_C^2}\right) \qquad \text{in the interior region } r \leq R_C$$

$$V_C = \frac{ZZ'\,e^2}{r} \qquad \text{in the external region } r > R_C \qquad 2.9$$

e being the electron charge, $R_C = r_C\ A^{1/3}$ the charge distribution radius and r_C an input parameter.

Compound Nucleus Reactions

CERBERO II utilizes the transmission coefficients generated from the optical potential to calculate both discrete and continuum level excitation as well as capture.

The formalism is based on the Hauser-Feshbach treatment (Phys. Rev. 87, 366 (1952)) as modified by Moldauer (Rev. Mod. Phys. 36, 1079 (1964), Phys. Rev. 135B, 642 (1964), and Phys. Rev. C11, 426 (1975)).

The compound nucleus is formed by an incident particle of Energy E, leaving the residual nucleus at an excitation E' and proceeding through channels C, C' with the same total angular momentum J and parity Π.

The cross section is represented as:

$$d\langle\sigma_{cc'}(E,E')\rangle = \frac{\langle\Theta_c(E)\times\Theta_{c'}(E')\rangle\rho_{c'}(E,E')dE'}{\langle\Theta(E)\rangle} W_{cc'}(E)$$

where $W_{cc'}(E)$ is the width fluctuation correction factor.

3. CRAPONE

Name of Program - CRAPONE: A Fortran IV Code for the Automatic Search for Local and Non-Local Optical Potential Parameters for Neutrons. CNEN Rpt. RT/FI (77) 3. The fitting procedure is described in detail in this report.

Authors: F. Fabbri, G. Fratamico, G. Reffo

Establishment: CNEN, Bologna, Italy

Nature of Problem Solved: CRAPONE is an automatic search program designed to produce neutron optical model parameters. The fitting procedure may be applied to various sets of experimental data using either local or non-local potentials.

Program Language: Fortran IV (IBM 360/175)

Program Size: Not specified

Introduction

CRAPONE employs the same optical model potentials as described in CERBERO-II (RT/FI (77) 6).

All experimental data forms that can be analyzed by CERBERO-II may be used. In addition S & P wave strength functions and scattering radii may be considered.

4. RAROMP

Name of Code: RAROMP (Regular and Reformulated Optical Model Program)

Author: G.J. Pyle

Establishment: University of Minnesota, Minneapolis, Minnesota

Present Address - Phys. Dept., Univ. of Birmingham, England.

Nature of Problem Solved: RAROMP is a general purpose search code, which performs optical model calculations using the reformulated optical model of Greenlees et al.

Program Language: FORTRAN II (CDC-6600)

Size: 32 K

Introduction

RAROMP (Regular And Reformulated Optical Model Program) is a general purpose search code which performs optical model calculations using the reformulated optical model of Greenlees, Pyle and Tang (Phys. Rev. 171, 1115 (1968) and also the standard form of the optical model. A brief discussion of the formalism was presented in section (3) of the main paper.

When the neutron and matter distributions are parameterized in terms of Woods-Saxon distributions and a Yukawa shape is used to describe the two-body potentials, the integrals are of the form:

$$I_j(r) = \frac{1}{r}\int_0^\infty \frac{x\,\rho_j(o)\left\{e^{-\beta_d|x-r|} - e^{-\beta_d(x+r)}\right\}}{1+\exp\left(\frac{x-R_j}{a_j}\right)}\,dx \qquad 4.0$$

where the subscript j refers to the neutron (n), proton (p) or matter (m) distribution.

The spin-orbit potential is given by:

$$U_s(r) = -V_s\, I_s(r), \qquad 4.1$$

where

$$I_s(r) = 2\pi\int_0^\infty G(r,x)\left\{\rho_n(x)+\rho_p(x)\right\}dx \qquad 4.2$$

The quantity G(r,x) is given by

$$G(r,x) = \frac{2x^2}{b\beta_s}\left\{\frac{x}{br}\left(e^{-\beta_s y}\left[\frac{y^2}{\beta_s}+\frac{2y}{\beta_s^2}-\frac{a}{\beta_s}+\frac{2}{\beta_s^2}\right]\right)_{\sqrt{a-b}}^{\sqrt{a+b}} + \left[\frac{e^{-\beta_s y}}{\beta_s}\right]_{\sqrt{a-b}}^{\sqrt{a+b}}\right\} \qquad 4.3$$

where

$$a = r^2 + x^2$$
$$b = 2rx \qquad 4.4$$

In Eq. (4.1) the strength V_s is left as an adjustable parameter to compensate for minor effects ignored in the model. As with the real central potential only 3 parameters of the spin-orbit potential are treated as search parameters. These are V_s, R_m and a_m, if the matter distribution is parameterized, and V_s, R_n and a_n, if the neutron distribution is parameterized.

The folding integrals for the real central potential Eq. (4.0) and the spin-orbit folding integral Eq. (4.2) involve numerical evaluation of integrals of the form,

$$I = \int_0^\infty \frac{x^n e^{-\gamma x}}{1+\exp\left(\frac{x-R}{a}\right)}\,dx \qquad 4.5$$

where n assumes the values 1, 2 and γ can take positive or negative values.

The speed and accuracy of the numerical evaluation of Eq. (4.5) can be greatly increased by expanding $\left[1+\exp\left(\frac{r-R}{a}\right)\right]^{-1}$ for parts of the range of integration, using

$$\left[1+\exp\left(\frac{r-R}{a}\right)\right]^{-1} = \sum_{m=0}^{\infty}(-1)^m e^{m\left(\frac{x-R}{a}\right)} \qquad 0 \le x \le R$$
$$= \sum_{m=0}^{\infty}(-1)^m e^{-(m+1)\left(\frac{x-R}{a}\right)} \qquad R < x \le \infty \qquad 4.6$$

Potential Options

RAROMP will carry out searches using the Regular Optical Model or the Reformulated Model.

The Optical Model Potential is given as usual as the sum of the various interacting potentials:

$$U_{op}(r) = U_c(r) + U_R(r) + i\,U_I(r) + U_s(r)\,\vec{l}\cdot\vec{\sigma} \qquad 4.7$$

Coulomb Potential

Two forms of the Coulomb potential are available:

(a) The Coulomb potential is that due to a uniformly charged sphere of radius R_c.

$$U_c(r) = \frac{Z_I Z_T e^2}{2 R_c}\left\{3 - \frac{r^2}{R_c^2}\right\} \qquad r \leq R_c$$

$$= \frac{Z_I Z_T}{r} \qquad r > R_c \qquad 4.8$$

(b) The Coulomb potential may also be taken as that due to a Woods-Saxon charge distribution of the form $\left[1 + \exp\frac{r-R_c}{a_c}\right]^{-1}$ 4.9

Imaginary Potential

The imaginary potential has the usual mixture of volume and surface parts given by

$$U_I(r) = -W_v f(r,R_I,a_I) + 4 a_I W_d \frac{d}{dr} f(r,R_I,a_I), \qquad 4.10$$

with

$$f(r,R_I,a_I) = \left[1 + \exp\frac{r-R_I}{a_I}\right]^{-1} \qquad 4.11$$

Regular Optical Model

(a) Real Potential

For the regular optical model calculations the real potential is written in the conventional form

$$U_R(r) = -V_R\left[1 + \exp\frac{r-R_R}{a_R}\right]^{-1} \qquad 4.12$$

with a radius parameter r_R defined as $R_R A^{-1/3}$.

(b) Spin-orbit potential

This is given by the usual Thomas form

$$U_s(r) = -\left(V_s + iW_s\right)\left(\frac{\hbar}{m_\pi c}\right)^2 \frac{1}{r}\frac{d}{dr} f(r,R_s,a_s) \qquad 4.13$$

with

$$f(r,R_s,a_s) = \left[1 + \exp\frac{r-R_s}{a_s}\right]^{-1} \qquad 4.14$$

radius parameter $r_s (=R_s A^{-1/3})$.

Reformulated Optical Model

(a) Real potential

For incident protons or neutrons the real potential can be written in the form

$$U_R(r) = -V_R \frac{I(r,R_n,a_n)}{I(o,R_n,a_n)}, \qquad 4.15$$

where $I(r,R_n,a_n)$ is given by

$$I(r) = \left\{I_n(r) + I_p(r)\right\} + \xi\left\{I_n(r) - I_p(r)\right\}\tau_z \qquad 4.16$$

with,

$$I_n(r) = \int \rho_n(r') V_d(|\bar{r} - \bar{r}'|)\, d\bar{r}' \qquad 4.17$$

$$I_p(r) = \int \rho_p(r') V_d(|\bar{r} - \bar{r}'|)\, d\bar{r}' \qquad 4.18$$

and τ_z has the eigen value +1 for incident protons and -1 for incident neutrons.

$$\rho_n(r) = \frac{N}{A}\rho_m(r),$$

$$\rho_p(r) = \frac{Z}{A}\rho_m(r),$$

$\rho_m(r)$ = matter density.

The code will also evaluate the real potential using the alternate form

$$U_R(r) = -\frac{V_R \; I_M(r,R_m,a_m)}{I_m(o,R_m,a_m)} \qquad 4.19$$

$$I_m(r) = \int \rho_m(r') V_d(|\bar{r}-\bar{r}'|)\, d\bar{r}. \qquad 4.20$$

Spin-orbit potential

Two forms of the spin orbit potential are possible.

For incident neutrons or protons the spin orbit potential can be of the form (eq. 2.1)

$$U_s(r) = -(V_s + iW_s)\; I_s(r,R_n,a_n) \qquad 4.21$$

with $I_s(r,R_n,a_n)$ given by equation 4.2. Note that this form of the spin-orbit potential can only be used for incident protons or neutrons and the real potential must be of the form given by 4.15. Again there are four search parameters V_S, W_S, r_n, a_n (symbols VS, WS, RN, and AN) and the parameters r_p, a_p and $\langle r^2 \rangle_S$ (symbol RSQS) are also required to evaluate 4.2.

For incident protons, neutrons or complex particles requiring a spin-orbit potential an alternate form can be used given by

$$U_S(r) = -(V_S + i\,W_S)\left(\frac{\hbar}{m_\pi c}\right)^2 \frac{1}{r}\frac{d}{dr} f_m(r,R_m,a_m), \qquad 4.22$$

with

$$f_m(r,R_m,a_m) = \frac{\rho_m(r)}{\rho_m(o)} = \frac{1}{1+\exp\left(\frac{r-R_m}{a_m}\right)} \qquad 4.23$$

5. JUPITOR

Name of Program: JUPITOR

Author: T. Tamura

Establishment: Oak Ridge National Laboratory, USA

Documentation: ORNL 4152 (1967)

Nature of Physical Problem: A coupled-channel code that may be used for incident particles of spin 0, 1/2, or 1, interacting with vibrational or rotational nuclei. Both non-adiabatic or adiabatic approximations may be performed. Up to six states can be coupled at one time. Calculates shape-elastic, total, and reaction cross sections and polarizations. (Also spin-spin interactions.)

Program Language: Fortran IV

Program Size: Approx.72K

Status: Converted for PDP-10 (overlay version), CDC 6600, IBM 360.

Introduction:

The formalism and equations necessary to describe the contents of JUPITOR are explained in detail in T. Tamura, Rev. Mod. Phys. 37, 679 (1965).

The interaction to which the incident particle is subjected is described by generalized optical model potential $V(r,\Theta,\phi)$. The potential includes spin-orbit and Coulomb interactions and has a Saxon-Woods radial dependence:

$$V(r,\theta,\phi) = -(V + iW)\,(1+e)^{-1} - 4i\,W_D\,\bar{e}\,(1+\bar{e})^{-2}$$

$$-V_{so}(\bar{\sigma}\cdot\bar{\lambda})\;(\lambda^2/ar)\;e\,(1+e)^{-2} + V_{Coul}$$

with $e = \exp\left[(r-R)/a\right]$, $\bar{e} = \exp\left[(r-\bar{R})/\bar{a}\right]$ 5.1

If R and $\bar{R}$ are taken as independent of angle, equ. 5.1 becomes the usual spherical optical model potential. R and $\bar{R}$ are, however, chosen as functions of the polar angles θ and ϕ and provide a phenomenological description of the collective nature of the target nucleus.

If the target is spherical, but able to undergo vibrations about its spherical shape, R and $\bar{R}$ become

$$\left.\begin{matrix}\bar{R}\\ R\end{matrix}\right\} = \left\{\begin{matrix}\bar{R}_o\\ R_o\end{matrix}\right\}\left(1 + \sum_{\lambda\mu} \alpha_{\lambda\mu} Y_\lambda^\mu(\theta,\phi)\right) \qquad 5.2$$

where the α_λ's are operators of rank λ and the $Y_\lambda^\mu(\theta,\phi)$ are spherical harmonics. The Boson creation and annihilation operators, $b^+_{\lambda\mu}$ and $b_{\lambda\mu}$, can be introduced and $\alpha_{\lambda\mu}$ may be written

$$\alpha_{\lambda\mu} = \left(\beta_\lambda/\hat{\lambda}\right)\left(b^+_{\lambda\mu} + (-)^\mu b_{\lambda-\mu}\right) \qquad 5.3$$

If, however, the target is permanently deformed (with axial symmetry), R and $\bar{R}$ may be expressed as

$$\left.\begin{matrix}\bar{R}\\ R\end{matrix}\right\} = \left\{\begin{matrix}\bar{R}_o\\ R_o\end{matrix}\right\}\left(1 + \sum_\lambda \beta_\lambda Y_\lambda^\circ(\theta')\right) \qquad 5.4$$

where θ' refers to the body-fixed coordinate system and the β_λ's become parameters. R_o and $\bar{R}_o$ are

$$\left.\begin{matrix}\bar{R}_o\\ R_o\end{matrix}\right\} = \left\{\begin{matrix}\bar{r}_o\\ r_o\end{matrix}\right\} A^{1/3}, \qquad 5.5$$

where r_o and $\bar{r}_o$ are parameters and A is the mass of the target.

The various possibilities afforded by JUPITOR are many and a brief description is given below. (Abbreviations used - see T. Tamura, ORNL 4152, 1967, and T. Tamura, Rev. Mod. Phys. 37, 679 (1965)).

CC = coupled-channel calculations

ACC = adiabatic coupled-channel calculations

NACC = non-adiabatic coupled-channel calculations

RFF = real form factor

CFF = complex form factor.

(i) Spin s of the projectile can be either 0, $\frac{1}{2}$, or 1 (s = 0 or $\frac{1}{2}$ for ACC).

(ii) Targets can be anything, though those with some collectivity are of primary interest. They can be either vibrational (spherical) or rotational (permanently deformed), and of either even or odd A.

(iii) When the target is deformed, either NACC or ACC can be made.

(iv) When the target is deformed, excitation of states belonging to higher (vibrational) bands can be considered. (Of course, NACC is to be used in this case.)

(v) Coulomb excitation can be included.

(vi) The form factor can be either real (RFF) or complex (CFF).

(vii) Up to six states can be coupled at one time.

(viii) Up to thirty partial waves can be coupled at one time. (Up to twenty-five partial waves, if the projectile energy becomes negative in some excited channels.)

(ix) The maximum value of the orbital angular momentum, ℓ_{max}, is 69, though it is not difficult to modify the program so as to make ℓ_{max} larger.

(x) Can compute the differential cross sections for up to 100 angles for any number of states (Up to 35 angles if a polarized beam or target is considered.). Total and reaction cross sections and s- and p-wave strength functions can also be computed (Only differential and total cross sections for ACC.).

(xi) If the projectile is a neutron, its energy in some excited channels can be negative.

(xii) Automatic plot of the theoretical and experimental differential cross sections and polarizations can be made. (Up to six states for cross sections and up to two states for polarizations.)

STATISTICAL THEORY OF NEUTRON NUCLEAR REACTIONS*

P.A. MOLDAUER
Argonne National Laboratory,
Argonne, IL,
United States of America

ABSTRACT The statistical theory of average neutron nucleus reaction cross sections is reviewed with emphasis on the justification of the Hauser Feshbach formula and its modifications for situations including isolated compound nucleus resonances, overlapping and interfering resonances, the competition of compound and direct reactions, and continuous treatment of residual nuclear states.

1. STATISTICS

We shall review theories of certain statistical properties of neutron reaction cross section data. Statistics is a method for the partial description of sets of data. Specifically it relies on averages of the data and of functions of the data. If $\{\sigma_i\}$, 1, 2, ... N is a set of cross section data, then one familiar set of statistics is the average $\langle\sigma\rangle = \Sigma_i\sigma_i/N$ and the central moments $m_\nu(\sigma) = \Sigma_i(\sigma_i - \langle\sigma\rangle)^\nu/N$ where $m_2(\sigma)$ is the square of variance s of $\{\sigma_i\}$. For two sets of data $\{\sigma_i\}$, $\{\tau_i\}$ one has a matrix of central moments $m_{\mu\nu}(\sigma,\tau) = \Sigma_i(\sigma_i - \langle\sigma\rangle)^\mu(\tau_i - \langle\tau\rangle)^\nu/N$ where m_{11} is the covariance of σ and τ and the correlation of σ and τ is $\rho = m_{11}(\sigma,\tau)/(s(\sigma)s(\tau))$. One obtains the autocovariance and the autocorrelation ρ_n for a single set of data $\{\sigma\}$ by stubstituting in the above expression σ_{i+n} for τ_i. These statistics are, of course, also applied to continuous variables by substituting integrals for the summations.

The basic statistics that we will be interested in will be the energy averages of fluctuating neutron cross sections. Fig. 1 shows an example of such a cross section and its energy average. Clearly, the value of an energy averaged cross section depends upon the averaging interval, both its size and its location. Each point in the average cross section curve in Fig. 1 represents the average obtained over an interval of 200 keV which is centered on the point in question. This is how we interpret an energy-dependent average cross section. Clearly one can discuss also the variance of such a cross section curve, its autocorrelation, or other statistics which describe the fluctuations about the average. In addition one can discuss the correlation between different cross sections, such as the elastic and inelastic cross section, or the cross sections for scattering at different angles, etc. These fluctuation statistics are, however, of minor interest in applications.

Reaction theory describes the complicated energy fluctuations of cross sections in terms of discrete sets of parameters, the "resonance" or "pole" parameters. The aims of statistical theory are to relate the average cross sections and their fluctuations to the statistics of resonance or pole parameters, and to further relate the latter to physical models and to basic principles. Some of these basic principles on the distributions and correlations of resonance spacing and the distributions of partial resonance widths were already discussed in the lectures of Sec. II.6. And the relations of resonance statistics to physical models were discussed in Sec. III on the optical model. We will briefly review these matters as we need to.

2. NOTATION

A neutron nuclear reaction proceeds by the interaction of an incident neutron of a certain energy with a target nucleus (Z,A) which together comprise a compound system (Z,A+1). Following the interaction the system breaks up into one of several possible reaction channels consisting of one, two, or more nuclei or nuclides having various internal and relative states. A Roman lower case subscript a,b,c, etc. will be used to label a specific such channel, that is the fragments present, their internal states, and their relative states. In the case of a two-product channel, e.g., neutron scattering, the channel index incorporates the relative orbital angular momentum ℓ of the fragments, the total angular momentum $j = \ell + s$ of one (usually the lighter) fragment, where s is that fragment's spin angular momentum and the sum is, of course, the quantitized vector sum, and the total angular momentum $J = j + I$ where I is the spin angular momentum of the heavier fragment. The relative energy of frag-

*This work supported by the U.S. Department of Energy.

ments is not included in the channel index as it will usually be the parameter to be averaged over. The Greek subscript γ will be reserved for gamma-ray channels in which all possible gamma rays are lumped together. The Greek subscripts α,β will be reserved to indicate the alternatives specifying only the fragments and their internal states.

States of the compound system (Z,A+1) will be labeled by lower case Greek subscripts μ,ν, etc. These incorporate all internal quantum numbers including the total angular momentum J and parity π.

3. ISOLATED RESONANCES [1]

When a low energy neutron interacts with a nucleus, one of two types of things can happen. Either the neutron is scattered elastically without involving the internal degrees of freedom of the target nucleus. This is potential scattering. Or the neutron is absorbed by the target, forming a compound system in one of a number of metastable resonance states. These are states consisting primarily of bound single particle configurations whose total energy is above the neutron threshold at the energy of the scattering system. However, because of its coupling to the neutron scattering channel and possible other open channels, having positive channel energies, these resonance states do decay with a mean lifetime which is τ_μ for the μth such state. The inverse of this lifetime $1/\tau_\mu \equiv 2\pi\Gamma_\mu/h$ is the probability of decay of the state per unit time. Here h is Planck's constant. The width Γ_μ is the energy uncertainty of the μth state in accordance with Heisenberg's uncertainty principle and it is proportional to the decay probability per unit time of the μth state. If this state can decay into any one of several channels a,b,c, etc., then there will be decay probabilities proportional to partial widths $\Gamma_{\mu a}$, $\Gamma_{\mu b}$, $\Gamma_{\mu c}$, etc. for each of these channels so that $\Gamma_\mu = \Gamma_{\mu a} + \Gamma_{\mu b} + \Gamma_{\mu c} + \cdots$

By reciprocity, the probability of formation of the compound state μ by absorption of an incident neutron in, say, channel a is also proportional to $\Gamma_{\mu a}$, and the relative probability for decay into channel b is clearly $\Gamma_{\mu b}/\Gamma_\mu$. The cross section for the reaction proceeding from incident channel a to exit channel b through the compound state μ is then proportional to the product of $\Gamma_{\mu a}$ and $\Gamma_{\mu b}/\Gamma_\mu$ and is in units of π/k_a^2

$$\sigma_{ab}^{(\mu)} \cong 2\pi\Gamma_{\mu a}\Gamma_{\mu b}/\Gamma_\mu. \tag{3.1}$$

From this it is clear that the average compound nuclear cross section for the reaction a,b within the energy interval Δ is

$$\bar{\sigma}_{ab}^{c.n.} = \frac{2\pi}{D}\left\langle \frac{\Gamma_{\mu a}\Gamma_{\mu b}}{\Gamma_\mu} \right\rangle_{\mu\in\Delta} \tag{3.2}$$

Where D is the mean energy spacing of compound states with correct J and π in Δ and the bracket signifies the average over compound states within Δ. The average absorption cross section into the compound system from channel a is called the transmission coefficient T_a.

$$\bar{\sigma}_a^{c.n.} = \Sigma_b \bar{\sigma}_{ab}^{c.n.} = \frac{2\pi}{D}\left\langle \Gamma_{\mu a} \right\rangle_\mu \equiv T_a. \tag{3.3}$$

These transmission coefficients are specified by various physical models for different types of channels, the optical model for neutron, proton and other nuclear channels, and corresponding models for fission and capture channels. These models are discussed elsewhere in these lectures. We shall return to the optical model later.

With the definition (3.3), Eq. (3.2) can be rewritten as

$$\bar{\sigma}_{ab}^{c.n.} = \sigma_{ab}^{H.F.} W_{ab} \tag{3.4}$$

where the well-known Hauser-Feshbach formula

$$\sigma_{ab}^{H.F.} \cong T_a T_b / \Sigma_c T_c \tag{3.5}$$

is completely specified by the transmission coefficients of all open channels, and hence by the physical models for these channels. The second factor in (3.4) is the width fluctuation correction

$$W_{ab} = \left\langle \frac{\Gamma_{\mu a}\Gamma_{\mu b}}{\Gamma_\mu} \right\rangle \Big/ \frac{\langle \Gamma_{\mu a} \rangle \langle \Gamma_{\mu b} \rangle}{\langle \Gamma_\mu \rangle} \tag{3.6}$$

This factor depends upon the distributions and correlations of the partial widths and we shall discuss it further in the next section.

The total average reaction cross section consists of the sum of the potential or direct scattering cross section and the average compound cross section. In the absence of direct reactions, which will be treated later, the only potential cross section is the shape elastic contribution

$$\bar{\sigma}_{ab} = \delta_{ab}\sigma_a^{s.e.} + \bar{\sigma}_{ab}^{c.n.}. \tag{3.6}$$

Here $\sigma_a^{s.e.} = \sigma_{aa}^{dir.}$ is also determined by the optical model, as will be seen below.

4. WIDTH FLUCTUATION CORRECTION

It has become well established that the distribution of partial widths for a channel as defined in Sec. 2 is given by the Porter-Thomas distribution law. According to it the probability that for some state μ the quantity $\Gamma_{\mu a}/\langle\Gamma_{\mu a}\rangle_\mu$ has a value between x and x + dx is

$$F_{P.T.}(x)\,dx = (2\pi x)^{-\frac{1}{2}}e^{-\frac{1}{2}x}dx. \tag{4.1}$$

This Porter-Thomas distribution belongs to the class of chi-squared distributions with ν degrees of freedom

$$F_\nu(x) = \frac{(\frac{1}{2}\nu)^{\frac{1}{2}\nu}}{\Gamma(\frac{1}{2}\nu)}\,x^{\frac{1}{2}\nu-1}\,e^{-\frac{1}{2}\nu x} \tag{4.2}$$

where $F_{P.T.}(x) = F_1(x)$ is the chi-squared distribution with one degree of freedom. In Eq. (4.2) ν can have any real positive value. If the states of a given J, π can decay into n channels, all having the same $\langle\Gamma_{\mu a_i}\rangle$, then we can consider the partial widths for decay into the alternative α consisting of any one of these n channels. Clearly $\langle\Gamma_{\mu\alpha}\rangle = n\langle\Gamma_{\mu\alpha_i}\rangle$ and the $\Gamma_{\mu\alpha}$ are distributed according to the chi-squared distribution with n degrees of freedom F_n. For example, if neutrons are scattered by a $\frac{1}{2}$+ target nucleus, then compound states of total angular momentum and parity 1- can be formed by the absorption of either a $p_{\frac{1}{2}}$ or a $p_{3/2}$ neutron. If the average partial widths for these two channels were the same, then the total neutron widths for these 1- states would be distributed according to the chi-squared distribution with two degrees of freedom $F_2(x) = \frac{1}{2}e^{-\frac{1}{2}x}$. If the transmission coefficients for $p_{\frac{1}{2}}$ and $p_{3/2}$ neutrons were not equal, the neutron widths of 1- states would not have exactly any chi-squared distribution but could still be well approximated by $F_\nu(x)$ with ν somewhere between 1 and 2.

Analyses of fission widths have shown that their distributions can be approximated by chi-squared distributions with between one and four degrees of freedom, depending on isotope and J. The gamma-ray radiation alternative consists generally of a large number of possible gamma-ray transition channels and is therefore best represented by a chi-squared distribution of perhaps 10 or 20 or more. Since such distributions involve only very small fluctuations about the average value, the total radiation width is often assumed not to be fluctuating at all.

From Eq. (4.2) it follows that if x is distributed according to $F_\nu(x)$ then

$$\langle x^k\rangle = \frac{\Gamma(k + \frac{1}{2}\nu)}{(\frac{1}{2}\nu)^k\Gamma(\frac{1}{2}\nu)} \tag{4.3}$$

and the variance of x is $(2/\nu)^{\frac{1}{2}}$.

It is useful to factor the width fluctuation correction into

$$W_{ab} = G_{ab}C_{ab}, \tag{4.4}$$

where

$$G_{ab} = \frac{\langle\Gamma_{\mu a}\Gamma_{\mu b}/\Gamma_\mu\rangle}{\langle\Gamma_{\mu a}\Gamma_{\mu b}\rangle/\langle\Gamma_\mu\rangle} \tag{4.5}$$

and

$$C_{ab} = \frac{\langle\Gamma_{\mu a}\Gamma_{\mu b}\rangle}{\langle\Gamma_{\mu a}\rangle\langle\Gamma_{\mu b}\rangle}. \tag{4.6}$$

Here G_{ab} arises from the correlation between $\Gamma_{\mu a}\Gamma_{\mu b}$ and Γ_μ^{-1} which is due to the fact that both contain $\Gamma_{\mu a}$ and $\Gamma_{\mu b}$. It is easily shown that if the $\Gamma_{\mu c}$ are distributed according to the chi-squared distribution with ν_c degrees of freedom, then G_{ab} can be expressed as the following single integral

$$G_{ab} = \int_0^\infty dt \prod_c \left(1 + \frac{2}{\nu_c}\frac{\langle\Gamma_{\mu c}\rangle}{\langle\Gamma_\mu\rangle}t\right)^{-(\frac{1}{2}\nu_c+\delta_{ac}+\delta_{bc})}. \tag{4.7}$$

A capture channel which is assumed to have a non-fluctuating partial width Γ_γ will contribute a factor $\exp(-t\Gamma_\gamma/\langle\Gamma_\mu\rangle)$ to the integral of Eq. (4.7). Some examples of numerical values are shown in Fig. 2. The factor C_{ab} which arises from correlations between the partial widths of channels a and b for chi-squared distributions can be expressed in terms of the partial

widths correlation coefficient ρ_{ab}

$$C_{ab} = 1 + \frac{2\rho_{ab}}{(\nu_a \nu_b)^{\frac{1}{2}}} . \qquad (4.8)$$

In the absence of a direct reaction between channels a and b, ρ_{ab} is expected to vanish for $a \neq b$ and of course $\rho_{aa} = 1$. Therefore

$$C_{ab} = 1 + 2\delta_{ab}/\nu_a \qquad \text{(no direct reactions.)} \qquad (4.9)$$

The case of direct reactions will be discussed in greater detail later.

The factor C_{ab} is seen to enhance the average elastic compound cross section by a factor of 3 for the case of the Porter-Thomas distribution and by a factor of 2 for the case of the $\nu = 2$ exponential distribution. This enhancement is compensated by a reduction of all cross sections due to the factor G_{ab} of Eq. (4.7) so that the sum (3.3) is preserved.

It is, however, also possible for G_{ab} to be greater than unity [2]. This will occur where the transmission factors for channels a and b are both very small (weak cross section) and when the total width is dominated by one of a very few competing channels. In that case it is useful to factor G_{ab} once more into

$$G_{ab} = \frac{\langle \Gamma_{\mu a}\Gamma_{\mu b}\Gamma_\mu^{-1}\rangle}{\langle \Gamma_{\mu a}\Gamma_{\mu b}\rangle\langle\Gamma_\mu^{-1}\rangle} \times \langle\Gamma_\mu^{-1}\rangle\langle\Gamma_\mu\rangle . \qquad (4.10)$$

Here the first factor is close to unity because $\Gamma_{\mu a}$ and $\Gamma_{\mu b}$ do not contribute appreciably to the magnitude of Γ_μ^{-1}. The second factor can be evaluated

$$\langle\Gamma_\mu^{-1}\rangle\langle\Gamma_\mu\rangle = \frac{1}{1 - 2/\nu_t} \quad \text{for } \nu_t > 2 \qquad (4.11)$$

where Γ_μ is distributed according to F_{ν_t}. When $\nu_t \leq 2$ this factor diverges, though of course G_{ab} will always be finite. It can be seen that large enhancements of small cross sections are possible in this way. Examples of calculations of this effect are shown in Fig. 3.

5. S-MATRIX THEORY

The discussion of Sec. 3 is reliable only in the case of very low neutron energies, typically up to several tens of keV. With increasing energy, neutron partial widths increase and the number of open channels also increases, while the level spacing decreases. As a result at higher energies the total widths become comparable to the spacings and the different resonances begin to interfere with one another. A neutron can then be absorbed coherently by two or more resonance states and this situation must be discussed quantum mechanically.

In quantum mechanics, the scattering system is described by the Schrödinger equation

$$(H - E)\Psi = 0 \qquad (5.1)$$

where H is the Hermitean Hamiltonian describing the interactions of the system, E is the energy, and the wave function Ψ describes all properties. We are interested in scattering solutions of the Schrödinger equation with boundary conditions at infinity which specify an incoming spherical wave of unit flux I_a in channel a only and outgoing waves of unit flux O_c in all open channels c. The asymptotic wave function for this boundary condition has the form

$$\Psi_a^{as.} = I_a - \Sigma_c S_{ac} O_c \qquad (5.2)$$

where the S-matrix components S_{ac} give the amplitude for transitions from channel a to channel c. From time reversal invariance of H it follows that S is symmetric

$$S_{ab} = S_{ba}, \quad S = \tilde{S} \qquad (5.3)$$

where $\tilde{S}$ is the transpose of S.

For a general asymptotic wave $\Psi^{as.} = \Sigma_a x_a \Psi_a^{as.}$ the incident flux is $\Sigma_a |x_a|^2$. The total outgoing flux is $\Sigma_{ab} x_a^* S_{ca}^* S_{cb} x_b$ which must equal the incident flux if no flux is absorbed or created. This leads to the unitarity property of S

$$S_{ca}^* S_{cb} = \delta_{ab}, \quad S^\dagger S = 1 \qquad (5.4)$$

A third property of the S-matrix follows from the causality principle. According to it the S-matrix considered as a function of energy has an analytic continuation without singularities in the upper half plane. This requirement can be understood by remembering that the time dependence of the wave function has the form $\exp(-iEt/\hbar)$ where E is the energy of the

system. A complex energy state at a singularity of the S-matrix will have an exponentially growing time dependence for a singularity in the upper half plane and an exponentially decaying behavior in the lower half plane. The causality principle requires us to exclude exponentially growing states.

In the absence of any scattering $S_{ac} = \delta_{ac}$ and $\psi_a^{as.} = I_a - O_a$. Then we can write (5.2) in the general case as

$$\psi_a^{as.} = (I_a - O_a) - \Sigma_c (S_{ac} - \delta_{ac}) O_c$$

where the first parentheses represent the unscattered wave and the sum represents the scattered wave. The cross section for the process $a \to b$ is now just the scattered flux in channel b for incident unit flux in channel a which in our units is

$$\sigma_{ab} = |\delta_{ab} - S_{ab}|^2. \tag{5.5}$$

I will generally discuss this cross section (5.5) because it is the simplest example of the kind of bilinear expression in the S-matrix elements that occurs in all observable cross sections. On the other hand, it is important to remember that the expression (5.5) which represents a reaction proceeding from one particular partial wave to another is seldom of practical interest. The quantities that are of practical interest are the following.

The differential cross section for the process originating with an incident wave in the alternative α and a scattered wave in the differential solid angle $d\Omega$ at scattering angle θ in the alternative β is given by

$$\frac{d\sigma_{\alpha\beta}(\theta)}{d\Omega} = \frac{1}{4\pi} \Sigma_L B_L P_L(\cos\theta) \tag{5.6a}$$

where the P_L are the Legendre polynomials of integer order L. For the case where the projectile in both alternatives α or β has either spin 0 or spin ½, B_L can be written

$$B_L = \left(\frac{\hat{L}}{\hat{I}_\alpha \hat{s}_\alpha}\right)^2 \sum \hat{j}^2 \hat{j}'^2 A(\alpha,L) A(\beta,L) \left(\delta_{\ell_\alpha \ell_\beta} \delta_{j_\alpha j_\beta} - S^{J\Pi}_{\ell_\alpha j_\alpha, \ell_\beta j_\beta}\right)$$

$$\times \left(\delta_{\ell'_\alpha \ell'_\beta} \delta_{j'_\alpha j'_\beta} - S^{J'\Pi'*}_{\ell'_\alpha j'_\alpha, \ell'_\beta j'_\beta}\right) \tag{5.6b}$$

and

$$A(\alpha,L) = (-1)^{s_\alpha + I_\alpha + j_\alpha + j'_\alpha} \hat{j}_\alpha \hat{j}'_\alpha \begin{pmatrix} j'_\alpha & j_\alpha & L \\ s_\alpha & -s_\alpha & 0 \end{pmatrix} \begin{Bmatrix} j'_\alpha & j_\alpha & L \\ J & J' & I_\alpha \end{Bmatrix} \tag{5.6c}$$

and the karet means $\hat{k} = (2k+1)^{\frac{1}{2}}$. The round bracket in (5.6c) is a Wigner 3j coefficient, the curly bracket is a 6j coefficient, and the sum in (5.6b) is over total angular momenta J,J' and parities Π,Π' as well as over all four orbital angular momenta ℓ and all four projectile angular momenta j, primed, unprimed, α, and β. s_α and I_α are the projectile and target spins in α.

Integrating Eq. (5.6) over all solid angles, we obtain the integrated cross section

$$\sigma_{\alpha\beta} = \Sigma_{J,\Pi,\ell_\alpha,j_\alpha,\ell_\beta,j_\beta} g_J \left|\delta_{\ell_\alpha \ell_\beta} \delta_{j_\alpha j_\beta} - S^{J,\Pi}_{\ell_\alpha j_\alpha, \ell_\beta j_\beta}\right|^2 \tag{5.7}$$

which is a sum over terms (5.5) with coefficients

$$g_J = (\hat{J}/\hat{I}_\alpha \hat{s}_\alpha)^2. \tag{5.7}$$

Summing (5.7) over all β yields the total cross section

$$\sigma_\alpha^{tot.} = \Sigma_{J,\Pi,\ell_\alpha,j_\alpha} 2 g_J \left(1 - \mathrm{Re} S^{J\Pi}_{\ell_\alpha j_\alpha, \ell_\alpha, j_\alpha}\right) \tag{5.9}$$

which depends linearly on the real part of the diagonal S-matrix elements.

6. S-MATRIX PARAMETERS AND THE OPTICAL MODEL

The energy variations of the S-matrix elements arise from two types of singularities in the finite energy plane: Branch points at the thresholds of channels and poles or other singularities in the lower half plane. The threshold branch points won't concern us here. We can always arrange all branch cuts so that they do not fall along our averaging interval. Also the energy dependences produced by these branch points are generally very weak. Only in the immediate vicinity of an s or p-wave neutron threshold is it generally necessary to be cautious. Similar statements apply to the contribution of entire functions to the S-matrix elements. Among singularities in the lower half plane, single poles are of greatest interest to us because, as we shall see, they correspond to the compound

state resonances of Sec. 3. Accordingly we write the S-matrix for a given J, Π in the form of the pole expansion

$$S_{ab} = S^B_{ab} + S^P_{ab}$$

$$S^P_{ab} = -i \sum_\mu \frac{g_{\mu a} g_{\mu b}}{E - E_\mu + \frac{1}{2} i \Gamma_\mu} . \qquad (6.1)$$

This formula requires some discussion. The justification for the factorized form of the pole residues will emerge later. The background term S^B_{ab} is smoothly varying in the energy interval of interest and arises from distant singularities as well as the contribution of entire functions. Generally we shall assume that S^B can be approximated by an energy-independent constant matrix in our energy interval. For purposes of statistical analysis it will be useful to be able to consider the poles of S^P to consist of an infinite ergodic sequence extending from $\mathrm{Re}E = -\infty$ to $+\infty$ with constant statistical properties, i.e. constant averages, distributions and correlations of the pole parameters E_μ, Γ_μ and $g_{\mu c}$. This can be done by defining a region in the energy plane such that poles within that region (near poles) contribute to the energy variation in our interval, but singularities outside that region (distant poles) do not contribute significantly to that energy variation. Then we define a statistical S-matrix which has the form (6.1), where the pole parameters form an infinite ergodic extension of the actual parameters of the near poles. Then S^B contains the contribution within the energy interval of interest of the difference between the actual distant poles and the distant poles belonging to the ergodic sequence. In what follows I shall always assume such a statistical S-matrix [3].

We first confirm that the S-matrix (6.1) yields isolated resonances as in Sec. 3. Considering only the simplest situation where $S^B_{ab} = \delta_{ab}$, we obtain from Eqs. (5.5) and (6.1) for the μth isolated resonance

$$\sigma^{(\mu)}_{ab}(E) = \frac{|g_{\mu a}|^2 |g_{\mu b}|^2}{(E - E_\mu)^2 + \frac{1}{4}\Gamma^2_\mu} , \qquad a \neq b$$

and integrating this over energy the total contribution of the μth resonance to the cross section is

$$\sigma^{(\mu)}_{ab} = 2\pi |g_{\mu a}|^2 |g_{\mu b}|^2 / \Gamma_\mu$$

which by comparison with Eq. (3.1) yields

$$\Gamma_{\mu a} = |g_{\mu a}|^2, \quad \Gamma_{\mu b} = |g_{\mu b}|^2.$$

It is also easily verified that this identification with $\Gamma_\mu = \Gamma_{\mu a} + \Gamma_{\mu b} + \ldots$ guarantees the unitarity of the S-matrix when only a single resonance term is included.

When more than one resonance term is included in the sum of Eq. (6.1), and in particular when the widths of such resonances are comparable or greater than their spacing, the conditions which unitarity of S imposes on all the resonance parameters become exceedingly complex. We return to that problem later. Of course the S-matrix of Eq. 6.1 is symmetric provided S^B is symmetric and it is causal if all Γ_μ are non-negative.

In order to calculate the average cross sections from the S-matrix (6.1) we write

$$S = \overline{S} + S^{f\ell} \qquad (6.2)$$

where $\overline{S}$ is the energy averaged S-matrix and since we regard S^B as constant we have

$$\overline{S} = S^B + \overline{S^P}$$

$$S^{f\ell} = S^P - \overline{S^P} \qquad (6.3)$$

and averaging Eq. (5.5) we have

$$\overline{\sigma}_{ab} = \sigma^{\mathrm{dir.}}_{ab} + \sigma^{f\ell}_{ab} \qquad (6.4)$$

where

$$\sigma^{\mathrm{dir.}}_{ab} = |\delta_{ab} - \overline{S}_{ab}|^2 \qquad (6.5)$$

$$\sigma^{f\ell}_{ab} = \overline{|S^{f\ell}_{ab}|^2}. \qquad (6.6)$$

The problem has evidently been split into two parts, finding the average S-matrix for Eq. (6.5) and finding the average absolute square of $S^{f\ell}$ for Eq. (6.6).

Considering first the problem of the average S-matrix we have from Eqs. (6.3) and (6.1)

$$\bar{S}^{P}_{ab} = -\frac{\pi}{D}\langle g_{\mu a} g_{\mu b}\rangle_{\mu} \tag{6.7}$$

where now D is the mean spacing of the E_μ and the bracket $\langle\ \rangle_\mu$ indicates an average with respect to μ. We now demonstrate a result [4] about $\bar{S}^{P}$ by means of integration around the two contours in Fig. 4. The contour in Fig. 4a encloses no singularities and therefore the integral of S(E) around this contour vanishes. If we assume that on the average the contributions from the two vertical members of the contour cancel and that S(E + iW) on the upper horizontal member is sufficiently constant for sufficiently large W, then we have

$$\bar{S} = S(E + iW) \tag{6.8}$$

where in fact W is of order of the averaging interval for $\bar{S}$. The contour of Fig. 4b encloses the poles in the interval ΔE. Assuming again that the contributions from the vertical members cancel, we have

$$2\pi\Sigma_\mu g_{\mu a} g_{\mu b} = \Delta E[S_{ab}(E - iW) - S_{ab}(E + iW)],$$

which together with the analytic continuation of the unitarity relation

$$S(E^*) = S^{*-1}(E),$$

gives using Eq. (6.7)

$$\bar{S}^{P} = \tfrac{1}{2}(\bar{S} - \bar{S}^{*-1}), \tag{6.9a}$$

from which

$$S^{B} = \tfrac{1}{2}(\bar{S} + \bar{S}^{*-1}). \tag{6.9b}$$

This allows us to express each part of $\bar{S}$ in Eq. (6.7) in terms of $\bar{S}$ itself.

Next we note that Eq. (6.5) looks just like the cross section formula (5.5). We may suppose therefore that there exists an interaction Hamiltonian $H^{O.M.}$ that gives rise to $\bar{S}$ in the same way that H of Eq. (5.1) gives rise to S. This optical model Hamiltonian $H^{O.M.}$ produces then the direct cross section $\sigma^{dir.}$ in the same way that H produces σ. Provided the fluctuation cross section $\sigma^{f\ell}$ does not vanish, $\bar{S}$ cannot exhaust the incident flux and is therefore non-unitary and hence $H^{O.M.}$ must be non-Hermitean, causing absorption of flux. Subtracting

$$\bar{\sigma}^{tot}_{a} = 2(1 - \mathrm{Re}\bar{S}_{aa}) \tag{6.10}$$

from the sum over b of Eq. (6.6) we find that the unitarity defect of $\bar{S}$ gives

$$1 - \Sigma_b|\bar{S}_{ab}|^2 = \Sigma_b\sigma^{f\ell}_{ab} \equiv T_a. \tag{6.11}$$

By the unitarity of S, the optical model transmission coefficients T_a cannot exceed unity

$$T_a \leq 1 \qquad \text{(unitarity)}. \tag{6.12a}$$

Similarly causality, which limits absorption into decaying states only, requires that $\bar{S}$ be absorptive rather than emissive, thus limiting T_a to be positive

$$T_a \geq 0 \qquad \text{(causality)}. \tag{6.12b}$$

For the present we will restrict ourselves to the case where $\bar{S}$ is diagonal. Then the optical model is a separate scattering model in each channel a with an absorptive complex potential. Then there are also no direct reactions $\sigma^{dir.}_{ab}$, only an elastic potential scattering cross section $\sigma^{dir.}_{aa} = \sigma^{s.e.}_{a}$ and

$$T_a = 1 - |\bar{S}_{aa}|^2, \qquad (\bar{S}\ \text{diagonal}). \tag{6.13}$$

From this and Eqs. (6.7) and (6.8) we have [4]

$$2|\bar{S}^{P}_{aa}| = \frac{2\pi}{D}|\langle g^2_{\mu a}\rangle| = T_a/\sqrt{1 - T_a}. \tag{6.14}$$

Another relationship valid for diagonal $\bar{S}$ is

$$\frac{2\pi}{D}\langle\Gamma_{\mu a}\rangle = -\ln(1 - T_a). \tag{6.15}$$

For the isolated resonance limit Eqs. (6.14) and (6.15) reduce to

$$\frac{2\pi|\langle g^2_{\mu a}\rangle|}{D} = \frac{2\pi\langle\Gamma_{\mu a}\rangle}{D} = T_a, \qquad (T \ll 1) \tag{6.16}$$

which verifies Eq. (3.3).

We give the proof of Eq. (6.15) in the form given by Simonius [5]. Since S is unitary, det S is unimodular and since it is assumed to have only simple poles and the pole residues factor, forming a rank 1 matrix, we can write it in the form

$$\det S = e^{2i\phi}\prod_\mu \frac{E - E_\mu - \frac{1}{2}i\Gamma_\mu}{E - E_\mu + \frac{1}{2}i\Gamma_\mu}$$

then to first order in the inverse averaging interval W^{-1}

$$\ln \det\langle S\rangle = \ln \det S(E + iW) = \Sigma_\mu \frac{-i\Gamma_\mu}{E - E_\mu + iW} + 2i\phi$$

$$= -\frac{\pi}{D}\langle \Gamma_\mu \rangle - i\left(\Sigma_\mu \frac{\Gamma_\mu(E - E_\mu)}{(E - E_\mu)^2 + W^2} - 2\phi\right).$$

The last sum vanishes for the case of the statistical S-matrix because the terms are odd in $(E - E_\mu)$ and from the real part of this equation the channel sum of Eq. (6.15) follows.

Eqs. (6.11), (6.14) and (6.15) relate averages of S-matrix parameters to the optical model. To evaluate the fluctuation cross section requires also knowledge about the distributions of these parameters. We now turn to this question.

7. R-MATRIX THEORY

The unitarity condition imposes severe restrictions on the S-matrix parameters. This can be seen from the fact that a unitary symmetric matrix has only half as many independent components as a general complex symmetric matrix. Since S(E) must be unitary for each value of the energy E and since some Γ/D resonance terms contribute to S at each energy, it is clear that unitarity must impose complicated correlations upon the resonance parameters. One way of avoiding this difficulty is by defining the S-matrix in terms of R-matrix states. The R-matrix states are solutions of the Schrödinger equation (5.1), subject to a boundary condition at the nuclear surface so that the solutions are stationary, real states ϕ_μ with real energies E_μ. The real symmetric R-matrix formed with these states is

$$R_{ab} = R^B_{ab} + \Sigma_\mu \frac{\gamma_{\mu a}\gamma_{\mu b}}{E - E_\mu} \qquad (7.1)$$

where

$$\gamma_{\mu a} = \int_S ds \psi_a^* \phi_\mu$$

is the real overlap on the nuclear surface of the solution ϕ_μ with the channel wave function ψ_a. The background R-matrix R^B is assumed to be constant in a statistical R-matrix in the same way that S^B was constant in the statistical S-matrix.

It is generally expected that the statistical distributions of the E_μ and the $\gamma_{\mu a}$ are represented by the distributions of the eigenvalues and the eigenvectors of the orthogonal matrix ensemble as discussed in Sec. II.6. Therefore the spacings of the E_μ follow the Wigner distribution and the $\gamma_{\mu a}$ are normally distributed with zero mean for varying state index μ and given channel a. The $\gamma_{\mu a}$ for different channels are expected to be statistically independent.

A relation between the R and the S-matrices is obtained by expanding the solution of the Schrödinger equation with scattering boundary conditions (5.2) in terms of the R-matrix states with boundary conditions at the nuclear surface. This expansion inside the nuclear surface is then fitted to the known channel wave functions in the exterior. In this procedure the channel wave functions are described by channel phase shift χ_c and by channel shift and penetration factors S_c^0 and P_c. These make up the two complex diagonal channel matrices

$$\Omega = e^{-i\chi}, \qquad L^0 = S^0 + iP. \qquad (7.2)$$

With the help of these the relationship between R and S is expressed by the following channel matrix equation

$$S = \Omega P^{\frac{1}{2}}(1 - RL^0)^{-1}(1 - RL^{0*})P^{-\frac{1}{2}}\Omega \qquad (7.3)$$

We can establish the connection between the R-matrix parameter statistics and the optical model by evaluating Eq. (7.3) at the energy E + iW and assuming Ω and L^0 to be constant within the averaging interval W. Then we get for diagonal $\overline{S}$

$$\bar{S}_{cc} = e^{-2i\chi_c} \frac{1 - L_c^{0*}\tilde{R}_{cc}}{1 - L_c^{0}\tilde{R}_{cc}} \tag{7.4}$$

where

$$\tilde{R}_{cc} \equiv R_{cc}(E + iW) = R^B_{cc} + i\pi \frac{\langle \gamma^2_{\mu c} \rangle_\mu}{D} \tag{7.5}$$

and where D is the mean spacing of R-matrix states E_μ. Since χ_c and L_c^0 are known functions of the energy in channel c, Eqs. (7.4) and (7.5) uniquely determine the two statistical R-matrix parameters R^B_{cc} and $\langle \gamma_{\mu c}^2 \rangle / D$ in terms of the real and imaginary parts of the optical model S-matrix $\bar{S}_{cc}$. This, together with the statistical assumptions discussed above, and an appropriate choice of the level density D makes it possible to construct a unitary statistical S-matrix and cross sections from the optical models for any number of competing channels with arbitrarily large values of Γ/D.

The steps in such a procedure are outlined in Fig. 5. First the Schrödinger equations with the optical model potentials are integrated to give the optical model S-matrices $\bar{S}_{cc}$ in all channels. Then Eqs. (7.4) and (7.5) are solved for R^B_{cc} and $\langle \gamma_{\mu c}^2 \rangle / D$ for all channels. Then R-matrix parameters E_μ and $\gamma_{\mu c}$ are selected by a random number generator, so as to agree with the above value of $\langle \gamma_{\mu c}^2 \rangle / D$ and to yield the appropriate level density and distribution laws. From these parameters an energy dependent R-matrix is constructed, using Eq. (7.1) from which our energy dependent S-matrix is calculated using Eq. (7.3). Energy-dependent cross sections are then calculated using Eqs. (5.5) to (5.9). These energy-dependent cross sections can then be compared with experimental high energy resolution measurements, or they can be averaged and statistically analyzed to compare with theoretical predictions. A computer program STASIG has been written to perform such calculations [6]. Fig. 6 shows an example of differing cross section fluctuations obtained with two optical models which yield equivalent average total cross sections.

With the help of the R-matrix formalism it is also possible to determine numerically the pole parameters E_μ and $g_{\mu a}$ of a unitary S-matrix. This is done with the aid of the level matrix L with components

$$L_{\mu\nu} = E_\mu \delta_{\mu\nu} - \Sigma_{ab} \gamma_{\mu a} \left[L^0 (1 - R^B L^0)^{-1} \right]_{ab} \gamma_{\nu b} \tag{7.6}$$

whose eigenvalues are the S-matrix poles $E_\mu - \frac{1}{2} i\Gamma_\mu$ and whose eigenvectors $T_\nu^{(\mu)}$ specify the S-matrix pole amplitudes by

$$g_{\mu a} = e^{-i\chi_a} \; 2P_a \, \Sigma_{\nu,b} T_\nu^{(\mu)} \left[(1 - R^B L^0)^{-1} \right]_{ab} \gamma_{\nu b} \, . \tag{7.7}$$

One important parameter that arises in the level matrix formalism is the level normalization

$$N_\mu = \Sigma_\nu |T_\nu^{(\mu)}|^2 \geq 1 \tag{7.8}$$

which enters into a relationship between the pole width Γ_μ and the pole amplitudes $g_{\mu a}$

$$\Gamma_\mu = \Sigma_a |g_{\mu a}|^2 / N_\mu \tag{7.9}$$

for every pole μ. This formula permits the definition of partial widths

$$\Gamma_{\mu a} = |g_{\mu a}|^2 / N_\mu \tag{7.10}$$

which add up to the total width.

The difficulty encountered in using this level matrix formalism numerically arises from the fact that it cannot be applied to a statistical S-matrix, but only to one with a finite set of poles. Here one encounters systematic end effects and large level matrices must be constructed in order to yield a satisfactory sample of poles in the middle of the energy interval where they are not disturbed by end effects [7]. However the method has been successfully applied in the computer program MATDIAG to confirm the relations (6.14) and (6.15) over a wide range of parameters [8]. It has also been learned from such studies that for large Γ/D, the level correlations of the Wigner distribution tend to disappear and the E_μ tend to be distributed only with an exponential spacing distribution

(see Fig. 7). On the other hand the widths in such cases tend to have a broader distribution than would be expected from sums of partial widths, each having the Porter-Thomas distribution law (see Fig. 8). It was also found that the average of N_μ increases with increasing Γ/D. We shall return to further applications of this method in the next section.

8. THE FLUCTUATION CROSS SECTION

Our aim here is to evaluate the average reaction cross section in terms of optical model transmission coefficients and general statistical laws. Since the direct cross section (6.5) is, for diagonal $\bar{S}$, already given by the optical model, we turn to the fluctuation cross section (6.6). By Eqs. (6.1), (6.3) and (6.7) we find that [3]

$$\sigma_{ab}^{f\ell} = \frac{2\pi}{D}\left\langle \frac{|g_{\mu a}|^2 |g_{\mu b}|^2}{\Gamma_\mu} \right\rangle - M_{ab}$$

$$M_{ab} = 2|\bar{S}_{ab}^{P}|^2 - \frac{2\pi i}{D}\left\langle \frac{g_{\nu a} g_{\nu b} g_{\mu a}^* g_{\mu b}^*}{(E_\mu - E_\nu) + \frac{1}{2}i(\Gamma_\mu + \Gamma_\nu)} \right\rangle_{\mu \neq \nu} \tag{8.1}$$

with the definition

$$\Theta_{\mu a} = \frac{2\pi}{D} N_\mu |g_{\mu a}|^2, \tag{8.2}$$

where N_μ is the normalization parameter of Eq. (7.8), we can rewrite (8.1)

$$\sigma_{ab}^{f\ell} = \left\langle \frac{\Theta_{\mu a}\Theta_{\mu b}}{\Theta_\mu} \right\rangle - M_{ab} \tag{8.3}$$

where

$$\langle \Theta_{\mu a} \rangle = T_a + \Sigma_b M_{ab} \tag{8.4}$$

and

$$\langle \Theta_\mu \rangle = \Sigma_c \langle \Theta_{\mu c} \rangle. \tag{8.5}$$

The similarity of the first term in Eq. (8.3) with Eq. (3.2) suggests that we use the notation of Sec. 4 to write

$$\sigma_{ab}^{f\ell} = \frac{\langle \Theta_{\mu a} \rangle \langle \Theta_{\mu b} \rangle}{\langle \Theta_\mu \rangle} G_{ab} C_{ab} - M_{ab} \tag{8.6}$$

with

$$G_{ab} = \left\langle \frac{\Theta_{\mu a}\Theta_{\mu b}}{\Theta_\mu} \right\rangle \Big/ \frac{\langle \Theta_{\mu a}\Theta_{\mu b} \rangle}{\langle \Theta_\mu \rangle} \tag{8.7}$$

$$C_{ab} = \frac{\langle \Theta_{\mu a}\Theta_{\mu b} \rangle}{\langle \Theta_{\mu a} \rangle \langle \Theta_{\mu b} \rangle} = 1 + 2\frac{\rho_{ab}}{\sqrt{\nu_a \nu_b}} \tag{8.8}$$

where we have assumed that the distribution of $\Theta_{\mu a}$ can be described by the chi-squared distribution with ν_a degrees of freedom and where the channel correlation coefficient ρ_{ab} is given by

$$\rho_{ab} = \frac{C_{ab} - 1}{\sqrt{(C_{aa} - 1)(C_{bb} - 1)}} \tag{8.9}$$

At this point one might hope that the term M_{ab} might vanish at least in the limit of large Γ/D, leaving again a simple Hauser-Feshbach formula. Unfortunately, as was pointed out by Weidenmüller [9], this is not possible. For, comparing the average of (8.2) with Eq. (6.14) and substituting this with Eq. (8.4), we find that

$$\Sigma_b M_{ab} \geq T_a \left(\frac{1}{\sqrt{1 - T_a}} - 1 \right) \tag{8.10}$$

which diverges as T_a approaches unity.

To make further progress it is useful to analyze a simple case which is described by a limited number of parameters and yet has arbitrarily large Γ/D. This is the case of n statistically equivalent channels [10]. By this we mean that

$$\begin{aligned} &T_c \equiv T, \qquad \nu_c \equiv \nu \quad \text{for all} \quad c = 1,2,3, \ldots n \\ &\rho_{cd} \equiv \rho \quad \text{for all} \quad c \neq d. \end{aligned} \tag{8.11}$$

Then also for all distinct c and d from 1 to n

$$\begin{aligned} C_{cc} &= 1 + 2/\nu \equiv C \\ C_{cd} &= 1 + 2\rho/\nu \equiv D \\ M_{cc} &\equiv M \\ M_{cd} &\equiv P \\ G_{cc} &= G_{cd} = \frac{n}{C + (n-1)D} \end{aligned} \tag{8.12}$$

Upon substitution into Eqs. (8.7) and (8.8) we find that

$$\sigma_{cc}^{f\ell} = \frac{\frac{C}{D}T}{\frac{C}{D} + n - 1} - \frac{n - 1}{\frac{C}{D} + n - 1}\left(M - \frac{C}{D}P\right) \tag{8.13a}$$

$$\sigma_{cd}^{f\ell} = \frac{T}{\frac{C}{D} + n - 1} + \frac{1}{\frac{C}{D} + n - 1}\left(M - \frac{C}{D}P\right). \tag{8.13b}$$

The actual behavior of these parameters was studied by means of MATDIAG calculations using channel numbers which varied from 5 up to 15 and using various values of channel transmission coefficients T distributed between 0 and 1. In all cases the results indicated the relationship [10]

$$C' \equiv \frac{C}{D} = \frac{M}{P} \tag{8.14}$$

which makes the second terms in Eqs. (8.13) vanish and leaves

$$\sigma_{cd}^{f\ell} = \frac{1 + \delta_{cd}(C' - 1)}{C' + n - 1}\ T \tag{8.15}$$

which is precisely the width-fluctuation corrected Hauser-Feshbach formula for n equivalent channels each having transmission coefficient T and partial widths that are uncorrelated between different channels and are distributed according to a chi-squared distribution with ν' degrees of freedom where

$$C' = 1 + 2/\nu'. \tag{8.16}$$

Furthermore, the values of ν' deduced from the MATDIAG calculations showed that ν' varied from a value of 1 for small values of T to a value of 2 for values of T near unity. Tepel, Hofmann and Weidenmüller [11] have given the following empirical formula for the dependence of ν_c' on T_c

$$\nu' = 1 + \sqrt{T}. \tag{8.17}$$

Another slightly different graphical relationship is shown in Fig. 9.

The Porter-Thomas distribution $\nu' = 1$ characterizes a random variable which is the square of a real normally distributed variable with zero mean. The exponential $\nu' = 2$ distribution characterizes a variable that is the sum of squares of two such real normally distributed variables with equal dispersions, or in other words the absolute square of a complex number with normal real and imaginary parts, isotropically distributed in the complex plane about the origin. This suggests that we consider a complex random variable $t_{\mu a}$ for every channel a, having normally distributed real and imaginary parts with zero means such that

$$T_a = \left\langle |t_{\mu a}|^2 \right\rangle_\mu \tag{8.18}$$

and

$$x_a = \left\langle (\mathrm{Im}t_{\mu a})^2 \right\rangle_\mu \Big/ \left\langle (\mathrm{Re}t_{\mu a})^2 \right\rangle_\mu. \tag{8.19}$$

If we now require

$$\frac{(1 + x_a)^2}{1 + x_a^2} = \nu_a' \tag{8.20}$$

then $|t_{\mu a}|^2$ has the same dispersion as the chi-squared distribution with ν_a' degrees of freedom, and is in fact quite close to it.

We can now summarize the development which started with the consideration of n competing equivalent channels in Eq. (8.11) by saying that

$$\sigma_{ab}^{f\ell} = \left\langle |S_{ab}^{f\ell}|^2 \right\rangle = \left\langle \frac{|t_{\mu a}|^2 |t_{\mu b}|^2}{\Sigma_c |t_{\mu c}|^2} \right\rangle_\mu \tag{8.21}$$

with the specifications (8.18) through (8.20) and with ν_a' given by (8.17). The final calculation of Eq. (8.21) proceeds then exactly in the way discussed in Sec. 4 for the Hauser-Feshbach formula with width fluctuation correction. Analogously we can evaluate other averages, such as

$$\left\langle S_{aa}^{f\ell} S_{bb}^{f\ell *} \right\rangle = \left\langle \frac{t_{\mu a}^2 t_{\mu b}^{*2}}{\Sigma_c |t_{\mu c}|^2} \right\rangle = \sqrt{\left(\frac{2}{\nu_a'} - 1\right)\left(\frac{2}{\nu_b'} - 1\right)}\ \sigma_{ab}^{f\ell}. \tag{8.22}$$

while for the case where $\overline{S}$ is diagonal, all averages such as $\left\langle S_{ab}^{f\ell} S_{ac}^{f\ell *} \right\rangle$ which involve indices that are not repeated vanish.

These results have been found consistent with MATDIAG calculated samples also in cases of inequivalent competing channels. They will be referred to as the M-cancellation formulas because they depend crucially on the cancellation of the M term in Eq. (8.6) by the channel-channel correlation effect as expressed in Eq. (8.14).

In evaluating average differential cross sections, we average Eqs. (5.6) which requires the evaluation of averages of the type

$$\left\langle S_{ab}^{J\pi f\ell} S_{a'b'}^{J'\pi' f\ell *} \right\rangle . \tag{8.23}$$

According to the above we have three types of nonvanishing contributions from (8.23). The first comes from terms of the type of Eq. (8.21):

$$\delta_{JJ'}\delta_{\pi\pi'}\delta_{aa'}\delta_{bb'} \frac{T_a T_b}{\sum_{c\epsilon J,\pi} T_c} G_{ab} C_{ab} . \tag{8.24}$$

The second contribution comes from terms of the type of Eq. (8.22)

$$\delta_{JJ'}\delta_{\pi\pi'}\delta_{ab}\delta_{a'b'} \sqrt{\left(\frac{2}{\nu_a} - 1\right)\left(\frac{2}{\nu_{a'}} - 1\right)} \; \frac{T_a T_{a'}}{\sum_c T_c} G_{aa'} C_{aa'} \tag{8.25}$$

The third contribution occurs for compound elastic scattering of neutrons from odd-A targets and arises from spin-flip elastic scattering

$$\delta_{JJ'}\delta_{\pi\pi'}\delta_{ab'}\delta_{ba'} \frac{T_a T_b}{\sum_c T_c} G_{ab} C_{ab} . \tag{8.26}$$

Besides the M-cancellation formula of Hauser-Feshbach times width fluctuation correction, there exists an empirically derived formula based on calculation of the STASIG type which in many instances gives results very similar to the M-cancellation formula. According to Tepel, Hofmann and Weidenmüller [11]

$$\begin{aligned} \sigma_{ab}^{f\ell} &= X_a X_b + 2\delta_{ab} X_b^2/\nu_b \\ T_a &= X_a \Sigma_c X_c + 2X_a^2/\nu_a \end{aligned} \tag{8.27}$$

This formula also depends only on the channel transmission coefficients and the channel parameters ν_c which have essentially the same numerical values as in the width fluctuation correction. Instead of evaluating the integrals (4.7) of the width fluctuation correction, Eq. (8.27) requires the solutions of the coupled equations for X_a in terms of the transmission coefficients which are then used to evaluate the fluctuation cross section. Numerically there appears to be little advantage of either procedure. The major difference arises in cases such as discussed in Eqs. (4.10) and (4.11) which give rise to enhanced nonelastic cross sections. This effect is not predicted by Eqs. (8.27). In the limit of large Γ/D when $\nu_a = 2$ for all channels, Eq. (8.27) becomes identical to a formula proposed by Kawai, Kerman, and McVoy [12].

9. DIRECT REACTION EFFECTS

We now give up the assumption that $\bar{S}$ is diagonal. Then the optical model becomes a coupled channels model in which, in addition to the complex potential for each channel there are coupling potentials between channels. Such a generalization is particularly important in the excitation by neutron inelastic scattering of vibrational or rotational collective states of the target nucleus.

One immediate effect of a nonvanishing $\bar{S}_{ab}$ is suggested by Eq. (6.7). Unless only S_{ab}^B contributes to $\bar{S}_{ab}$, there will also be contributions from $\bar{S}_{ab}^P = -\pi \left\langle g_{\mu a} g_{\mu b} \right\rangle / D$ and hence the pole amplitudes $g_{\mu a}$ and $g_{\mu b}$ for the two channels a and b will be correlated. In the isolated resonance limit this produces a nonvanishing correlation ρ_{ab} between the partial widths $\Gamma_{\mu a} = |g_{\mu a}|^2$ and $\Gamma_{\mu b} = |g_{\mu b}|^2$, which, by the width fluctuation correction factor C_{ab} of Eq. (4.8), causes an enhancement of the average compound cross section between channels a and b. In the isolated resonance limit this enhancement can be calculated from the coupled channels optical model value of $\bar{S}$. But for appreciable Γ/D we must again turn to S-matrix theory.

The crucial technique for treating such cases is the Engelbrecht-Weidenmüller transformation [13] which permits one to transform to the case of a diagonal $\bar{S}$, calculate $\sigma^{f\ell}$ for that diagonalized $\bar{S}$ in the manner of Sec. 8, and then transform the result back to the non-diagonal case. This transformation is best described in terms of Satchler's Hermitean

penetration matrix P which is a generalization of the optical model transmission coefficient for non-diagonal $\overline{S}$ [14]

$$P_{ab} = \delta_{ab} - \Sigma_c \overline{S}_{ac} \overline{S}^*_{bc}, \qquad P = 1 - \overline{S}\overline{S}^{\dagger}. \tag{9.1}$$

The transmission coefficients (6.11) are then just the diagonal elements of the P-matrix. Unitarity still requires these transmission coefficients to be no greater than unity

$$T_a = P_{aa} \leq 1 \quad \text{(unitarity)} \tag{9.2}$$

It can also be shown that causality now requires that

$$P \text{ is positive semidefinite} \quad \text{(causality)} \tag{9.3}$$

which means that all eigenvalues of P are non-negative. I shall refer to the case where P is a singular matrix, i.e., has a vanishing eigenvalue as the causality limit.

The Engelbrecht-Weidenmüller transformation is the unitary transformation U that diagonalizes P

$$UPU^{-1} = P' \text{ is diagonal.} \tag{9.4}$$

It follows that

$$U\tilde{S}\tilde{U} = S' \text{ is unitary if S is unitary and symmetric,} \tag{9.5}$$

and that

$$\overline{U}\overline{S}\tilde{\overline{U}} = \overline{S}' \text{ is diagonal.} \tag{9.6}$$

In the case of two coupled channels we can write

$$\overline{S} = \begin{pmatrix} f_1 e^{i\Theta_1} & f_3 e^{i\Theta_3} \\ f_3 e^{i\Theta_3} & f_2 e^{i\Theta_2} \end{pmatrix} \tag{9.7}$$

and

$$U = \begin{pmatrix} \cos\beta & -\sin\beta \\ \sin\beta & \cos\beta \end{pmatrix} \begin{pmatrix} e^{i\alpha} & 0 \\ 0 & e^{-i\alpha} \end{pmatrix} \tag{9.8}$$

and find that

$$\tan 2\alpha = \frac{f_2 \sin\Theta_{23} - f_1 \sin\Theta_{13}}{f_2 \cos\Theta_{23} + f_1 \cos\Theta_{13}}$$

$$\tan 2\beta = \frac{2f_3}{f_2 \cos(\Theta_{23} - \alpha) - f_1 \cos(\Theta_{23} - \alpha)}. \tag{9.9}$$

where

$$\Theta_{13} = \Theta_1 - \Theta_3, \qquad \Theta_{23} = \Theta_2 - \Theta_3.$$

For three or more coupled channels the direct effect will in general not be very significant as we shall see. In such cases numerical diagonalization of P is required.

Using Eq. (9.5) the fluctuation cross section $\sigma_{ab}^{f\ell}$ can be written in terms of the elements of S'. In this expression averages of the form $\left\langle S'^{f\ell}_{ab} S'^{f\ell *}_{cd} \right\rangle$ occur. From the discussion in Sec. 8 we know that the only non-vanishing such averages are of this form

$$\sigma'^{f\ell}_{ab} = \left\langle |S'^{f\ell}_{ab}|^2 \right\rangle \tag{9.10}$$

which is evaluated in terms of the elements T' of P' by means of the width fluctuation corrected Hauser-Feshbach formula as in Eq. (8.21), or they are of the form

$$\left\langle S'^{f\ell}_{aa} S'^{f\ell}_{bb} \right\rangle = \left(\frac{2}{\nu'_a} - 1\right)^{\frac{1}{2}} \left(\frac{2}{\nu'_b} - 1\right)^{\frac{1}{2}} \sigma'^{f\ell}_{ab} \tag{9.11}$$

by Eq. (8.22). With these results we get [15]

$$\begin{aligned} \sigma^{f\ell}_{ab} = {} & \Sigma_c |U_{ca}|^2 |U_{cb}|^2 \sigma'^{f\ell}_{cc} \\ & + \Sigma_{d \neq c} \Big[U^*_{ca} U^*_{db} (U_{ca} U_{db} + U_{da} U_{cb}) \\ & + \left(\frac{2}{\nu'_c} - 1\right)^{\frac{1}{2}} \left(\frac{2}{\nu'_d} - 1\right)^{\frac{1}{2}} U^*_{ca} U^*_{cb} U_{da} U_{db} \Big] \sigma'^{f\ell}_{cd}. \end{aligned} \tag{9.12}$$

Hofmann et al. [16] have evaluated a very similar formula differing only in the evaluation of the matrix elements (9.11) and employing the

Tepel formula (8.27) for the evaluation of $\sigma'^{f\ell}_{cd}$, instead of the width fluctuation corrected Hauser-Feshbach formula. Kawai et al. [12] have given the following formula which gives equivalent results only in the limit when all $\nu' = 2$

$$\sigma^{f\ell}_{ab} = X_{aa}X_{bb} + X_{ab}X_{ba}$$
$$P_{ab} = \Sigma_c(X_{ab}X_{cc} + X_{ac}X_{cb}). \qquad (9.13)$$

In addition to the fluctuation cross section (9.12) we will in general also have a direct contribution to the average reaction cross section due to Eq. (6.5).

For $a \neq b$ the cross section (9.12) can be enhanced over the value one would obtain with the ordinary width fluctuation corrected Hauser-Feshbach formula. This is because of the occurrence of the correlation-enhanced elastic fluctuation cross section $\sigma'^{f\ell}_{cc}$ in the primed channels in the first sum of Eq. (9.12). The enhancement of $\sigma'^{f\ell}_{cc}$ will be greatest when the relative contribution of this first term is greatest. The maximum effect will occur when P has only one non-vanishing eigenvalue, for then only one diagonal primed cross section $\sigma'^{f\ell}_{cc}$ can contribute, all others vanishing. In this case, clearly, the direct enhancement is of the order of the elastic enhancement, namely $1 + 2/\nu$. The above situation where eigenvalues of P vanish is what we have called the causality limit. It is likely to be achieved only in the case of two strongly coupled channels.

We have investigated the behavior of the direct enhancement for two classes of average S-matrices involving only pairs of coupled channels

$$\overline{S}_A = 5 \otimes A, \qquad A = \begin{pmatrix} F & iD \\ iD & -F \end{pmatrix}$$
$$\overline{S}_B = 5 \otimes B, \qquad B = \begin{pmatrix} F & D \\ D & -F \end{pmatrix} \qquad (9.14)$$

Here $5 \otimes A$ means that $\overline{S}_A$ is a 10×10 matrix consisting of five identical 2×2 blocks A along the diagonal. Both $\overline{S}_A$ and $\overline{S}_B$ represent two parameter families of average S-matrices depending on F and D. The non-trivial submatrices of the P matrix in the two cases are

$$P_A = \begin{pmatrix} T & 2iFD \\ -2iFD & T \end{pmatrix}$$
$$P_B = \begin{pmatrix} T & 0 \\ 0 & T \end{pmatrix} \qquad (9.15)$$

with $T = 1 - F^2 - D^2$ in both cases. In case B the causality limit $\det P_B = 0$ coincides with the usual limit $T = 0$ and imposes no separate restriction beyond $F^2 + D^2 \leq 1$. However in case A, the causality condition requires

$$F + D \leq 1 \qquad \text{(case A)} \qquad (9.16)$$

and we expect a maximum enhancement of the non-elastic cross sections between any two directly coupled channels. Fig. 10 shows the parameter space of the two average S-matrices of Eq. (9.14) and the calculated compound enhancements over the Hauser-Feshbach formula according to Eq. (9.12). As expected the enhancements are largest and comparable to elastic enhancements along the causality limit (9.16) and the enhancements quickly drop off as one moves away from this limit. In the case of $\overline{S}_B$ where the causality limit imposes no restriction on the available parameter space, there are no appreciable enhancements except along the line $F = 0$ which case B shares with case A.

The predictions of the direct enhancement in these and other cases have been confirmed by computer studies with randomly generated unitary S-matrices. In Fig. 10 the parameters of such computer studies are indicated by black dots.

10. CONTINUOUS CHANNELS

With increasing neutron energy the number of open exit channels increases rapidly until it is either impossible or undesirable to enumerate all such channels and discuss their cross sections in detail. It then becomes necessary to discuss the differential cross section for leaving the residual nucleus with an excitation energy within a differential interval at E_d.

$$\frac{d\sigma^{f\ell}_{cd}(\text{cont.})}{dE_d} = \sigma^{f\ell}_{cd}(\text{discr.})\rho_d(E_d) \qquad (10.1)$$

where $\sigma_{cd}^{f\ell}$(discr.) is the cross section for excitation of a discrete channel with residual nuclear excitation E_d, and $\rho_d(E_d)$ is the level density at excitation E_d of the residual nucleus in channel d for states having spin and parity specified by the channel index d.

If the dependence of ρ_d upon the relevant residual spins I_d is given by the factor $(2I_d + 1)$, then it can be shown that the fluctuation cross section (10.1) summed over I_d is isotropic. Though this spin dependence of ρ_d is not correct, the anisotropies of fluctuation cross sections at such high energies are expected to be small and can often be ignored.

Also, in the presence of large numbers of competing channels, the width fluctuation correction and direct effect upon non-elastic fluctuation cross sections becomes negligible. On the other hand for $\Gamma >> D$ we expect an elastic width fluctuation correction factor of 2, so that in the present domain we expect that

$$\sigma_{cd}(\text{discr.}) \cong (1 + \delta_{cd})\sigma_{cd}^{H.F.}. \tag{10.2}$$

The transmission factor sum $\Sigma_e T_e$ which occurs in the denominator of $\sigma_{cd}^{H.F.}$, Eq. (3.5), must also be evaluated statistically

$$\Sigma_e T_e = \Sigma_e \int_0^{E_e(\max)} dE T_e(E_e)/D_e(E_e) \tag{10.3}$$

which involves the level spacings D_e for the residual nuclei in all competing channels. Again, if D_e depends on the residual nucleus spin through a factor $(2I_e + 1)^{-1}$, then the transmission sum (10.3) is given by

$$\Sigma_e T_e = (2J + 1)G/\pi$$

where J is the total angular momentum and G depends only upon excitation energy of the compound nucleus.

Another empirical method for determining the transmission factor sum makes use of the relation

$$\Sigma_e T_e \cong 2\pi\Gamma^{corr}/D \tag{10.4}$$

where Γ^{corr} is the correlation width and ρ is the compound nucleus level spacing for states of the same total angular momentum and parity as the channels e that are summed over. The correlation width can under some circumstances be estimated from fluctuation experiments [17]. The validity of the relation (10.4) was recently confirmed by numerical studies [10]. Comparison of Eqs. (6.15) and (10.4) shows that the correlation width is not the same as the average of the widths Γ_μ .

Difficulties remain the reliable treatment of compound nucleus cross sections at high energies. These are caused by a number of different circumstances. First, there is the uncertainty regarding the effects of gamma-ray transitions between highly excited compound nuclear states in softening the spectrum of emitted neutrons and protons. Secondly, there are empirical results which disagree with the shapes of the particle spectra predicted by the above statistical picture. This indicates a breakdown of our basic statistical assumptions which is dealt with in the lectures on preequilibrium decay.

Finally, at neutron energies exceeding 10 to 20 MeV, residual nuclear levels become unstable and emit secondary particles which further add to the particle flux generated by the reaction. From a theoretical viewpoint, such physically continuous channels pose a three or more-body problem in the channel portion of configuration space, not just in the compound nucleus. While theoretical methods exist now for treating three-body problems [18], they are complicated and time-consuming and have not yet been applied to neutron-induced reactions in heavy nuclei. It is therefore generally assumed that above the threshold for three-body breakup, the breakup proceeds sequentially. That is, in addition to the particle spectrum produced according to Eq. (10.1), there are additional particles produced by the breakup of the residual nuclei in each channel d which is given by

$$\int_0^{E_d(\max)} dE_d \sigma_{cd}^{f\ell}(\text{discr.})\rho_d(E_d)T_{d'}\rho_{d'}(E_{d'})/\Sigma_{e'}T_{e'} \tag{10.5}$$

where the channels d' are decay channels of the residual nucleus of channel d, considered as a new compound system, etc.

REFERENCES

1. Most of the older subjects dealt within these talks are covered excellently in J. E. Lynn, The Theory of Neutron Resonance Reactions (Clarendon Press, Oxford, 1968) where all original references can be found. We will cite here only more recent references.
2. P. A. Moldauer, Phys. Rev. 14 (1976) 764.
3. P. A. Moldauer, Phys. Rev. 135 (1964) B642.
4. P. A. Moldauer, Phys. Rev. Lett. 19 (1967) 1047.
5. M. Simonius, Phys. Lett. 52B (1974) 279.
6. P. A. Moldauer, Statistical Properties of Nuclei, edited by J. B. Garg (Plenum, New York, 1972) p. 335.
7. P. A. Moldauer, Phys. Rev. Lett. 23 (1969) 708.
8. P. A. Moldauer, R. N. Huang, B. S. Garbow, Argonne National Laboratory report ANL-7590 (1969).
9. H. A. Weidenmüller, Phys. Rev. C9 (1974) 1202.
10. P. A. Moldauer, Phys. Rev. C11 (1975) 426.
11. J. W. Tepel, H. M. Hofmann, and H. A. Weidenmüller, Phys. Lett. 49B (1974) 1.
12. M. Kawai, A. K. Kerman, and K. W. McVoy, Ann. Phys. (N. Y.) 75 (1973) 156.
13. C. A. Engelbrecht and H. A. Weidenmüller, Phys. Rev. C8 (1973) 859.
14. G. R. Satchler, Phys. Lett. 7 (1963) 55.
15. P. A. Moldauer, Phys. Rev. 12 (1975) 744.
16. H. M. Hofmann, J. Richert, J. Tepel, and H. A. Weidenmüller, Ann. Phys. (N.Y.), 90 (1975) 403.
17. T. Ericson and T. Mayer - Kuckuk, Ann. Rev. Nucl. Sci. 16 (1966) 183.
18. L. D. Faddeev, Mathematical Aspects of the Three-Body Problem in Quantum Scattering Theory (D. Davey, N.Y. 1965).

FIGURE CAPTIONS

1. High resolution neutron total cross section of iron from 0.5 to 1.0 MeV, together with a running 200 keV energy average. (Data and average courtesy of Dr. A. B. Smith).
2. Width fluctuation correction for two channels having Porter-Thomas distributed partial widths, when these are the only channels (bottom), and when they compete with a large number of channels having a lumped non-fluctuating partial width (top).
3. Enhancement of weak average cross sections for values of ν ranging from 1 to 2 and various combinations of channels. The Tepel curves refer to the results obtained from Ref. 11; the points are the results of STASIG calculations.
4. Integration contours used in deriving Eqs. (6.8) and (6.9).
5. Method used in STASIG to generate statistical cross sections.
6. Example of STASIG generated cross sections for inelastic neutron scattering in titanium. The top curve is the experimental result. The middle curve was generated from a coupled channels optical model, the bottom for a single channel optical model.
7. MATDIAG-generated changes in the level spacing distribution with increasing numbers of competing strongly absorbed channels. (histograms).
8. MATDIAG-generated changes in the total width distribution with increasing numbers of competing strongly absorbed channels. (histograms). The curves are the distributions that would be expected from independently Porter-Thomas distributed partial widths.
9. Relation between ν and T obtained from numerical calculations (Ref. 15) compared to the prediction of the formula of Ref. 16 (H).
10. Distribution of enhancements of average compound cross sections due to competing direct reactions for two classes of average S-matrices.

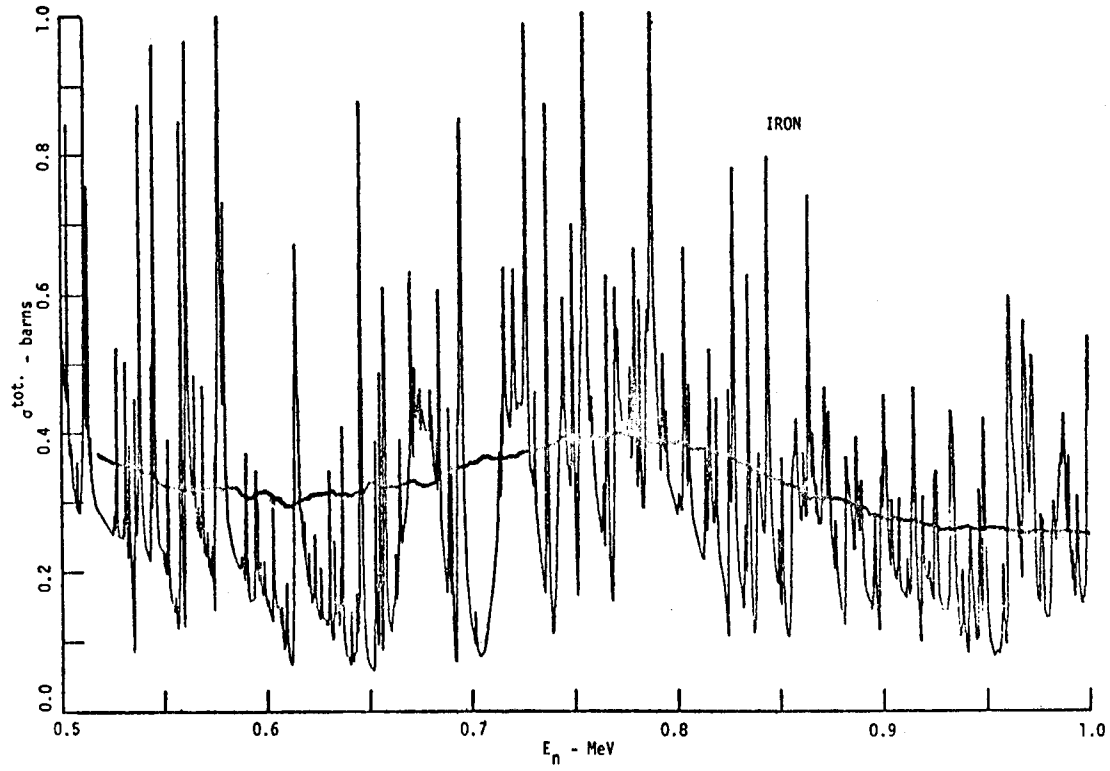
IRON
$\sigma^{tot.}$ - barns
E_n - MeV
0.0
0.2
0.4
0.6
0.8
1.0
0.5
0.6
0.7
0.8
0.9
1.0

FIG. 1.

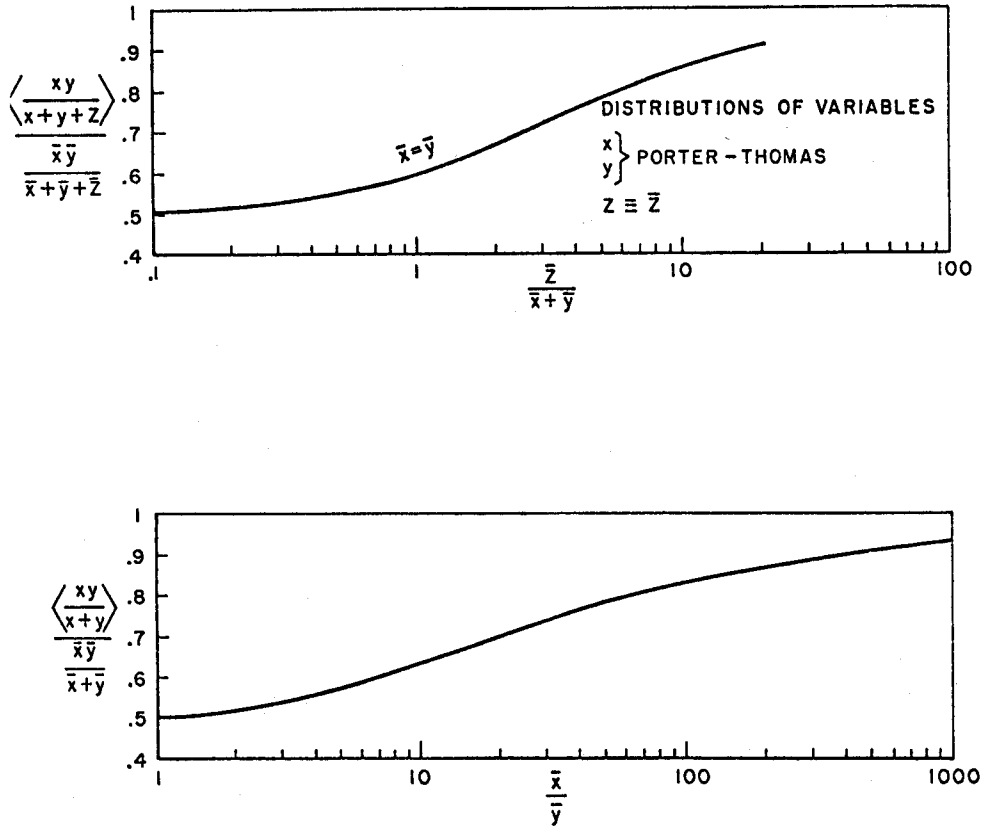
$\left\langle \frac{xy}{x+y+Z} \right\rangle \Big/ \frac{\bar{x}\bar{y}}{\bar{x}+\bar{y}+\bar{Z}}$
$\bar{x}=\bar{y}$
DISTRIBUTIONS OF VARIABLES
x, y } PORTER-THOMAS
$Z \equiv \bar{Z}$
$\frac{\bar{Z}}{\bar{x}+\bar{y}}$
$\left\langle \frac{xy}{x+y} \right\rangle \Big/ \frac{\bar{x}\bar{y}}{\bar{x}+\bar{y}}$
$\frac{\bar{x}}{\bar{y}}$
.4
.5
.6
.7
.8
.9
1
.1
10
100
1000

FIG. 2.

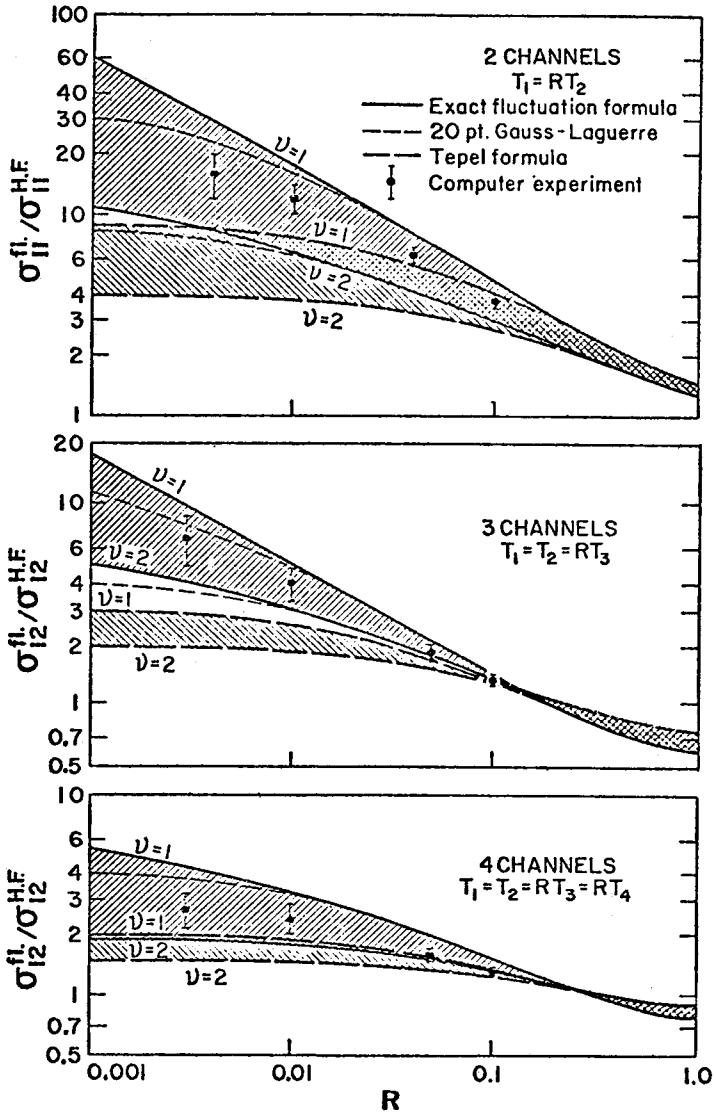

FIG. 3.

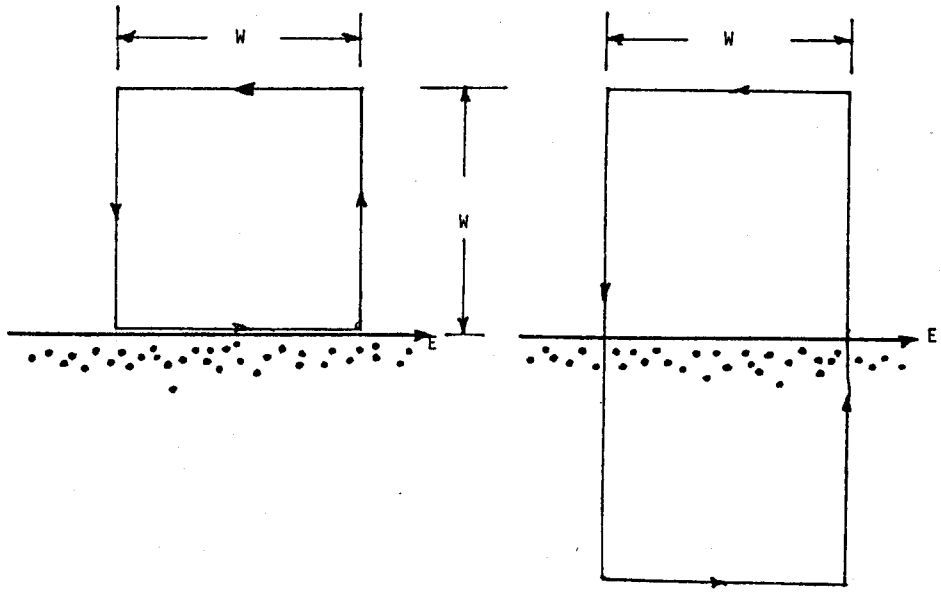

FIG. 4.

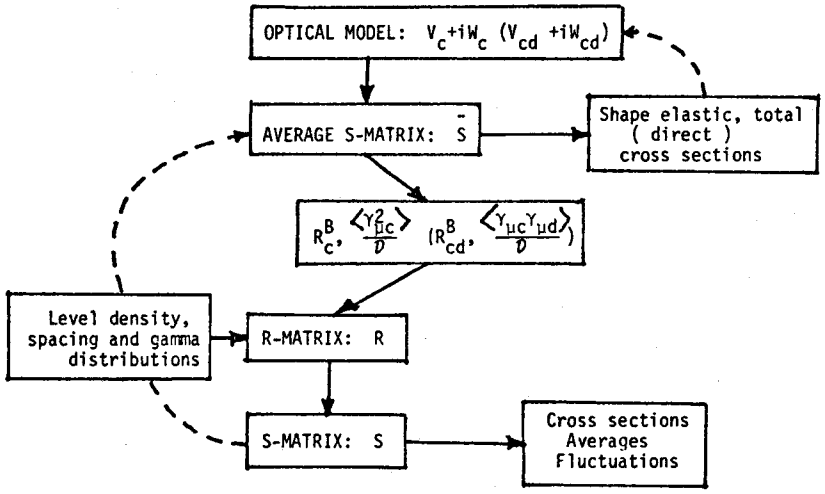

FIG. 5.

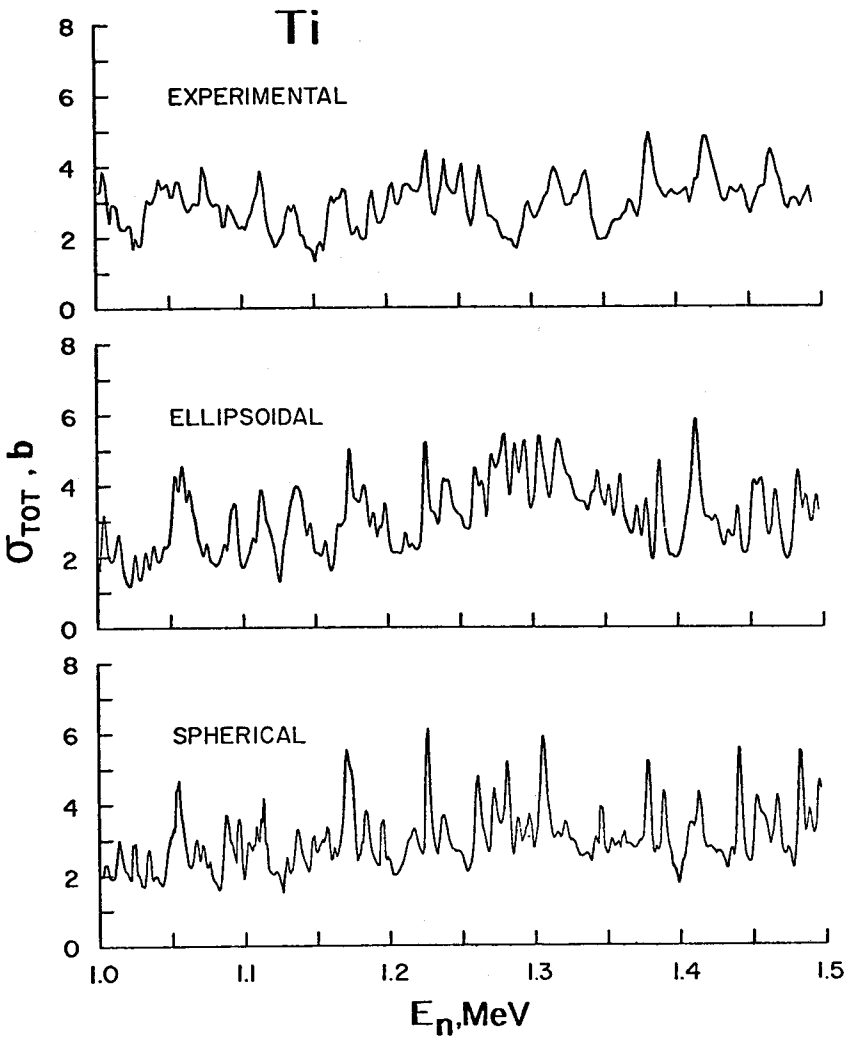
Ti
EXPERIMENTAL
ELLIPSOIDAL
SPHERICAL
σ_{TOT}, b
E_n, MeV

FIG. 6.a.

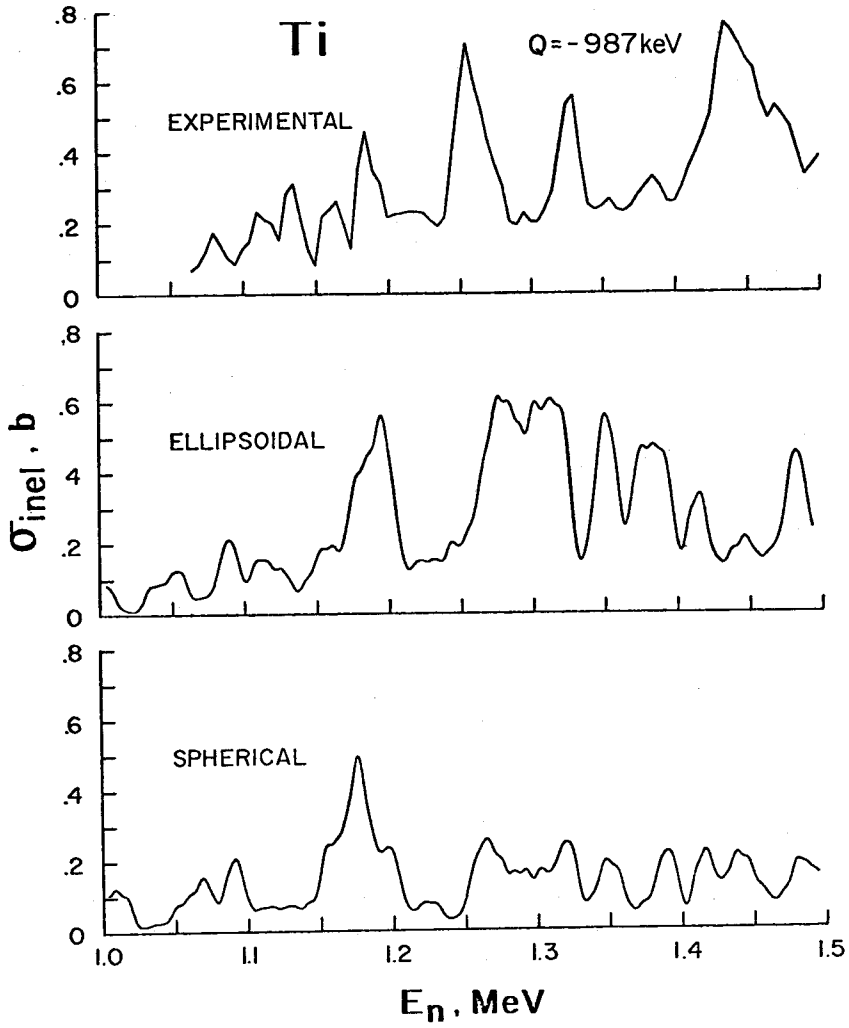
Ti
Q=-987keV
EXPERIMENTAL
ELLIPSOIDAL
SPHERICAL
σ_{inel}, b
E_n, MeV

FIG. 6.b.

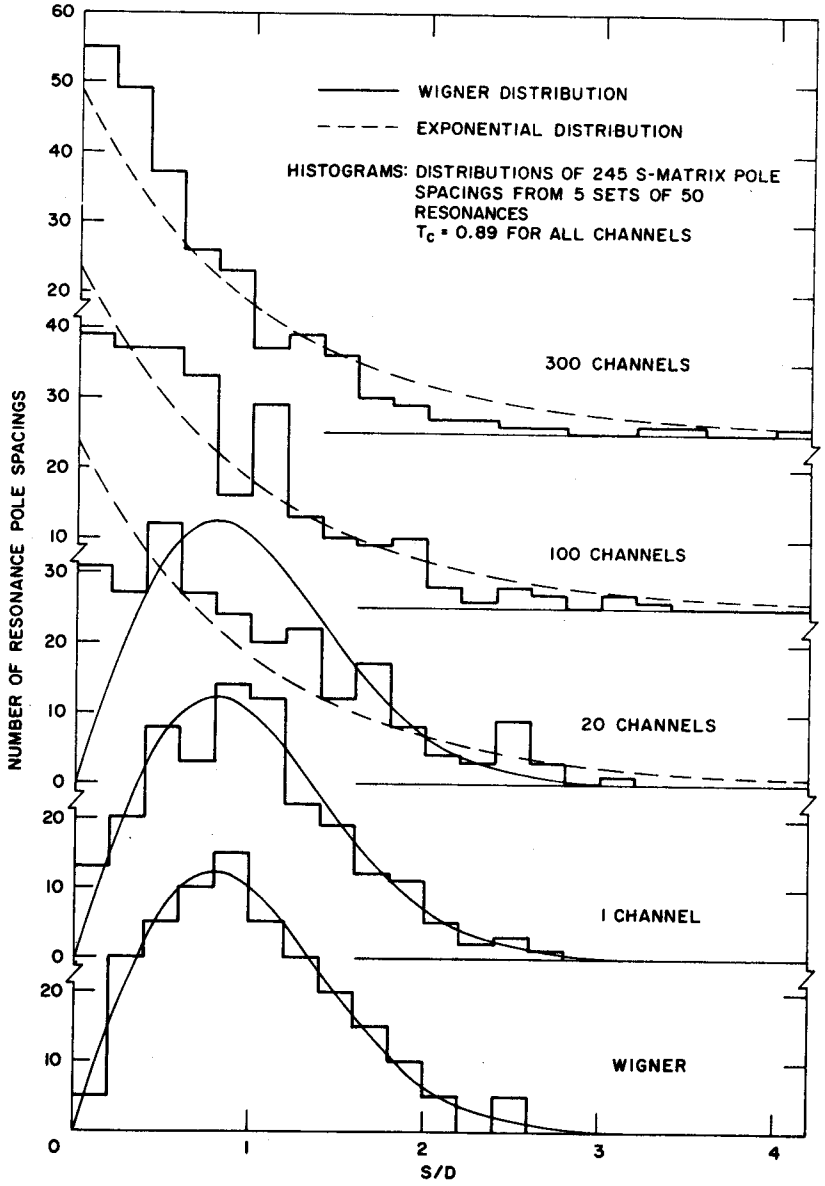

FIG. 7.

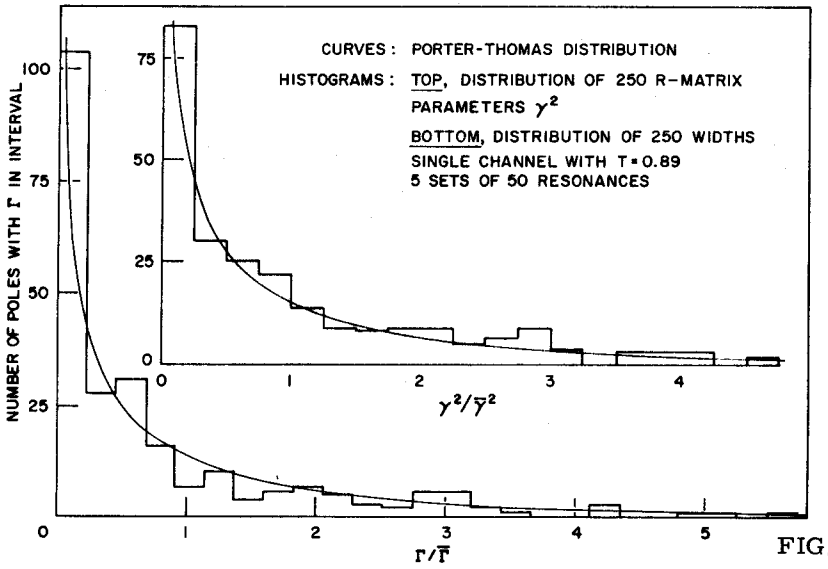

FIG. 8. a.

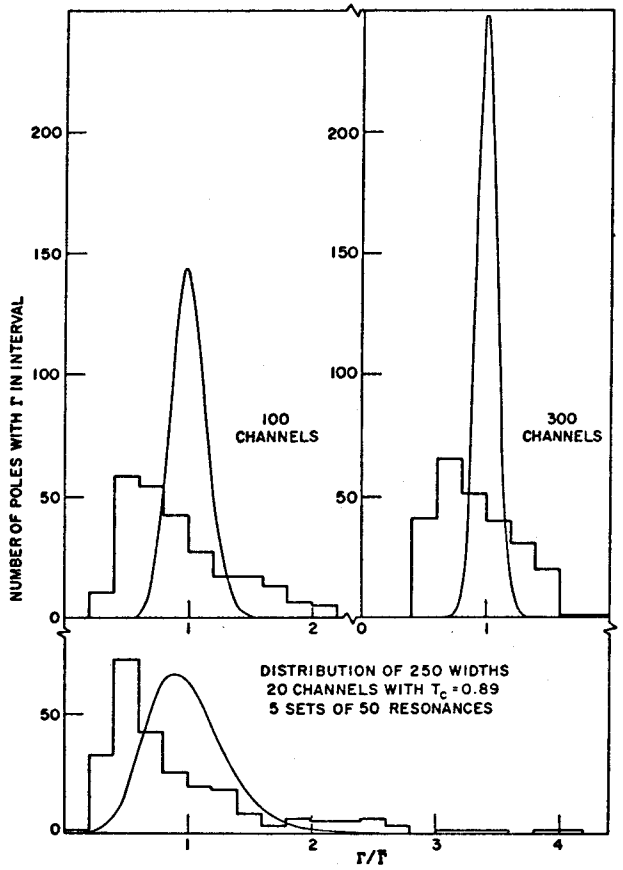

FIG. 8. b.

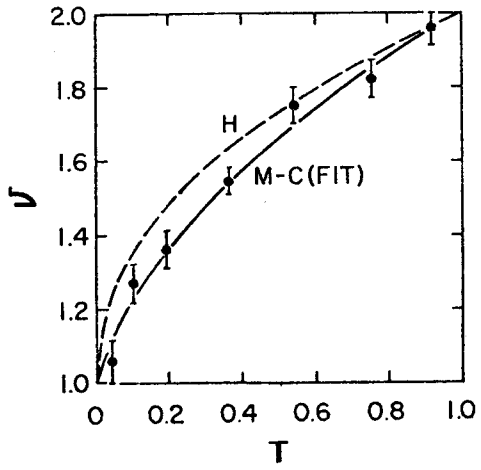
2.0
1.8
1.6
1.4
1.2
1.0
ν
H
M-C(FIT)
0
0.2
0.4
0.6
0.8
1.0
T

FIG. 9.

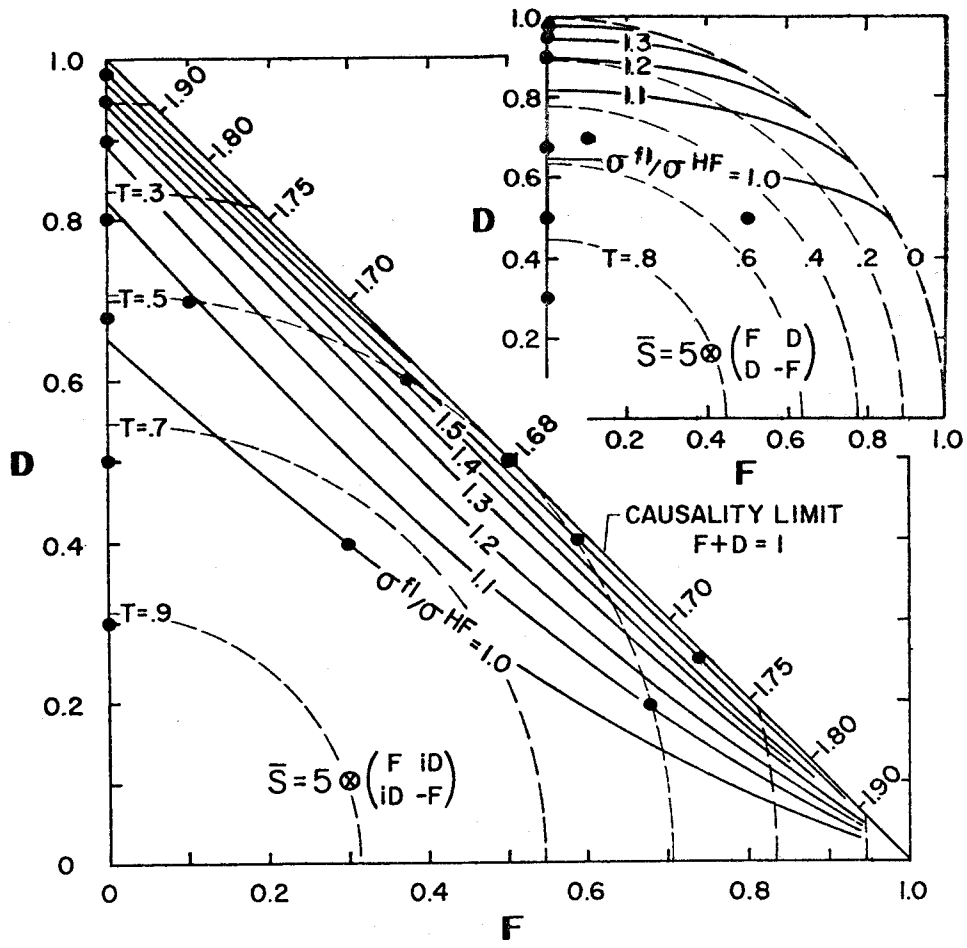
1.0
0.8
0.6
0.4
0.2
0
D
F
1.90
1.80
1.75
1.70
1.68
1.5
1.4
1.3
1.2
1.1
T=.3
T=.5
T=.7
T=.9
CAUSALITY LIMIT
F+D=1
σ fl/σ HF = 1.0
S̄=5⊗(F iD / iD -F)
T=.8
.6
.4
.2
0
S̄=5⊗(F D / D -F)

FIG. 10.

THEORIES AND APPROXIMATIONS OF NUCLEAR LEVEL DENSITIES

V.S. RAMAMURTHY
Bhabha Atomic Research Centre,
Trombay, Bombay,
India

ABSTRACT

Outstanding experimental features of nuclear level densities are their extremely rapid increase with excitation energy and dependence on nuclear shell and pairing effects. The rapid increase of the number of levels with energy is a general characteristic of any system with many degrees of freedom. In the case of a Fermion system like a nucleus, these degrees correspond to the elementary excitations with additive energies. The mathematical formulation of the level density problem for such a system is well known in statistical mechanics. The first part contains a detailed discussion of the method of calculation of nuclear level densities with particular emphasis on the partition function approach. Some of the recent generalizations of the method to include the effects of residual interactions between the nucleons such as the pairing interaction are also discussed. In the second part we give a brief description of some of the recent calculations of level densities starting from shell model single particle level schemes. The possible sources of error in such calculations of absolute level densities are also discussed. In the third part, two recently developed semiempirical level density formulae are described which retain the simplicity of approximate analytical formulae but at the same time include nuclear shell effects in a more realistic manner. A brief discussion of some of the open problems is also given.

1. GENERAL INTRODUCTION

The rates of many nuclear reactions, except at very low energies depend on the phase space available after the reaction. A dominating part in the phase space is the density of levels in the residual nucleus [1,2]. By far the most reliable experimental information on nuclear level densities comes from a study of neutron resonances. Many groups have estimated the average level spacing D_o of the nucleus from the rather irregularly located neutron resonance capture peaks [3-9]. The average level spacing is computed by fitting the first N observed resonance levels by least squares to the formula $E_n = E + nD$, $n = 1, 2 \ldots, N$ where E_o and the average spacing D_o are parameters to be determined and E_n is the energy of the n-th observed level. The inverse value D_o of the average spacing thus fixed represents the density of the nuclear levels of the compound nucleus at an excitation energy E and with a given value of the spin j. The binding energy B_n of the neutron gives with a good approximation the excitation energy E of the compound nucleus except for a few nuclides in which the low-lying levels are extremely rare and therefore higher levels are necessarily included in the analysis. The spin dependent level density $\rho(E, j)$ is related to the observed level spacing through the relations

$$D_o^{-1} = \tfrac{1}{2}\rho(E, j = \tfrac{1}{2}) \text{ for } I = 0$$

$$= \tfrac{1}{2}\left[\rho(E, j = I + \tfrac{1}{2}) + \rho(E, j = I - \tfrac{1}{2})\right] \text{ for } I \neq 0$$

where I is the target spin, E is the excitation energy of the compound nucleus and j is its spin. Since the initial state has a well defined parity the observed levels have only one of the two possible parities. This introduces the factor $\frac{1}{2}$ in the right hand side of the above equations. For a few cases where the l values of the neutron is different from zero the necessary alterations are to be added. On the assumption that no levels have been missed or wrongly attributed to the nucleus studied this method is the best source of information available at present for the level densities. The number of nuclei for which such an analysis has been performed is about 200 in and around the beta stability line. Some information has also been obtained from studies of proton resonances [10]. Nucleon evaporation spectra also provide information on nuclear level densities but only relative values and carry with them uncertainties associated with the reaction theories. Thus, the main experimental information on absolute nuclear level densities is confined to a narrow band of nuclei around the beta stability line and almost at one excitation energy equal to the neutron binding energy.

The type of level density information required in calculations relevant for nuclear data is however quite varied and can be split into the following categories:

i) Calculation of decay widths and particle evaporation spectra

The calculation of decay widths and the energy and angular distribution of the emitted particles involves the knowledge of the level densities of the daughter nuclei after the emission of the particles in a wide range of excitation energies. Such information is not experimentally available and one has to rely on theoretical extrapolation into all excitation energy ranges.

ii) Calculations involving nuclei beyond the beta stability line:

The best examples of this category are the fission product nuclei and the heavy transuranium nuclei. Of 80 major fission products causing reactor poisoning, 40% have no measurements. These involve therefore extrapolation into new regions of nucleon numbers.

iii) Calculations involving new nuclear configurations:

Such a situation is encountered in the calculation of fission widths. According to the Bohr-Wheeler theory [11], the fission width is proportional to the number of open channels on the top of the highly deformed fission barrier which in turn is decided by the density of levels of the highly deformed fission saddle point nucleus. Direct experimental information on this can not be obtained and one has to fully rely on extrapolation.

iv) Another requirement which does not directly concern the nuclear data evaluator but all the same is of fundamental importance is the extrapolation into new regions of angular momentum. The spin values encountered in neutron resonances are in general quite small and the experimental information therefore relates to these small values of j. However there are instances where one would like to predict the level densities for high angular momentum states, as in the case of reactions involving heavy ions. Here again one has to rely on theoretical extrapolations.

It is therefore clear that however extensive is the experimental information on nuclear level densities, there is a need for a reliable theoretical estimate of the same. The required sophistication of the theoretical basis of the formula, however, depends on the application where it is required. For example, in case (i) where an extrapolation into new regions of excitation energy was required it is necessary to obtain only a reliable functional form of the formula as a function of the excitation energy. The constants of the formula can then be obtained by a fit to the level density values at the neutron binding energy and the formula can be used at higher and lower excitation energies with reasonable confidence. On the other hand an extrapolation into new regions of nucleon numbers or deformations as in cases (ii) and (iii) require a better understanding of the theoretical basis of the formula since the constants of the formula should also contain the dependence on the composition of the nucleus and its shape.

Outstanding experimental features of nuclear level densities are their extremely rapid increase with excitation energy and dependence on nuclear shell and pairing effects. Any theoretical description of nuclear level densities must explain and reproduce the above basic features.

2. MATHEMATICAL FORMULATION

The rapid increase of the number of levels with excitation energy is a general characteristic of any system with many degrees of freedom. In the case of a nucleus which can very roughly be considered as a gas of A nucleons contained in a volume, these degrees correspond to elementary excitations which have additive energies. The mathematical formulation of the level density problem for such a system is well known. A plausible excitation energy dependence of the level density can be derived purely from the thermodynamical considerations [12]. For not too large excitation energies, the nucleons in a nucleus are in a state of high degeneracy and the third law of thermodynamics demands that the specific heat of this system is zero, for T should approach zero as the temperature of the system tends to zero. Therefore, if an expansion of the average excitation energy E_x of the nucleus near T = 0 in powers of T is possible, it must startat least with a quadratic term. Neglecting higher powers of T one can write $E_x = \underline{a}T^2$, where $\underline{a}$ is a constant. The thermodynamic entropy S of the nucleus can then be obtained from the relation $S = \int dE_x/T = 2\sqrt{\underline{a}E_x} = \log(w)$. The level density w is therefore $w = C \exp(2\sqrt{\underline{a}E_x})$. By a suitable adjustment of the constants C and $\underline{a}$, it is possible to reproduce qualitatively the exponential increase of nuclear level densities with excitation energy. The above formula should only be considered as a first rough approximate orientation to the general features of the density of nuclear levels. A more general approach can be given on the basis of the thermodynamics of excited Fermi systems and has been extensively reviewed in literature [13]. An outline of the approach is given below.

2.1 Dependence on excitation energy and mass number of the nucleus

Consider a system of N noninteracting Fermions with total energy E. The particles occupy the single particle states ϵ_i of an average potential. For such a system the following relations hold.

$$N = \sum n_i \qquad (1)$$

$$E = \sum \epsilon_i n_i \qquad (2)$$

where n_i are the occupation numbers of the single particle states.

For a system of Fermions, n_i can take values 0 or 1.

The level density problem is one of finding the number of ways in which the nucleons can be distributed among the available single particle levels for a fixed energy of the system. The very definition suggests a combinatorial approach, and has been used by a few authors in limited calculations [14-18]. While this approach has some definite advantages, the calculations can be performed only with large computers and are limited to small excitation energies because of the extremely high values that the level densities can reach especially for heavy nuclei. The most common method of level density calculation is therefore the partition function method, a well known tool in statistical mechanics.

Following the general terminology of statistical mechanics [19] the grand partition function for this system is defined as

$$e^{\Omega} = \sum_{N',E'} \exp(\alpha N' - \beta E') \qquad (3)$$

All the statistical properties of the system are contained in the grand partition function. Replacing the sum by an integral, one gets

$$e^{\Omega} = \sum_{N'} \int dE' \, \rho(E', N') \exp(\alpha N' - \beta E') \tag{4}$$

here the weighting function $\rho(E', N')$, assumed to be a continuous function, can be identified with the level density of the system. It is seen that $\rho(E', N')$ can be obtained as the inverse Laplace Transform of the coefficient of $\exp(\alpha N')$ in the grand partition function.

$$\rho(E, N) = \frac{1}{(2\pi i)^2} \int d\beta \int d\alpha \; \exp(S) \tag{5}$$

where $S = \Omega - \alpha N + \beta E$. The integrals in eqn. (5) can be calculated approximately by the method of steepest descent. The exponent S has a saddle point at

$$N = \frac{\partial \Omega}{\partial \alpha} \quad ; \quad E = -\frac{\partial \Omega}{\partial \beta}$$

Then the level density is approximately given by

$$\rho = \frac{\exp(S)}{2\pi\sqrt{D}} \tag{6}$$

where

$$D = \begin{vmatrix} \frac{\partial^2 \Omega}{\partial \alpha^2} & \frac{\partial^2 \Omega}{\partial \alpha \partial \beta} \\ \frac{\partial^2 \Omega}{\partial \alpha \partial \beta} & \frac{\partial^2 \Omega}{\partial \beta^2} \end{vmatrix}$$

all evaluated at the saddle point. The level density can thus be obtained if Ω is known as a function of α and β. Combining eqns. (1) - (3), we get

$$e^{\Omega} = \sum_{n_s} \exp \beta \left[\sum_s n_s (\mu - \epsilon_s) \right] \tag{7}$$

$$\Omega = \sum_s \log \left[1 + \exp \beta (\mu - \epsilon_s) \right] \tag{8}$$

$$S = \sum_s \log \left[1 + \exp \beta (\mu - \epsilon_s) \right] + \beta \frac{\epsilon_s - \mu}{1 + \exp(\epsilon_s - \mu)\beta} \tag{9}$$

The saddle point conditions are given by

$$N = \sum_s \frac{1}{1 + \exp \beta(\epsilon_s - \mu)}$$

$$E = \sum_s \frac{\epsilon_s}{1 + \exp \beta(\epsilon_s - \mu)} \tag{10}$$

The set of second derivatives in the determinant D are given by

$$\frac{\partial^2 \Omega}{\partial \beta^2} = \frac{1}{4} \sum_s \epsilon_s^2 \, \mathrm{Sech}^2 \beta(\epsilon_s - \mu)$$

$$\frac{\partial^2 \Omega}{\partial \alpha^2} = \frac{1}{4} \sum_s \mathrm{Sech}^2 \beta(\epsilon_s - \mu)$$

$$\frac{\partial^2 \Omega}{\partial \alpha \partial \beta} = -\frac{1}{4} \sum_s \epsilon_s \, \mathrm{Sech}^2 \beta(\epsilon_s - \mu) \tag{11}$$

Note that the independent variables α and β are related to the familiar thermodynamical variables μ and T by the relations $\beta = 1/T$ and $\alpha = \beta\mu = \mu/T$, where T is the thermodynamic temperature and μ is the chemical potential. It can also be seen that the function

$$f(\epsilon_s) = \frac{1}{1 + \exp(\beta\epsilon_s - \alpha)} = \frac{1}{1 + \exp(\epsilon_s - \mu)/T}$$

which is the Fermi-Dirac weighting function of ordinary statistical mechanics has the same interpretation of being the probability of a state of energy ϵ_s being occupied.

The above formulation of the level density problem can be easily generalised for two components, protons and neutrons in nuclei. For a system with N neutrons and Z protons with total energy E, the following relations analogous to Eqns. (1) and (2) hold

$$N = \sum_s n_{ns} \quad ; \quad Z = \sum_s n_{ps}$$

$$E = \sum_s \left(n_{ns} \epsilon_{ns} + n_{ps} \epsilon_{ps} \right) \tag{12}$$

where $\epsilon_{n\beta}$ and $\epsilon_{p\beta}$ are the energies of the single particle states and $n_{n\beta}$ and $n_{p\beta}$ are the occupation numbers for neutrons and protons respectively. The corresponding grand partition function for the system is

$$e^{-\Omega} = \sum_{Z',N',E'} \exp\left(\alpha_n N' + \alpha_p Z' - \beta E'\right) \tag{13}$$

α_n and α_p are some Lagrange multipliers to be determined by specifying the number of neutrons, protons and the energy of the nucleus. Again, replacing the summation over energies by an integral with a proper weighting function $\rho\ (E', Z', N')$ which is the level density, one can write

$$e^{-\Omega} = \sum_{Z',N'} \int dE'\, \rho(E',Z',N') \exp\left(\alpha_n N' + \alpha_p Z' - \beta E'\right) \tag{14}$$

The level density $\rho\ (E', Z', N')$ can be obtained by taking the inverse Laplace transform of the coefficient of $\exp(\alpha_n N + \alpha_p Z)$ in the grand partition function. This is

$$\rho(E,N,Z) = \frac{1}{(2\pi i)^3} \int d\beta \int d\alpha_n \int d\alpha_p\ e^{S} \tag{15}$$

Where

$$S = \Omega - \alpha_n N - \alpha_p Z + \beta E$$

As before the integrals in the above equation can be evaluated approximately by the method of steepest descent. The exponent S has a saddle point at

$$N = \frac{\partial \Omega}{\partial \alpha_n} \; ; \quad Z = \frac{\partial \Omega}{\partial \alpha_p} \; ; \quad E = -\frac{\partial \Omega}{\partial \beta}$$

The resulting expression for the level density is

$$\rho(E,Z,N) = \frac{\exp(S)}{(2\pi)^{3/2}\sqrt{D}} \tag{16}$$

where D is the second order partial derivative matrix

$$D = \begin{vmatrix} \frac{\partial^2\Omega}{\partial\alpha_n^2} & \frac{\partial^2\Omega}{\partial\alpha_n\partial\alpha_p} & \frac{\partial^2\Omega}{\partial\alpha_n\partial\beta} \\ \frac{\partial^2\Omega}{\partial\alpha_n\partial\alpha_p} & \frac{\partial^2\Omega}{\partial\alpha_p^2} & \frac{\partial^2\Omega}{\partial\alpha_p\partial\beta} \\ \frac{\partial^2\Omega}{\partial\alpha_n\partial\beta} & \frac{\partial^2\Omega}{\partial\alpha_p\partial\beta} & \frac{\partial^2\Omega}{\partial\beta^2} \end{vmatrix} \tag{17}$$

all evaluated at the saddle point.

The level density can thus be obtained if Ω is known as a function of α_n, α_p and β. Combining equations (12) and (13)

$$e^{-\Omega} = \sum_{n_{n\beta}, n_{p\beta}} \exp\left[\sum_\beta n_{n\beta}(\alpha_n - \beta\epsilon_{n\beta}) + \sum_\beta n_{p\beta}(\alpha_p - \beta\epsilon_{p\beta})\right] \tag{18}$$

so that

$$\Omega = \sum_\beta \log\left[1 + \exp(\alpha_n - \beta\epsilon_{n\beta})\right] + \sum_\beta \log\left[1 + \exp(\alpha_p - \beta\epsilon_{p\beta})\right] \tag{19}$$

It is apparent from the above equation that the proton and neutron contributions and its derivatives are additive giving rise to some simplifications.

$$\Omega = \Omega_n + \Omega_p$$

$$N = \frac{\partial \Omega_n}{\partial \alpha_n} \; ; \quad Z = \frac{\partial \Omega_p}{\partial \alpha_p}$$

$$E = E_n + E_p$$

where $E_n = -\frac{\partial \Omega_n}{\partial \beta}$; $E_p = -\frac{\partial \Omega_p}{\partial \beta}$

Similarly

$$S = S_n + S_p$$

where $S_n = \Omega_n - \alpha_n N + \beta E_n$

and $S_p = \Omega_p - \alpha_p Z + \beta E_p$

$$D = \frac{\partial^2 \Omega_n}{\partial \alpha_n^2} D_p' + \frac{\partial^2 \Omega_p}{\partial \alpha_p^2} D_n'$$

where

$$D_n' = \frac{\partial^2 \Omega_n}{\partial \alpha_n^2} \cdot \frac{\partial^2 \Omega_n}{\partial \beta^2} - \left(\frac{\partial^2 \Omega_n}{\partial \alpha_n \partial \beta} \right)^2$$

$$D_p' = \frac{\partial^2 \Omega_p}{\partial \alpha_p^2} \cdot \frac{\partial^2 \Omega_p}{\partial \beta^2} - \left(\frac{\partial^2 \Omega_p}{\partial \alpha_p \partial \beta} \right)^2$$

Consequently, until we get to the point of writing the level density as a function of N, Z and E, we can consider, with no loss of generality, a system with only one kind of particle. We thus have a complete formulation of the level density problem. In the most general case, the system of the three equations in the variables α_n, α_p and β is highly non-linear and has to be solved numerically. In a practical calculation one takes β as an independent variable to which any desired value can be assigned. Then α_n and α_p can be obtained by solving two uncoupled non-linear equations and the energy can be obtained by knowing α_n, α_p and β. To evaluate the level density for a given energy, interpolative techniques are to be used.

At this point it is worthwhile to note that the method used to derive the level density formula is of general use in statistical mechanics. The only difference between the problem considered here and one ordinarily encountered in statistical mechanics is the small number of particles in the nucleus. In the ordinary statistical mechanics, the particle number is so large that the entropy S is simply given by log ρ. In the present situation, the term in the denominator of equations (6) and (16), although much less important than the exponential, cannot be neglected. For the same reason, the thermodynamic temperature T($= 1/\beta$) is not identical to the nuclear temperature defined sometimes as the inverse of $\partial/\partial E (\log \rho)$. In ordinary statistical mechanics the two temperatures would be identical.

2.2 Dependence on angular momentum

In addition to the numbers of protons and neutrons and the total energy, there is at least one other good quantum number for the nucleus, namely the total angular momentum J. It is actually simpler to deal with the total magnetic quantum number M; this is just the sum of the single-particle magnetic quantum numbers, whereas the total angular momentum has no such simple additive property. The J dependence of the level density can be obtained in a simple way from its M dependence as shown below.

In this case, a nuclear level is defined by four constants

$$N = \sum_s n_{ns} \quad ; \quad Z = \sum_s n_{ps} \qquad (20)$$

$$E = \sum_s \left(n_{ns} \epsilon_{ns} + n_{ps} \epsilon_{ps} \right)$$

$$M = \sum_s \left(n_{ns} m_{ns} + n_{ps} m_{ps} \right)$$

where m_{ns}, m_{ps} are the single-particle magnetic quantum numbers for protons and neutrons respectively and the other symbols are the same as in equation (12). We can now define a grand partition function

$$e^{\Omega} = \sum_{N',Z',E',M'} \exp\left(\alpha_n N' + \alpha_p Z' + \gamma M' - \beta E' \right) \qquad (21)$$

The calculation would then proceed just as in the previous section. The level density has the form

$$\rho(E, N, Z, M) = \exp(S) / \left[(2\pi)^2 \sqrt{D} \right] \qquad (22)$$

where $S = \Omega - \alpha_n N - \alpha_p Z - \gamma M + \beta E$

and D_M is the 4 by 4 determinant of second derivatives of Ω, all evaluated at the saddle point of S.

Once ρ is known as a function of M, the J dependence is obtained using the relation

$$\rho(E, J) = \rho(E, M = J) - \rho(E, M = J + 1)$$

In the absence of an external magnetic field there is a degeneracy in the sign of the magnetic quantum numbers; there are pairs of single

particle states with the same value of ϵ_s (referring to either protons or neutrons) and opposite signs of m_s. Making use of this fact, it has been shown [20] that the dependence of the entropy S on M can be written as

$$S(E, M) = S(E, 0) - M^2/2\langle M^2\rangle + 0(M^4) \qquad (23)$$

where

$$\langle M^2\rangle = \frac{1}{4}\sum_{s} m_{ns}^2 \operatorname{Sech}^2 \frac{1}{2}(\beta\epsilon_{ns} - \alpha n) \qquad (24)$$

+ similar terms for protons.

The denominator term is given by

$$D_M = D\langle M^2\rangle + 0(M^2)$$

where D is the 3 by 3 determinant given by equation (17). Neglecting terms of order M^4 in S and terms of order M^2 in D_M gives the approximate expression

$$P(E,M) = P(E,0)\exp\left(-M^2/2\langle M^2\rangle\right)/\sqrt{2\pi\langle M^2\rangle} \qquad (25)$$

The J-dependence is then given by

$$P(E,J) = P(E,0)\,\frac{2J+1}{2\langle M^2\rangle}\exp\left(-J(J+1)/2\langle M^2\rangle\right)/\sqrt{2\pi\langle M^2\rangle}\,. \qquad (26)$$

It can be shown that the semiclassical WKBJ approximation applied to a gas of fermions in a spherical potential leads to a value of $\langle m^2\rangle$ given by $\langle m^2\rangle = IT/\hbar^2$, where I is the rigid body moment of inertia of the nucleus. However, one would expect deviations from this simple behaviour at low energies, where the detailed properties of the single particle spectrum are important. A rigid body with the dimensions of a heavy nucleus would have a spin dispersion factor $\langle m^2\rangle$ of the order of 150T. Such high values of $\langle m^2\rangle$ would render the exponential factor $\exp(-J(J+1)/(2\langle M^2\rangle))$ relatively unimportant for the levels studied in low energy neutron spectroscopy. Thus, the density of neutron resonances is expected to be very nearly proportional to the factor $(2J+1)$ according to this model. Lynn has tabulated [6] available data on the low energy resonances of some nuclei with ground state angular momentum $I = \frac{1}{2}$ and 3/2. For target nuclei with $I = \frac{1}{2}$ the number of resonances observed with J = 1 ranges from twice to three times the number with J = 0. (the expected ratio is 3). For target nuclei with I = 3/2 the observed ratios of the numbers of J = 2 resonances to J = 1 resonances range from 1 to 3 while the expectation is 1.67. Thus, the (2J + 1) law seems to be confirmed at least for the lowest values of J.

2.3 Effects of residual interactions and Odd-even effect in level densities

In the formulation presented so far, the nucleus is treated as an assembly of non interacting nucleons confined to the nuclear volume by an average potential. This is only the first approximation to the behaviour of a system of particles interacting via two-body forces and for a realistic description one has to include the correlations amongst the motions of the particles which inevitably arise from the short range components of the two body forces. A mathematically simple form for the residual force which has been successfully used in describing the well known odd-even effects in nuclear ground state masses [21] is the so called pairing force, defined by the value of its matrix element between the initial and the final states of the scattering of a pair of particles. Qualitatively the introduction of this force also explains the odd-even effect in the low energy behaviour of nuclear level densities. The partition function approach described in the previous section for calculating the statistical properties of the nuclei has been generalized also to include the pairing force [22-25]. As before, the grand partition function is first determined and is then restricted to conserve energy, number of particles and any other constants of motion such as the angular momentum projection.

We start with a Hamiltonian of the system in the following second quantization form

$$H = \sum_{\pm k} \epsilon_k a_k^+ a_k - \sum_{kk'} G_{kk'} a_{-k'}^+ a_{k'}^+ a_k a_{-k}$$

where ϵ_k are the unperturbed single particle energy levels, $G_{kk'}$ is the pairing interaction matrix element, and a_k^+, a_k are the single particle creation and annihilation operators. It has been shown by Moretto and Kataria [25] that for level density calculations, it is a good approximation to replace the matrix elements $G_{kk'}$ by a constant value G.

The logarithm of the grand partition function in this approximation (for one component only) is obtained as

$$\Omega = -\beta\sum_k(\epsilon_k - \mu - E_k) + \sum_k \ln\left[1+\exp(-\beta(E_k - \gamma m_k))\right] + \sum_k \ln\left[1+\exp(-\beta(E_k + \gamma m_k))\right] - \frac{\beta\Delta^2}{G} \qquad (27)$$

where $E_k = \left[(\epsilon_k - \mu)^2 + \Delta^2\right]^{1/2}$

The quantities $\Delta, \mu, \gamma, \beta$ are related to each other through the gap equation

$$\frac{2}{G} = \sum_k \frac{1}{2E_k}\left[\tanh\frac{\beta}{2}(E_k-\gamma m_k) + \tanh\frac{\beta}{2}(E_k+\gamma m_k)\right] \quad (28)$$

The level density of the system is as before the inverse Laplace transform of the grand partition function. The saddle point conditions give for the constants of motion

$$N = \sum_k \left[1 - \frac{\epsilon_k-\mu}{2E_k}\left\{\tanh\frac{\beta}{2}(E_k-\gamma m_k) + \tanh\frac{\beta}{2}(E_k+\gamma m_k)\right\}\right] \quad (29)$$

$$M = \sum_k m_k\left[\frac{1}{1+\exp\beta(E_k-\gamma m_k)} - \frac{1}{1+\exp\beta(E_k+\gamma m_k)}\right] \quad (30)$$

$$E = \sum_k \epsilon_k\left[1 - \frac{\epsilon_k-\mu}{2E_k}\left\{\tanh\frac{\beta}{2}(E_k-\gamma m_k) + \tanh\frac{\beta}{2}(E_k+\gamma m_k)\right\}\right] - \frac{\Delta^2}{G}. \quad (31)$$

The system of equations (28)-(31) defines the saddle point values of Δ, μ, γ and β. The entropy S is then given by

$$S = \sum_k \ln\left[1+\exp\left(-\beta\left(E_k-\gamma m_k\right)\right)\right] + \sum_k \ln\left[1+\exp\left(-\beta\left(E_k+\gamma m_k\right)\right)\right] + \beta\sum_k \frac{E_k-\gamma m_k}{1+\exp\beta(E_k-\gamma m_k)} + \beta\sum_k \frac{E_k+\gamma m_k}{1+\exp\beta(E_k+\gamma m_k)} \quad (32)$$

Expressions for the second derivative matrix can similarly be obtained by simple differentiation. The generalization to two components, protons and neutrons, is also straight forward. A complete presentation of the formalism can be found, for example, in reference [24].

The formalism has been recently extended [26] to include, for the residual interactions, both Hartree-Fock and pairing type effects also.

3. APPROXIMATION AND SEMI-EMPIRICAL FORMULAE

3.1 The constant spacing model and the Bethe formula

In the formulation of nuclear level densities presented above, nuclear structure enters only through the single particle states ϵ_s. The simplest possible model is one in which the densities of neutrons and protons are constant. We again start with the grand partition function and replace the sum over single particle states in equation (19) by integrals

$$\Omega = \int_0^\infty d\epsilon\, g_n(\epsilon)\log\left[1+\exp(\alpha_n-\beta\epsilon)\right] \quad (33)$$

+ similar terms for protons

where $g_n(\epsilon)$ and $g_p(\epsilon)$ are, by definition, the densities of neutron and proton single particle states respectively. Further modification of the above equation leads to

$$\Omega = \beta\int_0^\mu d\epsilon\, g_n(\epsilon)(\mu_n-\epsilon) + \int_0^\mu d\epsilon\, g_n(\epsilon)\log\left[1+e^{\beta(\epsilon-\mu)}\right] + \int_0^\infty d\epsilon\, g_n(\epsilon)\log\left[1+e^{\beta(\mu-\epsilon)}\right] + \text{Similar terms for protons.} \quad (34)$$

the nuclear Fermi level μ is of the order of 30 MeV, whereas the temperature T is usually of the order of a few MeV. Thus, $e^{-\mu\beta} \ll 1$ and with negligible error

$$\Omega = \beta\int_0^\mu d\epsilon\, g_n(\epsilon)(\mu_n-\epsilon) + \int_0^\infty d\upsilon\left[g_n(\mu+\upsilon)+g_n(\mu-\upsilon)\right] \times \log\left[1+e^{-\beta\upsilon}\right] + \text{Similar terms for protons,} \quad (35)$$

for $g_n(\epsilon) = g_n = \text{const.}$ and $g_p(\epsilon) = g_p = \text{const.}$

$$\therefore \Omega = \frac{g_n\mu_n^2}{2T} + \frac{\pi^2 g_n T}{6} + \frac{g_p\mu_p^2}{2T} + \frac{\pi^2 g_p T}{6}$$

Then, $N = g_n \mu_n \; ; \; Z = g_p \mu_p$

$$E = \frac{1}{2}(g_n \mu_n^2 + g_p \mu_p^2) + \frac{\pi^2}{6}(g_n + g_p) T^2$$

$$S = \frac{\pi^2}{3}(g_n + g_p) T$$

$$D = \frac{2}{3} g_n g_p (g_n + g_p) T^5$$

The first term in the E equation is just the ground state energy E_o. The excitation energy is then

$$E_x = E - E_o = \underline{a} T^2$$

where $\underline{a} = \pi^2 (g_n + g_p)/6$

Making the approximation $(g_n + g_p)^2 = 4 g_n g_p$ leads to the familiar formula

$$\rho = \frac{\sqrt{\pi}}{12} \frac{\exp \sqrt{\underline{a} E_x}}{\underline{a}^{1/4} E_x^{5/4}} \qquad (36)$$

It can be shown that even if the density of single particle states is a slowly varying function of energy, the results of the constant spacing model are still approximately valid if the densities of single particle states are evaluated at the Fermi level. For nucleons in nuclei with nearly constant density, the single particle spectrum has the form $g(\epsilon) \propto \epsilon^{\frac{1}{2}}$. The Fermi level μ is given by

$$\mu = \left(\frac{3}{\pi}\right)^{2/3} \frac{9}{4} \frac{\hbar^2}{2 m_o r_o^2}$$

where r_o is the radius parameter and m_o is the nucleon mass. The densities of neutron and proton states at the Fermi level are

$$g_n(\mu) = \frac{3N}{2\mu}$$

$$g_p(\mu) = \frac{3Z}{2\mu}$$

The parameter $\underline{a}$ is thus proportional to the mass number A of the nucleus. It has been possible to fit the experimentally derived level densities of a large number of nuclei over the periodic table to an expression of the form given by eqn. (36), by allowing the level density parameter $\underline{a}$ to be essentially a free parameter. However, the values of $\underline{a}/A$ obtained from these fits show considerable deviations from a constant value expected on the basis of the Bethe model, especially in the region of closed shell. Moreover, in some cases [27, 28] as in the analysis of fission excitation functions, it has also been found necessary to assume the parameter $\underline{a}$ to be excitation energy dependent.

These anamolies in the "experimental" values of $\underline{a}$ have been qualitatively attributed to the effect of nuclear shell structure on level densities.

3.2 The Newton, Cameron, Gilbert-Cameron formulae

It is clear from a comparison of neutron resonance data with the free gas model level density expression that such a simple theory with its one more or less adjustable parameter is an inadequate explanation of nuclear level densities at moderate excitation energies. Simple study of the data reveals strong correlations with nuclear magic numbers. Various attemps have been made to improve the situation, due mainly to Newton, Cameron, and Gilbert and Cameron. All these authors stayed within the framework of the constant spacing model, putting all their effort into obtaining effective values of the parameter $\underline{a}$.

Newton's analysis [3] begins with the realization that the level density depends mainly on a few states in the neighbourhood of the Fermi level and the shell model single particle spectrum has gaps at the magic numbers resulting in a complex energy dependence of the single particle state density. In the integral approximation for the partition function and its derivatives, the integrand is a product of the single particle level density and a function

$$W(\epsilon) = \log \left[1 + \exp(-|\epsilon - \mu|/T)\right]$$

which has a sharp maximum at the Fermi energy and is of a width roughly equal to the temperature T. Therefore, instead of using the free gas model single particle level density value in the formula, Newton suggested the use of an average value, obtained by averaging the discrete levels of the shell model with the weighing function $W(\epsilon)$. In the spherical shell model, the Fermi energies correspond to the energy of the last unfilled subshells for neutrons and protons. If the angular momenta of these subshells are j_N and j_Z respectively, the single particle level densities are proportional to $(j_N + j_Z + 1)$ at very low temperature. At higher temperatures this proportionality is modified by the averaging procedure; the result can be represented by using a notation of effective angular momenta j_N and j_Z. Newton showed that the spherical shell model calculation results in more structure in the level density at excitations equivalent to neutron

separation energies than the resonance data reveal. The structure between the major shells is removed by using the spheroidal model of Nilsson in the mass number regions where nuclei are known to be deformed. The effective angular momenta calculated using the spherical shell model close to magic nucleon numbers and the spheroidal model in the deformed region are given in the form of a table by Newton. Also, for a spherical well potential of radius R, the energy eigen values have an R dependence which is R^{-2}. Therefore if the nuclear radius varies as $A^{1/3}$ the density of neutron or proton states should have the form

$$g_n = \alpha A^{2/3} (2\bar{j}_N + 1)$$

$$g_p = \alpha A^{2/3} (2\bar{j}_Z + 1) \qquad (37)$$

$$g = 2\alpha (\bar{j}_N + \bar{j}_Z + 1) A^{2/3}$$

The final formula for the density of levels of zero angular momentum and one parity is

$$\rho(u, J=0) = K_s (g_n g_p)^{-1/2} (2E_x + 3T)^{-2} \exp\left[\left(\frac{2\pi^2}{3} g E_x\right)^{1/2}\right] \qquad (38)$$

The dependence of the level density on angular momentum is assumed to be proportional to 2J+1. The numerical values determined by Newton for the proportionality constants α and K_s by fitting to the neutron resonance spacings of 52 nuclei are $\alpha = 0.01886$ and $K_s = 3,0/A$. Newton has tested the equation by the following statistical criterion. The quantity γ was defined as the logarithm of the ratio of the observed level spacing to the calculated spacing: $\gamma = \ln[D_{obs}/D_{cal}]$. Then the quantity $X^2 = (n-1)^{-1} \sum \gamma_R^2$ was formed, where n is the number of nuclei for which γ was determined. For 52 nuclei X^2 was found to be 1.11; this is to be compared with a value of $X^2 = 5.4$ found in fitting the same data to a Fermi gas form. The former value is equivalent to an expected error of a factor of 3. Lynn [6] has carried out an analysis of a more extensive set of data than those that were available to Newton with the same formula. It was found that most of the data lie above the theoretical curve by a considerable factor; only at some of the closed shells and amongst the lighter nuclei is there reasonable agreement. It was also found that overall agreement cannot be obtained by a simple adjustment of the constant α. There are, however, some serious defects with Newton's method. Newton assumes that the Fermi level μ always has its ground state value. As we will see, this is not the case except for constant densities of single particle states. A more serious flow in Newton's treatment is that it leaves out the main feature of the shell model, namely the presence of gaps at closed shell.

To remedy some of those defects, it was suggested by Cameron [4] that one should obtain the single particle spacings from second differences of nuclear binding energies after removing the Coulomb and pairing terms rather than get them from the shell model. If M'(Z,A) is the mass excess after removing the Coulomb and the pairing terms, the proton orbit spacing is defined as

$$d(Z) = M'(Z,A) - 2M'(Z-1,A-1) + M'(Z-2,A-2)$$

A similar relation holds for the neutron spacing d(N). This procedure would be exact if the single particle spacings were constant as a function of N or Z: it proves adequate if these spacings are slowly varying and the formulae are applied close to the valley of beta stability. Then there is no adjustable constant as in the case of Newton's formula. In practice, it was also necessary to smooth out the results in the transition regions between spherical and deformed nuclei.

Having obtained single particle spacings as a function of N and Z Cameron proceeds to average them out using the same weighting function $W(\epsilon)$ as Newton. Using these average spacings in the equation (38) to calculate neutron resonance spacings, Cameron achieved a notable improvement over Newton, the calculated resonance spacings are off by a factor of 1.8 on the average, as compared to a factor of 3 for Newton's method.

Both the calculational schemes of Newton and Cameron are quite complicated. Nevertheless, these results indicate that shell effects in level densities could be predicted by a proper calculation based on the shell model.

We will now discuss one other method proposed by Gilbert and Cameron [5]. This method while being mainly semiempirical is very simple and has been widely used in nuclear data calculations. In the free gas model one would expect that the ratio $\underline{a}/A$ is a constant. Since appreciable deviations from the expected constancy occur near closed shell nuclei, it is reasonable to try to relate shell effects in resonance spacings to the shell correction to the nuclear ground state masses. While there is no unique way of doing this, Gilbert and Cameron demonstrated that a linear relationship exists between the ratio $\underline{a}/A$ as obtained from neutron resonances and the shell correction energy S to the nuclear masses. Specifically, it was found that two linear relations $\underline{a}/A = 0.00917S + 0.120$ and $\underline{a}/A = 0.00917S + 0.142$ can be obtained for the deformed and spherical nuclei. The average error was a factor of 1.8 as before.

In a subsequent analysis, Cameron has shown [29] that if one takes into account the deformation energy contribution to the ground state mass of nuclei it is possible to obtain a single universal linear relation for all nuclei.

3.3 Other semiempirical prescriptions

While the prescriptions of Newton, Cameron, and Gilbert - Cameron described above have stayed within the framework of Bethe formula, there have also been several studies based on mocked up shell model level schemes, such as a set of equally spaced levels of constant degeneracy [30] or a bunched periodic single particle level spectrum [31-35] in place of the equally spaced single particle level scheme of the Bethe model. Simple analytical results which could account for some of the most relevant experimental results were also derived in most cases. Without going into the details of the calculations, one of the significant features brought out by all these calculations is that in the high excitation energy limit, the shell effects manifest themselves as an energy shift. It was also found [36] that the magnitude of the energy shift is correlated with the ground state shell correction energy. A global fit to the neutron resonance data has also been attempted by Dilg et al [9] incorporating an energy shift and an adjustment of the level density parameter. However, the main problem in all these calculations is the significance of the parameter and the region of validity of these. For instance, the energy shift, while being a good asymptotic approximation, is not guaranteed to be given a good description at low excitation energies. The logical way is therefore, to go directly to a single particle spectrum given by the shell model and to calculate all the necessary quantities. The availability of high speed computers and reliable shell model single particle level schemes has made a procedure practical.

4. NUMERICAL CALCULATIONS OF LEVEL DENSITIES FROM SHELL MODEL SINGLE PARTICLE LEVELS

In the last few years, several calculations of shell model single particle level schemes have been carried out both as a function of nucleon numbers and as a function of nuclear shape in connection with the studies of nuclear deformation potential energy surfaces [37, 38]. Simple global parameters for the underlying shell model potential have also been estimated on the basis of fits to nuclear ground state masses and fission barrier heights [39, 40]. Based on these and other single particle level schemes and the partition function approach, several numerical calculations of nuclear level densities have been carried out and used in nuclear reaction rate calculations [41, 53]. However, only a few systematic comparisons of the level spacings thus calculated with the available experimental data have been undertaken. We refer here to two such comparisons carried out by Dossing and Jensen [54] and Huizenga et al [55, 56]. Starting from a realistic set of single particle levels generated for a Woods-Saxon potential, Dossing and Jensen have calculated the level spacings of nuclei in the mass range $100 < A < 253$, and compared it with the available experimental data from neutron resonances. It was found that for all nuclei except in the region of the doubly closed shell nucleus ^{208}Pb, the calculated level densities were systematically underestimated by a factor of nearly 100. This discrepancy was partly resolved by noting that most of the nuclei included in the analysis are deformed in their ground state and that nuclei having deformed shapes have been predicted earlier to have an enhanced density of levels due to the available extra collective degrees of freedom [57, 58]. However, the discrepancy for nuclei with $A < 138$ whose ground state shapes are spherical remained unresolved.

The analysis of Huizenga et al, on the other hand, included nuclei in a somewhat wider mass range $50 < A < 250$. Spherical and deformed nuclei were separately considered for the analysis. Starting from the single particle level scheme of Seeger and Perisho [39], Huizenga et al [55] calculated the level spacings of about 100 spherical nuclei at neutron binding energy and showed that in more than 66% of the cases studied, the calculated level spacings agree within a factor of two with the experimental values. In the case of deformed nuclei, the single particle level scheme of Nilsson et al [59] was used for the calculation of the level spacings and it was again shown that good agreement with experimental data could be obtained if one includes the enhancement due to collective degrees of freedom. It is therefore believed on the basis of the comparisons of Dossing and Jensen and Huizenga et al that numerical calculations of level densities starting from shell model single particle level schemes lead to fairly reliable estimates of the same and that there is an evidence for the enhancement of the level densities due to collective degrees of freedom for deformed nuclei.

Two important features of the above comparisons are, however, worth pointing out here. While in the analysis of Dossing and Jensen the single particle level scheme used for the level density calculations is the same for spherical and deformed nuclei, Huizenga et al have used two different single particle level schemes for the two classes of nuclei. It was also found that the calculated level densities were systematically underestimated by an average factor of about 30-40 at excitation energies of the order of neutron binding energies when the Nilsson level scheme was used. Significantly this factor is quite close to the collective enhancement factor introduced for deformed nuclei. In the analysis of Dossing and Jensen, the discrepancy for nuclei with $A < 138$ is disturbing since the number of spherical nuclei for which agreement is obtained is quite small. Thus, it is not quite

clear whether one can make reliable estimates of level densities from single particle levels over the full periodic table. In addition, if two sets of single particle level schemes yield different results for the level densities, it is not clear which of the two should be taken as reliable.

A more intrinsic objection to a direct calculation of level densities from shell model single particle level schemes is as follows. It is now well known that a static shell model cannot be expected to describe adequately the ground state properties and deformation energies of nuclei. Instead, one replaces the smooth component of the total nuclear shell model energy by a phenomenological liquid drop expression to obtain the potential energy of a nucleus. It is therefore natural that one may doubt the reliability of numerical calculations of level densities also in the absence of a renormalization procedure as in the case of deformation energy calculations. In particular, in any shell model calculation the quantity on which the calculated level density crucially depends is the density of single particle states near the Fermi level. This is not a quantity which is crucially adjusted in any calculation of shell model energy level scheme. In fact, differences to the extent of 10-20% are known to exist between the calculated average single particle level density near the Fermi level corresponding to various level schemes currently being used in literature for the calculation of nuclear shell correction energies. The major shell spacing is to first order a measure of this quantity and has a value $(35\text{-}50)/A^{1/3}$ in literature. Even though the ground state shell correction energies evaluated from different single particle level schemes are found to be appreciably different. It is therefore necessary to adopt a normalization procedure which ensures that the shell independent parts of the calculated level densities are consistent with a liquid drop model estimate and the shell dependent part is consistent with experimental shell correction energies. In the absence of such a normalization the calculated level densities from different single particle level schemes are expected to exhibit appreciable differences.

Another objection which can be raised against the numerical calculations of level densities is that these calculations are carried out in the independent particle model approximation. Some earlier studies [60] have shown that if one takes into consideration that the shell model potential is an effective potential generated by two-body interactions the calculated level densities as a function of excitation energy differ significantly from those calculated in the independent particle approximation.

Based on similar arguments, Gottschalk and Ledergerber [61] have proposed an extension of the Strutinsky method in order to describe the level densities of excited nuclei. Starting from a shell correction expansion for the Hartree-Fock grand partition function, the smooth components of the grand partition function are replaced by a phenomenological expression constructed from the deformation energy of the liquid drop model nucleus. The remaining oscillations are calculated directly from the shell model level scheme.

The proposed method has been used for a calculation of the fission probabilities. More extensive calculations covering a wide range of nuclei have, however, not yet been carried out. In spite of the above cited uncertainties in direct numerical calculations of level densities from shell model single particle levels, these calculations have contributed greatly to our understanding of the excitation energy dependence of shell effects on the level densities, particularly the washing out of shell effects on level densities with increasing excitation energy [62, 63]. One of the important conclusions that has been drawn from such numerical calculations is that the Bethe form for the level density is inadequate to satisfactorily describe the influence of shell effects on level densities even if the level density parameter is treated as a free parameter since this parameter shows an explicit excitation energy dependence. In particular it was shown that the excitation energy dependence of the thermodynamic entropy of a nucleus with shell effects deviates considerably from the form expected on the basis of the Bethe model. Instead a behaviour of the form

$$S^2 = 4\left[\underline{a}^{LDM} + \Delta_a(E_x)\right]\left[E_x + \Delta_E(E_x)\right] \tag{39}$$

was found where Δ_a and Δ_E are excitation energy dependent parameters and $\underline{a}^{LDM}$ is the liquid drop model value of the level density parameter. The asymptotic behaviour of Δ_a and Δ_E are such that, as the excitation energy increases, Δ_a decreases approaching an asymptotic value of zero, while Δ_E increases approaching an asymptotic value Δ, where Δ is the ground state shell correction energy of the nucleus. It was also found that these asymptotic values are reached at excitation energies of the order of 30-40 MeV.

Purely from the point of a mathematical representation equation (39) can also be written in the equivalent forms

$$S^2 = 4\left[\underline{a}^{LDM} + \Delta_a(E_x)\right]E_x \tag{40}$$

$$S^2 = 4\left[E_x + \Delta_E(E_x)\right]\underline{a}^{LDM} \tag{41}$$

Equation (40) implies that the deviation of the plot of the square of the entropy versus the excitation energy from a straight line passing through the origin can be represented by a shell and an excitation energy dependent level density parameter. In other words, one can take into account the shell effects on nuclear level densities by introducing an energy dependent shell correction $\Delta a(E_x)$ into the liquid drop model level density parameter. This procedure is somewhat similar to the conventional method of taking into account shell effects on level densities where the level density parameter is treated as a free parameter. On the other hand, equation (41) implies the introduction of an effective excitation energy to be measured from a reference mass surface which coincides with the actual ground state for small excitation energies and with the liquid drop model ground state for small excitation energies and with the liquid drop model ground state for high excitation energies. This procedure is quite similar to the Hurwitz-Bethe empirical prescription [64] where one subtracts from the excitation energy the ground state shell correction energy for the calculation of nuclear level densities. Of these three equivalent expressions, equation (39) is preferred since in this case, by a proper choice of Δa and ΔE, not only the magnitude of S^2 but also its derivative with respect to the excitation energy can be correctly represented. Equation (41) though is not very well suited for low excitation energies, exhibits the correct asymptotic high energy behaviour, Equation (40) does not show any asymptotic behaviour and is not suitable to be used in any excitation energy range.

Similar conclusions have also been drawn regarding the excitation energy dependence of pairing effects on nuclear level densities. At low excitation energies, pairing effects manifest themselves in all the thermodynamic properties of nuclei. As the excitation energy increases, the effect of pairing weakens and at temperature above a critical temperature T_c the pairing effects completely vanish. The only remembrence of pairing at these temperatures is an energy shift equal to the ground state condensation energy, equal to the ground state energy difference with and without pairing. Angular momentum of the nucleus plays a similar role as the excitation energy in weakening pairing effects and tend to reduce the critical temperature at which pairing is fully wiped out.

5. NEW SEMIEMPIRICAL LEVEL DENSITY FORMULAE WITH SHELL EFFECTS

It is clear from the discussions presented in the previous sections that while all the currently available nuclear level density formulae based on the traditional Bethe model with one or more parameters is inadequate to satisfactorily describe the influence of nuclear shell effects; the more recent direct numerical calculations of level densities starting from shell model single particle level schemes have not yet achieved the required level of reliability. In view of these, attempts have been made in the recent years to develop new semiempirical formulae which while retaining the simplicity of the earlier analytical formulae take into account nuclear shell effects in a more realistic manner. We briefly describe some of these investigations here.

5.1 Ignatyuk, Smirenkin and Tishin formula

It is known that the experimental values of the level density parameters of nuclei as evaluated from neutron resonance density data show considerable deviations from the predictions of the simple Bethe model and that these deviations are correlated with the shell correction energies to the ground state masses of nuclei. Ignatyuk et al [65] have proposed, on the basis of the above observations, the following energy dependence of the level density parameter

$$\underline{a}(E_x) = \underline{a}^{LDM}\left[1 - f(E_x)\,\Delta / E_x\right]$$

where $\underline{a}^{LDM}$ is the asymptotic value of $\underline{a}$ at high excitation energies, and Δ is the ground state shell correction energy of the nucleus. The dimensionless function $f(E_x)$ determines the excitation energy dependence of $\underline{a}$. $f(E_x) \rightarrow 1$ as $E_x \rightarrow \infty$ and $f(E_x)/E_x \rightarrow$ constant as $E_x \rightarrow 0$.

The above functional form is chosen on the basis of arguments similar to our earlier discussion on the excitation energy dependence of the thermodynamic entropy of a nucleus with shell effects. The following functional form was chosen for $f(E_x)$ on the basis of the numerically calculated entropy values versus the excitation energy for different nuclei.

$$f(E_x) = \left[1 - \exp(-\gamma E_x)\right]$$

In order to allow for possible deviations of the asymptotic behaviour of the level density parameter from the Bethe expression $\underline{a}^{LDM}$ was expressed in the form [66]

$$\frac{\underline{a}^{LDM}}{A} = \alpha + \beta A^{-1/3}$$

By a least square fit to the experimental level density parameters of about 200 nuclei the following values for the coefficients were obtained.

$$\alpha = 0.114$$
$$\beta = 0.162$$
$$\gamma = 0.054 \text{ MeV}^{-1}$$

5.2 Kataria, Ramamurthy and Kapoor formula

Another effort in the same direction is the semiempirical formula for level densities proposed by Kataria et al. It is known that the single particle states in nuclei exhibit appreciable fluctuations from the equidistant level scheme and these fluctuations are the source of the observed shell effects in nuclear masses and other observables. It has also been shown [13] that the systematics of shell correction energies to nuclear ground state masses can be reasonably well understood if the shell fluctuations to the single particle level density are approximated by a simple cosine term. Ramamurthy et al have shown [67] that for the same type of single particle level density, the following simple relations for the entropy and excitation energy of a nucleus as a function of the temperature can be obtained:

$$S = 2\underline{a}T + \frac{\Delta}{T}\left[\frac{\pi^2 w^2 T^2 \cosh \pi w T}{\sinh^2 \pi w T} - \frac{\pi w T}{\sinh \pi w T}\right] \quad (42)$$

$$E_x = \underline{a}T^2 + \Delta\left[\frac{\pi^2 w^2 T^2 \cosh \pi w T}{\sinh^2 \pi w T} - 1\right] \quad (43)$$

where $\underline{a}$ is the liquid drop model value of the level density parameter, given by $\underline{a} = \alpha A$. Δ is the ground state shell correction energy of the nucleus and w is the fundamental frequency of oscillation of the shell fluctuations to the single particle level density. By definition w is characteristic of the major shell spacing in nuclei and is represented as $w = w_0 A^{1/3}$, where w_0 is a mass independent parameter. A comparison of the calculated level spacings on the basis of the above equations with the experimental data for about 100 spherical nuclei yielded the following values for α and w_0 in the least square sense:

$$\alpha = 0.14 \text{ MeV}^{-1} \quad \text{and} \quad w_0 = 0.185 \text{ MeV}^{-1}$$

A further analysis of the data showed that the liquid drop model value of the level density parameter $\underline{a}$ itself exhibits a mass dependence of the form

$$\underline{a} = \gamma A\left(1 - \beta A^{-1/3}\right)$$

The second term represents the effect of the finite size of the nucleus on the density of single particles at the Fermi level and therefore on the level density parameter. Generalized to deformed nuclei, the above equation can be rewritten as

$$\underline{a} = \gamma A\left(1 - \beta A^{-1/3} B_s\right)$$

where B_s is the nuclear surface area relative to spherical shape. The best values of γ and β obtained by a least squares fit to the experimental data are $\gamma = 0.175$ MeV^{-1} and $\beta = 1.0$

It should be pointed out here that, while the functional form for $\underline{a}$ chosen by Ignatyuk et al [65] and Kataria et al [68] are the same, the coefficients of the $A^{-1/3}$ term obtained by them on the basis of a fit to the experimental data are different and are in fact of opposite sign. While the precise reason for this discrepancy is not clear, we show in figure 1 a plot of $\underline{a}/A$ versus $A^{-1/3}$ obtained by Kataria et al for various nuclei. The $\underline{a}$ values were obtained from the measured level spacings using equations (42) and (43). The negative slope is quite apparent.

Further details of the work are found in reference [68]. Kataria et al have also shown that the above formula when applied to deformed nuclei lead to calculated level spacings which are reasonably close to the experimental data within an average factor of 2-3. Fig. 2 and 3 show plots of the ratio of the calculated to the experimental level spacings as obtained by Kataria et al for spherical and deformed nuclei. As can be seen from the figures, there was no evidence for any significant enhancement of the level densities of deformed nuclei over the corresponding values obtained for spherical nuclei. As indicated in an earlier section such an enhancement has been deduced in earlier analysis of Dossing and Jensen [54] and Huizenga et al [56] and has been interpreted as a consequence of additional rotational degrees of freedom available to deformed nuclei if one assumes that rotational degrees are totally decoupled from intrinsic excitation. The results of Kataria et al may imply that the assumption of totally decoupled rotational degree is not valid at excitation energies of the order of neutron binding energies.

Another important implication of the proposed two parameter form for the level density parameter $\underline{a}$ is that the level density parameter for the fission saddle point shape is predicted to be smaller by

about 5% as compared to that for the spherical shape- a fact which is important for any reliable analysis of fission excitation functions. Evidence for such an effect has already been reported by Ramamurthy and Kapoor [69] in an analysis of the fission excitation function for the alpha particle induced fission of ^{208}Pb.

6. COLLECTIVE CONTRIBUTIONS TO NUCLEAR LEVEL DENSITIES

It is well known that nuclei exhibit near their ground state many low energy collective levels, rotational and vibrational. In general, each intrinsic level may therefore be expected to give rise to a band of collective levels and the total level spectrum for a given angular momentum is to be obtained as a sum over a set of intrinsic states. Such an analysis has been performed by Ericson [57] and Björnholm et al [58] and shown that in nuclei that have static deformations in their ground state the level densities are enhanced over those for spherical nuclei because of the contributions from the available rotational degrees of freedom. We present only a summary of the analysis here. For the case of a spherical nucleus it has been shown earlier that the level density considered as a function of the angular momentum can be written as

$$\rho(E,I) = \frac{2I+1}{\sqrt{8\pi}\,\sigma^3} \exp\left[-\frac{I(I+1)}{2\sigma^2}\right] \rho(E)$$

where σ is the spin cut-off parameter.
In a deformed nucleus each intrinsic state gives rise to a rotational band and the total level spectrum for a given angular momentum is to be obtained by summing over a set of intrinsic states. Let us consider the simple case of a nucleus having a ground state deformation shape with axial symmetry and invariance with respect to a rotationa R of 180° about an axis perpendicular to the symmetry axis. Axial symmetry implies that the intrinsic states can be specified by a quantum number K representing the component of I along the symmetry axis. The intrinsic states are also degenerate with respect to the sign of K as a result of the R invariance. Decomposing the total level density of intrinsic states into partial densities with specified K

$$\rho_{intr}(E) = \sum_{K=-\infty}^{\infty} \rho_{intr}(E,K)$$

Assuming a normal distribution for $\rho_{intr}(E;K)$ with a variance σ_K the level density for specified I is obtained by summing over intrinsic states with $|K| \leq I$.

$$\rho(E,I) = \frac{1}{2} \sum_{K=-I}^{I} \rho_{intr}(E - E_{rot}(K,I), K)$$

where $E_{rot}(K, I)$ is the rotational energy.

For values of I such that $E_{rot}(K, I)$ is small compared with the temperature and $I < \sigma_K$ one can neglect the dependence of E_{rot} as well as the exponential factor in $\rho_{intr}(E, K)$ to obtain

$$\rho(E,I) = \frac{(2I+1)}{\sqrt{8\pi}\,\sigma_K} \rho_{intr}(E)$$

It is thus seen that the level density in the case of a deformed nucleus exceeds that for a spherical nucleus by a factor of the order of σ^2. In general, any further loss of rotational symmetry leads to a corresponding increase in the total level density by a factor of the order of the total number of states in the collective spectrum with energies less than the temperature. One can also include in a similar way the vibrational contributions to the level densities.

The above analysis assumes that it is possible to fully decouple the collective and the intrinsic degrees of freedom of the nucleus. However, this approximation is expected to break down when the nuclear temperature becomes comparable to the energies associated with single particle excitation and it is no longer possible to speak of fully decoupled collective and intrinsic motion.

The dependence of the absolute level density on the asymmetry of the nucleus can be quite appreciable since the spin cut-off factors are about 5 for a heavy nucleus with excitation energies in the region of a few MeV. It is generally believed that there is experimental evidence for such a collective enhancement of the level densities on the basis of the analysis of Dossing and Jensen [54] and Huizenga et al [56] . However, as mentioned in the earlier section, independent analyses by Kataria et al [68] and Ignatyuk et al [65] have shown that such an enhancement is not demanded by the experimental data. It was also shown that the reason for this contradictory conclusion is the possible uncertainities in the numerically calculated level densities from shell model single particle levels with no normalization to liquid drop model values.

7. MISCELLANEOUS TOPICS

We have so far assumed that the nuclear levels are characterized by only the energy and the angular momentum. However, in some cases it may be necessary to specify other constants. One frequently encountered example is the preequilibrium emission of particles in nuclear reactions [70] . In describing the hard portion of the energy spectrum of particles emitted in the decay of a nucleus preequilibrium models have been extensively used. One of the principal nuclear inputs to the model is the density of excited states with a given number of particles and holes. This density is usually calculated using the simple relations derived from the model of noninteracting particles for an equispaced single particle level scheme. As was mentioned earlier it is possible to generalize the partition function approach to calculate the density of particle - hole states on the basis of a shell model level scheme. Such a generalization has been reported by Ignatyuk et al [71, 72] and shown that this approach enables one to study the manifestation of shell and pairing effects in the par - ticle-hole densities and also to evaluate the approximations used in different simplified studies. However, at present no direct experimental data exist to test the predictions of the formulae.

Another similar constraint which is likely to be encountered in preequilibrium reactions is the isospin constancy. In view of the small reaction times involved in preequilibrium emission as compared to the isospin mixing times, it is necessary to include only states of definite isospin in the calculated level densities. Jensen [73] has recently reported a calculation of level densities with specified values of isospin. The expression is given in terms of the ordinary level density where the total isospin is not specified and therefore contains both the shell and pairing effects. One of the main conclusions of Jensen's analysis is that the level density for a given isospin decreases with increasing value of the isospin itself. Again, for reactions where there are strong isospin selection rules, an exact decomposition of the level density into components with specific isospins is necessary.

8. SUMMARY AND OPEN PROBLEMS

A summary of the present state of art in nuclear level density calculations is as follows. The traditional Bethe expression with empirical adjustments of the level density parameter and the effec - tive excitation energy does not fully satisfy our present requirements especially when extrapolations into new regions of excitation energies and nucleon numbers are involved. The exact numerical calculations based on shell model single particle level schemes and the partition function approach, on the other hand, have not yet reached a level of reliability where they can be directly used for reaction rate calculations. Development of new semiempirical formulae for level density calculations which explicitly take into account some of the important features of numerical calculations are therefore quite relevant. While a beginning has already been made in this direction with the development of shell-dependent formulae, more attention is to be devoted to a more realistic treatment of nuclear pairing effects, composition dependence, shape dependence etc. In the numerical calculations, apart from the need to refine the formalism to include self-consistency effects, an immediate requirement is to provide a reliable set of single particle level schemeswhich can be used for routine level density calculations.

I thank my colleagues Drs. S.S. Kapoor and S.K. Kataria for many helpful discussions. My thanks are also due to Dr. M.K. Mehta for his keen interest in this work.

REFERENCES

1. WEISSKOPF, V.F., Phys. Rev. 52 (1937) 295.
2. WEISSKOPF, V.F., EWING, D.H., Phys. Rev. 57 (1940) 672.
3. NEWTON, T.D., Can. J. Phys. 34 (1956) 804.
4. CAMERON, A.G.W., Can. J. Phys. 36 (1958) 1040.
5. GILBERT, A., CAMERON, A.G.W., Can. J. Phys. 43 (1965)1446.
6. LYNN, J.W., The Theory of Neutron Resonance Reactions, Clarendon Press, Oxford, 1968.
7. FACCHINI, U., SAETTA-MENICHELLA, E., Energia Nucleare 15 (1968) 54.
8. BABA, H., BABA, S., JAERI - 1183 (1969).
9. DILG, W., SCHANTLE, W., VONACH, H., UHL, M., Nucl. Phys. A217 (1973) 269.
10. ENDT, P.M., VAN DER LEUN, C., Nucl. Phys. A105 (1967) 1.
11. BOHR, N., WHEELER, J.A., Phys. Rev. 56 (1939) 426.
12. BLATT, I.M., WEISSKOPF, V.M., Theoretical Nuclear Physics John Willey & Sons, New York, (1952).
13. BOHR, A., MOTTELSON, B.R., Nuclear Structure, Vol. I, Benjamin, New York, 1969.
    HUIZENGA, J.R., MORETTO, L.G., Ann. Rev. Nucl. Science 22 (1972) 427. and references cited therein.
14. HILLMAN, M., GROVER, J.R., Physics. Rev. 185 (1969) 1303.
15. MOTZ, L., FEINBERG, E., Phys. Rev. 54 (1938) 1055.
16. CRITCHFIELD, C.L., OLESKA, S., Phys. Rev. 83 (1951) 243.
17. GROVER, J.R., 157 (1967) 832.
18. KLUGE, K., Nucl. Phys. 51, (1967) 41.
19. See for instance FOWLER, R.H., Statistical Mechanics, 2nd Edition, University Press, Cambridge (1966).

20. BLOCH, C., Phys. Rev. 93 (1954) 1094.
21. BOHR, A., MOTTLESON, B.R., PINES, D., Phys. Rev. 110)(1958) 936.
22. SANO, M., YAMASAKI, S., Prog. Theor. Phys. 29 (1963) 397.
23. DECOWSKI, P., GROCHULSKI, W., MARCINKOWSKI, A., SIEWEK, K., WILHELMI, Z., Nucl. Phys. A110 (1968) 129.
24. MORETTO, L.G., Nucl. Phys. A182 (1972) 641; Nucl. Phys. A185 (1972) 145.
25. MORETTO, L.G., KATARIA, S.K., Lettere al Nuovo Cimento 9 (1974) 190.
26. CHOUDHURY, F.N., DAS GUPTA, S., Phys. Rev. C16 (1977) 757.
27. JARY, J., JAERI - M5984 (1975) 76.
28. THOMPSON, S.G., Ark. Fys. 36 (1966) 267.
29. BRANCAZIO, P.J., CAMERON, A.G.W., Can. J. Phys. 47 (1969) 1029.
30. ROSENZWEIG, N., Phys. Rev. 108 (1957) 817.
31. ROSENZWEIG, N., Nuovo Cimento 43B (1966) 227.
32. ROSENZWEIG, N., Phys. Letters 22 (1966) 307.
33. KAHN, P.B., ROSENZWEIG, N., Phys. Rev. 187 (1970) 1193.
34. GILBERT, A., UCRL - 18095 (1968).
35. BABA, H., Nucl. Phys. A159 (1970) 625.
36. RAMAMURTHY, V.S., KAPOOR, S.S., KATARIA, S.K., Phys. Rev. C5 (1972) 1124.
37. BRACK, M., DAMAGAARD, JENSEN, A.S., PAULI, H.C., STRUTINSKY, V.M., WONG, C.Y., Rev. Mod. Phys. 44 (1973)320.
38. NIX, J.R., Ann. Rev. Nucl. Sc. 22 (1972) 65.
39. SEEGER, P.A., PERISHO, R.C., LA - (1967).
40. SEEGER, P.A., HOWARD, W.M., Nucl. Phys. A238 (1975) 491.
41. IGNATYUK, A.V., SHUBIN, Y.N., Sov. J. Nucl. Phys. 8 (1969) 660.
42. IGNATYUK, A.V., Sov. J. Nucl. Phys. 9 (1969) 208.
43. IGNATYUK, A.V., STAVINSKI, V.S., SHUBIN, Y.N., Sov. J. Nucl. Phys. 11 (1970) 563.
44. MORETTO, L.G., Nucl. Phys. A180 (1972) 337.
45. MORETTO, L.G., THOMPSON, S.G., ROUTI, J., GATTI, R.C., Phys. Letters 38B (1972) 471.
46. WILLIAMS, F.C., CHAN, G., HUIZENGA, J.R., Nucl. Phys. A187 (1972) 225.
47. DECOWSKI, P., GROCHULSKI, W., MARCINKOWSKI, A., Nucl. Phys. A194)(1972) 380.
48. VANDENBOSCH, R., MOSEL, U., Phys. Rev. Letters 28 (1972) 1726.
49. BRITT, H.C., BOLSTERLI, M., NIX, J.R., NORTON, J.L., Phys. Rev. C7 (1973) 801.
50. METAG, V., LEE, S.M., LIUKKONEN, E., SLETTEN, G., BJORNHOLM, S., JENSEN, A.S., Nucl. Phys. A213 (1973) 397.
51. JENSEN, A.S., DAMGAARD, J., Nucl. Phys. A210 (1973) 282.
52. FREISLEBEN, H., BRITT, H.C., HUIZENGA, J.R., Physics and Chemistry of Fission, Rochester, IAEA (1973).
53. JENSEN, A.S., DOSSING, T., Physics and Chemistry of Fission, Rochester, IAEA, Vol.I (1973)
54. DOSSING, T., JENSEN, A.S., Nucl. Phys. A222 (1973) 493.
55. HUIZENGA, J.R., BEHKAMI, A.N., SVENTEK, J.S., ATCHER, R.W., Nucl. Phys. A223 (1973) 577.
56. HUIZENGA, J.R., BEKHAMI, A.N., ATCHER, R.W., SVENTHEK, J.S., BRITT, H.C., FREIESLEBEN, H., Nucl. Phys. A223 (1973) 589.
57. ERICSON, T., Nucl. Phys. 6 (1958) 62.
58. BJORNHOLM, S., BOHR, A., MOTTELSON, B.R., Physics and Chemistry of Fission, Rochester, IAEA, (1973) Vol.I, 367.
59. NILSSON, S.G., TSANG, C.F., SOBICZEWSKY, A., SZYMANSKI, Z., WYCHEC, S., LAMM, I.L., MOLLER, P., NILSSON, B., Nucl. Phys. A131 (1969) 1.
60. KATARIA, S.K., RAMAMURTHY, V.S., Pramana 7 (1976) 407.
61. GOTTSCHALK, P.A., LEDERGERBER, T., Nucl. Phys. A278 (1977) 16.
62. RAMAMURTHY, V.S., KAPOOR, S.S., KATARIA, S.K., Phys. Rev. Letters 25 (1970) 386.
KAPOOR, S.S., RAMAMURTHY, V.S., Physics and Chemistry of Fission, Rochester, IAEA, Vol. I (1973) 375.
KAPOOR S.S., RAMAMURTHY, V.S., Pramana, 5 (1975) 124.
63. JENSEN, A.S., DAMGAARD, J., Nucl. Phys. A210 (1973) 282.
64. HURWITZ, H., BETHE, H.A., Phys. Rev. 81 (1951) 898.
65. IGNATYUK, A.V., SMIRENKIN, G.N., TISHIN, A.S., Sov. J. Nucl. Phys. 21 (1975) 255.
66. IGNATYUK, A.V., ITKIS, M.G., OKOLOVICH, V.N., SMIRENKIN, G.N., TISHIN, A.S., Sov. J. Nucl. Phys. 21 (1975) 612.
67. RAMAMURTHY, V.S., KATARIA, S.K., KAPOOR, S.S., IAEA - 190 II(1975) 117.
68. KATARIA, S.K., RAMAMURTHY, V.S., KAPOOR, S.S., Phys. Rev. 18C (1978) 549.
69. RAMAMURTHY, V.S., KAPOOR, S.S., Pramana 10 (1978) 319.
70. BLANN, M., Ann. Rev. Nucl. Sc. 25 (1975) 1.
71. IGNATYUK, A.V., SOKOLOV, Yu. V., Sov. J. Nucl. Phys. 16 (1973) 155.
72. IGNATYUK, A.V., SOKOLOV, Yu. V., Sov. J. Nucl. Phys. 17 (1973) 376.
73. JENSEN, A.S., Phys. Letters 68B (1977) 105.

FIGURE CAPTIONS

Fig. 1 Plot of $\underline{a}/A$ versus $A^{-1/3}$. The bars represent the uncertainty in the deduced values of $\underline{a}$ due to differences in the compiled values of D_{exp} for the same nucleus. The straight line is the least square fit to the points.

Fig. 2 Plot of the ratio of the theoretical to the experimental level spacing versus the mass number A for spherical nuclei. The values of parameters used are α = 0.14, γ = 0.176, β = 1.0 and w_o = 0.185.

Fig. 3 Plot of the ratio of the theoretical to the experimental level spacing versus the mass number A for deformed nuclei. The values of parameters used are α = 0.14, γ = 0.176, β = 1.0 and w_o = 0.185.

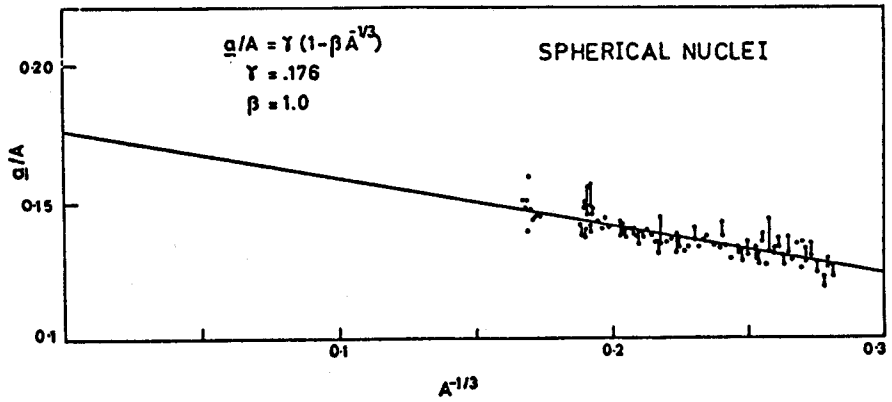

Figure 1

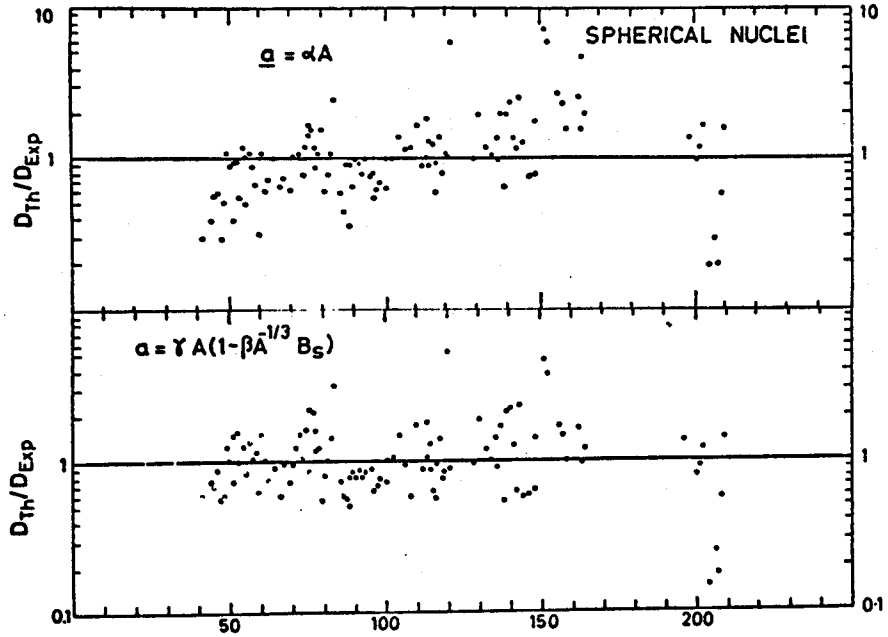

Figure 2

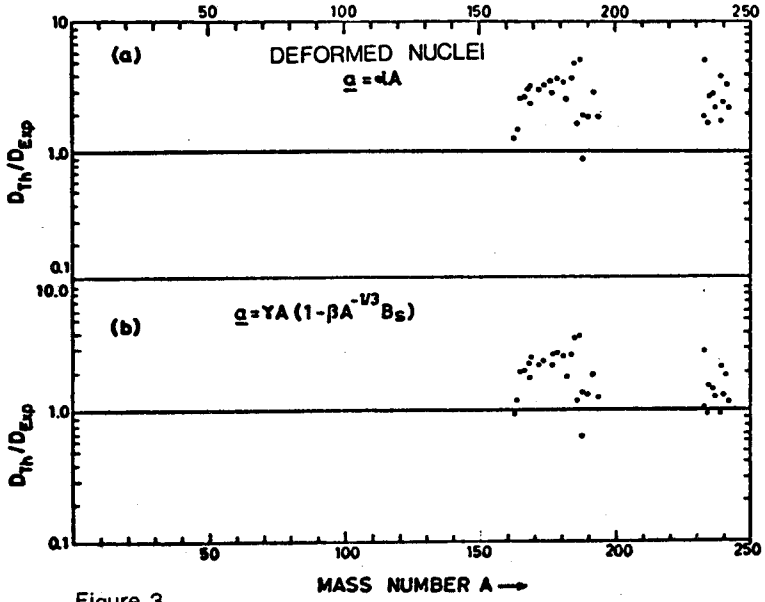

Figure 3

PARAMETER SYSTEMATICS FOR STATISTICAL THEORY CALCULATIONS OF NEUTRON REACTION CROSS-SECTIONS

G. REFFO*
Comitato Nazionale per l'Energia Nucleare,
Centro di Calcolo,
Bologna, Italy

Abstract

The problem of determining the parameters relevant to statistical model calculation of cross sections failing experimental information is reviewed from the point of view of the evaluation of nuclear data for reactor needs.

The level density problem in the whole energy range of interest is considered with emphasis on the systematic behaviour of the level density parameters "a", nuclear temperature T and matching energy U_x. A consistent determination of spin cut-off parameter is discussed.

The results of radiative decay width calculations according to most familiar approximations are investigated as well as its energy spin and parity dependence. Use of the Brink-Axel hypothesis is suggested and to this end the systematic trend of giant resonance parameters is shortly illustrated.

The systematic behaviour of neutron capture cross sections at lower energies as predicted by the statistical model is shown at 25 keV.

The degree of uncertainty in interpolating parameters on the systematic curves is given.

INTRODUCTION

There is a gap between the degree of sophistication of the models adopted in the calculation of cross sections for reactor needs and the degree of accuracy attached to parameters necessary for the models themselves.

Where one has no experimental information from which to deduce parameters or to normalize model calculations of parameters, one has to resort to model-guided systematics to interpolate or extrapolate parameters, or to "kitchen recipes" coupled with intuition and experience.

The purpose of these lectures is to illustrate what one can do in practice when the necessary parameters cannot be deduced from experiment and to show the accuracies obtained when the parameters needed are deduced from systematics.

Chapter 1. LEVEL DENSITY PROBLEM

Sect. 1. LEVEL DENSITY PARAMETERS

1.1. High Energy Level Density

The theoretical assumptions underlying commonly adopted level density formulae at high energies are based on the Fermi Gas Model (FGM).

Starting from the analogy which can be established between nucleon systems and gaseous systems, the model establishes:

a) that single particle states (sps) contributing to nuclear state excitations are those falling in the neighbourhood of Fermi's top for the order of thermodynamic temperature $(sps)_{FT}$;

b) a relation between $(sps)_{FT}$ density and nuclear state density;

c) a relation between quantum characteristics of nuclear states and the statistical averages of the corresponding quantities characterizing the ensemble of $(sps)_{FT}$.

It immediately appears that the model can only be valid where the excitation energies involved are high enough for the systems to be considered as being of a statistical nature.

Each nuclear state is completely characterized by the set of quantum numbers (E,J,M,π) .

In practice, one observes the nuclear levels, each level being completely determined by the set of quantum numbers (E,J,π) .

Because each nuclear level is $(2J+1)$ times degenerate in M , the relation between total density of states $\tilde{\rho}(E)$ and total density of levels $\rho(E)$ is given by eqs. 1 and 2 below,

$$\tilde{\rho}(E) = \Sigma_J \Sigma_\pi (2J+1)\, \rho(E,J,\pi) \qquad (1)$$

$\rho(E,J,\pi)$ being the density of levels of quantum characteristics (E,J,π) and

$$\rho(E) = \Sigma_J \Sigma_\pi \rho(E,J,\pi) \qquad (2)$$

Under the assumption of random coupling of sps parities, T. Ericson [1] has shown that nuclear states are equally distributed between the two parities, thus

$$\rho(E,J,\pi) \simeq \tfrac{1}{2} \rho(E,J) \ . \qquad (3)$$

By means of the central limit theorem of statistics and again under the assumption of random coupling of the projections m of sps angular momenta, it can be shown [1] that the distribution law for spin projections M of nuclear states is a Gaussian one

$$g(E,M) = e^{-M^2/2\sigma^2} \ . \qquad (4)$$

Consequently the distribution law for the spins J of nuclear levels becomes

$$f(E,J) \simeq \frac{(2J+1)\ \exp\left[-(J+\tfrac{1}{2})^2/2\sigma^2\right]}{2\sigma^2} \qquad (5)$$

where σ^2 is the so-called spin cut-off factor, a parameter which characterizes the spin distribution and establishes its energy dependence (the most probable value of J is given by $J \sim \sigma - \tfrac{1}{2}$).

According to the model

$$\sigma^2 \simeq g\ t(E)\ \langle m^2 \rangle \qquad (6)$$

t(E) being the thermodynamic temperature and $\langle m^2 \rangle$ an average taken over angular momentum projections of $(sps)_{FT}$.

From the distribution law (5) one has

$$\rho(E,J,\pi) = \tfrac{1}{2} \rho(E)\ f(E,J) \qquad (7)$$

and

$$\tilde{\rho}\ (E) = \rho(E)\ \Sigma_J (2J+1)\ f(E,J) = \rho(E)\ \sqrt{2\pi}\ \sigma \qquad (8)$$

thus giving the relation between total density of nuclear states $\tilde{\rho}(E)$ and total density of nuclear levels $\rho(E)$.

The recipe for model density calculations most widely adopted in available codes for neutron cross section evaluation is that given by Gilbert and Cameron (GC) [2]. The reasons for this universal choice are because the GC formula works reasonably well, it is simple enough to introduce into most sophisticated and time-wasting codes and it takes account of the description of level density also at low energies.

For these reasons in what follows all considerations are consistent with the GC formula, i.e. at high energies

$$\tilde{\rho}(E) = \frac{\sqrt{\pi}}{12} \frac{\exp\left[2\sqrt{a(E-\Delta)}\right]}{a^{1/4}(E-\Delta)^{5/4}} \qquad (9)$$

$$\rho(E,J) = \frac{\tilde{\rho}(E)}{\sqrt{2\pi}\ \sigma}\ f(E,J) \qquad (10)$$

where "a" is the level density parameter and Δ is the pairing energy correction.

1.2. Experimental Determination of Level Density Parameter "a"

The parameter "a" has a very well-defined physical meaning: it is proportional to the density of $(sps)_{FT}$ lying in a neighbourhood of the Fermi level for the order of thermodynamic temperature.

In practice, however, because of rough approximations of the model, wherever possible "a" is taken as a free parameter to be determined in general from mean level spacings of neutron resonances or more rarely from particle spectra analysis as well.

Excluding very exceptional cases (e.g. Pb^{208}) only s-wave and p-wave resonances can be excited. Analysis of s-wave resonances is much more accurate so in general only s-wave mean spacing of observed levels is taken into account.

Once the statistical analysis of one resonance scheme has been made and the value for $\bar{D}_{OBS}$ has been obtained, the following equation is solved to give the level density parameter "a",

$$\frac{1}{\bar{D}^{\ell=o}_{OBS}} = \tfrac{1}{2} \sum_{|I-s|}^{I+s} J\, \rho(B_n + \tfrac{\delta}{2}, J) \ , \qquad (11)$$

where the factor $\tfrac{1}{2}$ comes from considering only one-parity-type resonances, I is the target nucleus spin, $s=\tfrac{1}{2}$ is the neutron spin,

B_n is the neutron binding energy, $\frac{\delta}{2}$ accounts for the spread of the resonance energy interval.

On the one hand the procedure outlined is intended to meet the requirement of an experimental determination of "a" and a normalization of the model at the excitation energy $B_n+\frac{\delta}{2}$ to reproduce the observed mean level spacings; on the other hand the effects due to the model approximations give rise to an increase in the uncertainty in "a" which cannot be determined.

In addition questions may arise where one is faced with several variants of the model each of which gives more or less different expressions for $\rho(E,J)$. In fact, different expressions for $\rho(E,J)$ in eq. (11) obviously give different solutions for "a" . Furthermore even if two formulae are normalized at the same energy point, they may nevertheless yield divergent predictions for the energy behaviour of the level density, far from the normalization point. As an example one might mention the various conventions adopted for the pairing energy Δ .

According to the Fermi gas model in the elaboration by GC, Δ is a quantity to be subtracted from the total excitation energy, and is given as follows

$$\Delta = -\left[\Delta_{protons} + \Delta_{neutrons}\right] \quad \text{even even nuclei}$$

$$= -\Delta_{protons} \quad \text{N=odd, Z=even}$$

$$= -\Delta_{neutrons} \quad \text{N=even, Z=odd}$$

$$= 0 \quad \text{odd-odd nuclei.}$$

According to the back-shifted (BS) Fermi gas model, on the contrary, Δ is assumed to be added to the excitation energy.

The effects of these two conventions have been investigated in the case of Mo^{100}.

A value $\bar{D}_{OBS} = 670$ eV was assumed, while in addition $\Delta = 1.28$ MeV and $B_n = 5.39$ MeV were taken.

The spin cut-off parameter was determined consistently with the adopted conventions. In spite of the physical meaning of "a", the values for the level density parameters were

$a = 20.67\ MeV^{-1}$ G.C. model

$a = 13.5\ MeV^{-1}$ B.S. gas model .

In the table below the ratios

$$R(E) = \frac{\rho^{BS}\left[J=\frac{1}{2},\ B_n+E+\Delta\right]}{\rho^{GC}\left[J=\frac{1}{2},\ B_n+E-\Delta\right]}$$

are given for several values of E .

E(MeV)	0	1	2	3	4	5	6
R(E)	1	.45	.25	.16	.104	.069	.048

Similarly, because $\bar{D}_{OBS}$ depends on specific spin values of resonances and because "a" and σ are related to each other, different assumptions in the determination of σ lead to different distributions of levels according to spin, and consequently to different values for "a" .

Because of all these circumstances one must be very careful in using tabulated data of "a" or σ^2 and be certain that all adopted formulae and parameters are consistent.

1.3. Overall Systematic trend of "a"

Where the necessary experimental information is not available and the determination of "a" is not possible according to eq. (11), because a model determination of "a" is still affected by too large uncertainties one has to resort to systematics.

Several types of systematics are available. In all cases they are obtained by plotting the experimental values of "a" as obtained from the extensive use of eq. (11) in all cases where reliable resonance schemes are available.

In the literature almost every author has plotted a^{EXP} vs A . This systematic treatment, which is very rough, is consistent with the conclusions of the very simple Free Gas Model [1] which predicts an "a"-dependence on the mass number A of the type $a=const.\cdot A$.

In practice one observes large fluctuations of the experimental points around this theoretically predicted behaviour. This can be explained in that the model is much too rough to be able to account for the fluctuations in the density of $(sps)_{FT}$ due to shell and subshell closures, deformations, etc.

Alternatively one may assume the nucleus is a gas of nucleons of one type only (thus distinguishing neutrons and protons only by their isospin). Due to neutron excess ($T_z >> 0$ for medium and heavy nuclei) one expects the neighbourhood of the Fermi level for this gas to be mostly populated by neutron sps.

Accordingly one would expect the level density parameter to depend mostly on neutron number, at least for heavier nuclei.

In fig. 1 the plot $a^{EXP}(MeV^{-1})$ vs N is shown for neutron numbers $40<N<100$ typical of fission products (^).

Owing to the particularly stable configuration of magic nuclei the number of degrees of freedom of the nucleon gas is progressively greatly reduced at nearly magic numbers. This produces marked valleys in the "a"-trend (see fig. 1).

The plateau observed between two successive magic numbers is a deformation effect which will be better understood later on.

The plot given in fig. 1 is called "overall systematic" (OS) of the level density parameter because it can be used to estimate "a"-values of all nuclei.

The plotted curve fits experimental points to within 15%.

(^) Of course the plot can be extended to higher values until resonance schemes become available. On the contrary, one should not use data for light nuclei (say $N<28\div25$) . In this case the neutron excess tends to vanish and furthermore the number of sps can be so low that the statistical assumptions implied by eq. (11) do not hold any longer.

One commonly assumes that a comparable uncertainty may also be estimated for unknown "a"-values determined by use of the OS. (^)

What appears in statistical model formalism is the level density $\rho(E,J)$, therefore what one needs to know is the uncertainty in ρ . Unfortunately uncertainty in ρ results from the composition of

i) uncertainties as to the experimental data used in the O.S.;

ii) uncertainties due to the approximations implicit in the simple dependence of "a" on N which was assumed in the O.S.;

iii) uncertainties due to the model approximations (which can be energy dependent).

Because it is impossible to estimate all these uncertainties exactly and partly because they are incorporated in O.S. uncertainty, all one can do is to investigate how the O.S. uncertainty affects the ratios $\bar{D}^{CALC}_{OBS}/\bar{D}^{EXP}_{OBS}$ (mean level spacings calculated by means of "a" taken from O.S. over experimental ones). The results are shown in fig. 2. Error bars are those of D^{EXP}_{OBS} . Some 85% of cases fall between .5 and 1.5 ; if one takes into consideration the very large uncertainty of certain points lying outside this range, 50% appears to be a reasonable uncertainty over D^{CALC}_{OBS} when "a" is taken from O.S., and 100% can be considered an upper limit.

Greater accuracies than these are needed for cross section evaluation.

1.4. Local Systematic Trends in "a"

A further improvement in the determination of "a" can be obtained by taking into account deformation effects and proton contributions

(^) The OS given in fig. 1 is based on experimental data of stable nuclei. It is very likely that for nuclei far from the stability valley extrapolated "a"-values are affected by uncertainties greater than 15%.

to the density of $(sps)_{FT}$. Because the Nilsson model is able to predict sps characteristics (ε j m) in principle it appears to be a valid means of investigation.

To check this assumption a rough application of the model was carried out. Harmonic oscillator sps were considered. No Coulomb term was introduced, an approximation which is strictly valid only for low mass nuclei (say below $A \simeq 100$).

The staircase plot of the cumulative number of sps $N(\varepsilon)$ vs Fermi energies E_F in $\hbar\omega(\delta)$ units is shown in fig. 3 for spherical nuclei ($\delta=0$). [$\hbar\omega(\delta) = 41\ A^{-1/3} G(\delta)$, $G(\delta)$ being a function of δ which is related to deformation parameter β].

Introduction of the concept of an average occupation number according to Fermi statistics allows for a smoothing of the staircase into a set of curves that are continuous and derivable everywhere, each characterized by a given thermodynamic temperature t .

The level density parameter, disregarding a constant factor, is then given by the slope of the curves $N(\varepsilon,t)$

$$a \propto \frac{d\ N(\varepsilon)}{d\ \varepsilon}\bigg|_{\varepsilon=E_F} \qquad (12)$$

where $d\varepsilon \simeq t$.

As can be seen in fig. 3 the parameter "a" is very sensitive to the choice of t . A more thorough application of the model by use of a proper potential well would show that the parameter "a" is also very sensitive to the adopted well depth.

In fig. 4 the level density parameter $g=6/\pi^2 \cdot a$ in $\hbar\omega(\delta)$ units is plotted for several deformation values β = .1 ; .2 ; .3 ; -.1 as a function of neutron number N or proton number Z .

In all, 30% of the $\bar{D}_{OBS}$ values calculated according to these curves were in fair agreement with experimental ones within error bars.

In addition due to the rough approximations adopted, systematic deviations were observed in the slope of "a" curves.

This result, however, seems encouraging in view of all that can still be done in order to improve the application of the model.

To this end, a special mention must also be made of the problem of effective energy determination.

In addition useful information can be drawn from fig. 4 on the local and overall systematic behaviour of "a" . A glance at the figure allows one to conclude that

i) the typical shell closure effects already seen in the OS are punctually reproduced;

ii) "a" is a sum of neutron and proton contributions and the latter in some cases may be of comparable magnitude to the neutron ones. Accordingly one expects that the "a" trend for families of isotopes should be given by families of curves characterized by the same behaviour, more or less close to each other, with the amount of the splitting corresponding to the difference in proton contributions;

iii) the deformation effects can be very large. At high values of deformation β shell effects tend to be washed out (because of a uniform mixing of sps due to removal of degeneracies). In fact if one considers the curve $\beta=.3$ one sees that the characteristic fluctuations due to shell closure have disappeared, whereas the curves tend to be more consistent with an equidistant sps model and with predictions of FGM which gives $a \propto A$.

Because deformation effects play against shell effects, for highly deformed nuclei one observes a depression of the OS curve which results in a plateau-like trend (see fig. 1).

From the above points one may conclude that the OS finds its most significant explanation from the results of applying the Nilsson model, but also that deviations from OS are expected in the sense of local behaviours of "a" for those nuclei where more pronounced proton and deformation effects are present.

Because the model is not able, in this preliminary rough application, to predict D_{OBS}^{EXP} values, pending a more thorough application of the model, on the basis of the above conclusions it appears justified to investigate how the situation is improved by use of local systematics (LS) for "a".

In fig. 5 "a"-values are plotted against N for some isotope-rich families. In this way both proton and deformation effects are empirically taken into account.

A procedure which can be useful to extrapolate "a" is to normalize the trend of the model curves to experimental data. In practice it can be estimated that LS improve the accuracy in "a" determination by ~5%, which corresponds to a residual uncertainty in D_{OBS}^{CALC} ≈30%÷50%.

1.5. Choice of Spin Cut-off Factor at High Energies

In principle the spin cut-off factor could be determined from experiments e.g. from isomeric ratios of cross sections or by comparison of sequences of resonances with different J. Because these situations occur very seldom and in many cases the accuracies obtainable are not satisfactory, one commonly resorts to models.

In the model relation given by eq. (6) σ depends on g, $\langle m^2 \rangle$ and t(E), quantities which vary from nucleus to nucleus. Whereas g and t(E) can be related to each other,

$$E - \Delta = a\,t^2 - t \qquad (13)$$

$$a = \pi^2/_6 \cdot g \qquad (14)$$

$\langle m^2 \rangle$ must be determined independently for each case.

Again, because the Nilsson model provides us with a detailed microscopic description, its application appears promising in determining the averages $\langle m^2 \rangle$ over $(sps)_{FT}$. Results are shown in fig. 6, where $\langle m^2 \rangle$ are plotted against particle number for several deformations. One observed that $\langle m^2 \rangle$ depends on N, Z and β but it does not exhibit the usual shell effects. Again fluctuations are greatly reduced at high deformations.

Most authors adopt the average value for $\langle m^2 \rangle \simeq .146\ A^{2/3}$ given by G.C. and represented by the dashed straight line. This value has been obtained by averaging $\langle m^2 \rangle$ over all sps. An average value consistent with the model prescription to perform averages only over $(sps)_{FT}$ is represented by the solid straight line and is $\simeq .24\ A^{2/3}$. Owing to the large fluctuations in $\langle m^2 \rangle$ no average value should be used for $\langle m^2 \rangle$ in determination of "a". To conclude, this application of the Nilsson model can be assumed to be only qualitatively valid in order to determine the "a" values. On the contrary, one expects that predicted $\langle m^2 \rangle$ are much less sensitive to the adopted approximations. In fact, whereas including or excluding a few sps from the Fermi neighbourhood can sensibly change sps density, the same should not appreciably alter the average over m values. It is also worth noting how the Nilsson model, in principle, provides us with a consistent way of dealing both with "a" and σ^2 determinations.

Sect. 2. LOW ENERGY LEVEL DENSITY AND PARAMETERS

2.1. Total Level Density

Formulae (9) and (10) cannot be extrapolated to low energies because the underlying statistical assumptions cease to be valid and because, when $E<\Delta$, the quantity $\sqrt{a(E-\Delta)}$ becomes imaginary.

On the other hand, unfortunately experimental level schemes are not always known and in most cases even if they are available they stop below ~2 MeV excitation energy.

In practice one is again forced to resort to some more or less arbitrary recipe. The general philosophy advisable is to account for all experimental information as far as possible.

GC observed that in a very general way the staircase plot of low-lying level schemes in a semilog scale can be fitted by straight lines. They thereby assumed a law of the type

$$N(E) = e^{(E-E_o)/T} \qquad (15)$$

N(E) being the cumulative number of levels, E_o and T two free parameters to be deduced from the fitting conditions.

Let us henceforth give low-lying level density the label 1 and high-energy level density the label 2.

According to (15) the total observable level density of low-lying levels is given by

$$\rho_1(E) = \frac{d\,N(E)}{d\,E} = \frac{1}{T}\, e^{(E-E_o)/T} \qquad (16)$$

One must observe that from the concepts of classical thermodynamics the nuclear temperature is given by

$$\frac{d}{dE}\,\ell n\,\rho_1(E) = \frac{1}{T} \qquad (17)$$

thus assumption (16) implies parameter T has the physical meaning of a nuclear temperature and is constant in the region of discrete levels.

One does not know up to what energy law (16) can be extrapolated. Nonetheless, according to GC, one assumes that a point exists inbetween the range of validity of ρ_1 and ρ_2 where the two laws match. It seems reasonable to assume that a satisfactory description of total level density in the whole energy range is achieved if the following requirements are met:

i) a good fit of low-lying levels is obtained;

ii) observed resonance level spacing at the neutron binding Bn is exactly reproduced;

iii) a matching point E_x is found between $E=0$ and $E=Bn$, where

$$\rho_1(E_x) = \rho_2(E_x) \qquad (18)$$

and

$$\left.\frac{d\,\ell n\,\rho_1(E)}{d\,E}\right|_{E=E_x} = \left.\frac{d\,\ell n\,\rho_2(E)}{d\,E}\right|_{E=E_x} \qquad (19)$$

Condition i) is expressed by

$$N(E_p)-\tfrac{1}{2} = \left[N(E_1)-\tfrac{1}{2}\right](1-\delta_{o;E_1}) + e^{-E_o/T}\left[e^{E_p/T} - e^{E_1/T}\right] \qquad (20)$$

where E_p = energy of last level to be fitted

$N(E_p)$ = cumulative number of levels at E_p

E_1 = energy of the first level to be fitted

$N(E_1)$ = cumulative number of levels at E_1.

Condition ii) is expressed by eq. (11) if D_{OBS}^{EXP} is known (alternatively one can merely take "a" from the systematics).

The first of conditions iii) implies

$$E_o = E_x - T\,\ell n\,\rho_2(E_x) \qquad (21)$$

whereas the second of conditions iii) establishes that in E_x the constant nuclear temperature T of low-lying excited states is equal to the energy-dependent nuclear temperature $\tau(E)$ of high energy excited states

$$\frac{1}{T} = \frac{1}{\tau(E_x)} \qquad (22)$$

where

$$\frac{1}{\tau(E_x)} = \sqrt{\frac{a}{U_x}} - \frac{3}{2U_x}\ , \qquad (23)$$

with $U_x = E_x - \Delta$.

Solution of the set of eqs. (11), (20), (21), (22) gives the values of E_o, T, U_x, a, which completely determine the problem.

As an example, fig. 7 shows the fitting of a cumulative number of low-lying levels in Mo^{98}.

2.2. Systematic Trends in Nuclear Temperature T and Matching Energy U_x

Results of calculations performed in the F.P. range according to the above outlined procedure are shown in fig. 8. T appears as a smooth function of N, characterized by small fluctuations representative of weak shell effects.

The uncertainty in interpolating unknown T values can be estimated to within 15% when using the solid straight line, and reduces to 10% if the dashed curve is used.

Nuclear temperature is useful for the determination of evaporative spectra.

To the extent that the relation between T, "a" and the matching energy U_x

$$1/T \simeq (a/U_x)^{\frac{1}{2}} \qquad (24)$$

is valid, a correlation among the systematic trends of "a" , T and U_x is expected. Results of the investigation are shown in fig. 8. Marked shell closure effects appear as well as the local behaviour of SN isotopes (represented by dotted circles).

The uncertainty over unknown U_x taken out of the systematics, can be estimated to within 25%.

It is important to have a systematics of U_x because knowledge of it is sufficient for a complete determination of the total level density, at low energies.

2.3. Low-Energy Spin Distribution Law

Again not much information is available from models for us to give the spin distribution law for low-lying levels.

All that one can do is to resort to experimental level schemes and empirically try to find how experimental levels are distributed with respect to J .

The level schemes of about 100 isotopes in the fission product mass range have been analyzed (see as an example fig. 9). From this analysis it turns out that the spin distribution law at low energies can be approximately fitted by the law (5), provided σ^2 is appropriately chosen in each case, in order to get the best fit (see fig. 9).

In 40% of the cases considered a very good fit was obtained. In the remaining 60% of the cases either discrete level schemes were not well known, or the extrapolation really failed to work (e.g. Zr^{90} in fig. 9).

In general the position is harder to hold for even-even nuclei near shell closures, where it happens that some spin values are not assigned at all (In Zr^{92} J=1 does not appear up to 3 MeV). On the contrary the approximation works reasonably well in deformed nuclei (e.g. Tb^{160} in fig. 9).

A very fast procedure for determining the value of σ^2_{LEVELS} which better fits experimental spin distribution is given by the maximum likelihood method.

In fact one has

$$\sigma^2_{LEVELS} = \frac{1}{2N} \sum_1^N (J_i+\tfrac{1}{2})^2 \qquad (25)$$

N being the cumulative number of known levels (ground state excluded) and J_i their spins.

It is interesting to notice that results of the maximum likelihood method for σ^2 do not change much even if a large percentage of known spin values are randomly skipped. This means that even if many levels are missed, the resulting σ^2_{LVL} is still meaningful. Of course, where less than ≈5 levels are available the method does not apply. In these cases when possible one could analyse the spin distribution of isobars with similar characteristics.

2.4. Energy Dependence of Spin Cut-Off Parameter

To investigate a possible energy dependence of the spin distribution i.e. of the spin cut-off parameterr, an analysis was performed over the most level-rich schemes which spread up in energy as high as possible.

As an example of this analysis, in fig. 10 the cumulative number of observed levels of all J vs. E in Zr^{90} is compared with the cumulative number of levels of spin J=0 and J=2 . As can be seen all staircases can reasonably be fitted in a semilog scale by parallel straight lines. This means that in this case, within uncertainties, σ^2_{LEVELS} can be considered to be energy independent up to 3 MeV.

If one now assumes σ^2 is constant in the level region and energy dependent as given by (6) at high energies the following questions may be asked:

i) where shall we assume high energies start?
ii) where shall we assume the level region stops?
iii) how to fill the gap in between, where we do not know anything?

All of these questions have an arbitrary answer. In practice it is assumed that high energies start above the matching point E_x ; the level region stops at E_{cut} , which is the energy where the first le-

vel of unknown characteristics is assumed to be found (E_{cut} may be too low to be reasonable). The present writer suggests filling the gap between E_{cut} and E_x with a linear interpolation of σ^2 between σ^2_{LEVELS} at E_{cut} and $\sigma^2 = g\, t(E_x) \langle m^2 \rangle$ at E_x. In fig. 11 the case of Mo^{100} is considered. The full line illustrates the method proposed above for $\sigma^2(E)$ determination.

Extrapolation of high-energy formulae below E_x down to Δ is given by the dotted curve. From the comparison one can see that the straight-line interpolation is very close to the model extrapolation.

Several authors do not consider the information coming from low-lying level schemes and assume σ^2 is a constant $= \sigma^2(E_x)$ below E_x (dashed line in fig. 11). As can be seen, this approximation is very rough and in practice can give rise to serious drawbacks. As an example let us consider neutron capture in Mo^{100}, see fig. 11. [Fig. 13 gives an idea how well the distribution law (5) fits experimental spin distribution. Figs. 14 and 15 give the result of the analysis of total level density in Mo^{100} and Mo^{101}, respectively].

If below E_x a constant value $\sigma^2 \simeq 26.7$ is adopted corresponding to a spin distribution in the Mo^{100} target nucleus, peaked at $J=4.7$, the corresponding neutron capture cross section is given in fig. 12 by the dotted curve; whereas linear interpolation between $\sigma^2(E_x)$ and the value $\sigma^2_{LVL} \simeq 4.7$ corresponding to a most probable spin value $J \simeq 1.5$ gives the full curve. Because the ground state target spin is $I=0$, only lower values of compound nucleus spin are possible. In these conditions inelastic channels are at an advantage when target level spin distribution is peaked at lower J values. Thus even if neutron inelastic scattering is a dominant competition (i.e. to a large extent independent of level density) a small depression in inelastic channels produces a large bump in capture.

2.5. Parity Distribution Law

All that one knows about parity distribution is that at high excitation energy levels are equally distributed between the two parities and at low energies we know only what we can deduce from known level schemes. Nothing is known at intermediate energies.

From the analysis of a large number of cases it has been seen that the cumulative number of levels of a given parity too can be fitted by an exponential law at low energies. This means that one can assume

$$\rho_1(E,\pi) = \rho_1(E) \cdot p(E,\pi) \tag{26}$$

where

$$p(E,\pi) = e^{a^\pi E + b^\pi} \tag{27}$$

i.e. the parity distribution law is energy dependent, behaves exponentially and depends on two free parameters a^π and b^π to be determined from the fitting condition of low-lying levels.

A median $E_{\frac{1}{2}}$ of the distribution can be found above which the probability must be taken to be $\frac{1}{2}$ for both parities.

The best one can do is separately to fit positive parity levels and negative parity levels and iterate until the medians $E^+_{\frac{1}{2}}$ and $E^-_{\frac{1}{2}}$, as deduced from the two independent fits, converge.

As an example in fig. 16 the case of In^{116} is illustrated, where the fit of $N(E)$, $N(E,\pi=+)$, $N(E,\pi=-)$ is achieved with a value for the median $E^+_{\frac{1}{2}} = E^-_{\frac{1}{2}} = 4.433$ MeV. Unfortunately this procedure can be applied only where a sufficient number of levels of both parities are available, whereas nothing at all can be done where levels of only one parity are known. In this case any assumption above E_{cut} is arbitrary. Nevertheless, Igarasi [3], on the assumption that the probability of unassigned parity should exponentially tend to $\frac{1}{2}$, suggests a law of the type:

$$p(\pi,E) = \frac{N_\pi + .5 \exp\left[(E-E^*)/\delta\right]}{1+\exp\left[(E-E^*)/\delta\right]} \tag{28}$$

where N_π stands for the fraction of discrete levels with parity π and

$$E^* = (E_x + \tilde{E})/2 \tag{29}$$

$$\delta = (E_x - \tilde{E})/8 \tag{30}$$

where $\tilde{E}$ is the energy where continuum is assumed to start; in general $\tilde{E} = E_{cut}$ if E_{cut} is not too low.

Conclusions.

The method of analysis illustrated, though very simple and mostly empirical, can be very useful in the determination of level density and its spin and parity distributions. An example is given in fig. 17, where the neutron inelastic scattering in Zr^{90} is considered; the full line was obtained by using the full experimental level scheme up to 3 MeV, while the dashed line was obtained by replacing the level scheme by a description of level density according to the above outlined methods.

This methodology, besides fitting the gap at intermediate energies can also be used to some extent to give statistical average estimates of missing levels and/or of their unknown characteristics. In a very general way one expects that the level density problem should not greatly affect dominant competition calculations. On the contrary it may affect non-dominant process calculations both directly and indirectly.

In particular, neutron capture calculations and radiative width calculations can be strongly affected by spin and parity distribution due to E_1 selection rules.

Heavy-ion reactions can also be strongly influenced by the distribution of total level density and, owing to the higher angular momenta involved, also depends on the level spin distribution.

Chapter 2. RADIATIVE WIDTH PROBLEM

Sect. 1. MODELS AND FORMULAE MOST OFTEN USED IN LITERATURE

1.1 Brink-Axel model

Radiative widths have been measured for several stable nuclei in the slow-neutron resonance region. In spite of the large experimental uncertainties, these data constitute an important test for the validity of the various theoretical estimates of the radiative width at the neutron binding energies.

Among the various models Brink's estimate, which is also referred to as "Axel's estimate", and Weisskopf's estimate are those most frequently adopted to account for the statistical contributions to the total radiative widths, $\overline{\Gamma}_\gamma(E)$.

It is known that Weisskopf's estimate proved to give unsatisfactory predictions of the absolute magnitude of $\overline{\Gamma}_\gamma$ for all nuclei.

As far as the energy dependence of $\overline{\Gamma}_\gamma$ is concerned, it should be noticed that a realistic energy dependence of the radiative width should not be expected in the whole range, since Weisskopf's estimate neither accounts for the photoabsorption giant resonance phenomenon nor satisfies any sum rule. For these reasons, the Brink-Axel (B.A.) estimate is being more and more frequently adopted.

The cross section for the absorption of one photon of electric E (or magnetic M) character and of multipole order ℓ by an initial level i to a final single isolated level f is

$$\sigma^{E(M),\ell}(i\to f)=2\pi\lambda\!\!\!^{-2} g \frac{\varepsilon^2 \Gamma_\gamma^{E(M),\ell}(f\to i)\Gamma_f}{(\varepsilon^2-E_f^2)^2+\varepsilon^2\Gamma_f^2} \qquad (1)$$

where

i and f denote also the quantum numbers of the initial and final levels (E_i,J_i,π_i) and (E_f,J_f,π_f) respectively.

$\varepsilon = E_f - E_i$ is the photon energy

$\lambda\!\!\!^{-} = \frac{\hbar c}{\varepsilon}$ is the photon wavelength

$g = \frac{2J_f+1}{2J_i+1}$ is a statistical factor

$\Gamma_\gamma^{E(M),\ell}(f\to i)$ is the partial width for the inverse process of de-excitation of the level f via a photon emission of electric E or magnetic M character and multipole order ℓ .

Γ_f is the total width of the resonance (E_f,J_f,π_f) .

The cross section integrated over the whole range containing the resonance (E_f,J_f,π_f) is

$$I(i,f) = \int \sigma^{E(M),\ell}(i\to f)d\varepsilon = \pi^2\lambda\!\!\!^{-2} g \Gamma_\gamma^{E(M),\ell}(f\to i) \qquad (2)$$

By way of definition, the cross section averaged over a photon energy interval containing n resonances all characterized by the same spin and parity, as for f , is

$$\langle\sigma^{E(M),\ell}(i\to f)\rangle_{\Delta\varepsilon} = \frac{\sum_r^n I_r(i,f)}{\Delta\varepsilon} \quad , \tag{3}$$

while the integrated cross section $I(i,f)$ averaged in the same interval $\Delta\varepsilon$ is

$$\langle I(i,f)\rangle_{\Delta\varepsilon} = \frac{\sum_r^n I_r(i,f)}{n} \quad . \tag{4}$$

We thus have

$$\langle\sigma^{E(M),\ell}(i\to f)\rangle_{\Delta\varepsilon} = \frac{n}{\Delta\varepsilon}\langle I(i,f)\rangle_{\Delta\varepsilon} \quad , \tag{5}$$

where $\frac{\Delta\varepsilon}{n}$ is the mean spacing $D(E_f,J_f,\pi_f)$ of the resonances with spin J_f and parity π_f at the energy E_f , while

$$\langle I(i,f)\rangle_{\Delta\varepsilon} = \pi^2\lambda\!\!\!^{-2} g \langle\Gamma_\gamma^{E(M),\ell}(f\to i)\rangle_{\Delta\varepsilon} \quad . \tag{6}$$

By combining Eq. (5) and Eq. (6) one gets

$$\langle\sigma^{E(M),\ell}(i\to f)\rangle_{\Delta\varepsilon} = \pi^2\lambda\!\!\!^{-2} g \langle\Gamma_\gamma^{E(M),\ell}(f\to i)\rangle_{\Delta\varepsilon} / D(E_f,J_f,\pi_f) \tag{7}$$

which connects the average radiative width for the transition $(f\to i)$ to the average photo-cross section for the absorption inverse process $(i\to f)$.

The B-A estimate is based on the result expressed by eq. 7 in the light of the following assumptions:

i) only electric dipole photo-absorption contributes to the excitation of the levels in the continuum energy region.

ii) The average photo-absorption cross section is known and its energy dependence may be represented by a Lorentzian curve.

iii) The average photo-absorption cross section does not depend on the initial state excitation energy.

Assumptions i), ii) are confirmed by the experimental evidence that the giant resonance is a general property of the ground state photo-absorption cross section which results primarily as built up from electric dipole absorption and its experimental shape is fairly well fitted by one or more Lorentzian curves

$$\sigma_\gamma(0,\varepsilon) \approx \sigma_L(\varepsilon) = \Sigma_R \sigma_R \frac{\varepsilon^2\Gamma_R^2}{(\varepsilon^2-E_R^2)^2+\varepsilon^2\Gamma_R^2} \quad , \tag{8}$$

σ_R, E_R, Γ_R being fit parameters corresponding to the peak cross section, peak energy and half maximum width respectively.

As regards the absorption of photons by nuclei in an excited state in accordance with assumption iii) Rosenzweig [4] has shown that there is some experimental evidence for the mean energy of the dipole strength distribution built on an excited state of energy E_i (relative to the ground state) being displaced upwards in energy by an amount E_i .

This fact supports the idea that the total photo-absorption cross section built up on an excited state E_i with one photon of energy ε is related to the ground state photo-absorption by the relation

$$\sigma(E_i\to E_f) = \sigma(0\to E_f-E_i) \quad , \tag{9}$$

$E_f = E_i+\varepsilon$ being the excitation energy of the final state.

According to the above hypothesis summation of eq. (7) over all final states f related to the initial state i by E1 selection rules gives the relation

$$\sigma_L(\varepsilon) = \pi^2\lambda\!\!\!^{-2}\Sigma_f g\langle\Gamma_\gamma^{E1}(f\to i)\rangle_{\Delta\varepsilon}/D(E_f,J_f,\pi_f) \tag{10}$$

In addition, if the assumption is made that the radiative strength function $\langle\Gamma_\gamma^{E1}(f\to i)\rangle_{\Delta\varepsilon}/D(E_f,J_f,\pi_f)$ does not depend on J_f, the average radiative width for the transition $(f\to i)$ may be written as

$$\langle\Gamma_\gamma^{E1}(f\to i)\rangle_{\Delta\varepsilon} = \varepsilon^2\sigma_L(\varepsilon)D(E_f,J_f,\pi_f)/3(\pi\hbar c)^2 \qquad (11)$$

The total radiative width is obtained by assuming eq. (11) over all the lower states i permitted by the E1 selection rules

$$\overline{\Gamma}_\gamma(E_f,J_f,\pi_f) = \Sigma_i \langle\Gamma_\gamma^{E1}(f\to i)\rangle_{\Delta\varepsilon} \qquad (12)$$

The summation in eq. (12) was split into two parts to account for the transitions to the discrete level and to the levels in the continuum, separately, so that the formula adopted is

$$\overline{\Gamma}_\gamma(E_f,J_f,\pi_f) = \frac{2}{3(\pi\hbar c)^2\rho(E_f,J_f)}\Sigma_i\Sigma_{J_i}\,\delta_{\pi_i,-\pi_f}(E_f-E_i)^2\sigma_L(E_f-E_i) + \\ + \frac{1}{3(\pi\hbar c)^2\rho(E_f,J_f)}\int_0^{E_f-E_{cut}}\varepsilon^2\sigma_L(\varepsilon)\Sigma_J\rho(E_f-\varepsilon,J)d\varepsilon \qquad (13)$$

where E_i are the energies of the discrete levels.

1.2 The Weigmann-Rohr formula

Some years ago, Weigmann and Rohr [5] carried out a systematic analysis of total radiative widths of low-energy neutron resonances for a large number of nuclei, using the following formula

$$\Gamma_\gamma(B) = \xi A^{2/3}(B^*)^{5/4}e^{-2\sqrt{aB^*}}\int_0^B (B-\varepsilon)^3\tilde{\rho}(E^*)dE + s\,A^{2/3}g'D_{obs}S_\ell \qquad (14)$$

The quantity S_ℓ represents the ℓ-wave neutron strength function and $\tilde{\rho}$ the energy dependent part of the level density, for which the Gilbert-Cameron formula is assumed.

The first term of the R.H.S. of the above formula derives from a manipulation of the well known Weisskopf estimate of the radiation width, whereas the second term takes into account the valency nucleon contribution. The ξ is an adjustable parameter, and

$$s = \begin{cases} 3.9\ .\ 10^{-3} & \text{for s-waves, } A\leq 63 \\ 3.82\ .\ 10^{-4} & \text{for p-waves, } 88\leq A\leq 125 \\ 4.9\ .\ 10^{-2} & \text{for s-waves, } 196\leq A\leq 204 \\ 0 & \text{otherwise} \end{cases}$$

In addition,

$$E^* = E + \Delta + \eta$$
$$B^* = B + \Delta + \eta$$

where Δ and η are excitation energy corrections for shell and pairing effects, which are assumed to be given by the formulae of Kahn-Rosenzweig [6] and Nemirovsky-Adamchuk [7], respectively. The results obtained with these formulae are multiplied by the constants C_Δ and C_η, respectively, which are obtained from a simultaneous best fit of the experimental Γ_γ's. Thus, formula (5) contains three (adjustable) constants (C_Δ, C_η, ξ), for which the following values are suggested by Weigmann and Rohr:

$$C_\Delta = 0.07$$
$$C_\eta = 0.75$$
$$\xi = 3.72\ .\ 10^{-3}$$

1.3 The Musgrove formula

The empirical formula suggested by Musgrove [8] is based on the Weisskopf estimate and is

$$\Gamma_\gamma(B) = K\,a^x\left[D_{obs}(B)\right]^y U^z f(Z) \qquad (15)$$

with $U=B-\Delta$.

When Γ_γ and D_{obs} are given in eV and B in MeV, the following numerical values of the parameters have to be adopted

$$K = \begin{cases} 1.13\times10^{-3} & \text{for isomeric nuclei} \\ 1.43\times10^{-3} & \text{for non-isomeric nuclei} \end{cases}$$

$x = 0.02$

$y = 0.21$

$z = 2.08$

In addition,

$$\Delta = \begin{cases} 11\sqrt{A} & \text{for odd-A nuclei} \\ 22\sqrt{A} & \text{for even-even nuclei} \\ 0 & \text{for odd-odd nuclei} \end{cases}$$

The quantity f(Z) is an empirical correction factor which depends on the atomic number and ranges between 0.3 and 10. Such a factor is given for $21 \leq Z \leq 82$ in Ref. [8].

1.4 Comparison of the results obtained according to the three recipes outlined.

An extensive check of B-A model was performed [9] by using formula (13). Calculations were made for all fission products for which Γ_γ in the resonance region was known. Calculations were also performed according to formulae (14) and (15) and results were intercompared. Whereas formula (13) can account for spin and parity dependence of $\overline{\Gamma}_\gamma(B_n)$ neither formula (14) nor formula (15) can do so; thus, the comparison was only possible among the $\overline{\Gamma}_\gamma(B)$ values averaged over all spins and parities. This analysis showed that 56% of the average radiative widths calculated according to the B-A model fall within experimental error bars and 18% differ from experimental data by more than 30%.

If one bears in mind, that important valency contributions have been demonstrated for certain isotopes, and considers the large uncertainties in relevant parameters and particularly in the level density description at intermediate energies (which play a determinant role in this type of calculation), one concludes that, although the full degree of the model's validity can only be ascertained after the parameters involved are more precisely determined, the B-A method is the only model which may approach absolute values of statistical contributions to $\overline{\Gamma}_\gamma(B,J,\Pi)$.

As for the comparison among the three formulae in a large number of cases the calculated values were in reasonable agreement with the experimental ones, independently of the formula adopted.

For this reason, it does not seem possible to select the "best" formula among the three considered on the basis of the results obtained. It should be noted, however, that these conclusions refer to the case of $\Gamma_\gamma(B)$. If the energy dependence of Γ_γ has to be considered, as in the case of statistical model calculations, the above conclusions are no longer valid. For example, in many cases, the Musgrove formula gives a decreasing trend of Γ_γ vs. E , which does not seem acceptable on a physical basis.

In addition, one should expect the Weigmann formula to fail at high energies because the Weisskopf estimate does not account for the giant resonance phenomenon.

1.5 Energy, spin and parity dependence of Γ_γ

As an illustration of application of the B.A. model and to draw some conclusions let us consider the example of Zr-92.

Zr-92 has a very well known level scheme up to 3 MeV, it is an even-even quasi-magic nucleus, neutron binding is pretty high, $B_n = 8.641$ MeV, and very recent experimental values of $\Gamma_\gamma(B_n,J,\Pi)$ are available.

In fig. 18 the spin distribution of low levels is shown. The spin value J=1 is not assigned up to 3 MeV.

Because σ^2 is an increasing function of excitation energy (i.e. the peak of the distribution is shifted toward high spin values at increasing energies), the probability, that J=1, decreases with energy.

Accordingly it was assumed that the spin distribution law is more reliable if J=1 is dropped at all energies. (were this not so, too large a fraction of predicted levels would be attributed the spin J=1 , see fig. 18).

In fig. 19 the analysis of the cumulative number of levels is shown. In fig. 20 the same is shown for the cumulative number of positive parity levels.

In table 1 results of the calculations are given. Radiative decay width to single levels as well as continuum contribution are separately given for both s-and p-wave resonances.

As one can see, a strong spin dependence and parity dependence appear owing to spin and parity E_1 selection rules. In addition, on account of the E^5 dependence predicted by the B.A. model which tends to favour long transitions, the strongest contribution comes from long transitions to ground states and first excited states.

From the particular level scheme of Zr-92 one can see that up to 3 MeV, only one level can be reached from compound nucleus levels $J=2^+$ and $J=3^+$, whereas nearly all levels can be reached from the levels $J=1^-$. In addition if one observes results for continuum contribution one can deduce that spin and parity dependence of $\Gamma_\gamma(B_n)$ come for the most part from the features of the level scheme. Such particularities make Zr-92 a good example for both experimental and theoretical investigations into the strength and spin dependence of transitions.

In table 2 it is shown how results of calculations compare with most recent measurements.

Many authors use Weisskopf's estimate for capture and total radiative width calculations both normalized at the experimental radiative width $\Gamma_\gamma(B_n)$ as known from neutron resonances.

In fig. 21 the ratios

$$R_a = \frac{\left[\Gamma_\gamma^{\text{TOTAL}}(B_n + E)\right]^{\text{B-A}}_{\text{NORMALIZED}}}{\left[\Gamma_\gamma^{\text{TOTAL}}(B_n + E)\right]^{\text{WEISSKOPF}}_{\text{NORMALIZED}}}$$

$$R_b = \frac{\left[\Gamma_\gamma^{\text{CAPTURE}}(B_n + E)\right]^{\text{B-A}}_{\text{NORMALIZED}}}{\left[\Gamma_\gamma^{\text{CAPTURE}}(B_n + E)\right]^{\text{WEISSKOPF}}_{\text{NORMALIZED}}}$$

versus incident energies E up to 15 MeV are shown for Nb-94. As can be seen the two models diverge at increasing energies, the effect being much stronger for capture widths.

Sect. 2. SYSTEMATICS

2.1. Γ_γ Systematics

In many cases the B-A model does not meet the accuracy requirements for cross section evaluation, because the uncertainty of the calculated radiative width may far exceed 30%.

For this reason there is a great need for Γ_γ experimental data in order to achieve model normalization.

On the other hand the problem of finding a good systematics for the radiative widths has not yet been solved satisfactorily.

According to the B.A. model one has seen that, for the most part, the contributions to total radiative widths at the neutron binding are due to γ-ray transitions to levels lying below the matching energy E_x. This implies that the success of the model in particular depends on the knowledge of low-lying level densities and of their spin and parity distributions. Because no systematic behaviour of spin and parity distributions of low levels can be envisaged, no systematic behaviour of $\Gamma_\gamma(B,J,\Pi)$ should be expected to be found valid for all nuclei.

A very rough systematic trend of the experimental values of $\Gamma_\gamma(B_n)$ as averaged over all spins and parities is shown in fig. 22 where $\Gamma_\gamma(B_n)$ is plotted against neutron number. The uncertainty of this systematics is estimated to range between 50% and 100%.

One must note that knowledge of Γ_γ is very important because uncertainties in Γ_γ are heavily propagated to capture calculations (see eq. 6, Chap. 3 below).

2.2. Giant resonance parameter systematics

The systematic trend of all giant resonance parameters (G.R.P.) both for spherical and deformed nuclei has been determined [10] on the basis of the hydrodynamic model. This model is able consistently to describe data for all medium and heavy nuclei, provided the deformation parameter β is known.

Fig. 23 shows the systematic trend of peak energies E_o, half maximum widths Γ_o and peak cross sections σ_o for magic nuclei. Maximum uncertainties for unknown values of E_o, Γ_o/E_o, σ_o can be taken as less than 3%, 20% and 15%, respectively.

In fig. 24 the trends are shown of the characteristics of the split giant resonances in deformed nuclei. Labels a and b refer to semi-major and semiminor axes, respectively.

Uncertainties in determining unknown values for E_a/E_o, E_b/E_o can be estimated at less than 10%, while for Γ_a/E_a, Γ_b/E_b and for $\sigma_a E_a$, $\sigma_b E_b$ to within 30%.

G.R.P. do not play an important role in neutron capture calculations when $\overline{\Gamma_\gamma(B)}$ is known and when the excitations involved are far from giant resonance peak energy.

On the contrary an important role is played in calculations of absolute values of Γ_γ with the B.A. model.

Conclusion

A weak point of the B.A. estimate is the approximation by which the inverse photoabsorption cross section is estimated by means of the Lorentzian approximation.

In fact experimental data are given around the maximum of the giant resonance. This implies that the Lorentzian description fits data only at high photon energies and that we do not know anything about the more important low-energy tail.

M_1 and E_2 γ-ray transitions are not considered in general because they are assumed not to contribute significantly to the radiative decay of compound nucleus states. In any case the parameters for calculating these types of transitions are mostly unavailable.

Even if it is difficult to check the validity of the B.A. model, comparison among results obtained by various methods suggests that at the present time the B.A. model should nevertheless be recommended.

Chapter 3. NEUTRON CAPTURE CROSS SECTION SYSTEMATICS

Sect. 1. STATISTICAL CAPTURE

At very low energies where only s-wave neutron captures are involved and for values of the radiative transmission coefficients $T_\gamma(E)$ which are negligible with respect to neutron transmission coefficients T_o the statistical model formula,

$$\langle\sigma_{n,\gamma}(E)\rangle = \frac{\pi\lambda^2}{2(2I+1)} \cdot \Sigma_J \left\langle \frac{T_o T^J_{\gamma cap}}{T_o + T^J_{\gamma tot}} \right\rangle$$

can be approximated by

$$\langle\sigma_{n,\gamma}(E)\rangle \simeq \frac{\pi\lambda^2}{2(2I+1)} \Sigma_J \langle T^J_{\gamma capt}\rangle \qquad (1)$$

At a given incident energy, which for this purpose was chosen as 25 KeV, one has

$$\langle\sigma_{n,\gamma}\rangle_{25} = \frac{C}{2I+1} \Sigma_J \frac{\Gamma^J_\gamma(B_n)}{D^J(B_n)} \qquad (2)$$

Assuming i) a value $\overline{\Gamma}_\gamma(B_n)$ averaged over all spins and ii) a $(2J+1)$-dependence of $\rho(E,J)$ on spin (which is reasonable at high energies owing to high values of the spin cut-off factor), one has

$$\frac{1}{D^J(B_n)} = \frac{1}{D_{OBS}(B_n)} \frac{2J+1}{2(2I+1)} \qquad (3)$$

and

$$\langle \sigma_{n,\gamma} \rangle_{25} = c \frac{\bar{\Gamma}_\gamma(B_n)}{(2I+1)D_{OBS}} \qquad (4)$$

eq.(4) is very significative because it gives an idea of how uncertainties in $\bar{\Gamma}_\gamma$ and D_{OBS} propagate to capture cross sections, at least at low energies.

The statistical model predictions have been checked with experimental data of capture cross sections at 25 KeV.

In fig. 25 experimental data renormalized according to the most recent standards are plotted vs $\frac{\bar{\Gamma}_\gamma(B_n)}{\bar{D}_{OBS}(2I+1)}$.

As can be seen the model predictions are verified to within 40%-50% which is consistent with the experimental uncertainties in $\sigma_{n,\gamma}$, $\bar{\Gamma}_\gamma$ and $\bar{D}_{OBS}$.

This systematics may be very important when it is necessary to check the consistency of the adopted values, or to get first guess values, and in any case to determine one of $\sigma_{n,\gamma}, \bar{\Gamma}_\gamma, \bar{D}_{OBS}$ when the other two are known.

It is worthwhile to note that owing to the relation between $\bar{\Gamma}_\gamma$ and $\bar{D}_{OBS}$ established by the B-A model, the ratio $\frac{\bar{\Gamma}_\gamma}{\bar{D}_{OBS}}$ is a function of $\bar{D}_{OBS}$.

Conclusion

Models and codes are very nice things, but where one does not have the necessary parameters, they do not help much. This is the case sometimes where no experimental information is available for deducing parameters or normalizing models. In these cases one needs to resort to systematics.

Systematics are sometimes model guided, sometimes empirical, and sometimes one is left to pure intuition.

Thus, while the adopted formalism for neutron cross section calculations is going to be increasingly sophisticated and very much standardized in most laboratories, parameterology is still the Cinderella of evaluation and substantial disagreement still appears in the methodology of determining recommended sets of parameters in the absence of experimental information.

For these reasons greater efforts are needed in the study and development of models aimed at improving parameter accuracy and consistency.

REFERENCES

[1] T. Ericson: Advances in Phys. 9, 425(1960)

[2] A.G.W. Cameron, G. Gilbert: Can. J. of Phys. 43(1965)

[3] S.I. Igarasi et al.: JAERI Report N° 75984, 103(1975)

[4] N. Rosenzweig: Nucl. Phys. 118, 650(1968)

[5] H. Weigmann, G. Rohr: Proc."Tripartite Symp. on Nucl. Phys. with Thermal and Resonance Energy Neutrons"(1973)

[6] P.B. Kahn, N. Rosenzweig: Phys. Rev. 187, 1193(1969)

[7] P.E. Nemirovsky, Yu.V. Adamchuk: Nucl. Phys. 39, 553(1962)

[8] A.R. de L. Musgrove: Report AAEC/E 211(1970)

[9] V. Benzi et al.: Report IAEA 169, 123(1974)

[10] G. Reffo: Contributed Paper to "Second IAEA Advisory Group Meeting on Fission Product Nuclear Data", Petten, Netherlands, 5-9 Sept. 1977

Table 1

PARTIAL AND TOTAL RADIATIVE DECAY WIDTHS IN Zr-92 (mev)
(Level and excitation energies in Mev)

LEVEL SCHEME N	Q(N)	SPIN	EXC= 8.641 J= 2.0 +	EXC= 8.641 J= 3.0 +	EXC= 8.641 J= 1.0 -	EXC= 8.641 J= 2.0 -	EXC= 8.641 J= 3.0 -	EXC= 8.641 J= 4.0 -
0	0.0	0+	0.0	0.0	118.6503	0.0	0.0	0.0
1	0.9350	2+	0.0	0.0	65.2472	41.7495	32.8421	0.0
2	1.3830	0+	0.0	0.0	48.4117	0.0	0.0	0.0
3	1.4950	4+	0.0	0.0	0.0	0.0	22.5812	19.9746
4	1.8470	2+	0.0	0.0	35.1500	22.4913	17.6927	0.0
5	2.0670	2+	0.0	0.0	30.0600	19.2344	15.1307	0.0
6	2.1500	0+	0.0	0.0	28.3126	0.0	0.0	0.0
7	2.3400	3-	15.7651	12.4015	0.0	0.0	0.0	0.0
8	2.3960	3+	0.0	0.0	0.0	15.1240	11.8973	10.5240
9	2.4800	5-	0.0	0.0	0.0	0.0	0.0	0.0
10	2.4860	2+	0.0	0.0	22.0989	14.1404	11.1235	0.0
11	2.6500	0+	0.0	0.0	19.5153	0.0	0.0	0.0
12	2.7440	2+	0.0	0.0	18.1532	11.6156	9.1374	0.0
13	2.8190	2+	0.0	0.0	17.1246	10.9575	8.6197	0.0
14	2.8510	2+	0.0	0.0	16.7009	10.6864	8.4064	0.0
15	2.8980	2+	0.0	0.0	16.0946	10.2984	8.1012	0.0
16	2.9030	0+	0.0	0.0	16.0312	0.0	0.0	0.0
17	2.9090	3+	0.0	0.0	0.0	10.2093	8.0311	7.1041
LEVEL CONTR. SUM			15.7651	12.4015	451.5493	166.5068	153.5632	37.6027
CONTINUUM CONTR.			153.3450	160.7838	278.8757	283.2310	282.5205	230.8690
TOTAL WIDTH			169.1101	173.1854	730.4250	449.7378	436.0835	268.4714

Table 2

COMPARISON BETWEEN CALCULATED AND EXPERIMENTAL RADIATIVE DECAY WIDTHS IN Zr-92

ℓ	J	Γ_γ^{EXP} (mev) ± stand. deviation	N° of Res.s	Ref	Γ_γ^{EXP} (mev) ± stand. deviation	N° of Res.s	Ref	Γ_γ^{CALC} without J=1 (mev)
0	2	140±12	3	1	162±12	4	2	169
0	3	122±7	2	1	152±18	6	2	173
1	1	413±40	1	1	1040±410	2	3	730
1	2	480±50	4	1	691±482	2	2	450
1	3	193±20	1	1	409±157	2	2	436
1	4		0	1	230±66	2	2	268

References to Table 2 :

/1/ A.R. de L. MUSGROVE et al.: Aust. J. of Phys. 30, 391, (1977).

/2/ Time-of-flight + capture yields at GEEL Linac (BCMN); private communication by G. Rohr and A. Brusegan, 1978

/3/ Transmission measurements at GEEL Linac (BCMN); private communication by C. Coceva, P. Giacobbe, M. Magnani, 1978
+ capture γ-ray spectra by F. Corvi (BCMN).

FIGURE CAPTIONS

Fig. 1 : Level density parameter a (MeV^{-1}) vs neutron number N .

Fig. 2 : Ratio $\overline{D}^{calc}/\overline{D}^{OBS}$ of calculated to experimental mean level spacings vs mass number A .

Fig. 3 : Plot of cumulative number of sps vs Fermi's energy in $\hbar\omega(\delta=0)$ units for spherical nuclei. Smooth curves are obtained according to Fermi statistics: full line curve corresponds to a nuclear temperature $t_1=.0825$ in $\hbar\omega(0)$ units, dashed line curve corresponds to a value $t_2 = t_{1/2}$. The stair-case plot is also given for comparison.

Fig. 4 : Single particle level density g in $\hbar\omega(\delta)$ units vs neutron or proton numbers N and Z respectively, for typical deformations $\beta=.1, .2, .3, -.1$.

Fig. 5 : Local trends of level density parameter a(MeV^{-1}) vs N for Mo, Ru, Pd isotope families.

Fig. 6 : Variance of angular momentum projection of single particle state $\langle m^2\rangle$ vs neutron or proton numbers N and Z , respectively, for typical deformations $\beta=.1, .2, .3, -.1$. Straight solid line gives $\langle m^2\rangle$ as suggested here and dashed straight line gives $\langle m^2\rangle$ as suggested by [2] .

Fig. 7 : Cumulative number of known discrete levels vs excitation energy E(MeV) in Mo-98.

Fig. 8 : Systematic trend of nuclear temperature T(MeV) vs neutron number N at low excitations, and systematic trend of matching energies U_x(MeV) vs N . Dotted circles represent tin isotopes.

Fig. 9 : Comparison between the spin distributions of known discrete levels and the predictions according to the law $f(J) = (2J+1)\exp\left[-(s+\frac{1}{2})^2/2\sigma^2\right]$, when σ^2 is obtained according to maximum likelihood estimation.

Fig.10 : Trends of the cumulative number of levels N(E), N(E,J=0), N(E,J=2) vs E , according to all J, J=2 , J=0 in Zr-92.

Fig.11 : Energy dependence of spin cut-off factor $\sigma^2(E)$. (See text.).

Fig.12 : Neutron capture cross section $\sigma_{n,\gamma}$(mb) vs E(KeV) in Mo-100. Solid line represents calculations of Hauser-Feshbach theory with width fluctuation correction and a value $\sigma^2(E)$ linearly interpolated between $\sigma^2_{LVL}(E_{cut})$ and $\sigma^2(E_x)$. Dotted curve is obtained with a constant spin cut-off $\sigma^2(E_x)$ below E_x .

Fig.13 : Spin distribution of known discrete levels in Mo-100.

Fig.14 : Cumulative number of known discrete levels vs excitation energy E(MeV) in Mo-100.

Fig.15 : Cumulative number of known discrete levels vs excitation energy E(MeV) in Mo-101.

Fig.16 : Cumulative number of known discrete levels N(E) , N(E,π=+) , N(E,π=-) vs E(MeV) in In-116.

Fig.17 : Neutron inelastic scattering cross sections $\sigma_{n,n'}$(barn) vs incident neutron energy E_n(MeV) in Zr-90. Calculations obtained with Hauser-Feshbach theory with width fluctuation correction. The full line was obtained by considering the complete known discrete level scheme. The dashed curve was obtained by replacing the level scheme above E_{cut}= 1.5 MeV with a continuum description according to the methods proposed in chap. 1, sect. 2.

Fig.18 : Spin distribution of known discrete levels in Zr-92.

Fig.19 : Cumulative number of known discrete levels vs E(MeV) in Zr-92.

Fig.20 : Cumulative number of known discrete levels with positive parity vs E(MeV) in Zr-92.

Fig.21 : A comparison of the energy dependence of radiative (curve a) and capture widths (curve b) calculated according to Brink-Axel and Weisskopf.

Fig.22 : Trend of experimental radiative width $\Gamma_\gamma(B_n)$ in mV vs neutron number N .

Fig.23 : Trend of giant resonance parameters for spherical nuclei. E_o(MeV) , Γ_o/E_o, σ(barn) vs mass number A .

Fig.24 : Trend of giant resonance parameters $E_{a \text{ or } b}/E_o$, $\frac{\Gamma_a}{E_o}$, $\frac{\Gamma_b}{E_o}$ vs deformation parameter β , and trends of $\sigma_a E_o$, $\sigma_b E_o$ vs mass number A for deformed nuclei.

Fig.25 : Systematics of 25 keV experimental neutron capture cross section vs $\overline{\Gamma}_\gamma^{EXP}/\left[\overline{D}^{EXP}(2I+1)\right]$, I being the target spin.

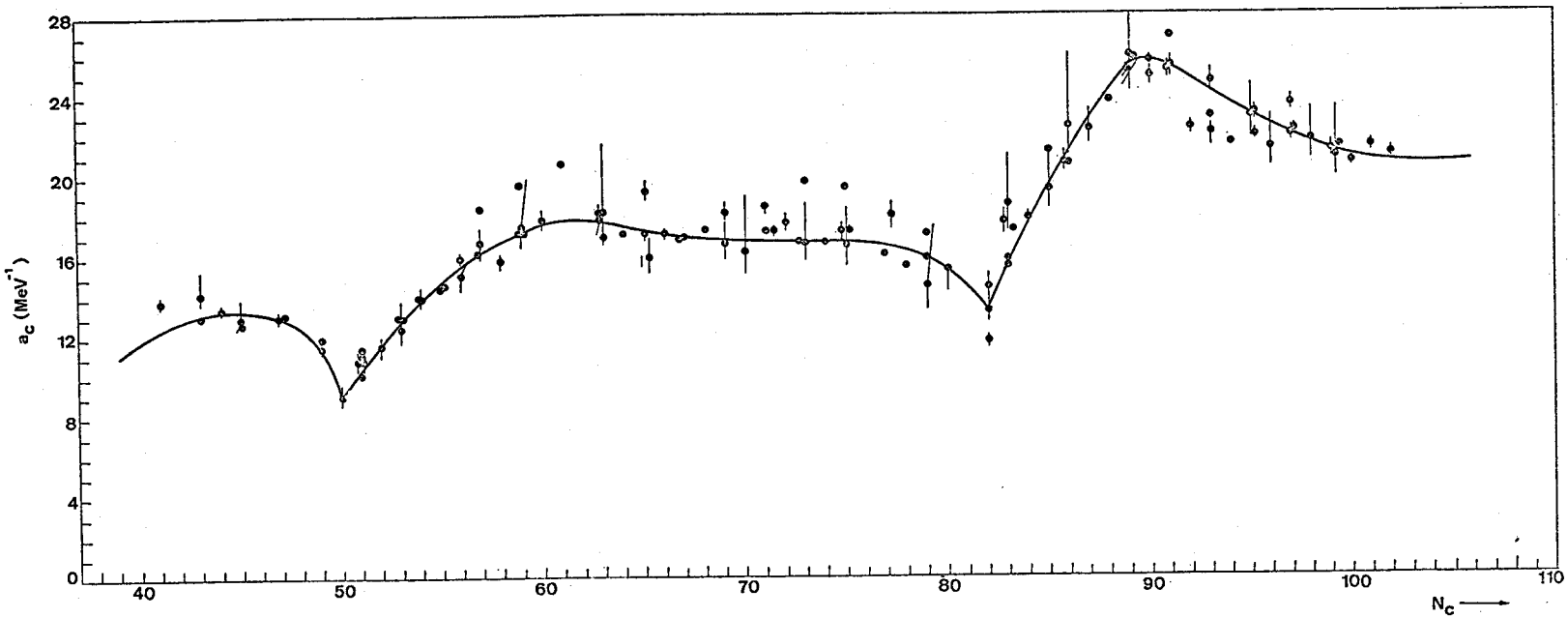
28
24
20
16
12
8
4
0
a_c (MeV^{-1})
40
50
60
70
80
90
100
110
N_c

FIG. 1.

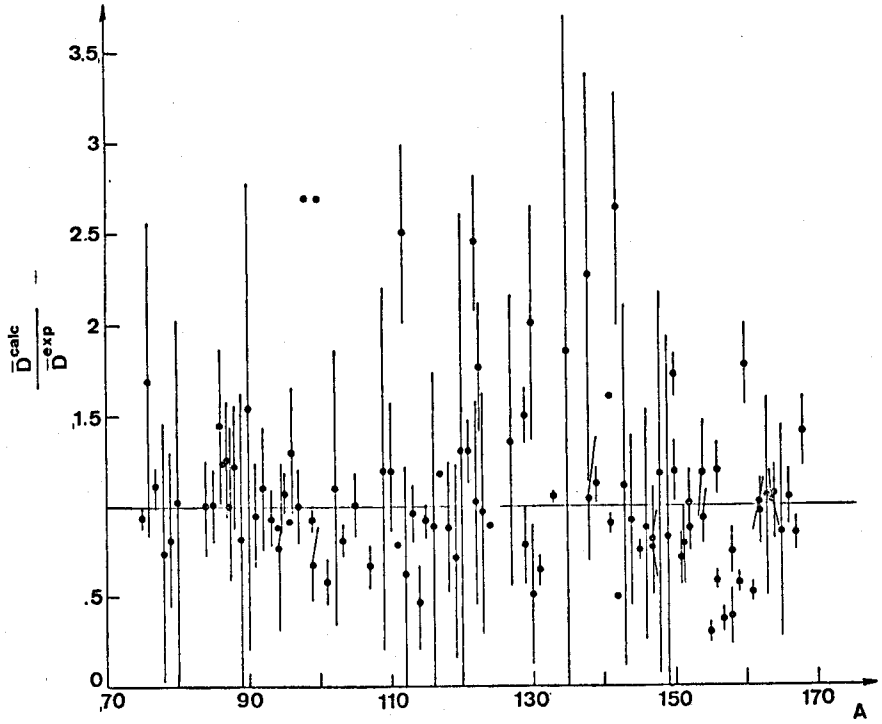
3.5
3
2.5
2
1.5
.5
0
$\frac{\bar{D}^{calc}}{\bar{D}^{exp}}$
70
90
110
130
150
170
A

FIG. 2.

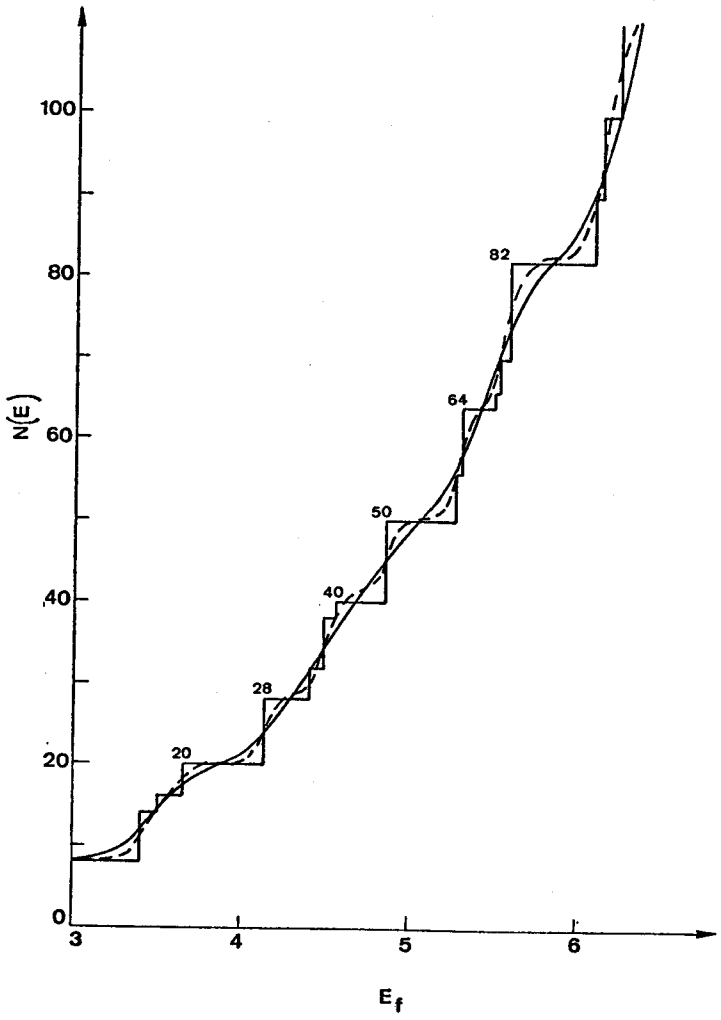

FIG. 3.

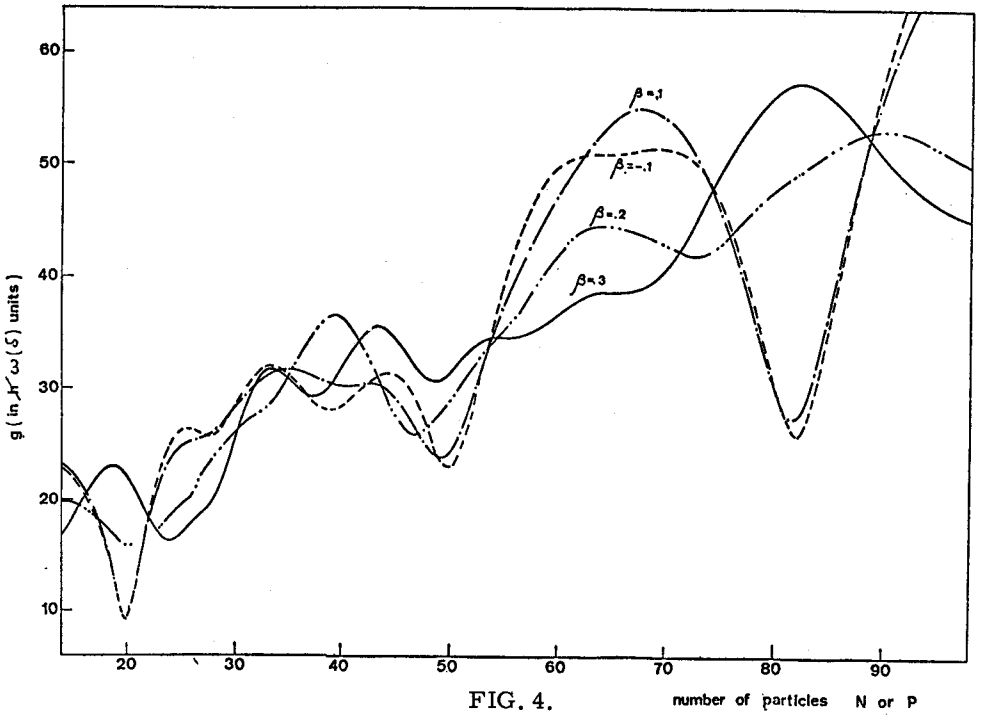

FIG. 4.

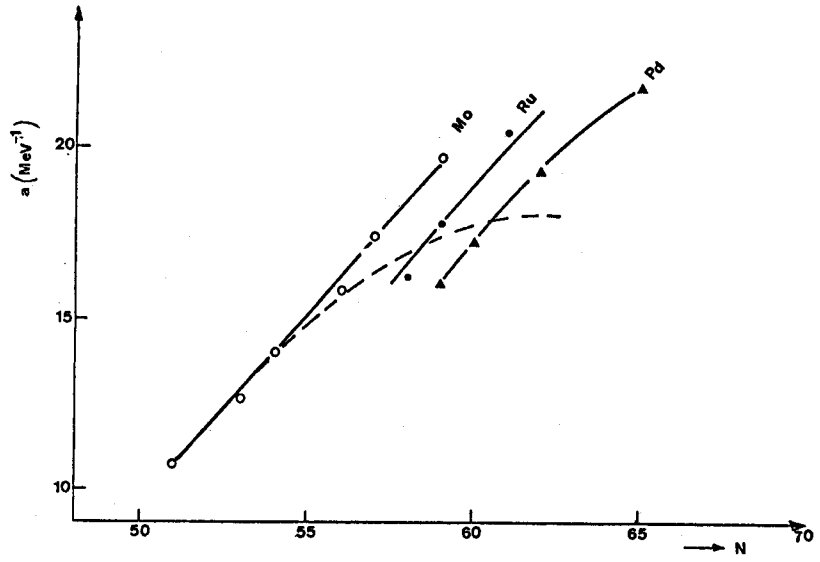

FIG. 5.

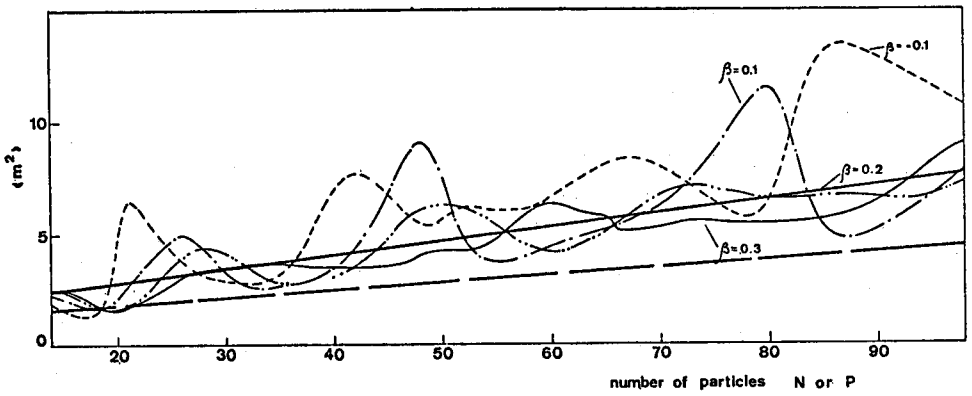

FIG. 6.

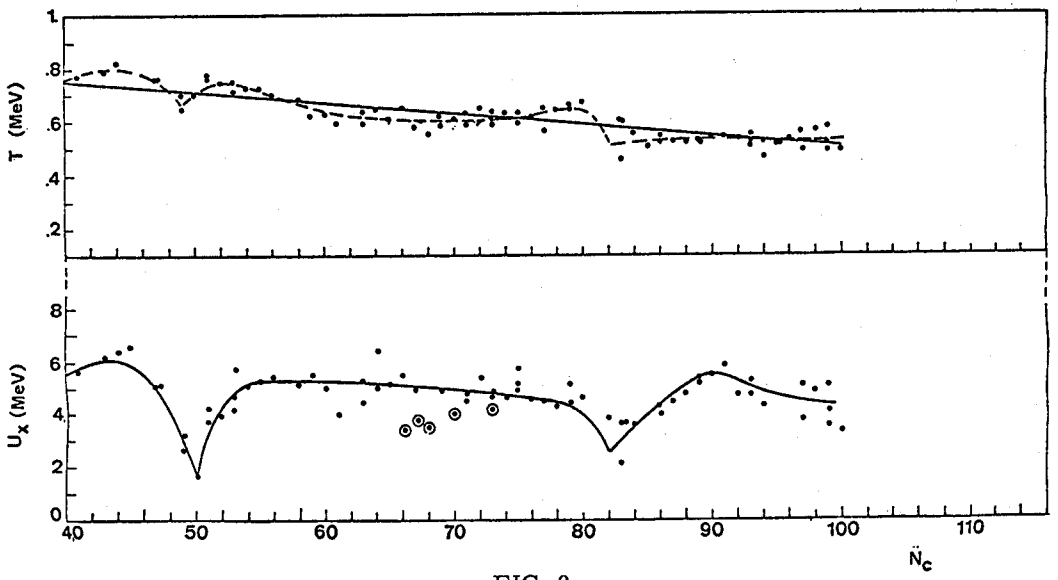

FIG. 8.

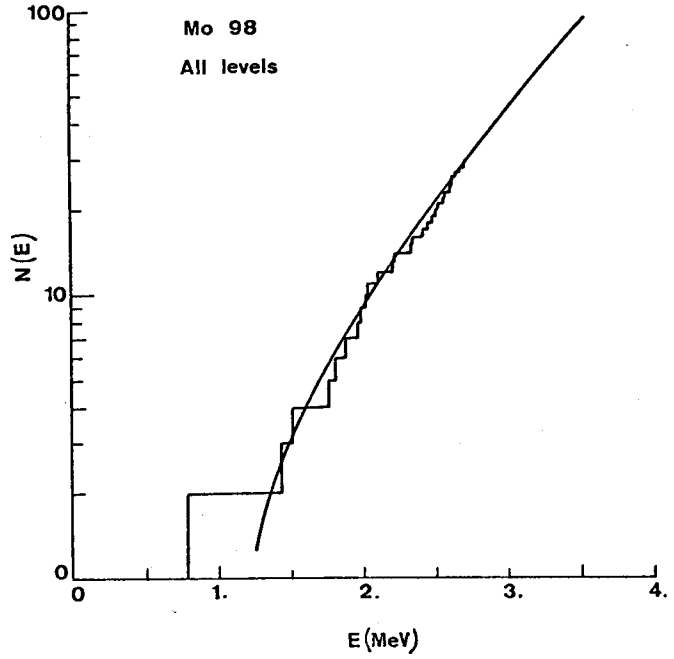

FIG. 7.

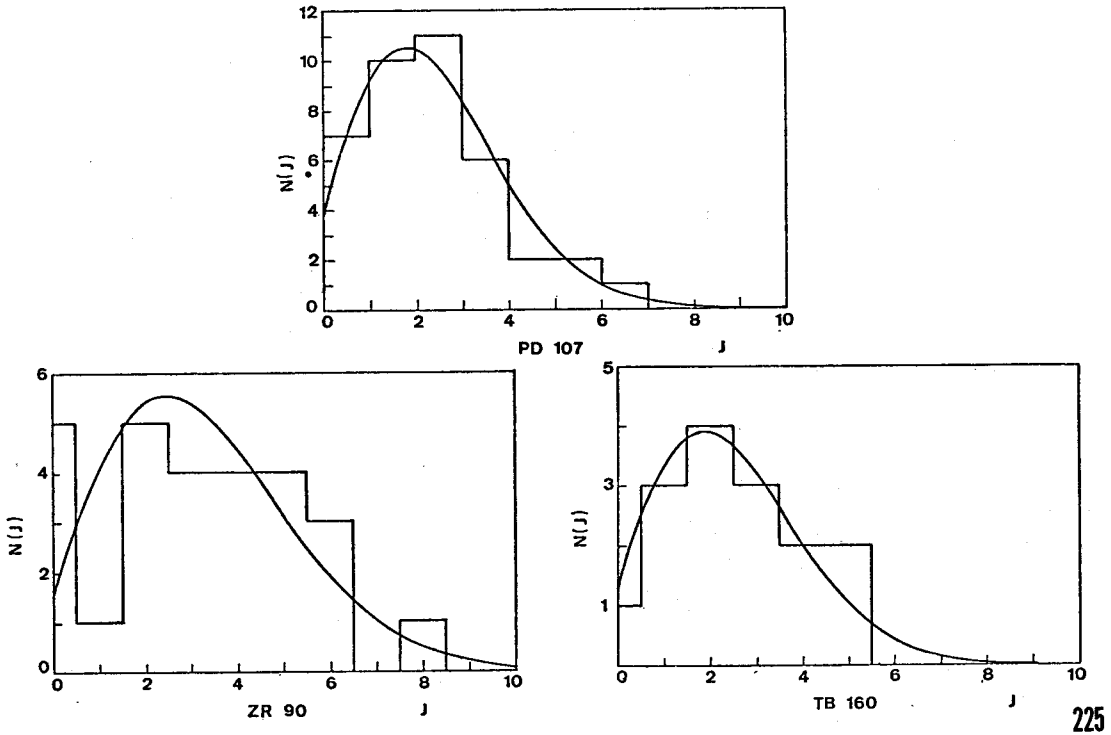

FIG. 9.

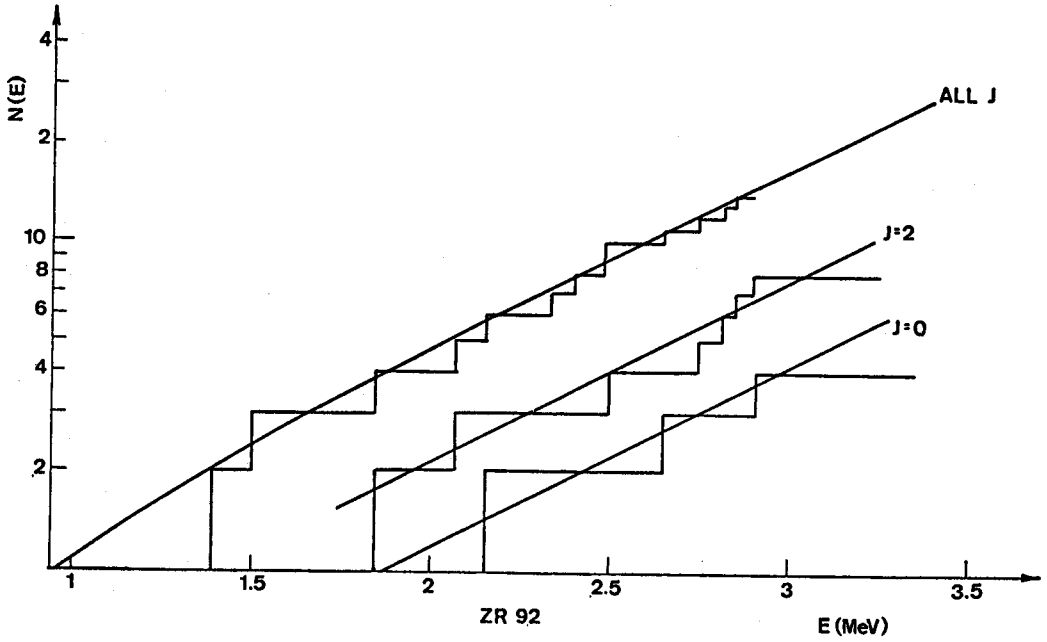

FIG. 10.

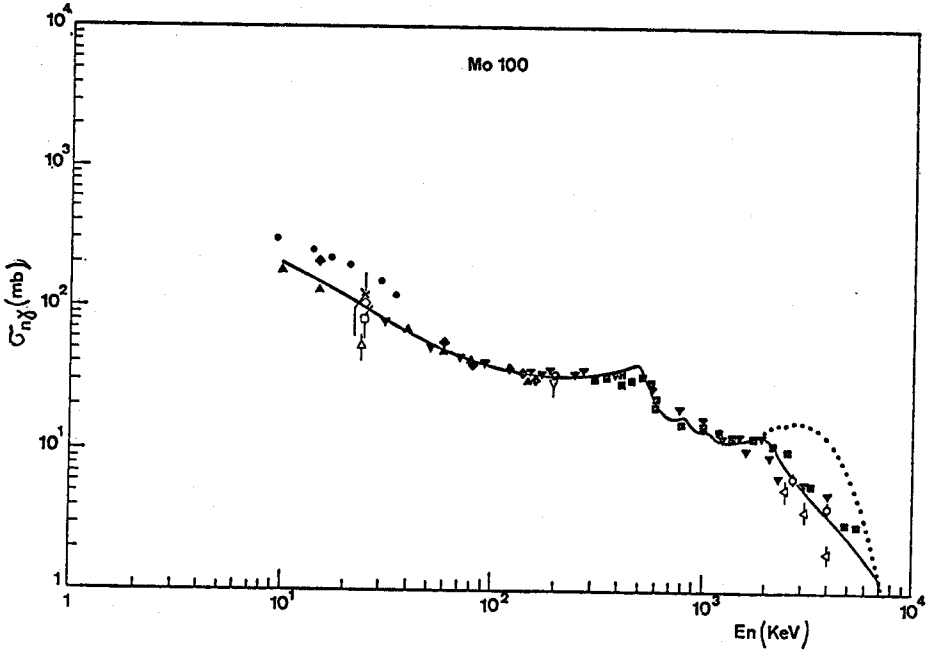

FIG. 12.

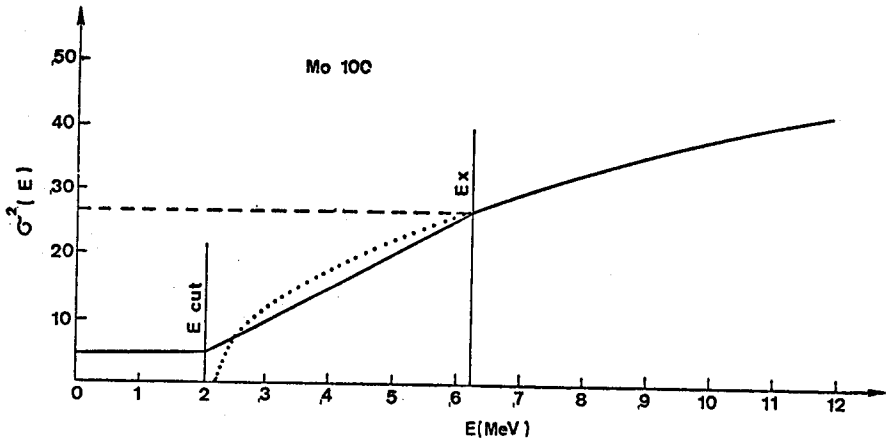

FIG. 11.

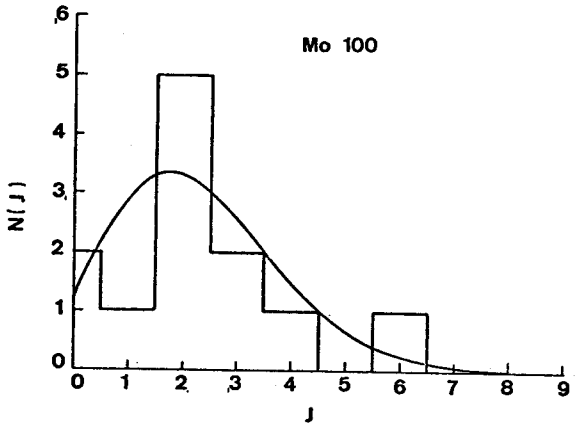

FIG. 13.

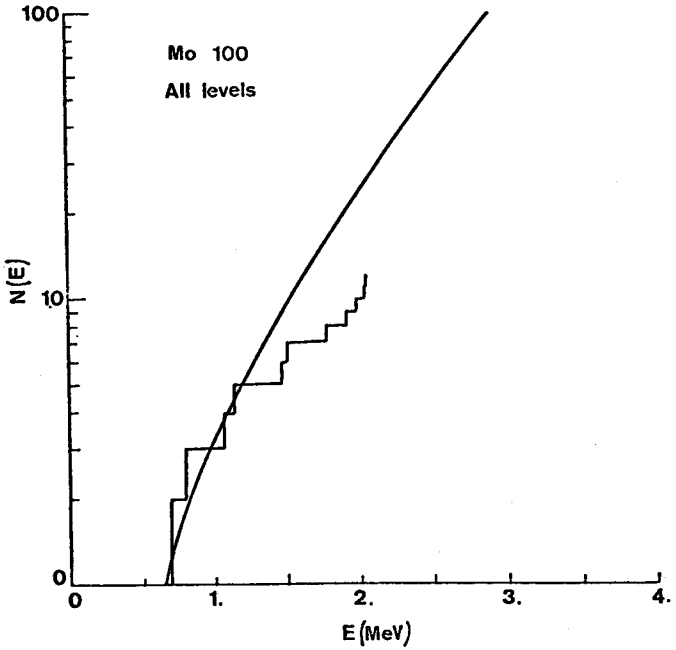

Fig.14

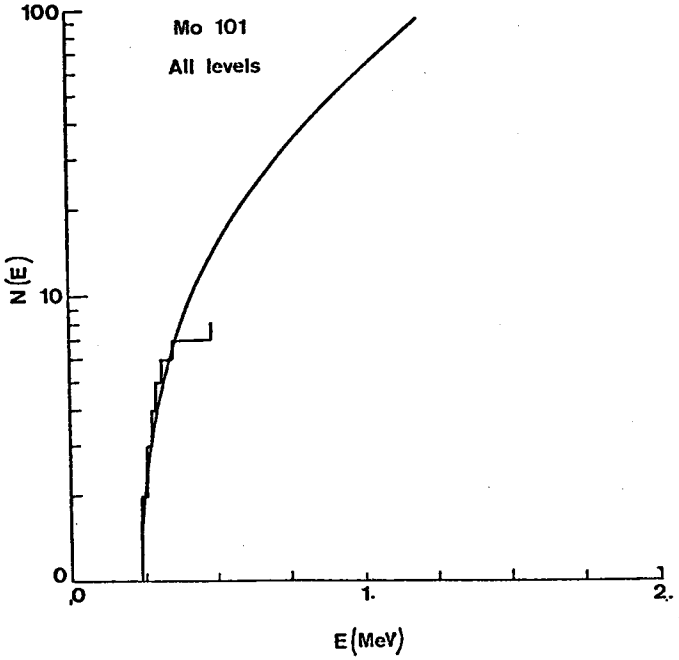

Fig.15

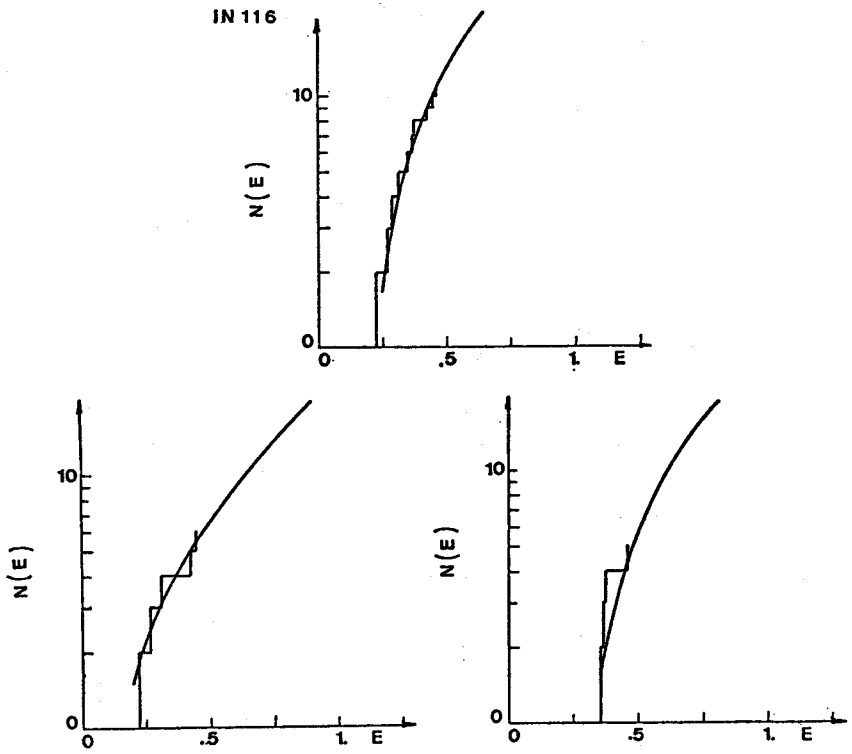

Fig.16

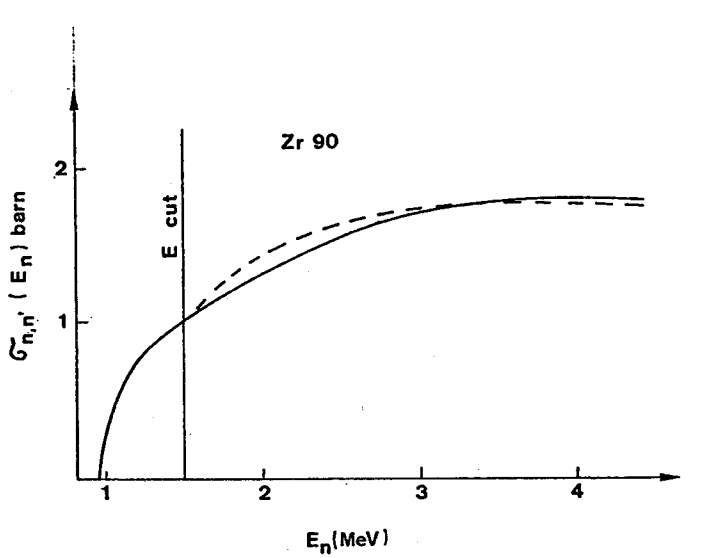

Fig. 17

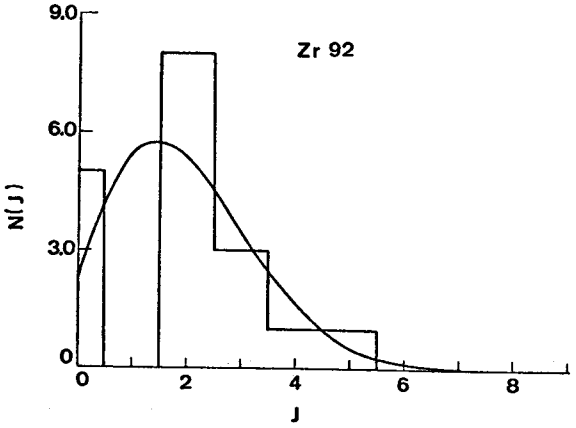

Fig. 18

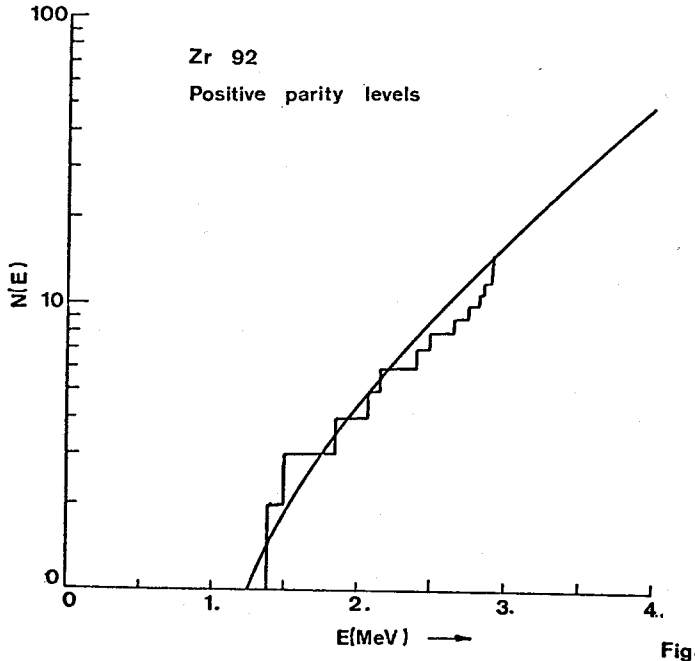

Fig. 20

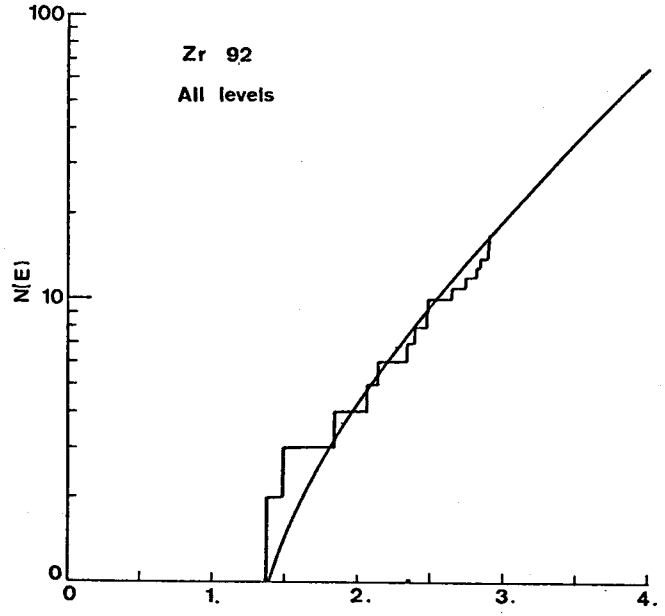

Fig. 19

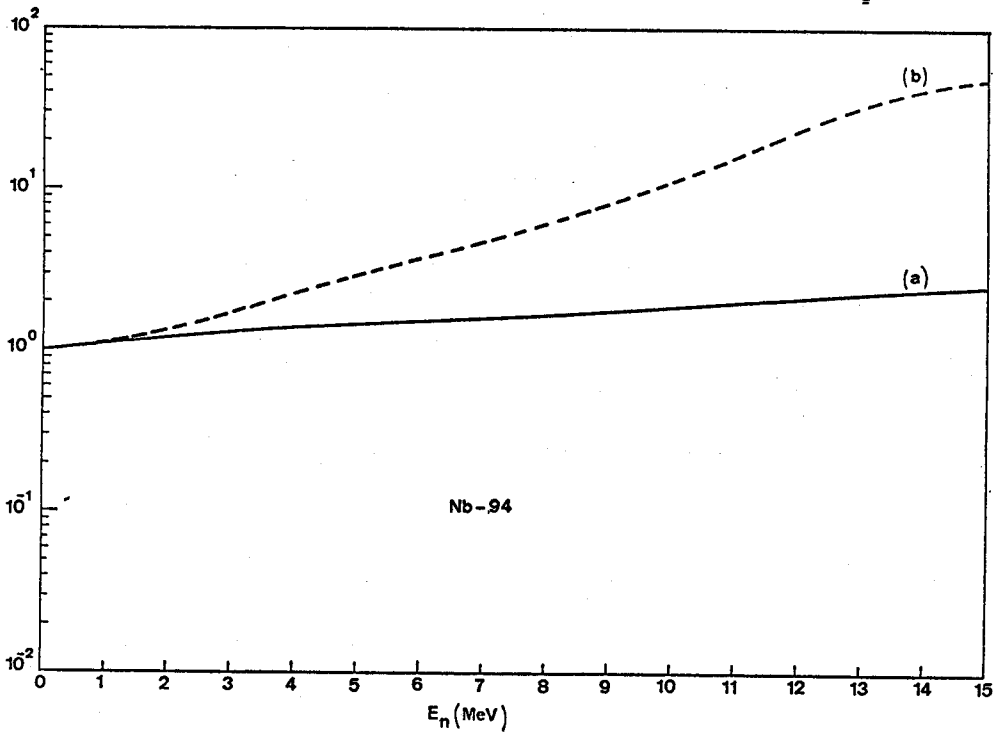

Fig. 21

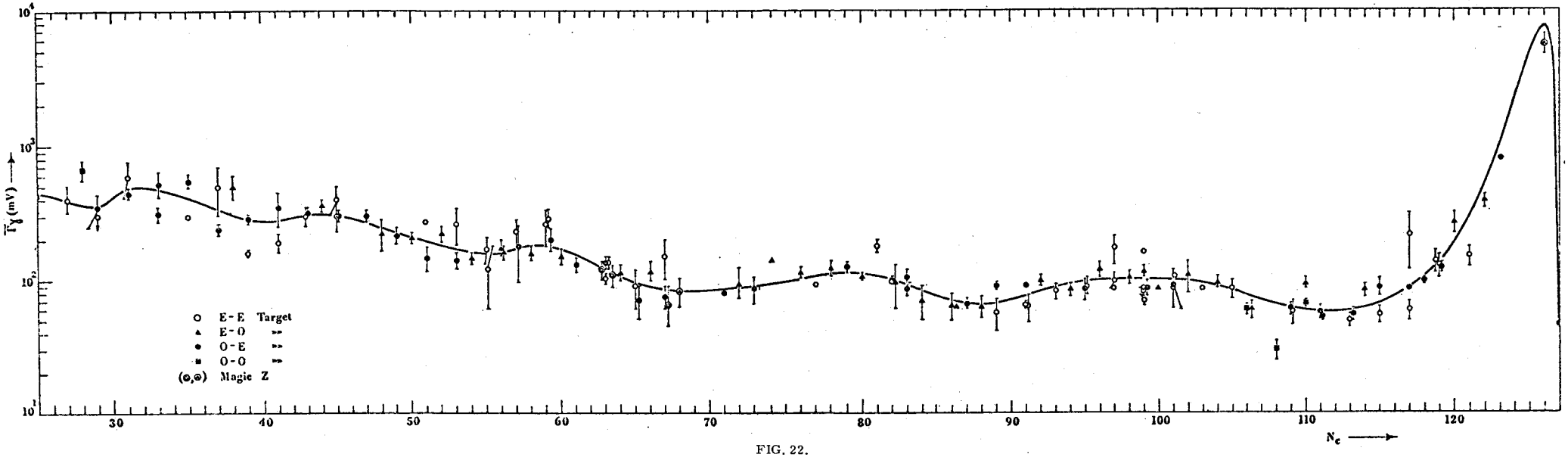
$\overline{\Gamma\gamma}$ (mV)
E-E Target
E-O
O-E
O-O
(e,e) Magic Z
N_e

FIG. 22.

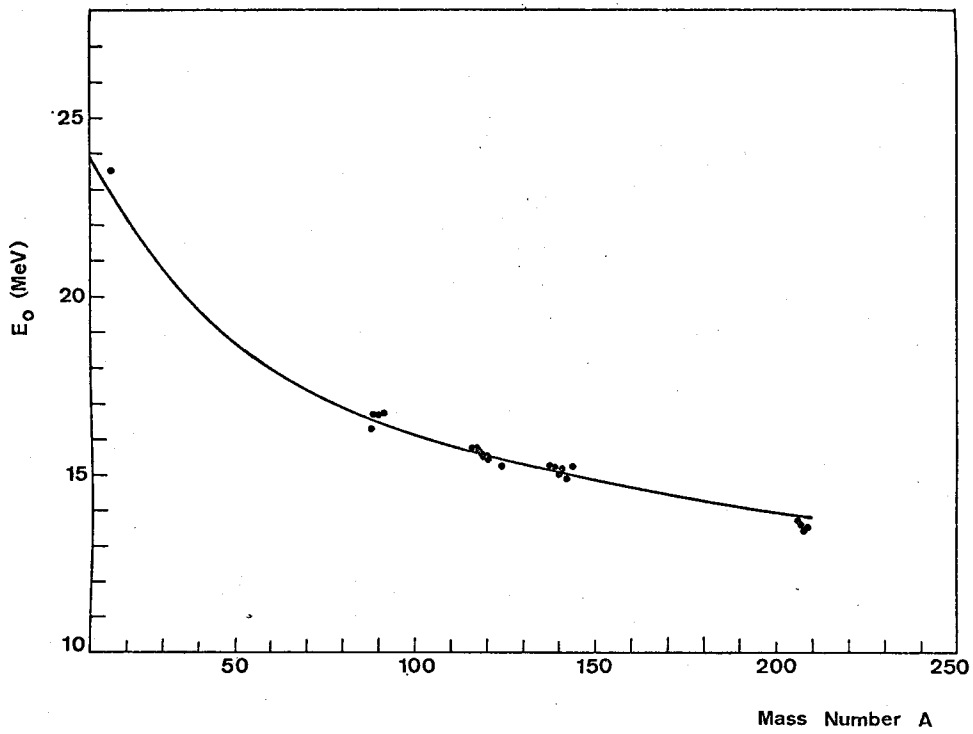
E_o (MeV)
Mass Number A

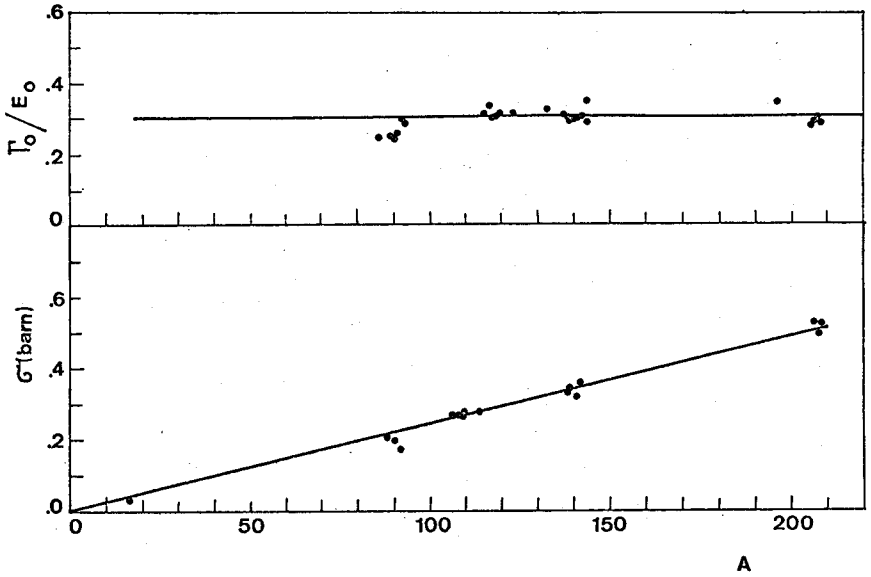
Γ_o / E_o
σ (barn)
A

FIG. 23.

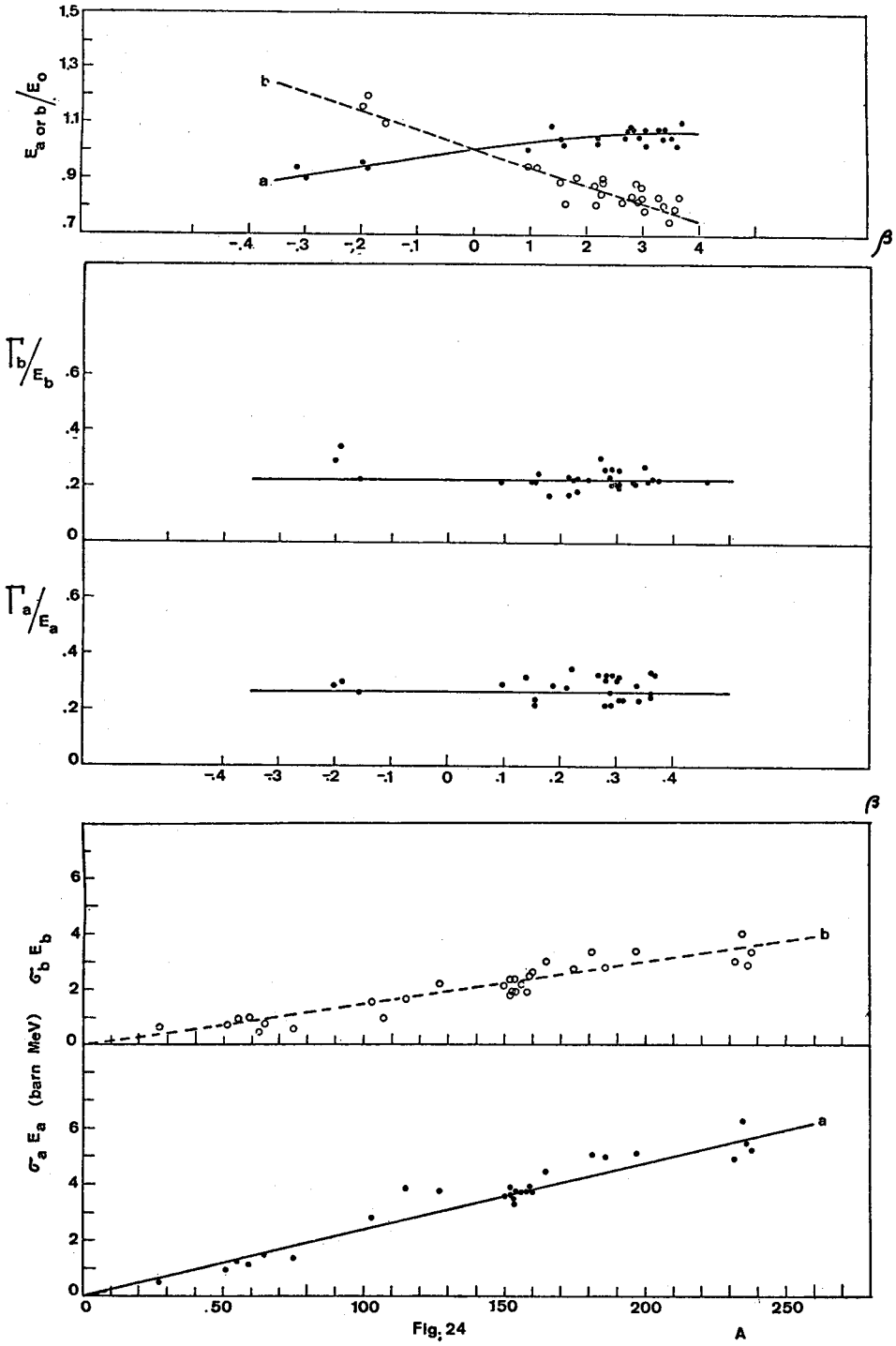
E_a or b/E_o
b
a
β
Γ_b/E_b
Γ_a/E_a
β
$\sigma_b E_b$
b
$\sigma_a E_a$ (barn MeV)
a
A

Fig. 24

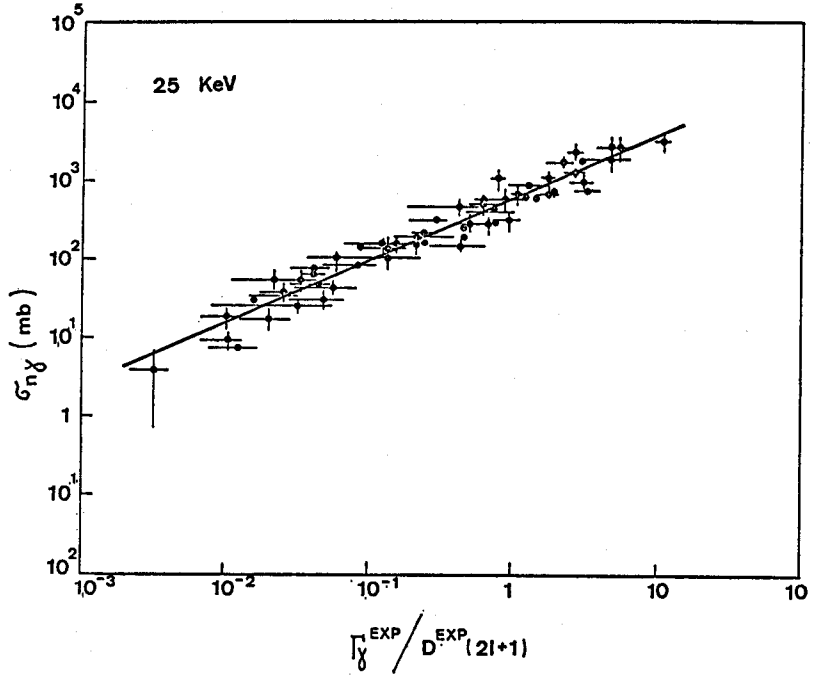
25 KeV
$\sigma_{n\gamma}$ (mb)
$\Gamma_\gamma^{EXP}/D^{EXP}(2I+1)$

Fig. 25

STATISTICAL THEORY APPLICATIONS AND ASSOCIATED COMPUTER CODES

A. PRINCE
National Nuclear Data Center,
Brookhaven National Laboratory,
Upton, NY,
United States of America

ABSTRACT

A. Theoretical Description

The general format is along the same lines as that used in the O.M. Session, i.e. an introduction to the nature of the physical problems and methods of solution based on the statistical model of the nucleus.

Both binary and higher multiple reactions are considered.

B. Workshop (Problem Session)

The computer codes used in this session are a combination of optical model and statistical theory.

As with the O.M. sessions, the preparation of input and analysis of output are thoroughly examined. Again, comparison with experimental data serves to demonstrate the validity of the results and possible areas for improvement.

A. Introduction

1.0 Purpose and Nature of Physical Problems

The statistical model given here is due to Wolfenstein [1] and Hauser and Feshbach.[2]

The theory is based on the assumption that all states of the compound nucleus which can be excited according to the conservation of energy, angular momentum and parity do take part in the reaction, however, the formation and decay of the compound nucleus takes place in an incoherent manner. The result of this evaporation theory for the cross section $\sigma<\alpha|\alpha'>$ integrated over all angles of the outgoing particle pairs and averaged over the resonance structure may be written.

$$\sigma<\alpha|\alpha'> = \pi\lambda^2 \sum_{J,j,\ell,j'\ell'} \{(2J+1)/(2i+1)(2I+1)$$

$$\times \{T^J_{\alpha'j'\ell'} T^J_{\alpha,j\ell} / \sum_{\alpha''j''\ell''} T^J_{\alpha''j''\ell''}\} \qquad 1.0$$

where ℓ is the orbital angular momentum of the incoming particle, $j = I + i = J - \ell$ its channel spin, while ℓ' and $j' = J - \ell$ are the corresponding values for the emitted particle. The symbols α and α' define a set of values characterizing the entrance and the exit channels, respectively. T stands for transmission coefficients; they are related to the optical-model phase shifts $\delta_{\ell j\alpha}$ by

$$T^J_{\alpha j\ell} \equiv \{1 - |e^{-2i\delta_{\ell j\alpha}}|^2\} \qquad 1.1$$

The factor

$$T^J_{\alpha'j'\ell'} / \sum_{\alpha''j''\ell''} T^J_{\alpha''j''\ell''} \propto \Gamma'/\Sigma\Gamma'' \qquad 1.2$$

since the transmission coefficients are proportional to the widths for decay to a given state. The sum in the denominator of (1.2) includes Γ' plus the widths of all possible decay modes competing with Γ'. When the spin-orbit interaction is absent, the transmission coefficients involve only ℓ and are independent of j and J. For incident and emerging particles of spin 1/2, j can have at most only two values $j_{1,2} = I \pm 1/2$ where I is the spin of the target nucleus in its ground state.

Under these circumstances, the cross section may be represented as a sum over ℓ of the contributions from the various J values possible for each ℓ. Thus, Eq. (1.1) now becomes:

$$\sigma<\alpha|\alpha'> = \frac{\pi\lambda^2}{2(2I+1)} \sum_{\ell} T_{\alpha\ell} \sum_{j} \frac{\epsilon^J_{j\ell} (2J+1) \sum_{\ell'} \epsilon^J_{j'\ell'} T_{\alpha'\ell'}}{\sum_{\ell''} \epsilon^J_{j''\ell''} T_{\alpha''\ell''}} \qquad 1.3$$

Here $\epsilon^J_{j,\ell}$ is a quantity such that

$$\epsilon^J_{j,\ell} = \begin{cases} 2, \text{ if both values of j are included in the range } |J-\ell| \le j \le (J+\ell), \\ 1, \text{ if one of the values of j is included in the range } |J-\ell| \le j \le (J+\ell), \\ 0, \text{ if neither value of j is included in the range } |J-\ell| \le j \le (J+\ell), \end{cases}$$

The channel designation α includes the energy of the incident particle and excitation state of the target nucleus, while α' is the similar designation for the final system which includes the type and energy of the emergent particle and the state of excitation of the residual nucleus.

Eq. (1.3) may also be used to describe fission and capture by ewriting it in simple form as

$$\sigma_r = \frac{\pi \lambda^2}{2(2I+1)} \sum_{l=0}^{\infty} T_n(l,E) \frac{\sum_{j=0}^{\infty} \epsilon_{j,l}^{J} (2J+1) T_r(J,E)}{\sum_r T_r(J,E) + \sum_{j',l'} \epsilon_{j',l'} T_n(l',E')} \qquad 1.4$$

(r refers to either capture or fission). The transmission coefficients for the fission and radiation channels are given by:

$$T_r(J,E) = 2\pi \frac{\langle \Gamma_r(J,E) \rangle}{\langle D(J,E) \rangle} \qquad 1.5$$

where $\Gamma_r(J,E)$ is the partial width of a level of spin J formed by a neutron of energy E. D(J,E) is the spacing of levels of spin J.

For radiative capture T_r in the denominator of Eq. (1.4) is the total probability of radiative decay of the compound nucleus, T_γ. This radiation term $T_\gamma(J,E)$ differs from the radiation transmission coefficient $T_c(J,E)$ which is used in the numerator of Eq. (1.4) and gives the neutron radiative capture probability.

For fission the transmission coefficient $T_f(J, ,E)$ is interpreted in terms of the Hill-Wheeler model [3] expressed as:

$$T_f(J,\pi,E) = \sum_k N(J,\pi, E-E_{fk}) P(E-E_{fk}) \qquad 1.6$$

where $N(J,\pi,(E-E_{fk}))$ is the number of transitional states in the saddle point of the fissioning nucleus above the $k^{\underline{th}}$ fission barrier with energy E_{fk}, and the penetrability $P(E-E_{fk}(J,\pi)$ of the $k^{\underline{th}}$ fission barrier is given as

$$P\{E-E_{fk}(J,\pi)\} = \frac{1}{1+\exp\left\{\frac{2\pi(E_{fk}-E)}{\hbar\omega}\right\}} \qquad 1.7$$

where ω is the circular frequency of the inverted harmonic oscillator.

Recently [4] a more detailed analysis of the fission process has incorporated the concept of a double-hump fission barrier.[5] This treatment allows the transmission coefficient to be expressed in terms of the coefficients for transmission across two peaks instead of one. Thus the fission probability is denoted by

$$P_F = \frac{T_A T_B}{T_A T_B + T'(T_A + T_B)} \qquad 1.8$$

where T' is the summation of all the other decay channels from the compound nucleus. T_A and T_B have the same form of Eq. (1.7) but different values for the barrier heights and curvature.

In Eqs. (1.0) and (1.3) the effect of fluctuations of the compound nucleus-level widths about their average values has been ignored. However, even though the widths in different channels might be independent, the fluctuations in the numerator Eqs. (1.0) and (1.3) are correlated to fluctuations in the denominator. Thus, following Lane and Lynn[6] and Moldauer[7,8], the Hauser-Feshbach equation should be multiplied by a fluctuation correction factor given by

$$R_{\alpha\alpha'} = \left\langle \frac{\Gamma_\alpha \Gamma_{\alpha'}}{\Gamma} \right\rangle \Big/ \frac{\langle \Gamma_\alpha \times \Gamma_{\alpha'} \rangle}{\langle \Gamma \rangle} \qquad 1.9$$

The particle widths Γ_α are related to the optical model transmission coefficients by

$$T_\alpha^{OM} \approx 2\pi \frac{\langle \Gamma_\alpha \rangle}{D}$$

Thus Eq. 1.8 may be written as

$$R_{\alpha\alpha'} = \left\langle \frac{T_\alpha T_{\alpha'}}{T} \right\rangle \Big/ \frac{\langle T_\alpha \rangle \langle T_{\alpha'} \rangle}{T} \qquad 1.10$$

Recent theoretical developments offer different interpretations of this correction factor where under certain conditions $R_{\alpha\alpha'}$ may become greater than unity for non-elastic processes (i.e. $\sigma_{n\gamma}$, $\sigma_{nn'}$). (See Refs. 9-11).

This effect may be interpreted in terms of the distribution laws for the various particle decay widths.

Programs were written[12] to [14] to be used in computer experiments that produced synthetic cross sections analagous to those encountered in experimental measurements. The results were interpreted so as to determine the limitations imposed on the average values of the various quantities (e.g. matrix elements) used to generate these synthetic cross sections.

The values of these variables as obtained from the statistics were compared with those resulting from the conventional Hauser-Feshbach theory.

These numerical experiments have shown that in the presence of direct reactions, it is necessary that the fluctuation corrections to the cross sections and polarization data be analyzed in a much more sophisticated and generalized form.

A recent paper by Gruppelaar and Reffo[12] reviews some of various properties of the width fluctuation factor and the effect on decay channels.

These various treatments for the reinterpretation of the Hauser-Feshbach formula differ in certain respects and are still open to question; nonetheless, the results are encouraging and upon application to a real situation the validity of the assumptions will be further tested.

1.2 Multiple Reactions

The foregoing treatment of the Hauser-Feshbach method was devoted to binary reactions only, however, it can be extended to include many particle reactions.

Of special interest to dosimetry and CTR application are the so called "rare" nuclear reactions such as (n,nγ), (n,γn) or (n,np) and (n,pn) which necessitate a three-particle analysis.

This tertiary reaction is assumed to proceed as

$$\alpha + A \longrightarrow A^* \longrightarrow B^* + \beta$$
$$\searrow\ C^* + \gamma$$

where β and γ are the emitted particles (n,p,d,t,He^3,He^4) and α is the particle incident on nucleus A leading to the compound nuclei A^* and B^*. Thus

$$\sigma^J_{\alpha,\beta\gamma} = \pi \lambda^2_\alpha \frac{(2J+1)}{(2i_\alpha+1)(2I_\alpha+1)} T^J_{J_\alpha \ell_\alpha}(\epsilon_\alpha)$$
$$\times\ \omega^J_{J_\alpha \ell_\beta I_\beta}(E_o; E_\beta, \epsilon_\beta)\, \omega^{I_\beta}_{J_\gamma \ell_\gamma I_\gamma}(E_o; E_\gamma, \epsilon_\gamma) \qquad 1.11$$

where $T^J_{J_\alpha \ell_\alpha}(\epsilon_\alpha)$ represents the transmission coefficient of particle α (e.g. a neutron) which has kinetic energy ϵ_α, total angular momentum J_α, orbital angular momentum ℓ_α, and total angular momentum J that is produced jointly with the target nucleus; $W^J_{J_\alpha \ell_\alpha I_\alpha}(E_o; E_\beta \epsilon_\beta)$ is the probability of disintegration of the compound nucleus with spin J and excitation energy E_o into a residual nucleus with spin I_β and excitation energy E_β and a particle with kinetic energy ϵ_β, total angular momentum J_β, and orbital angular momentum ℓ_β; $W^{I\beta}$ is the probability of disintegration of the compound nucleus following the emission of particle β.

An exact calculation of the cross section given in Eq.(1.11) reduces to the determination of the probability of disintegration of the compound nuclei.

By assuming the lifetime of all the compound nuclei to be sufficiently long and by writing the set of detailed balance equations for the series decay, one obtains the following equation for the three-particle reaction:

$$\sigma_{\alpha,\beta\gamma} = \pi \lambda^2_\alpha \sum_{J,J_\alpha,\ell_\alpha} \frac{(2J+1)}{(2i_\alpha+1)(2I_\alpha+1)} T^J_{J_\alpha \ell_\alpha}(\epsilon_\alpha)$$
$$\times \left\{ \sum_{J_\beta \ell_\beta} T^J_{J_\beta \ell_\beta}(\epsilon_\beta) \Big/ \sum_{\beta'} \sum_{E_{\beta'}=0}^{E_o - Q_{\beta'}} \sum_{J_{\beta'} \ell_{\beta'} I_{\beta'}} T^J_{J_{\beta'} \ell_{\beta'}}(\epsilon_{\beta'}) \right\}$$
$$\times \left\{ \sum_{J_\gamma \ell_\gamma} T^J_{J_\gamma \ell_\gamma}(\epsilon_\gamma) \Big/ \sum_{\gamma'} \sum_{E_{\gamma'}=0}^{E_o - Q_{\gamma'}} \sum_{J_{\gamma'} \ell_{\gamma'} I_{\gamma'}} T^{J_\beta}_{J_{\gamma'} I_{\gamma'}}(\epsilon_{\gamma'}) \right\} \qquad 1.12$$

The expressions for the n-particle reaction (n > 3) are similar.

If the density of final states is a continuous function of energy, then by summing or integrating over a definite range of energy, Eq.(1.0) becomes

$$\sigma_{a,\upsilon}(\epsilon_o,\epsilon)\,d\epsilon = \pi\lambda^2 \sum_{J,j,\ell} \frac{(2J+1)}{(2i+1)(2I+1)} \times \frac{\left\{ T^J_{a,\ell}(\epsilon_o) \sum_{J',\ell'I'} T^J_{\upsilon j' \ell'}(\epsilon)\rho_\upsilon(I',E)\,d\epsilon \right\}}{\sum_{\upsilon'' j'' I''} \int_0^{\epsilon_o - Q_{\upsilon''}} d\epsilon\; T^J_{\upsilon'' j'' \ell''}(\epsilon)\,\rho_{\upsilon''}(I'',E'')\,dE''} \qquad 1.13$$

where the symbols α and α' for these incoming and outgoing channels have been replaced by a and υ, respectively.

In Eq.(1,13) the sum in the denominator is taken over all energetically possible emitted particles υ'' (usually taken as n, P,d, t, He^3 and α) and ρ_υ (I;E) is the density of the residual nucleus at an excitation energy

$$E = \epsilon_o - \epsilon - Q \qquad 1.14$$

where Q is the Q value of the reaction.

It should also be noted that for simplicity the competing channels υ' leading to fission or radiactive capture have been neglected.

2.0 Parametrization Methods

In analyzing nuclear reactions using the statistical model, one of the most important aspects is a knowledge of the level density.

Empirical information on the level density is usually obtained by analyzing

a. levels of residual nuclei from reactions such as (n,n'), (p,p'), (d,p), (d,α) etc.,
b. spectral shape of emitted particles,
c. slow neutron resonances and associated widths.

Some of these experimental data provide direct information on the level density while in others, it is provided indirectly. The latter method, in many instances, provides only rough estimates since the results are influenced by estimation of other nuclear quantities.

The most commonly used expressions for the level densities are due to Ericson[15] and Lang and LeCouteur.[16]

$$\rho(E,J) = \text{const.}\,(2J+1)\exp\left(-\frac{J(J+1)}{2\sigma^2}\right)\frac{a^{1/2}\exp(2\sqrt{aU})}{\mathcal{I}^{3/2}U^2} \qquad 2.1$$

or

$$\rho(E,J) = \text{const.}\,(2J+1)\exp\left(-\frac{J(J+1)}{2\sigma^2}\right)\frac{a^{1/2}\exp(2\sqrt{aU})}{\mathcal{I}^{3/2}(U+t)^2} \qquad 2.2$$

which give a density of levels of spin J of a nucleus excited to an energy U.

Eqs. 2.1, 2.2 are derived on the basis of the Fermi gas model of the nucleus where σ is the so called spin cut-off parameter and is related to the nuclear moment of inertia by

$$\sigma^2 = \frac{\mathcal{I}t}{\hbar^2} \qquad 2.3$$

The nuclear temperature T is related to the nuclear thermodynamic temperature t by

$$\frac{1}{T} = \frac{1}{t} - \frac{2}{U} \qquad 2.4$$

$$\frac{1}{T} = \frac{1}{t} - \frac{2}{U+t} \qquad 2.5$$

corresponding to either 2.1 or 2.2, respectively.

The quantity a is a characteristic parameter related to the spacing of single particle nucleon states near the top of the Fermi sea and is related to the thermodynamic temperature by

$$at^2 - t = U \qquad 2.6$$

where U is the effective excitation energy, given by $U = (E + \Delta)$; E being the excitation energy and Δ is a negative term representing the pairing energy of the last two protons when Z is even; of the last two neutrons when N is even; and the sum of both pairing energies for even-even A; $\Delta = 0$ for odd-odd nuclei.

The parametrization has been carried out by several investigators using experimental neutron resonance data. (Refs. 17-20).

This produced meaningful results only for a narrow range in the region where the fit was carried out. The a-parameters determined at the neutron binding energies predicted level densities which were too high at excitations near the ground state and much too large level densities for energies greater than 15 MeV.

Gilbert and Cameron[21] introduced a four-parameter formula in which they used a shifted Fermi gas[22] formula at higher excitations which was smoothly joined to a constant temperature formula at lower energies. The fictive ground state was obtained from experimental mass differences, thus only the level density parameter, a, was left as the adjustable constant.

Carrying out a fit to the four constants in both the high and low regions produced fairly good results.

Another approach has employed the so-called "back-shifted" Fermi gas model[23-25] where the Fermi gas formula was used with both a and the ground state shift as adjustable parameters.

Dilg et al.[26] show that using the "back-shifted" Fermi gas produces rather large negative Δ values for odd mass nuclei and moderately positive Δ values for even nuclei.

The a values while not showing any drastic odd-even effects, do show strong shell effects similar to the one parameter fits.

While the use of the four-parameter (e.g. Gilbert and Cameron) or the two-parameter (e.g. Dilg et al.) formula has produced fair to excellent fits to experimental data, one must still be cognizant of the fact that the semi-empirical formulas do not necessarily justify the adopted energy dependence of the level density.

Also for nuclei near closed shells the values of a and Δ resulting from the parametrization can only be a coarse approximation and extrapolation beyond the range of validity can produce absurd results.

References

1. Wolfenstein, L., Phys. Rev. 82 (1951) 690.
2. Hauser, W., Feshbach, H., Phys. Rev. 87 (1952) 366.
3. Hill, D. L., Wheeler, J. A., Phys. Rev. 89 (1953) 1102.
4. Lynn, J. E., Bech, B. B., J. Phys. A. Math. Nucl. Gen. 7 (1974) 395. Also see Michaudon, A., Proc. of Conf. Nuclear Cross Sections and Tech., Wash. D. C. I (1975) 202.
5. Strutinsky, V. M., Nucl. Phys. A95 (1967) 420.
6. Lane, A. M., Lynn, J. E., Proc. Phys. Soc. (London) A70 (1957) 557.
7. Moldauer, P. A., Rev. Mod. Phys. 36 (1964) 1079.
8. Moldauer, P. A., Phys. Rev. 135B (1964) 642.
9. Moldauer, P. A., Phys. Rev. C14, 764 (1976).
10. Gruppelaar, H. and Reffo, G., Nucl. Sci. and Eng. 62, 756 (1977).
11. Hofmann, H. M. et al., Ann. Phys. 90, 403 (1975).
12. Tepel, J. W., et al., Phys. Lett. 49B (1974) 1.
13. Weidenmüller, H. A., Nukleonika 19 (1974) 387.
14. Moldauer, P. A., Phys. Rev. C12 (1975) 744.
15. Ericson, T., Ann. Phys. (NY) 23 (1963) 390.
16. Lang, J. M. B., Le Couteur, K. J., Proc. Phys. Soc. (London) A67 (1954) 586.
17. Erba, E., et al., Nuovo Cim. 22 (1961) 1237.
18. Facchini, U., Saetta-Menichella, E., Energia Nucl. 15 (1968) 54.
19. Buba, H., Nucl. Phys. A159 (1970) 625.
20. Gadioli, E., Iori, I., Nuovo Cimento 51 (1967) 100.
21. Gilbert, A., Cameron, A. G. W., Can. J. Phys. 43 (1965) 1446.
22. Erba, E., et al., Nuovo Cim. 22 (1961) 1237.
23. Gadioli, E., Zetta, L., Phys. Rev. 167 (1968) 1016.
24. Huizenga, J. R., et al., Phys. Rev. 182 (1964) 1149.
25. Vonach, H., Hille, M., Nucl. Phys. A127 (1969) 289.
26. Dilg, W., et al., Nucl. Phys. A217 (1973) 269.

B. Workshop (Problem Session)

The following codes have been chosen for calculating reaction cross sessions using a combined optical model and statistical theory.

a) ABACUS (See my lecture on optical model codes)
b) HAUSER-5; F. M. Mann, HEDL-TME 76-80 (1976)
c) CERBERO 2 (See my lecture on optical model codes)
d) ERRINI; F. Fabbri and G. Reffo RT/FI (77)4 (1977)

1. HAUSER - 5

Name of Code: HAUSER

Author: F. M. Mann

Establishment: Hanford Engineering Development Laboratory, Richland, WA., USA.

Nature of Problem Solved: Program HAUSER calculates the total reaction cross section for T(a,bc)F where T is the target nucleus, a is the projectile (any particle-charged or uncharged), b and c are emitted particles or gamma rays, and F is the final nucleus. The statistical model is employed with allowance for angular momentum and parity effects. The transmission coefficients can either be calculated (without spin-orbit interaction) or read-in. Width fluctuation corrections can be included through the method of Tepel, Hofmann, and Weidenmüller. Cross sections can be printed for discrete states, two-body or three-body reactions.

Program Language: FORTRAN IV

Size: 170 K for 7 values of bc, 6 values of b, 100 discrete states. Can be considerably reduced by reducing size of tables.

Status: Has run on IBM 370 and CDC 6600 and 7600.

Introduction

HAUSER-5 is a recent statistical model code which handles both binary and tertiary processes along with capture and fission.

Two basic equations are solved given as

$$\sigma_{\alpha\beta} = \frac{\pi \lambda^2_\alpha}{(2I_{\alpha_1}+1)(2I_{\alpha_2}+1)} \sum_{J^\pi} \frac{\sum_{\ell s} (T_\alpha)^{J^\pi}_{\ell s} \sum_{\ell' s'} (T_\beta)^{J^\pi}_{\ell' s'}}{T^{J^\pi}} W^{J^\pi}_{\alpha\beta} \quad 1.1$$

for conventional two-body reactions and

$$\sigma_{\alpha(\beta\gamma)} = \sum_{J^\pi} \left| \frac{\pi \lambda^2_\alpha}{(2I_{\alpha_1}+1)(2I_{\alpha_2}+1)} \sum_{\ell s} (T_\alpha)^{J^\pi}_{\ell s} \right| * \left| \frac{\sum_{\ell' s'} (T_\beta)^{J^\pi}_{\ell' s'}}{T_1^{J^\pi}} W^{J^\pi}_{\alpha\beta} \right| * \left| \sum_{\ell'' s''} \frac{(T_\gamma)^{J^\pi}_{\ell'' s''} W^{J^\pi}_{\beta\gamma}}{T_2^{J^\pi}} \right| \quad 1.2$$

for three body (e.g., n,2n, n, n etc.) ($W^{J^\pi}_{\alpha\beta}$ is the fluctuation correction factor). The particle transmission coefficients $T^{J^\pi}_{\ell s}$ are obtained from the optical model.

Transmission coefficients for gamma-ray channels are calculated by assuming E and M transitions exist between all possible states consistent with the appropriate energy and selection rules,

$$T^{J^\pi}_{E\ell \text{ or } M\ell}(E) = 2\pi \Gamma^{J^\pi}/D^{J^\pi}_\gamma = N_\ell \int_0^E \rho(E')(E-E')^n S(E')\, dE' \quad 1.3$$

where N_ℓ is a normalization varying smoothly with A,

ρ is the level density, $n=\ell+2$, and
S is the form factor (usually taken to be unity or of a Lorentzian shape to represent giant resonances).

Because higher multipolarity transitions are unlikely, usually only E1 and M1 transitions are included in the calculations.

Transmission coefficients for fission channels are given in the Hill-Wheeler formalism as

$$(T_\ell)^{J\pi} = \frac{1}{\exp\left[(E-E_1)/\hbar\omega\right] + 1} \qquad 1.4$$

where E_1 is the barrier height and $\hbar\omega$ is the width. With the advent of fission isomers, the potential is often taken to be doubly humped with an intermediate well. No simple equation like Eq. 1.4 exists for such a case. However, a closed form can be obtained if the two barriers and intermediate well are taken to be harmonic oscillator potentials.

In order to handle both discrete and continuum regions, the total transmission coefficient is given by

$$T^{J\pi} = \sum_{\substack{i \\ \text{discrete}}} T_i^{J\pi} + \int_{E_1}^{E_2} T^{J\pi}(E)\,\rho^{J\pi}(E)\,dE \,. \qquad 1.5$$

Two forms of the level density are often used, the constant temperature formula

$$\rho(E) = \exp\left[(E-E')/T\right]/T \qquad 1.6$$

and the Fermi gas formula

$$\rho(E) = \exp\left[2\sqrt{a(E-\Delta)}\right]/\left[12\sqrt{2}\,\sigma\, a^{1/4}\,(E-\Delta)^{5/4}\right]. \qquad 1.7$$

Spin and parity dependence is included by a multiplication factor

$$\rho(E)^J = \rho(E)\,(2J+1)\exp\left[-(J+1/2)^2/2\sigma^2\right]/(2\sigma^2). \qquad 1.8$$

The width fluctuation factor $W^{J\pi}$ for channels other than capture is

$$W_{\alpha\beta}^{J\pi} = (1+2\delta_{\alpha\beta}/\nu_\beta)\int_0^\infty \frac{\exp(-T_\gamma^{J\pi}\,t)\,dt}{(1+2t\,\frac{T_\alpha^{J\pi}}{\nu_\alpha})(1+2t\,\frac{T_\beta^{J\pi}}{\nu_\beta})\prod_{\varepsilon\neq\gamma}(1+2t\,\frac{T_\varepsilon^{J\pi}}{\nu_\varepsilon})^{\nu_\varepsilon/2}} \qquad 1.9$$

and for capture

$$W_{\alpha\gamma}^{J\pi} = \int_0^\infty \frac{\exp(-T_\gamma^{J\pi}\,t)\,dt}{(1+2t\,\frac{T_\alpha^{J\pi}}{\nu_\alpha})\prod_{\varepsilon\neq\gamma}(1+2t\,\frac{T_\varepsilon^{J\pi}}{\nu_\varepsilon})^{\nu_\varepsilon/2}} \qquad 1.10$$

The Tepel et al.[1] approximation is used for determining the width fluctuation factors. Transmission coefficients are interpolated from a table of previously calculated transmission coefficients, which can either be read as input or calculated internally.

The real spherical potential is taken to be the Woods-Saxon shape, and the imaginary potential can be a sum of potentials of the Woods-Saxon shape and the derivative Woods-Saxon shape, or can be a Gaussian shape. If the user desires, default potentials (shown in Table 1) can be used. However, (j,ℓ,s) dependent transmission coefficients ($T^s_{\ell j}$) must first be averaged

$$T = \sum_{j=\ell=s}^{\ell+s} (2j+1)\,T^s_{\ell,j}/(2\ell+1)(2s+1) \qquad 1.11$$

over j before they can be input.

TABLE 1

DEFAULT OPTICAL PARAMETERS

(Real potential is Woods-Saxon shape, imaginary potential is sum of Woods-Saxon and derivative Woods-Saxon shapes)

	Neutron[a]	Proton[b]	Deuteron[c]	Triton[d]	^{3}He[d]	Alpha[e]
V_{WS}(MeV)	47.01-0.267E -0.0018E^2	54+24*(N-Z)/A +0.4*Z/A$^{1/3}$-0.32E	81+2*Z/A$^{1/3}$	136.4+55*(N-Z)/A -0.17E	165-7*(N-Z)/A -0.17E	185.00
W_{WS}(MeV)	0.00	-2.7+0.22E	0.00	41.3+63*(N-Z)/A -0.33E	56-110*(N-Z)/A -0.33E	25.00
W_{der}(MeV)	9.52-0.053E	11.8+12*(N-Z)/A -0.25E	14.40	0.00	0.00	0.00
R_R(fm)/A$^{1/3}$	1.322-0.0076*A (1-0.005*A)	1.17	1.15	1.20	1.20	1.40
R_I(fm)/A$^{1/3}$	1.266-0.0037*A (1-0.005*A)	1.26	1.34	1.40	1.40	1.40
a_R(fm)	0.66	0.75	0.81	0.72	0.72	0.52
a_I(fm)	0.48	0.58	0.68	0.68	0.86	0.52

(a) Wilmore, D.; Hodgson, P.E.; Nucl. Phys. 55 (1964) 673
(b)(d) Becchetti, F.D., Jr.; Greenlees, G.W.; Phys. Rev. 182 (1969) 1190
(c) Perey, C.M.; Perey, F.G.; Atomic and Nuclear Data Tables 13 (1974) 293
(e) McFadden, L.; Satchler, G.R.; Nucl. Phys. 84 (1966) 177

2. ERRINI

Name of Code: ERRINI (An Optical Model Fortran IV Code for the calculation of multiple cascading particle emissions) Rpt. CNEN RT/FI (77) 4

Authors: F. Fabbri and G. Reffo

Establishment: CNEN, Bologna, Italy

Program Language: Fortran IV

Size: 240 K - bytes (overlay structure)

Status: IBM 375, modified for CDC

Introduction

ERRINI is a multiple emission code based on Hauser-Feshbach analysis and is primarily for high-energy condensing particles.

The transmission coefficients are calculated similar to those in CERBERO II, except no width fluctuation corrections are applied.

a) First step decay calculations

The total transmission coefficients $T_a^{J\pi}$ are first calculated for all J and π, then the various binary cross sections $\sum_{J\pi} \sigma_{x,a}^{J\pi}$ are calculated, where

$$\sigma_{cc'}^{x.a} \propto \frac{T_c^x \, T_{c'}^a}{T^a} \qquad 2.1$$

and

$$T_a = \sum_{c''} T_{c''}^a \qquad 2.2$$

For each channel c" and c' leading to excitation of levels in a continuum band, the corresponding transmission coefficients are weighted according to the number $\rho \, dU$ of levels in the band:

$$T_{c''} \rightarrow T_{c''} \, \rho_{c''}^a \, dU_{c''}^a \qquad 2.3$$

$\rho_{c''}^a$ being the density of levels available to channels c" in the residual nucleus corresponding to emission of particle a.

This part of the code calculates the same quantities as CERBERO II does, from which it is taken. As ERRINI was devised for use at high energies, no width fluctuation correction is introduced.

For any binary process, for which the cross section $\sigma^{x.a}$ is greater than 10^{-5}b.

b) Second step decay processes are accounted for by starting with the calculations of total transmission coefficients $T_b^{J\pi}$ for each J and π, then working out the branching ratios P_b^J for each J and π.

Formula (1) is generalized to describe a two step cascade as follows:

$$\left[d^2\sigma_{c,c'}^{x.ab} \propto \frac{T_c^x T_{c'}^a \, \rho_{c'}^a \, dU_{c'}^a \, \sum_{J'\pi'} (P_b(U_{c'}^a) \, dU_{c''}^b)_{J'\pi'}}{T^a} \right]_J \qquad 2.4$$

where

$$\left[P_b(U_{c'}^a) dU_{c''}^b = \frac{\sum_{c''} T_{c''}^b \rho_{c''}^b \, dU_{c''}^b}{T_b} \right]_{J'\pi'} \qquad 2.5$$

When channels c" lead to excitation of an isolated level, the code assumes $\rho_{c''}^b \, dU_{c''}^b = 1$.

Whenever second emission leaves the residual nucleus excited above the neutron binding, a neutron is assumed to be emitted.

THE ROLE OF DESK CALCULATORS IN NUCLEAR DATA EVALUATION

M. MOTTA
Comitato Nazionale per l'Energia Nucleare,
Bologna, Italy

Abstract

The performances of the modern Desk Calculators are more and more increasing. Consequently, the best feature for the definition of a Desk Calculator seems to be prices and volume occupation. The interactive operating mode and the low installation and maintaining costs make the use of these computing machines very likely and economical. A list of tasks which are profitably performed in nuclear data preparation are presented here. A lot of practical applications are given through the formulas and the list of codes written in BASIC language, which is commonly adopted for these small computers.

WHAT IS A DESK CALCULATOR ?

In the last few years a considerable improvement has been obtained in technologies for the construction of electronic computers.

Looking back in time, we can remember that twenty years ago a computer of the "first generation" used vacuum tubes, with a space occupation of many rooms. High power freezing plants were also needed for dissipation of the consumed thermal energy.

More recently, about ten years ago, the volume of a box of not many cubic meters could contain a computer of the "second generation" with equivalent calculating power and a number of about ten thousand transistors.

The same number of components can today be assembled on a small silicium plate of about 20 square millimeters.

Table 1 briefly summarizes the evolution of packing ability in assembling the computer components and the corresponding scale of information in bits/cubic centimeter [1].

TABLE 1

Evolution of computers (about 10000 components are assumed)

SYSTEM	VOLUME(m↑3)	PRICE($)	BITS/CUBIC CM
Vacuum tubes (1955)	20	10↑6	10↑(-2)
Transistors (1965)	2	10↑5	1
LIS-MOS (1975)	10↑(-7)	10↑2	10↑8

The improvement is self evident, mainly due to the adoption of Large Scale Integrated (LSI) microprocessors with Metal Oxide Semiconductors (MOS) and bipolar technologies.

In short, the functions of transistors and logical circuits are now directly implemented on silicium plates, starting from a plotted design of the circuits, which is later reduced by a factor of about 500 with a photolithographic process.

It is not our aim to describe this technical art of manufacturing and assembling computers. Nevertheless, it can be pointed out that the improvement will continue in the near future because the physical limit for information density is far from being reached. The human brain has an estimated information density of 10↑10 bits/cubic centimeters, the genetic memory of DNA elements has a density of the order 10↑19 bits/cubic cm, while a theoretical limit was set by Feynmann [2] and Landauer [3] at around 10↑21 bits/cubic cm. Thus, the bit commutation between two states 0,1 could still be shared by thermal agitation, at least in theory, in a cubic space of about 5 atoms each side, or 125 piled atoms.

The above considerations show that it is practically impossible to define what is a desk calculator by measuring its computing power, even if the power is only defined in terms of the high speed Central Memory capability.

Where application to our sphere of interest is concerned - i.e. the preparation and manipulation of nuclear data - we can define a desk calculator as a computing machine having two essential qualities:

1 - It is dimensioned, more or less, as a normal typewriting machine and can therefore be put on a normal writing table and started by turning a switch.

2 - The price lies approximately between ten and twenty thousand dollars, so that it can easily be bought even by a small Research Center.

NUCLEAR DATA AND DESK CALCULATORS

The neutron motion inside a reactor is described by assuming neutrons as classical particles. Balance equations, such as diffusion or transport equations, are therefore taken for motion description. But the interactions between neutrons and materials are governed by the laws of quantum theory. Quantum theory enters in the balance equations through the equation coefficients, which are essentially macroscopic cross sections. Thus, the importance of neutron cross sections and of the other nuclear data is evident in the design, construction and economy of nuclear reactors.

Let us now try to define the field of applications for nuclear data. To this end, a general view of the work which must be done, will be useful.

The preparation of nuclear data for reactor calculations and experiences is a job which runs through the following steps:

1 - Collection of the most recent data, both experimental and evaluated, which can be found in literature or by private communications, for each of the following energy regions:

a) Resolved resonances;
b) Unresolved resonances;
c) The continuum.

2 - Selection and evaluation of the most reliable data for each energy region (cross sections or parameters for a proper theoretical model).

3 - Compilation of the final selected data by writing them in a prefixed sequence given by some rules on position and formats, resulting in the so called "FILES".

It is well known that the FILES most commonly used are those named by the initials ENDF/B, LLL, UKNDL, KEDAK and SOKRATOR which indicate the American (Brookhaven & Livermore), English, German and Russian FILES respectively.

The above mentioned steps may be very cumbersome because collection, evaluation and printing regard a very large number of data, even if only one isotope is considered.

To give an idea of the volume of data which must be considered and written usually on punched cards in rows of 80 columns, let us remember some dimensions of files for elements in ENDF/B, edition iv:

Si	-	10523	cards
Cr	-	8321	cards
Fe	-	8285	cards
U-235	-	6759	cards

Such a large number of data can only be stored and manipulated by means of a big computer which has large volumes of memories with a capability of many megabytes, both of RAM (Random Access Memory) and of permanent type, using magnetic tapes and disks of peripheral units. The last storages, being "permanent", can be used as archives for data which are continually renewed and modified by up to date information.

Nevertheless, in order to arrive at the final compilation of a file, even of one isotope, all the data must be evaluated one by one with the best possible accuracy. At this point, it is essential that a set of calculation programs of quite easy access and usage should be available.

The programs must apply to the calculations in order to check the good agreement between theoretical calculations and experimental data in special energy ranges.
Most frequently we observe large discrepancies among experimental data of different Authors and Laboratories. Hence, theoretical calculations are needed for a good evaluation of data which are to be put in file.

Moreover, the theoretical models always make use of parameters which are obtained by a systematic analysis of experimental data, mainly in the energy region of resolved resonances.

The principal parameters which must be determined are the following:

a) Thermal cross sections (capture,absorption,fission and total);
b) Resonance integrals with and without 1/v contribution (reduced);
c) Potential scattering amplitude and cross section for slow neutrons;
d) Average level spacing (D) and Level Density Parameter "a";
e) s- and p-wave neutron Strength Functions;
f) Individual resonance parameters (l-state,energy Er,spin J, widths Γ);
g) Neutron and radiative average widths, for s- and p-waves.

The preparation of these data and the checking of their consistency with each other, as well as their ability to fit the experimental data correctly, must be done with a procedure of "trial and error" which can best be done with an interactive Unit of calculation and storage.
With such a Unit, the evaluator talks and works better in that he has a step by step execution which permits changes of data, a quick calculation and plotting of results with comparison of sources and models.
The "BATCH" mode of feeding a computer of high power with inputs and programs (for the sake of simplicity henceforth called Maxicomputer), is commonly used procedure; but it does not permit an interactive mode of operation which is instead obtained if Time Sharing Operation (TSO) is used.

The operation mode of the modern desk computers (henceforth called Minicomputers) is quite similar to the TSO mode of a Maxicomputer.

So, for a better understanding of the advantages given to the evaluator at some stages of nuclear data preparation by the use of a minicomputer, let us summarize the characteristics most commonly found in the two types of computers or operation modes.

TABLE 2

	MAXICOMPUTER (batch)	MINICOMPUTER (or TSO)
RAM capacity:	megabytes	8-48 kilobytes
PERIPHERALS:	disks and tapes	disks(floppy),tapes(cartridges)
PLOT:	by peripheral units	and/or by integrated printing unit
LANGUAGE:	Fortran, etc.	extended BASIC,etc.
INPUT:	Cards,tapes	keyboard,disks,tapes
WORKING MODE:	multiprogramming	by operator's decision
STOP:	only by program statements	and/or by keyboard command
DEBUG:	only by program statements	step by step execution
TRACE:	only by program statements	and/or by keyboard command
DATA CHANGING:	none during execution	in execution too (step condition)
CHAIN/LINK:	only by program statements	and/or by keyboard command
SYNTAX CONTROL:	on the whole program	at each entered line

The above table clearly shows that the decisional power of the operator is greatly increased by the use of a minicomputer, since at each time he can use the keyboard to stop the program, check the value of any variable, change it, restart, or ask for a printed trace of the logical flow of the program.

Such flexibility is particularly appreciated when checking a new input or a new code, as it often happens in preparation of nuclear data files.

The same interactive operating mode of a minicomputer is obtained with a TSO (Time Sharing Operation) working mode of a maxicomputer. Nevertheless, there are at least two good reasons to prefer the use of a minicomputer.

The first one is that the entering procedures and instruction manual of a TSO terminal are usually more complex (passwords needed, out of service intervals, long replication time in some periods crowded with users, etc.)

The second one is that the existence of TSO terminal units implies the existence of a big master calculation center with expensive transmission lines (wireless, telephone cable) for efficient communication.
Such apparatus may have too high an installation and mantainance cost.

On the other hand, for nuclear data preparation, there are a lot of applications which can efficiently be done by a small computer.

It will be useful to write down a list of tasks which are profitably performed with the aid of a desk calculator.

(1) The list of parameters of resolved resonances, their grouping in s-, p- or d-wave classes and the shift from one group to the other after comparison with experimental cross sections or after application of statistical tests.
(2) The quick modification on the keyboard of some file parameters which must be changed as a consequence of the above mentioned "trial and error" procedure.

(3) Statistical analysis of the resonance widths and spacings, with determination of average values, standard deviation and errors, and a comparison with theoretical distribution.
(4) Strength function determination, for s- and p-wave resonances.
(5) Calculation of thermal cross sections and resonance integrals (total and reduced).
(6) Cross section calculations in some energy checking points, mainly in the resolved and statistical region.
(7) Random generation of resonances from the proper spacing and width distributions, for all the isotopes without experimental data, for which a reasonable evaluation of cross section is needed.
(8) Estimation of levels of negative energy, in order to take into account the 1/v part of the cross section due to missed resonances.
(9) Probability tests for estimation of unknown spin and parity of the resonances.
(10) Numerical integrations for averaging tabulated cross sections, weighted over special functions such as a given flux.
(11) Doppler broadening of resonances in narrow energy ranges, by means of analytical calculation of the well known ψ and χ functions [4].
(12) General applications, running routines in common use, e.g. least square fits, tabulation of functions, plots of data and statistical distributions, etc.

This list of actions clearly gives an idea of the important role which a desk calculator can have in the preparation of nuclear data.

In order to see some of the above calculations in a practical way, let us look at some programs which regard data determination of the resolved resonance region.

Table 3 presents a typical list of calculations which can be obtained by the operator by manually pushing some special keys on the desk computers. Such special keys are present in almost all the computers of this type. They transfer the control of a running code to every prefixed statement. Thus, by going to the statements of a main program which recalls and links the requested routines, the operator can select any calculation required.

TABLE 3

Typical options for calculation in resolved region

FKEY# 1	Menu of the program
FKEY# 2	Input file from the keyboard
FKEY# 3	Input correction
FKEY# 4	Store input on disk or tape
FKEY# 5	Recall file from disk or tape
FKEY# 6	Print the input file
FKEY# 7	Cross sections tabulation vs. energy
FKEY# 8	Plot of one cross section vs. energy
FKEY# 9	Resonance integral calculation
FKEY#10	Staircase and linear statistics
FKEY#11	Statistics of neutron widths
FKEY#12	Statistics of spacings
FKEY#13	Statistics of selected parameters
FKEY#14	Test for probability of being a p-wave (Bayes)
FKEY#15	Level density parameter "a" from D and viceversa.
FKEY#16	Stop of the program

Some practical suggestions can here be given for calculations started with FKEY# 7, 9 and 15 which are largely used.

BREIT-WIGNER SINGLE LEVEL AND MULTILEVEL CALCULATION.

As an example, FKEY# 7 may calculate a single level and multilevel Breit-Wigner, starting from the resolved resonance parameters.

Table 4 gives a set of resonance parameters printed by the desk calculator following the ENDF/B format and symbols. The parameters are those of Ba-138. The names of the quantities are in reference [5].

Let us now try to have a better understanding of the single and multilevel Breit Wigner formulas and forget the R and S matrices till now considered. A short analysis of the formalism will help us to write down the program in a more compact form and even to give a new explanation of what the formula means.

The usual way of writing the elastic, radiative, capture and fission (or x-reaction) cross sections is given in Appendix D (from ref.[5]). The elastic cross section is formally the most general one and includes three parts:

(1) Potential scattering (hard sphere scattering);
(2) Resonance scattering (compound nucleus elastic reaction);
(3) Interference between (1) and (2).

Thus, it can be written in matrix form as a common quadratic expression, e.g., (we shall use the BASIC syntax for formula representation):

$$(2*x+3*y)\uparrow 2 = 4*x\uparrow 2 + 9*y\uparrow 2 + 12*x*y = \langle x \;\; y \rangle * \begin{vmatrix} 4 & 6 \\ 6 & 9 \end{vmatrix} * \begin{Bmatrix} x \\ y \end{Bmatrix}$$

in which the interpretation of the central matrix is well known. It introduces a metrization of the space (is a "metric" or a fundamental tensor of the reference space) where the diagonal elements give the metric scale on the axes, while the off diagonal elements give the interference between the axis scales due to their "non-orthogonality". In fact, orthogonality means independence among the reference axes.

Having clarified the concepts, let us go back to the BW formula. If we introduce the quantities:

DEj = E-Ej (j=resonance index)

aj=(DEj)+i*(Γj/2) ; aj`=(DEj)-i*(Γj/2) ( ` is the complex conjugate)

zj=1/aj ; zj`=1/zj`

uj=SQR(gj)*SQR(Γnj)*SQR(Γxj)=SQR(g*Γn*Γx)j

c(j,k)=uj*uk symmetric matrix n*n (j,k=1,2,3,...,n resonances)

With these notations we can write the resonance part of the single or multilevel BW cross section in the very synthetic form:

cross section for x-reaction = Z`*C*Z

where capital Z is the column vector of zj, Z` is the row vector of zj` and the central (n*n) matrix C is the space metric with elements uj*uk.

In the vector*matrix*vector product the contribution of the diagonal elements gives a sum of pure single level Breit-Wigner formulas, while the off-diagonal elements give the interference between resonances.

The energy space is n-dimensioned with an axis for every width Γj more or less orthogonal to each other depending upon the amount of interference among the resonances.

The matricial formalism can be extended to the potential scattering representation by introducing the widths of special type:

DE1=E×cos(ϕ) (ϕ is the phase shift depending on l quantum number)

1 =-2×E×sin(ϕ)

a1=(DE1)+i×(Γ1/2) ; a1`=(DE1)-i×(Γ1/2)

z1=1/a1 ; z1`=1/a1`

so that, for example, the elastic cross section for isolated resonance can be written as given in Appendix C.
More clearly than in the formula given in Appendix D appears the interferential term between the resonant and potential scattering.
We cannot here explain such a representation in much detail; but let us merely observe the following points:

1) The central matrix C is essentially the product of the reduced width amplitude (i.e. square root of Γ) of each resonance.
2) The Z vectors are curvilinear axes (Riemann space). Each element zj is geometrically a "reflection" of the point aj on the complex plane (E,Γ) with respect to a unit circle centered in resonance energy Ej (see fig.1).
3) The products of all the reduced width amplitudes SQR(Γn×Γx) form a sequence which has an uncertainty in the algebraic sign (+ or -) exept for the elastic reaction which is a full positive sequence, as can easily be verified.

   In fact, if we suppress the off-diagonal elements of the resonance scattering, assuming a sum of pure BW shapes, but conserve the interferential part between resonance and potential, we can obtain a negative cross section at some energy points. The quadratic form is no longer "complete" in the absence of some off-diagonal terms. An example of such a case is given in table 5 and fig.2 where the tabulation and plot of a single level total cross section is presented.
   For more details on this problem see ref.[6],[7].

As an example, the list of instructions with the summation, through nested loops, over the tabulation energies, the l-states, and resonances, is given in Appendix A. Statement 1430 of BW code recalls the internal function RND for the random generation of signs of the reduced amplitude when the multilevel calculations are performed and the sequence of signs has not been assigned.
The list is in BASIC language (Beginners All-purpose Symbolic Instruction Code) for an OLIVETTI P/6060 desk calculator with 16 to 48 Kbytes of central memory, totally available to the user.

RESONANCE INTEGRAL CALCULATION

The resonance integral is the integral of the capture cross section weighted over a standard 1/E flux from the Cadmium cutoff energy 0.5 eV to infinity. It is usually experimentally measured and must therefore be checked by calculation, starting from the resonance parameters.
But the resonances which were missing in experimental measurements contribute to the integral with a 1/v tail in the thermal group. Thus, if the thermal cross section is known, the resonance integral can be normalized to the capture cross section at the thermal energy, 0.0253 eV or 2200 meter per second, which is the most probable speed.
The formula which can be used for analytical integration of BW formula 1a (ref.[8]), is given in Appendix B.
When the integration problem does not concern isolated resonances and 1/E weighting flux, the integration must be done numerically, from a grid of unequally spaced points because the resonance shape requires a denser set of points near the peaks.
In all these cases it is very important to have a good general routine of numerical integration. One of the best and most up to date is the Romberg method [10] but it is applicable only to equally spaced points.
Nevertheless, an extension of the method to the general case has been obtained [11], which proves to be very efficient for any numerical integration. It can be written easily for a desk calculator and can often be used in the problems of resonance integral calculations or in flux averaging within energy groups.
The usual Romberg quadrature method for evenly spaced points is a particular case of the generalized Romberg method. The same happens for the trapezoidal, Simpson and Villarceau rules which correspond to a Romberg integration of order 1, 2 and 3 respectively (for evenly spaced points).
For numerical integration the file of x,y values is always more conveniently recorded on tape or disk, which is later recalled by the integration code (Romberg, etc.). The BASIC list of "ROMB" code for Olivetti P/6060 computer is given in Appendix A.
Some useful simplifications were given by Walker [12] for calculation of the resonance integral of a Breit-Wigner weighted over the 1/E flux both in the resolved and unresolved regions. The formulas given are applicable to the resonances not too near to thermal energy (say) 1 eV) because the integration is performed under the hypothesis that the resonance lies essentially to the right of cutoff (i.e.:E-Er))Γ/2). In the unresolved region the contribution of one resonance is multiplied by the number of resonances in the integration interval, as given by an assumed average spacing D. Walker's formulas are easily programmed even for a pocket calculator and greatly help the evaluator in every circumstance.

LEVEL DENSITY PARAMETER "a" AND SPACING D

It has been seen, in the previous lectures, that the level density is related to the special level density parameter "a" through a formula given in Appendix E from ref.[11].
The systematic behaviour of "a" for different isotopes has been studied and a general trend can be given vs. Z and A. Briefly, we can give a "systematic", which will help us to check or adjust the value of a spacing D, mainly when only poor informations can be obtained by the resonances.
If very few or no resonances have been measured, the spacing D can only be deduced by an estimated value of "a" taken by an overall and local (i.e. by isotopes with nearest Z and A) systematic. Caution must be used in such evaluation of "a" (an exponent in the formula!).
Thus, the direct and inverse calculations, from a to D and from D to a, can be included among the most important part of the evaluation work.
The inverse calculation D - a implies the solution of the transcendental equation by an iterative method. The code DADI, in Appendix A, is written in BASIC language for the Olivetti P/6060 desk calculator, and performs both the direct and inverse calculations. For the latter, a subroutine is recalled which gives D for any "a". An iterated loop changes the "a" of each iteration in such a way that for a requested spacing D5 we have:

$$a(i+1)=a(i)-\log(D5/D0)$$

where D0 is the actual value from iteration i. Iterations are stopped when:

$$ABS((D5-D0)/D5) < 1.E-6$$

The convergence is quickly obtained.

TEST FOR PROBABILITY OF BEING A P-WAVE (Bayes' theorem)

The observed D (=Dobs) is normally deduced by the s-wave resonance spacing. It is therefore important to eliminate any p-wave resonance in the s-wave set. Except for isotopes with a great p-wave strength function, p-wave resonances are very small and often cannot be detected. Moreover, the l-assignment is not always given by experimentors and some criteria have to be adopted by the evaluator for such attribution.

A method suggested by Bollinger and Thomas [13] assigns to each resonance a probability of being a p-wave on the basis of its size. Once the probability P is found, on the basis of Bayes theorem the resonance is assigned to the p-wave group if P) 0.5. The suggested formula for P is given in Appendix F. The formula can be programmed on a desk calculator thus immediately giving the evaluator the opportunity to check if the residual set of s-wave resonances is consistent with other experimental data, e.g. the thermal cross section and resonance integral.

The probability test can help the evaluator to select the resonances but, in our experience, the Bayes limit P=0.5 must be shifted for many cases to higher values. It is better to eliminate spurious p-waves progressively starting with the limit, say, of P=0.8, and iterating the procedure, checking the consistency each time and lowering P little by little.

DEFORMATION BETA FROM QUADRUPOLE ELECTRIC MOMENT

It has been seen in the lectures concerning the systematic of parameters, that the deformed status of nuclei can explain some of their behaviour. The deformation can be deduced by the quadrupole electric moment Q or intrinsic electric quadrupole momentum Q0 through a formula given in Appendix G.

A procedure is there suggested to solve the non linear equation in unknown BETA by splitting it into three parts which form a quadratic equation. Iterations are needed to complete the procedure.

CONCLUSIONS

We have given a panoramic view of what it is possible to do by means of a desk calculator. A very long list of many other actions could be given. Hence, it will be better to stop the description and go back to the characteristics which can be required, at the present time, of a desk calculator efficiently used in our field of interest.

1) A RAM memory of 32 to 48 Kbytes
2) A silent printing unit of high speed (about 1 row/sec or more)
3) Plotting facilities included in the language system
4) Floppy disk unit (better with 2 drives)
5) BASIC extended language permitting string manipulations
6) Facilities for peripherals (cartridge tape and plotting units)
7) Interfaces for usage as a TSO terminal, for power expansion.

The above features will probably be found in a pocket calculator in five or six years. But how much work could we do in the same period ?

NOTE: The present typescript has been written corrected and stored on floppy disk as a file "Text" of an Olivetti P/6060 desk calculator.

$z_j = \dfrac{1}{(E-E_j)+i\,\frac{\Gamma}{2}}$ **is a reflection with respect to the unit circle**

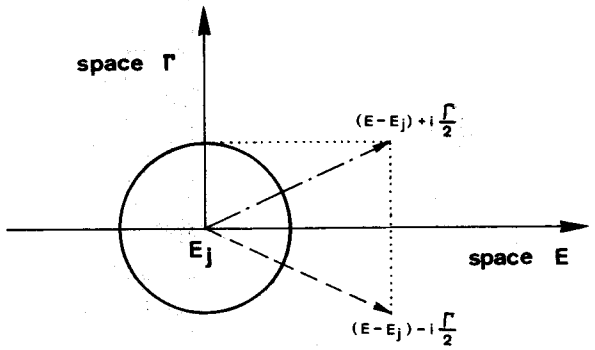

Fig. 1 - The space of Breit-Wigner representation

TABLE 4

Resolved resonance data of Ba-138, ENDF/B format

FKEY# 6: PRINT OF THE RECALLED FILE (ENDFA)

ZAI	ABN	b	LFW	NER	b
5.61380E+04	1.00000E+00	0.00000E+00	0.00000E+00	1.00000E+00	0.00000E+00
EL	EH	LRU	LRF	b	b
1.00000E-05	9.00000E+04	1.00000E+00	1.00000E+00	0.00000E+00	0.00000E+00
SPI	AP	b	b	NLS	b
0.00000E+00	6.23350E-01	0.00000E+00	0.00000E+00	3.00000E+00	0.00000E+00
AWRI	AM	L	b	6*NRS	NRS
1.36720E+02	0.00000E+00	0.00000E+00	0.00000E+00	7.20000E+01	1.20000E+01
ER	AJ	GT	GN	GG	GF
3.09100E+04	5.00000E-01	2.25350E+02	2.25000E+02	3.50000E-01	0.00000E+00
3.65000E+04	5.00000E-01	2.83100E+01	2.80000E+01	3.10000E-01	0.00000E+00
4.02500E+04	5.00000E-01	1.50250E+02	1.50000E+02	2.50000E-01	0.00000E+00
5.04000E+04	5.00000E-01	2.50320E+02	2.50000E+02	3.25000E-01	0.00000E+00
5.91000E+04	5.00000E-01	7.03600E+01	7.00000E+01	3.60000E-01	0.00000E+00
6.30000E+04	5.00000E-01	1.00200E+02	1.00000E+02	2.00000E-01	0.00000E+00
6.90000E+04	5.00000E-01	4.00590E+02	4.00000E+02	5.87000E-01	0.00000E+00
7.40000E+04	5.00000E-01	1.00240E+02	1.00000E+02	2.45000E-01	0.00000E+00
7.98000E+04	5.00000E-01	1.50220E+02	1.50000E+02	2.23000E-01	0.00000E+00
8.18000E+04	5.00000E-01	2.02840E+01	2.00000E+01	2.84000E-01	0.00000E+00
8.94000E+04	5.00000E-01	2.02800E+01	2.00000E+01	2.80000E-01	0.00000E+00
9.09000E+04	5.00000E-01	2.03100E+01	2.00000E+01	3.10000E-01	0.00000E+00
AWRI	AM	L	b	6*NRS	NRS
1.36720E+02	0.00000E+00	1.00000E+00	0.00000E+00	1.14000E+02	1.90000E+01
ER	AJ	GT	GN	GG	GF
4.71400E+03	5.00000E-01	8.50000E-02	3.50000E-02	5.00000E-02	0.00000E+00
7.87600E+03	1.50000E+00	3.04500E+00	3.00000E+00	4.50000E-02	0.00000E+00
1.40400E+04	1.50000E+00	3.03400E+00	3.00000E+00	3.40000E-02	0.00000E+00
1.97000E+04	5.00000E-01	1.04300E+00	1.00000E+00	4.30000E-02	0.00000E+00
1.99000E+04	1.50000E+00	7.55000E+00	7.50000E+00	5.00000E-02	0.00000E+00
2.34400E+04	1.50000E+00	1.00460E+01	1.00000E+01	4.60000E-02	0.00000E+00
2.43000E+04	5.00000E-01	5.04600E+00	5.00000E+00	4.60000E-02	0.00000E+00
2.92500E+04	1.50000E+00	5.05000E+00	5.00000E+00	5.00000E-02	0.00000E+00
3.26300E+04	5.00000E-01	1.40440E+01	1.40000E+01	4.40000E-02	0.00000E+00
3.54200E+04	1.50000E+00	1.00410E+01	1.00000E+01	4.10000E-02	0.00000E+00
4.37500E+04	1.50000E+00	5.03900E+00	5.00000E+00	3.90000E-02	0.00000E+00
4.98500E+04	1.50000E+00	1.07300E+00	5.00000E+00	7.10000E-02	0.00000E+00
5.13000E+04	5.00000E-01	1.07300E+00	1.00000E+00	7.30000E-02	0.00000E+00
5.34000E+04	1.50000E+00	1.00730E+01	1.00000E+01	7.30000E-02	0.00000E+00
5.55000E+04	1.50000E+00	2.00790E+01	2.00000E+01	7.90000E-02	0.00000E+00
6.16000E+04	1.50000E+00	2.00760E+01	2.00000E+01	7.60000E-02	0.00000E+00
6.55000E+04	1.50000E+00	5.09400E+00	5.00000E+00	9.40000E-02	0.00000E+00
7.29000E+04	1.50000E+00	5.08600E+00	5.00000E+00	8.60000E-02	0.00000E+00
8.35000E+04	1.50000E+00	5.06800E+00	5.00000E+00	6.80000E-02	0.00000E+00
AWRI	AM	L	b	6*NRS	NRS
1.36720E+02	0.00000E+00	2.00000E+00	0.00000E+00	4.80000E+01	8.00000E+00
ER	AJ	GT	GN	GG	GF
9.95600E+03	2.00000E+00	1.12000E-01	1.20000E-02	1.00000E-01	0.00000E+00
2.62400E+04	2.00000E+00	1.12000E-01	1.20000E-02	1.00000E-01	0.00000E+00
3.13100E+04	2.00000E+00	1.24800E-01	2.48000E-02	1.00000E-01	0.00000E+00
3.28300E+04	2.00000E+00	1.18000E-01	1.80000E-02	1.00000E-01	0.00000E+00
3.33500E+04	2.00000E+00	1.20000E-01	2.00000E-02	1.00000E-01	0.00000E+00
6.10000E+04	2.00000E+00	1.44000E-01	4.40000E-02	1.00000E-01	0.00000E+00
7.33000E+04	1.50000E+00	3.40000E-01	2.40000E-01	1.00000E-01	0.00000E+00
7.80000E+04	1.50000E+00	1.07500E+00	1.00000E+00	7.50000E-02	0.00000E+00

TABLE 5

Tabulated total cross section of Ba-138 in resonance region

FKEY# 8: TAB. AND PLOT OF A REQUESTED CROSS SECTION
DATA ON (ENDFA) FILE HAVE BEEN RECALLED FROM DISK

REQUESTED CROSS SECTION

62500	2.3432577	62525	2.2355384	62550
2.1192732	62575	1.9934130	62600	1.8567796
62625	1.7080684	62650	1.5458735	62675
1.3687578	62700	1.1754154	62725	.96502128
62750	.73796628	62775	.49740841	62800
.25261492	62825	2.6412258E-02	62850	-.12742145
62875	-8.1220431E-02	62900	.47895081	62925
2.3580019	62950	7.5995770	62975	19.979218
63000	36.979691	63025	41.022471	63050
33.933011	63075	26.673830	63100	21.545472
63125	18.064664	63150	15.640631	63175
13.889162	63200	12.578538	63225	11.567449
63250	10.766976	63275	10.119193	63300
9.5851021	63325	9.1376557	63350	8.7575882
63375	8.4308517	63400	8.1469875	63425
7.8980635	63450	7.6779641	63475	7.4819038
63500	7.3060882			

CROSS SECTION G(7 , 4) STORED FOR PLOT ON FILE (FIPLO)
ABSCISSA min= 62500 max= 63500 ORDINATE min=-.12742145 max= 41.022471

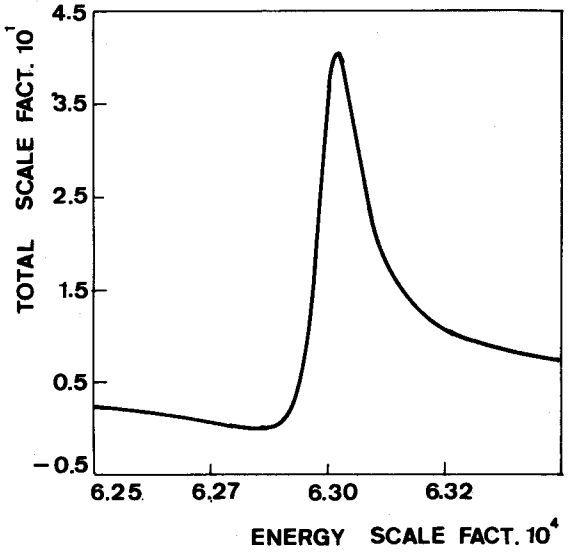

FIG. 2 - Plot of the total cross section from table 5

REFERENCES

[1] PELLEGRINI U. - Tecnologie e strutture dei microprocessori LSI - Informatica, vol.V,n.3/4,sept./dic. 1974.

[2] FEYNMANN R.P. - There is plenty of room at the bottom - Eng.Scient. (Calif.Inst.of Techn.),february 1960,p.22.

[3] LANDAUER R.W. - IBM J.Res.Develop.,1961,vol.5,p.183.

[4] BELL V.J.,BUCKLER P.A.C.,PULL I.C. - The calculation of generalized Doppler functions - AEEW R 266.

[5] DRAKE M.K. (Editor) - Data format and procedures for the ENDF neutron cross section library - ENDFB 102, vol I.

[6] MOTTA M. - The effect of the reduced width amplitude signs in the multilevel calculation of neutron cross section - CNEN RT/FI(72)37.

[7] MARTINELLI T.,MOTTA M. - The PIUME code for the multilevel two channel cross section calculations - CNEN RT/FI(72)50.

[8] STORY J.S. - AERE T/M 77.

[9] BAUER F.L.,RUTISHAUER H.,STIEFEL E. - New aspects in numerical quadrature - Proc.Simp.Appl.Mathem.,15,1963.

[10] MOTTA M. - The Romberg quadrature method for not evenly spaced points (unpublished).

[11] CAMERON A.G.W. and GILBERT G. - Can.Jour.of Phys.,43,1965.

[12] WALKER W.H. - AECL 3037 (Part I).

[13] BOLLINGER L.M. and THOMAS G.E. - Phys.Rev.171,(1968)1293.

APPENDIX A

```
0010 REM  * BW CODE :  CHAINED TO (ENDFB) FOR CROSS SECTION CALCULATION *
0020 DIM A(6),B(3,6),C(3,6),D(3,6),E(200,6),S(6),P(6),F(3),G(7,4)
0030 FILES ENDFA;FIPLO
0050 :'cccccccccc'cccccccccc'cccccccccc'cccccccccc'cccccccccc'cccccccccc
0060 :##,#####^^^^##,#####^^^^##,#####^^^^##,#####^^^^##,#####^^^^
0100 DISP " RECALL DATA FROM (ENDFA) FILE"
0110 RESTORE :1
0120 FOR J=1 TO 6 STEP 1
0130 READ :1,A(J)
0140 NEXT J
0150 FOR J0=1 TO A(5) STEP 1
0160 FOR J4=1 TO 6 STEP 1
0170 READ :1,B(J0,J4)
0180 NEXT J4
0190 FOR J4=1 TO 6 STEP 1
0200 READ :1,C(J0,J4)
0210 NEXT J4
0220 LET J9=1
0230 FOR J1=1 TO C(J0,5) STEP 1
0240 FOR J4=1 TO 6 STEP 1
0250 READ :1,D(J1,J4)
0260 NEXT J4
0270 FOR J2=J9 TO J9+D(J1,6)-1 STEP 1
0280 FOR J4=1 TO 6 STEP 1
0290 READ :1,E(J2,J4)
0300 NEXT J4
0310 NEXT J2
0320 LET J9=J9+D(J1,6)
0330 NEXT J1
0340 NEXT J0
0350 PRINT "DATA ON (ENDFA) FILE HAVE BEEN RECALLED FROM DISK"
0360 DISP "INITIAL ENERGY= ";
0370 INPUT E1
0380 DISP "FINAL ENERGY= ";
0390 INPUT E2
0400 LET J5=E0=0
0410 FOR J0=1 TO A(5) STEP 1
0420 IF (E1)B(J0,2))OR (E2(B(J0,1)) THEN 1990
0430 LET J5=J0
0450 DISP "TABULATION STEP FOR ENERGY= ";
0460 INPUT E3
0470 DISP "0,0=no plot ||| I,K for plot G(I,K)";
0480 INPUT N1,N2
0490 IF N1*N2=0 THEN 560
0500 LET W0=0
0510 SCRATCH :2
0520 WRITE :2,INT((E2-E1)/E3+1),W0
0530 LET Y1=1E63
0540 LET Y2=-Y1
0550 PRINT TAB(26);"REQUESTED CROSS SECTION"
0560 REM          *  CROSS SECTION CALCULATION  *
0570 REM      |||| LOOP ON ENNERGY  ||||
0580 FOR E0=E1 TO E2 STEP E3
0590 LET J0=J5
0600 IF (E0-B(J0,1))*(E0-B(J0,2)))0 THEN 1920
0610 FOR J=1 TO 7 STEP 1
0620 FOR J6=1 TO 4 STEP 1
0630 LET G(J,J6)=0
0640 NEXT J6
0650 NEXT J
0660 LET J9=1
0670 REM      ||||  LOOP ON L-STATES  ||||
0680 FOR J1=1 TO C(J0,5) STEP 1
0690 LET K1=FNA(D(J1,1),E0)
0700 LET L1=1/K1
0710 LET R0=(1.23*D(J1,1)^(1/3)+0.8)/10
0720 LET R1=K1*R0
0730 LET S(1)=0
0740 LET Q1=1+R1^2
0750 LET S(2)=-1/Q1
0760 LET Q2=9+3*R1^2+R1^4
0770 LET S(3)=-(18+3*R1^2)/Q2
0780 LET P(1)=R1
0790 LET P(2)=R1^3/Q1
0800 LET P(3)=R1^5/Q2
0810 LET R2=C(J0,2)*K1
0820 LET F(1)=R2
```

```
0830 LET F(2)=R2-ATN(R2)
0840 LET F(3)=R2-ATN(3*R2/(3-R2^2))
0850 LET G(1,1)=4*PI*L1*L1*SIN(F(1))^2
0860 LET G(1,2)=12*PI*L1*L1*SIN(F(2))^2
0870 LET G(1,3)=20*PI*L1*L1*SIN(F(3))^2
0880 LET G(1,4)=G(1,1)+G(1,2)+G(1,3)
0890 REM      LOOP ON RESONANCE
0900 FOR J2=J9 TO J9+D(J1,6)-1 STEP 1
0910 DISP "E=";E0;"   Er(";J2;")=";E(J2,1)
0920 LET L=D(J1,3)+1
0930 LET K2=FNA(D(J1,1),E(J2,1))
0940 LET L2=1/K2
0950 LET R3=K2*R0
0960 LET Q3=1+R3^2
0970 LET Q4=9+3*R3^2+R3^4
0980 LET P(4)=R3
0990 LET P(5)=R3^3/Q3
1000 LET P(6)=R3^5/Q4
1010 LET S(4)=0
1020 LET S(5)=-1/Q3
1030 LET S(6)=-(18+3*R3^2)/Q4
1040 LET E4=P(L)*E(J2,4)/P(L+3)
1050 LET E5=E4+E(J2,5)+E(J2,6)
1060 LET E6=E(J2,1)+E4*(S(L+3)-S(L))/(2*P(L+3))
1070 LET W1=2*SIN(F(L))*(2*(E0-E6)*COS(F(L))-E5*SIN(F(L)))
1080 LET W=(2*E(J2,2)+1)/(2*(2*C(J0,1)+1))
1090 LET W=W/((E0-E6)^2+E5^2/4)
1100 REM "W=";W;"AJ=";E(J2,2);"L1*L2";L1*L2;"E'=";E6;"nr";E4
1110 REM "P(";L+3;")=";P(L+3)
1120 FOR J=2 TO 6 STEP 1
1130 ON J-1 GOTO 1140,1260,1280,1300,1330
1140 LET G(2,L)=W*E4*E(J2,4)+G(2,L)
1150 ON B(J0,4) GOTO 1450,1160
1160 IF D(J1,6)=1 THEN 1450
1170 FOR J7=J2+1 TO J9+D(J1,6)-1 STEP 1
1180 LET E7=P(L)*E(J7,4)/P(L+3)
1190 LET E8=E7+E(J7,5)+E(J7,6)
1200 LET E9=E(J7,1)+E7*(S(L+3)-S(L))/(2*P(L+3))
1210 LET W2=(2*E(J7,2)+1)/(2*C(J0,1)+1)
1220 LET W2=W2/((E0-E9)^2+E8^2/4)
1230 LET G(2,L)=G(2,L)+2*SQR(W*W2*E4*E7*E(J2,4)*E(J7,4))
1240 NEXT J7
1250 GOTO 1450
1260 LET G(3,L)=W*E4*W1+G(3,L)
1270 GOTO 1450
1280 LET G(4,L)=G(1,L)+G(2,L)+G(3,L)
1290 GOTO 1450
1300 LET G(5,L)=W*E4*E(J2,5)+G(5,L)
1320 GOTO 1450
1330 LET G(6,L)=W*E4*E(J2,6)+G(6,L)
1340 ON B(J0,4) GOTO 1450,1350
1350 IF D(J1,6)=1 THEN 1450
1360 REM      INTERFERENTIAL PART
1370 FOR J7=J2+1 TO J9+D(J1,6)-1 STEP 1
1380 LET E7=P(L)*E(J7,4)/P(L+3)
1390 LET E8=E7+E(J7,5)+E(J7,6)
1400 LET E9=E(J7,1)+E7*(S(L+3)-S(L))/(2*P(L+3))
1410 LET W2=(2*E(J7,2)+1)/(2*C(J0,1)+1)
1420 LET W2=W2/((E0-E9)^2+E8^2/4)
1430 LET G(6,L)=G(6,L)+2*SQR(W*W2*E4*E7*E(J2,6)*E(J7,6))*SGN(RND-1)
1440 NEXT J7
1450 LET G(7,L)=G(4,L)+G(5,L)+G(6,L)
1460 REM "G(";J;",";L;")=";G(J,L);"W1=";W1
1470 NEXT J
1480 NEXT J2
1490 REM      END OF LOOP ON RESONANCES
1500 LET L3=L1*L1
1510 LET G(2,L)=PI*G(2,L)*L3
1520 LET G(3,L)=PI*G(3,L)*L3
1530 LET G(5,L)=PI*G(5,L)*L3
1540 LET G(6,L)=PI*G(6,L)*L3
1550 LET G(4,L)=G(1,L)+G(2,L)+G(3,L)
1560 LET J9=J9+D(J1,6)
1570 NEXT J1
1580 REM      END OF LOOP ON L-STATES
1590 FOR J=1 TO 7 STEP 1
1600 LET G(J,4)=G(J,1)+G(J,2)+G(J,3)
1610 NEXT J
1620 LET G(4,4)=G(3,4)+G(2,4)+G(1,4)
1630 FOR J=1 TO 4 STEP 1
1640 LET G(7,J)=G(4,J)+G(5,J)+G(6,J)
1650 NEXT J
1660 IF N1*N2()0 THEN 1860
1670 PRINT
1680 PRINT "ENERGY","wave no.","wave length","channel radius"
1690 PRINT E0,K1,L1,R0
1700 PRINT "PARAMETERS","l=0","l=1","l=2"
1710 PRINT "shift factors",S(1),S(2),S(3)
1720 PRINT "pen.factors",P(1),P(2),P(3)
1730 PRINT "Phase shift",F(1),F(2),F(3)
1740 ON B(J0,4) GOTO 1750,1770
1750 PRINT "CROSS SECTIONS","(single level Breit-Wigner)","","  SUM"
1760 GOTO 1780
1770 PRINT "CROSS SECTIONS","(multilevel Breit-Wigner)","","  SUM"
1780 PRINT "pot.scattering",G(1,1),G(1,2),G(1,3),G(1,4)
1790 PRINT "res.scattering",G(2,1),G(2,2),G(2,3),G(2,4)
1800 PRINT "res*pot scatt.",G(3,1),G(3,2),G(3,3),G(3,4)
1810 PRINT "total elastic",G(4,1),G(4,2),G(4,3),G(4,4)
1820 PRINT "capture",G(5,1),G(5,2),G(5,3),G(5,4)
1830 PRINT "fission",G(6,1),G(6,2),G(6,3),G(6,4)
1840 PRINT "total",G(7,1),G(7,2),G(7,3),G(7,4)
1850 IF N1*N2=0 THEN 1920
1860 WRITE :2,E0,G(N1,N2)
1870 IF G(N1,N2)<=Y2 THEN 1890
1880 LET Y2=G(N1,N2)
1890 IF G(N1,N2))=Y1 THEN 1910
1900 LET Y1=G(N1,N2)
1910 PRINT E0,G(N1,N2),
1920 NEXT E0
1930 REM      END OF LOOP ON ENERGY
1940 IF N1*N2=0 THEN 2050
1950 PRINT
1960 PRINT "CROSS SECTION G(";N1;",";N2;")STORED FOR PLOT ON FILE(FIPL0)"
1970 PRINT "ABSCISSA min=";E1;" max=";E2;"ORDINATE min=";Y1;" max=";Y2
1980 LET E1=E0
1990 NEXT J0
```

```
2000 IF J5)0 THEN 2050
2010 DISP "        ENERGY OUT OF RANGE"
2020 DELAY 50
2030 GOTO 360
2040 DEF FNA(A,E0)=2.19685E-3*SQR(E0)*(A/(A+1))
2050 CHAIN "ENDFB"
2060 END
0010 REM  * BW2 CODE :  CHAINED TO (ENDFB) FOR RESONANCE INTEGRAL CALCULATION *
0020 DIM A(6),B(3,6),C(3,6),D(3,6),E(200,6),S(6),P(6),F(3),G(7,4)
0030 FILES ENDFA
0050 :'eeeeeeeeee'eeeeeeeeee'eeeeeeeeee'eeeeeeeeee'eeeeeeeeee'eeeeeeeeee
0060 :##.#####^^^^##.#####^^^^##.#####^^^^##.#####^^^^##.#####^^^^##.#####^^^^
0100 DISP " RECALL DATA FROM (ENDFA) FILE"
0110 RESTORE :1
0120 FOR J=1 TO 6 STEP 1
0130 READ :1,A(J)
0140 NEXT J
0150 FOR J0=1 TO A(5) STEP 1
0160 FOR J4=1 TO 6 STEP 1
0170 READ :1,B(J0,J4)
0180 NEXT J4
0190 FOR J4=1 TO 6 STEP 1
0200 READ :1,C(J0,J4)
0210 NEXT J4
0220 LET J9=1
0230 FOR J1=1 TO C(J0,5) STEP 1
0240 FOR J4=1 TO 6 STEP 1
0250 READ :1,D(J1,J4)
0260 NEXT J4
0270 FOR J2=J9 TO J9+D(J1,6)-1 STEP 1
0280 FOR J4=1 TO 6 STEP 1
0290 READ :1,E(J2,J4)
0300 NEXT J4
0310 NEXT J2
0320 LET J9=J9+D(J1,6)
0330 NEXT J1
0340 NEXT J0
0350 PRINT "DATA ON (ENDFA) FILE HAVE BEEN RECALLED FROM DISK"
0360 DISP "LOWER INTEGRATION ENERGY= ";
0370 INPUT E1
0380 DISP "UPPER INTEGRATION ENERGY= ";
0390 INPUT E2
0400 DISP "Ther.CROSS SECTION (for 1/v) = ";
0410 INPUT S
0420 FOR J0=1 TO A(5) STEP 1
0460 REM          *  RESONANCE INTEGRAL CALCULATION  *
0470 PRINT
0480 LET S0=S2=0
0490 LET J9=1
0500 PRINT "Res.#","  INTEGRAL","  SUM TOTAL"
0510 FOR J1=1 TO C(J0,5) STEP 1
0520 FOR J2=J9 TO J9+D(J1,6)-1 STEP 1
0530 LET L1=1/FNE(D(J1,1),E(J2,1))
0540 IF E(J2,1)(=0 THEN 820
0550 LET G1=(2*E(J2,2)+1)/(2*(2*C(J0,1)+1))
0560 LET S1=4*PI*L1*L1*G1*(E(J2,4)*E(J2,5)/E(J2,3)^2)
0570 LET X1=E1/E(J2,1)
0580 LET X2=E2/E(J2,1)
0590 LET M=SQR(1+E(J2,3)^2/(4*E(J2,1)^2))
0600 LET H=E(J2,3)*E(J2,3)/(4*M*M*E(J2,1)*E(J2,1))
0610 LET H1=S1*H
0620 LET H2=FNA(X2,M)
0630 LET H3=FNA(X1,M)
0640 LET S0=2*FNC(X1)-FNC(X2)+(2+M)/M/SQR(2*(M+1))*(FNB(H2)-FNB(H3))
0650 LET H4=ATN(FND(X2,M))
0660 LET H5=ATN(FND(X1,M))
0670 IF FND(X2,M))=0 THEN 700
0680 IF  (H4)=PI/2)AND  (H4(=PI) THEN 700
0690 LET H4=H4+PI
0700 IF FND(X1,M))=0 THEN 730
0710 IF  (H5)=PI/2)AND  (H5(=PI) THEN 730
0720 LET H5=H5+PI
0730 LET S0=S0+(2-M)/M/SQR(2*(M-1))*(H4-H5)
0740 LET S2=S2+S0*H1
0750 PRINT J2,S0*H1,S2
0820 NEXT J2
0830 LET J9=J9+D(J1,6)
0840 NEXT J1
0850 NEXT J0
0860 PRINT
0870 PRINT "RESONANCE INTEGRAL   = :",S2;" between";E1;" and";E2
0880 LET T=S2
0890 IF S=0 THEN 930
0900 LET V=2*S*SQR(0.0253)*(1/SQR(E1)-1/SQR(E2))
0910 LET T=V+S2
0920 PRINT "1/v part of INTEGRAL =",V;"(th.cross sec.=";S;"barns)"
0930 PRINT
0940 PRINT "TOTAL RESONANCE INTEGRAL =",T;" between";E1;" and";E2
0960 DEF FNA(X,M)=SQR(2*X*(M+1))/(M+X)
0970 DEF FNB(X)=0.5*LOG((1+X)/(1-X))
0980 DEF FNC(X)=1/SQR(X)
0990 DEF FND(X,M)=SQR(2*X*(M-1))/(M-X)
1000 DEF FNE(A,X)=2.19685E-3*SQR(X)*(A/(A+1))
1010 PRINT
1020 CHAIN "ENDFB"
1030 END
0010 REM      *  ( D A D I )  CODE, FROM a TO (D) AND VICEVERSA  *
0020 PRINT "                  *  ENTER  ( D A D I )   CODE *"
0030 PRINT
0040 :####.##  ###.##  #####.###   #####.###        ########.##     ####.###
0050 FKEY #1,START 130:
0060 FKEY #2,START 220:
0070 FKEY #3,START 490:
0080 FKEY #4,START 440:
0090 FKEY #16,START 1090:
0100 LET Z0=0
0110 DISP "    SELECT A KEY OPTION";
0120 STOP
0130 REM             *   KEY OPTIONS  *
0140 PRINT TAB(28);"KEY OPTIONS"
0150 PRINT TAB(20);"KEY #1: MENU"
0160 PRINT TAB(20);"KEY #2: INPUT"
0170 PRINT TAB(20);"KEY #3: FROM a TO Dobs"
0180 PRINT TAB(20);"KEY #4: FROM Dobs TO a"
0190 PRINT TAB(20);"KEY #16:THE END  PROGRAM EXIT"
0200 PRINT
0210 GOTO 110
0220 ON Z0+1 GOTO 230,260
0230 PRINT "   A";TAB(13);"I";TAB(22);"Bn[MeV]";TAB(33);"Pairing[MeV]";TAB(50);
0240 PRINT "D(a)[eV]";TAB(64);"a[1/eV]"
0250 LET Z0=1
0260 REM                    *      INPUT    *
0270 LET C1=0.146
0280 DIM F(2)
```

```
0290 LET C9=1
0300 DISP "  TARGET MASS NUMBER = ";
0310 INPUT A1
0320 IF A1=9999E63 THEN 1100
0330 LET A1=A1+1
0340 DISP "       TARGET SPIN = ";
0350 INPUT F1
0360 DISP "  BINDING ENERGY (MEV): B1=";
0370 INPUT B1
0380 DISP "  PAIRING ENERGY (MEV)= ";
0390 INPUT D1
0400 DISP "  QUANTUM NUMBER 1 = ";
0410 INPUT L
0420 GOTO 110
0430 STOP
0440 REM                    *  From Dobs to a  *
0450 LET C9=2
0460 DISP "FIRST GUESS LEVEL DENSITY : a= ";
0470 INPUT A2
0480 GOTO 570
0490 REM                    *  From a to Dobs  *
0500 LET C9=1
0510 DISP "LEVEL DENSITY a =";
0520 INPUT A2
0530 ON C9 GOTO 540,570
0540 GOSUB 690
0550 PRINT USING 40,A1-1,F1,B1,D1,D0,A2
0560 GOTO 110
0570 DISP "  REQUESTED  Dobs  = ";
0580 INPUT D0
0590 LET D5=D0
0600 LET N0=0
0610 GOSUB 700
0620 LET N0=N0+1
0630 DISP N0;"## a=";A2;" D=";D0
0640 IF ABS((D5-D0)/D5)<1E-6 THEN 670
0650 LET A2=A2-LOG(D5/D0)
0660 GOTO 610
0670 PRINT USING 40,A1-1,F1,B1,D1,D0,A2
0680 GOTO 110
0690 REM              *  SUBROUTINE FROM a TO Dobs  *
0700 LET U=B1-D1
0710 LET A3=2/3
0720 LET S1=C1*SQR(A2*U)*A1^A3
0730 LET S2=2*S1
0740 LET R=EXP(2*SQR(A2*U))
0750 LET R=R/(12*SQR(S2))
0760 LET R=R/(U*(A2*U)^0.25)
0770 LET S3=0
0780 LET I1=0
0790 IF F1<>0 THEN 830
0800 LET N1=1
0810 LET F(1)=0.5
0820 GOTO 860
0830 LET N1=2
0840 LET F(1)=F1+0.5
0850 LET F(2)=F1-0.5
0860 LET I1=I1+1
0870 LET F3=F(I1)
0880 LET E1=ABS(F3-L)
```



```
0890 LET E2=F3+L
0900 LET F4=E1-1
0910 LET S4=0
0920 LET F4=F4+1
0930 IF F4>E2 THEN 980
0940 LET A3=(F4+0.5)^2/S2
0950 LET H=(2*F4+1)*EXP(-A3)/S2
0960 LET S4=S4+H
0970 GOTO 920
0980 LET S3=S3+S4
0990 IF I1<N1 THEN 860
1000 LET B2=0.5*R*S3
1010 LET D0=1E6/B2
1020 REM                    *  SUBROUTINE RETURN *
1030 RETURN
1090 PRINT
1100 PRINT "                  *  THE END. < D A D I >  CODE EXIT *"
1110 END
0010REM  * ROMBERG INTEGRATION FOR EVEN AND NOT EVENLY SPACED POINTS *
0020 PRINT "                              *  <ROMB> CODE *"
0030 FKEY #1,START 290:
0040 FKEY #2,START 430:
0050 FKEY #3,START 590:
0060 FKEY #4,START 740:
0070 FKEY #5,START 740:
0080 FKEY #6,START 1480:
0090 FKEY #16,START 1650:
0100 GOSUB 120
0110 GOTO 170
0120 PRINT
0130 PRINT
0140 RETURN
0150 DISP "KEY OPTIONS, KEY #1 = MENU";
0160 STOP
0170 REM NUMERICAL ROMBERG INTEGRATION FOR EVEN & NOT EVENLY SPACED POINTS
0180 REM
0190 DIM C(5,5),D(5)
0200 DATA 1,0,0,0,0,4,-1,0,0,0,64,-20,1,0,0,4096,-1344,84,-1,0,1048576
0210 DATA -348160,22848,-340,1,1,3,45,2835,722925
0220 LET R=0
0230 RESTORE
0240 READ C(1,1),C(1,2),C(1,3),C(1,4),C(1,5),C(2,1),C(2,2),C(2,3),C(2,4),C(2,5)
0250 READ C(3,1),C(3,2),C(3,3),C(3,4),C(3,5),C(4,1),C(4,2),C(4,3),C(4,4)
0260 READ C(4,5),C(5,1),C(5,2),C(5,3),C(5,4),C(5,5)
0270 READ D(1),D(2),D(3),D(4),D(5)
0280 GOTO 150
0290 PRINT
0300 PRINT TAB(9);"ROMBERG INTEGRATION FOR X,Y PAIRS"
0310 PRINT
0320 PRINT TAB(5);"KEY OPTIONS"
0330 PRINT
0340 PRINT TAB(5);"KEY #1: Menu"
0350 PRINT TAB(5);"KEY #2: Input from keyboard"
0360 PRINT TAB(5);"KEY #3: Input from disk file (FIPLO)"
0370 PRINT TAB(5);"KEY #4: Integral calculation"
0380 PRINT TAB(5);"KEY #5: Change of integration order and interval"
0390 PRINT TAB(5);"KEY #6: Input print from disk"
0400 PRINT TAB(5);"KEY #16:The end, Program exit"
0410 GOTO 150
0420 REM
0430 REM                      *  INPUT FROM KEYBOARD  *
0440 REM
```

```
0450 LET R8=0
0460 DISP "NUMBER OF POINT PAIRS = ";
0470 INPUT N
0480 DIM X(100),Y(100)
0490 PRINT " I","X(I)","Y(I)"
0500 FOR I=1 TO N STEP 1
0510 DISP "X(";I;") = ";
0520 INPUT X(I)
0530 DISP "Y(";I;") = ";
0540 INPUT Y(I)
0550 PRINT I,X(I),Y(I)
0560 NEXT I
0570 GOTO 150
0580 REM
0590 REM                    *  INPUT FROM DISK FILE  *
0600 REM
0610 GOSUB 120
0620 FILES FIPLO
0630 LET R8=0
0640 RESTORE :1
0650 READ :1,N,E1
0660 PRINT "NUMBER OF POINTS FROM DISK FILE = ";N
0670 FOR I=1 TO N STEP 1
0680 IF E1)0 THEN 710
0690 READ :1,X(I),Y(I)
0700 GOTO 720
0710 READ :1,X(I),Y(I),E
0720 NEXT I
0730 REM
0740 REM                     *  INTEGRAL CALCULATION  *
0750 REM
0760 LET R=0
0770 PRINT
0780 DISP "LOWER LIMIT INDEX =";
0790 INPUT N1
0800 DISP "UPPER LIMIT INDEX =";
0810 INPUT N2
0820 DISP "INTEGRATION ORDER =";
0830 INPUT I1
0840 PRINT "INTEGRATION ORDER = ";I1
0850 IF (I1)5)OR (I1(1) THEN 900
0860 GOTO 910
0870 REM
0880 REM
0890 REM
0900 LET I1=1
0910 LET I2=I1-1
0920 LET M1=2^I2
0930 LET N3=N2-N1
0940 LET N4=N1
0950 LET I3=0
0960 LET R2=0
0970 ON I1 GOTO 1080,1060,1040,1020,980
0980 IF N3)16 THEN 1100
0990 LET I1=I1-1
1000 LET M1=2^(I1-1)
1010 GOTO 970
1020 IF N3)=8 THEN 1100
1030 GOTO 990
1040 IF N3)=4 THEN 1100
1050 GOTO 990
1060 IF N3)=2 THEN 1100
1070 GOTO 990
1080 IF N3)=1 THEN 1100
1090 GOTO 1350
1100 LET N5=N4+M1
1110 LET N6=N4
1120 LET M3=2^I3
1130 LET I3=I3+1
1140 LET N7=N6+M3
1150 LET R1=0
1160 IF N7)N5 THEN 1220
1170 LET T=(X(N7)-X(N6))*((Y(N6)+Y(N7))/2)
1180 LET R1=R1+T
1190 LET N6=N6+M3
1200 LET N7=N7+M3
1210 GOTO 1160
1220 LET R2=R2+R1*C(I1,I3)
1230 IF I3)=I1 THEN 1300
1240 LET I4=I3+1
1250 IF (I4)5)OR (I4(1) THEN 1280
1260 ON I4 GOTO 1080,1060,1040,1020,980
1270 GOTO 1300
1280 LET I4=1
1290 GOTO 1260
1300 LET R2=R2/D(I1)
1310 LET R=R+R2
1320 LET N4=N5
1330 LET N3=N2-N5
1340 GOTO 950
1350 LET R8=R8+R
1360 PRINT "INTEGRAL BETWEEN X(";N1;")=";X(N1);"and";"X(";N2;")=";X(N2);"R=";R
1370 PRINT "AND CUMULATIVE INTEGRAL = ";R8
1380 DISP "INTEGRAL = ";R;
1390 STOP
1400 STOP
1410 GOSUB 120
1420 PRINT "I","X(I)","Y(I)"
1430 FOR I=1 TO N STEP 1
1440 PRINT I,X(I),Y(I)
1450 NEXT I
1460 GOTO 150
1470 REM
1480 REM                    *  INPUT PRINT FROM DISK  *
1490 REM
1500 GOSUB 120
1510 RESTORE :1
1520 READ :1,N,E1
1530 PRINT TAB(8),"NUMBER OF POINTS FROM DISK = ";N
1540 PRINT
1550 PRINT " I","  X(I)","  Y(I)","  DY(I)"
1560 FOR I=1 TO N STEP 1
1570 IF E1)0 THEN 1610
1580 READ :1,X(I),Y(I)
1590 PRINT I,X(I),Y(I)
1600 GOTO 1630
1610 READ :1,X(I),Y(I),E
1620 PRINT I,X(I),Y(I),E
1630 NEXT I
1640 GOTO 150
1650 GOSUB 120
1660 PRINT TAB(25);"*  THE END OF PROGRAM (ROMB)  *"
1670 END
```

APPENDIX B

RESONANCE INTEGRAL CALCULATION

The integration of a Breit-Wigner cross section, weighted over a standard flux 1/E, can be carried through explicitly. Assuming the cross section given by

$$\sigma(E) = \sigma_r \frac{E_r}{E} \cdot \frac{\Gamma^2/4}{(E-E_r)^2 + \Gamma^2/4} \qquad \text{with } \sigma_r,\ E_r,\ \Gamma \text{ constants}$$

we have, for integration between the limits E_1 and E_2 :

$$I(E_1,E_2) = \int_{E_1}^{E_2} \frac{\sigma(E)}{E}\, dE =$$

$$= \frac{\sigma_r \Gamma^2}{4\mu^2 E_r^2}\left[\frac{2}{\sqrt{X_1}} - \frac{1}{\sqrt{X_2}} + \frac{2+\mu}{\mu\sqrt{2(\mu+1)}}\left\{\tanh^{-1}\frac{\sqrt{2X_2(\mu+1)}}{\mu+X_2} - \tanh^{-1}\frac{\sqrt{2X_1(\mu+1)}}{\mu+X_1}\right\}\right.$$

$$\left. + \frac{2-\mu}{\mu\sqrt{2(\mu-1)}}\left\{\mathrm{tg}^{-1}\frac{\sqrt{2X_2(\mu-1)}}{\mu-X_2} - \mathrm{tg}^{-1}\frac{\sqrt{2X_1(\mu-1)}}{\mu-X_1}\right\}\right]$$

with the proviso that E_r is positive and, when either of the inverse tangents has negative argument, it lies in the quadrant $\pi/2$ to π .

In the above expression

$$\mu = \sqrt{1 + \Gamma^2/(4E_r^2)} \quad ; \quad X_1 = E_1/E_r \quad ; \quad X_2 = E_2/E_r \quad .$$

APPENDIX C

MATRIX FORM OF THE BREIT-WIGNER CROSS SECTION

The elastic cross section given in Appendix D can be written in matrix form as follows

$$\sigma^{\ell}_{n,n} = (2\sin\phi_\ell \quad \frac{1}{e^{-i\phi_\ell}.a_j^*}) \cdot \begin{vmatrix} 2\ell+1 & \Gamma_{nj} \\ \Gamma_{nj} & \Gamma_{nj}^2 \end{vmatrix} \cdot \begin{Bmatrix} 2\sin\phi_\ell \\ \frac{1}{e^{i\phi_\ell}.a_j} \end{Bmatrix}$$

from which, by the identity

$$2\sin\phi_\ell = \frac{2E\sin\phi_\ell}{e^{-i\phi_\ell}\left[E\cos\phi_\ell - i(-E\sin\phi_\ell)\right]} = \frac{2E\sin\phi_\ell}{e^{+i\phi_\ell}\left[E\cos\phi_\ell + i(-E\sin\phi_\ell)\right]}$$

and introducing the fictitious width and the energy distance

$$\Gamma_\ell = -2E\sin\phi_\ell \qquad ; \qquad \Delta E_\ell = E\cos\phi_\ell$$

which are "energy dependent", we can write down the elastic cross section including potential, resonance and res.xpot. interference terms of one isolated resonance:

$$\sigma^{\ell}_{n,n} = \pi\lambda^2 \sum_j g_j \left(\frac{1}{e^{-i\phi_\ell}.a_\ell^*} \quad \frac{1}{e^{-i\phi_\ell}.a_j^*}\right) \begin{vmatrix} (-\Gamma_\ell)^2(2\ell+1) & -\Gamma_\ell\Gamma_{nj} \\ -\Gamma_\ell\Gamma_{nj} & \Gamma_{nj}\Gamma_{nj} \end{vmatrix} \begin{Bmatrix} \frac{1}{e^{i\phi_\ell}.a_\ell} \\ \frac{1}{e^{i\phi_\ell}.a_j} \end{Bmatrix}$$

where

$$a_\ell = \Delta E_\ell + i\frac{\Gamma_\ell}{2} \quad ; \quad a_\ell^* = \Delta E_\ell - i\frac{\Gamma_\ell}{2}$$

APPENDIX D

D.1. THE RESOLVED RESONANCE REGION

D.1.1. Single-Level Breit-Wigner Formula: LRU=1, LRF=1

The formulae appearing in Gregson, et al.,[1] omitting the resonance-resonance interference terms are adopted. These formulae, written in the laboratory system for all ℓ-values and without Doppler broadening, are (for a particular isotope):

1. Elastic Scattering Cross Section

$$\sigma_{n,n}(E) = \sum_{\ell=0}^{NLS} \sigma_{n,n}^{\ell}(E),$$

where

$$\sigma_{n,n}^{\ell}(E) = (2\ell+1)\frac{4\pi}{k^2}\sin^2\varphi_\ell + \frac{\pi}{k^2}\sum_J g_J \sum_{r=1}^{NR_J} \frac{\Gamma_{nr}^2 \cos 2\varphi_\ell - 2\Gamma_{nr}(\Gamma_{\gamma r}+\Gamma_{fr})\sin^2\varphi_\ell + 2(E-E_r')\Gamma_{nr}\sin 2\varphi_\ell}{(E-E_r')^2 + \frac{1}{4}\Gamma_r^2}$$

2. Radiative Capture Cross Section

$$\sigma_{n,\gamma}(E) = \sum_{\ell=0}^{NLS} \sigma_{n,\gamma}^{\ell}(E)$$

where

$$\sigma_{n,\gamma}^{\ell}(E) = \frac{\pi}{k^2}\sum_J g_J \sum_{r=1}^{NR_J} \frac{\Gamma_{nr}\Gamma_{\gamma r}}{(E-E_r')^2 + \frac{1}{4}\Gamma_r^2}$$

3. Fission Cross Section

$$\sigma_{n,f}(E) = \sum_{\ell=0}^{NLS} \sigma_{n,f}^{\ell}(E),$$

where

$$\sigma_{n,f}^{\ell}(E) = \frac{\pi}{k^2}\sum_J g_J \sum_{r=1}^{NR_J} \frac{\Gamma_{nr}\Gamma_{fr}}{(E-E_r')^2 + \frac{1}{4}\Gamma_r^2},$$

where

$$g_J = \frac{2J+1}{2(2I+1)}$$

I is the spin of the target nucleus and J is the spin of the compound nucleus for the resonance state.

I = SPI, as given in File 2 data for each isotope

The summation on ℓ extends over all ℓ-states described. There will be NLS terms in the summation.

NLS is given in File 2 for each isotope

The summation on J extends over all possible J-states for a particular ℓ-state. NR_J is the number of resonances for a given pair of ℓ and J values.

$$NRS = \sum_J NR_J$$

NRS is given in File 2 for each ℓ-value

APPENDIX E

The formula for level density parameter "a" is the following

$$\frac{1}{D_{obs}^{exp}} = \frac{1}{2} \sum_{|I-s|}^{I+s} \rho(E) f(E,J)$$

$$\rho(E) = \frac{1}{12\sqrt{2}} \quad \frac{\exp 2\sqrt{a(E-\Delta)}}{a^{1/4}(E-\Delta)^{5/4}} \cdot \frac{1}{\sigma}$$

$$f(E,J) = (2J+1) \quad \frac{\exp\left[-(J+1/2)^2/(2\sigma^2)\right]}{2\sigma^2}$$

$$\sigma = \text{cutoff} = 2K \sqrt{a(E-\Delta)} \cdot A^{2/3}$$

K = cutoff factor = 0.146 (or other values)

APPENDIX F

Probability to be p-wave

$$P(g\Gamma_n) =$$

$$= \left\{ 1+\alpha \sqrt{\frac{\langle g\Gamma_n^1 \rangle}{\langle g\Gamma_n^o \rangle}} \exp\left[\frac{g\Gamma_n}{2} \left(\frac{1}{\langle g\Gamma_n^1 \rangle} - \frac{1}{\langle g\Gamma_n^o \rangle} \right) \right] \right\}^{-1}$$

where

$$\langle g\Gamma_n^o \rangle = \sqrt{E} \quad D_{obs} \; S_o$$

$$\langle g\Gamma_n^1 \rangle = \sqrt{E} \quad v_1(kr) D_{obs} \; S_1$$

S_o = strength function for $\ell=0$

S_1 = " " " $\ell=1$

$v_1(kr) = 10^{-7} A^{2/3} E$ eV = penetration factor ($\ell=1$)

α = constant (see ref. 13)

APPENDIX G

DEFORMATION β FROM ELECTRIC QUADRUPOLE MOMENTUM

$$Q_o = \frac{3}{(5\pi)^{\frac{1}{2}}} R_o Z \left[\frac{\beta_n + 0.36\ \beta_n^2 + 0.34\ \beta_{n-1}^2\ \beta_n}{1 + 0.24\ \beta_{n-1}^2} \right]$$

n is the iteration index.

$$\boxed{0 = a\ \beta_n^2 + b\ \beta_n + c}$$ eq. to be solved

where:

$$a = \text{coeff of } \beta_n^2 = \left[\frac{3}{(5\pi)^{\frac{1}{2}}} R_o^2 Z \frac{0.36}{1+0.24\beta_{n-1}^2} \right] = \frac{0.2725\ R_o Z}{1+0.24\beta_{n-1}^2}$$

$$b = \text{coeff of } \beta_n = \left[\frac{3}{(5\pi)^{\frac{1}{2}}} R_o^2 Z \frac{1+0.34\beta_{n-1}^2}{1+0.24\beta_{n-1}^2} \right] = \frac{0.75694 + 0.25735\beta_{n-1}^2}{1 + 0.24\beta_{n-1}^2} R_o^2 Z$$

$c = -Q_o$ = intrinsic quadrupole momentum

$Q = Q_o \frac{3K - I(I+1)}{(I+1)(2I+3)}$ K = magnetic projection of I

$Q \simeq Q_o \frac{I(2I-1)}{(I+1)(2I+3)}$ if K=I

$Q = 0$ if $K = I = \frac{1}{2}$ then experimentalists give Q_o .

FOUNDATIONS AND MODELS OF PRE-EQUILIBRIUM DECAY

V.E. BUNAKOV
Leningrad Nuclear Physics Institute,
Gatchina, Leningrad,
Union of Soviet Socialist Republics

Abstract

A review is given of the presently existing microscopic, semi-phenomenologic and phenomenologic models used for the description of nuclear reactions. Their advantages and drawbacks are analyzed. A special attention is given to the analysis of pre-equilibrium decay phenomenological models based on the use of master equations (time-dependent versions of exciton models, intranuclear cascade, etc.). A version of the unified theory of nuclear reactions is discussed which makes use of quantum master equations for finite open systems. The conditions are formulated for the derivation of these equations from the time-dependent Schrödinger equation for the many-body problem. The various models of nuclear reactions used in practice are shown to be approximate solutions of master equations for finite open systems. From this point of view the analysis is carried out of these models' reliability in the description of experimental data. Possible modifications are considered which provide for better agreement between the different models and for the more exact description of experimental data.

I. Introduction

A general rule in theoretical physics says that it is much simpler to describe the extreme cases than the intermediate one. This comes from the fact that the extreme case allows to neglect a lot in favour of one specific feature and therefore to introduce a simple model. The intermediate phenomena should be at any rate an interpolation between the two extreme points which demands a more general description including both extremes only as particular points. Therefore in speaking about the foundations of the pre-equilibrium decay one should try to construct a general theory which includes the fast direct process and the equilibrium compound nucleus theory as particularly simple cases. Thus we are forced to consider in our lectures the present situation in nuclear reaction theory as a whole rather than confine ourselves to what is commonly known as pre-equilibrium models.

In the first part of our course we shall briefly consider the main classes of models used in nuclear reaction theory. In doing this one can immediately see that these models might be subdivided into two unfortunately almost nonoverlapping groups. One of these groups contains the theoretically refined microscopic approaches showing how the reaction theory should be done in principle. The second group consists of the phenomenological and semi-phenomenological models which are used in practical calculations of nuclear reactions. Unfortunately the pre-equilibrium models fall into the second class and up to recently had no connections with the fundamental approaches. It was pointed by Feshbach / 1 / in 1972 that "the interesting problem of incorporating the pre-equilibrium theory into the quntum mechanical reaction theory remains". All this makes our task of giving the foundations of pre-equilibrium theory even harder. Lucky enough some progress was done in

this respect recently by several theoretical groups, including ours / 2-5 /. Therefore after speaking about the existing models in general and about phenomenological models in particular, we shall explain our opinion on why do these models work. In the last part of our course we shall speak briefly on the accuracy of the existing models and on possible modifications which can make them work better.

In the fundaments of each proper reaction theory lies the time-dependent Schrödinger equation for many-body system:

$$i\hbar \frac{\partial \Psi}{\partial t} = H\Psi \qquad (1)$$

with the proper initial and boundary conditions. In order to describe even the simplest case of potential scattering one should construct the wave packets out of the solutions of the stationary Schrödinger equation

$$H\psi = E\psi \qquad (2)$$

and trace their evolution in space and time. This is a rather complicated mathematical procedure which is considered only in very few textbooks (see e.g. / 6,7 /). Lippmann-Schwinger formalism uses the approximation of very long (in time) wave-packets and allows to reduce the problem to the stationary one with specific boundary conditions. This formalism underlies the R-matrix theory and Feshbach's unified reaction theory which gave life to the majority of microscopic approaches in nuclear reactions. In all these approaches the total Hamiltonian H is split essentially into two parts: $H = H_0 + V$ (3)

The part H_0 defines the system of basic wave functions in the average field, while the "residual interactions" part V defines the transition intensities between the states of the basis. The different choices of basis correspond to the different microscopic models like shell-model in continuum / 8 /, eigenchannel method / 9 /, Soloviev's model of low-lying resonant states /10/, etc., but, these methods are usually too complicated for practical use. First of all it is rather difficult to find a solution (diagonalize the Hamiltonian matrix) for a sufficiently complete basis. Secondly, even if this basis is complete enough the accuracy in calculated position of each resonance never exceeds several hundred keV while the average resonance spacing D in the majority of real nuclei is much smaller ($D \sim 1$ ev for the medium and heavy nuclei). This leads to a paradox: both in theory and in experiment one can estimate the positions and widths of the individual resonances, but the comparison is possible only for the characteristics averaged over large groups of resonances occupying the intervals $\Delta E \sim$ MeV.

11. Practical approaches based on semi- and purely phenomenological models.

Because of the difficulties mentioned the practical description of nuclear reactions makes use of the other group of models. All of them are either semi- or purely phenomenological. One of the most popular among them is the optical model. It describes the elastic cross-section averaged over energy using the single-particle Schrödinger equation with complex potential. The use of this simple model can be justified theoretically (see the lectures of Mahaux in the present course or ref./11- 14,7 /) in the frame-work of the microscopic description. The extinction

rate for the incident beam is given in this model by the imaginary part W of the optical potential which is defined by the matrix elements of residual interaction V averaged over sufficiently large energy interval ΔE. The optical model makes a nice combination of practical simplicity which allows still to trace its connection to the basic equations of the microscopic approach. Therefore it is out of competition in the description of the averaged elastic (or total reaction) cross-section. It is not possible, however, to use this model without modifications for inelastic processes.

One of these modifications is given by the distorted-wave Born approximation (DWBA) where the amplitude T_{if} of the inelastic process is given in a Born-like form:

$$T_{if} \sim \langle \bar{\psi}_f | V | \bar{\psi}_i \rangle \qquad (4)$$

Here $\bar{\psi}_i$ and $\bar{\psi}_f$ are the elastic and inelastic channel wave-functions calculated in the optical model potential. DWBA (and its high energy-modifications - the eikonal theory and Glauber theory) belongs also to a semi-phenomenological class because expression (4) might still be derived from the microscopic approach (see e.g. /7/, /8/). This derivation shows however that eq.(4) is valid only for the direct part of the reaction process, which proceeds immediately after the initial particle strikes the target. Therefore the DWBA cross-section should be complemented by the contributions coming from the compound and pre-compound processes. It is almost impossible to estimate these contributions and in practice it is considered to be a free parameter to fit the theory and experiment.

Because of this incompleteness of the optical model and DWBA description a number of purely phenomenological models is used in practice which stand completely apart from the basic Schrödinger equations. All of them are based on intuitive postulates and therefore contain a good deal of fitting parameters whose physical meaning depends on the interpretation of the model.

The most well known model decribing the energy and angular distributions of the secondary particles is the intranuclear cascade one (INC). There is a good deal of review-papers on this model (see e.g. / 15 /). For a long time it was applied essentially to describe the reactions caused by high-energy particles (hundreds of MeV). But recently some attempts were done with reasonable sucess to describe within this model the reactions with lower-energy incident beams / 16,17 /.

The INC is usually assumed to give a simple classical imitation of the history of nucleon-nucleus collision obtained with the aid of the computer. The algorithm of this method, suggested long ago / 18 / is as follows. Using the computer we "stage" a number of cases when the incident particle collides with the nucleus. In each of these cases the initial particle causes the cascade of secondary nucleons which leave the nucleus with a certain energy and momentum. The number of these secondary particles and their momentum distribution varies sharply from one case to another. But if we imitate a great number of collisions and average over all of them, the results obtained would give us the most probable distribution of emitted particles. The history of each incident particle transition through the nucleus is characterized by a number of parameters. Part of them (e.g. the impact parameter) are purely random numbers.

The choice of these parameters in the computer is performed with the aid of random number generators. There are, however, parameters whose probabilities depend on the properties of the nucleus and nucleons (e.g. the distance a nucleon passes in the nucleus without collisions which is defined by the nucleon-nucleon cross-section and the density of nuclear matter). In order to obtain these parameters one should attach to each value of the parameter its probability weight, subdivide the whole range of parameter variation into steps with equal probabilities and only then apply the random choice procedure within these steps. In this way we follow the classical trajectory of the incident nucleon inside the nucleus till the first collision which produces a couple of secondary nucleons and a hole in the Fermi-sea of the target. Then each secondary nucleon is followed along the classical trajectory separately until it leaves the nuclear volume or makes a new collision. The sum of the hole energies generated in the cascade defines the excitation energy of the residual nucleus. INC is practically the only phenomenological model which predicts the angular distribution of the secondary nucleons. Another advantage of INC is that it uses the nucleon-nucleon cross-section taken from experiment and not as a fitting parameter. Although the INC algorithm sprang to life in 1948 (see / 18 /), its main disadvantage is that practically nobody considered which equation underlies this algorithm or how it is connected with the basic Schrödinger equation. The only obvious point in it is that it uses the classical trajectories concept which is valid for sufficiently high-energy particles. This disadvantage leaves ample space for the introduction of a number of fitting parameters into the algorithm (like the cut-off energy for the secondary particles / 15 /), and allows to use some vague modifications (like the reflection and refraction, the specific Pauli principle / 17 /, etc.).

Although the cascade model covers a wider scope of reactions than DWBA it seems to describe only the fast stage of the reaction process and is usually complemented in practice by the evaporation model which gives a reasonable description of the low-energy particle spectra. This model is based on the analogy with the heated electron gas in metals or with evaporation of atoms from heated liquid. It is supposed that the excitation energy left in the nucleus after the first stage is distributed over a great number of nucleons (compound nucleus model) so that one can use the concept of temperature distribution for Fermi-gas of nucleons inside the residual nucleus (see e.g. / 13,19 /. Then one might apply the hypothesis / 20 /, / 21 / of thermodynamic equilibrium between the heated nucleus and saturated vapor of emitted nucleons to obtain the following expression for the emission probability per unit time $I(\varepsilon)$ of a nucleon with energy ε from nucleus A forming a nucleus B with excitation energy $E_B = E_A - \varepsilon - \varepsilon_{binding}$:

$$I(\varepsilon)\,d\varepsilon = \frac{\rho_B(E_B)}{\rho_A(E_A)}\,\sigma(E_B,\varepsilon)\,\frac{\bar{g}\,M\varepsilon}{\pi^2\hbar^3}\,d\varepsilon \qquad (5)$$

where $\rho(E)$ is the density of states for excitation energy E, σ is the cross section of the absorption of a nucleon with energy ε by a compound nucleus B (excited up to E_B)forming the compound system A with excitation E_A (this cross section is usually substituted by the optical model absorption cross section $\sigma_{abs}(\varepsilon)$ by the nonexcited nucleus B), $\bar{g} = 2s + 1$ is

the spin factor and M - the reduced mass of the system B + nucleon. Now using the relation between temperature T and level density ρ:

$$\left.\frac{d\ln\rho}{dE}\right|_{E=E_0} = T(E_0)^{-1} \qquad (6)$$

One can obtain the approximate Maxwell-like expression for the evaporation spectrum:

$$I(\varepsilon)\,d\varepsilon = C(\varepsilon,T)\,e^{-\frac{\varepsilon}{T}}\,d\varepsilon \qquad (7)$$

Here T means either initial temperature T_A (if $E_A \gg \varepsilon_{binding}$, $E_B \gg \varepsilon$) or final temperature T_B (if $\varepsilon \ll E_A - \varepsilon_{binding}$) and the factor $C(\varepsilon, T)$ is supposed to depend smoothly on ε, T and some other properties of systems A and B. Because of this ambiguities eq. (7) is almost never used for the calculation of the absolute cross-sections and T serves as a parameter to fit the experimental data to eq. (7). These drawbacks of the model on fundamental level arise again from the fact that it has no connection with the basic Schrödinger equation. This gives rise to many questions: is it possible to apply the thermodynamic equilibrium condition when there is no saturated vapour in the system, which temperature characterizes the evaporation spectrum (7), when each new particle leaving the system causes a considerable decrease of excitation energy (and this is just the normal case for the nucleus) etc. Still this model proved to be very useful in the description of the low-energy part of emitted particle spectrum. This gave rise to the combined cascade-evaporation theory (see e.g. / 15 /), where all the energy remaining in the residual nucleus (essentially in the form of hole excitation) was considered to be transformed into the temperature and to cause only evaporation. In other words the nucleus immediately after the cascade stage was considered to be in equilibrium state. But these attempts did not allow to reproduce the experimental spectra.

Therefore a new group of so called pre-equilibrium models appeared. Its introduction was based on the following reasoning. The cascade stage produces a number of holes in the Fermi- sea of the target nucleus and some particles above the Fermi surface. But the distribution of these quasi-particles is still far from a temperature one. It takes time for the system to come to the temperature equilibrium state via the exchange of nucleon energy in the two-body collisions. During this time a number of particles might be emitted and a certain part of excitation energy lost. Historically the first version of this group of models was suggested by Griffin / 22 / (the exciton model). But we shall rather consider in our lectures the more sophisticated time-dependent versions of the pre-equilibrium models, because as we shall see later one can trace the connection of these models with the fundamental Schrödinger equations easier than in the case of simplified closed (time-integrated) forms of pre-equilibrium models.

The most detailed version of these time-dependent models is the Harp-Miller-Berne (HMB) model / 23, 16 / which makes use of master equations. The guiding idea of the model is quite transparent . If we believe in the success of evoparation model and in the idea that the particles in the nucleus can be thermalized like any quantal or classical gas then one should look for the equation which describes this thermalization process in statistical physics. This description is given by master equations

of Uehling-Uhlenbeck / 24 / in quantum mechanics or by Boltzmann kinetic (master) equations in classical approach. Therefore the HMB model considers a target nucleus as a box filled with Fermi-gas at zero temperature which forms a Fermi-sea. In describing the reaction induced by a nucleon they say that at the initial moment t = 0 the incident particle is inserted into this box on one of the empty high-energy levels (see Fig. 1a). For the sake of computational simplicity all the energy space of the single-particle levels is divided into the bins of energy $\Delta\varepsilon$ (Fig.1b). Each i-th bin contains a number g_i of single-particle states

$$g_i = \int_{\varepsilon_i - \frac{\Delta\varepsilon}{2}}^{\varepsilon_i + \frac{\Delta\varepsilon}{2}} \rho(\varepsilon)\, d\varepsilon \qquad (8)$$

where the Fermi-gas state density is

$$\rho(\varepsilon)d\varepsilon = \frac{\bar{g} V_0 d^3p}{(2\pi\hbar)^3} = \frac{4\pi V_0 (2M)^{3/2} \varepsilon^{1/2} d\varepsilon}{(2\pi\hbar)^3} \qquad (9)$$

Here $\bar{g} = (2s + 1)$ is the spin factor, V_0 means nuclear volume, M is the nucleon mass, while p and ε mean momentum and energy (counted from the bottom of the nuclear well).

Assuming the occupation number of the bin to be n_i one can express the number of particles in the i-th bin as:

$$N_i = n_i g_i \qquad (10)$$

Now this system of particles would remain stable in time unless we allow them to collide with each other exchanging their energies. The transition probability (per unit time) for the collision $i + j \longrightarrow k + l$ is taken to be

$$\omega_{ij\to kl} = \frac{\sigma_N(\varepsilon_i+\varepsilon_j)\,[2(\varepsilon_i+\varepsilon_j)/M]^{1/2}}{V_0 \sum_{k,l} g_k g_l \,\delta(\varepsilon_i+\varepsilon_j-\varepsilon_k-\varepsilon_l)} \qquad (11)$$

Here σ_N is the nucleon-nucleon elastic scattering cross-section averaged over angles (or simply taken for 90° velocity vectors). The sum in the denominater due to the Kronecker symbol δ goes over the states that are allowed within the nucleus in nucleon-nucleon scattering.

Now in order to obtain the master equation one only needs to trace the change of particle number N_i in each bin. This change is caused by the following reasons:

The collision of the particles in k-th and l-th bins brings one particle into the i-th bin and the other into the j-th one

$$k + l \longrightarrow i + j$$

The particle change due to this process, taking into account Pauli principle, eq. (11) and energy conservation is

$$\frac{dN_i}{dt}(k+l\to i+j) = \sum_{kl} \omega_{kl\to ij}\, n_k g_k n_l g_l (1-n_i) g_i g_j (1-n_j) \times \delta(\varepsilon_k+\varepsilon_l-\varepsilon_i-\varepsilon_j) \qquad (12)$$

The collision $i + j \longrightarrow k + l$ causes the decrease of N_i:

$$\frac{dN_i}{dt}(i+j\to k+l) = -\sum_{kl} \omega_{ij\to kl}\, n_i g_i n_j g_j g_k g_l (1-n_k) \times (1-n_l)\,\delta(\varepsilon_i+\varepsilon_j-\varepsilon_k-\varepsilon_l) \qquad (13)$$

Now summing up the "gain" and "loss" terms (12)+(13) one obtains the well-known usual quantum master equation:

$$\frac{dn_i}{dt} = \sum_{jk\ell} \omega_{ijk\ell}\, \delta(\varepsilon_i+\varepsilon_j-\varepsilon_k-\varepsilon_\ell)\, g_k g_\ell g_j \left[n_k n_\ell (1-n_i)(1-n_j) - n_i n_j (1-n_k)(1-n_\ell)\right] \qquad (14)$$

(We assume as usual that in elementary collisions $\omega_{ij\to k\ell} = \omega_{k\ell\to ij} \equiv \omega_{ijk\ell}$). This equation describes the process of thermalization in statistical physics and we know that its solution for large times gives the equilibrium temperature distribution of Fermi-gas:

$$n_i^{eq} = \frac{1}{e^{\frac{\varepsilon_i-\varepsilon_F}{T}}+1} \qquad (15)$$

This means that particles confined in a closed system (even if it is a very large box) will interchange their energies in two-body collisions until the system reaches a temperature equilibrium.

But a nucleus is not a closed system - it might emit particles with sufficiently high energy to be in continuum ($\varepsilon > \varepsilon_F + \varepsilon_{binding}$). Therefore in HMB model a new sink term was introduced artificially into eq. (14), namely the particle loss due to the emission of particles from nuclear volume V_0 into the "laboratory" volume Ω, where their energy is $\varepsilon_{i'} = \varepsilon_i - U$ (U is the depth of the nuclear well):

$$\frac{dN_i}{dt}(i\to i') = -n_i g_i\, \omega_{i\to i'}\, g_{i'}\, \delta(\varepsilon_i - U - \varepsilon_{i'}) \qquad (16)$$

The probability $\omega_{i\to i'}$ was (in the spirit of evaporation model) taken to be proportional to the optical model absorption cross-section $\sigma_{abs}(\varepsilon_{i'})$:

$$\omega_{i\to i'} = \sigma_{abs}(\varepsilon_{i'})\left[2\varepsilon_{i'}/M\right]^{1/2}/g_i\Omega \qquad (17)$$

$g_{i'}$ is defined in analogy to g_i as the number of single-particle states in the external "laboratory" volume Ω.

Thus in HMB model one needs to solve a system of coupled equations:

$$\frac{dn_i}{dt} = \sum_{jk\ell} \omega_{ijk\ell}\, g_j g_k g_\ell\, \delta(\varepsilon_i+\varepsilon_j-\varepsilon_k-\varepsilon_\ell)\left[n_k n_\ell \times (1-n_i)(1-n_j) - n_i n_j (1-n_k)(1-n_\ell)\right] - n_i g_i\, \omega_{i\to i'}\, g_{i'}\, \delta(\varepsilon_i - U - \varepsilon_{i'}). \qquad (18)$$

The practical disadvantage of this model is its computational complexity. In addition to it, the model does not predict the angular distributions (but this is true practically for all the pre-equilibrium models, except the cascade one). On the other hand, this model contains no free parameters and seems to be quite close to the microscopic description of reactions. Unfortunately, it still belongs to a pure phenomenological class because it was not derived from Schrödinger equations. But it seems to be quite general in two senses: 1) in principle, it seems to cover the description of all the reaction process from the beginning to the end; 2) other versions of pre-equilibrium models seem to be simplified and less detailed forms of this model. One should also point out that in principle master equations of the type of eq.(14) can be derived from Schrödinger equations though under some special conditions, and a good deal of famous scientists contributed to this derivation in various ways (for instance, Pauli, Landau, Bogolyubov, Van Hove, Prigogine, Ehrenfest). But it still remains to prove that these special conditions can be fulfilled in nuclear reactions. Another

difficulty arises from the fact that these derivations were performed for closed systems and therefore led to eq.(14) without the specific sink term (16) which occurs in HMB equations. As a guess, the form (16), (17) of this term also does not seem to be a good one. First, the division of space into interior and exterior regions seems to be rather classical. In quantum mechanics each continuum state with non-vanishing wave function is defined in all the coordinate space ($0 \leq r \leq \infty$). Second, let us consider the cross-section in the elastic channel as defined by HMB master equation (18). This cross-section should by definition be proportional to the number of particles with initial energy $\mathcal{E}_0$ emitted from the nucleus. From eqs. (16), (17) we see that this number $N_0 \sim \sigma_{abs}(\mathcal{E}_0)$. On the other hand, we know from quantum mechanics that $N_0 \sim \sigma_{elastic}(\mathcal{E}_0)$ and that the elastic cross-section is a part of the total cross-section which remains after subtracting the absorption. Thus, if we assume that eqs.(16),(17) are good, we are forced to believe that the increase of σ_{abs} leads to the increase of $\sigma_{elastic}$, whereas our common sense and quantum mechanics say the inverse. Therefore, the form of the sink term (16),(17) looks suspicious.

As mentioned above, the HMB model gives a rather detailed description of pre-equilibrium process using realistic parameters which are fixed outside the model (radius and depth of the average nucleon well, free nucleon-nucleon elastic scattering cross-sections). One pays for this detailed description by solving a number of coupled differential equations (18). In order to simplify the computations (and the model) one can leave the detailed occupation number description and specify the nuclear state by the excitation energy E and by the total number of particles (above the Fermi-surface) and holes (n = p + h) without bothering much how this energy is shared between these particles and holes, i.e. assuming that all the possibilities to share this energy between them are equal. Although usually the common name for particles above the Fermi-surface and for holes is quasiparticles, it turned out historically that in pre-equilibrium models they were called excitons, and the models specifying the nucleon state by exciton number n were called exciton models. Instead of the occupation number evolution $n_i(t)$, in the exciton model one traces the evolution of the probabilities P(n,t) that there are n excitons in a nucleus (see Fig.2). The initial state in the nucleon-induced reaction is characterized by the exciton number $n_0=1$. Then the two-body collision of the incident particle with one of the target nucleons might change the energy of the incident particle and produce a particle-hole pair creating a system with n=3 (in the exciton model all the possible n=3 configurations are assumed to be created equally likely). The next collision between one of the two excited particles and a nucleon in Fermi-sea or between two excited particles might create the following states: 1) n = 5 (creation of a new pair), 2) n = 1 (one of the particles fills the hole), 3) n = 3 (a different $3p$ 1 h state is formed). The probability (λ_+, λ_- or λ_0) of each occurrence is assumed to be defined by the average matrix element of two-particle collision $\bar{M}$ and by the density of accessible final states:

$$\lambda_{n\to n'} = \frac{2\pi}{\hbar} |\bar{M}|^2 \rho_{n'}(E) \qquad (19)$$

The accessible number of states $\rho_{n'}$ for each type of transitions was calculated by Williams /25/ in the case of equidistant single-particle spectrum with density g :

$$\lambda_{n\to n+2} \equiv \lambda_+(n) = \frac{2\pi}{\hbar} |\bar{M}|^2 \frac{g^3 E^2}{p+h+1}$$

$$\lambda_{n\to n-2} \equiv \lambda_-(n) = \frac{2\pi}{\hbar}|\bar{M}|^2 g p h (p+h-2) \qquad (20)$$

$$\lambda_{n\to n} \equiv \lambda_0(n) = \frac{2\pi}{\hbar}|\bar{M}|^2 g^2 E \frac{3(p+h)-2}{4}$$

It is obvious that the equilibrium should be reached when the rates of increase λ_+ and decrease λ_- of the exciton number become equal. From this condition and eqs.(20) one can define (in the typical case of $gE \gg 1$) the equilibrium exciton number $\bar{n} \approx \sqrt{2gE}$. One can also see from (20) that for small exciton numbers $n \ll \bar{n}$ the increase of complexity prevails: $\lambda_+ \gg \lambda_-$. Thus from the initial excited state the system prefers to go in the direction of equilibrium sharing its excitation among more and more particles.

Using now the probabilities P (n,t) one can write instead of equations (14) another set of master equations /26/ :

$$\frac{dP(n,t)}{dt} = P(n-2,t)\lambda_+(n-2) + P(n+2,t)\lambda_-(n+2) - P(n,t)[\lambda_+(n) + \lambda_-(n)] \qquad (21)$$

For a given exciton number there might exist some configurations in which at least one particle has excitation energy ε in excess of its binding energy $\varepsilon_{binding}$. This particle might be emitted from the nucleus. The probability per unit time of this emission is defined in the exciton models as:

$$I(n,\varepsilon') = \frac{\rho_{n-1}(E-\varepsilon)g(\varepsilon)}{\rho_n(E)} \cdot \frac{\sigma_{abs}(\varepsilon')[2\varepsilon'/M]^{1/2}}{g(\varepsilon)\Omega} \cdot \frac{4\pi\Omega(2M)^{3/2}(\varepsilon')^{1/2}}{(2\pi\hbar)^3} d\varepsilon' \qquad (22)$$

Here $\varepsilon' = \varepsilon - U$ is the "asymptotic" energy of the emitted particle (in the external region), $g(\varepsilon)$ is the density of single-particle states inside the nucleus, the last factor is the number of single-particle states in the laboratory volume Ω (equal to $g_{i'}$ in eq.(16) of the HMB model). The first factor in (22) defines the relative statistical weight of configurations with one particle having energy ε in excess of the binding energy among all the n-exciton configurations in a nucleus. This factor substitutes the n_i probability of the HMB model (see eq.(16) because of the exciton model simplifying assumption that all the ways of sharing energy between the excitons are statistically equal. This assumption seems to be rather dubious because, if one takes the Ericson /27/ expression for densities $\rho_n(E)$, then :

$$\frac{\rho_{n-1}(E-\varepsilon)g(\varepsilon)}{\rho_n(E)} \sim p(p+h-1)$$

This shows that the particle emission is favoured for more complicated configurations with large exciton numbers n, while one should rather expect the inverse. The other two factors in (22) mean the emission probability of a particle ε' from the excited nucleus (compare with eqs.(16), (17)). Our doubts concerning the use of absorption cross-section σ_{abs} in (22) were expressed earlier in connection with HMB expression (17).

In more refined versions of exciton master equations /28/ the emission of particles is taken into account (it was neglected in eq.(21)):

$$\frac{dP(n,t)}{dt} = P(n-2,t)\lambda_+(n-2) + P(n+2,t)\lambda_-(n+2) - P(n,t)\left\{[\lambda_+(n)+\lambda_-(n)] + \sum_x \int I_x(n,\varepsilon')\,d\varepsilon'\right\} \qquad (21\,a)$$

Here x means the type of emitted particle and $I_x(\varepsilon')$ is defined by eq.(22). From the computational point of view, it is much easier to solve a system of equations (21a) than the HMB system (18). But the penalty for this simplification is rather heavy. The matrix element $\bar{M}$ (see eq.(20)) is now a free parameter of the theory which is very difficult to relate to the experimental nucleon-nucleon cross-sections used in ICM and HMB models (for more detailed studies of this problem see e.g. /29/, /30/, /31/). Therefore, the exciton models do not predict the absolute yields and are normalized to fit the experiment better. Since it is impossible to define the absolute energy loss during the pre-equilibrium process, it is difficult to assign the temperature of the equilibrium part of spectra within the exciton model. Therefore, the lack of knowledge about $\bar{M}$ allows to vary freely not only the absolute magnitude, but also the shape of the spectrum. In addition to all these ambiguities, even the initial number of excitons n_0 is also considered to be a free parameter for fitting experiments. For the nucleon-induced reactions the best fit parameters n_0 vary from 2 to 5 (see e.g. /26/, /30/). All these points make the exciton models at the present stage to be rather descriptive than predictive.

Although eq.(21a) is easier in computation than eq.(18), it still requires some time to solve this system. In order to circumvent this difficulty, one can use a wide class of closed-form exciton models. Since for the computation of particle yields

$$Y(\varepsilon')d\varepsilon' \sim \sum_n d\varepsilon' \int dt\, P(n,t) I(n,\varepsilon')$$

one still needs knowledge about P (n,t), all these closed-form models use some additional assumptions concerning the quantities $\int P(n,t)\,dt$. I will not consider all these models, since their detailed treatment will be given in the following lectures of Prof. Seeliger and other lecturers (for further details of the pre-equilibrium models considered one can also look through ref./2, 29-33/). In my opinion (taking into account the above mentioned descriptive character of the exciton models) and from the point of view of the application to the experiment, these closed forms are not much inferior to the time-dependent exciton versions. On the other hand, they are much simpler in computation and give a reasonable description of the experimental data.

To sum up our brief review of the present situation in the nucleon reaction theory, I would like to show a schematic picture in Fig.3. (I did not include the statistical theory into the scheme of Fig.3 and into my discussion, although it presents good examples of practical semi-phenomenological models for several reasons. First of all, you have already listened to lectures on the subject by Dr. Moldauer. Secondly, I am going to advocate in the following a version of statistical approach to nuclear reactions which provides a good bridge between the Schrödinger equation (1) and the phenomenological models and which overlaps partially /4/ with the more conventional statistical approaches).

From the previous discussion we see that the main disadvantage of the microscopic models is that they are not valid (or too complicated) for practical calculations. The semi-phenomenological models are quite practical but they do not cover the whole process of reaction. The phenomenological models are quite practical but they lack the fundamental derivation connecting them to the microscopic approach. This is bad not only from the puristic theoretical point of view, but also because it does not allow to define the

domains of their application and leave ample space to vaguely defined (or simply free) parameters and to further modifications caused rather by the choice of their authors than by physical reasoning. In spite of all that, they still work and give a reasonable description of experimental data. Therefore, it presents a challenge to a theorist to find why they do work.

III. Why do the phenomenological models work?

In order to build a bridge connecting the most general time-dependent Schrödinger equation with phenomenological models, let us inspect both sides again. As has been mentioned in the Introduction, the microscopic theory of reactions usually employs almost monochromatic ($\Delta E \to 0$) wave-packets that allow to make use of the stationary equation (2). The solution of this equation ψ is obtained by diagonalizing the Hamiltonian matrix using the basis φ_λ of the H_0 eigenfunctions:

$$\psi = \sum_\lambda c_\lambda \varphi_\lambda \qquad (23)$$

The S symbol means the sum over bound states and integral over continuum. The Lippmann- Schwinger formalism allows to connect the c_λ coefficients with S-matrix and reaction cross-sections. Usually (see e.g. /8/) H_0 is taken to be a shell-model Hamiltonian for non-interacting particles. Then φ_λ are the antisymmetrized products of single-particle shell-model wave-functions corresponding to a given configuration λ.

In treating the phenomenology we pointed out that the HMB master equation seems to stand closer to quantum mechanics than all the other models. We also mentioned in discussing the sink term (16) that the continuum state wave-function in quantum mechanics is defined in all the coordinate space. A good example is provided by the plane-wave

$$\varphi_E(r,t) = e^{i\kappa r - \frac{i}{\hbar}Et} \qquad (24)$$

which shows that the particle in this state might be found with equal probability everywhere ($-\infty \le r \le \infty$). On the other hand, our common sense and physics say that the particle should move in space and time. In order to observe this motion in quantum mechanics, one needs to construct a wave-packet $\tilde{\varphi}$ out of the plane-waves (24) :

$$\tilde{\varphi}_E(r,t) = \int A(E,E')\,\varphi_{E'}(r,t)\,dE' \qquad (25)$$

It is assumed and proved (see e.g./6/) that physical results depend only on the average energy E and characteristic width Δ E of the distribution A (E, E') and not on its particular shape (e.g. step-like, Lorenzian or Gaussian). If one takes for simplicity a step-like A function where the width Δ E (A(E,E')) equals $\frac{1}{2\Delta E}$ for $E-\Delta E \le E' \le E+\Delta E$ and 0 elsewhere), then eq.(25) will give us (provided that $E = \frac{K^2\hbar^2}{2M}$):

$$\tilde{\varphi}_E(r,t) = \frac{1}{2\Delta E}\int_{E-\Delta E}^{E+\Delta E} dE'\, e^{i\kappa' r - i\frac{E'}{\hbar}t} \approx$$

$$\approx e^{i\kappa r - i\frac{E}{\hbar}t}\cdot\frac{\sin(r-vt)\Delta K}{(r-vt)\Delta K} \equiv \bar{\varphi}_E(r,t)\cdot G(r,t) \qquad (26)$$

Here $v = \frac{K\hbar}{M}$ is the velocity of the particle, $\bar{\varphi}_E$ is the plane-wave function at average packet energy E and $G(r,t) = \frac{\sin(r-vt)\Delta K}{(r-vt)\Delta K}$ is the function which describes the evolution of the packet as a

whole. It shows that at a given moment of time the packet particle might be localized in space with the accuracy $\Delta r \sim \frac{1}{\Delta K}$, while in time it moves along the classical trajectory $r = vt$. (We made a Taylor expansion of E' (k') in the exponential of integral (26) and neglected the second-order terms which cause the spread of the packet and might be made small /6/ provided $\Delta K < K$). Now, if we insert this packet into a volume of radius $R \gg \Delta r$ (i.e. $\Delta K \cdot R \gg 1$), it will propagate through the volume like a classical particle and leave it after time $t \approx \frac{R}{v}$. But if the volume is small with respect to the packet length $R << \Delta r$ (i.e. $\Delta K \cdot R << 1$), then the packet will leave this volume after time $t \approx \frac{\Delta r}{v} = \frac{\hbar}{\Delta E} = \tau$ (τ is the packet duration in time). This latter case ($\tau \to \infty$) is treated in the conventional stationary description of reactions. With a bit of skill one can show (see e.g. /2/) that the same situation takes place when we use the potential scattering wave functions instead of plane waves, provided the potential phase-shifts δ vary smoothly with energy (to be exact, $\frac{\partial \delta}{\partial K} \lesssim R_o$ where R_o is the radius of nuclear potential), i.e. provided there are no single-particle potential resonances (which is a good approximation for the realistic Woods-Saxon potential , as we shall see later).

These preliminaries show that if one wishes to see the emission of particles occupying the continuum states from the internal nuclear volume, one needs to use the wave-packet technique. It also shows that the rate of emission of a sufficiently long ($\Delta K \cdot R < 1$) packet from the interior potential region is defined by the packet time $\tau = \frac{\hbar}{\Delta E}$. Therefore, in our approach we used instead of the stationary functions φ_λ the wave-packets $\tilde{\varphi}_\lambda$ (t):

$$\tilde{\varphi}_\lambda(t) = \int A(E_\lambda, E_\lambda') \varphi_\lambda(E_\lambda', t)\, dE_\lambda' = \bar{\varphi}_\lambda(t)\, G_\lambda(t) \qquad (27)$$

Here $\varphi_\lambda(t) = \varphi_\lambda e^{-\frac{i}{\hbar} E_\lambda t}$, and the meaning of $\bar{\varphi}$ and G is the same as in eq. (26). Then instead of the conventional expansion (23) one obtains the non-stationary expansion:

$$\tilde{\Psi}(t) = \sum_\lambda \bar{C}_\lambda(t) \tilde{\varphi}_\lambda(t) = \sum_\lambda \tilde{C}_\lambda(t)\, \bar{\varphi}_\lambda(t) \qquad (28)$$

which is the solution of the time-dependent eq.(1). Here $\bar{C}_\lambda$ are averaged over energy Δ E, while

$$\tilde{C}_\lambda(t) \equiv \bar{C}_\lambda(t)\, G_\lambda(t) \qquad (29)$$

describes both the evolution $\bar{C}_\lambda(t)$ of the particular component $\bar{\varphi}_\lambda$ in the wave-function Ψ, as well as the evolution $G_\lambda(t)$ of the packet as a whole.

Now the master equation is of statistical origin. Therefore, in all the standard derivations of master equations from the Schrödinger one it is necessary to operate with quantities averaged over large statistical ensembles. In our case of nuclear reaction we consider an ensemble which consists of a large number of pairs: "one target nucleus + one particle of the incident beam". This seems to be the most obvious ensemble generated in each nuclear reaction experiment. Then following the usual ways (see /2/ for details) one might derive from eq.(1) the master equation for the coefficients (29):

$$\frac{\partial \langle |\tilde{C}_\lambda|^2 \rangle}{\partial t} = \frac{2\pi}{\hbar} \sum_{\lambda'} |\bar{V}_{\lambda\lambda'}|^2 \delta^{\Delta E}(E_\lambda - E_{\lambda'}) \left[\langle |\tilde{C}_{\lambda'}|^2 \rangle - \langle |\tilde{C}_\lambda|^2 \rangle \right] \qquad (30)$$

Here $\bar{V}_{\lambda\lambda'} = \langle \bar{\varphi}_\lambda | V | \bar{\varphi}_{\lambda'} \rangle$ is the residual interaction matrix element, $\delta^{\Delta E}(E) = \frac{1}{\pi E} \sin \frac{E}{2\Delta E}$ is a "finite" delta-function (which is non-zero in the range Δ E around E), the index $\langle\ \rangle$ means averaging over statistical ensemble.

Master (or balance) equations (30), as all the master equations, seem to be quite transparent from the classical point of view: the change of probability is defined by the balance between the gain and the loss caused by residual interactions. But this in general is not true in quantum mechanics because successive collisions should interfere with each other, and in addition to mere probabilities $|\bar{V}_{\lambda\lambda'}|^2$ in eq. (30) one should get the interference cross-terms. Therefore, eq.(30) is derived /2/ from the Schrödinger eq. (1), only provided the following two conditions are fulfilled: 1) The wave packets employed are sufficiently broad in energy (short in time), so that $\Delta E > \Gamma_{spread}$, where Γ_{spread} characterizes the change of $\bar{C}_\lambda$ during the time period $\tau \sim \frac{\hbar}{\Delta E}$. At the first stages of the reaction Γ_{spread} equals approximately the imaginary part W of the optical model potential. Then it gradually decreases due to thermalization down to the inverse life-time of the compound state (to $\Gamma_{compound}$ in the case of isolated compound resonances).

2) The members of our statistical ensemble are uncorrelated, i.e. there is no correlation between the particles in the incident beam.

The meaning of the first condition becomes obvious if one recollects that the time between the two successive collisions $t_{coll} \approx \frac{\hbar}{W} = \frac{\hbar}{\Gamma_{spread}}$. Then this condition means $\tau < t_{coll}$. Indeed, if the packets are shorter in time than the interval between successive collisions, the amplitudes of these successive collisions will not interfere (there is no interference between the non-overlapping wave-packets in quantum mechanics).

The second condition is a bit deeper. As it was pointed out by Austern /34,7/ in his discussion on Freedman's and Weisskopf's time-dependent interpretation of the optical model /14/, each of the physical wave-packets in the accelerator is very narrow in energy (long in time). The poor resolution experiment means only that the accelerator beam consists of the incoherent (uncorrelated) mixture of these long wave-packets. Just this incoherency allows to use in the theoretical description of these poor-resolution measurements the short wave packets $\tau = \frac{\hbar}{\Delta E}$.

Summing up these two conditions, we see that the master equation approach (30) is valid for the description of poor resolution experiments with sufficiently large ΔE. Therefore, the cross-sections obtained with the aid of $\bar{C}_\lambda$ coefficients (see below) will describe only the averaged behaviour of the experimental cross-sections. But this is the price we pay for substitution of the complicated Schrödinger equation (1) by the much simpler eq.(30).

Our eq. (30) differs from the usually derived master equations of the type (14) in one significant detail. The $\partial/\partial t$ symbol in it means $|G_\lambda|^2 \, \partial |\bar{C}_\lambda|^2/\partial t$. Using the terminology of gas and fluid dynamics, this is a "substantive" derivative which describes the change of $|\bar{C}_\lambda|^2$ in a moving wave-packet. We are sitting inside the moving packet and observe the particle changes in it caused only by the two-body collisions. In order to see the total changes which occur inside a fixed volume in space (say, inside the nuclear volume V_0), one must switch over to the "local" derivative $\frac{d|\tilde{C}_\lambda|^2}{dt}$ which is related to the "substantive" one $\frac{\partial |\tilde{C}_\lambda|^2}{\partial t}$ as follows:

$$\frac{\partial |\tilde{C}_\lambda|^2}{\partial t} = \frac{d|\tilde{C}_\lambda|^2}{dt} - |\bar{C}_\lambda|^2 \frac{\partial |G_\lambda|^2}{\partial t} \qquad (31)$$

Thus, if we are going to describe with eq.(30) what happens inside the nuclear volume (use $\frac{d}{dt}$ in eq.(30)), then we shall find

in addition to the usual collision term (r.h.s. of eq.(30)) a "sink" term $|\bar{C}_\lambda|^2 \frac{\partial |G_\lambda|^2}{\partial t}$ which shows that even in the absence of collisions the continuum wave-packet particle leaves the nuclear volume after a time defined by the packet duration $\tau = \frac{\hbar}{\Delta E}$. This is a specific property of the open finite systems compared to the closed systems treated in all the previous derivations of master equations. If ΔE is small enough to provide for inequality $R \Delta K < 1$ (see discussion following eq.(26) where R is a nuclear radius), then the continuum configuration (i.e. that which contains at any rate one particle in continuum) wave packet $G_\lambda(t)$ inside the volume $r < R$ might be approximated by a step-like wave function

$$G_\lambda(t_i, t) = \begin{cases} 1 & \text{for } t_i \leq t \leq t_i + \tau \\ 0 & \text{otherwise} \end{cases} \qquad (32)$$

Then for the interval τ one can substitute $\bar{C}_\lambda$ for $\tilde{C}_\lambda$ in eq.(30). The presence of the "sink" term in this equation will lead to a special type of initial conditions in the solution of (30), namely the integration of (30) for each successive new interval should be carried with the zero initial condition for $\bar{C}_\lambda$ belonging to the continuum configurations. This means that by the end of each interval τ the continuum configuration wave packets leave the nucleus, and their population at the next stage should start with zero. Each wave packet $\tilde{\varphi}_\lambda$ that left the interior region during the interval $t_0 \leq t \leq t_0 + \tau$ might be detected at $r \to \infty$ contributing to the first stage cross-section for the transition from the initial state λ_0 into the final state λ . By definition, this cross-section is equal to the transition probability $|\bar{C}_\lambda(t_0, t_0+\tau)|^2$ per unit time per unit incident flux times the number of accessible final state $d\rho_\lambda$:

$$\frac{d\sigma^{t_0}_{\lambda_0 \to \lambda}}{d\rho_\lambda} = \frac{|\bar{C}_\lambda(t_0, t_0+\tau)|^2}{\tau \cdot F} \qquad (33)$$

Here F means the incident flux.

The bound state configurations are all localized within the nucleus, therefore their $G_\lambda(t)$ = const. for all the t values, and the corresponding $\bar{C}_\lambda(t)$ change monotonously (no sink terms).

During the next interval $t_0 + \tau \leq t \leq t_0 + 2\tau$ the continuum configurations will be populated again by transitions from the bound state configurations that were excited during the first stage (mind that, due to the two-body character of V interactions, these are essentially the doorway configurations of the 3-quasiparticle type). By the end of this new interval the continuum wave packets will leave the nucleus again contributing to the cross-section (33) of the first stage. Thus, the total cross-section by the time $t_0 + 2\tau$ will be a sum of two components

$$\sigma^{t_0}_{\lambda_0 \to \lambda} + \sigma^{t_0+\tau}_{\lambda_0 \to \lambda} \qquad (33a)$$

which might be called the direct-reaction and doorway components, respectively. We can proceed in this way for further time intervals t_i bringing the new contributions to the total cross-section from excitation of more and more complicated configurations:

$$\sigma_{\lambda_0 \to \lambda} = \sum_i \sigma^{t_i}_{\lambda_0 \to \lambda} \qquad (33b)$$

The corresponding S-matrices are related to $\bar{C}_\lambda$ coefficients in a conventional (see e.g./6/) way:

$$|\bar{S}^{t_i}_{\lambda\lambda_0}|^2 = |\bar{C}_\lambda(t_i, t_i+\tau)|^2 \qquad (34)$$

In using eqs. (33), (34), one should keep in mind that the expansions (23), (28) usually employ $\varphi_\lambda^{(+)}$ wave-functions for the continuum states' configurations, while the final states in (33), (34) are naturally defined in terms of $\varphi_\lambda^{(-)}$ functions which are related to $\varphi_\lambda^{(+)}$:

$$\varphi_K^{(-)} = \sum_\lambda S_{K\lambda}^{pot}\, \varphi_\lambda^{(+)} \tag{35}$$

Here S^{pot} is the potential scattering S-matrix in the average field H_0.

Now we are able to show /3/ that our master equations will give under various approximations the results known in the microscopic and semi-phenomenological models.

First we can see that in the limiting case V = 0 (no residual interactions between nucleons) eq.(30) describes just the potential elastic scattering. Indeed, consider the initial condition $|\bar{C}_\lambda(t_0)|^2 \sim \delta_{\lambda\lambda_0}$ (λ_0 is the entrance channel characterized by the configuration $\varphi_{\lambda_0}^{(+)}$). Taking into account eqs.(34) and (35), one obtains the total S-matrix in this case:

$$|\bar{S}_{K\lambda_0}|^2 = \sum_\lambda |\bar{S}_{K\lambda}^{pot}|^2 \delta_{\lambda\lambda_0} = |\bar{S}_{K\lambda_0}^{pot}|^2 \tag{36}$$

Now let us consider the first order perturbation (in V) solution of eq.(30) for the first stage of the reaction $t_0 \le t \le t_0 + \tau$. Again let us assume the initial conditions $|\bar{C}_\lambda(t_0)|^2 \sim \delta_{\lambda\lambda_0}$. In the entrance elastic channel we then can neglect the reverse transitions to λ_0 from inelastic channels λ :

$$\frac{d\,|\bar{C}_{\lambda_0}(t_0,t)|^2}{dt} = -\frac{2\pi}{\hbar}\,|\bar{C}_{\lambda_0}(t_0,t)|^2 \sum_\lambda |\bar{V}_{\lambda\lambda_0}|^2\, \delta^{\Delta E}(E_\lambda - E_{\lambda_0}) \tag{37}$$

Introducing the matrix element $\bar{V}$ averaged over λ and the density ρ_λ of inelastic states, we get the extinction law for the incoming packet:

$$|\bar{C}_{\lambda_0}(t_0,t)|^2 = |\bar{C}_{\lambda_0}(t_0)|^2 e^{-\frac{W}{\hbar}(t-t_0)} \tag{38}$$

The rate of absorption W is here defined in the same way (see e.g. /7/) as the imaginary part of the optical model potential

$$W(E_{\lambda_0}) = 2\pi |\bar{V}|^2 \rho\,(E_{\lambda_0}) \tag{39}$$

where $\rho(E_{\lambda_0})$ is the sum of the doorway configurations state densities ρ_λ .

In order to find the reaction $\lambda_0 \to \lambda$ cross-section in the same approximation, we neglect in (30) all the transitions except $\lambda_0 \to \lambda$:

$$\frac{d\,|\bar{C}_\lambda(t_0,t)|^2}{dt} = \frac{2\pi}{\hbar}\,|\bar{C}_{\lambda_0}(t_0,t)|^2 \left|\langle \bar{\varphi}_\lambda^{(+)} | V | \bar{\varphi}_{\lambda_0}^{(+)} \rangle\right|^2 \delta^{\Delta E}(E_\lambda - E_{\lambda_0}) \tag{40}$$

This equation with the aid of eqs.(33), (35) leads to the following cross-section:

$$\frac{d\bar{\sigma}_{\lambda\lambda_0}}{d\rho_\lambda} = \frac{2\pi M}{\hbar^2 K_{\lambda_0}}\, |\langle \bar{\varphi}_\lambda^{(-)} | V | \bar{\varphi}_{\lambda_0}^{(+)} \rangle|^2 \tag{41}$$

This is the Born expression which takes into account the distortion of the initial and final states in the average field H_0 . One can take into account the results of eqs. (37), (38) and introduce absorption in channels λ_0, λ . Then (41) will completely coincide with DWBA expression (see eq.(4)).

Let us now demonstrate that the purely phenomenological models might also be obtained as special approximate solutions of eq.(30) under different conditions. In order to do this, it is better to make a transition from the configuration probabilities representation $|\bar{C}_\lambda(t)|^2$ to the single-particle state occupation numbers $\bar{n}_k(t)$ (the technique of this transition is given e.g. in ref. /35/). Then, instead of eq. (30), one gets:

$$\frac{\partial \langle \tilde{n}_\kappa \rangle}{\partial t} = \frac{\pi}{\hbar} \sum_{ij\ell} |\bar{V}_{ij\kappa\ell}|^2 \delta^{\Delta E}(\varepsilon_i+\varepsilon_j-\varepsilon_\kappa-\varepsilon_\ell) [\langle \tilde{n}_i \rangle \langle \tilde{n}_j \rangle (1-\langle \tilde{n}_\kappa \rangle) \times \tag{30a}$$

$$\times (1-\langle \tilde{n}_\ell \rangle) - \langle \tilde{n}_\kappa \rangle \langle \tilde{n}_\ell \rangle (1-\langle \tilde{n}_i \rangle)(1-\langle \tilde{n}_j \rangle)]$$

Here $\langle \ \rangle$ means again the ensemble averaging and will be omitted further on, $\tilde{n}_\kappa(t) = \bar{n}_\kappa(t)\,|G_\kappa(t)|^2$ in analogy with (29), and $G_k(t)$ describes the evolution of the single-particle wave packet with quantum numbers k. The "substantive" derivative $\frac{\partial}{\partial t}$ on the left hand side of (30a) is related to the local derivative $\frac{d}{dt}$ in the same way as it is done in eq.(31) :

$$\frac{\partial \tilde{n}_\kappa}{\partial t} \equiv |G_\kappa|^2 \frac{\partial \bar{n}_\kappa}{\partial t} = \frac{d\tilde{n}_\kappa}{dt} - \bar{n}_\kappa \frac{\partial |G_\kappa|^2}{\partial t} \tag{31a}$$

Thus we obtained the master equation of the Uehling-Uhlenbeck type (14) with the additional "sink" term $\bar{n}_\kappa \frac{\partial |G_\kappa|^2}{\partial t}$ we were looking for in the discussion of HMB equations. Now the exact shape of this term is defined by the exact shape of the packet A (E_k, E'_k) (see eqs. (25), (26)), but it obviously differs from the sink term (16), (17) of the HMB model. Let us consider first the case of ΔE fulfilling the condition $R\cdot\Delta K < 1$. Then, as we have seen earlier, the rate of emission is defined by the packet time τ . One can take, for instance, the Lorentzian shape of A (E, E'). This leads to:

$$|G_\kappa(t)|^2 = e^{-\frac{t}{\tau}} \qquad \tau = \frac{\hbar}{\Delta E} \tag{32a}$$

Then the "sink" term would be:

$$\bar{n}\,\frac{\partial |G|^2}{\partial t} = -\frac{\tilde{n}}{\tau} \tag{42}$$

And one can write (30a) in the internal region of the nucleus:

$$\frac{d\tilde{n}_\kappa}{dt} = \sum_{ij\ell} \omega_{ij\kappa\ell}\, \delta(\varepsilon_i+\varepsilon_j-\varepsilon_\kappa-\varepsilon_\ell)\, g_i g_j g_\kappa g_\ell [\tilde{n}_i \tilde{n}_j (1-\tilde{n}_\kappa)(1-\tilde{n}_\ell) - \tag{30b}$$

$$-\tilde{n}_\kappa \tilde{n}_\ell (1-\tilde{n}_i)(1-\tilde{n}_j)] - \frac{\tilde{n}_\kappa}{\tau}$$

(For the bound states, as usual, $\frac{\partial |G|^2}{\partial t} = 0$, and there is no sink term). We have introduced here the transition probabilities $\omega_{ij\kappa\ell} = \frac{\pi}{\hbar} |\langle \overline{\varphi_i \varphi_j} | V | \overline{\varphi_\kappa \varphi_\ell} \rangle|^2 = \frac{\pi}{\hbar} |\overline{V_{ij\kappa\ell}}|^2$ which are related to the matrix elements of two-body interactions between the single-particle states φ in the central field of H_0 averaged over $\vec{p}$ directions (for continuum) and magnetic quantum numbers (for bound states). We have also approximated the integrals over continuum by the sums which led to the appearance of the single-particle state numbers g and Kronecker symbols instead of finite δ^Δ-functions. Comparing this equation with the HMB eq.(18), we see that they differ in two respects: 1) The form of the sink term is defined by τ in our case and merely reflects the fact that the packet of continuum states leaves the fixed volume during the time

$\tau = \frac{\hbar}{\Delta E}$. 2) The single-particle state densities ρ , necessary to calculate g (see eq.(8)), for continuum states differ very much from those employed by the HMB model. In principle, they are defined by the single-particle potential phase-shifts $\partial\delta/\partial K$ (see e.g./36/) but if one neglects them ($\frac{\partial\delta}{\partial K} <$ R, which means essentially the absence of the narrow single-particle potential resonances), then one can use /36/ the Fermi-gas expression for them which is similar to eq.(9):

$$\rho(\varepsilon)d\varepsilon = \frac{(2s+1)V_0\, d^3p_a}{(2\pi\hbar)^3} = \frac{4\pi V_0 (2M)^{3/2}\varepsilon_a^{1/2}\, d\varepsilon}{(2\pi\hbar)^3} \qquad (9a)$$

but contains the asymptotic energy ε_a and momentum p_a which are much smaller than the local energies ε employed in HMB equations:

$$\varepsilon_a = \varepsilon - U \qquad (43)$$

where U is the depth of the nuclear well.

Both points of deviation between eqs.(30b) and (18) are caused by a more proper treatment of the boundary conditions of the open systems in eq.(30b). Later on we shall show numerically the significance of these deviations. But now let us turn to the evaporation stage. If instead of the shape (32a) one uses the step-like expression (32) for G_K (we again point out that the physical results should not depend on the particular choice of A(E, E')), then for each time interval τ one can use instead of (30a) the Uehling-Uhlenbeck equations (14), but with specific initial conditions of "cleaning" the continuum states after each integration over time. As we know, the Uehling-Uhlenbeck equations lead to thermal equilibrium with temperature distribution (15) for Fermi gas. In our case this equilibrium might exist for a time interval τ . After this interval the particles in the continuum will leave the nucleus giving contribution to the yield dN_ε which is proportional to n_ε^{eq} (see (15)) and the continuum state density $d\rho(\varepsilon) \sim \sqrt{\varepsilon}\, d\varepsilon$:

$$dN_\varepsilon \sim \sqrt{\varepsilon}\, e^{-\frac{\varepsilon}{T}}\, d\varepsilon \qquad (44)$$

This is just the formula used in the evaporation theory (see eq.(7)). During the next interval the equilibrium might be reached again, but the temperature of the system would be lower, because part of the excitation energy was carried away at the previous stage by the emitted particles. Therefore, in our version of evaporation model the temperature would gradually go down and the complete equilibrium will be reached when all the excitation energy is emitted from the system leaving the cold residual nucleus. This is a realistic result which appears in our master equations because we consider a finite open system.

Let us now consider the case of large Δ E, so that RΔK > 1. Then we are able to localize the particle wave-packet inside the nucleus with the accuracy of $\Delta r \sim \frac{1}{\Delta K}$. As soon as Δr becomes smaller than the characteristic length (mean free path for homogeneous nuclear matter distribution or surface diffuseness in the Fermi distribution model), one can use the local momentum approximation assigning the momentum $\vec{p}(\vec{r})$ to the particles between successive collisions. Then the role of quantum number K in eq.(30a) is performed by the momentum $\vec{p}_K$, $G_K(\vec{r}, t)$ has the form (26) and the occupation numbers $\tilde{n}_K(t)$ become just the classical distribution function $\rho(\vec{p}_K, \vec{r}, t)$:

$$\tilde{n}_K(t) = \bar{n}_{\vec{p}_K}(t)\,|G_K(\vec{r}, t)|^2 = \rho(\vec{p}_K, \vec{r}, t) \qquad (45)$$

Then, instead of master equations (30a), we obtain the Boltzmann-like equations:

$$\frac{\partial \rho(\vec{r},\vec{p}_k,t)}{\partial t} = \int d\vec{p}_i\, d\vec{p}_j\, d\vec{p}_e\; P_{ijke}\{\rho(\vec{r},\vec{p}_i,t)\rho(\vec{r},\vec{p}_j,t)[1-\rho(\vec{r},\vec{p}_k,t)]\times$$
$$\times[1-\rho(\vec{r},\vec{p}_e,t)] - \rho(\vec{r},\vec{p}_k,t)\rho(\vec{r},\vec{p}_e,t)[1-\rho(\vec{r},\vec{p}_i,t)][1-\rho(\vec{r},\vec{p}_j,t)]\} \qquad (46)$$

The collision term $P_{ijke} = \frac{\pi}{\hbar}|\langle\varphi_{\vec{p}_i}\varphi_{\vec{p}_j}|V|\varphi_{\vec{p}_k}\varphi_{\vec{p}_e}\rangle|^2\delta^{\Delta E}(\varepsilon_i+\varepsilon_j-\varepsilon_k-\varepsilon_e)$ contains integration in the matrix element over the volume $\Delta V \sim \frac{1}{(\Delta K)^3}$. The derivative $\partial\rho/\partial t$ is a usual substantive one which is related to the local derivative $\frac{d}{dt}$ in a usual way:

$$\frac{\partial \rho}{\partial t} = \frac{d\rho}{dt} + \frac{\vec{p}}{m}\vec{\nabla}\rho + \frac{\partial U}{\partial \vec{r}}\cdot\frac{\partial \rho}{\partial \vec{p}} \qquad (47)$$

The third term here takes into account the change of ρ due to the existence of the nuclear average potential field $U(r)$. Eq. (46) differs from the Boltzmann kinetic equation only because it takes into account the Pauli principle. Now we can learn something from gas dynamics which uses the Boltzmann equation as the fundamental one. It is well known there (see e.g./37/) that a good approximate way to solve this equation is given by the random choice procedure which coincides with Goldberger's algorithm of the intranuclear cascade model. To end up with the derivation of the phenomenological models, I would like to mention that in order to obtain the exciton master equation (21) or (21a), one should start with our eq.(30), recollecting that $|C_\lambda(t)|^2 = P_\lambda(t)$ is the probability for the existence of configuration λ. Averaging eq.(30) over configurations containing the same number of excitons, one immediately arrives at the form (21a) where again one should modify the continuum state densities appearing in λ_+ through (19) in a way similar to (9a). As to the emission rates (22), one might claim in analogy to eqs.(32), (32a) that they should be inversely proportional to τ.

Thus we have proved that our master equations for finite open systems overlap strongly with the semi-phenomenological models and produce a good bridge connecting the existing phenomenological models with the fundamental Schrödinger equation (1). Therefore, instead of the scheme in Fig.3 we are able to suggest a scheme of Fig.4. I do not include again the statistical theory into the scheme. As we have seen, our master equations are of statistical character because we average the time-dependent Schrödinger equations over a statistical ensemble of colliding pairs - "incident nucleon + target nucleus". This led us to the time-dependent form of master equation (30). As has been mentioned above, the group of Agassi, Weidenmüller and Mantzouranis /5/ got results on the lines somewhat similar to ours. They started with the stationary Lippmann-Schwinger approach in the microscopic theory of reactions. Instead of our statistical ensemble, they introduced the statistical ensemble of the residual interaction matrix elements and in averaging over this ensemble assumed a version of random phase approximation (which should correspond to our assumption concerning the absence of correlations between the samples of our ensemble). In complete analogy to our approach, they also introduced the condition for averaging interval $\Delta E > \Gamma_{spread}$. In this way they obtained from the microscopic reaction theory an equation which coincides with the exciton model master equation (21a) integrated over time ($\int_0^\infty dt$). This necessity of time integration in their approach is obviously caused by the fact that they started with the Lippmann-Schwinger equation which is obtained from the Schrödinger equation (1) with the aid of time-integration over a very long wave-packet ($\tau \to \infty$). The use of the

Lippmann-Schwinger equation caused additional limitation in this theory - it does not allow to treat the case of several nucleons in the continuum (i.e. the incident nucleon energy larger than $\sim$ 10 Mev). This limitation arises basically from the fact that the solutions of the Lippman-Schwinger equation are not unique for the case of more than 2 bodies (one of them is the target nucleus) in continuum. (This well-known fact brought to life Faddeev's equations). But it is also known (see e.g./6/) that in the time-dependent wave-packet theory this difficulty does not appear with the solutions of eq.(1). Therefore, our approach is in principle free from this limitation and allows to understand the high-energy INC model. In addition to the two previously mentioned conditions, Agassi and Weidenmüller /4/ used in their derivation the condition $\Gamma_{spr} > D$ (D is the average spacing of the states considered). This brought one more limitation in their theory - it can be applied only to initial states with exciton numbers $n \geq 3$, i.e. it cannot describe the initial stages of the reaction. We do not need this rather severe condition in our derivation. Therefore, as it has been demonstrated, our master equations describe also the initial stages of reaction including elastic scattering and direct processes. On the other hand, the stationary approach in /4/, /5/ is closer to the microscopic theory underlying the conventional statistical models. This allowed to obtain a number of results of the conventional statistical theory (i.e. the Hauser-Feshbach formula) in a more general way than usual. Perhaps I am not objective in comparing our approaches, but both theories were developed independently during the recent two years, and unfortunately we have not had so far an occasion for a personal meeting and discussion.

Now a few words about the choice of the basis (i.e. about H_o) in our approach. Our only condition in the derivation of eq.(30) was $\Delta E > \Gamma_{spread}$. Obviously, one should choose the basis in such a way that ΔE is smaller than the characteristic distance between the basic states. In the case of the single-particle shell-model basis this characteristic distance is of the order of $2\hbar\omega \approx 20$ Mev, while Γ_{spread} for the single-particle states is, as we have seen (eq.(37)-(39)), equal to the imaginary part of the optical model potential W. This shows that one can use this basis for the description of nucleon-induced reactions at all energies before the meson-production starts to contribute considerably. (Actually, the creation of the optical model was caused just by this fact . Otherwise, we shall still be confined to the archaic black nucleus approaches). Speaking about the shell-model basis, I should mention that in our discussion we used the fixed shell-model potential and did not consider the fact that this potential should be defined self-consistently by the nuclear density. One can easily find (see e.g. /38/) that, adding to our master equations this self-consistency condition, we shall get a new type of solutions, namely the zero-sound (i.e. collective excitations of the giant multipole type). In practice, this addition would mean the necessity to make the time-dependent Hartree-Fock calculations simultaneously with the solution of master equations. Obviously, this straightforward solution is too complicated numerically and should be performed in some approximate way. Presently one can neglect this effect because the existing theoretical /39/ and experimental /40/ estimates show that the contribution of zero-sound excitation to the cross-sections of nucleon-induced processes is quite small.

We can also choose a larger ΔE and switch over to the quasi-classical or local momentum approximation basis, as we have done in the derivation of the Boltzmann-like eq.(46). The condition for the validity of this basis is $\Delta E \prec E$. As we shall see later, one might try to combine the features of several bases.

We have restricted ourselves to the description of reactions with outgoing nucleons. Formally one can easily include the cluster emission into the theory, provided the microscopic theory would give us the appropriate basis. Unfortunately, up to now this basis does not exist.

Thus, we have shown that the existing phenomenological models are at any rate the bastards of the high-brow theory. Let us now examine the portion of noble blood they do contain and what are the ways to make them quite lawful.

IV. To what extent should one believe in these models?

As we have already mentioned, the exciton models rather describe the already obtained experiments than predict the results. Since the matrix elements $\bar{M}$ are not fixed, one can easily vary the magnitude and the shape of the emission spectrum. If this does not help, one can vary n_0 as well. Therefore, I highly appreciate the above mentioned attempts /28-32/ to define $\bar{M}$ in one way or other. From the above mentioned derivation of the exciton master equation one sees that $\bar{M}$ is the residual interaction matrix element $V_{\lambda\lambda'}$ averaged over all the configurations λ, which might appear in the nucleus. The experience of microscopic calculations of $V_{\lambda\lambda'}$ shows that they vary within very wide limits. Therefore, even if we get the average value $\bar{M}$, the dispersion might still be comparable with this value because the model is oversimplified.

Now there are two other types of phenomenological models that predict the absolute cross-sections: the HMB model and the cascade one. The parameters of these models are in principle fixed (i.e. can be defined with a reasonable degree of accuracy in the independent experiments). To save time, I shall not demonstrate numerous pictures comparing experimental data and theoretical calculations in these models (one can find them e.g. in ref./30, 41, 16/). These pictures just show that these models give an order-of-magnitude agreement with the experiment for the incident nucleon energies in the intervals 18 ÷ 60 Mev. Usually the HMB model underestimates the experimental data by a factor of 2-3. The cascade model sometimes shows better agreement. It seems to me that in order to estimate the validity of the models, one should rather compare them with each other. Some examples of such a comparison are shown in Figs.5, 6 borrowed from /30/. The dashed histogram presents the BNL cascade version, while the solid one corresponds to the ORNL cascade. One can easily see that the ORNL version reproduces the experiment much nicer than the BNL one. On the other hand, the main difference between these two versions is that ORNL uses a three-step approximation for nuclear density and does not take into account the reflections and refractions of particles, while the BNL version employs the seven-step representation to reproduce the nuclear potential better and considers refraction and reflection of the particles on the border of each step. The question arises immediately: why should the more sophisticated (and seemingly more realistic) model give poorer results? The other question is why should the classical ORNL cascade work better than the quantum-mechanical description of the HMB model (which is also presented in Figs.5,6) ?

I would like to discuss both questions using the general approach of the previous part of these lectures and the results obtained by our group /42/.

As we have seen (Fig.4), both the HMB and INC models are solutions of master equations (30) for different ΔE assumptions. The other difference between them arises because the HMB model solves the master equations exactly, while the cascade is only an approximate solution of the Boltzmann-like eq.(46). The last source of difference is that one uses in HMB the angular independent (averaged over angles between colliding particles) nucleon-nucleon cross-sections σ_N (see eq.(11)) and never takes into account the refraction of particles on the edges of potential, while all the INC models consider the angular-dependent σ_N and some of them (BNL version) also take into account the refraction. This last point of angular averaging simplifies HMB to a great extent, but may cause difficulties in comparing the results with the experiment. Therefore, we decided to start with intercomparison of the models under the same assumptions of angular independence and lack of refraction leaving the experimental data aside for a while. The aims of this intercomparison of models within the same approximations (aside from testing our scheme in Fig.4) are as follows. First, it is interesting to understand to what extent the proper solution of an open system by master eq.(30b) with the continuum state densities (9a), (43) differs numerically from solutions of the HMB master eq.(18) with the sink term (16),(17) and state densities (9). On obtaining the exact solution of master eq.(30b), one can compare it to the approximate INC solution and see the accuracy of cascade approximations in order to find possible ways to increase it. Therefore, we have performed the numerical solution of eq.(30b) for the model cases of 39 Mev protons incident on ^{56}Fe and ^{209}Bi targets, considering these targets as a mixture of proton and neutron Fermi-gases in a square nuclear well with radius R_o. As has been mentioned above, we neglected the reflection and refraction (considering the case $\frac{\partial \delta}{\partial \kappa} < R_o$) and used therefore eqs. (9a), (43) for continuum state densities. In accordance with eqs.(33), (33b), the inelastic cross-section was defined as follows:

$$\frac{d\sigma_\varepsilon}{d\varepsilon} = \frac{\int \bar{n}_\varepsilon(t)\, dt\, \rho(\varepsilon)}{\tau^2 F} \qquad (48)$$

Fig.7a shows how the lowest energy part ($\varepsilon \approx 2$ Mev) of the inelastic neutron spectrum is formed in time for the ^{56}Fe case. One can see that the reaction process is separated into 2 well-defined stages. The fast pre-equilibrium stage lasts about 5-10 t_{coll} (the mean free time between successive collisions $t_{coll} \approx \frac{\hbar}{W} \approx 10^{-22}$sec). By the end of this period one can see numerically that the bound state occupation numbers are nicely described by the equilibrium temperature distribution, while the continuum occupation numbers demonstrate a faster decrease with energy, contrary to the HMB results (Fig.3 of ref./23/). The second evaporation stage corresponding to the plateau of Fig.7a is characterized by much larger relaxation times (integrating our equations up to $t \sim 10^{-19}$sec gains only a percent additional contribution to the fast process cross-section at $t \simeq 3 \cdot 10^{-21}$sec, although the total evaporation cross-section in this energy bin is by an order of magnitude larger than the pre-equilibrium one). This result is also different from the HMB one /23/ shown in Fig.7b. Although they claim that at

$t \approx 35\ t_{coll}$ a complete equilibrium is reached, we do not see in Fig.7b any hints of the cross-section formation slowing down to the evaporation stage. It seems that the HMB equation underestimates the role of emission term relative to the collision term for continuum states. In other words, the HMB box is much more closed than the actual nucleus. In any case, the behaviour of our system allows to separate unambiguously the fast and slow stages. This is important, since the INC approximate solution of eq.(46) might obviously be valid only for the fast stage. This approximation is based essentially on the assumption that the densities ρ on the right-hand side of eq.(46) are time-independent. The standard INC never considers either the hole deexcitation (historically just this fact caused the appearance of the first exciton model of Griffin). The knowledge of eq.(46) underlying the INC algorithm allowed us to modify the standard INC in this respect. Indeed, eq.(46) is seen to be symmetric with respect to the particle-hole exchange. Therefore, we fix all the holes excited in the usual cascade process and then apply the cascade algorithm to trace the hole deexcitation, while the hole rises up to energy $\mathcal{E}_F - \mathcal{E}_{binding}$. The hole deexcitation in higher shells would cause the temperature smearing of the Fermi-surface rather than the particle emission. Now the second modification which we introduced into INC originally was done for the sake of inter-consistency in our two models. Indeed, in calculating the continuum state density of eq.(9a) necessary for solutions of eq.(30b), we neglected the narrow potential resonances which might exist for $l > k_a R_o$ (l is the angular momentum, $k_a = \frac{p_a}{\hbar}$, $R_o = r_o A^{1/3}$ is the nuclear radius). Therefore, in our cascade calculations we fixed the l value of the secondary particle after each collision and excluded the collisions giving rise to particles with $l > k_a R_o$. This additional selection caused a drastic change in the spectrum of emitted particles (see Fig.8). There is a great number of high-l potential resonances in a square well because the sum of the centrifugal potential and a square well produces a step-like barrier at $r = R_o$ for all the values of l. In the classical INC with refraction (the solid line in Fig.8) the corresponding high-l particles are reflected at this step and rotate inside the nucleus till the next two-body collision slows them down. Therefore, the inclusion of our $l < k_a R_o$ criterion enriches the high-energy part of the emitted particle spectrum (see the dashed line in Fig.8) and lowers the excitation energy of the residual nucleus which appears after the cascade stage.

To end up with the intercomparison of the exact master equation solution and our modified INC, we can look at Fig.9. Here the emitted neutron spectra are shown for the Fe and Bi cases by solid lines corresponding to the exact solution of master eq.(30b). Dashed lines correspond to INC modified only by $l < k_a R_o$ criterion without the contribution of the hole deexcitation. The dash-dotted line takes into account the contribution of the hole deexcitation as well. We see here that our modified INC allows to obtain the inelastic cross-section within the 20-30 % accuracy even for sufficiently low incident energies (in our case, the incident protons with $E_p = 39$ Mev). The agreement for the secondary proton spectra is essentially the same.

Thus we see that proper treatment of continuum states in open systems modifies the HMB and INC models to such an extent that the

agreement between them becomes considerably better than it was in purely phenomenological approaches (mind that, if we used in Fig.9 the semi-logarithmic scale of Figs.5,6 employed in all the comparisons of phenomenological models, then our master equation and the INC spectra would be quite indistinguishable).

It has been a great pleasure to learn that the INC model reproduces fairly well the pre-equilibrium process because the INC algorithm is much simpler in the computation than the exact integration of master equations. To our great surprise, the contribution of the hole deexcitation to the pre-equilibrium spectra has turned out to be far less significant than one might expect. As one can see from Fig.9, it might contribute only to the low-energy part of the spectrum which is completely dominated by the evaporation process (the evaporation contribution is not shown in Fig.9, but, as we have already mentioned, it usually is by an order of magnitude larger in the low energy region than the pre-equilibrium one).

Now one can come back to the drastic role of the $\ell < k_a R_o$ criterion in our modified INC (Fig.8). In case the actual nuclear potential possesses the high-ℓ resonances dropped out by our additional selection, this criterion, although necessary for our model intercomparison, would be of no practical use. But one can see from crude balance estimates of centrifugal repulsion and diffused Woods-Saxon attraction that the narrow high-ℓ neutron resonances are very rare phenomena in actual nuclei. The same fact is demonstrated by numerical calculations /43/ of neutron resonances in the realistic Woods-Saxon potential: the diffuse border of the nuclear potential contrary to the square well hardly ever provides for the existence of a sufficiently high barrier to keep a narrow resonance. Therefore, our $\ell < k_a R_o$ criterion serves a simple but efficient way to take into account this diffuseness. In a way, this is a possibility to take into account the shell-model effects into the INC algorithm. This allows us to understand why the simplified ORNL cascade version reproduces the experimental data much better than the sophisticated BNL one. The reflection of particles on the borders of step-like potential in the BNL version does not allow them to leave the nucleus. This leads to a large decrease of the high-energy spectra clearly seen in Figs.5,6.

As has been mentioned earlier, our main point in obtaining Fig.9 was to compare the exact and approximate (cascade) ways of the master equation solution within the same model rather than to fit the experimental data. Therefore, the cascade curves in Fig.9 were obtained for angular-averaged collision terms $P_{ijk\ell}$. However, we also made modified cascade calculations for ^{209}Bi case with classical refraction (but still with the $\ell < k_a R_o$ criterion) and the realistic angular dependence of $P_{ijk\ell}$ (see /44/). In the Bi case the Coulomb barrier is large enough to damp the evaporation stage contribution, and one can compare the calculated INC results with experimental data of ref./45/ (see Fig.10 where our INC results are given by a dashed histogram, while the solid line is an experimental one averaged over 4 Mev intervals). The quasi-elastic maximum in the experiment corresponds to the low-energy collective state excitation in ^{209}Bi which is not included in the cascade model. Otherwise, the agreement is fairly good taking into account that we used a crude step-like Coulomb barrier penetrability (mind again that we do not need to use the semi-logarithmic scale in Fig.10).

All this gives us a rather optimistic feeling that a properly modified cascade algorithm might be the most practical approximation for the solution of our master equations, i.e. for the description of the pre-equilibrium process. Obviously, one cannot use the classical trajectory concept describing the diffraction of a low-energy emitted particle on the border of the potential. Presently we are completing the investigation of this problem, which also allows to incorporate the shell-model features into the INC and gives a more rigorous proof to our $l < k_a R_o$ criterion. In a complete analysis of the experimental data one practically cannot separate the pre-equilibrium part from the equilibrium one. Therefore, we are also cross-examining the evaporation stage on the basis of our master equations.

We all feel that nuclear physics is reaching the stage of becoming a mature science. And this means that, in addition to the already existing qualitative understanding, we are able and need to start quantitative description based on sound foundations rather than on pure phenomenology and bright guesses.

References

1. H. Feshbach in Proceedings of the Europhysics Study Conference on Intermediate Processes in Nuclear Reactions, August 31-September 5, Plitvice Lakes, Yugoslavia. Lecture notes in physics. vol.22, Springer-Verlag, 1973.
2. V.E.Bunakov. Nucl. Phys. (Russian) 25, 505 (1977).
   (Sov. Journ. Nucl. Phys. 25 , 271 (1977)).
   V.E.Bunakov, M.M.Nesterov. Proceedings of X Winter School of LINP in nuclear physics and elementary particles. Part I. Leningrad, 1975 (Russian).
3. V.E.Bunakov, M.M.Nesterov. Phys. Lett. 60 B, 417 (1976).
4. G.Agassi, N.Weidenmüller. Phys. Lett 56 B , 305 (1975).
5. G.Agassi, H.Weidenmüller, G.Mantzouranis. Phys. Reports 22 C, 147 (1975).
6. M.L.Goldberger, K.M.Watson. Collision Theory. N.Y., 1964.
7. N.Austern. Direct Nuclear Reaction Theories. N.Y., 1970.
8. C.Mahaux, H.Weidenmüller. Shell-model approach to nuclear reactions. Amsterdam, 1969.
9. R.F.Barrett, L.Biedenharn, M.Danos, P.Delstano, W.Greiner. Rev. Mod. Phys. 45 , 44 (1973).
10. V.G.Soloviev. Proc. International School in Nuclear Structure. Alushta, 1972.
    V.G.Soloviev, L.A.Malov. Nucl. Phys. A 196 , 433 (1972).
11. H.Feshbach. Ann. of Phys. 5 , 357 (1958).
12. G.E.Brown. Rev. Mod. Phys. 31 , 893 (1959).
13. A.Bohr, B.Mottelson. Nuclear Structure. v.1, N.Y., 1969.
14. F.Friedman, V.Weisskopf in "Niels Bohr and the Development of Physics", London, 1955.
15. V.S.Barashenkov, A.S.Ilynov, N.M.Sobolevsky, V.D.Toneev in Proc. of International JINR-CERN School on High-Energy Physics, E 2-5813, Dubna, 1971.
    V.S.Barashenkov, H.V.Bertini, K.Chen, G.Friedlander, G.D.Harp, A.S.Iljinov, J.M.Miller, V.D.Toneev. Nucl. Phys. A 187, 531 (1972).
16. G.D.Harp, J.M.Miller. Phys. Rev. C 3 , 1847 (1971).
17. H.W.Bertini, G.D.Harp, F.E.Bertrand. Phys. Rev. C 10, 2472 (1974).
18. M.L.Goldberger. Phys. Rev. 74 , 1268 (1948).

19. L.D.Landau. Phys. Zs. Sovjetunion. 11 , 556 (1937).
20. J. Frenkel. Phys. Zs. Sovjetunion. 9 , 533 (1936).
21. V.Weisskopf. Phys. Rev. 52 , 295 (1937).
22. J.J.Griffin. Phys. Rev. Lett., 17 , 478 (1966).
23. G.D.Harp, J.M. Miller, B.J.Berne. Phys. Rev., 165 , 1166 (1968).
24. E.A.Uehling, G.E. Uhlenbeck., Phys. Rev., 43 , 552 (1933).
25. F.C.Williams. Phys. Lett. 31 B , 184 (1970).
26. C.K.Cline, M.Blann. Nucl. Phys. A 172 , 225 (1971).
27. T. Ericson. Advan. Phys. 9 , 423 (1960).
28. C.K.Cline. Nucl. Phys. A 193 , 417 (1972).
K.K.Gudima, G.A.Ososkov, V.D.Toneev. Nucl. Phys. (Russian) 21, 260 (1975).
29. E.Gadioli, L.Milazzo-Colli in Proceedings of the Europhysics Study Conference on Intermediate Processes in Nuclear Reactions. Plitvice Lakes. Yugoslavia. Lecture Notes in Physics. vol.22, Springer-Verlag, 1973.
30. M.Blann in Proceedings of the Europhysics Study Conference on Intermediate Processes in Nuclear Reactions. Plitvice Lakes, Yugoslavia. Lecture Notes in Physics, vol.22, Springer-Verlag, 1973.
31. E.Gadioli, E.Gadioli-Erba, G.Tagliaferri, J.J.Hogan. Phys. Lett. 65 B , 311 (1976).
32. C.Kalbach in Proceeding of II International School on Neutron Physics. Alushta, 1974, D3-7991, Dubna, 1974.
33. K.Seidel, D.Seeliger, R.Reif, V.D.Toneev. Elem. Part. and Nucl. Struct. (review article in Russian) 7 , 499 (1976).
34. N.Austern in Selected Topics in Nuclear Theory. IAEA, Vienna, 1963.
35. P.M.Matthews, I.Shapiro, D.Falkoff. Phys. Rev. 120 , 1 (1960).
N.Dresden. Rev. Mod. Phys., 33 , 265 (1961).
36. L.D.Landau, E.M.Lifshitz. Statistical physics. 1958.
37. J.K.Haviland. Methods in Computational Physics. Advances in Research and Application, 4 , 109 (1965).
G.A.Bird. Journ. of Fluid Mechanics, 30 , 479 (1967).
38. D.Thouless. The Quantum Mechanics of Many-Body Systems. N.Y.- London, 1972.
39. G.Bertsch, S.F.Tsai. Phys. Rev. C 11 , 1634 (1975).
G.Satchler et al. Nucl. Phys. A 245 , 189 (1975).
40. F.T.Kuchnir. Phys. Rev. 161 , 1236 (1967).
41. H.W.Bertini, G.D.Harp, F.E.Bertrand. Phys. Rev. C 10, 2472(1974).
42. V.E.Bunakov, M.M.Nesterov, N.A.Tarasov. Izvestia AN SSR (ser. phys.) (Russian), 41 , 2187 (1977).
V.E. Bunakov, M.M.Nesterov, N.A.Tarasov (to be published in Phys. Lett.).
43. V.E.Kolesnikov, V.L.Korotkih. Izvestia AN SSR (ser. Phys.) (Russian), 27 , 900 (1963).
44. K.Chen, Z.Fraenkel, G.Friedlander, J.R.Grover, J.M.Miller, J.Shimamoto. Phys. Rev. 166 , 949 (1968).
45. F.E.Bertrand, R.W.Peelle. Phys. Rev. C 8 , 1045 (1973).

Figure Captions

Fig.1. Harp-Miller-Berne model

Fig.2. Exciton model scheme

Fig.3. A scheme of present situation in nuclear reaction theory

Fig.4. Present situation in nuclear reaction theory including master equations for finite open systems

Fig.5. Typical case of intercomparison between different pre-equilibrium models predicting the absolute cross-sections (ref. / 30 /) for Fe target

Fig.6. Same as in Fig.5 for Bi target

Fig.7. Cross-section formation in time obtained by solving:
a) our master equations / 42 /,
b) HMB equations / 23 /

Fig.8. INC model spectrum of secondary protons with (dashed line) $\ell < K_a R_0$ criterion and without it (solid line).

Fig.9 Neutron spectra obtained by exact solution of master equations (solid line) and by modified INC with (dash-dotted) and without (dashed line) hole de-excitation

Fig.10. Inelastic proton spectrum for ^{209}Bi (p,p') case (E_p = 39 MeV). Solid line corresponds to experimental data of ref. / 45 / averaged over 4 MeV intervals. Dashed line is a result of our modified INC calculations.

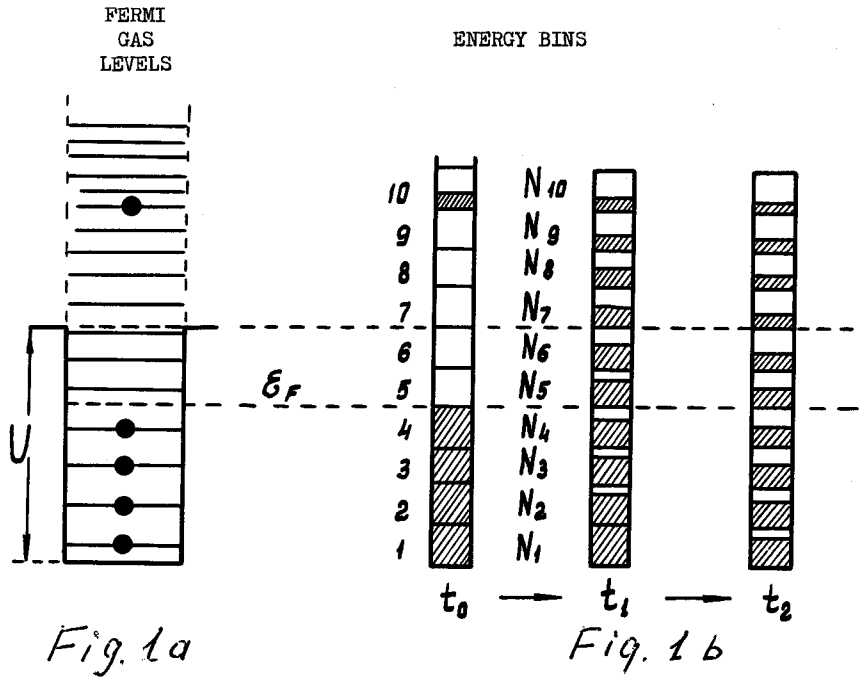

Fig. 1. Harp-Miller-Berne model

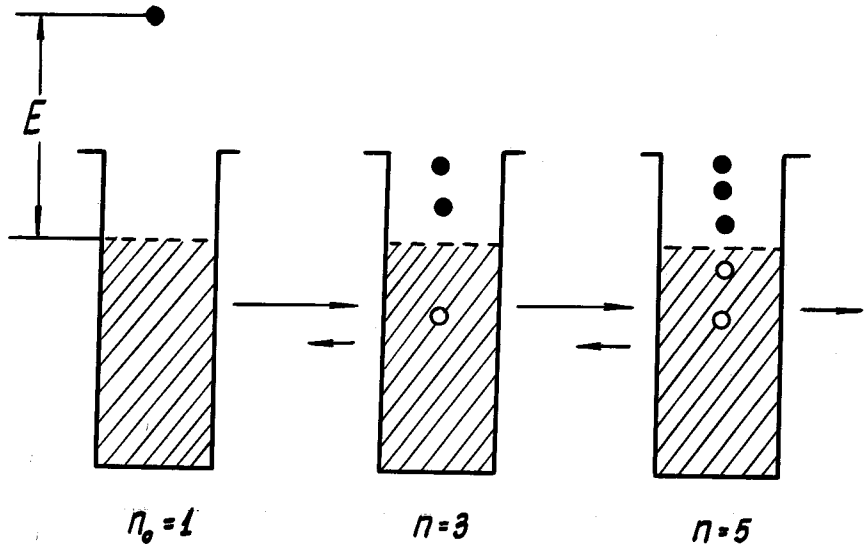

Fig. 2. Exciton model scheme

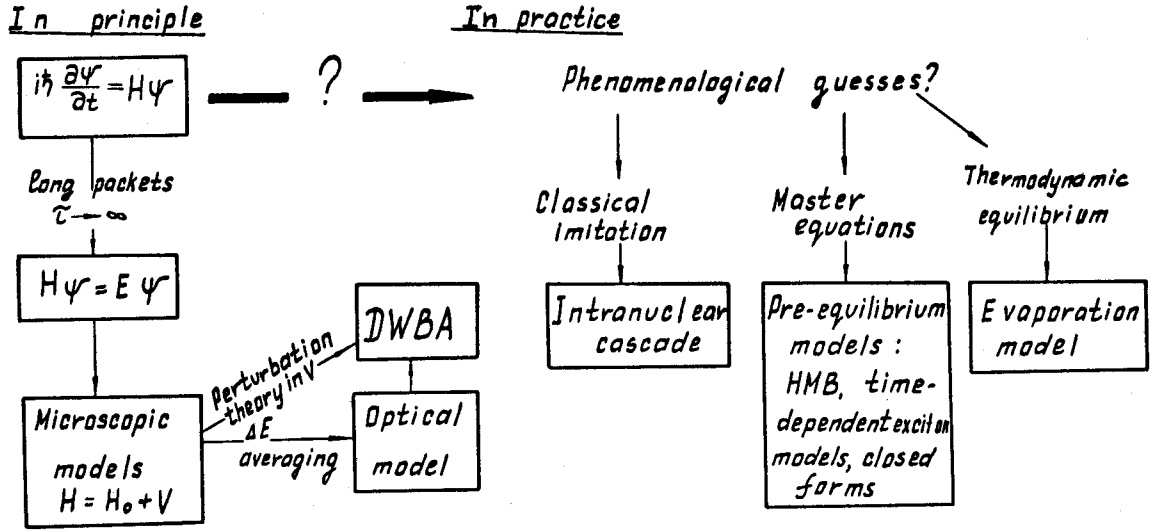

Fig.3. A scheme of present situation in nuclear reaction theory

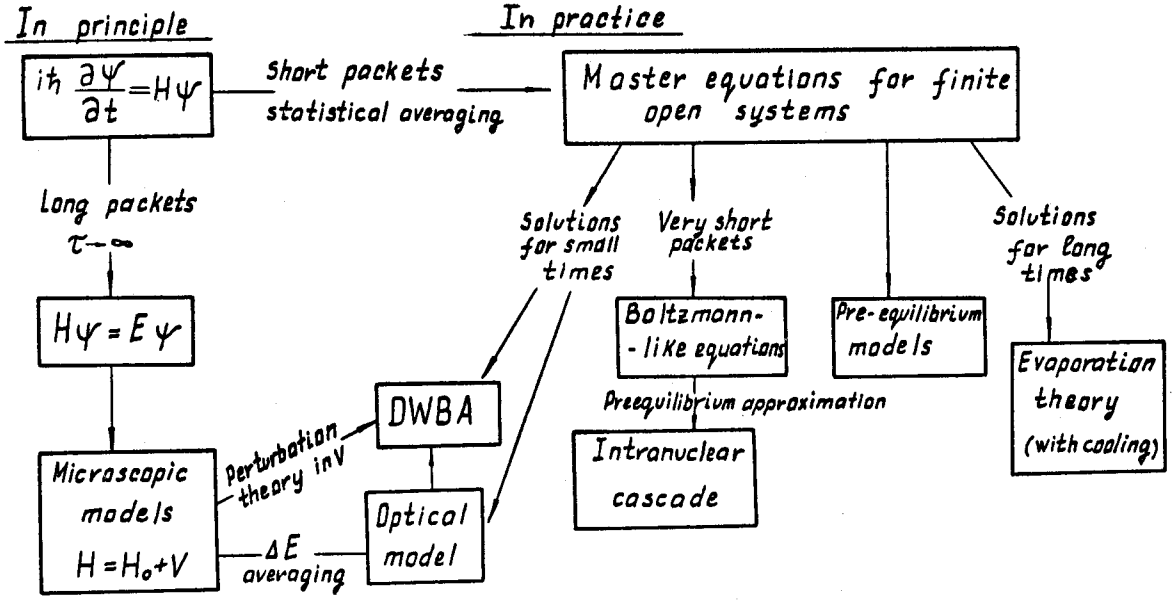

Fig.4. Present situation in nuclear reaction theory including master equations for finite open systems

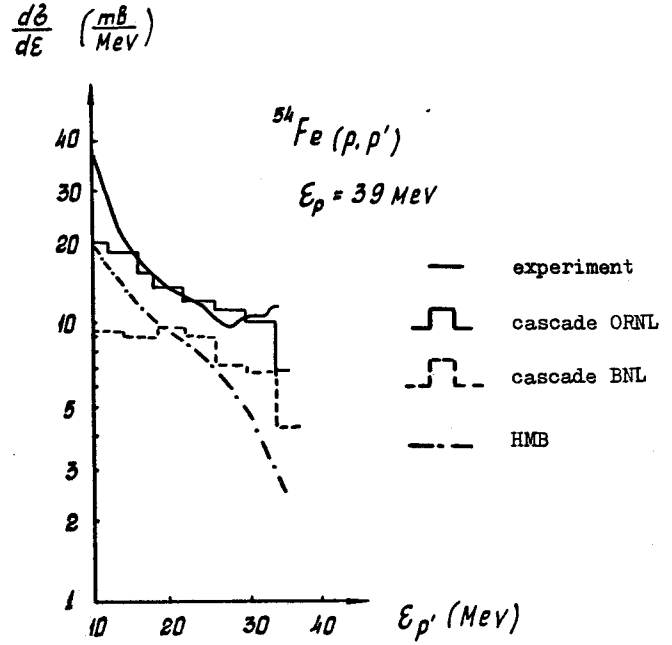

Fig.5. Typical case of intercomparison between different pre-equilibrium models predicting the absolute cross-sections (ref. / 30 /) for Fe target

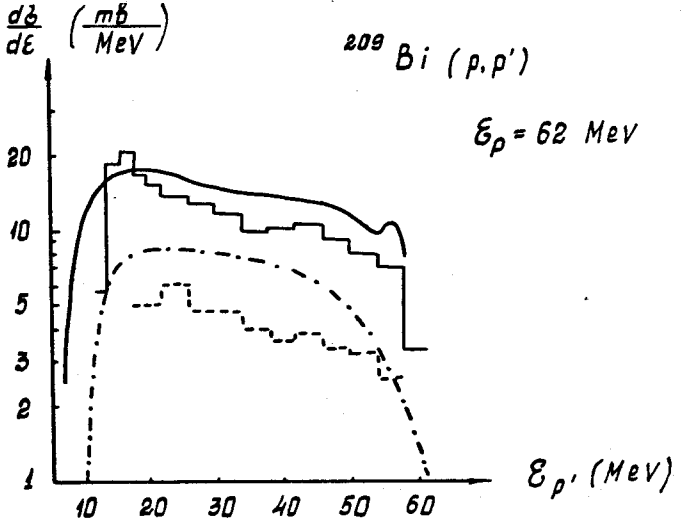

Fig.6. Same as in Fig.5 for Bi target

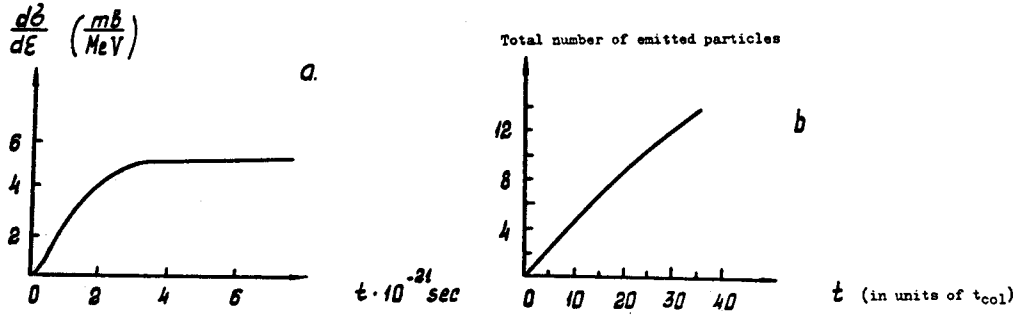

Fig.7. Cross-section formation in time obtained by solving:
a) our master equations / 42 /,
b) HMB equations / 23 /

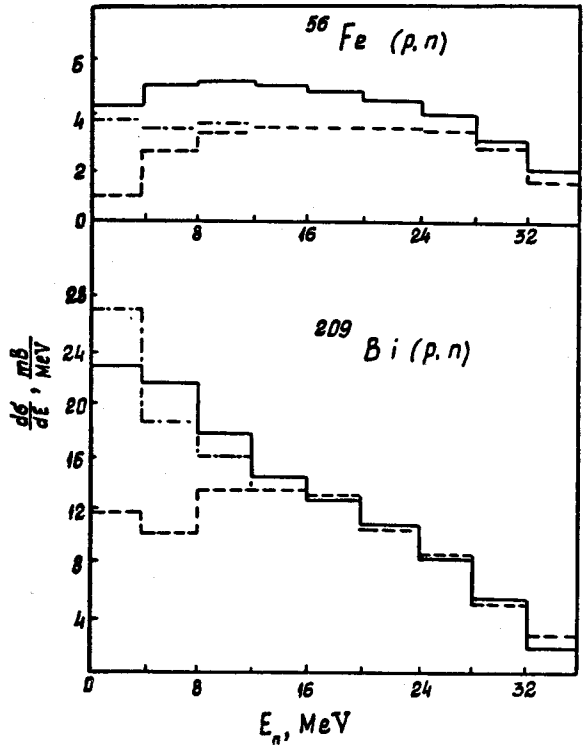

Fig.9. Neutron spectra obtained by exact solution of master equations (solid line) and by modified INC with (dash-dotted) and without (dashed line) hole de-excitation

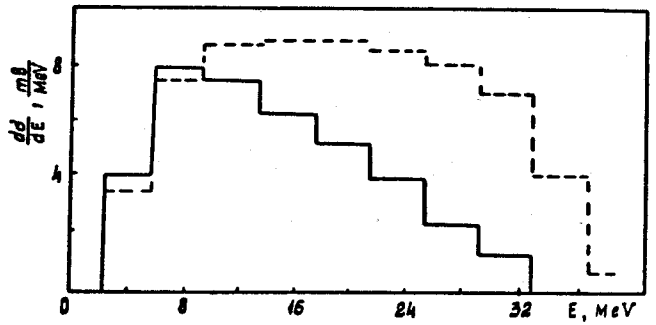

Fig. 8. INC model spectrum of secondary protons with (dashed line) $\ell < K_a R_o$ criterion and without it (solid line).

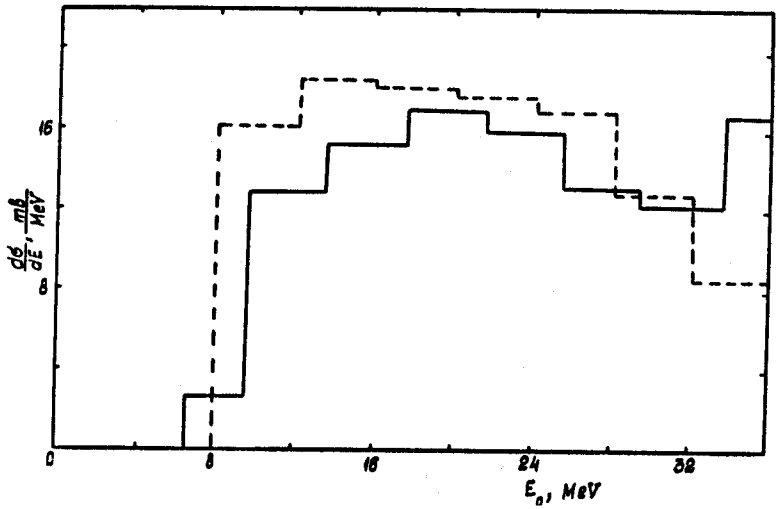

Fig.10. Inelastic proton spectrum for ^{209}Bi (p, p') case (E_p = 39 MeV). Solid line corresponds to experimental data of ref. / 45 / averaged over 4 MeV intervals. Dashed line is a result of our modified INC calculations

APPLICATION OF PRE-EQUILIBRIUM DECAY MODELS TO THE CALCULATION OF NEUTRON REACTION DATA

D. SEELIGER
Technical University Dresden,
Dresden,
German Democratic Republic

ABSTRACT

The basic assumptions of the concept of pre-equilibrium decay during the initial phase of nuclear reactions in the framework of the phenomenological exciton model are briefly reviewed. Recent approaches to the problem of angular distribution calculation are discussed.

1. INTRODUCTION

Pre-equilibrium emission of particles from highly excited compound systems during the initial phase of nuclear reactions seems to be an experimentally well established fact, independent of the kind of theoretical description of these processes. It is indicated by the smooth 'high energy tail' of emitted particle spectra as well as by the anisotropic forward-directed angular distributions of secondary particles. Assuming the formation of a long-lived compound nucleus, i.e. an equilibrated statistical system, the mentioned experimental behaviour cannot be understood. The only physically meaningful explanation is the assumption of occurrence of fast 'pre-equilibrium processes', i.e. nuclear reactions are finished before the statistical equilibrium in the compound system is reached.

The well established direct reaction theories for many years have been proved as a very useful tool for description of such pre-equilibrium reactions, in which isolated low-lying states of residual nuclei are excited. In the recent years, introducing suitable averaging procedures over single-particle excitations and involving multiple collisions, with these direct reaction theories was obtained also a good description of spectra and angular distributions in cases, when the residual nuclei are left in the continuum of states. However, in these cases two completely different reaction theories - the direct and the statistical reaction theory - have to be linked together for obtaining a satisfactory description of the complete experimental results. To overcome this situation, many attempts have been undertaken to generate a time-dependent description of the whole reaction process on a unique, more or less microscopic base. The most successful attempts in this direction, from the view-point of application for realistic cross section calculations, are made with comparatively simple phenomenological approaches to this problem, such as for instance

- the model of partial equilibrium (Bethe, Izumo),
- the exciton model (Griffin), and
- the Fermi gas equilibration model (Harp, Miller).

So far, the most intensive and successful application to calculations of neutron-induced reactions is coming from the exciton model (EM), including its different modifications. The present lectures therefore are mainly dealing with some aspects of these reaction models. Although the EM succeeds in predictions of fast neutron and other nuclear reactions, it represents a classical treatment of nuclear reactions only. The problems of quantuum-mechanical foundation of the EM are discussed in the lectures by Dr. Bunakov at the present course. Several comprehensive reviews have been published in recent years on the subject of EM and other pre-equilibrium models / 1 - 6 /. Interested people are directed to these reviews for more profound studies and for complete lists of references, whereas in the present paper only basic ideas and some recent results are discussed.

2. THE EXCITON MODEL

2.1. BASIC ASSUMPTIONS

In the EM nuclei are considered as a Fermi gas with a small two-particle residual interaction. Therefore, the excited states of nuclei can be classified by the number of particles p above plus the number of holes below the Fermi energy at a given excitation energy E. In the original formulation the angular momentum is not considered as a quantuum number, i.e. the information on angular distribution of emitted particles is lost.

Successive two-body residual interactions between particles p and holes h lead through a sequence of transitions with increasing average exciton number n=p+h to the statistical equilibrium state, where $n=\bar{n}=(gE)^{1/2}$ remains constant (see fig.1).

In every moment of this equilibration process there takes place a competition between the intranuclear transitions $n \rightarrow n+\Delta n$ to more or less complex states at the same excitation energy E and particle emission to the continuum. The EM includes the ad-hoc statistical assumption, that every partition of excitation energy for a given exciton number n occurs with equal probability during the equilibration process.

2.2. QUANTITATIVE FORMULATION

The most general quantitative formulation of the EM is given by the master equations (1), which describe the time evolution of the nuclear equilibration as a stochastic process of Kolmogorov - Chapman type:

$$\frac{\partial P(n,t)}{\partial t} = \lambda_+(n-2,E)P(n-2,t) + \lambda_-(n+2,E)P(n+2,t) - \left[\lambda_+(n,E) + \lambda_-(n,E) + \sum_i \Gamma_i(n,E)\right] P(n,t) \qquad (1)$$

Equation (1) connects the change of the occupation probability $P(n,t)$ of states with n excitons at the time t with the intranuclear transition rates $\lambda_{\Delta n}(n,E)$ for transitions $n \rightarrow n+\Delta n$ (where $\Delta n = 0, \pm 2$) and the emission probability $\Gamma_i(n,E)$ for particles of type i to the continuum from states with n excitons.

$\Gamma_i(n,E)$ is determined by the spectral emission probability $W_i(n,\epsilon)$ through

$$\Gamma_i(n,E) = \int_0^{E-B} W_i(n,\epsilon)\, d\epsilon \quad . \qquad (2)$$

The following notations are used for the occurring energies:

B_o, B_i - binding energies for incoming and emitted particles,
ϵ_o, ϵ - corresponding kinetic energies,
E, U - compound system and residual nucleus excitation energies.

They are connected by

$$E = \epsilon_o + B_o = \epsilon + B_i + U \; . \qquad (3)$$

The initial conditions for eq.(1) are given by

$$P(n, t=0) = \delta(n-n_o) \; , \qquad (4)$$

where n_o is the initial number of excitons immediately after the first residual interaction between incoming particle and the target nucleus. In a nucleon-induced reaction, neglecting pairing effects, should be valid $n_o = 3$, i.e. n_o is generally not to be considered as a free parameter of EM.

With P(n,t) from solution of the coupled differential eqs.(1) (one equation for every n) the instantaneous spectral emission rate $I_i(E,t)$ for particles of type i from pre-equilibrium states within time- and energy-interval t...t+ dt resp. $\epsilon \ldots \epsilon + d\epsilon$ is obtained as

$$I_i(\epsilon,t)\, d\epsilon\, dt = \sum_{n=n_o}^{\bar{n}} P(n,t)\, W_i(n,\epsilon)\, d\epsilon\, dt \; , \quad (\Delta n = 2) \qquad (5)$$

whereas the full pre-equilibrium spectrum, which is emitted during the equilibration time $t = 0 \ldots t_{eq}$, is given by

$$N_i(\epsilon)\, d\epsilon = \int_0^{t_{eq}} I_i(\epsilon,t)\, dt \cdot d\epsilon = \sum_{n_o}^{\bar{n}} W_i(n,\epsilon)\, t_n\, d\epsilon \; , \qquad (6)$$

where t_n is the life-time of n-exciton states determined as

$$t_n = \int_0^{t_{eq}} P(n,t)\, dt \quad . \qquad (7)$$

The absolute differential pre-equilibrium cross section $\sigma_{oi}^{PE}(\epsilon_o,\epsilon)$ can be easily obtained from $N_i(\epsilon)$ and the absorption cross section $\sigma_o^{abs}(\epsilon_o)$, which usually is calculated with the optical model :

$$\sigma_{oi}^{PE}(\epsilon_o,\epsilon) = \sigma_o^{abs}(\epsilon_o)\, N_i(\epsilon) \qquad (8)$$

For practical calculations with the aid of eqs.(1) the following physical quantities are needed:

- the density of n-exciton states w(n,E),
- the particle emission probability $W_i(n,\epsilon) = W_i(p,h,\epsilon)$,
- and the intranuclear transition probabilities $\lambda_{\Delta n}(n,E) = \lambda_{\Delta n}(p,h,E)$.

The first quantity usually is derived from a simple Boltzmann gas approximation, involving the additional quantum number n and assuming an equidistant spacing of single particle states, i.e. $g(\varepsilon) = g = \text{const}$. The statistical distribution function in this case looks like

$$Z_{ph}(\beta) = \sum_k \exp(\beta E_k) = (g/\beta)^{p+h}\; p!h! \;, \qquad (9)$$

with $\beta = (kT)^{-1}$. From this distribution function Ericson and Strutinsky derived the density function of n-exciton states $w(n,E) \equiv w(p,h,E)$

$$w(p,h,E) = g(gE)^{p+h-1}/p!h!(p+h-1)!, \qquad (10)$$

which is used in most cases. Working with EM, one should bear in mind, that application of the density function (10) leads to limitations of accuracy at low excitation energy, especially for lighter and near-magic nuclei. More realistic approaches take into account Pauli-principle and deviations from g=const., caused by shell and pairing effects.

The second value, $W_i(p,h,\epsilon)$, is given by the principle of detailed balance in the same way as in the well-known statistical theory of nuclear reactions. Special problems arise, if the emission of complex particles is considered. They are not discussed in the present paper.

Making the assumption of weak two-particle residual interactions between the nucleons, the probabilities $\lambda_{\Delta n}$ are obtained with the first order perturbation theory:

$$\lambda_{\Delta n} = (2\pi/\hbar)\, \langle |M|^2 \rangle\, w_f^{\Delta n}(p,h,E) \;. \qquad (11)$$

In (11) $w_f^{\Delta n}(p,h,E)$ describes the density of accessible final states for transitions $n \rightarrow n+\Delta n$ (with $\Delta n = 0, \pm 2$), which is less than the full density w(p,h,E), due to limitations by the selection rules of two-particle interactions. Since analytic expressions for $w_f^{\Delta n}$ are derived by Williams, the most critical value in eq.(11) is the average matrix element $\langle |M|^2 \rangle$ for intranuclear transitions. In some earlier works on EM the matrix element has been considered as a free, adjustable parameter for every case analysed. Later on, by systematic comparisons between experiments and calculations empirical functions in E and A have been evaluated. Using a function

$$\langle |M|^2 \rangle = k\, E^{-1}\, A^{-3}, \qquad (12)$$

with a constant factor $k \simeq 200\ \text{MeV}^3$, particle spectra and excitation functions can be calculated without any additional parameter adjustment. An independent way to determine $\langle |M|^2 \rangle$ consists of replacing $\lambda_+(1,0,E)$ by the collision rate λ_{coll} for the quasi-free moving incident particle. In that case λ_{coll} is obtained from considerations of nucleon-nucleon-scattering in nuclear matter or from the imaginary part of the optical potential. By choosing λ_{coll} reasonable agreement between experiment and EM calculations can be achieved without any free parameter [3].

2.3. SOLUTION OF MASTER EQUATIONS

From the application of EM we learned interesting features about the dynamics of nucleon-induced reactions. The main point is, that by the master eqs.(1) both pre-equilibrium and equilibrium emission spectra of neutrons, protons and other particles are described on a unique, phenomenologic basis, from which arises without any additional assumptions the division of reaction events in two, corresponding to the time-scale strongly different groups: a fast pre-equilibrium part dominated by particles emitted very early, mainly after one or two residual interactions only (usually these events are called direct reactions), and a compound nucleus part, which is growing up on a much longer time scale.

Really, on figs.2 and 3 the instantaneous and the full neutron spectra resulting from solution of (1) for a compound system with A=64 and E=96MeV or 24 MeV, respectively, are shown. In this case $\langle |M|^2 \rangle$ has been obtained from λ_{coll} in nuclear matter. The time increments indicated on the curves are equal to about 10^{-23} sec. The fast reaction component is emitted within about 400 time increments, i.e. in less

than 5.10^{-21} sec. The slow component needs between two and three orders of magnitude more time [3].
And so, starting from the time-dependent description of nuclear reactions by eqs.(1) in the framework of EM the resulting physical picture of the reaction process is not so different from that obtained by the alternative way, i.e. using direct reaction theory and statistical model calculations (including two-step direct processes). However, one should mention two differences: The EM in its present formulation does not include any collective excitation effects, which are known to be important for the excitation of low-lying residual levels. Differences should occur also at high incident and low emission energy of particles due to pre-equilibrium contributions from states of higher complexity in the range $n \geq 7$. Further careful comparative analyses of emission spectra at incident energies $\epsilon_0 > 20$MeV by the two alternative ways are needed to establish, whether really contributions from states with higher complexity are evident in the experimental spectra, supporting the EM description.

2.4. ANALYTIC APPROXIMATIONS TO THE MASTER EQUATIONS

It can be shown [3], that neglecting transitions with $\Delta n = 0$ and -2, i.e. assuming $\lambda_+ \gg \lambda_0 \gg \lambda_-$, simplified eqs.(1) have a simple analytic solution. Such assumption is valid only during the first residual interactions, consequently in this approximation only the pre-equilibrium emission is described. Indeed, for a compound nucleus the opposite condition $\lambda_+ = \lambda_0 = \lambda_-$ is valid.
The resulting pre-equilibrium particle spectrum becomes

$$N_i(\epsilon)\, d\epsilon = \sum_{\substack{n=\bar{n} \\ \Delta n=2}}^{n_0} W_i(n, \epsilon) \left[\frac{D(n)\ d\epsilon}{\lambda_+(n,E) + \sum_i \Gamma_i(n,E)} \right], \qquad (13)$$

where D(n) is the so-called depletion factor, which accounts for particle emission from less complex states.
By additional assumptions, such as $\lambda_+ \gg \sum_i \Gamma_i(n,E)$ and others, from (13) the widely used expressions of Blann and Williams are obtained. The 'hybrid model' of Blann [2] is also based on (13), but it entails additional assumptions, which are not inherent in the original EM: $W_i(n, \epsilon)$ is substituted by the emission probability $\lambda_i^c(\epsilon)$ of particles in the continuum and $\lambda_+(n,E)$ is replaced by $\lambda_{coll}(\epsilon + B_i)$, again only for the particles in the continuum.
Altogether, the overwhelming majority of applications of EM to neutron cross section calculations is based on analytic approximations to the master equations. This simplification is justified, due to the similarity of results from eq.(6) and (13), as shown on fig.4. However, spectra at low energy are not identical, but they differ up to 30% from each other. Moreover, using the analytic expressions one of the most appealing features of the EM is lost, the nuclear reaction process again has to be described by two completely different reaction theories (in the general case). Nevertheless this way of calculation of neutron cross sections, which is now widely used in computer programmes, presents a real progress in neutron data prediction in comparison with former calculations, which have been based on the statistical theory only. One of the most striking results in this sense have been recent calculations of (n,2n), (n,pn) and (n,np) cross sections taking into account pre-equilibrium emission [6,8] (see fig.5).

3. ATTEMPTS OF ANGULAR DISTRIBUTION DESCRIPTION

One of the most serious shortcomings of the original EM is the loss of information on angular distributions of emitted particles. In recent years a lot of attempts to overcome this difficulty have been published. Some of them are reviewed here briefly.

3.1. MIXED EM - DI - DESCRIPTION

Irie et al. [9] considered the pre-equilibrium emission spectrum by an analytic expression based on (13), but with emission rates $\lambda_c^{l_i}$ separately accounted for every orbital momentum l_i. Thus, energy distribution of emitted particles is calculated with EM, whereas the angular distribution is coming from the plane-wave Born approximation (PWBA), the simplest modification of direct reaction theory. Following this way, the double-differential pre-equilibrium cross

section $\sigma^{PE}_{oi}(\epsilon_o, \epsilon, \vartheta)$ is calculated with the formula

$$\sigma^{PE}_{oi}(\epsilon_o,\epsilon,\vartheta) = \sigma^{abs}_{o}(\epsilon_o) \sum_{l_i} \sum_{\substack{n=n_{\bar{n}} \\ \Delta n=2^o}} \sum_{\substack{J_= \\ I\mp I_o+s}}^{I+l_o+s} \sum_{I_R=0,1/2} H \cdot$$

$$\cdot \frac{\lambda^{l_i}_{c}(\epsilon)}{\lambda^{l_i}_{c}(\epsilon) + \lambda_+(n,E)} \cdot \frac{w(p-1,h,U,I_R)}{w(p,h,E,J_c)} \cdot \sigma_{PWBA}(\epsilon,\vartheta) \qquad (14)$$

where the PWBA cross section $\sigma_{PWBA}(\epsilon_o, \vartheta)$ determines the shape of the angular distribution

$$\sigma_{PWBA}(\epsilon_o,\vartheta) \sim (2l_i+1) \sum_{l} (l_o l_i 00 \,/\, 1\,0)\, j_l(QR) \,. \qquad (15)$$

H is a free normalisation factor.
In several cases with this approach a good description of experimental angular distributions of emitted neutrons has been obtained (see figs.6 and 7). From a physical point of view this 'hybrid' of two different models is not satisfying.

3.2. GENERALISATION OF MASTER EQUATIONS

Weidenmüller and Mantzouranis [10] introduced the information on scattering angle into the master equations (1). They assumed, that anisotropy of pre-equilibrium angular distribution is determined by the direction of motion of a 'leading particle'. States are characterized by n, E and the angle of leading particle $\vec{\Omega}$. Consequently occupation probabilities are also functions of three parameters $P = P(n,E,\vec{\Omega})$, and transition probabilities must include information on the angle of leading particle before and after the collision $\vec{\Omega}$ and $\vec{\Omega}'$ (i.e. only those transitions are selected, in which leading particle participates). Further it is assumed, that transition rates can be factorized in two functions

$$\lambda_{\pm}(n,E,\vec{\Omega} \to \vec{\Omega}') = \lambda_{\pm}(n,E) \cdot g(\vec{\Omega} \to \vec{\Omega}') \,, \qquad (16)$$

where function g does not depend on n.
The eqs.(1) without emission are changed to the following equations:

$$\frac{\partial P(n,t,\vec{\Omega})}{\partial t} = \int d\vec{\Omega}' \left\{ \lambda_+(n-2,E,\vec{\Omega}' \to \vec{\Omega}) \, P(n-2,t,\vec{\Omega}') + \lambda_-(n+2,E,\vec{\Omega}' \to \vec{\Omega}) \, P(n+2,t,\vec{\Omega}') \right\} -$$

$$- \int d\vec{\Omega}' \, P(n,t,\vec{\Omega}) \left\{ \lambda_+(n,E,\vec{\Omega} \to \vec{\Omega}') + \lambda_-(n,E,\vec{\Omega} \to \vec{\Omega}') \right\} \qquad (17)$$

With $P(n,t,\vec{\Omega})$, determined from (17), the double-differential cross section $\sigma^{PE}_{oi}(\epsilon_o, \epsilon, \vartheta)$ is derived through an expression, which is equivalent to (6):

$$\sigma^{PE}_{oi}(\epsilon_o,\epsilon,\vartheta) \sim \sum_{n_o}^{\bar{n}} W_i(n,\epsilon) \int_{o}^{t_{eq}} P(n,t^*,\vec{\Omega}) \, dt^* \qquad (18)$$

The used concept of one leading particle among all excited particles p is not inherent in the original EM, but it is similar to the 'philosophy' of the hybrid model. In several cases a satisfactory agreement with experimental angular distributions has been achieved.

3.3. IMPULSE AS ADDITIONAL QUANTUUM NUMBER

In an approach by Mädler and Reif (published in [7]), the states of compound system are characterized by quantum numbers n, E and the total impulse $\vec{P}$. The statistical sum of the Boltzmann gas (9) in this case includes a second term

$$Z_{ph}(\beta, \vec{v}) = \sum_{k} \exp\left[\beta E_k + \vec{v}\vec{P}_k\right] \,, \qquad (19)$$

which depends on the average velocity $\vec{v}$ and the impulse $\vec{P}$ of excitons. From the statistical distribution function the state density $w(p,h,E,p_{\parallel}, p_{\perp})$ is determined, which is now a function of the impulse components parallel and perpendicular to the direction of the incoming particle. Having state densities of the intermediate and final system, $w(p,h,E,p^{\parallel},0)$ and $w(p-1,h,U,p^{\parallel},p_{\perp})$ resp., the double-differential cross section $\sigma^{PE}_{oi}(\epsilon_o, \epsilon, \vartheta)$ is calculeted from one of the analytic expressions (13), completely remaining in the framework of the EM. There does not excist limitation for introduction of the extended state densities into eqs.(17). However, the additional splitting of the phase space generates serious restrictions on the applicability of statistical treatment.

Results, obtained with this approach are shown in figs.6 and 7. In the case ^{93}Nb (n,n') at E_n = 14 MeV this approach fails at backward angles, due to the limited number of 1p1h-states of the residual nucleus within the corresponding energy and impulse interval. A much better agreement is obtained for $^{27}Al(p,p')$ at higher incident energy E_p = 62MeV, demonstrating the adequacy of this approach.

3.4. DI - THEORY APPROACHES

A scheme of parametrisation for angular distributions of inelastic scattered neutrons based on the direct PWBA reaction theory linked with the Maxwellian evaporation theory was elaborated by Lukyanov et al. [11]. Roughly speaking, in this approach the shape of angular distributions is determined by σ_{PWBA} (15), calculated for single-particle transitions in the target nucleus within an averaging energy interval near $U = \epsilon_0 - \epsilon$, which corresponds to the experimental energy resolution. The energy dependence of the spectra is determined by a factor

$$(\epsilon / \epsilon_0)^{1/2} \cdot (\epsilon_0 - \epsilon) = (\epsilon / \epsilon_0)^{1/2} \cdot (U), \qquad (20)$$

which was obtained empirically by comparison with the shape of integrated (n,n')-spectra. (It is noticeable that this is not far away from the shape of the first and main term of the analytic EM spectrum, which is proportional to $\epsilon \cdot \sigma_{inv}(\epsilon)\ U$).
The absolute value of cross sections is determined by a normalization factor. In this way for many cases both double-differential and angular-integrated scattering cross sections have been parametrized and typical structures in the angular distributions could be connected with the quantuum numbers of a comparatively small number of transitions between shell model single-particle states.
Similar results have been obtained by Jahn [12].
A more rigorous DI-theory treatment by several groups is based on DWBA, one of them was elaborated by Reif [13]. In this case direct excitation of 1p1h states through two-particle residual interactions of Gaussian type $\sum_{i=1}^{A} v_{io}$ is calculated on an absolute base, starting from the wave functions for the ground state and excited states

$$/\ IM\pi U\ > = \sum_{p,h} c_{ph}^{I\pi}(U)\ /\ 1p1h\ IM\pi> + /c>. \qquad (21)$$

Calculated DWBA matrix elements

$$T_{fi}^{DWBA} = \sum_{p,h} c_{ph}^{I\pi}(U)\ (\chi_f^{(-)} / <(1p1h) IM\pi /\ \sum_{i=i}^{A} v_{io} / 0> \chi_i^{(+)}) \qquad (22)$$

are averaged over a suitable energy interval ΔU. Distorted waves result from an optical model analysis of the elastic scattering. Calculated double-differential cross sections for several cases investigated are in agreement with the experiment.
An application of multi-step direct reaction (MSDR) theory to the description of continuous spectra recently was presented by Tamura and Udagawa [14]. In this approach the excitation of both 1p1h and 2p2h states in the target nucleus, i.e. one-step and two-step direct two-particle excitation processes, have been taken into account. In fig.8 the obtained results for the reaction $^{208}Pb(p,n)$ at ϵ_0 =45 MeV are shown. It can be concluded, that the MSDR approach is in fact a rather powerful tool in describing cross sections with continuous spectra. The lower the energy of the outgoing particle and the larger the angle of observation, the larger is the relative contribution of the two-step processes. Nevertheless one may suspect that this approach can only fit the portion of spectra in which the outgoing particles still retain comparatively high energy. At lower emission energy contributions from more complex and compound nucleus processes are expected.

4. CONCLUSIONS

At present within the EM and DI-theory there exist several more or less founded approaches to the description of the high-energy

forward-directed products of fast neutron-induced nuclear reaction products, which are considered as a result of pre-equilibrium processes. The most detailed semi-microscopic description at present is achieved from the well established formalism of direct reaction theories, especially with the MSDR method. However, calculations of this kind are rather difficult and the principal physical drawback of this way is, that only the fast component of the reaction process is seized.

Within the framework of EM by the aid of the master equations (1) nuclear reactions are followed during the whole time scale, but on a simple phenomenologic base. Comparatively easily different reaction channels can be calculated, including processes, in which two or more particles are emitted. With the widely used analytic expressions of EM similar results for the pre-equilibrium part of cross sections as with the master equations are obtained, but the main advantage of the EM is lost.

As an open problem remains the quantum mechanical foundation of the EM and the creation of a microscopic unique theory of nuclear reactions.

REFERENCES

/1/ J.M.Miller, Proc.Int.Conf.Munich; ed.De Boer and Mang, Vol.2, p.597

/2/ M.Blann, Ann.Rev.of Nucl.Sci. Vol.25, 1975, 123-166

/3/ K.Seidel, D.Seeliger, R.Reif, V.D.Toneev
Particles and Nuclei, Richland, Vol.7, 1976, 499-552

/4/ C.Kalbach, Acta Phys.Slovaca Vol.25, 1975, 1oo-125

/5/ Proc.Vth Intern.Symp.on the Interactions of fast Neutrons with Nuclei, Gaußig, Nov.1975; ed.D.Seeliger, ZfK-324, 1976

/6/ Nuclear Theory in Neutron Nuclear Data Evaluation
Proc.Consultants Meeting, ICTP Trieste, Dec.1975, Vol.I+II
ed. IAEA-190, Vienna, 1976

/7/ Proc.VIIth Intern.Symp.on the Interactions of fast Neutrons with Nuclei, Gaußig, Nov.1977; ed.H.G.Ortlepp and D.Seeliger, ZfKreport 1978, to be published

/8/ A.Meister et al., Kernenergie Vol.20, 1977, 395

/9/ Y.Irie et al., Phys.Lett.Vol.26b, N.1, 1976, 9

/10/ G.Mantzouranis et al., Z.Physik A276, 1976, 145

/11/ A.A.Lukyanov et al., Journ.of Nucl.Phys.(Sov.) 21, 1975, 67

/12/ H.Jahn, p.315 in Vol.II of /6/

/13/ R.Reif, Kernenergie 20, H.6, 1977, 177

/14/ T.Tamura, T.Udagawa in Proc.Symp.on Neutron Cross Sections from 10 to 40 MeV, Brookhaven, 1977
ed.by M.R.Bhat and S.Pearlstein, BNL-NCS-50681, p.533

FIGURE CAPTIONS

Fig.1 Scheme of a nucleon-induced reaction in the framework of EM.

Fig.2 Instantaneous neutron spectra calculated fron (1) and (5) for a compound system with A=64 and excitation energy 96 MeV resp. 24MeV; the time increments are about 10^{-23}sec./3/.

Fig.3 As on fig.2, but spectra are integrated over the time.

Fig.4 Comparison between pre-equilibrium spectra shape resulting from (1) (solid line) and two analytic expressions by Blann (dash-dotted line) and Williams (dashed line), both based on (13).

Fig.5 Change of calculated (n,2n), (n,pn) and (n,np) cross sections taking into account pre-equilibrium emission by an analytic expression of EM; crosses - results obtained by the statistical theory only, points - results after accounting for pre-equilibrium emission /8/.

Fig.6 Comparison between experimental angular distributions of neutrons from the reaction ^{93}Nb(n,n') at ϵ_o=14.1 MeV with calculations based on the approach of Irie et al./9/ (dashed lines) and Mädler et al./7/ (solid lines).

Fig.7 As on fig.6, but for the reaction ^{27}Al (p,p') at ϵ_o = 62MeV.

Fig.8 Comparison of experimental angular distributions of neutrons from ^{208}Pb(p,n) at ϵ_o = 45 MeV with the results of the MSDR method /14/; dashed lines - one-step direct excitations, full lines - one-step plus two-step reactions.

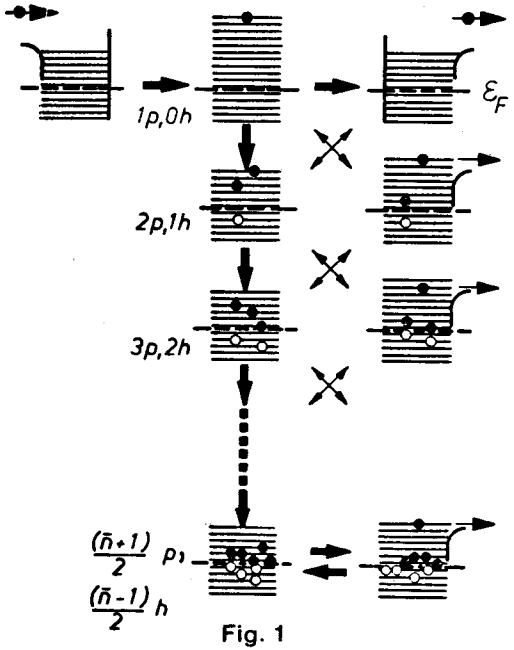

Fig. 1

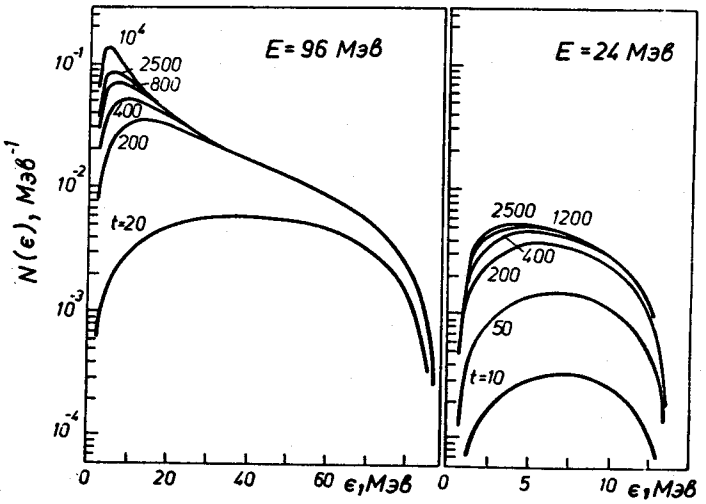

Fig. 3

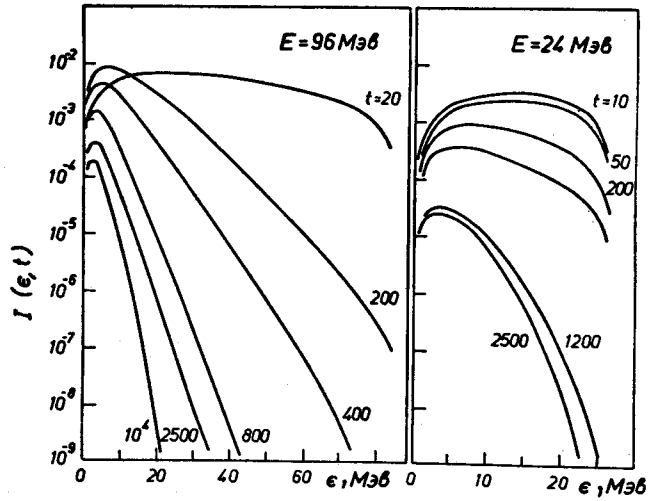

Fig. 2

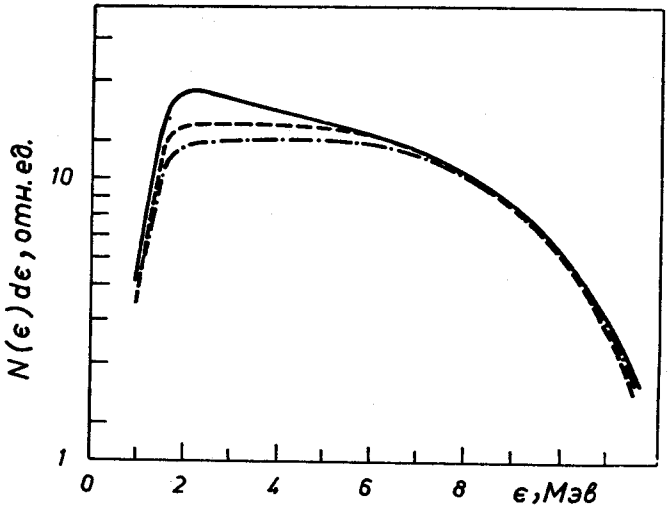

Fig. 4

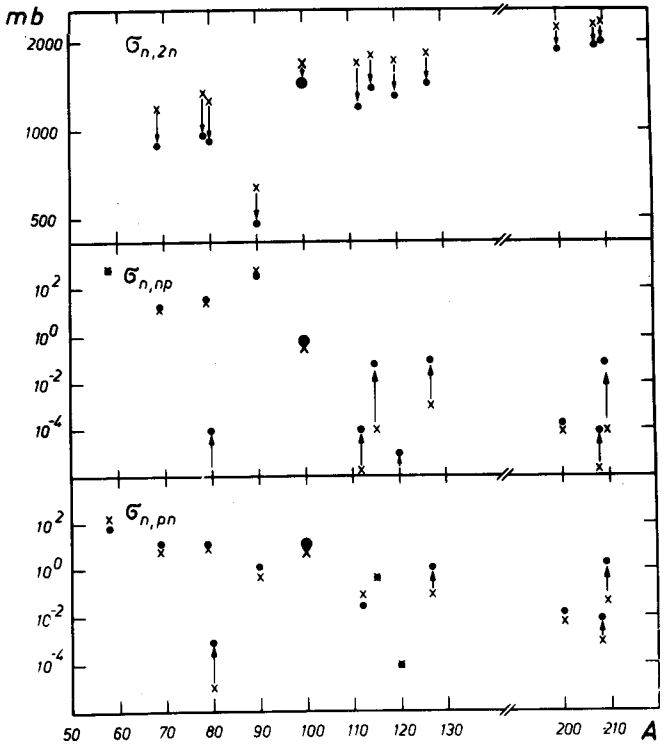

Fig. 5

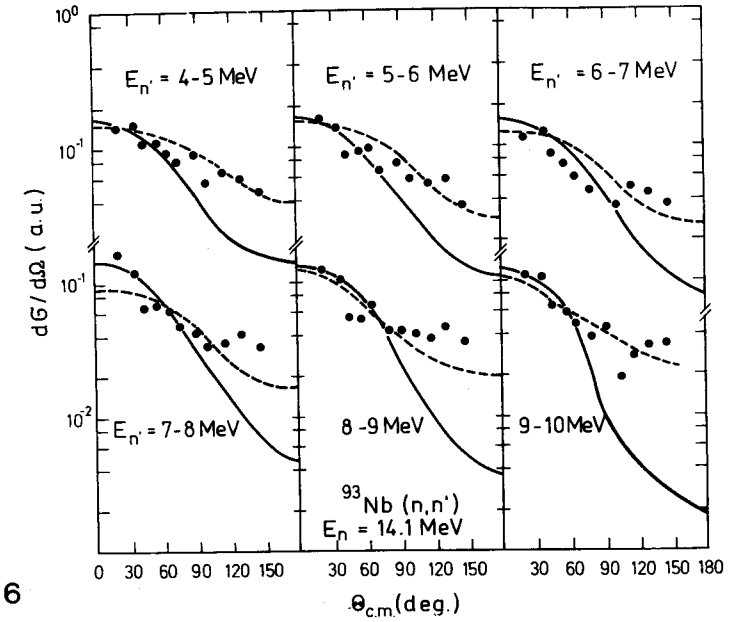

Fig. 6

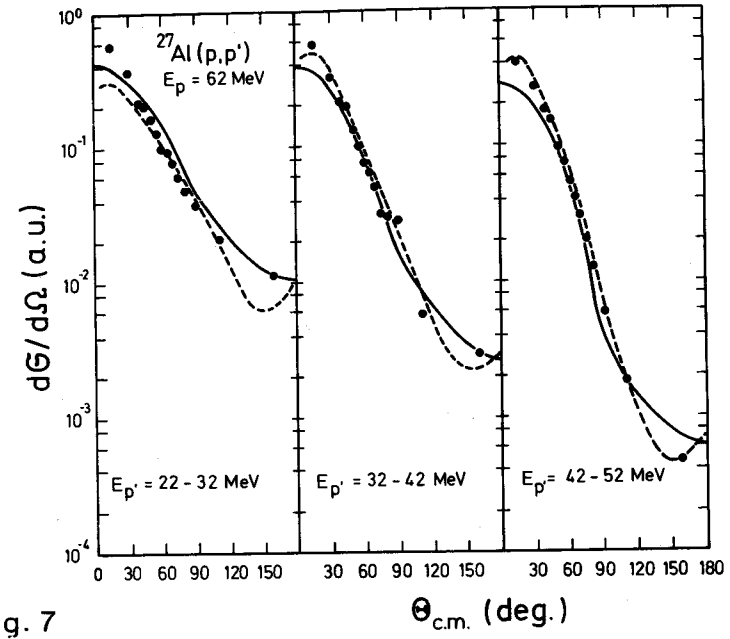

Fig. 7

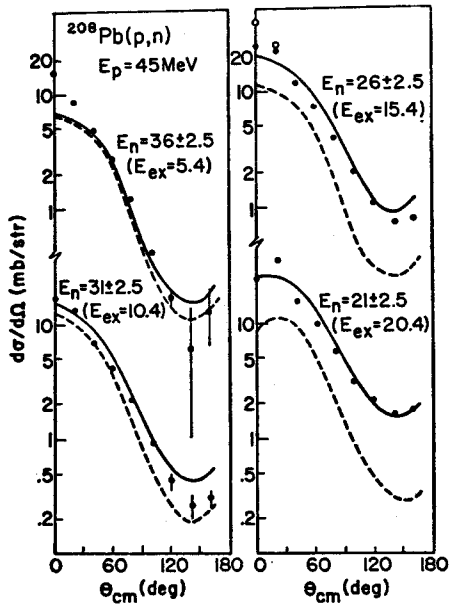

Fig. 8

ABSOLUTE VALUES OF INELASTIC NEUTRON SCATTERING CROSS-SECTIONS CALCULATED WITH ACCOUNT TAKEN OF THE PRE-EQUILIBRIUM MECHANISM

H. JAHN
Institut für Neutronenphysik und Reaktortechnik,
Kernforschungszentrum Karlsruhe G.m.b.H., and
Fakultät für Physik der Universität Karlsruhe,
Karlsruhe,
Federal Republic of Germany

Abstract

Absolute values of secondary energy-dependent inelastic neutron scattering cross sections can be calculated either with the master equation pre-equilibrium formalism of Cline and Blann or with Blann's more recent geometry-dependent hybrid model. The master equation formalism was used at Dubna and Dresden to reproduce experimental results for 14 MeV incident energy. The geometry-dependent hybrid model was used at Karlsruhe to cover for a number of materials the whole range from 5 to 14 MeV incident energy and to reproduce smoothed experimental spectra at 7.45 and 14 MeV. Only the geometry-dependent hybrid model accounts for scattering in the diffuse nuclear surface and thus for a certain average over the direct interaction. It is also free of any fit parameters other than those of the usual optical model. The master equation calculations, on the other hand, are based on nucleon-nucleon scattering cross sections inserted into the high-energy approximation of Kikuchi and Kawai for the intranuclear transition rate. Other approaches require either mass- or energy-dependent or more global fit parameters for a satisfactory reproduction of experimental results, but a genuine prediction of the incident-energy dependence of the inelastic neutron cross section, especially below 14 MeV, is needed for transport and shielding calculations for instance in connection with fusion reactor design studies.

1. Exciton master equation approach, achievements and shortcomings

1.1. Master equation

The first successful reproductions of energy distributions of nucleons emitted by excited nuclei were obtained by Griffin /1/ and Blann /2/ who applied phase space considerations to a sequence of steps of statistically treated particle-hole configurations. Cline and Blann /3/ extended this description to a more complete formalism by writing down a balance or master equation for the equilibrating compound nucleus. This master equation is still more or less the basis of various presently used models and codes for the calculation of spectra of inelastically scattered neutrons. We therefore briefly review this approach, starting with the master equation

$$\frac{dP(n,t)}{dt} = P(n-2,t)\lambda_{+}^{n-2,n} + P(n+2,t)\lambda_{-}^{n+2,n} - P(n,t)(\lambda_{+}^{n,n+2} + \lambda_{-}^{n,n-2} + \lambda_{c}^{n,n-1}) \quad . \tag{1}$$

Here $P(n,t)$ is the probability per unit time that n excitons are excited at time t. The exciton number n is the sum of particles and holes,

$$n = p + h \quad . \tag{2}$$

This excitation process developing step by step is illustrated by the following picture.

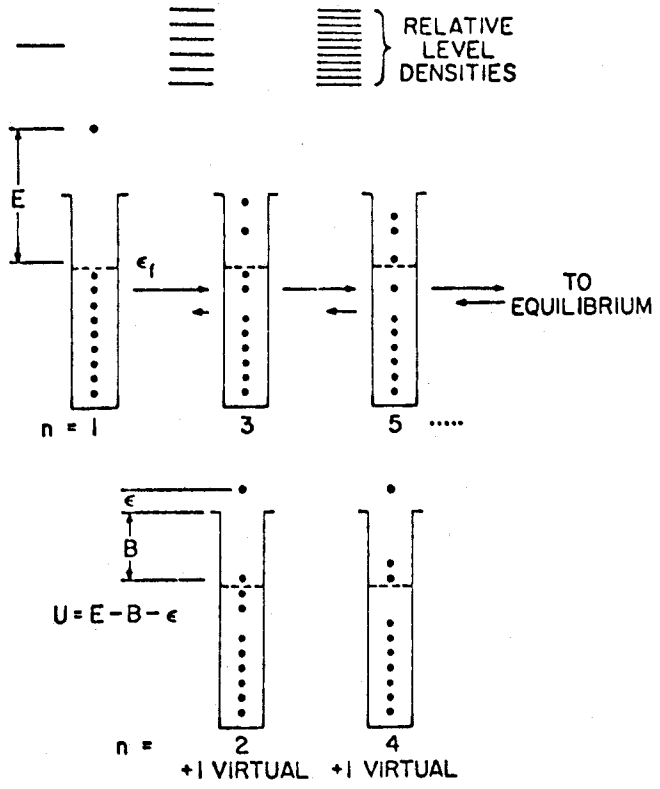

Fig. 1: Pictorial representation of the cascade equilibration process in the exciton model /4/.

Agassi, Weidenmüller and Mantzouranis /41/ showed how the master equation is related to the statistical theory of nuclear reactions. A different approach was developed by Bunakov (see Bunakov's lecture at this course).

The λ_+, λ_- in the master equation are the transition probabilities per unit time for an increase or decrease of the exciton number by one particle-hole pair while λ_c is the transition probability per unit time for the emission of a particle into the continuum from an n-exciton configuration.

If $w(n,\varepsilon)d\varepsilon$ is the probability for emission of a nucleon with an energy between ε and $\varepsilon+d\varepsilon$ from an n-exciton configuration then the total probability for emission of such a particle is given by

$$P(\varepsilon)d\varepsilon = \sum_n \int_0^\infty P(n,t)dt\, w(n,\varepsilon)d\varepsilon \,. \tag{3}$$

1.2. Closed-form approximation +)

Cline and Blann could show by full numerical calculation that the exact solution of the master equation can be approximated by

$$P(\varepsilon)d\varepsilon = \{C\, W(E,\varepsilon) + \sum_{n=n_0}^{\bar{n}} \tau_n\, w(n,\varepsilon)\}d\varepsilon \tag{4}$$

where τ_n is given by the expression

$$\tau_n = \frac{D_n}{\lambda_+^{n,n+2} + \lambda_-^{n,n-2}} \tag{5}$$

which shows that τ_n can be interpreted as the lifetime of an n-exciton state. D_n is the so-called depletion factor which still has to be determined, n_0 is the first-step exciton number - usually equal to 3 in the nucleon case - and $\bar{n}$ is the average exciton number when equilibrium is reached. Thus $\bar{n}$ is given by

$$\lambda_+^{\bar{n},\bar{n}+2} = \lambda_-^{\bar{n},\bar{n}-2} \,. \tag{5a}$$

The first term on the right-hand side of (4) is the equilibrium term with $W(E,\varepsilon)$ taken as the Weisskopf expression for the decay probability of an excited nucleus in equilibrium configuration /5/

$$W(E,\varepsilon)d\varepsilon = \sigma(E,\varepsilon)\frac{(2s+1)m\varepsilon}{\pi^2\hbar^3}\frac{\omega_B(U)}{\omega_A(E)}\,d\varepsilon \tag{6}$$

where s, m, ε are spin, mass and energy of the emitted particle.

The sum in (4) accounts for pre-equilibrium processes with $w(n,\varepsilon)$ chosen as the same Weisskopf expression, but now for the compound system in an n-exciton state instead of the equilibrium configuration. Thus (/2/, /4/, /5/)

$$w(n,\varepsilon)d\varepsilon = \sigma(E,\varepsilon)\frac{(2s+1)m\varepsilon}{\pi^2\hbar^3}\frac{\rho_{n-1}(U)}{\rho_n(E)}\,d\varepsilon \tag{7}$$

where $\rho_n(E)$ and $\rho_{n-1}(U)$ are the exciton state densities (number of states per energy interval) given by the Ericson expression /5a/

$$\rho_n(E) = \frac{g(gE)^{-1}}{p!h!(n-1)!} \tag{7a}$$

for the excitation energy E of the compound nucleus and the excitation energy U of the residual nucleus, corresponding to the state densities $\omega_A(E)$ and $\omega_B(U)$ of the target nucleus A and the compound nucleus B in Eq. (6). The quantity g is the single-nucleon level density at the Fermi energy. In both equations (6) and (7) $\sigma(E,\varepsilon)$ is the absorption cross section of the nucleon to be emitted. With the binding energy B of the emitted particle we have

$$E = U + \varepsilon + B \tag{8}$$

as indicated in Fig. 1. The transition probability per unit time $\lambda_c^{n,n-1}$ for emission into the continuum from an n-exciton configuration is then given by

$$\lambda_c^{n,n-1} = \sum_i \Big(\int_0^{E-B} w(n,\varepsilon)d\varepsilon \Big)_i \tag{9}$$

where the sum extends over all types of emitted nucleons (i = n or p). The depletion factor D_n of Eq. (5) can now be expressed as

$$D_n = \prod_{n'=n_0+2}^{n} \Big[1 - \sum_i \Big(\int^{E-B} w(n'-2,\varepsilon)d\varepsilon \Big)_i \Big] \,. \tag{10}$$

The cross section for inelastic neutron scattering is obtained by multiplication of the total emission probability $P(\varepsilon)d\varepsilon$ of Eqs. (3) or (4) with the neutron absorption (compound nucleus formation) cross section $\sigma(\varepsilon_0)$ for the incident energy ε_0,

$$\sigma(\varepsilon_0,\varepsilon)d\varepsilon = \sigma(\varepsilon_0)P(\varepsilon)d\varepsilon \,. \tag{11}$$

1.3. Intranuclear transition rates with fit parameters

The transition probabilities λ_+ and λ_- in the master equation (1) remain to be determined. They are often discussed in a form which was first derived by Williams /6/ from the golden rule for transition probabilities,

$$\lambda_+^{n,n+2} = \frac{2\pi}{\hbar}|M|^2\frac{g^3E^2}{n+1} \,, \qquad \lambda_-^{n,n-2} = \frac{2\pi}{\hbar}|M|^2 gph(n-2) \,. \tag{12}$$

Here $|M|^2$ is the absolute square of the corresponding matrix element averaged over initial and final exciton states of excitation energy E. The factors behind $|M|^2$ are the phase space averages of the Ericson expression (7a) over final exciton states (phase space averages for a finite potential depth have been calculated by Běták and Dobeš /6a/). From the equilibrium condition (5a) and from (12) one gets for large n (for which $p \approx h \approx n/2$)

$$\bar{n} \approx \sqrt{2gE} \,. \tag{13}$$

$|M|^2$ is frequently treated simply as a fit parameter. In this case only relative spectral shapes rather than absolute cross sections can be calculated. A more elaborate prescription for the determination of $|M|^2$ is due to Braga-Marcazzan, Gadioli-Erba, Milazzo-Colli and Sona /7/ who used the Fermi gas model. As a result of this analysis and on the basis of her own studies Kalbach-Cline /8/ has proposed the following mass number and energy dependence

$$|M|^2 = KA^{-3}E^{-1} \tag{14}$$

+) More detailed investigations about the master equation and its closed-form expression have been presented by Ribanský, Obložinský and Běták /42/.

which was also used by Strohmaier and Uhl /9/ for their own code STAPRE and by Young and Arthur /38/ for the code GNASH. The results of Kalbach-Cline for the constant K,

$$(15) \qquad K = \begin{cases} 95\ \text{MeV}^3 \pm 32\% & \text{for nucleon-induced reactions,} \\ 725\ \text{MeV}^3 \pm 36\% & \text{for } \alpha\text{-particle-induced reactions} \end{cases}$$

show such large fluctuations that Uhl /9/ considered K as an adjustable parameter.

1.4. Intranuclear transition rates, effort to calculate absolute values

Blann /10/ and Braga-Marcazzan et al./7/ attempted to remove all adjustable parameters and thus to obtain absolute cross sections. They write

$$(16) \qquad \lambda_+ = \rho v \langle\sigma\rangle$$

where ρ is the density of nucleons, v the particle velocity in nuclear matter and $\langle\sigma\rangle$ the effective cross section for an excited nucleon to interact with the other nucleons for which a Fermi gas momentum distribution is assumed. The average indicated by $\langle\ \rangle$ is taken over the free nucleon-nucleon scattering cross section with a method due to Goldberger /11/ and Hayakawa, Kawai and Kikuchi /12/ with the Pauli principle taken into account.

On this basis Gadioli, Gadioli-Erba and Sona /13/ calculated λ_+ for a truncated harmonic oscillator potential and for a square well, taking into account the finite potential depth not only for the exciton transition probabilities but also for the exciton state densities. For the harmonic oscillator well with 40 MeV Fermi energy at the center they found results which were only slightly different from those for the square well with 20 MeV Fermi energy. For the latter case their results are shown in Fig. 2.

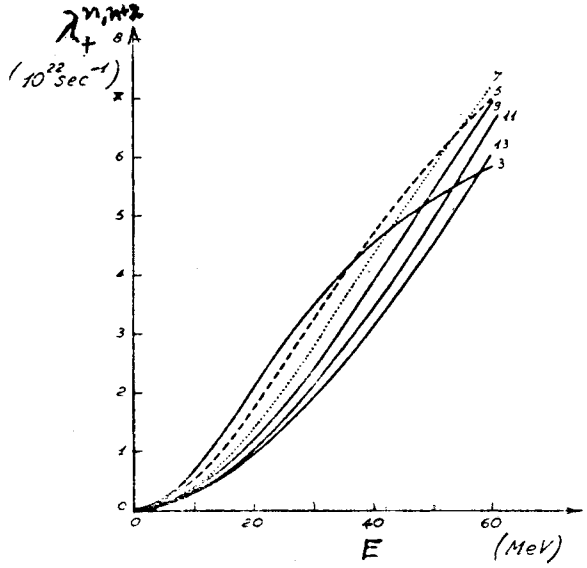

Fig. 2: Decay rates for the exciton-exciton interaction calculated in the framework of the Fermi gas model.

Fig. 2 shows a quadratic increase of $\lambda_+^{n,n+2}$ up to an excitation energy of 10 MeV and a linear increase above. This means that $|M|^2$ is independent of excitation below 10 MeV whereas above 10 MeV the energy dependence of Kalbach-Cline /8/ (see Eqs. (14), (15)) is confirmed.

In the case of the Fermi gas model and for a kinetic energy of relative motion higher than about 100 MeV $\langle\sigma\rangle$ can be represented by the following expression for a nucleon of type i (see /11/, /12/, /7/ and /13/),

$$(17) \qquad \langle\sigma(E+E_F)\rangle_i = \left[(A-Z)\bar{\sigma}_{ni}(E+E_F) + Z\bar{\sigma}_{pi}(E+E_F)\right]/A$$

where

$$(18) \qquad \bar{\sigma}_{ji}(E+E_F) = \sigma_{ji}(E+E_F)P(X); \qquad X = \frac{E_F}{E+E_F}$$

with

$$(19) \qquad P(X) = \begin{cases} 1 - \frac{7}{5}X & \text{if } X \leq \frac{1}{2} \\ 1 - \frac{7}{5}X + \frac{2}{5}X\,(2 - \frac{1}{X})^{5/2} & \text{if } X \geq \frac{1}{2} \end{cases}$$

and with the free nucleon-nucleon scattering cross section $\bar{\sigma}_{ji}$ which at the energy $E+E_F = mv^2/2$ can be represented as

$$(20) \qquad \begin{aligned} \sigma_{nn}(E+E_F) &= \sigma_{pp}(E+E_F) = (10.63\,\beta^{-2} - 29.92\,\beta^{-1} + 42.9)\text{mb} \\ \sigma_{np}(E+E_F) &= \sigma_{pn}(E+E_F) = (34.10\,\beta^{-2} - 82.2\,\beta^{-1} + 82.2)\text{mb} \end{aligned}$$

where $\beta = v/c$ and c is the velocity of light (Metropolis et al. /14/, see also /12/).

With the Fermi energy E_F, the excitation energy E and the incoming-particle velocity in nuclear matter

$$(20a) \qquad v = \sqrt{\frac{2(E+E_F)}{m}}$$

Gadioli, Gadioli-Erba and Sona /13/ were able to reproduce absolute values of secondary-energy-dependent (p,n) cross sections as well as excitation functions for a wide range of mass numbers ($89 \leq A \leq 169$) and excitation energies ($15\ \text{MeV} \leq E \leq 50\ \text{MeV}$) provided they reduced their λ_+ values generally by a factor 4 ± 1.

Gudima, Osokov and Toneev /15/ did not need such a reduction factor. These authors replaced $E+E_F$ in σ_{ji} and v by the relative kinetic energy

$$(21) \qquad T_n = \frac{8}{5}E_F + \frac{E}{n}$$

of the colliding particles in nuclear matter with n excitons and excitation energy E. Eq. (21) results from the so-called right-angle approximation. T_n is the sum of the mean kinetic energy of an excited particle (p)

$$(21a) \qquad T_n^{(p)} = E_F + \frac{E}{n}$$

and the kinetic energy of an intranuclear nucleon (N) averaged over the Fermi spectrum,

(21b) $$T_n^{(N)} = \frac{3}{5} E_F .$$

Gudima, Osokov and Toneev /15/ achieved a good reproduction of the absolute values of the secondary-energy-dependent cross sections for the reactions Ta(n,n') at 14.6 MeV, Cu(α,p)Zn at 43 MeV and Ta(p,n)Zn at 18 MeV incident energy. Absolute pre-equilibrium (n,n') cross sections at 14 MeV were calculated in the same way by Hermsdorf, Meister, Sassonov, Seeliger and Seidel /16/ in good agreement with experimental results in the mass range $30 \leq A \leq 200$. The absorption cross section σ in Eqs. (6), (7) and (11) was obtained from the optical model. No additional fit parameters were needed but a λ_0 term was added to the master equation with

(12a) $$\lambda_0^{n,n} = \frac{2\pi}{\hbar} |M|^2 g^2 E \frac{3n-2}{2} .$$

Tests for more incident energies below as well as above 14 MeV and additional secondary-energy-dependent cross sections for a wide range of mass numbers should be performed before the predictive power of the method can be judged conclusively. This seems necessary in particular because the approximations (17)-(21a) were originally derived for kinetic energies of the colliding particles above about 100 MeV, which means for incident neutron energies above about 55 MeV if we consider $E+E_F$ as a measure for the relative energy of the colliding particles. The applications just mentioned, on the other hand, were made for incident neutron energies well below 55 MeV. Meanwhile Toneev has created a new "cascade exciton model" which is explained in Seeliger's lecture at this course. This model is able also to describe the angular distribution of the secondary particles.

2. Hybrid model approach

2.1. Pure hybrid model

An alternative to the approximations (16)-(21a) for λ_+ has been obtained by Blann /17/ who used the method of Kikuchi and Kawai /12/ to get a binomial function for nucleon energies up to about 100 MeV with the result

(22) $$\lambda_+(\varepsilon) = \{1.4 \cdot 10^{21}\ \mathrm{MeV}^{-1}(\varepsilon+B) - 6 \cdot 10^{18}\ \mathrm{MeV}^{-2}(\varepsilon+B)^2\}\ \mathrm{sec}^{-1}$$

This expression depends on the energy ε of the emitted nucleon. This means that Eqs. (4), (5) and (7) can no longer be interpreted as a closed-form approximation to the solution of the master equation. Instead Blann /17/ used Eq. (22) to obtain a marriage between the exciton model and the Harp-Miller-Berne model /18/ (see Bunakov's lecture at this course). This marriage, called by Blann the "hybrid model", produces the following simple expression for the total pre-equilibrium emission probability for a nucleon with an energy between ε and ε+dε:

(23) $$P_{pr}(\varepsilon)d\varepsilon = \sum_{\substack{n=n_0 \\ (\Delta n=2)}}^{\bar{n}} \frac{p_n}{p} \frac{\rho_{n-1}(U) g}{\rho_n(E)} \frac{\lambda_c(\varepsilon)}{\lambda_c(\varepsilon)+\lambda_+(\varepsilon)} D_n d\varepsilon .$$

In this expression one has

(24) $$\lambda_c(\varepsilon) = \frac{(2s+1)}{\pi^2\hbar^3} \frac{m\varepsilon\sigma(\varepsilon)}{g}$$

from which it can be seen that the numerator of (23) is almost the same as in Eq. (4) upon insertion of (5) and (7). One can also show that λ_c is the familiar transition probability into the continuum. The Weisskopf estimate is

(25) $$\lambda_c = W_A \frac{\omega_c}{g}$$

with the compound nucleus formation probability

(26) $$W_A = \frac{\sigma v}{V} = \frac{\sigma}{V} \sqrt{\frac{2\varepsilon}{m}}$$

where V is the laboratory volume, $v = \sqrt{2\varepsilon/m}$ the particle velocity and σ the inverse absorption cross section. With the state density of the continuum corresponding to the laboratory volume V, viz.

(27) $$\omega_c = (2s+1) \frac{Vm^{3/2}}{\pi^2\hbar^3} \sqrt{\frac{\varepsilon}{2}}$$

and the single-nucleon level density g as given by (7a) one obtains in fact Eq. (24). Eq. (23) can be interpreted in the following way: The first factor in the sum is the fraction of nucleons of a given type (neutrons or protons) that is to be emitted. The second factor counts the number of allowed arrangements leading to emission into the secondary-energy interval between ε and ε+dε after scattering of the considered nucleon in the nuclear matter of the excited nucleus (with n excitons). Blann could show that the result of this counting for $n>5$ can be approximated by the result given by Ericson /5a/ or Williams /20/ for the n-exciton state density

(7b) $$\rho_n(E) = \frac{g(gE-\theta)^{n-1}}{p!h!(n-1)!}$$

with the constant single-particle level density g referring to an infinitely deep potential well, usually taken at the Fermi energy,

(7c) $$g = \frac{3A}{2E_F} .$$

The quantity θ is a correction term for the Pauli principle which could be neglected in all cases that have been investigated, and D_n in (23) is given by

(28) $$D_n = \prod_{n_0+2<n'<n}^{n} \left(1 - \sum_i \left\{ \int_0^{E-B} P_{n'}(\varepsilon)d\varepsilon \right\}_i \right)$$

where $P_{n'}(\varepsilon)d\varepsilon$ is the n-th sum term in (23) and the summation extends over nucleon types.

A successful reproduction of experimental emission cross sections for (α,p) reactions, integrated over angles but dependent on secondary energy, was obtained by Mignerey and Blann /4/ and by Chevarier et al. /21/ according to Eqs. (11), (23), (22), and (24) without any parameter adjustment except for n_0 (see Fig. 3).

2.2. Influence of nuclear surface diffuseness, ALICE and OVERLAID ALICE

Results for the angle-integrated secondary-energy-dependent cross section for the reaction $^{197}Au(p,p')$ are shown in Fig. 4 (from Ref. /22/). The calculated values obtained with the choice $n_0 = 3$ disagree very much with the measured

data. The choice $n_0 < 3$, however, appears quite unphysical unless we assume that at the nuclear surface one of the three excitons (a hole) is suppressed. Such an assumption can be understood in the framework of the Thomas-Fermi model,

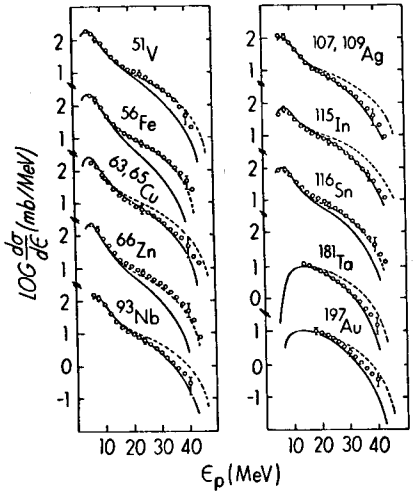

Fig. 3: Experimental and calculated (α,p) cross sections for 55 MeV incident α-particle energy (from Ref. /21/). The points represent experimental angle-integrated cross sections given as a function of secondary proton energy. The dashed lines are hybrid-model results with $n_0 = 4$, the solid lines with $n_0 = 5$. Equilibrium components are included in the calculated spectra.

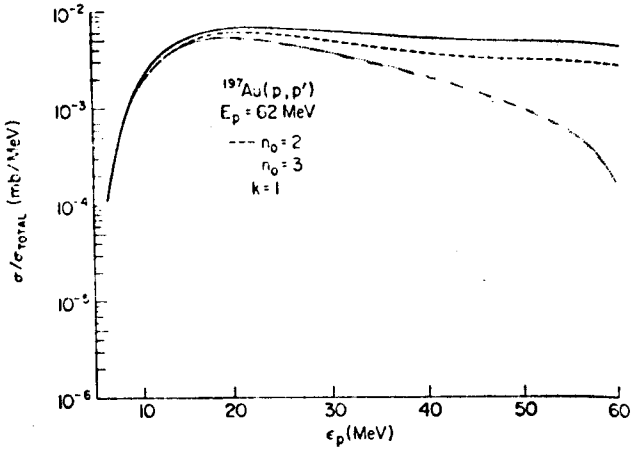

Fig. 4: Experimental and calculated $^{197}Au(p,p')$ cross sections for 62 MeV incident protons. Experimental results (Ref. /23/) are given by the solid curve, calculated results by the dashed line for $n_0 = 2$ and by the dotted line for $n_0 = 3$.

if the Fermi energy, as in the atomic case, is taken as decreasing with the nuclear density d(r) towards the surface according to

$$E_F(r) = \frac{\hbar^2}{2m}\left(\frac{3}{2}\pi^2 d(r)\right)^{2/3} \tag{29}$$

where the density follows the Fermi (or Woods-Saxon) distribution

$$d(r) = d_s\left(e^{(r-c)/z} + 1\right)^{-1} \tag{30}$$

with the nuclear half-density radius

$$c = c_0 A^{1/3}, \qquad c_0 = 1.07 \text{ fm}, \tag{30a}$$

the surface thickness

$$z = 0.55 \text{ fm} \tag{30b}$$

and the saturation density

$$d_s = \left(\frac{4\pi}{3} c_0^3\right)^{-1}. \tag{30c}$$

A reasonable way to account for the influence of the nuclear surface diffuseness can be obtained according to Blann /24/ by averaging along the particle trajectory taking the impact parameter

$$R_\ell = \ell\lambda \tag{31}$$

as the lower limit and the upper limit as

$$R_s = c + 5z \tag{32}$$

outside the nucleus where the density is practically zero. The quantities ℓ and λ in (31) are the orbital angular momentum quantum number and the de Broglie wave length,

$$\lambda = \frac{\hbar}{\sqrt{2m\varepsilon_0}}. \tag{33}$$

The averaged density is then defined by

$$d(R_\ell) = \frac{1}{R_s - R_\ell}\int_{R_\ell}^{R_s} d(r)dr. \tag{34}$$

Inserting this into the Fermi energy expression (29) one gets the geometry-dependent Fermi energy or potential depth

$$E_F(R_\ell) = E_F \cdot \left(\frac{d(R_\ell)}{d_s}\right)^{2/3} \tag{35}$$

where

$$E_F = \frac{\hbar^2}{2m}\left(\frac{3\pi^2}{2} d_s\right)^{2/3} \tag{36}$$

is the usual Fermi energy.

From the good results obtained without surface diffuseness for (α,p) reactions by Mignerey and Blann /4/ and Chevarier et al. /21/ with $n_0 = 4$ or 5 (see Fig. 3) and from the failure with $n_0 = 3$ in the case of $^{197}Au(p,p')^0$ (see Fig. 4) Blann /25/ concluded that only for $n_0 = 3$ (incident nucleons) must the surface diffuseness be taken into account because only then can an exciton acquire enough energy to sense the bottom of the potential well. In this way Blann /25/ found

$$(37)\qquad \rho_{1p1h} = gE_F(R_\ell), \qquad U > E_F(R_\ell);$$
$$\rho_{2p1h} = \frac{1}{4} g^2 E_F(R_\ell)\{2E-E_F(R_\ell)\}, \quad E > E_F(R_\ell).$$

The Ericson (7a) or Williams formula (7b) is used in all other cases.

In addition there is an influence of the surface diffuseness on the third factor in each sum term of Eq. (23): g in the expression (24) for $\lambda_c(\varepsilon)$ has to be taken as

$$(38)\qquad g(R_\ell) = \left(\frac{\varepsilon+B+E_F(R_\ell)}{E_F}\right)^{1/2} \frac{2N}{A} g$$

instead of (7c). Finally also the absorption and excitation rate $\lambda_+(\varepsilon)$ in the third factor of Eq. (23) can be affected by the surface diffuseness. This is the case if $\lambda_+(\varepsilon)$ is calculated from the imaginary part W(r) of the optical potential for neutron scattering according to

$$(39)\qquad \lambda_+^{(\ell)}(\varepsilon) = \frac{2W(R_\ell)}{\hbar} \quad \text{with} \quad W(R_\ell) = \frac{1}{R_s-R_\ell}\int_{R_\ell}^{R_s} W(r)dr \ .^{+)}$$

One can now calculate the pre-equilibrium component of the inelastic-scattering neutron cross section, integrated over emission angles but dependent on the secondary energy, by means of the Eqs. (23), (7b), (7c), (28), (31)-(39). These equations represent the hybrid model with surface diffuseness which was called by Blann the geometry-dependent hybrid model. Apart from general nuclear parameters such as nucleon numbers (N, Z, A), nuclear radius and surface thickness the model contains only the optical-model quantities W and σ(ε). In particular there are no additional fit parameters. Moreover, the geometry-dependent hybrid model is the only existing model that takes the diffuseness of the nuclear surface into account.

A computer code was developed by Blann /26/ on the basis of this model the first version of which was called ALICE /26/. In this code, as in Refs. /24/ and /25/, the expression

$$(40)\qquad g(R_\ell) = \frac{3A}{2E_F(R_\ell)}$$

was used instead of (38). This led to unrealistic results as described in Ref. /29/. The calculations of Hansen, Grimes, Howerton and Anderson (see Ref. /37/) were apparently based on Eq. (40) and therefore give too small pre-equilibrium components of the secondary-energy-dependent inelastic neutron-scattering cross section. Also our own first (n,n') calculations on ^{56}Fe and ^{238}U with the hybrid model code /26/ were only successful after re-introduction of a fit parameter /39/.

+) In (39) R_s is given by $R_s = r_o A^{1/3}+5a$ with $r_o = 1.32$fm and $a = 0.51+0.7(N-Z)/A$ which is somewhat different from (32).

This deficiency of ALICE was corrected in the version OVERLAID ALICE /27/ which was successfully applied to (p,p') reactions by Blann (see Ref. /4/) and to d-, ^{3}He- and ^{4}He-induced reactions by Bisplinghoff, Ernst, Machner, Mayer-Kuckuk and Jahn, Probst, Djaloeis, Davidson and Mayer-Böricke (see Ref. /4/).

Further applications to angle-integrated secondary energy distributions for the reactions $^{55}Mn(n,n')$, $^{56}Fe(n,n')$, $^{58}Ni(n,n')$ and $^{93}Nb(n,n')$ will be presented below (see Refs. /28/, /29/ and /30/).

2.3. Equilibrium component

Before comparison with experimental data is possible one has to add an equilibrium component to the pre-equilibrium expression (23). In ALICE and OVERLAID ALICE the Weisskopf evaporation formula is used. In our own calculations we used instead the more accurate angle-integrated Hauser-Feshbach expression for continuous channels,

$$(41a)\qquad \left(\frac{d\sigma(\varepsilon_0,\varepsilon)}{d\varepsilon}\right)_{eq} = \pi\lambda^2 \frac{\sum_\ell (2\ell+1)T_\ell(\varepsilon_0)\sum_{\ell'} T_{\ell'}(\varepsilon)\omega(\varepsilon_0-\varepsilon)/2}{\sum_{\ell''}\{\sum_{\nu'} T_{\ell''}(\varepsilon_0-U_{\nu'}) + \int_0^{\varepsilon_0-\varepsilon_c} T_{\ell''}(\varepsilon)\omega(\varepsilon_0-\varepsilon)d\varepsilon/2\}}$$

The neutron transmission coefficients T_ℓ were calculated with the Perey-Buck /31/ optical-model program and also used for the calculation of σ(ε) in Eqs. (11), (23) and (24). The density of residual excited states $\omega(\varepsilon_0-\varepsilon)$, with the excitation energy of the residual nucleus given by

$$(41b)\qquad \varepsilon_0-\varepsilon = \begin{cases} U & \text{for the continuum,} \\ U_{\nu'} & \text{for discrete levels,} \end{cases}$$

and ε_c being the continuum cut-off, was taken as

$$(41c)\qquad \omega(U) = \begin{cases} e^{(U-U_0)/T} & \text{for } U \le U_x \ , \\ \dfrac{e^{2\sqrt{a(U-\Delta)}}\, a^{3/2}}{12\sqrt{2c}\sqrt{(U-\Delta)^3}} & \text{for } U \ge U_x \ , \end{cases}$$

with

$$(41d)\qquad c/a = 0.0888\, A^{2/3}$$

and

$$(41e)\qquad a/A = (0.00917\ S + \begin{cases} 0.142 \\ 0.120 \end{cases}) \text{ MeV}^{-1} \text{ for } \begin{cases} \text{spherical nuclei} \ , \\ \text{deformed} \quad " \ . \end{cases}$$

The other constants in (41c)-(41e) are taken from tables presented by Gilbert and Cameron /32/ from whose work these level-density expressions were adopted in the HELENE program /33/.

2.4. Numerical results for inelastic neutron scattering

The final result ist obtained by adding equilibrium and pre-equilibrium components,

$$(42)\qquad \frac{d\sigma(\varepsilon_0,\varepsilon)}{d\varepsilon} = \left(\frac{d\sigma(\varepsilon_0,\varepsilon)}{d\varepsilon}\right)_{eq} + \left(\frac{d\sigma(\varepsilon_0,\varepsilon)}{d\varepsilon}\right)_{pr} .$$

The numerical results are presented in Figs. 5a-e for the target nuclei ^{52}Cr, ^{55}Mn, ^{56}Fe, ^{58}Ni and ^{93}Nb. The sum curves as well as the equilibrium and pre-equilibrium curves are plotted together with the experimental histograms. The incident energy in all these cases was $\varepsilon_0 = 14.6$ MeV. The histograms were obtained from experimental results by averaging over 1 MeV energy intervals of the scattered neutrons. In the case of ^{56}Fe the measurements were performed at Livermore /34/. The histograms for the other nuclei were obtained by angular integration of data measured at Dresden /35/ for angles of 40^o, 60^o, 90^o, 120^o and 150^o in the case of Cr and Nb, and for 52.9^o, 77.7^o, 89.9^o, 108.4^o and 131.1^o in the case of Mn and Ni. We carried out the angle integration after interpolating between the cross section data given at those angles with the help of

$$\frac{d^2\sigma(\varepsilon_0,\varepsilon,\theta)}{d\varepsilon d\Omega} = \sum_{\ell=0}^{5} a_\ell P_\ell(\cos\theta) , \tag{43}$$

The coefficients a_ℓ of the Legendre polynomials $P_\ell(\cos\theta)$ were determined by fitting the measured cross section values.

2.5. Discussion

The results given in Figs. 5a-5e show that the measured data are reproduced quite well by our calculations as far as the pre-equilibrium component is concerned. This is also true for the equilibrium component in the case of Fe, Cr and Mn, where the sum curve fits the experimental values over the whole range of secondary energies. For ^{58}Ni, however, the contribution of the (n,p) channels cannot be neglected in the Hauser-Feshbach denominator (eq. (41a)) as we have done. The Q-value for the (n,p) reaction is exceptionally low in this case. Therefore the calculated equilibrium part is too large compared with the measured data. On the other hand the relatively low negative Q-value of the (n,2n) processes for ^{93}Nb shows that these cannot be neglected as we did. The calculated equilibrium part in this case is too small. The completion of our calculations in this respect is underway.

2.6. Incident energy dependence

The data considered so far were obtained with 14.6 MeV neutrons. Below this incident energy there is a gap without data down to 8.56 MeV. Below the gap there are measurements again, performed at Oak Ridge between 4.19 and 8.56 MeV /36/. The gap must be filled by model calculations. Blann's geometry-dependent hybrid model appears to be a proper tool for this purpose because it yields absolute cross sections from the optical model alone without any undetermined parameters. A check against the data below the gap confirms the usefulness of the model: Fig. 6 shows calculated and measured cross sections for the reaction $^{56}Fe(n,n')$ as a function of residual excitation energy, for an incident energy of 7.54 MeV. Our model-calculated results are drawn as a smooth line through the fluctuating curve measured at Oak Ridge /36/. It can be seen that the calculated curve is close to an average of the measured values. This is at the same time a strong indication that the geometry-dependent hybrid model with Hauser-Feshbach term describes the dependence on incident energy of the angle-integrated, secondary-energy-dependent inelastic neutron cross section adequately. The model can therefore be used to close the gap, at least in the sense of averages over intermediate structure. For $^{56}Fe(n,n')$ this interpolation has been used to calculate the inelastic scattering cross section data which have been incorporated in the KEDAK library (see ref. /46/).

2.7. Direct component

Since especially the high-energy tails of the angle-integrated secondary spectra are quite well reproduced by our results it looks as if the direct scattering contribution is already included in Blann's geometry-dependent hybrid model.

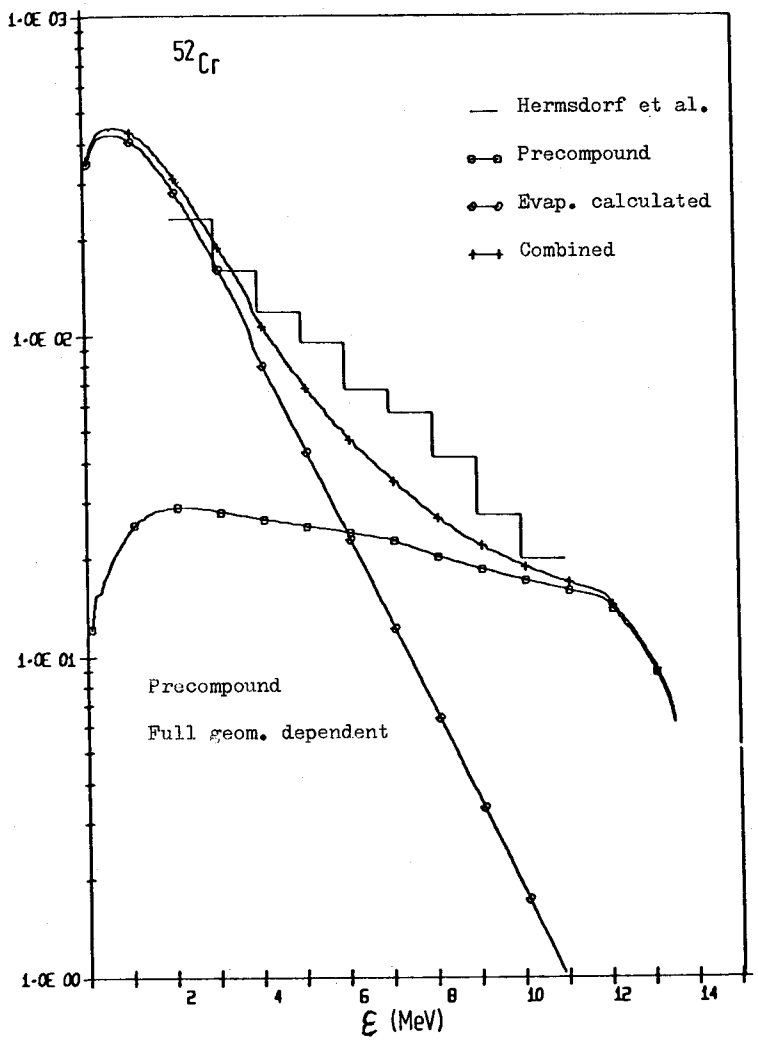

Fig. 5a: Angle integrated energy distribution of inelastic 14.6 MeV neutron cross section of ^{52}Cr.

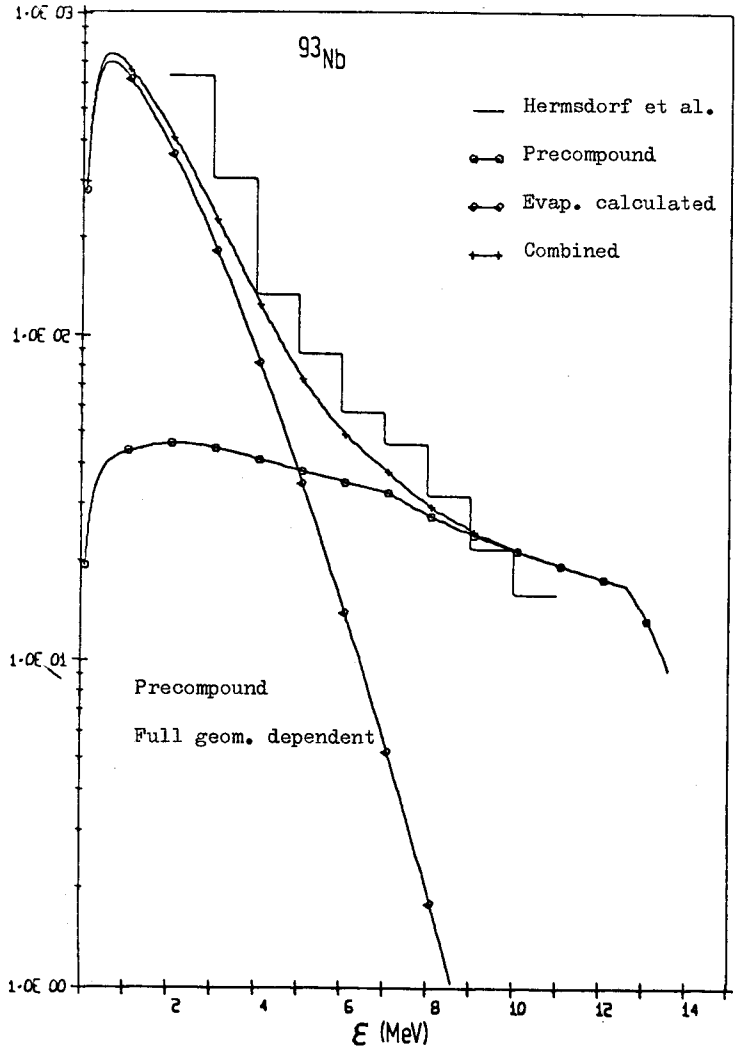

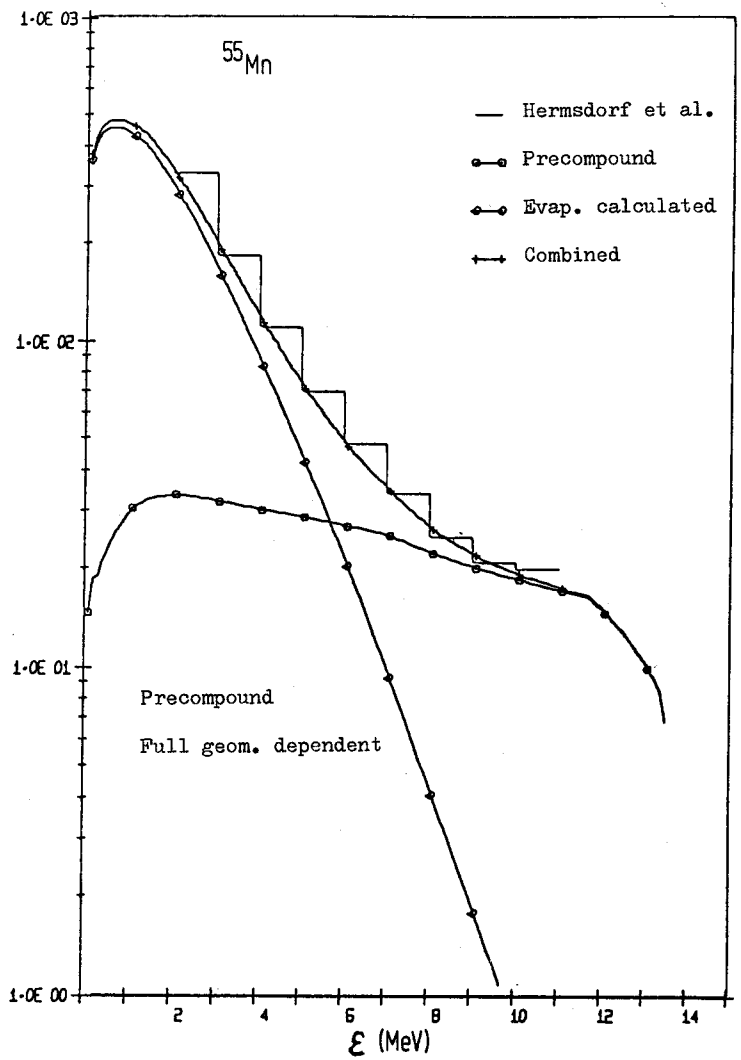

Fig.5b and c: Angle integrated energy distribution of inelastic 14.6 MeV neutron cross section of ^{93}Nb and ^{55}Mn.

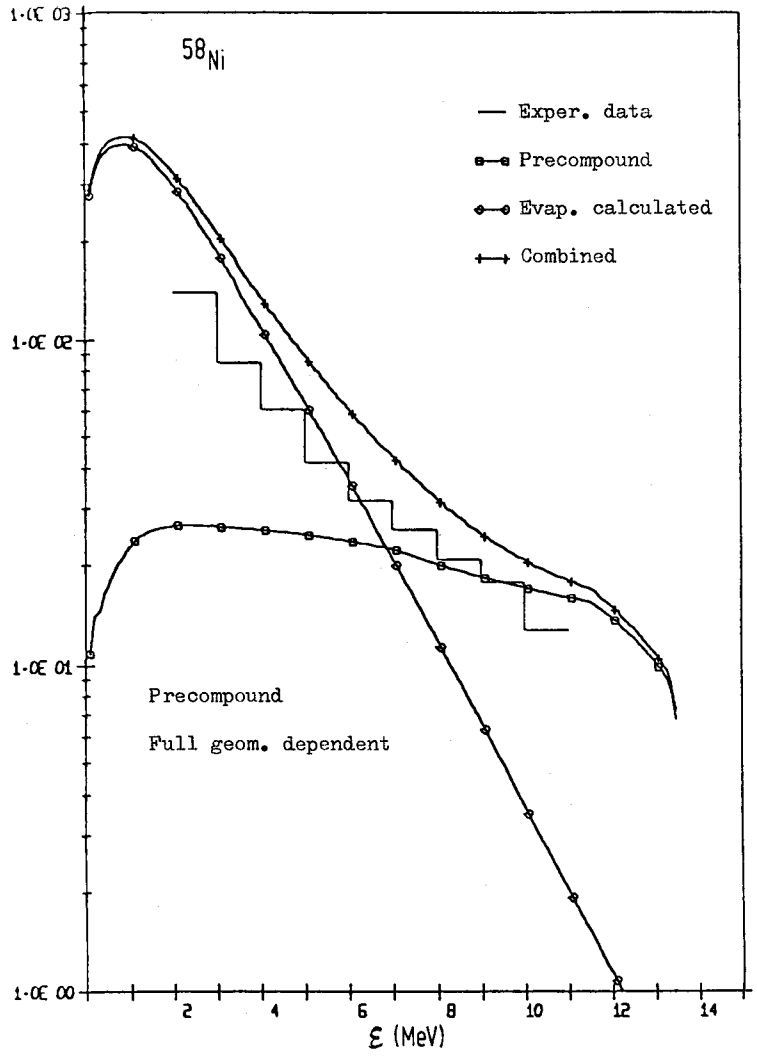

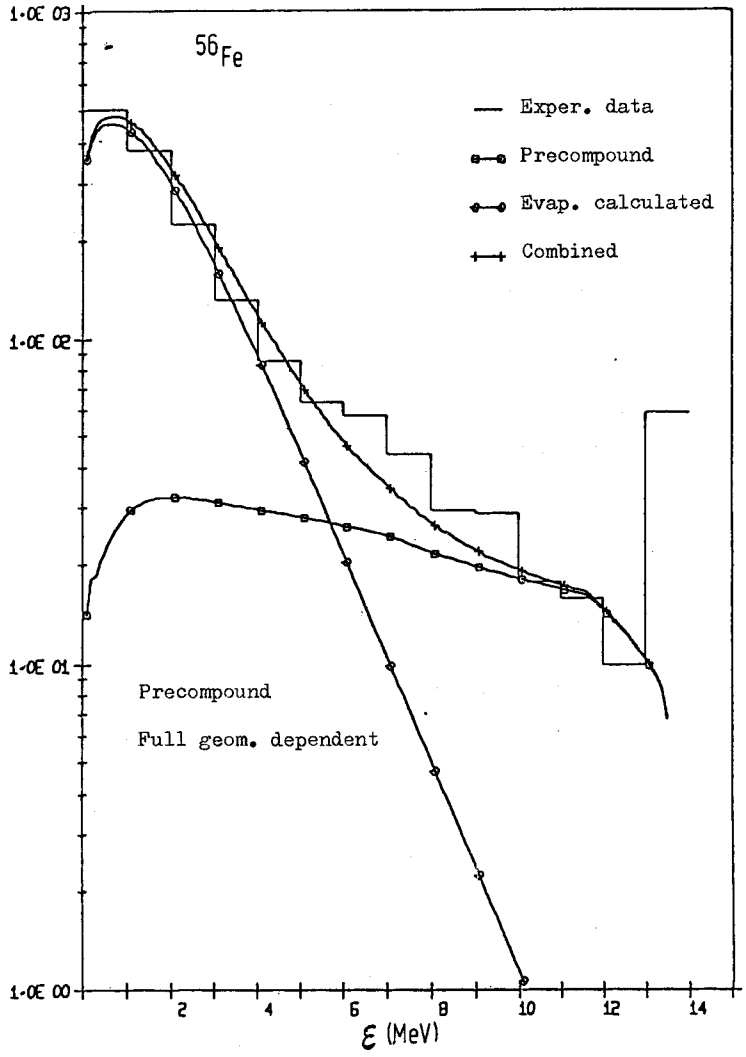

Fig.5d and e: Angle integrated energy distribution of inelastic 14.6 MeV neutron cross section of ^{58}Ni and ^{56}Fe.

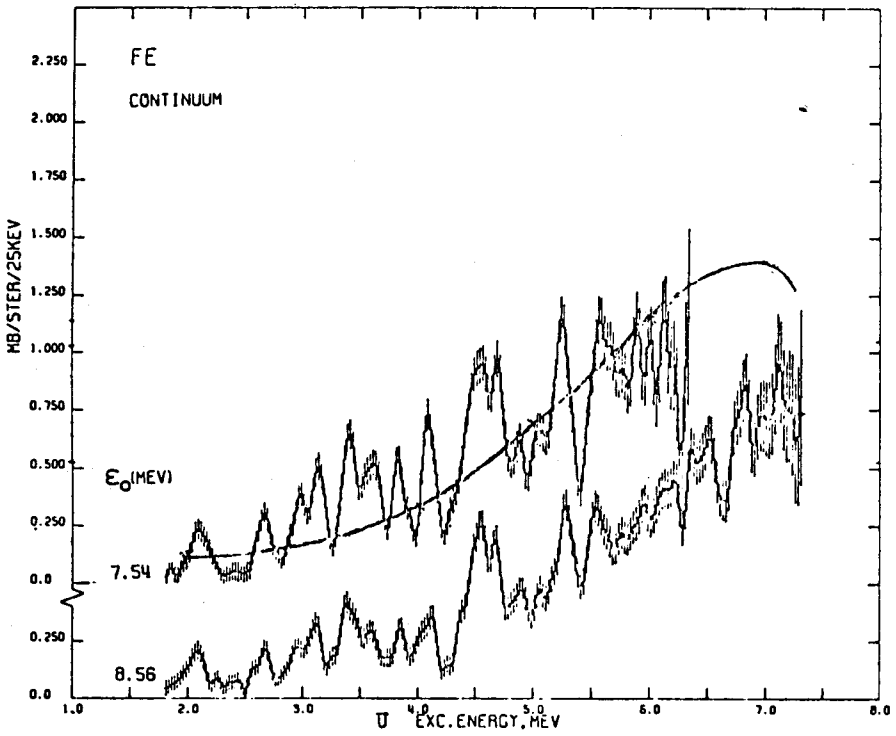

Fig.6: The angle-averaged continuum differential inelastic-scattering cross sections per 25 keV per atom of natural iron for the two contaminant-free sets of measurements of the Oak Ridge group /36/. The solid line represents the results of our calculations.

This point was discussed in a previous paper /29/. Actually, for the case of nucleon-induced reactions, Blann interprets the lowest-order ($n_0 = 3$) contribution from three-exciton pre-equilibrium states as a direct component in the geometry-dependent version of his hybrid model. We have tested this interpretation by checking whether the angular distribution of the high-energy tail (energy averaged over 1MeV intervals as before) can be described on this basis. For this purpose we have written down the energy- and angle-dependent differential cross section as composed of three components,

$$(44) \qquad \frac{d^2\sigma(\varepsilon_0,\varepsilon,\theta)}{d\varepsilon d\Omega} = \frac{1}{4\pi}\left(\frac{d\sigma(\varepsilon_0,\varepsilon)}{d\varepsilon}\right)_{eq} + \frac{1}{4\pi}\left(\frac{d\sigma(\varepsilon_0,\varepsilon)}{d\varepsilon}\right)_{n\geq 5} + \left(\frac{d^2\sigma(\varepsilon_0,\varepsilon,\theta)}{d\varepsilon d\Omega}\right)_{dir} .$$

The equilibrium component is considered as isotropic as well as the pre-equilibrium component from states with more than three excitons. The third component, however, is considered as the direct component, and consequently we choose for it the angular dependence given by the plane wave Born approximation,

$$(45) \qquad \left(\frac{d^2\sigma(\varepsilon_0,\varepsilon,\theta)}{d\varepsilon d\Omega}\right)_{dir} = F(\varepsilon_0,\varepsilon)\sqrt{\frac{\varepsilon}{\varepsilon_0}}\,(2\ell'+1)\sum_L C_{\ell\ell'}(L0,00)\,j_L^2(QR)$$

where $Q = |\vec{k}_0 - \vec{k}|$ is the absolute value of the momentum transferred to the target nucleus (in units of $\hbar$), the $j_L(QR)$ are spherical Bessel functions and the $C_{\ell\ell'}$ are Clebsch-Gordan coefficients. The factor $F(\varepsilon_0,\varepsilon)$ is determined by equating the angle-integrated direct part with the 3-exciton contribution of the geometry-dependent hybrid model according to

$$(46) \qquad \int d\Omega \left(\frac{d^2\sigma(\varepsilon_0,\varepsilon,\theta)}{d\varepsilon d\Omega}\right)_{dir} = \left(\frac{d\sigma(\varepsilon_0,\varepsilon)}{d\varepsilon}\right)_{n=3} .$$

The results are shown together with the measured angular distributions of the Dresden group /35/ in Fig. 7. Since many 2^+ states of ^{56}Fe are excited in the considered energy intervals we have put $L = 2$ for this rough test. In view of the approximations made the agreement is quite satisfactory. The lowest-order term in Blann's exciton expansion appears in fact to be responsible for the direct-reaction contribution. It is emphasized once more that our results with the geometry-dependent hybrid model were obtained, without any fit parameters, exclusively from conventional optical-model information. This remarkable success encourages further refinement of the model. The occurence of direct processes as indicated by Eqs. (44)-(46) and Fig. 7 can also be seen from recent work by Feshbach /40/. Also the similarity of the averaged spectral shape of DWBA - with geometry-dependent hybrid results at 90° scattering angle and 17 MeV incident energy which was found for the $^{116}Sn(p,p')$-process by Arndt and Reif /43/ supports his concept.
In contrast to the above outlined concept the direct component has been treated by Lukyanov, Salnikov and Saprykin /44/, by Fu /45/ and in ref. /28/ as unrelated to the pre-equilibrium component. While the pre-equilibrium compoent is completely omitted in the evaporation + DWBA-fit of Lukyanov et al. /44/ it has been shown very clearly by Fu /45/ that the experimental Livermore spectrum of Fig. 5e cannot be reproduced by absolute Hauser-Feshbach + DWBA-calculations alone unless a pre-equilibrium component is added. Fu has done it by fitting Blann's first exciton estimate /2/. As the other way around the pre-equilibrium component has been calculated absolutely using the pure hybrid model in ref. /28/ and the experimental energy spectral shape of Fig. 5e could very well be reproduced using in addition a PWBA-fit of the Dresden experimental angular distribution.

Acknowledgement

The author wants to express his best gratitude to his collegue Dr. F. Fröhner for much help by reading and preparing the manuscript. Informative discussions with Dr. D. Rusch are also gratefully acknowledged.

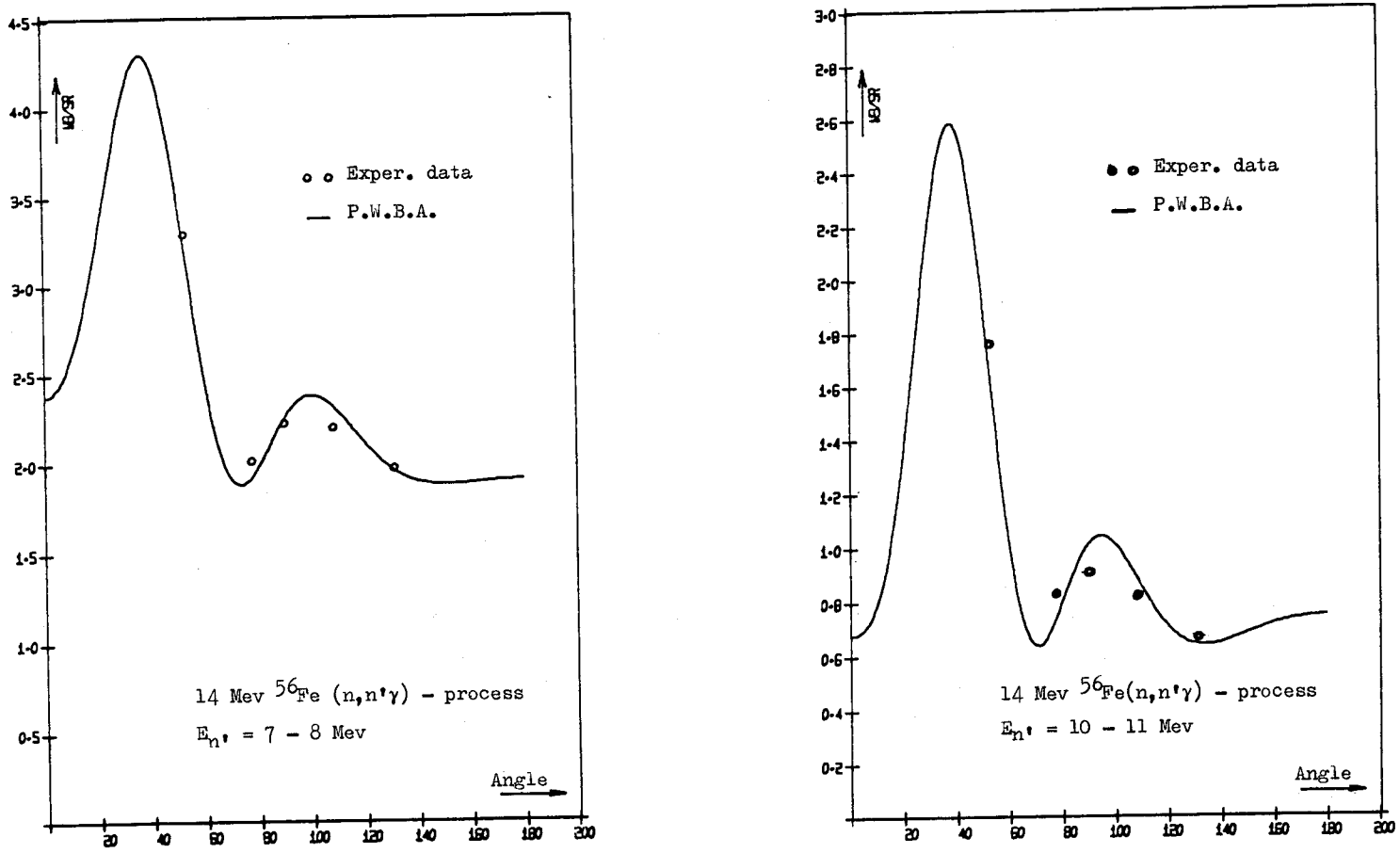

Fig.7: Angular distribution of 14 MeV neutrons scattered inelastically on ^{56}Fe. The curves represent a PWBA distribution with equilibrium + $n \geq 5$ pre-equilibrium background where the angle-integrated PWBA component is equated with the $n_o=3$ component of the geometry-dependent Hybrid model.

References

/1/ Griffin,J.J., Phys. Rev. Lett. 17,478 (1966); Int. Nucl. Phys. Conf., 1966, Gatlinburg Tenn. ed. R.L. Becker p.778, New York Academic; Intermediate Structure in Nuclear Reactions, ed. H.P. Kennedy, R. Schrils, Lexington: Univ. Kentucky Press, 219 pp. Phy. Lett.B, 24, 5 (1967)

/2/ Blann, M., Phys. Rev. Lett. 21, 1357 (1968); Blann, M., Lanzafame, F.M. Nucl. Phys. A 142.559 (1970)

/3/ Cline, C.K., Blann, M., Nucl. Phys. A 172, 225 (1971); Cline,C.K., Nucl.Phys.A.193, 417 (1972), Nucl. Phys. A.195, 353 (1972).

/4/ Blann, M., Ann. Rev. Nucl. Sci. 25, 123 (1975)

/5/ Weisskopf, V.F., Phys. Rev. 53, 295 (1937) Weisskopf V.F. and Ewing D. Phys. Rev. 57, 472 and 935 (1940)

/5a/Ericson, T., Adv. Phys. 9,423 (1960)

/6/ Williams, Phys. Lett. B31, 184 (1970)

/6a/Běták, E., Dobeš, J, Z. Phys. A. 279, 319 (1976)

/7/ Braga-Marcazan, G.M., Gadioli-Erba, E., Milazzo-Colli, L. and P.G. Sona, Phys. Rev. C6, 1398 (1972)

/8/ Kalbach-Cline, C., Nucl. Phys. A 210, 570, 1973

/9/ Strohmaier, B. and Uhl,M. see lectures of this courses and Uhl, M. in Nuclear Theory in Neutron Nuclear Data Evaluation, IAEA-190, Vol.II, p.361

/10/Blann, M., Phys. Rev. Lett., 27, 337 (1971), 700E, 1550 E

/11/Goldberger, M., Phys. Rev. 74, 1269 (1948)

/12/Kikuchi, K., Kawai, M. Nuclear Matter and Nuclear Interactions, North-Holland Publishing Comp., Amsterdam 1968, S.33-40

/13/Gadioli, E., Gadioli-Erba, E., and Sona, P.G., Nucl. Phys. A 217,589 (1973), see Proc. Int. Conf. on Nucl. Reaction Mechanism, Varenna, June 13-17,1977, p.24

/14/Metropolis, N., Bivins, R., Storm, M., Miller, J.M., Friedländer, G. and Turkevich, A., Phys. Rev.110, 204, 185 (1958); 166,949 (1968).

/15/Gudima, K.K., Osokov, G.A., Toneev, V.D., Sov.J.Nucl.Phys. 21, 138 (1975)

/16/Hermsdorf, D., Meister, A., Sassonov, S., Seeliger, D., Seidel, K. in Nuclear Theorie in Neutron Nuclear Data Evaluation 1975/76, IAEO-190, p.274,283; ATOMKI, Közlemények 18, 229 (1976)

/17/Blann, M. see ref. /10/ and Blann, M. and Mignerey, A., Nucl. Phy. A. 186, 245 (1972)

/18/Harp, G.D., Miller, J.M. Phys. Rev. C3, 1847 (1971)

/19/Blann, M., Mignerey, A. and Scobel W. Proc. 8th International Summer School in Nuclear Physics, Mikocaki, Poland (1975); Nukleonika 21, 335 (1976)

/20/Williams, F.C. Jr., Nucl. Phys. A 166, 231 (1971)

/21/ Chevarier, A., Chevarier, N., Demeyer, A., Hollinger, G. and Tran Minh Duc, Phys. Rev.C.8, 2155 (1973)

/22/ Blann, M., Mignerey, A. Nucl. Phys. A 186, 245 (1972)

/23/ Bertrand , F.E. and Peelle, R.W., see ref. /22/

/24/ Blann, M., Nucl. Phys. A 213,570 (1973)

/25/ Blann, M., Phys. Rev. Lett. 28, 757;see also the comments in Phys.Rev.C17,1871u.2238 (1978)

/26/ Blann, M., Hybrid Code, US-AEC Report No. COO-3494-9 (1973), see also ref. /24/, Blann, M. and Plasil, F., ALICE a Nuclear Evaporation Code, US-AEC Report No. COO-3494-10 (1973)

/27/ Blann, M., OVERLAID ALICE, USERDA Report No. COO-3494-29 (1976); Additions and Corrections to OVERLAID ALICE, USERDA Report No. COO-3494-32 (1975)

/28/ Jahn,H.,Broeders,C.H.M.,Broeders,I. , Proc. Conf. Nuclear Cross Sections and Technology, Washington D.C., March 3-7, 1975, p.350, N.B.S. Sp. Pub.425

/29/ Jahn,H., in Nuclear Theory in Neutron Nuclear Data Evaluation, Trieste, 1975/76, IAEA-190, Voll.II p.315

/30/ Jahn, H., C.H.M. Broeders and I. Broeders in Proc. Int. Conf. on Nucl. Reaction Mechanism, Varenna, June 13-17, 1977, p. 185

/31/ Perey, F., ORNL 3429, (1963)

/32/ Gilbert, A., Cameron, A.G.W., Can Journ. Phys. 43, 144 (1965)

/33/ Penny, S.K., HELENE, ORNL-TM-2590 (1969)

/34/ Hansen, L.F., Anderson, I.D., Brown, P.S., Howerton, R.I., Kamerdiener, I.L., Logan, C.M., Plechaty, E.F. and Wong, C., Nucl. Sc. Eng. 51, 278 (1973)

/35/ Hermsdorf, D., Meister, A., Sassonov, S., Seeliger, D., Seidel, V. and Shahin, F., Kernenergie 17, 259 (1974), ZfK-277

/36/ Kinney, W.E., and Perey, F.G., ORNL-4515 (1970)

/37/ Hansen, L.F., Grimes, S.M., Howerton, R.J. and Anderson, J.D., Nucl. Sc. Eng. 1,201 (1961)

/38/ Young, P.G. and Arthur, E.D., LA-6947, UC-34c, Nov.1977

/39/ C.H.M. Broeders,I.Broeders,H.Jahn and M.Lalovic AERE-R 8636,NEANDC(UK) 170L NEACRP L176(1977),Proc.Spec.Meeting on Inelastic Scattering and Fission Neutron spectra held at AERE, Harwell April 14-16 1975

/40/ Feshbach,H.,in Proc. Int. Conf.on Nucl. Reaction Mechanism, Varenna, June 13-17, 1977,

/41/ Agassi,D.,Weidenmüller,H.A.,Mantzouranis,G.,Physics Reports 22C,147 (1975)

/42/ Ribanský,I., Obložinský,P. and Běták,E., Nucl. Phys. A205,545 (1973); A226, 347 (1974)

/43/ Arndt,E. and Reif,R., see ref. /29/ p.353

/44/ Lukyanov,A.A., Salnikov, O.A. and Saprykin,E.M., Sov.J.Nucl.Phys.21, 35 (1975)

/45/ Fu,C.F., see ref. /28/ p. 328

/46/ Fröhner,F.H., Broeders,C., Broeders,I., Goel,B., Langer,I., Meyer,R., Wiese,H.W., KfK 2387/V.

COMPUTER CODES INCORPORATING PRE-EQUILIBRIUM DECAY

A. PRINCE
National Nuclear Data Center,
Brookhaven National Laboratory,
Upton, NY,
United States of America

ABSTRACT

A. Theoretical Description

After establishing the need to describe the high-energy particle spectrum which is evident in the experimental data, the various models used in the interpretation are presented.

This includes the following:
a) Cascade Model
b) Fermi-Gas Relaxation Model
c) Exciton Model
d) Hybrid and Geometry-Dependent Model

B. Workshop (Problem Session)

The codes description and preparation of input data for STAPRE was presented (Dr. Strohmaier). A simulated output was employed for a given input and comparison with experimental data substantiated the rather sophisticated treatment.

Selected Computer Codes for the Calculation of Neutron Reaction Cross Sections Combining Compound and Pre-Compound Reaction Mechanisms

A. Introduction

1.0 Purpose and Nature of Physical Problem (Pre-Equilibrium Model)

There are two extremes that are encountered in the energy distribution of nucleons resulting from a nuclear reaction mechanism. The high-energy end is usually described in terms of a combined direct (discrete) and compound nuclear process while the low end is explained in terms of the statistical theory where the Bohr independence hypothesis is assumed.

In between these extremes there exists a wide spectrum of intermediate stage processes characterized by what is commonly called a pre-equilibrium resulting from the sharing of the incoming energy with a small number of nucleons.

In order to explain these phenomena, several models based on classical and semi-classical ideas have evolved during the past few years.

The various methods range from rather simple to very complex treatments, with the basic assumption that the system in its decaying mechanism proceeds through a phase having relatively few degrees of freedom to a higher order configuration where equilibrium is reached.

During this time-dependent process, the emission of both particles and gamma-rays is possible with the mean energy of the particles being greater for emission from the pre-equilibrium configuration.

The time-dependent classical representation of particle emission may be expressed as

$$\frac{d^2\sigma_\nu}{d\Omega\, dE} = \sigma_r \sum_Q \int_0^{E_{max}} dE \int_0^\infty W(E,Q,t)\,\lambda(\nu,\varepsilon,\Theta \mid E,Q,t)\,dt \qquad (1)$$

where δ_R = reaction cross-section,

W (E,Q,t) = probability per unit energy that the reaction may be expressed in terms of the excitation energy E, in a state Q at a time t,

$\lambda(\nu, \varepsilon, \Theta / E,Q,t)$ = probability per unit time that the system in such a state will emit a particle of type ν at an angle Θ with a kinetic energy ε.

The quantity Q is rather general and its interpretation depends upon the particular model that is used, subject to the condition that

$$\sum_Q \int W(E,Q,t)\,dE = 1 \qquad (2)$$

Several review articles have appeared which go into great detail concerning the various models and their application in interpreting pre-equilibrium processes.[1-5]

2.0 General Description

2.1 Cascade Model

In this model the interaction is consistent as a quasi-free scattering process where the target nucleus is taken to be a Fermi gas. The mean free paths and energy transfers are based on nucleon-nucleon experimental scattering cross sections and angular distributions, with collisions between two particles with energy less than the Fermi energy being forbidden by the Pauli principle.

A Monte-Carlo simulation treatment of Eq. (1) by sampling many intra-nuclear cascades defines the momenta and coordinates of each nucleon involved in the cascade.

Bertini [6] developed a code in which the fastest moving particle in each cascade is followed from collision to collision, while the Brookhaven-Columbia group [7-9] followed the evolution of the intra-nuclear cascade in time.

In both cases the collisions are followed until all particle energies are below some prescribed minimum.

By following the reaction process explicitly, both equilibrium and pre-equilibrium spectra may be calculated. The angular distributions of emitted particles are also predicted.

2.2 Fermi-Gas Relaxation Model

This model encompasses another approach to the solution of the "master equation" Eq. (1) and is commonly referred to as the Harp-Miller-Berne Model. [10,11]

In this approach the single particle levels are computed with a Fermi gas spacing. The energy scale is divided into bins having a certain width (e.g. 1 MeV) and the number of available single particle levels in each bin is calculated and stored. The change in the population of states occurs as the result of two nucleons, which are in different single particle states, being scattered. The fractional change in each bin is calculated as a function of time.

The evolution process is carried out sequentially in units of time which are short compared to the nucleon-nucleon collision time.

An advantage of this model is that nuclear structure effects may be reproduced when a realistic set of single particle levels are used. However, the angular distribution of emitted particle cannot be met.

2.3 Exciton Model

This model is a phenomenological one and was proposed by Griffin [12,13]. The status of the system is classified according to the number of particles (p) and holes (h) that it contains. In this model a nucleon is assumed to enter the nucleus forming a one-particle (1p) zero-hole (0h) state. Upon interaction with one of the target nucleons a 2p - 1h state is formed. Further collisions create more particle-hole pairs (e.g. 3p - 2h, 5p - 4h, etc.).

The interaction of these excitons with the other nuclear particles permits various states to exist. For each group of states there is a certain number that can undergo particle emission. Therefore, a nuclear cascade is initiated which ends when statistical equilibrium is reached for a particular exciton number. The spectrum may then be calculated for each class of states.

The evolution of the system is described in terms of a set of coupled differential (master) equations, which have the form [14]

$$\frac{dP(n,t)}{dt} = P(n-2,t)\lambda_+(n-2,E) + P(n+2,t)\lambda_-(n-2,E) - P(n,t)\left[\lambda_+(n,E) - \lambda_-(n,E) + \sum_\nu \int_0^{E-B_\nu} W_\nu(n,\varepsilon)\,d\varepsilon\right] \quad (3)$$

There is one equation for each permissible n. The following quantities are defined:

$p(n,t)$	is the occupation probability of an n-exciton state at time t,
$\lambda^+(n,E)$	is the transition rate for the transition of an n-exciton state to an (n+2)-exciton state,

$\lambda^{-}(n,E)$ is the transition rate for the transition of an n-exciton state to an (n-2)-exciton state,

$w_\nu(n,\varepsilon)d\varepsilon$ is the emission rate for a particle ν with energy between ε and $\varepsilon+d\varepsilon$, for emission to the continuum from an n-exciton state,

E is the excitation energy,

B_ν is the binding energy of particle ν in the composite nucleus,

The pre-equilibrium spectrum for a particle ν is given by

$$N_\nu(\varepsilon) = \sigma_c(\varepsilon_\alpha) \sum_{\substack{n=n_0 \\ \Delta n=2}} w_\nu(n,\varepsilon) \int_0^{T_{eq}} P(n,t)\,dt \qquad (4)$$

where $\sigma_c(\varepsilon_\alpha)$ is the formation cross section for the composite nucleus. The pre-equilibrium cross section is obtained by integrating the spectrum over an appropriate energy range.

The emission rate of particles of type β with p_β nucleons and energy ε may be expressed as

$$w_\beta(\beta,\varepsilon,p,h)\,d\varepsilon = \frac{(2S_\beta+1)}{\pi^2\hbar^3}\mu_\beta\,\varepsilon\,\sigma_\beta(\varepsilon)R_\beta(p)(p_\beta)! \times \frac{W(p-p_\beta,h,U)}{W(p,h,E)}\,d\varepsilon \qquad (5)$$

where μ_β is the reduced mass, $\sigma_\beta(\varepsilon)$ the cross section for the inverse process, S_β the spin of the emitted particle. $R_\beta(p)$ is the probability of finding a particle of type β among the p particles, while W (p,h,E) is the density of the initial exciton state and W ($p-p_\beta$, h, U) is the density of the residual nucleus with an excitation energy U.

Several methods have been proposed for solving the master equations; they are reviewed in Refs. 2 & 4.

Recently a more unified approach has been made in which equilibrium is approached via a pre-equilibrium process, thus the evaporative component is a natural consequence of the method.

By using an exact matrix method to solve the set of master equations, the artificial time division between the pre-equilibrium and equilibrium processes is eliminated.

2.4 Hybrid and Geometry - Dependent Hybrid Model

The hybrid model [16,17] combines the features of the Fermi gas relaxation model and the exciton model. The excited particle populations during equilibrium are calculated assuming equally-spaced single particle states as in the exciton model. The states are classified according to the number of particle of holes they contain, and the intranuclear transition rates were determined by calculating the mean free paths of the nucleus in nuclear matter.

A further refinement in which nuclear geometry effects were considered led to the development of the "geometry-dependent Hybrid Model."[18]

The pre-equilibrium emission probability is given as

$$P_x(\varepsilon)d\varepsilon = \sum_{\substack{n=n_0 \\ \Delta n=2}}^{\bar{n}} \left[n P_x \frac{S_{p,h}(U,\varepsilon)g\,d\varepsilon}{\rho_{p,h}(E)} \right] \left[\frac{\lambda_c(\varepsilon)}{\lambda_c(\varepsilon)+\lambda_+(\varepsilon)} \right] D_n = \sum_{\substack{n=n_0 \\ \Delta n=2}}^{\bar{n}} n P_x(\varepsilon)\,d\varepsilon \qquad (6)$$

where np_x is the number of particles of type x (neutrons or protons) in the n-exciton state.

$\rho_{p,h}(U,\varepsilon)$ is the density of states with n-excitons such that if one is emitted, it would have an energy ε.

$\rho_{p,h}(E)$ is the density of n-exciton states and excitation energy E. $\lambda_c(\varepsilon)$ is the emission rate into the continuum of a particle with channel energy ε; g is the single particle level density of the composite nucleus.

$\lambda_+(\varepsilon)$ is the transition rate of a particle at energy ε+ V (V=real potential well depth).

The multiplication factor D_n is the fraction of reaction cross sections surviving decay from simpler states.

References

1. J. M. Miller; Proc. of Int'l Conf. on Nuclear Physis, Munich, 1973, Vol. II; J. DeBoer and H. J. Mang eds., North Holland/American Elsevier Publ. Co.
2. M. Blann; Ann. Rev. of Nuclear Science, Vol. 25, 1975, E. Segré et al, eds.
3. C. Kalbach, Int'l School on Neutron Physics, Alushta, 1974 (D3-7991).
4. F. J. Luider, ECN-17 (1977) Netherlands Energy Research Foundation, Petten.
5. K. Seidel et al., Sov. J. Part. Nucl. Vol. 7 (2) 192 (1976).
6. H. W. Bertini, Phys. Rev. 131, 1801 (1963).
7. K. Chen et al., Phys. Rev. 166, 949 (1968).
8. K. Chen et al., Phys. Rev. 176, 1208 (1968).
9. K. Chen et al., Phys. Rev. C 4, 2234 (1971).
10. G. D. Harp et al., Phys. Rev. 165, 1166 (1968).
11. G. D. Harp and J. M. Miller, Phys. Rev. C 3, 1847 (1971).
12. J. J. Griffin, Phys. Rev. Lett. 17, 478 (1966).
13. J. J. Griffin, Phys. Rev. Lett. 243, 5 (1967).
14. C. K. Cline and M. Blann, Nucl. Phys. A172, 225 (1971).
15. L. Fauger and O. Bersillon, NEANDC (E) 184 "L" 1977.
16. M. Blann, Phys. Rev. Lett. 27, 337 (1971).
17. M. Blann and A. Mignerey, Nucl. Phys. A186, 245 (1972).
18. M. Blann, Phys. Rev. Lett. 28, 757 (1972).

B. Workshop (Problem Session)

The following codes have been chosen as examples of calculating reaction cross sections and particle spectra resulting from both equilibrium and pre-equilibrium conditions.

STAPRE: M. Uhl and B. Strohmaier
OVERLAID ALICE: M. Blann

Abstracts and general information on other codes that also handle cross sections and particle spectra are given for the following codes:

GNASH: (A Multi-purpose Statistical Model Code) (Unpublished) P. G. Young and E. D. Arthur, LASL, U.S.A.

TNG: (A Two-Step Hauser-Feshbach Code with Precompound Decays and Gamma-Ray Cascades) (Unpublished) C. Y. Fu, ORNL, U.S.A.

MODESTY: W. Matthes, Ispra, Italy.

1. STAPRE

A detailed description of this code is given in the lecture by B. Strohmaier and M. Uhl on "STAPRE - a statistical model code with consideration of pre-equilibrium decay" delivered at this Course.

Name of Code: STAPRE (A computer code for particle induced activation cross sections and related quantities).

Authors: M. Uhl and B. Strohmaier

Institution: Institute for Radium Research and Nuclear Physics, Vienna, Austria.

Nature of Problem Solved: STAPRE is a statistical model code for calculating particle-induced cross sections using discrete (Hauser-Feshbach) evaporation and pre-equilibrium (exciton model) formalisms. Gamma decay is described by means of a cascade model.

Program Language: FORTRAN IV.

Program Size: CDC Cyber 61,400 words.

2. OVERLAID ALICE

Name of Code: OVERLAID ALICE

Author: M. Blann

Institution: Univ. of Rochester, Rochester, New York, USA

Documentation: COO-3494-29, 1975
COO-3494-32 (Revised) 1976

Nature of Problem Solved: Evaporation cascade including fission plus pre-equilibrium emission based on Hybrid Model using neutrons, protons, and deuterons as projectiles.

Program Language: Fortran H

Size of Program: 180K bytes - IBM 360/75
In overlay mode the code is designed to run with less 140k bytes of core.

OVERLAID ALICE

Types of Calculation

This computer code can perform several types of calculations and combinations of these types:

(1) a standard Weisskopf-Ewing evaporation calculation [1,2] with multiple particle emission. Emitted particles may be either neutrons; n and p; n, p, and α; or n, p, α and d. Excitation energies of the compound nucleus up to 200 MeV can be considered. Residual nuclei (evaporation residue yields) of a grid 11 mass units wide by 9 atomic numbers deep may be calculated as the code is presently dimensioned. Particle spectra may also be selected in the output.

The inverse reaction cross sections may either be read in from cards, or by default are computed by the optical model subroutine. The latter means that ∿ 95% of the total computation time is used in generating the inverse cross sections. For this reason the σ(inv)results are punched on cards for possible future use, unless the punching is suppressed.

The evaporation cascade is computed with 1 MeV bin width with the method previously described in the literature [2].

(2) An s-wave approximation [3,4] may be selected, which gives an upper limit to the enhancement of γ-ray deexcitation due to angular momentum effects. In this option the calculation of (1) is performed but for every partial wave in the entrance channel. In this approximation it is assumed that the rotational energy for each partial wave is irrevocably committed to rotational motion and therefore unavailable for particle emission. The rotational energy versus J may be selected either as the rigid rotor value, or from the equilibrium deformed rotating liquid drop model of Cohen et al.[5] The transmission coefficients for the partial waves to be used in the computation may be read in from cards or by default will be provided by the parabolic model[6] routine (projectile atomic number ≥ 2) or by the optical routine (n,p,d).

(3) The evaporation calculation can include fission competition according to the Bohr-Wheeler approach, using angular momentum dependent ground state and saddle point energies[7]. The latter values come from the Cohen et al[5] rotating liquid drop calculations. The calculations may be performed at every partial wave or by bins or partial waves which differ by 1 MeV in rotational energy. Default gives calculation over all partial waves, however, upper and lower limits on angular momentum may be selected (i.e. the calculation may be limited to an angular momentum 'window'). Provision is made in input to modify the liquid drop fission barrier by some factor, as well as the a_f/a_n ratio (default = 1). An option exists by which it is assumed that neutron emission carries an average of $2\hbar$ in angular momentum from the emitting nucleus, and proton emission $3\hbar$[7].

(4) Provision is made to permit precompound emission via the hybrid model[8] for the first neutron or protom emitted. Input for this aspect (including the geometry-dependent approach) is discussed in greater depth in report

COO-3494-27[9]. When this option is selected in conjunction with fission, the author has assumed that the fast precompound process will precede fission with no competition. As excitation energies increase and fission and evaporation widths increase, this assumption may become invalid. However, it should also be noted that the basic criteria of the compound nucleus model are not met, and the fission and evaporation calculations are of questionable theoretical validity. 'Let the buyer beware'!

The actual input variables are described on the comments cards preceding the main program. The CALL ERRSET subroutines in MAIN are overflow and underflow instructions (largest number and continue, zero and continue) and should be replaced by the hardware or software of the computer to be used.

The treatment of angular momentum is approximate.

References to OVERLAID ALICE

1) V. F. Weisskopf and D. H. Ewing, Phys. Rev. 57 (1940) 472.

2) M. Blann, Nucl Phys. 80 (1966) 223.

3) M. Blann and G. Merkel, Phys. Rev. B137 (1965) 367.

4) T. Ericson, Adv. in Physics 9 (1960) 425.

5) S. Cohen, F. Plasil and W. J. Swiatecki, Proceedings of the Third Conference on Reactions between Complex Nuclei, ed. A. Ghiorso, R. Diamond and H. E. Conzett (Univ. of Calif. Press, Berkeley 1963) p325.

6) T. D. Thomas, Phys. Rev. 116 (1959) 703.

7) M. Blann and F. Plasil, Phys. Rev. Lett-29 (1972) 303; F. Plasil and M. Blann, Phys-Rev. C11 (1975) 508.

8) M. Blann, Ann. Rev-Nucl. Sci 25 (1975) 123; M. Blann, Phys. Rev. Lett.27 (1971) 337; 28 (1972) 757.

9) M. Blann and J. Bisplinghoff, HYBRID CODE DESCRIPTION, COO-3494-27 (1975).

3. GNASH

A Multipurpose Statistical Theory Code

CODE NAME: GNASH (Gamma-ray, Neutron, and Asserted Particle Spectra from Neutron-Induced Reactions on Heavy Nuclei).

AUTHORS: P.G. Young and E.D. Arthur

COMPUTER: CDC 7600

CAPABILITY: GNASH calculates level activation cross section, discrete gamma-ray cross sections, isomer ratios, and neutron, gamm-ray and charged-particle spectra from almost any combination of neutron-induced reactions up to 20 MeV or higher. The code handles de-excitation of up to ten nuclei in the decay sequence, and each decaying nucleus can emit up to six types of radiation (neutrons, gamma-rays, protons, alphas, etc.). A maximum of 50 discrete levels can be included for each residual nucleus formed in the calculation, which provides great flexibility in calculations of activation cross sections, isomer ratios, etc. Examples of reactions that can be handled in a single calculation are (n,γ), $(n,n'\gamma)$, $(n,\gamma n')$, $(n,p\gamma)$, $(n,np\gamma)$, $(n,\alpha n\gamma)$, $(n,2n\gamma)$, $(n,3n\gamma)$, $(n,4n\gamma)$, etc.

METHOD: The calculation follows closely the statistical theory described by Uhl[1]. Widths for particle decay are computed from externally calculated optical model transmission coefficients. Gamma-ray widths are calculated using either the Weisskopf single-particle approximation[2] or the Brink-Axel giant dipole resonance model.[3] Gamma-ray emission by electric and magnetic dipole or quadrupole transitions are allowed, and gamma-ray cascades are followed in detail. The Gilbert and Cameron[4] form of level density function is used and is matched with inputted discrete data for up to 50 low-lying states per residual nucleus. A simple pre-equilibrium model is used to correct particle spectra and level excitation cross sections for semi-direct processes.

References

1. M. Uhl, Acta Physica Aust. 31, (1970) 245.
2. J.M. Blatt and V.F. Weisskopf, "Theoretical Nuclear Physics", Wiley, New York, (1952).
3. D.M. Brink, Thesis, Oxford University, 1955; P. Axel, Phys. Rev. 126, (1962) 671.
4. A. Gilbert and A.G.W. Cameron, Can. J. Phys. 43, (1965) 1446.

4. TNG

Name of Code: TNG (A Two-Step Hauser-Feshbach Code with Precompound Decays and Gamma-Ray Cascades)

Author: C.Y. Fu, ORNL

Computer for which Code is Designed: IBM 360/75 and 360/91

Nature of Physical Problems Solved: The code is designed for calculating nuclear reaction cross sections below 20 MeV. Binary-reaction, tertiary-reaction and gamma-ray-production cross sections such as (n,γ), (n,p), $(n,2n)$, $(n,n'\gamma)$, $(n,\alpha n\gamma)$ may be calculated. Energy distributions of secondary particles and gamma rays may be output in ENDF/B formats. Angular distributions of the first outgoing particles may be output in terms of Legendre coefficients.

Method of Solution: The Hauser-Feshbach formula[2] for compound binary reactions is extended to include tertiary reactions. Sequential decays without correlation between the two outgoing particles are assumed. Transmission coefficients needed for each step of the sequential decays are calculated with an in-house optical model without spin-orbit coupling. Binary-reaction part of the code, including width-fluctuation corrections, is based on the ORNL Hauser-Feshbach code HELENE.[3] A precompound model[4] may be included as a correction to the energy distributions of the first outgoing particles. Gamma-ray competition with the second outgoing particles and the gamma-ray-cascades calculations are spin- and parity-dependent, thus sensitive to the angular momentum effects of the Hauser-Feshbach method. Gamma-ray branching ratios, if not available experimentally, are estimated from the tails of electric giant dipole resonances.[5] The parity selection rule of electric dipole transitions may be partially relaxed as a means of including magnetic dipole transitions.

Restriction on Complexity: Present dimensioning restricts a maximum of three types of binary particles and three types of tertiary particles.

Representative running time: The running time is roughly proportional to $(E \times \Delta E)^2$ where E is the incident neutron energy and ΔE the continuum bin width. For E = 14 MeV, ΔE = 0.2 MeV and a case that includes $(n,n'x)$, (n,px) and $(n,\alpha x)$ with x = γ, n, p, or α, and gamma-ray-cascades for every residual nucleus, the running time would be roughly two minutes on IBM 360/91.

Related or Auxiliary Programs: Collective excitation cross sections from measurements and/or calculations may be input to TNG so that the collective effects are included in the calculated gamma-ray-production cross sections.

Status: In use at ORNL.

Machine Requirements: 300 K bytes of core.

Materials available: Complete code package will be available by July 1, 1975 from the Radiation Shielding Information Center at the Oak Ridge National Laboratory.

Acknowledgements: Work funded by the Defense Nuclear Agency and the Atomic Energy Agency under contract with the Union Carbide Corporation.

References:

1. C.Y. Fu, "TNG, A Two-Step Hauser-Feshbach Code with Precompound Decays and Gamma-Ray Cascades," Technical Memorandum, Oak Ridge National Laboratory (in preparation).
2. W. Hauser and H. Feshbach, Phys. Rev. 87, (1952) 366. A.M. Lane and R.G. Thomas, Rev. Mod. Phys. 30, (1958) 257.
3. S.K. Penny, "HELENE - A Computer Program to Calculate Nuclear Cross Sections Employing the Hauser-Feshbach Model, Porter-Thomas Width Fluctuation, and Continuum States," ORNL-TM-2590, Oak Ridge National Laboratory (1969).
4. J.J. Griffin, Phys. Rev. Lett. 17, (1966) 478.
   M. Blann, Phys. Rev. Lett. 21, (1968) 1357.
   M. Blann, Nucl. Phys. A213, (1973) 570.
5. P. Axel, Phys. Rev. 126, (1962) 671.
   P. Oliva and D. Prosperi, Nuovo Cimento ILB, (1967) 161.

5. MODESTY

Name of Code: MODESTY (Calculation of Nuclear Reaction Cross Sections with the Statistical Model) EUR 5722.e (1977)

Author: W. Matthes

Establishment: Joint Research Centre, Ispra, Italy

Nature of Problem Solved: Code MODESTY calculates all energetically possible reaction cross sections and particle spectra within a nuclear decay chain.

It is based on the statistical nuclear model following the method of Uhl [1] where the optical model is used in the calculation of partial widths and the Blatt-Weisskopf single particle model for γ decay.

The program is designed in the "modular concept in that all necessary nuclear data are automatically searched for from an external (tape or disc) library of fundamental data.

Plans are underway to modify the code to include pre-equilibrium effects and a more sophisticated treatment of γ-decay by including the Brink-Axel model.

Program Language: PL/1 (IBM 360/75)

Size: 130k bytes

Ref.

1) M. Uhl, Acta Physics Austriaoa 31, 245 (1970)

STAPRE – A STATISTICAL MODEL CODE WITH CONSIDERATION OF PRE-EQUILIBRIUM DECAY

B. STROHMAIER, M. UHL
Institut für Radiumforschung und Kernphysik,
Vienna, Austria

Abstract

A computer code based on the statistical compound nucleus model and the exciton model is described. The emission of up to six particles, intermediary gamma-ray cascades and fission are taken into account. The employed models, the proceeding of the code, the required input data and the output are discussed. By means of several neutron-induced reactions the influence of model parameters on the calculated cross sections is illustrated.

1. Introduction

The code STAPRE is designed to calculate energy-averaged cross sections for particle-induced nuclear reactions with several emitted particles and gamma-rays under the assumption of sequential evaporation. The different ways of populating a particular state of a final nucleus by such a reaction are illustrated in fig. 1.

Each evaporation step is treated within the framework of the statistical model with consideration of angular momentum and parity conservation. For the emission of the first particle preequilibrium decay is taken into account. For a specified sequence of up to six emitted particles the following quantities can be obtained for all nuclei involved in the cascade:

i. activation cross section
ii. population of isomeric states
iii. production cross sections for gamma-rays from low excited levels
iv. energy spectra for all emitted particles and γ-rays.

The angular distributions of the emitted particles and gamma-rays are not calculated.

A version of the STAPRE code with the above features has been made available to the NEA Programme Library in Ispra for general distribution. Lately the code has been modified in several respects. The most important extension is the inclusion of the fission process. Further improvements regard the width fluctuation correction for first chance emitted gamma-rays and some additional options for preequilibrium decay. Subject of this lecture is the most recent version because it will also be available before long.

First, we describe the employed models. Then, the input data of the code will be discussed. By means of examples their influence on the results will be illustrated. Finally, the output will be commented upon.

2. Models employed and proceeding of the code

The calculation of the above-named quantities is based on the following models:

The equilibration of the composite system formed by projectile and target nucleus is described in the frame of the exciton model; this is only one of the current models for this process. In the preequilibrium stage of the reaction particle emission is assumed to be the only decay mode; preequilibrium photon emission and fission are thus neglected. For the equilibrium portion of first chance particle and photon emission as well as for first chance fission the width fluctuation corrected Hauser-Feshbach (HF) formula is applied. Higher chance processes are treated as sequential evaporation steps. For fission either a single- or a double-humped barrier can be assumed.

As a guide for explaining the application of these models a schematic drawing (fig. 2) of the proceeding of the code is used as in this way it can be illustrated how the various models are combined.

In the following the term "i^{th} compound nucleus (CN)" means that nucleus resulting from emission of (i-1) of a specified sequence of emitted particles ($\pi_1, \pi_2, \pi_3, \ldots$). Hence, the system formed by incoming particle π_0 and target nucleus T is called first CN even if not yet in the equilibrium stage. Each CN is assumed to be subject to fission.

2.1. Hauser-Feshbach denominator and fission probability

The program at first generates a table containing for each CN the HF denominator $N_i(U,J,\Pi)$ and the fission probability $R_i^f(U,J,\Pi)$ for all excitation energies U (in steps defined by a grid of binsize DU) and all values of angular momentum J and parity Π which are required for the subsequent evaporation calculations. For the calculation of excitation functions these tabulated quantities are used for all incident energies.

The HF denominator is defined as the sum of transmission coefficients T_c for all open channels c

$$N(U,J,\Pi) = \sum_c T_c = N^{part}(U,J,\Pi) + N^{\gamma}(U,J,\Pi) + N^{f}(U,J,\Pi) \qquad (1)$$

and therefore consists of contributions resulting from particle, gamma-ray and fission decay.

The excited states of residual nuclei as well as the transition states at saddle-point deformation which both enter in the definition of the various channels are described by a level density $\rho(U,J,\Pi)$. At low excitation energy where complete information on the quantum numbers (E_j, I_j, Π_j) of "discrete levels" is available the level density reads:

$$\rho(U,J,\Pi) = \sum_j \delta(U-E_j)\,\delta_{JI_j}\,\delta_{\Pi\Pi_j} \qquad (2).$$

In the energy region above the discrete levels which will be referred to as "continuum" the level density has to be calculated by means of a model.

In the following we briefly describe how the various decay modes are treated.

i. Particles

The transmission coefficients are related to the optical model and have to be supplied as input data. In the code STAPRE the channel-spin coupling scheme is used. The transmission coefficients for particle of type π are assumed to depend on orbital angular momentum l and energy ε of relative motion only: $T_c^\pi = T_l^\pi(\varepsilon)$.

It is assumed that the emission of neutrons, protons, α-particles and deuterons contributes to the HF denominator. Of course this list of evaporated particles can be extended by minor modifications of the code.

ii. Photons

By assumption the gamma-ray transmission coefficients T_c^γ only depend on multipole type XL and transition energy ε. They are related to the gamma-ray strength function $f_{XL}^\gamma(\varepsilon)$ by $T_c^\gamma = T_{XL}^\gamma(\varepsilon) = 2\pi\,\varepsilon^{2L+1} f_{XL}^\gamma(\varepsilon)$.
For the energy dependence of the E1 strength function the Weisskopf or the Brink-Axel model can be used [1]. The strength functions for M1, E2, ... M3 radiation are for the present obtained from the Weisskopf model and normalized relative to $f_{E1}^\gamma(\varepsilon)$. The gamma-ray transmission coefficients are normalized by fitting the average total s-wave radiation width at the neutron binding energy.

iii. Fission

Fission channels are defined by transition states at saddle point deformation. The fission transmission coefficient T_c^f is related to the penetrability P_c through the fission barrier associated with the transition state c. In order to reduce the number of model parameters it is assumed that the fission motion along the "fission path" can be described by only one deformation coordinate and that barriers associated with different transition states have the same shape.

For a barrier with parabolic shape characterized by height E and curvature $\hbar\omega$ the penetrability P(U) as function of excitation energy U is given by the Hill-Wheeler formula [2]:

$$P(U) = \left\{1 + \exp\left[\frac{2\pi}{\hbar\omega}(E-U)\right]\right\}^{-1} \qquad (3).$$

Under the assumption of such a single-humped barrier the transmission coefficient $T_c^f(U,J,\Pi)$ for fission decay of compound nucleus states with (U,J,Π) via channel c reads:

$$T_c^f(U,J,\Pi) = \delta_{J\Pi,I_c\Pi_c} P_c(U) = \delta_{J\Pi,I_c\Pi_c}\left\{1+\exp\left[\frac{2\pi}{\hbar\omega}(E_c-U)\right]\right\}^{-1} \qquad (4).$$

Here (E_c, I_c, Π_c) are the excitation energy, spin and parity of the transition state specifying the channel c. Conservation of angular momentum and parity is accounted for by the factor $\delta_{J\Pi,I_c\Pi_c}$.

The fission contribution $N^f(U,J,\Pi)$ to the HF denominator and the fission probability $R^f(U,J,\Pi)$ are given by:

$$N^f(U,J,\Pi) = \sum_c T_c^f(U,J,\Pi); \qquad R^f(U,J,\Pi) = N^f(U,J,\Pi)/N(U,J,\Pi) \qquad (5).$$

The treatment of fission under consideration of a double-humped barrier closely follows the model proposed by Back et al. [3]. The shape of the barrier is essentially approximated by three smoothly joined parabolic sections and is therefore characterized by six parameters: the heights (E_A, E_B, E_{II}) and the curvatures $(\hbar\omega_A, \hbar\omega_B, \hbar\omega_{II})$ of the inner barrier A, the outer barrier B and the secondary minimum.

The following consequences of the secondary minimum in the deformation energy surface are taken into account:

a) Damping in the second well: Interaction of the fission mode with internal degrees of freedom excites compound nucleus states in the second well. Fission decay of these states provides an "indirect" contribution to fission.

b) Intermediate class II structure: Coupling between compound nucleus states in the first well (class I states) and those in the second well (class II states) enhances the indirect fission contribution for energies near a class II state. This intermediate structure is of importance mainly for sub-barrier fission.

Damping is accounted for by adding to the real deformation potential a negative imaginary part located at the position of the second well. Solution of Schrödinger's equation for the fission mode gives the directly transmitted flux $P^{AB}(U)$ and the absorbed flux $\mathcal{A}^{AB}(U)$. At the positions of quasibound vibrational levels both of them exhibit vibrational resonances with a width which increases with the extent of damping.

For partial damping the fission transmission coefficient T_c^f consists of a direct and an indirect contribution which are related to the transmitted and the absorbed flux, respectively:

$$\left.\begin{aligned} T_c^f(U,J,\Pi) &= \delta_{J\Pi,I_c\Pi_c}\left[P_c^{AB}(U) + N^{abs}(U,J,\Pi)\frac{P_c^B(U)}{N^A(U,J,\Pi)+N^B(U,J,\Pi)}\int^{J\Pi}(U'-U)\right] \\ N^{abs} &= \sum_c \delta_{J\Pi,I_c\Pi_c}\mathcal{A}^{AB}(U), \qquad N^A = \sum_c \delta_{J\Pi,I_c\Pi_c}P_c^A(U), \qquad N^B = \sum_c \delta_{J\Pi,I_c\Pi_c}P_c^B(U) \\ \frac{1}{2\Delta}&\int_{U-\Delta}^{U+\Delta} dU'\, \int^{J\Pi}(U'-U) = 1 \end{aligned}\right\} \qquad (6)$$

The quantities P^A and P^B are the penetrabilities through the separate barriers A and B and are calculated by means of the Hill-Wheeler formula (eq. (1)). The normalized weight function $\int^{J\Pi}(U'-U)$ describes the energy dependence due to intermediate class II structure in an interval $[U-\Delta, U+\Delta]$ small enough so that all other energy-dependent quantities are nearly constant therein. The expression for the indirect contribution to the fission transmission coefficient in eq. (6) is based on the assumption that the states in the second well which are excited by the ab-

sorbed flux decay either by penetration of barrier A or barrier B which leads to fission. Particle and gamma decay in the second well are neglected. Hence the cross sections for the population of "shape isomers" cannot be obtained.

The code STAPRE computes only cross sections which are averaged with respect to intermediate class II structure. The average values are calculated using a schematic model for the class II states which was proposed by Back et al. [3] and by Lynn [4]. In this model with equidistant class II states (spacing $D_{II}^{J\pi}$) of equal width $W^{J\pi}=(2\pi)^{-1}D_{II}^{J\pi}(N^A+N^B)$ the weight function $f^{J\pi}(U'-U)$ reads:

$$f^{J\pi}(U'-U)=\sinh\left(\frac{2\pi W^{J\pi}}{D_{II}^{J\pi}}\right)\Big/\left(\cosh\left(\frac{2\pi W^{J\pi}}{D_{II}^{J\pi}}\right)-\cos\left(\frac{2\pi(U'-U)}{D_{II}^{J\pi}}\right)\right) \qquad (7).$$

By means of eqs. (6) and (7) the average value of the fission probability and of the branching ratios for the other decay modes can be obtained in closed form.

Due to the growing density of class II states the damping in the second well increases with energy. In the limit of complete damping the directly transmitted flux can be neglected and the absorbed flux is given by the penetrability P^A through the inner barrier. Hence the fission transmission coefficient becomes:

$$T_c^f(U,J,\Pi)=\delta_{J\pi,I_c\pi_c}\,N^A(U,J,\Pi)\,\frac{P_c^B(U)}{N^A(U,J,\Pi)+N^B(U,J,\Pi)} \qquad (6').$$

In this limit barrier A and B act independently. For many practical applications the complete damping limit is also adequate at small energies and can therefore optionally be used for all energies. The calculations are simpler then but can, of course, not account for vibrational resonances.

2.2. Equilibration

The equilibration of the composite system formed by projectile π_0 and target T is treated in the framework of the "exciton model" [5] - [10].

Starting from a simple configuration the composite system is assumed to equilibrate through a series of two-body collisions and to emit particles from all intermediate stages. The states of the system are classified according to the number n of excitons or more specifically to the numbers p and h of the excited particle and hole degrees of freedom. The application of a two-body interaction to states of a (p,h)-configuration leads to states with (p+1, h+1),(p,h) or (p-1, h-1) excited particles and holes. In competition with these internal transition particles can be emitted from each state. For all these processes transition rates averaged over all states of a configuration are employed.

The population probability $b^{(k)}(n) = b^{(k)}(p,h)$ of the states of a (p,h)-configuration resulting from k internal transitions is obtained from:

$$\left.\begin{aligned} b^{(k)}(n) &= b^{(k-1)}(n+2)\,\frac{\lambda_-(n+2)}{\lambda(n+2)}+b^{(k-1)}(n)\,\frac{\lambda_0(n)}{\lambda(n)}+b^{(k-1)}(n-2)\,\frac{\lambda_+(n-2)}{\lambda(n-2)}\\ \lambda(n) &= \lambda_-(n)+\lambda_0(n)+\lambda_+(n)+\lambda^e(n); \qquad \lambda^e(n)=\sum_\nu\int d\varepsilon_\nu\,\lambda_\nu^e(n;\varepsilon_\nu)\end{aligned}\right\} \qquad (8).$$

in eq. (8) $\lambda_+(n)$, $\lambda_0(n)$ and $\lambda_-(n)$ are the average rates for internal transitions with a change of the exciton number by an amount of +2,0 and -2, respectively, and $\lambda_\nu^e(n;\varepsilon_\nu)d\varepsilon_\nu$ is the average rate for emission of particle ν with energy of relative motion ε_ν. The quantity $\lambda^e(n)$ therefore represents the total rate for emission of particles. Starting from an initial population probability

$$b^{(0)}(n)=\delta_{nn_0} \qquad \text{or} \qquad b^{(0)}(p,h)=\delta_{pp_0}\delta_{hh_0}$$

successive application of eq. (8) gives the populations of the various (p,h) configurations by processes with an arbitrary number k of internal transitions. With increasing k the ratio $b^{(k-1)}(n)/b^{(k)}(n)$ becomes independent of n and k what indicates that equilibrium has been reached and hence can be used to determine an upper limit K for the number of internal transitions to be considered for preequilibrium decay. The preequilibrium contribution $\frac{\partial\sigma_{\pi_0,\pi_1}^{pre}}{\partial\varepsilon_1}d\varepsilon_1$ to the differential cross section is given by

$$\frac{\partial\sigma_{\pi_0,\pi_1}^{pre}}{\partial\varepsilon_1}d\varepsilon_1=\sigma_{\pi_0}^{non}\sum_{k=0}^{K}\sum_n b^{(k)}(n)\,\frac{\lambda_{\pi_1}^e(n;\varepsilon_1)}{\lambda(n)}\,d\varepsilon_1 \qquad (9)$$

where $\sigma_{\pi_0}^{non}$ represents the optical model absorption cross section for the projectile π_0. The fraction q^{pre} of the initial population surviving preequilibrium emission is given by

$$q^{pre}=1-\sum_{k=0}^{K}\sum_n b^{(k)}(n)\,\frac{\lambda^e(n)}{\lambda(n)} \qquad (10).$$

$\frac{\partial\sigma_{\pi_0,\pi_1}^{pre}}{\partial\varepsilon_1}$ and q^{pre} are the quantities which are required for the further calculations as shown in fig. 2. In order to evaluate these two quantities actually one needs the rates $\lambda_+(n)$, $\lambda_0(n)$, $\lambda_-(n)$ for internal transitions and $\lambda_\nu^e(n;\varepsilon_\nu)$ for particle emission. The rates $\lambda_+(n)$, $\lambda_0(n)$ and $\lambda_-(n)$ are related by the formulas of Williams [11] to $|M|^2$, the absolute square of the average effective matrix element of residual interactions:

$$\left.\begin{aligned} \lambda_+(n) &\equiv \lambda_+(p,h,U)=\frac{2\pi}{\hbar}\,|M|^2\,\frac{g(gU)^2}{p+h+1}\\ \lambda_0(n) &\equiv \lambda_0(p,h,U)=\frac{2\pi}{\hbar}\,|M|^2\,g\,(gU)\,(p+h-1)\\ \lambda_-(n) &\equiv \lambda_-(p,h,U)=\frac{2\pi}{\hbar}\,|M|^2\,g\;p\,h\,(p+h-2)\end{aligned}\right\} \qquad (11)$$

where U is the excitation energy of the composite system and g the single particle state density. A Pauli-principle correction proposed by Cline [12] can be applied.
For the dependence of $|M|^2$ on mass number A and excitation energy U the expression

$$|M|^2 = FM\cdot A^{-3}U^{-1} \qquad (12)$$

proposed by Kalbach-Cline [13] is used; the quantity FM is an adjustable constant. The rates $\lambda_\nu^e(n;\varepsilon_\nu)$ for particle emission are calculated from detailed balance considerations:

$$\left.\begin{aligned} \lambda_\nu^e(n;\varepsilon_\nu)\,d\varepsilon_\nu &\equiv \lambda_\nu^e(p,h,U;\varepsilon_\nu)\,d\varepsilon_\nu=\\ &=\frac{2s_\nu+1}{\pi^2\hbar^3}\,\mu_\nu\varepsilon_\nu\sigma_\nu(\varepsilon_\nu)\,F_\nu\,\frac{\omega(p-p_\nu,h,U-B_\nu-\varepsilon_\nu)}{\omega(p,h,U)}\,d\varepsilon_\nu\\ F_\nu &=\left(\frac{Z}{A}\right)^{z_\nu}\left(1-\frac{Z}{A}\right)^{p_\nu-z_\nu}\binom{p_\nu}{z_\nu}\end{aligned}\right\} \qquad (13)$$

The symbols have the following meaning:

s_ν... spin
p_ν... number of nucleons
z_ν... number of protons
B_ν... binding energy
} of particle ν

μ_ν... reduced mass
ε_ν... energy of relative motion
σ_ν... inverse cross section
} in the exit channel

Z ... charge number of the composite system.

The quantity $\omega(p,h,U)$ represents the density of states with excitation energy U, p particles and h holes; these densities are related by means of a formula given by Williams [14] to the single particle state density g.
The factor F_ν is meant to take into account the nature of the emitted particle roughly in a combinatorial way.

In the recent version of the code charge conservation and α-preformation as proposed by Gadioli et al. [15] and by Milazzo-Colli [16] can be considered for nucleon-induced reactions. In case of nucleon emission charge conservation favours the emission of particles of the same type as the projectile. The factor F_ν in eq. (13) then reads:

$$F_\nu = \frac{n \pm 1}{n} \quad \left(\pm\right\} \ldots \text{projectile and emitted particle of} \left\{\begin{matrix}\text{same}\\ \text{different}\end{matrix}\right\} \text{type})$$

For α-particle emission $F_\nu = 1$ and the ratio of the particle-hole state densities depends on the preformation factor as described in ref. [16].

In the described treatment of the preequilibrium decay angular momentum and parity are not taken into account. Therefore, the population of levels with given angular momentum and parity cannot be calculated without additional assumptions.

2.3. Width fluctuation corrected HF formula

The decay modes of that part of the population of the first CN that survives preequilibrium decay are described by means of the equilibrium compound nucleus model, that is, the HF formula is used to calculate the cross sections for first-chance particle emission, γ-ray emission and fission of this portion of the population. For entrance channel c and exit channel c' and a total angular momentum J and parity Π the formula in well known notation reads:

$$\sigma_{cc'}^{(HF)J\Pi} = \frac{\pi}{k^2} g^J \frac{T_c T_{c'}}{N_\lambda(U,J,\Pi)} S_{cc'}^{J\Pi} \qquad (14).$$

The factor $S_{cc'}^{J\Pi}$ corrects the average with respect to fine structure for fluctuations of the partial width ("width fluctuation" (WF)); it depends on the transmission coefficients T_c and the fluctuation indices ν_c for all open channels and is given by the following integral [17]:

$$S_{cc'}^{J\Pi} = \left(1 + 2\frac{\delta_{cc'}}{\nu_{c'}}\right) \int_0^\infty dt \prod_{c''} \left(1 + \frac{2t}{\nu_{c''}} \frac{T_{c''}}{N_\lambda(U,J,\Pi)}\right)^{-\left(\frac{1}{2}\nu_{c''} + \delta_{cc''} + \delta_{c'c''}\right)} \qquad (15).$$

The product comprises all open channels compatible with angular momentum and parity conservation. The integral is calculated numerically under the hypothesis that, due to the large number of contributing channels, the total radiation width does not fluctuate. For the same reason it is assumed that $S_{cc'}^{J\Pi}$ does not depend on the exit channel c' if it is a photon channel. For the present the fluctuation indices ν_c have the same value ν (usually $\nu = 1$) for all channels.

If due to fission contributions the cross section $\sigma_{cc'}^{(HF)J\Pi}$ has to be averaged with respect to intermediate class II structure this is done by a further numerical integration over energy employing eq. (7) for the weight function $f^{J\Pi}(U'-U)$.

For inelastic processes the WF correction factor approaches unity with increasing number of open channels. In order to save computation time the calculation of the correction factor is then turned off by an internal criterion.

By means of eqs. (14) and (15) the contributions of the different decay modes to the respective cross sections are obtained as follows:

Equilibrium first-chance particle emission contributes a fraction

$$WB_2^{(HF)}(U,J,\Pi)\Delta U = q_1^{pre} \sum_{J'\Pi'} \sum_{cc'} \sigma_{cc'}^{(HF)J'\Pi'} \rho_2(U,J,\Pi)\,\Delta U \qquad (16)$$

to the population $WB_2^{(o)}(U,J,\Pi)\Delta U$ of levels with excitation energy in an interval ΔU around U and with angular momentum J and parity Π of the second CN. The sum $\sum_{J'\Pi'}$ is over all angular momenta and parities of the first CN and the sum $\sum_{cc'}$ refers to particle channels and is restricted by angular momentum and parity conservation. The quantity q_1^{pre} is defined in eq. (10) and corrects for loss of initial population by preequilibrium emission. Due to the definition (sec. 2.1.) of the level density the above expression for $WB_2^{(HF)}$ refers to the continuum as well as to discrete levels. The same holds true for all further equations defining populations, therefore no distinction between the region of discrete levels and the continuum will be made furtheron.

First chance gamma-ray emission defines the population $WB_1^{(o)}(U,J,\Pi)\Delta U$ of the first compound nucleus:

$$WB_1^{(o)}(U,J,\Pi)\Delta U = q_1^{pre} \sum_{J'\Pi'} \sum_{cc'} \sigma_{cc'}^{(HF)J'\Pi'} \rho_1(U,J,\Pi)\,\Delta U \qquad (17).$$

The sum $\sum_{c'}$ now refers to photon channels and is restricted by multipole selection rules; $\rho_1(U,J,\Pi)$ is the level density of the first CN.

For the first chance fission cross section one has to sum over all fission channels c^T:

$$\sigma_{\gamma_0,f} = q_1^{pre} \sum_{J'\Pi'} \sum_{cc'} \sigma_{cc'}^{(HF)J'\Pi'} \qquad (18).$$

2.4. Gamma-ray cascades

The states of the first CN populated by primary gamma-rays can undergo transitions to lower-lying states. Such γ-ray cascades populate the ground state or isomeric states. The problem of de-excitation by γ-ray cascades also occurs for the further CN as will be seen later on. An accurate treatment of

gamma-ray cascades is important for the calculation of activation cross sections, population of isomeric states, γ-ray production spectra and for the consideration of all processes where gamma emission precedes particle emission or fission. Therefore we give a general description of γ-ray cascades in this place suppressing the subscript denoting a particular CN.

The population of levels with quantum numbers (U',I',Π') by photon emission from levels (U,J,Π) is governed by the branching ratio for gamma-ray emission $R^{\gamma}(U,J,\Pi;U',J',\Pi')$:

$$R^{\gamma}(U,J,\Pi;U',J',\Pi') = \left(\sum_{xL} T^{\gamma}_{xL}(U-U')\right) / N(U,J,\Pi)$$

where the sum of the γ-ray transmission coefficients is restricted by the multipole selection rules.

The population $WB^{(n)}(U',J',\Pi')\Delta U'$ of levels with $J'\Pi'$ in an interval $\Delta U'$ around U' by n successive gamma transitions can be obtained by the following recursion relation:

$$WB^{(n)}(U',J',\Pi')\,\Delta U' = \sum_{J\Pi}\int_{U'}^{U_{max}} dU\; WB^{(n-1)}(U,J,\Pi)\,R^{\gamma}(U,J,\Pi;U',J',\Pi')\,\rho(U',J',\Pi')\,\Delta U'$$

where U_{max} is the maximum energy up to which the considered CN is populated. The recursion starts from a population $WB^{(0)}$ which for the 1st CN comes from primary gamma-ray emission, for all further CN from particle emission of the preceding CN. The cumulative population $\overline{WB}(U',J',\Pi')\Delta U'$ is the result of all possible γ-ray cascades:

$$\overline{WB}(U,J',\Pi')\,\Delta U' = \sum_{n} WB^{(n)}(U',J',\Pi')\,\Delta U' \qquad (19).$$

This quantity is of relevance for all further calculations and obeys the following relation:

$$\left.\begin{aligned}\overline{WB}(U',J',\Pi')\,\Delta U' = {} & WB^{(0)}(U',J',\Pi')\,\Delta U' + \\ & + \sum_{J\Pi}\int_{U'}^{U_{max}} dU\; \overline{WB}(U,J,\Pi)\,R^{\gamma}(U,J,\Pi;U',J',\Pi')\,\rho(U',J',\Pi')\,\Delta U'\end{aligned}\right\} \qquad (20).$$

For U' in the continuum this is an integral equation for the quantity $\overline{WB}$ which in the STAPRE code is approximately solved by introducing an energy grid with binsize DU:

If K is the number of the bin containing U_{max} and if γ-ray transitions between states lying in the same bin are neglected, the integral equation for $\overline{WB}$ can be reduced to the following system of successively to be solved linear equations:

$$\overline{WB}(K,J',\Pi') = WB^{(0)}(K,J',\Pi')$$

$$\overline{WB}(K-1,J',\Pi') = WB^{(0)}(K-1,J',\Pi') + \sum_{J\Pi}\overline{WB}(K,J',\Pi')\,R^{\gamma}(K,J,\Pi;K-1,J',\Pi')\,\rho(K-1,J',\Pi')\,DU$$

$$WB(K-2,J',\Pi') = WB^{(0)}(K-2,J',\Pi') + \sum_{J\Pi}\left\{\overline{WB}(K,J,\Pi)\,R^{\gamma}(K,J,\Pi;K-2,J',\Pi') + \overline{WB}(K-1,J,\Pi)\,R^{\gamma}(K-1,J,\Pi;K-2,J',\Pi')\right\}\rho(K-2,J',\Pi')\,DU$$

.....

As already explained, the quantities $WB^{(n)}(U,J,\Pi)\Delta U$ and $\overline{WB}(U,J,\Pi)\Delta U$ are understood as the populations of each single level $(E_{\gamma}, I_{\gamma}, \Pi_{\gamma})$ as far as the excitation energy U is in the region of discrete levels. For the γ-branching ratio for transitions between discrete levels the experimental values are used.

The γ-ray production spectrum is obtained by appropriate book-keeping in the course of the solution of eq. (20). The activation cross sections for ground state and isomeric states are given by their cumulative population.

2.5. Higher-chance particle emission and fission

Levels of the 1st CN which are populated by the different gamma-ray transitions can emit particles if this is allowed by energy conservation. As this higher-chance particle emission is equally treated for all CN the following description is not restricted to the 1st CN.

Emission of particle π_i from the i^{th} CN with cumulative population $\overline{WB}_i(U,J,\Pi)\Delta U$ leads to the population $WB^{(0)}_{i+1}(U',J',\Pi')\Delta U'$ of the $(i+1)^{th}$ CN:

$$WB^{(0)}_{i+1}(U',J',\Pi')\Delta U' = \sum_{J\Pi}\int_{U'+B_{\pi_i}}^{U_{max}} dU\; \overline{WB}_i(U,J,\Pi)\,R_i^{\pi_i}(U,J,\Pi;U',J',\Pi')\,\rho_{i+1}(U',J',\Pi')\Delta U' \qquad (21).$$

The branching ratio $R_i^{\pi_i}$ for emission of particle π_i is given by

$$R_i^{\pi_i}(U,J,\Pi;U',J',\Pi') = \left(\sum_{ls} T_{\ell}^{\pi_i}(U-U'-B_{\pi_i})\right) / N_i(U,J,\Pi)$$

The sum is over orbital angular momentum l and channel spin s and is restricted by angular momentum and parity conservation. The cumulative population $\overline{WB}_i$ on the right hand side of eq. (21) results from the gamma-ray cascades occurring before the emission of particle π_i.

Together with $WB^{(0)}_{i+1}$ the contribution to the emission spectrum of particles of type π_i is calculated.

The contribution of the i^{th} CN to the total fission cross section is calculated from the fission probability and the cumulative population as

$$\sigma_{\pi_0,\pi_1\ldots\pi_{i-1}f} = \sum_{J\Pi}\int_{0}^{U_{max}} dU\; \overline{WB}_i(U,J,\Pi)\,R_i^{f}(U,J,\Pi) \qquad (22).$$

In this way all processes where gamma-ray cascades are followed by fission are taken into account.

2.6. Combination of equilibrium and preequilibrium particle emission

To the population $WB^{(0)}_2$ of the 2nd CN contributes on one hand preequilibrium, on the other equilibrium decay. The equilibrium contribution consists of a portion describing 1st chance particle emission and a portion of particle evaporation after gamma-ray emission. The latter in general is negligible compared to the former. Since the preequilibrium model described in section 2.2. does not consider angular momentum and parity, it is assumed that the population $\frac{\partial\sigma^{pre}_{\pi_0,\pi_1}}{\partial U}\Delta U$ is distributed among the levels with different spin and parity in the same proportion as the equilibrium contribution is. Hence the population $WB^{(0)}_2$ is given by

$$WB^{(0)}_2(U,J,\Pi)\,\Delta U = WB^{eq}(U,J,\Pi)\Delta U + \frac{\partial\sigma^{pre}_{\pi_0,\pi_1}}{\partial U}\,\frac{WB^{eq}_2(U,J,\Pi)}{\sum_{J'\Pi'} WB^{eq}_2(U,J',\Pi')}\,\Delta U$$

where

$$WB^{eq}_2(U,J,\Pi)\,\Delta U = \left\{WB^{(HF)}_2(U,J,\Pi) + \sum_{J'\Pi'}\int_{U}^{U_{max}} dU'\,\overline{WB}_1(U',J',\Pi')\,R^{\pi_1}_{\lambda}(U',J',\Pi';U,J,\Pi)\,\rho_2(U,J,\Pi)\right\}\Delta U$$

This is certainly a crude approximation which has to be improved in future. Its consequences become the more important

the more the preequilibrium fraction increases, that is with increasing incident energy. Besides, this approximation affects the different calculated quantities to a different extent. The effect on total activation cross sections or on particle production spectra is smaller than on cross sections which critically depend on the spin and parity distribution as e.g. isomeric state population cross sections.

2.7. Succession of γ-ray cascades and particle emission or fission from the 2nd CN on

Once the starting population for γ-ray cascades $WB_i^{(0)}(U,J,\Pi)\Delta U$ for $i \geq 2$ has been defined, the possible decay modes are treated alike for all CN. The gamma-cascade model gives the cumulative population $\overline{WB}_i(U,J,\Pi)\Delta U$ from which the contribution to the fission cross section and the population $WB_{i+1}^{(0)}$ of the next CN are calculated by means of eqs. (21) and (22), respectively. The contributions of the various CN to the γ-ray production spectrum, to the fission cross section and, as far as particles of the same type are emitted, to the particle production spectrum are summed up.

In order to save computation time, the calculation of gamma-ray cascades can be suppressed for several CN. If N is the total number of CN for a particular reaction the γ-ray cascades optionally can be neglected for the CN with numbers $1,2,..,N_\gamma < N$. In this case, in eqs. (21) and (22) the cumulative population $\overline{WB}_i$ is replaced by $WB_i^{(0)}$.

3. Input data

We do not give a complete description of the input data here but only explain such quantities which control the calculations and such on which the results critically depend for physical reasons. This dependency will be illustrated by means of some examples for neutron-induced reactions.

3.1. Control parameters and energy binsize

The sequence of emitted particles has to be chosen by means of code numbers among the following particles: (n,p,α,d). The projectile, however, may be of arbitrary type. In addition, the number of particles contributing to the HF denominator can be restricted to a number less then four. If one is e.g. interested only in neutron emission from heavy nuclei where the evaporation of charged particles is strongly hindered by the Coulomb barrier, computation time can be saved by neglecting the charged particle contributions to the HF denominator.
The computation time can also be reduced by considering gamma-ray cascades not for all CN. E.g., at higher incident energies gamma-ray cascades for the first CN may be neglected by choosing $N_\gamma = 1$ (see sec. 2.7.) if one is only interested in particle emission and not in the capture reaction.

The calculation of the WF correction optionally can be turned off; in addition one can specify the fluctuation index and the accuracy up to which the correction factor (see eq. (15)) is computed.

As already mentioned in sec. 2.4. an energy grid whose binsize is DU is introduced for the approximate calculation of integrals with respect to energy in the continuum region. For the choice of DU one has to consider the numerical accuracy and, on the other hand, the central memory and computation time requirements. Values between 0.1 and 0.5 MeV for the binsize are recommended.

For the calculation of the excitation function the incident energy can be diminished automatically, starting from a given value. Since the HF denominator for each CN is stored binwise, the energy steps for the excitation function have to be chosen as integer multiples of DU.

3.2. Separation energies

The binding energy of the projectile and the separation energies of all particles whose emission is considered in the HF denominator have to be supplied. Tables of separation energies have been published by Wapstra and Gove [18,19] and Viola et al. [20].

3.3. Optical model transmission coefficients

The particle transmission coefficients have to be created by an optical model code and supplied as input data. For the most important particles, in particular for nucleons, there are global optical potentials which can be used for generating the transmission coefficients. To obtain as accurate results as possible the transmission coefficients should be calculated from optical potentials which well reproduce the available experimental data as e.g. total cross sections, differential elastic cross sections and strength functions. This may require an adjustment of the parameters of the above-mentioned global potentials. For permanently deformed nuclei the use of a coupled-channel code for generating the transmission coefficients is recommended as the excitation of the low-lying collective states by inelastic scattering constitutes a considerable part of the absorption cross section.

We don't discuss further details of the optical model here because several lectures of this course are devoted to this subject.

3.4. Data required for the creation of gamma-ray transmission coefficients

The maximum multipolarity of electric and magnetic radiation can be chosen less or equal three. If the E1 strength function f_{E1}^{γ} is calculated according to the Brink-Axel model, that is: derived from the E1 photo-absorption cross section, one has to specify the parameters for the E1 giant resonance (resonance energies, widths and peak cross sections). A compilation of such parameters for nuclei with $A \geq 90$ has been given by Bartholomew et al. [1]. Optionally the global parameters for the E1 giant resonance given by Axel [21] can be used.

According to the Weisskopf model the strength functions for M1,E2, ... M3 radiation are energy-independent. Their ratio to f_{E1}^{γ} at the neutron binding energy can be prescribed or optionally be taken according to Weisskopf's estimate [22].

For the final normalization of all gamma-ray transmission

coefficients the average s-wave neutron radiation width $\bar{\Gamma}_\gamma$ is required. Experimental data are compiled in the report BNL 325 [23]; more recent references on resonance data can be taken from CINDA [24]. If no experimental data are available, one has to interpolate between average s-wave radiation widths of neighbouring nuclei. Uncertainties in the normalization of the gamma-ray transmission coefficients show up most significantly in the capture cross sections.

Examples:

1. Fig. 3 illustrates the influence of the value of the average s-wave radiation width used for the normalization on the neutron capture activation cross section for ^{137}Ba. The three curves display the results of calculations with different values for $\bar{\Gamma}_\gamma$, but fixed values for all other model parameters. For the E1 strength function the Brink-Axel model was applied, using global parameters [21] for the E1 giant resonance.
2. The use of the Brink-Axel model for the E1 strength function leads, in comparison to the Weisskopf model, to a harder gamma-ray production spectrum as can be seen from fig. 4 for ^{138}Ba at an incident neutron energy of 8.5 MeV. For both calculations the normalization of the gamma-ray transmission coefficients was to $\bar{\Gamma}_\gamma$ = 80 meV. The overwhelming part of the gamma-ray production spectrum shown in this figure stems from (n,n'γ) processes. As the displayed experimental data by Perkin [25] have large errors, it is not evident that the Brink-Axel model is preferable, but in general it is. Therefore this model with global parameters for the E1-giant resonance [21] is used in the further examples.

3.5. Level densities

The level densities are calculated in the frame of the backshifted Fermi gas model by means of the expression by Lang [26]:

$$\rho(U,J,\pi) = \tfrac{1}{2}\,\rho(U,J)$$

$$\rho(U,J) = \omega(U,M=J) - \omega(U,M=J+1)$$

$$\omega(U,M) = \frac{1}{\sqrt{12}}\left(\frac{2\Theta_{eff}}{\hbar^2}\right)^{-1/2}\left[U-\Delta-\hbar^2M^2/2\Theta_{eff}+\tfrac{3}{2}t\right]^{-3/2}\exp\left\{2\left[a\left(U-\Delta-\hbar^2M^2/2\Theta_{eff}\right)\right]^{1/2}\right\}$$

$$U = at^2 - \tfrac{3}{2}t + \hbar^2M^2/2\Theta_{eff}$$

It is assumed that levels with positive and negative parity have the same density. The parameters of the model are the level density parameter a, the effective moment of inertia Θ_{eff} and the backshift Δ. In the recent version also a combination of Fermi gas and constant temperature forms can be used; the additional input parameters then are: transition energies between the different forms, temperatures and spin cutoff parameters.

It occurs that in many cases the calculated cross sections most critically depend on the level densities. As these formulas are of semiempirical nature it is important that the level density parameters are based on additional experimental information. For instance the parameters of the backshifted Fermi gas model can be determined so as to reproduce the cumulative density of low excited levels and resonance spacings. Level density parameters derived from such experimental information can be found in the literature; e.g. there are compilations by Dilg et al. [27] and by Gilbert and Cameron [28]. In cases where the level densities have a strong influence on the results it is better to redetermine the level density parameters by reproducing most recent data than to take them from such compilations. For nuclei for which no appropriate experimental data are available one has to interpolate between level density parameters of neighbouring nuclei. This may introduce considerable uncertainties in the calculated cross sections. In addition to uncertainties in the level density parameters there remains also the question how well such semi-empirical formulas reproduce the energy dependence of the level density in the rather wide energy region required for such calculations. An improvement may be achieved by using level densities derived from microscopic calculations which have been described in the lectures on level density.

A few qualitative statements on the dependence of the total probability of the various decay modes on the level densities can be given. For simplicity we consider only nuclei not subject to fission. For heavy nuclei neutron emission dominates. Therefore the neutron emission probability depends on the level densities only weakly. The emission probabilities of charged particles and photons depend on the level density of the respective residual nucleus and of that nucleus resulting from the competing neutron emission. For lighter nuclei, however, where charged particle emission is not hindered by the Coulomb barriers to such an extent things are more complicated. The emission probability for each decay mode depends on the level densities of all residual nuclei. The extent of this dependence is determined by the separation energies and heights of the Coulomb barriers.

Since total activation cross sections mainly depend on the total emission probabilities these considerations apply immediately to such activation cross sections.

Examples: We want to illustrate the dependence of activation cross sections on level densities for low incident energies where only equilibrium decay is relevant for which the level densities discussed above apply. Fig. 5 again shows the neutron capture activation cross section for ^{137}Ba for incident energies below 4 MeV calculated with three values of the a-parameter of ^{138}Ba; the back-shifted Fermi gas model was used for all excitation energies. All other parameters are kept unchanged, in particular the average s-wave radiation width used for the normalization of the γ-ray transmission coefficients. With fixed $\bar{\Gamma}_\gamma$, a variation of the level density changes the normalization constant for the γ-ray transmission coefficients.

3.6. Discrete levels

Excitation energies, spins and parities of the discrete levels for all residual nuclei must be prepared as input. For all CN for which gamma-ray cascades are taken into account, also the gamma-ray branching ratios are required. The information about

the level schemes can be found in the journal Nuclear Data Sheets [29] and in compilations by Endt and van der Leun [30] and Ajzenberg-Selove [31]. The level density formulas describe the actual spin and parity distribution the worse the lower the excitation energy is. Therefore, it is important to use discrete levels to as high an energy as complete information on them is available. The transition between discrete levels and level density can nevertheless lead to unphysical effects on the calculated cross sections. This has to be kept in mind when interpreting results at energies where this transition plays an important role.

Example: The consideration of discrete levels of the target nucleus is important not only for the calculation of cross sections for inelastic scattering but also for those reactions for which (n,n') processes represent a considerable competition. Fig. 6 shows the calculated capture activation cross section of ^{138}Ba compared with experimental data. One clearly sees the onset of additional neutron competition at 1.436 MeV and at 1.899 MeV where the first two excited levels (2^+,4^+) of ^{138}Ba lie. For the calculations we used neutron transmission coefficients generated by an optical potential which was obtained by fitting experimental data for elastic scattering, the total cross section and strength functions. The gamma-ray transmission coefficients were normalized to an average s-wave radiation width of 80 meV.

3.7. Preequilibrium model parameters

For the preequilibrium decay the parameter FM, which by eq. (12) defines the matrix element for the internal transition rates, and the initial numbers of particles and holes must be given. For the latter numbers, for nucleon-induced reactions the values 2 and 1, respectively, are recommended. By means of a control parameter one can choose between particle emission rates with and without charge conservation. If for α-particles preformation shall be considered the preformation factor has to be specified. The single particle state density g entering in the internal transition rates and in the particle hole state densities can either be taken as $6\pi^{-2}A/g$ (A ... mass number) or as $6\pi^{-2}a$ where a is the input a-parameter for the Fermi gas level density. A backshift in the particle-hole-state density can optionally be used.

Example: Preequilibrium emission has a marked influence on first chance particle spectra, in as far as the emission of high energetic particles is favoured. As a consequence, also the activation cross sections are affected. The amount of preequilibrium emission depends on how successful particle decay competes with internal transitions and is therefore determined by the respective rates. Fig. 7 displays the influence of the constant FM, that is of the internal transition rates on the falling part of the $^{56}Fe(n,p\gamma)$ excitation function. With increasing FM the precompound contribution decreases. Particle emission rates with consideration of charge conservation were employed. That this is important whenever proton and neutron emission shall be described simultaneously can be seen from fig. 8 which shows that the experimental neutron production spectrum [44] resulting from ^{56}Fe+n at 14.36 MeV can be well reproduced with the same precompound parameters as the $^{56}Fe(n,p\gamma)$ activation cross section. The internal transition rate of the three exciton state assumes with FM = 500 MeV^3 a value of $\lambda_+(p=2,n=1,U\approx 22\,MeV) = 0.7\,10^{22}\,s^{-1}$ and is in good agreement with the value obtained by E. Gadioli et al. [45].

3.8. Fission input

Fission input data have to be prepared for all CN. Besides the control numbers for single-or double-humped barrier and complete or partial damping in the second well the parameters which characterize the shape of the fission barrier must be given. As the symmetry properties of the saddle point shapes are different at the two barriers the spectrum of transition states can be specified separately for the inner and the outer barrier. For the discrete part of the spectrum, information (bandheads, rotational constants) for generating rotational bands has to be supplied, for the continuous part parameters for a level density formula which consists of constant temperature forms and a Fermi gas form are required. We do not discuss how to choose the fission input data since special lectures of this course deal with this problem.

Example: We merely show in fig. 9 as an example the calculated fission cross section for ^{238}U for neutron energies up to 10 MeV compared with ENDF/B-IV. The parameters were chosen similar to those proposed by Lynn [46]. For the transition states of ^{238}U four rotational bands in the first MeV of excitation energy were considered, while for ^{239}U all transition states were treated as continuum. In general, the calculations were performed under the assumption of complete damping; only for incident energies below 1.4 MeV partial damping was assumed. Complete damping in this energy region, however, gives a fit of comparable quality. Neutron transmission coefficients were derived by means of a version of the IUPITOR 1 code from the optical potential proposed by Lagrange [47].

4. Output evaluation

By specific control parameters intermediary results can be printed out. If none of these control parameters has a non-zero value, the standard output is obtained.

It contains the population of discrete levels by particle emission and the contribution to the total fission cross section for all CN. For those CN, for which γ-ray cascades are considered, also the population of the levels by gamma-ray cascades starting from the continuum, and the activation cross sections for ground and isomeric states are printed.

Further the standard output comprises the sum of the gamma-ray spectra and - if all emitted particles are of same type - the sum of the particle spectra resulting from the decay of

each CN. For (n,xn) reactions for heavy nuclei, where charged particle emission is strongly hindered, these sums represent practically the total photon and neutron production spectrum. For lighter nuclei the contributions of (n,pn), (n,αn) ... reactions to the photon and neutron production spectra have to be considered, too. As the code treats only one sequence of emitted particles at one time, several runs are required in this case. For fissile nuclei, on the other hand, one has to be aware that the contributions of the fission products to the photon and neutron production spectra are not calculated.

The standard output also contains some intermediary results for the WF correction and the information whether the correction factor is calculated or set equal to unity by an internal criterion.

In addition, the precompound fraction ($1-q^{pre}$) and the integrals over all first chance emission spectra are part of the standard output.

The output can be extended by setting one or more of the above-mentioned controls to a non-zero value. The most important intermediary results that can be obtained in this way are the following:

i. The γ-ray spectrum and the particle emission spectrum resulting from the decay of each single CN. For first chance particle emission in this case the preequilibrium and the equilibrium spectrum are output both separate and combined.

ii. Production cross sections for gamma transitions between discrete levels of all CN.

iii. Level densities, contributions of the various decay modes to the HF denominator, fission probabilities and populations ($W\beta^{(o)}$, $\overline{W\beta}$) of the continuum. The knowledge of these quantities is helpful if one wants to judge how critically the competing reactions influence the accuracy of the calculated cross sections.

Example: From the additional output further information of interest can be extracted. As an example for such an output evaluation we illustrate the influence of gamma competition on (n,2n) excitation functions for heavy nuclei, in particular for ^{198}Pt (fig. 10). The solid and the dashed curve were obtained under consideration of γ-ray cascades in ^{198}Pt and ^{197}Pt, using the Brink-Axel and the Weisskopf model, respectively, and an average s-wave radiation width of 100 meV. For the dash-dotted curve gamma-ray cascades in ^{198}Pt were neglected; it displays only the sum of all populations of ^{197}Pt below the neutron binding energy. Therefore this curve represents the (n,2n) cross section under the assumption that gamma-ray emission is negligible compared with neutron emission. The results show, that this is not the case. Gamma competition has a marked influence on (n,2nγ) activation cross sections whenever the competing (n,n'γ) and (n,3nγ) processes are of importance.

5. Conclusion

The code STAPRE is apt to calculate a variety of cross sections for processes which can be described in the compound nucleus model as an evaporation sequence. In particular, γ-ray cascades are treated in great detail. By the inclusion of preequilibrium decay in the first step processes for which the compound nucleus model is not adequate are, at least partially, comprehended. Nevertheless, there is a number of cross sections of practical importance which cannot be calculated reliably. The excitation of low-lying collective states by inelastic scattering, especially for deformed nuclei, is not adequately represented by the preequilibrium contribution, but has to be described by direct reaction models. Another type of reaction where direct processes play an important role is the capture reaction at energies above some MeV. As the direct and semidirect capture mechanism is not included to the code, capture cross sections and the high-energy part of gamma-ray production spectra are underestimated by far at high incident energies.

When applying the results of the code one has to make sure of the adequacy of the underlying models. Besides that, one has to be aware of the dependency of the results on quantities - such as level densities, level schemes, gamma-ray strength functions, fission barrriers and others - which frequently are not known very well. The influence of uncertainties in these quantities on the cross section differs from reaction to reaction. Therefore in unfavourable cases inaccurate results may be obtained even if the reaction is adequately described by the models employed. The accuracy of the result has to be investigated in each individual case. Quite general, however, the accuracy of a particular cross section can be improved by fitting as many experimental data for competing reactions as possible with one set of model parameters.

References

[1] BARTHOLOMEW, G.A., EARLE, E.D., FERGUSON, A.J., KNOWLESS, J.W., LONE, M.A., Advances in Nuclear Physics, Vol. 7, Ch. 4, Plenum Press, New York (1973).

[2] HILL, D.L., WHEELER, J.A., Phys. Rev. 89 (1953) 1102.

[3] BACK, B.B., HANSEN, O., BRITT, H.C., GARRETT, J.D., Phys.Rev. C9 (1974) 1924.

[4] LYNN, J.E., BACK, B.B., J. Phys. A7 (1974) 395.

[5] GRIFFIN, J.J., Phys. Lett. 17 (1966) 478.

[6] CLINE, C.K., BLANN, M., Nucl. Phys. A 172 (1971) 225.

[7] BRAGA-MARCAZZAN, G.M., GADIOLI-ERBA, E., MILAZZO-COLLI, L., SONA, P.G., Phys. Rev. C6 (1972) 1398.

[8] MILLER, J., "Preequilibrium Processes", Proceedings of the Int. Conf. on Nuclear Physics, Munich, Sept. 1973, Vol.II, DE BOER, J., MANG, H.J., Edts., North-Holland-American Elsevier Publ. Co. (1974).

[9] KALBACH, C., Acta phys. slov. 25 (1975) 100.

[10] BLANN, M., Ann.Rev.Nucl.Sc. 25 (1975) 123.
[11] WILLIAMS, F.C., Jr., Phys.Lett. 31B (1970) 184.
[12] CLINE, C.K., Nucl. Phys. A 195 (1972) 353.
[13] KALBACH-CLINE, C., Nucl. Phys. A 210 (1973) 590.
[14] WILLIAMS, F.C., Jr., Nucl. Phys. A 116 (1971) 231.
[15] GADIOLI, E., GADIOLI-ERBA, E., SONA, P.G., Nucl. Phys. A 217 (1973) 589.
[16] MILAZZO-COLLI, L., BRAGA-MARCAZZAN, G.M., Nucl.Phys. A210 (1973) 297.
[17] MOLDAUER, P.A., Revs. of Mod. Phys. 36 (1964) 1079.
[18] WAPSTRA, A.H., GOVE, N.B., Nucl. Data Tables 9 (1971) No 4-5.
[19] GOVE, N.B., WAPSTRA, A.H., Nucl. Data Tables 11 (1972) No 2-3.
[20] VIOLA, V.E., Jr., SWANT, J.A., GRABER, J., Atomic and Nucl. Data Tables 13 (1974) No 1.
[21] AXEL, P., Phys. Rev. 126 (1962) 671.
[22] WEISSKOPF, V.F., Phys. Rev. 83 (1951) 1073.
[23] MUGHABGHAB, S.F., GARBER, D.J., BNL 325 (1973).
[24] CINDA, An Index to the Literature on Microscopic Neutron Data, IAEA, Vienna (1977).
[25] PERKIN, J.L., Nucl.Phys. 60 (1964) 561.
[26] LANG, D.W., Nucl. Phys. 77 (1966) 545.
[27] DILG, W., SCHANTL, W., VONACH, H., UHL, M., Nucl. Phys. A 217 (1973) 269.
[28] GILBERT, A., CAMERON, A.G.W., Can. J. Phys. 43 (1965) 1446.
[29] Nuclear Data Sheets, ed. by the Nuclear Data Group, Academic Press (New York).
[30] ENDT, P.M., VAN DER LEUN, C., Nucl. Phys. A 214 (1973) 1.
[31] AJZENBERG-SELOVE, F., Nucl. Phys. A 281 (1977) 1.
[32] STAVISSKII, Yu. Ya., TOLSTIKOV, V.A., Sov. J. Atomic Energy 10 (1962) 498.
[33] JOHNSRUD, A.E. SILBERT, M.G., BARSHALL, H.H., Phys. Rev. 116 (1959) 927.
[34] PASECHNIK, M.V., BARCHUK, I.F., TOTSKY, I.A., STRIZHAK, V.I., KOROLOV, A.M., HOFMAN, Y.V., LOVCHIKOVA, G.N., KOLTYNIN, E.A., YNKOV, G.B., 2nd Int. Conf. Peaceful Uses At. Energy (Proc. Conf. Geneva, 1958) 15, UN, New York (1958) 18.
[35] LEIPUNSKY, A.I., KAZACHKOVSKY, O.D., ARTYUKHOV, G.Y., BARYSHNIKOV, A.I., BELANOVA, T.S., GALKOV, V.N., STAVISSKY, Y.Y., STUMBUR, E.A., SHERMAN, L.E., 2nd Int. Conf. Peaceful Uses At. Energy (Proc. Conf. Geneva, 1958) 15, UN, New York (1958) 50.
[36] LYON, W.S. MACKLIN, R.L., Phys. Rev. 114 (1959) 1619.
[37] PETÖ, G., MILIGY, Z., HUNYADY, I., J. Nucl. Energy 21 (1967) 797.
[38] HUGHES, D.J., GARTH, R.C., LEVIN, J.S., Phys. Rev. 91 (1953) 1423.
[39] COLDITZ, J., HILLE, P., Anz. Österr. Akad. Wiss., math.-naturw. Kl. 105 (1968) 236.
[40] LISKIEN, H., PAULSEN, A., J. Nucl. Energy AB19 (1965) 73.
[41] LISKIEN, H., PAULSEN, A., Nukleonik 8 (1966) 315.
[42] VONACH, H.K., VONACH, W.G., MUENZER, H., SCHRAMEL, P., EANDC(E)-89(1968) 37.
[43] SMITH, D.L., MEADOWS, J.W., ANL/NDM-10 (1975).
[44] STENGL, G., UHL, M., VONACH, H., Nucl. Phys. A 290 (1977) 109.
[45] GADIOLI, E., GADIOLI-ERBA, E., TAGLIAFERRI, G., Phys. Rev. C14 (1976) 573.
[46] LYNN, J.E., Harwell Report AERE-R7468 (1974).
[47] LAGRANGE, C., Acta phys. slov. 26 (1976) 32.
[48] BISSEM, H.H., BORMANN, M., MAGIERA, E., WARNEMUENDE, R., Nucl. Phys. A 157 (1970) 481.

Figure Captions

Fig. 1: A schematic representation of the different ways of populating final states (E_d, I_d, Π_d) in the reaction $T(J_0, \pi_1, \pi_2\gamma)F$.

Fig. 2: A schematic representation of the proceeding of the code STAPRE.

Fig. 3: The influence of the average s-wave radiation width used for the normalization of the gamma-ray transmission coefficients on the neutron capture activation cross section of ^{137}Ba.

Fig. 4: The gamma-ray production spectrum for ^{138}Ba+n at 8.5 MeV calculated with the Brink-Axel and the Weisskopf model for $T^{\gamma}_{J\pi}(\varepsilon_\gamma)$. In both cases the gamma-ray transmission coefficients were normalized to an average s-wave radiation width of 80 meV.

Fig. 5: The neutron capture activation cross section for ^{137}Ba calculated with three different values of the level density parameter a for ^{138}Ba. The back-shifted Fermi gas model was used for all excitation energies in the continuum region.

Fig. 6: The calculated neutron capture cross section for ^{138}Ba compared with experimental data.

Fig. 7: The influence of the parameter FM which determines the internal transition rates for preequilibrium decay on the high energy part of the ^{56}Fe(n,pγ) excitation function.

Fig. 8: The neutron production spectrum for ^{56}Fe+n at 14.36 MeV compared with experimental data; contributions from (n,n'), (n,2n) and (n,pn) processes were taken into account.

Fig. 9: The calculated total fission cross section for ^{238}U compared with ENDF/B-IV.

Fig. 10: The influence of gamma-ray competition on the ^{198}Pt(n,2nγ) activation cross section.

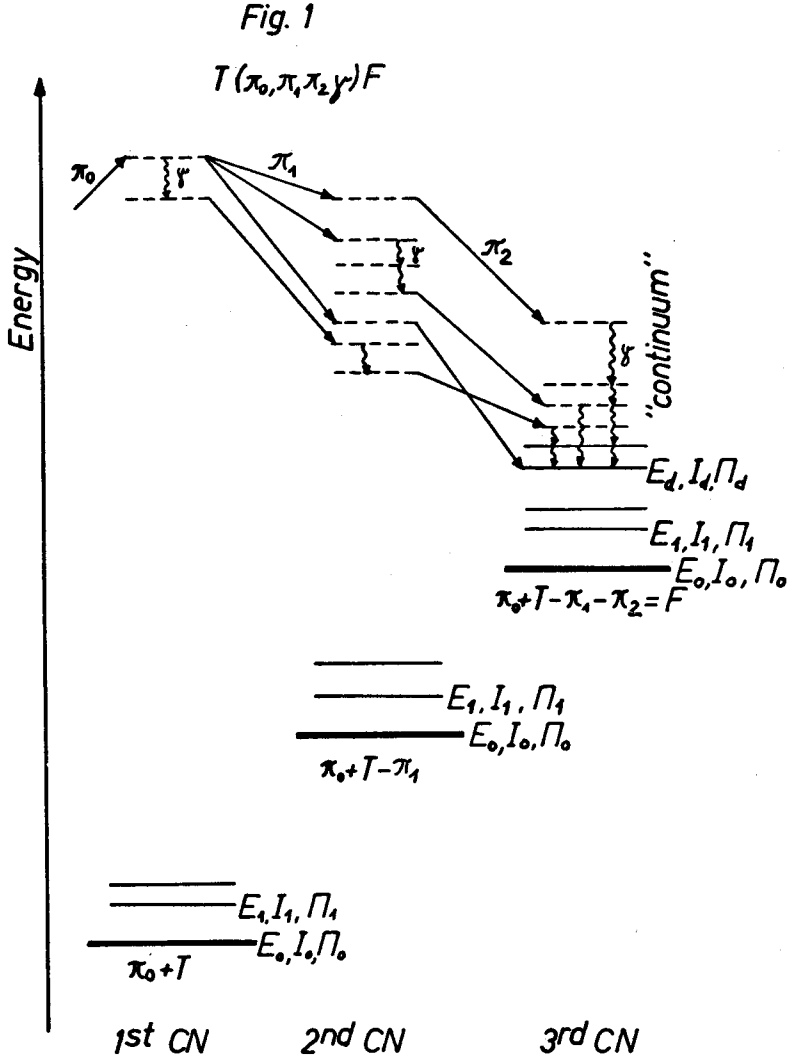

Fig. 1: A schematic representation of the different ways of populating final states (E_d, I_d, Π_d) in a reaction $T(\pi_0, \pi_1, \pi_2, \gamma)F$.

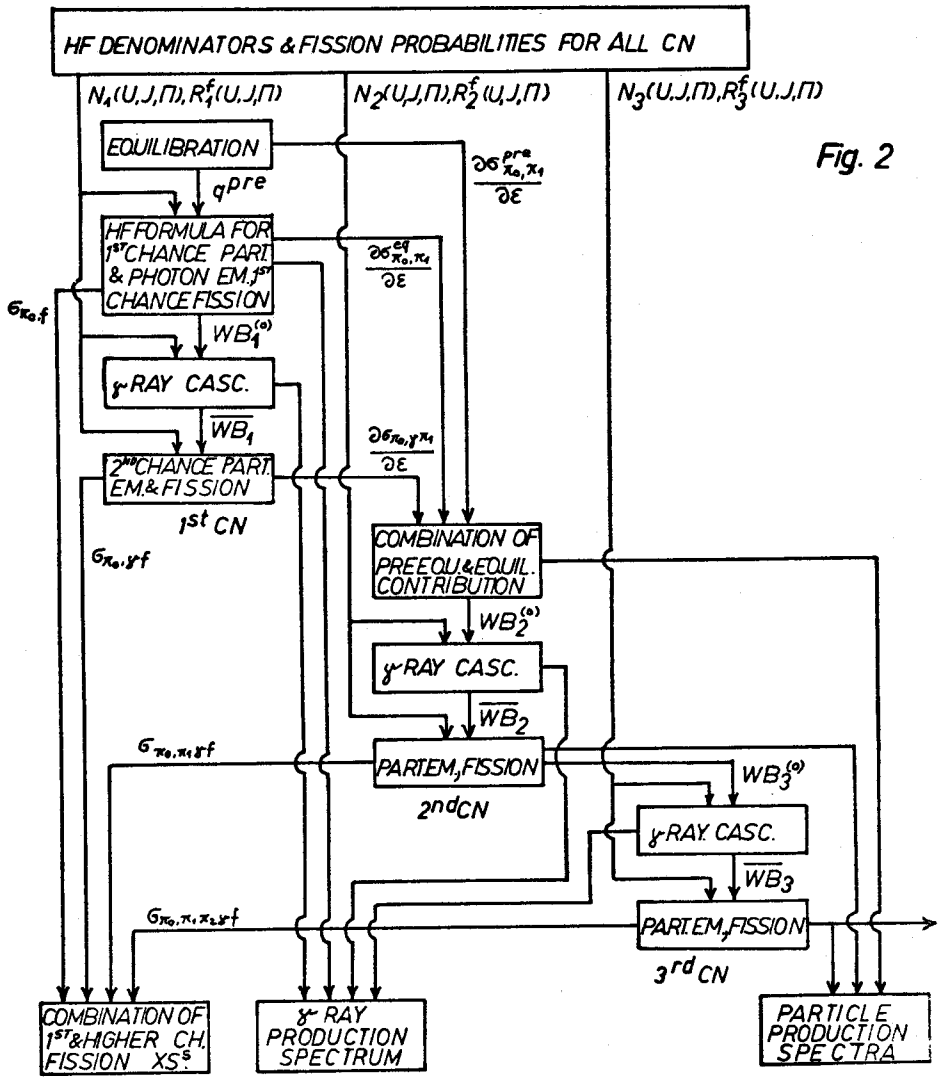

Fig. 2

Fig. 2: A schematic representation of the proceeding of the code STAPRE.

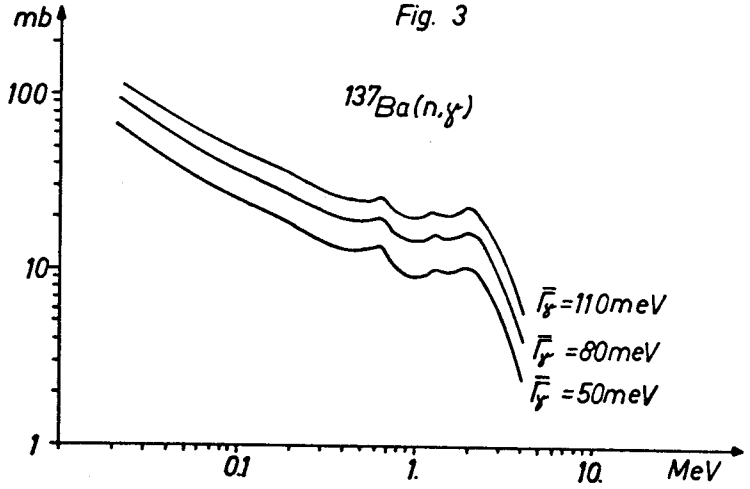

Fig. 3: The influence of the average s-wave radiation width $\bar{\Gamma}_\gamma$ used for the normalization of the gamma-ray transmission coefficients on the neutron capture activation cross section of ^{137}Ba.

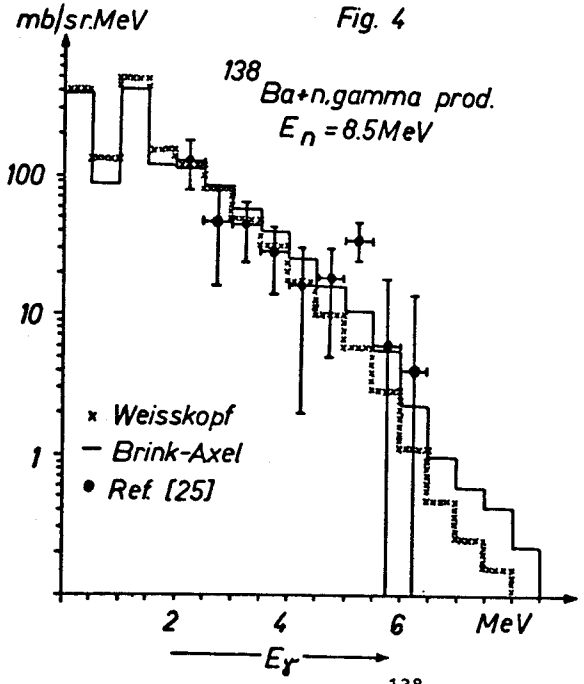

Fig. 4: The gamma-ray production spectrum for ^{138}Ba+n at 8.5 MeV calculated with the Brink-Axel and the Weisskopf model for $f^{\gamma}_{E1}(\varepsilon_\gamma)$. In both cases the gamma-ray transmission coefficients were normalized to an average s-wave radiation width of 80 meV.

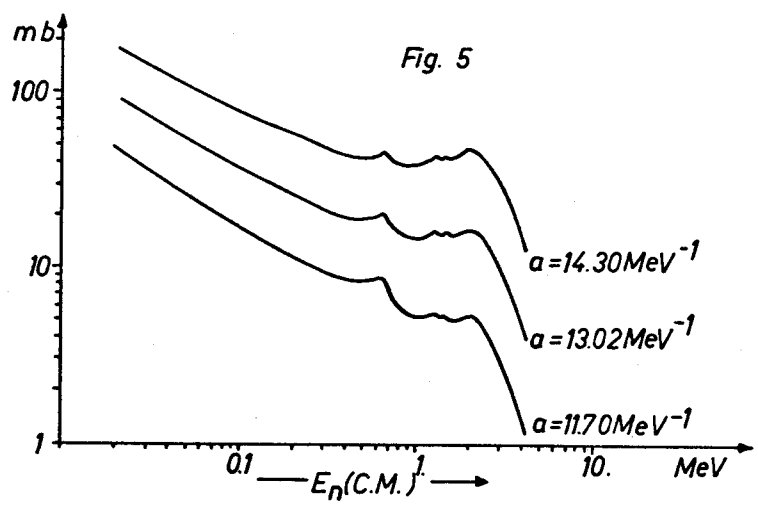

Fig. 5: The neutron capture activation cross section for ^{137}Ba calculated with three different values of the level density parameter a for ^{138}Ba. The back shifted Fermi gas model was used for all excitation energies in the continuum region.

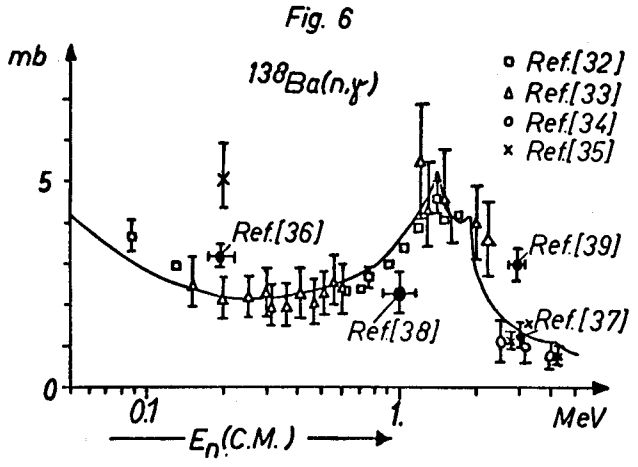

Fig. 6: The calculated neutron capture activation cross section for ^{138}Ba compared with experimental data.

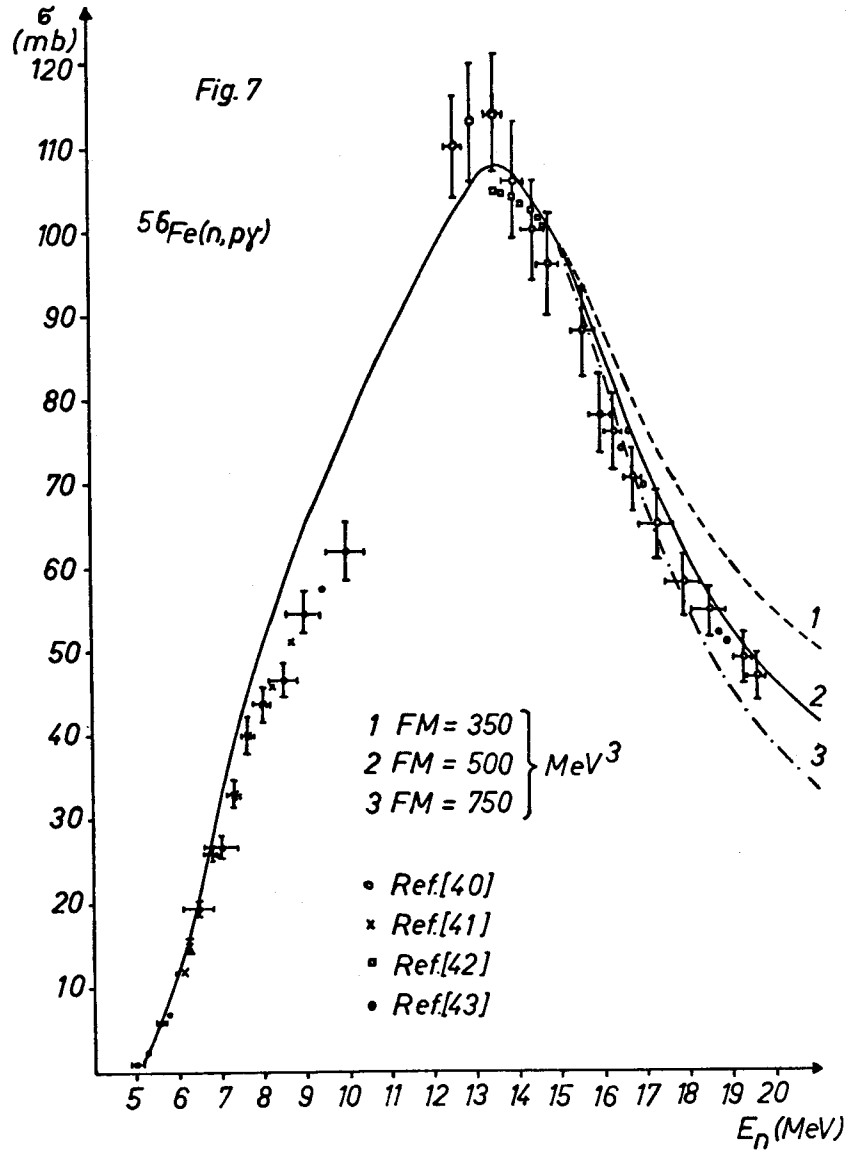

Fig. 7: The influence of the parameter FM which determines the internal transition rates for preequilibrium decay on the high energy part of the $^{56}Fe(n,p\gamma)$ excitation function.

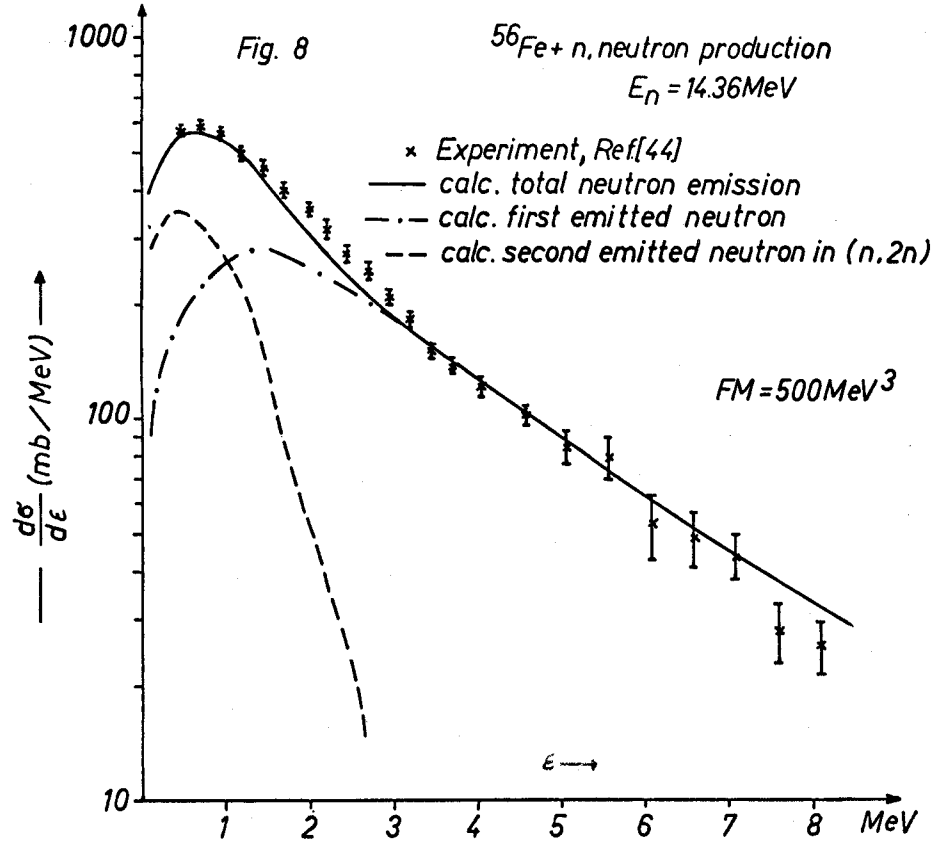

Fig. 8: The neutron production spectrum for $^{56}Fe+n$ at 14.36 MeV compared with experimental data; contributions from (n, n'), (n, 2n) and (n, pn) processes were taken into account.

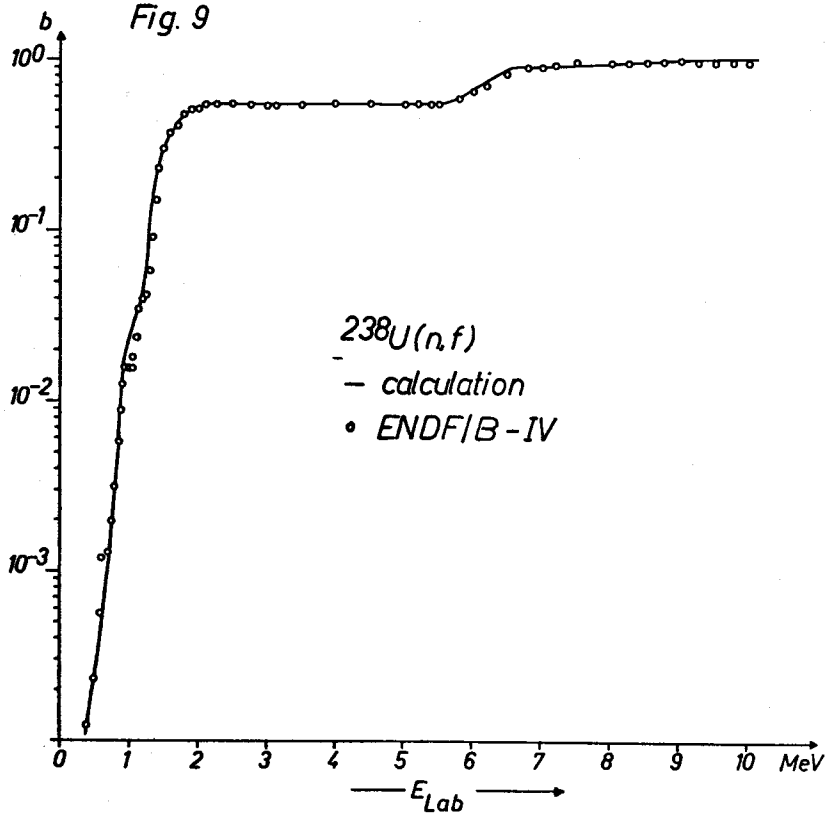

Fig. 9: The calculated total fission cross section for ^{238}U compared with ENDF/B-IV.

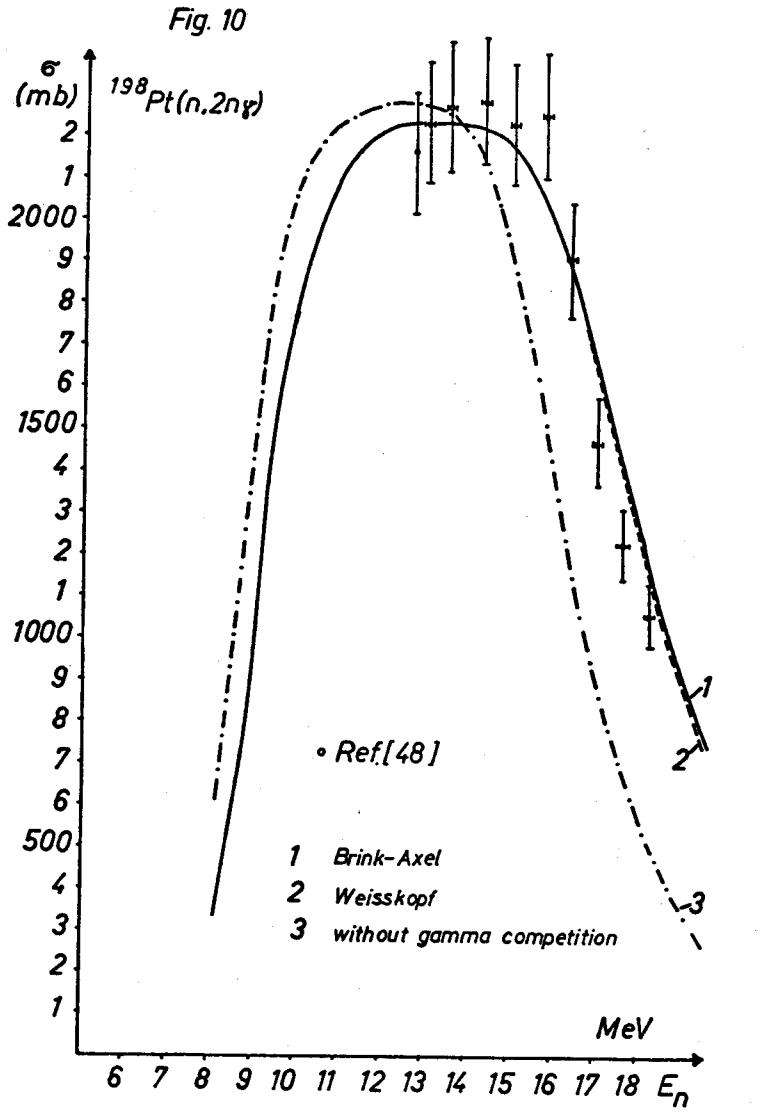

Fig. 10: The influence of gamma-ray competition on the $^{198}Pt(n, 2n\gamma)$ activation cross section.

FUNDAMENTALS OF THE DOUBLE-HUMPED FISSION BARRIER

M. BRACK
Institut Laue-Langevin,
Grenoble, France

ABSTRACT

We review the development of the theory of the fission barrier over the past forty years. Special emphasis is put on the shell-correction method of Strutinsky and its foundation and numerical verification from microscopical Hartree-Fock calculations. The different practical realisations of the method and its applications to the calculation of deformation energy surfaces are reviewed. The influence of the different shape degrees of freedom of the nucleus on the form of the fission barrier is discussed. Finally, we summarize some more recent developments concerning both experimental and theoretical aspects of the double-humped fission barrier.

INTRODUCTION

These notes cover the contents of six lectures presented at the Winter Course on Nuclear Theory for Applications, held at the ICTP in 1978.

Almost all of what was discussed in the lectures has been published before extensively; we shall therefore not repeat here details of mathematical derivations or numerical computations. For these, we refer to the literature. The main purpose of these notes is to give the reader an introduction to the different physical models which are employed in the theory of the fission barrier. With the help of illustrative examples, we shall summarize the results of different calculations and give an impression of their reliability and their agreement with experimental results.

1. HISTORICAL REVIEW OF THE FISSION BARRIER

1.1. Discovery of Fission

A nice historical account of the discovery of fission is given in the book of Hyde, 1964, p.3 (with detailed references). Fermi and collaborators in Rome (1934/5)[1] bombarded uranium (Z = 92) with paraffin-slowed neutrons. They tried to explain the resulting radioactivity as coming from a new element (Z = 93) or even several "transuranium" elements. However, too many activities were seen and the radiochemical properties were too unexpected to be explained in this way. The situation remained confused, until in 1939, Hahn and Strassmann [2] and Meitner and Frisch[3] recognized the new process as the fissioning of the nucleus into (normally two) fragments.

Immediately after the discovery of fission, Meitner and Frisch[3] also gave a qualitative theoretical explanation of the process using the analogy of a charged liquid drop. Still in the same year, 1939, two independent theoretical papers appeared, using and developing the same basic picture: a short one of Fraenkel [Fr39], and an extensive one of Bohr and Wheeler [BW39], which became and remained a classic for many years to come.

1.2. The liquid drop model

This model uses an idealization of the nucleus as a uniformly charged liquid drop. The attractive nuclear forces are summarized by a (classical) surface tension. The stability or decay (fissioning) of the nucleus is governed by the interplay between this attractive surface tension and the repulsive Coulomb force.

This same model underlies the semi-empirical mass formula developed by Weizsäcker[We35] and Bethe[BB36,Be37] (see also [BK37]), in which the total mass (binding energy) of a nucleus is written in the form

[1] E. Fermi, Nature 133 (1934) 898; E. Amaldi et al. Proc. Roy. Soc. A149 (1935) 522.
[2] O. Hahn and F. Strassmann , Naturwiss. 27 (1939), p.11 and p.89.
[3] L. Meitner and O.R. Frisch, Nature 143 (1939) p.239 and p.471

$$E(N,Z) = a_v(1+\kappa_v I^2)A + a_s(1+\kappa_s I^2)A^{2/3} + \dots$$
$$+ C_d Z(Z-1)A^{-1/3} + C_{ex} Z^{4/3} A^{-1} + \dots \qquad (1.1)$$
$$+ P(N,Z) + \delta E(N,Z)$$

with

$$A = N+Z \ , \quad I = \left(\frac{N-Z}{A}\right).$$

Here a_v and a_s are the so-called volume and surface energies, κ_v and κ_s the asymmetry coefficients, the terms with C_d and C_{ex} are the direct and exchange Coulomb energies, P(N,Z) is a (relatively small) pairing energy ($\sim \pm 2$ MeV) and δE the so-called shell-correction energy. All terms but δE are smooth functions of N and Z and constitute the main part ($\gtrsim$ 99% in a heavy nucleus) of the binding energy. We express this by writing (1.1) in the form

$$E(N,Z) = E_{LDM}(N,Z) + \delta E(N,Z). \qquad (1.2)$$

The LDM accounts for all terms included in E_{LDM} (except for P(N,Z) which we include for convenience).

In the application of this model to the fission process, one is interested in the deformation energy, i.e. the difference $E^{dif}_{LDM}(\beta)$ between the energy at a given deformation (we summarize all possible deformation parameters by β) minus that of the spherical shape $\beta = 0$. To this difference, only the surface and Coulomb terms contribute in E_{LDM}; the volume term falls out due to the fact that nuclear matter is (almost) incompressible. The deformation energy is thus written as the sum of a surface and a Coulomb energy:

$$E^{def}_{LDM}(\beta) = E_{Surf}(\beta) + E_{Coul}(\beta) \qquad (1.3)$$

(both normalized to zero at $\beta = 0$, i.e. spherical shape).

We come back to the parametrization of the nuclear shape (i.e. the exact meaning of β) in lesson 4.

In his book on "Theories of Nuclear Fission", 1964, Wilets presents the LDM and results of deformation energy calculations very extensively, summarizing both the original papers [BW39, Fr39] and later extensions, the last of which [CS63] containing large-scale numerical computer calculations. Not mentioned there is another important paper [SL63].

The critical parameter in the LDM is the so-called "fissionability" (or fissility) parameter X, defined as the ratio of the Coulomb energy and twice the surface energy of a charged sphere with radius R_0:

$$X = E_{Coul}(0) / 2E_{Surf}(0) \qquad (1.4)$$

with

$$E_{Coul}(0) = \tfrac{3}{5} \cdot Z^2 e^2 / R_0 \; ; \quad E_{Surf}(0) = 4\pi R_0^2 \tau . \qquad (1.5)$$

Here τ is the surface tension. Using the experimentally known A-dependence of the nuclear radius

$$R_0 = r_0 A^{1/3} \quad , \quad r_0 \simeq 1.2 \text{ fm} , \qquad (1.6)$$

we can relate τ to the surface term in the mass formula (1.1):

$$\tau = a_s (1 + \kappa_s I^2) / 4\pi r_0^2 . \qquad (1.7)$$

Combining eqs.(1.5)-(1.7) we see that the fissility parameter X, apart from the relatively weak I^2-dependence of τ , goes like Z^2/A. One therefore frequently puts

$$X = (Z^2/A) / (Z^2/A)_{crit} . \qquad (1.8)$$

With the above constants and the empirical values $a_s \simeq 18$ MeV, $\kappa_s \simeq -2.5$, one obtains

$$(Z^2/A)_{crit} \approx 45 - 50 . \qquad (1.9)$$

In most early LDM calculations, one used the multipole expansion of the deformed nuclear surface [BW39]:

$$R(\vartheta,\varphi) = R_0 \left[1 + \sum_{\lambda,\mu} a_{\lambda\mu} Y_{\lambda\mu}(\vartheta,\varphi) \right] . \qquad (1.10)$$

The $\{a_{\lambda\mu}\}$ thus represent one possible set of deformation parameters β.

Main results of LDM calculations:

1) For $X < 1$, the spherical configuration (all $a_{\lambda\mu} = 0$) is a stable local minimum. Thus, the LDM predicts spherical groundstates for all stable nuclei. For $X > 1$, the spherical shape becomes unstable against quadrupole (a_{20}) deformation, the nucleus then is spontaneously deforming itself until it fissions. Thus, the LDM predicts spontaneous fission for all nuclei with $X > 1$. (N.B. A heavy actinide nucleus has $X \simeq 0.8$, i.e. $(Z^2/A) \simeq 40$).

2) For $0.7 \lesssim X < 1$ the deformation energy surface, $E^{def}_{LDM}(a_{\lambda\mu})$ has a saddle point with positive energy E_f relative to the ground state. This result is qualitatively already found if only a_{20} and a_{40} deformations are used, see Fig. 1.1. The saddle point has always positive (prolate) quadrupole deformation. Along a static path over the saddle point (way of steepest descent), one obtains thus a fission barrier with height E_f. Numerical calculations including multipoles up to $\lambda \simeq 16$ in eq.(1.10) lead to [CS63]

$$E_f \approx 0.83 E_{Surf}(0) (1-X)^3 , \quad 0.67 < X < 1 . \qquad (1.11)$$

In Table 1.1 we show a comparison of the calculated values of E_f with the experimental barriers measured up to $\sim$ 1960 (assuming a single-humped form of the barrier). The agreement is bad. Whereas E_f^{LDM} varies from $\sim$ 15 to $\sim$9 MeV, the experimental barriers are all around $\sim$ 5.5 to 6.5 MeV. The LDM thus gives the wrong quantitative behaviour of the barrier heights.

3) For $X > 0.39$, the deformation energy is always stable against rotationally asymmetric ($\mu \neq 0$) and reflection (left/right) asymmetric (λ odd) deformations. In other words, only the parameters $a_{\lambda 0}$ with λ even are different from zero. As a consequence, the LDM cannot explain the asymmetric mass split in fission.

The main failures of the LDM (no static deformations, wrong fission barriers, no asymmetric fission) are due to the missing of quantum mechanical effects (shell effects). As a hint we may take the order of magnitude of the empirical shell-corrections δE to the goundstate masses [MS66]:

$$|\delta E| = |\delta M| \simeq 5 - 15 \text{ MeV} . \qquad (1.12)$$

This is very small compared to the total binding energies of heavy nuclei ($\sim$ 1000 - 2000 MeV), but it becomes important when compared to the heights of the fission barriers E_f!

The LDM provides thus a nice qualitative description of the fission process, but for a quantitative theory the shell effects have to be included.

1.3 The (deformed) shell model

The shell model [HJ49, Ma49] emphasizes the quantum mechanical structure of the nucleus as a system of Z protons and N neutrons. The mutual nuclear interaction between the neutrons (protons) is summarized by an average potential V_n (V_p) in which the particles are assumed to move independently. For each kind (n or p), a Schrödinger equation is solved

$$\left[-\frac{\hbar^2}{2m}\Delta + V(\underline{r})\right]\varphi_i(\underline{r}) = \varepsilon_i\,\varphi_i(\underline{r}) \qquad (1.13)$$

to obtain the levels ε_i and wavefunctions of the individual nucleons. In the g.-s., the lowest N(Z) states are filled. The potentials $V_n(\underline{r})$ and $V_p(\underline{r})$ contain a local (central) and a spin-orbit part. $V_p(\underline{r})$ includes also a Coulomb potential.

In connection with fission, we are mostly interested in the extension of the shell model to deformed nuclei, which was introduced by Nilsson [Ni55]. In the Nilsson model, the potentials V_n and V_p are deformed along with the shape of the nucleus. The solutions of the Schrödinger equation (1.13) then depend also on the deformation parameters; this gives the familiar Nilsson level schemes, see Fig. 1.2.

In the independent particle model, the total energy is

$$E(\beta) = \sum_{i=1}^{N}\varepsilon_i^n(\beta) + \sum_{i=1}^{Z}\varepsilon_i^p(\beta). \qquad (1.14)$$

Strictly, the justification of the shell model is given in Hartree-Fock theory, where eq.(1.14) is not equal to the total binding energy (see lesson 2). However, for harmonic oscillator potentials (and thus also approximately for the Nilsson model), the total energy is still proportional to (1.14).

A comprehensive description of the Nilsson model is given in the book of Preston and Bhaduri.

Minimisation of the energy E(β) (1.14) with respect to β leads to the groundstate deformation β_0. Good agreement with the experimental deformations of rare earth and actinide nuclei is obtained[1,2]. From the Nilsson spectra $\varepsilon_i(\beta_0)$ at the groundstate, other properties such as spin, magnetic moment and single particle spectra of odd-A nuclei can be derived.

When extended to large deformations, the model fails. The deformation energy (1.14) was found to increase too steeply and not to lead to any reasonable fission barrier[3] (see also [NT69]). Similar results were also found in the two-center shell model (e.g.[SG71]).

The reason for this breakdown is the lack of self-consistency of the used average deformed potentials and of the expression (1.14) for the total energy. At small (groundstate) deformations, the experimental spectroscopic information allows to parametrize the shell model potentials sufficiently well. But when extrapolating to large deformations, the results depend very crucially on the parameters and on the way in which the potentials are deformed.

Myers and Swiatecki [MS66] discussed the connection between the non-uniformities of the shell model spectra ε_i and the magnitude of the empirical shell corrections δE in (1.1). Large gaps in the spectrum ("magic" nucleon numbers) lead to increased binding (negative δE). This is not only restricted to spherical nuclei [St66,67]; deformed shells exist as well (Fig. 1.2)

The first quantitative prescription to calculate δE from the spectrum ε_i was given by Strutinsky [St66-68].

1.4 The shell-correction method (SCM) ("Strutinsky method")

Strutinsky defines the shell-correction δE for each kind of particles by

$$\delta E_{p(n)} = \sum_{i=1}^{Z(N)}\varepsilon_i^{p(n)} - \tilde{E}_{p(n)}\,, \qquad (1.15)$$

i.e. the difference between the sum of occupied levels and its average part

$$\tilde{E}_{p(n)} = \left\langle \sum_{i=1}^{Z(N)}\varepsilon_i^{p(n)} \right\rangle. \qquad (1.16)$$

(The precise definition of the average energies $\tilde{E}_{p(n)}$ will be given in lesson 4). The total energy of the nucleus is then the LDM energy plus the shell-corrections:

$$E(N,Z,\beta) = E_{LDM}(N,Z,\beta) + \delta E_p(Z,\beta) + \delta E_n(N,\beta). \qquad (1.17)$$

This means a renormalization of the average parts of the single-particle energies by the LDM energy. One is thus combining the correct average energy of the LDM with the (at least at small deformations) correct fluctuating part δE of the shell model energy (1.14).

[1] B. Mottelson and S.G. Nilsson, K.gl. Dan. Vid. Selsk. Mat. Fys. Skr. 1, no.8 (1955)
[2] D. Bès and Z. Szymanski, Nucl. Phys. 28 (1961) 42.
[3] S.A.E. Johansson, Nucl. Phys. 22 (1962) 529.

The theoretical quantitative justification of eq.(1.17) can be given in the Hartree-Fock theory and will be discussed in lesson 3.

Main Results of SCM calculations: (Details see lessons 4-6)

1) Explanation of the fission isomers, which had been known long ago [Po62] but not understood, in terms of a double-humped fission barrier which turns out for most actinide nuclei.

2) Quantitative agreement between theoretical and experimental barrier heights; usually within ∿ 1-2 MeV (except for neutron-poor lighter actinides; so-called "Th-anomaly").

3) Ground-state deformations in excellent agreement with experimental ones. The g.s. mass corrections δE(δM) agree with the empirical ones within ∿1-2 MeV (except sometimes in the Pb^{208} region; so-called "Pb-anomaly").

4) Qualitative explanation of mass asymmetry of the fission products due to shell effects, both at the outer saddle point and at the scission point (see lesson 6).

5) Prediction of a possible island (or several) of stable nuclei with $Z \sim 114$-126 or larger; "superheavy nuclei"?

In summary, the Strutinsky method brought a break-through in the theory of the fission barrier, allowing for the first time a quantitatively satisfactory calculation of barrier heights and giving the explanation of the fission isomers as shape isomers. In this method, both the LDM and the shell model are given their balanced role.

1.5 The Hartree-Fock method (HF)

The HF method allows to calculate nuclear properties starting from an effective nucleon-nucleon interaction $V_{eff}(r_1-r_2)$. This is a basically microscopic, quantum mechanical theory, in which only the parameters of the interaction V_{eff} are adjustable. The HF method is the subject of lesson 2.

Fission barriers were calculated with the HF method using the Skyrme force [VB72] for the first time in 1973 [FQ73b, 74]. The obtained barrier heights do not agree with the experimental ones as well as those calculated with the shell-correction method; the reasons for this are mostly understood.

Nevertheless, it was a very essential step to prove that the double-humped barrier can be obtained in a purely microscopical approach.

2. HARTREE-FOCK (HF) THEORY OF NUCLEAR BINDING ENERGY

2.1 Effective nucleon-nucleon interaction: $V_{eff}(\underset{\sim}{r}_1,\underset{\sim}{r}_2)$

With $V_{eff}(\underset{\sim}{r}_1,\underset{\sim}{r}_2)$ we mean the interaction (potential,"force") which acts between two nucleons (placed at $\underset{\sim}{r}_1$ and $\underset{\sim}{r}_2$) in the nuclear medium, i.e. in the presence of the other nucleons of the same nucleus.

V_{eff} thus contains not only the basic interaction between the nucleons considered; it also summarizes the influence of the mutual interactions with all other nucleons of the same nucleus: Reduction of a many (A = N + Z)-body problem to a two-body problem.

Different from V_{eff} is the basic, so-called "free" nucleon-nucleon interaction $V(r_1,r_2)$ which acts between two isolated nucleons. With V one attempts to describe the scattering of two free nucleons by fitting phase shifts (phenomenological potentials V: e.g. Hamada and Johnston [HJ62]and Reid [Re68]. Theoretically, V can be derived from meson exchange processes (see e.g. [BJ76]).

The way from the free potential $V(r_1,r_2)$ to the effective one, $V_{eff}(r_1,r_2)$, in a finite nucleus is long and difficult: One has to solve a many (A)-body problem, which can only be done approximately. A succesful theory was developed by Brückner [Br55, Da67] for infinite nuclear matter; in the so-called "local density approximation" (LDA) [BG58, Be71] it could be applied to finite nuclei.

Extensive numerical calculations, starting with the "Reid soft core potential" $V(r_1,r_2)$ [Re68], were done in order to derive effective potentials $V_{eff}(r_1,r_2)$ which describe nuclear ground state properties well in the Hartree-Fock (HF) approximation (see below) [Ne70, CS72].

Another possibility is to design phenomenological effective interactions V_{eff} which have a simple mathematical form and adjustable parameters [Sk56, 59; Wi58, BB68, Mo70, KC73, NV70, EM72, Go75]. The most successful Hartree-Fock calculations were done in the last decade with the so-called Skyrme forces [Sk56,59], re-discovered by Vautherin and Brink[Va69, VB72, Va73] and further developed by the Orsay group [FQ73a,b; BF74, Fl75, Qu75a]. For extensive reviews of the results, see [Fl75,76; Qu75a,b]. A lecture series on the Skyrme forces was given in Trieste by Vautherin[1].

More recently, Gogny [Go73,75] developed a phenomenological force which allows also the self-consistent inclusion of pairing effects (Hartree-Fock-Bogolyubov method). This is probably at present the most refined effective force, which reproduces many nuclear groundstate properties extremely well.

The connection between the phenomenological Skyrme-type forces and the ones derived from the more basic Brückner-LDA-HF-calculations [Ne70, CS72] was made by Negele and Vautherin [NV72,75] : they justify not only the form, but also the approximate values of the parameters of the Skyrme force (see also [Ne75]).

[1] D. Vautherin, Trieste lectures 1975 (IAEA Vienna, 1975, SMR-14/39)

In the following, we summarize the HF theory; to study it, see e.g. the text book of G.E. Brown[1].

2.2 Hartree-Fock Approximation (HF)

We start from an effective two-body potential $V_{eff}(r_1,r_2)$. In general, it depends not only on the distance r_1-r_2 between the nucleons, but also on their velocities and on the local density $\rho(\frac{r_1+r_2}{2})$ of the nucleus.

The HF approximation consists in extracting from V_{eff} an average one-body potential $V_{HF}(r)$ in which the nucleons move independently. The wave-function[†] is written as an antisymmetrized product of single-particle wave-functions $\phi_i(\underset{\sim}{r})$:

$$\Phi_{HF} = \frac{1}{\sqrt{N!}} \det \left| \phi_i(\underset{\sim}{r}_j) \right|_{i,j=1,\dots N} \qquad \text{(Slater determinant)}. \tag{2.1}$$

The Hamilton operator is

$$\mathcal{H} = T + V_{eff} = \sum_{i=1}^{N} \frac{\hat{p}_i^2}{2m} + \sum_{i<j}^{N} V_{eff}(\underset{\sim}{r}_i, \underset{\sim}{r}_j, \hat{\underset{\sim}{p}}_i, \hat{\underset{\sim}{p}}_j). \tag{2.2}$$

The HF energy is then

$$E_{HF} = \langle \Phi_{HF} | \mathcal{H} | \Phi_{HF} \rangle . \tag{2.3}$$

2.3 Density matrix ρ

$$\rho_{\alpha\beta} = \sum_{i=1}^{N} \langle \alpha | i \rangle \langle i | \beta \rangle ; \qquad (2.4)$$

$|\alpha\rangle, |\beta\rangle$ is an arbitrary basis; $\langle \alpha | i \rangle$ are the expansion coefficients of the wavefunction $\phi_i(\underline{r})$ in this basis:

$$\phi_i(\underline{r}) = \sum_{\alpha} \langle \alpha | i \rangle \langle \underline{r} | \alpha \rangle . \qquad (2.5)$$

In terms of $\rho_{\alpha\beta}$, the HF energy (2.3) can be written as

$$E_{HF} = \sum_{\alpha\beta} T_{\alpha\beta} \rho_{\beta\alpha} + \frac{1}{2} \sum_{\alpha\beta} \sum_{\gamma\delta} \bar{v}_{\alpha\beta,\gamma\delta} \rho_{\delta\beta} \rho_{\gamma\alpha} , \qquad (2.6)$$

or, using matrix notation (tr ≡ trace)

$$E_{HF} = \mathrm{tr}\, T\rho + \frac{1}{2} \mathrm{tr}\left(\mathrm{tr}\, \bar{v} \rho \right) \rho . \qquad (2.7)$$

The matrices $T_{\alpha\beta}$ and $\bar{v}_{\alpha\beta,\gamma\delta}$ are the basic matrix elements:

$$\left.\begin{aligned} T_{\alpha\beta} &= \langle \alpha | -\tfrac{\hbar^2}{2m} \Delta | \beta \rangle \\ \bar{v}_{\alpha\beta,\gamma\delta} &= \langle \alpha\beta | v_{eff} | \gamma\delta \rangle - \langle \alpha\beta | v_{eff} | \delta\gamma \rangle . \end{aligned}\right\} \qquad (2.8)$$

[1] G.E. Brown, "Unified Theory of Nuclear Models", North Holland 1967

† We neglect spin and isospin coordinates and consider N nucleons of one kind only (e.g. neutrons).

The "best" set of s.p. wavefunctions $\phi_i(\underline{r})$ is found using the Ritz variational principle by minimizing the total energy E_{HF} with respect to the individual variations of all the ϕ_i:

$$\frac{\delta}{\delta \phi_i(\underline{r})} \left\{ E_{HF} - \varepsilon_i \int d^3\underline{r}\, |\phi_i(\underline{r})|^2 \right\} = 0 . \qquad (2.9)$$

The second term in the brackets { } is a Lagrange multiplier which guarantees the normalization of the $\phi_i(\underline{r})$. Performing the variation (2.9) leads to a set of equations:

$$\hat{H}_{HF} \phi_i = \left(\hat{T} + V_{HF} \right) \phi_i = \varepsilon_i \phi_i . \qquad \text{"HF equations"} \qquad (2.10)$$

In coordinate space, V_{HF} is in general a nonlocal, velocity-dependent potential, and the HF eqs. are very difficult to solve. (They are integro-differential equations).

In matrix notation, eq.(2.10) means a diagonalization :

$$H_{ij} = \varepsilon_i \delta_{ij} \qquad (i,j = 1, \ldots N) , \qquad (2.11)$$

and the matrix H is defined from (2.7) as

$$H_{\alpha\beta} = \frac{\partial E_{HF}}{\partial \rho_{\beta\alpha}} . \qquad (2.12)$$

If v_{eff} does not depend on the density, then V_{HF} in eq.(2.10) is equal to $\mathrm{tr}\, \bar{v} \rho$. T in eq.(2.10) is the kinetic energy operator $-\hbar^2/2m\,\Delta$.

For the Skyrme force, the HF equations are relatively simple†, of the type of a Schrödinger equation with an effective mass $m^*(\underline{r})$ and a spin orbit potential $\underset{\sim}{W}_{so}(\underline{r})$:

$$\hat{H}_{Sky} \phi_i(\underline{r}) = \left\{ -\frac{\hbar^2}{2} \underset{\sim}{\nabla} \cdot \frac{1}{m^*(\underline{r})} \underset{\sim}{\nabla} + U_{HF}(\underline{r}) - i \underset{\sim}{W}_{so}(\underline{r}) \cdot (\underset{\sim}{\nabla} \times \underline{\sigma}) \right\} \phi_i(\underline{r}) = \varepsilon_i \phi_i(\underline{r}) . \qquad (2.13)$$

The potentials U_{HF} and W_{so} and the eff. mass m^* depend in a relatively simple way on the local density $\rho(\underline{r})$ and the kinetic energy density $\tau(\underline{r})$ and thus the wavefunctions ϕ_i:

$$\rho(\underline{r}) = \sum_{i=1}^{N} |\phi_i(\underline{r})|^2 \; ; \quad \tau(\underline{r}) = \sum_{i=1}^{N} |\underset{\sim}{\nabla} \phi_i(\underline{r})|^2 . \qquad (2.14)$$

Through this dependence, the HF eqs. are non-linear and present a self-consistency problem. It is solved by starting from an initial set $\{m^{*(o)}, U_{HF}^{(o)}, W_{so}^{(o)}\} = H^{(o)}$; solving then eq.(2.13), from the ϕ_i calculating (2.14), from them new $H^{(1)}$ etc.etc.... until convergence, i.e. $H^{(n)} \equiv H^{(n+1)}$ (input ≡ output). ("HF iterations").

The ground state energy E_{HF} and wavefunction Φ_{HF} are obtained by including the N states ϕ_i with the lowest eigenvalues ε_i in the summations of eqs. (2.4) and (2.14).

2.4 Deformation energies

To obtain a solution with a given deformation, one has to add in eq.(2.10) an external field (constraint); otherwise one finds automatically a solution for which the energy is locally a minimum (ground state or eventually, an isomeric state).

The shape of the nucleus may be characterized by the multipole moments of the density:

$$Q_{\lambda\mu} = \mathrm{tr}\, \rho q_{\lambda\mu} ; \qquad (2.15)$$

here $q_{\lambda\mu}$ is the matrix element $\langle \alpha | \hat{q}_{\lambda\mu} | \beta \rangle$ of the multipole operator $\hat{q}_{\lambda\mu}$

$$\hat{q}_{\lambda\mu} = r^{\lambda} Y_{\lambda\mu}(\vartheta, \varphi) . \qquad (2.16)$$

Let us choose for instance the quadrupole moment $Q_{20} = Q_2$. If the HF equation

$$\left[\hat{T} + V_{HF} - \lambda \hat{q}_2 \right] \phi_i = \varepsilon_i \phi_i \qquad (2.17)$$

† see the classical paper [VB72].

is solved, one obtains a solution with a quadrupole moment Q_2. The Lagrange multiplier λ gives then the local derivative of the deformation energy at the point Q_2 (i.e. the negative driving force, which wants to bring the nucleus back to the minimum):

$$\lambda = \frac{dE(Q_2)}{dQ_2} . \qquad (2.18)$$

In this way, one can, however, only obtain those regions of the curve $E_{HF}(Q_2)$ which have a positive curvature. To obtain the full curves, one can use a quadratic constraint (for details, see [FQ73a]) .

2.5. Main results of Skyrme-HF calculations : [F175,76; Qu75a,b]

Note: The Skyrme force has 6 adjustable parameters; for the pairing effects (in BCS approximation [Va73]) one more parameter is used. Thus, a total of 7 free parameters are used in all calculations.

1. Ground-state masses (binding energies) are reproduced within $\sim$2-5 MeV for spherical and $\sim$5-10 MeV for deformed nuclei. Nuclear radii (r.m.s.) fit within $\sim$2%; quadrupole moments of lanthanides and actinides within $\sim$2-4%.

2. Deformation energy curves: Have the correct qualitative properties. For Pu^{240}, a double-humped barrier was obtained, see Fig. 2.1 [FQ73b,74]. The barrier heights are too big, compared to the experimental ones. The differences are (mostly) due to the following shortcomings of constrained-HF-calculations:

- The HF equations are solved by diagonalization (eq.2.11) in a finite (truncated) harmonic-oscillator basis [Va73]. This leads to truncation errors in the total energy which affect the deformation dependence.

- Slater determinants (eq.2.1) are not good eigenstates of the centre of mass momentum and of the total angular momentum. This leads to spurious c.m. and rotational energies, which also affect the deformation-behaviour.

- For reasons of computer time, one must restrict the shapes to axial and left/right symmetry, which is known from Strutinsky-calculations to give too high barriers (see lesson 5).

- For the Coulomb exchange energy, the Slater approximation was used [NV72, Va73]; it was newly found to lead to an error which increases at larger deformations[1].

All the above deficiencies of the constrained HF method are (ideally) avoided in the Strutinsky method; see the following lessons.

Nevertheless, the merit of these HF calculations was to demonstrate that fission barriers can in principle be obtained purely microscopically. The HF calculations could furthermore be used to test and justify numerically the Strutinsky method [BQ73, 75a-d], see lesson 3.

[1] P. Quentin, private communication, 1978.

3. THE BASIS OF THE STRUTINSKY METHOD

3.1. Extraction of an average part of the HF energy :

We want to extract a smooth part of the HF energy, which varies slowly with particle number and deformation, as does the LDM energy. This means we want to derive microscopically the LDM from HF theory with effective interactions.

We saw in lesson 2 that the HF energy is given as a functional of the density matrix ρ (2.4), see expression (2.7) for E_{HF}. The proposition of Strutinsky [St68,74,75] was to split ρ into a smooth part $\tilde{\rho}$ which contains the average information (in the LDM sense) and an oscillating part $\delta\rho$:

$$\rho = \tilde{\rho} + \delta\rho \; ; \qquad (3.1)$$

Without specifying $\tilde{\rho}$ quantitatively, Strutinsky derived [St68] what has been called the "energy theorem" [Be71](see also [BD72, BK72a, BK72b]), which we will discuss below. We give here a slightly different derivation (see also [Di72]); a discussion of different derivations may be found in [Br74b, BQ75a].

To define $\tilde{\rho}$ quantitatively, we use here Strutinsky's energy averaging method, which was originally introduced in order to define the average part of the single-particle level density of a given potential [St66-68]; see details in lesson 4. The same technique may be used to extract average parts of expectation values of any single-particle operator [BD72, BQ73], using the average occupation numbers $\tilde{n}_i$ determined by a given s.p. spectrum ε_i. The precise definition will be given in eq.(4.13) in the next lesson.

The average density matrix $\tilde{\rho}$ is defined as

$$\tilde{\rho}_{\alpha\beta} = \sum_i \langle\alpha|i\rangle\langle i|\beta\rangle \tilde{n}_i \; , \qquad (3.2)$$

thus replacing the "HF" occupation numbers (1 below and 0 above the Fermi energy λ) in eq.(2.4) by the $\tilde{n}_i$. This means an energy smoothing around the Fermi level λ in a range $\pm \sim\hbar\Omega$, the distance of main shell spacing in the spectrum ε_i.

The average part of any observable O - we are always speaking within the independent particle, i.e. HF approximation - is given through $\tilde{\rho}$ (3.2) and the corresponding operator $\hat{O}^{(1)}$ (one-body) or $\hat{O}^{(2)}$ (two-body) in matrix form:

$$\tilde{O} = \mathrm{tr}\,\tilde{\rho}\,\hat{O}^{(1)} \; ; \quad \tilde{O} = \mathrm{tr}\left(\mathrm{tr}\,\tilde{\rho}\,\hat{O}^{(2)}\right)\tilde{\rho} . \qquad (3.3)$$

In terms of the HF matrix elements (e.g. one-body)

$$O_i = \langle i \,|\, \hat{O}^{(1)} \,|\, i \rangle$$

we thus get

$$\tilde{O} = \sum_i O_i \tilde{n}_i . \qquad (3.4)$$

The average density matrix in coordinate space $\tilde{\rho}(r,r')$ - the diagonal part of which is the ordinary density $\tilde{\rho}(r)$ - is

$$\tilde{\rho}(\underline{r},\underline{r}') = \sum_{\alpha\beta} \tilde{\rho}_{\alpha\beta} \langle \underline{r}|\beta\rangle\langle\alpha|\underline{r}'\rangle = \sum_i \phi_i(\underline{r})\phi_i^*(\underline{r}')\tilde{n}_i \,. \tag{3.5}$$

The average level density (see eq.(4.3)) is

$$\tilde{g}(E) = \frac{d}{d\lambda}\int d^3r\, \tilde{\rho}(\underline{r},\underline{r})\Big|_E \,. \tag{3.6}$$

The average part of the HF energy E_{HF} (2.7) is thus simply

$$\tilde{\tilde{E}}_{HF} = \mathrm{tr}\, T\tilde{\rho} + \tfrac{1}{2}\mathrm{tr}\left(\mathrm{tr}\, \bar{v}\tilde{\rho}\right)\tilde{\rho} \,. \tag{3.7}$$

(If the interaction V depends itself on ρ, it is understood in eq.(3.7) that it has to be taken at the average value $\tilde{\rho}$!)

By construction, $\tilde{E}_{HF}$ should behave like a LDM energy. Numerical checks see below.

3.2. The Strutinsky Energy Theorem

(see also [St68,74,75; BD72, BK72a,b; Di72, Be71, Br74b, BQ75a]).

The aim is to derive from the microscopical HF-theory a quantitative expression for the fluctuating part δE of the total nuclear binding energy, see eq.(1.2), that is, for the shell-correction.

The easiest way is to expand the HF energy functional $E_{HF}[\rho]$ eq.(2.7) around the average part of ρ:

$$E_{HF}[\rho] = E_{HF}[\tilde{\rho}] + \mathrm{tr}\left(\frac{\partial E_{HF}}{\partial \rho}\Big|_{\rho=\tilde{\rho}} \delta\rho\right) + \mathcal{O}[(\delta\rho)^2] \,. \tag{3.8}$$

This Taylor expansion is - hopefully ! - justified by the relative orders of magnitude of the average (LDM) energy ($\sim$ 1-2 GeV) and the shell-correction($\pm$ $\sim$5-15 MeV).

The first term on the r.h.s. of eq.(3.8) is identical to $\tilde{E}_{HF}$ (3.7). The second term contains the derivative of E_{HF} with respect to ρ - which is a matrix - and which is equal to the HF one-body Hamiltonian H_{HF} (2.12) taken at the smooth value of ρ . We call it

$$H_{HF}[\tilde{\rho}] = \tilde{H}_{HF} = \hat{T} + \tilde{V}_{HF} \,. \tag{3.9}$$

We have thus

$$E_{HF} = \tilde{\tilde{E}}_{HF} + \mathrm{tr}\,\tilde{H}_{HF}\delta\rho + \mathcal{O}[(\delta\rho)^2] \,. \tag{3.10}$$

Now, the difference between V_{HF} and $\tilde{V}_{HF}$ is of order $\delta\rho$ and thus small relative to V_{HF} :

$$\delta V_{HF} = V_{HF} - \tilde{V}_{HF} = \mathcal{O}[\delta\rho] \,. \tag{3.11}$$

Let us call the spectrum and eigenstates of $\tilde{V}_{HF}$: $\tilde{\varepsilon}_i$ and $\tilde{\phi}_i$ respectively:

$$\tilde{H}_{HF}\tilde{\phi}_i = \left[\hat{T} + \tilde{V}_{HF}\right]\tilde{\phi}_i = \tilde{\varepsilon}_i\tilde{\phi}_i \,. \tag{3.12}$$

Using perturbation theory, we find easily that

$$\mathrm{tr}\,\tilde{H}_{HF}\delta\rho = \sum_i \tilde{\varepsilon}_i \delta\tilde{n}_i + \mathcal{O}[(\delta\rho)^2] \,. \tag{3.13}$$

[The $\delta\tilde{n}_i$ are defined in terms of the average spectrum $\tilde{\varepsilon}_i$ and not identical to those obtained from the HF spectrum ε_i, unless the averaging is done self-consistently by iteration; see below. We ignore the difference, however, which is again of higher order.] The quantity in eq.(3.13) is thus just the usual shell-correction (see lesson 4, eq. 4.14) :

$$\delta E_1 = \sum_i \tilde{\varepsilon}_i \delta n_i = \sum_{i=1}^{N} \tilde{\varepsilon}_i - \sum_i \tilde{\varepsilon}_i \tilde{n}_i \,. \tag{3.14}$$

We arrive thus at the Strutinsky energy theorem

$$E_{HF} = \tilde{\tilde{E}}_{HF} + \delta E_1 + \delta E_2 + \ldots \tag{3.15}$$

The important point is that all shell effects of lowest (i.e. first) order in $\delta\rho$ are given by expression (3.14); the remaining higher-order terms should be small (δE_2 etc).

The practical importance of this is that δE_1 is given by the spectrum ($\tilde{\varepsilon}_i$) of an average potential $\tilde{V}_{HF}$ (3.12), which may be approximated by the standard (deformable) shell model potential V_{SM} (which by construction varies smoothly with N, Z and deformation!). With this assumption one does not need to know the effective interaction v_{eff} for calculating δE to lowest order. (The terms of $\delta E_2, \ldots$ depend explicitly on v_{eff}!). If, furthermore, E_{HF} is close to the LDM energy E_{LDM} and the higher order terms $\delta E_2, \ldots$ are negligible, the approximation (SCM = shell correction method)

$$E_{SCM} = E_{LDM} + \delta E_1 \tag{3.16}$$

should replace a HF calculation, which in the later sixties was not available for fission barriers!

[We left out here the pairing effects. In principle the energy theorem can be derived from HFB-theory, [see Ko73]].

The derivation of the energy theorem (3.15) given here is true for any density and velocity-dependent effective two-body interaction v_{eff}.

3.3. Basic assumptions of the Shell-Correction Method (SCM)

1. The average HF energy $\tilde{E}_{HF}$ can be parametrized and well approximated by the LDM energy E_{LDM} (in the form e.g. eq.(1.1)), both as a function of nucleon numbers N, Z and of deformation β. In particular, it should thus

be a smooth function of N, Z and β (no shell effects).

2. The average HF potential $\tilde{V}_{HF}$ can be well approximated by a phenomenological shell model potential V_{SM} (Nilsson, Woods-Saxon etc). What counts is not so much the radial dependence of $V_{SM}(r)$, but that the shell-correction δE_1 extracted from its spectrum is the same as that obtained from $\tilde{V}_{HF}$.

3. The higher-order shell-corrections $\delta E_2 \ldots$, are small compared to δE_1 (i.e. $|\delta E_2| < 1$-2 MeV), so that they can be neglected.

If these assumptions are true, the energy E_{SCM} (3.16) replaces the HF-energy.

3.4. Numerical test of the SCM with HF-calculations

(see [BQ73-75], also [BK73]).

Idea: Perform numerically the program used above to derive the energy theorem and check individually each term.

Results: Figs. 3.1 and 3.2 show deformation energy curves obtained with HF calculations (interactions Skyrme III [BF74] and Negele-DME [NV72]) with a constraint on the quadrupole moment Q_2. The average energy $\bar{E}(= \tilde{E}_{HF})$ is seen to behave exactly like a smooth LDM energy. Shown also is the LDM energy E_{LD} with the parameters of [MS66]. The differences between $\bar{E}$ and E_{LD} could easily be removed by a re-adjustment of the LDM parameters.

Fig. 3.3 shows shell-corrections δE_1 and δE_2; the latter is found as $\delta E_2 = E_{HF} - \tilde{E}_{HF}$ and contains thus all higher-order terms. δE_1 agrees for both interactions and also with the one found in a usual Woods-Saxon potential [BD72] (no adjustment of parameters!) within $\sim$1-1.5 MeV. $|\delta E_2| \lesssim 2$ MeV everywhere; the oscillations are only $\pm \sim$1-1.5 MeV.

Fig. 3.4 shows the sum of 2. and higher order shell-corrections, δE_2, for 14 different nuclei with $100 \lesssim A \lesssim 250$ in their groundstates. The average value of δE_2 is $\sim$2 MeV and could easily be renormalized into the LDM energy; the fluctuations in δE_2 are less than $\pm \sim$1 MeV.

More results, see [BQ73-75].

Conclusions:

1) The series $E_{HF} = \tilde{E}_{HF} + \delta E_1 + \delta E_2 + \ldots$ converges very rapidly. In nuclei with $A \gtrsim 100$, $|\delta E_2|$ is always less than $\sim$ 2 MeV; its oscillations are less than $\pm \sim$1-1.5 MeV.

2) The shell-correction δE_1 is well reproduced by a phenomenological shell-model potential within $\pm \sim$1-1.5 MeV; it seems to depend little on the effective interaction.

3) The average energy $\tilde{E}_{HF}$ ($\bar{E}$ in figs. 3.2, 3.3 and 3.6 below) has the features of a LDM energy: Minimum at spherical shape, no rapid oscillations (shell structure). It can be fitted by a standard LDM energy within less than $\sim$ 1 MeV.

4) In light nuclei, δE_2 is not small, but of the same order as δE_1 (see [BQ75a,c]). Thus: attention for shell-correction calculations with not-self-consistent potentials for light nuclei!

5) Since all these differences of $\sim$1-2 MeV seem to be rather random (not in phase as functions of N, Z and Q_2), they should normally not add up. Thus, in heavy nuclei, the total error (compared to a self-consistent HF calculation) should not exceed $\sim$1-2 MeV.

6) If the average quantities $\tilde{\rho}$, $\tilde{E}_{HF}$ and $\tilde{V}_{HF}$ are determined self-consistently (by iteration), then $|\delta E_2|$ is less than 0.5-1 MeV for all N, Z and Q_2 tested [BQ75b]. The approximation

$$E = \tilde{E}_{HF} + \delta E_1(\tilde{\rho}_i) \qquad \text{(self-consistent)} \quad (3.17)$$

converges thus extremely well. This is even the case for light nuclei, see e.g. ^{40}Ca in Fig. 3.5!

7) The ideal shell-correction method should thus use LDM parameters and shell-model potentials $\tilde{V}$ which are determined self-consistently from one and the same effective interaction V_{eff}. This needs to be done!

8) All these results are derived from the HF framework. For tests with Migdal's theory, which exceeds in principle the HF-approximation, see [BK72a].

9) Self-consistency is important mostly for the average energy and potential. The shell-effects can be treated perturbatively. This motivates the use of semiclassical methods to solve the average self-consistency problem with a given interaction (see e.g. [BC76, CJ77]).

4. PRACTICAL DETAILS OF THE SHELL-CORRECTION METHOD

The "program" of a Strutinsky calculation is summarized in the following.

1) Parametrization of nuclear shape $\{\beta_i\}$
2) Parametrization of LDM energy
3) Parametrization of shell-model potential
4) Calculation of the shell-correction δE; pairing correction δP
5) Add up: $E_{def}(\beta_i) = E_{LDM}(\beta_i) + \delta E(\beta_i) + \delta P(\beta_i)$ †)

We cannot possibly mention all the different choices of parameters and potentials, which were used by different groups. Table 4.1 shows a list of the most active groups (especially in the years 1968-1974) and their potentials.

We go quickly through the above points, mention only the essentials and refer to literature for details. Good review articles, covering both technical details and results are [TN70, BD72, Ni72, Pa73, MN73].

† We omit from now on the index "1" used in lesson 3 to denote the first order shell-correction δE_1

For illustrative examples, we shall use nomenclature and results of the Strutinsky group (Moscow-Copenhagen-Basel), published in [BD72].

4.1. Shape parametrization

From the LDM studies, we have learned that the two most important degrees of freedom in the fission process are:

1) Elongation of the nucleus (c)
2) Neck-formation (constriction) (h)

In accordance with LDM results, these deformations are always chosen axially symmetric (around the fission axis) and left-right (mass-)symmetric (with respect to a perpendicular plane through the neck).

In the Copenhagen-Basel [BD72] and Los Alamos [Ni72] groups, these two degrees of freedom were parametrized such as to closely reproduce the family of optimized saddle-point shapes obtained in the numerical LDM calculations [CS63, SL63]. In the {c,h} parametrization [BD72], the LD fission path goes (for actinides) approximately along $h \neq 0$. The {c,h} shapes are shown in Fig. 4.1 by the solid lines. (Spherical shape: c = 1.0, h = 0).

In Nilsson-model and related potentials, these two degrees are reproduced by a mixture of ε_2, ε_4 and ε_6 deformations. Close to sphericity, $c \sim \varepsilon_2$ and $h \sim \varepsilon_4$.

The other two important types of deformations, which do not occur in the statistical LDM and are pure shell effects, are:

3) left/right (mass-, octupole-) asymmetry (α)

4) non-axial (tri-axial ellipsoid), γ-deformation

The asymmetry (α) is defined quite differently from group to group (Lund: a mixture of ε_3 and ε_5). γ is always the traditional tri-axial deformation parameter.

4.2. LDM energy

At early stages, the classical parameters of Myers and Swiatecki [MS66] were used. Later (> 1969), all groups oriented themselves more or less towards the "droplet model" [My69, MS69] ; with details to be found in the different references.

The essentials of the LDM deformation energy have already been discussed in lesson 1.

4.3. Shell model potential (deformed) V(r)

We give here the potentials of the main groups, with references for details:

1) Nilsson-model: (modified harmonic oscillator) with $\varepsilon_2 - \varepsilon_6$ and γ deformations: [St66-68, NT69, Mö72, MN73]

2) Two-centre-model: (two joined harmonic oscillators): [GM71, SG71, SM72, AD72, MM73, Ju74].

3) "folded Yukawa potential" (a deformable density with sharp surface, folded with a short-range Yukawa force to generate a diffuse surface) : [Ni69, BF72, Ni72, MN73].

4) generalized Woods-Saxon potential with constant surface thickness: [DP69a,b; BD72, GP72, Pa73, BL74, Ju75, JH77].

Some main common points are:

- The surfaces of constant potential V(r) (but, due to lack of self-consistency, not necessarily exactly of constant density!) are chosen to be the same as those of the drops (droplets) of the corresponding LDM.

- The volume within an equipotential surface is independent of deformation (incompressibility of nucleus).

In fig. 4.2 we see an example of the single-particle levels ε_i for the deformed Woods-Saxon potential of ref. [BD72, Pa73].

4.4. The Strutinsky energy averaging method [St66-68; Ts69, BP73].

This is the main technical ingredient of all practical shell-correction calculations. There exists a wide literature of descriptions, criticisms and alternative suggestions. The situation up to spring 1975 is covered in [BQ75a]; we refer to this paper and to [Br74b] for most of that literature and present here only shortly the main points.

One wants to define the average part of the total single-particle energy E_{sp} of one kind of particle:

$$E_{sp} = \sum_{i=1}^{N} \varepsilon_i . \tag{4.1}$$

This is done over the level density

$$g(E) = \sum_i \delta(E-\varepsilon_i) . \tag{4.2}$$

The smooth level density $\tilde{g}(E)$ is defined by averaging the exact one over an energy range γ with a certain averaging function $f_M(\chi)$:

$$\tilde{g}(E) = \frac{1}{\gamma} \int_{-\infty}^{+\infty} dE' g(E') f_M\left(\frac{E-E'}{\gamma}\right) = \frac{1}{\gamma} \sum_i f_M\left(\frac{E-\varepsilon_i}{\gamma}\right) . \tag{4.3}$$

(M is an even integer, see below).

The function $f_M(\chi)$ has the following properties [BP73]:

1) $f_M(\chi)$ is even in χ, has its maximum at $\chi = 0$ and goes to zero for $\chi \to \pm\infty$

2) Folding an arbitrary polynomial $P_M(E)$ (of degree M) leaves this polynomial unchanged for any value of γ :

$$\frac{1}{\gamma}\int_{-\infty}^{+\infty} P_M(E')\, f_M\left(\frac{E-E'}{\gamma}\right) dE' \equiv P_M(E). \qquad (\forall\,\gamma) \tag{4.4}$$

3) In the limits $\gamma \to 0$ and $M \to \infty$, $f_M(\chi)$ gives a delta function:

$$\frac{1}{\gamma} f_M(\chi/\gamma) \xrightarrow[\text{or } M\to\infty]{\gamma\to 0} \delta(\chi). \tag{4.5}$$

In order to smooth out the shell effects in (4.2), one has to choose γ slightly larger than the distance $\hbar\Omega$ of the main shells in the spectrum:

$$\gamma \gtrsim \hbar\Omega. \tag{4.6}$$

Fig. 4.3 shows as an example the level density g(E) for a deformed Woods-Saxon potential [BD72]. The dashed lines are the averaged level densities $\tilde{g}(E)$.

The condition (4.4) guarantees that the results do not depend on γ if the (true) average part of g(E) is a polynomial of degree M.

The average single-particle energy $\tilde{E}_{sp}$ is now given by

$$\tilde{E}_{sp} = \int_{-\infty}^{\tilde{\lambda}} E\,\tilde{g}(E)\, dE, \tag{4.7}$$

where the Fermi energy $\tilde{\lambda}$ is determined by

$$N = \int_{-\infty}^{\tilde{\lambda}} \tilde{g}(E)\, dE. \tag{4.8}$$

If the (true) average density $\tilde{g}(E)$ is a polynomial of degree M_o, then the energy $\tilde{E}_{sp}$ (4.7) will not depend on γ as soon as $M > M_o + 2$ and eq.(4.6) is fulfilled. If the spectrum ε_i is unlimited, then the function $\tilde{E}_{sp}(\gamma)$ has an ideal "plateau" in the region

$$\hbar\Omega \lesssim \gamma \ll \tilde{\lambda} - \varepsilon_o. \tag{4.9}$$

This is the case for the harmonic oscillator potential (in 3 dimensions: $M_o = 2$), see Fig. 4.4. It is also approximately true for Nilsson-model potentials: the plateau is constant within $\sim \pm 0.2$-0.3 MeV.

For an arbitrary average density, the Strutinsky procedure approximates the average part locally into a Taylor series which stops after M/2 + 1 terms. The error is minimised by the "local plateau condition" [BP73] for γ

$$\frac{\partial \tilde{E}_{sp}}{\partial \gamma} = 0 \tag{4.10}$$

and for M:

$$\tilde{E}_{sp}(M) = \tilde{E}_{sp}(M+2). \tag{4.11}$$

In Fig. 4.5 is an example where eqs.(4.10, 11) are only fulfilled for $M \gtrsim 16$; this is rather exceptional. In most cases, local plateaux are found with $6 < M < 10$ and $\hbar\Omega \lesssim \gamma \lesssim 1.5\ \hbar\Omega$.

In potentials with finite depth (e.g. Woods-Saxon), the range γ may reach into the continuum region ($E > 0$). There, ideally the resonances should be included [RB72]. In praxis, one uses artificial unbound states up to $\sim +20$ MeV which are obtained by diagonalizing the potential in a harmonic oscillator basis. In doing so, the uncertainties in the plateau values of E_{sp} are usually not larger than ~ 1-1.5 MeV. In some exceptional cases, especially at larger deformations with high local level density[1,2] - see e.g. Fig. 4.6 at c = 1.6 and 1.72 - or for small nuclei where $\hbar\Omega$ is bigger than the distance of λ from the continuum [SG77] ($A \lesssim 80$-100), the uncertainty may be somewhat larger.

At the plateau point where eq.(4.10) is fulfilled, the smooth energy $\tilde{E}_{sp}$ (4.7) can also be written as

$$\tilde{E}_{sp} = \sum_i \varepsilon_i \tilde{n}_i \tag{4.12}$$

with the smooth occupation numbers $\tilde{n}_i$ being defined by

$$\tilde{n}_i = \int_{-\infty}^{(\tilde{\lambda}-\varepsilon_i)/\gamma} dx\, f_M(x). \tag{4.13}$$

[1]R.R. Chasman, Phys. Rev. Lett. 33 (1974)544
[2]V.S. Ramamurthy et al. Phys. Lett. 62B (1976)124

The shell-correction is thus

$$\delta E = E_{sp} - \tilde{E}_{sp} = \sum_i \varepsilon_i \delta n_i, \tag{4.14}$$

where

$$\delta n_i = n_i^{(o)} - \tilde{n}_i\ ; \qquad n_i^{(o)} = \begin{cases} 1 & \text{for } i = 1,2,\ldots N \\ 0 & \text{for } i > N \end{cases}. \tag{4.15}$$

In Fig. 4.7 we show the values of δn_i in a typical case (the value of δn_i is the length of each vertical line, located at the energy ε_i). That figure also demonstrates that the shell-correction δE is mostly determined by the levels inside an interval $\tilde{\lambda} \pm \sim\gamma$. Thus, the deep-lying levels do not contribute to δE (4.14).

Of various methods proposed as alternatives to the Strutinsky averaging (see references in [BQ75a]), the only one which completely avoids the continuum problem is the semiclassical method developed by Bhaduri and Jennings [BR71, Je76]. Detailed comparisons of both methods show that they lead to identical results within ~ 1-2 MeV [JB75b,c], thus essentially confirming the Strutinsky method using artificial unbound states in finite potentials.

Strutinsky and Ivanjuk [SI75] proposed a modified averaging method which uses only bound states. Here, too, some uncertainties in the plateau values of $\tilde{E}_{sp}$ of $\sim$1-1.5 MeV are found. Improvements of this method seem, however, possible [SB77][1].

4.5. Pairing correlations

They have to be included in medium and heavy nuclei. This is done in the BCS formalism; a pairing correction is calculated (δP) which is determined as the ocsillating part of the difference between a paired and an unpaired ($\Delta = 0$) system. Definitions see [BP72, Pa73].

4.6. Numerical uncertainties in the shell-corrections (in praxis)

a) due to numerical energy averaging: (this lesson)

- in infinite potentials (Nilsson, square box) : $|\Delta\tilde{E}| < 0.5$ MeV
- in finite potentials (Woods-Saxon, folded Yukawa):

  for A $\gtrsim$ 100 : $|\Delta\tilde{E}|$ usually $\lesssim$ 1-1.5 MeV
  for light nuclei, or in situations with extremely high level density (e.g. at second barrier without mass-asymmetry):
  $|\Delta\tilde{E}|$ maybe $\sim$ 1.5-2.5 MeV (?)

b) due to lack of self-consistency of potential used :

(see lesson 3)

- in heavy nuclei and deformations up to second fission barrier:

[1]see also Ivanjuk and Strutinsky, Kiev-preprint (1978)

  $|\Delta\delta E| \lesssim$ 1-1.5 MeV

- in light nuclei: up to several MeV!
- at very large mass asymmetry and large separation (mostly in application to heavy-ion-reactions) :[1,2]

  $|\Delta\delta E|$ up to several MeV!

c) due to lack of self-consistency between potential and LDM:

- $|\Delta\delta E|$ easily $\sim$2-3 MeV; but smooth as function of N, Z and deformation!
- "Pb-anomaly" : $\Delta\delta E \sim -4$ to -7 MeV !! (see lesson 5)

This error can be removed by a renormalization of the LDM parameters. It does not occur, if the potential V(r) and the LDM parameters are derived from the same effective interaction and self-consistently [BQ75b] (see also lesson 3) - but this has not been done in the praxis so far!

[1] P. Möller and J.R. Nix, Nucl. Phys. A281 (1977) 354
[2] H. Gick et al., Z. Physik A282 (1977) 417

5. RESULTS OF SCM CALCULATIONS

In this lecture we will summarize the results of realistic deformation energy calculations using the SCM. As illustrations, we will show some typical results which we have taken - for pure convenience - from refs. [BD72, Pa73]. Unless particularly stated otherwise, all the results discussed here have been obtained independently and with excellent overall agreement by the different groups using different potentials, as discussed in sect. 4.3.

We shall restrict ourselves to static aspects, since the dynamics of fission is still at a rather early theoretical stage. The only exception will be the fission life time estimates (sect. 5.6), where a "minimal dynamical information" is needed in the form of inertial parameters; there, too, the static deformation energy is however the main ingredient.

5.1. Deformation energy surfaces

The basic problem in representing the deformation energy of a nucleus is that the deformation space $\{\beta\}$ has an infinite dimensionality. One thus has to select the most important deformation degrees of freedom - mostly using intuition.

From the LDM calculations (see sect. 1.2) we know that elongation (c) and necking (h) are important collective modes during the fission process. A practical way towards an approximate solution of the multidimensional problem consists in calculating the deformation energy E(c,h) and minimizing it at each point (c,h) with respect to other possible deformations.

Fig. 5.1 shows as examples the energy surfaces E(c,h) obtained in ref. [BD72] for the nucleus Pu^{240} for axially and mass symmetric shapes ($\gamma = \alpha = 0$). The contributions E_{LDM}, δE_n and δE_p (including pairing) are shown separately; on the lower r.h.s. is the sum of the three, i.e. the total energy (normalized, as usual, to $E_{LDM}(0) = 0$). Note that the inclusion of the shell effects moves the ground state minimum to a deformed shape ($c \simeq 1.2$, $h \simeq -0.15$). At the same time, a secondary minimum is created ($c \simeq 1.4$, $h \simeq 0$) which lies about 2 MeV above the ground state and is separated between ground state and the fission valley by two saddles.

This secondary minimum is found in most actinides and explains the nature of the long-known fission isomers [Po62] as shape isomers. Their deformation corresponds roughly to that of an ellipsoid with axis ratio 2/1. The shapes of the four stationary points in this symmetric energy surface E(c,h) are shown in Fig. 5.2.

Spontaneous fission from the second minimum is much more likely (only one barrier) than from the ground state (two barriers, lower energy). Thus, the fission life times from isomers are typically 10^{20}-10^{22} times shorter than those from ground states.

We shall return later to some of the consequences of the existence of these fission isomers (sect. 5.4).

5.2. Influence of non-axial and mass-asymmetric deformations

When mass-asymmetric shapes ($\alpha \neq 0$, see Fig. 4.1) are included, one finds that in the region around the second saddle point and beyond it, the energy is lowered by several MeV. The energetically most favorable path leads thus over a mass-asymmetric second saddle. This is a pure shell effect (in the LDM α is always zero!) and indicates the building up of asymmetric fragments.

Fig. 5.3 shows the second saddle region; in the upper part with $\alpha = 0$ and in the lower part after minimizing E with respect to α in each point (c,h). Note that the barrier height is decreased by $\sim$2.5 MeV! The isomer minimum is stable ($\alpha = 0$). The mass asymmetry thus increases rapidly between the isomer minimum and the outer saddle; beyond the saddle it stays constant in such a way that the ratio of the nascent fragments approaches a more or less constant value as the nucleus approaches the scission point. This value agrees qualitatively well with the most probable mass ratio observed in the fragment distribution. (For a recent comparison, see [JH77]).

This is particularly well demonstrated in a calculation using the two-centre-model (see sect. 4.3) which is especially well suited for the shapes between saddle and scission point. Fig. 5.4 shows as an example the energy surface of U^{236} as a function of neck radius (D) and mass asymmetry [MM73]. One sees the valley which leads down from the saddle with an approximately constant mass ratio ($\sim$140:96 near scission). The fact that this agrees well with the experimental (most probable, kinetic energy averaged) mass ratio, should of course be taken with caution. Here we considered only the potential energy (i.e. static) aspect of the problem, ignoring dynamical (inertial) effects which may play an important role especially on the way down towards scission!

Still, it is interesting that the mass ratio of the future fragments is already indicated after the saddle point by a purely static shell effect.

Another important deformation degree of freedom is the non-axial (γ) deformation. In the same way as mass asymmetry lowers the second saddle, one finds that inclusion of γ-deformation lowers the first saddle by up to $\sim$2 MeV for actinides with $A \gtrsim 232$. This effect, which increases through the actinide region with increasing mass number, considerably improves the agreement between theoretical and experimental heights of the first barrier (see e.g. Fig. 11 in ref. [MN73](Rochester) p.125).

Recently, an instability against γ-deformation was also found around the second barrier [GB77, JH77]. It leads to a "second outer" saddle which is γ-deformed but mass symmetric and lies $\sim$1-2 MeV higher than the usual, mass asymmetric but axially symmetric outer saddle. This "new channel" may affect the fission cross section at larger excitation energies (see [GB77]), especially in the mass-symmetric mode.

5.3 Systematics of barrier heights

We refer to the lectures of E. Lynn[1] for the extraction of barrier heights from an analysis of fission cross sections. In Fig. 5.5 we see a comparison[1] of the most up-to-date experimental barrier heights (E_A = inner, E_B = lowest outer barrier) with the theoretical values obtained using three different shell model potentials (see sect. 4.3).

In general, there is a pretty good agreement, amongst the different theoretical results as well as between theory and experiment. A systematic deviation is found for E_A in light actinides with low neutron number ($N \lesssim 140$). This discrepancy, first observed in Th-isotopes, has obtained the name "Th-anomaly". Otherwise, the calculated barriers agree with the experimental ones within $\sim$1-2 MeV. As we have seen in the previous lesson (sect. 4.6), this is the general kind of uncertainty which we expect in SCM calculations; so we cannot expect the agreement to be much better.

A possible explanation of the Th-anomaly may be the fact that in some calculations [MN73] a splitting of the second barrier into two small humps, separated by a shallow (third) minimum, has been found. This would completely change the analysis of fission cross sections (see Lynn's lectures). However, the fluctuations of this split second barrier are only of the order of $\sim$1-2 MeV, and have thus to be taken with caution. Furthermore, it seems that the picture of the triple-humped barrier (with a second minimum at $\sim$2-3 MeV and a third minimum at $\sim$4-5 MeV) is not compatible with photofission data of Th^{232} [2,3]. (See lesson 6 for more discussion about Th).

5.4 Physics of the fission isomers

We quickly summarize here the kind of experiments that allow to learn about the nature and details of the fission isomers. Extensive reviews were given by Specht [Sp74][4].

a) The fission cross sections (excitation functions) are modified by the isomers in a characteristic way: they show resonances which correspond to vibrational states in the second well. (See the lectures of Lynn for details).

b) The rotational band built on the lowest 0^+ state in the second well of Pu^{240} was measured in a rather spectacular experiment [SW72]. The deduced moment of inertia $\mathcal{J}$ is about 2.5 times larger than that of the g.s. band. This was the first direct evidence of the large deformation of an isomer. The measured value of $\mathcal{J}$ agrees well with the theoretical one, obtained from the single particle wavefunctions with the cranking model (although the latter one has an uncertainty of $\sim$5-10%). A similar experiment was recently finished for U^{236} [BP77a].

c) The most direct determination of the deformation of an isomer was obtained in a recent measurement of the quadrupole moments Q_2 of Pu^{239} [HM77] and Pu^{236} [MS77] in the isomer state. The agreement of Q_2 (within the experimental error limits) with the theoretical values [BL74] is excellent.

[1] D. Habs et al., Heidelberg Preprint 1978 (Z. Physik, in press).
[2] C.D. Bowman et al., Phys.Rev. C17 (1978) 1086.
[3] M. Asghar, Z. Physik A, in print (1978).
[4] and H. Specht, Nukleonika Vol. 20 (1975) 717 (Summer School Mikolajki, 1974).

[1] E. Lynn, these proceedings

d) The only directly (and precisely) measured energy of the fission isomeric state known up to date is the one of U^{238}, deduced from observed γ-transitions between the 0^+ state in the second well and the lowest 2^+ and 1^- states in the ground state well[1]. The energy $E_{II}-E_I$ = 2.559 MeV agrees well with the theoretical values within their error limits.

e) Spectroscopy in the isomeric well was attempted for Pu^{237} [2]. Here, two isomeric states are known with half lives 100 ns and 1.1 μs. Since this is an odd-A nucleus, these states have spin J, K ≠ 0. Their g-factors were measured with the spin-precession method in an external field. The spin assignments were, however, not unique.

5.5. Ground-state masses

The SCM can of course also be used to calculate the total ground-state mass (binding energy) of a nucleus. The empirical corrections δM to the LDM energies were determined systematically for the first time by Myers and Swiatecki [MS66]. More recent compilations, using different versions of semi-empirical mass formulae or the droplet model[3], may be found in Nuclear Data Tables[4]. In Fig. 5.6 we see a comparison of the empirical values of δM^3 with the theoretical ones, obtained with the folded Yukawa potential [MN73]. The agreement is in general good, within ± ∿1-2 MeV, except in the Pb region. Especially using a Woods-Saxon potential [BD72], one obtains a discrepancy of ∿5 MeV for Pb^{208}.

This "Pb-anomaly" is much smaller, when one uses the Nilsson model. In the most recent mass fit using Nilsson levels[5], an agreement
- 2 MeV ≲ $(\delta M_{th} - \delta M_{exp})$ ≲ + 2 MeV was reached (although here, too, the most systematic deviations occur around Pb^{208}). On the other hand, the too large (negative) value of δM obtained for Pb^{208} with the Woods-Saxon potential has been substantiated[6] by HF-calculations [BQ75b] in which the exact total energy of Pb^{208} is reproduced. The discrepancy must therefore be due to the lack of self-consistency between the smooth (LDM) energy and the W-S. potential used. This is the point we made at the end of sect. 4.3 above (point c).

If both the average energy and the average potential are derived self-consistently from the same interaction, as was done in ref.[BQ75b], the Pb-anomaly does not exist; see the results discussed in sect. 3.4, especially point 6), and eq.(3.17)! It is possible that the Th-anomaly discussed above is due to the same reason.

[1] P.A. Russo et al., Rochester 1973, Vol. I, p.271.
[2] R. Kalish et al., Phys. Rev. Lett. 32 (1974) 1009.
[3] W.D. Myers and W.J. Swiatecki, Ann. Phys. (N.Y.) 84 (1974) 186.
[4] Atomic Data and Nuclear Data Tables, Vol. 17 (1975) 411.
[5] P.A. Seeger and W.M. Howard, Nucl. Phys. A238 (1975) 491
[6] see also Y. Yariv et al., Z. Physik A278 (1976) 225.

5.6. Life time estimates for spontaneous fission

We just sketch here a simple semiclassical method which allows to calculate life times using WKB barrier penetration. The first systematic studies of this kind were done by Ledergerber and Pauli[1] [PL73]. For more recent similar studies, see refs.[2,3]

If the fission path is represented as a one-dimensional trajectory q(c,h,a...) in the deformation space, the probability (width) Γ for barrier penetration between points q_1 and q_2 is in the WKB approximation (see e.g. [BW39])

$$\Gamma \simeq \hbar\omega_f \cdot e^{-\frac{2}{\hbar}S} \qquad (S \gg \hbar),$$

where $\hbar\omega_f \approx$ 1 MeV (within a factor of ∿2) is the frequency of "assault" in the fission mode (q), and S is the action integral along the chosen trajectory:

$$S = \int_{q_1}^{q_2} \sqrt{|E-V(q)|\,2B_q(q)}\; dq .$$

Here V(q) is the potential energy of collective deformation, i.e. the deformation energy obtained with the SCM along the path q(c,h,α...); $B_q(q)$ is the inertial parameter which in the adiabatic approximation can be obtained using the "cranking model" [4]; E is the total energy of the system.

The most probable path is the one which minimizes the action S, i.e. the "least action trajectory". An example of such a trajectory is shown in Fig. 5.7 (from [PL73]).

This method applies only if one is well below the barrier; it can therefore only be used with reasonable justification for spontaneous (g.s. or isomeric) fission. Hereby, q_1 is a point in the g.s. (or isomeric) minimum and q_2 a point in the "fission valley" on the other side of the barrier at the same energy. The life time is then given simply by

$$t_{1/2} \simeq \frac{\hbar}{\Gamma} .$$

Since Γ is extremely sensitive to the barrier heights (through the exponential dependence), the inaccuracy in the latter (∿1-2 MeV) leads to theoretical error limits in $t_{1/2}$ of several orders of magnitude.

Fig. 5.8 shows the results obtained in [PL73] for ground state fission of the actinides. (Hereby, the LDM parameters a_s and κ_s were readjusted in three different regions, as shown in the figure). There is a very clear correlation between theoretical and experimental values within each isotope series.

Similar results were obtained by Randrup et al.[2] using a phenomenological (classical) inertial function $B_q(q)$ (instead of the cranking value) with one adjustable parameter. Extended life time calculations with microscopical inertias $B_q(q)$ using the Nilsson model will soon be published by the Warsaw group (Sobiczewski et al.).

[1] T. Ledergerber and H.C. Pauli, Nucl. Phys. A207 (1973) 1.
[2] J. Randrup et al., Phys. Rev. C13 (1976) 229.
[3] A. Sobiczewski et al., to be published.
[4] D.R. Inglis, Phys. Rev. 96 (1954) 1059 and 103 (1956) 1786.

6."HOT TOPICS" - SOME OPEN QUESTIONS

We mention here some open problems related to the static barrier picture discussed above and its possible limitations. Rather than presenting a detailed discussion and reproducing many figures, we shall just give some key arguments and refer to the relevant literature.

6.1. Th-anomaly: triple-humped barriers?

We have already mentioned (in sect. 5.3) the so-called Th-anomaly and a possible interpretation in terms of a triple-humped barrier [MN73]. If this interpretation is correct, one has to consider other possible consequences of the existence of a third minimum. In a recent experiment at Saclay[1], a shape-vibrational resonance in the fission of the Th^{233} compound-nucleus was investigated with high resolution. Some fine structures with rotational band-like nature were observed. The corresponding moments of inertia are larger than the typical values found in the second wells of Pu^{240} and U^{236} (see sect. 5.4.b) and would be compatible with the deformation of the second saddle point, if one interpolates between the values of the neighbouring even-A isotopes. However, in Th^{233}, the blocking effect of the odd neutron has to be taken into account which will give larger moments of inertia, also in the case of rotational bands built on quasiparticle states in the usual second well. Thus, the values of $\mathcal{J}$ do not prove the existence of a third minimum.

A recent analysis of photo-fission data on Th^{232} [2] seems to favour the usual double-humped barrier with the second minimum at $\sim$ 3 MeV (and not one at $\sim$4.5 MeV).

If the usual double-humped barrier picture is to be maintained in the lighter neutron-poor actinides, one has to explain why the calculated inner barriers are several MeV too low. It is possible that this defect is related to the "Pb-anomaly", which we attributed (in sect. 5.5) to the missing self-consistency between the LDM energies and the average potentials used in the SCM calculations.

6.2. Superheavy Elements?

Already since the first successes of the SCM, one has speculated about the possibility, that an "island" of stable nuclei exists with $Z \sim 114\text{-}126$ and $A \sim 300\text{-}350$. Although the LDM part of the deformation energy does not give a stable ground state for such nuclei ($X \gtrsim 50$), a sufficiently strong shell effect (preferably at the spherically magic numbers Z = 114; N = 184,226) might produce a barrier which is high enough to lead to an experimentally detectable fission lifetime. Indeed, barriers of $\sim$7-12 MeV were obtained in the calculations for such nuclei. However, the main problem is here the unreliability of extrapolating LDM and shell model potential parameters to unknown regions. Indeed, the different models and parameter sets give differences of several MeV in the predicted barrier heights (which means ten or more orders of magnitude uncertainty in the life times!). We refer to conference reports for details of these calculations (Ronneby, 1974 and ref.[1]).

The use of the HF method with effective interactions might be more reliable for such extrapolations, since relatively few parameters ($\sim$7) are used here which are the same for all known nuclei from $A \sim 16$ to $A \sim 250$. But the constrained HF calculations are too time consuming - at least at the moment - for systematic studies for these superheavy nuclei, so that further approximations are necessary which lead to further uncertainties.

As to the experimental searches for "superheavies", both in nature and in the laboratory (heavy-ion accelerators), which all have been negative so far, we also refer to the above-mentioned proceedings.

6.3. Fragment mass and kinetic energy distributions

We saw in section 5.2 that already at the second saddle, a preference for mass-asymmetric shapes exists due to the shell effects in the deformation energy. Although this is certainly connected to the asymmetric fragment masses, we cannot explain the mass distributions knowing the potential energy only. One should expect that dynamics play an essential role in the determination of the fragment distributions.

Therefore, it is rather astonishing that it is still possible to explain the qualitative features of the fragment distributions reasonably well without doing dynamical calculations. We shall not discuss here the statistical model of Fong[2] which is known since more than two decades. We will, however, quickly mention the so-called static scission point models used in connection with the Strutinsky SCM[3 4 5]. Here the scission configuration is described by two fragments (so far usually rotational ellipsoids) kept at a finite distance d (which is the distance between the closest points of the two surfaces). The total potential energy of this configuration, $V(N_1,Z_1, N_2,Z_2,\beta_1,\beta_2,d)$, is calculated including interaction and shell-correction energies. Based on the arguments of Nörenberg[6] one assumes a partial equilibrium between collective degrees of freedom (here mainly the asymmetry determined by the nuclear numbers $N_i Z_i$ and the deformations β_i) and negligible coupling between collective and intrinsic degrees (in constrast to the model of Fong, where total statistical equilibrium is assumed, also between collective and intrinsic degrees). The probability for a certain fragment distribution is then given either by a Boltzmann factor[4] $\exp[-V(Z_i,N_i,\beta_i)/T_{coll}]$ where the collective temperature T_{coll} is an adjustable parameter, or - which thermodynamically is probably more correct - by minimizing the free energy[5]. In either case, the fragment distributions are determined by the static potential energy at scission (plus the assumed partial statistical equilibrium).

[1] J. Blons et al., Phys. Rev. Lett. 35 (1975) 1749. The experiment was redone at Geel with even better resolution; the rotational structures seem to be confirmed (J. Blons et al., to be published).

[2] M. Asghar, Z. Physik (in print).

[1] Proceedings of International Symposium on Superheavy Elements, Lubbock, Texas, March 9-11, 1978.

[2] P. Fong, Statistical Theory of Nuclear Fission, Gordon and Breach, N.Y., 1969; see also Phys. Rev. C16 (1977) 251 for recent references.

[3] F. Dickmann and K. Dietrich, Nucl. Phys. A129 (1969) 241.

[4] B.D. Wilkins et al., Phys. Rev. C14 (1976) 229.

[5] M. Prakash et al., Nucl. & Solid State Physics Symp. (India) 19B (1976) 127.

[6] W. Nörenberg, Rochester 1973, Vol. I, p.547 and Vienna 1969, p.51.

Such calculations reproduce many features of fragment mass and kinetic energy distributions, including shell effects, in a qualitative and in some cases even semiquantitative way (see especially the extended calculations of ref.[4] above). Clearly, all the shell effects, which play an essential role in these distributions for low-energy fission, are determined by the shells in the fragments at the scission point, in particular also the asymmetry of the mass distribution (where it occurs). Above in section 5.2 we saw that the most probable mass ratio is also coming out as the result of a shell effect in the parent nucleus at the outer saddle. Thus, the asymmetric mass split seems to be affected very little during the descent from the saddle to the scission point. This was indeed confirmed in approximate dynamical calculations using the two centre model[1]. It was found there that at least the gross features of the mass distribution are mainly determined by the potential energy surface.

The success of the static scission point model makes it worth while investigating somewhat more its theoretical justification. In particular, the choice of the constant distance d has to be justified. The underlying assumption of the presence of a scission barrier must be checked and its dependence on the shape parametrization of the fragments must be investigated. Also, in a more rigorous thermodynamical treatment, the collective temperature T_{coll} and the intrinsic temperature T_{int} given to the fragments are not free parameters, but should be determined by the total energy balance of the system. Some promising work along these lines is under way[2].

It is interesting to note that many of the features of the fragments can be understood from purely static and statistic considerations at the scission point. The fissioning system seems to have lost most of its memory of what happened between the saddle and the scission point, except for the establishment of the partial equilibrium.

6.4. The role of dynamics

After the above discussion, one cannot withhold any longer the obvious question: where and how do the dynamical aspects come in at all? Certainly they must play a role in the descent between the saddle and the scission point. But the qualitative success of the static scission point model puts at least some boundaries on this role. In particular, it seems to confirm the underlying assumption of this model that the fragments have a negligible pre-scission kinetic energy at the moment of the rupture of the neck. Recent measurements of long range α-particle emission in the fission of U^{236} and Cf^{252} and their analysis[3] also seem to confirm the assumption of a small pre-scission kinetic energy ($\lesssim 5 - 10$ MeV). This is in contradiction with dynamical liquid-drop calculations[4] which predict this energy to be larger and to increase with increasing mass number ($\sim 20 - 50$ MeV for actinides).

The dissipation during the descent from the saddle must be small enough not to destroy the superfluidity of the lighter actinides, where the preference for the formation of fragments with even Z is a well-known experimental fact[1] (for low-energy fission).

At this point we would have to enter into a discussion of dynamical theories, of the question: one-body or two-body viscosity, etc., which goes beyond the boundaries of our lectures. But this is the field where most theoretical work must be done in the near future. We conclude by referring to a recent article[2] in which both macroscopic and microscopic dynamical models and dissipation mechanisms are discussed and many references to the recent literature can be found.

ACKNOWLEDGEMENT

I am indebted to M. Asghar, C. Guet and H. Nifenecker for many illuminating discussions on the present experimental situation.

LITERATURE

Schools and Conferences

Hirschegg 1974: Second International Workshop on Gross Properties of Nuclei and Nuclear Excitations, Hirschegg (Austria) 1974 (Technische Hochschule Darmstadt, 1974)

Munich 1973: International Conference on Nuclear Physics (Eds. J. de Boer and H.J.Mang, North-Holland, 1973)

Paris 1975 Fifth International Conference on Atomic Masses and Fundamental Constants (Eds. J.H.Sanders and A.H.Wapstra, Plenum Press, 1976)

Rochester 1973 Physics and Chemistry of Fission 1973 (IAEA Vienna 1974)

Ronneby 1974 Nobel Symposium 27 on Superheavy Elements; Proceedings published in Physica Scripta 10A (1974)

Trieste 1971 The Structure of Nuclei, Trieste Lectures 1971 (IAEA Vienna 1972)

Trieste 1975 International Conference on Nuclear Self-Consistent Fields, ICTP Trieste 1975 (Eds. G.Ripka and M.Porneuf, North-Holland, 1975)

[1] J.A. Maruhn and W. Greiner, Phys. Rev. C13 (1976) 2404.
[2] M. Prakash et al., Preprint Bombay (1978), and ref. [5] above.
[3] C. Guet et al., submitted to Journ. de Physique, Lettres (1978), and references therein.
[4] J.R. Nix, Nucl. Phys. A130 (1969) 241.

[1] See e.g. R. Brissot et al., Nucl. Phys. A282 (1977) 109 and references therein.
[2] J.W. Negele et al., Phys. Rev. C17 (1978) 1098.

Varenna 1965 Many-Body Description of Nuclear Structure and Reactions, Varenna Lectures 1965 (Academic Press, 1966)

Vienna 1963 Second International Conference on Nuclidic Masses (Ed. W.H.Johnston Jr., Springer, 1963)

Vienna 1969 Physics and Chemistry of Fission 1969 (IAEA Vienna, 1969)

Books

E.K. Hyde: Nuclear Properties of the Heavy Elements, Vol. III: Fission Phenomena, Prentice-Hall, 1964.

L. Wilets: Theories of Nuclear Fission, Clarendon Press, Oxford, 1964.

R. Vandenbosch and J.R. Huizenga: Nuclear Fission, Academic Press, New York and London, 1973.

M. Preston and R.K. Bhaduri: Structure of the Nucleus, Addison-Wesley, 1975.

AD 72 B.L.Andersen, F.Dickmann and K.Dietrich, Nucl.Phys. A159 (1972) 337

AS 68 M.Abramowitz and I.A.Stegun, Handbook of Mathematical Functions (Dover, N.Y., 1968)

Ba 63 M.Baranger, Cargèse Lectures in Theoretical Physics, 1962 (W.A.Benjamin, New York, 1963)

BB 36 H.A.Bethe and F.Bacher, Rev.Mod.Phys. 8 (1936) 82

BB 68 K.A.Brückner, J.R.Buchler, S.Jorna and R.J.Lombard, Phys.Rev. 171 (1968) 1188

BB 70 R.Balian and C.Bloch, Ann. Phys. (N.Y.) 60 (1970) 401

BB 71 " " " " " 64 (1971) 271

BB 71a " " " " " 63 (1971) 592

BB 72 " " " " " 69 (1972) 76

BC 76 O.Bohigas, X.Campi, H.Krivine and J.Treiner, Phys.Lett. 64B (1976) 381

BD 72 M.Brack, J.Damgaard, H.C.Pauli, A.S.Jensen, V.M.Strutinsky and C.Y. Wong, Rev. Mod. Phys. 44 (1972) 320

BD 73 R.K.Bhaduri and S.DasGupta, Phys.Lett. 47B (1973) 129

Be 37 H.A.Bethe, Rev.Mod.Phys. 9 (1937) 69

Be 68 " Phys.Rev. 167 (1968) 879

Be 71 " Ann.Rev.Nucl.Sci. 21 (1971) 93

Be 72 R.Bengtsson, Nucl.Phys. A198 (1972) 591

Be 73 " Rochester 1973, Vol.I, p. 203

BF 72 M.Bolsterli, E.O.Fiset, J.R.Nix and J.L.Norton, Phys.Rev. C5 (1972) 1050

BF 74 M.Beiner, H.Flocard, N.V.Giai and P.Quentin, Nucl.Phys. A238 (1975) 29; see also M.Beiner, H.Flocard, M.Veneroni and P.Quentin, Ronneby 1974, p.84

BG 58 K.A.Brückner, J.L.Gammel and H.Weitzner, Phys.Rev. 110 (1958) 431

BH 73 B.B.Back, O.Hansen, H.C.Britt, G.D.Garrett and B.Leroux, Rochester 1973, Vol. I, p. 3

Bh 77 R.K.Bhaduri, Phys.Rev.Lett. 39 (1977) 329

BJ 76 G.E.Brown and A.D.Jackson, The Nucleon-Nucleon-Interaction (North-Holland/ Amer.Elsevier, New York, 1976)

BJ 76a M.Brack and B.K.Jennings, Nucl.Phys. A258 (1976) 264

BJ 76b " " and Y.H.Chu, Phys.Lett. 65B (1976) 1

BK 37 N.Bohr and F.Kalckar, Kgl.Dan.Vid.Selsk., Mat.-Fys.Medd. 14 (1937) No. 10

BK 72a G.G.Bunatian, V.M.Kolomietz and V.M.Strutinsky, Nucl.Phys. A188 (1972) 225

BK 72b W.H.Bassichis, A.K.Kerman, C.F.Tsang, D.R.Tuerpe and L.Wilets, "Magic without magics: John Archibald Wheeler" (Freeman, San Francisco, 1972)

BK 73 W.H.Bassichis, A.K.Kerman and D.R.Tuerpe, Phys.Rev. C8 (1973) 2140

BL 74 M.Brack, T.Ledergerber, H.C.Pauli and A.S.Jensen, Nucl.Phys. A234 (1974)185

BL 75 R.Bengtsson, S.E.Larsson, G.Leander, P.Möller, S.G.Nilsson, S.Åberg and Z.Szymanski, Phys.Lett. 57B (1975) 301

BM 55 A.Bohr and B.Mottelson, Kgl.Dan.Vid.Selsk., Mat.-Fys.Medd. 30 (1955) No. 1

BM 69 " " Nuclear Structure, Vol. I (Benjamin, 1969)

BM 75 A.Bohr and B.Mottelson, Nuclear Structure, Vol. II (Reading, 1975)

Bo 57 N.N.Bogolyubov et al., Doklady (Sovjet Phys.) 2 (1957) 535

BP 73 M.Brack and H.C.Pauli; Nucl.Phys. A207 (1973) 401

BP 77a J.Borggreen, J.Pedersen, G.Sletten, R.Heffner and E.Swanson, Nucl.Phys. A279 (1977) 189

BP 77b N.Balazs and H.C.Pauli, Preprint Heidelberg, 1977

BQ 73 M.Brack and P.Quentin, Rochester 1973, Vol. I, p. 231

BQ 74a " " Ronneby 1974, p. 163

BQ 74b " " Phys.Lett. 52B (1974) 159

BQ 75a " " Trieste 1975, p. 353

BQ 75b " " Phys.Lett. 56B (1975) 421

BQ 75c " " Paris 1975, p. 257

BQ 75d " " Trieste 1975, p. 399

Br 55 K.A.Brückner, Phys.Rev. 97 (1955) 1353

Br 67 B.H.Brandow, Rev.Mod.Phys. 39 (1967) 771

BR 71 R.K.Bhaduri and C.K.Ross, Phys.Rev.Lett. 27 (1971) 606

Br 74a M.Brack, Hirschegg 1974, p. 14

Br 74b " Lectures given at the International School of Nuclear Physics, Predeal (Romania) 1974

Br 76 M.Brack, Seminar given at Orsay, 1976

Br 77 " Phys.Lett. 71B (1977) 239

BS 69 S.Bjørnholm and V.M.Strutinsky, Nucl.Phys.A136 (1969) 1

BW 39 N.Bohr and J.A.Wheeler, Phys.Rev. 56 (1939) 426

BW 55 R.A.Berg and L.Wilets, Proc.Phys.Soc.Lon. A68 (1955) 229

BW 56 " " Phys.Rev. 101 (1956) 201

BW 69 W.H.Bassichis and L.Wilets, Phys.Rev.Lett. 22 (1969) 79

BW 71 " " " " " 27 (1971) 1451

BZ 73 N.Balazs and G.Zipfel, Ann.Phys.(N.Y.) 77 (1973) 139

Ch 77 Y.H.Chu, Doctoral Thesis, Stony Brook, 1977

CJ 77 Y.H.Chu, B.K.Jennings and M.Brack, Phys.Lett. 68B (1977) 407

CP 74 S.Cohen, F.Plasil,and W.J.Swiatecki, Ann.Phys.(N.Y.) 82 (1974) 557

CS 63 " and W.J.Swiatecki, Ann.Phys.(N.Y.) 22 (1963) 406

CS 72 X.Campi and D.W.Sprung, Nucl.Phys.A194 (1972) 401

Da 67 B.D.Day, Rev.Mod.Phys. 39 (1967) 719

DB 77 M.Durand, M.Brack and P.Schuck, Preprint ILL Grenoble, 1977

De 68 J.Des Cloiseaux in "Many Body Physics", Les Houches 1967 (Gordon and Breach, New York, 1968)

Di 72 K.Dietrich, Trieste 1971, p. 373

DJ 74 T.Døssing and A.S.Jensen, Nucl.Phys. A222 (1974) 493

DM 73 K.T.R.Davies, R.J.McCarthy and P.U.Sauer, Phys.Rev. C7 (1973) 943

DM 75 M.Dworcecka and S.A.Moszkowski, Phys.Rev. C12 (1975) 619

DP 69a J.Damgaard, H.C.Pauli, V.V.Pashkevich and V.M.Strutinsky, Nucl.Phys. A135 (1969) 432

DP 69b J.Damgaard, H.C.Pauli, V.M.Strutinsky, C.Y.Wong, M.Brack and A.S.Jensen, Vienna 1969, p. 213

DR 74 S.DasGupta and S.Radhakant, Phys.Rev. C9 (1974) 1775

EM 72 D.Ehlers and S.A.Moszkowski, Phys.Rev. C6 (1972) 217

Fl 75 H.Flocard, Trieste 1975, p. 219

Fl 76 " Thèse d'Etat, Orsay, 1976

FQ 73a H.Flocard, P.Quentin, A.K.Kerman and D.Vautherin, Nucl.Phys. A203 (1973) 433

FQ 73b H.Flocard, P.Quentin, D.Vautherin and A.K.Kerman, Rochester 1975, Vol. I, p. 221

FQ 74 H.Flocard, P.Quentin, D.Vautherin, M.Véneroni and A.K.Kerman, Nucl. Phys. A231 (1974) 176

Fr 39 J.A.Frenkel, Zhur.Eksptl. i Teor.Fyz. 9 (1939) 641

GB 57 M.Gell-Mann and K.A.Brückner, Phys.Rev. 106 (1957) 364

GB 77 A.Gavron, H.C.Britt, P.D.Goldstone, J.B.Wilhelmy and S.E.Larsson, Phys.Rev.Lett. 38 (1977) 1457

GM 71 J.Grumann, T.Morovic and W.Greiner, Z.Naturforsch. 26a (1971) 643

Go 48 P.Gombas, Die Statistische Theorie des Atoms, (Springer, Vienna, 1948)

Go 73 D.Gogny, Munich 1973, Vol. I, p. 48

Go 75 " Trieste 1975, p. 333

GP 72 U.Götz, H.C.Pauli, K.Junker and K.Alder, Nucl.Phys. A192 (1972) 1

Gr 72 D.H.E.Gross, Phys.Lett. 42B (1972) 41

GS 69 M.Gaudin and A.M.Sajot, Vienna 1969, p. 229

GS 77 G.Gumpertsberger and P.Schuck; Phys.Lett. 66B (1977) 219

GV 77 B.Grammaticos and A.Voros, private communication, 1977

HJ 49 O.Haxel, J.H.D Jensen and H.E.Suess, Phys.Rev. 75 (1949) 1766

HJ 62 T.Hamada and T.D.Johnston, Nucl.Phys. 34 (1962) 382

HK 64 P.Hohenberg and W.Kohn, Phys.Rev. 136 (1964) B864

HM 72 J.K.Huizenga and L.G.Moretto, Ann.Rev.Nucl.Sci. 22 (1972) 427

HM 77 D.Habs, V.Metag, H.J.Specht and G.Ulfert, Phys.Rev.Lett. 38 (1977) 387

HN 77 P.Hoodbhoy and J.W.Negele, Nucl.Phys. A288 (1977) 23

Ho 73 C.H.Hodges, Can.J.Phys. 51 (1973) 1428

HS 73 R.W.Hasse and W.Stocker, Phys.Lett. 44B (1973) 26

Hu 57 J.Hubbard, Proc.Roy.Soc. (London) A243 (1957) 336

HW 53 D.L.Hill and J.A.Wheeler, Phys.Rev. 89 (1953) 1102

JB 75a B.K.Jennings and R.K.Bhaduri, Nucl.Phys. A237 (1975) 149

JB 75b B.K.Jennings, R.K.Bhaduri and M.Brack, Phys.Rev.Lett. 34 (1975) 228

JB 75c " " " Nucl.Phys. A253 (1975) 29

JD 73 A.S.Jensen and J.Damgaard, Nucl.Phys. A203 (1973) 578

Je 73 B.K.Jennings, Nucl.Phys. A207 (1973) 538

Je 74 " Ann.Phys. (N.Y.) 84 (1974) 1

Je 76 " Ph.D. Thesis, McMaster University, 1976

JH 77 K.Junker and J.Hadermann, Z.Physik A282 (1977) 391

JN 70 T.Johansson, S.G.Nilsson and Z.Szymanski, Ann.Phys. (Paris) 5 (1970) 377

Ju 74 K.Junker, Atomkernenergie (ATKE) Vol. 23 (1974) 57

Ju 75 " Acta Phys. Austr. 43 (1975) 221

KB 61 K.Kumar and R.K.Bhaduri, Phys.Rev. 122 (1961) 1926

KC 73 D.Kolb, R.Y.Cusson and M.Harvey, Nucl.Phys. A215 (1973) 1

Ki 33 J.G.Kirkwood, Phys.Rev. 44 (1933) 31

Ki 57 D.A.Kirzhnits, Sovj.Phys. JETP 5 (1957) 64

Ko 73 V.M.Kolomietz, Yad.Fiz. 18 (1973) 288 [Sov.J.Nucl.Phys. 18 (1974) 147]

KP 73 C.M.Ko, H.C.Pauli, M.Brack and G.E.Brown, Phys.Lett. 45B (1973) 433

KP 74 " " " " Nucl.Phys. A236 (1974) 269

KR 69 P.B.Kahn and R.Rosenzweig, Phys.Rev. 187 (1969) 1193

KS 65 W.Kohn and L.J.Sham, Phys.Rev. 137 (1965) A1697; ibid. 140 (1965) A1133

KW 72 S.J.Krieger and C.Y.Wong, Phys.Rev.Lett. 28 (1972) 690

La 37 R.E.Langer, Phys.Rev. 51 (1937) 669

La 64 A.M.Lane, Nuclear Theory (Benjamin, New York, 1964)

LL 74 S.E.Larsson, G.Leander, I.Ragnarsson and J.Randrup, Ronneby 1974, p. 65

LL 75 S.E.Larsson and G.Leander, Nucl.Phys. A239 (1975) 93

Lo 73 R.J.Lombard, Ann.Phys. (N.Y.) 77 (1973) 380

Ma 49 M.G.Mayer, Phys.Rev. 75 (1949) 1969

Ma 77 R.S.Mackintosh, Rep. Prog. Phys. 40 (1977) 731

MG 53 S.C.Miller Jr. and R.H.Good, Phys.Rev. 91 (1953) 174

Mi 67 A.B.Migdal, Theory of finite Fermi systems and properties of atomic nuclei (Moscow, 1965; Interscience, New York, 1967)

MM 73 M.G.Mustafa, U.Mosel and H.W.Schmitt, Phys.Rev. C7 (1973) 1519

MN 70 P.Möller and S.G.Nilsson, Phys.Lett. 31B (1970) 283

MN 73 P.Möller and J.R.Nix, Rochester 1973, Vol. I, p. 103; see also Nucl. Phys. A229 (1974) 269

Mo 70 S.A.Moszkowski, Phys.Rev. C2 (1970) 402

Mo 72 L.G.Moretto, Phys.Lett. 38B (1972) 393

Mö 72 P.Möller, Nucl.Phys. A192 (1972) 529

MS 66 W.D.Myers and W.J.Swiatecki, Nucl.Phys. 81 (1966) 1

MS 69 " " Ann.Phys. (N.Y.) 55 (1969) 395

MS 70 L.G.Moretto and R.Stella, Phys.Lett. 32B (1970) 558

MS 77 V.Metag and G.Sletten, Nucl.Phys. A282 (1977) 77

My 69 W.D.Myers, Nucl.Phys. A145 (1969) 387

MZ 74 U.Mosel, P.Zint and K.Passler, Nucl.Phys. A236 (1974) 252

Ne 70 J.W.Negele, Phys.Rev. C1 (1970) 1260

Ne 75 " Trieste 1975, p. 113

Ni 55 S.G.Nilsson, Kgl.Dan.Vid.Selsk., Mat.-Fys.Medd. 29 (1955) No. 16

Ni 69 J.R.Nix, Nucl.Phys. A130 (1969) 241

Ni 72 " Ann.Rev.Nucl.Sci. 22 (1972) 65

NP 58 P.Nozières and D.Pines, Phys.Rev. 111 (1958) 442

NT 69 S.G.Nilsson, C.F.Tsang, A.Sobiczewski, Z.Szymanski, S.Wychec, C.Gustafsson, I.L.Lamm, P.Möller and B.Nilsson, Nucl.Phys. A131 (1969) 1

NV 70 J.Nemeth and D.Vautherin, Phys.Lett. 32B (1970) 561

NV 72 J.W.Negele and D.Vautherin, Phys.Rev. C5 (1972) 1472

NV 75 " " " " C11 (1975) 1031

OZ 77 S.R.Ofengenden, V.F.Zavarzin and V.M.Kolomietz, Phys.Lett. 69B (1977) 264

Pa 73 H.C.Pauli, Phys.Reports (Phys.Lett.C) 7 (1973) 35

PL 71 H.C.Pauli, T.Ledergerber and M.Brack, Phys.Lett. 34B (1971) 264

PL 73 " and T.Ledergerber, Rochester 1973, Vol. I, p. 463

Po 62 S.Polikanov et al., JETP (Sov.Phys.) 15 (1962) 1016

Qu 75a P.Quentin, Trieste 1975, p. 297

Qu 75b " Thèse d'Etat, Orsay, 1975

RB 72 C.K.Ross and R.K.Bhaduri, Nucl.Phys. A188 (1972) 566

Re 68 R.V.Reid, Ann.Phys. (N.Y.) 50 (1968) 411

RK 72 V.S.Ramamurthy and S.S.Kapoor, Phys.Lett. 42B (1972) 399

Sa 75 P.U.Sauer, Trieste 1975, p. 89

SB 73 W.Stocker and J.Burzlaff, Nucl.Phys. A202 (1973) 265

SB 77 V.M.Strutinsky, private communication; M.Brack, unpublished results (1977)

SC 76 G.Sauer, H.Chandra and U.Mosel, Nucl.Phys. A264 (1976) 221

SG 71 D.Scharnweber, W.Greiner and U.Mosel, Nucl.Phys. A164 (1971) 275

SG 77 A.Sobiczewski, A.Gyurkovich and M.Brack, Nucl.Phys. A289 (1977) 346

SI 75 V.M.Strutinsky and F.A.Ivanjuk, Nucl.Phys. A255 (1975) 405

Sk 57 T.H.R.Skyrme, Proc.Phys.Soc. A70 (1957) 433

Sk 56 " Phil.Mag. 1 (1956) 1043

Sk 59 " Nucl.Phys. 9 (1959) 615

SL 63 V.M.Strutinsky, N.Ljashchenko and N.A.Popov, Nucl.Phys. 46 (1963) 639

SM 72 H.W.Scmitt and U.Mosel, Nucl.Phys. A186 (1972) 1

SM 77 V.M.Strutinsky, A.G.Magner, S.R.Ofengenden and T.Døssing, Z.Physik A283 (1977) 269

Sp 74 H.J.Specht, Rev.Mod.Phys.46 (1974) 773

SS 72 P.J.Siemens and A.Sobiczewski, Phys.Lett. 41B (1972) 16

St 66 V.M.Strutinsky, Yad.Fiz. 3 (1966) 614 [Sov.J.Nucl.Phys. 3 (1969) 449]

St 67 " Nucl.Phys. A95 (1967) 420

St 68 " " " A122 (1968) 1

St 74 V.M.Strutinsky, Nucl.Phys. A218 (1974) 169

St 75 " " " A254 (1975) 197

Sw 55 W.J.Swiatecki, Proc.Phys.Soc. A65 (1955) 285

SW 72 H.J.Specht, J.Weber, E.Konecny and D.Heunemann, Phys.Lett. 41B (1972) 43

SY 63 M.Sano and S.Yamasaki, Progr.Theor.Phys. 29 (1963) 397

Ta 64 F.Tabakin, Ann.Phys. (N.Y.) 30 (1964) 51

Ts 69 C.F.Tsang, Ph.D. Thesis, Berkeley, 1969

Ty 70 A.S.Tyapin, Sov.J.Nucl.Phys. 11 (1970) 401

Ty 72 " " " " 14 (1972) 50

UB 36 G.E.Uhlenbeck and E.Beth, Physica 3 (1936) 729

Va 69 D.Vautherin, Thèse d'Etat, Orsay, 1969

Va 73 " Phys.Rev. C7 (1973) 296

VB 72 " and D.Brink, Phys.Rev. C5 (1972) 626

Vo 77 A.Voros, Thèse d'Etat, Saclay, 1977

WC 72 F.C.Williams, G.Chan and J.R.Huizenga, Nucl.Phys. A187 (1972) 225

We 35 C.F.v.Weizsäcker, Z.Physik 96 (1935) 431

Wi 32 E.P.Wigner, Phys.Rev. 40 (1932) 749

Wi 34 " Phys.Rev. 40 (1934) 1002

Wi 58 L.Wilets, Rev.Mod.Phys. 30 (1958) 542

Wi 69 " Vienna 1969, p. 179

Yu 35 H.Yukawa, Proc.Phys.-Math.Soc.,Japan 17 (1935) 48

Table 1.1 Comparison of theoretical LDM barriers (E_{th}) and measured barriers (E_{exp}), both in MeV. Values of X calculated with $(Z^2/A)_{crit} = 50$. (From Wilets, 1964).

Nucleus	X	E_{th}	E_{exp}
Th^{233}	0.694	15.58	6.44
Th^{232}	0.697	15.08	5.95
U^{239}	0.707	13.51	6.15
U^{238}	0.710	13.06	5.80
Ra^{232}	0.713	12.68	6.18
U^{237}	0.713	12.63	6.40
U^{235}	0.719	11.79	5.75
U^{233}	0.725	10.96	5.49
Np^{238}	0.725	10.92	6.04
Np^{237}	0.729	10.53	5.49
Pu^{239}	0.738	9.39	5.48

FIGURE CAPTIONS

Fig. 1.1: LDM energy surface as function of a_{20} and a_{40} deformations for a nucleus with x = 0.8. Equidistance of contour lines in units of the surface energy $E_{surf}(0)$. (From Wilets, 1964).

Fig. 1.2: Nilsson levels for protons, $82 < Z < 126$. (From Vandenbosch and Huizenga, 1973).

Fig. 2.1: Fission barrier of Pu^{240} obtained with a constrained HF calculation with the force Skyrme III [FQ 736]. Dashed and solid lines correspond to different ways of including pairing. Dots (with arrows) give the energies (and slopes of the curve) at the two minima and the 2. saddle when the basis is increased (to demonstrate convergence). For details see [FQ 74].

Fig. 3.1: Exact HF energy (E_{HF}) and its average part ($\bar{E}$; $\tilde{E}_{HF}$ in the text above) obtained with force Sky III. E_{LD} shows the LDM energy (adjusted at $Q_2 = 0$) obtained with the parameters of [MS 66].

Fig. 3.2: Same as Fig. 3.1 with force Negele - DME.

Fig. 3.3: Shell-corrections δE_1 and δE_2 corresponding to the two previous figures, and δE_1 from usual WS potential [BD 72] for comparison.

Fig. 3.4: Values of δE_2 for various nuclei in their ground-states.

Fig. 3.5: As in Fig. 3.1, but here $\tilde{E}$ is calculated selfconsistently.

Fig. 4.1: Axially symmetric shapes as functions of elongation (c) and necking (h) parameters. The shapes along $h = 0$ correspond to the LDM fission valley in a typical actinide nucleus. The dotted curves include some left/right asymmetry ($\alpha \neq 0$) typical at the second saddle ($c \sim 1.6$) [Pa 73].

Fig. 4.2: Neutron levels ε_i^n of the Pu^{240} (N = 146) obtained with the deformed Woods-Saxon potential [BD 72, PA 73] versus elongation c ($n = \alpha = 0$). Numbers in circles show "magic" numbers (note the deformed shell $n = 146$ at $c \simeq 1.4$ which leads to the shape isomer in Pu^{240}!). Odd parity states are dotted; the numbers inserted correspond to twice the K value (projection of ang. momentum along symmetry axis).

Fig. 4.3 Density of single-particle states g(E) in Pu^{240} at different deformations c ($h = \alpha = 0$). At the top, some nucleon numbers are indicated (magic numbers for $c = 1$). The dashed lines represent the uniform level density $\tilde{g}(E)$.

Fig. 4.4: Shell-correction δE for a spherical harmonic oscillator well with 70 particles, versus smoothing width γ. The numbers in parentheses are M/2. Note that the length of the plateau increases with the number of levels (shells) included [BP 73].

Fig. 4.5: As in Fig. 4.4, for a spherical Woods-Saxon potential [SG 77]. The inserted plot shows the stationary value $\delta E(\gamma_o)$ according to eq. 4.10 versus order M of curvature correction.

Fig. 4.6: As in Fig. 4.4, for Z = 94 protons in WS potential at different deformations c [BP 73].

Fig. 4.7: Proton levels ε_i^p in deformed WS potential and values of the occupation number differences δn_i in a region $\sim \pm\hbar\omega$ around the Fermi level λ [BP 73].

Fig. 5.1 Deformation energy surface for Pu^{240} for symmetric shapes ($\alpha = \gamma = 0$). Upper right: LDM energy. Left side: proton and neutron shell-corrections δE_p, δE_n (including pairing). Lower right: total energy. Numbers along contour lines show energy in MeV.

Fig. 5.2: Shapes of Pu^{240} nucleus at the four stationary points in the (c,h) surface. Dashed line at second saddle: asymmetry $\alpha \neq 0$ included.

Fig. 5.3: Total energy of Pu^{240} in region including isomer minimum and outer saddle. Upper part: symmetric shapes. Lower part: energy minimized with respect to α in each point (c,h).

Fig. 5.4: Potential energy surface of U^{236} calculated with the two-centre model [MM 73], as function of neck radius D and mass ratio. Energy contours in MeV (relative to g.-s.). The region between ground-state and second minimum (at $\sim$1 MeV) is only indicated partially. The asymmetry reduces the second saddle from 8 to 5.7 MeV.

Fig. 5.5: Comparison of experimental and theoretical barriers of actinide nuclei. The figure includes two newly measured barriers E_A of Pu^{232} and Pu^{234} using β-delayed fission [D. Habs et al., to be published in Z. Physik A, 1968]. I am indebted to H. Specht for providing me with this figure prior to its publication.

Fig. 5.6: Comparison of experimental $\delta M_{exp.}$ (top) and theoretical shell-corrections δM_{th} (middle) to ground-state masses. (Bottom: $\delta M_{exp.} - \delta M_{th}$). From [MN 73].

Fig. 5.7: Potential energy surface of Pu^{240} obtained with WS potential [BD 72]. Upper part: as in Fig. 5.1. Lower part: as function of elongation c and asymmetry α. The solid heavy line is the projection of the least action trajectory onto the corresponding surfaces. Crosses show the locus of constant mass ratio 1.43 of the nascent fragments (from [PL 73]).

Fig. 5.8: Comparison of calculated (dots) and measured (crosses) life times for spontaneous fission. (From [PL 73]).

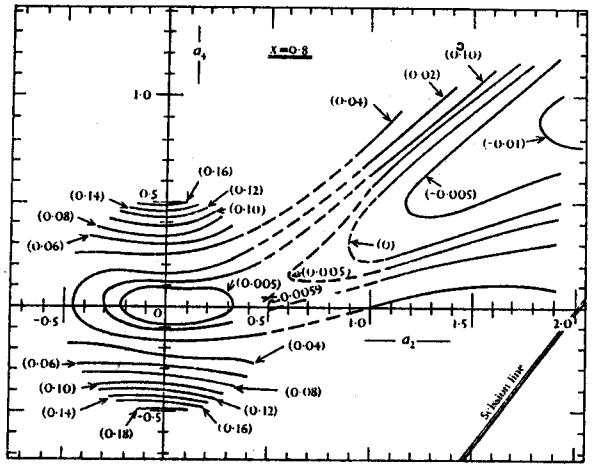

Fig. 1.1

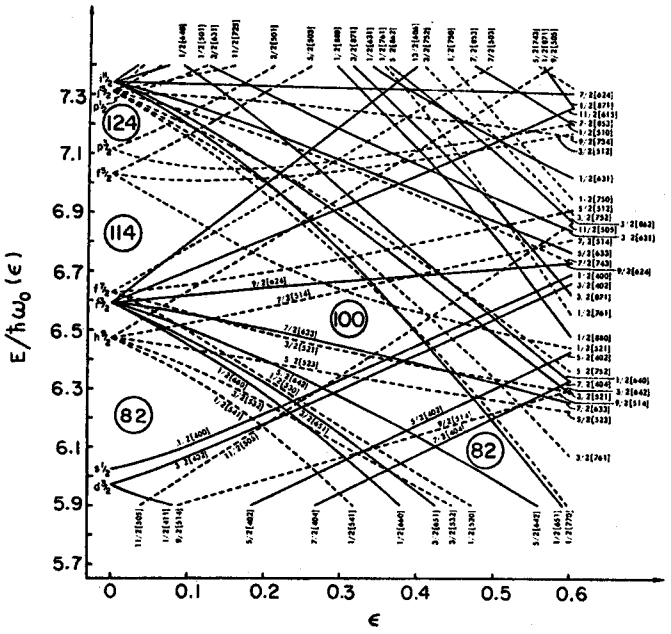

Fig. 1.2

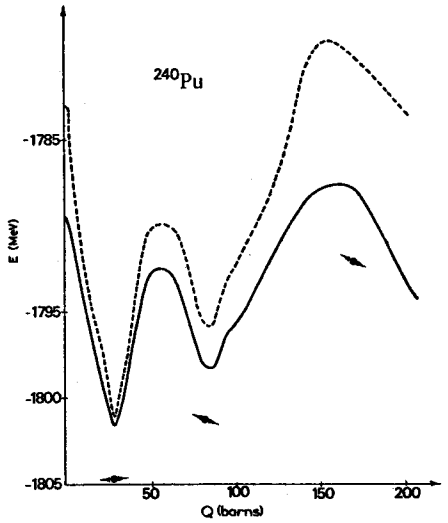

Fig. 2.1

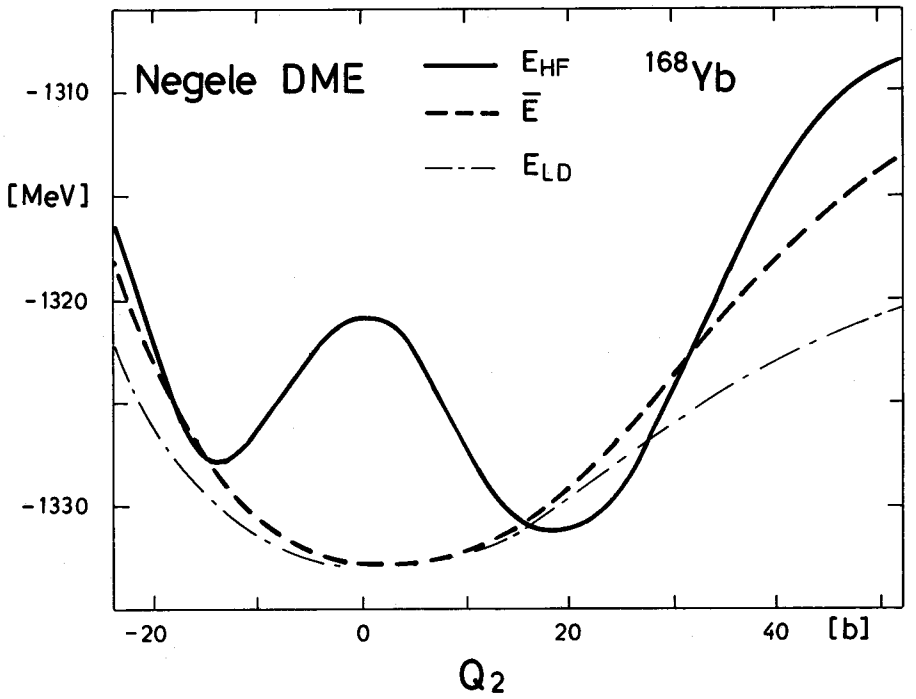

Fig. 3.2

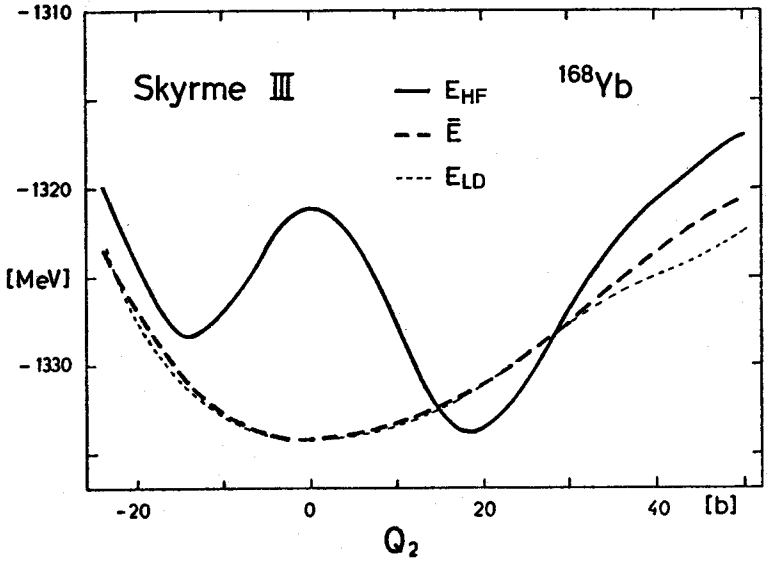

Fig. 3.1

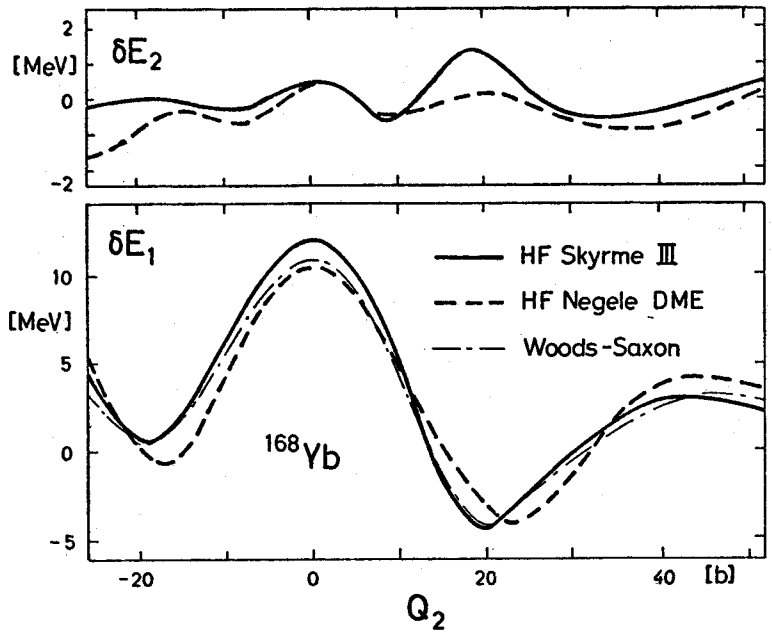

Fig. 3.3

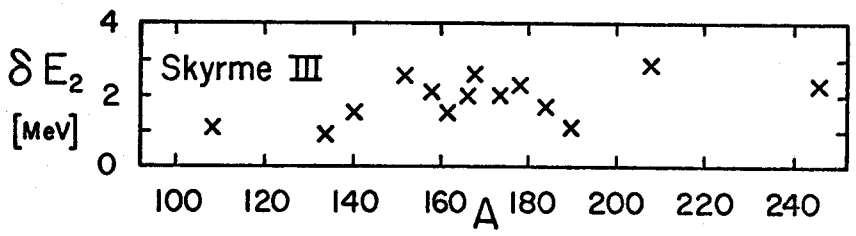

Fig. 3.4

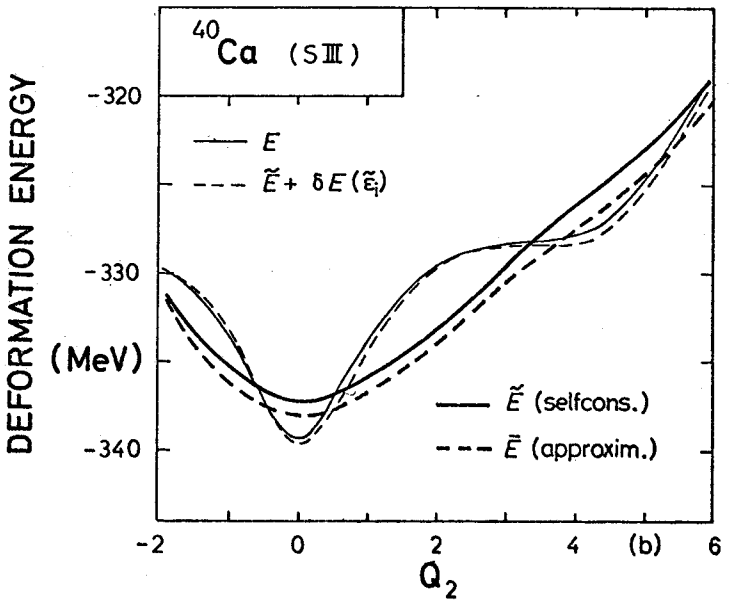

Fig. 3.5

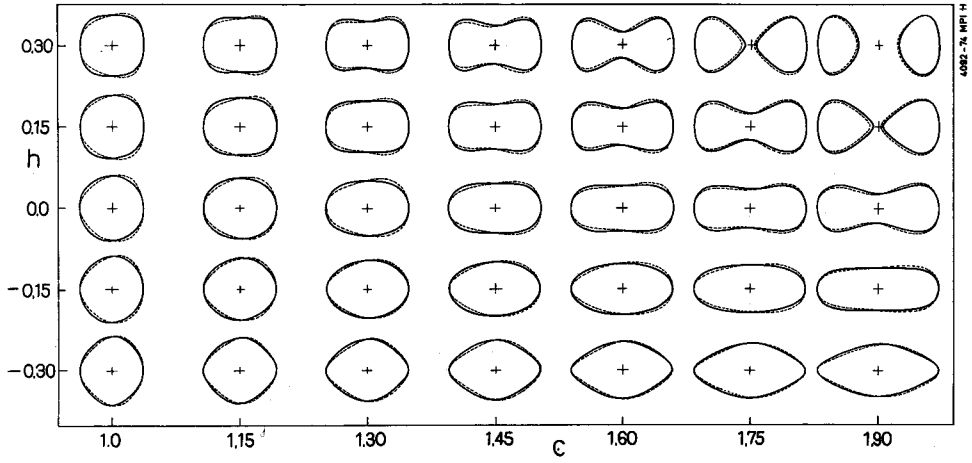

Fig. 4.1

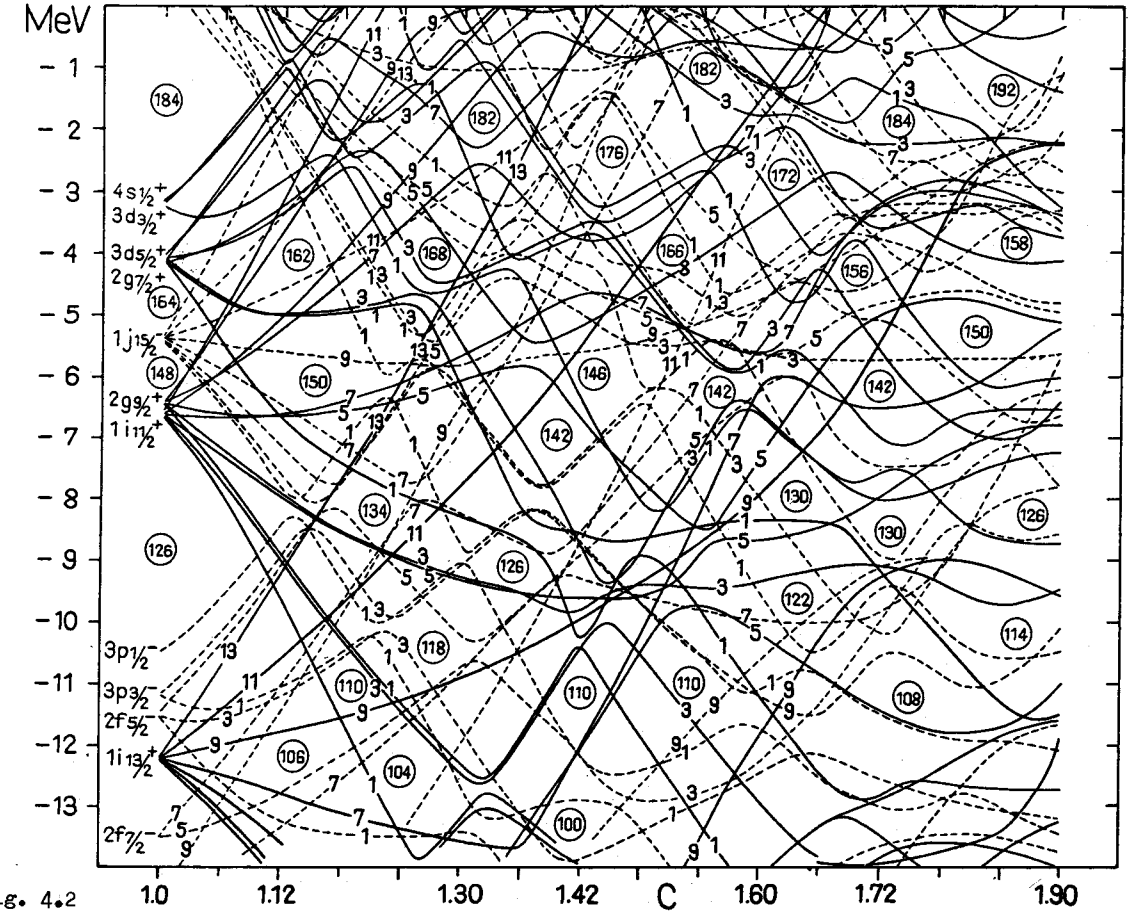

Fig. 4.2

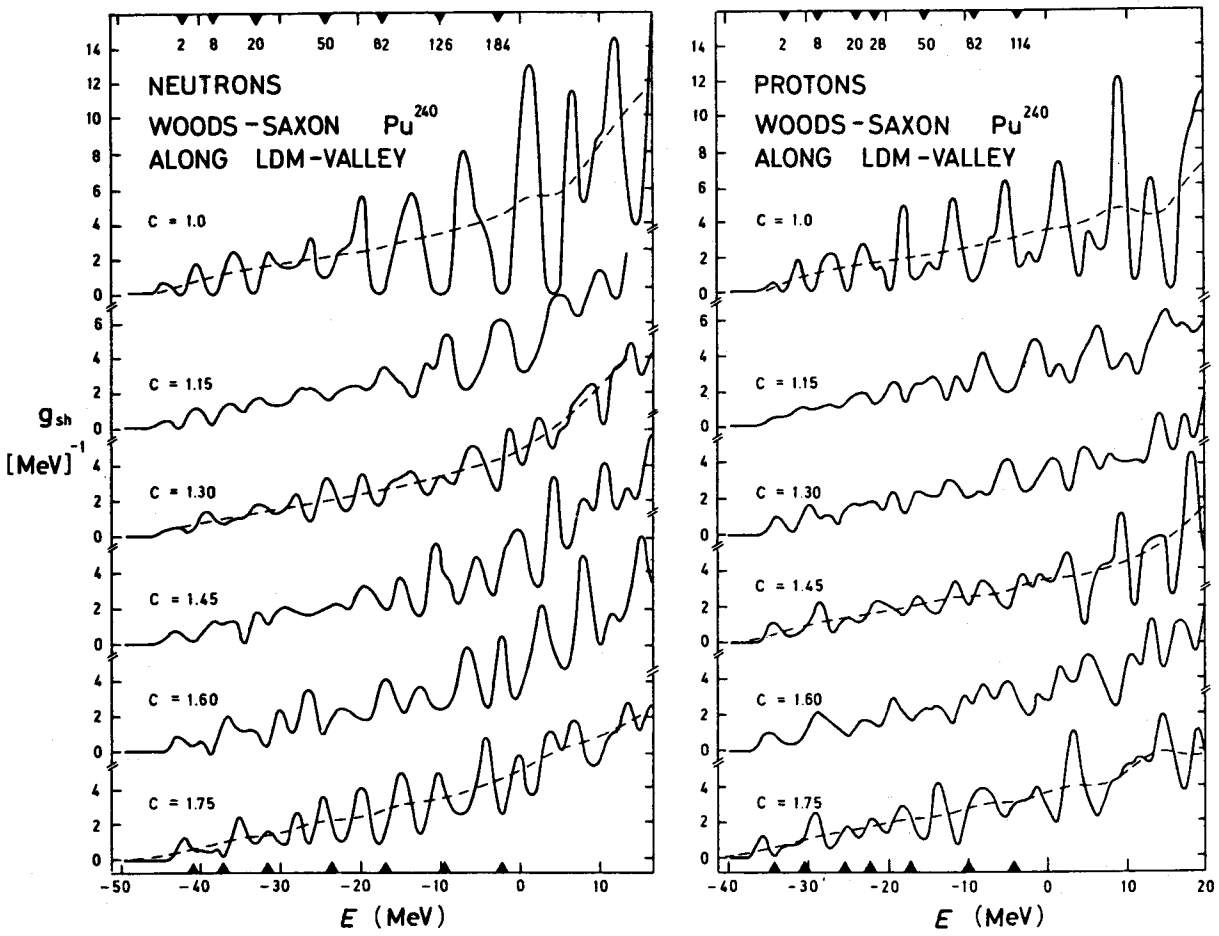

Fig. 4.3

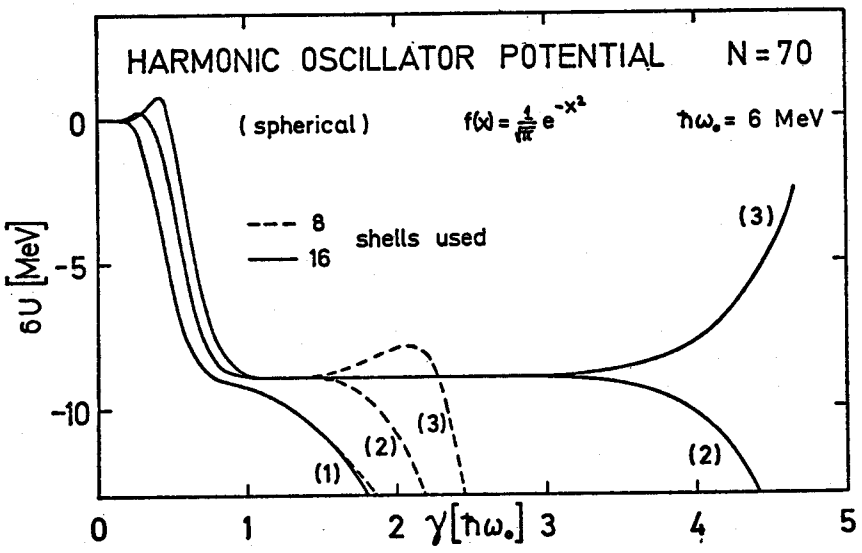

Fig. 4.4

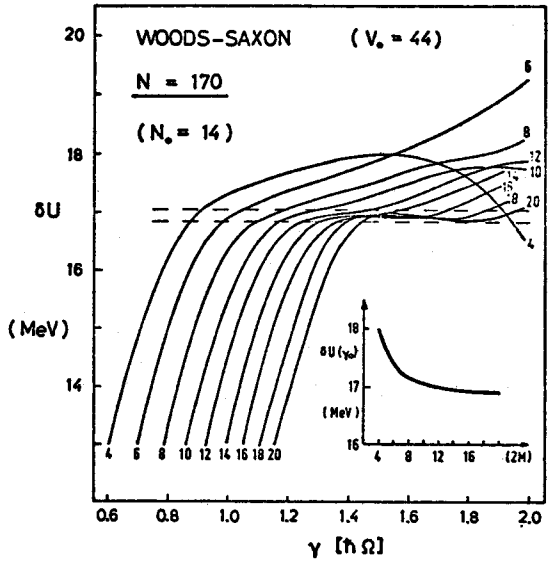

Fig. 4.5

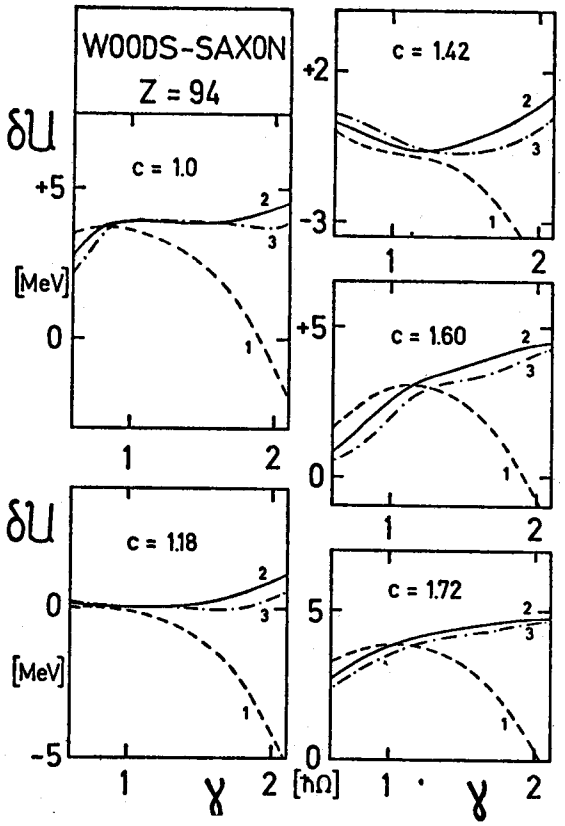

Fig. 4.6

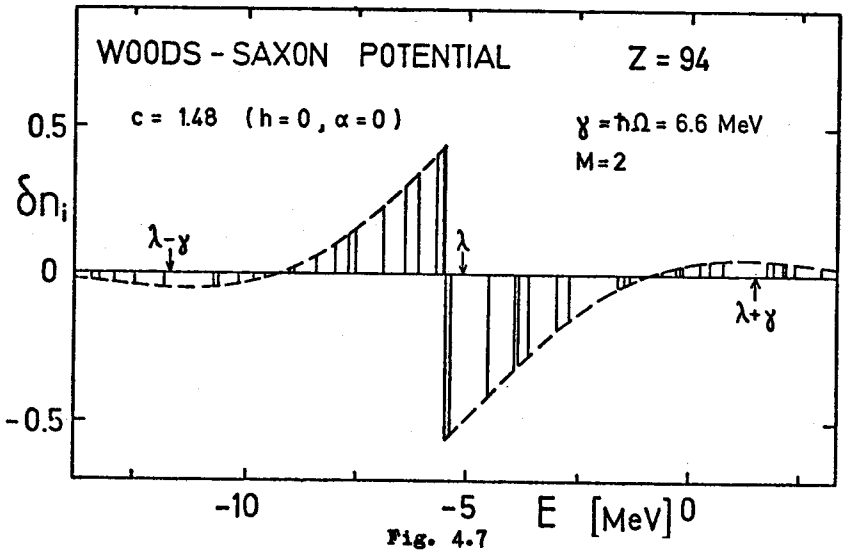

Fig. 4.7

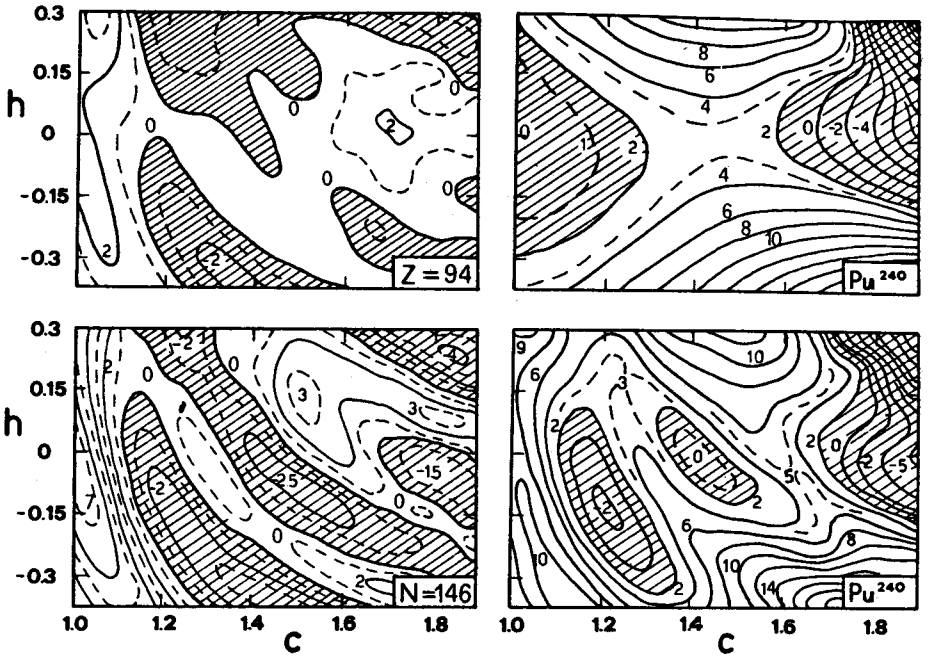

Fig. 5.1

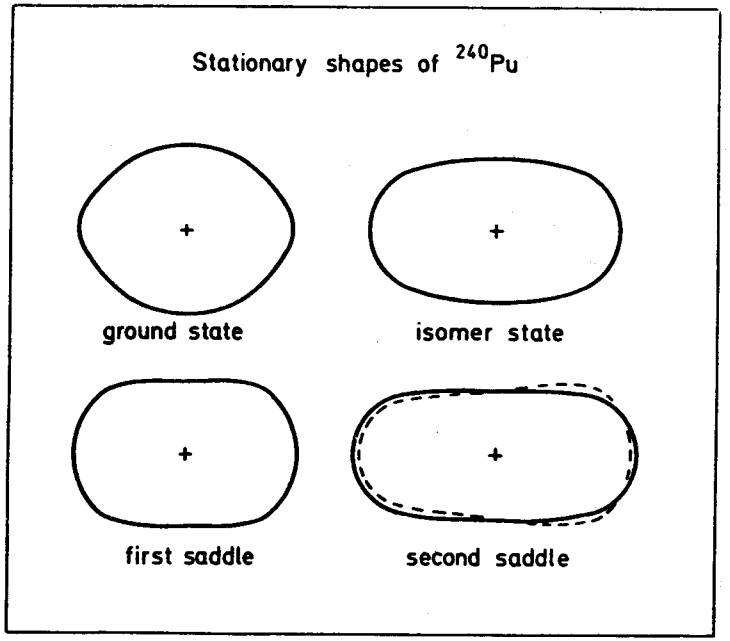

Fig. 5.2

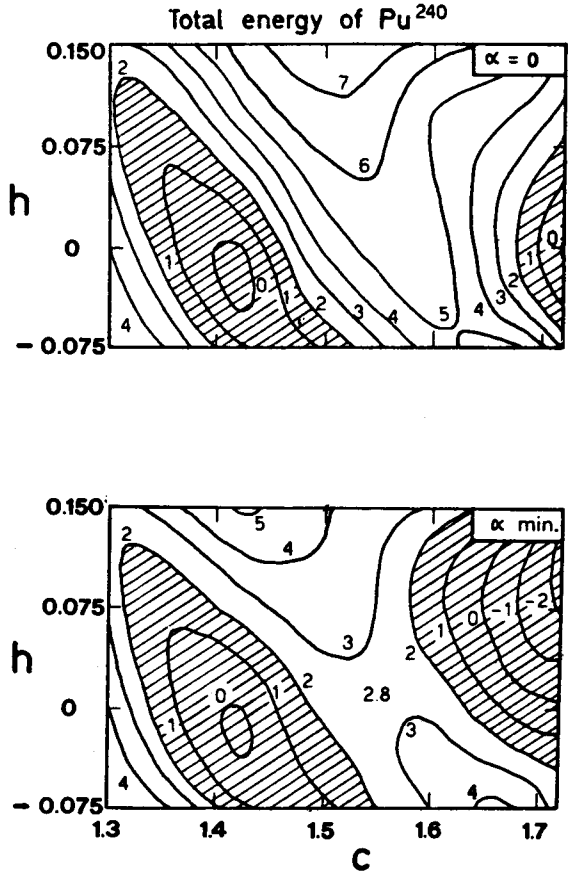

Fig. 5.3

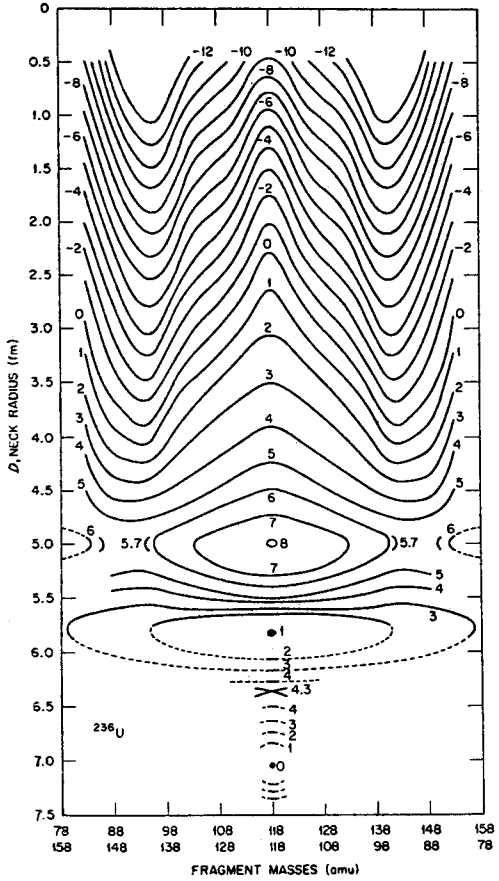

Fig. 5.4

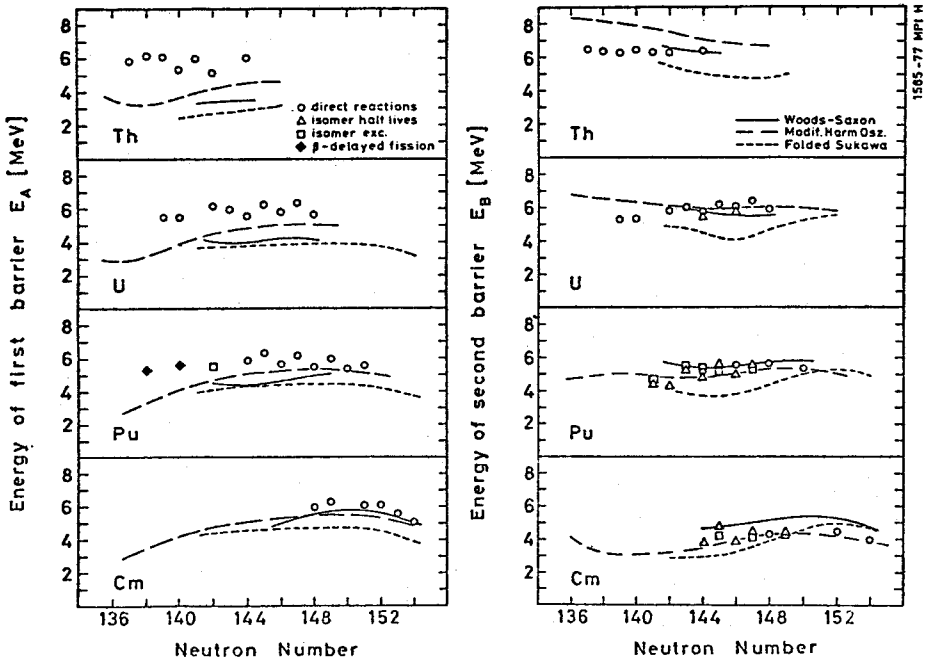

Fig. 5.5

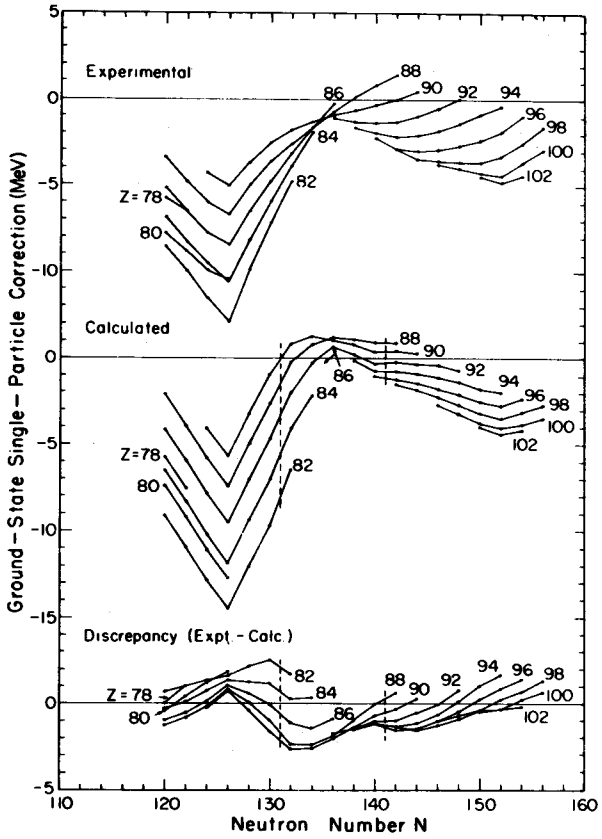

Fig. 5.6

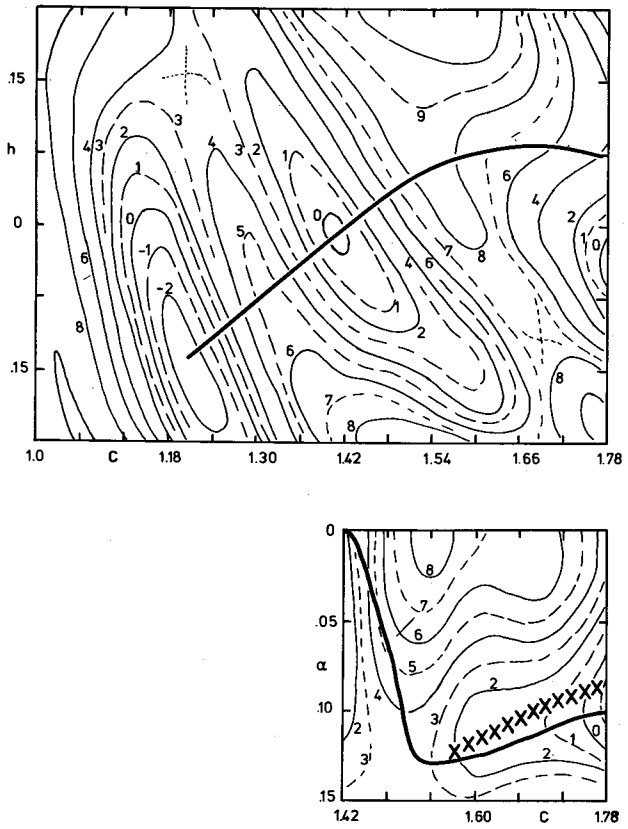

Fig. 5.7

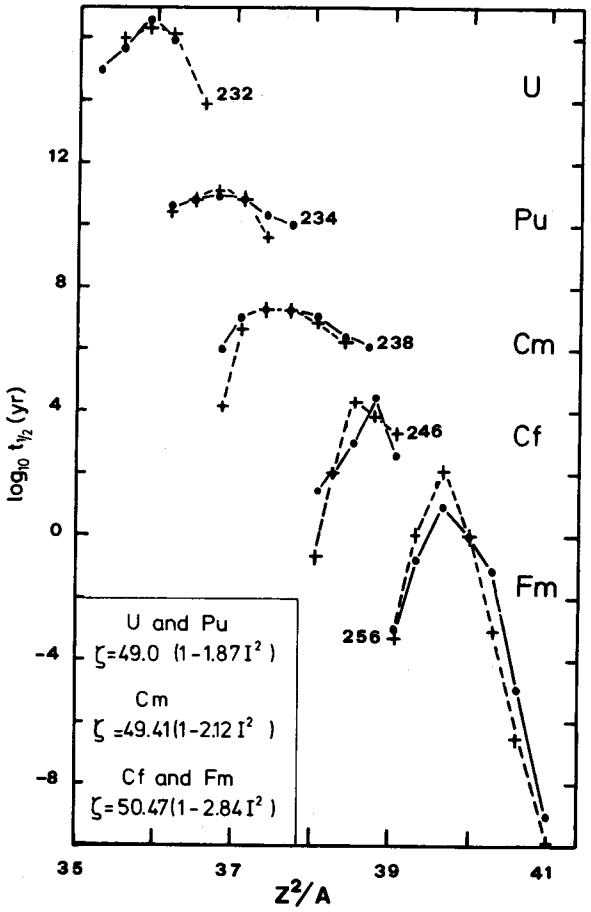

Fig. 5.8

FISSION BARRIER THEORY AND ITS APPLICATION TO THE CALCULATION OF ACTINIDE NEUTRON CROSS-SECTIONS

J.E. LYNN
UKAEA,
Atomic Energy Research Establishment,
Harwell, United Kingdom

Abstract

The lectures discuss the possibilities and realisations of applying nuclear fission theory to the calculation of unknown nuclear data required for applications, principally in the nuclear power field. A brief description of the fundamentals of fission theory, the nature of the potential energy surface in the deformation plane, and of the inertial tensor, is given, and the accuracy of the theoretical calculations is discussed. It is concluded that it is impracticable to obtain required quantities such as neutron cross-sections from such fundamental calculations at present. On the other hand the fundamental theory reveals a wealth of phenomenological aspects of the fission process which can be incorporated into nuclear reaction theory. It is then shown how reaction theory thus extended to take correct account of the structured ("double-humped") fission barrier can be used to parametrise the barrier by analysis of experimental data, and subsequently to calculate new data. Descriptions of computer programmes and illustrations of the application of the methods to actual physical examples are included in this account.

1. INTRODUCTION

This lecture course is aimed at describing the perspectives in using the theory of nuclear fission to provide data that are of use for applications, particularly in nuclear power technology, and to outline the methods for calculating such data. The background to the use of fission theory in this context is to be found in the great effort, costly in both scientific man-power and money, in providing the relevant data by experimental methods alone. As examples of the scale of the experimental effort required, decades of work have resulted in the cross-sections of the three commonest fissile nuclides being known to better than 1% only for neutrons of energy 0,025 eV, the differential fission cross-sections of fast neutrons of ^{235}U, ^{239}Pu and ^{238}U are now known to between 3 and 5%, whereas for reactor physics purposes an accuracy of better than 1% is desirable; and these are nuclides for which high quality samples are readily available for experimental measurement. In all countries there are now severe economic constraints on the amount of effort that can be put into nuclear data measurement while at the same time the range of fissionable, heavy nuclei for which sophisticated data are required is increasing rapidly as the full implications of the nuclear fuel cycle need to be studied. Clearly it is not going to be possible to provide the bulk of such data from experiment in the readily foreseeable future, especially as many of the nuclides for which data are required are either very difficult to obtain in suitable form or are so radioactive that the desired measurement cannot readily be carried out.

In these circumstances it is pertinent to ask the extent to which fission theory can be used to alleviate the situation. As a first step to this in the present Winter School Matthias Brack has been presenting the fundamentals of fission theory. The first lecture in my own course briefly summarises some of these more basic matters with a view to assessing the likely accuracy of data that can be produced by the present theoretical techniques. The remaining seven lectures deal in turn with the development of theoretical methods, available computer codes, and examples of data.

2. BASIC FISSION THEORY; OUTLINE AND ACCURACY

2.1 Potential energy surfaces

The primary pre-occupation of fission theory has been the determination of the potential energy surface in the space of the various collective co-ordinates defining the shape of a deforming nucleus. Prior to about 1966 efforts in this direction concentrated on the liquid drop model. While this gave a qualitative account of the phenomenon of fission and simultaneously an overall semi-quantitative description of nuclear binding energies it also had many difficulties (e.g. no obvious likelihood, in the light of the potential energy surface, of explaining asymmetric mass division, wrong trend of fission barrier heights). Myers and Swiatecki (1) first attempted to improve this situation by superposing shell effects in a semi-empirical way onto the liquid drop model, but it was Strutinsky (2) who made the real breakthrough in this direction by developing a more fundamental way of calculating the shell effects in such an approach, thus enabling the theory to be extrapolated to large deformations.

The basis of Strutinsky's method of calculating nuclear energies, either as a function of nuclear mass or as a function of deformation is now well-known. Very briefly outlined it is this: in a pure independent-particle shell model, particles (neutrons and protons) are filled into the levels of a deformed potential well (the deformation assumed static) up to a certain level (the Fermi energy) at which the particular nucleus of interest is obtained. The energies of the filled levels are then summed to give the nuclear ground state energy at the chosen well deformation. It is well-known of course that because of the residual interactions, and hence the correlated motions, among the nucleons, which cannot be described in the framework of a simple potential well model, this is a quite hopeless procedure for extracting the absolute energy of a real nucleus. For this the liquid drop model with semi-empirically adjusted parameters gives much more realistic estimates of the nuclear binding energies - within 15 MeV or so at worst relative to binding energies of hundreds of MeV, over the whole periodic table; but it does not give any of the correlations with nuclear shell closures that appear in the observed binding energies.

Strutinsky's way of obtaining accurate estimates of absolute nuclear energies is to hypothesize that summing the single-particle state energies as shown in the left half of Fig. 1 will reproduce the change in energy from nucleus to nucleus (at a given deformation) due to the shell structure, and to obtain this change, denoted by $E_{\text{Shell Correction}}$, it is only necessary to subtract from the independent-particle energy a similar sum calculated from the independent

particle levels smeared out in some way to remove the shell structure, as illustrated schematically in the right half of Fig. 1. The gross energy that is thus removed is then replaced by a realistic energy term calculated from the liquid drop model E_{LDM}. Thus,

$$E = E_{LDM} + E_{SC} \qquad (2.1)$$

Strutinsky's method when applied to the broad mass of nuclei, with the energy minimised as a function of deformation for every nucleus, was immediately successful in reproducing accurately the nuclear binding energies. Furthermore, when the energy was calculated as a function of extended deformation for the actinide nuclei, in order to calculate fission barrier saddle heights to compare with observation, he discovered a secondary dip (Fig. 2) in the energy at deformations corresponding roughly to the traditional liquid drop saddle point. It is now well recognized that this deformation corresponds roughly to a spheroidal shape with a ratio of major to minor axes of about 2:1, and this gives almost as much shell structure (and hence great stability for particular nuclei like the actinides) as spherical potential wells (see Fig. 3 from ref. (3)). The dip or secondary well offered an explanation for the spontaneously fissioning isomers that had been known for a few years and for the phenomena of intermediate structure in fission cross-sections that were being discovered about that time, and Strutinsky's theory therefore became spectacularly successful.

Since Strutinsky's original work a tremendous amount of effort has been put into the calculation of potential energy surfaces as a function of deformation. Some of this has been devoted to discovering the possibility of new meta-stable shapes among the lighter nuclei, and much to the estimation of the stability of super-heavy nuclei with respect to alpha, beta and fission decay. As far as the subject matter of these lectures is concerned, which is principally the fission properties, especially cross-sections, of the actinide nuclei, the theoretical work that is most important concerns the potential energy landscape in the region of the liquid drop saddle point, giving the double-humped barrier properties that control cross-sections.

2.1.1 Basis and technical treatment of Strutinsky theory

The justification of the Strutinsky method for determining nuclear energies, the technical method for carrying it out, and the physical nature of the results have been reviewed in detail by Brack et al (4). A comprehensive review containing less detail but with a complete bibliography of work carried out up to 1972 has been written by Nix (3).

Basic justifications of the Strutinsky method start from the Hartree-Fock theory. In ref. (4) it is shown how the expression for the energy of a nucleus in Hartree-Fock theory (in which the single-particle potential is self-consistent with the single-particle density matrix generated by that potential) can be written in terms of shell-model single particle energies and densities to second order in the difference between the shell-model and the self-consistent densities. The significant feature of the new expression for the Hartree-Fock energy is that apart from the simple sum over occupied shell-model levels the remaining principal term is expressed in terms of averaged single-particle densities, and is therefore smooth in its dependence on nucleon numbers and nuclear shape. It is this smooth term plus a smooth component extracted from the sum over occupied single particle levels that is replaced by a liquid drop expression for the energy, E_{LDM}.

Most of the methods for extracting the smooth component from the sum of occupied energy levels are based on Strutinsky's own technical procedures for averaging over the shell-model energy levels with a suitable weighting function (see refs. (2,4)). This weighting function can be expressed as sums of products of Gaussians and Hermite polynomials, the width of the Gaussian being governed mainly by the energy spacing between major shells just below the Fermi energy. Such averaging procedures can run into conceptual if not practical difficulties however if the shell-model potential is a realistic one i.e. it permits unbound eigenstates, as with the Woods-Saxon potential for instance. Bengtsson (5) has therefore initiated a method in which each individual shell-model level as a function of deformation is smoothed by fitting it with the cube root of a fourth-order polynomial in the deformation parameter; this particular form of the fitting function is suggested by the Thomas-Fermi statistical model. The smooth component of the sum of occupied energy levels is then simply given by the sum of the occupied smoothed energy levels resulting from this fitting procedure, and the unbound levels thus require no consideration. The shell correction energy, E_{SC}, thus defined for neutrons in ^{238}Pu is shown in Fig. 4 in comparison with the result from the same set of shell-model levels using the Strutinsky procedure. The overall agreement, especially for prolate deformations in which we are most interested in fission theory, is seen to be remarkably good, although local differences of up to 1 MeV can occur.

2.1.2 Comparison with Hartree-Fock calculations

Apart from work on the justification of the Strutinsky theory in a basic way, there have been attempts to calculate nuclear deformation energies directly from Hartree-Fock theory. These employ the Skyrme effective nucleon-nucleon interaction (6) with parameters adjusted to reproduce gross nuclear properties, as given in ref. (7). The result of the work of Flocard et al (21) showing the binding energy for ^{240}Pu as a function of the quadrupole moment of the nucleon density is presented in Fig. 5. No allowance is made for axial asymmetry or reflection asymmetry in the nuclear shape in this calculation. It looks qualitatively very similar to the deformation energy curves that result from calculations using the Strutinsky method, but the energy differences between the extrema are greater. For example the first barrier height (V_A) is at about 9 MeV relative to the

primary well depth (V_I) whereas Strutinsky calculations with a similar restriction on the range of nuclear shapes explored would give about 6 MeV for this quantity. However, there are recognized sources of error in the present Hartree-Fock calculation that approach the order of one MeV; they arise from the necessity to project out the 0^+ ground state from the calculated state with no constraint on angular momentum, and from the truncation of the harmonic oscillator basis states used in the numerical work.

2.1.3 Nuclear models employed in Strutinsky calculations

Apart from the possible source of error arising from the actual principle of the Strutinsky theory, and possible errors from the technical treatment of smoothing procedures, the basic parametrisations of the models used in the theory contain uncertainties that will give rise to errors in calculations based on the theory. The main source of this kind of error is likely to come from the liquid drop model, which provides the basic (or macroscopic) energy term in the Strutinsky theory, but there are also likely to be significant uncertainties from the shell model adopted, and smaller errors from the treatment of the pairing interaction, which is shell dependent and is also normally incorporated into the Strutinsky theory. This last term depends not only on the choice of shell model but also on the hypothesis assumed for the dependence of the interaction strength on surface area.

Notice, in this connection, that virtually all calculations with the Strutinsky method have been made for even nuclei.

2.1.3.1 Liquid drop and droplet models

The nuclear energy in the basic liquid drop model of the nucleus is characterised by a volume term proportional to the mass number A, a surface energy term proportional to the surface area, and hence to $A^{2/3}$ for a spherical nucleus, and a Coulomb energy term, proportional to $A^{-1/3}$ for a spherical nucleus:

$$E_{LD} = -C_V A + C_S A^{2/3} B_S(\text{shape}) + \frac{3}{5}\cdot\frac{e^2 Z^2}{r_0 A^{1/3}} B_c(\text{shape}) \qquad (2.2)$$

where B_S (shape) is the ratio of the surface area of the deformed nucleus of specified shape to that of a spherical nucleus, and B_c (shape) is the ratio of the Coulomb energy of the deformed nucleus to that of the sphere. The quantities e and r_0 are the proton charge and the nuclear radius constant of proportionality, respectively. The coefficients C_V and C_S contain a dependence on the neutron-proton asymmetry I = (N - Z)/A:

$$C_V = a_V(1 - k_V I^2) \qquad (2.2a)$$

$$C_S = a_S(1 - k_S I^2) \qquad (2.2b)$$

So far as the fission barrier is concerned, the important terms in equation (2.2)are the surface energy and Coulomb energy terms, and the sum of their contributions to the liquid drop energy relative to the energy of a spherical liquid drop can be written as

$$E_{LD}(\text{shape}) - E_{LD}(0) = \left\{\left[B_S(\text{shape}) - 1\right] + 2x\left[B_c(\text{shape}) - 1\right]\right\} E_S(0) \qquad (2.3)$$

where $E_S(0)$, the surface energy of a spherical liquid drop, is $C_S A^{2/3}$ and x the fissility parameter is defined as the ratio of the Coulomb energy of a spherical drop to $2E_S(0)$:

$$x = \left(\frac{3}{5}\right)\left(\frac{e^2}{r_0}\right)\cdot\frac{(Z^2/A)}{2a_S(1 - k_S I^2)} \qquad (2.4)$$

The fissility parameter, and hence the values of the coefficients a_S and k_S, are crucial in determining the shape dependence of the liquid drop energy and therefore of fission barriers. These coefficients have to be determined empirically from an overall fit to nuclear binding energies and, where possible, to experimental fission barrier data. For reliable determination of the coefficients equation (2.2) is too crude as it stands, and it is recognized that in that formula the volume and surface terms are only the leading terms of a systematic expansion of the nuclear energy of a finite body with a relatively thin surface region in which the matter density falls to zero. The ratio of surface diffuseness to nuclear radius is of order $A^{-1/3}$, so a refinement of equation (2.2) takes the expansion to higher powers in $A^{-1/3}$; this is the droplet model of Myers and Swiatecki (8). In this, terms in $A^{1/3}$ are associated with energy of curvature of the surface and redistribution of Coulomb energy in the surface, and other terms are associated with the compressibility of nuclear matter. The many parameters involved are determined partly from fitting to experimental data and partly from statistical calculations based on Thomas-Fermi theory; fitting to experimental data has to take account of shell effects both in ground-state masses and in fission barriers, and this is generally done in the empirical way outlined in ref. (1). Values of the liquid drop (or droplet) coefficients actually used for calculations of fission barriers by the Strutinsky method vary. One common set is that due to Myers and Swiatecki (9) (liquid drop model):

$$\begin{aligned} r_0 &= 1.2249 \text{ fm}, \\ \left(\frac{3}{5}\right)\left(\frac{e^2}{r_0}\right) &= 0.7053 \text{ MeV}, \\ a_S &= 17.9439 \text{ MeV}, \\ k_S &= 1.7826 \end{aligned} \qquad (2.5)$$

Another set coming into vogue is derived from a redetermination of droplet model coefficients in unpublished work of Myers and Swiatecki referred to in ref. (10); from these an equivalent set of liquid drop coefficients can be determined, among which an effective neutron-proton asymmetry coefficient, $k_{s,eff}$, turns out to have the value 2.8. This implies a distinct lowering of the calculated values of the fission barriers of neutron-rich nuclei from those that would be calculated with the set (2.5), and at present it can be stated that the precise value of the surface neutron-proton asymmetry coefficient is probably the main uncertainty arising from the liquid drop or the droplet model in calculating fission barrier heights.

2.1.3.2 Shell models

There is a wide variety in the choice of shell model for calculating the shell-correction energy entering fission barrier calculations. Strutinsky's own calculations (2), (5) employed a deformed Woods-Saxon potential which has the advantage of physical realism for nuclear shapes that are not too strongly deformed; the potential is defined in such a way as to have a constant skin thickness about an effective surface defining the shape. Such a potential encounters difficulties for strongly necked-in shapes, and here a variation suggested by physical notions of the effect of finite range nucleon forces has advantages; this is the diffuse-surface potential obtained by folding a Yukawa function over a square-well potential of the nuclear shape required (11):

$$V(\vec{r}) = -\frac{V_0}{4\pi a^3}\int d^3\vec{r}\,' \frac{\exp\left[-|\vec{r}-\vec{r}\,'|/a\right]}{|\vec{r}-\vec{r}\,'|/a} \qquad (2.6)$$

where V_0 is the square well depth. The range, a, of the Yukawa function can be chosen to give the desired surface diffuseness. Parameters of such potentials are generally chosen to reproduce a given set of experimental data on single particle levels. Nix and his collaborators chose to fit their potential to the levels of ^{208}Pb in their earlier calculations (11), but in a later set they have adjusted their parameters to fit the levels of heavy deformed actinide nuclei (12). The difference in the two sets of potential well parameters amounts to about 11% in the surface diffuseness parameter (smaller in ref (12)) and 12% and 6% in the neutron and proton spin-orbit interaction (greater in ref. (12)).

The other class of shell model potentials in common use is based on the harmonic oscillator. In general these have distinct computational advantages and permit the exploration of a greater variety of nuclear shapes. Calculations of the potential energy landscape in the region of the barrier are generally performed within the framework of the one-centre modified oscillator model with the shell model potential having, typically, the following form:

$$V = V_{osc} + V_{corr} \qquad (2.7)$$

$$V_{osc} = \tfrac{1}{2}\hbar\omega_0\rho^2\left[1 - \tfrac{2}{3}\varepsilon\sqrt{\tfrac{4\pi}{5}}\cdot\cos(\gamma)Y_{20} + 2\varepsilon_4 P_4 + \tfrac{2}{3}\varepsilon\sqrt{\tfrac{4\pi}{5}}\sin(\gamma)\left(\frac{Y_{22}+Y_{2-2}}{\sqrt{2}}\right)\right] \qquad (2.7a)$$

$$V_{corr} = -k\hbar\omega_0\left[2\vec{l}_t\cdot\vec{s} + \mu\left(\vec{l}_t^{\,2} - \langle\vec{l}_t^{\,2}\rangle\right)\right] \qquad (2.7b)$$

The correction term, depending principally on the square of the orbital angular momentum l_t, has the effect of flattening the potential towards its outer edges and also contains a spin-orbit interaction. The parameters k and μ are adjustable for optimal reproduction of experimental single particle level schemes. The variable ρ is the radius vector length in "stretched" co-ordinates and is thus defined by

$$\rho^2 = \frac{M}{\hbar}\left(\omega_x x^2 + \omega_y y^2 + \omega_z z^2\right) \qquad (2.8)$$

The oscillator frequencies for the principal ellipsoidal axes are related to the parameter ω_0 (itself governed by the shape parameters ε, ε_4 and γ) through the relations

$$\omega_x = \omega_0\left[1 - \tfrac{2}{3}\varepsilon\cdot\cos\left(\gamma + \tfrac{2\pi}{3}\right)\right]$$

$$\omega_y = \omega_0\left[1 - \tfrac{2}{3}\varepsilon\cdot\cos\left(\gamma - \tfrac{2\pi}{3}\right)\right]$$

$$\omega_z = \omega_0\left[1 - \tfrac{2}{3}\varepsilon\cdot\cos\gamma\right]$$

and ω_0 is related to the spherical oscillator frequency $\overset{\circ}{\omega}_0$ through a volume conservation condition. A typical numerical value adopted for the last parameter is (13)

$$\hbar\overset{\circ}{\omega}_0 = \frac{41.0}{A^{1/3}}\left[1 \pm \frac{1}{3}\frac{(N-Z)}{A}\right] \qquad (2.9)$$

the plus and minus signs referring to proton and neutron potentials respectively.

The deformation parameters ε, ε_4 and γ refer to quadrupole deformation (nuclear elongation), hexadecapole deformation (waistline "necking-in" or broadening) and degree of axial asymmetry, respectively. The parameter γ is generally treated through its range of values 0° to 60°, 0° representing axial symmetry of a prolate body and 60° the opposite extreme of axial symmetry of an oblate body. Other degrees of freedom in the shape can be introduced within this framework, still allowing practical computation, and two such important parameters are the deformations associated with the third and

fifth Legendre polynomials; these parameters allow the description of reflection asymmetry in the nuclear shape (often referred to as mass or volume asymmetry).

More sophisticated shell-model effects can be incorporated within the Strutinsky theory. One of these is a shell-correction term to the Coulomb energy (14) which is normally computed simply as a liquid drop term with uniform charge density over the nucleus. For this, the Coulomb repulsion energy is calculated directly from the single particle wave-functions; the proton densities arising from these can change sharply with changing deformation giving rise to changes in the occupation of single particle levels near the Fermi energy with very different radial and angular distributions. The treatment of pairing correlation energies can also contain elaborations. One of these is the dependence of the pairing interaction strength on surface area, as already mentioned. Another is the introduction of the quadrupole pairing force (14). This arises from the well-known expansion of a delta-force in terms of spherical harmonics,

$$\delta(\vec{r}_1 - \vec{r}_2) = \sum_{\lambda\mu} \frac{\delta(r_1 - r_2)}{r_1 r_2} Y_{\lambda\mu}(1) Y_{\lambda\mu}(2) \qquad (2.10)$$

only terms in $\gamma = 0,2$, $\mu = 0$ being retained.

2.1.4 Results of calculations

2.1.4.1 Inner barrier

The shell correction as a function of deformation is obviously correlated with the local density of single particle levels in the shell model around the highest occupied level (in the absence of pairing correlations), the Fermi energy. High single particle densities give rise to a positive shell correction (less stability) and vice versa. An oscillating shell correction (with the correct phase) superimposed on or close to the liquid drop saddle point gives rise to the double-humped barrier. Variation of the shell-correction amplitude or phase with changing proton and neutron number, together with the variation of the liquid drop potential barrier with changing fissility parameter, gives rise to variation of the double-humped barrier from nucleus to nucleus. The contribution to the shell correction from the pairing correlation effect is opposite in sign, being negative at high single particle densities, but is much smaller in magnitude than the main shell effect.

The phrase "double-humped barrier" expresses the main feature of the potential energy of deformation of the nucleus as a function of elongation of the nucleus towards fission. Early calculations assumed a maximum degree of symmetry in the shape in the course of this elongation. Pashkevich (15) first investigated the potential energy as a function of axial asymmetry along this path and noted that the secondary well in the barrier was stable with respect to this. Later work (16,17,18) has concentrated on investigating the potential energy surface in the plane of elongation and the γ-degree of freedom more carefully, and has established in general that the nucleus has axial asymmetry at the first saddle point (A) but has regained axial symmetry at the secondary well (II). Typical results of Larsson and Leander from ref. (18) are shown in Fig. 6. For ^{236}Th the inner barrier occurs at a value of $\gamma \approx 10^{\circ}$ but the potential energy on the axially symmetric path is only ~0.4 MeV higher than the saddle; whereas for ^{250}Cm the barrier energy drop at an axial asymmetry $\gamma \approx 17^{\circ}$ is a substantial 1.8 MeV. There is a trend for increasing stability of axially asymmetric shape at the inner barrier both with increasing neutron number and increasing mass number as shown in Fig. 7 (from ref. (18)). As far as the actual magnitudes of the barrier heights are concerned, the axially asymmetric values of Fig. 7 tend to be a little lower in general (on average ~0.5 MeV) than experimental data (after making allowance for zero-point β-vibration energy of the ground state). For the Th nuclei they are considerably lower, but there may be special reasons in theory and interpretation of experimental data for this. For each element the trend of the calculated value with neutron number is greatly peaked at N ≈ 150. The experimental data (see Fig.50) show similar trends but with the peaking 2 to 3 neutron units lower.

The agreement of this kind of calculation with data seems to be improved if the quadrupole pairing interaction is included (14), particularly for Th nuclei for which the inner barrier is raised by about 1 MeV. For Pu nuclei quadrupole pairing raises the inner barrier by about 0.5 MeV. It should be noted that in the calculation of Larsson et al (14) the liquid drop energy has been refitted so that the calculation reproduces experimental data on the secondary well.

2.1.4.2 Secondary well

Calculations on the energy of the second minimum relative to that of the first minimum, this time due to Möller and Nix (12) (using still the modified harmonic oscillator shell-model potential), are shown in Fig. 8. In general these energies are in the range 2 to 3 MeV and agree with available experimental data on spontaneously fissioning isomers to this extent. However, interpretation of experimental fission cross-section data on Th isotopes (see for example ref. (37)) indicates that the secondary well is higher than 4 MeV for these light nuclei and so disagrees with the trends of the calculation.

The overall trend of the curves in Fig. 8 (with a minimum about N ≈ 145 and a peak about N ≈ 152) is also given by calculations using the folded Yukawa model (12). However, there are discrepancies in absolute value of up to ~0.5 MeV between the two sets of calculations, changing in sign between Th and Fm.

2.1.4.3 Outer barrier

Early calculations in which the nuclear shape was assumed axially and reflection symmetric indicated that the outer barrier was higher than the inner one in the actinides by some 3 to 4 MeV (see Fig. 2). Experimental data on spontaneous fission isomer half-lives and excitation cross-sections and intermediate structure in fission cross-sections refuted this; indeed analysis of data on plutonium and higher nuclei suggested that experimentally the outer barrier is the lower. The discrepancy was removed at least qualitatively by the calculations of Möller and Nilsson (19,20) demonstrating that reflection asymmetry in the nuclear shape (included in the shell-model

potential as third- and fifth-order Legendre polynomials) gave potential energy minima at the elongations corresponding to the outer barrier. There is no calculational evidence for axial asymmetry also existing at the outer barrier. Indeed, the existence and explanation of strong angular distributions of fission products is held to be evidence against axial asymmetry.

More recent calculated values of the outer barrier height (12) are shown in Fig. 9. The curves for individual elements do not show marked structure or trends (except for the highest elements) but there is a strongly falling tendency with increasing nuclear charge, which is borne out by experimental data on fission isomer excitation yields. These calculations employ a modified harmonic-oscillator shell model potential, and they show discrepancies of up to ~1 MeV (changing sign in going from Th to Fm) with calculations based on a folded Yukawa potential (eq. 2.6).

The calculations based on the folded Yukawa shell-model potential (12) show a new feature in the potential energy curve in the second barrier region; this is a tendency in the low Z, moderate N nuclei for the outer barrier to be further split into two subsidiary peaks with shallow minimum between them (see Fig. 10). If this is a real physical effect it will explain experimental fission data on Th isotopes which demand an interpretation involving a double barrier peak of nearly equal height with a very shallow well between them.

2.1.4.4 Probable accuracy of quantitative calculations on fission barrier parameters

In Table 1 the theoretical results on fission barriers for two specific nuclei are compared. These are both nuclei that are quite central to the nuclear stability line and to the actinide group of elements and therefore ought to provide reasonable tests for theoretical calculation. Some of the differences in the numbers are of course due to very significant differences in the physics assumed, e.g. degree of asymmetry in shape allowed, but even where sets of numbers are comparable, because differences are confined to the choice of shell-model, as in rows 1 and 3 (columns 3 to 5) or rows 1 and 2 (column 6) differences of the order of 1 MeV in the estimated quantity occur. This can probably be taken as a measure of the accuracy of the theory at the present time. This statement is supported by a comparison of the measured nuclear ground state masses of the actinidies and lower nuclei with the values calculated by Möller and Nix (12) using the folded Yukawa shell-model within the Strutinsky theory; the average discrepancy is about zero, but there are systematic trends of the discrepancy curves as a function of neutron number, the trends having a slope of ~0.5 MeV per neutron. The accuracy of the theory is extremely good when set against the nuclear binding energies of well over 1000 MeV, but they are not accurate to supply on their own the relevant barrier parameters for the nuclear cross-sections required by technology. This can be seen at its simplest by considering the effect on calculation of the one-group fission cross-section in the neutron spectrum for an oxide-fuelled fast reactor (mean neutron energy) for a fissionable nucleus.

If the pseudo-threshold energy of the fission cross-section is in the region of 1 MeV, an error of one MeV in the estimate of barrier height could lead to an error grossly over-estimating the one group cross-section in one direction, or giving a negligible value in the other direction (see Fig. 11). The estimates of other cross-sections (such as capture and inelastic scattering) which depend on a knowledge of fission competition will be in error in related amounts.

2.2 Dynamical considerations

2.2.1 General remarks

The potential energy landscapes for deformation of the nucleus discussed in Section 2 provide the essential foundation for discussing the fission process and suggest already many of the most striking phenomena to be observed, but, with such complicated potential energy surfaces, and with the consideration that the nucleus is a microscopic body, strongly influenced by the motion of a single or a few nucleons, it is apparent that the dynamics of fission is still a major problem. The difficulties are compounded in two main ways. Firstly, for large deformations from a spherical shape, a description of the deformation in normal modes, based on a Legendre polynomial expansion of the surface, is not practicable; the choice of suitable deformation parameters is somewhat arbitrary, although based on physical intuition, and as a result the inertial tensor can take a complicated non-diagonal form. Furthermore, the inertial tensor is strongly affected by single particle effects as well as being a measure of "collective motion". Secondly, the effects of "viscosity" in the nuclear motion obviously play an important role. Viscosity is itself a classical concept and its transference to the nuclear case is not yet clearly defined, although there is much current work on this topic (see e.g. ref. (21)). Many of the quantities observable in fission (e.g. cross-sections at low energies, properties of spontaneously fissioning isomers) do not require such an all-embracing concept as viscosity for their explanations; these can be based on extensions of normal quantal ideas. On the other hand, some fission phenomena involve such a large number of degrees of freedom that statistical or thermodynamic treatments seem to be demanded.

2.2.2 Inertial tensor calculations

The dynamical requirement of an expression for the kinetic energy in terms of generalised collective co-ordinates q_i,

$$T = \frac{1}{2} \sum_{i,j} B_{ij}(q)\, \dot{q}_i \dot{q}_j \qquad (2.11)$$

demands the knowledge of the inertial tensor as a function of the collective co-ordinates. This is the essential complement to the potential energy and can be either modelled according to hydrodynamic

concepts [22] or can be computed microscopically from the same shell model level schemes used to construct the shell-correction to the potential energy in the Strutinsky method. The classical liquid drop model is already sufficiently complex that straightforward analytical expressions for the inertia have not been derived except for very small deviations from a sphere, in which case the inertial parameter associated with the lowest normal mode (the quadrupole term in the spherical harmonic expansion of the surface) for irrotational flow is

$$B_\beta = 3MR_o^2/8\pi \qquad (2.12)$$

β being the coefficient for the second spherical harmonic Y_{20} in the expansion of the surface, M the nuclear mass and R_o the nuclear radius. For his studies of the later stages of fission towards the scission point Nix [23] used the Werner-Wheeler numerical method, in which the internal hydrodynamic flow is approximated by the flow of circular layers of fluid perpendicular to the symmetry axis.

Phenomenological expressions for the inertia have also been employed; for example if the fragment separation r is employed as the fission variable the asymptotic inertial parameter at large separations, r, is the reduced mass of the fragments, μ, while at the other extreme of small deformation it tends toward eq. (2.12) for irrotational flow. A typical expression for B_{rr}, due to Randrup, quoted by Szymanski [24], is

$$B_{rr} = \left\{1 + \frac{17}{5} k . \exp\left[-(r - 0.75R_o)/d\right]\right\} \qquad (2.13)$$

where R_o is the spherical nuclear radius, and k and d are parameters that describe deviations from the irrotational value (for irrotational flow $k = 1$, $d = R_o/2.542$).

Microscopic calculations of the inertial tensor are normally based on the cranking model, originally developed by Inglis [25] for calculation of nuclear moments of inertia, in which the independent particle or quasi-particle system is assumed to be driven in a specific form of collective motion by an external force, and the inertial parameter is determined from the generated kinetic energy and the collective velocity. Its application to fission was first developed by Sobiczewski et al [26] and Damgaard et al [27]. The cranking model expression involves virtual excitations from the ground state $|o\rangle$ of the deforming system to excited states $|m\rangle$:

$$B_{ij} = 2\hbar^2 \sum_{m \neq 0} \frac{\langle o|\partial/\partial q_i|m\rangle\langle m|\partial/\partial q_j|o\rangle}{E_m - E_o} \qquad (2.14)$$

For a pure independent particle system this expression, literally evaluated, contains singularities at single-particle level crossings. Within the shell-correction framework of the Strutinsky theory, however, pairing forces are included in the shell-model treatment; the resulting energy gap separating the ground-state from other states removes these singularities and permits the inertial tensor to have a behaviour of reasonable physical magnitude. A simple statistical expression for the dependence of the inertia on the energy gap, Δ, and the density of single particle states, g_{eff}, at the Fermi energy is developed in ref. [27]:

$$B \sim \frac{\hbar^2}{2} \overline{\left|\frac{\partial H}{\partial q}\right|^2} \frac{g_{eff}}{\Delta^2} \qquad (2.15)$$

A typical detailed calculation of the inertia from the cranking model is shown in Fig. 12; this is due to Pauli and Ledergeber [28]. As to be expected from eq. (2.15) it is strongly correlated with the shell-correction to the potential energy of deformation of the nucleus. This strong structure in the inertial parameter already implies that the potential energy alone does not provide a simple guide to the dynamical motion of the system through deformation space.

This is demonstrated by Pauli and Ledergeber's treatment of spontaneous fission half-lives. The half-life is proportional to the Gamov barrier tunnelling factor

$$\tau \sim \frac{1}{\omega} \exp\left[-2S/\hbar\right]$$

$$S = \int_{q_1}^{q_2} dq \sqrt{2B_q |E - V(q)|} \qquad (2.16)$$

The integral S, the action integral, is calculated along a trajectory q through deformation space, defined to give the least value of S. The inertial parameter B_q for this trajectory is determined from the inertial tensor by

$$B_q = \sum_{i,j} B_{ij} \left(\frac{\partial q_i}{\partial q}\right)\left(\frac{\partial q_j}{\partial q}\right) \qquad (2.17)$$

The trajectory calculated from this prescription for symmetric deformations in ^{240}Pu is shown in Fig. 13. It is apparent that the "dynamic" barrier for this trajectory is higher than the static barrier. Calculations of spontaneous fission half-lives of ground states using these calculations of the inertia and the least action principle give remarkably close agreement with data provided that the surface energy constant of the liquid drop model is suitably adjusted (see Fig. 14). This, as shown in the diagram, differs for different elements.

Agreement is poorer (discrepancy up to four orders of magnitude) if it is attempted to use a universal surface energy constant. Half-lives of spontaneously fissioning isomers are shown in Fig. 15.

Pauli and Ledergeber suggest as a hypothesis that the least action trajectory determined for spontaneous fission should also be the path for near-barrier fission. While this would have the attraction of explaining the high intermediate barriers observed for Th isotopes (the dynamic barriers found for these are particularly high compared to the static barriers [29]), it is certainly a very

controversial idea and needs to be properly tested by a calculation of the development of the wave-function over the barrier in a two- or few-dimensional deformation space.

2.3 The role of basic fission theory

It is apparent that greater uncertainty exists in the understanding of the dynamics of strongly deformed nuclei than of the potential energy behaviour; consequent uncertainties will ensue in the attempt to calculate cross-section and related data from fundamentals. The strategy is therefore clear. Basic fission theory alone is not sufficient for the required applications. The role of basic fission theory has to be on the one hand to suggest the modifications and refinements necessary when incorporating the fission reaction into the nuclear reaction theory required for calculating cross-sections. This fully developed reaction theory can be used for analyzing existing experimental data to extract fission barrier parameters. Systematic trends that may exist among these parameters will be suggested by basic fission theory in its second role. Finally, by using the body of new parametrisations (by drawing from it, or by extrapolation or interpolation) within the reaction theory framework, new cross-section data can be calculated. This is the programme the remaining lectures will describe.

3. FISSION REACTION THEORY

The first phase in our strategy for calculating fission data is the development of a useful nuclear reaction theory incorporating or exploiting the features of the double-humped fission barrier. This can be done at a number of levels. At the simplest level the only degree of freedom considered is the deformation of the nucleus as it passes through the barrier; these are the phenomenological barrier transmission models. At the opposite extreme the deformation of the nucleus is considered as only one of very many degrees of freedom and is therefore treated within a statistical framework. At an intermediate level the deformation degree of freedom is treated explicitly and in detail, but the possibility of excitation of other degrees of freedom is treated in a gross way through the intermediary of a complex potential. Finally, exact formal treatments of all degrees of freedom in the reaction process can be developed. In this and the following two lectures these reaction theories are developed.

3.1 One-dimensional barrier-transmission theories

In these theories the single degree of freedom is only treated as such in the barrier region and beyond; for the internal region, the compound nucleus, an expression must still be developed for the width of a compound nucleus state in the absence of the barrier. A simple semi-classical expression for the partial level width was developed long ago by Blatt and Weisskopf [30]. Consider a quantal system with N uniformly spaced energy levels, $E_n = E_o + nD$. The time dependence of the wave-function can be written

$$\psi(t) = \sum_{n=1}^{N} a_n \phi_n e^{-iE_n t/\hbar}$$

$$= e^{-iE_o t/\hbar} \sum_{n=1}^{N} a_n \phi_n e^{-inDt/\hbar} \qquad (3.1)$$

where the ϕ_n contain the spatial dependence of the wave-functions. The period of motion, P, of this system is obviously

$$P = 2\pi\hbar/D \qquad (3.2)$$

i.e. this is the time taken to reconstitute its configuration at the entrance to any given channel, f, and would be its lifetime if there were no barrier of any kind against escaping through that channel. The width in that case would be $\Gamma_f = \hbar/\tau_f = D/2\pi$. However, if the barrier in that channel can only be penetrated or overcome with a probability denoted by the transmission coefficient T_f, the lifetime is $\tau_f = P/T_f$ and the width is

$$\Gamma_f = \frac{\hbar}{\tau_f} = \frac{D}{2\pi} \cdot T_f \qquad (3.3)$$

The barrier transmission coefficient can in principle be calculated very simply. The principle is illustrated for a rectangular barrier in Fig. 16 with a travelling wave from the left incident upon the barrier, with velocity v_o, wave number k_o, giving rise to a reflected wave, and an "interior" wave-function, leading finally to a transmitted wave on the right with velocity v_{oo}, wave number k_{oo}. Matching of the wave-functions shown on Fig. 16 will allow the calculation of the coefficient D of the transmitted wave giving the transmission coefficient (for the flux) $T = |D|^2 v_{oo}/v_o$. For a rectangular barrier the result is a standard one given in quantum mechanic textbooks. Some numerical curves of the energy behaviour for values of barrier parameters that could roughly correspond to actinide fission are given in Fig. 17. The oscillating behaviour of the transmission coefficient found for wave energies greater than the barrier height is characteristic only of the sharp edges found in the rectangular barrier, and is absent for more realistic behaviour of the potential energy.

A very common barrier form for realistic phenomenological analysis is the parabolic barrier. Denote the circular frequency of the barrier oscillator to be obtained by inverting this by ω, then Hill and Wheeler [31] showed, on the same principle as above, matching the combination of parabolic cylinder functions that describe the wave-functions that

$$T = \frac{1}{1 + \exp\left[\frac{2\pi(V_F - E)}{\hbar\omega}\right]} \qquad (3.4)$$

where V_F is the peak of the parabolic barrier. The typical behaviour of this transmission coefficient is also shown in Fig. 17 and is clearly very different, well below the barrier, from that of the rectangular form.

In general, the transmission coefficients for single-humped barriers are quite featureless showing only a strong monotonic rise with energy well below the barrier, flattening off to an asymptotic value of unity above the barrier. For the double-humped barrier, which the Strutinsky theory suggests is appropriate for actinide fission, the transmission through a single barrier is irrelevant in the one-dimensional treatment but plays an important role in more advanced analyses.

For the transmission through a double-humped barrier all the important features are displayed by the results obtained from the JWKB approximation. These are dominated by the virtual states of the potential well that lies between the two peaks; these states give rise to resonances in the transmission function, and the effect of the potential maxima on either side of the well is felt mainly in the widths of these resonances, and in the minima between the resonances. Within the secondary well of the barrier, where the kinetic energy is positive, the quasi-classical approximation to the wave-function is

$$\phi(\eta) \sim \frac{1}{\sqrt{2B[E-V(\eta)]}} \left\{ C_1 \exp\left[\frac{i}{\hbar}\int d\eta \left[2B(E-V)\right]^{1/2}\right] + C_2 \exp\left[-\frac{i}{\hbar}\int d\eta \left[2B(E-V)\right]^{1/2}\right]\right\} \tag{3.5}$$

Between the two turning points η_b and η_c where E=V (see Fig.18), this wave-function reduces to the form of either

$$\frac{C}{\sqrt{2B[E-V(\eta)]}} \sin\left[\frac{1}{\hbar}\int_{\eta_b}^{\eta} d\eta \left[2B(E-V)\right]^{1/2} + \frac{\pi}{4}\right]$$

or

$$\frac{C}{\sqrt{2B[E-V(\eta)]}} \sin\left[\frac{1}{\hbar}\int_{\eta}^{\eta_c} d\eta \left[2B(E-V)\right]^{1/2} + \frac{\pi}{4}\right]$$

if the condition is imposed that the solution of the exact Schrödinger equation vanishes as $\eta \to \pm\infty$. For these two expressions to be identical at η, the sum ϕ of their phases must equal an odd-integral multiple of $\pi/2$:

$$\phi = \frac{1}{\hbar}\int_{\eta_b}^{\eta_c} d\eta \left[2B(E-V)\right]^{1/2} = \left(n+\tfrac{1}{2}\right)\pi \tag{3.6}$$

which is Bohr's quantisation condition. When the barriers on either side of the secondary well are finite, so that the wave-function does not vanish for $\eta \to \pm\infty$, the condition on ϕ for discrete solutions is no longer required for the general solution, but the amplitude of the wave-function between the wells is maximised at an energy close to the above quantisation condition, i.e. resonance occurs. Fröman and Dammert (32) give the general approximate form for the general solution

$$T \approx \frac{\exp\left\{-2\left(K_A+K_B\right)\right\}}{\left(S-1\right)^2 + 4S\cos^2\alpha} \tag{3.7a}$$

$$S = \left[1+\exp\left(-2K_A\right)\right]^{1/2}\left[1+\exp\left(-2K_B\right)\right]^{1/2} \tag{3.7b}$$

with expressions for K_A and K_B in higher order phase integral approximations, which reduce in first-order to the expressions

$$K_A \approx \int_{\eta_a}^{\eta_b} d\eta \left[\frac{2B(E-V)}{\hbar^2}\right]^{1/2}$$

$$K_B \approx \int_{\eta_c}^{\eta_d} d\eta \left[\frac{2B(E-V)}{\hbar^2}\right]^{1/2}$$

while the phase angle α has correction terms on ϕ, resulting in

$$\alpha \approx \int_{\eta_b}^{\eta_c} d\eta \left[\frac{2B(E-V)}{\hbar^2}\right]^{1/2} - \sigma_A - \sigma_B \tag{3.7c}$$

with $$\sigma_A \approx \frac{1}{2}\left[\frac{K_A}{\pi}\ln\left|\frac{K_A}{\pi}\right| - \frac{K_A}{\pi} + \arg\Gamma\left(\frac{1}{2}-\frac{iK_A}{\pi}\right)\right] \tag{3.7d}$$

and a similar formula for σ_B in terms of K_B. The final term in the formula for the correction phases σ has been given approximately by Ford et al (33) as

$$\frac{1}{2}\arg\Gamma\left(\frac{1}{2}-\frac{iK}{\pi}\right) \approx -\frac{iK}{2\pi}\ln\left[\left(\frac{K}{\pi e}\right)^2 + \left(\frac{1}{4\gamma}\right)^2\right]^{1/2}$$

where γ is the Euler constant. Notice that the two factors in the numerator of T are approximately the JWKB approximations for transmission through the two barriers A and B separately.

The resonance condition for equation (3.7) is discussed in some detail by Fröman and Dammert. They note that for a symmetric double barrier the resonance condition is exactly

$$\alpha = \left(n + \frac{1}{2}\right)\pi \qquad (3.8)$$

where n is an integer, and at this energy the transmission is exactly unity. For energies far below the peaks of both barriers this same condition for resonance is approximately true; in fact the quantity $4S\cos^2\alpha$ is the dominant term in the denominator of equation (3.7a) except when cos α is very close to zero and hence in this strongly sub-barrier situation the transmission function has the appearance of high, very narrow peaks on a low but exponentially increasing base. In the case of a symmetric double barrier these peaks rise to a transmission value of unity. Equation (3.7a) can be written approximately

$$T \approx \frac{\cosh^{-2}(K_A - K_B)}{1 + \left[\dfrac{\cos\alpha}{\frac{1}{4}\exp(-2K_A) + \frac{1}{4}\exp(-2K_B)}\right]^2} \qquad (3.9)$$

giving $T_{max} \approx \cosh^{-2}(K_A - K_B)$ at resonance. Close to the resonance condition cos α can be written $\alpha - (n + 1/2)\pi$ thus demonstrating that the half-width of the resonance is $\Delta\alpha \approx 1/2(\exp(-2K_A) + \exp(-2K_B))$ which, in terms of energy, is

$$T \approx \hbar\left[\exp(-2K_A) + \exp(-2K_B)\right] \Big/ \int_{\eta_b}^{\eta_c} d\eta \left[\frac{(E-V)}{2B}\right]^{-\frac{1}{2}} \qquad (3.10)$$

The denominator in this expression is the reciprocal of the classical oscillation frequency between the two barriers. The resonance width therefore is simply interpreted through the Heisenberg uncertainty principle, i.e. it is Planck's constant (divided by 2π) multiplied into the escape probability (oscillation frequency times probability of tunnelling the barriers) from the intermediate well.

Other points to be noted about the JWKB formula are, firstly, that, well below the peaks, replacement of α by φ gives rise to very small error in α, but this nevertheless implies a large shift in the resonance in comparison with its width. Secondly, between resonances, the transmission has minima close to the value

$$T \approx \frac{1}{4}\exp\left\{-2\left(K_A + K_B\right)\right\} \approx \frac{T_A T_B}{4} \qquad (3.11)$$

3.2 Barrier transmission with absorption

The one-dimensional treatment of the fission process can be extended to take some account of other degrees of freedom by treating excitation of the latter as a simple absorption out of the fission mode. This method is very familiar in the treatment of nucleon scattering by complex nuclei, being just the optical model of nuclear reactions. In the application of the optical model to the fission process it is necessary to include the well(s) in addition to the barrier in the potential energy function for the deformation mode.

In the original application of this method to fission through a single-peaked barrier [34] there is no difficulty in principle in obtaining the transmission function, and hence the fission strength function. An imaginary component is introduced into the potential well representing the internal compound nucleus region (see Fig. 19). This can be either a constant component between certain adopted limits of deformation, or have some functional form attenuating to zero in the region of the potential barrier. An incident wave of form $(\exp(-ik_0\eta))$ in the deformation mode is now considered to fall on this potential, and the result of the interaction gives an outgoing wave with amplitude S_{ff}; beyond a deformation value η_0 expressing the range of the potential barrier beyond the internal region, the wave function has the form

$$\phi = \exp(-ik_0\eta) + S_{ff}\exp(ik_0\eta), \qquad (\eta > \eta_0) \qquad (3.12)$$

The amplitude S_{ff} is calculated by solving the Schrödinger equation (usually by numerical integration), the governing boundary condition to give the correct solution being that the wave function is real and regular at some value of the deformation η_{min} sufficiently far on the low deformation side of the potential well. A resulting value of S_{ff} with modulus unity implies pure scattering of the fission wave. The difference between unity and $|S_{ff}|^2$ gives the absorption into the internal region i.e. compound nucleus formation; the cross-section for compound nucleus formation from an "inverse-fission" channel is proportional to $1 - |S_{ff}|^2$, and this expression is normally defined as the transmission coefficient T_f corresponding exactly to the simple barrier transmission already considered

$$T_f = 1 - |S_{ff}|^2 \qquad (3.13)$$

Typical calculations of this transmission coefficient are shown in Fig. 20. It is seen that resonance effects can be found, but these are due to small damping of vibrations in the deep potential well. Such small imaginary components are not normally expected at the excitation energies considered here.

Such a treatment has also been applied to the double-humped potential barrier [35]. If the imaginary component of the potential is confined to the primary well, transmission coefficients that display the vibrational resonance peaks described above can occur. These are undamped vibrational resonances (zero damping in the secondary well), and spreading the imaginary potential across both the primary and secondary well is not a strictly correct way of treating the damping in the secondary well.

The difficulty in this model is that absorption into the secondary well has to be considered separately from that in the primary well; use of an imaginary potential in both wells simply

lumps together the absorption in the two wells. The picture here is that an incident inverse-fission wave penetrates the secondary well with attenuation, and this attenuated direct component is absorbed in the primary well, while the component absorbed in the secondary well can be re-emitted into the fission channel, or suffer a transition irrevocably into some other degree of freedom, or be emitted into the primary well. The total flux reaching, and being absorbed, into the primary well is the quantity of interest here. Bondorf (35) and Back et al (36) have modified the model to obtain the transmission coefficient correctly by making the simplifying assumption that all the flux reaching the primary well is absorbed completely. The wave function at some deformation η_1 close to the entry (at barrier A) into the primary well therefore has no returning wave and is given by

$$\phi = a \exp(-ik_1\eta), \qquad (\eta \leq \eta_1) \tag{3.14}$$

(or, more exactly, to take the attenuation distance $1/K$ in the primary well into account, $\phi = a \exp(-K(\eta_1 - \eta) - ik_1\eta)$; the factor $\exp(-K(\eta_1 - \eta))$ is required if the imaginary potential starts at η_1 with a non-zero value). The flux that is absorbed directly into the primary well is thus $k_1|a|^2/k_\infty$, while that absorbed in the secondary well is $1 - |S_{ff}|^2$. Of the secondary well absorption a fraction

$$P_A = \frac{T_A}{T_A + T_B + T_\gamma} \tag{3.15}$$

is emitted into the primary well, T_A and T_B being transmission coefficients from the secondary well across barriers A and B, and T_γ the transmission probability for de-exciting radiation across compound levels (class-II states) associated with the secondary well deformation. Thus

$$T_f = \frac{k_1|a|^2}{k_\infty} + P_A\left(1 - |S_{ff}|^2\right) \tag{3.16}$$

Of the two terms on the right hand side of this equation the first can be interpreted as a "direct" one, being the fraction of the wave that is transmitted right across the secondary well without absorption. The second term corresponds to re-emission after absorption into the compound motion of the secondary well and hence is expected to have a microscopic structure corresponding to the class-II compound states associated with this motion. The detailed structure of the first term is expected to be just the much broader one of the vibrational resonances in the secondary well.

An example of the transmission coefficient of equation (3.16) is shown in Fig. 20 in comparison with the result for zero damping in the secondary well.

3.3 Statistical model

When absorption out of the fission mode is very strong, a limit has been reached that is just the opposite of the simple undamped barrier transmission models of the double-humped barrier. This limit can be treated by assuming statistical equilibrium among all the degrees of freedom of the nucleus. Such a model is therefore appropriate to moderately high excitation energies ('hot' nuclei), in distinction to the barrier transmission model which can only be expected to describe low excitations in the secondary well.

In a hot nucleus with very many degrees of freedom only a relatively small amount of excitation energy will be concentrated on motion in the deformation mode; this amount will be of the order of the nuclear temperature θ. If this temperature is much less than the barrier between the wells in the potential energy of deformation the nuclear system will survive for a relatively long time in one or other equilibrium shape before changing shape, or decaying by particle emission, radiation or break-up by fission. Thus, in first approximation, two sets of states, associated with each equilibrium shape, and denoted by class I for the first well and class-II for the second, exist in the nucleus. The probability of decay of these states can be represented by transmission coefficients that take account of barriers (deformation, centrifugal or coulomb) as well as the internal nature of the states in the energy region under consideration. These transmission coefficients can be defined through the reciprocity theorem in terms of the probability of the formation of such states of the compound nucleus in the inverse process to the given decay mode. Thus, for a formation process α, the maximum possible average cross-section is $\pi\lambda\!\!\!^{-2}_\alpha g_J$ where $\lambda\!\!\!^{-}_\alpha$ is the de Broglie wavelength (divided by 2π) of the relative motion of projectile and target, and g_J is the statistical weighting factor for formation of the compound nucleus with total angular momentum J. The actual cross-section for compound nucleus formation is denoted by

$$\sigma_{\alpha(CN)} = \pi\lambda\!\!\!^{-2}_\alpha g_J T_\alpha \tag{3.17}$$

where T_α is the transmission coefficient for this mode of formation. When the ratio of partial width to level spacing Γ_α/D is small, $T_\alpha = 2\pi\Gamma_\alpha/D$, and it has been established fairly conclusively (37) that, in general,

$$T_\alpha = 1 - \exp\left[-2\pi\Gamma_\alpha/D\right] \tag{3.18}$$

Transmission coefficients for making transitions from shape I to shape II, denoted by $T_{I(A)}$, and vice versa, denoted by $T_{II(A)}$, can be defined in analogy with the decay coefficients.

From the transmission coefficients the probability of decay of a class-I state by process α is

$$P_{I(\alpha)} = \frac{T_{I(\alpha)}}{\sum_\beta T_{I(B)} + T_{I(A)}} \tag{3.19}$$

and the probability of a transition from a class-I to a class-II state is

$$P_{I\to II} = \frac{T_{I(A)}}{\sum_{\beta} T_{I(\beta)} + T_{I(A)}} \qquad (3.20)$$

Similarly, probabilities for decay or shape transition of a class-II state are

$$P_{II(\alpha')} = \frac{T_{II(\alpha')}}{\sum_{\beta'} T_{II(\beta')} + T_{II(A)}} \qquad (3.21)$$

$$P_{II\to I} = \frac{T_{II(A)}}{\sum_{\beta'} T_{II(\beta')} + T_{I(A)}} \qquad (3.22)$$

Given these probabilities the overall decay of the nucleus can be calculated. Let us assume that the nucleus is initially populated entirely in class-I states. The initial stage of decay consists of a fraction $P_{I(d)} = \Sigma_\beta P_{I(\beta)}$ decaying to all residual systems allowed to class-I decay (these will principally be, according to the Franck-Condon principle, class-I states of lower excitation in the same nucleus, reached by gamma transitions, and residual nuclei of class-I shape reached by neutron emission) and a fraction $P_{I\to II}$ changing to shape II. The second stage of decay therefore consists of a fraction $P_{I\to II}\cdot P_{II(d')}$ (where $P_{II(d')} = \Sigma_{\beta'} P_{II(\beta')}$) decaying by processes allowed by the Franck-Condon principle for class-II state decay (this is either fission, over barrier B, or formation of residual nuclei in shape II) and a fraction $P_{I\to II}\cdot P_{II\to I}$ changing back to shape I. The third stage consists of this new fraction $P_{I\to II}\cdot P_{II\to I}$ dividing as in the first stage, and if the process is followed through and the infinite series thus generated are summed we have for the final decay fractions appropriate to shapes I and II respectively

$$F_{(d_I)} = \sum_{n=0}^{\infty} \left(P_{I\to II}\cdot P_{II\to I}\right)^n P_{I(d_I)} = \frac{P_{I(d_I)}}{1 - P_{I\to II}\,P_{II\to I}}$$

$$= \frac{T_{I(d)}\left(T_{II(A)} + T_{II(d')}\right)}{\left(T_{I(d)} + T_{I(A)}\right)\left(T_{II(A)} + T_{II(d')}\right) - T_{I(A)}\,T_{II(A)}} \qquad (3.23)$$

$$F_{(d_{II})} = \sum_{n=0}^{\infty} \left(P_{I\to II}\cdot P_{II\to I}\right)^n P_{I\to II}\,P_{II(d')} = \frac{P_{I\to II}\,P_{II(d')}}{1 - P_{I\to II}\,P_{II\to I}}$$

$$= \frac{T_{I(A)}\,T_{II(d')}}{\left(T_{I(d)} + T_{I(A)}\right)\left(T_{II(d')} + T_{II(A)}\right) - T_{I(A)}\,T_{II(A)}} \qquad (3.24)$$

The fractions for individual decay processes are contained within these expressions. Thus, the fraction of decay by prompt fission, for example, is given by

$$F_{(f)} = \frac{T_{I(A)}\,T_{II(B)}}{\left(T_{I(d)} + T_{I(A)}\right)\left(T_{II(d')} + T_{II(A)}\right) - T_{I(A)}\,T_{II(A)}} \qquad (3.25)$$

For decay of the compound nucleus excited initially in a class-I shape the ratio of decay either by fission or to residual nuclei of shape II, relative to decay to shape I states is therefore

$$\frac{F_{(d_{II})}}{F_{(d_I)}} = \frac{T_{I(A)}\,T_{II(d')}}{\left(T_{II(A)} + T_{II(d')}\right)T_{I(d)}} \qquad (3.26)$$

This expression is remarkable for the factor $T_{I(A)}/(T_{II(A)} + T_{II(d')})$ by which the ratio is reduced below that expected for completely mixed compound nucleus motion, $T_{II(d')}/T_{I(d)}$. For the kind of fission barrier exhibited by the actinide nuclei fission decay ($T_{II(B)}$) completely dominates particle or radiative decay. If the barrier A is much lower than B then it is expected that $T_{II(A)} \gg T_{II(B)}$, and since, according to the theory of reaction rates over a single barrier (Wigner [78]) $T_{I(A)} = T_{II(A)}$, equation (3.26) reduces consequently to the complete mixing expression. If, on the other hand, B is much lower than A, the factor $T_{I(A)}/(T_{II(A)} + T_{II(B)})$ is much less than unity; and this implies a partial decoupling persisting between the class-I and class-II states.

3.4 Formal reaction theory

To achieve sophisticated analysis and calculation the role of other degrees of freedom must be considered in more detail than the extreme phenomenological picture so far considered will allow. A formal reaction theory treats other degrees of freedom explicitly from the start. The choice of formal theory for these lectures is R-matrix theory.

The basic physical idea of R-matrix theory is the isolation of the region in configuration space where all the specifically nuclear forces in a nuclear reaction are operating; this "internal region" incorporates the compound system formed from the merging of the projectile in the reaction with the target. The internal region is formally defined by introducing a channel radius, set outside (usually fairly closely outside) the range of nuclear forces, for

each channel defining the separation of the compound system into two residual nuclei with specific excitation and angular momentum properties. The wave-functions in the channels can be specified closely, and hence the cross-sections obtained once the values and derivatives at the channel radius are given. These are given in principle by the solution of the Schrödinger equation for the compound system in the internal region.

In principle, fission is formally incorporated in R-matrix theory, in the sense that every pair of fission products (in a specific state of excitation and angular momentum) constitutes a channel. In practice it has been known for more than two decades following the intuitive analysis by A. Bohr (38) that fission cross-sections are governed to a large extent by conditions at the saddle point where the nucleus can be in one or relatively few states of intrinsic excitation while slowly elongating. It is this intuitive idea of a fission or deformation channel that now has to be incorporated into the formal R-matrix theory.

To do this the coordinates describing the degrees of freedom of the system have to be recast for that part of configuration space that encompasses the description of fission. Specifically a deformation coordinate, describing increasing elongation and ultimately separation into two large fragments, must be defined, and the remaining coordinates modified to be orthogonal with this. Different deformation channels are defined by the state of excitation for these remaining coordinates, and this corresponds with A. Bohr's physical idea of a fission channel. For these channels a channel deformation parameter is defined, and for this to be physically significant it must be set close to the saddle point in the fission barrier.

3.4.1 Separation of the nuclear Hamiltonian

This procedure will now be set down more explicitly. The deformation coordinate (describing increasing elongation of the system) is denoted by η. This coordinate can be defined in a statistical manner in terms of the individual nucleon coordinates. After extraction of the deformation coordinate the remaining ('intrinsic') degrees of freedom are denoted collectively by ξ.

It is now assumed that the kinetic energy operator of the nuclear Hamiltonian can be separated into components referring explicitly to the deformation parameter η and the intrinsic coordinate ξ respectively. While it is possible to choose a deformation parameter η that allows its kinetic energy operator to be independent of the intrinsic degrees of freedom, it is not in general possible at the same time to free the remaining components of the kinetic energy from all dependence on deformation. Thus

$$T = T_\eta + T_\xi(\eta) \tag{3.27}$$

Likewise the potential energy $V(\eta,\xi)$ will not, in general, be a separable function of η and ξ, and it is necessary to find a prescription that will give an approximation to the overall dependence of the potential energy on η. The prescription that we choose is in the spirit of Strutinsky's theory of the deformation energy, and consists of representing the potential energy for the deformation by the minimum total intrinsic energy surface. More precisely, of the eigenvalues $\varepsilon_\mu(\eta)$ of the operator

$$H_\xi(\eta) = T_\xi(\eta) + V(\eta,\xi) \tag{3.28}$$

for a fixed value of η, the lowest eigenvalue $\varepsilon_0(\eta)$ is taken as the deformation potential energy $\mathcal{V}(\eta)$. An intrinsic Hamiltonian term H_{int} can now be defined for some chosen value of deformation η_0, and also a 'coupling' term H_c depending on both deformation and intrinsic variables. Thus

$$H = H_\eta + H_{int}(\xi,\eta_0) + H_c(\eta,\xi;\eta_0) \tag{3.29}$$

where

$$H_\eta = T_\eta + \mathcal{V}(\eta) \tag{3.30a}$$

$$H_{int}(\xi,\eta_0) = T_\xi(\eta_0) - \varepsilon_0(\eta_0) + V(\eta_0,\xi) \tag{3.30b}$$

$$H_c = T_\xi(\eta) - \varepsilon_0(\eta) + V(\eta,\xi) - H_{int}(\xi,\eta_0) \tag{3.30c}$$

It is useful to be able to generalize the intrinsic Hamiltonian to any other value of deformation η. Therefore, we shall denote the eigenvalues and eigenfunctions of $H_{int}(\eta)$ by $\varepsilon_\mu(\eta)$ and $\chi_\mu(\eta)$, and from the definition of H_{int} the eigenvalues $\varepsilon_\mu(\eta)$ are just $\varepsilon_\mu(\eta) - \varepsilon_0(\eta)$, the intrinsic excitation energies with respect to 'ground' at the fixed deformation η. The eigenfunctions and eigenvalues of H_η are denoted by $\Phi_\nu(\eta)$ and ϵ_ν.

In phenomenological models of the liquid drop type, the usual procedure in setting up the Hamiltonian is to write the kinetic and potential energy terms for irrotational flow in terms of the shape parameters (denoted here by α_λ). The quantal operator for the kinetic energy term is then written according to the Schrödinger prescription:

$$T = -\frac{\hbar^2}{2}\sum_{\lambda,\mu}\frac{1}{\sqrt{B}}\frac{\partial}{\partial\alpha_\lambda}\left(\sqrt{B}\,B^{\lambda\mu}\frac{\partial}{\partial\alpha_\mu}\right) \tag{3.32}$$

where $B_{\lambda\mu}$ is the relevant element of the covariant inertial tensor, B is the determinant of this tensor, and $B^{\lambda\mu}$ is the element of the related contravariant tensor:

$$\sum_\nu B^{\lambda\nu}B_{\nu\mu} = \delta^\lambda_\mu \tag{3.33}$$

Discussions of the ambiguities of this procedure, particularly when the shape variables constitute only a part of the total degrees of freedom of the system, have been given by Jensen and Koffe [39], Dietrich [40], Hofmann [41] and Nörenberg [42]. Briefly, it turns out that the ambiguity in the kinetic energy term for any single variable is equivalent to a curvature term to be added to the potential energy.

As an example of the phenomenological procedure we can take the simple quadrupole deformation parameter β from the expansion of the nuclear surface in Legendre polynomials. For small values of β the kinetic energy operator is

$$T_\beta = -\frac{\hbar^2}{2B_\beta}\frac{\partial^2}{\partial\beta^2} \tag{3.34}$$

The inertial parameter B_β for the irrotational liquid drop is

$$B_\beta = 3AmR_o^2/8\pi \tag{3.35}$$

where m is the nucleon mass, so that Am is the liquid drop mass, and R_o is the radius of the drop. If the potential energy has the quadratic form

$$V_\beta = \tfrac{1}{2}C_\beta\beta^2 \tag{3.36}$$

with stiffness parameter C_β, as expected in the liquid drop model, the solutions of the Schrödinger equation in the β-variable are the well-known Hermite functions with eigenvalues

$$E_n = \left(n+\tfrac{1}{2}\right)\hbar\omega_\beta = \left(n+\tfrac{1}{2}\right)\hbar\left(C_\beta/B_\beta\right)^{\frac{1}{2}} \tag{3.37}$$

The form of the kinetic energy operator for statistical deformation parameters can be derived without ambiguity from the Schrödinger form for the Cartesian coordinates of a system of particles (here assumed to have equal mass, m):

$$T = -\frac{\hbar^2}{2m}\sum_i\left(\frac{\partial^2}{\partial x_i^2}+\frac{\partial^2}{\partial y_i^2}+\frac{\partial^2}{\partial z_i^2}\right) \tag{3.38}$$

The general equation for transforming the second derivative in a particular coordinate, say x_i, into the second derivatives of a new set of coordinates ξ_j is

$$\frac{\partial^2\psi}{\partial x_i^2} = \sum_j\left\{\frac{\partial^2\psi}{\partial\xi_j^2}\left(\frac{\partial\xi_j}{\partial x_i}\right)^2+\frac{\partial\psi}{\partial\xi_j}\frac{\partial^2\xi_j}{\partial x_i^2}\right\}+\sum_{j\neq k}\frac{\partial^2\psi}{\partial\xi_j\partial\xi_k}\left(\frac{\partial\xi_j}{\partial x_i}\right)\left(\frac{\partial\xi_k}{\partial x_i}\right) \tag{3.39}$$

Hence the generalised Laplacian term of equation (3.38) is

$$\sum_i\left(\frac{\partial^2\psi}{\partial x_i^2}+\frac{\partial^2\psi}{\partial y_i^2}+\frac{\partial^2\psi}{\partial z_i^2}\right) = \sum_j\left\{\frac{\partial^2\psi}{\partial\xi_j^2}\sum_i\left[\left(\frac{\partial\xi_j}{\partial x_i}\right)^2+\left(\frac{\partial\xi_j}{\partial y_i}\right)^2+\left(\frac{\partial\xi_j}{\partial z_i}\right)^2\right]+\frac{\partial\psi}{\partial\xi_j}\sum_i\left(\frac{\partial^2\xi_j}{\partial x_i^2}+\frac{\partial^2\xi_j}{\partial y_i^2}+\frac{\partial^2\xi_j}{\partial z_i^2}\right)\right\}$$
$$+\sum_{j\neq k}\frac{\partial^2\psi}{\partial\xi_j\partial\xi_k}\sum_i\left(\frac{\partial\xi_j}{\partial x_i}\frac{\partial\xi_k}{\partial x_i}+\frac{\partial\xi_j}{\partial y_i}\frac{\partial\xi_k}{\partial y_i}+\frac{\partial\xi_j}{\partial z_i}\frac{\partial\xi_k}{\partial z_i}\right) \tag{3.40}$$

The condition of orthogonality for the new coordinates ξ_j is

$$\sum_i\left(\frac{\partial\xi_j}{\partial x_i}\frac{\partial\xi_k}{\partial x_i}+\frac{\partial\xi_j}{\partial y_i}\frac{\partial\xi_k}{\partial y_i}+\frac{\partial\xi_j}{\partial z_i}\frac{\partial\xi_k}{\partial z_i}\right) = \delta_{jk}$$

Hence the summation over j = k on the right-hand side of equation (3.40) vanishes for an orthogonal coordinate system.
Equation (3.40) can be formally expressed in terms of the scale factors h_j,

$$h_j^2 = \left[\sum_i\left\{\left(\frac{\partial\xi_j}{\partial x_i}\right)^2+\left(\frac{\partial\xi_j}{\partial y_i}\right)^2+\left(\frac{\partial\xi_j}{\partial z_i}\right)^2\right\}\right]^{-1} \tag{3.41}$$

or

$$\sum_i\left(\frac{\partial^2\psi}{\partial x_i^2}+\frac{\partial^2\psi}{\partial y_i^2}+\frac{\partial^2\psi}{\partial z_i^2}\right) = \frac{1}{\Pi_k h_k}\sum_j\frac{\partial}{\partial\xi_j}\left[\frac{\Pi_k h_k}{h_j^2}\frac{\partial\psi}{\partial\xi_j}\right] \tag{3.42}$$

for an orthogonal system.

As an example of the application of equation (3.42) if the deformation parameter η of a new coordinate set is taken to be the mass quadrupole moment Q, the kinetic energy operator is

$$T_Q = -\frac{\hbar^2(4Q+8A\overline{r^2})}{2m}\frac{\partial^2}{\partial Q^2} \tag{3.43}$$

where $\overline{r^2}$ is the mean square of the radial position of the nucleon (with respect to the centre of mass). The inertial parameter appropriate to the quadrupole moment appears in this operator as

$$B_Q = \frac{m}{4Q+8A\overline{r^2}} \tag{3.44}$$

For asymptotically large separation, ℓ, of the two fission products the quadrupole moment is

$$Q = \frac{2A_1A_2}{A_1 + A_2}\ell^2 = \frac{2M}{m}\ell^2 \qquad (3.45)$$

where A_1 and A_2 are the mass numbers of the products and M is their reduced mass. In this asymptotic situation the kinetic energy operator of equation (3.43) becomes

$$T_Q = -\frac{\hbar^2}{2M}\frac{\partial^2}{\partial\ell^2} \qquad (3.46)$$

For near-spherical spheroidal deformation on the other hand, the quadrupole moment can be related to the spheroidal deformation parameter β

$$Q \approx \frac{3AR_o^2}{\sqrt{5\pi}}\beta \qquad (3.47)$$

and the inertial parameter $B_Q \sim (5m/24AR_o^2)\{1 - (5/4\pi)^{\frac{1}{2}}\beta\}$. The kinetic energy operator transformed into its form for β in this limit is just

$$T_\beta = -\frac{\hbar^2}{2B_\beta}\frac{\partial^2}{\partial\beta^2} \qquad (3.48)$$

with the inertial parameter of equation (3.35) appropriate to irrotational flow.

The most easily handled of statistical deformation parameters is the mean square radius parameter

$$\mathcal{R} = \sqrt{\sum_i \left(x_i^2 + y_i^2 + z_i^2\right)} \qquad (3.49)$$

which has a kinetic energy term

$$T_{\mathcal{R}} = -\frac{\hbar^2}{2m\mathcal{R}^{3A-1}}\frac{\partial}{\partial\mathcal{R}}\left(\mathcal{R}^{3A-1}\frac{\partial}{\partial\mathcal{R}}\right) \qquad (3.50)$$

3.4.2 Summary of R-matrix theory

The above definitions for the deformation channel, the deformation variable, the intrinsic degrees of freedom (giving rise to labelling of deformation channels) and so on, allow R-matrix theory to incorporate the physically interesting aspects of fission. R-matrix theory [44,45] has been fully described in earlier courses in the present series (see the course by Moore and by Fröhner). Here, just sufficient summary is included to provide a framework for the extra notation required for fission.

The basic tool for constructing R-matrix theory is the Green's theorem relationship

$$(E_2 - E_1)\int_\tau d\tau\,\Psi_2^*\Psi_1 = \sum_c\left(V_{2c}^*D_{1c} - V_{1c}D_{2c}^*\right) \qquad (3.51)$$

where τ is the internal region, Ψ_1, Ψ_2 (eigenvalues E_1, E_2) are solutions of the Schrödinger equation for the nuclear Hamiltonian in the internal region, V_{1c}, V_{2c}, D_{1c}, D_{2c} are value and derivative quantities of the wave-functions Ψ_1, Ψ_2 at the channel radius (delimiting the internal region) of every channel c. For the part of configuration space which is relevant to fission the appropriate channels c are now deformation channels with entrances to the internal region set at deformation η_o and labelled by the state of intrinsic excitation χ_μ, at deformation η_o.

The discrete R-matrix eigenstates X_λ (eigenvalues E_λ) are defined by imposing boundary conditions (normally real and energy-independent) at every channel entrance. The value and derivative quantities of the eigenstates X_λ are denoted by $\gamma_{\lambda(c)}$, $\delta_{\lambda(c)}$ respectively, for each channel c, and the imposed boundary condition is written

$$\frac{\delta_{\lambda(c)}}{\gamma_{\lambda(c)}} = \mathcal{B}_c \qquad (3.52)$$

The central R-matrix relationship is obtained by expanding a general solution of the Schrödinger equation in the internal region Ψ for energy E, without imposition of special boundary conditions, as a superposition of the R-matrix states

$$\Psi(E) = \sum_\lambda A_\lambda X_\lambda \qquad (3.53)$$

The expansion coefficients are obtained from Green's theorem. Substitution leads to a relationship between the value and derivative quantities of Ψ:

$$V_{c'} = \sum_c R_{c'c}\left(D_c - \mathcal{B}_c V_c\right) \qquad (3.54)$$

with $R_{c'c}$, the element of the R-matrix, given by

$$R_{c'c} = \sum_\lambda \frac{\gamma_{\lambda(c')}\gamma_{\lambda(c)}}{E_\lambda - E} \qquad (3.55)$$

The external wave-functions in the channels can be written as superposition of waves that have the character of incoming flux I_c and outgoing flux O_c. The form of these wave functions depend on the kinetic energy available in the channel and on the potential energy behaviour (including Coulomb and centrifugal barriers). The logarithmic derivatives of the incoming and outgoing wave-functions at the channel entrances a_c are required for matching to the internal wave-function, Ψ, and the logarithmic derivatives of the outgoing waves appear explicitly in final expressions for the collision matrix and cross-

sections; it is denoted by

$$L_c \equiv S_c + iP_c = \left[\frac{k_c r_c}{O_c}\frac{\partial O_c}{\partial(k_c r_c)}\right]_{r_c = a_c} \qquad (3.56)$$

(r_c is the channel coordinate defining separation of the two nuclei in the channel for particle channels, but is to be replaced by the deformation variable η_μ for deformation channels). The quantity k_c is the wave-number corresponding to the kinetic energy in the channel.

The complete wave-function in the channel is conveniently written in terms of quantities ϑ_c, θ_c, which are products of the wave-functions of internal excitation (including angular momentum relationships) of the products in the channel, and the functions I_c, O_c respectively. So, in the external region, the complete wave-function is

$$\Psi_{ext} = \sum_{c,c'}\left(\delta_{c'c}\vartheta_c - U_{c'c}\theta_{c'}\right)y_c \qquad (3.57)$$

The scattered wave into any channel c' is

$$\Psi_{scat,\,in\,c'} = \sum_c y_c\left(\delta_{c'c} - U_{c'c}\right)\theta_{c'} \qquad (3.58)$$

The quantities $U_{c'c}$ are the elements of the collision matrix and govern the magnitude of the cross-section for the reaction c in, c' out, the result being obtained after substituting for y_c from the expansion for a plane wave:

$$\sigma_{cc'} = \frac{\pi}{k_c^2} g_J \left|\delta_{c'c} - U_{c'c}\right|^2 \qquad (3.59)$$

This is over the full solid angle. The quantity g_J is the factor containing all the spin variables relating to the reaction. The quantity $\delta_{c'c} - U_{c'c}$ is often denoted simply by $-S_{c'c}$ and is referred to as the element of the scattering or S-matrix.

The collision matrix is obtained in terms of the R-matrix $\underset{\sim}{R}$ by matching the internal and external wave-functions at all channel entrances to give

$$\underset{\sim}{U} = \underset{\sim}{\Omega}\,\underset{\sim}{P}^{\frac{1}{2}}\left\{\underset{\sim}{1} - \underset{\sim}{R}\left(\underset{\sim}{L} - \underset{\sim}{B}\right)\right\}^{-1}\left\{\underset{\sim}{1} - \underset{\sim}{R}\left(\underset{\sim}{L}^{*} - \underset{\sim}{B}\right)\right\}\underset{\sim}{P}^{-\frac{1}{2}}\,\underset{\sim}{\Omega} \qquad (3.60)$$

in matrix notation. The matrices $\underset{\sim}{\Omega}$, $\underset{\sim}{P}$, $\underset{\sim}{L}$ and $\underset{\sim}{B}$ are diagonal matrices with elements, respectively, representing hard-sphere phase shift, penetration factor, outgoing wave logarithmic derivative and boundary condition for the channels.

In these expressions the channels c, as stated above, contain not only the conventional particle channel, but also the newly defined deformation channels μ. Although great advantages are to be gained in physics concepts in placing the entrances to these channels close to the fission barrier saddle point, there are also some minor calculational disadvantages. Definition of the outgoing wave-functions and hence of the shift and penetration factors becomes a little awkward because (i) the potential energy in the channel is not precisely known, and (ii) the deformation channels contain an interaction zone of nuclear forces before the scission point is reached.

3.4.3 Approximate forms and other representations

This expression for the collision matrix, and hence the cross-sections, is normally too intractable for general use. Approximations must be sought.

The simplest approximation is the retention of only one level in the R-matrix sum. This leads to the single-level Breit-Wigner formula

$$\sigma_{cc'} = \frac{\pi}{k_c^2} g_J \frac{\Gamma_{\lambda(c)}\Gamma_{\lambda(c')}}{\left(E_\lambda - \Delta_\lambda - E\right)^2 + \frac{1}{4}\Gamma_\lambda^2} \qquad (3.61)$$

where $\Gamma_{\lambda(c)}$, $\Gamma_{\lambda(c')}$ are the partial widths for channels c and c', Γ_λ is the total width and Δ_λ the level shift. These are defined in terms of the R-matrix reduced widths $\gamma_{\lambda(c)}^2$ and the penetration and shift factors by

$$\Gamma_{\lambda(c)} = 2P_c\gamma_{\lambda(c)}^2 \qquad (3.62a)$$

$$\Gamma_\lambda = \sum_{c''}\Gamma_{\lambda(c'')} \qquad (3.62b)$$

$$\Delta_\lambda = \sum_{c''}\left(S_{c''} - B_{c''}\right)\gamma_{\lambda(c'')}^2 \qquad (3.62c)$$

The reduced width amplitudes $\gamma_{\lambda(c)}$ are just the value quantities at the channel entrances of the R-matrix eigenstate X_λ.

More levels can be handled practically by manipulation of the form of the collision matrix into one involving the inversion of a level matrix rather than a channel matrix. The collision matrix element becomes

$$U_{c'c} = \Omega_{c'}\Omega_c\left\{\delta_{c'c} + 2iP_{c'}^{\frac{1}{2}}\sum_{\lambda\lambda'}\gamma_{\lambda(c')}\gamma_{\lambda'(c)}A_{\lambda\lambda'}P_c^{\frac{1}{2}}\right\} \qquad (3.63)$$

$$\underset{\sim}{A} = \underset{\sim}{C}^{-1}$$

and $\underset{\sim}{C}$ has elements

$$C_{\lambda\lambda'} = (E_\lambda - E)\delta_{\lambda\lambda'} - \Delta_{\lambda\lambda'} - \tfrac{1}{2}i\Gamma_{\lambda\lambda'} \qquad (3.64)$$

The generalised level shift and width quantities here are defined by

$$\Delta_{\lambda\lambda'} = \sum_{c''} (S_{c''} - B_{c''})\gamma_{\lambda(c'')}\gamma_{\lambda'(c'')} \qquad (3.65a)$$

$$\Gamma_{\lambda\lambda'} = 2\sum_{c''} P_{c''}\gamma_{\lambda(c'')}\gamma_{\lambda'(c'')} \qquad (3.65b)$$

Alternatively the number of channels explicitly included in the calculation may be reduced. In this, the reduced R-matrix formulation, all the closed channels and most of those only slightly open (expressed by their partial widths being very much smaller than the spacing between levels) are eliminated in explicit reference in the expression for the collision matrix. The collision sub-matrix U_{rr} referring only to the explicitly retained channel has the same form as the full matrix

$$\underset{\sim}{U}_{rr} = \underset{\sim}{\Omega}_r \underset{\sim}{P}_r^{\frac{1}{2}}\left[\underset{\sim}{1} - \underset{\sim}{R}_{rr}\left(\underset{\sim}{L}_r - \underset{\sim}{B}_r\right)\right]^{-1}\left[\underset{\sim}{1} - \underset{\sim}{R}_{rr}\left(\underset{\sim}{L}_r^* - \underset{\sim}{B}_r\right)\right]\underset{\sim}{P}_r^{-\frac{1}{2}}\underset{\sim}{\Omega}_r \qquad (3.66)$$

but the reduced R-matrix $\underset{\sim}{R}_{rr}$ now has a complex form:

$$(\underset{\sim}{R}_{rr})_{cc'} \approx \sum_\lambda \frac{\gamma_{\lambda(c)}\gamma_{\lambda(c')}}{E_\lambda - \Delta_\lambda^e - E - \frac{1}{2}i\Gamma_\lambda^e} \qquad (3.67)$$

where the level shift and width quantities are sums only over eliminated channels, denoted as a sub-set by e:

$$\Delta_\lambda^e = \sum_{c'' \text{ in } e} (S_{c''} - B_{c''})\gamma_{\lambda(c'')}^2 \qquad (3.68a)$$

$$\Gamma_\lambda^e = 2\sum_{c'' \text{ in } e} P_{c''}\gamma_{\lambda(c'')}^2 \qquad (3.68b)$$

Finally, we make mention of the S-matrix formulation of reaction theory (46). This is obtained from the expansion of the collision matrix in the complex energy plane about its poles at the complex energies $E_\ell^{(H)} - \frac{1}{2}i\Gamma_\ell^{(H)}$

$$U_{c'c} = \delta_{c'c} + \Omega_{c'}\Omega_c\left\{Q_{c'c} - i\sum_\ell \frac{G_{\ell(c)}G_{\ell(c')}\exp\left[i(\xi_{\ell(c')} + \xi_{\ell(c)})\right]}{|\Omega_{c'}(E_\ell)\Omega_c(E_\ell)|\left(E - E_\ell^{(H)} + \frac{1}{2}i\Gamma_\ell^{(H)}\right)}\right\} \qquad (3.69)$$

Here the Ω_c are threshold factors containing the explicit energy dependence on centrifugal and Coulomb potential barriers, $Q_{c'c}$ is a background function, regular and slowly-varying, the $G_{\ell(c)}$ are partial width amplitudes associated with the pole ℓ, and the $\xi_{\ell(c)}$ are associated phase factors. The numerator of each item in the sum of equation (3.69) is the residue of the pole at $E_\ell^{(H)} - \frac{1}{2}i\Gamma_\ell^{(H)}$.

The quantities that appear in this S-matrix formulation have been analytically related to the parameters of the R-matrix theory in only a few relatively simple cases. For example, in the single-level approximation $E_\ell^{(H)} \sim E_\lambda - \Delta_\lambda$, $\Gamma_\ell^{(H)} \sim \Gamma_\lambda$, $G_{\ell(c)}^2 \sim \Gamma_{\lambda(c)}$ and $\xi_{\ell(c)} \sim n\pi$ where n is an integer. In many-level cases however, the relationship between R-matrix and S-matrix parameters can be found numerically and computer programmes have been written for this. In one programme the S-matrix poles are determined by finding the zeros, in the complex energy plane, of the determinant of the level matrix $\underset{\sim}{C}$. In another, the numerical integration of the collision matrix (for different pairs of channels c,c') around a small circular contour enclosing the pole is carried out thus leading to a determination of the partial width quantities $G_{\ell(c)}$, $\xi_{\ell(c)}$. For overlapping levels the energy and width quantities of the S-matrix representation can be very different from the single-level R-matrix quantities as given in equation (3.62). A calculated example of just two overlapping levels is given in Fig. 21. These both have R-matrix single level widths of the order of 0.5 eV and are separated by 0.11 eV. The S-matrix poles are separated by only 0.019 eV real energy, one has a width of only 0.039 eV and appears as a strong narrow-resonance, the other has a width of 0.87 eV and is apparent as little more than a background feature; level repulsion has occurred in the imaginary energy direction!

3.4.4 Introduction of the double-humped barrier

The potential $\Psi(\eta)$ of the deformation Hamiltonian cannot, as yet, be calculated from first principles. It is necessary to deduce it by using theories that have some phenomenological aspects. The original theory of this kind was the liquid drop model. If this is taken to provide the classical analogue of the term $T_\xi(\eta) + V(\eta,\xi)$ of equation (3.28), which is just $\varepsilon_o(\eta)(\equiv \Psi(\eta))$ in the classical limit, it gives a function for Ψ that has a minimum at values of η corresponding to the sphere, rises and passes on through a maximum (the fission barrier) for prolate, axially symmetric deformations, and finally reaches (asymptotically, for the separation into two smaller particles) a value that is considerably lower than the spherical value (for nuclei heavier than iron). Particle shell effects are included in a semi-empirical way in the droplet model of Myers and Swiatecki (1) (see under Section 2). These oscillate for small deformations but are attenuated for larger ones. They affect the position and magnitude of the minimum of $\Psi(\eta)$ but do not affect the qualitative nature of its maximum.

Shell effects have a much more dramatic influence on Ψ (so far as fission effects are concerned) in the theory of Strutinsky (2). The principal term of $T_\xi(\eta) + V(\eta,\xi)$ is taken to be the static liquid drop energy for deformation η. To this is added the sum of single particle energies computed on the assumption that $V(\eta,\xi)$ is a static, single particle potential well of fixed deformation η, and from it is subtracted a similar sum computed over a suitably "smoothed-out" (shell-averaged) single particle spectrum. The Strutinsky prescript-

ion for the deformation potential $v(\eta)$ results in a double-humped fission barrier for nuclei in the general range of thorium to curium and, to a less dramatic extent, on either side of these limits. It is the purpose of the remainder of this section to survey, using the R-matrix developments given above, the more detailed theoretical consequences for fission reactions of this kind of barrier.

It is useful, at this point, to recall the definition of some quantities which can be used to characterise the barrier, at least in an approximate fashion. The value of the potential at η_I is labelled v_I, at η_A it is v_A, at η_{II}, v_{II} and at η_B, v_B. In the neighbourhood of each of these deformations it is generally assumed, for calculational purposes, that the potential energy v is harmonic, and that the four harmonic segments join smoothly to each other; thus, in the region of η_I,

$$v = v_I + \tfrac{1}{2} C_I (\eta - \eta_I)^2 \qquad (3.70)$$

around η_A,

$$v = v_A - \tfrac{1}{2} C_A (\eta - \eta_A)^2 \qquad (3.71)$$

and similar equations are assumed for the regions around η_{II} and η_B. The joining point η_x is given by

$$\eta_x = \eta_A - \sqrt{\frac{2(v_A - v_I) C_I}{C_A (C_A + C_I)}} \qquad (3.72a)$$

with the condition

$$\eta_I = \eta_x + \frac{C_A}{C_I} (\eta_x - \eta_A) \qquad (3.72b)$$

The other joining points are given by equations (3.32).
The curvature coefficient is seldom referred to directly, but rather through the real or imaginary vibrational frequencies,

$$\hbar\omega_I = \left(C_I / B_\eta(\eta_I) \right)^{\frac{1}{2}} \qquad (3.73a)$$

$$\hbar\omega_{II} = \left(C_{II} / B_\eta(\eta_{II}) \right)^{\frac{1}{2}} \qquad (3.73b)$$

$$i\hbar\omega_A = \left(-C_A / B_\eta(\eta_A) \right)^{\frac{1}{2}} \qquad (3.73c)$$

$$i\hbar\omega_B = \left(-C_B / B_\eta(\eta_B) \right)^{\frac{1}{2}} \qquad (3.73d)$$

The last two appear in the expressions for the transmission coefficient of a wave through an inverted harmonic barrier. For the barriers A and B separately, the relevant transmission coefficients are

$$T_A = \frac{1}{1 + \exp\left[-2\pi \left(\frac{E - v_A}{\hbar\omega_A} \right) \right]} \qquad (3.74)$$

$$T_B = \frac{1}{1 + \exp\left[-2\pi \left(\frac{E - v_B}{\hbar\omega_B} \right) \right]} \qquad (3.75)$$

and can be used in the semi-quantitative discussion of fission rates through the double-humped barrier as parametrised above provided the energy is not too much below the heights of the barrier peaks.

3.4.4.1 Illustration of vibrational states of the double potential well: class-I and class-II vibrational states

The nature of the wave functions $\Phi(\eta)$ of the quasi-discrete states of the deformation node that occur for the double potential well that thus appears in the Strutinsky picture of the deformation energy of actinide nuclei is graphically illustrated by numerical calculations for a double rectangular well (Fig. 22). The striking degree of clustering of the wave-function within either one well or the other leads to the classification of the wave-function; those with major amplitude within the deeper, primary well are class-I vibrational states and those concentrated in the secondary well are class-II vibrational states. Note that the energy eigenvalues of states of either class are very little perturbed from the values they would have if the opposite well were filled in. Note also that the total number of nodes of the wave-function no longer gives the ordering of the vibrational state within its class. Thus, the "zero-point" vibration in the class-II well $\Phi_0(II)$ has 3 nodes, indicating that it is weakly connected with the fourth class-I vibrational state $\Phi_3^{(I)}$.

3.4.4.2 Amplitude relationships of class-I and class-II vibrational states

The numerical illustration of the last section suggests a systematic way of calculating the special features of the vibrational wave-functions of a double potential well of more general shape. From the double well separate primary and secondary wells (denoted by $\psi_1(\eta)$ and $\psi_2(\eta)$ respectively) are constructed in the manner shown in Fig. 23 so that $\psi_1(\eta) + \psi_2(\eta) = \psi(\eta)$, the origin of the energy scale being taken as zero. The modified asymptotic end-values are equal to the height of the intermediate maximum of the double well. The eigenvalues $\epsilon_{\nu_n}^{(n)}$ and eigenfunctions $\phi_{\nu_n}^{(n)}$ of the Schrödinger equations for the separated wells n,

$$\left[T(\eta) + v_n(\eta) \right] \phi_{\nu_n}^{(n)} = \epsilon_{\nu_n}^{(n)} \phi_{\nu_n}^{(n)} \qquad (3.76)$$

are calculated, and the solutions for the Schrödinger equation of the double well are written approximately

$$\Phi_\nu \approx a_\nu \phi^{(1)}_{\nu_1} + b_\nu \phi^{(2)}_{\nu_2} \qquad (3.77)$$

the two wave-functions appearing on the r.h.s. being (usually) a pair closest in energy. Normally one of the two coefficients a_ν, b_ν is close to unity (giving the class of Φ_ν) and the other is small. Occasionally more than one of the small amplitude terms will contribute commensurately, and equation (3.77) will need to be generalised accordingly; in this case a perturbation treatment will normally suffice.

In the approximate solution of the Schrödinger equation with the wavefunction 3.77 the values of the coefficients a_ν and b_ν are usually close to the values given by 1st order perturbation theory. For a class-I vibrational state, $a_\nu \approx 1$ and

$$b_\nu \approx \frac{\langle \phi^{(1)}_{\nu_1} | U_2 | \phi^{(2)}_{\nu_2} \rangle}{\epsilon^{(1)}_{\nu_1} - \epsilon^{(2)}_{\nu_2}} \qquad (3.78)$$

For a class-II vibrational state, $b_\nu \approx 1$ and

$$a_\nu \approx \frac{\langle \phi^{(2)}_{\nu_2} | U_1 | \phi^{(1)}_{\nu_1} \rangle}{\epsilon^{(2)}_{\nu_2} - \epsilon^{(1)}_{\nu_1}} \qquad (3.79)$$

The small contributions to the wave-function that might arise from other states of the potential ψ_n can clearly be calculated in the same way.

The matrix elements of ψ_n are quite readily and accurately calculable by straightforward digital computer methods. From the WKB approximation to the wave-functions $\phi_{\nu 1}{}^{(1)}$ and $\phi_{\nu 2}{}^{(2)}$ in the barrier region it can be shown that the strongest factor in the amplitude expression of equation (3.78),(3.79) is the square root of the transmission coefficient through the intermediate barrier. This is borne out by the numerical computations. A graphical display for all the eigenvalues of a typical double potential well is shown in Fig. 24. If the empirical results are expressed in the form

$$b_\nu^2 \approx \frac{KT_A}{(\epsilon^{(1)}_{\nu_1} - \epsilon^{(2)}_{\nu_2})^2} \qquad (3.80a)$$

for class-I states and

$$a_\nu^2 \approx \frac{KT_A}{(\epsilon^{(2)}_{\nu_2} - \epsilon^{(1)}_{\nu_1})^2} \qquad (3.80b)$$

for class-II states, the constant K is found to have the empirical value 0.006.

3.4.5 Specialisation of R-matrix theory to the double-humped barrier

3.4.5.1 Class-I and class-II compound R-matrix states

The form of the double-humped potential energy barrier in the elongation mode lends itself readily to special treatment within the extended R-matrix reaction theory outlined above. In this the R-matrix internal eigenstates are expanded in terms of two auxiliary sets of eigenstates, the class-I and class-II states (43). In this treatment the channel deformations are chosen close to the outer barrier B. Physically, the class-I states are largely confined to deformations within the region of the primary well of the double-humped barrier, and the class-II states are similarly located within the region of the secondary well.

Formal definition of these auxiliary states follows from the expansion of the R-matrix internal state in terms of products of vibrational wave-functions $\Phi_{\nu(\mu)}$ and intrinsic states χ_μ of the intrinsic Hamiltonian for channel deformation η_μ

$$\chi_\lambda = \sum_{\mu,\nu} C^\lambda_{\mu\nu} \chi_\mu \Phi_{\nu(\mu)} \qquad (3.81)$$

Here, the vibrational wave-functions $\Phi_{\nu(\mu)}$ are subject to a real energy-independent boundary condition at the selected channel deformations η_μ and this can depend on the channel label μ; the vibrational wave-functions $\Phi_{\nu(\mu)}$ are themselves discrete, and if their eigenvalues ϵ_ν are lower than the intermediate barrier of the double-humped barrier they fall into the classes I and II described in Section 3.4.4. The class-I and class-II R-matrix states are therefore conveniently defined by the incomplete expansions,

$$\chi^{(I)}_{\lambda_I} = \sum_{\mu,\nu} C^{\lambda_I}_{\mu\nu} \chi_\mu \Phi^{(I)}_{\nu(\mu)} \qquad (3.82)$$

$$\chi^{(II)}_{\lambda_{II}} = \sum_{\mu,\nu} C^{\lambda_{II}}_{\mu\nu} \chi_\mu \Phi^{(II)}_{\nu(\mu)} \qquad (3.83)$$

with eigenvalues E_{λ_I}, $E_{\lambda_{II}}$ respectively.

Physical properties of the class-I and class-II compound states follow quite simply from the expansions (3.82) and (3.83). Class-I states can be expected to contain significant amounts of components $\chi_\mu \Phi^{(I)}_{o(\mu)}$ where $\Phi^{(I)}_{o(\mu)}$ corresponds to zero-point vibrational motion within the primary well and the χ_μ are highly excited intrinsic states. The latter will include unbound states corresponding to the motion of free neutrons or protons, or more complex particles such as α-particles, against the appropriate residual nucleus, and the zero-point vibrational state becomes an essential part of the description of the ground (or even a low excited state) of the residual nucleus. Thus class-I states will have neutron and proton reduced widths for decay into these particular channels. They will also have reduced widths for alpha-decay to the ground and low excited states. The

limitation of the expansion to class-I vibrational states with (extremely likely) very small amplitudes at the channel deformation η_μ, even for comparatively high quantum numbers ν, also implies that the class-I states have very small, although not quite negligible, fission widths.

By contrast, the class-II states, by virtue of their components of class-II vibration, particularly those of high quantum number ν, have much larger reduced fission widths, but have zero reduced nucleon widths to ground and normal low-lying states of residual nuclei. Another important difference for fission barrier potentials calculated for actinide nuclei by the Strutinsky method lies in the density of the two kinds of state (for the same available excitation energy). This arises from the density of the basis product states $\chi_\mu\Phi^{(I)}_{\nu(\mu)}$ $\chi_\mu\Phi^{(II)}_{\nu(\mu)}$. The intrinsic states can be envisaged as combinations of single-particle or hole states with spacing of the order of 100 keV. Furthermore, rotational bands with spacing of the same order will be built on them. By contrast, the vibrational states will have separations of the order of 1 MeV. Thus the principal contribution to density of class-I and class-II levels will come from the combinations $\chi_\mu\Phi^{(I)}_{0(\mu)}$ and $\chi_\mu\Phi^{(II)}_{0(\mu)}$ respectively. For the actinides the potential energy calculations (see Section 2) and the experimental evidence of spontaneously fissioning isomers (see Section 3.4.5.3) and fission cross-section intermediate structure (see Section 6) indicate that the secondary well is at least about 2 MeV above the primary well, so that this amount of excess energy is tied up in the vibrational state $\Phi^{(II)}_{0(\mu)}$ and is not available for the excitation of intrinsic degrees of freedom in the class-II compound states. Consequently the density of class-II states can be expected to be some two or more orders of magnitude lower than the class-I density.

Radiation spectra for the two classes of states will differ. The class-II spectra will terminate at lower gamma-ray energies and show structure at much lower energies than those of class-I states. This is shown in Fig. 25. Radiative widths (total) will be of the same order of magnitude for both classes, the exact ratio depending on the mechanism for primary radiative transitions, although partial radiative widths for single transitions will differ by a factor that is of the order of the ratio of the spacings of the two classes of states.

3.4.5.2 Final R-matrix compound states

The final R-matrix states X_λ can now be constructed from the auxiliary class-I and class-II compound states (43). The expansion (3.81) is substituted into the Schrödinger equation

$$HX_\lambda = E_\lambda X_\lambda \qquad (3.84)$$

in the internal region of configuration space (defined in Section Both sides are multiplied by $\chi_\mu^*\Phi_\nu^*$ and integration over all variables gives

$$(\epsilon_\nu + \mathcal{E}_\mu - E_\lambda)C^\lambda_{\mu\nu} + \sum_{\mu'\nu'} C^\lambda_{\mu'\nu'}\langle\chi_\mu\Phi_{\nu(\mu)}|H_c|\chi_{\mu'}\Phi_{\nu'(\mu')}\rangle = 0 \qquad (3.85)$$

using the split of the Hamiltonian into deformation, intrinsic and coupling (H_c) terms as defined in equation (3.64). This is a representative row of a matrix equation, the eigenvalues of which are determined from the secular equation

$$\det\left(H_{\mu\nu,\mu'\nu'} - E_\lambda\delta_{\mu\nu,\mu'\nu'}\right) = 0 \qquad (3.86)$$

The determination of the eigenvalues of the matrix $\underset{\sim}{H}$ is also conventionally expressed as finding the unitary matrix $\underset{\sim}{U}$ which transforms $\underset{\sim}{H}$ by the operation $\underset{\sim}{U}\,\underset{\sim}{H}\,\underset{\sim}{U}^{-1}$ into the diagonal form $\underset{\sim}{E}$. We now specifically consider only the eigenstates of a particular set of good quantum numbers (these are normally total angular momentum J and parity π).

The matrix $\underset{\sim}{H}$ can now be partitioned into sub-matrices depending on whether the index of an element refers to a class-I (ν_I) or class-II (ν_{II}) vibrational function. Thus,

$$\underset{\sim}{H} = \begin{pmatrix} \underset{\sim}{H}_{I,I} & \underset{\sim}{H}_{I,II} \\ \underset{\sim}{H}_{II,I} & \underset{\sim}{H}_{II,II} \end{pmatrix} \qquad (3.87)$$

The sub-matrices $\underset{\sim}{H}_{I,I}$ and $\underset{\sim}{H}_{II,II}$ may now be separately diagonalised by operation with matrices

$$\begin{pmatrix} \underset{\sim}{S} & 0 \\ 0 & \underset{\sim}{T} \end{pmatrix} \quad \text{and} \quad \begin{pmatrix} \underset{\sim}{S}^{-1} & 0 \\ 0 & \underset{\sim}{T}^{-1} \end{pmatrix}$$

where $\underset{\sim}{S}$ and $\underset{\sim}{T}$ are unitary operators within the sub-space of functions of class-I and II respectively. So we have

$$\begin{pmatrix} \underset{\sim}{S} & 0 \\ 0 & \underset{\sim}{T} \end{pmatrix}\begin{pmatrix} \underset{\sim}{H}_{I,I} & \underset{\sim}{H}_{I,II} \\ \underset{\sim}{H}_{II,I} & \underset{\sim}{H}_{II,II} \end{pmatrix}\begin{pmatrix} \underset{\sim}{S}^{-1} & 0 \\ 0 & \underset{\sim}{T}^{-1} \end{pmatrix} = \begin{pmatrix} \underset{\sim}{S}\,\underset{\sim}{H}_{I,I}\,\underset{\sim}{S}^{-1} & \underset{\sim}{S}\,\underset{\sim}{H}_{I,II}\,\underset{\sim}{T}^{-1} \\ \underset{\sim}{T}\,\underset{\sim}{H}_{II,I}\,\underset{\sim}{S}^{-1} & \underset{\sim}{T}\,\underset{\sim}{H}_{II,II}\,\underset{\sim}{T}^{-1} \end{pmatrix} \qquad (3.88)$$

The eigenvalues of $\underset{\sim}{H}_{I,I}$ are just the class-I compound states defined in equation (3.82), and those of $\underset{\sim}{H}_{II,II}$ are the class-II compound states of equation (3.83). The unitary matrices $\underset{\sim}{S}$ and $\underset{\sim}{T}$ required to effect this sub-space diagonalisation are themselves the expansion coefficients of the class-I and class-II compound states respectively:

$$S_{\lambda_I,\mu\nu_I} = \langle\lambda_I|\mu\nu_I\rangle \equiv C^{\lambda_I}_{\mu\nu_I}$$

$$T_{\lambda_{II},\mu\nu_{II}} = \langle\lambda_{II}|\mu\nu_{II}\rangle \equiv C^{\lambda_{II}}_{\mu\nu_{II}} \qquad (3.89)$$

Thus the sub-matrices $\underset{\sim}{S}\,\underset{\sim}{H}_{I,II}\,\underset{\sim}{T}^{-1}$ and $\underset{\sim}{T}\,\underset{\sim}{H}_{II,I}\,\underset{\sim}{S}^{-1}$ have elements of the form

$$\left(\underset{\sim}{S}\,\underset{\sim}{H}_{I,II}\,\underset{\sim}{T}^{-1}\right)_{\lambda_I\lambda_{II}} = \sum_{\mu''\nu_{II}}\sum_{\mu'\nu_I}\langle\lambda_I|\mu'\nu_I\rangle\langle\mu'\nu_I|H_c|\mu''\nu_{II}\rangle\langle\mu''\nu_{II}|\lambda_{II}\rangle$$

$$= \left\langle X^{(I)}_{\lambda_I}\middle|H_c\middle|X^{(II)}_{\lambda_{II}}\right\rangle \qquad (3.90a)$$

$$\left(\underset{\sim}{T}\,\underset{\sim}{H}_{II,I}\,\underset{\sim}{S}^{-1}\right)_{\lambda_{II}\lambda_I} = \left\langle X^{(II)}_{\lambda_{II}}\middle|H_c\middle|X^{(I)}_{\lambda_I}\right\rangle \qquad (3.90b)$$

For compound states rather lower in energy than the intermediate maximum A in the deformation potential energy barrier, it is expected that the admixture of vibrational states Φ from above the maximum, with comparable amplitude in both regions of deformation I and II, will be very small. In this case the matrix elements of equation (3.90) are very small because of the attenuation of the vibrational components through the intermediate peak. At low enough energies it is clearly possible for these matrix elements describing the coupling between class-I and class-II states to be so small that the eigenstates X_λ can be described to a very good approximation as being either class-I or class-II states. Good physical examples of such a clean separation are provided by the slow neutron resonances in the cross-sections of ^{240}Pu and ^{238}U.

Very rough estimates of the magnitude of the coupling matrix elements can be made from equation (3.90) for the slow neutron case (resonance states at an excitation energy of ~ 5 MeV with a density $D_I^{-1} \sim 10^5\ MeV^{-1}$). Observations of the neutron-induced fission cross-sections of fissile nuclei indicate that the high vibrational states (quantum number $\nu \sim 5$ to 10) are mixed fairly uniformly over the compound states. The magnitude of the matrix element for mixing of a vibrational state into a class-I state in the absence of attenuation through the intermediate barrier can thus be deduced from the spreading width value $W \gtrsim \hbar\omega_I$ (see section 3.4.5.3 for discussion of Lorentzian mixing) to be $\gtrsim (D_I\hbar\omega_I/2\pi)^{\frac{1}{2}}$. The attenuation through the intermediate barrier will reduce this by a factor $(T_A/2\pi)^{\frac{1}{2}}$. The fractionation of a class-II vibrational state into the class-II compound states will be given by $\langle\mu\nu_{II}/\lambda_{II}\rangle \sim (D_{II}/\hbar\omega_{II})^{\frac{1}{2}}$ where D_{II} is the class-II compound state spacing. Thus

$$\left|\left\langle X^{(I)}_{\lambda_I}\middle|H_c\middle|X^{(II)}_{\lambda_{II}}\right\rangle\right| \sim \left(\frac{D_I}{2\pi}\cdot\frac{D_{II}}{2\pi}\cdot\frac{T_A}{2\pi}\right)^{\frac{1}{2}} \qquad (3.91)$$

3.4.5.3 Specific coupling modes for class-I and class-II states

With small matrix elements in the off-diagonal sub-matrices for coupling class-I and class-II states the final diagonalisation of the Hamiltonian of equation (3.87), and the insertion of the resulting eigenstates into the R-matrix reaction theory, becomes possible by a number of methods corresponding to distinct physical situations. In most of them the approximation is made that the coupling matrix elements are sufficiently small that the effects of all but one class-II state on a localised group of class-I states can be neglected.

(i) Very weak coupling; narrow class-II states

Here narrowness of the class-II state is defined by the product of penetrability and squared amplitude at the channel deformation (the fission width) being much smaller than the energy interval δ between the class-II state and its nearest class-I neighbour. (It will be shown in sub-section (v) that although this condition does not affect the diagonalisation of $\underset{\sim}{H}$ it has a drastic effect on the properties of the resonances in the cross-section.) Very weak coupling is defined as the average magnitude of the coupling matrix element $\langle\lambda_I|H_c|\lambda_{II}\rangle$ being much smaller than the energy interval δ. This condition allows the Hamiltonian of (3.87) to be diagonalised by perturbation theory. Second order perturbation theory in the region of a single class-II state gives

$$X_{\lambda'} \approx \left[1 - \frac{\left\langle X^{(I)}_{\lambda_I}\middle|H_c\middle|X^{(II)}_{\lambda_{II}}\right\rangle^2}{2\left(E_{\lambda_I} - E^{(II)}_{\lambda_{II}}\right)^2}\right]X^{(I)}_{\lambda_I}$$

$$+ \frac{\left\langle X^{(I)}_{\lambda_I}\middle|H_c\middle|X^{(II)}_{\lambda_{II}}\right\rangle}{\left(E_{\lambda_I} - E_{\lambda_{II}}\right)}X^{(II)}_{\lambda_{II}} + \sum_{\lambda'_I}\frac{\left\langle X^{(I)}_{\lambda_I}\middle|H_c\middle|X^{(II)}_{\lambda_{II}}\right\rangle\left\langle X^{(II)}_{\lambda_{II}}\middle|H_c\middle|X^{(I)}_{\lambda'_I}\right\rangle}{\left(E_{\lambda_I} - E_{\lambda'_I}\right)\left(E_{\lambda_I} - E_{\lambda_{II}}\right)}X^{(I)}_{\lambda'_I} \qquad (3.92a)$$

$$E_{\lambda'} \approx E_{\lambda_I} + \frac{\left\langle X^{(I)}_{\lambda_I}\middle|H_c\middle|X^{(II)}_{\lambda_{II}}\right\rangle^2}{E_{\lambda_I} - E_{\lambda_{II}}} \qquad (3.92b)$$

for the states that remain essentially class-I in character, and

$$X_{\lambda''} \approx \left[1 - \sum_{\lambda_I}\frac{\left\langle X^{(I)}_{\lambda_I}\middle|H_c\middle|X^{(II)}_{\lambda_{II}}\right\rangle^2}{2\left(E_{\lambda_{II}} - E_{\lambda_I}\right)^2}\right]X_{\lambda_{II}}$$

$$+ \sum_{\lambda_I}\frac{\left\langle X^{(I)}_{\lambda_I}\middle|H_c\middle|X^{(II)}_{\lambda_{II}}\right\rangle}{E_{\lambda_{II}} - E_{\lambda_I}}X_{\lambda_I} \qquad (3.93a)$$

$$E_{\lambda''} \approx E_{\lambda_{II}} + \sum_{\lambda_I}\frac{\left\langle X^{(II)}_{\lambda_{II}}\middle|H_c\middle|X^{(I)}_{\lambda_I}\right\rangle^2}{E_{\lambda_{II}} - E_{\lambda_I}} \qquad (3.93b)$$

for the remaining states.

From these relations simple results are obtained for the resonance widths (see Section 3g(i)). If $\Gamma_{\lambda_{II}(f)}$ is the fission width an unperturbed class-II state would have if it appeared as a resonance in a suitable cross-section, and the fission widths for unperturbed class-I states are assumed to be negligible, we have immediately that

$$\Gamma_{\lambda'(f)} \approx \frac{\langle X^{(I)}_{\lambda_I} | H_c | X^{(II)}_{\lambda_{II}} \rangle^2}{(E_{\lambda_I} - E_{\lambda_{II}})^2} \Gamma_{\lambda_{II}(f)} \qquad (3.94)$$

for quasi-class-I resonance states, while

$$\Gamma_{\lambda''(f)} \approx \left[1 - \sum_{\lambda_I} \frac{(H_c)^2_{\lambda_I \lambda_{II}}}{(E_{\lambda_I} - E_{\lambda_{II}})^2}\right] \Gamma_{\lambda_{II}(f)} \qquad (3.95a)$$

$$= \Gamma_{\lambda_{II}(f)} - \sum_{\lambda'(\neq\lambda'')} \Gamma_{\lambda'(f)} \qquad (3.95b)$$

is the fission width of the quasi-class-II resonance.

Exactly similar relations hold for the partial radiation widths for electromagnetic transitions to lower class-II states, so we see that each admixed level has exactly the same pattern, in terms of relative intensities, of class-II spectrum superimposed on the normal class-I spectrum. This "fingerprint" spectrum could be used to identify the second minimum phenomenon in resonance behaviour when the class-II states themselves cannot fission (because the saddle-point is too high). The "fingerprint" behaviour is of course quite different from the normal spectrum behaviour which varies strongly (at least in the high transition energy region where discrete transitions can be observed) from one resonant state to the next. Each class-II "fingerprint" spectrum will also vary strongly from one class-II group of resonances to the next group. Radiative transitions are treated in greater detail in Section 4

Neutron (or other particle) widths cannot be given so unambiguously. The expressions for reduced neutron widths (in the experimenters' convention: neutron width divided by penetration factor) are

$$\Gamma^{(o)}_{\lambda'(n)} \approx \left\{\left[1 - \frac{\langle X^{(I)}_{\lambda_I} | H_c | X^{(II)}_{\lambda_{II}} \rangle^2}{2(E_{\lambda_I} - E_{\lambda_{II}})^2}\right] \sqrt{\Gamma^{(o)}_{\lambda_I(n)}} + \sum_{\lambda'_I(\neq\lambda_I)} \frac{\langle X^{(I)}_{\lambda_I} | H_c | X^{(II)}_{\lambda_{II}} \rangle \langle X^{(II)}_{\lambda_{II}} | H_c | X^{(I)}_{\lambda'_I} \rangle}{(E_{\lambda_I} - E_{\lambda'_I})(E_{\lambda_I} - E_{\lambda_{II}})} \sqrt{\Gamma^{(o)}_{\lambda'_I(n)}}\right\} \qquad (3.96)$$

$$\Gamma^{(o)}_{\lambda''(n)} \approx \left\{\sum_{\lambda_I} \frac{\langle X^{(I)}_{\lambda_I} | H_c | X^{(II)}_{\lambda_{II}} \rangle}{E_{\lambda_{II}} - E_{\lambda_I}} \sqrt{\Gamma^{(o)}_{\lambda_I(n)}}\right\}^2 \qquad (3.97)$$

where $\Gamma^{(o)}_{\lambda(n)} = 2P_n$ (at 1 eV) $\gamma^2_{\lambda(n)}$.

The signs of the square roots (the reduced width amplitudes) are random from one resonant state to another, and generally will be unknown. This gives a number of possibilities for the value of $\Gamma_{\lambda''(n)}$ in relation to the values of the $\Gamma_{\lambda'(n)}$. A maximum value of $\Gamma_{\lambda''(n)}$ can be stated (this would occur if the signs of the $\sqrt{\Gamma_{\lambda I(n)}}$ were fully correlated) and a mean expected value of this width can also be given; the latter is

$$\langle \Gamma^{(o)}_{\lambda''(n)} \rangle \approx \sum_{\lambda'(\neq\lambda'')} \frac{\Gamma_{\lambda'(f)} \Gamma^{(o)}_{\lambda'(n)}}{\Gamma_{\lambda_{II}(f)}} \qquad (3.98)$$

Physical examples of such coupling between class-I and class-II states are to be found in the slow neutron cross-sections of ^{240}Pu and ^{238}U. In the former, three now well-studied class-II states occur below a neutron energy of 2000 eV, and in this energy range the average class-I level spacing is ~ 14 eV. For each of the class-II states, identified by the comparatively high fission cross-sections of the resonances in their immediate vicinity (see Fig. 26), the class-II fission width is about 2 eV. In two of the cases (at 800 eV and 1900 eV) the bulk of this fission width is to be found in a single weak, but broad, resonance at the centre of a cluster of strong fission resonances. The quasi-class-II resonance thus identified has a reduced neutron width less than one-tenth of the average value of its neighbours.

(ii) Very weak coupling with accidental degeneracy

The perturbation theory of sub-section (i) above does not cover the possibility of an accidental degeneracy or near-degeneracy between a class-I state and a class-II state. This situation, with weak-coupling to the remaining class-I states can be dealt with quite easily. The sub-section H_s of the Hamiltonian matrix around a given class-II state (moved into the row 1, column 1 position) is

$$\begin{pmatrix} E_{1_{II}} & \langle X^{(II)}_1 | H_c | X^{(I)}_2 \rangle & \langle X^{(II)}_1 | H_c | X^{(I)}_3 \rangle & \cdots \\ \langle X^{(I)}_2 | H_c | X^{(II)}_1 \rangle & E_{2_I} & 0 & \cdots \\ \langle X^{(I)}_3 | H_c | X^{(II)}_1 \rangle & 0 & E_{3_I} & \cdots \\ \cdot & 0 & 0 & \cdot \\ \cdot & \cdot & \cdot & \cdot \\ \cdot & \cdot & \cdot & \cdot \end{pmatrix} \qquad (3.99)$$

Here, E_{2_I} is the nearly-degenerate class-I eigenvalue. The top left-hand sub-matrix of order two can be diagonalised by a matrix with a unitary sub-matrix $\underset{\sim}{W}$ in that position and partitioned otherwise as

$$\begin{pmatrix} \underset{\sim}{W} & 0 \\ 0 & \underset{\sim}{1} \end{pmatrix}$$

By operating with this matrix and its reciprocal on the sub-matrix H_{ss} using perturbation theory detailed results for the widths can be obtained (43). These are not quoted here. It is sufficient to say that the class-II and nearest class-I states are shared almost equally between two fine-structure resonances (but with opposite signs in the relative amplitude), so that these two resonances appear with almost equal fission and neutron widths, and interference in the fission cross-section is constructive between the resonances. This phenomenon is exemplified almost perfectly in the 1405 eV class-II resonance in the neutron fission cross-section of ^{240}Pu (Fig. 27).

From the results on the neutron fission cross-section of ^{240}Pu it appears that the average class-II fission width is 2.5 eV and the mean squared coupling matrix element is 5.1 eV^2.

It is normal to express the value of the latter in the form of the coupling width

$$\Gamma_{\lambda_{II}(c)} = \frac{2\pi\overline{(H_c)^2_{\lambda_I\lambda_{II}}}}{D_I}$$

because, as will be seen in the next section that for somewhat stronger coupling, this is the width of the Lorentzian profile of fission widths. From the expressions (3.74),(3.75) information on the barrier heights of ^{241}Pu can be obtained. From these equations we find

$$2\pi(V_A - S_n)/\hbar\omega_A = 3.8$$

$$2\pi(V_B - S_n)/\hbar\omega_B = 3.6$$

These values are special to states of spin and parity $J^\pi = \frac{1}{2}^+$; the conventional barrier height expressed irrespective of spin will almost certainly be lower than this.

(iii) Moderately weak coupling: narrow class-II states

Moderately weak coupling may be defined as the magnitude of the coupling matrix elements lying within the range

$$D_I^2 \gtrsim \overline{\langle\lambda_I|H_c|\lambda_{II}\rangle^2} \ll D_I D_{II}/2\pi \qquad (3.100)$$

With these conditions it is a good approximation to consider only the mixing of a single class-II state with a group of class-I states in its vicinity. However, the coupling is too strong to permit a perturbation treatment.

The limitation to a single class-II state allows the diagonalisation of the matrix on the right-hand side of equation (3.88) to be reduced to the solution of

$$C^\lambda_{\lambda_I}(E_{\lambda_I} - E_\lambda) + C^\lambda_{\lambda_{II}}\langle\lambda_I|H_c|\lambda_{II}\rangle$$

$$\sum_{\lambda_I} C^\lambda_{\lambda_I}\langle\lambda_I|H_c|\lambda_I\rangle + C^\lambda_{\lambda_{II}}(E_{\lambda_{II}} - E_\lambda) \qquad (3.101)$$

for a single class-II state λ_{II}, together with the normalisation condition

$$\sum_{\lambda_I}(C^\lambda_{\lambda_I})^2 + (C^\lambda_{\lambda_{II}})^2 = 1 \qquad (3.102)$$

Here the $C^\lambda_{\lambda I}$, $C^\lambda_{\lambda II}$ are the expansion coefficients of the class-I and class-II states in the diagonalised states λ:

$$X_\lambda = \sum_{\lambda_I} C^\lambda_{\lambda_I} X^{(I)}_{\lambda_I} + C^\lambda_{\lambda_{II}} X^{(II)}_{\lambda_{II}} \qquad (3.103)$$

The solution of these equations (43,49) is

$$C^\lambda_{\lambda_I} = -\frac{\langle\lambda_I|H_c|\lambda_{II}\rangle}{E_{\lambda_I} - E_\lambda} C^\lambda_{\lambda_{II}} \qquad (3.104a)$$

$$E_{\lambda_{II}} - E_\lambda = \sum_{\lambda_I} \frac{\langle\lambda_I|H_c|\lambda_{II}\rangle^2}{E_{\lambda_I} - E_{\lambda_{II}}} \qquad (3.104b)$$

$$(C^\lambda_{\lambda_{II}})^2 = \left(\sum_{\lambda_I} \frac{\langle\lambda_I|H_c|\lambda_{II}\rangle^2}{(E_{\lambda_I} - E_\lambda)^2} + 1\right)^{-1} \qquad (3.104c)$$

This result is exact and incorporates the results of perturbation theory for the very weak coupling case. Equations (3.104) are most easily surveyed for the uniform, or picket-fence, model of level structure. Class-I levels are assumed to be equally spaced (with interval D_I) and the squared matrix element of H_c is assumed independent of λ_I. Thus

$$E_{\lambda_{II}} - E_\lambda = -\frac{\pi H_c^2}{D_I}\cot\left(\frac{\pi E_\lambda}{D_I}\right) \qquad (3.105a)$$

(the origin of the energy scale coinciding with a class-I level) and

$$(C^\lambda_{\lambda_{II}})^2 = \frac{H_c^2}{(E_{\lambda_{II}} - E_\lambda)^2 + \frac{\pi^2 H_c^4}{D_I^2} + H_c^2} \qquad (3.105b)$$

In the familiar Lorentzian form of equation (3.105b) the half-width of the profile of squared admixture coefficients (defined as half-width at half-maximum) is

$$W = \frac{\pi H_c^2}{D_I}\sqrt{1 + \frac{D_I^2}{\pi^2 H_c^4}} \qquad (3.106)$$

The first factor is the well-known "golden rule", and for all but very weak coupling the second factor is nearly unity. It must be remembered, however, that, according to equation (3.105a), eigenvalues are densest close to the spreading class-II state λ_{II} (Fig.28 is a schematic diagram of the solution 3.105a), hence the half-width of suitably averaged strength of the $C^{\lambda}_{\lambda_{II}}{}^2/D_I$ as a function of energy is less than the result given in equation (3.106). In fact it has been shown (Lane et al [81]) that $W = \pi H_c^2/D_I$ is the exact result for the locally averaged intensity coefficient if the average mixing of λ_{II} into the states λ is defined by an ensemble procedure in which the members of the ensemble are all possible patterns of E_λ and $(C^{\lambda}_{\lambda_{II}})^2$ resulting from prescribed mean values and statistical distributions of the class-I level spacings and the matrix elements.

An estimate of the value to be expected for the Lorentzian half-width in terms of the intermediate barrier transmission coefficient T_A can be obtained from equation (3.106), with the result

$$2W = \frac{D_{II}}{2\pi}\,T_A \qquad (3.107)$$

The coefficients of mixing of the class-II state into the states λ, as expressed by equation (3.104c), can be used immediately to give the fission widths in the narrow resonance approximation;

$$\Gamma_{\lambda(f)} = \left(C^{\lambda}_{\lambda_I}\right)^2 \Gamma_{\lambda_{II}(f)} \qquad (3.108)$$

In the uniform model the resonance fission widths would therefore follow the Lorentzian profile of equation (3.105b). Entrance channel widths must be deduced from the coefficients of equation (3.104a). Far from the class-II state the entrance channel widths are very little disturbed from the original pattern possessed by the class-I states. Near the original class-II state there is considerable dislocation of the original pattern, but, except in the case of very weak coupling, there will be no strong reduction in expected value, and anti-correlation between fission width and entrance channel width will only be weak.

Physical examples of moderately weak coupling have been observed in the fission reaction in a few cases. The best explored is the slow-neutron-induced fission cross-section of ^{234}U (50). Fission and neutron widths have been measured for all the resonances in the region of 580 eV and the former show (Fig. 29) a Lorentzian type of profile about this energy, but with very considerable scatter about the ideal form owing to the Porter-Thomas fluctuations normally expected for compound states. The half-width of the profile has been assessed as 64 eV, a factor of 6 times the mean class-I level spacing (D_I = 10.6 eV). The deduced barrier heights are V_A = 5.53 MeV (with $\hbar\omega_A$ assumed to be 0.8 MeV) and V_B = 5.86 MeV ($\hbar\omega_B$ assumed to be 0.52 MeV). Another example, in which the fine structure resonances have not been experimentally resolved, occurs in the fission cross-section (see Fig. 28) for neutrons bombarding ^{230}Th (51). In this case the class-II state appears to be of particularly simple character (see Section 6).

(iv) Weak coupling; broad class-II states

The expression

$$\Gamma_{\lambda(f)} = \frac{H_c^2\,\Gamma_{\lambda_{II}(f)}}{\left(E_\lambda - E_{\lambda_{II}}\right)^2 + \left(\frac{1}{2}\Gamma_{\lambda_{II}}\right)^2} \qquad (3.109)$$

which stems from equation (3.108) combined with (3.105b), also describes the fission widths of the fine-structure resonances in the cross-section when the class-II fission width is greater than the class-I level spacing. In this case the class-II width in the denominator is the sum of the coupling width and fission width of the state. It is important to note, however, that the fission widths in this new case are the partial widths of the S-matrix poles describing the fine-structure resonances. In the case of weak coupling the sum of widths of the resonances encompassed by equation (3.109) falls far short of the total class-II fission width. The difference is encompassed by an extra pole with very small partial width for the entrance channel; this pole is not manifested by an obvious fine structure resonance, but, rather, by a very weak slowly varying background effect.

The effect is demonstrated by a numerical experiment (52). R-matrix levels of class-I type were generated with Porter-Thomas statistics for reduced neutron widths and squared coupling matrix elements $(H_c)^2_{\lambda_I\lambda_{II}}$ in the region of a postulated class-II R-matrix state. The coupling between the states was accomplished according to the formulation of section (iii) above to give the final R-matrix states, and from this simulated set the R-matrix and collision matrix were generated. Numerical methods were then used to find the poles and residues of the S-matrix. Also, the cross-section was generated and the apparent R-matrix levels were determined by fitting procedures (Fig. 30). Some results for the central resonances produced by this procedure are shown in Table 2. It is apparent that the true R-matrix states bear little resemblance to either the apparent (fitted) R-matrix states or to the S-matrix poles; the latter sets are very similar however, except that the set of apparent R-matrix states do not contain the very broad S-matrix pole. The apparent R-matrix states have very similar neutron widths to the class-I R-matrix states.

(v) Class-II coupling and fission widths of similar magnitude

When the width of the class-II state is greater than the class-I level spacing, but its fission width is of the same magnitude as the coupling width, Lorentzian patterns of fission widths in the resulting fine-structure resonances break down. A typical case, in which the partial fission widths of the S-matrix poles are plotted, is shown in Fig. 31. This case is now becoming so complicated that even the S-matrix poles do not always give a clear indication of the pattern of fine-structure resonances. In a case simulated, as in (iv) above, this is shown by the results of Table 3. The generated cross-section is shown in Fig. 32; fitting with a set of R-matrix levels based on the observed resonances in the cross-section is now clearly unsatisfactory.

4. AVERAGE CROSS-SECTIONS OF FISSIONABLE NUCLEI

4.1 Introduction

With a formal reaction theory, developed to include fission channels and specialised to display explicitly the extra features introduced by the double-humped barrier, we are now in a position to study the expressions required for calculating the energy-averaged cross-sections of fissionable nuclei. In these lectures we shall restrict the discussion to the compound nucleus mechanism, so the expressions required are of the Hauser-Feshbach or statistical type; this theory has been discussed in earlier components of the present course. It is not anticipated that fission cross-sections themselves will proceed by any other than a compound nucleus mechanism, but it must be borne in mind that competing reactions (in the compound nucleus sense) may also be influenced by more direct or pre-equilibrium mechanisms, particularly at higher projection energies, and also that fission which is not the primary stage in a reaction (i.e. n,n'f or n,xnf) can be influenced by such direct processes operating in the earlier stages.

4.2 Hauser-Feshbach formalism

Since the general material has been covered in Moldauer's lectures only a brief summary of the basic material is given here. The simplest derivation of Hauser-Feshbach stems from the narrow-resonance approximation. If the Breit-Wigner single-level form of the cross-section is averaged for an energy interval equal to the level spacing D the result, for the total compound nucleus formation cross-section is

$$\bar{\sigma}_{CN} = 2\pi^2 \lambda^2 g(J, I) \frac{\Gamma_{(n)}}{D} \qquad (4.1)$$

and for the reaction cross-section in channel c is,

$$\bar{\sigma}_c = 2\pi^2 \lambda^2 g(J, I) \frac{\Gamma_{(n)} \Gamma_{(c)}}{D \Gamma} \qquad (4.2)$$

where $\lambda (= 1/k)$ is the neutron de Broglie wavelength divided by 2π. These expressions can be recast using transmission coefficients defined for narrow resonances by

$$T_c = \frac{2\pi \Gamma_{(c)}}{D} = \frac{4\pi P_c \gamma^2_{(c)}}{D} \qquad (4.3)$$

The recast expressions are in the simplest Hauser-Feshbach form:

$$\bar{\sigma}_c = \pi \lambda^2 g(J, I) \frac{T_n T_c}{\sum_{c'} T_{c'}} \qquad (4.4)$$

For larger energy intervals than a single level spacing the fluctuations of the widths from resonance to resonance must be taken into account. For the total compound nucleus formation cross-section averaging over resonances makes no formal difference; the neutron width for a particular resonance is simply replaced by its average. For a specific reaction cross-section the whole factor $\Gamma_{(n)}\Gamma_{(c)}/\Gamma$ must be averaged, and as a result the cross-section can no longer be written simply as equation (4.4) with the transmission coefficients each proportional simply to an average width. It is normal however to retain the form of equation (4.4) and simply to multiply in an extra factor $\mathcal{S}$ which takes account of the distortion introduced by averaging over Porter-Thomas distributions:

$$\sigma_c = \pi \lambda^2 g(J, I) \frac{T_n T_c}{\sum_{c'} T_{c'}} \mathcal{S}_{nc} \qquad (4.5)$$

The fluctuation factors $\mathcal{S}$ normally lie between about 0.5 and 1.5 for Porter-Thomas distribution of partial widths.

This method for deriving the Hauser-Feshbach form breaks down when resonances become broad. For moderately broad (not completely overlapping) resonances Lane and Thomas (45) have shown that the transmission coefficients in equation (4.5) must be replaced by

$$T_c = \frac{2\pi \bar{\Gamma}_{(c)}/D}{\left(1 + \pi \bar{\Gamma}_{(c)}/D\right)^2} \qquad (4.6)$$

For still broader resonances it is necessary to use the S-matrix formulation to retain some resemblance to the cross-section as a superposition of single-level forms. With this the interference between the single-level resonances can be made more explicit. A study of a range of picket-fence models by Moldauer (53) has shown that the transmission coefficients for the Hauser-Feshbach expression can be written

$$T_c = 1 - \exp\left[-\frac{2\pi |\bar{\Gamma}^{(1)}_{(c)}|}{D}\right] \qquad (4.7)$$

Furthermore, the S-matrix widths in this term can be written in terms of R-matrix quantities:

$$\frac{2\pi\,|\bar{\Gamma}^{(H)}_{(c)}|}{D} = 4\tanh^{-1}\left(\frac{\pi\bar{\Gamma}_{(c)}}{2D}\right), \qquad \left(\text{if } \frac{\pi\bar{\Gamma}_{(c)}}{2D} < 1\right)$$

$$= 4\coth^{-1}\left(\frac{\pi\bar{\Gamma}_{(c)}}{2D}\right), \qquad \left(\text{if } \frac{\pi\bar{\Gamma}_{(c)}}{2D} > 1\right) \tag{4.8}$$

As far as practical calculation is concerned the difference between S-matrix and R-matrix widths only becomes large when $\Gamma_{(c)}/D$ approaches unity, but then the difference in inserting the latter rather than the former in equation (4.7) for the transmission coefficient is quite small.

It should be noted here that special attention must be paid to the treatment of elastic scattering (see (54)).

All the above comments are for conventional particle channels. Important modifications can arise when the fission channels are introduced. First of all, however, it should be noted that the more elementary forms of fission reaction theory give expressions for fission transmission coefficients that can be substituted directly into the Hauser-Feshbach expressions. Thus, the expression from one-dimensional barrier penetration theory (equation 3.7) is exactly the fission transmission coefficient to be provided by this theory for the average cross-section.

4.3 Statistical expressions for very many channels

4.3.1 Neutron channels

We start from the compound nucleus formation cross-section through an individual channel with neutron energy ϵ (to which corresponds a de Broglie wavelength divided by 2π, $\lambda\!\!\!^{-}_n$) as given by the transmission coefficient $T_{J^\pi(n)}$:

$$\sigma^{J^\pi}_{n,CN}(\epsilon) = \pi\lambda\!\!\!^{-2}_n g(J,I)\, T_{J^\pi(n)}(\epsilon) \tag{4.9}$$

where g(J,I) is the statistical spin weighting factor for bombardment of a target with spin I to form a compound nucleus with total angular momentum J and parity π.

The full compound nucleus formation cross-section is, from (4.4),

$$\sigma_{n,CN}(\epsilon) = \pi\lambda\!\!\!^{-2}_n \sum_J \sum_{s=|I-\frac{1}{2}|}^{I+\frac{1}{2}} \sum_{\ell=|J-s|}^{J+s} g(J,I)\, T_{J^\pi(n,ls)}(\epsilon) \tag{4.10}$$

s being the channel spin for the given entrance channel and l the neutron orbital angular momentum. Generally, the transmission coefficient depends, for given energy ϵ, most strongly on l. Hence, ignoring the dependence on J and the channel spin s, we may write

$$\sigma_{n,CN}(\epsilon) = \pi\lambda\!\!\!^{-2}_n \sum_{\ell=0}^{\infty}(2\ell+1)\,T_{(\ell)}(\epsilon) \tag{4.11a}$$

or

$$\sum_{\ell=0}^{\infty}(2\ell+1)\,T_{(\ell)}(\epsilon) = \frac{2m\epsilon\,\sigma_{n,CN}(\epsilon)}{\pi\hbar^2} \tag{4.11b}$$

where m is the reduced neutron mass. The summed transmission coefficient for total elastic and inelastic scattering at excitation energy E can be written in terms of the level density of states of the residual nucleus as follows:

$$T_{J^\pi(n,tot)}(\epsilon) = \int_0^{E-S_n} d\varepsilon \sum_I \sum_{s=|I-\frac{1}{2}|}^{I+\frac{1}{2}} \sum_{\ell=|J-s|}^{J+s} T_{J^\pi(\ell s)}(\epsilon)\,\rho^{(R)}(E-S_n-\varepsilon, I^{\pi_I}) \tag{4.12}$$

Here the parity π_I of the residual nucleus is given by $\pi_I = (-1)^{\ell}\pi$, and S_n is the neutron separation energy of the compound nucleus. A common and convenient assumption for the dependence of level density on angular momentum is the (2I+1) proportionality. This allows the reduction of equation (4.12) to

$$T_{J^\pi(n,tot)} = (2J+1)\int_0^{E-S_n} d\varepsilon\,\rho^{(R)}_{eff}(E-S_n-\varepsilon)\sum_{\ell=0}^{\infty}(2\ell+1)\,T_{(\ell)}(\epsilon) \tag{4.13a}$$

$$= \frac{2m}{\pi\hbar^2}(2J+1)\int_0^{E-S_n} d\varepsilon\,\sigma_{n,CN}(\varepsilon)\,\varepsilon\,\rho^{(R)}_{eff}(E-S_n-\varepsilon) \tag{4.13b}$$

with the use of equation (4.11b). Here ρ_{eff} is the level density for an effective angular momentum value of zero (i.e. is $\rho(U,0)$ for an even or odd nucleus, $\frac{1}{2}\rho(U,\frac{1}{2})$ for an odd-mass nucleus) and both parities. In the use of equation (4.13b) σ_{CN} is generally assumed to be virtually independent of the neutron energy ε.

A more accurate representation of the spin dependence of the level density is

$$\rho(U,I) \propto (2I+1)\exp\left[-\frac{(I+\frac{1}{2})^2}{2\sigma^2}\right] \tag{4.14}$$

where σ is a spin dispersion coefficient. The introduction of this into equation (4.12) prohibits the simple derivation of equation (4.13b). We now have, approximately

$$\sum_{I}\sum_{s=|I-\frac{1}{2}|}^{I+\frac{1}{2}}\sum_{l=|J-s|}^{J+s}{}' \rho(U,I)T_{(l)}(\varepsilon) \approx 2\sum_{l=0}^{\infty}\sum_{I=|J-l|}^{J+l}(2I+1)e^{-(I+\frac{1}{2})^2/2\sigma^2}\rho^{(R)}(U,0)T_{(l)} \qquad (4.15)$$

$$\approx 2\sum_{l=0}^{\infty}(2l+1)(2J+1)f(J,l)\ \rho^{(R)}(U,0)T_{(l)}$$

With this expression, equation (4.12) is cast into the form of (4.13b) but with an additional factor $f_{eff}(J,\varepsilon)$ in the integrand:

$$T_{J\pi(n,tot)} = \frac{2m}{\pi\hbar^2}(2J+1)\int_0^{E-S_n} d\varepsilon\ \sigma_{CN}(\varepsilon)\,\varepsilon\, f_{eff}(J,\varepsilon)\rho_{eff}^{(R)}(E-S_n-\varepsilon) \qquad (4.16)$$

For rough calculations a simple prescription for $f_{eff}(J,\varepsilon)$ is to make it equal to $f(J,l_{max})$ where l_{max} is the partial wave contributing the most to the compound nucleus formation cross-section in equation (4.11a). This will vary with energy, and to remove it from the integrand of equation (4.16) l_{max} should be calculated for the approximate mean energy $\bar{\varepsilon}$ of neutron emission:

$$\bar{\varepsilon} = \int_0^{E-S_n} d\varepsilon\ \varepsilon^2\rho_{eff}^{(R)}(E-S_n-\varepsilon)\Big/\int_0^{E-S_n} d\varepsilon\ \varepsilon\,\rho_{eff}^{(R)}(E-S_n-\varepsilon) \qquad (4.17)$$

If the level density contains the usual well-known temperature factor $e^{U/\theta}$, then $\bar{\varepsilon} \approx 2\theta$. Some values of f(J,1) are given in Table 4.

The same assumption of a constant temperature level density behaviour allows the evaluation of the integral in equation (4.16). Using

$$\rho_{eff}^{(R)}(U) = C_R\, e^{U/\theta_R} \qquad (4.18)$$

for the level density of the residual nucleus, we find

$$T_{J\pi(n,tot)} = \frac{2m\sigma_{CN}C_R\theta_R}{\pi\hbar^2}(2J+1)f_{eff}(J,2\theta_R)\left[\theta_R e^{E_n/\theta_R} - (E_n+\theta_R)\right] \qquad (4.19)$$

for neutron energy E_n. For more complicated level density laws equation (4.19) can still be used in numerical work by breaking up the level density function into regions of constant temperature.

4.3.2 Electromagnetic radiation

An individual transmission coefficient for γ-ray emission of energy ε_γ from highly excited states of energy E and total angular momentum and parity J^π can be written

$$T_{J^\pi(\gamma)}(E) = \frac{2\pi T_{J^\pi(\gamma)}}{D_{J^\pi}} = 2\pi f(E,\varepsilon_\gamma) \qquad (4.20)$$

where $f(E,\varepsilon_\gamma)$ contains the energy dependence of the transition matrix element (structure effects) as well as the phase space dependence $\varepsilon_\gamma^{2\ell+1}$ depending on the multipolarity of the transition concerned ($\ell = 1$ for the most important multipolarity, electric dipole radiation). The total radiative transmission coefficient is therefore

$$T_{J^\pi(\gamma,tot)}(E) = \frac{2\pi T_{J^\pi(\gamma,tot)}}{D_{J^\pi}} = \int_0^E d\varepsilon_\gamma f(E,\varepsilon_\gamma)\sum_{J_f=|J-1|}^{J+1}\rho^{(c)}(E-\varepsilon,J_f) \qquad (4.21)$$

in which $\rho^{(c)}(U,J_f)$ is the level density of the normal states of the compound nucleus at excitation U. The straightforward relationship between T and Γ/D given in equations (4.20) and (4.21) can be used because of the weak perturbation effect of the electromagnetic coupling on the nuclear system.

4.3.3 Fission

For a one-humped fission barrier, of height V_F, the total fission transmission coefficient is the sum of coefficients for all channels μ, each having intrinsic excitation $\mathcal{E}_\mu$, which effectively increases the barrier height for that channel by the amount $\mathcal{E}_\mu$:

$$T_f(E) = \sum_\mu T_\mu(V_F,\mathcal{E}_\mu) = \sum_\mu T(E-V_F-\mathcal{E}_\mu)$$

$$\approx \int d\mathcal{E}\ \rho^{(F)}(\mathcal{E})T(E-V_F-\mathcal{E}) \qquad (4.22)$$

where $\rho^{(F)}(\mathcal{E})$ is the density, at the deformation of the barrier, of intrinsic excitation states. This simple concept of a total fission transmission coefficient cannot be applied immediately to the double-humped barrier unless there is no interaction with other degrees of freedom in the secondary well region. If the class-II states associated with the secondary well deformation are effective compound nucleus states thoroughly mixing the degrees of freedom then the statistical theory of Section 3.3 gives a first orientation for the fission transmission coefficient; by expressing the right-hand side of equation (3.25) in the form $T_{eff,f}/\Sigma_c,T_c$, it is seen that

$$T_{eff,f} \approx \frac{T_A T_B}{T_A + T_B} \qquad (4.23)$$

(neglecting all particle and electromagnetic decay processes of the class-II states). The individual coefficients T_A, T_B that appear in this expression are now to be understood as total transmission coefficients across the individual barriers A and B, and can be expressed in the form (4.22) with A, B, respectively, substituted for the subscripts and superscript F. The form of T in the integrand of equation (4.22) will be that of equation (3.74), (3.75) respectively, for parabolic forms of the barriers.

With this specialised form for T in the integrand of (4.22), the expression can be reduced to a form suitable for simple approximation by adoption of the constant temperature level density relation

$$\rho^{(F)}(U, J^\pi) = \frac{(2J+1)}{2} \exp\left[-\frac{(J+\frac{1}{2})^2}{2\sigma^2}\right] \rho^{(F)}_{eff}(U) \qquad (4.24a)$$

$$\rho^{(F)}_{eff}(U) = C_F e^{U/\theta_F} \qquad (4.24b)$$

(where U is the effective excitation energy relative to the barrier) and suitable expansions for the tunnelling factor of equation (4.22). In this way it is deduced that

$$T_{J^\pi(f)} = \frac{(2J+1)\, e^{-(J+\frac{1}{2})^2/2\sigma^2}}{2} \theta_F C_F \left\{ \left[e^{(E-V_F)/\theta_F} - 1 \right] + 2e^{(E-V_F)/\theta_F} \left(\frac{\hbar\omega_F}{2\pi\theta_F}\right)^2 \left[\frac{\pi^2}{12} + \cdots\right] + \left[\sum_{n=1}^{n_{cut}} (-)^{n+1} \frac{\hbar\omega_F}{2\pi n\theta_F + \hbar\omega_F} e^{-2\pi n(E-V_F)/\hbar\omega_F} + \cdots\right] \right\} \qquad (4.25)$$

for $E - V_F > 0$. The terms neglected in the second square bracket of the right-hand side are of order $(\hbar\omega_F/2\pi\theta_F)^4$ and higher, and those neglected in the third square bracket are those left after cutting the summation at $n = n_{cut}$. For $E - V_F < 0$

$$T_{J^\pi(f)} = \frac{(2J+1) e^{-(J+\frac{1}{2})^2/2\sigma^2}}{2} \theta_F C_F \sum_{n=1}^{\infty} (-)^{n+1} \frac{\hbar\omega_F}{2\pi n\theta_F - \hbar\omega_F} e^{2\pi n(E-V_F)/\hbar\omega_F} \qquad (4.26)$$

More drastic modification to the transmission coefficient is required for energies below the barrier where the class-II resonances do not overlap (55). We consider first the case in which the class-II resonance widths encompass many class-I level spacings. Then a local fission transmission coefficient can be defined (from equation 3.109),

$$T_f = \frac{2\pi \Gamma_{\lambda(f)}}{D} = \frac{\Gamma_{\lambda_{II}(c)} \Gamma_{\lambda_{II}(f)}}{(E_{\lambda_{II}} - E)^2 + \frac{1}{4}\left(\Gamma_{\lambda_{II}(c)} + \Gamma_{\lambda_{II}(f)}\right)^2} \qquad (4.27)$$

for an energy interval small compared to the class-II state width. This is to be substituted into the expression for the fission probability

$$P_f = \frac{T_f}{\sum_{c'} T_{c'}} \qquad (4.28)$$

giving

$$P_f = \frac{D_{II}^2}{4\pi^2} \left(\frac{T_A T_B}{T'}\right) \left[(E_{II} - E)^2 + \frac{D_{II}^2}{4\pi^2} \left(\frac{T_A T_B}{T'} + \frac{(T_A + T_B)^2}{4} \right) \right]^{-1} \qquad (4.29)$$

where $T_A = \dfrac{2\pi\, \Gamma_{\lambda_{II}(c)}}{D_{II}}$, $T_B = \dfrac{2\pi\, \Gamma_{\lambda_{II}(f)}}{D_{II}}$

and $T' = \sum_{c' \neq f} T_{c'}$

(For narrow class-II resonances $\Gamma_{\lambda_{II}} \ll D_{II}$, T_A and T_B can be equated to the barrier transmission expressions in equations 3.74, 3.75.) This is a local fission probability with Lorentzian form. If it is averaged over the level spacing D_{II} we obtain the expression to be used in statistical theory:

$$\bar{P}_f = \frac{1}{\pi} \frac{T_A T_B}{T'} Y \arctan(\pi Y) \qquad (4.30a)$$

$$Y = \left(\frac{T'}{T_A T_B + \frac{1}{4} T' (T_A + T_B)} \right)^{\frac{1}{2}} \qquad (4.30b)$$

For a sequence of uniform class-II levels the averaged fission probability is

$$\bar{P}_f = \left\{1 + \left(\frac{T'}{T_{eff,f}}\right)^2 + 2\left(\frac{T'}{T_{eff,f}}\right)\coth\left[\tfrac{1}{2}\left(T_A + T_B\right)\right]\right\}^{-\frac{1}{2}} \qquad (4.31)$$

The large differences that can transpire between the results given in equation (4.30) and the statistical theory result that contains the implicit assumption of overlapping class-II levels,

$$P_f = \frac{T_{eff,f}}{T_{eff,f} + T'} = \frac{T_A T_B}{T_A T_B + T'\left(T_A + T_B\right)} \qquad (4.32)$$

are shown in Fig. 33.

When the class-II resonances become even narrower than the class-I level spacing, the departure from the statistical expression becomes even greater. This is because the quasi-class-II state carrying the bulk of the class-II fission width has an anti-correlated entrance channel width. The relevant expressions can be obtained from the perturbation theory developed in Section 3.4.5.3, and are given in ref. (55). The effect is illustrated in Fig. 34.

4.4 Level densities for statistical transmission coefficients

4.4.1 Remarks on the independent-particle model

The above "gross" transmission coefficients depend strongly not only on barrier heights, if they exist, but also on the magnitude of the level density and its dependence on energy. All the level density factors appearing in the above expressions are different. The neutron scattering and radiative coefficients differ in the level density factor through the kind of nucleus (number of nucleons) but the deformation will be similar; in these cases the level density behaviour is quite well-known. The level density factor for fission depends on a quite different concept - the density of intrinsic states at the deformation of the barrier.

The methods for calculating level density have been described by Ramamurthy in his lectures at this Winter School. Here most of my remarks will be concerned with the extension of these concepts to the strong deformations associated with the fission barrier. Modern theory and computational methods for level density are based on the picture of build-up of independent-particle states from superpositions of excited quasi-particles, which are the states in the region of the Fermi level occupied by single nucleons not involved in the correlated motion caused by the pairing interaction. The main effect of the pairing interaction in modifying the structure of the single quasi-particle levels is to introduce an energy gap denoted by 2Δ, the magnitude of which is proportional to the density ρ_s of single particle states at the Fermi energy as well as to the strength of the pairing force. In even nuclei no states of single-particle character appear within the energy gap; immediately above the gap two-quasi-particle states are found. In odd-mass nuclei, single-quasi-particle states are found within the energy gap, but at the top of the gap there is a sudden increase in density as three-quasi-particle states appear. At a sufficiently high excitation energy (believed to be several MeV) sufficient single-particle orbitals in the vicinity of the Fermi energy are occupied by single quasi-particles that a pair-correlated state cannot be formed (the blocking effect). Above this energy the density of independent-particle states is calculated from the simple single-particle state energies, rather than from the modified quasi-particle state energies. However, excitation energies are calculated from the ground state of the correlated system, and this is estimated to be an amount $\frac{1}{4}\rho_s\Delta^2$ below the energy of an equivalent true independent-particle system. Consequently, the effective excitation energy to be used in the independent-particle model calculation is to be reduced below the true excitation energy by this amount.

The discussion of the density of states in the above-outlined independent-particle model can be based on the expression for the level density of the Fermi-gas, an idealisation of the independent-particle system. The form of the Fermi-gas expression as a function of effective excitation energy is

$$\rho(U, J^\pi) = \frac{(2J+1)e^{-(J+\frac{1}{2})^2/2\sigma^2}}{4\sigma^3\sqrt{2\pi}}\,\rho(U) \qquad (4.33a)$$

$$\rho(U) = \frac{\sqrt{\pi}}{12}\,\frac{e^{2\sqrt{aU}}}{a^{\frac{1}{4}}\,U^{5/4}} \qquad (4.33b)$$

$$\sigma^2 = 0.0888\,a\,t\,A^{2/3} \qquad (4.33c)$$

$$t = \sqrt{U/A} \qquad (4.33d)$$

$$a = \pi^2\rho_s/6 \qquad (4.33e)$$

Here the quantity ρ_s is the density of single-particle states in the region of the Fermi energy of the nuclear system (with mass number A). The predominant Fermi-gas parameter a governing the exponential-type rise of the level density with excitation energy is proportional to ρ_s.

We are thus led to a first intuitive expectation of the level density at the barrier deformations compared with those of normally-deformed nuclei. It will be remembered that the Strutinsky shell correction term is dependent on the same density of single-particle

states at the Fermi energy, being a minimum when ρ_s is low and maximum when ρ_s is high. Consequently at the barrier deformations (both inner and outer) ρ_s, hence a, will be high, and the level density of intrinsic excitations at moderate to high excitation energies is expected to be correspondingly higher than for normal deformations.

Detailed calculations [56,57] do not confirm this expectation. For moderate excitations the barrier densities are found, if anything, to be slightly lower than the normal level density. The reason is the role played by the energy gap. This is increased for the barrier deformations and the effective excitation energy is thereby decreased. It also appears that in the lower energy region where the correlated pair motion is of fundamental importance, the energy variation of the Fermi-gas form is too extreme; a simple exponential form, as already used in the derivation of expressions for the total fission transmission coefficient, equation (4.24), is a closer approximation,

$$\rho(E,J^\pi) = \frac{(2J+1)}{2}\, e^{-(J+\frac{1}{2})^2/2\sigma^2}\, \rho_{eff}(0)\, e^{E/\vartheta} \qquad (4.34)$$

4.4.2 Rotational states

The independent-particle model, however, does not contain the entire spectrum of excited nuclear levels. It is well-known that collective states, vibrations and, especially, rotations predominate at low excitation energies and are believed to persist in importance to energies of at least several MeV. Although their description ultimately must be in terms of individual particle degrees of freedom the current theoretical interpretation of this description is that it involves excited single particle states from energies well above the first few MeV of excitation. In this energy range therefore these collective states involve extra degrees of freedom other than those involved in the independent-particle states. The latter, therefore, are to be taken as the band-heads for groups of rotational states when calculations are made of the level densities of deformed nuclei; the deformation removes the magnetic sub-state degeneracy (the total angular momentum of an independent-particle state is no longer a good quantum number), and, for a cylindrically symmetric nucleus the projection of the independent-particle spin on the axis of symmetry gives the K-value of the band-head. Since the wave-functions of these band-head states are constructed from symmetric top functions of both positive and negative K to give correct invariance properties, the density obtained from the calculation of independent-particle state density must finally be divided by two (except in the case of K = 0, but this point is ignored below).

The K-dependence of the band-head states is not given explicitly in these level density theories but it is generally assumed to be Gaussian in nature with maximum probability at zero:

$$\rho_{BH}(U,K) = \frac{2\,\rho_{BH}(U)}{\sigma_K\sqrt{2\pi}}\, e^{-K^2/2\sigma_K^2} \qquad (4.35)$$

(zero or positive K values only, on the assumption of cylindrical symmetry). Examination of the Nilsson model of single particle schemes in the actinide region indicates that for single-particle neutron levels $\sigma_K^{(N)} \approx 3.5$ and for single particle proton levels $\sigma_K^{(K)} \approx 3$, giving an average value $\sigma_K \approx 3.25$. This will be the band-head dispersion coefficient for odd-A nuclei below the energy gap excitation level of 2Δ, but in the region of 2Δ above the energy gap it will tend to $\sqrt{3}$ times this value (3p-2h states) and to $\sqrt{5}$ times 3.25 in the subsequent energy region in a pure independent particle picture. An odd nucleus will be expected to have $\sigma_K \approx \sqrt{2} \times 3.25$ in the lowest energy region, and $\sigma_K \approx \sqrt{4} \times 3.25$ in the next range, while an even nucleus will have $\sigma_K \approx \sqrt{2} \times 3.25$ in the energy region immediately above the energy gap, and only a very low value contributed by sparse collective vibrational levels (like the gamma-vibration) within the gap itself. Indeed, within the energy gap of an even nucleus it is straining to breaking point the whole concept of a statistical picture to attempt to describe the energy states in this way.

The total density of nuclear states is finally determined by adding to the band-head density the contribution of collective states. The principal component of the latter comprises the rotational states, and in this report collective states of other kinds are neglected. Thus, the density of states of angular momentum I is

$$\rho(U,I) = \rho_{BH}(U,K=I) + \sum_{K=K_{min}}^{I-1} \rho_{ROT}(U,K,I) \qquad (4.36)$$

where $K_{min} = 0$ or $\frac{1}{2}$ depending on the odd-even character of the nucleus, and

$$\rho_{ROT}(U,K,I) = \rho_{BH}\left[U - \{I(I+1) - K(K+1)\}\frac{\hbar^2}{2\mathcal{J}},\ K\right] \qquad (4.37)$$

where $\mathcal{J}$ is the effective rotational moment of inertia of the nucleus about an axis perpendicular to the cylindrical symmetry axis. If the band-head density has the simple exponential dependence of equation (4.34) then we obtain

$$\rho(U,I) = \frac{2C e^{U/\vartheta}}{\sigma_K\sqrt{2\pi}}\, e^{-I(I+1)\hbar^2/2\mathcal{J}\vartheta} \sum_{K=K_{min}}^{I} e^{K^2\left(\frac{\hbar^2}{2\mathcal{J}\vartheta} - \frac{1}{2\sigma_K^2}\right) + K\hbar^2/2\mathcal{J}\vartheta} \qquad (4.38)$$

For small values of the coefficients $(\hbar^2/2\mathcal{J}\vartheta - 1/2\sigma_K^2)$ (compared with I^{-2}) and $\hbar^2/2\mathcal{J}\vartheta$ (compared with I^{-1}) this expression tends to the form

$$\rho(U,I) \approx (2I+1)\, e^{-I(I+1)/2\sigma^2}\, \rho_0(U) \qquad (4.39a)$$

where $$\sigma = \left(\mathcal{J}\Theta/\hbar^2\right)^{\frac{1}{2}} \qquad (4.39b)$$

and $$\rho_o(U) = \frac{C}{\sigma_K\sqrt{2\pi}}\, e^{U/\Theta} \qquad (4.39c)$$

As explained above, σ_K increases with energy and if its value at low energies is inserted here, its overall (smoothed) energy variation being included in the exponential, there will be a temperature increase of about 7%. The actual departure of the K-summation term of equation (4.38) from the value of (2I+1)/2 can be offset to some extent by modifying the spin dispersion coefficient σ of equation (4.39). For example, for $\hbar^2/2\mathcal{J}$ = 7.5 keV, Θ = 0.5 MeV, σ_K = 4.6, the effective spin dispersion coefficient is modified from its rotational value $(\mathcal{J}\Theta/\hbar^2)^{\frac{1}{2}}$ = 5.77 to a value of about 5.3. A set of effective σ values, evaluated for angular momentum I ≈ 13/2, is given in Table 5.

The semi-quantitative estimates of level density of the actinides from pairing correlation theory (58), adjusted to observed low-lying band-head states of odd-A nuclei, like ^{235}U and ^{234}Pu are:

(i) for odd-A nuclei

$$\rho_o(E) \approx 1.8 e^{E/\Theta}, \quad (E > 2\Delta) \qquad (4,40a)$$

$$\sigma \approx 4.1 + 1.2E \qquad (4.40b)$$

(ii) for even nuclei

$$\rho_o(E) \approx 0.45 e^{E/\Theta}, \quad (E > 2\Delta) \qquad (4.41a)$$

$$\sigma \approx 3.4 + 1.2E \qquad (4.41b)$$

(iii) for odd nuclei

$$\rho_o(E) \approx 7.5 e^{E/\Theta} \qquad (4.42a)$$

$$\sigma \approx 4.8 + 1.2E \qquad (4.42b)$$

with $\Theta \approx 0.44$ MeV.

For the values of moment of inertia and temperature met with in practice for the actinide nuclei, the addition of the rotational states as developed above provides a considerable enhancement factor to the total level density, but further increase of the moment of inertia with increasing prolate deformation will not in itself give any significant increase in this rotational enhancement. In fitting fission cross-section data to statistical theory expressions it has been observed (59) that an extra enhancement factor of between 2 and 5 is required on the barrier densities to explain the overall magnitudes of the cross-sections. The larger factor appears to be appropriate to the inner barrier A and the smaller to the outer barrier B.

The cause of this extra enhancement factor has been explained as further deviation of the nuclear shape from a symmetric form at the barrier deformations (60). The outer barrier is the simpler to consider. Calculations of the energy of deformation using the Strutinsky method indicate that at the outer barrier reflection asymmetric shapes are energetically favoured. The result of this is that for any rotational band-head state a whole rotational band of opposite parity becaomes possible, thus doubling the level density. For the inner barrier the Strutinsky calculations indicate, generally, that axial symmetry is lost although reflection symmetry is retained. In this case the nucleus can rotate about the three principal axes of the ellipsoidal shape. The enhancement factor over the level density of the axially symmetric shape is expected to be $\sigma_K(\pi/2)^{\frac{1}{2}}$ which is numerically ≈ 4.

4.4.3 Experimental data on level densities

In some analyses of fission data using the statistical model the level density behaviours involved have been purely theoretical ones, based on the independent-particle model as described above (56), with rotational enhancement factors introduced at later stages of the work (61); the single-particle states required for such models have also been drawn from theoretical calculations. The opposite philosophy is to draw the level density behaviour from observation as far as possible, and hopefully to understand its main features from theory. This is the approach adopted in ref. (59) and described here.

For level densities of the normally deformed nuclei the basic expressions adopted follow the lines recommended by Gilbert and Cameron (62). Above a specified energy E_{IP} the Fermi-gas formulation, equation (4.38), is adopted and the dominant parameter a is, usually, fixed by observations of neutron resonance spacings. To account for residual odd-even effects in these spacings the effective excitation energy is adjusted to U = E-P(Z)-P(N). The P-factors are drawn from the compilation in ref. (62). Below E_{IP} the constant temperature form, equation (4.34), is adopted, but below the energy gap 2Δ, taken to be 1.2 MeV, for even and odd-A nuclei, a simple constant value is adopted as being more realistic. The parameters for the constant temperature form are based on the semi-theoretical estimates given in equations (4.40) to (4.42), but with modified numerical parameters.

The numerical modifications consist of replacing the energy dependent spin dispersion coefficient by a simple constant evaluated from equations (4.40b), (4.41b), (4.42b) at an excitation energy between 2Δ and 3Δ. The reason for this is that this coefficient would otherwise be considerably greater than the value given by equation (4.33) of the independent particle model at the transition energy, E_x, between the two forms. In addition, the temperature Θ is increased to at least

0.5 MeV. This second adjustment is necessary for two reasons. Firstly, with the lower temperature the level density rises too fast to meet the independent particle formula; indeed, equations (4.40) to (4.42), extrapolated into the neutron resonance region, give much smaller resonance spacings than any observed. Secondly, detailed calculation of the capture cross-sections of ^{238}U and ^{232}Th up to neutron energies greater than 3 MeV and the capture gamma-ray spectra of these nuclei demand temperatures of 0.5 MeV to reproduce the available experimental data; in this analysis the model of the electro-magnetic transition process is important, and for this the giant dipole resonance model of Brink (86) was chosen. A temperature of 0.5 MeV is adopted in ref. (59) whenever this allows the simple constant temperature model to meet the independent particle formulation at an energy, E_x, below the neutron separation energy of the nucleus concerned. When this does not occur the temperature is adjusted to reproduce the observed neutron resonance spacing. Among the actinides, the highest temperature required by this procedure is 0.544 MeV for ^{247}Cm.

At the excitation energies at which neutron resonances are found it is normally assumed that the independent particle model of level densities is valid, and hence the neutron resonance data are used to determine the Fermi-gas parameter, a.

At the lowest excitation energies a simple extrapolation of the constant temperature level density form is generally inappropriate to allow reliable calculations of inelastic scattering transmission coefficients at low to moderate incident neutron energy. It is particularly important for such calculations that the local trends and jumps associated with the energy gap at 2Δ are reproduced reasonably accurately by the level density formulation adopted. A simple first approach is to choose, for even and odd-mass nuclei, a constant level density within the energy gap, 2Δ, the numerical value of which is normally taken to lie between 1.0 and 1.2 MeV for normally deformed actinides. The value of this constant level density can be evaluated from low-lying level spectra. For even nuclei, the data indicate $\rho_{eff} \approx 0.5$ MeV^{-1}, $\sigma \approx 4$. For odd-mass nuclei, $\rho_{eff} \approx 1.25$ MeV^{-1}, $\sigma \approx 4.5$. For odd nuclei the rather sparse level spectra available indicate that extrapolation of the constant temperature form down to zero excitation energy is a reasonably valid procedure.

5. COMPUTER CODES FOR CALCULATING AVERAGE CROSS-SECTIONS

5.1 Introduction

This section is not intended to be a review of available computer codes that exploit, for the fission channels, the theory that includes the effects of the double-humped fission barrier; unlike other families of codes for cross-section calculations, such as optical model codes, such fission codes are not generally available. Here I shall only describe in general terms a few of my own computer codes for fission problems. These are not yet in a form in which they can be released for general use, but I hope to be able to make them generally available in the not too distant future.

The first code described is FISRA; with it the fission probability is calculated for the case in which the only competition comes from radiative de-excitation. For somewhat higher excitation energies at which competition can also come from neutron emission through a limited number of channels, fission and other cross-sections can be calculated using the code AVXC. At higher energies still, or for other cases in which only statistical knowledge of de-excitation channels is available, or for cases in which partial or complete cascades of de-excitation particles or gamma-rays must be followed the fission probability, or probability for other processes, can be calculated with the code EVAPF. In all three of these codes the fission transmission coefficient is calculated according to the principles described in Section 4.3.3.

5.2 The code FISRA

This code calculates the fission probability for decay of the compound nucleus when there is competition only between fission and radiative decay. Since the latter process is weak there is effective competition from it only at sub-barrier energies, at which the fission transmission coefficient, $T_f = 2\pi\overline{\Gamma_{\lambda(f)}}/D$ is effectively modulated by the intermediate class-II structure. This modulation has an important effect on the calculation of the fission probability P_f as described in Section 4.3.3. The basic formula employed by the code is equation (4.30).

The physical cases for which this code is likely to be of most value are those of fissioning even compound nuclei at sub-barrier energies, so the code embodies simple structural models for these cases. The relevant compound nuclei will usually be excited by particle transfer reactions, such as (d,p) or (t,p), causing a considerable range of angular momentum states to be populated. To allow for this a rotational model for the transition states at the barrier is adopted i.e. for each component of angular momentum J the effective barrier energies to be adopted in equation (4.30) are

$$V_A(J) = V_A(0) + \frac{\hbar^2}{2\vartheta_A} J(J+1) \qquad (5.1a)$$

$$V_B(J) = V_B(0) + \frac{\hbar^2}{2\vartheta_B} J(J+1) \qquad (5.1b)$$

The weightings for each angular momentum component (i.e. fraction of compound nuclei formed with angular momentum J) and the moments of inertia ϑ_A, ϑ_B are input quantities to the program, the latter being entered in the form $\hbar^2/2\vartheta_A$, $\hbar^2/2\vartheta_B$. The basic barrier quantities $V_A(0)$, $\hbar\omega_A$, $V_B(0)$, $\hbar\omega_B$ are also input parameters.

The radiative transmission coefficient T_γ is assumed to have the form

$$T_{\gamma(J)} = T_{\gamma(0)}(0)(2J+1)e^{-J(J+1)/2\sigma^2} e^{E/\theta} \qquad (5.2)$$

that would follow, as the leading term, from a constant temperature level density form for the residual states, such as equation (4.34). The values of the constants $T_{\gamma(o)}(0)$ and the level density parameters σ, Θ are chosen from an appropriate model for the radiative emission process and adjustment to experimental data, as described in Section 6. These are input data.

Two options are also available. The behaviour of the code as outlined above calculates the fission probability on the assumption of complete damping of the vibrational states of the second well. One option available in the code is a schematic damped vibrational model. This is introduced through the following sequence of equations, introduced into equation (4.30) for each J component:

$$T_A = \sum_{n=1}^{n_v} \frac{\Gamma_{v(D)}\,\Gamma_{v(A)}}{(E-E_v)^2 + \frac{1}{4}\left(\Gamma_{v(D)} + \Gamma_{v(A)} + \Gamma_{v(B)}\right)^2} \qquad (5.3a)$$

$$T_B = \sum_{n=1}^{n_v} \frac{\Gamma_{v(D)}\,\Gamma_{v(B)}}{(E-E_v)^2 + \frac{1}{4}\left(\Gamma_{v(D)} + \Gamma_{v(A)} + \Gamma_{v(B)}\right)^2} \qquad (5.3b)$$

$$E_v(J) = E_{II} + \left(n-\tfrac{1}{2}\right)\hbar\omega_{II} + \frac{\hbar^2}{2\mathcal{J}_{II}} J(J+1), \quad (n = 1,2 \ldots n_v) \qquad (5.3c)$$

$$\Gamma_{v(A)} = \frac{\hbar\omega_{II}}{2\pi} \frac{1}{1 + \exp\left[-\frac{2\pi(E-V_A)}{\hbar\omega_A}\right]} \qquad (5.3d)$$

$$\Gamma_{v(B)} = \frac{\hbar\omega_{II}}{2\pi} \frac{1}{1 + \exp\left[-\frac{2\pi(E-V_B)}{\hbar\omega_B}\right]} \qquad (5.3e)$$

$$\Gamma_{v(D)} = \Gamma_{(D)} \qquad (5.3f)$$

The quantities E_{II}, $\hbar\omega_{II}$, $\frac{1}{2}\Gamma_{(D)}$, $\hbar^2/2\mathcal{J}_{II}$ and n_v are all program input.

The second option is the introduction of Porter-Thomas statistics for the class-II fission and coupling widths. This is done on a purely numerical basis. Mean values of T_A and T_B are calculated as above (either option). Individual values of T_A and T_B appropriate to a local class-II level are obtained by independent random sampling from the Porter-Thomas distribution and substituted into equation (4.30). This is repeated a large number of times (100 times in the standard version of the code, but this can be very simply changed), and the resulting values of P_f are averaged.

The calculation can be carried out for a sequence of energy values spaced by a specified interval. An example of the calculated results is given in Fig. 35.

5.3 The code AVXC

The code AVXC is designed to calculate neutron cross-sections for all specified channels on the basis of Hauser-Feshbach theory as outlined in Section 4.2. It is suitable for use when the detailed properties (intrinsic excitation energy, angular momentum, parity) of all energetically available channels (including deformation channels) are known or can be inferred from principles of nuclear structure. The neutron energy is a specified input to the calculation, and is re-specified for every energy value for which the calculation is required. At each neutron energy the total radiation width (assumed independent of angular momentum) is also specified. This is converted into the radiation transmission coefficient $T_{\gamma J} = 2\pi\Gamma(\gamma)/D_J$. The level spacing D_J is obtained from that for zero angular momentum and neutron energy (an input quantity) by extrapolation, using the level density expression, (4.33); for this the level density parameter, a, and spin dispersion coefficient σ are specified.

For inelastic neutron channels the cross-section has the form

$$\sigma_{nn'} = \pi\lambda^2 \sum_J g(J,I) \sum_{s=|I-\frac{1}{2}|}^{I+\frac{1}{2}} \sum_{\ell=|J-s|}^{J+s} \sum_{s'=|I'-\frac{1}{2}|}^{I'+\frac{1}{2}} \sum_{\ell'=|J-s'|}^{J+s'} \frac{T_{n(J^\pi;\ell s)}\, T_{n'(J^\pi;\ell' s')}}{\sum_c T_{c(J^\pi)}} \delta_{nn'} \qquad (5.4a)$$

$$g(J,I) = \frac{(2J+1)}{2(2I+1)} \qquad (5.4b)$$

where I (an input quantity) is the spin of the target nucleus, the total angular momentum J ranges over all integer or half-integer values, whichever is appropriate to the nature of the compound nucleus, but a practical upper limit of the order of 10 is set in the code, s is the entrance channel spin, s' the exit channel spin, ℓ the entrance channel orbital angular momentum, ℓ' the exit channel orbital angular momentum, and I' (input quantity) is the angular momentum of the state of the residual nucleus reached after inelastic neutron emission. The parity π of the compound nucleus is determined by the

parity π_I of the target nucleus and the orbital angular momentum of the entrance channels

$$\pi = (-1)^{\ell} \pi_I \qquad (5.5)$$

Since the parity $\pi_{I'}$ of the residual state is fixed (another input quantity) the possible values of orbital angular momentum in the exit channel ℓ' are controlled by this, i.e.

$$\pi_{I'} = (-1)^{\ell'} \pi \qquad (5.6)$$

The numerical values of the transmission coefficients are calculated from equation (4.3), the values of the strength-function $\gamma^2_{(n')}/D$ being input quantities; in the present version of the code these are dependent only on the orbital angular momentum of the neutron channel, there being one value for even values of ℓ' and another for odd values. The penetration factors $P_{\ell'}$ of equation (4.3) are calculated from the standard R-matrix expressions (45) a channel radius (suitable for the actinides) of 9 fm being builtinto the code, and the neutron energies required are calculated from the initial neutron energy and the specified energies of the states of the residual nucleus.

For fission channels, too, the total angular momentum and parity must be specified, as well as the intrinsic excitation plus barrier energy (relative to the neutron separation energy of the compound nucleus) for each barrier. In addition, the barrier penetrability parameters $\hbar\omega_A$, $\hbar\omega_B$ are to be specified for each channel, these quantities being allowed to vary from channel to channel. One difficulty with calculations that include fission in Hauser-Feshbach theory is that there is no true threshold for the opening of a fission channel, only a barrier. Thus there is no definite cut-off in the number of channels that should be included in the calculation, and, of course, our knowledge of the channel properties, already mainly theoretical even for the lowest channels, can only be statistical at best. Fission channels (of given J^{π}) that cannot be explicitly described and have energies close to or somewhat higher than the neutron energy stipulated for the calculation are therefore lumped together to form a single effective channel the strengh of which is calculated from the leading term of equation (4.26 or (4.25), and the energy of which is based on the expected spacing of the low-lying barrier states (this is an input quantity for J = 0, and is adjusted for higher J according to the usual spin-dependent factor given in equation (4.33a)). The barrier A level density constant (C_F of equation (4.24)) and temperature (Θ_F) are input quantities, while the barrier B density is assumed to be half the A density. These effective channels are not intended to have any more significance than correction factors, so for simplicity the code calculates one effective channel, according to the above prescription, for each specific channel that is entered.

The transmission coefficients across each barrier for the deformation channel are calculated in the form,

$$T_{A,B} = 2 p_{A,B} s_{A,B} \qquad (5.7)$$

where the "penetration" factors $p_{A,B}$ have the Hill-Wheeler form (3.74), (3.75), and the strength functions $s_{A,B}$ normally have the value 0.5 for strong-damping of the class-II vibrational modes, but can be written in a damped (or pure) vibrational form through use of a subroutine FISST.

Cross-sections are calculated by the program, both with and without the effect of fluctuations in the resonance partial widths. In the latter case the procedure for calculating corss-sections from the transmission coefficients is straightforward. The summed values (for given J^{π}) of both T_A and T_B over all deformation channels are taken, and the value of the fission probability P_f is calculated from equation (4.31). This is multiplied into the compound nucleus formation cross-section to obtain the fission cross-section,

$$\sigma_{nf} = \pi \lambda_n^2 \sum_J g(J,I) \sum_{s=|I-\frac{1}{2}|}^{I+\frac{1}{2}} \sum_{\ell=|J-s|}^{J+s} T_{n(J,\ell)} P_{f(J^{\pi})} \qquad (5.8)$$

This quantity is printed in the output as 'Total fission, with class-II structure'.

Alternatively, and more crudely, but necessarily in the present version of the program, the total fission transmission coefficient T_f is constructed from the summed values of T_A and T_B using equation (4.23); this is required for calculation of the inelastic and radiative capture cross-sections by equation (5.4).

In the case that includes fluctuations the procedure is not so clear, because, in addition to the Porter-Thomas fluctuations of resonance fission widths about the local expected value, the latter quantity is modulated by the intermediate structure at sub-barrier energies. This in turn is affected by Porter-Thomas fluctuations of the class-II level parameters. The code does not attempt to deal with all these complications exactly, but includes fluctuations on an over-simplified basis, so that, by comparison with the cross-sections calculated without fluctuations the likely importance of the fluctuation effect can be ascertained.

Let us first consider the likely physical situations that will be dealt with by the code. First of all there are nuclei, like the even actinide targets, which are fissionable but not fissile; the fission barrier is at a comparatively high neutron energy. At low neutron energies fission widths even near the centre of class-II resonances will normally be small compared to neutron widths. Hence it will be a reasonable approximation to use equation (4.23) rather than (4.31) to obtain the average fission cross-section. At the higher neutron

energies closer to the barrier fission widths will be increasing rapidly, but at these energies total resonance widths (including inelastic neutron widths) will still probably be larger, so equation (4.23) will still probably be a good approximation. Above the barrier the class-II resonance widths will approach the class-II spacing in value, and equation (4.23) is correct in any case. For fissile nuclei, all neutron energies are usually well above the barrier and equation (4.23) will apply.

For the purpose of the fluctuation calculation the class-II modulation effect is therefore ignored. If now the fission channels can be ordered in an obvious hierarchy of strength, fission through the first being much stronger than that through the second and so on, the transmission coefficient can be written, very approximately, as a sequence,

$$T_{f,eff} \approx \sum_{\mu} T_{f,\mu} = \sum_{\mu} \frac{T_{A_\mu} T_{B_\mu}}{T_{A_\mu} + T_{B_\mu}} \qquad (5.9)$$

provided also that either $T_{A\mu} \gg T_{B\mu}$ or $T_{B\mu} \gg T_{A\mu}$, for all μ. In the code the individual $T_{B\mu}$ are formed for all channels and these are then treated in the Hauser-Feshbach calculation with fluctuations in the same way as the particle channels (equation (5.4)):

$$\sigma_{nf} = \sum_{\mu} \sigma_{nf,\mu} = \pi\lambda^2 \sum_{J} g(J,I) \sum_{s=|I-\frac{1}{2}|}^{I+\frac{1}{2}} \sum_{l=|J-s|}^{J+s} \frac{T_{n(J,l,s)}\, T_{f,\mu(J^\pi)}}{\sum_c T_{c(J^\pi)}} \delta_{n\mu} \qquad (5.10)$$

The calculation of the fluctuation factors δ is done by simple numerical integration of the one-dimensional integral to which δ can be reduced for Porter-Thomas distributions (see e.g. ref. [53] p.329).

An example of cross-section curves calculated by AVXC is shown in Fig. 36. The parameters for the calculation are shown in Table 6.

5.4 The code EVAPF

This code is of much more general use than AVXC. It can be used not only to calculate cross-sections but also to calculate spectra of emitted neutrons and gamma-rays. It can be used to calculate cross-sections to much higher energy than AVXC because it is based on statistical concepts of level density rather than detailed specification of the energy levels, but on the other hand it is limited in its precision at low (neutron) energies because it cannot (in its present form) exploit precise information on level structure when it is available, and (in aiming at calculations in which large numbers of levels are normally involved) it does not include the effects of width fluctuations.

The excitation energy scales of the compound nucleus and of the residual nucleus following neutron scattering are divided into constant energy intervals (bins) of width ΔE. The initial compound nucleus (at a given energy of excitation E^*) is started, in the code, within the appropriate energy interval. The total angular momentum and parity of the initial compound nucleus are also specified. An available option is to specify a range of spin and parity, together with the population of each spin-parity combination. The populations are not required to sum to unity; they can, for instance, be the compound nucleus formation cross-sections for each spin-parity, in which case the final results of the calculations are automatically cross-sections for the various decay processes considered.

For each energy-spin-parity bin the partial widths for transitions to all lower energy bins (with individual spin-parity labelling) are calculated. These comprise neutron emission channels (over a range of orbital angular momentum, which is cut off when the penetration factor becomes excessively weak), and electromagnetic radiation channels. A choice of model is available for the latter, for electric dipole transitions either the strong-coupling dipole (SCD) model (see Section 6) or the giant dipole resonance model (GDR) being available. Magnetic dipole and electric quadrupole transitions can also be included (as an option), the simple SCD model being used for these. All these partial widths are calculated by means of the subroutine GAMMT, which finally sums them. In this subroutine individual partial widths are calculated for a final state at the centre of the residual bin $E^* - n\Delta E$ where n is an integer. This is then multiplied by the number of final states within the bin, calculated from the bin width ΔE multiplied by the level density at $E^* - n\Delta E$. The level density is computed by means of the subroutine LEVD. The summed partial widths to each residual bin are stored for further use.

The probability of fission from the initial bin at E^* is also calculated. This is done on the basis of equation (4.31), the transition probabilities for the two barriers being calculated from equations (3.74, 3.75) (the strong damping model). These transition probabilities are calculated by the subroutine GHIF. The density of states at the barrier deformations required for these calculations are also calculated by LEVD, but start from a different entry point LEVD2. The population of the bin at E^* that decays by fission is thus calculated (by multiplying the initial population by the fission probability) and is registered as part of the final output. The population remaining (for decay by neutron and gamma-emission) then replaces the initial population.

At this point the populations in the lower energy bin resulting from the neutron and radiation decay processes from the energy E^* are calculated (multiplication of the initial population after fission by the ratio of the sum of partial widths to the residual bin and the total width). The code then moves on (if required) to the calculation of the decay of the bins with central energy $E^* - \Delta E$, using the same process as above, and can subsequently proceed to the decay at $E^* - 2\Delta E$, and so on, as far down the chain as desired; this is controlled by input of a simple integer at the start of the programme.

From the stored results of the calculation the emission probabilities and the spectra of emitted neutrons and gamma-rays can be printed out. These can be partial or total spectra. For example if

the chain is cut after the de-population of the initial bin at E^* is calculated, the spectra calculated are simply primary spectra. If the calculation is continued to below the neutron separation energy, the total neutron spectrum, including those neutrons emitted in the $(n,\gamma n')$ reaction, is available. If the chain of de-population is completed (to zero energy in the compound nucleus) the total capture gamma-ray spectrum becomes available. Details of special two-stage reactions are also calculated. The $(n,\gamma n')$ reaction has already been mentioned, and the spectrum of neutrons from this is retained in memory for subsequent printing out. Likewise the $(n,\gamma f)$ reaction is tracked; in this case it is the spectrum of gamma-rays followed by fission that is printed.

If required the cascade calculation can be made for the residual nucleus resulting from neutron emission in just the same way as for the initial compound nucleus, the initial populations in the energy bins being those that result from the compound nucleus de-decitation.

A schematic flow-chart of the computer code is shown in Fig. 37. Calculated cross-sections from the code are shown in Fig. 38.

6. ANALYSIS OF EXPERIMENTAL DATA TO OBTAIN BARRIER PARAMETERS

6.1 General

In Section 2 the basic theory of nuclear reactions involving fission was set up, and in Section 4 it was used to derive the basic expressions for calculating average cross-sections, through the compound nucleus mechanism, when fission channels are involved. An important set of data for these calculations was seen to be level density data, and the analysis of experimental data to obtain these crucial quantities at normal deformations was also described in Section 4. In the present section the analysis of experimental data is extended to obtain information on the fission barrier parameters.

Relevant experimental data fall into several categories. In the first category are the spontaneous fission half-lives both of ground states and of isomers. These give information on barrier penetrability and height, but since they presuppose adherence to a specified functional form of barrier over a large range of deformation and also to a well-behaved inertial parameter they are not given any weight in the analysis described here, except as a crude qualitative indication of the barrier penetrability parameters $\hbar\omega_A$ and $\hbar\omega_B$.

In the second category are the data on the excitation of spontaneously fissioning isomers. The functional dependence on excitation energy gives the energy of the isomer, and hence the depth of the secondary well, while the magnitude of the excitation cross-section can be interpreted to give information on the height of the outer fission barrier in the nucleus containing one extra neutron.

The third category of data is the intermediate structure to be found in fission cross-sections. Interpretation of these data to give estimates of barrier heights has already been mentioned (in Section 3).

The fourth category is the fission cross-section data from many different reactions in which the energy resolution is usually quite poor but the range of excitation energy is large and encompasses the barrier region. These give information generally on the greater of the two barrier heights. The computer codes used for analysing such data have been described in Section 5.

6.2 Shape isomer formation yields and excitation functions

Information on the barriers containing the shape isomer, particularly on the outer barrier, can be obtained from the experimental data on the cross-sections for formation of the isomer, and especially from the dependence of such cross-sections on excitation energy. Specifically, it is expected that extrapolation backwards of a sharply rising excitation curve to its threshold point will yield the isomer excitation energy, while the maximum value of the excitation curve, in the case of neutron evaporation reactions, will give information on the relative transmission coefficients (and hence barrier heights) of the inner and outer barriers of the penultimate nucleus in the evaporation process (i.e. that nucleus with one more neutron than that of the shape isomer itself); the drop in yield with further increasing excitation energy ought to be governed by the outer barrier (and its penetrability parameter, $\hbar\omega_B$) of the final nucleus.

6.2.1 Threshold excitation curves from neutron evaporation theory

Most of the experimental data on shape-isomer excitation curves are from neutron evaporation reactions, a highly excited nucleus being formed, usually, from charged particle bombardment, and the isomer results from this after emission of a specified number of neutrons. The relevant widths (or more accurately transmission coefficient) for the last stage neutron evaporation leading to the states in the final nucleus that feed the isomer is expected to be very small in comparison with the total for all other modes of decay. It is then possible to derive simple statistical theory expressions that describe to first-order the expected features of the excitation curve in the neighbourhood of its threshold [64,65]. These are related to the features of (x,n) evaporation reactions first discussed in terms of the statistical theory by Jackson [66].

6.2.1.1 One-neutron evaporation process

In the case of one-neutron evaporation from an initial nucleus of mass number A excited by a mono-energetic reaction to a precise excitation energy E^*, we calculate the transmission coefficient for neutron emission to the residual class-II states (in the nucleus A-1) that can feed the isomer. The density of these states is denoted by $\rho_{II}^{(A-1)}(U,I)$, so the transmission coefficient can be written (from equation 4.13) as

$$T_{n\to II}(E^*) \approx \frac{2m}{\pi\hbar^2}(2J+1)\int_0^{E^*-S_1} d\varepsilon\, \sigma_{n(CN)}(\varepsilon)\,\varepsilon\,\rho_{II,eff}^{(A-1)}(E^*-S_1-\varepsilon) \quad (6.1)$$

where S_1 is the separation energy of a neutron from the nucleus A. If it is assumed that the class-II state density has the simple

(constant temperature Θ_{II}) exponential form (as in equation 4.18), but with an effective excitation energy lower than the total excitation energy in the nucleus A-1 by the isomer excitation energy E_{II} then the integration in equation (6.1) is simply performed to give

$$T_{n\to II}(E^*) \approx \frac{2m\sigma_{inv(CN)}\rho_{II,eff}^{(A-1)}(0)\Theta_{II}}{\pi\hbar^2}(2J+1)\left[\Theta_{II}e^{(E^*-S_1-E_{II})/\Theta_{II}} - (E^*-S_1-E_{II}+\Theta_{II})\right] \qquad (6.2)$$

If the isomer energy is considerably greater than the nuclear temperature Θ for the totality of states in the residual nucleus A-1 then the transmission coefficient to the class-II states will certainly be small. The transmission coefficient for total neutron emission is given in equation (4.19), so the ratio, for excitation energies above the isomer excitation threshold is

$$Y_{II}(E^*) = \frac{T_{n\to II}}{T_{n(tot)}} = \frac{\rho_{II,eff}^{(A-1)}(0)\Theta_{II}^2}{\rho_{eff}^{(A-1)}(0)\Theta^2}\exp\left[-\frac{E_{II}}{\Theta_{II}} + E_1^*\left(\frac{1}{\Theta_{II}} - \frac{1}{\Theta}\right)\right]$$

$$\times\left[1-\left(1+\frac{E_1^*-E_{II}}{\Theta_{II}}\right)e^{-(E_1^*-E_{II})/\Theta_{II}}\right] \qquad (6.3)$$

where $E_1^* = E^* - S_1$. For the simple case of $\Theta_{II} = \Theta$ this function is shown in Fig. 39. By contrast, the excitation function of the ground state of the residual nucleus, on the assumption that it is fed uniformly from all states reached by neutron evaporation and that there are no competing reactions, is simply a step function at the ground state threshold energy.

6.2.1.2 Two-neutron evaporation process

For isomers reached by a two-stage neutron emission process from the nucleus A the population of states excited in the nucleus A-1 by emission of one neutron must first be obtained. From equation (6.1) this is just

$$P_1(\varepsilon_1)d\varepsilon_1 \propto \frac{(E_1^*-\varepsilon_1)\rho_{eff}^{(A-1)}(\varepsilon_1)}{\int_0^{E_1^*} d\varepsilon\,\varepsilon\,\rho_{eff}^{(A-1)}(E_1^*-\varepsilon)}\,d\varepsilon_1 \qquad (6.4)$$

for the probability of exciting states, within the interval of excitation energy $d\varepsilon_1$ at ε_1 in residual nucleus A-1. If now the isomer is fed from a set of class-II states in the residual nucleus A-2 reached after emission of a second neutron as in Fig. 39, and the density of these states is denoted by $\rho_{II}^{(A-2)}(U,I)$, the probability of forming the isomer is

$$Y_{II}(E^*) = \int_{S_2+E_{II}}^{E_1^*} d\varepsilon_1\,P_1(\varepsilon_1)\,\frac{T_{n\to II}(\varepsilon_1)}{T_{tot}(\varepsilon_1)} \qquad (6.5)$$

where the transmission coefficients now refer to the compound nucleus A-1. These expressions can be evaluated readily under the constant temperature assumption. The expression of fullest generality for the isomer yield is

$$Y_{II}(E^*) = \frac{T_{n(tot)}(E^*)\rho_{II,eff}^{(A-2)}(0)}{T_{tot}(E^*)\rho_{eff}^{(A-2)}(0)}\left[\frac{\Theta_{II}^{(A-2)}\Theta}{\Theta^{(A-2)}\Theta^{(A-1)}}\right]$$

$$\times\exp\left[E_2^*\left(\frac{1}{\Theta_{II}^{(A-2)}} - \frac{1}{\Theta^{(A-2)}}\right) - \frac{E_{II}}{\Theta_{II}^{(A-2)}}\right]\left\{1 - \left(1+\frac{E_{II}^*}{\Theta}\right)e^{-E_{II}^*/\Theta} - \left[\frac{\Phi^2}{\Theta^2}\left(1+\frac{E_{II}^*}{\Theta_{II}}\right)\left(1-\left\{1+\frac{E_{II}^{**}}{\Phi}\right\}e^{-E_{II}^*/\Phi}\right)\right.\right.$$

$$\left.\left. - \frac{\Phi^3}{\Theta_{II}\Theta^2}\left(2-\left\{\frac{E_{II}^{*2}}{\Phi^2}+\frac{2E_{II}^*}{\Phi}+2\right\}e^{-E_{II}^*/\Phi}\right)\right]e^{-E_{II}^*/\Theta_{II}}\right\} \qquad (6.6)$$

where $\Theta = (1/\Theta_{II} + 1/\Theta^{(A-1)} - 1/\Theta^{(A-2)})$ and $\Phi = (1/\Theta^{(A-1)} - 1/\Theta^{(A-2)})$, $E_2^* = E^* - S_1 - S_2$, $E_{II}^* = E^* - E_{II} - S_1 - S_2$. The energy relations are shown in Fig. 40. The special case of the yield function when all temperatures are equal is shown in Fig. 39.

The arguments outlined above can be developed further to give the result for isomer excitation following 3-neutron evaporation. A typical calculation, again for all temperatures equal is also shown in Fig. 39.

6.2.1.3 Isomer energies

As apparent from Fig. 39 if the isomer yields are measured to low enough excitation energy an estimate of the isomer energy can be obtained. It is also apparent that the most sensitive estimates will come from single neutron evaporation reactions. Such reactions can only be initiated in practice, for the actinides, by neutron excitation, charged particles being very effectively blocked at such low excitations by the Coulomb barrier. The detection of very low delayed fission yields following neutron bombardment is very difficult experimentally, because of the fission background that can be caused by room-return neutrons. Therefore most of the data on isomer yield curves have come from 2-neutron evaporation reactions initiated by protons and alpha-particles. Some typical data and the fitted curve are shown in Fig. 41.

In spite of the difficulty of the neutron-initiated reactions a few of these have been measured. One example is the (n,n') reaction leading to the shape isomer of ^{238}U (67). In this case the statistical representation of the density of class-II states leading to the result (6.3) above is inapplicable; the spectrum of class-II states for one MeV or so above the isomer is expected to be limited to two rotational bands based on the $K^{\pi} = 0^{+}$ isomer state and a $K^{\pi} = 0^{-}$ reflection asymmetric vibration. The numerically calculated curve for the isomer excitation (68) is shown in Fig. 42 fitted to the data of Wolf and Meadows (67). The isomer energy for this fit is 2.56 MeV. (The broken curves are based on simple constant temperature level densities, and give lower isomer energies.) This agrees well with the interpretation of some delayed gamma-ray data of Russo et al (69), which has been interpreted as the gamma-decay branch to the ^{238}U ground state of a shape isomer at 2.559 MeV (see Fig. 43). (It should be noted that the lowest data points on the delayed fission yield curve imply a lower isomer energy however, and reconciliation of all the data and the theoretical fit can be maintained only if it is assumed that these lowest points are distorted by background.)

6.2.2 Fission barriers

The expressions for the yields given in Section 6.2.1 ignore the details of competing reactions. The most important competing reaction is prompt fission, and this occurs at every evaporation stage of the reaction. Consequently there will be a combination of such competition factors to multiply into the yield expressions. In addition the final branch for neutron emission to class-II states is, according to the statistical theory of Section 3.3, to be attenuated by the decoupling factor $T_A/(T_A + T_B)$ that is appropriate for the evaporating nucleus at this final stage i.e. containing one more neutron than the isomer nucleus. Therefore, if the other competition factors are known, the strength of the reaction leading to the isomer can be used to give an estimate of the relative heights of the inner and outer barriers.

The measured yield of the isomers by delayed fission will also be affected by any appreciable branching of the isomer decay, particularly by gamma-ray emission to the ground state. Gamma-branching is normally expected to be weak however (estimates are given in ref. (70)) unless the inner barrier is markedly lower or more transparent than the outer barrier. For most of the known actinide shape isomers this does not appear to be the case. One exception is the ^{238}U isomer mentioned above, for which the gamma-branch appears to be an order of magnitude stronger than the fission branch.

6.2.3 (n,γ) reactions for isomer excitation

Some americium spontaneously fissioning isomers have been observed and their yield as a function of excitation energy measured by means of the neutron capture reaction. Data for the $^{241}Am(n,\gamma)^{242si}Am$ reaction are shown in Fig. 44 together with calculated yield curves. The latter have been calculated with the computer code EVAPF described in Section 5.4 which follows a statistical model representation of the gamma-ray cascades allowing for competition from neutron emission and prompt fission.

6.2.4 Examples of collected results from isomer data

Examples of extracted barrier parameters for americium and curium nuclides are shown in Table 6.

6.3 Vibrational resonances

6.3.1 Introduction

Structure in fast neutron-induced fission cross-sections had been observed at a comparatively early stage in fission physics. For example, unpublished measurements at Los Alamos dating from about 1950, show clear structure in the fission cross-section of ^{232}Th for neutrons above 1 MeV energy (see Fig. 44). This structure certainly had nothing to do with resonance fine-structure, the energy resolution of these measurements being about four orders of magnitude coarser than the expected resonance fine spacing. First published explanations of the effect were based on an extension of A. Bohr's ideas (38) of channels over the fission barrier for the fission process.

At later dates structure was also found in the fission yield of certain (d,pF) reactions. In this reaction the proton energy following the deuteron stripping process is measured so that the excitation energy of the resulting fissioning nucleus is known. The reaction is particularly useful for observing fission in the barrier region of even compound nuclei in which the barrier lies below the neutron separation energy. At these energies the only competition against the fission process is the very weak electromagnetic de-excitation. Hence structure in the fission probability curve v. excitation energy could not be ascribed to competition unless the fission process is far from attaining saturation. Early observations of the structure (71) suggested a series of steps and plateaux, and these were explained as the effect of the initial channel opening for a set of states of particular spin and parity. Later observations (72) showed that some of these "plateau" levels really dipped with increasing excitation, and the explanation was advanced that this was due to structure (probably residual single particle effects) in the (d,p) formation probability for states of the same spin and parity as the opening fission channel.

Changes in the angular distribution of fission products with changing excitation energy in such reactions were also held to be manifestations of the channel structure of the fission barrier (73).

Later observations and more quantitative analysis, particularly of the structure in fast fission cross-sections, showed such explanations to be virtually estimable. The principal evidence came from measurements of the fission cross-section of ^{230}Th (74,75). This showed a distinct peak in the cross-section at a neutron energy of 720 keV; in the higher resolution measurements of Evans and Jones (75) the peak cross-section was observed to be about 4 times higher than the minimum value at higher neutron energy (see Fig. 45). At these comparatively low neutron energies for bombardment of an even target nucleus, there is only a very limited number of inelastic scattering thresholds. On the basis of very plausible assumptions about the residual states in ^{230}Th for inelastic scattering, it was computed on the competition theory (34) that the fission cross-section should only drop at most some 10% below the peak value (see Fig. 45); the peak in this value was clearly a resonance effect of some kind. An analysis of the peaks in the fission cross-section at higher neutron energies (~ 1.4 MeV) in the cross-section of ^{232}Th showed that there would have to be a very strong onset of states in ^{232}Th above 1.5 MeV for them to be explained by the channel competition theory; the density of states above this energy would have to increase at a rate about five times greater than acceptable on current knowledge of level densities, and it was also established experimentally (76) that no strong onset of inelastic scattering was to be observed at that energy.

Channel analysis of angular distributions of the fission products released in fast neutron-induced fission had fallen into similar difficulties. Sharp changes in the angular distribution with changing neutron energy were attributed to new fission channels opening but an attempt at quantitative analysis for the ^{234}U target nucleus by Vandenbosch (77) showed that the various channels would need to have very different tunnelling characteristics ($\hbar\omega$ ranging from ~0.1 to ~ 1 MeV).

It was apparent therefore that intermediate resonance effects existed in the fission transmission coefficient, the structure not being attributable to the neutron entrance channel, since no sign of systematically related structure existed in other fast neutron reactions on these nuclei.

The theoretical work of Strutinsky (2) introducing the double-humped fission barrier of the actinide nuclei provided the understanding for this. The weakly damped beta-vibrational states responsible for the resonance structure in the fission transmission coefficient could be explained, not indeed as a many-phonon state in the oscillator well centred on the normal beta deformation associated with the nuclear ground state, but as a few-phonon state oscillating about the mean deformation value of the secondary well. The weak damping observed is due to the combination of the low effective excitation energy available in the secondary well and the inhibition provided by the intermediate barrier. When this barrier is energetically overcome, as it is for the slow neutron cross-sections of the fissile nuclei, there is a dramatic increase in the mixing of this special vibrational state into the compound nucleus, and the broad resonance features in the fission transmission coefficient largely disappear. In this picture, the dramatic changes in angular distribution of fission products with changing excitation energy that are often observed are due more to the dominance of individual vibrational resonances, each associated with spin-parity quantum numbers given by coupling with simple states in the other degrees of freedom (single-particle, gamma-vibrations, rotations etc.), rather than the opening of fresh fission channels at the barrier. The "steps" in the fission probability curves measured from (d,pF) and similar reactions are now also largely understood as vibrational resonances, rather than the energies at which the lowest channel of each spin and parity become effectively open at the barrier.

In this section the various phenomena associated with fission vibrational resonances are interpreted within the framework of the double-humped barrier.

6.3.2 Pure vibrational resonances

6.3.2.1 Definition as barrier transmission resonances

When there is no damping of the vibrational motion by the other degrees of freedom, the vibrational resonances can be treated by the simple transmission theory of Section 3.1. The fission transmission coefficient to be substituted in the cross-section, equation (4.4), is calculated directly from the flux transmitted through the double-humped barrier if an incident wave of unit flux progressing from low to higher deformation is incident on the barrier. It is found for a symmetric barrier that the narrow peaks in the transmission coefficient reach a value of unity. The resonant condition is given approximately by equation (3.6). For a harmonic oscillator form of potential for the secondary well, $V = V_{II} - \frac{1}{2}C_{II}\eta^2$, and an inertial parameter independent of deformation thus gives the familiar beta-phonon condition $E - V_{II} = (n + \frac{1}{2})\hbar\omega$. Forms for the transmission coefficient in the region of resonance are given by equation (3.7a), and from this it can be shown (equation 3.10) that the resonance width is proportional to the sum of the transmission coefficients T_A and T_B through the inner and outer barriers, respectively considered as separate entities, and is also proportional to the oscillation frequency between the two barriers:

$$\Gamma \approx \left(T_A + T_B\right)\hbar\omega_{II} \tag{6.7}$$

The peak transmission at the resonance is

$$T_{res} \approx \frac{4T_A T_B}{\left(T_A + T_B\right)^2} \tag{6.8}$$

Between vibrational resonances the transmission reaches a low value of

$$T_{min} \approx \frac{T_A T_B}{4} \tag{6.9}$$

Examples of calculated transmission curves have been shown in Fig. 20. These certainly bear a close qualitative resemblance to the best experimental examples of vibrational resonances (c.f. the neutron fission cross-section of ^{230}Th, Fig. 46). Considerable use has been made of the simple transmission theory in analysing such data.

6.3.2.2 Formal definition of vibrational states in R-matrix theory

The comprehensive formal reaction theory for treating fission cross-sections expounded in Section 3.4 includes the special case of pure vibrational resonances. The R-matrix theory described there is based on the concept of eigenstates of the internal region of the reaction system. It was shown that if the fission barrier is of the double-humped character the R-matrix internal eigenstates can be constructed from the auxiliary sets of states with only a limited degree of coupling between them. The second set of these states, the class-II states associated with vibrational motion mostly within the secondary well, are largely responsible for governing the magnitude of the fission cross-section.

The class-II internal states are defined in equation (3.83) in terms of the vibrational and intrinsic wave functions of the components of the Hamiltonian introduced in Section 3.4.1 (equations 3.29,3.30). It is immediately apparent that a sufficient condition for a class-II state of vibrational nature is that it contains only one term in the expansion (3.83), namely

$$\chi^{(II)}_{\lambda_{II}} \approx \chi_{\mu} \Phi^{(II)}_{\nu(\mu)} \qquad (6.10)$$

with eigenvalue

$$E_{\lambda_{II}} \approx \epsilon_{\nu} + \Omega^{(II)}_{\nu(\mu)} \qquad (6.11)$$

For a physically observable resonance, the distribution of energy here should be high for the vibrational and low for the intrinsic state. The wave-function χ_{μ} describing the state of motion in the intrinsic degrees of freedom is defined at a fixed value of deformation η_o, generally taken to be the channel deformation close to the outer barrier, B. In the case of an absolutely pure vibrational state this choice of deformation is not important, because the coupling term H_c in the Hamiltonian (equation 3.30) must then vanish, implying that the intrinsic term H_{int} is independent of deformation. This can never be completely true of course, or fission would be practically unobservable in particle-induced reactions. There must at least be considerable interaction in the primary well region.

It is to be expected in a number of situations that equation (6.10) might be very nearly satisfied for intrinsic states defined at a deformation η_o near the centre of the secondary well, but nevertheless the description in terms of a basis defined at the outer or inner barrier might be more fragmented. Thus a nearly pure vibrational state in the configurational sense may not be outstanding in its fission strength. The criteria for the appearance of pure vibrational fission resonances in fission cross-sections or yield curves are clearly very tight; they demand the near-fulfilment of equation (6.10) at both the inner and outer barriers (so that the coupling width as well as fission width is minimised). It is to be expected that such resonances will normally be found only at energies equivalent to excitations in the second well that are within the energy gap for even nuclei or that are very close to "ground" in odd-A and odd nuclei. Because of this the interpretation of data that appear to constitute a vibrational resonance, with the particular objective of giving information on barrier heights, must be made with care. It is to be expected in general that such analyses will tend to over-estimate the barrier heights.

Although it is the vibrational factor in equation (6.10) that governs the magnitude of the cross-section resulting from the class-II state, the nature of the intrinsic states entering the expansion is important for special features of the fission process such as the angular distribution of the fission products. Analysis of angular distributions for the observed case of fast neutron induced fission of ^{230}Th is described in Section 6.3.2.4.

6.3.2.3 Cross-sections in the region of vibrational resonances

With the definition of the vibrational state as a relatively simple type of class-II auxiliary R-matrix state (equation 6.10) all cross-section formulae resulting from coupling this class-II state to the much denser and more complex class-I auxiliary states, associated with normal deformation, to give the complete R-matrix states can be taken over from Section 3.4.5. At the higher neutron energies sometimes involved these cross-section formulae will have to be generalised (straight-forwardly) to include inelastic scattering channels. All degrees of coupling strength are possible in principle, but only one - moderately weak coupling - has been reasonably well established by observation; this is the ^{230}Th neutron-induced fission cross-section.

The magnitude of the matrix element for the coupling of the vibrational state to the class-I states is given immediately by equation (3.91) with $D_{II} = \hbar\omega_{II}$ where ω_{II} is the circular frequency of vibrations in the secondary well. The result for the matrix element is

$$\left|\langle \chi^{(I)}_{\lambda_I} | H_c | \chi^{(II)}_{\nu_{II}} \rangle\right| \sim \frac{1}{2\pi}\left(D_I \hbar\omega_{II} T_A\right)^{\frac{1}{2}} \qquad (6.12)$$

and the coupling width of the Lorentzian profile for admixture of the vibrational states into the complete compound nucleus state is (from equations 3.105,3.106)

$$\Gamma^{\downarrow}_{\nu_{II}(c)} = 2W \approx \frac{\hbar\omega_{II}}{2\pi} T_A \qquad (6.13)$$

The actual profile of fission widths of the fine structure resonances that appear in fission yields or cross-sections of reactions that are initiated by populating the class-I states also depends on the fission width of the vibrational state. The estimate for this is commonly based on the statistical theory methods of Wigner (78) or Blatt and Weisskopf (30) (see Section 3.1), giving

$$\Gamma_{\nu_{II}}(f) \approx \frac{\hbar\omega_{II}}{2\pi} T_B \qquad (6.14)$$

6.3.2.4 Experimental data on pure vibrational resonances

No experimental evidence on broad resonance behaviour in fission cross-sections or fission probabilities has so far been found that is completely conclusive in proving the existence of a pure vibrational state. Nevertheless I shall describe here a typical case that lends itself to this interpretation.

The most carefully studied candidate as a pure vibrational resonance is undoubtedly ^{231}Th in the region of 5.85 MeV excitation. Data on neutron-induced fission of ^{230}Th have been measured by Yuen et al (79) and James et al (51) and analysed by the latter authors. In this cross-section the resonance occurs at a neutron energy of 720 keV, and is apparently about 30 keV wide; this is about 4 orders of magnitude greater than the resonance fine spacing expected in the cross-section at this energy. A feature of the experimental studies is that the angular distribution of fission products with respect to the incident neutron beam direction has been measured at various energies across the resonance. The forward peaking of the angular distribution right across the resonance indicates that the intrinsic state (defined at the outer barrier η_B) in the resonance configuration (equation 6.) has angular momentum projection $K = \frac{1}{2}$ on the symmetry axis (see ref. (80)). The analysis of the data proceeds on the assumption that the observed resonance is a composite of peaks, each of $K = \frac{1}{2}$ but with different total angular momentum J, forming a rotational band of intrinsic states.

On this assumption the cross-section has been calculated using the Hauser-Feshbach formula, equation (4.4), and the fission transmission coefficient for a vibrational resonance, equation (4.27) in the code AVXC (Section 5.3). The major competition against fission in the decay of the compound nucleus is provided by elastic and inelastic scattering of neutrons to known and inferred rotational bands in ^{230}Th. Strength functions for the calculation of these neutron transmission coefficients were taken from the known s- and p-wave neutron strength functions determined by low-energy neutron studies. At 700 keV neutron energy the main neutron entrance channels to the compound nucleus are provided by s, p and d-wave neutrons (exciting total angular momenta and parity $J^\pi = 1/2^+, 1/2^-, 3/2^-, 3/2^+, 5/2^+$) and somewhat more weakly by f-wave neutrons ($J^\pi = 5/2^-, 7/2^-$). From the calculations of the various spin-parity components of the cross-section the angular distribution of fission products was obtained.

The main variables in fitting the data are the parity of the intrinsic state in the vibrational resonance configuration, and the effective moment of inertia $\mathcal{J}$ and decoupling parameter a that govern the relative spacing of the members of the $K = 1/2$ rotational band:

$$E_{\lambda_{II}}(J) = E_{\nu_{II}} + \frac{\hbar^2}{2\mathcal{J}}\left[J(J+1) - K(K+1) + \delta_{K,\frac{1}{2}} a_1 (-)^{J+\frac{1}{2}}\left(J+\tfrac{1}{2}\right)\right] \qquad (6.15)$$

The best fit was achieved with odd parity, and with $(\hbar^2/2\mathcal{J})$ lying between 1.8 and 2.7 keV and a_1 between -2.0 and -2.3 (see Fig. 46). The value of the moment of inertia thus determined is about twice that observed for any normally observed rotational bands in odd-A actinide nuclei, and this provided one of the first direct indications that the shape of the nucleus in the intermediate states acting in fission was indeed much different from normal, as postulated by the double-humped barrier theory.

What are the reasons for believing this remarkable resonance phenomenon to be a nearly pure vibrational resonance as distinct from a damped vibrational resonance as described in Section 6.3.3? Mainly, because it is very smooth. With neutron energy resolution of a few keV it is to be expected that any class-II compound state structure would not occur with a frequency greater than a few class-II states per resolution interval, and, because of the statistical fluctuations in strength and width inherent in compound states, this would cause large variations about any smooth curve that would describe the envelope of the vibrational resonance. On the other hand there is a feature in the fit to the data that suggests damping is playing a role. This is a variation in width and strength of the different spin components of the resonance (other than variations due to penetration through the centrifugal barrier). Strictly speaking these variations arise, in the analysis, from the neutron fission cross-section of each component, and could be attributed to the variation of neutron strength function with spin, but the magnitude of the variation makes this appear unlikely.

At higher energies in ^{231}Th no more peaks appear in the cross-section, but the angular distribution of fission products undergoes marked variations in character with changing neutron energy, becoming considerably sideways peaked with respect to neutron direction at about 960 keV and forward-peaked again at 1060 keV. The sideways peaking is attributed (51) to a $K = 3/2$ intrinsic state coupled to a much broader vibrational resonance. The general behaviour of the $K = 1/2$ component of the cross-section both at the sharp resonance at 720 keV and at higher energies can be satisfactorily explained by the choice of barrier parameters:

$$V_A \approx 6.02\,\text{MeV}, \hbar\omega_A \sim 0.9\,\text{MeV}, V_B \approx 6.27\,\text{MeV}, \hbar\omega_B \sim 0.57\,\text{MeV}$$

6.3.3 Damped vibrational resonances

In most actinide nuclei it is expected from theory that observable fission will only be met at excitation energies that are already a few MeV above the bottom of the secondary well. To this extent the apparently nearly pure vibrational resonance of ^{231}Th is already a

surprise; the implication that the secondary well is very shallow is called the "thorium anomaly" and has caused speculation that there may be a weak splitting of the second barrier giving rise to a third well. Be that as it may, it is to be expected that vibrational resonances, when they are found, will be damped. In the idealised situation the vibrational fission mode will be dissolved in an incomplete way (with Lorentzian profile) into class-II compound states, which are then coupled to the class-I compound states to give the situation illustrated schematically in Fig. 47.

So far no ideal case like that illustrated in Fig. 47 has been observed. In one case, the neutron fission cross-section of ^{234}U [84], fragments of the complete picture seem to have been assembled. There is a "giant" resonance some tens of keV in width at about 310 keV neutron energy. Fluctuations in the cross-section about the smoothed-profile through this resonance have been interpreted as due to the underlying intermediate resonances due to class-II levels, a few of these contributing to each energy resolution interval. At low neutron energies the study of the fine structure resonances reveals an intermediate resonance in the fission widths at 580 eV. This is believed to be due to a class-II level on the wing of the vibrational resonance at 310 keV, and its parameters are almost reconcilable with those of the vibrational resonance on this account. The barrier parameters required to explain this vibrational resonance are:

$$V_A = 0.2 \text{ MeV } (\hbar\omega_A \text{ assumed to be 1 MeV})$$

$$V_B = 0.67 \text{ MeV } (\hbar\omega_B \text{ assumed to be 0.56 MeV})$$

relative to the neutron separation energy S_n (equals 5.31 MeV in ^{235}U). The intermediate barrier height is considerably lower than the values suggested by systematics based on other data. In fact, vibrational character was not assumed for the class-II coupling width in this analysis. It can be shown that if vibrational character had been assumed, as for the fission width, the estimate of the barrier height would have been raised by a few hundred keV.

In ^{240}Pu a vibrational resonance of width 0.12 MeV has been observed at 5 MeV excitation by means of the (d,pf) reaction [85]. The energy resolution employed was extremely good for this reaction mechanism (3 keV), but is still only sufficient to isolate the intermediate (class-II) resonances and not the fine-structure ones. Angular correlations between the fission product and proton directions was also observed and the, at first sight, surprising result obtained that the observed intermediate resonances were all $J = 2$, $K = 0$ in angular momentum properties. Interpretation of the fission strength of these and extrapolation to give the properties of the expected $J = 0$ class-II levels showed that the latter would be practically featureless, contributing only to the underlying background cross-section. Interpretation of the vibrational resonance is consistent with barrier parameters of

$$V_A = 5.65 \text{ MeV } (\hbar\omega_A = 0.82 \text{ MeV})$$

$$V_B = 5.3 \text{ MeV } (\hbar\omega_B = 0.6 \text{ MeV}).$$

6.4 Average fission cross-sections

Although fission intermediate structure (including vibrational resonances) gives valuable complementary evidence, the main body of information on fission barrier heights (particularly on the dominating barrier) comes from the analysis of the wealth of information on the overall energy behaviour of fission cross-sections (including the fission probability functions obtained from charged particle reactions such as (t,pf)). But the analysis of such data particularly at above-barrier energies requires information, or assumptions, on level densities at the barrier deformations, as described in Section 4. In some approaches to analysis of fission cross-section data (e.g. [56,61]) the barrier level densities have been calculated within the framework of the independent-particle model, using single-particle states obtained from deformed shell-model potentials, and with rotational band enhancement (see Section 4.4.2). These analyses have been quite successful, but it is probably more reliable, in the current state of knowledge, to use empirical barrier densities extracted from analyses of a key set of particularly reliable fission cross-sections.

The latter approach was adopted in ref. [59]. Deduction of such level densities from fission cross-sections is very dependent on assumptions about the barrier height, however. In ref [59] simple constant temperature level density forms were found, for odd-mass and odd nuclei, that would satisfy the fission cross-sections of ^{246}Cm, ^{238}U, ^{232}Th, ^{237}Np and ^{241}Am. The fission cross-section of ^{246}Cm was chosen because fission isomer excitation data (see Section 6.2) suggest that the outer barrier is a long way below the intermediate barrier, which therefore completely dominates the cross-section behaviour. The cross-sections of ^{238}U and ^{232}Th are two of the best-known of fission cross-sections, while the appearance of strong intermediate structure in the uranium and thorium series cross-sections suggests the near-equality of the two barriers; thus, the outer barrier density can be inferred. Similar complementary considerations apply to ^{241}Am and ^{237}Np.

Barrier densities of even nuclei are more complex; an energy gap containing a limited spectrum of collective levels, different for barriers A and B, is to be expected. The difference in collective spectra lies chiefly in the postulated existence of a low-lying $K^\pi = 0^-$ band for barrier B, due to the expected reflection asymmetry of the nuclear shape, and a low-lying $K^\pi = 2^+$ (γ-vibration) band for barrier A (due to axial asymmetry). With the low-lying spectra thus postulated and barrier heights roughly fixed from particle-transfer induced fission reactions, the barrier densities above the energy gap for the nuclei ^{236}U and ^{240}Pu can be assessed from the neutron fission cross-sections of ^{235}U and ^{239}Pu, two of the most accurately known of all fission cross-sections.

The barrier spectra and level density parameters thus determined are presented in Tables 6 and 7. The reference barrier parameters of the nuclei ^{236}U and ^{240}Pu are as follows:

^{236}U:- $V_A = 5.63$ MeV, $\hbar\omega_A = 1.04$ MeV, $V_B = 5.53$ MeV, $\hbar\omega_B = 0.6$ MeV

^{240}Pu:- $V_A = 5.57$ MeV, $\hbar\omega_A = 1.04$ MeV, $V_B = 5.07$ MeV, $\hbar\omega_B = 0.6$ MeV

It is to be stressed that, although the barrier densities given in Table 7 seem in general reasonable, the barrier heights deduced by using them are clearly dependent to some degree on these densities; calculations using these deduced barrier parameters must also employ the reference barrier densities as part of a correlated set.

Typical fits to fission cross-section data are shown in Figs. 48 and 49 for ^{240}Pu and ^{241}Pu respectively. The codes AVXC and EVAPF were used for the calculations. These are examples in which the intermediate barrier plays the major role in determining the fission cross-section behaviour, although the part contributed by the outer barrier is by no means insignificant.

6.5 Fission barriers

The fission barriers determined from these various data are presented in Figs. 50 (intermediate barrier heights) and 51 (outer barrier heights). The tunnelling parameters associated with these barriers have been reasonably well determined from a few fission cross-sections that are well-known over a large dynamic range. Amongst these few a definite odd-even effect is apparent, and evidence contributing to this conclusion is apparent from the odd-even effects in spontaneous fission half-lives of both ground-states and shape isomers of actinide nuclei. For the purposes of analysing the bulk of the data the few directly determined tunnelling parameters have therefore been employed as a universal set for the actinides. Their values are:

(i) even nuclei - $\hbar\omega_A$ = 1.04 MeV, $\hbar\omega_B$ = 0.6 MeV

(ii) odd-mass nuclei - $\hbar\omega_A$ = 0.8 MeV, $\hbar\omega_B$ = 0.52 MeV

(iii) odd nuclei - $\hbar\omega_A$ = 0.65 MeV, $\hbar\omega_B$ = 0.45 MeV.

In Fig. 50 the intermediate barrier heights are shown as a function of neutron number, with different shading of symbols to indicate the odd-even character of the nuclide. Overall trends are apparent. One is the tendency for there to be a broad maximum around 147 neutrons. The second is the existence of a distinct odd-even effect in barrier height, odd nuclei having barriers 0.6 to 0.8 MeV higher than even nuclei (with similar neutron number). A third feature to note is that smooth trends appear to break down to some extent among the thorium nuclei.

Comparison of these data with theoretical values as discussed in Section 2 show certain similarities and a number of differences. The tendency for the intermediate barriers to maximise around 148 neutrons in the theory is broadly confirmed. However, the theoretical calculations indicate a much greater tendency to fall towards the lower charge (thorium) nuclides. (Likewise, the secondary well depth appears roughly constant in the theory but the interpretation of the data, particularly the existence of sharp vibrational resonances, suggests a shallow well in the thorium region; these discrepancies together are labelled the "thorium anomaly".) There is also an absolute numerical difference of the order of 0.5 MeV between the data and the best of the theoretical calculations. Very little theoretical work has been devoted to calculations of barriers of odd-mass and odd nuclei, so the only theoretical comment that can be made on the odd-even effect is a qualitative one. It is an effect to be expected on the basis of Strutinsky theory. The barrier heights presented here are differences between barrier and ground state energies. The energy gap, which lowers the minimum energy state of even nuclei with respect to odd nuclei, is proportional to the density of single particle states at the Fermi energy. In Strutinsky theory the single particle state density is high at the barriers (which are caused by positive shell correction energy) and hence the energy gap is higher; it is this difference in energy gap between normal and barrier deformations that gives rise to the observed effect.

In Fig. 51 the outer barrier heights are presented in a similar fashion. Again there appears an overall tendency for peaking around 148 neutrons (for constant proton number). The odd-even effect is also apparent. The main difference between Figs. 50 and 51 is the very considerable fall in outer barrier height with increasing proton number, and this is in general accord with the theoretical results presented in Section 2.

6.6 Fission barrier parameters and the calculation of cross sections

The existence of a body of information on barrier parameters, such as that shown in Figs. 50 and 51, together with the barrier level densities of Table 7, is of very considerable value for the calculation of the general fast neutron cross-section behaviour of the less available trans-actinium nuclei. Most compound nuclei of interest are already encompassed in the data sets presented here, but approximate values of the barriers may be obtained by interpolation or extrapolation of these data even for those that may be absent.

The tools for these calculations have been presented in Sections 4 and 5. Examples of calculations with the barrier parameters of Sections 6.4 and 6.5 are shown in Fig. 52 for ^{242}Am. The only experimental data available on this nucleus is a measurement of the fission cross-section with accuracy that is particularly poor above 1 MeV neutron energy. The likelihood of obtaining good capture and inelastic scattering cross-section data in the near future seems remote. The accuracy of the calculated cross-sections presented here is probably of the order of ±30%. This assessment comes from comparison of calculations (59), by these methods, of the capture cross-section of ^{233}U, ^{235}U, ^{239}Pu and ^{241}Am with the data that exist for these nuclei; in these cases agreement is better than 25%.

7. CONCLUDING REMARKS

Improvement of the calculation methods described in these lectures will depend mainly on further experimental confirmation and elucidation of the structured theory of the fission barrier. For example, the ordering of the barrier states of odd-mass nuclei is important for the calculation of fission cross-sections and competition with other reactions up to neutron energies of 1.5 MeV or so; the detailed energy variation will depend on spin through the centrifugal barriers in the neutron channel (59).

While such improvements are desirable in the detailed picture of the double-humped barrier, there are more qualitative aspects still to be explored at the lower end of the trans-actinium range. The thorium anomaly has been mentioned, and a lot of attention is now focussed on this, and, in particular, on the possibility that there is a third minimum in the fission barrier as first postulated by Möller and Nix [12]. Calculated cross-sections do become more difficult to reconcile with data on the scheme reported in ref. [59] and described here in detail. The structure due to resonances of a vibrational type makes for difficulties of course in comparison with cross-sections calculated from statistical theory, but apart from this the calculated fission cross-sections of the thorium nulcei tend to be too high (by up to a factor of 2), and the sub-barrier cross-sections tend to fall with energy more sharply than the data indicate. The third minimum, with two high barriers based on a split outer barrier B from the more conventional double-humped picture, would not only better account for the vibrational resonance structure but would be expected to have lower barrier level densities (giving lower fission transmission coefficients) and higher transparency at sub-barrier energies. Alternative explanations must also be explored for some of these discrepancies. One line of attack is the much weaker degree of axial asymmetry expected at the intermediate barrier deformation for the lower charge nuclei; again a lower barrier level density would result from this because of decreased rotational state enhancement, and lower fission transmission coefficients could be expected.

Beyond this, advances are to be expected from a better understanding of the vibrational states associated with the structured fission barrier. Recent calculations I have made suggest that reasonably pure vibrational states are only to be expected as a systematic feature in even compound nuclei. However, there does seem to be some possibility of calculating the properties of "pseudo-" vibrational states of odd-mass nuclei and relating them to observation. Such calculations may even have some bearing on the question of the third minimum.

These lectures have been devoted entirely to the calculation of cross-sections of fissionable nuclei. The questions of mass yields and other properties of the fission reaction that are of importance for technology are ones that are not yet amenable to treatment in the kind of detail required for applications. Statistical model and thermodynamic treatments of such phenomena have been developed and are capable of fair reproduction of data but generally at the cost of parameter adjustment; they are therefore more useful as tools for elucidating these aspects of the fission phenomenon than as formalisms calculating new data. But this situation will certainly improve with time, as application of Strutinsky methods to the calculation of both the potential energy surface and inertial tensor of the region between barrier and scission becomes more fully developed.

REFERENCES

[1] MYERS, W.D. and SWIATECKI, W.J., Nucl. Phys. 81 (1966) 1. Also Ark. Fys. 36 (1967) 343.
[2] STRUTINSKY, V.M., Nucl. Phys. A95 (1967) 420.
[3] NIX, J.R., Ann. Revs. Nucl. Sci. 22 (1972).
[4] BRACK, M., DAMGAARD, J., JENSEN, A.S., PAULI, H.C., STRUTINSKY, V.M. and WONG, C.Y., Revs. Mod. Phys. 44 (1972) 320.
[5] BENGTSSON, R., Physics and Chemistry of Fission (Conf. Proc. Rochester, 1973) IAEA, Vienna (1974) 1 203.
[6] SKYRME, T.H.R., Phil. Mag. 1 (1956) 1043.
[7] VAUTHERIN, D. and BRINK, D.M., Phys. Rev. C5 (1972) 626.
[8] MYERS, W.D. and SWIATECKI, W.J., Ann. Phys. 55 (1969) 395.
[9] MYERS, W.D. and SWIATECKI, W.J., Ark. Fys. 36 (1967) 343.
[10] HOWARD, W.M. and NIX, J.R., Physics and Chemistry of Fission (Conf. Proc. Rochester, 1973) IAEA, Vienna, (1974) 1 145.
[11] BOLSTERLI, M., FISET, E.O., NIX, J.R. and NORTON, J.L., Phys. Rev. C5 (1972) 1050.
[12] MÖLLER, P. and NIX, J.R., Physics and Chemistry of Fission (Conf. Proc. Rochester, 1973) IAEA, Vienna (1974) 1 103.
[13] NILSSON, S.G., TSANG, C.F., SOBICZEWSKI, A., SZYMANSKI, Z., WYCECH, S., GUSTAFSON, C., LAMM, I., MÖLLER, P. and NILSSON, B., Nucl. Phys. A131 (1969) 1.
[14] LARSSON, S.E. and LEANDER, G., RAGNARSSON, I. and RANDRUP, J., Physica Scripta 10A (1974) 65.
[15] PASHKEVICH, V.V., Nucl. Phys. A133 (1969) 40.
[16] LARSSON, S.E., RAGNARSSON, I. and NILSSON, S.G., Phys. Lett. 38B (1972) 269.
[17] SCHULTHEISS, H. and SCHULTHEISS, R., Phys. Lett. 34B (1971) 245.
[18] LARSSON, S.E. and LEANDER, G., Physics and Chemistry of Fission (Conf. Proc., Rochester, 1973) IAEA, Vienna (1974) 1 177.
[19] MÖLLER, P. and NILSSON, S.G., Phys. Lett. 31B (1970) 283.
[20] MÖLLER, P., Nucl. Phys. A192 (1972) 529.
[21] SCHIRMER, J., KNAAK, S. and SÜSSMANN, G., Nucl. Phys. A199 (1973) 31
SCHÜTTE, G. and WILETS, L., Physics and Chemistry of Fission (Proc. Conf. Rochester, 1973) IAEA, Vienna (1974) 1 503.
WIECZOREK, R., HASSE, R.W. and SÜSSMANN, G., Ibid, 523.
[22] NIX, J.R., Annals of Physics 41 (1967) 52.
[23] NIX, J.R., Nucl. Phys. A130 (1969) 241.
[24] SZYMANSKI, Z., Physica Scripta 10A (1974) 122.
[25] INGLIS, D., Phys. Rev. 96 (1954) 1059.
[26] SOBICZEWSKI, A., SZYMANSKI, Z., WYCECH, S., NILSSON, S.G., NIX, J.R., TSANG, C.F., GUSTAFSON, C., MÖLLER, P. and NILSSON, B., Nucl. Phys. A131 (1969) 67.
[27] DAMGAARD, J., PAULI, H.C., STRUTINSKY, V.M., WONG, C.Y., BRACK, M. and STENHOLM-JENSEN, A., Physics and Chemistry of Fission (Conf. Proc., Vienna, 1969) IAEA, Vienna (1969) 213.
[28] PAULI, H.C. and LEDERGEBER, T., Physics and Chemistry of Fission (Conf. Proc., Rochester, 1973) IAEA, Vienna (1974) 463.
[29] PAULI, H.C., Physica Scripta 10A (1974) 127.
[30] BLATT, J.M. and WEISKOPFF, V.F., Theoretical Nuclear Physics (1952) Wiley, New York.

(31) HILL, D.L. and WHEELER, J.A., Phys. Rev. 89 (1953) 1102.
(32) FRÖMAN, N. and DAMMERT, Ö, Nucl. Phys. A147 (1970) 627.
(33) FORD, K.W., HILL, D.L., WAKONO, M. and WHEELER, J.A. Ann. Phys. 7 (1959) 239.
(34) LYNN, J.E., Nuclear Data for Reactors, 2 (1966) 89.
(35) BONDORF, J.P., Phys. Lett. 31B (1970) 1.
(36) BACK, B.B., BONDORF, J.P., OSTROSCHENKO, G.A., PEDERSEN, J. and RASMUSSEN, B., Nucl. Phys. A165 (1971) 449.
(37) MOLDAUER, P.A., Phys. Rev. 157 (1967) 907.
(38) BOHR, A., International Conference on Peaceful Uses of Atomic Energy 2 (1955) 220, United Nations, New York.
(39) JENSEN, H. and KOPPE, M., Ann. Phys. 63 (1971) 586.
(40) DIETRICH, K., Structure of Nuclei (1972) 373, IAEA Vienna.
(41) HOFMANN, H., Z. Phys. 250 (1972) 14.
(42) NÖRENBERG, W., Z. Phys. 260 (1973) 165.
(43) LYNN, J.E., Harwell Report AERE-R5891 (1968).
(44) WIGNER, E.P. and EISENBUD, L., Phys. Rev. 71 (1947) 29.
(45) LANE, A.M. and THOMAS, R.G., Rev. Mod. Phys. 30 (1958) 257.
(46) HUMBLET, J. and ROSENFELD, L., Nucl. Phys. 26 (1961) 529.
(47) MIGNECO, E. and THEOBOLD, J.P., Nucl. Phys. A112 (1968) 603.
(48) AUCHAMPAUGH, G. and WESTON, L.W., Phys. Rev. C12 (1975) 1850.
(49) BOHR, A. and MOTTELSON, B., Nuclear Structure (Benjamin, New York, 1969) 1 302.
(50) JAMES, G.D., DABBS, J.W.T., HARVEY, J.A., HILL, N.W. and SCHINDLER, R.H., Phys. Rev. C15 (1977) 2083.
(51) JAMES, G.D., LYNN, J.E. and EARWAKER, L., Nucl. Phys. A189 (1972) 225.
(52) LYNN, J.E., Physics and Chemistry of Fission (IAEA, Vienna, 1969) 249.
(53) MOLDAUER, P.A., Phys. Rev. 157 (1967) 907.
(54) HOFMANN, H.M., RICHERT, J., TEPEL, J. and WEIDENMÜLLER, H.A., Ann. Phys. 90 (1975) 403.
(55) LYNN, J.E. and BACK, B.B., J. Phys. A 7 (1974) 395.
(56) BRITT, H.C., BOLSTERLI, M., NIX, J.R. and NORTON, J.L., Phys. Rev. C7 (1973) 801.
(57) METAG, V., LEE, S.M., LIUKKONEN, E., SLETTEN, G., BJØRNHOLM, S. and JENSEN, A.S., Nucl. Phys. A213 (1973) 397.
(58) KLUGE, G., Nucl. Phys. 51 (1964) 41.
(59) LYNN, J.E., Harwell Report AERE-R7468 (1974).
(60) BJØRNHOLM, S., BOHR, A. and MOTTELSON, B., Physics and Chemistry of Fission IAEA, Vienna, 1974) 367.
(61) GAVRON, A., BRITT, H.C., KONECNY, E., WEBER, J. and WILHELMY, J.B., Phys. Rev. C13 (1976) 2374.
(62) GILBERT, A. and CAMERON, A.G.W., Can. J. Phys. 43 (1965) 1446.
(63) LYNN, J.E., Theory of Neutron Resonance Reactions (Oxford, Clarendon Press, 1968).
(64) JÄGARE, S., Phys. Lett. 32B (1970) 571.
(65) VANDENBOSCH, R., Phys. Rev. C5 (1972) 1428.
(66) JACKSON, J.D., Can. J. Phys. 34 (1956) 767.
(67) WOLF, K.L. and MEADOWS, J.W., Bull. Am. Phys. Soc. 19 (1974) 595.
(68) LYNN, J.E., Proc. Int. Conf. on Interactions of Neutrons with Nuclei, Lowell, 1976.
(69) RUSSO, P.A., PEDERSEN, J. and VANDENBOSCH, R., Nucl. Phys. A240 (1975) 13.
(70) LYNN, J.E., Harwell Memorandum AERE-M2505 (1972).
(71) NORTHROP, J.A., STOKES, R.H. and BOYER, K., Phys. Rev. 115 (1959) 1277.
(72) SPECHT, H.J., FRASER, I.S. and MILTON, J.C.D., Phys. Rev. Lett. 17 (1966) 1187.
(73) HUIZENGA, J., Proc. of NATO Summer School, 1964.
(74) DUBROVINA, S.M. and SHIGIN, V.A., Dokl. Akad. Nauk. SSR 157 (1964) 561.
(75) EVANS, J.E. and JONES, G.A., Private Communication (1965).
(76) HOLMBERG, M., STRÖMBERG, L.G. and WALLIN, L., Nucl. Phys. A129 (1969) 149.
(77) VANDENBOSCH, R., Nucl, Phys. A101 (1967) 460.
(78) WIGNER, E.P., Trans. Faraday Soc. 34 (1938) 29.
(79) YUEN, G., RIZZO, G.T., BEHKAMI, A.N. and HUIZENGA, J.R., Nucl. Phys. A (1972)
(80) WILETS L. and CHASE, D.M., Phys. Rev. 103 (1956) 1296.
(81) LANE, A.M., LYNN, J.E. and MOSES, J.D., Nucl. Phys. A232 (1974) 189.
(82) BJÖRNHOLM, S., BORGGREEN, J., WESTGAARD, L. and KARNAUCHOV, V.A., Nucl. Phys. A95 (1967) 513.
(83) BRITT, H.C., BURNETT, S.C., ERKKILA, B.H., LYNN, J.E. and STEIN, W.E., Phys. Rev. C4 (1971) 1444.
(84) JAMES, G.D., DABBS, J.W.T., HARVEY, J.A., HILL, N.W. and SCHINDLER, R.H., Phys. Rev. C15 (1977) 2083.
(85) GLÄSSEL, P., RÖSLER, H. and SPECHT, H.J., Nucl. Phys. A256 (1976) 220.
(86) BRINK, D.M., D.Phil. Thesis (1955) Oxford.

TABLE 1

Comparative results on fission barrier heights from a range of calculations. The barrier heights are quoted in MeV relative to the primary minimum of the potential energy curve. For comparison with experimental data (normally quoted relative to the nuclear ground state) a zero-point beta-vibration energy should be subtracted from these numbers.

Reference	Remarks on calculation	$V_A(^{240}Pu)$	$V_A(^{244}Pu)$	$V_A(^{232}Th)$	$V_B(^{232}Th)$
Möller and Nix [12]	Folded Yukawa shell-model. No axial asymmetry in deformation but reflection asymmetry allowed.	5.45	6.3	2.9	5.7
Möller and Nix [12]	Modified harmonic-oscillator shell-model. No axial asymmetry but reflection asymmetry allowed.				8.0
Larsson and Leander [18]	Modified harmonic oscillator shell model. No axial asymmetry.	6.3	7.1	4.7	
Larsson and Leander [18]	Modified harmonic oscillator shell model. Axial asymmetry allowed.	5.6	5.9	4.7	
Flocard et al [21]	Hartree-Fock calculation. No axial asymmetry or reflection asymmetry. Pairing interaction strength proportional to surface area.	9.0			
Flocard et al [21]	Ditto, but pairing interaction strength constant	11.0			

TABLE 2

Resonance parameters resulting from the mixing of a broad-class-II level with class-I states to give fine structure resonances. The class-II state defines zero energy, its fission width $\Gamma_{\lambda_{II(f)}} = 20$, its coupling width $\Gamma_{\lambda_{II(c)}} = 4.3$.

CLASS I			COUPLED			POLES	
E_{λ_I}	$\Gamma_{\lambda_I(n)}$	$H''^2_{\lambda_I\lambda_{II}}$	E_λ	$\Gamma_{\lambda(n)}$	$\Gamma_{\lambda(f)}$	$E_m^{(H)}$	$\Gamma_m^{(H)}$
- .932	.0070	.387	- 1.011	.0089	.299	- .947	.091
- .037	.0147	.032	- .056	.0156	.222	- .038	.041
			.256	.(3)3	2.813	.792	15.154
.928	.0022	1.89				.903	.414
1.072	.0051	.0056	1.072	.0048	.(3)57	1.072	.025
			1.934	.0046	2.574		
2.246	.0070	.274				2.250	.082
			2.369	.(3)2	.605		
2.585	.0248	.577				2.577	.164
			3.141	.0353	4.503		
3.465	.0051	.015	3.478	.0016	.255	3.465	.028
4.632	.0158	.066	4.649	.0130	.084	4.635	.047

CROSS-SECTION FIT		
E'_λ	$\Gamma'_{\lambda(n)}$	$\Gamma'_{\lambda(f)}$
- .947	.0077	.0665
- .037	.0182	.0050
.928	.0024	.390
1.072	.0048	.009
2.25	.0070	.053
2.58	.0259	.125
3.47	.0049	.0036
4.64	.0128	.0125

TABLE 3

Resonance parameters resulting from the mixing of a broad class-II level with class-I states when the coupling width is of comparable magnitude to the fission width; $\Gamma_{\lambda_{II(f)}} = 25$, $\Gamma_{\lambda_{II(c)}} = 13.1$, $D_I = 1.2$.

CLASS-I STATES		COUPLED STATES			S-MATRIX POLES		ATTEMPTED R-MATRIX FIT		
E_{λ_I}	$\Gamma_{\lambda_I(n)}$	E_λ	$\Gamma_{\lambda(n)}$	$\Gamma_{\lambda(f)}$	$E_\ell^{(H)}$	$\Gamma_\ell^{(H)}$	E_λ'	$\Gamma'_{\lambda(n)}$	$\Gamma'_{\lambda(f)}$
2.822	.0110	2.822	(-) .0112	5×10^{-6}	2.822	.031	2.82	.011	4×10^{-5}
3.895	.0114	5.601	.0797	.146	5.632	.132	5.63	(-) .114	.011
5.626	.098	5.655	(-) .0263	.134	5.706	.241			
5.788	.0006	6.055	.0146	.306	6.053	.419	6.1	(-) .019	.379
6.421	.0217	7.788	(-) .0142	1.49	7.622	2.153			
8.015	.0036	8.047	3×10^{-4}	.202	8.019	.038	8.02	.003	.018
8.596	4×10^{-8}	8.598	(-) 4×10^{-6}	.0002	8.598	.035			
9.247	.0135								
9.638	.0087	9.624	.0129	.0104	9.627	.041	9.62	.012	.009
10.267	.0158	10.267	.0055	1.455	9.853	1.210	9.87	.0039	.791

TABLE 4

The factor f(J,ℓ) for correcting calculations of the total neutron transmission coefficient for departures of the level density law from linear dependence on angular momentum.

J \ ℓ	0	1	2	3	4
0	0.996	0.966	0.908	0.828	0.732
1/2	0.985	0.955	0.899	0.820	0.726
1	0.966	0.937	0.882	0.806	0.715
3/2	0.940	0.913	0.860	0.787	0.699
2	0.908	0.882	0.833	0.764	0.680
5/2	0.871	0.847	0.800	0.736	0.658
3	0.828	0.806	0.764	0.704	0.632
7/2	0.782	0.762	0.724	0.670	0.604
4	0.732	0.715	0.680	0.632	0.573
9/2	0.681	0.665	0.635	0.593	0.541
5	0.628	0.615	0.589	0.552	0.507
11/2	0.575	0.564	0.542	0.511	0.472
6	0.522	0.513	0.495	0.469	0.437

TABLE 5

Effective spin dispersion coefficients incorporating rotational bands built on independent particle band-head states.

$h^2/2\mathcal{J}\theta$ \ σ_K	3	3.5	4.6	5.5	6.5
-.004	7.15	8.29	11.59	15.81	25.5
.0006	6.05	6.74	8.32	9.63	11.1
.006	5.25	5.72	6.67	7.34	7.97
.012	4.66	5.00	5.67	6.10	6.48
.015	4.43	4.74	5.32	5.69	6.00

TABLE 6

Levels of ^{246}Cm used in the code AVXC for the calculation of the cross-sections of ^{246}Cm. Above 1 MeV the level scheme is schematic, and is based on the recommended level density.

E	I^π	E	I^π	E	I^π
0.0429	2^+	1.00	4^+	1.437	2^{+-}
0.1417	4^+	1.045	4^+	1.086	3^{+-}
0.296	6^+	1.375	0^+	1.172	3^{+-}
0.599	1^-	1.125	0^-	1.258	3^{+-}
0.66	3^-	1.164	1^{+-}	1.345	3^{+-}
0.78	5^-	1.328	1^{+-}	1.076	4^{+-}
0.863	0^+	1.492	1^{+-}	1.153	4^{+-}
0.903	2^+	1.109	2^{+-}	1.229	4^{+-}
0.945	2^+	1.218	2^{+-}	1.306	4^{+-}
0.990	3^+	1.328	2^{+-}	1.382	4^{+-}

TABLE 7

Barrier parameters extracted from isomer excitation data for some Am and Cm nuclei.

NUCLIDE	REACTION	E_{II}	V_A	V_B
^{244}Am	$^{244}Pu(p,2n)$		6.4	5.3
^{243}Am	"	2.3		
	$^{244}Am(n,2n)$		6.3	5.6
^{242}Am	"	2.9		
^{244}Cm	$^{242}Pu(\alpha,3n)$		5.8	4.3
^{243}Cm	"	1.9		

TABLE 8

Barrier spectra (channel structure) employed for fission calculations on even actinide nuclei (to 1 MeV)

K^π	I^π	Energy range above V_A	Energy range above V_B
0^+	0^+, 2^+, 4^+	0.0 - 0.1	0.0 - 0.1
	6^+	0.1 - 0.2	0.1 - 0.2
	8^+	0.3 - 0.4	0.3 - 0.4
	10^+	0.4 - 0.5	0.4 - 0.5
2^+	2^+, 3^+	0.9 - 1.0	0.9 - 1.0
0^-	1^-	0.6 - 0.7	0.0 - 0.1
	3^-	0.7 - 0.8	0.0 - 0.1
	5^-	0.8 - 0.9	0.1 - 0.2
	7^-	-	0.1 - 0.2
	9^-	-	0.3 - 0.4
1^-	1^-, 2^-, 3^-	0.9 - 1.0	0.9 - 1.0

TABLE 9

Barrier level density parameters employed for actinide nuclei. Level densities have the form of equation (4.24).

Type	Energy range (MeV)	C_A	θ_A	C_B	θ_B	σ
Even	1.0 - 2.5	0.02135	0.3005			5.7
	2.5 - 2.8	1.435×10^{-4}	0.1877			6.0
	2.8 - $\gtrsim$ 5	1.6	0.5			6.3
	1.0 - 1.4			0.02135	0.3005	5.7
	1.4 - 2.0			0.198	0.576	5.7
	2.0 - 3.05			0.00965	0.308	6.0
	3.05 - $\gtrsim$ 5			0.4265	0.5	6.3
Odd-A	0 - $\gtrsim$3	6.8	0.48	3.4	0.48	6.4
Odd	0 - ~2	11.5	0.36	5.75	0.36	6.4
	2 - $\gtrsim$5	54.5	0.5	27.2	0.5	6.4
		Suggested: no data analysed beyond ~2				

Figure Captions

Fig. 1 Schematic diagram of Strutinsky shell-correction method.

Fig. 2 Nuclear energy calculated as a function of deformation (for cylindrically symmetric shapes) for ^{240}Pu using Strutinsky's prescription. Arrow on outer barrier, B, gives lowering of barrier as calculated from reflection asymmetric deformation. Calculation from Nix (3).

Fig. 3 Energy levels of a harmonic oscillator potential for prolate spheroidal deformations. Numbers in diagram are numbers of particles filling the shell. From Nix (3).

Fig. 4 Comparison of two different technical procedures for calculating the Strutinsky shell-correction energy from the same set of shell-model levels. The solid curve is calculated using the normal energy-averaging procedure for every specific deformation. The dashed curve is from the summing of smoothed energy levels fitted to the actual shell model levels over a large range of deformation. Diagram from ref. (5).

Fig. 5 Binding energy of ^{240}Pu as function of deformation (the parameter Q is the quadrupole moment of the matter density) calculated with a Hartree-Fock method by Flocard et al (7). Dashed and solid curves correspond to pairing-interaction strength independent of nuclear surface area and proportional to surface area respectively.

Fig. 6 Potential energy landscapes for ^{236}Th and ^{250}Cm as calculated in ref. (18). The plane is one of nuclear elongation (ε) versus axial asymmetry (γ). The nuclear shape is chosen so that the energy is minimised as a function of the hexadecapole deformation parameter ε_4. Energy contours are at intervals of 0.2 MeV. The heavy solid line with arrows follows roughly the track of minimum potential energy with increasing elongation through barrier A and secondary well II.

Fig. 7 Inner barrier height as calculated from Strutinsky theory with a modified harmonic oscillator shell model with and without the axial asymmetry degree of freedom. Pairing interaction strength was assumed proportional to surface area, and the liquid-drop neutron-proton asymmetry constant $k_s = 1.78$. From ref. (18).

Fig. 8 Calculated energy of second minimum using Strutinsky theory with modified harmonic oscillator shell-model potential. The liquid-drop neutron-proton asymmetry constant $k_s = 2.8$. From ref. (12).

Fig. 9 Calculated outer barrier heights using modified harmonic-oscillator shell-model potential. From ref. (12).

Fig. 10 Calculated fission barrier potential energy curves, using folded Yukawa shell-model potential. From ref. (12). The dashed curves assume reflection symmetry in the nuclear shape, but the solid curves allow for minimization of the potential with respect to reflection asymmetry.

Fig. 11 Schematic indication of resulting calculation of fission cross-section if fission barrier is in error by 1 MeV either way. The full curve is the true cross-section.

Fig. 12 Inertial parameter B_{cc} corresponding to the collective parameter for nuclear elongation, c, compared to the shell correction energy E_{shell}. From ref. (28).

Fig. 13 Least action trajectory for ground-state spontaneous fission of ^{240}Pu through potential energy landscape in plane of elongation parameter c and neck constriction, h. From ref. (28).

Fig. 14 Least action calculations of ground-state spontaneous fission half-lives with optimised adjustments of surface energy constants for different groups of elements. From ref. (28).

Fig. 15 Least action calculation spontaneously-fissioning isomer half-lives. From ref. (28).

Fig. 16 Wave-functions in rectangular barrier transmission.

Fig. 17 Transmission coefficients as function of energy for rectangular barrier (full curve and dot-dash curve). The transmission coefficient for a parabolic barrier is shown as a dashed curve. Inertial parameter is $2B/\hbar^2 = 1200\ \text{MeV}^{-1}\text{s}^{-2}$.

Fig. 18 Notation for JWKB treatment of transmission through a double-humped barrier.

Fig. 19 Schematic diagram of complex potential well model for fission.

Fig. 20 Transmission coefficient for double-humped barrier with damping in secondary well compared with undamped transmission. Barriers are of equal height, $\hbar\omega_A = 1.5$ MeV, $\hbar\omega_D = 1.2$ MeV, $\hbar\omega_{II} = 0.6$ MeV, damping width $\Gamma_D = 0.06/2\pi$ MeV.

Fig. 21 Total and partial cross-sections for two close levels with R-matrix parameters $E_1 = 22.81$ eV, $\Gamma^{\frac{1}{2}}_{1(n)} = 0.35\ (\text{meV})^{\frac{1}{2}}$, $\Gamma^{\frac{1}{2}}_{1(f)} = -0.728\ (\text{eV})^{\frac{1}{2}}$, $E_2 = 22.92$ eV, $\Gamma^{\frac{1}{2}}_{2(n)} = 0.84\ (\text{meV})^{\frac{1}{2}}$, $\Gamma^{\frac{1}{2}}_{2(f)} = 0.574\ (\text{eV})^{\frac{1}{2}}$, $\Gamma_{1(\gamma)} = \Gamma_{2(\gamma)} = 0.025$ eV.

Fig. 22 Calculated vibrational wave-functions for a double rectangular well. The dimensions of the potential are given in the top part of the diagram. The inertial parameter is shown so that the wave number k ($= \sqrt{2B(E-V)/\hbar^2}$) is given by $15.7\sqrt{(B-E)}$ in MeV.

Fig. 23 Construction of separate potentials for discussion of amplitude relationships between class-I and class-II vibrational functions.

Fig. 24 Computed value of amplitude of class-I and class-II vibrational wave-function penetrating to the opposite well. Dimensions of the potential are shown in the left-half of the figure. The phonon energies are $\hbar\omega_I = \hbar\omega_{II} = 0.8$ MeV and the tunnelling parameter $\hbar\omega_A = 0.8$ MeV. Vibrational state energies are relative to intermediate barrier height.

Fig. 25 Schematic diagram of radiative capture spectra of class-I and class-II states.

Fig. 26 Neutron fission cross-section of ^{240}Pu in the resonance region. The upper diagram is the original measurement of the fission intermediate structure by Migneco and Theobald (47). The lower diagram is higher resolution data of Auchampaugh and Weston (48) for the class-II states at 1900 eV.

Fig. 27 Neutron fission cross-section of ^{240}Pu in region of 1405 eV class-II resonance (48).

Fig. 28 Schematic diagram of Lorentzian mixing of a class-II state with class-I states.

Fig. 29 Neutron resonance fission widths in the cross-section of ^{234}U (50) and fitted Lorentzian profiles.

Fig. 30 Simulated fission cross-section for broad class-II state with weak coupling to class-I states. The R-matrix parameters are given in Table 2.

Fig. 31 Fission widths of S-matrix poles for class-II fission widths similar in magnitude to coupling width $\Gamma_{\lambda_{II(f)}} = 25$, $\Gamma_{\lambda_{II(c)}} = 13.1$, $D_I = 1.2$.

Fig. 32 Simulated fission cross-section for broad class-II level with coupling of similar strength to the fission width. Parameters are given in Table 3. Notation as in Fig. 30.

Fig. 33 Differences in fission probability calculated from pure statistical theory (A',C') and microscopic theory (A,B,C). For the barrier parameters are as follows (energies in MeV):

Curves	V_A	$\hbar\omega_A$	V_B	$\hbar\omega_B$
1,1'	5.9	0.9	5.3	0.6
2	5.9	0.9	5.1	0.6
3,3'	5.9	0.9	4.9	0.6

Fig. 34 Average fission probability calculated from perturbation theory for coupling of class-II and class-I states (full curve). Parameters are $V_A = V_B = 5.5$ MeV, $\hbar\omega_A = 0.9$ MeV, $\hbar\omega_B = 0.6$ MeV, E_{II} (ground state of secondary well) = 2.5 MeV. Radiation widths (governing the amount of delayed fission through the spontaneously fissioning isomer) are calculated from the giant dipole resonance model. The broken curve is calculated from equation 3.137 for structured class-II states overlapping class-I states, and the chain curve is calculated from pure statistical theory.

Fig. 35 Average fission probability calculated from the code FISRA (for competition with radiative decay, barrier transition states limited to rotational band characteristic of even nuclei). The fissioning nucleus is ^{242}Pu excited in the reaction ^{240}Pu(t,p). Calculated curves are for $V_A = 5.6$ MeV, $\hbar\omega_A = 1.0$ MeV, $V_B = 5.1$ MeV, $\hbar\omega_B = 0.7$ MeV. The damping half-width for vibrational levels is 0.1 MeV (full curve), 0.025 MeV (short-deck curve) and is large (strong damping) for long-deck curve. Porter-Thomas fluctuations in class-I levels are not included.

Fig. 36 Typical set of neutron capture, inelastic and fission cross-sections calculated from the code AVXC. The target nucleus is ^{246}Cm. Circles in the top diagram are experimental data and the broken curve is a statistical calculation using the code EVAPF. Barrier parameters are $V_A = 0.94$ MeV, $\hbar\omega_A = 0.8$ MeV, $V_B = 0.345$ MeV, $\hbar\omega_B = 0.52$ MeV. Lowest channels are assumed to be $J^\pi = 3/2^{+-}$.

Fig. 37 Schematic flow-chart for the code EVAPF.

Fig. 38 Calculated cross-sections from the code EVAPF for the reactions resulting from neutron bombardment of ^{238}U; □ - - - fission cross-section data and calculated cross-section; O ——— capture cross-section data and calculated cross-sections.

Fig. 39 Typical calculated isomer excitation curves for reactions in which the isomer is formed after neutron evaporation.

Fig. 40 Schematic diagram of 2-neutron evaporation leading to formation of a shape isomer.

Fig. 41 Excitation function (ratio of cross-section for delayed fission to that for prompt fission) for spontaneously fissioning isomer of ^{240}Am (half-life 0.9 ms) resulting from the reactions ^{241}Pu(p,2n) (82) (open circles) and ^{240}Pu(d,2n) (83). The parameters for the fitted curve are $E_{II} = 3.0$ MeV, $V_B = V_A - 0.9$ MeV (for ^{241}Am).

Fig. 42 Excitation function for spontaneously fissioning isomer of ^{238}U (half-life 200 ns) resulting from the reaction ^{238}U(n,n')^{238}U. The fitted curve is described in the text.

Fig. 43 Transition diagram of gamma-rays attributed to decay of shape isomer of ^{238}U.

Fig. 44 Yield (relative to prompt fission) of the spontaneously fissioning isomer $^{242si}Am$ resulting from the reaction $^{241}Am(n,\gamma)^{242si}Am$ as a function of neutron energy.

Fig. 45 Neutron fission cross-section of ^{230}Th. These are early data (75). The attempted fit is based on the competition theory of structure in fission cross-sections.

Fig. 46 Neutron fission cross-section of ^{230}Th - more recent data (51). The fitted cross-sections are described in detail in ref. (51).

Fig. 47 Schematic diagram of damped vibrational resonance. The vibrational state (many-phonon β-vibration in secondary well) is mixed into the compound class-II states which in turn are coupled through the intermediate barrier to the class-I compound states - with the resulting cross-section pattern shown below.

Fig. 48 Neutron fission cross-section of ^{240}Pu. The continuous curve represents the experimental data. The points Δ are calculations from the statistical model code EVAPF and the points ∇ are calculated with the Hauser-Feshbach code AVXC.

Fig. 49 Neutron fission cross-section of ^{241}Pu. The full curve is a Hauser-Feshbach calculation (code AVXC), and the broken curve is a statistical model calculation (code EVAPF).

Fig. 50 Intermediate barrier heights as function of neutron number. Open symbols denote even nuclei, hatched denote odd-mass, block denote odd nuclei, O - Th,Cm; □ - Pa,Am; ◇ - U,Cf; Δ - Np,Bk; ∇ - Pu.

Fig. 51. Outer barrier heights as function of neutron number. Symbols as in Fig. 50.

Fig. 52 Some calculated cross-sections for the nucleus ^{242}Am (152y).

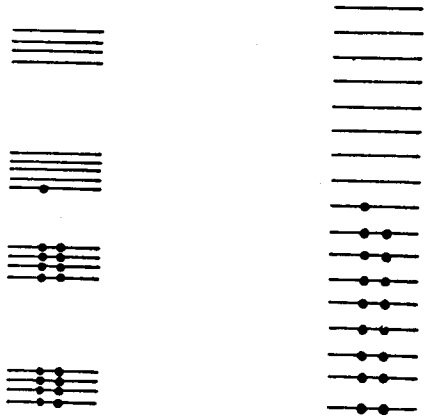

FIG. 1.

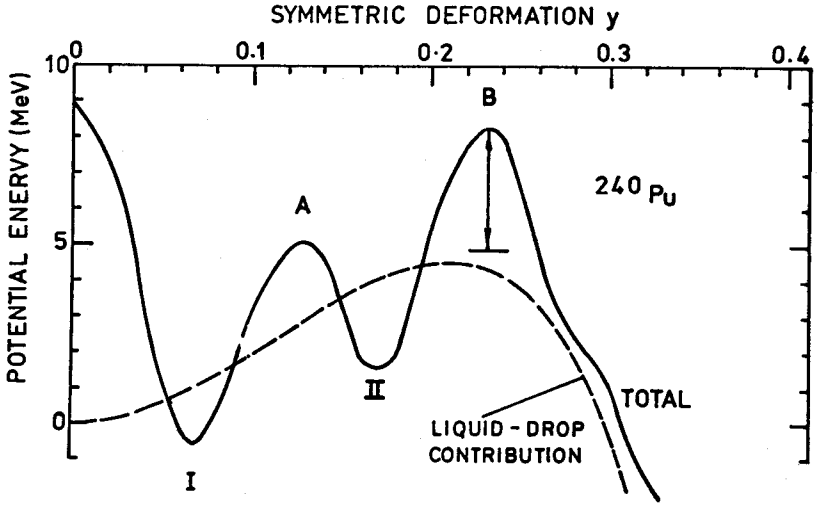

FIG. 2.

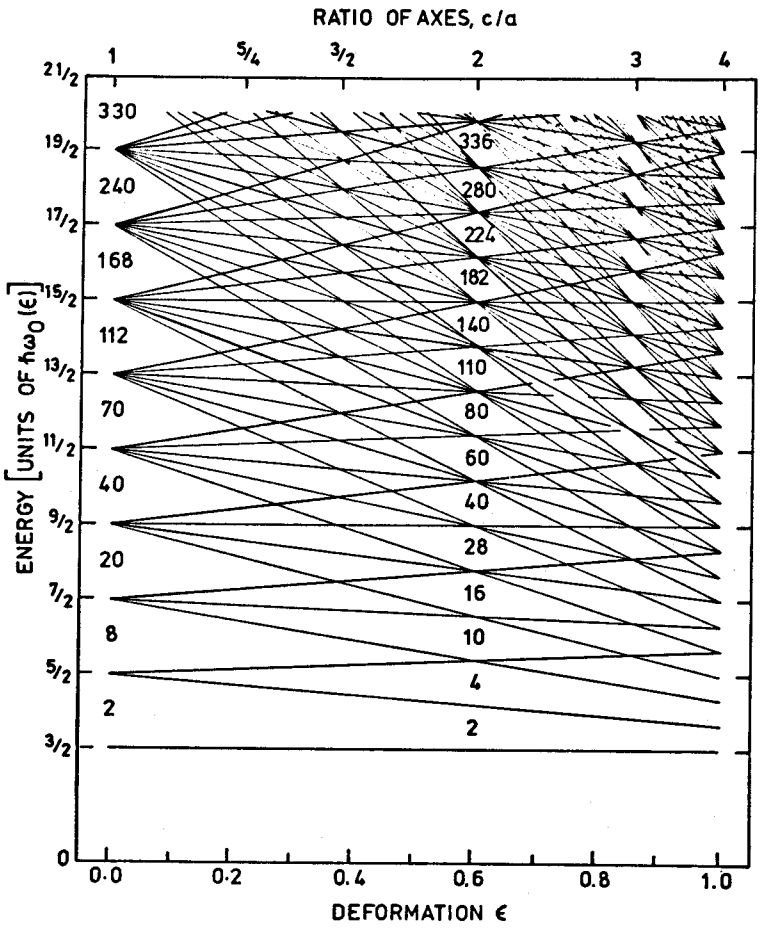

FIG. 3.

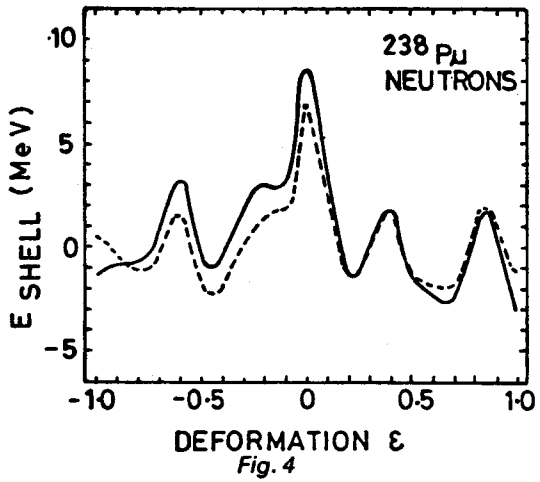

Fig. 4

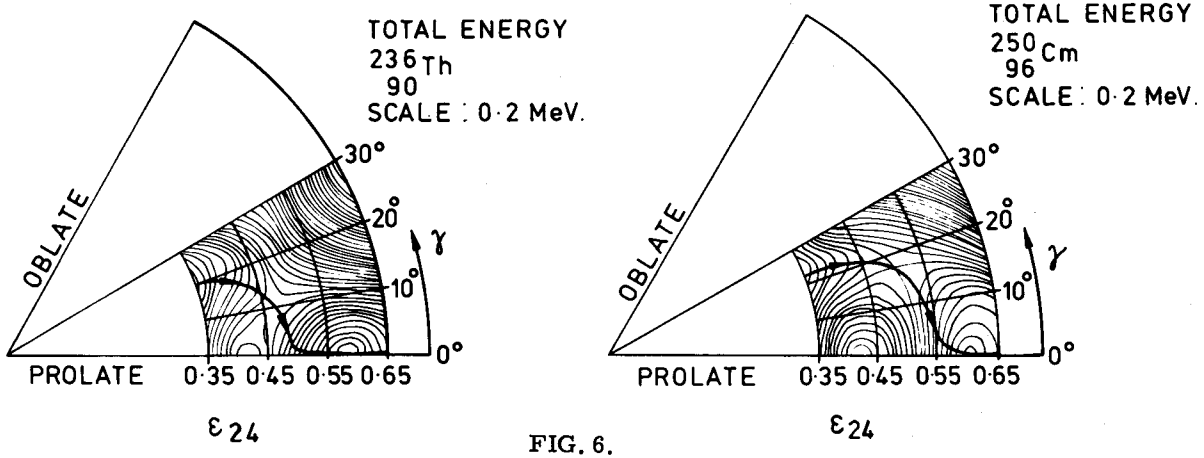

FIG. 6.

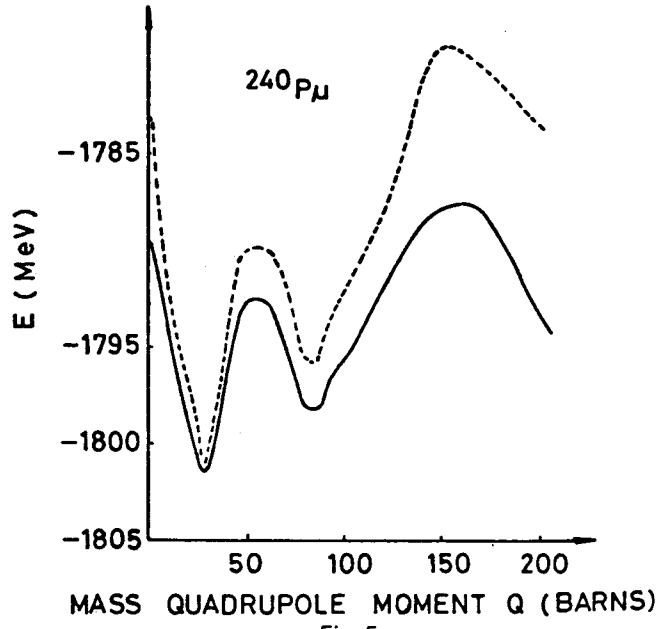

Fig. 5

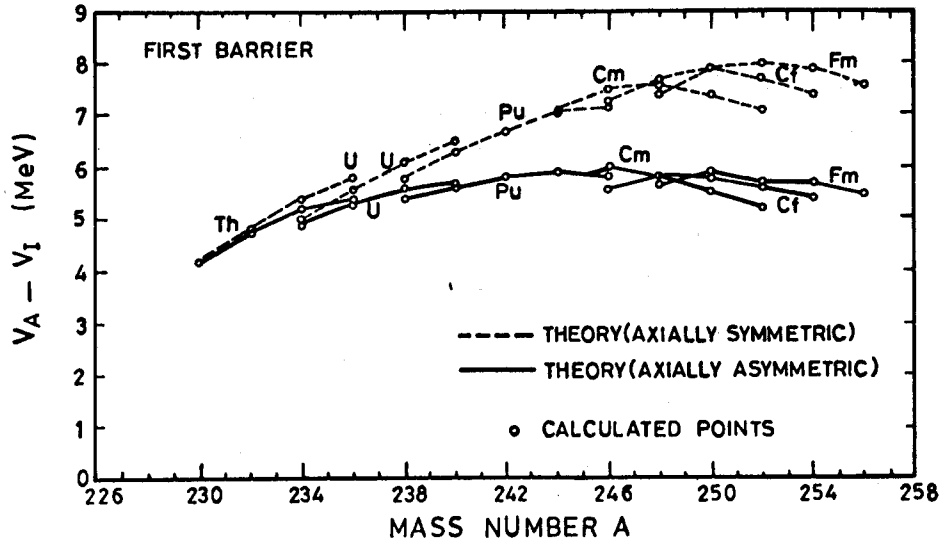

Fig. 7

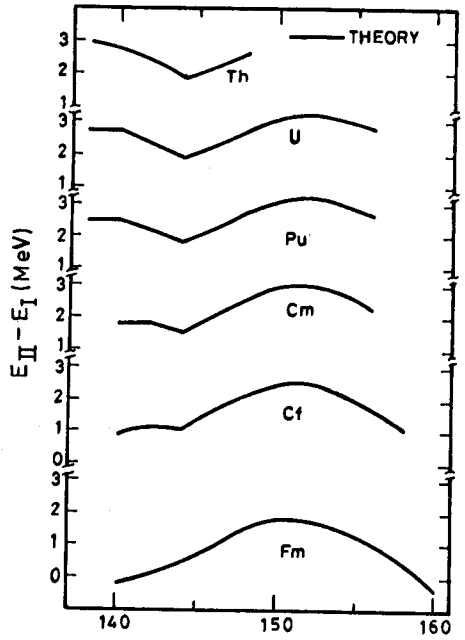

Fig. 8

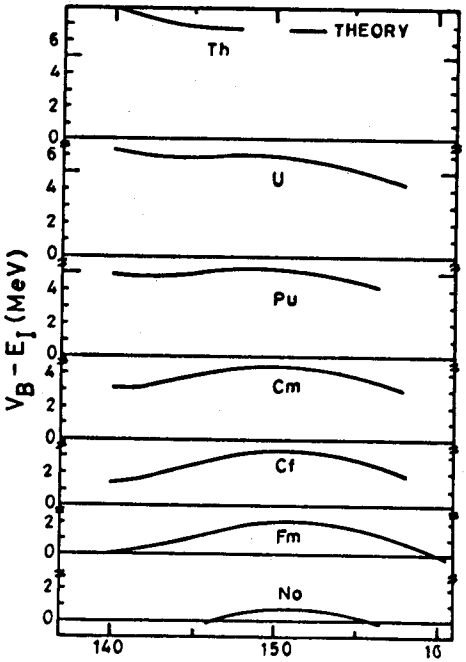

Fig. 9

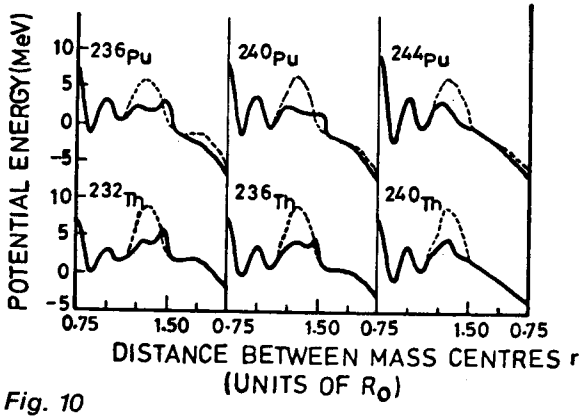

Fig. 10

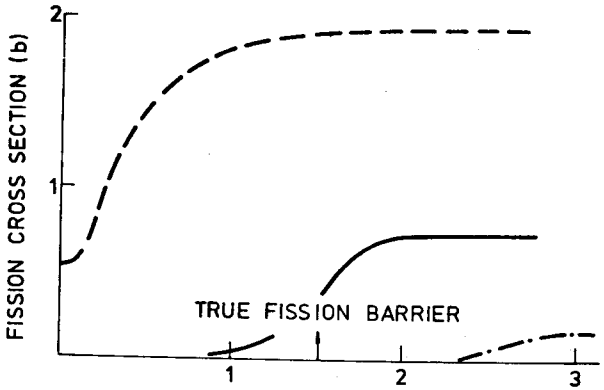

Fig. 11

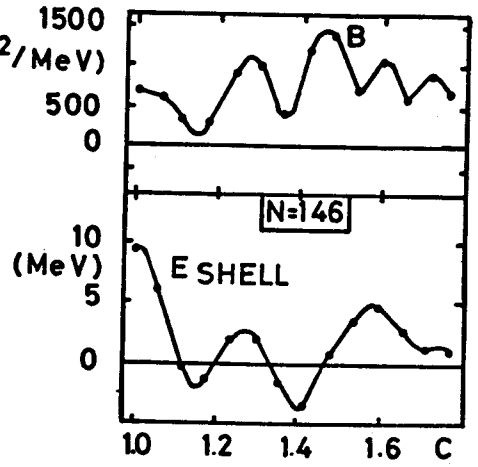

Fig. 12

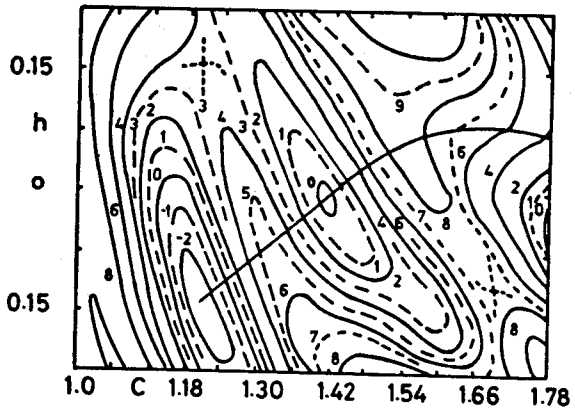

Fig. 13

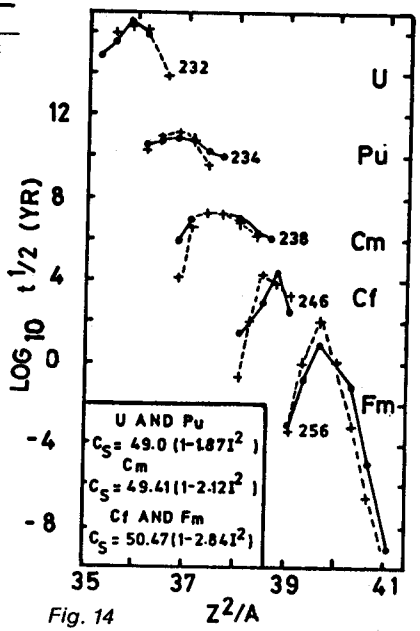

Fig. 14

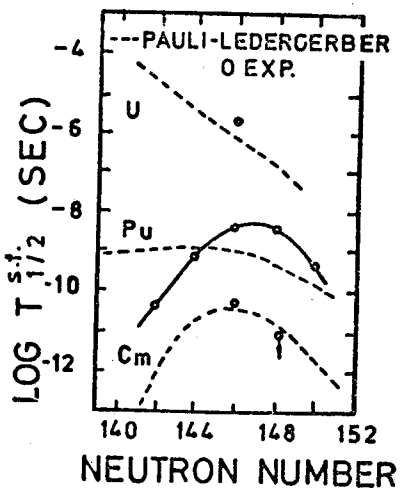

Fig. 15

BARRIER TRANSMISSION

Rectangular barrier

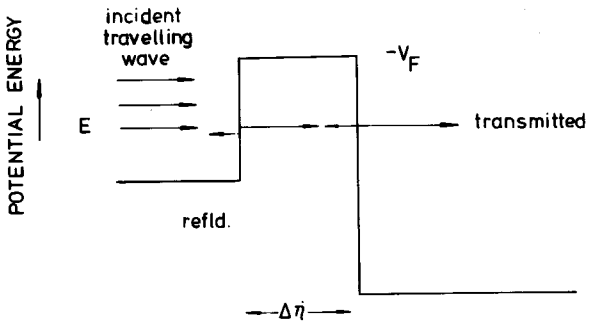

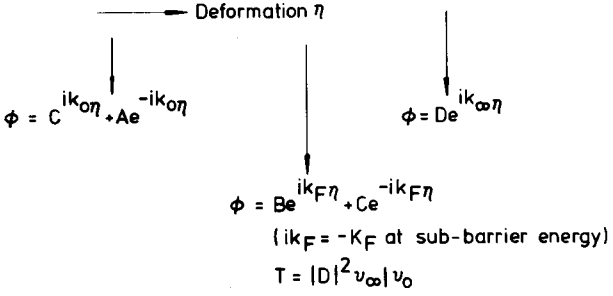

Fig. 16

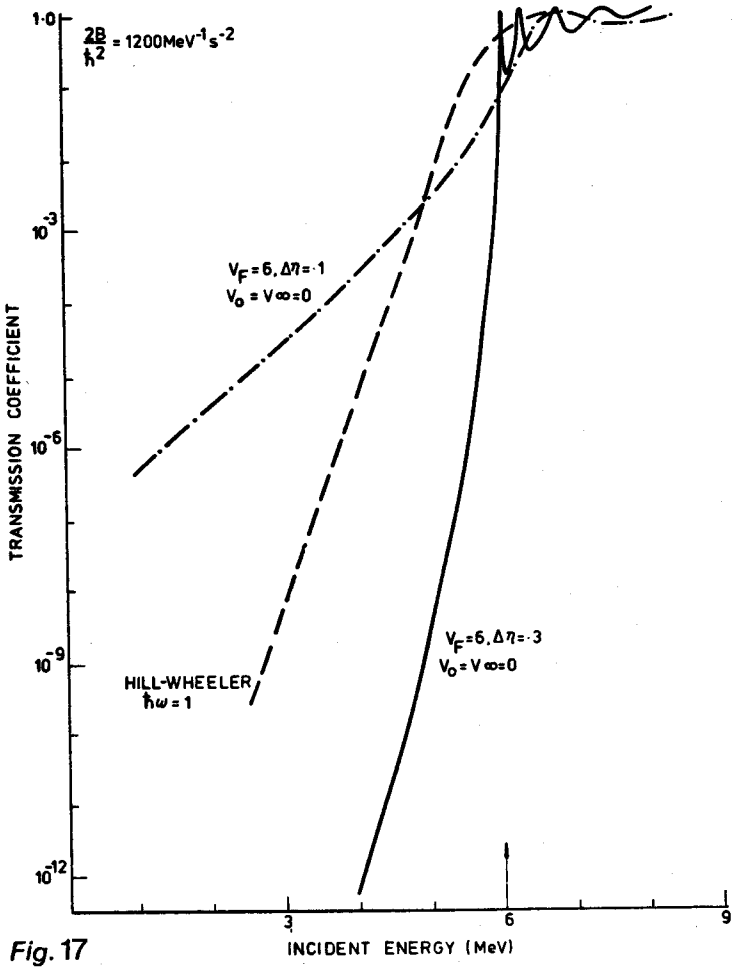

Fig. 17

$\eta a, \eta b, \eta c, \eta d$ are deformations where $V(\eta) = E$

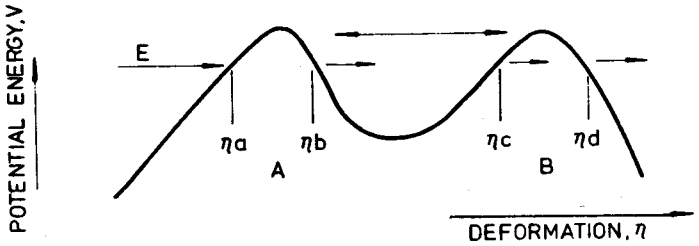

Fig. 18

1. SINGLE BARRIER

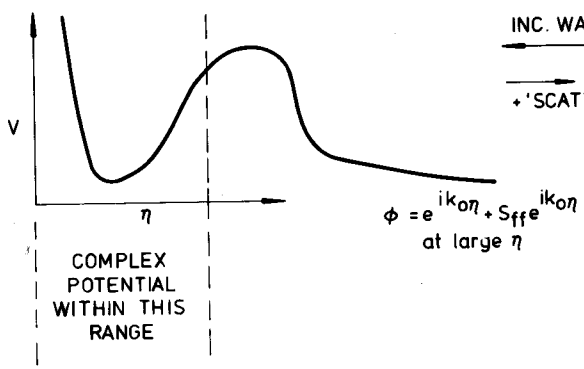

Cross-section for compound nucleus formation from "inverse-fission" channel $\propto 1-|S_{ff}|^2$ gives transmission coefficient

2. 2-HUMPED BARRIER

Treated with Bondorf assumption that all flux reaching primary well is absorbed

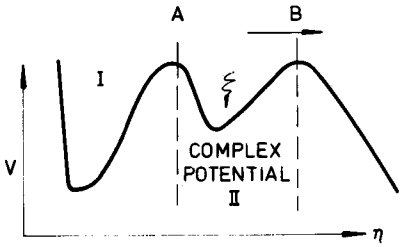

flux absd. in well $II \propto 1-(S_{ff})^2$

Fraction of this passed to I

$$P_A = \frac{T_A}{T_A + T_B + T_\gamma}$$

$\phi = a \exp(-ik_1\eta)$ ∴ flux absorbed $= k_1|a|^2/k_o$

Fig. 19

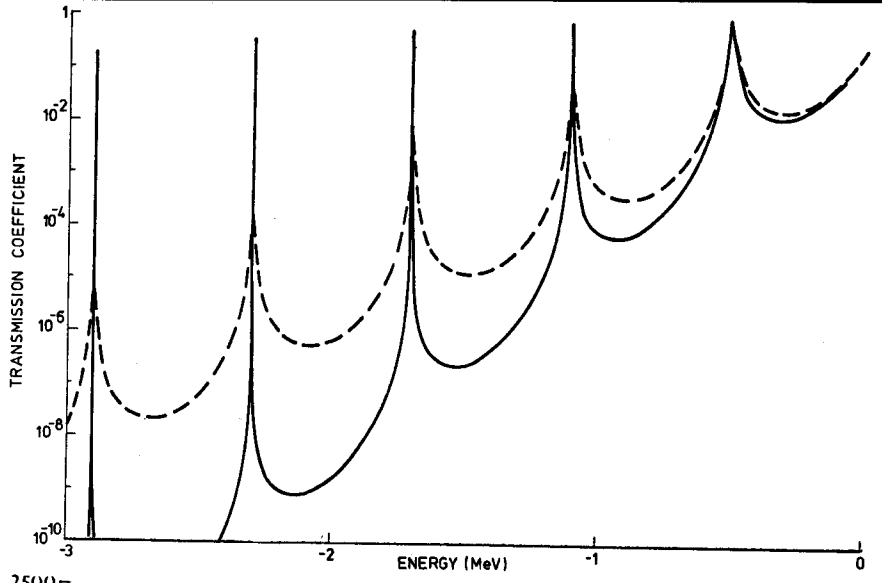

Fig. 20

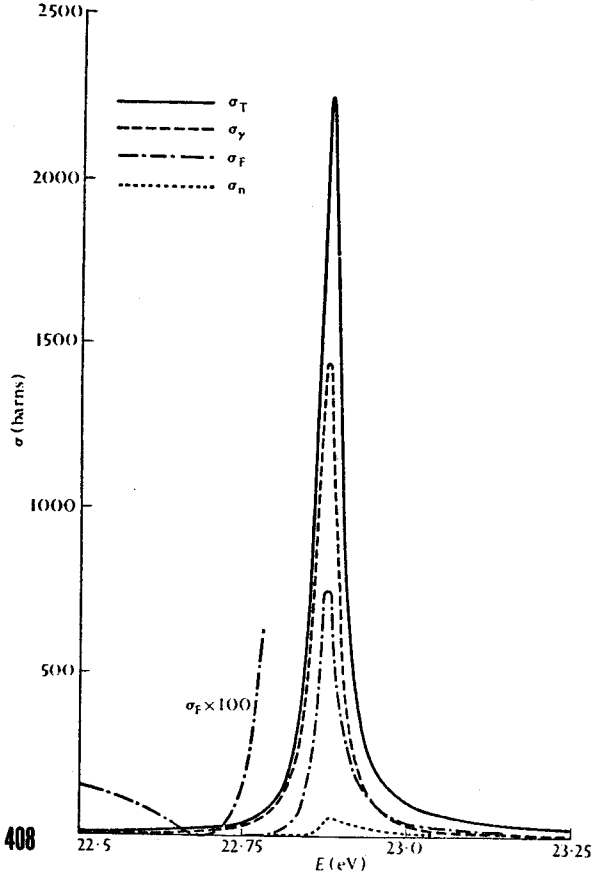

Fig. 21

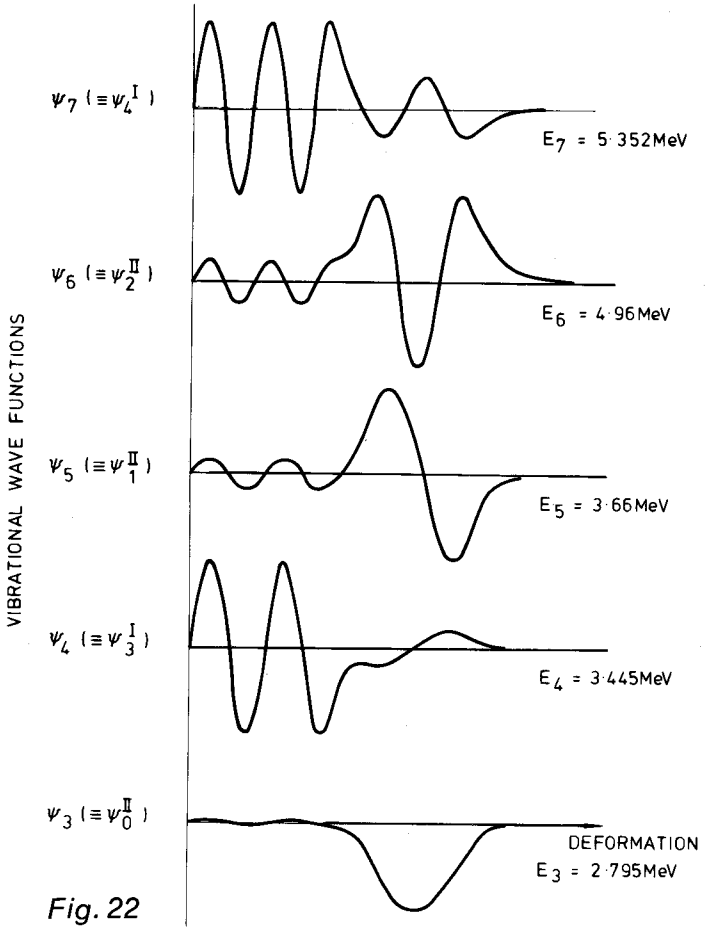

Fig. 22

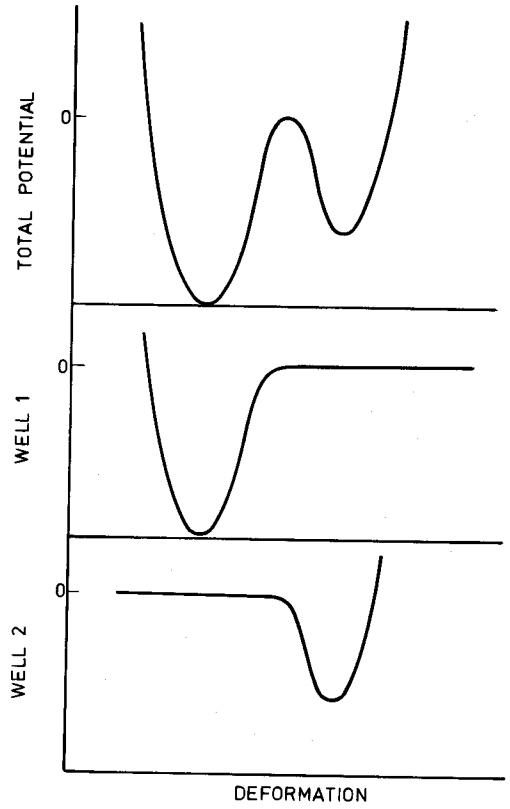

Fig. 23

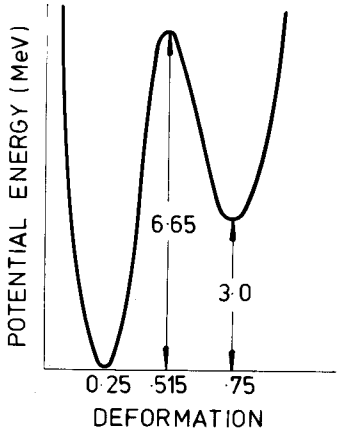

Fig. 24

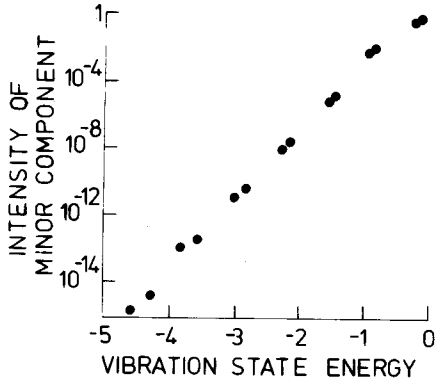

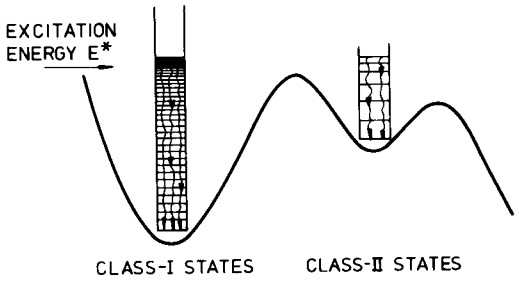

a. TYPICAL RADIATIVE CASCADES

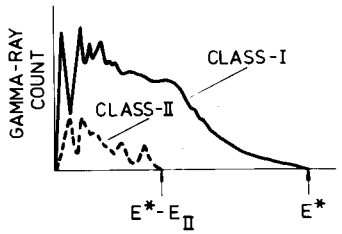

Fig. 25

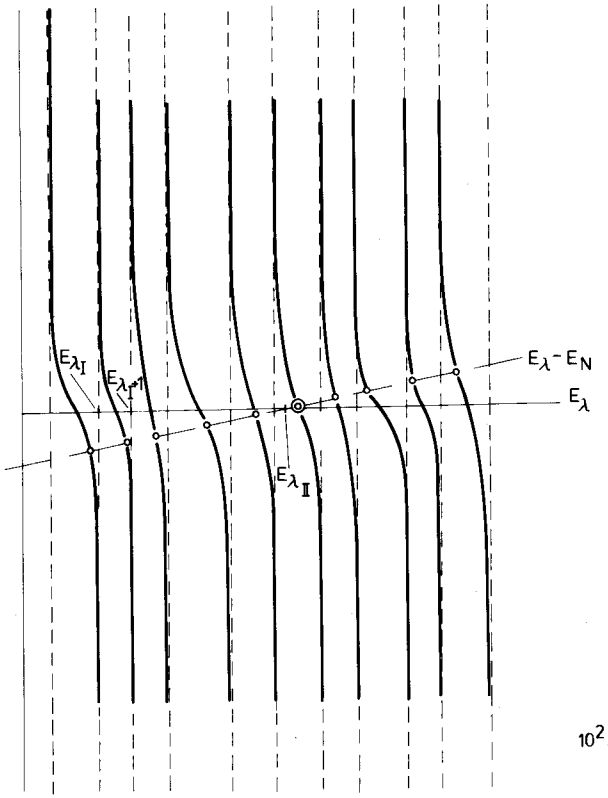

FIG. 28

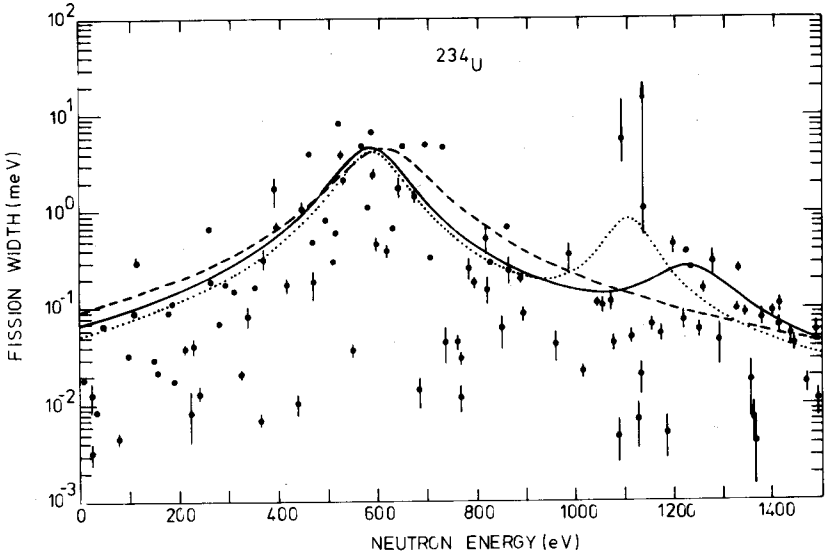

FIG. 29

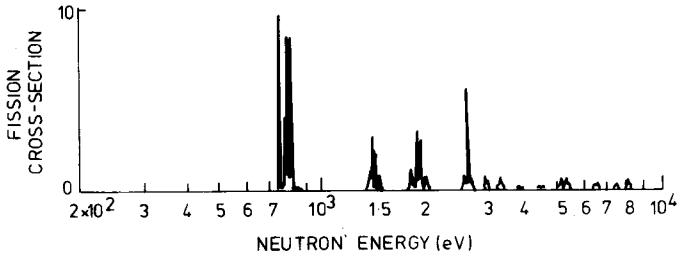

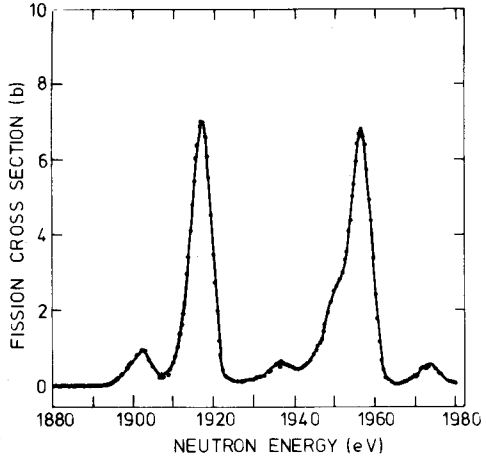

Fig. 26

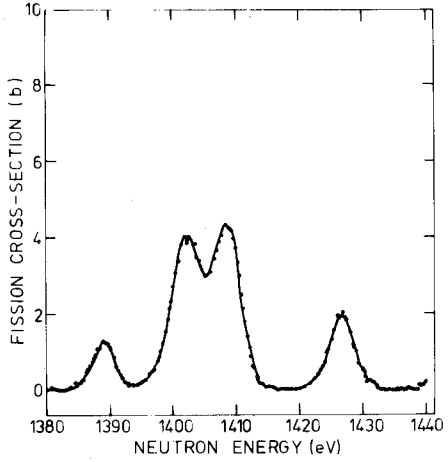

FIG. 27

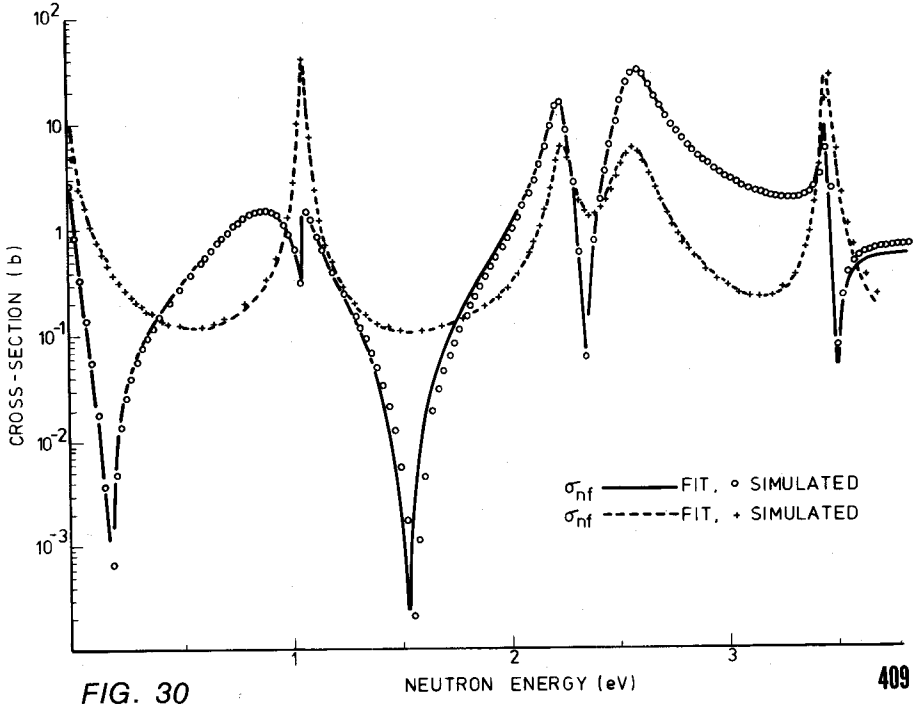

FIG. 30

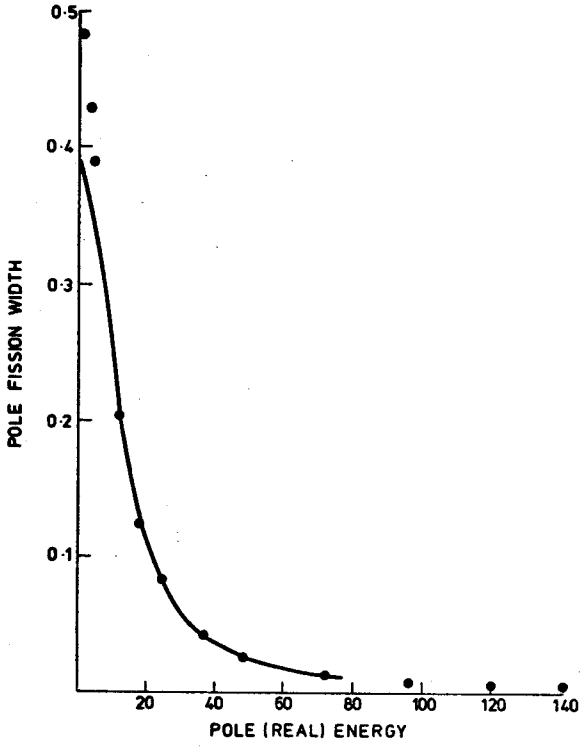

FIG. 31

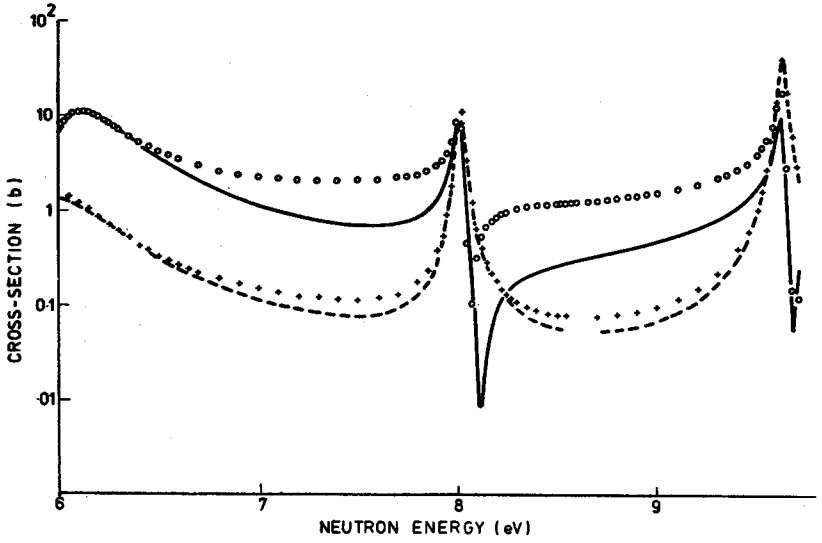

FIG. 32

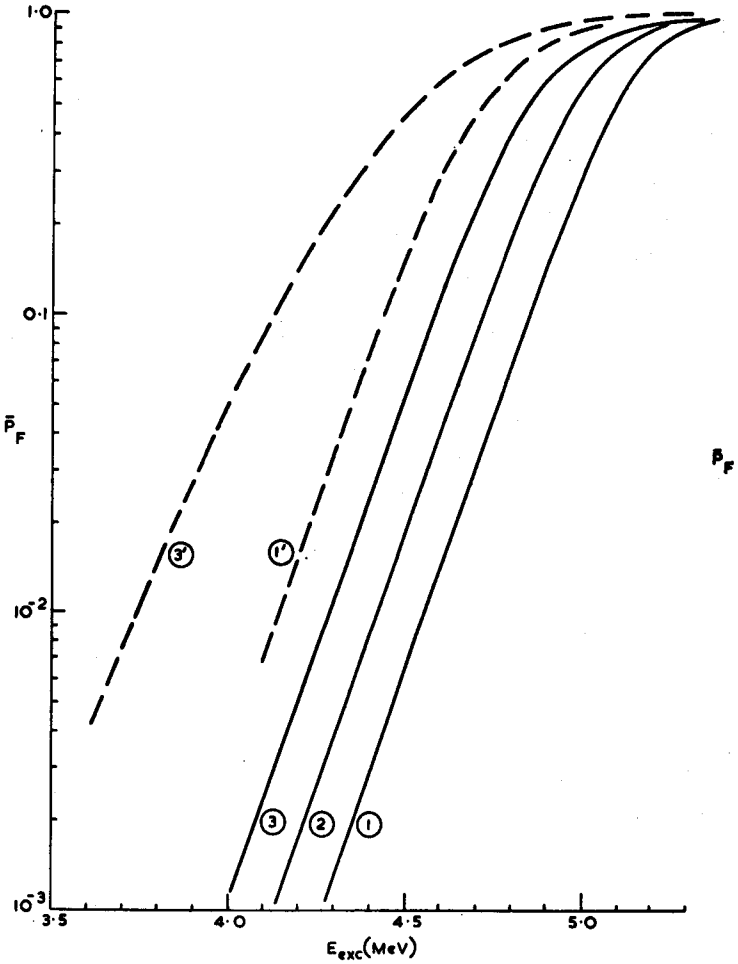

FIG. 33

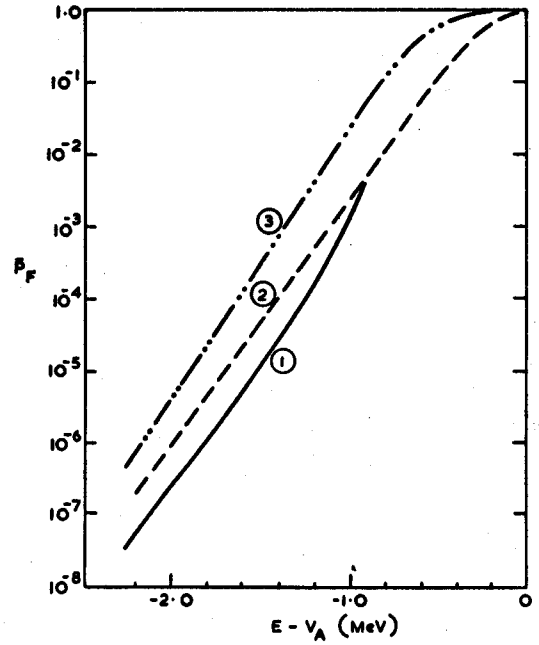

FIG. 34

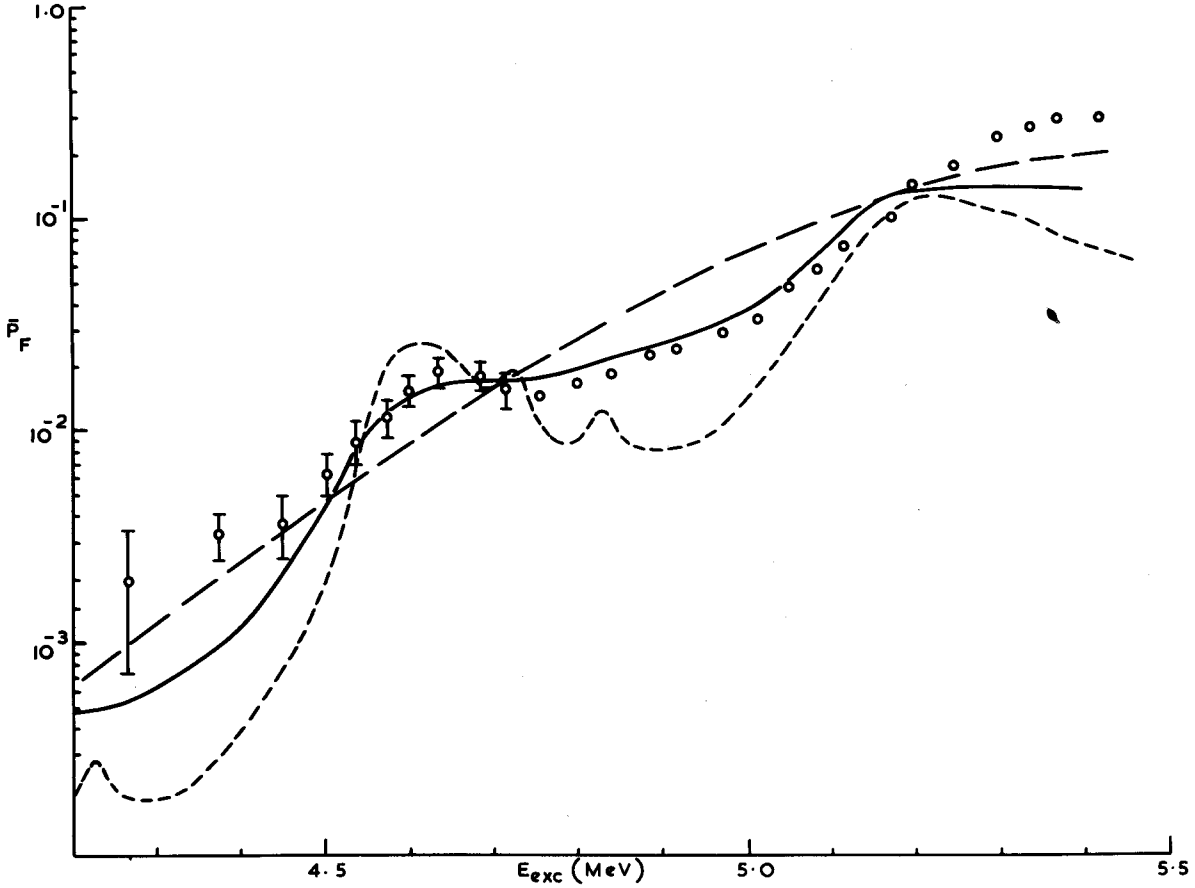
1·0
10^{-1}
10^{-2}
10^{-3}
$\bar{P}_F$
4·5
E_{exc} (MeV)
5·0
5·5

FIG. 35

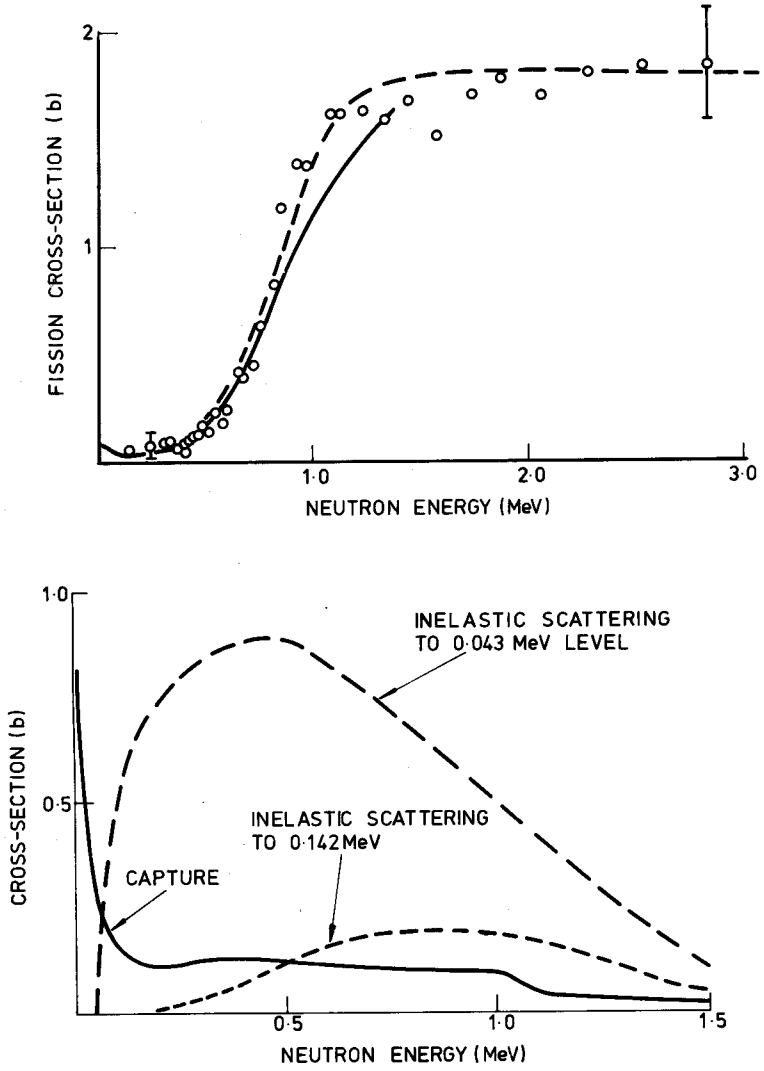
2
1
FISSION CROSS-SECTION (b)
1·0
2·0
3·0
NEUTRON ENERGY (MeV)
1·0
0·5
CROSS-SECTION (b)
INELASTIC SCATTERING
TO 0·043 MeV LEVEL
INELASTIC SCATTERING
TO 0·142 MeV
CAPTURE
0·5
1·0
1·5
NEUTRON ENERGY (MeV)

FIG. 36

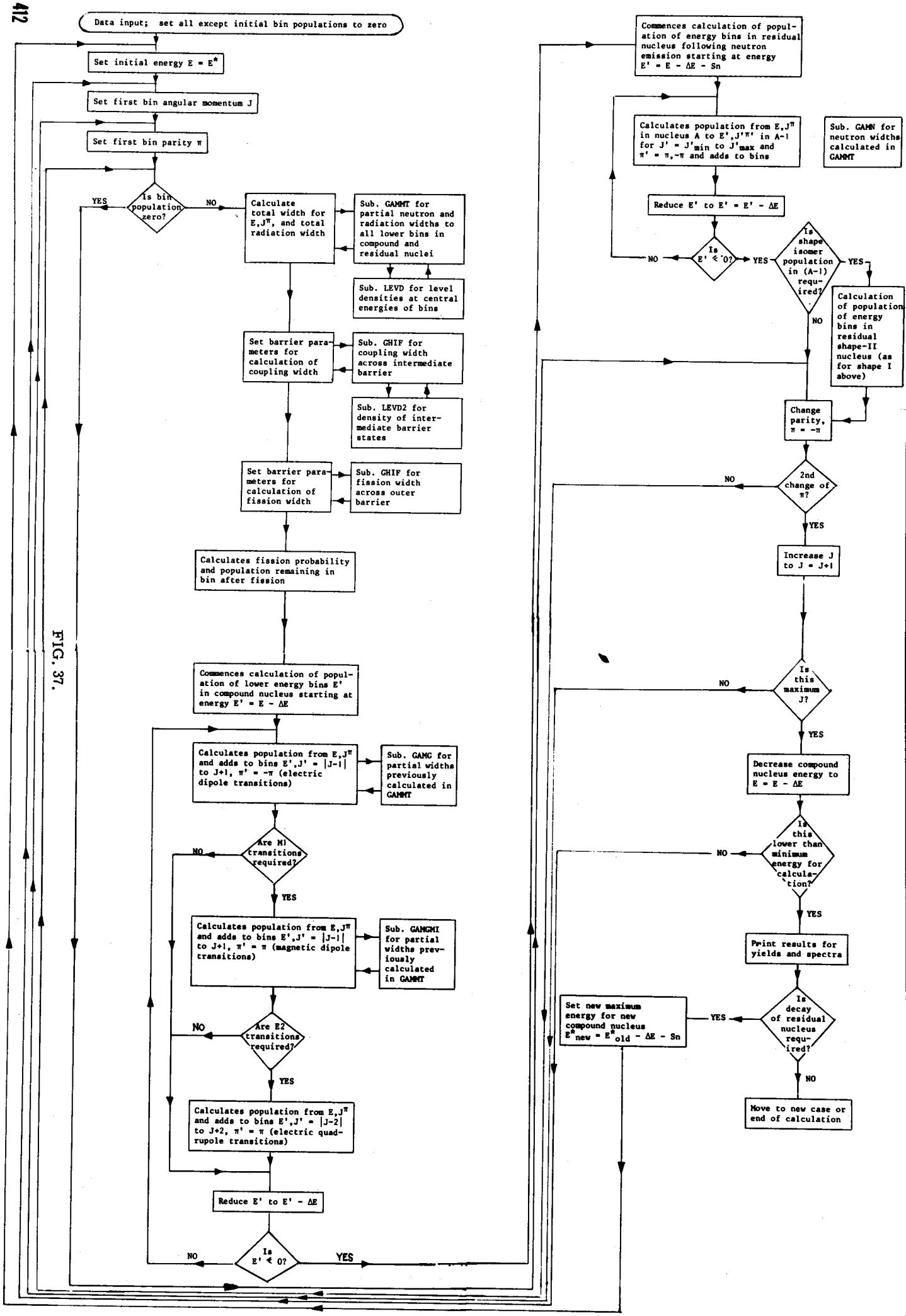
Data input; set all except initial bin populations to zero
Set initial energy E = E*
Set first bin angular momentum J
Set first bin parity π
Is bin population zero?
YES
NO
Calculate total width for E,Jπ, and total radiation width
Sub. GAMMT for partial neutron and radiation widths to all lower bins in compound and residual nuclei
Sub. LEVD for level densities at central energies of bins
Set barrier parameters for calculation of coupling width
Sub. GHIF for coupling width across intermediate barrier
Sub. LEVD2 for density of intermediate barrier states
Set barrier parameters for calculation of fission width
Sub. GHIF for fission width across outer barrier
Calculates fission probability and population remaining in bin after fission
Commences calculation of population of lower energy bins E' in compound nucleus starting at energy E' = E - ΔE
Calculates population from E,Jπ and adds to bins E',J' = |J-1| to J+1, π' = -π (electric dipole transitions)
Sub. GAMG for partial widths previously calculated in GAMMT
Are M1 transitions required?
NO
YES
Calculates population from E,Jπ and adds to bins E',J' = |J-1| to J+1, π' = π (magnetic dipole transitions)
Sub. GAMGMI for partial widths previously calculated in GAMMT
Are E2 transitions required?
NO
YES
Calculates population from E,Jπ and adds to bins E',J' = |J-2| to J+2, π' = π (electric quadrupole transitions)
Reduce E' to E' - ΔE
Is E' ≤ 0?
NO
YES
Commences calculation of population of energy bins in residual nucleus following neutron emission starting at energy E' = E - ΔE - Sn
Calculates population from E,Jπ in nucleus A to E',J'π' in A-1 for J' = J'min to J'max and π' = π,-π and adds to bins
Sub. GAMN for neutron widths calculated in GAMMT
Reduce E' to E' = E' - ΔE
Is E' ≤ 0?
NO
YES
Is shape isomer population in (A-1) required?
YES
NO
Calculation of population of energy bins in residual shape-II nucleus (as for shape I above)
Change parity, π = -π
2nd change of π?
NO
YES
Increase J to J = J+1
Is this maximum J?
NO
YES
Decrease compound nucleus energy to E = E - ΔE
Is this lower than minimum energy for calculation?
NO
YES
Print results for yields and spectra
Is decay of residual nucleus required?
YES
Set new maximum energy for new compound nucleus E*new = E*old - ΔE - Sn
NO
Move to new case or end of calculation

FIG. 37.

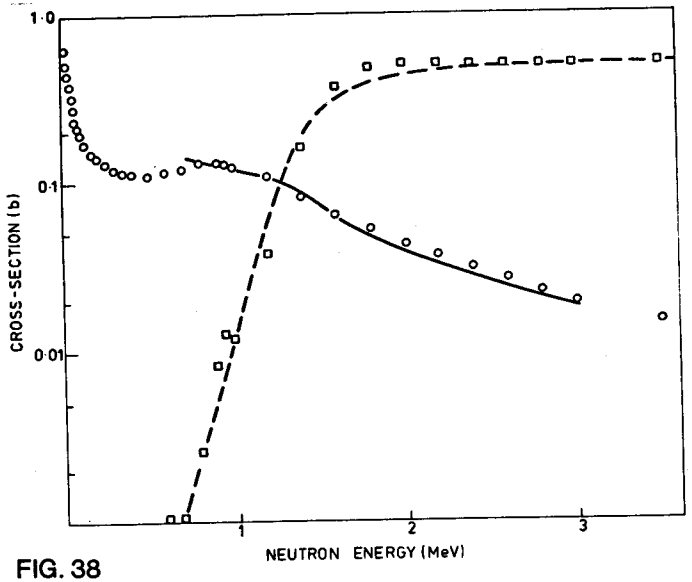

FIG. 38

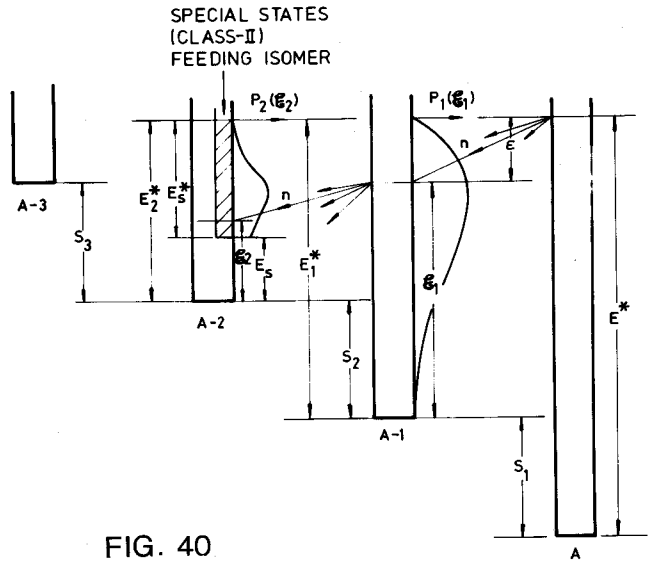

FIG. 40

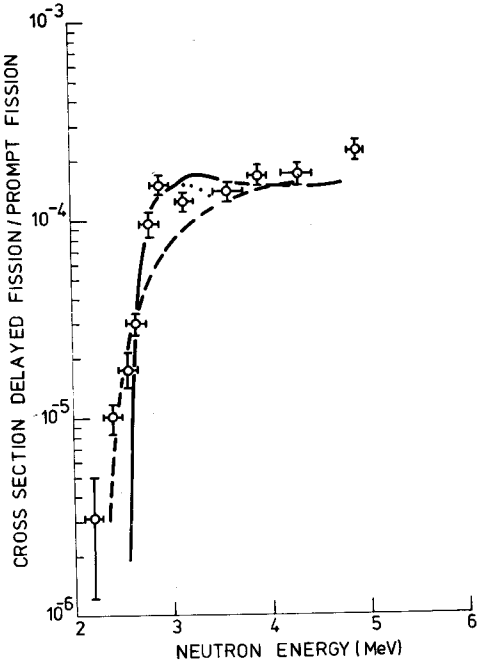

FIG. 42

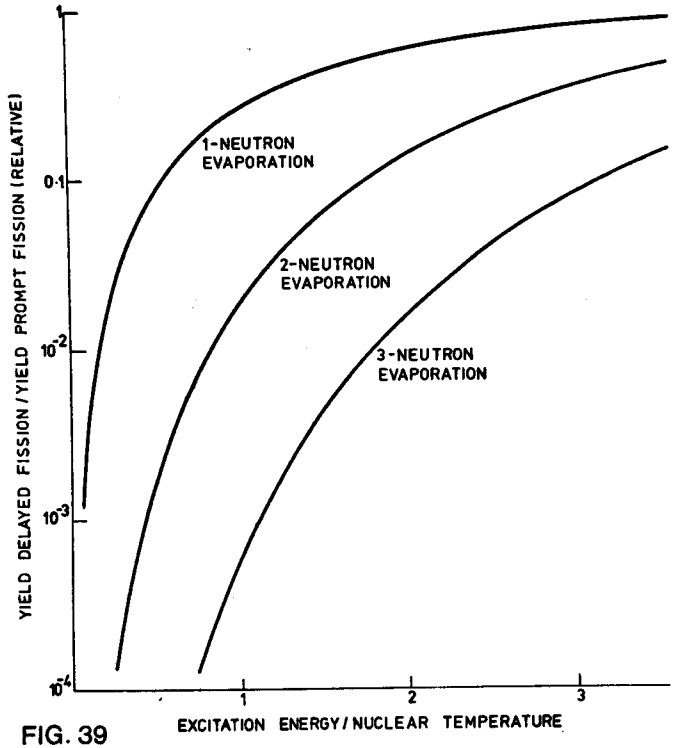

FIG. 39

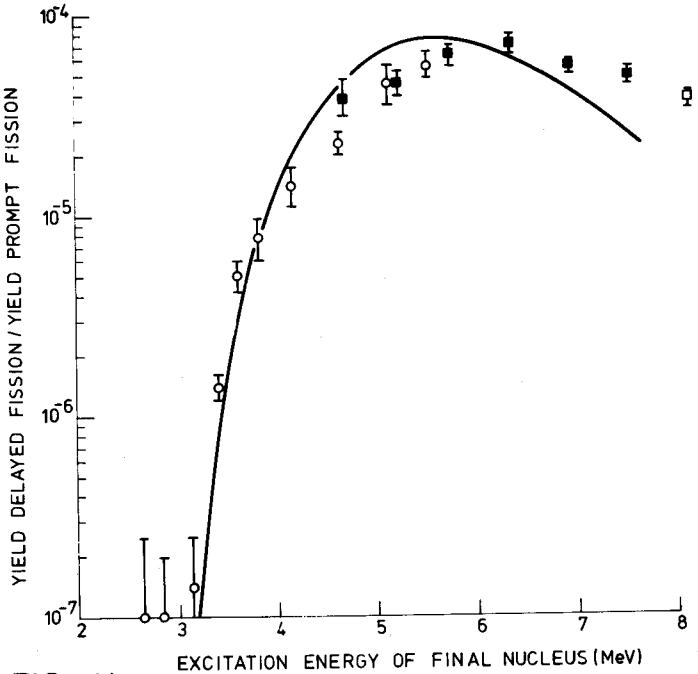

FIG. 41

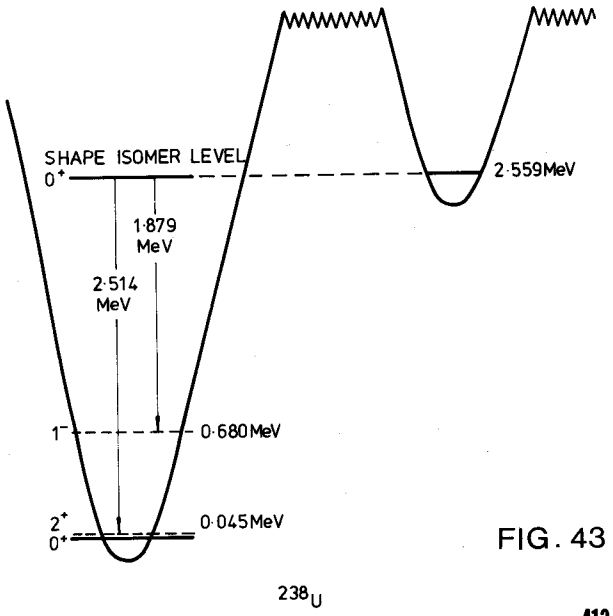

FIG. 43

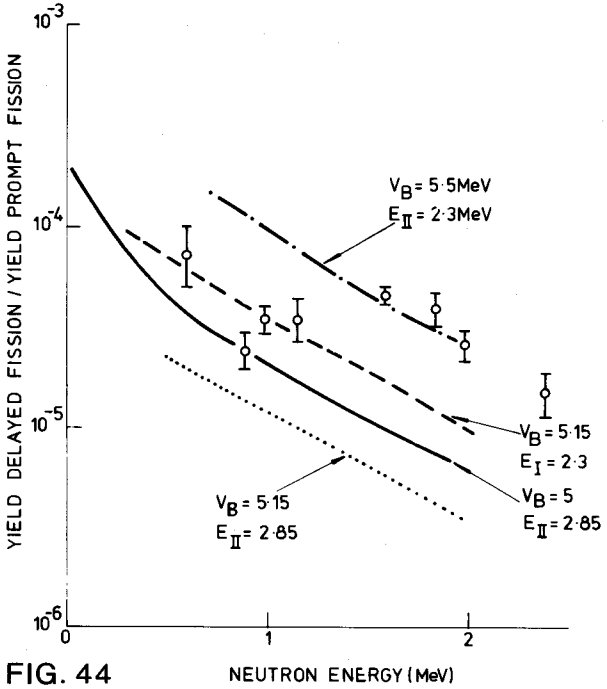

FIG. 44

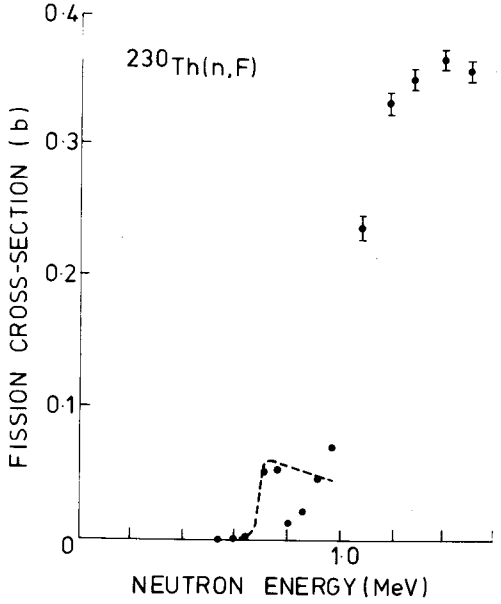

FIG. 45

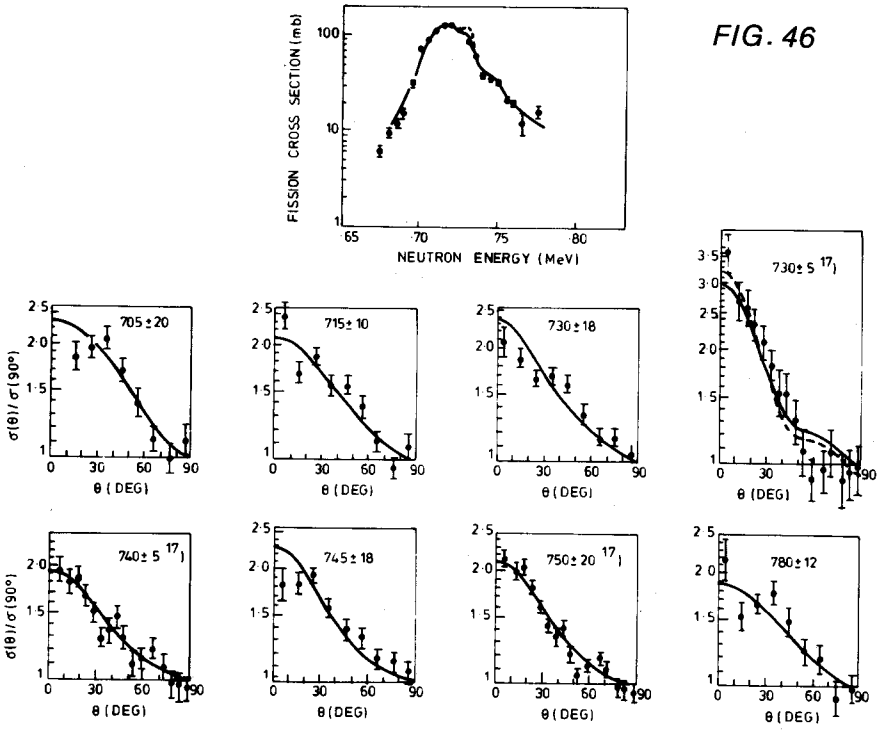

FIG. 46

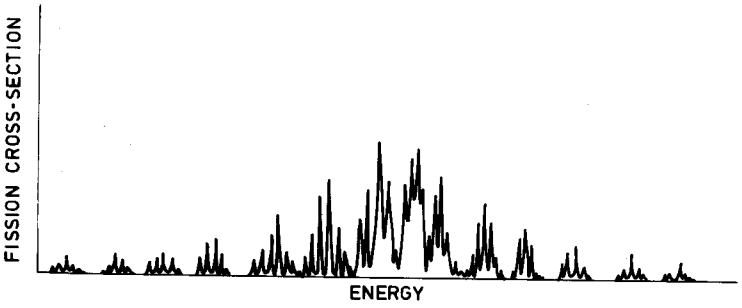

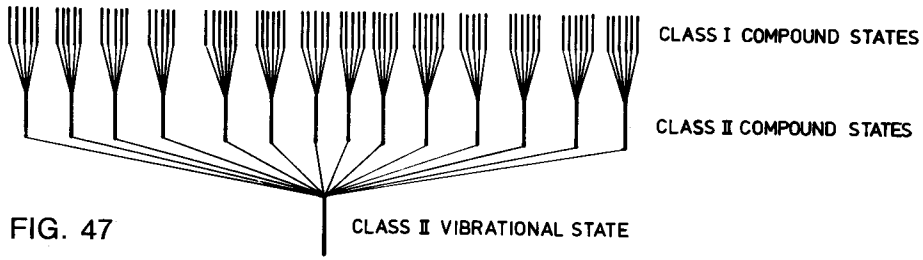

FIG. 47

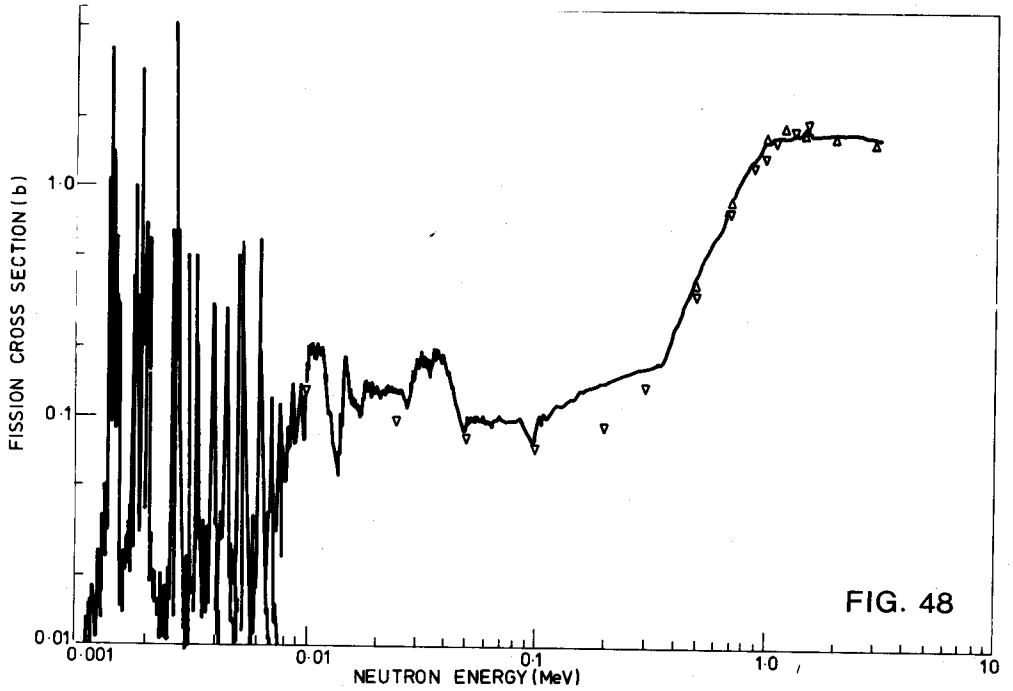

FIG. 48

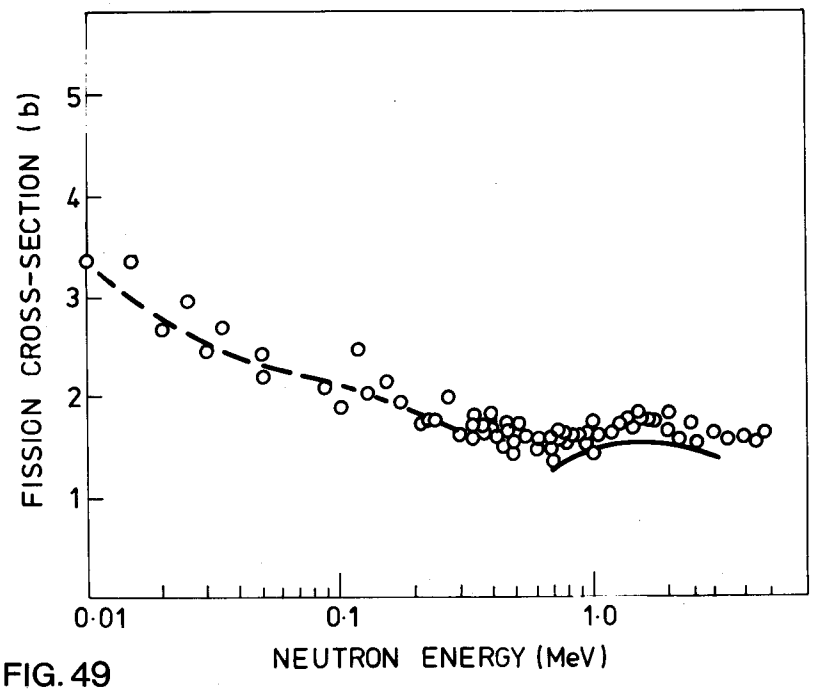

FIG. 49

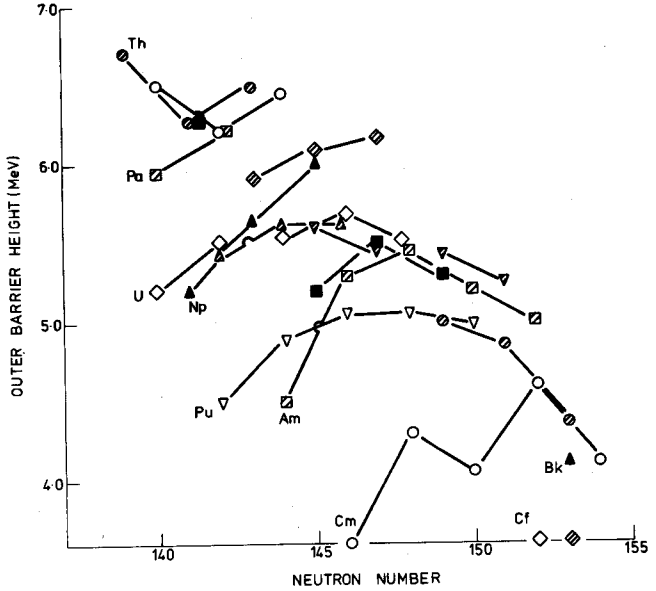

FIG. 51

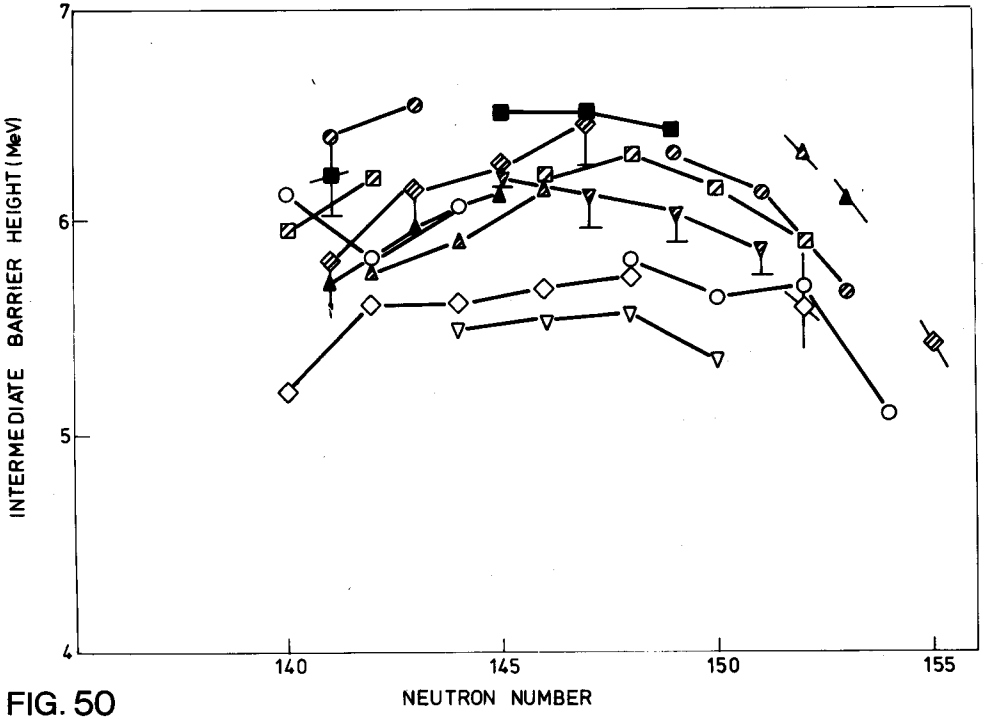

FIG. 50

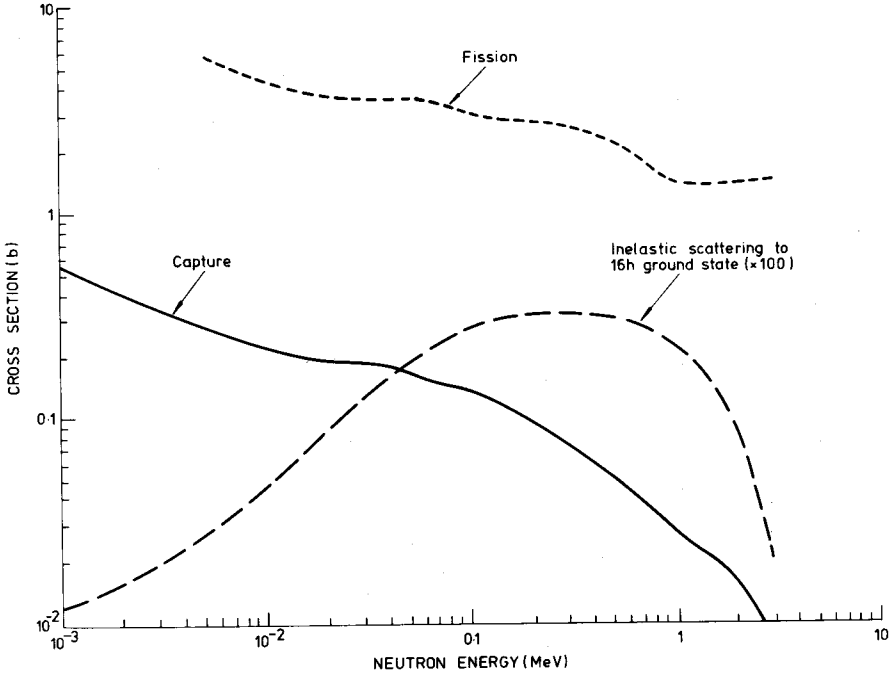

FIG. 52

List of special seminars

held by participants during the Course
on Nuclear Theory for Applications
(not published in these proceedings)[+]

I. General

M.K. Mehta, Bombay, India:
Importance of nuclear physics for developing countries.

R. Ricci, Legnaro, Italy:
Facilities and perspectives of nuclear physics in Italian laboratories.

II. Resonance theory

S. Ganesan, Kalpakkam, India:
On the treatment of the unresolved resonance region and Doppler effect calculations for fast power reactors.

D.B. Syme, Harwell, United Kingdom:
Recent analysis of Ni resonances including the description of a new R-matrix code (multilevel, one channel) used in the analysis.

S.S. Ahmed, Karachi, Pakistan:
Iterative R-matrix method for the exact calculation of reaction cross sections.

III. Optical model

D.C. Agrawal, Varanasi, India:
Characteristics of nuclear potentials.

Ch. Stoyanov, Dubna, USSR:
Description of neutron and gamma strength functions in the quasi-particle - phonon model.

W. Haider, Aligarh, India:
Dispersion relation and surface peaking in the real part of the nuclear optical potential.

A.H. Hussein, Dhahran, Saudi Arabia:
Scattering of 10 MeV polarized neutrons from Pb and Bi in the angular range 1 to 65°.

F.D. Santos, Lisbon, Portugal:
Polarization transfer in (d,n) reactions.

I.-T. Cheon, Seoul, Korea:
Phenomenological pion form factor and pionic atoms.

IV. Statistical theory and nuclear level densities

A. Marcinkowski, Swierk, Poland:
Comparison of nuclear level densities calculated with the super-conductivity model with experiment.

V. Pre-equilibrium decay

F. Shahin, Mansoura, Egypt:
Fluctuations connected with pre-compound emission in excitation functions for the $^{25}Mg(^{3}He,P)$ reaction.

R. Parthasarathy, Madras, India:
Pre-compound emission of neutrons in muon capture.

VI. Fission theory

M. Zielinska-Pfabe, Warsaw, Poland:
Angular momenta of fission fragments.

VII. Nuclear structure

A.M. Khan, Dacca, Bangladesh:
Isospin symmetry breaking in mirror beta decays.

B.P. Singh, Roorkee, India:
Triple angular correlation studies of the radiations from radio-active decay.

A.M. Osman, Cairo, Egypt:
Short-range correlations in nuclei.

VIII. Heavy ion physics

W. Nawrocka, Wroclaw, Poland:
Deep inelastic heavy ion collisions.

L. Satpathy, Bhubaneswar, India:
On the anomaly of high spin states.

[+] For further information on these special seminars interested people are advised to contact the relevant authors.

Course on Nuclear Theory for Applications

Programme schedule

First week: 17-20 January 1978

Tuesday	Wednesday	Thursday	Friday
9.30 Opening	9.30 J.J. Schmidt Lecture III	9.30 C. Mahaux Optical model theory I	9.30 C. Mahaux Lecture III
10.00 J.J. Schmidt Nuclear data importance I	10.45 J.J. Schmidt Lecture IV	10.45 C. Mahaux Lecture II	10.45 C. Mahaux Lecture IV
11.15 J.J. Schmidt Lecture II		12.00 F. Fröhner Applied resonance theory I	
2.30 M.S. Moore Multilevel resonance theory I	2.30 M.S. Moore Lecture III	2.30 F. Fröhner Lecture II	2.00 F. Fröhner Lecture III
3.45 M.S. Moore Lecture II	3.45 M.S. Moore Lecture IV	4.00 Fonda, Fröhner, Mehta, Schmidt - Interviews continued	3.15 F. Fröhner Lecture IV
	4.45 Fonda, Fröhner, Mehta, Schmidt - Interviews with participants		4.30 Working session on resonance theory (Tutors: Moore, Fröhner)
	5.30 Reception - Prof. A. Salam		

Second week: 23–27 January 1978

Monday	Tuesday	Wednesday	Thursday	Friday
9.15 V.S. Ramamurthy Nuclear level densities I	9.15 V.S. Ramamurthy Lecture III	9.15 V.S. Ramamurthy Lecture V	9.15 P.A. Moldauer statistical nuclear reaction theory I	9.15 P.A. Moldauer Lecture III
10.30 V.S. Ramamurthy Lecture II	10.30 V.S. Ramamurthy Lecture IV	10.30 V.S. Ramamurthy Lecture VI	10.30 P.A. Moldauer Lecture II	10.30 P.A. Moldauer Lecture IV
11.45 F. Fröhner Lecture V	11.45 F. Fröhner Lecture VII	11.45 A. Prince Phenomenological optical potentials I	11.45 A. Prince optical model computer codes	11.45 Workshop on optical model computer codes I (Tutors: Prince, Fabbri)
2.30 F. Fröhner Lecture VI	2.30 F. Fröhner Lecture VIII	2.30 A. Prince Lecture II	2.30 M.K. Mehta Special Seminar: Importance of nuclear physics for developing countries	2.30 Workshop on optical model computer codes II (Tutors: Prince, Fabbri)
4.00 S. Ganesan Special Seminar: Unresolved resonances and Doppler effect calculations	3.45 D.B. Syme Special Seminar: Ni resonance analysis with new R-matrix code	3.45 A. Marcinkowski Special Seminar: Comparison of theoretical and experimental nuclear level densities	3.30 W. Nawrocka Special Seminar: Deep inelastic heavy ion collisions	3.45 – 5.15 Special Seminars: B.P. Singh Triple angular correlation studies D.C. Agrawal Characteristics of nuclear potentials W. Haider Dispersion relation and surface peaking in real optical potential
	4.30 Working Session on resonance theory (Tutors: Moore, Fröhner)	4.30 Working session on nuclear level densities (Tutors: Ramamurthy, Dietrich)	4.30 L. Satpathy Special Seminar: Anomaly of high spin states	

Third week: 30 January - 3 February 1978

Monday	Tuesday	Wednesday	Thursday	Friday
9.15 P.A. Moldauer Lecture V	9.15 G. Reffo Statistical theory parameter systematics I	9.15 G. Reffo Lecture III	9.15 Workshop on statistical theory computer codes I (Tutors: Prince, Fabbri)	9.15 V. Bunakov Lecture III
10.30 P.A. Moldauer Lecture VI	10.30 G. Reffo Lecture II	10.30 G. Reffo Lecture IV	10.30 Workshop on statistical theory computer codes II (Tutors: Prince, Fabbri)	10.30 V. Bunakov Lecture IV
11.45 F. Dietrich (for J. Salvy)	11.45 F. Dietrich Lecture III	11.45 A. Prince Statistical theory applications and computer codes I	11.45 V. Bunakov Fundamentals of pre-equilibrium decay I	11.45 D. Seeliger Application of pre-equilibrium decay models I
2.30 F. Dietrich Lecture II	2.30 Workshop on optical model computer codes III (Tutors: Prince, Fabbri)	2.30 A. Prince Lecture II	2.30 V. Bunakov Lecture II	2.30 D. Seeliger Lecture II
3.45 - 5.00 Special Seminars: A.H. Hussein Scattering of polarized neutrons F.D. Santos Polarization transfer in (d,n) reactions I.-T. Cheon Pion form factors	5.00 S.S. Ahmed Special Seminar: Iterative R-matrix method In parallel: 5.00 A.M. Osman Special Seminar: Short range correlations in nuclei	3.45 M. Motta Desk computers in evaluation 4.45 Workshop with demonstration of typical desk computer (Olivetti P6060) (Tutor: M. Motta)	3.45 Ch. Stoyanov Special Seminar: Neutron and gamma strength functions 4.30 A.M. Khan Special Seminar: Isospin breaking in mirror beta decays In parallel: 3.45 Workshop on statistical theory computer codes III (Tutors: Prince, Fabbri)	3.45 F. Shahin Special Seminar: Pre-compound fluctuations in excitation functions 4.30 R. Parthasarathy Special Seminar: pre-compound neutron emission in muon capture

Fourth week: 6–10 February 1978

Monday	Tuesday	Wednesday	Thursday	Friday
9.30 D. Seeliger Lecture III	9.30 M. Brack Fission barrier fundamentals I	9.30 M. Brack Lecture III	9.30 M. Brack Lecture V	9.30 J.E. Lynn Lecture V
10.30 D. Seeliger Lecture IV	10.30 M. Brack Lecture II	10.30 M. Brack Lecture IV	10.30 J.E. Lynn Lecture VI	10.30 J.E. Lynn Lecture VI
11.45 H. Jahn Pre-equilibrium decay in absolute inelastic scattering cross section calculations I	11.45 M. Uhl STAPRE code with consideration of pre-equilibrium decay	11.45 J.E. Lynn Fission barrier theory and its applications I	11.45 M. Brac' Lecture VI	11.45 R. Ricci Special Seminar: Nuclear physics in Italy
2.30 H. Jahn Lecture II	2.30 M. Uhl Lecture II	2.30 J.E. Lynn Lecture II	2.30 J.E. Lynn Lecture IV	2.30 J.E. Lynn Lecture VII
3.45 Working session on pre-equilibrium decay (Tutors: Bunakov, Seeliger, Jahn)	3.45 Workshop on nuclear model codes with pre-equilibrium decay I (Tutors: Prince, Fabbri, Uhl, Strohmaier)	3.45 M. Zielinska-Pfabe Special Seminar: Fission fragment angular momenta In parallel 3.45 Workshop on nuclear model codes with pre-equilibrium decay II (Tutors: Prince, Fabbri, Uhl, Strohmaier)	3.45 Working session on fission theory (Tutors: Lynn, Brack)	3.45 J.E. Lynn Lecture VIII 5.00 Closing of course (J.J. Schmidt)

DIRECTORS

BENZI, V. (Part II)
C N E N
Dipartimento Ricerca Tecnologica
di Base e Avanzata
Divisione Fisica
Via Mazzini 2
C.P. 40138
Bologna
Italy

FONDA, L.
International Centre for Theoretical
Physics
Strada Costiera 11
P.O.B. 586
34100 Trieste
Italy

SCHMIDT, J.J. (Part I)
Nuclear Data Section
International Atomic Energy Agency
P.O.Box 590
A-1011 Vienna
Austria

LECTURERS

Brack, M.
Universität Regensburg
Fachbereich Physik
Institut für Physik I -
- Theoretische Physik
Universitätsstrasse 31
D-8400 Regensburg
Fed. Rep. of Germany

BUNAKOV, V.
Theory Division
Leningrad Nuclear Physics Institute
Academy of Sciences
Gatchina
Leningrad Region, 188350
U.S.S.R.

DIETRICH, F.S.
Lawrence Livermore Laboratory, L-405
University of California
P.O.Box 808
Livermore, California 94550
U.S.A.

FRÖHNER, F.
Institut für Neutronenphysik
und Reaktortechnik
Postfach 3640
D-7500 Karlsruhe
Fed. Rep. Germany

JAHN, H.
Institut für Neutronenphysik
und Reaktortechnik
Postfach 3640
D-7500 Karlsruhe
Fed. Rep. Germany

LYNN, J.E.
UK Atomic Energy Research Establishment
Harwell, OX11 ORA
U.K.

MAHAUX, C.
Institut de Physique
Université de Liege
Sart-Tilman
B-4000 Liege 1
Belgium

MEHTA, M.
Bhabha Atomic Research Centre
Trombay
Bombay 400 085
India

MOLDAUER, P.A.
Argonne National Laboratory
9700 South Cass Avenue
Argonne, Illinois 60439
U.S.A.

MOORE, M.S.
Los Alamos Scientific Laboratory
University of California
P.O.Box 1663
Los Alamos, New Mexico 87545
U.S.A.

MOTTA, M.
Divisione Fisica
Centro di Calcolo del CNEN
Via Mazzini 2
I-40138 Bologna
Italy

PRINCE, A.
National Nuclear Data Center
Brookhaven National Laboratory
Upton, New York 11973
U.S.A.

RAMAMURTHY, V.S.
Fission Physics Section
Bhabha Atomic Research Centre
Trombay
Bombay 400 085
India

REFFO, G.
Centro di Calcolo del CNEN
Via Mazzini 2
I-40138 Bologna
Italy

SALVY, J.
Centre d'Etudes de
Bruyeres-le-Chatel
B.P. No. 561
F-92542 Montrouge
FRANCE

Schmidt, J.J.
IAEA Nuclear Data Section
Vienna International Centre
P.O. Box 100
A-1400 Vienna
AUSTRIA

SEELIGER, D.
Sektion Physik
Technische Universität Dresden
Mommsenstra. 13
DDR-8027 Dresden
German, Dem. Rep.

UHL, M.
Institut für Radiumforschung und
Kernphysik
Boltzmanngasse 3
A-1090 Vienna
Austria

PARTICIPANTS

ABBOUD, A.A.
Reactor Technology Department
Atomic Energy Establishment
Cairo
Egypt

ABDULMOMEN, M.A.
Physics Department
Faculty of Science
Riyadh University
Riyadh
Saudi Arabia

ADAMSKI, L.K.
Department of Reactor Physics
Institute of Nuclear Research
05-400 Otwock-Swierk
Poland

AGRAWAL, D.C.
Department of Physics
Faculty of Science
Banaras Hindu University
Varanasi - 221 005
India

AGYEI, A.K.
Department of Physics
University of Cape Coast
Cape Coast
Ghana

AHMAD, M.
Technical Development Division
Pakistan Atomic Energy Commission
P.O.Box 1114
Islamabad
Pakistan

AHMAD, S.S.
C - 96
Staff Town
University Campus
Karachi 32
Pakistan

AHMED, F.
Department of Physics and
Astrophysics
University of Delhi
Delhi - 110007
India

AHMED, I.
Reactor Physics Group
Nuclear Engineering Division
PINSTECH
P.O.Nilore
Rawalpindi
Pakistan

ALAM, B.
Department of Physics
University of Dacca
Dacca - 2
Bangladesh

ALBINSKI, J. (Affiliate)
Department of Physics
University of Cracov
Cracov
Poland

ALVEAR, C.
Instituto de Fisica
Universidade Federal do
Rio de Janeiro
Ilha do Fundao
Rio de Janeiro - 20.000
Brazil

AMARANTE, J.A.A.
Centro Tecnico Aeroespacial
Instituto de Atividades Espaciais
12.200 Sao José dos Campos
Brazil

AMUSA, A.
Department of Physics
University of Ife
Ile-Ife
Nigeria

AUGUSTYNIAK, W.
Division I
Institute of Nuclear Research
Hoza 68
Warsaw
Poland

BAK, H.-I.
Department of Nuclear Engineering
College of Engineering
Seoul National University
Seoul
Korea

BARTAL, Y.
TECHNION
Haifa
Israel

BASTIAN, C.
B.C.M.N.
EURATOM
Steenweg Op Retie
2440 Geel
Belgium

BEN MOHAMED, A.K.
Departament de Physique
Université de Niamey
B.P. 237
Niamey
Niger

BRUSEGAN, A.
B.C.M.N. - EURATOM
Steenweg Op Retie
2440 Geel
Belgium

BUDNAR, M.G. (Affiliate)
Institut "Jozef Stefan"
Jamova 39
P.O.Box 199
Ljubljana
Yugoslavia

BURRA, G.S.
St. Xavier's College
30 Park Street
Calcutta - 700216
India

CHEON, I.-T.
Department of Physics
Yonsei University
Seoul 120-00
Korea

CINDRO, N.
"Ruder Bosković" Institute
P.O.B. 1016
41001 Zagreb
Yugoslavia

CRISTIAN, I.G.
Institute for Nuclear Power Reactors
Bucharest Magurele
P.O.Box 5203
Romania

D'OLIVEIRA, A.B.
Divisão de Estudos Avancados
CTA - IAE - EAV
12200 São José dos Campos
E.S. Paulo
Brazil

DYMARZ, R. (Affiliate)
Institute of Nuclear Physics
Radzikowskiego 152
31-342 Krakow
Poland

FABBRI, F.
Centro di Calcolo del CNEN
Via G. Mazzini 2
Bologna
Italy

FORT, E.
DRNR/SPNR
Bat 230
CEA, CEN-Cadarache
13115 Saint-Paul-lez-Durance
France

Ganesan, S.
Reactor Research Centre
Kalpakkam P.O.
Chingleput Dist.
Tamil Nadu
INDIA

GARG, S.B.
Bhabha Atomic Research Centre
Bombay 400 085
India

GOUMRY, N. (Affiliate)
Department of Physics
Faculty of Science
University of Jordan
Amman
Jordan

GUL, K.
PINSTECH
P.O.Nilore
Rawalpindi
Pakistan

GUPTA, H.P.
5th Floor, T.R.P.S.
Central Complex
Bhabha Atomic Research Centre
Trombay
Bombay 400 085
India

HAIDER, W.
Department of Physics
Aligarh Muslim University
Aligarh 202001
India

HAMDAN, M.A.
Physics Department
Basrah University
Basrah
Iraq

HAMID, K.
Neutron Physics Laboratory
Eötvös Lorand University
Puskin 5-7
1088 Budapest VIII
Hungary

HARRIS, M.J.
A.E.R.E., Harwell
Didcot
Oxfordshire, OX11 ORA
U.K.

HASNAIN, S.A.
PINSTECH
P.O.Nilore
Rawalpindi
Pakistan

HOSSAIN, M.H.
Department of Physics
Bangladesh Agricultural University
Mymensingh
Bangladesh

HUSAIN, D.
Department of Mathematics
Dacca University
Dacca - 2
Bangladesh

HUSAIN, M.M.
Atomic Energy Centre
P.O.Box 164
Ramna
Dacca
Bangladesh

HUSSEIN, A.H.
Dhahran International Airport
P.O.B. 144
UPM, 449
Dhahran
Saudi Arabia

HUSSEIN, H.
Department of Physics
Faculty of Science
University of Alepo
Alepo
Syria

KHADKIKAR, S.B.
Physical Research Laboratory
Navrangpura
Ahmedabad 380009
India

KHALID, Z.M.
Nuclear Engineering Division
PINSTECH
P.O. Nilore
Rawalpindi
Pakistan

KHAN, A.M.
Physics Department
University of Dacca
Dacca - 2
Bangladesh

KIM, C.H.
Nuclear Engineering Department
Seoul National University
Chungryang
P.O.Box 105
Seoul
Korea

KISS, A. (Affiliate)
Department of Atomic Physics
Roland Eötvös University
Puskin 5-7
1088 Budapest VIII
Hungary

KIZILTAN, H.
Institute of Physics, 83
Hacettepe University
Ankara
Turkey

KPONOU, A.E.F.
Department of Physics
Fourah Bay College
University of Sierra Leone
Freetown
Sierra Leone

LASIJO, R.S.
Bandung Reactor Centre
Jl. Tamansari 71
Bandung
Indonesia

LEES, E.W.
Atomic Energy Research Establishment
Nuclear Physics Division
Building 418, Harwell
Oxfordshire, OX11 ORA
U.K.

LOPAC, V.
Institute "Ruder Boskovic"
P.O.Box 1016
41001 Zagreb
Yugoslavia

MAHTABOALLY, Q.G.
Department of Physics
University of Rajshahi
Rajshahi
Bangladesh

MARCINKOWSKI, A.M. (Affiliate)
Institute of Nuclear Research
ul. Hoza 69
00-681 Warsaw
Poland

MARTINEZ, A.S.
COPPE
Universidade Federal do
Rio de Janeiro
Caixa Postal 1191
ZC 00 - 20.000 Rio de Janeiro
Brazil

MATTHES, W.K.
C.C.R. EURATOM
21020 Ispra
Italy

MEDRANO, G.
Internacional de Ingeniería y
Estudios Tecnicos (INTECSA)
Power Division
Condesa de Venadito I
Madrid 27
Spain

MENAPACE, E.
Centro Calcolo del CNEN
Via Mazzini 2
Bologna
Italy

MIKHAIL, M.L.
Reactor Department
Atomic Energy Commission
Cairo
Egypt

MUMBA, N.
National Council for Scientific
Research
P.O.Box Ch. 158
Chelston
Lusaka
Zambia

NAJAM, M.R.
GNS - PINSTECH
P.O.Nilore
Rawalpindi
Pakistan

NASEEM, H.A.
Department of Physics
Panjab University
Chandigarh 160014
India

NAWROCKA, W.
Institute of Theoretical Physics
University of Wroclaw
ul. Cybulskiego 36
50-205 Wroclaw
Poland

NONIE, S.E.B.
Department of Physics
Fourah Bay College
University of Sierra Leone
Freetown
Sierra Leone

NOTARI, C.
Comision Nacional de Energia Atomica
Av. Libertador 8250
Buenos Aires
Argentina

OSAE, E.K.
(Present - for 3 years)
Department of Physics
University of Kent
Canterbury, Kent
U.K.

(Permanent)
Ghana Atomic Energy Commission
P.O.Box 80, Legon
Ghana

OSMAN, A.M.
Physics Department
University of Cairo
Cairo
Egypt

PARTHASARATHY, R.
Institute of Mathematical Sciences
MATSCIENCE
Madras - 600020
India

PASCHOA, A.S.
Departamento de Fisica
Pontificia Universidade Catolica
Rua Marques de Sao Vicente, 209
Rio de Janeiro
Brazil

PAUL, O.P.K.
Bhabha Atomic Research Centre
CIRUS
Trombay
Bombay 400 085
India

PAVIOTTI CORCUERA, R.A.
Comision Nacional de Energia Atomica
Avda. del Libertador 8250
1249 Buenos Aires
Argentina

PICON, C.L.
Universidad Nacional de Ingenieria
Av. Tupamac Amaru Sin.
Apartado 1301
Lima
Peru

POCANIC, D.
Physics Department
Institute "Ruder Bošković"
P.O.Box 1016
41001 Zagreb
Yugoslavia

RAOOF, M.A.
Department of Physics
University of Karachi
Karachi 32
Pakistan

RATNA RAJU, R.D.
Department of Physics
Andhra University
Visakhapatnam 530 003
India

RAVANSHID, H.
Atomic Energy Organization
9 Rodsar Street
Hafez Street
Tehran
Iran

RIBANSKY, I. (Affiliate)
Institute of Physics
Slovak Academy of Sciences
89930 Bratislava
Czechoslovakia

ROBERTO, V.
Istituto di Fisica
Università di Trieste
Trieste
Italy

ROSATO, A.
Physics Department, ITA, CTA
S. José dos Campos
Sao Paulo
Brazil

SANTOS, F.D.
Laboratorio de Fisica
Facultade de Ciencias
R. Escola Politecnica
Lisbon - 2
Portugal

SANTOS, S.
Instituto di Fisica
Universidade Federal de
Rio de Janeiro
Bloco A
Ilma de Fundao
Rio de Janeiro
Brazil

SATPATHY, L.
Institute of Physics
A/105 Saheed Nagar
Bhubaneswar - 751007
India

SEFIDVASH, F.
Nuclear Engineering Department
Arya Mehr University
P.O.Box 3406
Tehran
Iran

SEN GUPTA, H. M.
Department of Physics
University of Dacca
Dacca - 2
Bangladesh

SHAHIN, F.
Department of Physics
Mansoura University
Mansoura
Egypt

SHARMA, M.L.
Reactor Research Centre
Kalpakkam 603102
India

SHARMA, S.K.
Physical Research Laboratory
Navarangpura
Ahmedabad 380 009
India

SHELLEY, R.
B.C.M.N., EURATOM
Steenweg Op Retie
2440 Geel
Belgium

SINGH, B.P.
Department of Physics
University of Roorkee
Roorkee - 247 672
India

STANCIC, V.A.
Boris Kidric Institute
P.O.Box 522
Beograd
Yugoslavia

STOYANOV, C.P.
Laboratory of Theoretical Physics
Joint Institute for Nuclear Research
Head Post Office, Box 79
Dubna, Moscow
U.S.S.R.

STROHMAIER, B.
Institut für Radiumforschung
und Kernphysik
Boltzmanngasse 3
A-1090 Vienna
Austria

SUBBA RAO, K.
Bhabha Atomic Research Centre
Bombay 400 085
India

SUMITRA, T.
Department of Nuclear Technology
Faculty of Engineering
Chulalongkorn University
Bangkok
Thailand

SYME, B.
Nuclear Physics Division
A.E.R.E., Harwell
Didcot
Oxfordshire OX11 ORA
U.K.

TADIC, D.
Prirodoslono-Matematicki Facultet
Zavod za Teorijsku Fiziku
Marulićev trg 19/I
41000 Zagreb
Yugoslavia

TAY, G.
Ghana Atomic Energy Commission
P.O.Box 80
Legon
Ghana

TELLO-DUQUE, V.M.
Departamento de Física
Facultad de Ingeniería
Universidad de San Carlos
Zona 12
Guatemala

TESTONI, J.E.
Comision Nacional de Energia
Atomica - Reactores
Avda. del Libertador 8250
Buenos Aires
Argentina

THUONG, T.Q.
DRNR/SPNR
Bat 230
CEA, CEN Cadarache
13115 St. Paul-lez-Durance
France

TRAORE, B.M.
Direction Générale de l'Hydraulique
et de l'Energie
Division Energie
B.P. 66
Bamako
Mali

VENTURA, A.
Centro di Calcolo del CNEN
Via G. Mazzini 2
Bologna
Italy

WAGHMARE, Y.R. (Associate)
Physics Department
Indian Institute of Technology
Kanpur - 208016
India

WAHEED, A.
Nuclear Physics Division
PINSTECH
P.O.Nilore
Rawalpindi
Pakistan

YALCIN, C.
Physics Department
Middle East Technical University
Inonu Bulvari
Ankara
Turkey

ZIELINSKA-PFABE, M.
Institute of Nuclear Research
Nuclear Theory Department
Hoza 69
00-681 Warsaw
Poland

80–00857